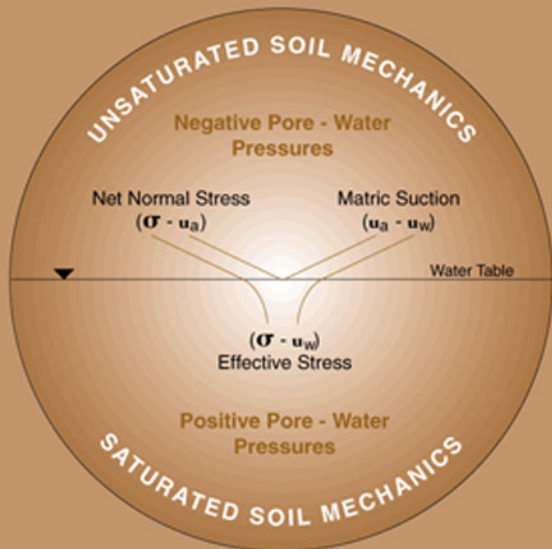


The Emergence of Unsaturated Soil Mechanics

Fredlund volume



Editors:

A.W. Clifton

S.L. Barbour

G.W. Wilson

The Emergence of Unsaturated Soil Mechanics

Fredlund Volume

Inquiries: Monograph Publishing Program, NRC Research Press, National Research Council of Canada, Ottawa, Ontario K1A 0R6, Canada.

Correct citation for this publication: Clifton, A.W., Wilson, G.W., and Barbour, S.L. (*Editors*). 1999. *The Emergence of Unsaturated Soil Mechanics: Fredlund Volume*. NRC Research Press, Ottawa, Ontario, Canada. 735 p.

The Emergence of Unsaturated Soil Mechanics

Fredlund Volume

Editors

A.W. Clifton

Clifton Associates Ltd., Regina, Saskatchewan

G.W. Wilson

Department of Civil Engineering,
University of Saskatchewan, Saskatoon, Saskatchewan

S.L. Barbour


Department of Civil Engineering,
University of Saskatchewan, Saskatoon, Saskatchewan

NRC-CNRC

NRC RESEARCH PRESS
Ottawa 1999

© 1999 National Research Council of Canada

All rights reserved. No part of this publication may be reproduced in a retrieval system, or transmitted by any means, electronic, mechanical, photocopying, recording or otherwise, without the prior written permission of the National Research Council of Canada, Ottawa, Canada K1A 0R6.

Printed in Canada on acid-free paper 

ISBN 0-660-17256-9

NRC No. 41645

Canadian Cataloguing in Publication Data

Main entry under title:

The emergence of unsaturated soil mechanics

“Fredlund volume”

Includes bibliographical references.

Issued by the National Research Council of Canada.

ISBN 0-660-17256-9

I. Soil mechanics.

I. Clifton, W.A. (Wayne)

II. Wilson, G. Ward (Gordon Ward), 1955–

III. Barbour, S.L. (S. Lee)

IV. National Research Council Canada.

TA710.E53 1999 624.1'5136 C99-980179-1

Contents

Abstract/Résumé	xi
Preface	xiii
Acknowledgments	xv

Part I

Delwyn G. Fredlund — An Appreciation

A.W. Clifton, S.L. Barbour, and G.W. Wilson	1
---	---

Part II

Stress State for Unsaturated Soils and the Measurement of Soil Suction

N.R. Morgenstern	7
Fredlund, D.G., and Morgenstern, N.R. 1977. Stress state variables for unsaturated soils. <i>Journal of the Geotechnical Engineering Division, Proceedings, American Society of Civil Engineering (GT5)</i> , 103 : 447–466.	13
Fredlund, D.G. 1987. The stress state for expansive soils. <i>Proceedings, Sixth International Conference on Expansive Soils, New Delhi, India</i> , pp. 1–9.	27
Krahn, J., and Fredlund, D.G. 1972. On total, matric and osmotic suction. <i>Soil Science</i> , 114 (5): 339–348.	35
Barbour, S.L., and Fredlund, D.G. 1989. Physico-chemical state variables for clay soils. <i>Proceedings, XII International Conference on Soil Mechanics and Foundation Engineering, Rio de Janeiro, Brazil</i> , pp. 1839–1843.	42
Fredlund, D.G., and Rahardjo, H. 1988. State-of-development in the measurement of soil suction. <i>Proceedings of the First International Conference on Engineering Problems of Regional Soils, Beijing, China</i> , pp. 582–588.	47
Fredlund, D.G. 1992. Background, theory, and research related to the use of thermal conductivity sensors for matric suction measurements. <i>In Advances in Measurement of Soil Physical Properties; Bringing Theory into Practice</i> . Soil Science Society of America, Special Publication No. 30, pp. 249–262.	53
Loi, J., Fredlund, D.G., Gan, J.K., and Widger, R.A. 1992. Monitoring soil suction in an indoor test track facility. <i>Transportation Research Board, Transportation Research Record 1362</i> , pp. 101–110.	60
Fredlund, D.G., Gan, J.K., and Rahardjo, H. 1991. Measuring negative pore-water pressures in a freezing environment. <i>Transportation Research Board, Transportation Research Record No. 1307</i> , pp. 291–299.	70
Guan, Y., and Fredlund, D.G. 1997. Direct measurement of high soil suction. <i>Proceedings, Third Brazilian Symposium on Unsaturated Soils, Rio de Janeiro, Brazil</i>	79
Fredlund, D.G., Gan, J.K.-M., Guan, Y., and Richardson, N. 1997. Suction measurements on a Saskatchewan soil using a direct measurement, high suction sensor. <i>Transportation Research Board 76th Annual Meeting, Washington, DC</i>	85
Fredlund, D.G., Gan, J.K.-M., and Gallen, P. 1995. Suction measurements on compacted till specimens and indirect filter paper calibration technique. <i>Transportation Research Board, Transportation Research Record 1481</i> , pp. 3–9.	96

Part III

Theoretical Framework for Unsaturated Soil Mechanics

A.W. Clifton	105
------------------------	-----

Fredlund, D.G. 1979. Second Canadian geotechnical colloquium: Appropriate concepts and technology for unsaturated soils. <i>Canadian Geotechnical Journal</i> , 16 (1): 121–139. . . .	111
Fredlund, D.G., and Rahardjo, H. 1985. Theoretical context for understanding unsaturated residual soil behavior. <i>Proceedings of the First International Conference on Geomechanics in Tropical Lateritic and Saprolitic Soils, Brazilia, Brazil</i> , pp. 295–306. . . .	127
Fredlund, D.G. 1985. Soil mechanics principles that embrace unsaturated soils. <i>Proceedings, 11th International Society for Soil Mechanics and Foundation Engineering, San Francisco, USA., Vol. 2</i> , pp. 465–473.	133
Fredlund, D.G. 1995. The scope of unsaturated soils mechanics: An overview. <i>Proceedings, 1st International Conference on Unsaturated Soils, Paris, France, Vol. 3</i> , pp. 1155–1177. . . .	140
Wulfsohn, D., Adams, B.A., and Fredlund, D.G. 1996. Application of unsaturated soil mechanics for agricultural conditions. <i>Canadian Agricultural Engineering</i> , 38 (3): 173–181. . . .	157
Fredlund, D.G. 1997. From theory to the practice of unsaturated soil mechanics. <i>Proceedings, 3rd Brazilian Symposium on Unsaturated Soils, Rio de Janeiro, Brazil</i>	166
Fredlund, D.G., and Xing, A. 1994. Equations for the soil-water characteristic curve. <i>Canadian Geotechnical Journal</i> , 31 (3): 521–532.	181
Fredlund, D.G. 1964. Comparison of soil suction and one-dimensional consolidation characteristics of a highly plastic clay. <i>National Research Council of Canada, Division of Building Research, Technical Report No. 245, Ottawa, Ontario</i>	193
Fredlund, M.D., Fredlund, D.G., and Wilson, G.W. 1997. Prediction of the soil-water characteristic curve from grain-size distribution and volume-mass properties. <i>Proceedings, Third Brazilian Symposium on Unsaturated Soils, NSAT'97, Rio de Janeiro, Brazil, April 22–25, Vol. 1</i> , pp. 13–23.	202
Fredlund, M.D., Sillers, W.S., Fredlund, D.G. and Wilson, G.W. 1996. Design of a knowledge-based system for unsaturated soil properties. <i>Proceedings, Third Canadian Conference on Computing in Civil and Building Engineering, Aug. 26–28</i> , pp. 659–677. . . .	207
 Part IV	
Shear Strength of Unsaturated Soils and its Application	
H. Rahardjo	217
Fredlund, D.G., Morgenstern, N.R., and Widger, R.A. 1978. The shear strength of unsaturated soils. <i>Canadian Geotechnical Journal</i> , 15 (3): 313–321.	223
Fredlund, D.G., Rahardjo, H., and Gan, J.K.-M. 1987. Non-linearity of strength envelope for unsaturated soils. <i>Proceedings, 6th International Conference on Expansive Soils, New Delhi, India</i> , pp. 49–54.	231
Ho., D.Y.F. and Fredlund, D.G. 1982. A multistage triaxial tests for unsaturated soils. <i>ASTM, Geotechnical Testing Journal</i> , 5 (1/2): 18–25.	237
Gan, J.K.-M., Fredlund, D.G., and Rahardjo, H. 1988. Determination of the shear strength parameters of an unsaturated soil using the direct shear test. <i>Canadian Geotechnical Journal</i> , 25 (8): 500–510.	244
Gan, J.K.-M., and Fredlund, D.G. 1996. Shear strength characteristics of two saprolitic soils. <i>Canadian Geotechnical Journal</i> , 33 : 595–609.	255
Oloo, S.Y., and Fredlund, D.G. 1996. A method for the determination of ϕ^b for statically compacted soils. <i>Canadian Geotechnical Journal</i> , 33 (2): 272–280.	269
Fredlund, D.G., Xing, A., Fredlund, M.D., and Barbour, S.L. 1996. The relationship of the unsaturated shear strength to the soil-water characteristic curve. <i>Canadian Geotechnical Journal</i> , 33 (3): 440–448.	277

Vanapalli, S.K., Fredlund, D.G., Pufahl, D.E., and Clifton, A.W. 1996. Model for the prediction of shear strength with respect to soil suction. *Canadian Geotechnical Journal*, **33**(3): 379–392. 286

Ho, D.Y.F., and Fredlund, D.G. 1982. Increase in shear strength due to soil suction for two Hong Kong soils. *Proceedings, ASCE, Geotechnical Conference on Engineering and Construction in Tropical and Residual Soils, Honolulu, Hawaii*, pp. 263–295. 300

Ching, R.K.H., Sweeney, D.J., and Fredlund, D.G. 1984. Increase in factor of safety due to soil suction for two Hong Kong slopes. *Proceedings, Fourth International Symposium on Landslides, Toronto*, pp. 617–623. 313

Fredlund, D.G. 1989. Negative pore-water pressures in slope stability. *Proceedings, South American Symposium on Slope Stability, Paipa, Colombia*. 320

Fredlund, D.G. 1995. The stability of slopes with negative pore-water pressures. *In The Ian Boyd Donald Symposium on Modern Developments in Geomechanics. Edited by C.M. Haberfield, Monash University, Department of Civil Engineering, Clayton, Australia*, pp. 99–116. 333

Hasan, J.U., and Fredlund, D.G. 1980. Pore pressure parameters for unsaturated soils. *Canadian Geotechnical Journal*, **17**(3): 395–404. 344

Fredlund, D.G., Rahardjo, H., and Ng, T. 1993. Effect of pore-air and negative pore-water pressures on stability at the end-of-construction. *Proceedings, International Conference on Dam Engineering, Johor Bahru, Malaysia*, pp. 43–51. 352

Pufahl, D.E., Fredlund, D.G., and Rahardjo, H. 1983. Lateral earth pressures in expansive clay soils. *Canadian Geotechnical Journal*, **20**(2): 228–241. 360

Oloo, S.Y., Fredlund, D.G., and Gan, J.K-M. 1997. Bearing capacity of unpaved roads. *Canadian Geotechnical Journal*, **34**(3): 398–407. 373

Part V

Steady State and Transient Flow Through Unsaturated Soils

S.L. Barbour 383

Fredlund, D.G., Xing, A., and Huang, S.Y. 1994. Predicting the permeability function for unsaturated soils using the soil-water characteristic curve. *Canadian Geotechnical Journal*, **31**(4): 533–546. 389

Papagianakis, A.T., and Fredlund, D.G. 1984. A steady state model for flow in saturated-unsaturated soils. *Canadian Geotechnical Journal*, **21**(3): 419–430. 399

Lam, L., Fredlund, D.G., and Barbour, S.L. 1988. Transient seepage model for saturated-unsaturated systems: A geotechnical engineering approach. *Canadian Geotechnical Journal*, **24**(4): 565–580. 411

Lim, T.T., Rahardjo, H., Chang, M.F., and Fredlund, D.G. 1996. Effect of rainfall on matric suction in a residual soil slope. *Canadian Geotechnical Journal*, **33**(4): 618–628. 426

Fredlund, D.G., and Hasan, J. 1979. One-dimensional consolidation theory: unsaturated soils. *Canadian Geotechnical Journal*, **16**(2): 521–531. 436

Fredlund, D.G., and Xing, A. 1997. The use of a rheological model for the visualization of unsaturated soils processes. *Proceedings, 6th National Congress on Mechanics, Hanoi, Vietnam*. 445

Fredlund, D.G., and Rahardjo, H. 1985. Unsaturated soil consolidation theory and laboratory experimental data. *In Consolidation of Soils: Testing and Evaluation, ASTM STP 892*. 450

Rahardjo, H., and Fredlund, D.G. 1996. Consolidation apparatus for testing unsaturated soil. *Geotechnical Testing Journal*, **19**(4): 341–353. 457

- Rahardjo, H., and Fredlund, D.G. 1995. Experimental verification of the theory of consolidation for unsaturated soils. *Canadian Geotechnical Journal*, **32**(5): 749–766. 468
- Barbour, S.L., and Fredlund, D.G. 1989. Mechanics of osmotic flow and volume change in clay soils. *Canadian Geotechnical Journal*, **26**: 551–562. 485
- Barbour, S.L., Lim, P.C. and Fredlund, D.G. 1996. A new technique for diffusion testing of unsaturated soils. *ASTM, Geotechnical Testing Journal*, **19**(3): 247–258. 498

Part VI

Volume Change Behavior of Unsaturated Soils

- R.L. Lytton 509
- Fredlund, D.G., and Morgenstern, N.R. 1976. Constitutive relations for volume change in unsaturated soils. *Canadian Geotechnical Journal*, **13**(3): 261–276. 515
- Ho, D.Y.F., Fredlund, D.G., and Rahardjo, H. 1992. Volume change indices during loading and unloading of an unsaturated soil. *Canadian Geotechnical Journal*, **29**(2): 195–207. 528
- Pereira, J.H.F., and Fredlund, D.G. 1997. Constitutive modelling of a metastable-structured compacted soil. *Proceedings, International Symposium on Recent Developments in Soil and Pavement Mechanics, Rio de Janeiro, Brazil*, pp. 317–326. 540
- Fredlund, D.G., Hasan, J.U., and Filson, H. 1980. The prediction of total heave. *Proceedings, Fourth International Conference on Expansive Soils, Denver, CO., June 16–18, Vol. 1*, pp. 1–17. 550
- Fredlund, D.G. 1987. The prediction and performance of structures on expansive soils. *Proceedings, International Symposium on Prediction and Performance in Geotechnical Engineering, Calgary, Canada*, pp. 51–60. 559
- Fredlund, D.G. 1969. Consolidometer test procedural factors affecting swell properties. *Proceedings, International Conference on Expansive Soils, Texas A & M, College Station, Texas*, pp. 435–456. 567
- Rao, R.R., Rahardjo, H., and Fredlund, D.G. 1988. Closed-form heave solutions for expansive soils. *Journal of Geotechnical Engineering*, **114**(5): 573–588. 582
- Yoshida, R.T., Fredlund, D.G., and Hamilton, J.J. 1983. The prediction of total heave of a slab-on-grade floor on Regina clay. *Canadian Geotechnical Journal*, **20**(1): 69–81. 590
- Ching, R.K.H., and Fredlund, D.G. 1984. A small Saskatchewan town copes with swelling clay problems. *Proceedings, 5th International Conference on Expansive Soils, Adelaide, Australia*, pp. 306–310. 602
- Sattler, P.J., and Fredlund, D.G. 1990. Numerical modelling of vertical ground movements in expansive soils. *Canadian Geotechnical Journal*, **28**(2): 189–199. 609
- Shuai, F., and Fredlund, D.G. 1997. Measured and simulated behavior of an expansive soil. *Proceedings, Third Brazilian Symposium on Unsaturated Soils, NSAT'97, Rio de Janeiro, Brazil, Vol. 1*, pp. 253–260. 620
- Tadepalli, R., and Fredlund, D.G. 1991. The collapse behavior of a compacted soil during inundation. *Canadian Geotechnical Journal*, **28**: 477–488. 626
- Fredlund, D.G., Bergan, A.T., and Wong, P.K. 1977. Resilient modulus constitutive relationships for cohesive soils. *Transportation Research Board, Transportation Research Record 642*, pp. 73–81. 639

Part VII

Moisture Flux Boundary Conditions at Ground Surface

- G.W. Wilson 651
- Wilson, G.W., Fredlund, D.G., and Barbour, S.L. 1994. Coupled soil-atmosphere modeling for soil evaporation. *Canadian Geotechnical Journal*, **31**(2): 151–161. 657

Wilson, G.W., Barbour, S.L., and Fredlund, D.G. 1997. The effect of soil suction on evaporative fluxes from soil surfaces. *Canadian Geotechnical Journal*, **34**(1): 145–155. . . . 670

Tratch, D.J., Fredlund, D.G., and Wilson, G.W. 1995. An introduction to analytical modeling of plant transpiration for geotechnical engineers. *Proceedings, 48th Canadian Geotechnical Conference, Vancouver, B.C., Vol. 2*, pp. 771–780.. . . . 681

Dakshanamurthy, V., and Fredlund, D.G. 1981. A mathematical model for predicting moisture flow in an unsaturated soil under hydraulic and temperature gradients. *Water Resources Journal*, **17**(3): 714–722. 687

Part VIII

Epilogue

A.W. Clifton and D.G. Fredlund. 699

Part IX

Bibliography of Publications. 705

Part X

Graduate Students Supervised 725

Index 731

Abstract

Unsaturated soil mechanics developed considerably later than saturated soil mechanics. Most of the basic theories for unsaturated soil behaviour were formulated in the 1960s and 1970s. By the end of the 1970s, a classical soil mechanics for unsaturated soils was emerging. The primary categories of unsaturated soil behaviour involved were the flow of water, the shear strength, and the volume change characteristics of an unsaturated soil. Constitutive relationships for these areas, along with appropriate boundary conditions, formed the basis for deriving formulating for practical geotechnical engineering problems.

One of the main differences between saturated soil mechanics and the mechanics required for unsaturated soil behaviour was the non-linearity of the unsaturated soil properties. It became necessary to develop practical means estimate or predict unsaturated soil property functions. The key to accomplishing this task lay in the use of the soil–water characteristic curve, which quantifies the amount of water in the voids of a soil corresponding to a particular soil suction. Soil–water characteristic curves can be readily measured in the laboratory. This information, along with a knowledge of the saturated soil properties, has provided a means of quantifying unsaturated soil property functions.

The decade of the 1980s witnessed the use of numerical models to solve a variety of engineering problems. The problems ranged from analyzing seepage through saturated/unsaturated soil systems to computing the factor of safety of slopes. The computer played an important part in the emergence of unsaturated soil mechanics because of the high non-linearity of most unsaturated soils formulations. The procedures involved in the study of engineering problems has taken on the form of a variety of scenerios that can quickly be analyzed.

The analysis of climatic conditons above the soil surface allows the moisture flux boundary conditions to be assessed. Precipitation conditions are approximated from monitoring station data. The “actual” evaporation conditions can now be approximated based upon coupled heat and mass transport solutions that incorporate the upper portion of the ground as part of the model.

It is anticipated that the next millenium will witness the continued emergence of unsaturated soil mechanics into geotechnical engineering practice. It has become practical to measure soil suction over a wide range, in the laboratory and in situ. The elements required for bringing unsaturated soil mechanics into engineering practice have been developed; however, the implementation process will still require years of study.

Résumé

La mécanique des sols non saturés a une histoire beaucoup plus récente que celle des sols saturés. En effet, la plupart des théories sur le comportement des sols non saturés ont été formulée dans les années 1960 et 1970. Et ce n'est que vers la fin des années 1970 que le domaine de la mécanique des sols non saturés a pu s'enorgueillir de véritables fondations. Les principales catégories de comportements examinées étaient l'écoulement de l'eau, la résistance au cisaillement et les caractéristiques de changement de volume des sols non saturés. Les relations constitutives dans ces domaines, conjuguées à l'application des conditions limites, ont formé la base de l'extraction de formules permettant de résoudre des problèmes géotechniques pratiques.

Une des principales distinctions entre la mécanique des sols saturés et celle des sols non saturés est la non-linéarité des propriétés des sols non saturés. À la lumière de ce fait, il est devenu nécessaire d'établir des moyens pratiques d'estimer ou de prédire les fonctions des propriétés des sols non saturés. La clé d'une telle approche était d'utiliser la courbe caractéristique sol–eau, qui permet de quantifier la quantité d'eau dans les vides du sol selon la force de succion du sol. Les courbes sol–eau peuvent être facilement calculées en laboratoire. Cette information, savamment associée à la connaissance de propriété de sols saturés, a permis de quantifier les fonctions des propriétés des sols non saturés.

Les années 1980 ont marqué l'émergence de l'utilisation de modèles numériques pour résoudre divers problèmes techniques. Les problèmes variaient de l'analyse du suintement dans les sols saturés/non saturés au calcul du coefficient de sécurité des pentes. L'ordinateur a beaucoup contribué à l'enrichissement de la mécanique des sols non saturés étant donné la non-linéarité de

la plupart des compositions de sols non saturés. Grâce à l'informatique, les problèmes techniques de très nombreuses situations peuvent être analysés rapidement et efficacement.

L'étude des conditions climatiques au-dessus de la surface du sol permet d'évaluer les conditions limites de flux d'humidité. Les conditions de précipitation sont approximées à la lumière des données des stations de surveillance. Les conditions d'évaporation «réelles» peuvent maintenant être approximées selon des solutions de transfert conjugué de chaleur et de masse qui incorporent au modèle la couche supérieure du sol.

On s'attend à ce que le nouveau millénaire continue d'être la scène de l'essor de la mécanique des sols non saturés dans la pratique de la géotechnique. Il est devenu pratique de mesurer la succion du sol sur un territoire dispersé, en laboratoire et *in situ*. Les éléments nécessaires pour que la mécanique des sols non saturés soient appliqués à la géotechnique existent bel et bien, cependant il faudra encore des années d'étude avant que ceux-ci ne soient pleinement déployés et mis en pratique.

Preface

The Emergence of Unsaturated Soil Mechanics is an assemblage of selected papers dealing with unsaturated soil mechanics that have been authored or co-authored by D.G. Fredlund. The substance of these papers documents the milestones of both the science of unsaturated soil mechanics and the career of the author. While some of this research was performed by Professor Fredlund when he was a student, his major accomplishments occurred during his tenure as a faculty member in the Department of Civil Engineering at the University of Saskatchewan.

The contents of the monograph provides the reader with a snapshot of the breadth and depth of the contributions of Professor Fredlund to unsaturated soil mechanics. It is of interest, however, to provide a brief historical review of the way in which this field of engineering science has developed with respect to his contributions.

Interest in unsaturated soils from an engineering perspective can easily be traced to K. Terzaghi and his textbook, *Theoretical Soil Mechanics*. However, unsaturated soil mechanics never became a force majeure in North American classical soil mechanics. Even today, the number of textbooks available that deal with unsaturated soils is indeed restricted. Limited research was conducted in countries such as Australia, South Africa, England, Israel, the United States, and others including Canada during the 1950s and 1960s. Globally, interest in this area waned during the 1970s. By contrast, the past decade has enjoyed a renewed interest in unsaturated soil mechanics as witnessed by the 1995 Paris Conference on Unsaturated Soils and the 1998 Conference in China, the 2002 Conference in Brazil and the national annual Conference of the Canadian Geotechnical Society, as well as the specialty conferences of the American Society of Civil Engineering, to cite only a few examples.

Even though research may have flagged in the 1970s and 1980s, there were a handful of researchers throughout the world who never gave up the quest for knowledge in this area of geotechnical engineering. Professor Fredlund was one such researcher, and he quickly developed an international reputation in unsaturated soil mechanics. If North Americans showed only modest interest in this field of research, areas like Hong Kong with its steep slopes of residual unsaturated soils were eager to embrace this emerging science.

One of the major developments in unsaturated soils technology was the introduction of stress state variables. This concept, which emerged from the research carried out by D.G. Fredlund in the 1970s, provided the cornerstone for describing the behaviour of these soils on a rational basis. This concept has now gained acceptance in most quarters.

Each year, from the 1970s onward, research projects at the University of Saskatchewan were initiated to better understand the basic behaviour of these unsaturated soils. Slowly it became evident to geotechnical engineers that the upper soils remained unsaturated throughout the year. While precipitation affected the shear strength, volume change, and permeability functions, these soils had to be analyzed from an “unsaturated soil perspective” if rational engineering decisions were to be made about their behaviour or performance.

Flow in unsaturated soils emerged as an important concept in the 1980s with publication of some of the first numerical solutions showing steady state flow in the unsaturated zone above the line of seepage in embankments impounding water. Later, transient seepage in unsaturated soils was addressed and the required technology was introduced.

While the soil–water characteristic curve had been a well-known concept to soil scientists for almost 100 years, its common utility was not apparent to geotechnical engineers until the past decade. Research at the University of Saskatchewan has shown that the numerical quantification of the soil–water characteristic curve can be used to predict unsaturated soil shearing resistance, unsaturated coefficient of permeability functions, and the general behaviour of unsaturated soils. The soil–water characteristic curve allows predictions of behaviour of unsaturated soils without the time-consuming laboratory testing that was required in the past. As a result, there is growing optimism that many of the concepts that remained in the realm of research because of complex testing procedures will be more and more accepted by practicing geotechnical engineers.

The rational design of covers for waste containment systems in the domestic, industrial, and resource sectors has required the application of unsaturated soil principles and the use of moisture flux boundary conditions at ground surface. In particular, covers for waste rock to prevent

acid mine drainage has captured the imagination of the mining industry. Unsaturated permeability functions and moisture flux boundary conditions are major factors in these applications.

Finally, knowledge-based systems based on large databases appear to hold promise in the application of unsaturated soils technology to engineering practice. It is apparent that if the soil-water characteristic curve can be obtained from existing soils data, preliminary and perhaps final designs can be performed with a minimum of time-consuming, costly testing procedures.

One of the final existing impediments to complete adoption of unsaturated soils design technology is a reliable field device for measuring soil suction. If long-term reliable measurements of soil suction are not available, confidence in the design is greatly diminished. Research into this area has been a priority at the University of Saskatchewan for several years. While a reliable device for monitoring changes in suction in the field is not yet available, it is only a matter of time before an instrument that is reliable, sufficiently rugged, and durable is developed.

As we proceed into the new millennium, the focus on unsaturated soils will continue. Much of the theory has already been formulated. The mandate now is to put this theory into common engineering practice and to follow each project as an engineering case history.

D.E. Pufahl
Head, Department of Civil Engineering
University of Saskatchewan
Saskatoon, Saskatchewan, Canada

Acknowledgments

As I assembled this monograph, it became obvious to me that many researchers and engineers had worked over several decades to write the included conference and journal papers and had contributed greatly to my research into the behaviour of unsaturated soils. Therefore, the monograph is not the work of one person. I would like to acknowledge the graduate students, research engineers and practicing engineers who contributed to the publication of the original papers. This monograph is a credit to all who were involved.

The idea of compiling this monograph originated in a meeting of Dr. S. Lee Barbour, Dr. A. Wayne Clifton and Dr. G. Ward Wilson. They investigated the feasibility of publishing such a document and ensured that the task got underway. Their role in the selection of papers, the preparation of the “Appreciation” and the “Introduction” to each chapter is acknowledged. They also put into place most of the finances necessary to produce the monograph. I wish to acknowledge their efforts and express my gratitude for their generosity. I also appreciate the trust and confidence that they have placed in the research with which I have been involved.

Each chapter is introduced by a researchers who had a major influence on my research studies. Dr. Norbert R. Morgenstern was instrumental in setting the direction for the development of a sound theoretical basis for understanding unsaturated soil mechanics. The two years spent on my research at the University of Alberta established the basis for a career of studying unsaturated soil behaviour and its application to the engineering practice. Dr. A. Wayne Clifton has been involved in the geotechnical and geo-environmental consulting engineering fields for several decades. During this time he served as an adjunct professor at the University of Saskatchewan and has provided guidance and direction to the university research program. Dr. Harianto Rahardjo studied at the University of Saskatchewan in the M.Sc. and Ph.D. programs. He spend several years at the University of Saskatchewan as a post-doctoral fellow before he went to teach at Nanyang Technological University in Singapore. His devotion to the subject of unsaturated soil mechanics is acknowledged.

Dr. Robert L. Lytton has been an encouragement to me since the first day we discussed theoretical aspects of unsaturated soil behaviour. His in-depth knowledge of the continuum mechanics and physics has provided a check and verification for many of the ideas that have come forward over the years. Dr. S. Lee Barbour gained his M.Sc. and his Ph.D. at the University of Saskatchewan. His research program focused on geo-environmental aspects of unsaturated soils as well as numerical modelling in saturated/unsaturated soil systems. Dr. G. Ward Wilson also studied at the University of Saskatchewan in the M.Sc. and Ph.D. programs. His research focused on the quantification of the moisture flux boundary conditions for geotechnical and geo-environmental problems. Both researchers have played an important role in establishing the Unsaturated Soils Group, USG, at the University of Saskatchewan, and thereby provided a critical mass for research into a wide range of unsaturated soils problems.

The University of Saskatchewan, Saskatoon, Canada, has provided a supportive home for my research efforts over many years. I acknowledge the support given to the Unsaturated Soils Group by the Department of Civil Engineering and the College of Engineering.

Many people were involved in the assemblage of the research papers into a uniform format. The text was scanned into the computer, verified, and formatted for the monograph. The equations were retyped, and the figures were scanned in and redrawn electronically. The organization of this effort was monumental and was undertaken from beginning to end by Brigitte Boldt-Leppin (Research Engineer, M.Sc.). She was meticulous for detail and able to keep everyone focused on the final manuscript. Several persons assisted in the redrawing of the figures. I would like to acknowledge the efforts of Rachelle Hounjet (3rd year Education Student), Dale Pavier (Laboratory Assistant), Kritsana Sujinukul (2nd year Computer Science Student), and Nicola Wiig (4th year Civil Engineering Student). The task was enormous and all remained dedicated to preparing the monograph.

Finally, I would like to acknowledge the staff at the National Research Council, Ottawa, Canada, for their guidance and help in preparing the monograph.

Delwyn G. Fredlund

Part I
Delwyn G. Fredlund —
An Appreciation



Dr. D.G. Fredlund
Professor, Department of Civil Engineering
University of Saskatchewan
Saskatoon, Saskatchewan, Canada

by A.W. Clifton, S.L. Barbour, and G.W. Wilson

Personal and Work History

Delwyn G. Fredlund was born in 1940, the second child of George and Esther Fredlund. His grandparents emigrated from Sweden and later his father and mother would establish a small farm near Norquay, Saskatchewan. A small stream passed through the woods on the farm and became the place where Del would spend much of his time. As a young boy he loved to be outdoors, hiking in the woods and building small dams across streams. The dams never got much higher than one metre before they were washed away because of “an inadequate spillway design.” The spillway was always a challenge, but he learned “from the beaver” that rocks, sticks, and mud provided a spillway that would withstand the flows from most rainfalls. It became axiomatic that, in the hands of skilled practitioners, wise and appropriate use of even these common materials would serve the builders well.

Del attended a small country school called Moss Lake and later went to Norquay High School. He was selected as Valedictorian of the 1958 grade 12 graduating class. He then began his engineering education at the University of Saskatchewan in Saskatoon. He graduated with his B.Sc. degree in 1962. He then attended the University of Alberta in Edmonton where he obtained his M.Sc. degree in 1964. His Master’s thesis was entitled *Comparison of soil suction and one-dimensional consolidation characteristics of a highly plastic clay*, making him one of the earliest researchers in this field. He later returned to the University of Alberta and completed his Ph.D. degree in 1973. His Ph.D. thesis was *Volume change behaviour of unsaturated soils*.

Del worked as a Research Assistant with the Division of Building Research of the National Research Council in Saskatoon during the summers of 1962 and 1963. It was here that he was first introduced to the foundation problems associated with expansive soils in Western Canada. His work involved monitoring the movement of light buildings as well as instrumentation of test plots in expansive soils.

Following completion of his M.Sc. degree, Del was employed by R.M. Hardy and Associates Ltd. as a geotechnical engineer. He was involved in a wide range of geotechnical studies encompassing the investigation, design, and analyses of slopes, dams, and underground structures, as well as rather unique problems of vibration analyses, hydrocarbon spills, contaminant migration, and freezing and thawing of soils.

In 1966, Del accepted an offer from the University of Saskatchewan to join the Department of Civil Engineering to teach and undertake research in the geotechnical area. He remains in the Department as a Professor of Civil Engineering at the time of this publication.

Del married JoAnne and they had four children: Murray, Jocelyn, Kenton, and Brendon. At the time of publication of this monograph, Murray had graduated in Civil Engineering from the University of Saskatchewan with a B.Sc. degree, had completed his M.Sc. degree, and was working towards a Ph.D. degree in geotechnical engineering. Jocelyn had graduated from veterinary medicine at the University of Saskatchewan. Kenton was studying optometry at Pacific College in Oregon and Brendon was attending Walter Murray High School in Saskatoon. The Fredlund family enjoys and participates in music. Del plays the saxophone and JoAnne has her ARCT and Licentiate degrees in Piano Performing. They were joined by other members of the family for many years as they traveled and performed musical concerts. They also produced two long-play records of sacred music.

University and Professional Activities

Del has always enjoyed teaching, at both the undergraduate and the graduate levels. He puts his teaching first, maintaining that “to be a successful professor, one must be able to reduce the most complex of mechanisms into simple pictures which can be envisioned by the students”. He has also served his department and college on numerous committees, such as the Executive Committee of the College of Engineering, the University Review Committee, and the International Committee.

From 1989 to 1995 Del was Head of the Department of Civil Engineering at the University of Saskatchewan. He led the department into several new areas of research, including a focus on geo-environmental engineering, at the time a new, emerging area in civil engineering practice. Del maintained that “now more than ever before, Civil Engineers are called upon to be faithful stewards of the environment”.

Del has served on a number of national and international technical committees and conference committees. In 1997 he was appointed Chair of the Geotechnical Research Board of Canada. He was Regional Director for the Canadian Geotechnical Society, Chair of the Canadian Geotechnical Society Expansive Soils Subcommittee and a member of the Landslides Committee of the International Society for Soil Mechanics and Foundation Engineering. He served as a member of the Computer Application Division of the Canadian Society of Civil Engineering, the Natural Sciences and Engineering Research Council Grant Selection Committee. He was also appointed a fellow of the Engineering Institute of Canada.

Del served as an Associate Editor for the *Canadian Geotechnical Journal* for seven years and was a member of the Association of Professional Engineers of Saskatchewan committee to review all applications for registration received from foreign countries.

Del was also a member of a number of international technical committees and organizations. These included the Soils Properties Committee and the Committee on Embankments, Dams and Slopes of the American Society for Civil Engineering (ASCE), and the advisory board of Expansive Soil Research Centre at the University of Colorado. He served on the Scientific Committee and editorial board of the Vietnamese Geotechnical Journal.

Del was Chair of the Expansive Soils Committee of the International Society for Soil Mechanics and Foundation Engineering (ISSMFE) from 1989 to 1997. During his appointment he orchestrated the change in name of the committee from the Expansive Soils Committee to the Unsaturated Soils Committee. He felt a name change was necessary to broaden the scope of the committee to include all soils that had negative pore-water pressures and were unsaturated. He also was a member of the ISSMFE Residual Soils and Computer Applications in Geotechnical Engineering Committees.

Awards

Del has received numerous awards and delivered many prestigious lectures in the area of unsaturated soils. In 1996 he won three important awards, including the University of Saskatchewan's most prestigious research award, the Distinguished Researcher Award; the Spencer Buchanan Award of Texas A & M University; and the Saskatoon Engineer of the Year Award. Del also received the highest honour of the Association of Professional Engineers and Geoscientists of Saskatchewan, the Gold Medal signifying the Distinguished Service Award. The Saskatoon Geotechnical Achievement Award and Canadian Geotechnical Colloquium Award were the other honours conferred on him.

During 1998, Del received even more recognition in Canada and internationally. He received the highest award of the Canadian Geotechnical Society, the R.F. Leggett Award, presented annually to the person who has made exceptional contribution to Geotechnical Engineering in Canada. He was further recognized by being a keynote speaker at the 2nd International Conference on Unsaturated Soils in Beijing, China, and he received the Kassif Medal from the State of Israel for his research on unsaturated soils. In 1999, he received the Scotiabank–AUCC Award for Excellence in Internationalization. In particular, the award was for "Contribution of Research to Internationalization," resulting from a CIDA project on Land and Water Management in the Red River Basin of Vietnam.

He was the prestigious Cross-Canada Lecturer of the Canadian Geotechnical Society in 1995, one of many such honours. He was the keynote speaker for many international forums, among them the First International Conference on Unsaturated Soils, Paris, 1995; INFOGEO'96 Conference on Computers in Geotechnical Engineering, 1996; Third Brazilian Symposium on Unsaturated Soils, 1997; ASCE Geo-Logan Conference on Unsaturated Soils, 1997; and the Second International Conference on Unsaturated Soils, Beijing, 1998. He has been an invited lecturer at more than 80 geotechnical seminars, professional associations and organizations, and other public forums in Canada and around the world.

Research and Consulting

Del developed a balanced program of fundamental and applied research funded from private industry, provincial and national government agencies, and international organizations. This research funding grew progressively in the 1980s and 1990s. As a result, he supervised graduate

students from many countries on M.Sc., M.Eng., and Ph.D. programs. By 1998, he had supervised at least 55 M.Sc. and 15 Ph.D. students. Del also trained several research engineers and postdoctoral fellows. Visiting scholars came from several countries of the world to spend at least one term studying unsaturated soil behaviour at the University of Saskatchewan. These highly qualified personnel became the leaders of this relatively new, but important, field of unsaturated soils, around the world. Del was also interested in collaborative research work. He was the founder and chairperson of the Unsaturated Soils Group (USG) at the Department of Civil Engineering at the University of Saskatchewan.

In 1978 he was awarded a strategic NSERC grant to study the behaviour of expansive soils. He was also given access to research data from the Division of Building Research, NRC, Saskatoon. He held a NSERC grant from the Government of Canada that continuously increased during his tenure at the University of Saskatchewan. In 1994 he received, along with Professors S.L. Barbour and G.W. Wilson, a three-year strategic grant for study of fractured, unsaturated clay behaviour.

The focus of Del's research program was in two key areas: the behaviour of unsaturated soils and modelling the stability of slopes. These research studies were theoretical and analytical, while at the same time including case histories and retaining a relevancy to geotechnical engineering practice. The theoretical developments subsequently led to analytical procedures that were accepted for practice in numerous countries.

Research papers, study reports, and journal papers were presented in many international outlets. By 1998, he had published approximately 180 conference papers, 90 journal papers, as well as numerous research reports and other articles. About 70% of the papers relate to the behaviour of unsaturated soils and about 30% to slope stability studies. In addition, he offered numerous short courses and workshops on understanding and applying unsaturated soil mechanics. Other research personnel assisted in these courses, which were offered to practicing engineers nationally and internationally. Del is a strong believer of transferring theory into practice and the need for life-long learning.

Del has written chapters in books and edited several other books. He realized there was a need to synthesize research information available on the behaviour of unsaturated soils. Since much of the research had been done at the University of Saskatchewan, he set out to produce such a document. With the assistance of Dr. Harianto Rahardjo of Nanyang Technological University, Singapore, he wrote a book on unsaturated soil behaviour. The work, which took almost ten years to complete, was published by John Wiley & Sons, New York, in 1993. *Soil Mechanics for Unsaturated Soils* is 560 pages in length and was the first book to address the engineering behaviour of unsaturated soils in arid and semi-arid regions of the world. It was translated into Chinese and sold by a publisher in Beijing. The topic unsaturated soil mechanics provided a unified theoretical context for analyzing soils around the world that had become known as "Problematic Soils," including expansive soils and collapsing soils such as loess, residual soils, and other soils in arid regions.

In the late 1960s, Del recognized that the computer would have a significant influence on the future practice of geotechnical engineering. He wrote a comprehensive slope stability computer program, and in 1977 he and his brother Lorne, a computer science major, started a software company called Geo-Slope Programming Ltd. Initially their software was supported on mainframes through software bureaus. In 1984, the transition was made to the microcomputer environment. Their products expanded to embrace most types of numerical analyses required to support geotechnical engineering. Del maintained that classical, saturated soil mechanics was a special case of the more general area of unsaturated soil mechanics. The software distributed by Geo-Slope was developed to analyze both saturated and unsaturated soils problems. As such, it remains at the forefront of numerical modeling in geotechnical engineering. In 1998, Geo-Slope International Ltd. was the oldest and largest geotechnical software company of its kind, marketing to more than 80 countries.

Del consulted on projects locally, nationally and internationally. In 1979, he was asked by a Hong Kong consulting engineering firm to assist in slope stability studies in Hong Kong. This led to a number of research studies over a period of several years, including research contracts from the Geotechnical Engineering Office (GEO) Government of Hong Kong, on specialized testing of Hong Kong residual soils. Domestically, Del was a staff consultant to several engi-

neering consulting firms. Internationally, he was called as an expert witness on a number of litigation cases. Over a period of about ten years, he acted as a research review consultant to the Corps of Engineers at the Waterways Experimental Station, Vicksburg, Mississippi, and the Cold Regions Research Laboratory, Hanover, New Hampshire.

International Cooperation

Much of the research conducted on the behaviour of unsaturated soils was of particular interest to the more arid regions of the world. As a result, his research led him to Australia, Brazil, China, Colombia, Hong Kong, India, Israel, Japan, Kenya, Malaysia, and most countries in Europe. Technological interaction with the United States was also extensive. Two sabbatical leaves were spent at universities in the United States: 1977 to 1978 at the University of Texas, Austin, Texas and 1984 to 1985 at Colorado State University, Fort Collins, Colorado. He was subsequently appointed as an Adjunct Professor at Colorado State University. From 1992 to 1993, he spent his sabbatical leave at Nanyang Technological University in Singapore.

Del held the view that training highly qualified personnel from developing countries was one of the best forms of assistance that could be given to those countries. He supported and trained graduate students, visiting scholars, and technicians from many countries including Brazil, China, Greece, Hong Kong, India, Iran, Kenya, Malaysia, Pakistan, Singapore, and Vietnam.

Research on behaviour of unsaturated soils, along with a personal interest in developing countries, led to the establishment of two International Development Research Centre (IDRC) exchange research programs. An IDRC exchange program was established with Tsinghua University, Beijing, China in 1990. A second IDRC exchange program was established with the University of Nairobi, Kenya, in 1992. Each of the programs extended over a three-year period and led to international linkages through the transfer of technology. The exchange program with China emphasized design of shallow foundations on expansive soils while the exchange program with Kenya focused on the design of highways on expansive soils. Both exchange programs resulted in exchange visits by engineers from the respective countries. In 1996, a technology exchange program sponsored by the Canadian International Development Agency (CIDA) was undertaken with Vietnam. This five-year program, "Land and Water Management in the Red River Basin," was in cooperation with the College of Agriculture at the University of Saskatchewan.

Del has traveled extensively promoting the technology for unsaturated soils as developed at the University of Saskatchewan. He maintains that it is not enough to do research, but that the work ought to be "tested" in the research arena and then transferred to areas of need. He is recognized internationally as the person who established the stress state variable approach to unsaturated soils and subsequently derived the theory to establish the engineering behaviour on a scientific basis. He maintained the same categorization for soil mechanics problems as was historically developed for saturated soils.

Closure

This appreciation would not be complete without a final comment on the philosophy of life that had been Del's motivation throughout his life. One heard this philosophy come through quite clearly in many of his most common sayings:

"If I live for myself, I will feed the ego.
If I live for others, I will feed the soul."

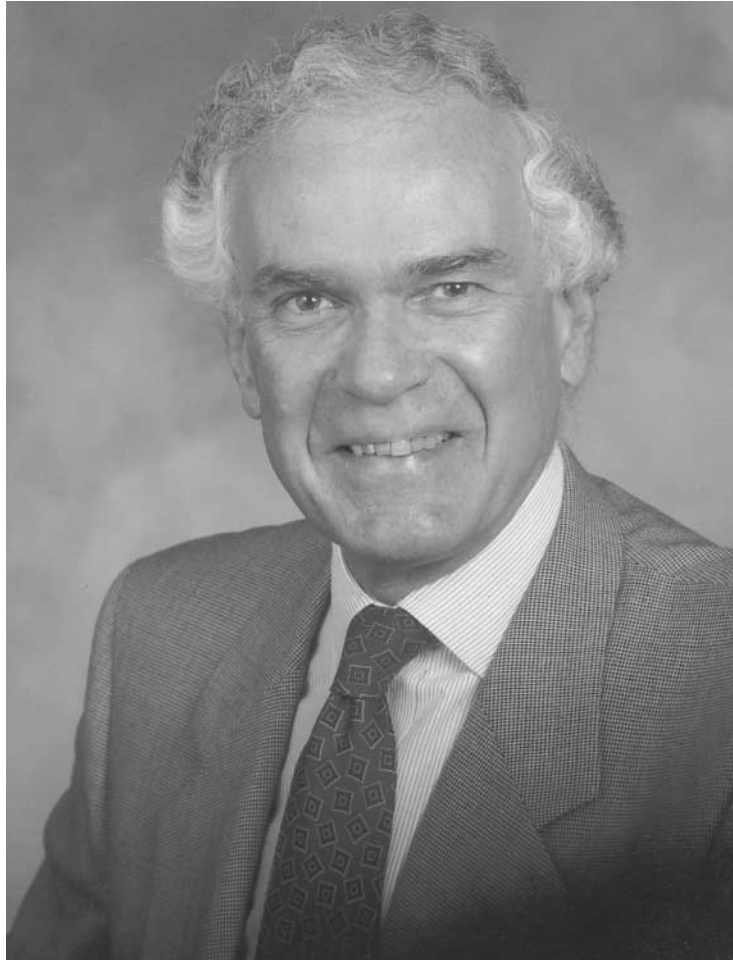
"We make a living by what we get,
we make a life by what we give." (Winston Churchill)

"The person who has never had a problem to solve is indeed a poor person.
The person who has never had a need, is indeed a poor person.
I have found rich countries, because I have found places with many problems and many needs."

This philosophy sprang from deep rooted faith in Jesus Christ, who said: "Freely you have received, freely give." Del's life-long commitment to meeting human needs is not only a response to a moral responsibility, but rather the response of a grateful heart.

Part II

Stress State for Unsaturated Soils and the Measurement of Soil Suction



Dr. N.R. Morgenstern
Department of Civil Engineering
University of Alberta
Edmonton, Alberta, Canada

Introduction and Overview

The description of the state variables for a multiphase material, such as an unsaturated soil, becomes the fundamental building block upon which an engineering science can be built. The universal acceptance of unsaturated soil mechanics depends largely upon how well the stress state variables can be defined and justified. Historically, the lack of certainty regarding the description of the stress state for an unsaturated soil appears to be largely responsible for the slow emergence of unsaturated soil mechanics.

Researchers began recognizing the need to use two independent stress state variables for an unsaturated soil as early as the 1950s. This realization could be seen in the three-dimensional plots of the volume change constitutive surfaces for an unsaturated soil. However, it was not until the 1970s that D.G. Fredlund provided a theoretical basis and justification for the use of two independent stress state variables. The justification was based on the superposition of equilibrium stress fields for each of the phases of a multiphase system. While the analysis has little direct application towards solving engineering problems, it provided the confidence needed to unite researchers in various countries of the world with respect to describing the stress state of an unsaturated soil.

Three possible combinations of independent stress state variables could be justified from the theoretical continuum mechanics analysis. However, it was the net normal stress (i.e., $(\sigma - u_a)$ where σ = total net normal stress and u_a = pore-air pressure) and the matric suction (i.e., $(u_a - u_w)$ where u_w = pore-water pressure) stress state variable combination that proved to be most easily applied in engineering practice. The net normal stress primarily embraces the activities of man which are dominated by applying and removing total stress (i.e., excavations, fills, and applied loads). The matric suction stress state variable primarily embraces the impact of the climatic environment above the ground surface.

The stress state of a saturated soil was completely defined in terms of effective stress variables by Terzaghi in 1936 and can be written in the form of a tensor.

$$[1] \quad [\sigma'] = \begin{bmatrix} (\sigma_x - u_w) & \tau_{yx} & \tau_{zx} \\ \tau_{xy} & (\sigma_y - u_w) & \tau_{zy} \\ \tau_{xz} & \tau_{yz} & (\sigma_z - u_w) \end{bmatrix}$$

where:

$\sigma_x, \sigma_y, \sigma_z$ = total stresses in x, y, z -directions, respectively, and
 u_w = pore-water pressure.

Using a similar approach, the stress state for an unsaturated soil can be defined using two sets of independent stress state variables. There are three sets of possible stress state variables, of which only two are independent. The stress tensors associated with the three sets of independent stress state variables are

Stress state set No. 1:

$$[2a] \quad \begin{bmatrix} (\sigma_x - u_a) & \tau_{yx} & \tau_{zx} \\ \tau_{xy} & (\sigma_y - u_a) & \tau_{zy} \\ \tau_{xz} & \tau_{yz} & (\sigma_z - u_a) \end{bmatrix}$$

Stress state set No. 2:

$$[2b] \quad \begin{bmatrix} (\sigma_x - u_w) & \tau_{yx} & \tau_{zx} \\ \tau_{xy} & (\sigma_y - u_w) & \tau_{zy} \\ \tau_{xz} & \tau_{yz} & (\sigma_z - u_w) \end{bmatrix}$$

and

Stress state set No. 3:

$$[2c] \quad \begin{bmatrix} (u_a - u_w) & 0 & 0 \\ 0 & (u_a - u_w) & 0 \\ 0 & 0 & (u_a - u_w) \end{bmatrix}$$

In the special case of a saturated soil, the pore-air pressure, u_a , is equal to the pore-water pressure, u_w , and the three stress tensors reduce to one single stress tensor (i.e., eq. [1]).

The stress state variables most often used in the formulation of unsaturated soils problems are as follows:

$$[3a] \quad \begin{bmatrix} (\sigma_x - u_a) & \tau_{yx} & \tau_{zx} \\ \tau_{xy} & (\sigma_y - u_a) & \tau_{zy} \\ \tau_{xz} & \tau_{yz} & (\sigma_z - u_a) \end{bmatrix}$$

and

$$[3b] \quad \begin{bmatrix} (u_a - u_w) & 0 & 0 \\ 0 & (u_a - u_w) & 0 \\ 0 & 0 & (u_a - u_w) \end{bmatrix}$$

The direct measurement of matric suction values (*in situ* and in the laboratory) from zero up to several atmospheres has proven to be a great challenge to geotechnical engineers. Recent developments have given new hope that the direct measurement of matric suction may become a part of engineering practice. The key to producing the direct measurement, high range suction sensor has been the conditioning of the water used in the sensor and the care in manufacturing the sensor.

The indirect measurement of soil suction is also of great value in implementing unsaturated soil mechanics. The use of thermal conductivity sensors has shown encouraging success, and recent research has solved many of the previous problems associated with these sensors. The research has dealt with all aspects of the sensor design ranging from the manufacturing of the ceramic to the performance of the electronic components.

The measurement of total suction is also practical in cases where the soil suctions are relatively large. Both thermocouple psychrometers and the filter paper technique have been used with similar degrees of success in practice. The techniques are simple to use but produce considerable scatter in the data. Psychrometers require a precise temperature controlled environment and as a result have limited use *in situ*. The suctions must also be more than several atmospheres in magnitude. The filter paper method is quite technique dependent but continues to become more and more commonly applied in engineering practice. More research, particularly on the use of the filter paper technique, is justified. The calibration curve for the filter paper is in reality a soil-water characteristic curve for filter paper. The osmotic suction does not appear to be commonly measured but can be successfully determined using the squeezing technique.

The research papers in this section provide a state-of-the-art synthesis on the definition of the stress state for an unsaturated soil, as well as the measurement of soil suction.

Part II
Stress State for Unsaturated Soils and the Measurement of Soil Suction

Fredlund, D.G., and Morgenstern, N.R. 1977. Stress state variables for unsaturated soils. Journal of the Geotechnical Engineering Division, Proceedings, American Society of Civil Engineering (GT5), 103 : 447–466.	13
Fredlund, D.G. 1987. The stress state for expansive soils. Proceedings, Sixth International Conference on Expansive Soils, New Delhi, India, pp. 1–9.	27
Krahn, J., and Fredlund, D.G. 1972. On total, matric and osmotic suction. Soil Science, 114 (5): 339–348	35
Barbour, S.L., and Fredlund, D.G. 1989. Physico-chemical state variables for clay soils. Proceedings, XII International Conference on Soil Mechanics and Foundation Engineering, Rio de Janeiro, Brazil, pp. 1839–1843	42
Fredlund, D.G., and Rahardjo, H. 1988. State-of-development in the measurement of soil suction. Proceedings of the First International Conference on Engineering Problems of Regional Soils, Beijing, China, pp. 582–588	47
Fredlund, D.G. 1992. Background, theory, and research related to the use of thermal conductivity sensors for matric suction measurements. <i>In</i> Advances in Measurement of Soil Physical Properties; Bringing Theory into Practice. Soil Science Society of America, Special Publication No. 30, pp. 249–262.	53
Loi, J., Fredlund, D.G., Gan, J.K., and Widger, R.A. 1992. Monitoring soil suction in an indoor test track facility. Transportation Research Board, Transportation Research Record 1362, pp. 101–110	60
Fredlund, D.G., Gan, J.K., and Rahardjo, H. 1991. Measuring negative pore-water pressures in a freezing environment. Transportation Research Board, Transportation Research Record 1307, pp. 291–299.	70
Guan, Y., and Fredlund, D.G. 1997. Direct measurement of high soil suction. Proceedings, Third Brazilian Symposium on Unsaturated Soils, Rio de Janeiro, Brazil	79
Fredlund, D.G., Gan, J.K.-M., Guan, Y., and Richardson, N. 1997. Suction measurements on a Saskatchewan soil using a direct measurement, high suction sensor. Transportation Research Board 76th Annual Meeting, Washington, DC	85
Fredlund, D.G., Gan, J.K.-M., and Gallen, P. 1995. Suction measurements on compacted till specimens and indirect filter paper calibration technique. Transportation Research Board, Transportation Research Record 1481, pp. 3–9	96

Stress state variables for unsaturated soils

Delwyn G. Fredlund and Norbert R. Morgenstern

Abstract: The stress state variables for an unsaturated soil find their origin in the equilibrium equations for the soil structure and the contractile skin. The contractile skin is the air–water interface which must be considered as a fourth phase in the study of the stress conditions of the unsaturated soil. The equilibrium equations are based on the superposition of coincident equilibrium stress fields for a multiphase system. The desired stress state variables appear as surface tractions in the equilibrium equations. The theoretically derived stress state consists of two stress tensors that may consist of any two of the following three stress variables; namely, $(\sigma - u_a)$, $(u_a - u_w)$, or $(\sigma - u_w)$.

Null tests were performed in which the individual components of the stress state variables were varied while the stress state variables were maintained constant. The experimental results showed that the theoretically derived stress state variables are acceptable for use in describing the mechanical *behavior* of an unsaturated soil.

Key words: stress state variables, matric suction, null tests, continuum mechanics, contractile skin, stress fields.

Introduction

Practicing engineers are well aware that many of the problems they encounter involve unsaturated soils. The construction of earthfill dams, highways, and airport runways all use compacted soils that are unsaturated. Also, large portions of the earth's land surface are subjected to desiccating influences that leave the upper portion of the profile cracked and unsaturated. The success of the effective stress concept in describing the behavior of saturated soils has led research workers into a search for a similar statement for unsaturated soils. During the last two decades, there have been numerous equations proposed in the literature; however, none has proven completely successful in practice.

This paper examines the description of the stress state of an unsaturated soil within the context of multiphase continuum mechanics. First, the physical nature of an element of unsaturated soil is described and special consideration is given to the air–water interphase. Second, equilibrium equations for each phase of an unsaturated soil are written in terms of measurable variables. On the basis of these equations, it is possible to identify the independent variables necessary to describe the stress state in an unsaturated soil. Third, theoretically proposed stress state variables are then verified experimentally.

The next steps in the analysis of an unsaturated soil involve the prediction of the deformation state variables and the proposal of suitable constitutive relationships to combine the stress and deformation state variables (not

dealt with in this paper). The constitutive equations can then be applied to the solution of practical engineering problems (Fredlund 1974; Fredlund and Morgenstern 1976).

Unsaturated soil element

Generally, an unsaturated soil is considered to be a three-phase system. Lambe and Whitman (1969) state that soil contains “three distinct phases; solid (mineral particles), gas and liquid (usually water)”. However, on the basis of the definition of a phase, the authors postulate that the air–water interface should be considered as a fourth and independent phase. The following characteristics (Gove 1967; Sisler et al. 1953) qualify a material as an independent phase of a mixture: (1) Differing properties than that of the surrounding material; and (2) definite bounding surfaces. Davies and Rideal (1963) clarify the nature of the air–water interface when they state:

The boundary between two homogeneous phases is not to be regarded as a simple, geometrical plane, upon either side of which extends the homogeneous phases, but rather as a lamina or film of a characteristic thickness. The material in this surface phase shows properties differing from those of the materials in the contiguous homogeneous phases.

The air–water interface is commonly referred to as the “contractile skin” in the surface chemistry literature (Paday 1969).

An element of an unsaturated soil can therefore be visualized as a mixture with two phases that come to equilibrium under applied stress gradients (i.e., soil particles and contractile skin) and two phases that flow under applied stress gradients (i.e., air and water) (Fig. 1). The terms “partly saturated” and “partially saturated” are generally used to designate the preceding case; however, the writers prefer the term “unsaturated,” since the inclusion of the smallest amount of free gas renders the system unsaturated.

Delwyn G. Fredlund. Professor, Civil Engineering Department, University of Saskatchewan, 57 Campus Drive, Saskatoon, SK, Canada S7N 5A9.

Norbert R. Morgenstern. Professor, Civil Engineering Department, University of Alberta, Edmonton, AB, Canada T6G 2G7.

Reproduced with permission from the *Journal of Geotechnical Engineering Division, Proceedings, American Society of Civil Engineers, GT5, 103: 447–466, 1977.*

Effective stress concept

The success of the effective stress equation for saturated soils (Terzaghi 1936) has led many researchers into a search for a similar equation for unsaturated soils (Table 1). The equations differ primarily in that some account for variations in air pressure and variations in solute suction. Common to all equations is the incorporation of a soil parameter characteristic of the soil behavior in the description of the stress state. This renders the equation a constitutive relationship rather than a description of the stress state (Fung 1969). The soil parameter has proven essentially impossible to evaluate uniquely and difficult to apply to practical problems (Bishop and Blight 1963; Blight 1965; Burland 1965; Coleman 1962; Jennings and Burland 1962). More recently, there has been an increased tendency to uncouple the effective stress equations and treat the stress variables independently (Aitchison 1967; Barden et al. 1969; Matyas and Radhakrishna 1968).

Theoretical equilibrium analysis of unsaturated soil element

The procedure used herein to propose suitable stress state variables for an unsaturated soil is based on multiphase continuum mechanics. A three-dimensional element (i.e., a cube) is selected for the free body diagrams, of a size such that it contains a large number of particles and qualifies as a continuum (Fung 1969). The equations of motion (or force equilibrium) are written for each phase of the element (i.e., water, air, soil particles, and contractile skin). In other words, it is assumed that each phase has an independent continuous stress field associated with each of the cartesian coordinate directions. The principle of superposition of coincident equilibrium stress fields is used in writing the equations of motion (Faizullaev 1969; Green and Naghdi 1965; Truesdall 1968; Truesdall and Toupin 1960). In addition to the stress fields for each phase, an overall or total stress field can be assumed. The number of independent equations however, is equal to the number of phases involved. The derivations must be conducted such that all surface tractions are physically measurable quantities.

The derivations of the equilibrium equations for the soil particles and the contractile skin are presented in the Appendix. The surface tractions in each equation can be extracted and written in the form of stress matrices. Each surface traction is referred to as a "stress state variable." The extracted stress state variables cannot be placed in one matrix since they are linked by differing porosity terms outside the partial differentials. In any case, the inclusion of a porosity term (i.e., a soil property) in the description of the state of stress is not in keeping with continuum mechanics. Two independent stress matrices can be extracted from the equilibrium equations for the soil particles and the contractile skin. They are (Fig. 2):

$$[1a] \quad \begin{bmatrix} \sigma_x - u_w & \tau_{yx} & \tau_{zx} \\ \tau_{xy} & \sigma_y - u_w & \tau_{zy} \\ \tau_{xz} & \tau_{yz} & \sigma_z - u_w \end{bmatrix}$$

and

$$[1b] \quad \begin{bmatrix} u_a - u_w & 0 & 0 \\ 0 & u_a - u_w & 0 \\ 0 & 0 & u_a - u_w \end{bmatrix}$$

The derivation in the Appendix used the water phase as a reference phase. However, if the air phase is used as a reference, the equilibrium equation is of a slightly different form. The first matrix will have substituted for u_w . The total stress can also be used as a reference. In this case, the normal stress variables are $(\sigma - u_a)$ and $(\sigma - u_w)$. Therefore, the analysis indicates that any two of three possible normal stress variables can be used to define the stress state. Possible combinations are: (1) $(\sigma - u_w)$ and $(u_a - u_w)$; (2) $(\sigma - u_a)$ and $(u_a - u_w)$; and (3) $(\sigma - u_a)$ and $(\sigma - u_w)$. Prior to their use in the formulation of constitutive relationships, they should be verified experimentally.

Experimental verification of stress state variables

It is now desirable to develop an experimental technique to verify the theoretically proposed stress state variables. The writers propose the following definition and proof for independent stress state variables:

A suitable set of independent stress state variables are those that produce no distortion or volume change of an element when the individual components of the stress state variables are modified but the stress state variables themselves are kept constant. Thus the stress state variable for each phase should produce equilibrium in that phase when a stress point in space is considered.

Any proposed stress tensor can be considered with respect to the following question. How can the individual components of the state variables be altered without changing the overall stress matrix? The alteration of any one stress state variable should destroy the equilibrium of the system.

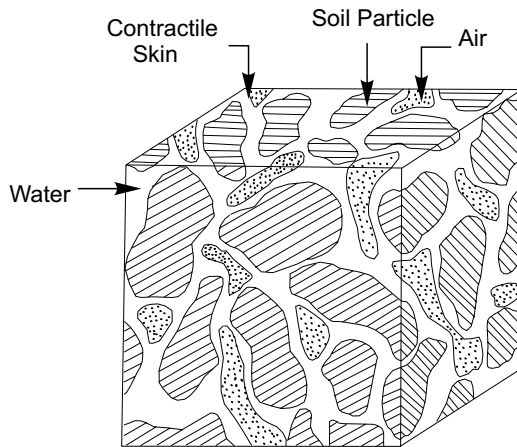
For a saturated soil, the test required to verify $(\sigma - u_w)$ as the stress state variable could be stated as follows: $\Delta\sigma_x = \Delta\sigma_y = \Delta\sigma_z = \Delta u_w$. If the deformation of the soil structure is zero during such a test, the proposed stress state variables are defined. In the case of an unsaturated soil, two stress matrices are proposed for both the soil particles and the contractile skin. For example, let the matrices be selected that contain the $(\sigma - u_w)$ and $(u_a - u_w)$ stress state variables.

To test the $(\sigma - u_w)$ matrix, the total stresses in all directions can be increased or decreased by an equal amount along with an equal increase or decrease in the water pressure. However, the change in the water pressure disturbs the equilibrium of the $(u_a - u_w)$ matrix. To

Table 1. Effective stress equations for unsaturated soils.

Reference	Equation	Description of variables
Bishop (1959)	$\sigma' = \sigma - u_a + \chi(u_a - u_w)$	σ = total normal stress u_w = pore-water pressure χ = parameter related to degree of saturation u_a = the pressure in gas and vapor phase
Cronley et al. (1958)	$\sigma' = \sigma - \beta' u_w$	β' = holding or bonding factor which is measure of number of bonds under tension effective in contributing to soil strength
Lambe (1960)	$\sigma = \bar{\sigma} a_m + u_a a_a + u_w a_w + R - A$	$\bar{\sigma}$ = mineral interparticle stress a_m = mineral particle contact area a_w = water phase contact area a_a = fraction of total area that is air-air contact R = repulsive pore fluid stress due to chemistry A = attractive pore fluid stress due to chemistry
Aitchison (1961)	$\sigma' = \sigma + \psi p''$	ψ = parameter with values ranging from zero to one p'' = pore-water pressure deficiency
Jennings (1960)	$\sigma' = \sigma + \beta p''$	β = statistical factor of same type as contact area; should be measured experimentally in each case
Richards (1966)	$\sigma' = \sigma - u_a + \chi_m(h_m + u_a) + \chi_s(h_s + u_a)$	χ_m = effective stress parameter for matric suction h_m = matric suction χ_s = effective stress parameter for solute suction h_s = solute suction

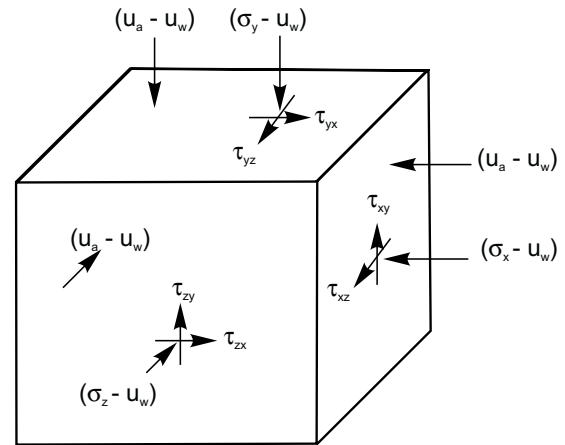
Fig. 1. Element of unsaturated soil.



maintain equilibrium in the $(u_a - u_w)$ matrix, the air pressure must also be increased or decreased by an amount equal to the water and total pressures. This test should satisfy the equilibrium of both the soil structure and the contractile skin. In other words, if all phases are operated as an open system (i.e., allowed to deform or flow if desired), there should be no tendency for volume change of the overall sample and no change in the degree of saturation. The test can be stated as $\Delta\sigma_x = \Delta\sigma_y = \Delta\sigma_z = \Delta u_w = \Delta u_a$. If the change in overall volume is zero and the change in degree of saturation is zero, equilibrium of the soil particles and contractile skin has been maintained.

These tests are termed null tests since the desired result of the changes in pressure is to not produce a process in the phase or phases under consideration. Thus, an attempt is being made to measure “no volume change” or a con-

Fig. 2. Stress state for soil particles and contractible skin in unsaturated soil.



tinuing equilibrium state. It is difficult to measure zero volume change over an extended period of time, and therefore slight volume changes would be anticipated. Similar null-type tests have been used in conjunction with shear strength tests on an unsaturated silt by Bishop and Donald (1961). Also, the axis-translational technique for measuring matric suction (Hilf 1956) is a special case of the null-type test where the total and air pressures are equal.

Description of equipment and test program

Four pieces of equipment were used in performing the null tests (Fredlund 1973a). Two employed modified

Anteus odometers (manufactured by Testlab Corporation in the United States) with one-dimensional loading conditions. The other two pieces of equipment allowed isotropic volume change testing conditions in modified 4-in. diameter Wykeham Farrance triaxial cells.

Air and water pressures were separated by means of a high air entry disk placed at the bottom of the sample [i.e., either 4 bar or 15 bar (400 kPa or 1,500 kPa)]. Although the high air entry disks do not leak air at pressure less than their air entry value, dissolved air diffuses through the water in the disk and collects below the base of the disk. For accurate water volume change measurements, it was necessary to measure the volume of diffused air and apply the appropriate correction. The diffused air volume was measured by periodically flushing the base plate and measuring the volume of air displacing water in an inverted burette (Fredlund 1975).

Figure 3 shows the layout of the modified Anteus oedometer and associated plumbing and equipment. The chamber of the oedometer, (normally filled with water for back pressuring the water phase of soils) was filled with air to regulate air pressure in the soil sample. All pressures were controlled using pressure regulators with an accuracy better than ± 0.14 kPa. The valves in Fig. 3 associated with the total, air, water, and diffused air pressure control are labeled with a *T*, *A*, *W*, and *D*, respectively.

The modified Wykeham Farrance triaxial cell (T-2) is shown in Fig. 4. Linear voltage displacement transducers (LVDT) were used to measure the vertical and lateral displacements. The cell was pressurized with air. A composite membrane consisting of slotted aluminum foil, vacuum grease, and two latex membranes was used to prevent the diffusion of air from the cell into the sample. The original Wykeham Farrance triaxial cell (T-1) had a double-walled cell with mercury between the sample and the inner cell. Fluctuations in mercury level were measured using a cathetometer. In the null test program, a series of tests was first performed on saturated samples, and then a series was performed on unsaturated samples. The properties of the soil tested are shown in Table 2. A summary of the test program is shown in Fig. 5.

Analysis of null tests

The key question considered during the analysis of the null tests is: Does any process or volume change occur as a result of the changes in pressure? If some volume change is measured, an attempt is made to ascertain its cause. Some of the main factors considered with respect to possible volume changes are: (1) test procedure; (2) air diffusion through the water or membrane; (3) water loss from the sample; and (4) secondary consolidation.

The first 15 tests on the saturated samples (Section I) involved changing the total and water pressures and monitoring the water and overall sample volume changes. These tests served to assess the reliability of the test procedure and equipment for a known case. The results are presented in Table 3. Col. 5 shows the amount by which the total and water pressures were changed while Cols. 3

and 4 show the final total and water pressures, respectively. In Cols. 6, 7, and 8, a positive sign designates a volume decrease and vice versa. The "estimated volume change" in Col. 10 is the volume change that would have occurred if only the total stress had been changed and drainage allowed.

The first few tests showed that small amounts of entrapped air in the sample resulted in significant total and water volume changes. After both the testing technique and the means of removing the initially entrapped air were improved (i.e., vibration and a vacuum pump), the results were more satisfactory. The last set of null tests indicated a total or overall volume change of approximately 1.8% of that estimated for a corresponding effective stress increase. The corresponding water volume change was approximately 0.5%. These volume changes are not interpreted as a limitation of $(\sigma - u_w)$, being the effective stress variable, for a saturated soil but rather as an indication of testing technique limitations. The immediate total volume changes are related to entrapped air and measuring system compliance. Long-term volume changes are related to slight amounts of secondary consolidation of the soil structure and compression of the pore air. The results are sufficiently accurate to verify the stress state variables for engineering purposes.

In the tests performed for Section II, the top of the saturated samples was subjected to an air pressure change in addition to the application of the total and water pressure changes (Table 4). The total and water volume changes were monitored on all tests. Air pressure was applied through a coarse corundum stone to create a differential between the pore-water pressure and the air pressure applied to the surface of the sample. Some difficulty occurred in applying all three pressures simultaneously. In the one-dimensional oedometer, the air pressure took a few seconds to increase. As a result, the sample underwent a slight immediate compression. A second problem was the diffusion of air through the water phase of the sample. This was reflected as water leaving the sample. However, the total or overall volume of the sample remained essentially constant (Fig. 6). The best test results show the total volume change over a period of several days as less than 0.1% for a 10 psi (69 kPa) pressure increase on a soft saturated soil. This is approximately 2% of that anticipated for a corresponding change in effective stress.

A total of 19 null tests were performed on unsaturated samples (Tables 5 and 6). Samples N-23 to N-28 were prepared at standard American Association of State Highway and Transportation Officials (AASHTO) compactive effort whereas the remaining samples were prepared at one-half standard AASHTO. The first few tests performed showed remarkably low volume changes. There was a slight tendency for some water to go into the sample during the early stages (i.e., up to 100 min) of the test, but later there was evidence of a small volume of water leaving the sample. The phenomenon is readily understood when it is realized that, at the moment the pressures are applied, two secondary transient processes

Fig. 3. Layout of modified Anteus odometer.

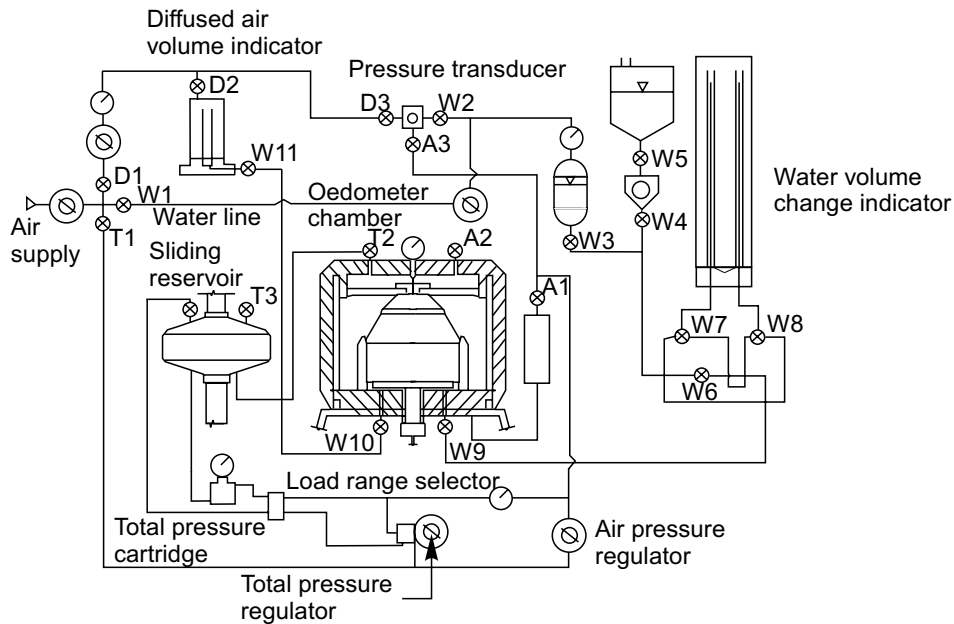
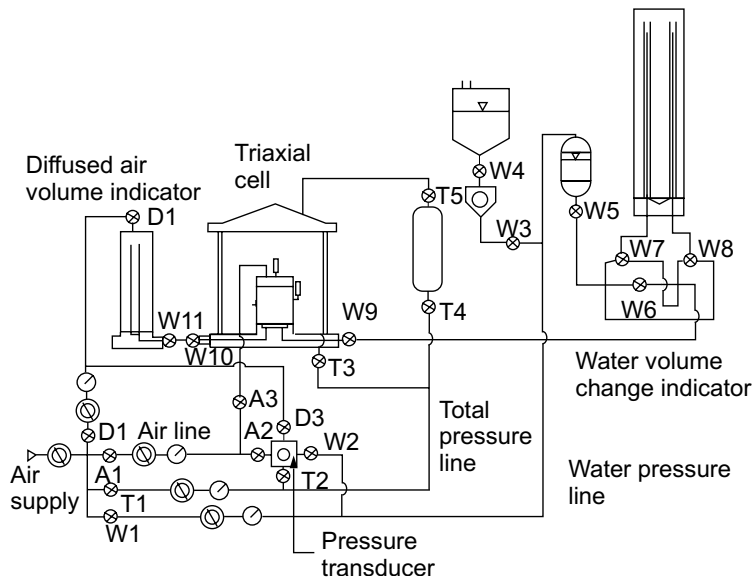


Fig. 4. Layout of modified triaxial apparatus.



commence. Air starts to diffuse through the water primarily from the top of the sample while water tends to compress the occluded air bubbles from the bottom of the sample. The entrapped air bubbles appear to equalize with time, whereas the diffusion process tends toward a steady state process.

Subsequent to the initial tests, a new triaxial apparatus (T-2) was designed with more complete data acquisition capabilities. The null test program was used to simultaneously assess the performance of the apparatus and perform further precise null tests. Two new problems were encountered. First, there was a delay in the application of the cell pressure which allowed the upper load cap to be lifted from the sample at the start of the test. Second,

there was a slow leakage of water through the rubber membranes surrounding the sample. The first problem was overcome by using a surge tank to rapidly increase cell pressure. The second problem was overcome by means of a composite membrane consisting of two rubber membranes separated by slotted aluminium foil and vacuum grease (Dunn 1965).

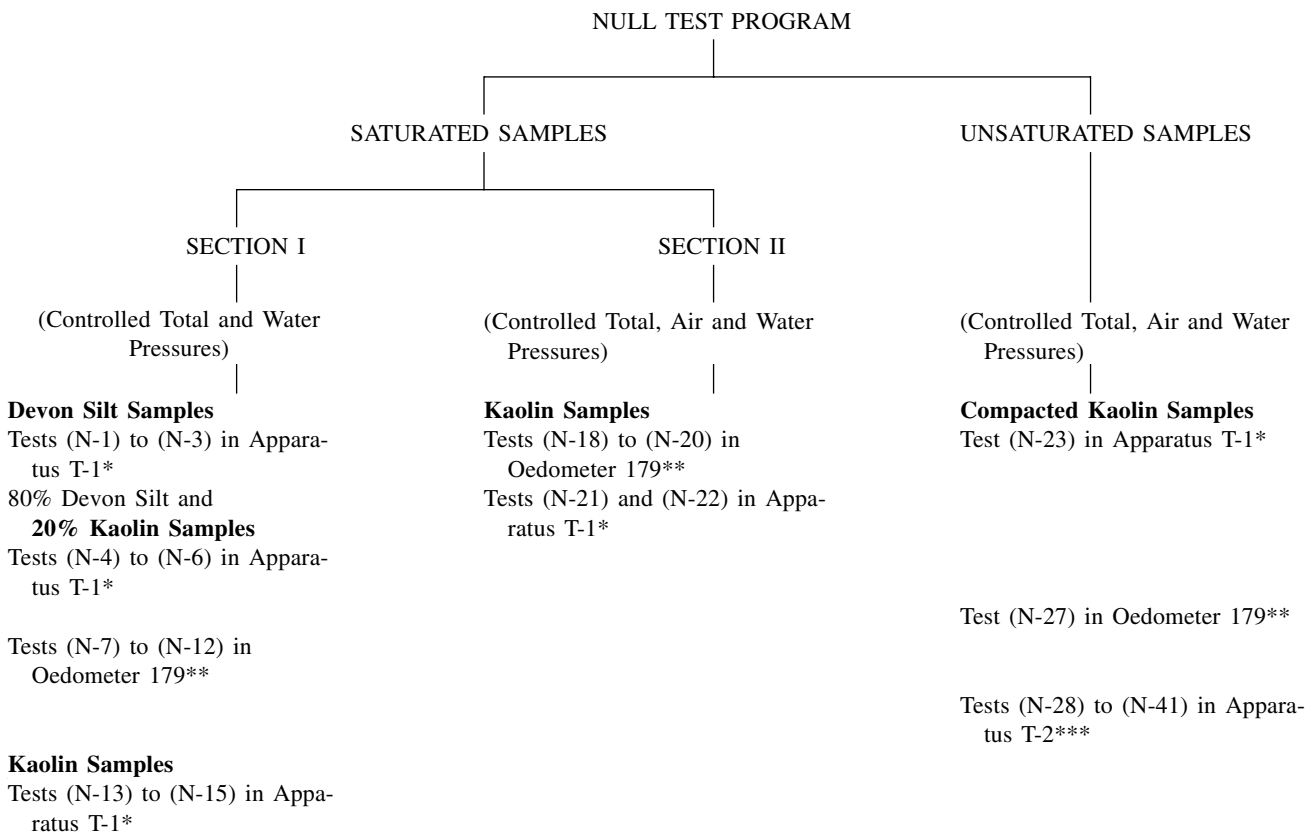
The last set of null tests (i.e., N-35 to N-41) were performed on Triaxial Apparatus No. 2 with the procedural problems solved. Fig. 7 shows the results of null tests N-39 and N-40. The results show essentially no volume change in either the total sample or the water phase. Expanding the volume change scale by 10 times on null test N-37 (Fig. 8) shows that the results are approaching the

Table 2. Soil properties of samples used for Null Tests

Soil type (1)	Samples tested (2)	Specific gravity (3)	Liquid limit in % (4)	Plastic limit in % (5)	Silt sizes ^a in % (6)	Clay sizes ^a in % (7)
Devon Silt	1	2.695	31	23	80	18
80% Devon Silt plus 20% Kaolin	2, 3	2.679	38	25	67	31
Kaolin	4, 6, 7, 9, 10, 11, 20, 22, 27, 30, 31	2.616	64	35	15	85

^aMIT Classification.

Fig. 5. Null test program.



*Apparatus T-1 is a 4-inch diameter (102 mm) double-walled triaxial cell where lateral displacements were monitored (using a cathetometer) by measuring fluctuations in the mercury level. Same as Bishop and Donald (1961).
 **Oedometers 177 and 179 were modified, one-dimensional Anteus Oedometer (Fredlund 1973).
 ***Apparatus T-2 is a 4-inch diameter (102cm) triaxial cell where LVDT's were used to measure lateral displacements (Fredlund 1975).

accuracy of the measuring systems. The volume changes after 1 day are within one part in 10,000. The total volume changes were approximately 0.3% of the volume change that would have occurred if only the total stress had been changed. The water volume changes were approximately 2.5% of those that would have occurred if only the water pressure had been changed. Even when taking into account the increased stiffness of the samples, the two stress state variables for the unsaturated soils are verified at least as conclusively as the effective stress variable was for the saturated samples.

These results are encouraging and supply evidence to state with assurance that the theoretically proposed stress state variables qualify as satisfactory stress state variables from an experimental standpoint.

Conclusions

Previous experimental evidence substantiates the consideration of the air–water interface (i.e., contractile skin) as an independent phase. It qualifies as an independent phase due to its distinct physical properties. Therefore, an

Table 3. Summary of Null Tests on saturated samples, controlling total and water pressures.

Test No. (1)	Sample No. (2)	After pressure change, in psi		Pressure change in psi (5)	Sample volume change, in %		Water volume change, in % (8)	Elapsed time, in minutes (9)	Estimated volume change for corresponding effective stress increase, in % (10)	Water content, in % (11)	Void ratio (12)
		Total (3)	Water (4)		Imme- diate (6)	At elapsed time (7)					
N-1 ^a	1	21.48	14.34	+10	—	—	-0.98	1710	4.28	24.24	0.672
N-2 ^b	1	31.41	24.87	+10	—	+0.72	-0.72	1010	4.54	24.82	0.678
N-3 ^b	1	41.72	1.47	-40	—	0.0	+2.37	1000	1.14	24.02	0.620
N-4	2	40.11	32.23	+10	+0.08	+0.08	-0.06	1000	5.02	28.53	0.783
					+0.08	+0.08	-0.11	6000	5.02		
N-5	2	69.51	31.76	-20	—	+0.125	+0.02	2000	2.77	24.32	0.655
N-6	2	44.66	6.93	-25	—	-0.22	+0.06	800	3.31	24.35	0.652
N-7 ^c	3	74.11	60.18	+10	+0.011	+0.014	—	190	3.36	27.55	0.738
N-8 ^c	3	83.71	69.78	+10	+0.021	+0.020	—	1035	3.36	27.53	0.738
N-9 ^c	3	73.92	59.99	-10	-0.003	-0.010	—	23	3.36	27.52	0.737
N-10 ^c	3	63.92	49.99	-10	-0.010	-0.002	—	70	3.36	27.52	0.737
N-11 ^c	3	53.5	39.57	-10	+0.003	+0.011	—	60	3.36	27.52	0.737
N-12 ^c	3	43.85	29.92	-10	-0.003	+0.006	—	65	3.36	27.52	0.737
N-13	4	25.73	15.62	+10	-0.02	+0.10	+0.03	1400	5.92	55.27	1.476
N-14	4	35.80	25.84	+10	+0.07	+0.10	+0.025	1170	5.92	55.25	1.473
N-15	4	45.89	35.8	+10	+0.11	+0.11	0.0	120	—	55.22	1.470
					+0.11	+0.13	+0.012	1470	5.92		

^aIncreased in 1 psi (6.89 Pa) increments.^bIncreased in 5 psi (34.5 kPa) increments.^cMeasured total volume change only.

Table 4. Summary of Null Tests on saturated soils, controlling total, air and water pressures.

Test No.	Sample No.	After pressure change, in psi			Pressure change in psi	Sample volume change, in %			Elapsed time, in minutes	Estimated volume change for corresponding effective stress increase, in %	Water content in %	Void ratio
		Total	Air	Water		Immediate	At elapsed time	Water volume change, in %				
(1)	(2)	(3)	(4)	(5)	(6)	(7)	(8)	(9)	(10)	(11)	(12)	(13)
N-16	6	56.40	39.27	30.08	+10	+0.054 -0.073	+0.063 -0.066	+0.168 +0.054	1410 100	2.93 —	49.91	1.309
N-17	6	66.53	49.36	40.33	+10	-0.073 -0.073	-0.069 -0.062	+0.19 +0.54	1000 4300	2.93 2.93	49.81	1.307
N-18	6	56.25	39.19	30.44	-10	0.0	+0.019	+0.28	2760	2.93	49.21	1.309
N-19	6	66.23	49.14	40.50	+10	+0.006 +0.006	0.00 -0.001	+0.05 +0.33	1000 7180	2.93 2.93	48.91	1.308
N-20	6	76.28	59.19	50.08	+10	+0.012	+0.027	+0.088	2770	2.93	48.56	1.305
N-21	7	74.04	54.43	53.99	+8	0.0	+0.129	-0.057	2870	3.07	50.37	1.309
N-22	7	83.90	64.22	44.06	+10	0.0	+0.110	+0.148	7170	2.14	44.95	1.203

Note: 1 psi 6.89 kPa.

Table 5. Summary of Null Tests on unsaturated soils: controlling total, air and water pressures.

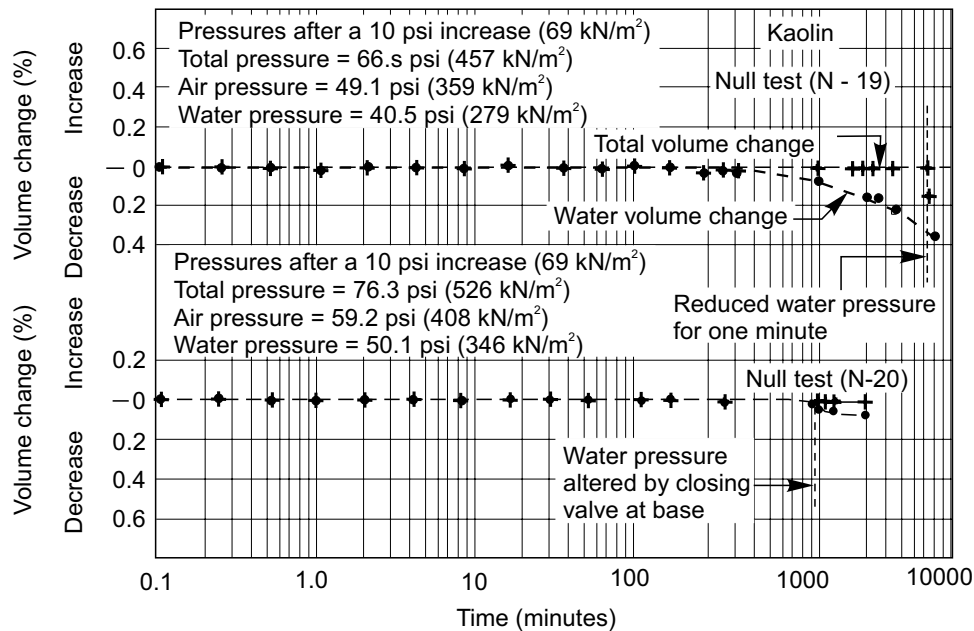
Test No. (1)	Sample No. (2)	After pressure change, in psi			Stress change, in psi (6)	Water content, in % (7)	Void ratio (8)
		Total (3)	Air (4)	Water (5)			
N-23	9	71.37	50.62	26.15	+10	31.56	1.087
N-24	10	71.84	59.00	20.81	+20	31.16	0.870
N-25	10	81.78	68.90	30.51	+10	31.21	0.870
N-26	10	72.14	59.30	42.56	-30	31.73	0.873
N-27	11	43.95	30.00	26.27	+10	32.20	0.902
N-28	20	88.67	77.16	24.68	+20	32.03	0.928
N-29	22	49.76	39.23	13.23	+10	34.59	1.062
N-30	22	59.74	49.17	23.34	+10	35.10	1.062
N-31	22	69.54	58.93	33.00	+10	35.82	1.028
N-32	22	79.62	69.09	43.11	+10	35.87	1.025
N-33	22	89.63	78.96	53.02	+10	35.90	1.022
N-34	27	49.27	38.88	20.19	+10	34.75	1.091
N-35	31	69.68	59.14	40.32	+10	34.01	1.026
N-36	31	79.41	68.70	49.88	+10	34.05	1.025
N-37	31	89.25	78.50	59.65	+10	34.07	1.026
N-38	31	79.69	69.19	50.41	-10	34.11	1.025
N-39	31	69.50	59.11	40.29	-10	34.10	1.025
N-40	31	59.84	49.41	30.66	-10	34.11	1.025
N-41	31	39.47	29.07	10.39	-20	34.09	1.025

Note: 1 psi 6.89 kPa.

Table 6. Sample volume change and water volume change during Null Tests on unsaturated soils: controlling total, air, and water pressures.

Test No. (1)	Sample volume change, in %		Water volume change, in % (4)	Elapsed time, in minutes (5)	Estimated volume change for corresponding effective stress change, in %	
	Immediate (2)	At elapsed time (3)			Overall sample (6)	Water phase (7)
N-23	0	-0.03	-0.05	5800	0.6	2.3
N-24	+0.04	+0.4	-0.07	1500	1.4	0.8
N-25	+0.01	0	-0.02	1650	0.7	0.4
N-26	-0.25	-0.2	—	4300	2.1	1.2
N-27	0	-0.1	-0.5	1880	0.8	0.5
N-28	≈-0.15	-0.15	-0.11	1900	1.6	1.8
N-29	≈-0.015	+0.012	-0.642	8700	1	1.2
N-30	≈-0.005	+0.012	-0.072	1350	1	1.2
N-31	—	+0.12	-0.06	1380	1.1	0.8
N-32	—	+0.17	-0.045	1390	1.1	0.8
N-33	—	+0.15	-0.02	410	1.1	0.8
N-34	≈+0.055	+0.060	-0.105	4350	1	2.5
N-35	+0.015	+0.033	-0.06	5800	0.9	1.9
N-36	+0.010	-0.02	-0.035	2800	0.9	1.9
N-37	0	-0.005	-0.05	5800	0.9	1.9
N-38	-0.015	+0.002	+0.010	2700	0.9	1.9
N-39	-0.01	+0.005	-0.005	1500	0.9	1.9
N-40	-0.007	-0.005	+0.015	5800	0.9	1.9
N-41	-0.03	+0.007	-0.04	2900	1.8	3.8

Fig. 6. Null tests (N-19) and (N-20) on sample No. 6.



unsaturated soil is a four-phase system, composed of two phases that come to equilibrium under applied stress gradients, (i.e., soil particles and contractile skin) and two phases that flow under applied pressure gradients (i.e., air and water phases).

Force equilibrium equations for each phase of an unsaturated soil are formulated within the context of multiphase continuum mechanics. They are arranged in such a manner that the stresses associated with each phase are written in terms of the physically measurable stresses (i.e., σ , u_a , and u_w). The stress state variables governing the behavior of an unsaturated soil (i.e., soil particles and contractile skin) are extracted from the equilibrium equations to form two independent stress matrices. The analysis indicates that any two of three possible normal stress variables can be used to define the stress state. Possible combinations are: (1) $(\sigma - u_w)$ and $(u_a - u_w)$; (2) $(\sigma - u_a)$ and $(u_a - u_w)$; and (3) $(\sigma - u_a)$ and $(\sigma - u_w)$.

Null tests were performed to experimentally test the proposed stress state variables. Experimental data from numerous tests on unsaturated soil samples indicated essentially no overall volume change or water volume change during the null tests. On the final set of tests, the overall and water volume changes were approximately 2% of the volume changes that would be associated with a change in either one of the stress state variables. The theoretically proposed stress state variables would appear to be verified for the soil structure and the contractile skin.

Appendix – Equilibrium analysis of unsaturated soil

The element most suitable for the equilibrium analysis of a multiphase system is a cube, completely enclosed by

imaginary unbiased boundaries (Biot 1955; Hubbert and Rubey 1959). However, many research workers in the area of soil mechanics have used static equilibrium across a wavy cross-sectional plane passed through the soil when justifying the use of a proposed effective stress equation (Bishop and Blight 1963; Lambe and Whitman 1969). The wavy plane constitutes a special type of free body diagram for which the spatial variation goes to zero. This is an equivalence statement in which one force system is substituted for another equivalent force system.

In this paper, the equilibrium of a cubical element is considered within the context of continuum mechanics applied to multiphase systems. An element of unsaturated soil can be disassembled into a water, air, soil particle, and contractile skin phase. Linear equilibrium equations can be written for each of the four phases (Fredlund 1973b). In addition, an overall or total equilibrium equation can also be written (Fig. 9) as,

$$[2] \quad \left(\frac{\partial \tau_{xy}}{\partial x} + \frac{\partial \sigma_y}{\partial y} + \frac{\partial \tau_{zy}}{\partial z} + \gamma \right) dx \, dy \, dz = 0$$

where:

- γ = total unit weight of saturated soil,
- σ_y = total stress in y direction,
- τ_{xy} = shear stress on x-plane in y direction,
- τ_{zy} = shear stress on z-plane in y direction, and
- dx, dy, dz = unit dimensions of element.

This gives rise to five equilibrium equations in each of the cartesian coordinate directions. Only four equations are independent. Since it is possible to measure only total, pore-water, and pore-air pressure, the equilibrium equations for the soil particles and contractile skin will be written in terms of the total, water, and air phase equilibrium equations.

Fig. 7. Null tests (N-39) and (N-40) on sample No. 31.

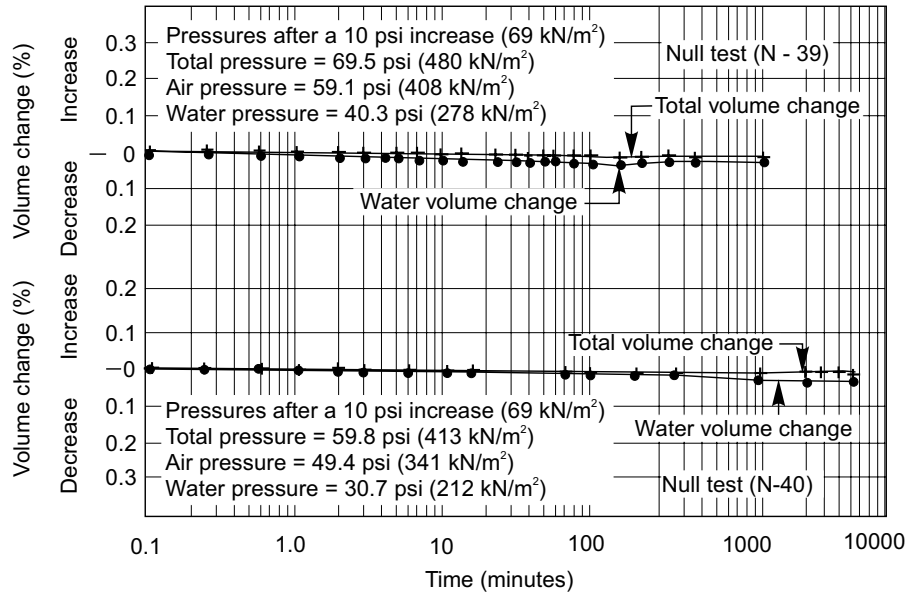


Fig. 8. Null tests (N-37) on unsaturated sample No. 31 (expanded scale).

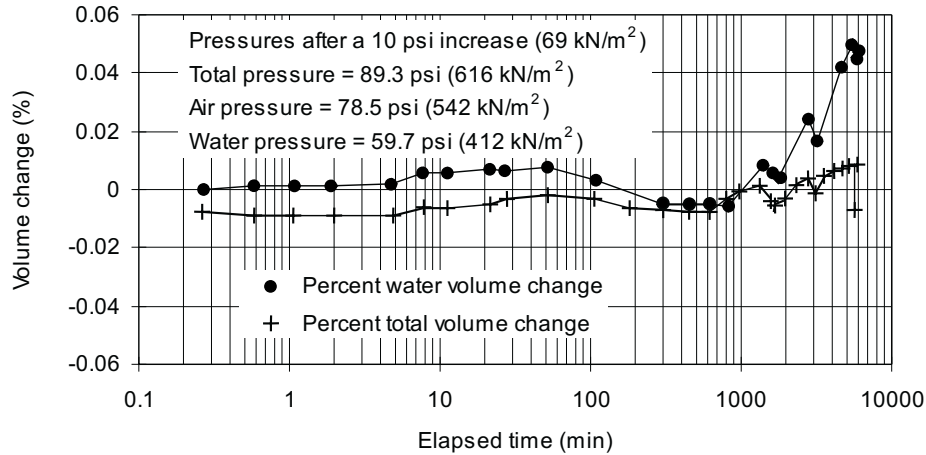


Figure 10 shows the forces in the y direction associated with the water phase. Assuming that the contractile skin behaves as a membrane that comes to equilibrium, there is an interaction force between the water and the contractile skin which can be represented by a body force, F_{cw} . There is also an interaction force between the water and the soil particles, F_{pw} . The equilibrium in the y direction is,

$$[3] \quad \left(n_w \frac{\partial u_w}{\partial y} + n_w \gamma + F_{cwy} + F_{pwy} \right) dx \, dy \, dz = 0$$

where:

- u_w = pressure in water phase,
- n_w = porosity with respect to water phase, and
- $n_w \gamma_w$ = gravity body force for water phase.

Figure 11 shows the forces associated with the air phase. Let the interaction force between the air and the

contractile skin be designated by a body force, F_{ca} . Summing in the y direction gives,

$$[4] \quad \left(n_a \frac{\partial u_a}{\partial y} + n_a \gamma_a + F_{cay} \right) dx \, dy \, dz = 0$$

where:

- u_a = pressure in the air phase
- n_a = porosity with respect to the air phase (i.e., percentage of the surface of the element going through air), and
- $n_a \gamma_a$ = gravity body force for the air phase.

The contractile skin is only a few molecular layers thick but can be described by an independent equilibrium equation since it qualifies as an independent phase and affects soil behavior. The contractile skin interacts with the soil particles producing an interaction force, X_{pc} . The drag of water and air on the contractile skin are F_{wc} and F_{ac} , respectively. Similarly, the soil particles can be de-

Fig. 9. Y-direction equilibrium for overall element of unsaturated soil.

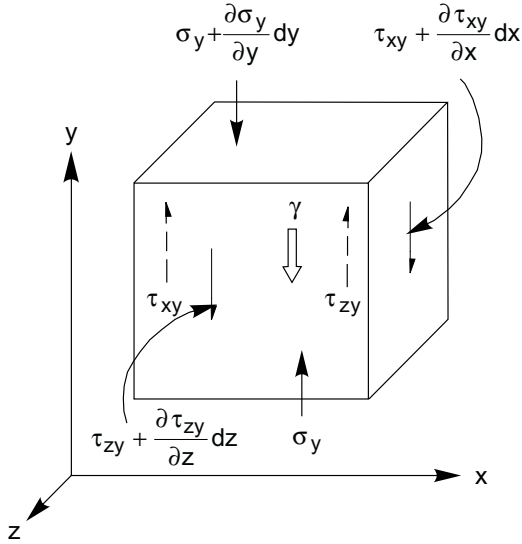
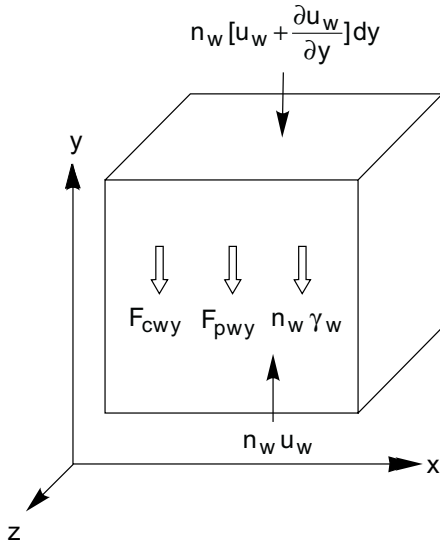


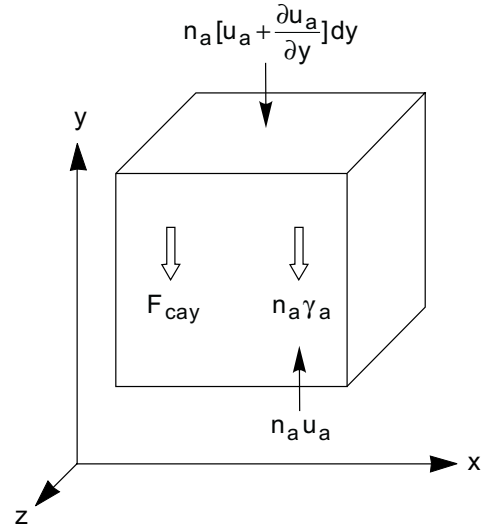
Fig. 10. Y-direction equilibrium for pore-water phase of unsaturated soil.



scribed by an independent equilibrium equation. There is an interaction force, X_{cp} , between the contractile skin and the soil particles. Also, there is the drag force of the water on the soil particles, F_{wp} .

Although the equilibrium equations for the contractile skin and the soil particles can be written assuming a general state of stress, the associated stresses cannot be physically measured. This difficulty is resolved by uncoupling the unsaturated soil element into a water-soil particle multiphase and an air-contractile skin multiphase. The fictitious element has all the air moved to one side of the element (Fig. 12), with the total and component stress fields remaining the same. (The rearrangement of the element is strictly for conceptual purposes.) Now let the unsaturated soil element be separated into two portions. The first portion contains only soil particles and water but has

Fig. 11. Y-direction equilibrium for pore-air phase of unsaturated soil.



additional forces applied to make it equivalent to the original system (Fig. 13). The stress field, $\partial T_y / \partial y$, accounts for the net normal effect of the air and contractile skin stress fields. Similar substitutionary stress fields must be set up on the sides of the element to replace the shear components. (These are omitted from Fig. 13 and the analysis in order to reduce the number of terms involved. They cancel out in the final equations.)

The body force, X_{cp} , must be applied to account for the interaction between the contractile skin and the soil particles. In addition, a unit weight term, γ_{ac} , must account for the air and contractile skin gravity force. The y direction equilibrium equation for the soil particles can be written as,

$$[5] \quad \frac{\partial \tau_{xy}}{\partial x} + \frac{\partial (\sigma_y - u_w)}{\partial y} + \frac{\partial \tau_{zy}}{\partial z} + (\gamma - n_w \gamma_w) + (n_p + n_a + n_c) \frac{\partial u_w}{\partial y} - F_{cwy} - F_{pwy} - X_{cp} + (n_a + n_c) \frac{\partial T_y}{\partial y} + \gamma_{ac} = 0$$

where:

- n_p = percentage of element surface that is soil particles, and
- n_c = percentage of element surface that is contractile skin.

Using the air-contractile skin portion of the element (Fig. 13), the equilibrium equation for the contractile skin is,

$$[6] \quad X_{cp} + (n_a + n_c) \frac{\partial T_y}{\partial y} + \gamma_{ac} - n_a \frac{\partial u_a}{\partial y} - n_a \gamma_a - F_{cay} = 0$$

Fig. 12. Rearrangement of unsaturated soil element.

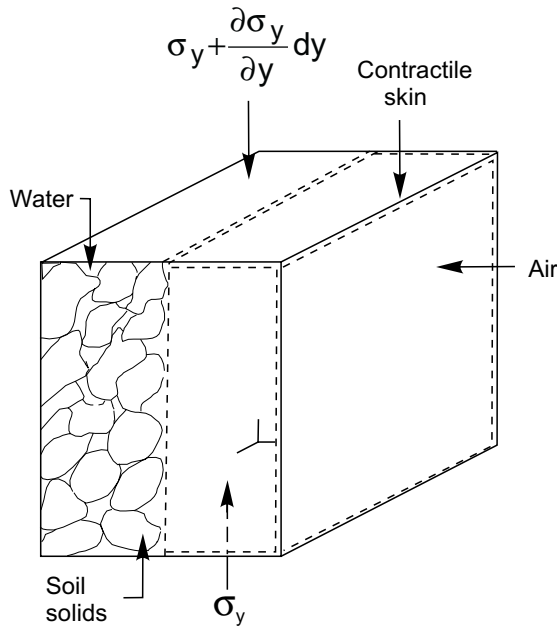
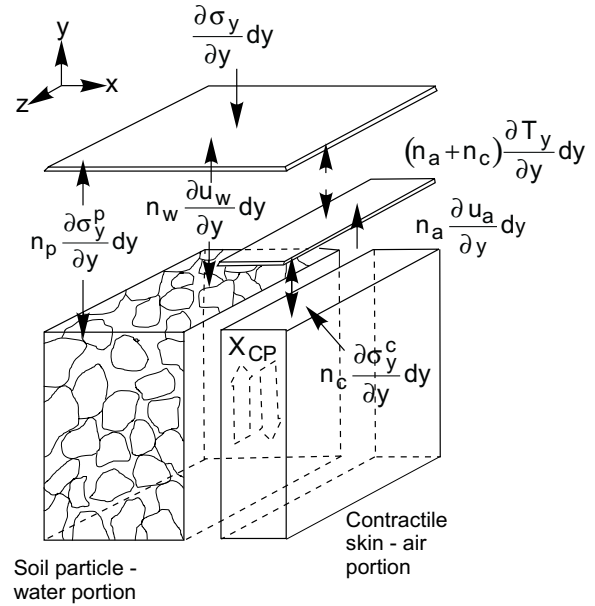


Fig. 13. Rearranged unsaturated soil element separated into two portions.



Substituting eq. [6] into eq. [5] gives,

$$\begin{aligned}
 [7] \quad & \frac{\partial \tau_{xy}}{\partial x} + \frac{\partial(\sigma_y - u_w)}{\partial y} + \frac{\partial \tau_{zy}}{\partial z} + (\gamma - n_w \gamma_w - n_a \gamma_a) \\
 & + (n_p + n_c) + \frac{\partial u_w}{\partial y} - F_{cwy} - F_{pwy} - F_{cay} \\
 & - n_a \frac{\partial(u_a - u_w)}{\partial y} = 0
 \end{aligned}$$

This equilibrium equation applies for both the soil particles and the contractile skin. Similar equilibrium equations can be written for the x and z directions.

An examination of the equilibrium equation reveals that it contains three independent sets of surface tractions [i.e., $(\sigma - u_w)$, $(u_a - u_w)$, (u_w)]. The u_w term can be eliminated when the soil particles are assumed incompressible. The equilibrium equation for the soil particles in the case of a saturated soil can be similarly derived by subtracting the water-phase equation from the total stress equilibrium equation:

$$\begin{aligned}
 [8] \quad & \frac{\partial \tau_{xy}}{\partial x} + \frac{\partial(\sigma_y - u_w)}{\partial y} + \frac{\partial \tau_{zy}}{\partial z} \\
 & + \gamma - n_w \gamma_w - F_{pwy} + n_p \frac{\partial u_w}{\partial y} = 0
 \end{aligned}$$

The normal stress components in the equilibrium equation are equivalent to the conventionally defined effective stress (i.e., the so-called effective stress law is actually a stress state variable extracted from an equilibrium equation).

References

Aitchison, G.D. 1961. Relationship of moisture and effective stress functions in unsaturated soils. *In Pore Pressure and Suction in Soils*, Conference, British National Society of the International Society of Soil Mechanics and Foundation Engineering at the Institution of Civil Engineering, Butterworths, London, England, pp. 47–52.

Aitchison, G.D. 1967. Separate roles of site investigation, quantification of soil properties, and selection of operational environment in the determination of foundation design on expansive soils. *Proceedings, 3rd Asian Regional Conference on Soil Mechanics and Foundation Engineering*, Haifa, Israel, Vol. 3, pp. 72–77.

Barden, L., Madedor, A.O., and Sides, G.R. 1969. Volume change characteristics of unsaturated clay. *ASCE, Journal of Soil Mechanics and Foundation Engineering Division*, **95**(SM1): 33–52.

Biot, M.A. 1955. Theory of elasticity and consolidation for a porous anisotropic solid. *Journal of Applied Physics*, **26**(2): 182–185.

Bishop, A.W. 1959. The principle of effective stress. Lecture delivered in Oslo, Norway, in 1955. *In Teknisk Ukeblad*, **106**(39): 859–863.

Bishop, A.W., and Blight, G.E. 1963. Some aspects of effective stress in saturated and unsaturated soils. *Géotechnique*, **13**(3): 177–197.

Bishop, A.W., and Donald, I.B. 1961. The experimental study of partly saturated soil in the triaxial apparatus. *Proceedings, 5th International Conference on Soil Mechanics and Foundation Engineering*, Paris, Vol. 1, pp. 13–21.

Blight, G.E. 1965. A study of effective stresses for volume change. *In Moisture equilibria and moisture changes in soils beneath covered areas*. Edited by G.D. Aitchison, Butterworths and Company (Australia) Ltd., Sydney, Australia, pp. 259–269.

- Burland, J.B. 1964. Effective stresses in partly saturated soils. Discussion of: Some aspects of effective stress in saturated and partly saturated soils, by G.E. Blight and A.W. Bishop, *Géotechnique*, **14**: 64–68.
- Burland, J.B. 1965. Some aspects of the mechanical behavior of partly saturated soils. In *Moisture equilibrium and moisture changes in soils beneath covered areas. A symposium in print. Edited by G.D. Aitchison*, Butterworths and Company (Australia) Ltd., Sydney, Australia, pp. 270–278.
- Coleman, J.D. 1962. Stress/strain relations for partly saturated soils. *Correspondence in Géotechnique*, **12**(4): 348–350.
- Crone, D., Coleman, J.D., and Black, W.P.M. 1958. The movement and distribution of water in soil in relation to highway design and performance. In *Water and its Conduction in Soils*, Highway Research Board Special Report No. 40, Washington, D.C., pp. 226–252.
- Davies, J.T., and Rideal, E.K. 1963. *Interfacial phenomena*. Second edition. Academic Press, New York, N.Y.
- Dunn, C.S. 1965. Developments in the design of triaxial equipment for testing compacted soils. *Proceedings, Symposium on the Economic Use of Soil Testing in Site Investigation*, Birmingham, Al., Vol. 3, pp. 19–25.
- Faizullaev, D.F. 1969. Laminar motion of multiphase media in conducts. Special Research Report. Translated from Russian by Consultants Bureau, New York, N.Y., pp. 144.
- Fredlund, D.G. 1973. Volume change behaviour of unsaturated soils. Ph.D. thesis, University of Alberta, Edmonton, AB, Canada.
- Fredlund, D.G. 1973. Discussion of: The second technical session, division two (flow and shear strength). *Proceedings, 3rd International Conference on Expansive Soils*, Jerusalem Academic Press, Haifa, Israel, Vol. 2, pp. 71–76.
- Fredlund, D.G. 1974. Engineering approach to soil continua. *Proceedings, 2nd Symposium on the Application of Solid Mechanics*, Hamilton, ON, Vol. 1, pp. 46–59.
- Fredlund, D.G. 1975. A diffused air volume indicator for unsaturated soils. *Canadian Geotechnical Journal*, **12**(4): 533–539.
- Fredlund, D.G., and Morgenstern, N.R. 1976. Constitutive relations for volume change in unsaturated soils. *Canadian Geotechnical Journal*, **13**(3): 261–276.
- Fung, Y.C. 1969. *A first course in continuum mechanics*. Prentice-Hall Inc., Englewood Cliffs, N.J.
- Gove, P.B. 1967. *Webster's Third New International Dictionary*. Edited by P.B. Gove, G. & C. Merriam Co., Springfield, Mass.
- Green, A.E., and Naghdi, P.M. 1965. A dynamical theory of interacting continua. *International Journal of Engineering Science*, **3**:231–241.
- Hilf, J.W. 1956. An investigation of pore water pressures in compacted cohesive soils. Technical Memorandum 654, United States Department of the Interior, Bureau of Reclamation, Design and Construction Division, Denver, CO.
- Hubbert, M.K., and Rubey, W.W. 1959. Role of fluid pressure in mechanics of overthrust faulting. *Bulletin of the Geological Society of America*, **70**: 115–166.
- Jennings, J. E. 1960. A revised effective stress law for use in the prediction of the behaviour of unsaturated soils. *Proceedings, Conference on Pore Pressure and Suction in Soils*, Butterworths, London, pp. 26–30
- Jennings, J.E., and Burland, J.B. 1962. Limitations to the use of effective stresses in partly saturated soils. *Géotechnique*, **12**(2): 125–144.
- Lambe, T.W. 1960. A mechanistic picture of shear strength in clay. *Proceedings, ASCE Research Conference on Shear Strength of Cohesive Soils*. University of Colorado, Boulder, CO, pp. 555–580.
- Lambe, T.W., and Whitman, R.V. 1969. *Soil mechanics*. John Wiley and Sons, Inc., New York, N.Y.
- Matyas, E.L., and Radhakrishna, H.S. 1968. Volume change characteristics of partially saturated soils. *Géotechnique*, **18**(4): 432–448.
- Padday, J.F. 1969. *Theory of surface tension: Surface and colloid science*. Vol. 1, Wiley-Interscience, Toronto, Canada.
- Richards, B.G. 1966. The significance of moisture flow and equilibria in unsaturated soils in relation to the design of engineering structures built on shallow foundations in Australia. *Symposium on Permeability and Capillarity*, American Society for Testing Materials, Atlantic City, N.J.
- Sisler, H.H., Vanderwerf, C.A., and Davidson, A.W. 1953. *General chemistry-a systematic approach*. The MacMillan Co., New York, N.Y.
- Terzaghi, K. 1936. The shear resistance of saturated soils. *Proceedings, 1st International Conference on Soil Mechanics and Foundation Engineering*, Cambridge, MA, Vol. 1, pp.54–56.
- Truesdell, C. 1966. *The elements of continuum mechanics*. Springer-Verlag, Inc., New York, N.Y.
- Truesdell, C., and Toupin, R.A. 1960. The classical field theories. In *Handbuch der Physik*. Edited by S. Flügge Vol.7/1, Springer-Verlag, Berlin, Germany.

The stress state for expansive soils

Delwyn G. Fredlund

Abstract: The description of the stress state in expansive soils is examined from historical, conceptual, experimental, and theoretical standpoints. From conceptual and theoretical considerations, there is strong evidence in favour of the use of two independent stress state variables. The development of principles associated with continuum mechanics assists in deciding on the most acceptable form for the description of the stress state.

Key words: stress state, matric suction, continuum mechanics, expansive soil.

Introduction

Expansive soils can be characterized as soils having a high swelling index, C_s , which are subjected to a change in matric suction ($u_a - u_w$). Matric suction can be defined as the difference between the pore-air, u_a , and pore-water, u_w , pressures. The pore-water pressures are negative relative to the pore-air pressures. Since the pore-air pressure remains essentially constant with time, it is the pore-water pressure which is generally a function of the microclimatic conditions. A change in the microclimate at a site results in a change in the negative pore-water pressure which in turn results in a change in the stress state of the soil.

Negative pore-water pressures in the soil are the result of the earth's surface climatic conditions. Significant portions of the earth's surface are classified as semi-arid, arid and extremely arid, because the annual potential evaporation of water from the region exceeds the annual precipitation. Regions with a Thornthwaite index (Meigs 1953) between -20 and -40 are classified as semi-arid areas. A Thornthwaite index less than -40 indicates arid areas. About 33% of the earth's surface is considered arid and semi-arid (Dregne 1976). Arid and semi-arid areas usually have a deep groundwater table. The soil located above the water table has negative pore-water pressures. The negative pore-water pressures cause the soil to desaturate, shrink, and crack. These changes are more dominant in the proximity of the ground surface. Upon subsequent wetting, the pore-water pressures increase (i.e., tending towards positive values), resulting in a swelling of the soil. In general, the overall soil mass involved in swelling is initially desaturated to some degree and therefore, the expansive soil must be considered as an unsaturated soil for purposes of analysis.

It is important in the study of the problem of heave, as well as other problems associated with expansive soils, to separate the soil properties and the state variables in-

involved, particularly the stress state variables. The emphasis in this paper will be on the description of the stress state for expansive soils. One needs only to examine the importance of the role of effective stress in the development of saturated soil mechanics in order to realize the importance of an acceptable description of the stress state for unsaturated soils. The paper briefly reviews descriptions of the stress state that have been proposed and then examines the potential for their usage from conceptual, experimental and theoretical standpoints. Although an attempt can be made to use any one of numerous stress state descriptions, the author will provide reasons substantiating the most acceptable description to use in practice. An overall view of how the description of the stress state can be applied to expansive soils is provided in a summary form.

Definition of variables

The author is reserved to introduce new variables and terminology. However, some of the terminology associated with saturated soils "lacks" when applied to unsaturated soils. As a result, a few more universally acceptable terms are proposed. These terms are common to continuum mechanics and are defined within a thermodynamic context. The following definitions, put in a succinct form, are based on numerous continuum mechanics and thermodynamic references:

- i) State: non material variables required for the characterization of the stress condition.
- ii) Stress state variable: the variables required for the characterization of the stress condition.
- iii) Deformation state variables: the variables required for the characterization of deformation conditions or deviations from an initial state.
- iv) Constitutive relations: single-valued equations expressing the relationship between state variables.

The International Dictionary of Physics and Electronics (Michels 1961) defines state variables as:

A limited set of dynamical variables of the system, such as pressure, temperature, volume, etc., which are sufficient to describe or specify the state of the system completely for the considerations at hand.

Fung (1965) describes the state of a system as that "information required for a complete characterization of the

Delwyn G. Fredlund. Professor, Department of Civil Engineering, University of Saskatchewan, 57 Campus Drive, Saskatoon, SK, Canada S7N 5A9.

Reproduced from the *Proceedings, Sixth International Conference on Expansive Soils*, Keynote Address, New Delhi, India, December 1-3, 1987. pp. 1-9.

system for the purpose at hand". Typical state variables for an elastic body are given as those variables describing the strain field, the stress field, and its geometry. The state variables must be independent of the physical properties of the material involved.

Constitutive relations are single-valued expressions which relate one state variable to one or more other state variables (Fung 1969).

A stress versus strain relationship is a constitutive relation which describes mechanical behaviour of a material. The material properties involved may be an elastic modulus and a Poisson's ratio. The ideal gas equation relates pressure to density and temperature and is called a constitutive equation. The gas constant is the material property involved. Three simple, idealized constitutive equations are those given for a nonviscous fluid, a Newtonian viscous fluid, and a perfectly elastic solid (Fung 1969).

Other examples of constitutive equations relating stress state variables are the shear strength equation and the pore pressure parameter equations. Examples of constitutive equations relating stress state variables to deformation state variables are the stress versus strain equations, stress versus volumetric change equations, and the moisture characteristic relation. From the above definitions, it is clear that the physical properties of a system are part of the constitutive relations for the system and are not to be a part of the description of the stress state. The use of the above concepts was advocated by Matyas and Radhakrishna in 1969.

Historical context

The first ISSMFE conference in 1936 provided a forum for the establishment of principles and equations relevant to saturated soil mechanics. These principles and equations have remained pivotal throughout subsequent decades of research. This same conference was also a forum for numerous research papers on unsaturated soil behaviour. Unfortunately, a parallel set of principles and equations did not immediately emerge for unsaturated soils.

It is of value to examine the evolution in our understanding of the stress state for both saturated and unsaturated soils. Few research papers have concentrated directly upon effective stress or the description of stress state. Those that have been written reveal new ideas and concepts which are worth considering within the context of continuum mechanics.

Stress state for saturated soils

An understanding of the meaning of effective stress proves to be valuable when considering the stress state description for unsaturated soils. Terzaghi's 1936 statement regarding effective stress defined the stress state variables necessary to describe the behaviour of saturated soils. He stated:

The stress in any point of a section through a mass of soil can be computed from the total principal stresses, σ_1 , σ_2 , σ_3 , which act at this point. If the voids of the

soil are filled with water under a stress, u , the total principal stresses consist of two parts. One part, u , acts in the water and in the solid in every direction with equal intensity The balance $\sigma_1' = \sigma_1 - u$, $\sigma_2' = \sigma_2 - u$ and $\sigma_3' = \sigma_3 - u$ represents an excess over the neutral stress, u , and it has its seat exclusively in the soil phase of the soil. All the measurable effects of a change in stress, such as compression, distortion and a change in shearing resistance are exclusively due to changes in the effective stress σ_1' , σ_2' and σ_3' .

Two aspects of Terzaghi's statement are of particular interest. The first assertion of interest is that the pore-water pressure "acts in the water and in the solid in every direction". This becomes meaningful when the concept of continuous stress fields in continuum mechanics, is applied to a multiphase system. The second assertion of interest is that "all the measurable effects ... are exclusively due to changes in the effective stress". There is no suggestion that the effective stress variable is an approximation. If anything, the statement appears to leave no room for further refinement. This is of interest because re-evaluations of the concept of effective stress have led to attempts at refinement. The question as to whether these refinements are justifiable will be addressed later.

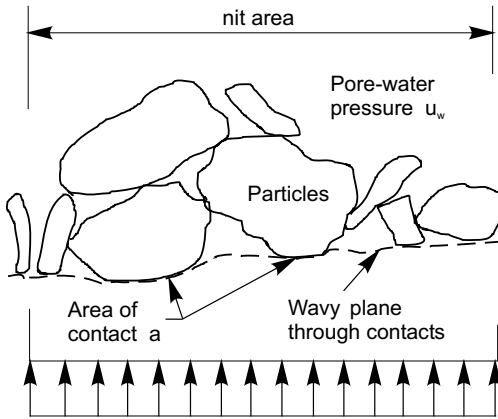
All aspects of "effective stress" have been highly regarded and treated as a sacrament to geotechnical engineers. While the significance of the "effective stress" concept cannot be questioned, it is of value to consider the basis for the "effective stress" term. The lone term "effective stress" is used at this point in order to delay making a commitment as to whether it is an equation, a principle, a law, a concept, a theory, etc. The following questions might be asked:

- i) What is the theoretical basis for the effective stress equation?
- ii) Should it be called an equation?
- iii) Is it right to call it a law?
- iv) A concept?
- v) A principle?
- vi) A theory?

It would appear that a lack of understanding as to the origin or basis of this relationship has led to much misunderstanding regarding effective stress. Attempts at verification and justification of "effective stress" have led to more rigor in its form which may not be of value. An attempt is made to answer the above questions later by considering the theoretical basis for "effective stress".

The view has been held that the simple effective stress equation is in reality more complex and Terzaghi's equation is an approximation. It has been proposed, for example, that the area of contact between the particles should have an influence on the effective stress equation and that a more accurate equation can be derived by considering statics across a wavy plane (Fig. 1).

Considering a unit projected area of the wavy plane and letting the sum of the parts equal the whole, the following equation can be written:

Fig. 1. Equivalence statement across a wavy plane.

$$[1] \quad \sigma_p a + u_w(1 - a) = \sigma$$

where:

- σ_p = interparticle stress
- a = area of contact between particles
- σ = total stress

Let us assume that:

$$[2] \quad \sigma' = \sigma_p a$$

where:

- σ' = effective stress

The area of contact, a , must be taken as a ratio of the unit area in order for σ' to be a stress. Equation [1] can then be written as:

$$[3] \quad \sigma' = (\sigma - u_w) + a u_w$$

It would at first appear that the area of contact between particles should be included in the effective stress statement. However, it should first be noted that a wavy plane through the soil mass does not constitute a legitimate free body diagram, the reason being that the spatial variation is zero. The wavy plane merely allows an equivalence statement to be written (Fung 1969). In order to complete the free body diagram, the plane must be made into a cube (or a two-dimensional shape) where spatial variations are taken into account. This is commonly done in continuum mechanics using the concept of continuous stress fields. Fung (1969) also suggests that the sides of the cubic element selected must be unbiased. In other words, the above exercise is not a proof. It is simply an equivalence statement where it has been decided to let one set of variables be equal to another. It does not constitute the relationship between independent forces.

Bishop and Eldin (1950) also concluded that the area of contact does not come into the effective stress description. Their conclusion was based on an analysis involving the superposition of two equivalent force systems on a plane. Hubbert and Ruby (1959) came to a similar conclusion by applying Archimedes' Principle to a soil. Skempton (1961) proposed more refined or rigorous forms for the effective stress equation. Independent forms

of the equation were suggested for compressibility and shear strength type analyses. Only the compressibility form is discussed in this paper. Assuming the soil particles to be compressible, the change in volume can be written as follows:

$$[4] \quad \frac{-\Delta V}{V} = C\Delta(\sigma - u_w) + C_s\Delta u_w$$

where:

- ΔV = change in volume of an elemental volume, V
- C = compressibility of the soil structure
- C_s = compressibility of the soil particles

This equation can be rearranged to give the form:

$$[5] \quad \frac{-\Delta V}{V} = C\Delta \left[\sigma - \left(1 - \frac{C_s}{C} \right) u_w \right]$$

This gives rise to the suggestion that the effective stress equation could be written as:

$$[6] \quad \sigma' = \sigma - \left(1 - \frac{C_s}{C} \right) u_w$$

Inherent in the above exercise is the assumption that one single-valued relationship can be written between the stress components. This formulation results in an effective stress equation for compressibility problems which incorporates soil properties into the description of the stress state. It could be argued that the stress state variables should be independent of the soil properties and that the soil properties make eq. [6] a constitutive relation. Effective stress equations proposed for use with fluid-saturated porous rocks have also incorporated soil properties (Nur and Byerlee 1971) and subsequently have limitations for application in practice.

Referring to eq. [4] it could be reasoned that it would be superior to envisage $(\sigma - u_w)$ and u_w as two independent stress state variables. All material properties could subsequently be incorporated in the formulation of constitutive relations. The end result of the application of the two formulations may be the same, but the independent stress state variable approach would appear to be more acceptable.

In summary, Terzaghi's description of "effective stresses" can be taken to be the description of the stress state variables which can be used to describe the behaviour of saturated soils. In a sense, it would not appear to be correct to write effective stress as an equation since the equation form is arrived at simply by letting one variable be equal to another. It would not appear to be correct to call Terzaghi's description a law. It can be shown that the effective stress variable appears as a surface traction in the application of Newton's equilibrium equations to a two phase system. The concept of effective stress, on the other hand, is most useful in explaining soil behaviour but should be extended to include the possibility of more than one stress state variable being involved.

Table 1. Proposed effective stress equations for unsaturated soils.

$\sigma' = \sigma - u_a + \chi(u_a - u_w)$	χ = parameter related to degree of saturation	Bishop (1959)
$\sigma' = \sigma - \beta' u_w$	u_a = the pressure in gas and vapour phase β' = holding or bonding factor which is measure of number of bonds under tension effective in contributing to soil strength	Croney, Coleman and Black (1958)
$\sigma = \bar{\sigma} a_m + u_a a_n + u_w a_w + R - A$	a_n = fraction of total area that is air-air contact $\bar{\sigma}$ = mineral interparticle stress a_m = mineral particle contact area a_w = water phase contact area R = repulsive pore fluid stress due to chemistry A = attractive pore fluid stress due to chemistry	Lambe (1960)
$\sigma' = \sigma + \psi p''$	ψ = parameter with values ranging from zero to one p'' = pore-water pressure deficiency	Aitchison (1961)
$\sigma' = \sigma + \beta p''$	β = statistical factor of same type as contact area; should be measured experimentally in each case	Jennings (1960)
$\sigma' = \sigma - u_a + \chi_m(h_m + u_a) + \chi_s(h_s + u_a)$	χ_m = effective stress parameter for matric suction h_m = matric suction h_s = solute suction χ_s = effective stress parameter for solute suction	Richards (1966)

Stress state for unsaturated soils

Numerous attempts have been made to extend stress concepts useful for saturated soils, into the unsaturated soil range. The proposed equations have taken the form of a single-valued effective stress equation. Table 1 contains a summary of the more common forms which have been proposed.

All of the equations in Table 1 propose a single-valued equation. Soil properties can also be identified in all equations. It could be argued that these equations are constitutive relations and as such “fall short” of meeting the conditions of a state variable. The difficulties are primarily conceptual in nature, and their adoption gives rise to a deviation from classical continuum mechanics. Practical difficulties have also been encountered in the use of these effective stress equations in practice.

Morgenstern (1979) amply summarized the difficulties associated with the use of the first equation listed in Table 1. (His comments would also apply to other single-valued equations.) Bishop’s effective stress equation

... proved to have little impact or practice. The parameter χ when determined for volume change behaviour was found to differ when determined for shear strength. While originally thought to be a function of the degree of saturation and hence bounded by 0 and 1, experiments were conducted in which χ was found to go beyond these bounds. As a result, the fundamental logic of seeking a unique expression for the effective stress independent of degree of saturation has been called into question (Fredlund 1973). The effective stress is a stress variable and hence related to equilibrium considerations alone.

Bishop’s effective stress equation

... contains a parameter, χ , that bears on constitutive behaviour. This parameter is found by assuming that the behaviour of a soil can be expressed uniquely in terms of a single effective stress variable and by

matching unsaturated behaviour with saturated behaviour in order to calculate χ . Normally, we link equilibrium considerations to deformations through constitutive behaviour and do not introduce constitutive behaviour directly into the stress variable.

Historically, the calling into question of a single-valued effective stress equation for unsaturated soils can be summarized as follows: Coleman (1962) suggested the use of “reduced” stress variables ($\sigma_1 - u_a$), ($\sigma_3 - u_a$) and ($u_a - u_w$) to represent the axial, confining and pore-water pressure, respectively, in triaxial tests. Constitutive relations for volume change were then formulated using the “reduced” stress variables. In 1963, Bishop and Blight re-evaluated the use of the single-valued effective stress equation and stated that a change in matric suction did not always result in the same change in effective stress. It was also suggested that volume change laboratory data be plotted in terms of the independent stress variables, ($\sigma - u_a$) and ($u_a - u_w$). This appears to have initiated a transition towards utilizing the stress variables in an independent manner. This approach was further reinforced by Blight (1965) and Burland (1964, 1965).

Matyas and Radhakrishna (1968) introduced the concept of “state parameters” in describing the volumetric behaviour of unsaturated soils. Volume change and degree of saturation were plotted versus ($\sigma - u_a$) and ($u_a - u_w$). Barden, Madedor and Sides (1969) also suggested analysing volume change in terms of independent stress state variables.

In 1977, Fredlund and Morgenstern presented a theoretical stress analysis basis for the use of independent stress state variables. The analysis used principles of multiphase continuum mechanics. The analysis concluded that the use of any two of three possible stress variables could be justified (i.e., ($\sigma - u_a$), ($\sigma - u_w$) and ($u_a - u_w$)). The possible combinations are: (1) ($\sigma - u_a$) and ($u_a - u_w$),

(2) $(\sigma - u_w)$ and $(u_a - u_w)$, and (3) $(\sigma - u_a)$ and $(\sigma - u_w)$. No analysis or experiment has been proposed to confirm which combination is most satisfactory. However, $(\sigma - u_a)$ and $(u_a - u_w)$ were shown to be the most satisfactory combination from a practical analysis standpoint. These can be written in the form of two independent stress tensors.

$$\begin{bmatrix} (\sigma_x - u_a) & \tau_{yx} & \tau_{zx} \\ \tau_{xy} & (\sigma_y - u_a) & \tau_{zy} \\ \tau_{xz} & \tau_{yz} & (\sigma_z - u_a) \end{bmatrix}$$

and

$$\begin{bmatrix} (u_a - u_w) & 0 & 0 \\ 0 & (u_a - u_w) & 0 \\ 0 & 0 & (u_a - u_w) \end{bmatrix}$$

The above brief history shows that initial attempts to describe the stress state of an unsaturated soil led to various proposed, single-valued equations. However, with time there has been a gradual transition towards the use of independent stress state variables. At present, the emphasis appears to be on the formulation of practical geotechnical applications using independent stress state variables.

Conceptual aspects

There are numerous types of state variables, but the discussions in this paper will be limited primarily to the state variables required to describe the stress state. It can be reasoned that any one or more variables can be designated as the state variables for a particular multiphase material. While this may be true, it can also be reasoned that state variables possessing certain characteristics provide a better basis for developing a practical science. Unfortunately, there does not appear to be any theory which can be used to derive or prove that one or more state variables are the only state variables that can be used. In the final analysis, the selection of state variables will come down to: (1) variables that can be experimentally tested, (2) variables that can be theoretically justified, (3) variables which are operational in practice, and (4) variables that have characteristics acceptable within the definition of state variables.

It is also possible that the above conditions can be met by more than one set of state variables. The final selection of state variables may come back to personal preference and in essence be a philosophical preference.

Most analyses associated with saturated soil mechanics are formulated in terms of effective stresses as the stress state variables. However, there are, for example, total stress slope stability analyses. This means that total stresses are being used as the stress state variables. While total stress, without reference to pore-water pressure, can be used as a stress state variable, it is well known that this is not the best, general approach. In other words, the total stress analysis has proven to be the exception rather than the rule. The total stress analysis has become known

as an approximate simulation of a specific situation. The soil mechanics discipline references its beginning as a science to Terzaghi's introduction of the effective stress variable because it was a superior definition of the stress state. The rapid development of this discipline has demonstrated that the effective stress variable was a good choice. The above discussion gives but one example to show that more than one choice can be made regarding stress state variables, but in general, one description will be superior. There are also several acceptance descriptions of deformation state variables (e.g., Lagrangian, Eulerian, etc.) but generally one set of deformation state variables will prove to be superior for a particular class of problems.

On the basis of the definition of state variables, it is not prudent to incorporate soil properties into the definition of the stress state. Developments within continuum mechanics have, in general, adhered to this condition. Continuum mechanics has proven to be an all-encompassing and unifying theory embracing the behaviour of many types of materials. Therefore, it is incumbent upon us to give careful consideration to continuum mechanics principles in formulating the stress state variables for unsaturated soils.

Experimental evidence

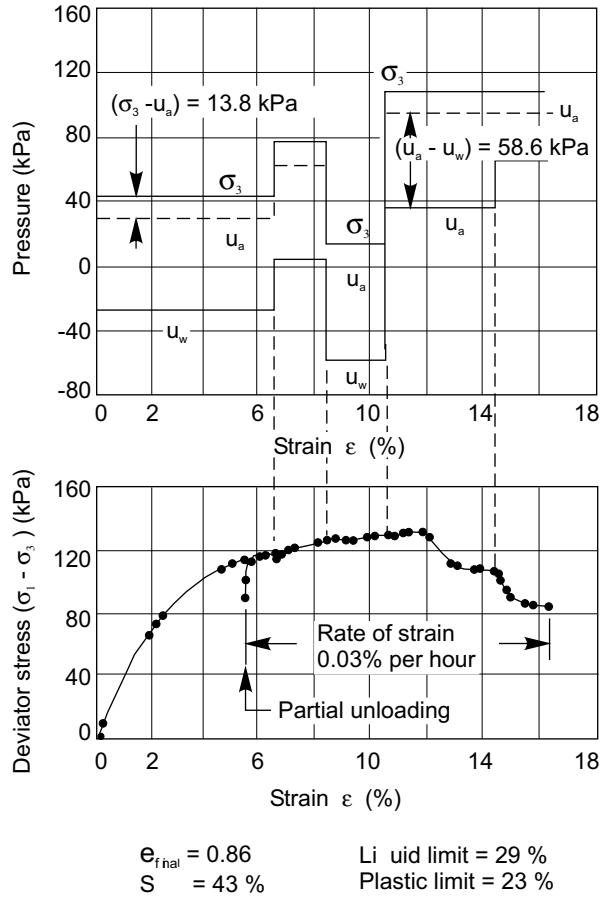
Numerous laboratory experiments have been performed which assist in understanding the description of the stress state in unsaturated soils. Mention is made of a few earlier experiments which are of relevance.

A key experiment on unsaturated soils was performed by Bishop and Donald (1961) (Fig. 2). In this experiment, a Braehead silt was subjected to drained triaxial compression with independent control of σ_3 , u_a and u_w . These pressures were changed during the experiment with the restriction that: $\Delta(\sigma_3 - u_a) = 0$; and $\Delta(u_a - u_w) = 0$. Both deviatoric stresses and volumetric strain were monitored and found to vary monotonically with axial strain as shown in Fig. 3. The results illustrate that the single-valued effective stress variable remained constant. An alternate interpretation is that each of the independent stress variables (i.e., $(\sigma_3 - u_a)$, $(u_a - u_w)$ and $(\sigma_3 - u_w)$) was not altered and therefore the behaviour was not influenced.

While the experiment supports the validity of the independent stress state variables, one cannot be exclusive in the interpretation of the data. It is also possible to suggest that any one of three possible combinations of the stress state variables are experimentally justifiable.

In 1956, Hilf proposed the axis-translation testing technique along with data from several soils. This laboratory technique made it possible to measure matric suctions greater than one atmosphere. Results in Fig. 3 show that the measured pore-water pressure reaction was always the same as the applied air pressure change. This meant that the measured matric suction remained at a constant value. Examination of the axis-translation procedure would indicate that the test is a special type of Null Test under

Fig. 2. Drained test on partially saturated loose silt in which σ_3 , and u_a and u_w are varied so as to keep $(\sigma_3 - u_a)$ and $(u_a - u_w)$ constant (from Bishop and Donald 1961).



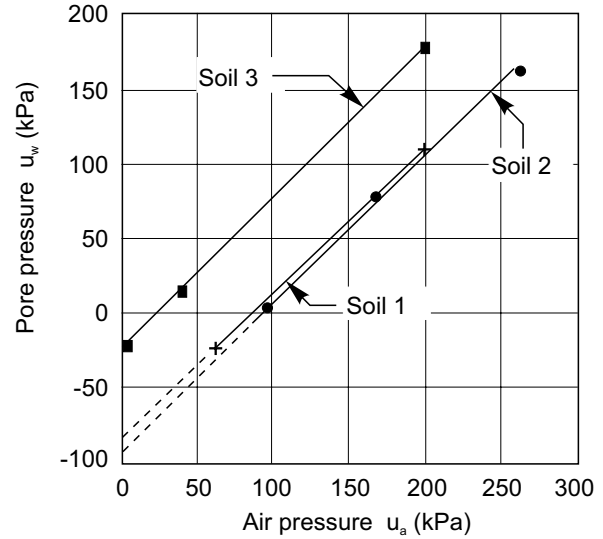
which the stress state remained constant. In this test the total pressure is equal to the applied air pressure. The stress variables $(\sigma - u_a)$ and $(u_a - u_w)$, remain constant throughout the test and for this reason the test can successfully measure the stress state of the soil.

In 1977, Fredlund and Morgenstern reported a series of Null Tests on compacted and natural clays. The Null Tests allowed for the equal change in the total, pore-air and pore-water pressure while the overall volume and water volume of the specimen were monitored. The Null Tests were interpreted in view of the following definition of independent stress state variables.

A suitable set of independent stress state variables are those that produce no distortion or volume change of an element when the individual components of the stress state variables are modified but the stress state variables themselves are kept constant. Thus the stress state variable for each phase should produce equilibrium in that phase when a stress point in space is considered.

The experimental data indicated extremely small overall volume change and net water flow from the specimens (Fig. 4). The overall and water volume changes were approximately 2% of the volume changes that would be associated with a similar change in either one of the stress

Fig. 3. Determination of capillary pressure by translation of the origin (Hilf 1956).



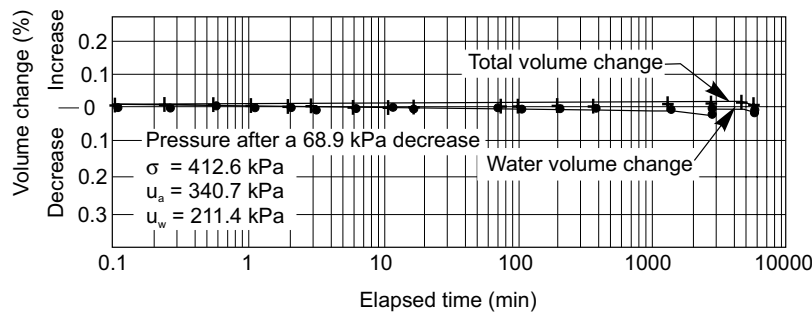
state variables. These tests demonstrate that the differences in the stress components form stress state variables that can be used to define the behaviour of unsaturated soils. At the same time, it is impossible to experimentally prove an exclusive form for the definition of the stress state. The shear strength testing of unsaturated soils has also supported the use of independent stress state variables (Escario 1980; Gulhati and Satija 1981).

Theoretical evidence

The state of a system is generally defined within the context of thermodynamic considerations. For the problem under consideration (i.e., an unsaturated soil element) the system is also assumed to be isothermal and the state variables of interest are those related to stress. The thermodynamic considerations are therefore reduced to the conservation of momentum. Since we are dealing with a static system with negligible velocities, this further reduces to considering Newton's second law of statics (i.e., summation of forces in orthogonal directions).

The force equilibrium equations for the solid phases of a multiphase system are of interest. The surface tractions appearing in these equilibrium equations are the stress state variables which must be kept constant in order to maintain the equilibrium of the system. The principle involved in viewing the force equilibrium equation is essentially the same as the principle or concept of effective stress. That is, if the surface tractions (or stress state variables) in the equilibrium equation remain unchanged, there will be no change in the state of the solid (i.e., no change in volume, distortion, or shear strength).

In 1977, Fredlund and Morgenstern used the concept of multiphase continuum mechanics to write the equations of action for the solid phase of an unsaturated soil. The principle of the superposition of coincident equilibrium stress fields was used as described in continuum mechanics (Truesdell and Toupin 1960; Green and Naghdi 1965;

Fig. 4. Null test on unsaturated sample (N-40).

Truesdell 1966). The assumption is made that an independent continuous stress field is associated with each phase of the multiphase system. The number of independent force equilibrium equations that can be written is equal to the number of cartesian coordinate directions multiplied by the number of phases constituting the continuum. The equilibrium equation can be written for various combinations of the phases.

As a result of the above analysis, it was possible to demonstrate that the surface tractions appearing in the force equilibrium equations for the soil solids (and the contractile skin or air-water interphase) were the same as those previously suggested for use for unsaturated soils. It was also explained that three possible sets of stress state variables could be combined in the form of two stress tensors; each one being a function of the reference phase used in deriving the equations.

The force equilibrium equations can be taken as convincing evidence in support of the proposed stress state variables. However, the derivation cannot be viewed as exclusive proof of the proposed stress state variables.

The selection of the most suitable combination of stress state variables must be based on practical preference rather than theoretical considerations. There has been a central consensus that $(\sigma - u_a)$ and $(u_a - u_w)$ are the best combination of stress state variables. This combination allows for the independent consideration of the effects of externally applied total stresses and the internally applied pore-water pressure. Each of these stresses are referenced to the pore-air pressure, which in most cases is equal to atmospheric pressure.

Application of stress state variables to geotechnical engineering analyses

Theories associated with saturated soils relate the effective stress state to soil behaviour. For unsaturated soils, the theories have been extended to relate more than one independent stress state variable to soil behaviour. These formulations have proven to be easy-to-comprehend extensions of concepts well known to geotechnical engineers. In each case, a smooth transition has been demonstrated between the saturated and unsaturated formulations. Forms for the constitutive relations for volume change, seepage, and shear strength problems have been summarized by Fredlund (1985).

The concept of stress state variables for unsaturated soils is relevant to expansive soils. However, it is expedient to view the problem of expansive soils in terms of a broader context; that is, as one application of the broader subject of unsaturated soil behaviour. The limited scope associated with problems of expansive soil studies may prove in the long-run to be inferior to a broader study involving all aspects of unsaturated soil behaviour. This broader discipline would provide the necessary theoretical links between seepage, volume change, and shear strength type problems. This would appear to be the key challenge before us.

Conclusions

The use of $(\sigma - u_a)$ and $(u_a - u_w)$ holds the greatest promise for use in geotechnical engineering. There is convincing experimental and theoretical evidence in support of these stress state variables.

Formulations for most engineering analyses have already been published. These formulations have illustrated that there is a parallel to saturated soil mechanics which should be developed for unsaturated soils. The problems associated with expansive soils should be resolved as a special case of unsaturated soil mechanics. Further effort should be made towards accurately and readily measuring the *in situ* matric suction of soils. Once this is accomplished, a practical technology will be a reality for geotechnical engineers.

References

- Aitchison, G.D. 1961. Relationship of moisture and effective stress functions in unsaturated soils. *In* Pore Pressure and Suction in Soils, Conference, British National Society of International Society of Soil Mechanics and Foundation Engineering at the Institute of Civil Engineering, Butterworths, London, England, pp. 47–52.
- Barden, L., Madedor, A.D., and Sides, G.M. 1969. Volume change characteristics of unsaturated clay. *ASCE Journal of the Soil Mechanics and Foundation Division*, **95**(SM1): 33–52.
- Bishop, A.W. 1959. The principle of effective stress. Lecture delivered in Oslo, Norway, 1955; *Technisk Ukeblad*, **106**(39): 859–863.
- Bishop, A.W. and Blight, G.E. 1963. Some aspects of effective stress in saturated and unsaturated soils. *Géotechnique*, **13**(3): 177–197.

- Bishop, A.W. and Donald, I.B. 1961. The experimental study of partly saturated soil in the triaxial apparatus. Proceedings, 5th International Conference of Soil Mechanics and Foundation Engineering, Paris, France, Vol. 1, pp. 13–21.
- Bishop, A.W. and Eldin, G. 1950. Undrained triaxial tests on saturated sands and their significance in the general theory of shear strength. *Géotechnique*, **2**: 13–32.
- Blight, G.E. 1965. A study of effective stresses for volume change. A Symposium in Print. *In* Moisture equilibria and moisture changes in soils beneath covered areas. *Edited by* G.D. Aitchison, Butterworths, Sydney, Australia, pp. 259–269.
- Burland, J.B. 1964. Effective stresses in partly saturated soils. Discussion of: Some aspects of effective stress in saturated and partially saturated soils, by G.E. Blight and A.W. Bishop, *Géotechnique*, **14**: 65–68.
- Burland, J.B. 1965. Some aspects of the mechanical behavior of partly saturated soils. *In* Moisture equilibrium and moisture changes in soils beneath covered areas. A symposium in print. *Edited by* G.D. Aitchison, Butterworth and Company (Australia) Ltd., Sydney, Australia, pp. 270–278.
- Coleman, J.D. 1962. Stress/strain relations for partly saturated soils. Correspondance in *Géotechnique*, **12**(4): 348–350.
- Crone, D., Coleman, J.D., and Black, W.P.M. 1958. The movement and distribution of water in soil in relation to highway design and performance., Highway Research Board Special Report, Washington, D.C. No. 40, pp. 226–252.
- Dregne, H.E. 1976. Soils of arid regions. American Elsevier Publishing Company, Inc., New York.
- Escario, V. 1980. Suction controlled penetration and shear tests. Proceedings, 4th International Conference on Expansive Soils, Denver, CO, American Society of Civil Engineers, Vol. 2, pp. 781–797.
- Fredlund, D.G. 1973. Volume change behaviour of unsaturated soils. Ph.D. thesis, University of Alberta, Edmonton, AB, Canada.
- Fredlund, D.G. 1985. Soil mechanics principles that embrace unsaturated soils. Proceedings, International Society for Soil Mechanics and Foundation Engineering, San Francisco, CA., Vol. 2, pp. 465–473
- Fredlund, D.G., and Morgenstern, N.R. 1977. Stress state variables for unsaturated soils. ASCE, Journal of the Geotechnical Engineering Division, **103**(GT5): 447–466.
- Fung, Y.C. 1965. Foundations of solid mechanics. Prentice-Hall, Inc., Englewood Cliffs, N.J.
- Fung, Y.C. 1969. A first course in continuum mechanics. Second edition, Prentice-Hall Inc., Englewood Cliffs, NJ.
- Green, A.E., and Naghdi, P.M. 1965. A dynamical theory of interacting continua. *International Journal of Engineering Science*, **3**: 231–241.
- Gulhati, S.K., and Satija, B.S. 1981. Shear strength of partially saturated soils. Proceedings, 10th International Conference for Soil Mechanics and Foundation Engineering, Stockholm, Sweden, Vol. 1, pp. 609–612.
- Hilf, J.W. 1956. An investigation of pore water pressures in compacted cohesive soils. Technical Memorandum 654, United States Department of Interior, Bureau of Reclamation, Design and Construction Division, Denver, CO.
- Hubbert, M.K., and Rubey, W.W. 1959. Role of fluid pressure in mechanics of overthrust faulting. *Bulletin of the Geological Society of America*, **70**: 115–166.
- Jennings, J.E.B. 1960. A revised effective stress law for use in the prediction of the behaviour of unsaturated soils, pore pressure and suction in soils. Proceedings, Conference on Pore Pressure and Suction in Soils, British National Society of International Society of Soil Mechanics Foundation Engineering at the Institute of Civil Engineering, Butterworths, London, England, pp. 26–30.
- Lambe, T.W. 1960. A mechanistic picture of shear strength in clay. Proceedings, ASCE Research Conference on Shear Strength of Cohesive Soils, University of Colorado, Boulder, CO, pp.555–580.
- Matyas, E.L. and Radhakrishna, M.S. 1968. Volume change characteristics of partially saturated soils. *Géotechnique*, **18**(4): 432–448.
- Meigs, P. 1953. World distribution of arid and semi-arid homoclimates. *In* UNESCO, Reviews of Research on Arid Zone Hydrology, Arid Zone Research, pp. 203–210.
- Michels, W.C. 1961. The international dictionary of physics and electronics. Second edition, *Edited by* Van Nostrand Co., Princeton, New Jersey.
- Morgenstern, N.R. 1979. Properties of compacted soils. Proceedings, 6th Pan-American Conference on Soil Mechanics and Foundation Engineering. Contribution to panel discussion Session IV, Lima, Peru, Vol. 3, pp. 349–354.
- Nur, A., and Byerlee, J.D. 1971. An exact effective stress law for elastic deformation of rock with fluids. *Journal of Geophysical Research*, **76**(26): 6414–6419.
- Richards, B.G. 1966. The significance of moisture flow and equilibria in unsaturated soils in relation to the design of engineering structures built on shallow foundations in Australia. Symposium on Permeability and Capillarity, American Society for Testing and Materials, Atlantic City, N.J.
- Skempton, A.W. 1961. Effective stress in soils, concrete and rocks. Proceedings, Pore pressure and suction in soils. Butterworths, London, pp. 4–16.
- Terzaghi, K. 1936. The shear resistance of saturated soils. Proceedings, 1st International Conference on Soil Mechanics and Foundation Engineering, Cambridge, MA, Vol. 1, pp. 54–56.
- Truesdell, C. 1966. The elements of continuum mechanics. Springer-Verlag, Inc., New York, NY.
- Truesdell, C., and Toupin, R.A. 1960. The classical field theories. *In* Handbuch der Physik. *Edited by* S. Flüge, Vol. 7/1, Springer-Verlag, Berlin, Inc., Germany.

On total, matric and osmotic suction

J. Krahn and D.G. Fredlund

Abstract: The total suction of a soil is generally considered to consist of two components; namely, matric suction and osmotic suction. To verify this assertion experimentally, independent measurements of total, matric and osmotic suction were performed on samples of a low plasticity glacial till and a high plasticity clay. The total suction was measured with a psychrometer, the matric suction with a modified consolidometer operating on the same principles as the pressure plate, and the osmotic suction was determined from an analysis of the pore fluid squeezed from the sample using a high pressure hydraulic squeezer. The osmotic suction values were compared with results obtained using the saturation extract technique. Tests were performed for a wide range of water contents and densities on statically, compacted samples.

The results indicate good correlation between the total suctions and the sum of the matric and osmotic suctions. The total and matric suctions are shown to be primarily functions of water content and therefore essentially independent of dry density.

Key words: soil suction, matric suction, total suction, osmotic suction, pressure plate, psychrometer.

Introduction

Most of the basic research associated with the role played by the pore fluid in a soil was initiated by soil physicists and agronomists during the late 1800's and later transferred to engineering. Probably the first group to recognize its importance in civil engineering was Croney et al. (1948, 1950) at the Road Research Laboratory in London, England. They borrowed their terminology from soil science and observed the effect of soil moisture deficiency on soil behaviour. Later research workers (Croney et al. 1958; Bishop 1959; Jennings 1960; Aitchison 1961) attempted to incorporate the soil suction term into an effective stress equation that could be used to describe the volume change and shear strength behaviour of a soil.

The Review Panel for the soil mechanics symposium, "Moisture Equilibria and Moisture Changes in Soils" (Aitchison 1964), adopted the subdivision of soil suction and the definitions quoted by the International Society of Soil Science.¹

The definitions state that total suction is equal to the sum of the matric and osmotic suction and may be determined by the measurement of the vapour pressure in equilibrium with the soil water. The fact that the vapour

pressure is controlled by the dissolved salts in the pore fluid and the hydrostatic tension of the pore-water lends credence to this subdivision of total suction (Edlefsen and Anderson 1943).

Although numerous methods are available for the measurement of each component of suction, few documented cases are available in which independent measurements of matric and osmotic suction have been performed and their sum compared with the measurement of total suction on the same sample. Richards and Ogata (1961) found that their measurements of total suction were not the same. It should be noted that their samples were prepared as a slurry. A small amount of extract was removed for the osmotic suction measurement and then the samples were brought to equilibrium under relatively high matric suction values (pressure membrane technique). Their analysis of the data assumes that the concentration of the salts in the pore fluid and, therefore, the osmotic suction, remains the same as the pore fluid is being squeezed out of the sample.

Oster et al. (1969) devised a technique which allowed the independent measurement of matric suction and osmotic suction. They compared the difference of the measured osmotic suction (psychrometric measurement on pore fluid) with the osmotic suction predicted by electri-

J. Krahn. Professor, Department of Engineering, University of Alberta, Edmonton, AB, Canada T6G 2G7.

D.G. Fredlund. Professor, Department of Civil Engineering, University of Saskatchewan, 57 Campus Drive, Saskatoon, SK, Canada S7N 5A9.

Reproduced with permission from *Soil Science*, **114**(5): 339–348, 1972.

¹Matric suction is the negative gauge pressure relative to the external gas pressure on the soil water, to which a solution identical in composition with the soil water must be subjected in order to be in equilibrium through a porous permeable wall with the soil water. The osmotic suction is the negative gauge pressure to which a pool of pure water must be subjected in order to be in equilibrium through a semipermeable (i.e., permeable to water molecules only) membrane with a pool containing a solution identical in composition with the soil water. The total suction is the negative gauge pressure relative to the external gas pressure on the soil water to which a pool of pore water must be subjected in order to be in equilibrium through a semi-permeable membrane with the soil water. Total suction is thus equal to the sum of matric, or soil water suction, and osmotic suction.

cal conductivity measurement on the salt solution used to saturate the samples. The latter values were smaller than those determined by the psychrometer. Their work indicates the importance of the procedure used when attempting to predict osmotic suction.

This paper presents data on the independent measurements of matric, osmotic, and total suction where dry density and water content are used as the basis for comparison of all soil suction components. The osmotic suction was computed from electrical conductivity measurements on the saturation extract as well as an extract of the pore fluid at the actual water content under consideration (squeezing method).

The matric and total suctions were measured only at the "as prepared" water contents and dry densities. No attempt was made to vary suction and measure changes in volume or water content since this involves the area of constitutive relationships. The purpose of this research was to verify the existing state variables under static conditions. The research literature contains some information on the variation of matric suction with density and water content; however, the results are somewhat conflicting. Croney et al. (1958) showed that for an incompressible material such as sand or chalk, the matric suction was affected by dry density. He also stated that a compressible, compacted clay is not affected by changes in dry density. Croney and Coleman (1961) showed a unique relationship between the suction of a "continuously disturbed" clay and water content. In other words, the density did not affect the suction measurements. Natural undisturbed samples, however, had a suction-water content relationship dependent upon density. Box and Taylor (1961) used a null-point tensiometer and showed that at constant water contents, higher densities resulted in a decrease in matric suction. The variations appear to be small, however, from an engineering stand-point. For example, the suction decreased 1 psi (6.895 kPa) for an increase in dry density of 30 lb/ft³ (480 kg/m³). Their testing was performed in the low suction range. Olson and Langfelder (1965) presented considerable data on the effect of changing dry density and method of compaction of the soil. They tested five soil types and measured matric suctions (null-technique) up to 280 psi (1931 kPa). On all soil types, it can be concluded that the variation of matric suction with dry density appears to be of a secondary interest.

Apparatus and technique

a) Matric suction

The apparatus used in this investigation was a Modified Anteus consolidometer (Fig. 1) developed at the University of Saskatchewan (Pufahl 1970). The chamber of the consolidometer was filled with air at a pressure regulated by the back pressure valve (axis-translation technique). Any tendency for movement of water through the stone was detected by a pressure transducer (null-point technique). The air-entry value of the ceramic disk was 15 bars (1,500 kPa).

This technique should not measure the osmotic suction since the dissolved salts in the pore fluid are able to pass through the porous disk. Mitchell (1960) and Pufahl (1970) have shown that this type of porous disk does not act like a semi-permeable membrane.

b) Osmotic suction

The osmotic suction can be determined from the electrical conductivity of an extract of the pore fluid. The saturation extract technique (USA Agricultural Handbook No. 60, 1950) generally used in soil science involves wetting the soil to a slurried paste and measuring the electrical conductivity of a portion of the pore fluid.

The osmotic suction determined by the saturation extract technique corresponds to the water content of the slurried soil at the time of extraction. However, there is no theoretical procedure for back-calculating to obtain the osmotic suction at lower water contents. The most reasonable procedure for back-calculating would be to assume an inverse linear relationship between cation concentration and volume of water in the soil. In other words, the electrical conductivity is assumed to be inversely proportional to the water content during the wetting of a soil (i.e., linear dilution).

Alternatively, the pore fluid in the soil at a particular water content can be retrieved using a squeezer or pressure plate apparatus. A heavy-walled cylinder and piston squeezer employing pressures up to 5,000 psi (35 MPa) was used in this investigation. The squeezer is essentially the same in design as described by Manheim (1966), but considerably larger. The pore fluid was then analyzed in the same manner as in the saturation extract technique.

c) Total suction

The total suction was measured with a psychrometer. The theory and operational technique upon which the psychrometer is based has been well documented by Spanner (1951); Dalton and Rawlins (1968); and Richards (1969). Basically, the psychrometer measures relative humidity inside a closed chamber containing the soil sample. The total suction of the soil is computed from the relative humidity measurement (Edlefsen and Anderson 1943).

The most difficult aspect in using the psychrometer is related to the temperature control (Fig. 2). In order to measure total suction to an accuracy of 10.13 kPa, the constant temperature bath must be maintained to within ± 0.001 degrees centigrade and it is estimated that the soil temperature was maintained within the same degree of accuracy due to the buffering effect of the glass beaker.

The thermocouple probe and the sample container are shown in Fig. 3. The sample containers are considerably larger than those reported elsewhere in the literature. The only effect of the large containers appeared to be in the length of time required for the vapour pressure to equalize. Figure 4 is a plot of the galvanometer deflection versus time after the calibrating solution in the containers was placed in the bath. From the graph, it can be seen that there was little change after approximately 24 hours. However, it was found that in order to obtain consistent

Fig. 1. Modified Anteus consolidometer (after Pufahl 1970).

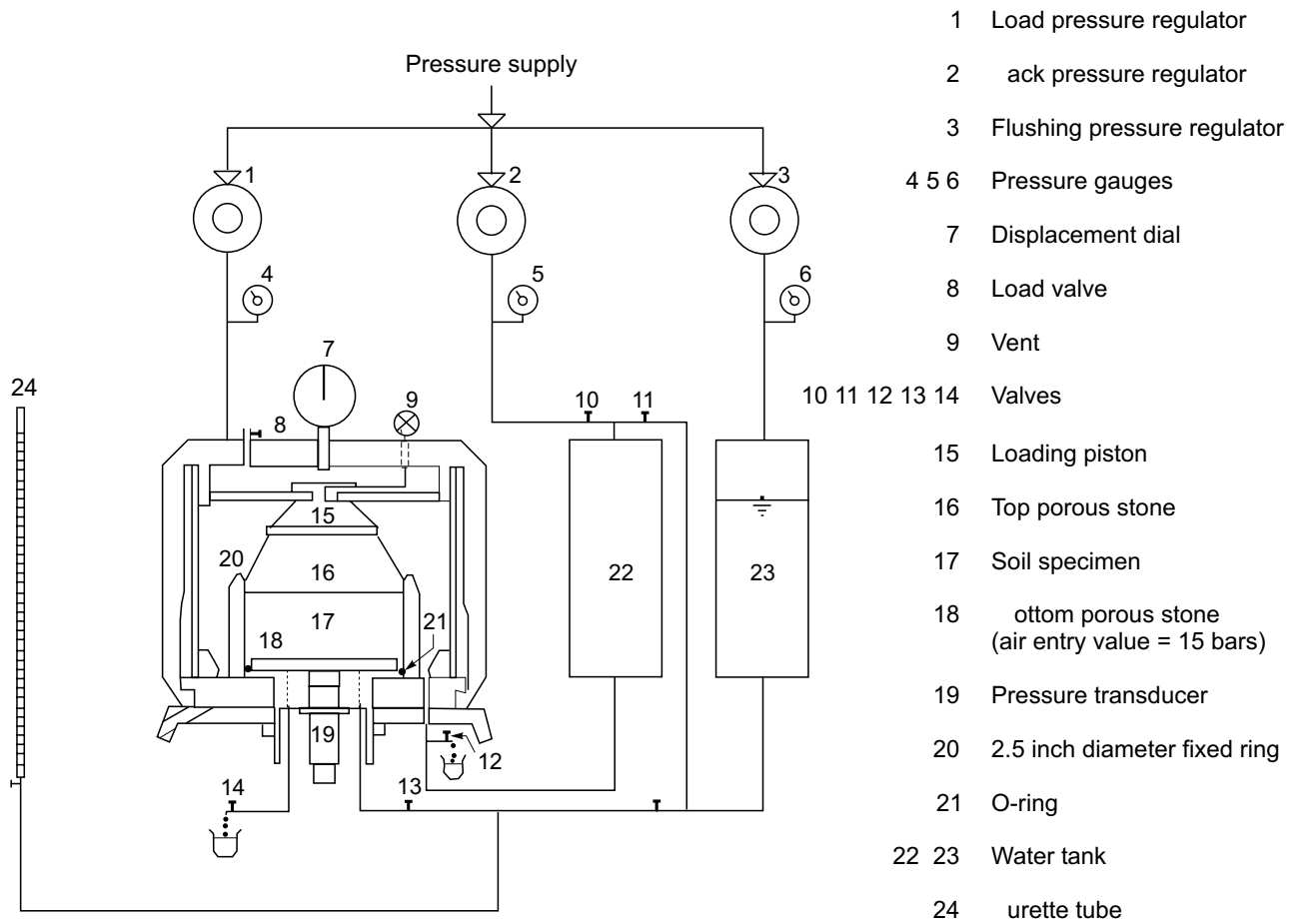
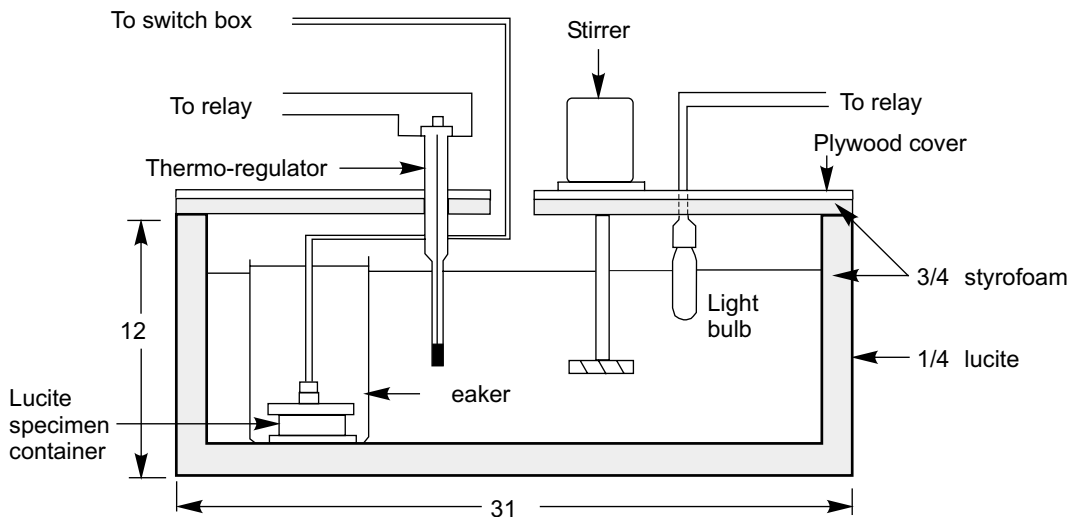


Fig. 2. Schematic diagram of constant temperature bath.

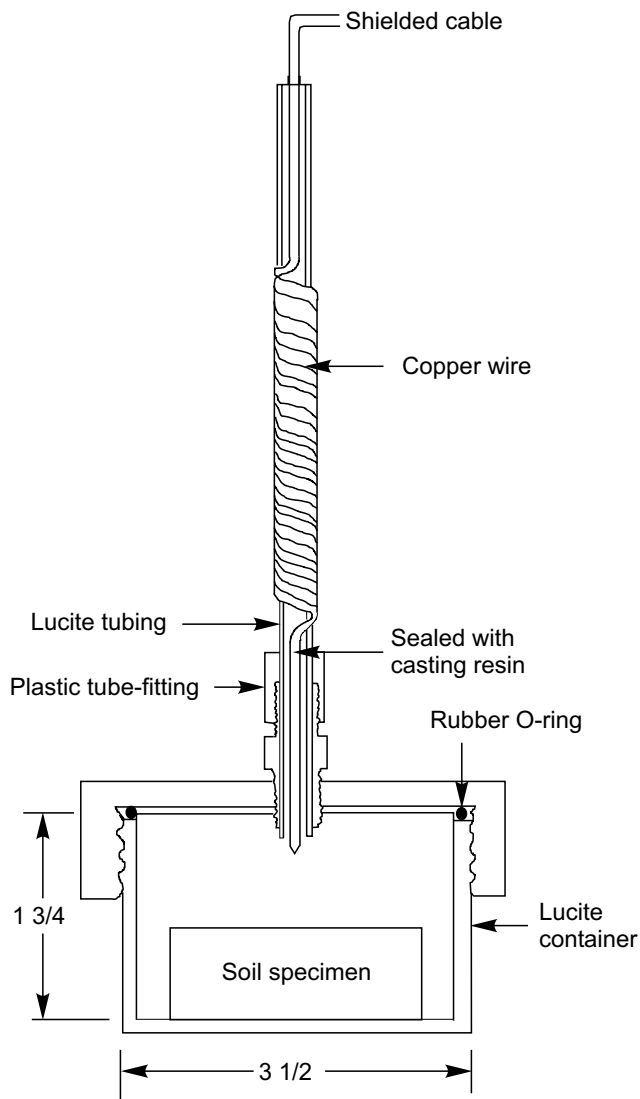


results, the containers had to be left in the bath until the slow decrease after 24 hours had ceased. As a result, the samples and calibrating solutions were left in the bath for approximately three days. The bath was operated at 25°C and the thermocouple probes were calibrated using solutions of potassium chloride.

Materials tested and sample preparation

Two types of soil were used in this project, a low and a high plasticity clay. The low plasticity, sandy clay is typical of the glacial till found in central and southern Sas-

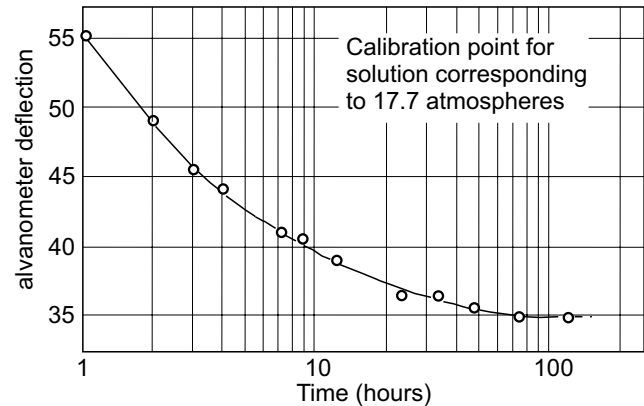
Fig. 3. Schematic diagram of sample container and thermocouple psychrometer.



katchewan, Canada. The high plasticity clay is from a highly swelling, lacustrine deposit found beneath the city of Regina, Saskatchewan (commonly referred to as Regina clay). Classification test results, together with the mineralogical composition and the cations in the pore-water are presented in Table 1.

The till was screened through a number 10 sieve, oven-dried and then mixed with the required amount of distilled water for a desired water content. The Regina clay samples were initially air-dried, crushed and passed through a number 10 sieve. The prepared soil was stored in a plastic container for at least 24 hours after which the samples were formed by static compaction. The samples were compressed in the compaction mold for at least 24 hours, then removed from the mold, wrapped in plastic wrap and waxed. They were cured for a minimum of seven days prior to testing.

Fig. 4. Galvanometer deflection versus time after solution was placed in the bath.



Experimental results

a) Comparison of total and matric suction

Figure 5 shows the results of the total and matric suction measurements on the till at various water contents and a dry density of 110.1 lb/ft^3 (1760 kg/m^3). Similar results for the Regina clay at a dry density of 88.5 lb/ft^3 (1420 kg/m^3) are shown in Fig. 6. Although some scatter is evident, the trends are clear. The matric and total suction curves show similar shapes. The difference between the two curves (the osmotic suction) decreases with increasing water content as anticipated.

b) The osmotic suction

The results of the electrical conductivity measurements on the saturation extract and the pore fluid from the squeezer are shown in Figs. 7 and 8. Also shown are the computed osmotic suction values, assuming a linear dilution up to the water content of the saturation extract. These results are compared with the difference between the measured total and matric suction.

The osmotic suctions obtained for the Regina clay by the squeezer technique show an excellent correlation with the difference between the total and matric suction measurements. A good correlation was also obtained for the till at the higher water contents. The osmotic suction obtained from the saturation extracts is lower than the actual osmotic suction at lower water contents. This is as anticipated since the concentration of salts in the pore-water increases with decreasing water content. The computed osmotic suctions, assuming a linear dilution up to the saturation extract water content, give values that are much higher than those obtained by the squeezing technique. For the two soils tested, the difference is substantial (in the order of 100%). It appears that a linear dilution of the pore fluid does not occur upon wetting. However, to assume a more realistic, non-linear dilution theory would require more data than is obtained during the saturation extract test. From these results, it is obvious that the squeezing technique is a superior procedure.

Table 1. Classification tests.

	Till	Regina clay
Specific Gravity	2.74	2.83
Atterberg Limit		
Liquid Limit (%)	33.9	78.4
Plastic Limit (%)	17	30.6
Plasticity Index	16.9	47.8
Grain Size Distribution ^a		
Percent Sand	31.8	5.6
Percent Silt	38.5	27.2
Percent Clay	29.7	67.2
Standard Compaction		
Maximum Dry Density (lb/ft ³)	122.9	91.8
Maximum Dry Density (kg/m ³)	1970	1470
Optimum Water Content (%)	11.8	27.8
Modified AASHO		
Maximum Dry Density (lb/ft ³)	122.5	—
Maximum Dry Density (kg/m ³)	1800	—
Optimum Water Content (%)	15.6	—
Mineralogical Composition (of minus 2 micron fraction) ^b		
Montmorillonite (%)		
Illite (%)	14	20
Kaolinite (%)	50	42
Mixed (12A) Mineral Layer (%)	14	14
Cations in Pore Water (Saturation Extract) (meq/100 grams dry soil)		
Sodium	1.03	1.05
Calcium	3.17	3.16
Magnesium	4.84	1.66
Potassium	0.11	0.33

^a MIT Grain Size Scale

^b X-ray Diffraction

The difference between the total and matric suctions on the till (Fig. 7) deviate somewhat from the “squeezing technique” values at lower water contents. Several factors may be involved, but it is most probable that the matric suction measurements are low since the measurements are approaching the air-entry value of the porous disk. However, the dispersion in data is relatively small, and the results would appear to reinforce the validity of the subdivision of soil suction.

c) Relationship between dry density, water content and suction

The suction versus water content curves at various dry densities are shown in Figs. 9 and 10. It does not appear that the suction (matric or total) is significantly affected by a change in dry density. For the sake of interest, some loose soil was placed in the psychrometer container and tested. The results showed close agreement with those ob-

Fig. 5. Comparison of total and matric suction for the till.

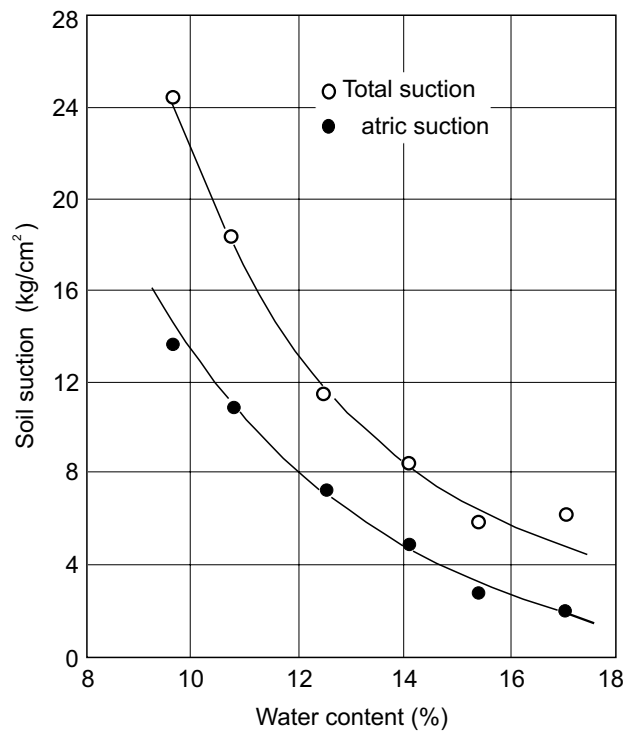
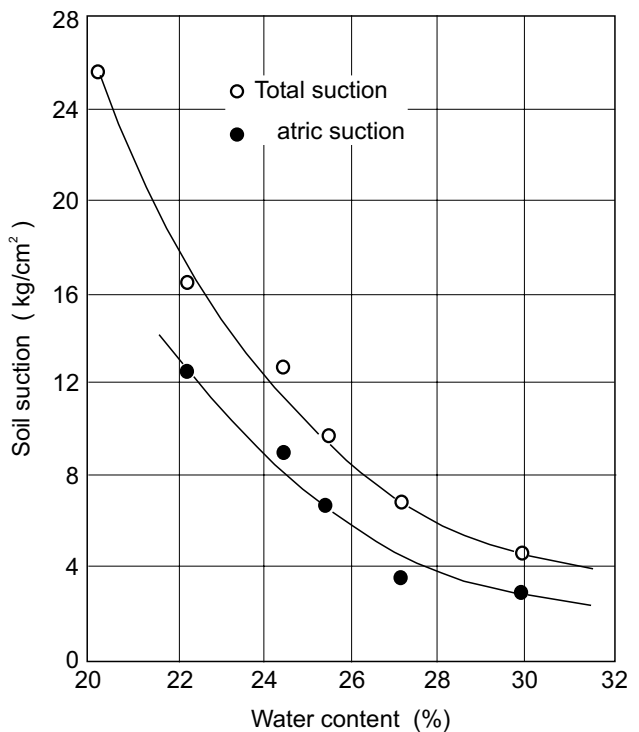


Fig. 6. Comparison of total and matric suction for the Regina clay.



tained on the compacted soil (see Fig. 9). The results are similar to those obtained by Olson and Langfelder (1965) and further verify that a variation in dry density has little effect on the matric suction of remolded, compacted soils.

Fig. 7. Comparison of osmotic suctions for the till.

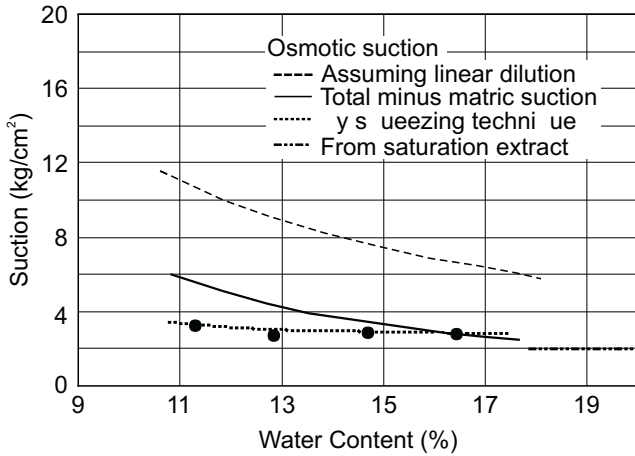
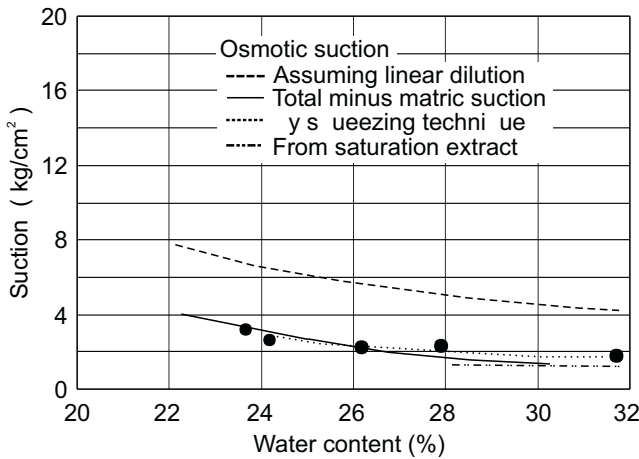


Fig. 8. Comparison of osmotic suctions for the Regina clay.



The results obtained in this investigation also substantiate this for the total suction measurements. Croney and Coleman (1961) also emphasized the existence of a unique water content versus suction relationship for remolded soils. Although this unique relationship has repeatedly occurred, its explanation is not presently clear.

Conclusions

The conclusions which can be made on the basis of the soils tested and procedures used are as follows:

a) The values of osmotic suction determined on a saturation extract differ significantly from values obtained by using pore-water obtained by squeezing. Applying a linear dilution factor to the saturation extract values also produces values that are substantially different from those obtained by the squeezer technique. The values obtained on the squeezed pore fluid were in much closer agreement with the difference between matric and total suction than were the values obtained using the saturation extract technique. The squeezer technique appears to be a satisfactory way of obtaining pore fluid for the determination of the osmotic suction.

Fig. 9. Suctions at various densities for the till.

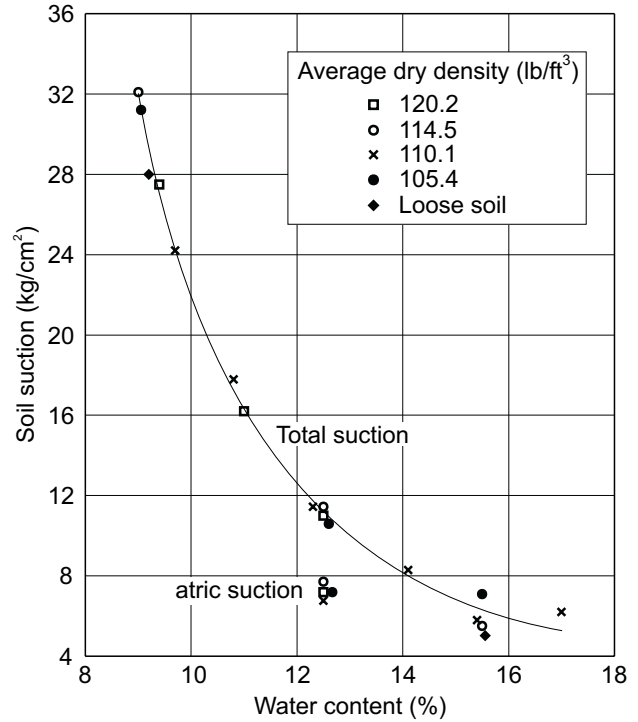
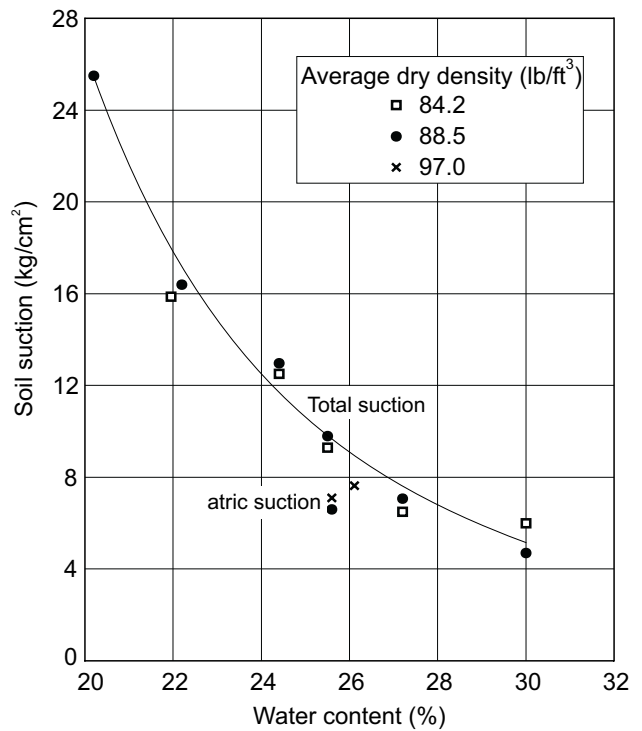


Fig. 10. Suctions at various densities for the Regina clay.



b) The sum of independent measurements of matric and osmotic suction is equal to the measured total suction. Therefore, the generally accepted subdivision of total suction is experimentally verified.

c) For remolded, compacted soils, the matric and total suction are dependent on the molding water content but essentially independent of the dry density.

Acknowledgements

The authors are grateful to Dr. N.R. Morgenstern, Department of Civil Engineering, University of Alberta, for his helpful suggestions in the preparation of this report. Special thanks is extended to D. Pufahl for the development of the modified consolidometer used to measure matric suction and to B. Balasubramonian for the use of the pore-water squeezer.

The research for this investigation (except for the pore fluid squeezing) was conducted at the University of Saskatchewan, Saskatoon, Saskatchewan, as partial fulfillment of a Master of Science Degree by the senior author.

The financial assistance of the National Research Council is gratefully acknowledged.

References

- Aitchison, G.D. 1961. Relationship of moisture and effective stress functions in unsaturated soils. *In* Pore Pressure and Suction in Soils, Conference, British National Society of the International Society of Soil Mechanics and Foundation Engineering at the Institution of Civil Engineering, Butterworths, London, England, pp. 47–52.
- Aitchison, G.D. 1964. Engineering concepts of moisture equilibria and moisture changes in soils. Statement of the Review Panel. *In* Moisture Equilibria and Moisture Changes in Soils Beneath Covered Areas, Butterworths, Australia, pp.7–21.
- Bishop, A.W. 1959. The principle of effective stress. Lecture delivered in Oslo, Norway, 1955; *Technisk Ukeblad*, **106**(39): 859–863.
- Box, J.E., and Taylor, S.A. 1961. Influence of soil bulk density on matric suction. *Soil Science Society of America Proceedings*.
- Croney, D., and Coleman, J.D. 1948. Soil thermodynamics applied to the movement of moisture in road foundations. *Proceedings, 7th International Congress Applied Mechanics*, Vol. 3, pp. 163–177.
- Croney, D., Coleman, J.D., and Lewis, W.A. 1950. Calculation of the moisture distribution beneath structures. *Cov. Eng. (L.)*, Vol. 45, pp. 524.
- Croney, D., Coleman, J.D., and Black, W.P.M. 1958. The movement and distribution of water in soil in relation to highway design and performance. *In* Water and its Conduction in Soils, Highway Research Board Special Report No. 40, Washington, D.C., pp. 226–252.
- Croney, D., and Coleman, J.D. 1961. Pore pressure and suction in soil. *Proceedings, Conference on Pore Pressure and Suction in Soils*. Butterworths, London, pp. 31–37.
- Dalton, F.N., and Rawlins, S.L. 1968. Design criteria for Peltier-effect thermocouple psychrometers. *Soil Science*, **105**(1):12–17.
- Edlefsen, N.E., and Anderson, A.B.C. 1943. *Thermodynamics of soil moisture*. Hilgardia, Berkeley, California, **15**(2): 31–298.
- Jennings, J. E. 1960. A revised effective stress law for use in the prediction of the behaviour of unsaturated soils. *Proceedings, Conference on Pore Pressure and Suction in Soils*, Butterworths, London, pp. 26–30
- Manheim, F.T. 1966. A hydraulic squeezer for obtaining interstitial water from consolidated and unconsolidated sediment. U.S. Geological. Survey, Professional Paper 550 C, pp. 256–261.
- Mitchell, J.K. 1962. Components of pore water pressure and their engineering significance. *Proceedings, 9th National Conference Clays and Clay Minerals (1960)*, Vol. 9, pp. 162–184.
- Olson, R.E., and Langfelder, L.J. 1965 Pore-water pressures in unsaturated soils. *ASCE, Journal of Soil Mechanics and Foundation Division*, **91**(SM4): 127–160.
- Oster, J.D., Rawlins, S.L., and Ingvalson, R.D. 1969. Independent measurement of matric and osmotic potential of soil water. *Soil Science of America Proceedings*, **33**: 188–191.
- Pufahl, D.E. 1970 Components of effective stress in non-saturated soils. M.Sc. Thesis, University of Saskatchewan, Saskatoon, SK, Canada.
- Richards, B.G. 1969. Psychrometric techniques for measuring soil water potential. Department of Soil Mechanics, CSIRO, Victoria, Australia, pp 39–46.
- Richards, L.A., and Ogata, G. 1961. Psychrometric measurements of soil samples equilibrated on pressure membranes. *Soil Science Society of America, Proceedings*, **25**(6): 456–459.
- Spanner, D.C. 1951. The Peltier effect and its use in measurement of suction pressure. *Journal of Experimental Botany*, **11**(5): 145–168.
- United States Department of Agriculture. 1950. *Agricultural Handbook No. 60. Diagnosis and improvement of saline and alkali soils*.

Physico-chemical state variables for clay soils

S.L. Barbour and D.G. Fredlund

Abstract: The classic principle of effective stress does not provide a complete description of the stress state that controls volume change or shear strength of a clay if a change in pore fluid chemistry is involved. In this paper, a more complete set of stress state variables are developed using a multiphase continuum mechanics approach. It is shown that for saturated soils two stress state variables are required to describe the stress state. These include the classic effective stress and a physico-chemical stress state variable which represents the net electrostatic repulsive stresses between the soil particles. Laboratory test results are used to illustrate a three-dimensional constitutive surface for volume change that is described by a relationship between void ratio, effective stress, and the physico-chemical stress state variable.

Key words: physico-chemical, state variables, multi-phase continuum mechanics, volume change, shear strength.

Introduction

The development of the principle of effective stress by Terzaghi (1936) heralded the beginning of theoretical soil mechanics. This principle stated that changes in the volume or shear strength of a soil occur as the result of changes in the effective stress, that is, the difference between the total stress, σ , and the pore-water pressure, u_w . This principle is consistent with, and can be shown to be based on continuum mechanics. In this approach the "state" and "stress state" of a soil system is defined for a Representative Elementary Volume (REV) of the continuum as follows (Fredlund 1987):

- (1) State: non material variables required for the characterization of a system.
- (2) Stress state variable: the variables required for the characterization of the stress condition.

Changes in the stress state of the system can be linked to the deformation and the shear strength of the system through constitutive relationships which contain material properties. It follows that the effective stress principle can be extended to assert that no change in behaviour will occur unless there is a change in the stress state variable.

When clay soils are subject to changes in pore fluid chemistry a difficulty arises with the use of the classic effective stress state variable for saturated soils (i.e., $\sigma - u_w$). Although there may be no changes in the total stress or pore fluid pressure in a specimen, changes in the strength, volume change, and permeability have been observed (Bolt 1956; Mesri and Olson 1971; Dunn and Mitchell 1984; Kenney 1967). In practice, these changes in soil behaviour have usually been incorporated into the soil properties by ensuring that tests conducted in the lab-

oratory duplicate the pore fluid chemistry present in the field. This approach, however, cannot account for transient changes in soil behaviour during changes in pore fluid chemistry and may not prove to be the best approach for geotechnical practice. In modern geotechnique more and more engineers are being faced with design of waste containment systems in which the natural and compacted soils routinely experience wide variations in pore fluid chemistry over their design life. Consequently, a more general approach is needed to allow changes in the "chemical" stress state to be incorporated into conventional analyses.

Diffuse double layer theory

Most clay minerals have a net negative surface charge. In order to obtain electroneutrality, a diffuse double layer of cations and anions develops around the clay particle. The negatively charged clay surface and the charge distribution adjacent to the clay particle is termed the diffuse double layer. Theoretical descriptions of the diffuse double layer were first proposed by Gouy (1910) and Chapman (1913) and later modified by Stern (1924). Mitchell (1976) has shown that the distance to the center of charge density surrounding a semi-infinite negatively charged clay particle, that is, the "thickness" of the double layer, changes in response to changes in pore fluid chemistry such as concentration, cation valence, and dielectric constant.

Interparticle stresses

Changes in the volume or shear strength of soil occur in response to changes in stresses transmitted directly between particle contacts. These interparticle stresses include; long range stresses due to electrostatic repulsion (i.e., stresses resulting from diffuse double layer effects) and van der Waals stresses, and short range stresses that result from Born repulsion and surface hydration or primary valence and cementation bonds. In most clays the

S.L. Barbour and D.G. Fredlund. Department of Civil Engineering, University of Saskatchewan, 57 Campus Drive, Saskatoon, SK, Canada S7N 5A9.

Reproduced with permission from the *Proceedings, XII International Conference on Soil Mechanics and Foundation Engineering*, Rio de Janeiro, Brazil, 1989, A.A. Balkema, Rotterdam, The Netherlands, pp. 1839–1843.

dominant long range stress between particles is electrostatic repulsion (Bailey 1965, Mitchell 1976).

Numerous attempts have been made to predict the net repulsive stress, $(R - A)$, for pure clay systems using the assumption that all interparticle stresses are transmitted by the electrostatic stresses. The conceptual model applied in these calculations is called the osmotic pressure concept. The clay system is assumed to exist as a series of perfectly dispersed, parallel, clay particles. The equation describing the charge density distribution and electric potential around a single particle can be integrated to obtain the mid-plane electrolyte concentration and the potential half way between the clay particles. The overlapping diffuse layers are considered to behave as semi-permeable osmotic membranes. The difference in osmotic pressure between the bulk pore fluid and the fluid between the clay particles is then taken to be equivalent to the net repulsive stresses between the particles. Detailed developments of the osmotic pressure concept are provided by Bolt (1956) and Mitchell (1976).

During the 1950's and 1960's a number of researchers attempted to use the osmotic pressure concept to predict the compressibility of pure clays under varying pore fluid concentrations (Bolt 1956, Bolt and Miller 1955, Warkentin et al. 1957, Aylmore and Quirk 1962, Blackmore and Miller 1962, Warkentin and Schofield 1962, Mesri and Olson 1971). The result of these studies, however, was that with the exception of pure homoionic clays at high void ratios, the osmotic pressure concept only provided a qualitative description of soil compressibility. The major limitations with this technique were that the assumptions of a perfectly dispersed particle arrangement and the dominance of the electrostatic stress between particles were not generally satisfied.

“True effective stress”

The work described above dealt with the physico-chemical stresses at a microscopic level rather than the macroscopic level used in the definition of classic effective stress for a saturated soil. During the 1960's and 1970's several researchers, including Lambe (1960), Balasubramonian (1972) and Chattapadhyay (1972), attempted to extend the effective stress equation to include the net long range electrostatic stress as follows:

$$[1] \quad \sigma^* = (\sigma - u_w) - (R - A)$$

where:

σ^* = “true” effective stress

σ = total stress

u_w = pore-water pressure

$(R - A)$ = net long range electrostatic stress

This “true effective stress” was developed from an analysis of static equilibrium of normal forces perpendicular to a wavy plane passing between soil particles. Although it provides a statement of the equivalence of stress, it is not based on an appropriate free body diagram

and consequently is not an appropriate means of developing stress state variables (Fredlund 1987).

To be an appropriate stress state variable, the components of the stress state must be shown to be equally effective in controlling soil behaviour. Fredlund and Morgenstern (1977) demonstrated this concept for stress states for unsaturated soil through the use of null tests. Similar tests for “true” effective stress were conducted by Balasubramonian (1972) on clay shales. Morgenstern and Balasubramonian (1980) demonstrated that during leaching of a dense clay shale, changes in the predicted $(R - A)$ stress were balanced by changes in the total stress required to maintain a constant specimen volume. It is important to note that the shale used was predominately montmorillonitic and consequently the assumption regarding the dominance of electrostatic repulsion is likely valid. This would not be true for clay soils in general.

Physico-chemical stress state from continuum mechanics

In the continuum mechanics of multiphase mixtures the behaviour of each phase is dictated by the stresses acting on that phase. Fredlund (1973) states that the first two steps in this approach are the description of the physical multiphase element or Representative Elementary Volume (REV), and the establishment of the state variables associated with each phase.

Representative elementary volume (REV)

An element of saturated soil can be considered as a three phase system consisting of the soil particles, the pore fluid, and the diffuse double layer or adsorbed fluid hull surrounding each soil particle (Fig. 1). The diffuse double layer includes the surface charge along the clay particles. By definition, a phase must possess differing properties from the contiguous homogeneous phases and must have a continuous bounding surface throughout the element. The unique properties of the diffuse double layer have been documented by Mitchell (1976). The existence of a distinct boundary surface is not as well defined but the extent of the adsorbed fluid phase is described by double layer theory.

The porosities of each phase of the elementary volume may be defined as follows:

n_p = volume of soil particles/total elemental volume

n_f = volume of bulk pore fluid/total elemental volume

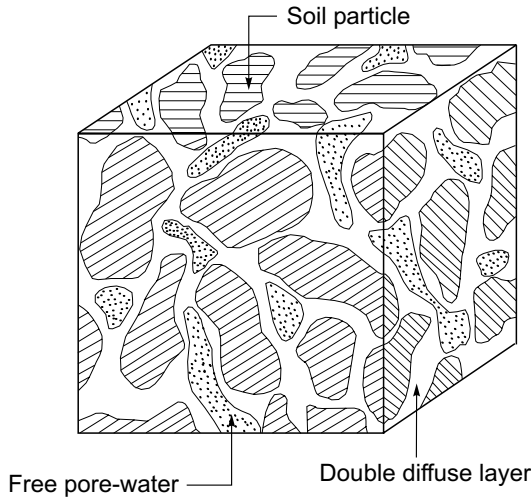
n_d = volume of diffuse double layer/total elemental volume

The sum of the phase porosities is equal to unity.

Equilibrium equations for each phase

The principle of superposition of coincident equilibrium stress fields may be used as described in continuum mechanics (Truesdell 1966). The assumption is made that an independent continuous stress field is associated with each phase of the multiphase system. The number of independent force equilibrium equations that can be written is equal to the number of cartesian coordinate directions

Fig. 1. Element of saturated soil illustrating the diffuse double layer.



multiplied by the number of phases constituting the continuum (Fredlund 1987).

Force equilibrium for the element is ensured by independently considering equilibrium for each phase. The elemental forces consist of surface tractions, gravity body forces and interaction forces between the phases. The interaction body forces between the phases are as follows: F_f = interaction force between the diffuse double layer and pore fluid

F_d = interaction force between the soil particles and the diffuse double layer

Equilibrium stress systems acting on the overall element and the diffuse double layer and bulk pore fluid phases are considered.

We can assume that the electrostatic interactions between particles can be described by the net repulsive minus attractive stress ($R-A$) acting within the diffuse double layer. This is conceptually similar to the osmotic pressure concept, in which the repulsive stress is equated to the osmotic pressure difference within the pore fluid. A second assumption is that when ($R-A$) is expressed as a stress tensor it is isotropic and does not contain shear stresses. The density of the diffuse double layer is assumed to be equal to the density of the pore fluid.

Equilibrium equations can be written for the overall soil element as well as for each phase. A one-dimensional form of the equilibrium equations in the y -direction can be written as follows:

Overall element:

$$[2] \quad \left(\frac{\partial \tau_{xy}}{\partial y} + \frac{\partial \sigma_y}{\partial y} + \frac{\partial \tau_{zy}}{\partial y} + \rho_t g \right) dx \, dy \, dz = 0$$

Pore fluid:

$$[3] \quad \left(n_f \frac{\partial u_f}{\partial y} - F_f + n_f \rho_f g \right) dx \, dy \, dz = 0$$

Diffuse double layer:

$$[4] \quad \left(n_d \frac{\partial (R-A)}{\partial y} - F_d - F_f + n_d \rho_f g \right) dx \, dy \, dz = 0$$

where:

σ_y = normal stress in the y -direction

τ_{xy} = shear stress on the x -plane in the y -direction

τ_{zy} = shear stress on the z -plane in the y -direction

u_f = pore fluid pressure

ρ_t = total density of the soil

ρ_f = fluid density

Equations [2] through [4] are statements of equilibrium for the overall element, the pore fluid, and the double layer. Volume change of the soil structure is controlled by the interparticle interactions between the soil particles. However these interactions cannot be measured directly. An equation for the stresses effective at the interparticle contacts can be written as the difference between the statement of equilibrium for the entire element, and those for the pore fluid and double layer phases. This equation is then written as follows:

$$[5] \quad \frac{\partial \tau_{xy}}{\partial y} + \frac{\partial \sigma_y}{\partial y} + \frac{\partial \tau_{zy}}{\partial y} + \rho_t g - n_f \frac{\partial u_f}{\partial y} - n_d \frac{\partial (R-A)}{\partial y} + 2F_f + F_d - \rho_f g (n_d + n_f) = 0$$

By adding and subtracting $[n_d(\partial u_f/\partial y)]$ and $[n_f \partial (R-A)/\partial y]$ and combining terms, the following equilibrium equation for the soil particles can be obtained:

$$[6] \quad \frac{\partial \tau_{xy}}{\partial y} + \frac{\partial (\sigma_y - u_f - (R-A))}{\partial y} + \frac{\partial \tau_{zy}}{\partial y} + \rho_t g + (1 - n_f) \frac{\partial u_f}{\partial y} + (1 - n_d) \frac{\partial (R-A)}{\partial y} + 2F_f + F_d - (n_f + n_d) \rho_f g = 0$$

An examination of this equation reveals the presence of three sets of surface tractions (i.e., $(\sigma_y - u_f - (R-A))$, u_f , $(R-A)$). In a similar development for the stress state variables for unsaturated soils Fredlund and Morgenstern (1977) suggested that the u_f term can be eliminated if the assumption is made that the soil particles are incompressible. If the diffuse double layers in the soil are extensive and completely overlapping then a similar assumption for the $(R-A)$ term would also be valid. The remaining stress state variable is identical to that of true effective stress (i.e., $(\sigma_y - u_f - (R-A))$). The test results of Morgenstern and Balasubramonian (1980) provide verification for this combination of stresses as a single stress state variable for the case of a montmorillonitic clay shale.

In a more general case, it is likely that the diffuse double layers will not be extensive and consequently two stress state variables remain (i.e., $(\sigma_y - u_f - (R-A))$ and $(R-A)$). It is not appropriate to include $(R-A)$ in both stress state variables. If only the term $(n_d \partial u_f/\partial y)$ is added and subtracted from eq. [5] the resulting equilibrium equation is as follows:

$$[7] \quad \frac{\partial \tau_{xy}}{\partial y} + \frac{\partial (\sigma_y - u_f)}{\partial y} + \frac{\partial \tau_{zy}}{\partial y} + \rho_f g + (1 - n_f) \frac{\partial u_f}{\partial y} - n_d \frac{\partial (R - A)}{\partial y} + (n_f + n_d) \rho_f g + 2F_f + F_d = 0$$

From this equation two stress state variables emerge (i.e., $(\sigma_y - u_f)$ and $(R - A)$) if the u_f term is again eliminated as before. Two stress state variables then control soil behaviour; the effective stress, $(\sigma - u_f)$, and the physico-chemical stress represented by $(R - A)$. This is similar in form to the stress state variables for unsaturated soil (i.e., $(\sigma_y - u_a)$ and $(u_a - u_w)$) proposed by Fredlund and Morgenstern (1977). Fredlund and Morgenstern (1976) used a three-dimensional constitutive surface for volume change to relate changes in void ratio to changes in matric suction and net total stress. A similar constitutive surface for the physico-chemical stress state variables drawn from the compressibility data of Mesri and Olson (1971) is illustrated in Fig. 2. Two variables are essential because changes in matric suction are not as "efficient" in producing changes in volume change and shear strength as are changes in total stress. This has also been shown to be true for $(R - A)$ and $(\sigma_y - u_f)$. As illustrated in Fig. 2 each stress state variable is linked to volume change through a separate modulus. Laboratory testing to obtain the osmotic compressibility modulus for two clay soils (Regina Clay and a Sand/Na-montmorillonite mixture) was conducted by Barbour (1987a) and reported by Barbour (1987b) and Barbour and Fredlund (1988).

Practical physico-chemical stress state variables

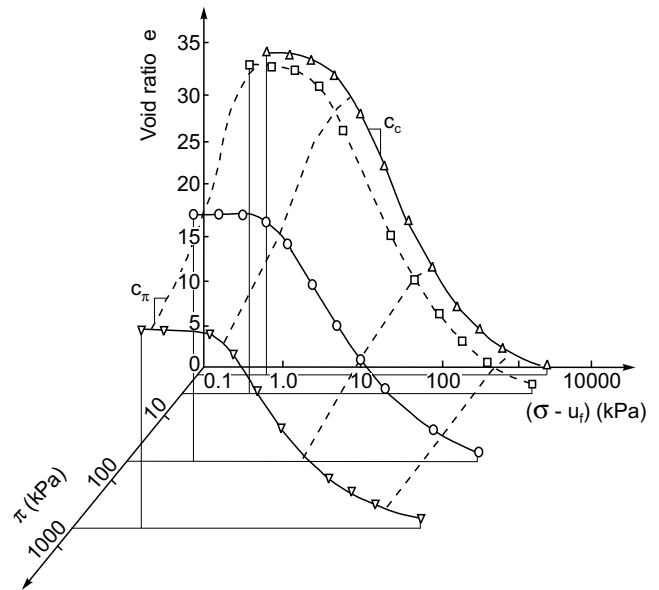
A difficulty remains in the practicality of the physico-chemical stress state variables. Fredlund (1987) suggested that the choice of an appropriate set of stress state variables has to also consider whether:

- (1) the variables can be experimentally tested,
- (2) the variables can be theoretically justified,
- (3) the variables are operational in practice, and
- (4) the variables that have characteristics acceptable within the definition of stress state variables.

$(R - A)$ is not a stress which can be directly measured in laboratory testing. In addition, the prediction of $(R - A)$ is possible only under ideal conditions. This is a severe restriction to the use of $(R - A)$ as a component of the stress state variable. Because of this, it may be necessary that a deduced quantity, which is more easily measured than $(R - A)$, be used.

The osmotic pressure concept relates the change in repulsive stress between clay particles, to the osmotic pressure difference between the interparticle fluid and the bulk external fluid. Mitchell (1962) suggested that "double layer interactions and the consequent repulsion between opposing particles are reflected by the osmotic pressure". The osmotic pressure is described as having two components; one associated with the free salt in the bulk solution and the other caused by the additional ions required to satisfy double layer requirements. The osmotic pressure of the bulk solution can be readily evalu-

Fig. 2. Three-dimensional constitutive surface for Na-montmorillonite as drawn from the data of Mesri and Olson (1971).



ated using samples of the pore fluid, however the difference between the osmotic pressure of the bulk fluid and that between the clay particles cannot be measured directly.

In most practical problems, the change of osmotic pressure is of more interest with respect to volume change and shear strength than the absolute value of the components of osmotic pressure. Consequently, it can be assumed that the osmotic pressure of the bulk solution can be used as an independent stress state variable. The osmotic pressure satisfies the requirements listed above because it is a measurable quantity which is theoretically related to the $(R - A)$ stress through the osmotic pressure concept.

Conclusions

The design of waste containment facilities requires that the behaviour of soils subjected to changing pore fluid chemistries be incorporated into conventional geotechnical analyses. The microscopic mechanistic conceptual models such the diffuse double layer theory and the osmotic pressure concept have provided valuable qualitative insight into the role that pore fluid concentrations have on soil behaviour, however, it is unlikely that these theories can be applied in a quantitative manner into routine geotechnical design.

The macroscopic phenomenological model of stress state variables presented in this paper provides a framework which can be extended into conventional geotechnical analyses. Further work is required to verify the use of physicochemical stress states (i.e., $(R - A)$ or osmotic pressure) and to define the material properties associated with the constitutive relations for volume change and shear strength.

References

- Aylmore, L.A.G., and Quirk, J.P. 1962. The structural status of clay systems. *Clays and Clay Minerals*, **9**:104–130.
- Bailey, W.A. 1965. The effect of salt content on the consolidation behaviour of saturated remoulded clays. United States Army Engineer Waterways Experimental Station, Vicksburg, Contract Report 3–101.
- Balasubramonian, B.I. 1972. Swelling of compaction shale. Ph.D. thesis, Department of Civil Engineering, University of Alberta, Edmonton, AB, Canada.
- Barbour, S.L. 1987a. Osmotic flow and volume change in clay soils. Ph.D. thesis, Department of Civil Engineering, University of Saskatchewan, Saskatoon, SK, Canada.
- Barbour, S.L. 1987b. The Role of physico-chemical effects on the behaviour of clay soils. Proceedings, 40th Canadian Geotechnical Conference, Regina, SK, pp. 323–342.
- Barbour, S.L., and Fredlund D.G. 1989. Mechanics of osmotic flow and volume change in clay soils. *Canadian Geotechnical Journal*, **26**(4): 551–562.
- Blackmore, A.V., and Miller, R.D. 1962. Tactoid size and osmotic swelling in calcium montmorillonite. *Soil Science Society of America Proceedings*, **25**: 169–173.
- Bolt, G.H. 1956. Physico-chemical analyses of the compressibility of pure clay. *Géotechnique*, **6**(2): 86–93.
- Bolt, G.H., and Miller, R.D. 1955. Compression studies of illite suspensions. *Soil Science Society of America Proceedings*, **19**: 285–288.
- Chapman, D.L. 1913. A contribution to the theory of electrocapillarity. *Philosophical Magazine* **25**(6): 475–481.
- Chattopadhyay, P.K. 1972. Residual shear strength of some pure clay minerals. Ph.D. thesis, Department of Civil Engineering, University of Alberta, Edmonton, AB, Canada.
- Dunn, R.J., and Mitchell, J.K. 1984. Fluid conductivity testing of fine grained soils. *ASCE, Journal of the Geotechnical Engineering Division*, **11**(110): 1648–1665.
- Fredlund, D.G. 1973. Volume change behaviour of unsaturated soils, Ph.D. thesis, University of Alberta, Edmonton, AB, Canada.
- Fredlund, D.G. 1987. The stress state for expansive soils. Proceedings, Sixth International Conference on Expansive Soils, Key Note Address, Additional papers, Centre Board of Irrigation and Power, New Delhi, India, December 1–3, pp. 1–9.
- Fredlund, D.G., and Morgenstern, N. 1977. Stress state variables for unsaturated soils. *ASCE, Journal of the Geotechnical Engineering Division*, **103**(GT5): 447–466.
- Fredlund, D.G., and Morgenstern, N.R. 1976. Constitutive relations for volume change in unsaturated soils. *Canadian Geotechnical Journal*, **13**(3): 261–276.
- Gouy, G. 1910. Sur la constitution de la charge électrique à la surface d'un électrolyte. *Annuaire Physique (Paris)*, **9**(4): 457–468.
- Kenney, T.C. 1967. The influence of mineral composition on the residual strength of natural soils. Proceedings, Oslo Geotechnical Conference, Vol. 1, reprinted in NGI Publ. (76), pp. 37–43.
- Lambe, T.W. 1960. A mechanistic picture of shear strength in clay. Proceedings, ASCE Research Conference on Shear Strength of Cohesive Soils, University of Colorado, Boulder, CO, pp. 555–580.
- Mesri, G. and Olson, R.E. 1971. Consolidation characteristics of montmorillonite. *Géotechnique*, **21**(4): 341–352.
- Mitchell, J.K. 1962. Components of pore water pressure and their engineering significance. Proceedings, 9th National Conference Clays and Clay Minerals (1960), Vol. **9**, pp. 162–184.
- Mitchell, J.K. 1976. Fundamentals of soil behaviour. John Wiley and Sons, New York.
- Morgenstern, N., and Balasubramonian, B.I. 1980. Effects of pore fluid on the swelling of clay-shale. Proceedings, 4th International Conference on Expansive Soils, Denver, CO, pp. 190–205.
- Stern, O. 1924. Zur Theorie der elektrolytischen Doppelschicht. *Zeitschrift Elektrochemie*, **30**: 508–516.
- Terzaghi, K. 1936. The shear resistance of saturated soils. Proceedings, First International Conference on Soil Mechanics, Vol. 1, pp. 54–56.
- Truesdell, C. 1966. The elements of continuum mechanics. Springer-Verlag, Inc., New York, NY.
- Warkentin, B.P., and Schofield, R.K. 1962. Swelling pressures of Na-montmorillonite in NaCl solution. *Soil Science*, **13**: 98–105.
- Warkentin, B.P., Bolt, G.H., and Miller, R.D. 1957. Swelling pressure of montmorillonite. *Soil Science Society of America Proceedings*, **21**: 495–497.

State-of-development in the measurement of soil suction

D.G. Fredlund and H. Rahardjo

Abstract: The measurement of soil suction is central to the application of unsaturated soil mechanics to geotechnical practice. Several devices for the measurement of soil suction are discussed in this paper. The working principles, typical results and state-of-development are presented for the most promising devices.

Key words: unsaturated soil, soil suction, measurement of soil suction.

Introduction

Surficial soils in many parts of the world are classified as expansive, collapsible, and residual soils. These soils are generally unsaturated with pore-water pressures that are negative relative to atmospheric conditions. There has been a significant increase in our understanding of unsaturated soil mechanics, concepts, theories, and formulations during the past two decades. However, the knowledge can only be put into practice as devices for measuring the negative pore-water pressures are available. The measuring devices should be accurate and economical for use in engineering practice. There has been a great need for such devices in order to expand soil mechanics' practice to arid and semi-arid regions of the world.

This paper summarizes some recent experiences in measuring negative pore-water pressure and soil suction. The emphasis is on measuring *in situ* soil suction. The paper first outlines a brief theoretical context for soil suction and then discusses devices showing the greatest promise for use in geotechnical engineering.

Theory and definitions of soil suction

The total suction of a soil can be related to the partial pressure of the pore-water vapour. From a thermodynamic standpoint, the total suction can be written,

$$[1] \quad \psi = -\frac{RT}{v_{w0}\omega_v} \ln \frac{\bar{u}_v}{\bar{u}_{v0}}$$

where:

ψ = total suction (kPa)
 R = universal (molar) gas constant (i.e., 8.31432 J/(mol K))

T = absolute temperature (i.e., $T = 273.16 + t^0$) (K)

t^0 = temperature ($^{\circ}\text{C}$)

v_{w0} = specific volume of water or the inverse of water density (i.e., $1/\rho_w$) (m^3/kg)

ρ_w = water density (i.e., 998 kg/m^3 at 20°C)

ω_v = molecular mass of water vapour (i.e., 18.016 kg/kmol)

\bar{u}_v = partial pressure of pore-water vapour (kPa)

\bar{u}_{v0} = saturation pressure of pore-water vapour over a flat surface at the same temperature (kPa)

The term in eq. 1 is also referred to as the relative humidity, RH (%). The relative humidity is commonly less than 100%, indicating a partial pressure lower than the saturation pure water vapour pressure over a flat surface at the same temperature (i.e., $\bar{u}_v < \bar{u}_{v0}$). The reduction in the water vapour pressure can be caused by a curved (i.e., concave) water surface such as is found in a capillary tube. The water vapour pressure or the relative humidity decreases as the radius of curvature of the water surface decreases. At the same time, the radius of curvature is inversely proportional to the difference between the air and water pressures across the surface [i.e., $(u_a - u_w)$]. The term is called the matric suction; where: is pore-air pressure and is pore-water pressure. This means that one component of the total suction in eq. 1 is matric suction which causes a reduction in the relative humidity.

The pore-water in a soil generally contains dissolved salts. The water vapour pressure over a flat surface of solvent is less than the vapour pressure over a flat surface of pure water. In other words, the relative humidity decreases with increasing dissolved salts in the pore-water in the soil. The decrease in relative humidity due to the presence of dissolved salts in the pore-water is referred to as the osmotic component of total suction. In summary, the total suction of a soil, ψ , can be considered as the sum of the matric suction, $(u_a - u_w)$, and the osmotic suction, π

$$[2] \quad \psi = (u_a - u_w) + \pi$$

The role of osmotic suction has commonly been associated more with unsaturated soils than with saturated soils. In reality, dissolved salts are present in both satu-

D.G. Fredlund. Professor, Civil Engineering Department, University of Saskatchewan, 57 Campus Drive, Saskatoon, SK, Canada S7N 5A9.

H. Rahardjo. Research Engineer, Civil Engineering Department, University of Saskatchewan, 57 Campus Drive, Saskatoon, SK, Canada S7N 5A9.

Reproduced from the *Proceedings of the International Conference on Engineering Problems of Regional Soils*, August 11–15, 1988, Beijing, China, pp. 582–588.

rated and unsaturated soils. Therefore, the role of osmotic suction is equally important in both saturated and unsaturated soils. Changes in osmotic suction due to changes in salt content will affect the mechanical behaviour of a soil. However, the osmotic suction change is not generally taken into account in an analysis if the change has been simulated during the laboratory measurement of soil properties.

Tensiometers

A tensiometer measures the negative pore-water pressure in a soil. The tensiometer consists of a porous ceramic, high air-entry cup connected to a pressure measuring device through a small bore capillary tube. The tube and the cup are filled with de-aired water. The cup can be inserted into a pre-cored hole until there is good contact with the soil. After equilibrium has been achieved, the water in the tensiometer will have the same negative pressure as the pore-water in the soil. The water pressure that can be measured in a tensiometer is limited to approximately negative 90 kPa due to the possibility of cavitation of the water in the tensiometer. The measured negative pore-water pressure is numerically equal to the matric suction when the pore-air pressure is atmospheric (i.e., equals to zero gauge). When the pore-air pressure is greater than atmospheric pressure, the tensiometer reading can be added to the pore-air pressure reading to give the matric suction of the soil. However, the matric suction must not exceed the air-entry value of the ceramic cup. The osmotic component of soil suction will not be measured by tensiometers since soluble salts are free to flow through the porous cup.

There are several types of tensiometers available from Soilmoisture Equipment Corporation, Santa Barbara, California, USA. Slow diffusion of air through the high air-entry cup is a problem common to all tensiometers. The Quick Draw tensiometer has proven to be a particularly useful portable tensiometer to rapidly measure negative pore-water pressures (Fig. 1). The water in the tensiometer is subjected to tension for only a short period of time during each measurement. Therefore, air diffusion through the ceramic cup with time is minimised. The Quick Draw tensiometer can repeatedly measure pore-water pressures approaching minus one atmosphere when it has been properly serviced. When it is not in use, the probe is maintained saturated in a carrying case which has water saturated cotton surrounding the ceramic cup. Figure 2 illustrates the distribution of matric suction along a trench excavated perpendicular to a railway embankment in British Columbia, Canada. The embankment soil consisted predominantly of unsaturated silt. The negative pore-water pressures were measured on the side-walls of the trench using a Quick Draw tensiometer.

Thermal conductivity sensors

A thermal conductivity sensor indirectly measures the matric suction in a soil. The sensor consists of a porous ceramic block containing a temperature sensing element

Fig. 1. Quick Draw tensiometer from Soilmoisture Equipment Corporation.

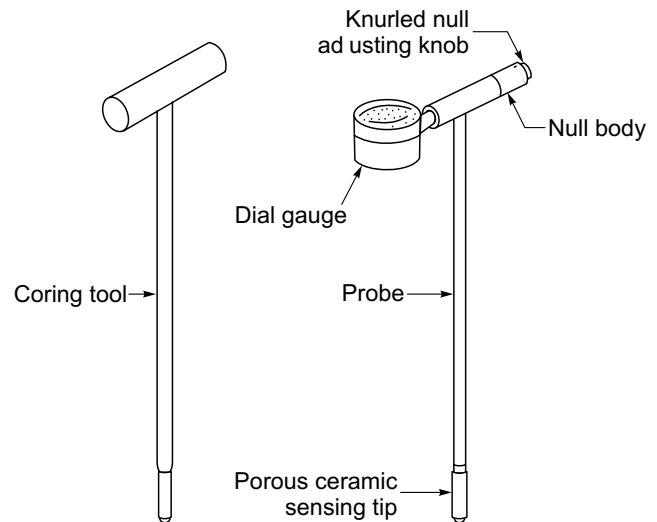
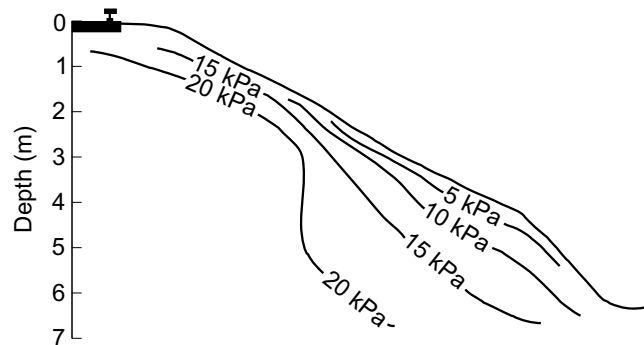


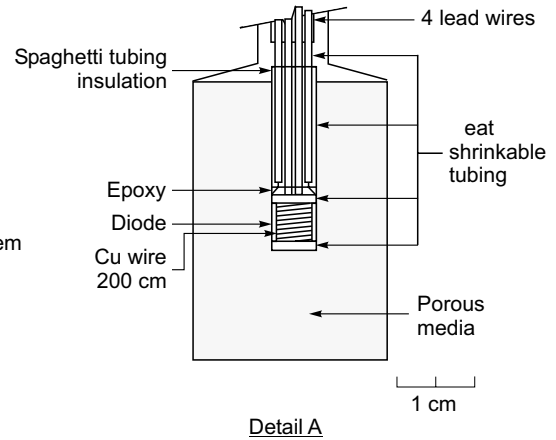
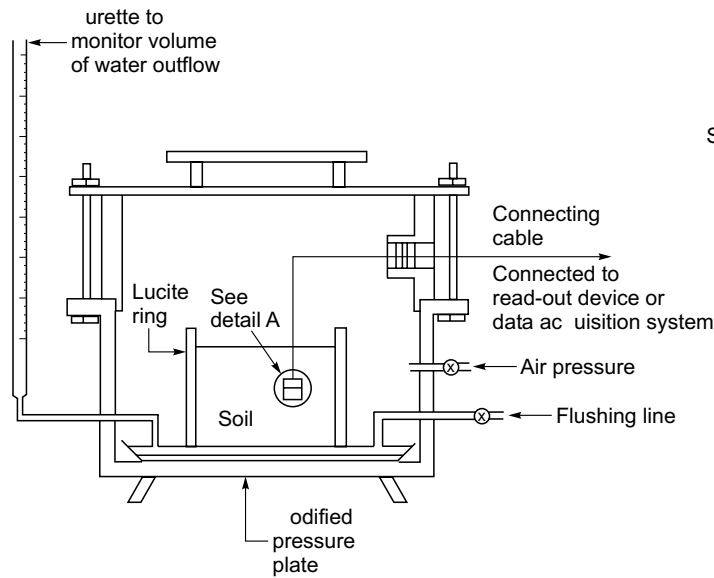
Fig. 2. Matric suction contours along a railway embankment (from Krahn et al. 1987).



and a miniature heater. Measurements are made by inserting the sensor into a pre-drilled hole in the soil and allowing the matric suction in the ceramic block to come to equilibrium with the matric suction in the soil. The equilibrium matric suction is related to the water content in the porous block. The amount of water in the porous block affects the rate of heat dissipation within the block. Therefore, the water content in the porous block can be measured indirectly by measuring the heat dissipation of the block. This is accomplished by generating a controlled amount of heat at the centre of the porous block and measuring the temperature rise at the same point after a fixed period of time. More heat will be dissipated throughout the block with increasing water content in the block. The undissipated heat causes a temperature rise that is inversely proportional to the water content in the porous block. As a result, the measured temperature rise can be calibrated to measure the matric suction in the soil.

The thermal conductivity sensor calibration can be conducted using a pressure plate apparatus. A pressure plate set up for calibrating the sensor is shown in Fig. 3 together with a cross-section of a sensor. The height of

Fig. 3. Pressure plate setup for calibrating thermal conductivity sensors (from Wong and Ho 1987).



the pressure chamber was increased in order to provide several circular holes along the chamber wall. The holes are used to connect several sensors to the read-out device or data acquisition system. Several sensors are first installed in a soil specimen which is placed in the pressure plate. A desired matric suction, $(u_a - u_w)$, is then applied to the soil specimen by applying an air pressure, u_a , and maintaining a zero water pressure below the ceramic disk. The pore-water will flow out from the soil specimen and collect in a volume change indicator. The water outflow will cease when equilibrium is attained. During calibration, the pressure plate set-up is contained within a temperature controlled box. The response of each sensor is monitored periodically until equilibrium is achieved. The reading at equilibrium is used in the calibration of the sensor. The above procedure is repeated for various applied matric suctions to provide a calibration curve.

A thorough calibration study on AGWA-II thermal conductivity sensors has been completed recently at the University of Saskatchewan, Canada (Wong and Ho 1987). The AGWA-II sensors used in the study were manufactured by Agwatronics Incorporation, Merced, California, USA. Typical results indicate a non-linear calibration curve which may be approximated by a bilinear curve as illustrated in Fig. 4. The breaking point of the calibration curve was found to be around 175 kPa. It has been found that relatively accurate measurements of matric suctions can be expected from the AGWA-II sensor in the range of 0 to 175 kPa. Matric suction measurements above 175 kPa correspond to a steeper calibration curve with a lower sensitivity. The sensors also produced consistent and stable output with time.

The AGWA-II thermal conductivity sensors have been used for laboratory measurements of matric suction on a highly plastic clay from Sceptre, Saskatchewan, Canada (Fig. 5). The measurements were performed using two sensors. One sensor was initially saturated while the other sensor was initially dry.

Fig. 4. Calibration curves for two AGWA-II thermal conductivity sensors from Agwatronics Incorporated (from Wong and Ho 1987).

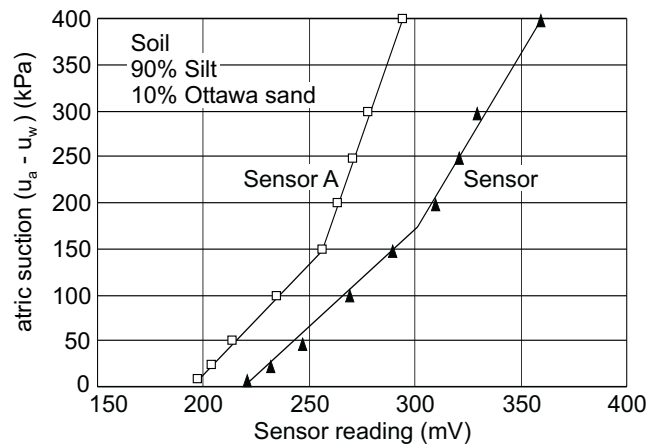


Fig. 5. Laboratory measurements of matric suction using the AGWA-II thermal conductivity sensors.

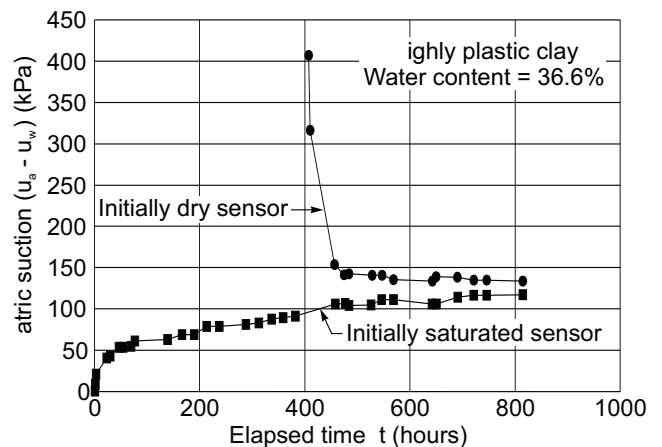
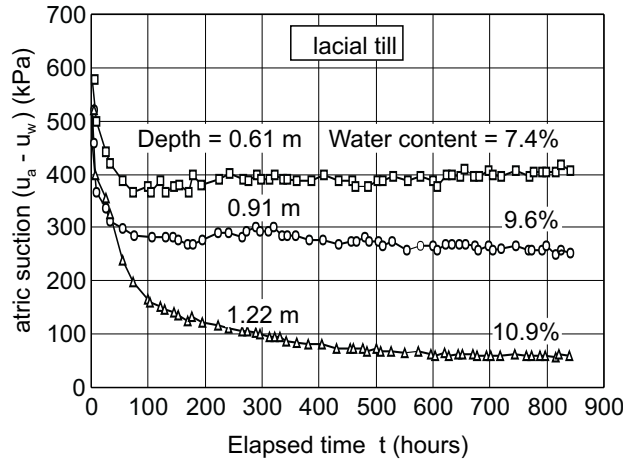


Fig. 6. Field measurements of matric suction using the AGWA-II thermal conductivity sensors under controlled environments.



were monitored immediately and at various elapsed times after their installation. The results indicate that the equilibrium time required for the initially dry sensor is less than the equilibrium time for the initially saturated sensor. The AGWA-II sensors have also been used for measuring matric suction in a highway test track with a controlled environment (i.e., controlled temperature and humidity). Typical results on a glacial till subgrade are presented in Fig. 6. The measured matric suctions are constant with time and the water contents show a reasonable decrease in matric suction with respect to depth.

Psychrometers

Thermocouple psychrometers are used to measure the total suction in a soil by measuring the relative humidity (RH) in the soil. Total suction is related to relative humidity in accordance with eq. 1 and is illustrated in Fig. 7. Details of the thermocouple psychrometer are shown in Fig. 8a. The measurements of total suction are carried out by placing a soil specimen in a small chamber together with the psychrometer (Fig. 8b). The relative humidity is then measured after equilibrium is attained between the air near the psychrometer and the pore-air in the soil. Equilibrium at relative humidities approaching 100 percent is difficult to obtain since the slightest lowering of temperature may cause condensation of water vapour. A controlled temperature environment of $\pm 0.001^\circ\text{C}$ is required in order to measure total suctions to an accuracy of 10 kPa (Krahn and Fredlund 1972). The lower limit of total suction measurements using a psychrometer is approximately 100 kPa under a controlled temperature environment. The thermocouple psychrometer is capable of measuring total suctions up to 8000 kPa (Edil and Motan 1984). Therefore, psychrometers are ideal for measuring high suctions in soils from arid regions. *In situ* measurements of total suctions using psychrometers are not recommended because of significant temperature fluctuations which occur in the field. However, laboratory measurements can be conducted in a

Fig. 7. Relative humidity versus total suction relationship.

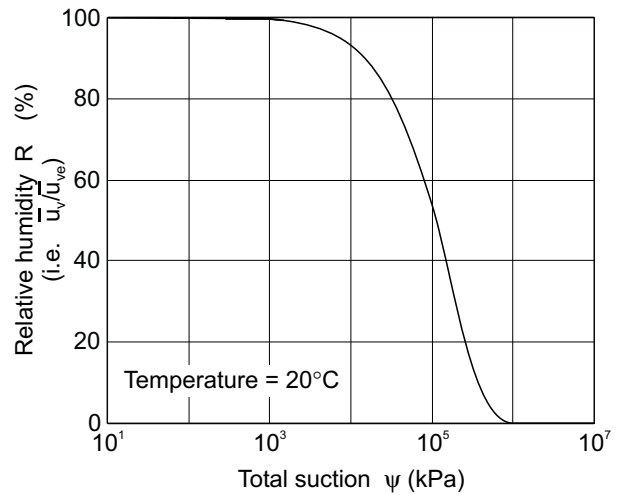
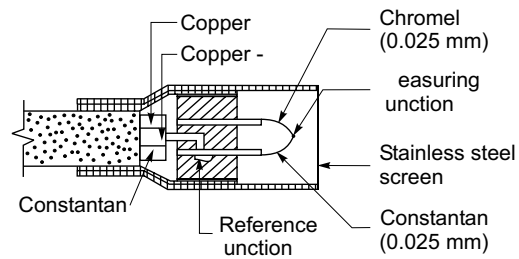
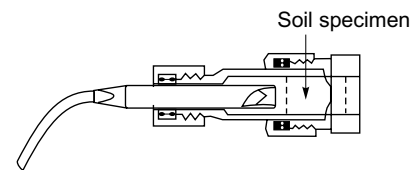


Fig. 8. Details of the thermocouple psychrometer manufactured by J.R.D. Merrill Specialty Equipment, Logan, Utah, USA; a) thermocouple psychrometer details, b) chamber with soil specimen and psychrometer.



a) Thermocouple psychrometer details



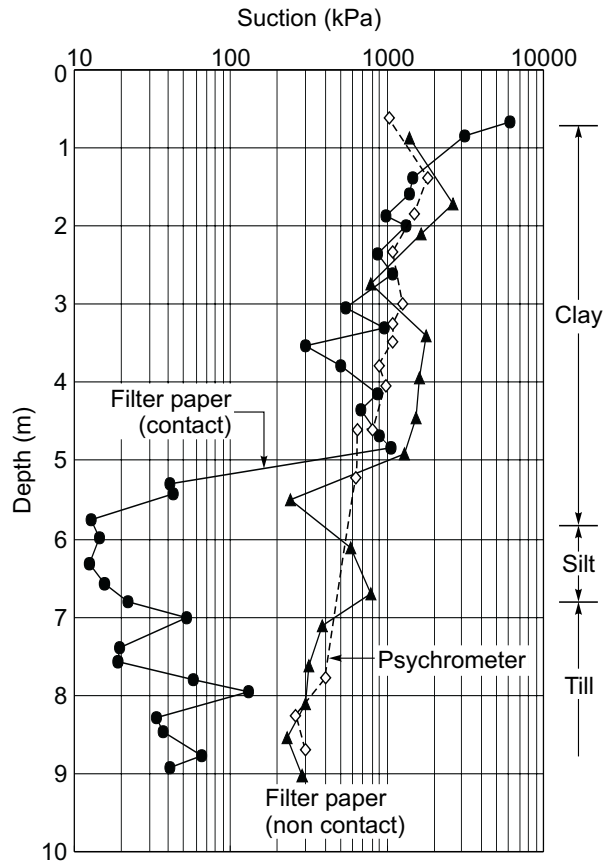
b) Chamber with soil specimen and psychrometer

controlled temperature environment using undisturbed soil specimens from the field. The specimens should not be covered with hot wax following sampling, since temperature changes alter the relative humidity in the soil. Figure 9 illustrates measurements of total suctions on soil samples from various depths at a location near Regina, Saskatchewan, Canada.

Filter paper

Theoretically, the filter paper method can be used to measure the total or matric suction of a soil. The method is based on the assumption that a filter paper can come to equilibrium (i.e., with respect to water flow) with a soil having a specific suction. The equilibrium can be reached

Fig. 9. Suction profile versus depth obtained using thermocouple psychrometers and the filter paper method (from van der Raadt et al. 1987).



by water exchange between the soil and the filter paper in a liquid or vapour form. When a dry filter paper is placed in contact with a soil specimen, moisture flow takes place from the soil to the filter paper until equilibrium is achieved (Fig. 10). When a dry filter paper is suspended above a soil specimen (i.e., no contact with the soil) the vapour flow of water should occur from the soil to the paper until equilibrium is obtained (Fig. 10). Having established equilibrium conditions, the water content in the filter paper can be measured. The filter paper water content is related to a suction value through use of the filter paper calibration curve as illustrated in Fig. 11. Theoretically, the equilibrium water content of the filter paper corresponds to the soil matric suction when the paper is placed in contact with the soil and liquid flow occurs. On the other hand, the equilibrium water content of the filter paper corresponds to the total suction of the soil if the paper is not in contact with the soil and only vapour flow occurs. The filter paper method can be used to measure almost the entire range of suctions.

A comparison between the results of suction measurements using filter papers and psychrometers is shown in Fig. 9. The results from the non-contact filter paper agreed closely with the psychrometer results indicating that total suction was measured. However, the contact filter paper did not exhibit consistent results with respect to

Fig. 10. Contact and non-contact filter paper method for measuring matric suction and total suctions, respectively (from Al-Khafaf and Hanks 1974).

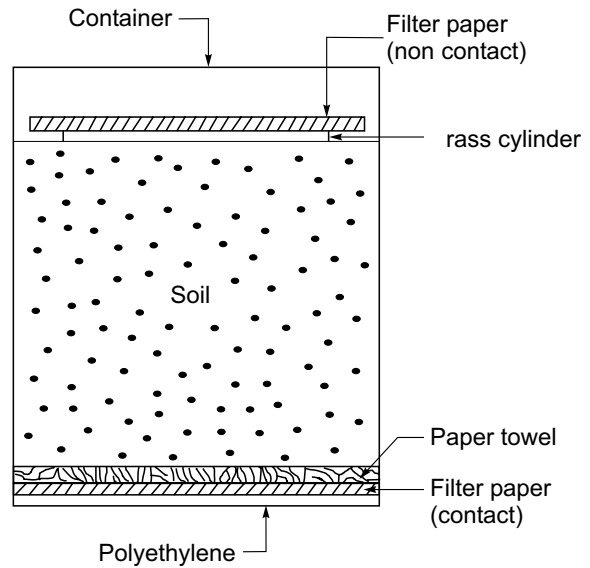
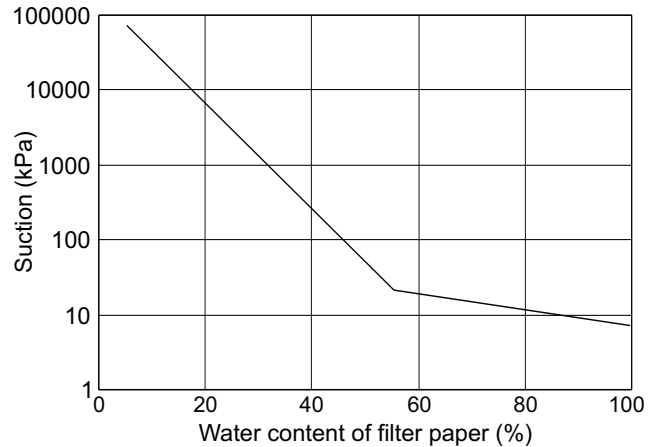


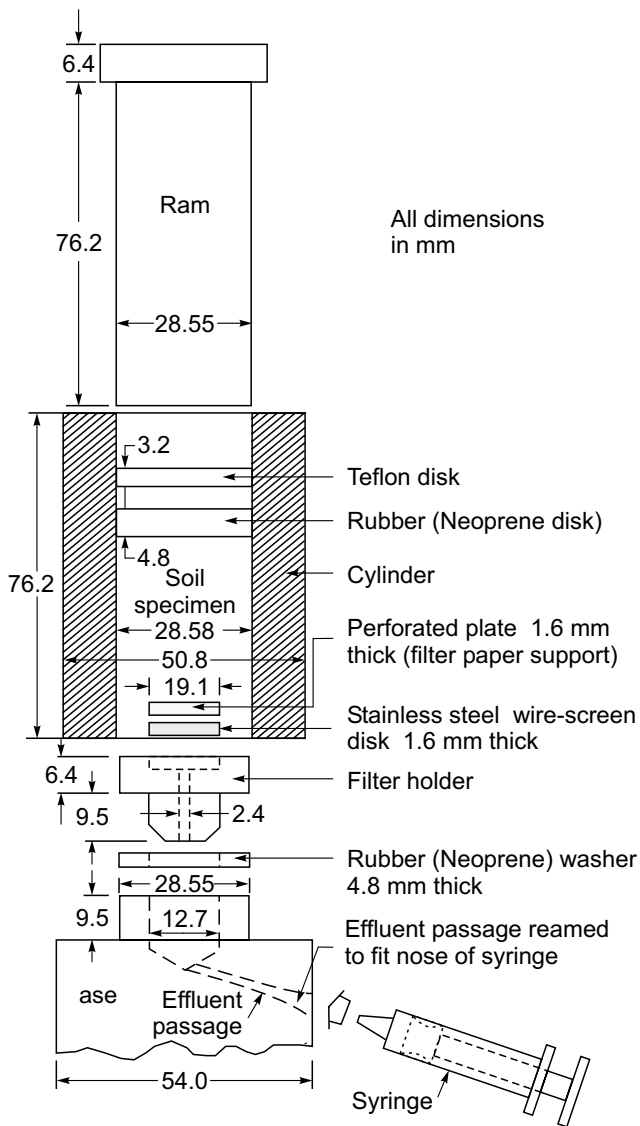
Fig. 11. A typical calibration curve for filter paper (from McQueen and Miller 1968).



depth. This is believed to be due to poor contact between the filter paper and the soil specimen that resulted in the total suction being measured instead of the matric suction (i.e., in the depth range of 0 to 5 m in Fig. 9).

Pore fluid squeezer

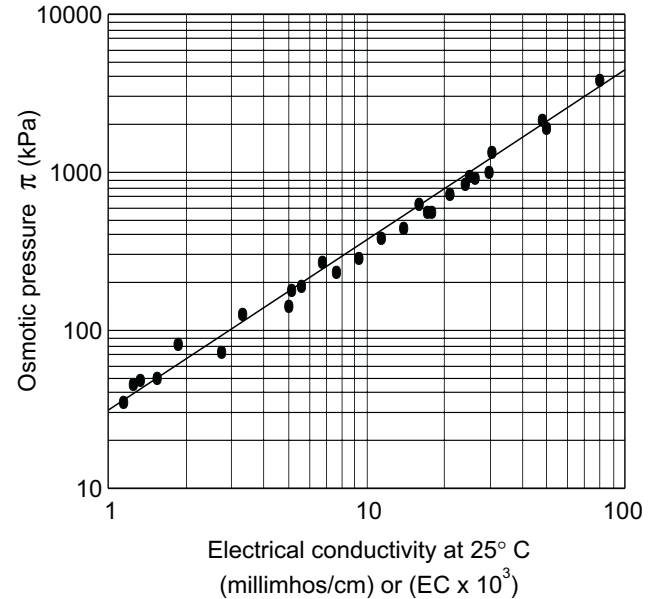
The osmotic suction of a soil can be determined by measuring the electrical conductivity of pore-water from the soil. Pure water has a low electrical conductivity in comparison to the pore-water that contains dissolved salts. Therefore, the electrical conductivity of the pore-water from the soil can be used to indicate the total concentration of dissolved salts which is related to the osmotic suction of the soil. The pore-water in the soil can be extracted using a pore fluid squeezer which consists of a heavy-walled cylinder and piston squeezer (Fig. 12).

Fig. 12. Pore fluid squeezer (from Manheim 1966).

The electrical resistivity (or electrical conductivity) of the pore-water is then measured. A calibration curve (Fig. 13) can be used to relate the electrical conductivity to the osmotic pressure of the soil.

Summary

Several devices for measuring total, matric, and osmotic suctions have been described in this paper. Techniques and limitations associated with each device are outlined. More research is required on the measurement of suction. It is not possible, however, to measure the components of soil suction for engineering projects. The best procedures and devices vary, depending primarily upon the range of suction being measured.

Fig. 13. Osmotic pressure versus electrical conductivity relationship for pore-water containing mixtures of dissolved salts (from U.S.D.A. 1950).

References

- Al-Khafaf, S., and Hanks, R.J. 1974. Evaluation of the filter paper method for estimating soil water potential. *Soil Science*, **117**(4): 194–199.
- Krahn, J., Fredlund, D.G., and Klassen, N.J. 1987. The effect of soil suction on slope stability at Notch Hill. Proceedings, 40th Canadian Geotechnical Conference, Regina, SK, Canada, Oct. 19–21, pp. 103–110.
- Manheim, F.T., 1966. A hydraulic squeezer for obtaining interstitial water from consolidated and unconsolidated sediment. U.S. Geological Survey, Professional Paper 550-C, pp. 256–261.
- McQueen, I.S., and Miller, R.F. 1968. Calibration and evaluation of a wide range method of measuring moisture stress. *Journal of Soil Science*, **106**(3): 225–231.
- Phene, C.J., Hoffman, C.J., and Rawlins, S.L. 1971. Measuring soil matric potential *in situ* by sensing heat dissipation within a porous body: I. Theory and Sensor Construction. II. Experimental Results. *Soil Science Society of America Proceedings*, **35**: 27–32.
- U.S.D.A. 1950. Diagnosis and improvement of saline and alkali soils. United States Department of Agriculture. Agricultural Handbook No. 60.
- van der Raadt, P., Fredlund, D.G., Clifton A.W., Klassen, M.J., and Jubien, W.E. 1987. Soil suction measurement at several sites in western Canada. Session on Geotechnical Problems in Arid Regions. Transportation Research Board, Committee A2LO6TRB, Washington, D.C., Transportation Research Record 1137, pp. 24–35.
- Wong, K.H., and Ho, A. 1987. An evaluation of a thermal conductivity sensor for the measurement of soil matric suction. Internal Report, Department of Civil Engineering, University of Saskatchewan, Saskatoon, SK, Canada.

Background, theory, and research related to the use of thermal conductivity sensors for matric suction measurement

D.G. Fredlund

Abstract: This chapter describes the history and use of thermal conductivity sensors to measure matric suction. The technique uses an indirect measurement which is correlated to matric suction. The sensors were initially developed and used primarily with irrigation control systems. More recently, attempts have been made to apply the sensors to geotechnical engineering problems. This has resulted in the development of more refined calibration procedures. The thermal conductivity sensors have now been applied on several engineering projects, but more case histories are still required for their complete evaluation.

Key words: thermal conductivity sensors, matric suction, geotechnical engineering, case histories.

Introduction

Various regions of the world are covered with soils which are often categorized as “problematic” soils from a geotechnical engineering standpoint. Soils in this category are (i) swelling soils, (ii) collapsing soils, and (iii) residual soils. Typically, their mechanical behavior does not adhere to classical soil mechanics behavior.

Common to all these problematic soils is the fact that their pore-water pressures are negative, relative to atmospheric conditions and most often, the soils are unsaturated. The negative pore-water pressures can be referenced to the pore-air pressure, [i.e., $(u_a - u_w)$] resulting in the definition of the term matric suction. Matric suction is now recognized as one of the stress state variables controlling the mechanical behavior of unsaturated soils (or soils with negative pore-water pressures). The development of techniques and devices for measuring matric suction is important to the advancement of soil mechanics for unsaturated soils. Of particular need is a device which will measure matric suction *in situ*.

Direct measurements of negative pore-water pressures are limited to less than one atmosphere below zero gauge pressure because of cavitation of water in the measuring system. An indirect method for measuring matric suction involving thermal conductivity measurements is described in this chapter. This method makes use of the thermal properties of a standard porous medium, which is placed in contact with the soil. The resulting device is called a thermal conductivity sensor to measure matric

suction. This chapter considers the potential of these sensors for use in geotechnical engineering.

History and development of thermal conductivity sensors

The thermal properties of a soil have been found to be indicative of the soil water content. Water is a better thermal conductor than air. The thermal conductivity of soil increases with increasing water content. This is particularly true where the change in water content is associated with a change in the degree of saturation of the soil.

Shaw and Baver (1939) developed a device consisting of a temperature sensor and heater which could be installed directly into the soil for thermal conductivity measurements. It was found that the presence of salts did not significantly affect the thermal conductivity of the soil. However, different soils would require different calibrations in order to correlate the thermal conductivity measurements to the water contents of the soil. Johnston (1942) suggested that the thermal conductivity sensor be enclosed in a porous medium that would result in a standard calibration curve. The porous material could then be brought into equilibrium with the soil under consideration. Johnston (1942) used plaster of paris to encase the heating element.

In 1955, Richards patented an electro-thermal element for measuring moisture in porous media. The element consisted of a resistance thermometer which was wrapped with a small heating coil. The electro-thermal element was then mounted in a porous cup and sealed with ceramic cement. Richards proposed the use of a sandy silt material for the porous block. It was suggested that the porous cup should have an air entry value less than 10 kPa.

Bloodworth and Page (1957) studied three materials for use as a porous cup for the thermal conductivity sensors. Plaster of paris, fired clay, or ceramic and castone (i.e., a commercially available dental stone powder) were

D.G. Fredlund. Professor, Civil Engineering Department, University of Saskatchewan, 57 Campus Drive, Saskatoon, SK, Canada S7N 5A9.

Reprinted with permission from *Advances in Measurement of Soil Physical Properties: Bringing Theory into Practice*. SSSA Special Publication No. 3, 1992, Soil Science Society of America, 677 S. Segoe Rd., Madison, WI 53711, USA. pp. 249–262.

used in the study. The castone was found to be the best material for the porous cup.

Phene et al. (1971) developed a thermal conductivity sensor using a Germanium P-N Diode as a temperature sensor. The sensor was wrapped with 40-gauge Teflon coated copper wire that served as the heating coil. The sensing unit was embedded in a porous block. The optimum dimensions of the porous block were calculated based on a theoretical analysis. The block must be large enough to contain the heat pulse (particularly for the saturated sensor) without being interfered with by the thermal properties of the surrounding soil. As well, it was found that the higher the ratio of thermal conductivity and diffusivity, the higher the precision with which the water content can be measured. The distribution of the pore size was also important.

Gypsum, ceramics, and mixtures of ceramics and castone were examined as potential porous block materials by Phene et al. (1971). It was found that the ceramic block exhibited a linear response and provided a stable solid matrix.

In the mid-1970's, Moisture Control System Inc., Findlay, OH, manufactured the MCS 6000 thermal conductivity sensors. The sensor was built using the same design and construction principles as developed by Phene et al. (1971). The manufactured sensors were subjected to a one point calibration. The suggested calibration curves were assumed to be linear from 0 to 300 kPa. Above 300 kPa the calibration curves were empirically extrapolated. In this region the calibration curves became highly non-linear and less accurate.

The MCS 6000 sensors have been used for matric suction measurements in the laboratory and in the field (Picornell et al. 1983; Lee and Fredlund 1984). The sensors appeared to be quite suitable for field usage, being insensitive to temperature and salinity changes. Relatively accurate measurements of matric suctions were obtained in the range below 300 kPa. Curtis and Johnston (1987) used the MCS 6000 sensors in a major groundwater recharge study. The sensors were found to be sufficiently responsive and sensitive. The results were in good agreement with piezometer and neutron probe data. However, Moisture Control System Inc. discontinued production in early 1980, and the MCS 6000 sensor is no longer commercially available.

In December 1981, Agwatronics Inc., Merced, CA, commenced production of the AGWA thermal conductivity sensors as designed and developed by Phene et al. (1971). There were several difficulties associated with the AGWA sensors that resulted in the replacement of the sensors by the AGWA-II sensors in 1984. A thorough calibration study on the AGWA-II sensors was completed at the University of Saskatchewan, Canada (Wong et al. 1989, Fredlund and Wong 1989). Several other difficulties have also been reported with the use of the AGWA-II sensors. These include the deterioration of the electronics and the porous block with time.

Typical calibration curves of the AGWA-II sensor are presented and discussed in this paper. The AGWA-II sen-

sors have been used for laboratory and field measurements of matric suctions (van der Raadt et al. 1987; Sattler and Fredlund 1989). Typical results are described in this paper together with techniques used in the measurements. The main consideration is given to the performance of the AGWA-II sensors which are the only sensors commercially available.

Theory of operation

A thermal conductivity sensor consists of a porous ceramic block containing a temperature sensing element and a miniature heater (Fig. 1). The thermal conductivity of the porous block varies in accordance with the water content in the block. The water content in the porous block is dependent on the matric suctions applied to the block by the surrounding soil. Therefore, the thermal conductivity of the porous block can be calibrated with respect to the applied matric suction.

A calibrated sensor can then be used to measure the matric suction in a soil mass by placing the sensor in the soil and allowing it to come to equilibrium with the state of stress in the soil (i.e., the matric suction of the soil). Thermal conductivity measurements at equilibrium are an indication of the matric suction of the soil.

Thermal conductivity measurements are performed by measuring heat dissipation within the porous block. A controlled amount of heat is generated by the heater at the center of the block. A portion of the generated heat will be dissipated throughout the block. The amount of heat dissipation is controlled by the presence of water within the porous block. The change in the thermal conductivity of the sensor is directly related to the change in water content of the block. Hence, more heat will be dissipated as the water content in the block increases.

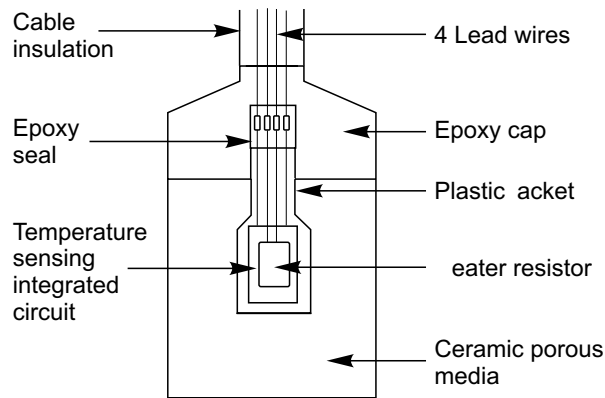
The undissipated heat will result in a temperature rise at the center of the block. The temperature rise is measured by the sensing element after a specified time interval and its magnitude is inversely proportional to the water content of the porous block. The measured temperature rise is expressed in terms of a voltage output.

Calibration of sensors

AGWA-II sensors are usually subjected to a two-point calibration prior to shipment from the factory. One calibration reading is taken with the sensors placed in water (i.e., zero matric suction). A second calibration reading is taken with the sensors subjected to a suction of approximately 100 kPa. This calibration procedure may be adequate for some applications, however, it has been suggested that a more rigorous calibration procedure is necessary when the sensors are used for geotechnical engineering applications (Fredlund and Wong 1989).

A more thorough calibration of thermal conductivity sensors can be performed by applying a range of matric suction values to the sensors while they are mounted in a soil. Readings of the change in voltage output from the sensor are taken at each applied suction. The change in

Fig. 1. Cross-sectional diagram of the AGWA-II thermal conductivity sensor.



voltage output is a measure of the thermal conductivity (or the water content) of the porous block under the applied matric suction. The matric suction can be applied to the sensor using a modified pressure plate apparatus (Wong et al. 1989, Fredlund and Wong 1989).

The sensor is embedded in a soil that is placed on the pressure plate (Fig. 2). The soil on the pressure plate provides continuity between the water phase in the porous block and in the high air entry disc. The matric suction is applied by increasing the air pressure within the pressure plate apparatus, but maintaining the water pressure below the pressure plate at atmospheric conditions.

The change in voltage output from the sensor can be monitored periodically until matric suction equilibrium is achieved. The above procedure is repeated for various applied matric suctions in order to obtain a calibration curve. A number of thermal conductivity sensors can be calibrated simultaneously on the pressure plate. During calibration, the pressure plate setup should be contained within a temperature controlled box.

At least 40 AGWA-II sensors have been purchased and calibrated at the University of Saskatchewan, Canada. Typical non-linear calibration curves for the AGWA-II sensors are shown in Fig. 3. The non-linear response of the sensors is likely related to the pore size distribution of the ceramic porous block. Similar non-linearities were also observed on the calibration curves for the MCS 6000 sensor.

The non-linear behavior of the AGWA-II sensors may be approximated by a bilinear curve as illustrated in Fig. 3. The breaking point on the calibration curve was found to be generally around 175 kPa. Relatively accurate measurements of matric suctions with the sensor can be expected using the AGWA-II, particularly within the range of 0 to 175 kPa. Matric suction measurements above 175 kPa correspond to the steeper portion of the calibration curve which has a lower sensitivity.

Times for equilibrium during calibration have ranged from a few days to several months. The longer equilibrium times are required when the soils surrounding the sensors is relatively dry. In general, only a few days are required for equilibrium at each applied suction. The

characteristic shape of the calibration curves remains the same as long as a reasonable calibration time is allowed. Equilibrium can best be assessed by observing the change in readings on the sensor over a period of several days.

A study on the AGWA-II sensors indicated consistent and stable output readings with time (Fredlund and Wong 1989). The sensors were found to be responsive to wetting and drying processes. However, some failures have been experienced with sensors particularly when they are subjected to a positive water pressure. The failures are attributed to the possibility of moisture coming into contact with the electronics sealed within the porous block (Wong et al. 1989). As well, there have been continual problems with the porous blocks being too fragile. Therefore, the sensor must be handled with great care. Even so, there is a percentage of the sensors which crack or crumble during calibration or installation.

Typical results of matric suction measurements

Laboratory and field measurements of matric suctions using the AGWA-II thermal conductivity sensors have been made in several types of soils (Rahardjo et al. 1989). The soils ranged from being highly plastic to essentially non-plastic and the sensors have been installed in either an initially wet, or initially dry state.

Results of laboratory measurements on highly plastic clays from Sceptre and Regina, Saskatchewan are shown in Figs. 4, 5, and 6. The soils were sampled in the field using Shelby tubes. Matric suction measurements on compacted soils have also been performed on silts from Brazil (Fig. 7).

Laboratory measurements were conducted using two sensors in each soil specimen. One sensor was initially saturated, while the other sensor was initially air-dried. The initially saturated sensor was submerged in water for about 2 days prior to being installed in the soil. The sensors were then inserted into predrilled holes in either end of the soil specimen. The specimen with the installed sensors were wrapped in a plastic film to prevent moisture loss during measurements.

The response of both sensors were monitored immediately, and at various elapsed times after their installation. The results indicate that the time required for the initially dry sensor to come to equilibrium with the soil specimen is less than the equilibrium time required for the initially saturated sensor to come to equilibrium.

On the basis of many laboratory experiments, it would appear that the AGWA-II sensors, which were initially dry, yield a matric suction value which is closest to the correct value. In general, the initially dry sensor should yield a value which is slightly too high. On the other hand, the initially wet sensor yields a value which is too low. The following table (Table 1) gives the author's interpretation of the results presented in Figs. 4 to 7, inclusive. Part or all of the difference in matric suction values measured by the dry and wet sensors could be the result of hysteresis in both the sensor and in the soil. The differ-

Table 1. Interpretation of laboratory matric suction measurements of four soils.

Soil type	Soil classification†	Water content (%)	Figure No.	Initially dry sensor (kPa)	Initially wet sensor (kPa)	Best estimate (kPa)
Sceptre clay	CH	39.3	4	120	100	114
Sceptre clay	CH	34.1	5	136	108	126
Regina clay	CH	35.1	6	160	150	157
Brazil silt	MH	15.2	7	100	68	90

†Unified classification system: CH-highly inorganic plastic clays; and MH-inorganic silts.

Fig. 2. Pressure plate calibration of thermal conductivity sensor.

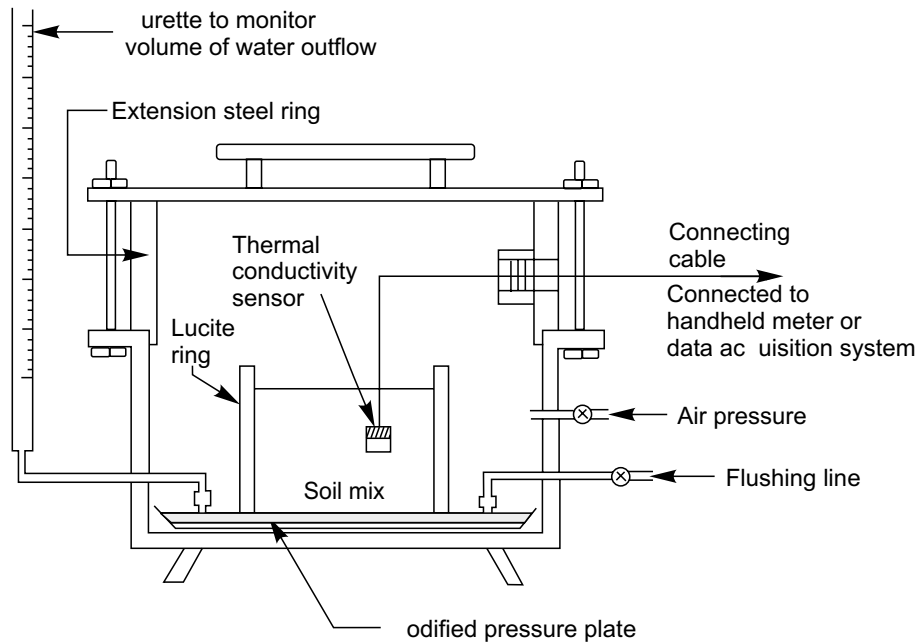
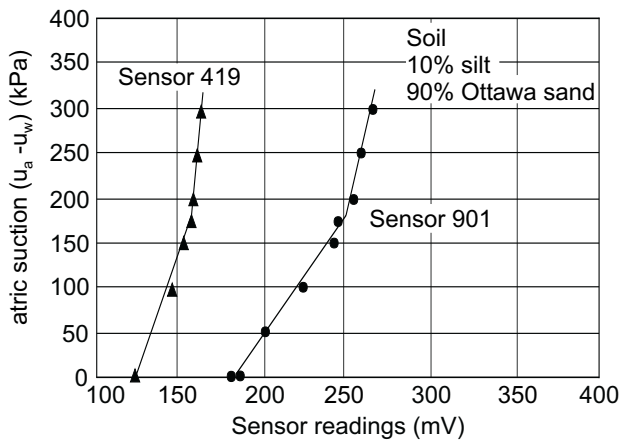


Fig. 3. Calibration curves for two AGWA-II thermal conductivity sensors.



ences are surprisingly small, and do not necessarily result from instrument error.

The sensors are calibrated along a drying mode, starting with a saturated sensor. It is recommended, however,

that the sensor be installed dry into the soil. The reason being that the amount of water entering the sensor is less when the sensor is dry than the amount of water that would be leaving the sensor if it were initially wet.

On the basis of many laboratory tests, the author would recommend that if only one sensor is installed in an undisturbed sample, the sensor should be initially dry. If the sensors have been calibrated using at least seven data points, the readings obtained in the laboratory should be accurate to within at least 15 kPa of the correct value provided the matric suction reading is in the range of 0 to 300 kPa. It may take 4 to 7 days before equilibrium has been achieved. If the sensors are left *in situ* for a long period of time, the measurements should be even more accurate.

Results from laboratory measurements of matric suction have been used to establish the negative pore-water pressures in undisturbed samples of Winnipeg clay taken from various depths within a railway embankment (Sattler et al. 1990). The samples were brought to the laboratory for metric suction measurements using the AGWA-II sensors. The measured matric suctions were corrected for the removal of the overburden stress and

Fig. 4. Laboratory measurements of matric suction on highly plastic clay from Sceptre, Saskatchewan, Canada ($w = 39.3\%$).

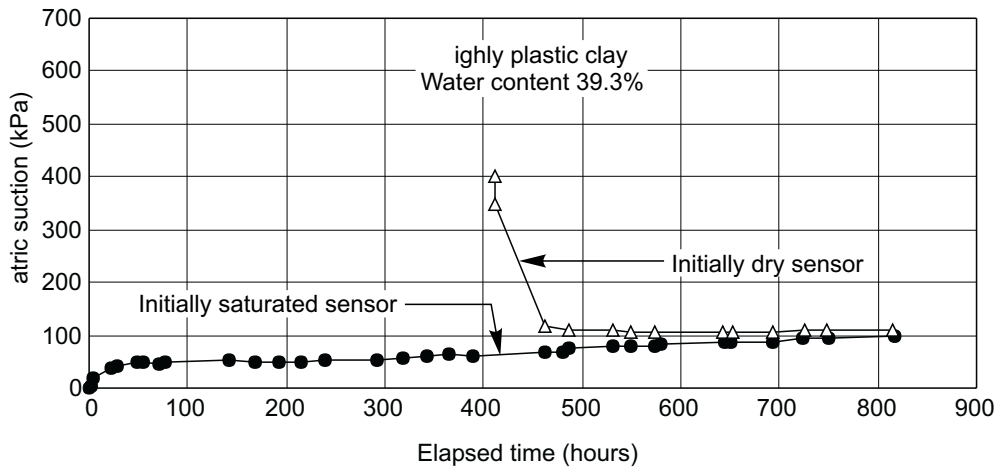


Fig. 5. Laboratory measurements of matric suction on highly plastic clay from Sceptre, Saskatchewan, Canada ($w = 34.1\%$).

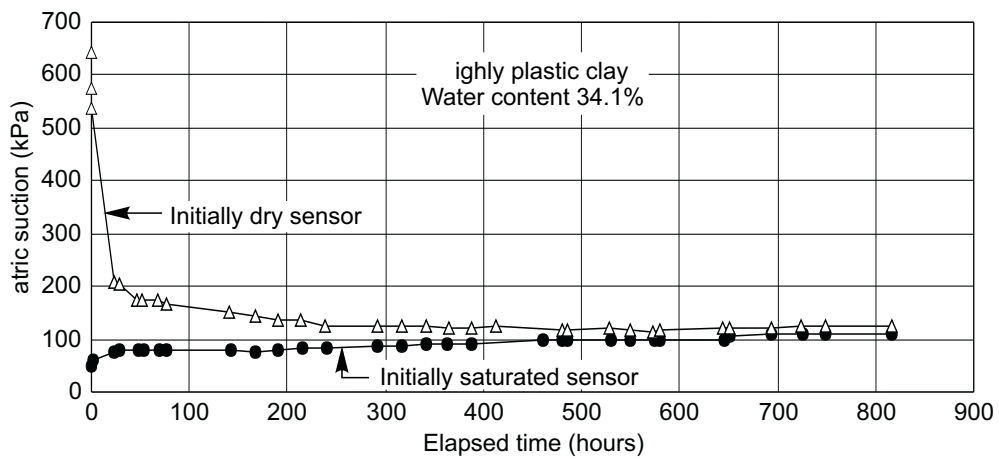
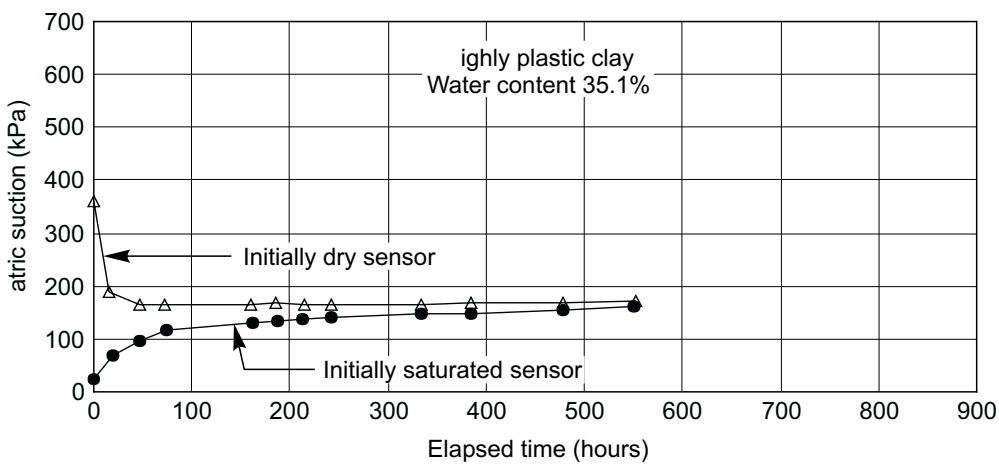


Fig. 6. Laboratory measurements of matric suction on highly plastic clay from Darke Hall, Regina, Saskatchewan, Canada ($w = 35.1\%$).



plotted as a negative pore-water pressure profile (Fig. 8). The results indicated that the negative pore-water pressures approached zero at the average water table and were, in general, more negative than the hydrostatic line above the water table.

Field measurements of matric suction under a controlled environment have been conducted in the subgrade soils of an indoor highway test track (Loi et al. 1989). The temperature and the relative humidity within the test track facility are controlled. Twenty-two AGWA-II sen-

Fig. 7. Laboratory measurements of matric suction on highly plastic clay from Brazil ($w = 15.2\%$).

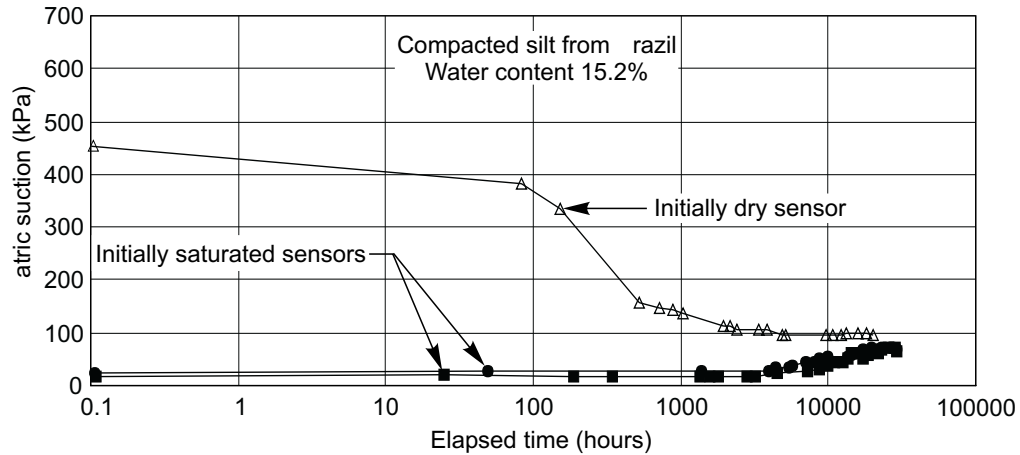
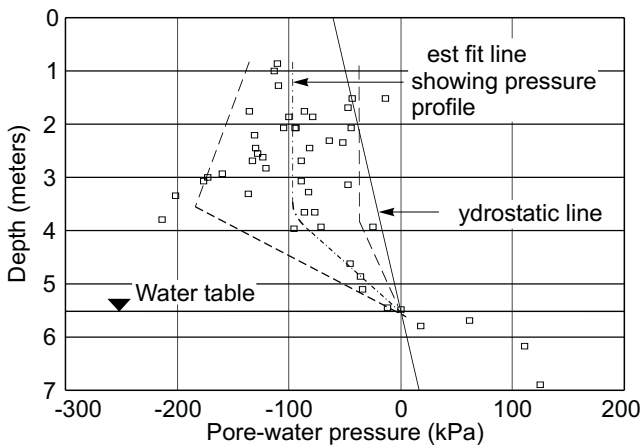


Fig. 8. Negative pore-water pressure profiles obtained using the AGWA-II thermal conductivity sensors (from Sattler and Fredlund 1989).



sensors were installed in the subgrade of the test track. The subgrade consisted of a highly plastic clay and glacial till. The sensors were initially air-dried and installed into pre-drilled holes at various depths in the subgrade. The sensor outputs were recorded twice a day.

Typical matric suction measurements on the compacted Regina clay and glacial till subgrade are presented in Fig. 9. Consistent readings of matric suction ranging from 50 to 400 kPa were monitored over a period of more than 5 months prior to flooding the test track. The sensors responded quickly upon flooding (data not shown in Fig. 9). The results demonstrated that the AGWA-II sensors provide stable measurements of matric suction over a relatively long period of time.

Matric suction variations in the field can be related to environmental changes. Several AGWA-II sensors have been installed at various depths in the subgrade below a railroad. The soil was a highly plastic Regina clay that exhibits high swelling potentials. Matric suctions in the soil were monitored at various times of the year. The results clearly indicate seasonal variations of matric

Fig. 9. Field measurements of matric suction using the AGWA-II thermal conductivity sensors under controlled conditions.

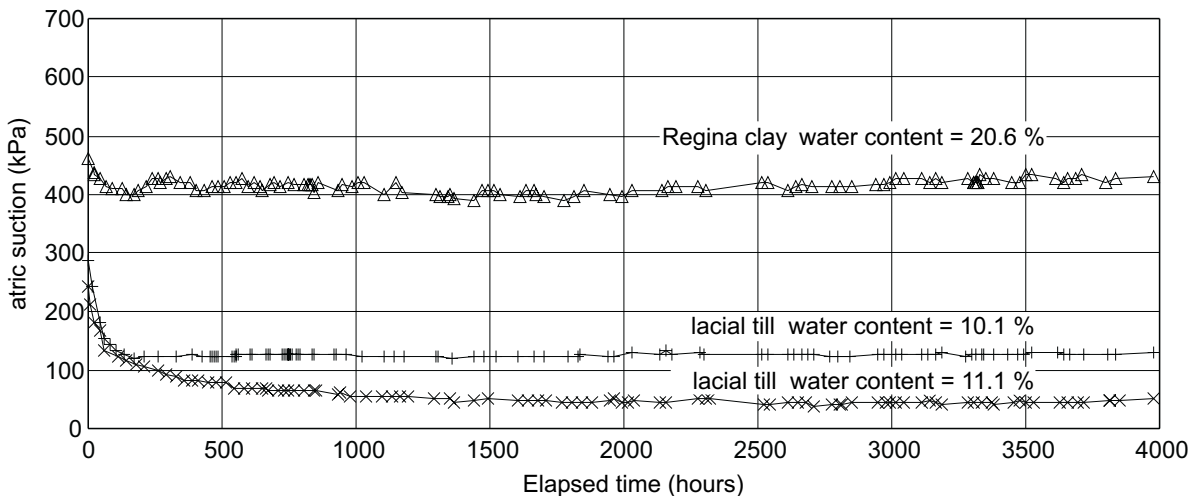
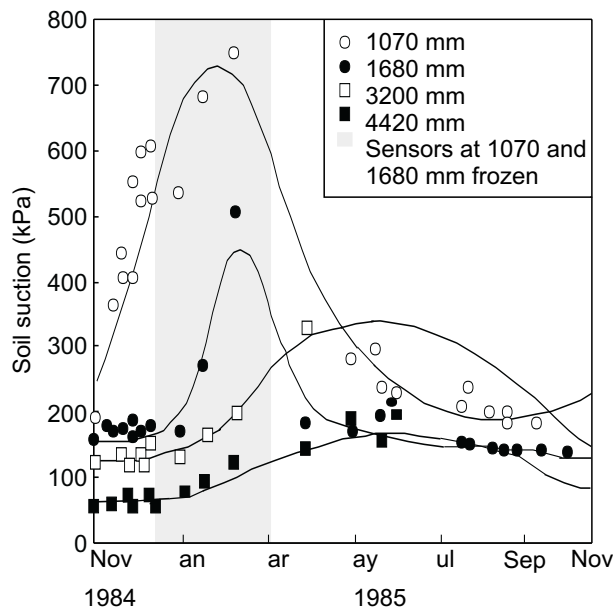


Fig. 10. Idealized plot of matric suction versus time of year for various depths of Regina clay in Saskatchewan (from van der Raadt 1988).



suctions in the field with the greatest variation occurring near ground surface (Fig. 10).

Conclusions

Thermal conductivity sensors appear to be a promising device for measuring matric suction either in the laboratory or in the field. However, proper calibration should be performed on each sensor prior to its use. The calibration study on the AGWA-II sensors revealed that the sensors are quite sensitive for measuring matric suctions up to 175 kPa.

It is possible that future improvements on the AGWA-II sensors will further enhance their performance. For example, a better seal around the electronics within the sensor could reduce the effect of soil water. As well, a stronger, more durable porous block would produce a better sensor for geotechnical engineering applications. These improvements would reduce the mortality rate of the sensor.

References

Bloodworth, M.E., and Page, J.B. 1957. Use of thermister for the measurement of soil moisture and temperature. *Soil Science Society of America Proceedings*, **21**: 11–15.

Curtis, A.A., and Johnston, C. D. 1987. Monitoring unsaturated soil water conditions in groundwater recharge studies. *Proceedings, International Conference on Measurement of Soil and Plant Water Status*, Utah State University, Logan, Utah, pp. 267–274.

Fredlund, D.G., and Wong, D.K.H. 1989. Calibration of thermal conductivity sensors for measuring soil suction. *Geotechnical Testing Journal*, GTJODJ, **12**(3): 188–194.

Johnston, C.N. 1942. Water permeable jacketed thermal radiators as indicators of field capacity and permanent wilting percentage in soils. *Soil Science*, **54**: 123–126.

Lee, R.K., and Fredlund, D.G. 1984. Measurement of soil suction using the MCS 6000 gauge. *Proceedings, 5th International Conference on Expansive Soils*, The Institution of Engineers, Adelaide, South Australia, 21–23 May, pp. 50–54.

Loi, J., Gan J., and Fredlund, D.G. 1989. An evaluation of AGWA-II sensors in measuring soil suction from full-scale testing at the Regina Test Track. Internal Report, Geotechnical Group of the Department of Civil Engineering, University of Saskatchewan, Saskatoon, SK, Canada.

Phene, C.J., Hoffman, G.J., and Rawlins, S.L. 1971. Measuring soil matric potential in situ by sensing heat dissipation with a porous body: theory and sensor construction. *Soil Science Society of America Proceedings*, **35**: 27–32.

Picornell, M., Lytton, R.L., and Steinberg, M. 1983. Matric suction instrumentation of a vertical moisture barrier. *Transportation Research Board, National Research Council*, Washington, DC, *Transportation Research Record* 945, pp. 16–21.

Rahardjo, H., Loi, J., and Fredlund, D.G. 1989. Typical matric suction measurements in the laboratory and in the field using thermal conductivity sensors. *Proceedings, Indian Geotechnical Conference on Geotechnics of Problematic Soils and Rocks: Characterization, Design, and Ground Improvements*, Visakhapatnam, Dec. 14–16, Sarita Prakashan, Meerut-New Delhi, Vol. 1, pp. 127–131.

Richards, L.A. 1955. Electro-thermal element for measuring moisture in porous media. U.S. Patent 2 718 141. Date issued: 20 September.

Sattler, P. J., and Fredlund D.G. 1989. Use of thermal conductivity sensors to measure matric suction in the laboratory. *Canadian Geotechnical Journal*, **26**(3): 491–498.

Sattler, P.J., Fredlund D.G., Lam, L.W., Clifton, A.W., and Klassen, M.J. 1990. Implementation of a bearing capacity design procedure for railway subgrades: a case study. *In Transportation Research Record No. 1288 — Soils, Geology, and Foundations*, Transportation Research Board, National Research Council, Washington, DC, pp. 191–197.

Shaw, B., and Baver, L.D. 1939. An electrothermal method for following moisture changes of the soil in situ. *Soil Science Society of America Proceedings*, **4**: 78–83.

van der Raadt, P. 1988. Field measurement of soil suction using thermal conductivity matric potential sensors. M.Sc. thesis, University of Saskatchewan, Saskatoon, SK, Canada.

van der Raadt, P., Fredlund, D.G., Clifton, A.W., Klassen, M.J., and Jubien, W.E. 1987. Soil suction measurement at several sites in western Canada, considerations in arid and semi-arid regions. *Geotechnical Problems in Arid Regions*, Transportation Research Board, Committee A2L06TRB, Washington, DC, pp. 24–35.

Wong, D.K.H., Fredlund, D.G., Imre, E., and Putz, G. 1989. Evaluation of AGWA-II thermal conductivity sensors for soil suction measurement. *Proceedings, Transportation Research Board Meeting, National Research Council*, Washington, DC, pp. 131–143.

Monitoring soil suction in an indoor test track facility

J. Loi, D.G. Fredlund, J.K. Gan, and R.A. Widger

Abstract: Tests on a full-scale pavement were conducted in an indoor controlled environment, the pavement track testing facility operated by the Saskatchewan Department of Highways and Transportation. The tests were conducted to evaluate the performance and reliability in using thermal conductivity sensors to measure matric suction in the subgrade under field conditions. Thermal conductivity sensors were installed at various locations and depths to monitor the matric suctions under the pavement structure. The thermal conductivity sensors were found to produce reliable and stable readings of the *in situ* matric suction over a long period of time. The effects of repetitive wheel loadings as well as ponding of the side slopes were investigated.

Key words: thermal conductivity sensors, matric suction, pavements, testing, wheel loadings.

Introduction

Highway embankments are elevated earth structures. The subgrades of the embankment are nearly always unsaturated. A knowledge of the negative pore-water pressures is necessary to the understanding of the behavior of the subgrade soils with respect to shear strength, volume change, and flow

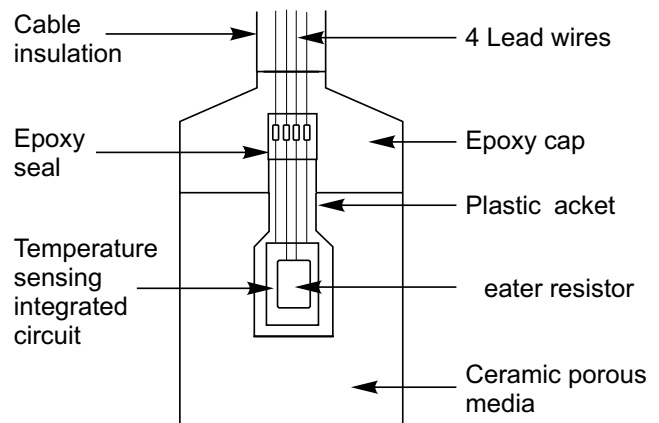
Thermal conductivity sensors appear to be a promising device for measuring matric suction. Two types of thermal conductivity sensors are currently available. One type uses a thermocouple; the other uses an integrated circuit as the temperature-sensing device. The integrated circuit-type sensors were used in this research program. A cross-sectional diagram of an integrated circuit-type thermal conductivity sensor is presented in Fig. 1. The thermal conductivity sensor uses an indirect method for measuring matric suctions on the basis of thermal conductivity of a standard porous ceramic. The development of the thermal conductivity sensors has been discussed by Fredlund.

Objective of research

The objectives of this program were as follows:

- (1) To evaluate the use of thermal conductivity sensors for measuring matric suctions in pavement subgrades over a long period of time,

Fig. 1. Cross-sectional diagram of integrated circuit-type thermal conductivity sensor.



- (2) To evaluate the effect of repetitive wheel loadings on the pavement structure and on the *in situ* matric suctions in the subgrade, and
- (3) To evaluate the response of the pavement structure and the *in situ* matric suctions of the subgrade to the ponding of water against the sideslopes of the embankment.

When a new sensor is being evaluated for its acceptability in measuring matric suction, it is important that laboratory studies be done on the sensor before its installation *in situ*. Many laboratory studies have been done on the thermal conductivity sensors, and their performances have been quite promising. It is fitting that the sensors be installed in the indoor test track for a study of their performance because this facility has a controlled environment. An evaluation can then be done on the acceptability of using these sensors *in situ* installations in highway subgrades.

J. Loi. Clifton Associates, 101-108 Research Drive, Saskatoon, SK, Canada S7N 3R3.

D.G. Fredlund and J.K. Gan. University of Saskatchewan, 57 Campus Drive, Saskatoon, SK, Canada S7N 5A9.

R.A. Widger. Saskatchewan Highways and Transportation, 1855 Victoria Avenue, Regina, SK, Canada S4P 3V5.

Reproduced from the *Proceedings, 71st Annual Meeting of the Transportation Board, Session 228, on Environmental Factors Except Frost*, Transport Research Record 1362, Washington, DC, January 12-16, 1992. pp. 101-110.

Description of test track facility

The test track facility of the Saskatchewan Department of Highways and Transportation is located in Regina, Saskatchewan, Canada. The facility is housed in a fully insulated, dome-shaped, ribbed-plywood building. The circular track is 15.84 m in diameter and is divided into five segments. These are labeled as Segments 0, 1, 2, 3, and 4 in Fig 2.

Segments 0, 2, 3, and 4 have concrete barrier walls that confine the track. Segment 1 has an unconfined outer sideslope that allows for the simulation of a typical shoulder with a sideslope embankment configuration. Only Segment 1 was instrumented for this study.

The test track carries normal dual-wheel tires mounted on a single-arm, twin parallel I-beam gantry. The lateral position of the wheels can be varied to simulate actual field conditions, because vehicles tend to wander across the width of the driving lane. The system can apply loads of up to 54 kN and can operate at speeds up to 32 km/hr. In this program, a wheel load of 40 kN and a tire pressure of 350 kPa were used with a speed of 6 to 7 km/hr.

Subsoil profile and installation of instrumentation

Segment 1 was constructed with a sideslope of 4:1 and was divided into two sections: Section 1A and Section 1B.

In Section 1A, the foundation material consists of 300 mm of sand underlain by 900 mm of highly plastic Regina clay. The upper 300 mm of the Regina clay was compacted to 100 percent maximum standard AASHTO density. The lower 600 mm of the Regina clay was compacted to 95 percent maximum standard AASHTO density. Below this structure was another 500 mm of Regina clay, which was nominally compacted.

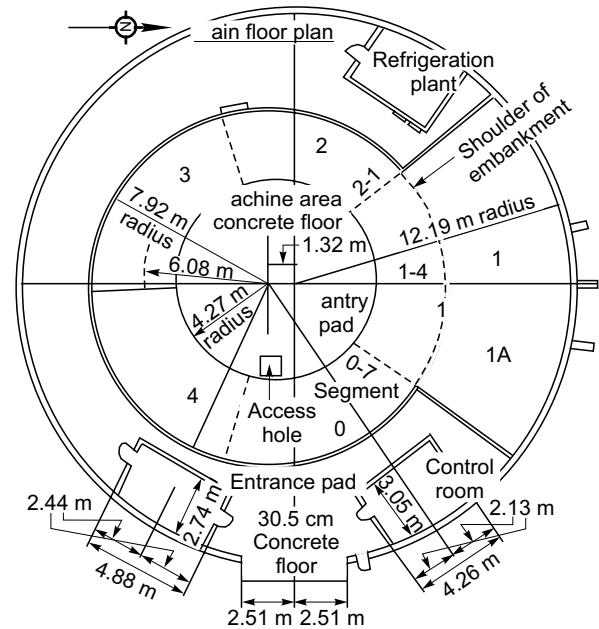
The foundation soil in Section 1B was made up of 1200 mm of a glacial till from the Indian Head area. The upper 600 mm of the till was compacted to 100 percent maximum standard AASHTO density. The lower 600 mm of the till was compacted to 95 percent maximum standard AASHTO density. This section was also underlain by 500 mm of nominally compacted Regina clay.

The Regina clay has a liquid limit of 66.5 percent, a plasticity index of 34.0 percent, and standard AASHTO maximum dry density of 1.410 Mg/m^3 at the corresponding optimum water content of 28.0 percent. The Indian Head till has a liquid limit of 34.5 percent, a plasticity index of 14.4 percent, and standard AASHTO maximum dry density of 1.765 Mg/m^3 at the corresponding optimum water content of 17.0 percent.

Both sections 1A and 1B were placed on 200 mm of sand with an embedded plastic membrane. On the top, both sections were overlaid with 40 mm of hot-mix asphaltic concrete.

Nineteen thermal conductivity sensors were installed in Section 1A and 1B. The locations of the 19 sensors are shown in Figure 3. The installation of the sensors proceeded as follows: first, a 76-mm-diameter hole was

Fig. 2. Plan of Saskatchewan Department of Highways and Transportation test track facility.



drilled vertically to within 50 mm of the intended level of the sensor. A smaller hole, the size of the sensor (which is 25 mm in diameter) was then drilled from the base of the 76-mm-diameter hole. The hole was cleaned using compressed air before the sensor was gently pushed into place in the smaller hole. This mode of installation ensured good contact between the sensor and the soil. The hole was backfilled in layers with cuttings from the drilling operation and was compacted with a compaction hammer.

The sensors were installed dry in each of the prepared drill holes. There were, however, some exceptions. Before the sensors were installed in some of the deep holes (e.g., Sensors 419, 427, 424, 426, and 425), some water was added to the hole. This unfortunate procedure was adopted at the discretion of the on-site engineer, because of the difficulty of installation at those depths.

Six neutron tubes were installed for water content measurements. Seven survey control points, each consisting of a 100-mm-long nail driven through the pavement surface, was established to monitor movements. The locations of this instrumentation are shown in Fig. 4.

Description of tests

Installation of the thermal conductivity sensors was completed on July 15, 1987. Suction readings were taken immediately and monitoring was continued for more than a year before the first wheel load test. The wheel load test consists of running the dual wheels at speed of 6 to 7 km/hr. The load on the dual wheels was 4000 kg (9000 lb), and the tire pressure was 350 kPa (50 psi). During the initial monitoring period, an automated data acquisition system was used to read the thermal conductivity sensors on an hourly basis.

Fig. 3. Location of thermal conductivity sensors in Section 1A and 1B.

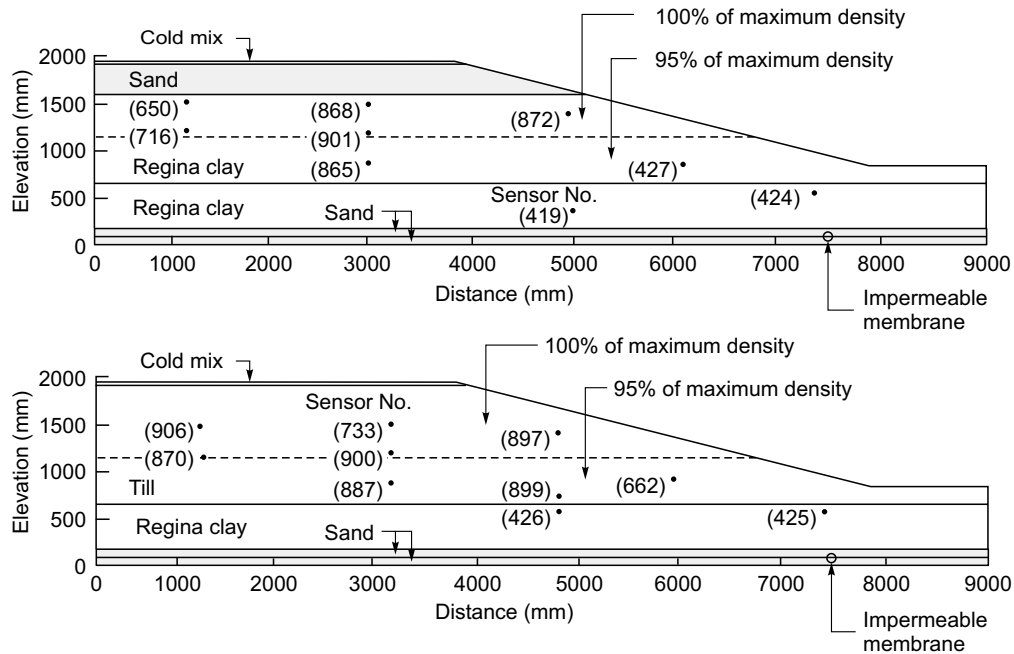
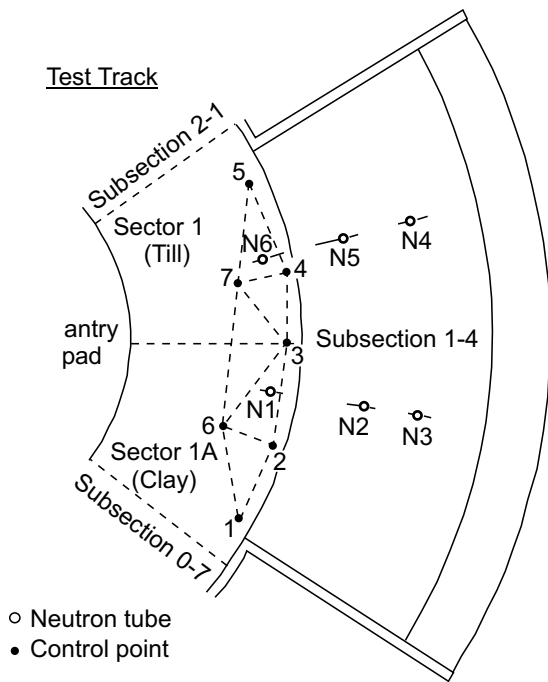


Fig. 4. Location of neutron tubes and survey control points.



The preliminary wheel load test was commenced on July 27, 1988. During this period the automated data acquisition system was programmed to record matric suction readings at the 100th, 200th, 400th, 800th, and 1,600th passes of the wheels. However, at the 58th pass excessive deformation of the subgrade occurred in Section 1B (till section) near the interface with Segment 2. The test was terminated to allow for the repair of the track.

Wheel load tests were resumed on October 17, 1988. This test continued to 613 passes, and excessive deformations of up to 25 mm were evident near the end of Section 1B.

Water was introduced into the ditch in Sections 1A and 1B. It took approximately 66 min to raise the water level to within 150 mm below the upper sand layer of Section 1A. In other words, no water was allowed to enter the upper sand layer just below the asphaltic pavement in Section 1A. The water level was checked frequently to ensure that it was maintained at the required level.

The area was drained on January 16, 1989, by pumping water from the flooded area. The water was discharged outside the building. Draining was completed in about 60 min.

A second wheel load test was performed on February 15, 1989. In this test, excessive deformations occurred in Section 1B. Excessive deformations also occurred at the boundary of Sections 1A and 1B after about 155 wheel passes. The deflection and the rebound of the pavement was as much as 20 mm.

Presentation of results

Long-term, stable measurements were obtained from the thermal conductivity sensors. Some typical data obtained over a monitoring period of one year are presented in Figs. 5, 7, and 8. These data were collected before the wheel loading tests and the infiltration test.

The data presented in Fig. 5 were from sensors installed in the Indian Head till subgrade in Section 1B. The sensors were initially air-dried and were installed in dry holes. The average water content of the till measured at that time was 11 percent. This water content is lower than the as-built water content of 18 percent, indicating that significant drying of the subgrade had occurred since

Fig. 5. Long-term matric suction readings in till subgrade of Section 1B.

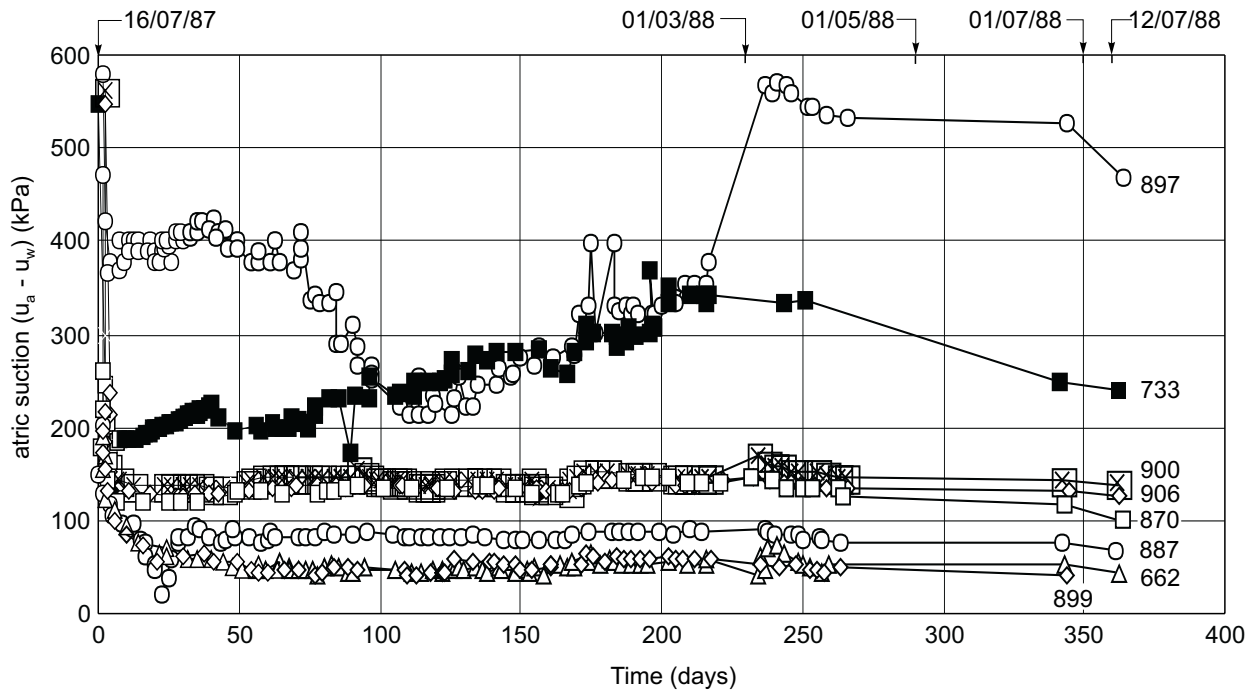
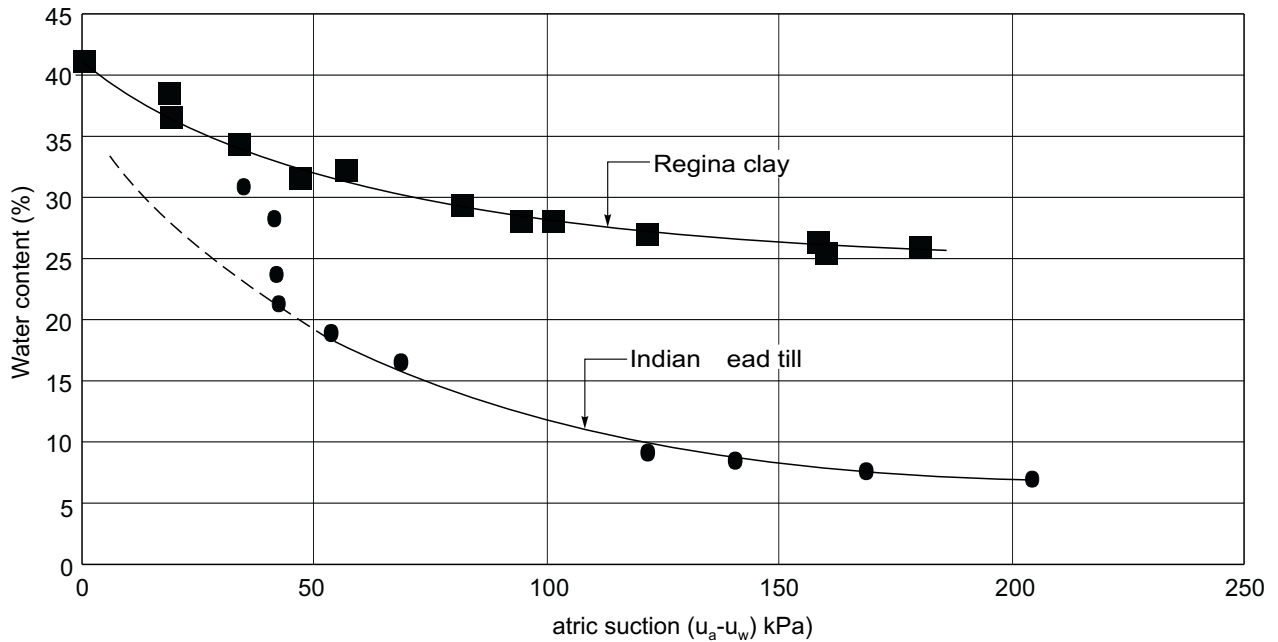


Fig. 6. Water content versus matric suction relationships of slurried samples of Regina clay and Indian Head till.



the section was constructed. A water content of 11 percent corresponds to a matric suction value of about 110 kPa (Fig. 6). The sensors took in water from the surrounding soil, and the matric suction of the sensors decreased until equilibrium was established between the sensors and the soil. With the exception of Sensors 897 and 733, stable consistent matric suction values of about 50 to 100 kPa were recorded. The higher matric suction values recorded by Sensors 897 and 733 could be due to the soil's being drier at these locations or to faulty func-

tioning of the sensor. Sensor 897 was near the exposed sideslope, and Sensor 733 was near the edge of the pavement, fairly close to the exposed sideslope. Water may have been lost from the soil at these locations because of evaporation, resulting in increased matric suction values.

The data presented in Fig. 7 were from sensors installed in the Regina clay subgrade of Section 1A. Again these sensors were installed in an air-dried state into dry holes. The long-term equilibrium matric suction values recorded by the sensors installed in the Regina clay sub-

Fig. 7. Long-term matric suction readings in Regina clay subgrade of Section 1A.

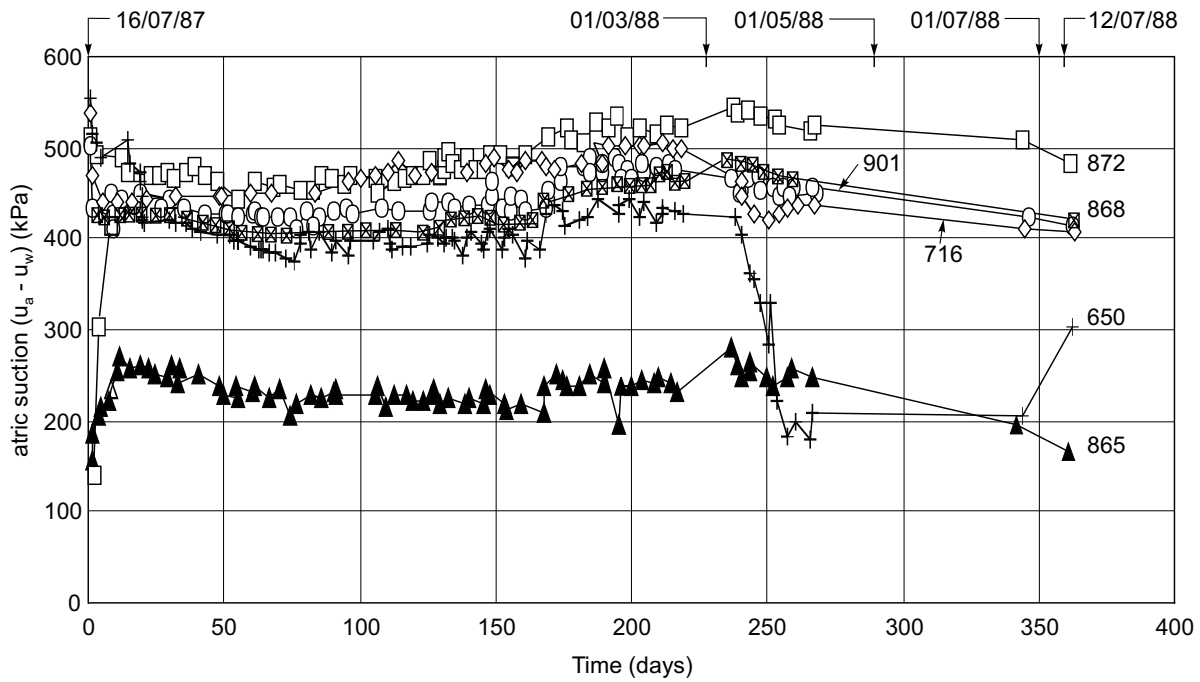
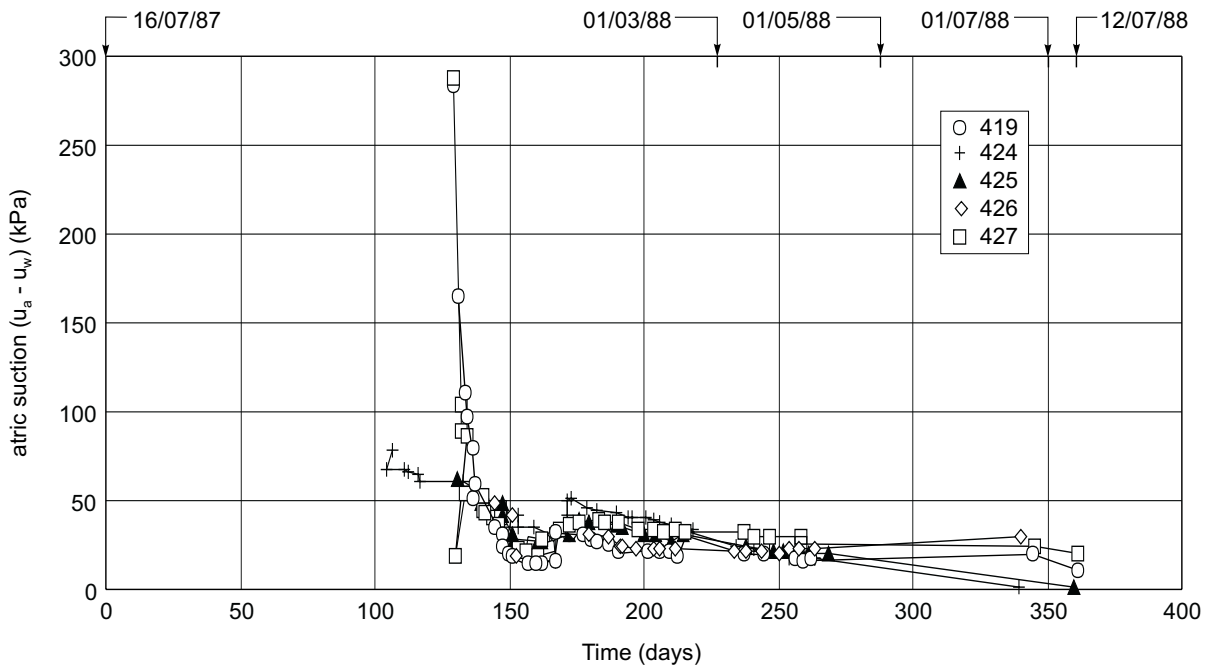


Fig. 8. Long-term matric suction readings from thermal conductivity sensors installed in prewetted holes.



grade of Section 1A were from about 400 to 500 kPa. These measurements were near the upper limit of the range of the sensor. The average water content measured was 15 percent, which was much lower than the as-built water content of 28 percent. This confirmed that significant drying of the subgrade had occurred since the section was constructed.

Sensor 865 recorded a consistently lower matric suction value of between 200 and 250 kPa. This could be

due to the soil's being wetter at the location of Sensor 865. Sensor 650 recorded matric suction values of approximately 400 to 425 kPa over about 250 days. The matric suction then decreased to a value of about 200 kPa and remained at that value for about 100 days before increasing and approaching the initial record value of about 400 kPa. Sensor 650 was located just below the upper sand layer and was close to the surface. The reduction in matric suction may have been due to the accidental spill-

Fig. 9. Response of thermal conductivity sensors in Section 1A to infiltration test.

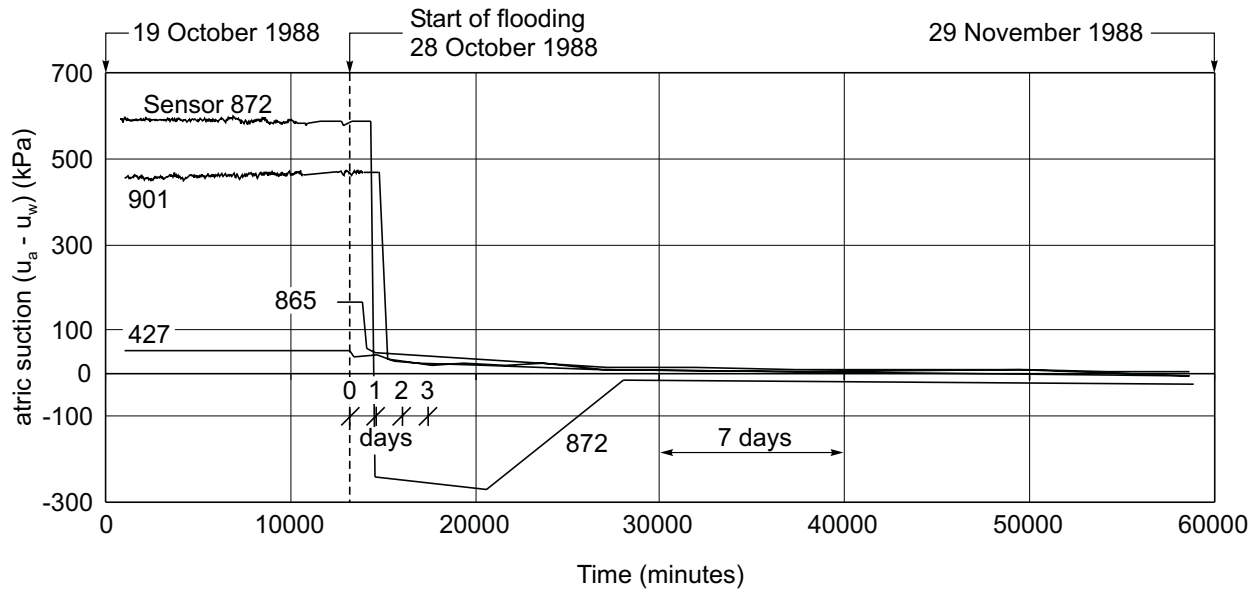
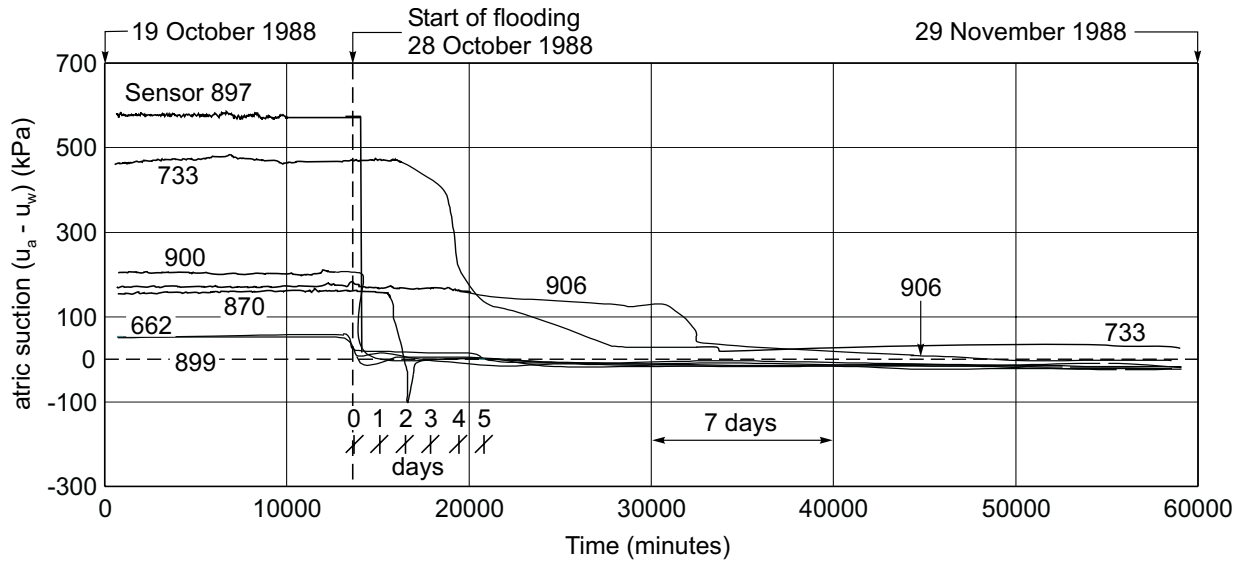


Fig. 10. Response of thermal conductivity sensors in Section 1B to infiltration test.



age of water on the pavement and the eventual seepage of the water to the sensor location. This suggests the possible existence of cracks in the pavement structure.

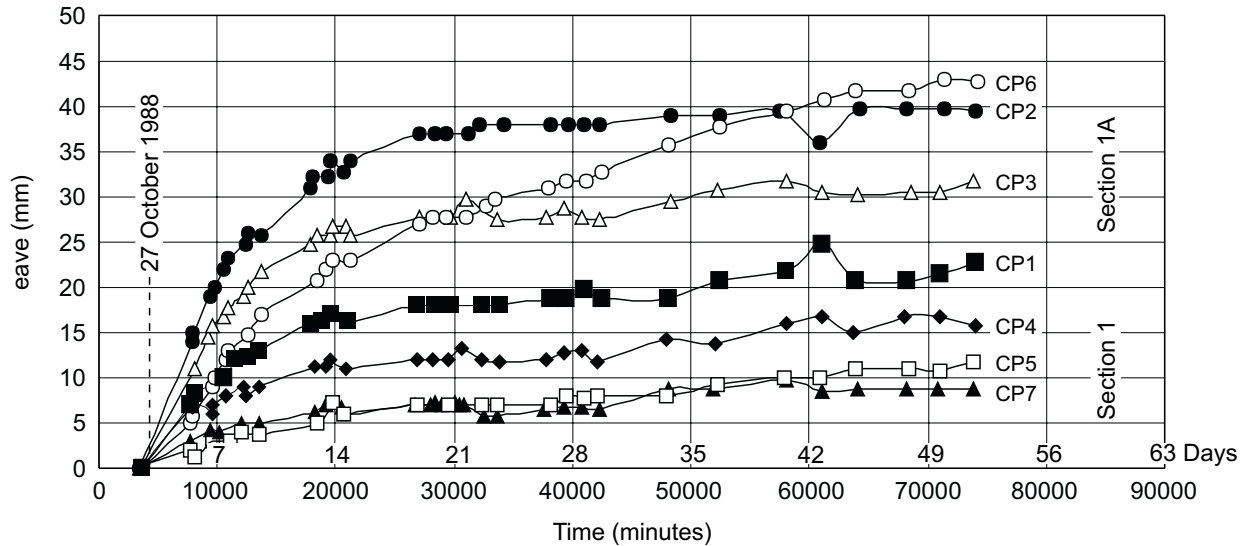
Data from sensors that were installed with prior wetting of the bottom of the drillholes are presented in Fig. 8. The matric suction values were observed to decrease rapidly to values of less than 30 kPa and remained low over the entire monitoring period. The prewetting of the hole was an unfortunate innovation to the installation procedure inasmuch as the added water appeared to redistribute slowly throughout the soils.

The responses of the thermal conductivity sensors during the filtration test are presented in Figs. 9 and 10. Data presented in Fig. 9 were obtained from sensors located in the Regina clay subgrade of Section 1A. The responses of these sensors showed that the water travelled to the sen-

sor locations in a matter of a few hours to a day after flooding. The matric suction values decreased to zero rapidly (less than one hour, in some cases). The high flow of water suggests an extensive network of secondary desiccation cracks in the clay. Extensive cracks will lead water into the sand layer at the base, conveying water rapidly to the interior section of the subgrade. In addition, observations made during the excavation to retrieve the sensors at the end of the program showed that there were preferential flows along the wires leading to the sensors. This was probably due to a poor backfilling procedure for the sensors.

In Section 1B, the responses of the sensors were more varied; some sensors showed a considerably slower and more gradual infiltration of water to the sensor locations (Fig. 10). The rapid reduction in matric suction recorded

Fig. 11. Heave measurements in Sections 1A and 1B.



by Sensors 899 and 662 suggests that there was preferential flow along the till-clay interface. Sensors 899 and 662 were in the till, close to the till-clay interface. Sensors 897 and 900 also registered a rapid response. Sensor 897 was located near the sideslope, and Sensor 900 was about 500 mm above the till-clay interface near the edge of the pavement structure. Sensors 733, 870, and 906 showed a gradual wetting, taking from 2 days to about 2 weeks to reduce to zero suctions. These sensors were located farthest from the sideslope and from the sand base. It may thus be concluded that secondary desiccation cracking is less widespread in the till than in the clay.

Heave measurements were conducted throughout the ponding period. The results are presented in Fig. 11. Results show that the swelling potential of Regina clay is substantially greater than that of Indian Head till. Cracks were observed on the pavement. Cracking was found to be more severe in Section 1A, which was constructed over the Regina clay subgrade. Cracks were as wide as 5 mm.

Neutron probe water content measurements obtained for the period of November 20, 1989, to February 16, 1990, confirmed that the soils were saturated as a result of the infiltration test.

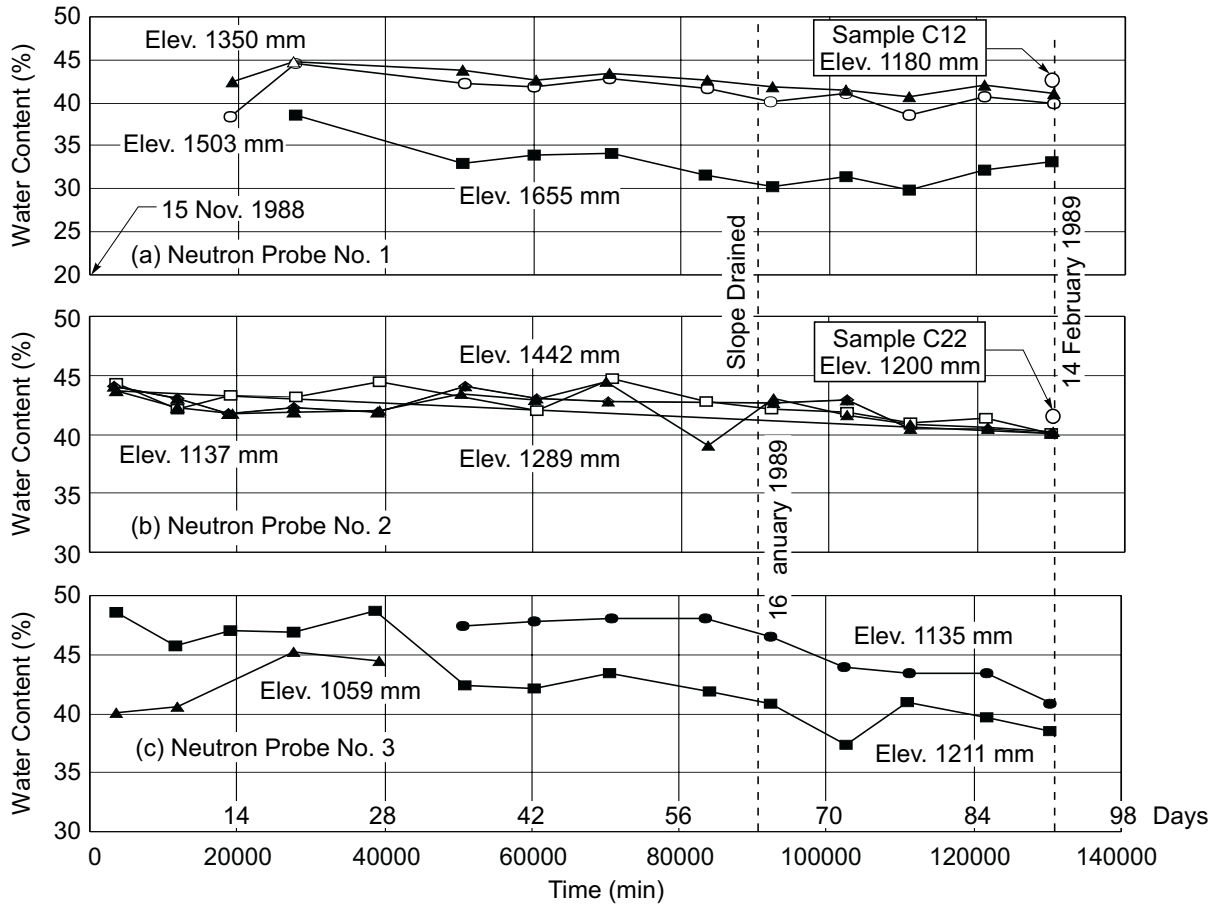
The average initial water content of the upper clay layer in Section 1A before the infiltration test was about 15 percent. Neutron probe measurement after infiltration test showed that the water content had increased to about 40 percent (Fig. 12) at elevations below the maximum ponding water level, which was at an elevation of 1600 mm. This corresponds closely to the saturation water content of the clay (a water content of 40 percent at saturation gives a void ratio of 1.1 assuming a specific gravity of 2.7 for the solids). Water content versus matric suction relationships presented in Fig. 6 showed that Regina clay had zero matric suction when the water content reached about 40 percent. This relationship was obtained from slurried samples using thermal conductivity sensors for the matric suction measurements. The water contents

obtained using the neutron probe device agreed well with the gravimetric water content measurements conducted on samples retrieved near the neutron tube locations on February 15, 1989, 1 day before the draining of the sideslopes. Sample C12 was taken from an elevation of approximately 1180 mm near Neutron Tube 1, and Sample C22 was taken from an elevation of about 1200 mm near Neutron Tube 2 (Figure 12). These samples showed water contents of 42.3 and 41.8 percent, respectively.

In the till section (i.e., Section 1B), the average initial water content before ponding was about 11 percent. Neutron probe measurements after the infiltration test showed that the water content had increased to values of 20 to 30 percent. Water content versus matric suction relationships presented in Fig. 6 showed that the till had matric suction values of zero when the water content reached about 30 percent. At Neutron Tube 5, which is on the sideslope, water contents of about 30 percent were measured (Fig. 13). Water content data at elevations 1612 and 1460 mm indicated that the soil near the surface was drying out. The wetting of the soil at these elevations, after drainage of the sideslope, might have been caused by the spraying of the pavement surface with water (for an unknown reason). Neutron Tube 6 was within the asphalt pavement section. Water content measurements from Tube 6 showed that the soils became progressively drier toward the surface, which is to be expected because of evaporation.

Matric suction values of less than zero were recorded for some of the sensors after ponding. Thermal conductivity sensors measure matric suction indirectly by correlating the temperature rise when a controlled heat pulse is applied for 1 minute. In the integrated circuit-type thermal conductivity sensor, the temperature rise is converted into a voltage reading. The calibration curve of a sensor used in this program is presented in Fig. 14. Because of the higher thermal conductivity of water in comparison to air, a saturated tip at zero matric suction will register the lowest temperature rise because of the high heat loss from

Fig. 12. Neutron probe water content and gravimetric water content measurements in Section 1A.



the water. The temperature rise is a function of the degree of saturation of the ceramic tip and not of the pressure of the water. The sensor, therefore, cannot measure positive pressures. Negative matric suction readings may be due to the following reasons:

- (1) The sensor tips were not large enough to contain the heat pulse completely within the porous ceramic. In this case, the heat loss will be affected by the surrounding soil medium. The calibration obtained will then be in error when installed in a different soil medium.
- (2) The sensor tips were broken in the process of installation, resulting in tips that were not large enough to contain completely the heat pulse.
- (3) With time, the ceramic deteriorated in the ground, particularly in a ponded condition under positive water pressures. The ceramic changes from a rigid structured medium to a structureless mass of soil-like material, altering the characteristics of the sensor tip.
- (4) The sensor tips were not fully saturated at zero matric suction during the calibration process. Positive water pressures will compress the air within the pores of the tip and force more air into water. Or, the tip simply got more saturated under prolonged submergence.
- (5) A gap existed between the sensor and the soil. A waterfilled gap, particularly in conjunction with tips

that were not large enough to contain the heat pulse, could result in higher heat loss.

- (6) Prolonged submergence caused a breakdown of the electronics.

Upon retrieval of the sensors at the end of the study, it was found that the sensor tips were quite soft and that most of them disintegrated upon handling.

There were no noticeable immediate or long-term effects on the matric suction readings due to wheel loadings, even though the loading tests resulted in severe deformations. The surface profiles before and after the wheel loading test of February 15, 1989, are presented in Figs. 15 and 16, respectively. The initial track surface was rougher over the Regina clay subgrade section. The deformations, however, were more severe over the till section. The till was compacted slightly wetter than optimum and had low matric suctions. The till section, in comparison, was inferior to the clay section, which had much higher matric suctions.

Conclusions

The conclusions from this research program can be summarised as follows:

- (1) Long-term stable and reliable matric suction readings in highway subgrades can be obtained using thermal

Fig. 13. Neutron probe water content and gravimetric water content measurements in Section 1B.

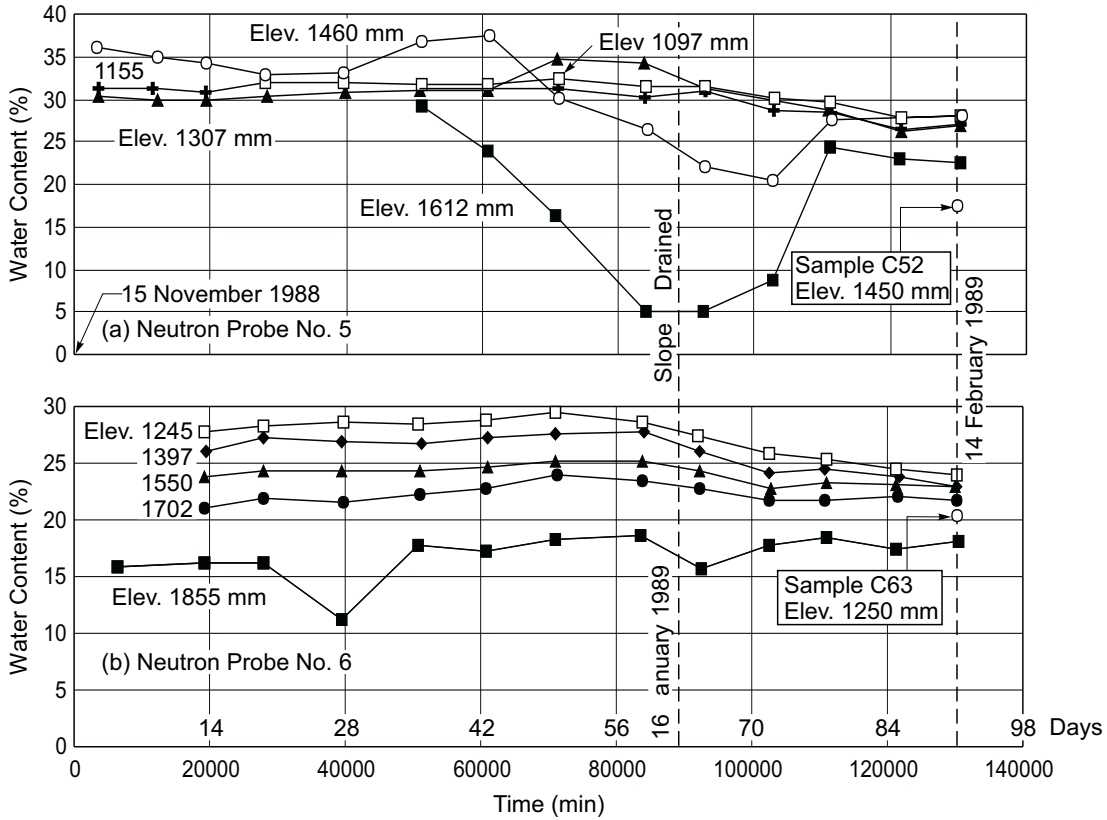


Fig. 14. Typical thermal conductivity sensor calibration curve.

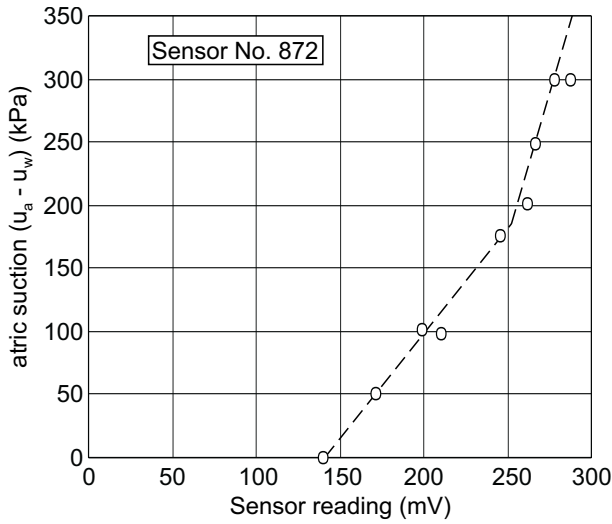


Fig. 15. Track surface elevation just before wheel load test on February 15, 1989.

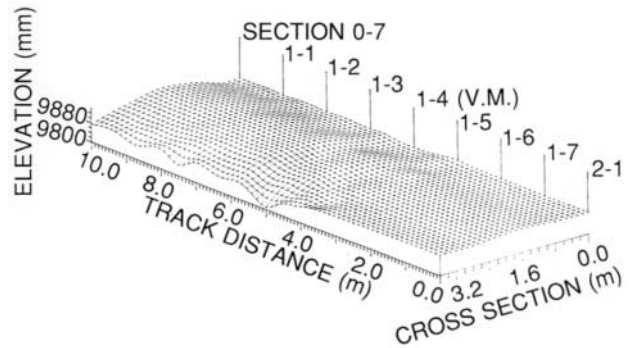
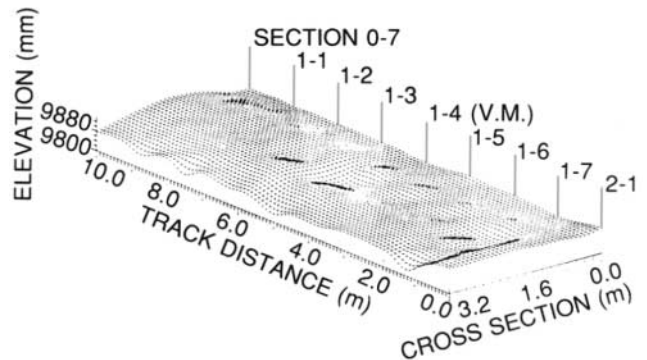


Fig. 16. Track surface elevation after wheel load test on February 15, 1989.



conductivity sensors, as long as the sensor is not subjected to prolonged positive pore-water pressures.

- (2) Poor backfilling procedures can result in preferential flow along the leads to the sensors. This problem is augmented by the vertical position of the installation boreholes. Secondary, dessication cracking also appeared to provide pathways for the rapid inflow of water to the subgrade.
- (3) Water introduced into the soil during installation of the sensors does not redistribute easily. It is easy to

put water into a hole. Once this water gets into the soil, it is difficult to remove.

- (4) Further investigations are required to ascertain the reasons for negative suction readings.
- (5) The deterioration of the sensor tips shows that there is an urgent need for the development of a more durable ceramic for the sensor tip.

References

- Fredlund, D.G. 1979. Appropriate concepts and technology for unsaturated soils. *Canadian Geotechnical Journal*, **16**(1): 121–139.
- Fredlund, D.G. 1985. Soil mechanics principles that embrace unsaturated soils. *Proceedings, 11th International Conference on Soil Mechanics and Foundation Engineering*, San Francisco, CA, Vol. 2, pp. 465–472.
- Fredlund, D.G. 1990. Background, theory and research related to the use of thermal conductivity sensors. *Proceedings, Symposium on Soil Physical Properties*, American Society of Agronomy, Crop Science Society of America, and Soil Science Society of America, 82nd Annual Meeting, San Antonio, TX.
- Sattler, P. and Fredlund, D.G. 1989. Use of thermal conductivity sensors to measure matric suction in the laboratory. *Canadian Geotechnical Journal*, **26**(3): 491–498.

Measuring negative pore-water pressures in a freezing environment

D.G. Fredlund, J.K. Gan, and H. Rahardjo

Abstract: The measurement of negative pore-water pressures is essential to the study of soil behaviour in a freezing environment. Various devices are now available for suction measurements in unfrozen, unsaturated soils. The possibility of using these devices in the measurement of negative pore-water pressures under freezing conditions is discussed in the paper.

The thermal conductivity sensor appears to be the most promising device for suction measurement. The thermal conductivity method of suction measurement in a freezing environment is examined. The theory of freezing soil and the thermal properties of soil are presented. Suction measurements in a freezing environment using thermal conductivity sensors from recent tests conducted at the University of Saskatchewan are also presented. The results are interpreted in the light of the theory of freezing soil and the thermal properties of soil. The latent heat of fusion associated with the water phase transformation of water has significant influence on the thermal conductivity reading of the sensor during freezing and thawing. The formation of ice on freezing makes the interpretation of sensor reading difficult due to the significantly higher thermal conductivity of ice to that of water.

Key words: negative pore-water pressure, freezing conditions, thermal conductivity, suction sensors.

Introduction

The negative pore-water pressures in a soil or soil suctions affect the moisture flow, volume change, shear strength and frost-heaving characteristics of a soil as it freezes. There is therefore a need for reliable techniques to measure negative pore-water pressures in a freezing environment. Various techniques are now available for measuring soil suction in unfrozen soils. Of these techniques, the thermal conductivity sensor appears to be one of the most promising devices. This paper evaluates the suitability of the thermal conductivity sensor, and other devices, for *in situ* suction measurements in a freezing environment.

Physics of the problem

As the temperature drops below 0°C, some soil water freezes producing ice in the soil. Let us consider the situation of a thermal gradient with the coldest temperature at the ground surface. Figure 1 (Konrad 1990) illustrates a

typical temperature gradient in a soil under freezing conditions. Water moves from the unfrozen zone to the frozen zone through a thin, partially frozen fringe. The frozen zone slowly advances to a greater depth below the ground surface.

The ability of water to move upward to the freezing fringe is attributed to the development of a negative pore-water pressure (suction) gradient through the frozen fringe as shown in Fig. 1 (Konrad 1990). The suction can be negligible in sands, but more significant in silts and clays depending on the temperature gradients and the rate of freezing (Williams 1982). The suction just below the frost front can range from 6 kPa in silt to 400 kPa in Leda clay (Williams 1967). The suction values in the frozen zone increases with decreasing temperatures below 0°C.

Water can exist in three phases as shown by a phase diagram (Fig. 2). The fusion curve, *OC*, is associated with the freezing and thawing processes. At a given temperature, *T*, ice and water can coexist under a specified pressure as determined by the fusion curve, *OC*. The slopes of the curves on the phase diagram in Fig. 2 are described by the Clausius-Clapeyron equation (Van Haveren and Brown 1972). For the fusion curve *OC*, the slope has the following relation:

$$[1] \quad \frac{dP}{dT} = -\frac{L}{Tv_w}$$

where:

dP = change in pressure,

dT = change in temperature,

L = latent heat of fusion which is the heat liberated when water turns to ice or the heat absorbed when ice turns to water (i.e., 333 kJ/kg),

D.G. Fredlund. Professor, Civil Engineering Department, University of Saskatchewan, 57 Campus Drive, Saskatoon, SK, Canada S7N 5A9.

J.K. Gan. Research Engineer, Civil Engineering Department, University of Saskatchewan, 57 Campus Drive, Saskatoon, SK, Canada S7N 5A9.

H. Rahardjo. Lecturer, School of Civil and Structural Engineering, Nanyang Technological Institute, Singapore, 2263.

Reproduced with permission from the *Session on Moisture Migration in Freezing and Thawing Soils*, Transportation Research Board, Transportation Research Record 1307, Washington, DC, January 1991. pp. 291-299.

Figure 1. Schematic description of a freezing system (after Konrad 1990).

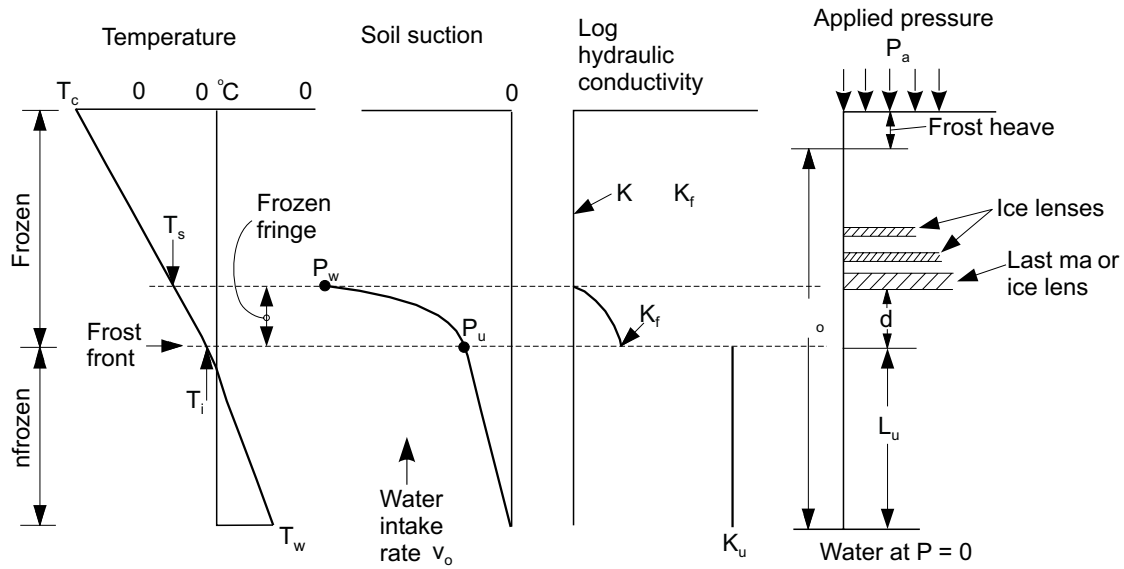
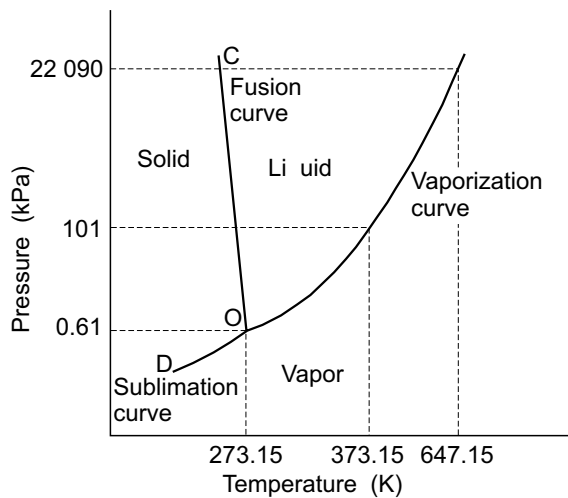


Figure 2. Phase diagram for water (not to scale); (after Van Haveren and Brown 1972).



T = temperature in degrees Kelvin, and
 v_w = specific volume of water (i.e., $1/\rho_w$ where:
 ρ_w = water density (1000 kg/m³)).

Equation [1] has commonly been used to calculate the suction developed in the freezing fringe. Williams (1982) defined the suction in the frozen soil as the difference between the ice and the pore-water pressures, $(u_i - u_w)$, where: u_i = ice pressure and u_w = pore-water pressure. The ice pressure, u_i , is usually assumed to be constant (e.g., atmospheric pressure or $u_i = 0$ gauge). This definition of suction is analogous to the matric suction definition in an unsaturated soil. The presence of suction results in a lower freezing temperature from that of the normal freezing temperature of 0°C or 273.15 K (Edlefsen and Anderson 1943). The suction in the frozen soil can be related to the lowering of the freezing temperature below 0°C (i.e., dT_0) using eq. [1].

$$[2] \quad \frac{d(u_i - u_w)}{dT_0} = -\frac{L}{T_0 v_w}$$

where:

T_0 = normal freezing temperature in Kelvin (i.e., 273.15 K or point 0 in Fig. 2), and
 dT_0 = freezing point depression, either in °C or K

Considering a constant ice pressure (i.e., $u_i = 0$) and rearranging eq. [2] yields an equation for the suction in the frozen soil:

$$[3] \quad d(-u_w) = -\frac{L}{T_0 v_w} dT_0$$

The $d(-u_w)$ term in eq. [3] refers to an increase in suction as the freezing temperature is lowered by dT_0 from 0°C. In other words, the suction increases as the temperature decreases below 0°C. Equation [3] together with typical experimental data are plotted in Fig. 3 (Williams 1982).

Relevant properties of partially frozen soils

Water in a porous medium, such as soil, does not all freeze at a single freezing temperature (Fig. 4), (Anderson and Morgenstern 1973). The freezing characteristics of the pore-water are dependent on many factors. Among these factors are: i) mineralogical composition, ii) specific surface area of soil solids, iii) surface forces, iv) osmotic potential of soil solution, v) grain size and grain size distribution, and vi) surface charged density. Generally, the smaller the particles, the greater the amount of unfrozen water present at any temperature below freezing (Fig. 4), (Anderson and Morgenstern 1973). As freezing progresses, it becomes increasingly more difficult to freeze the remaining water. The freezing point depression

Figure 3. Theoretical and experimental relationship between temperature and suction (at atmospheric pressure) (after Williams 1982).

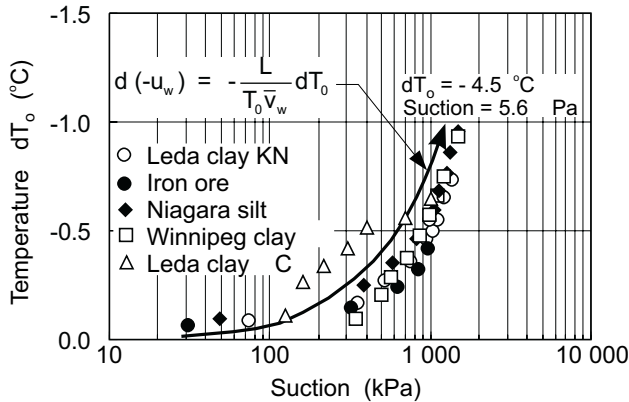
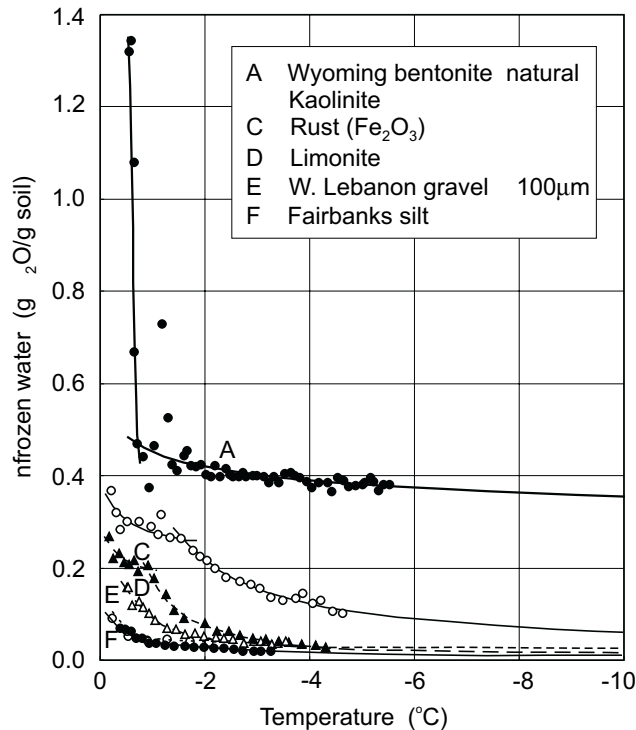


Figure 4. Variation of unfrozen water content with temperature for six representative soils and soils constituents (after Anderson and Morgenstern 1973).



is due to the increasing surface forces on the water as the freezing advances closer to the particle surface.

Thermal conductivity

In a soil, heat is transferred via direct conductivity, k . The thermal conductivity, k , of a soil is defined as the amount of heat that is transferred in a unit time through a unit length of the soil with a unit cross-sectional area under a unit temperature gradient. The thermal conductivities of the various constituents in a soil are different and must be combined to give the apparent thermal conductivity of the soil. As the proportions of the constituents

are changed, the apparent thermal conductivity of the soil will also change. Typical values of thermal conductivities of various constituents of a partially frozen soil are given in Tables 1, 2 and 3 (van Nijk 1963). For a given soil, the bulk density of the soil particles remains fairly constant. However, there are significant changes in the proportion of the frozen and unfrozen water contents as the water freezes.

The thermal conductivity of ice is approximately four times greater than that of water (Fig. 5). As the ice content in a soil increases, the unfrozen water content decreases. During freezing, it is anticipated that the apparent thermal conductivity of the soil will increase.

Heat capacity

The heat capacity of a soil refers to the quantity of heat that is required to raise the temperature of a unit mass of the soil by 1°C. The heat capacity of a partly frozen soil is simply the sum of the heat capacities of its constituents, including the latent heat of fusion that is required in the water-ice phase transformation when freezing occurs. The specific heat capacity, c , is the heat capacity of the soil expressed on a unit weight basis. Typical values of specific heat capacities of soil constituents are presented in Tables 1, 2 and 3 (van Nijk 1963).

Latent heat

The latent heat of fusion is the heat or energy that is required in a phase change (e.g., from a liquid phase to a solid phase or vice versa). For water, the latent heat of fusion, L , is 333 kJ/kg. This means that 333 kJ of heat is liberated when 1 kg of water turns to ice, or is absorbed when 1 kg of ice turns to water. The phase transformation takes place without any change in temperature. The latent heat of a soil is a function of its water content.

Thermal diffusivity

The thermal diffusivity, α , of a soil is given by

$$[4] \quad \alpha = \frac{k}{\rho c}$$

where:

- k = thermal conductivity,
- c = specific heat capacity, and
- ρ = density.

Thermal diffusivity controls the rate at which a temperature change spreads through a mass. The thermal conductivity of ice is approximately four times that of water. The specific heat capacity of ice is approximately half that of water. Consequently, the diffusivity of ice is about eight times the diffusivity of water. Therefore, in a frozen soil, temperatures can change faster and to a greater extent than in an unfrozen soil.

In a fine-grained soil, the water in the pores freezes gradually. Its latent heat is therefore released in stages (Fig. 6), (Johansen 1975). The rate of heat released reduces with decreasing temperatures. The result of a release in latent heat is a sudden change in the specific heat

Table 1. Thermal properties of soil constituents at 20°C and 1 atm (after Nijk 1963).

Material	Density, ρ (kg/m ³)	Specific heat, c (kJ/kg °C)	Thermal conductivity, k (W/m K)	Thermal diffusivity, α (10 ⁻⁷ m ² /s)
Quartz	2650	0.732	8.4	43
Many soil minerals*	2650	0.732	2.9	43
Soil organic matter*	1300	1.925	0.25	15
Water	1000	4.184	0.6	1.42
Air	1.2	1.004	0.026	0.21

*Approximate average values

Table 2. Physical properties of liquid water (after Nijk 1963).

Temperature, T (°C)	Density, ρ (kg/m ³)	Specific heat, c (kJ/kg °C)	Thermal conductivity, k (W/m K)	Latent heat of evaporation (kJ/kg)
-10	997.94	4.268	—	2523
-5	999.18	—	—	—
0	999.87	4.2150	0.561	2499
4	100.00	—	—	—
5	999.99	4.1995	0.574	2487
10	999.73	4.1894	0.596	2476
15	999.13	4.1832	0.595	2464
20	998.23	4.1790	0.603	2452
25	997.08	4.1769	0.611	2440
30	995.68	4.1756	0.620	2428
35	994.06	4.1752	0.628	2417
40	992.25	4.1756	0.632	2405
45	990.24	4.1765	0.605	2393
50	988.07	4.1777	0.645	2381

Table 3. Physical properties of ice (after Nijk 1963).

Temperature, T (°C)	Density, ρ (kg/cm ³)	Specific heat, c (kJ/kg °C)	Thermal conductivity, k (cal/cm s °C) (W/m K)	Latent heat of sublimation (kJ/kg)	Latent heat of fusion (kJ/kg)
-20	920	1.958	2.433	2836	289
-10	919	2.029	2.319	2835	312
0	917	2.105	2.24	2833	333

immediately below the temperature at which freezing begins (Fig. 7), (Low et al. 1968). The latent heat acts similarly to a large sink where heat is released or absorbed without any change in temperature. This sudden change in the specific heat causes a corresponding sudden change in the diffusivity (e.g., Fig. 8), (Hoekstra 1969).

Suction measurement techniques

Several techniques are available for suction measurements in an unfrozen soil. These techniques include: i) tensiometers, ii) psychrometers, iii) filter paper methods, and iv) thermal conductivity sensors. Some of these techniques have also been used for frozen soils. The psychrometric and filter paper techniques do not require intimate contact with the soil. The other techniques require the use of a porous medium in intimate contact with the soil and allowing the suction in the medium to come

to equilibrium with the suction in the soil. Water in the porous medium has different freezing characteristics from the water in the soil. Under sub-zero temperatures, the different freezing characteristics may present some problems in obtaining accurate suction measurement.

Tensiometers

Tensiometers have commonly been used to measure the negative pore-water pressures in an unsaturated soil. The tensiometer consists of a porous ceramic, high air-entry cup connected to a pressure measuring device through a small bore capillary tube. The tube and the cup are filled with de-aired water. The cup can be inserted into a pre-cored hole until there is intimate contact with the soil. After equilibrium has been achieved, the water in the tensiometer will have the same negative pressure as the pore-water in the soil. The water pressure that can be

Figure 5. Thermal conductivity of ice and water at various temperatures.

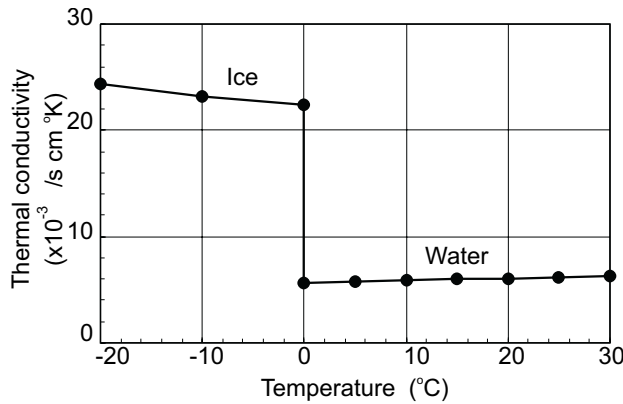
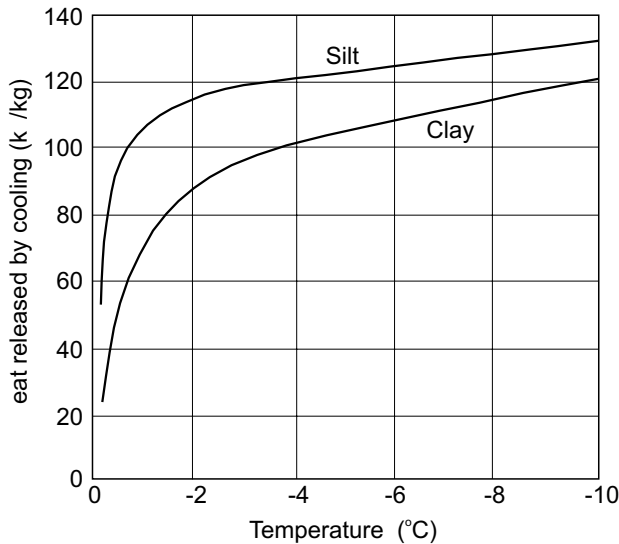


Figure 6. Latent heat released on cooling below 0°C (after Johansen 1976).



measured using a tensiometer is limited to approximately negative 90 kPa due to cavitation of water in the tensiometer.

Ingersoll and Berg (1981) have used tensiometers for measuring negative pore-water pressures under freezing conditions. The tensiometer cups were installed along a cylindrical soil column 1 m long and 14 cm diameter. The tensiometer tube was filled in with a solution of ethylene glycol and water to lower the freezing point of the tensiometer fluid. The soil suctions increased as the temperature decreased below 0°C. Typical results are plotted in Fig. 9 (Ingersoll and Berg 1981), along with the corresponding temperatures. The results indicate a distinct increase in soil suction with a decreasing temperature below 0°C.

Psychrometers

Thermocouple psychrometers are used to measure soil suction by measuring the relative humidity in the soil. Soil suction results in a decrease in the relative humidity. Measurements of soil suction are commonly conducted in

Figure 7. Relationship between heat capacity and temperature of a partially frozen bentonite (after Low et al. 1968).

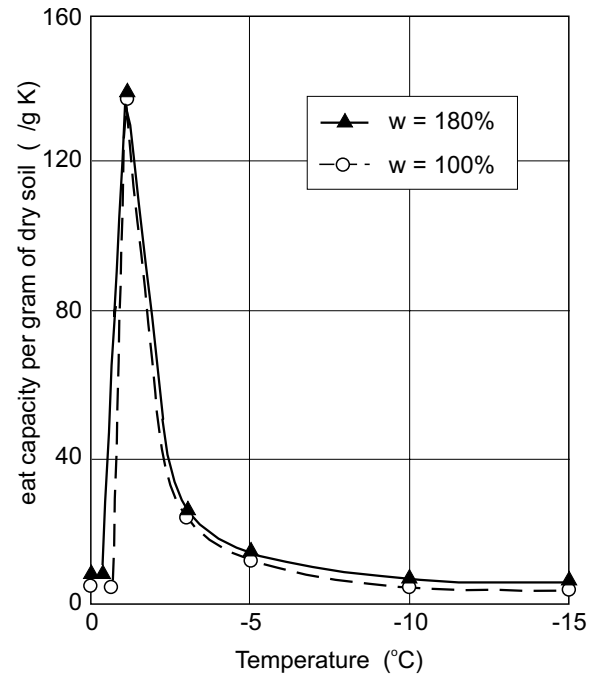
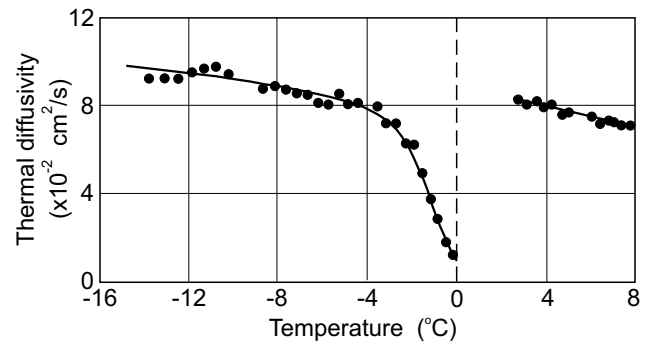


Figure 8. Variation of thermal diffusivity with temperatures for a kaolinite suspension (after Hoekstra 1969).



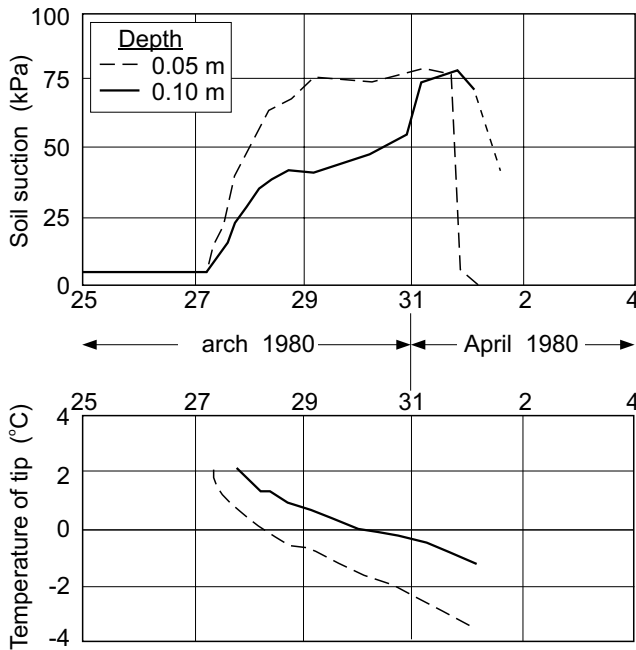
the laboratory by placing a small soil specimen in a chamber together with the psychrometer. The relative humidity is then measured after equilibrium is attained between the air near the psychrometer and the pore-air in the soil. The suction range that can be reliably measured by psychrometers in a controlled temperature environment is from 100 kPa to 8000 kPa.

The authors are not aware of the use of psychrometers in the measurements of soil suction in a freezing environment. However, psychrometers have been used to measure relative humidity (and therefore suction) in snow (van Haveren 1972). The results indicate a reduction in the relative humidity with decreasing temperatures below 0°C.

Filter paper technique

The authors are unaware of any attempts to use the filter paper technique to measure soil suction under frozen conditions. The vapour pressure associated with ice

Figure 9. Suction measurements using tensiometers in a freezing environment (after Ingersoll and Berg 1981).



would lead one to believe that there may be some possibilities in using this technique for frozen soils. Research is needed in this area.

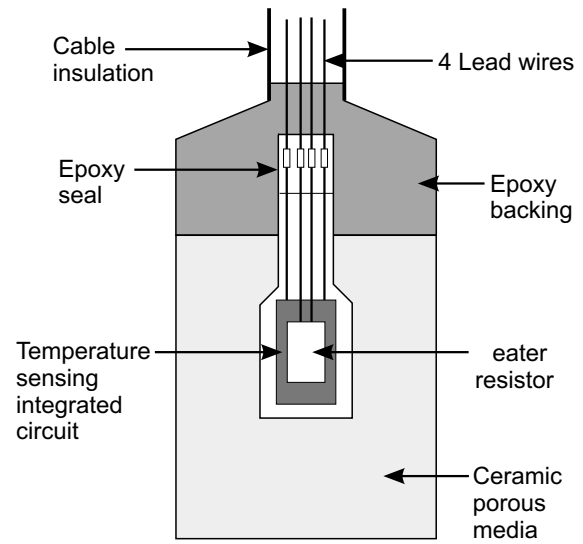
Thermal conductivity sensor

The operation of a thermal conductivity sensor is based on the principle of heat dissipation in a porous material. The rate of heat dissipation is dependent on the: i) thermal conductivity of the solid material and of the water, and ii) the mass of the solid and the water. The thermal conductivity of air can be considered negligible. For a particular sensor, the mass of the solid is a constant, and the rate of heat dissipated in the solid will be constant. Therefore, changes in the rate of heat dissipated in a sensor are directly related to the water content of the sensor.

When a sensor is inserted into a soil, water will move between the sensor and the soil. The movement of water takes place until stress equilibrium is attained between the soil and the sensor. The equilibrium water content of the sensor is an indication of the suction in the sensor and in the soil. The water content of the sensor can be calibrated against the applied suction using a modified pressure plate apparatus (Fredlund and Wong 1989).

A typical sensor is made up of two parts: i) a heating and heat sensing device enclosed within ii) a porous block (Fig. 10). The heater and the sensing devices are embedded within a porous ceramic of low thermal conductivity. The porous ceramic should be relatively small in order to ensure a rapid response. However, the porous ceramic must be sufficiently large so that the heat pulse generated is fully contained within the ceramic block,

Figure 10. A cross-sectional diagram of the AGWA-II thermal conductivity sensor.



otherwise the thermal conductivity reading will be affected by the type of the surrounding soil.

The reading operation consists of measuring the electrical output (current or voltage) before the heat pulse and the electrical output at a definite time lapse after the heat pulse. The change in voltage output is a function of the electrical resistance, which in turn is a function of the temperature rise. The heat pulse is a precisely controlled amount of heat applied at a fixed rate. The voltage outputs varies linearly with temperature, and therefore the difference is not affected by the temperature of the sensor. A single calibration is therefore adequate for all temperatures.

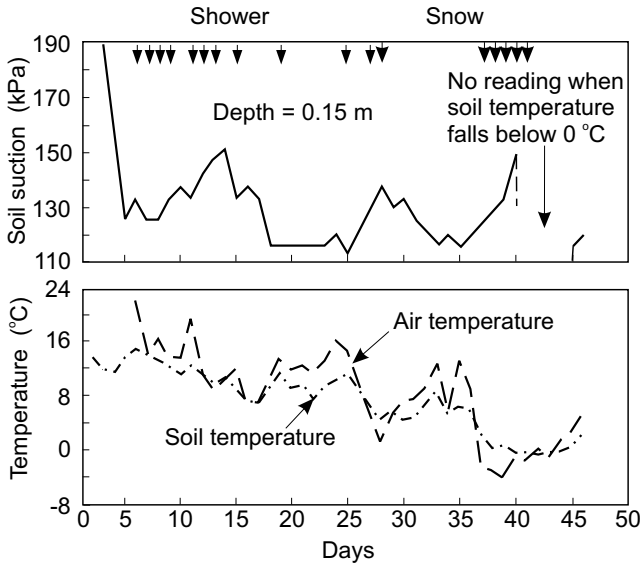
In an unfrozen soil, a low water content in the sensor, or high soil suction, would result in a high temperature rise in the thermal conductivity sensor. The high temperature rise indicates a low apparent thermal conductivity of the sensor due to its low water content. In a frozen, or partially frozen soil, the thermal conductivity of the sensor is not only a function of the unfrozen water content, but is also dependant upon the ice content. At a low unfrozen water content, the temperature rise recorded by the sensor would be expected to be low due to the high thermal conductivity of ice.

Results of suction measurements using thermal conductivity sensors

Lee (1983) used heat dissipation sensors (MCS 6000 sensors)¹ for both *in situ* and laboratory suction measurements. The results of *in situ* suction measurements conducted in a glacial till are presented in Fig. 11 (Lee 1983). The results show that suction variations closely followed the daily temperature variation. The soil suction increased as the temperature approached 0°C. When the

¹Manufactured by Moisture Control System Corporation, Findlay, OH.

Figure 11. Field measurements of matric suction in a glacial till using the MCS 6000 thermal conductivity sensors (after Lee 1983).



temperatures dropped below 0°C, the sensor was not able to record any suction reading.

Van der Raadt et al. (1988) used AGWA-II thermal conductivity sensors² for monitoring suction changes below railway subgrades. Results of suction measurements using the AGWA-II sensors from one site are presented in Fig. 12 (van der Raadt et al. 1988). The results also show that the suction readings increased as the temperature decreased below freezing. Several suction measurements were obtained for the soil in the frozen state.

Recent experience with the AGWA-II sensor in a freezing environment

Suction measurements have recently been made in a freezing environment at the University of Saskatchewan. The measurements were made using AGWA-II thermal conductivity sensors. A soil column was prepared by compacting a glacial till into a PVC cylinder.

The cylinder had a height of 300 mm and a diameter of 150 mm. A thermal conductivity sensor together with a thermocouple were embedded near the top, middle and bottom sections of the soil column (Fig. 13). The thermocouple was used to measure the temperature in the soil at the proximity of each thermal conductivity sensor. The column was insulated on all sides except for the top face. The top of the column was subjected to temperatures ranging from 22°C down to minus 20°C inside a freezing chamber.

The suction and temperature measurements with respect to time are presented in Figs. 14, 15 and 16. All three sensors appeared to respond in a similar manner. As the temperature decreased from above freezing to below

Figure 12. Variation of soil suction with time of year for various depths of Regina clay in Saskatchewan (after van der Raadt 1988).

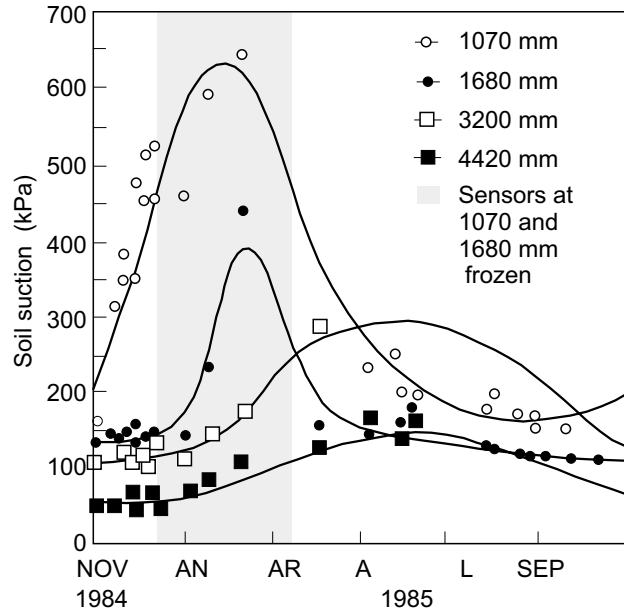
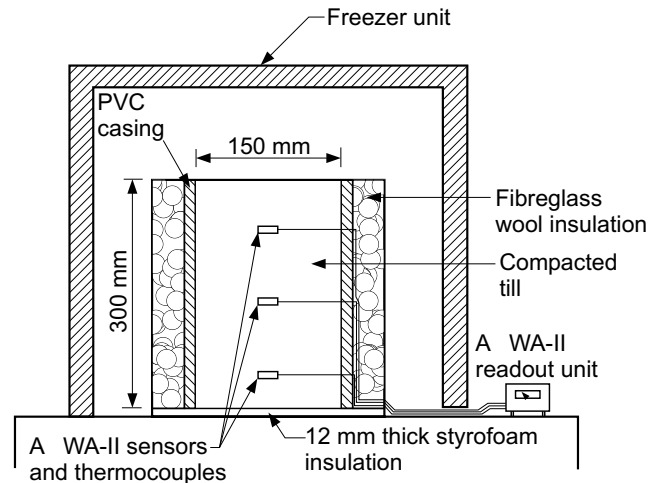


Figure 13. Set-up for Soil Suction measurements using the AGWA-II sensor in a freezing test.



freezing, the sensor readings dropped sharply and then increased rapidly to approximately the same readings. The same behaviour was observed as the temperature was increased from below freezing to above freezing. All three sensors showed that after thawing, the soil suctions dropped to a range of 0 to 40 kPa.

Interpretation of test results

The apparent thermal conductivity of the sensor is affected by the latent heat of fusion as the water in the sensor begins to freeze. During the freezing process, the

²Manufactured by Agwatronics Incorporated, Merced, CA.

Figure 14. Suction and temperature measurements at the top section of the soil column.

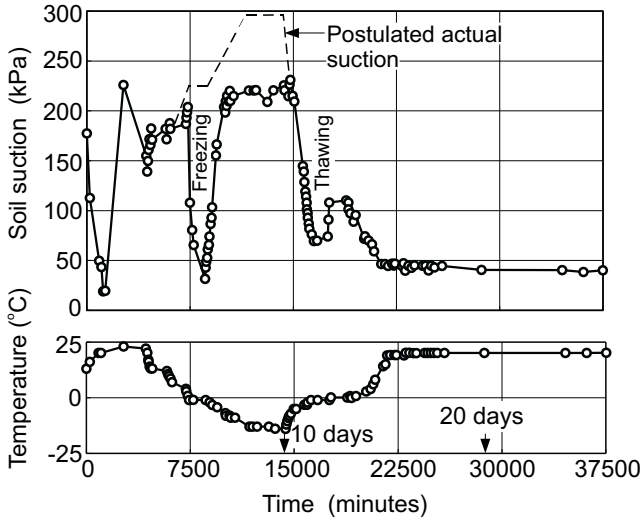
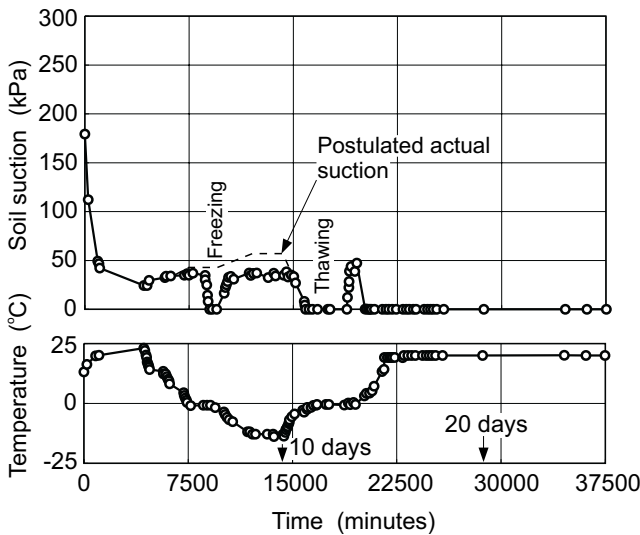


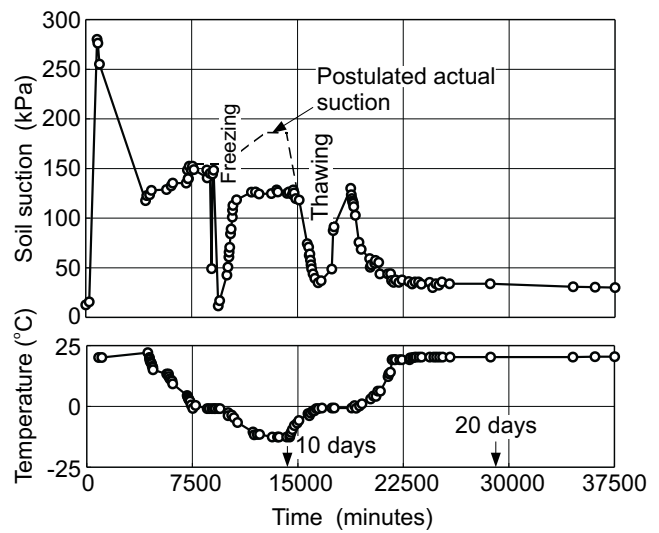
Figure 15. Suction and temperature measurements at the middle section of the soil column.



latent heat of fusion is released in stages at a constant temperature (Fig. 6). This is because the water in the sensor does not freeze simultaneously, but rather, it freezes in a gradual manner. During the freezing process, the heat capacity of the porous ceramic sensor peaks sharply as illustrated in Fig. 7. An increase in the heat capacity means a lower temperature rise for the same heat pulse. As a result, the temperature rise produced by the heat pulse will be smaller in a freezing sensor as compared to that registered in a non-freezing sensor.

The above phenomenon can be attributed to the tendency of the water to maintain a constant temperature during the phase transformation. The reduced temperature rise in a freezing sensor would then be interpreted from the calibration curve as a decreasing soil suction. This situation is demonstrated by the drop in soil suction readings as the temperature decreases to 0°C.

Figure 16. Suction and temperature measurements at the bottom section of the soil column.



After a major portion of the water in the sensor has frozen, the temperature rise measured due to the heat pulse depends upon the proportion of ice and unfrozen water, and also on the quantity of air bubbles which may be present. The higher sensor readings in the frozen state are probably due to the reduced thermal conductivity caused by the presence of air bubbles.

As the water in the sensor begins to thaw, the heat pulse released in the sensor is again affected by the latent heat of fusion. During the thawing process, the latent heat of fusion is adsorbed at a constant temperature. The thawing process also occurs gradually within the sensor. During the thawing process, the heat capacity of the porous ceramic sensor increases rapidly (Fig. 7) causing a lower temperature rise in response to the same heat pulse. In other words, the tendency to maintain a constant temperature will again reduce the temperature rise generated by the heat pulse. As a result the suction readings will drop again as the temperature increases towards 0°C.

During the freezing and the thawing processes (i. e., the phase transformation stage at around 0°C) the thermal diffusivity of the porous ceramic sensor will depend on the ice and water contents in the sensor. The thermal diffusivity, α , is expressed in eq. [4]. An increase in the heat capacity will result in a decrease in the thermal diffusivity. At the same time the higher thermal conductivity of ice will cause an increase in the thermal diffusivity of the freezing soil. The net effect of the changes in the heat capacity and the thermal conductivity on the thermal diffusivity is not known. A change in the thermal diffusivity will determine the change in the rate of temperature change. It is the lower temperature rise due to the increase in the heat capacity, however, that is predominant during the phase transformation stage.

The reduction in the sensor reading after a complete thawing of the ice, may be due to the following phenomenon, the porous ceramic sensor is not prone to change in volume upon freezing. The soil, however, tends to change

in volume upon freezing. The volume of the soil may increase or decrease depending upon the suction, as the suction increases the soil volume may decrease and the soil will shrink away from the sensor. As the suction decreases, the soil volume may increase. In addition, there are also volume changes associated with the formation of ice. At the end of the test, the soil column was found to have expanded vertically by approximately 5 mm. A gap was also discovered between the soil and the sensor. This gap was especially noticeable in the top section of the specimen. It appears, therefore, that there is a tendency for the soil to separate from the sensor after a cycle of freezing and thawing. Once the sensor has separated from the soil, the sensor will register a suction reading depending upon the remaining water content of the sensor.

Conclusion

Experimental evidence presented in the paper has identified the difficulties associated with the measurement of negative pore-water pressures in freezing soils. In particular, the emphasis is on the use of thermal conductivity sensors in freezing environments. Distinct drops in suction readings have been observed during the freezing and thawing processes. These drops are attributed to the effect of the latent heat of fusion on the thermal conductivity measurements. As a result, the sensor readings are difficult to interpret and convert to soil suctions. In addition, the rigid and brittle ceramic used for the thermal conductivity sensors is susceptible to cracking due to expansion on freezing, especially under high water content conditions.

References

- Anderson, D. M., and Morgenstern, N.R. 1973. Physics, chemistry and mechanics of frozen ground: A review. Proceedings, 2nd International Conference on Permafrost, Yakutsk, USSR, North American Contribution, US National Academy of Sciences, pp. 257–288.
- Edlefsen, N. E., and Anderson, A.B.C. 1943. Thermodynamics of Soil Moisture. *Hilgardia*, **15**(2): 31–298.
- Fredlund, D.G., and Wong, D.K.H. 1989. Calibration of thermal conductivity sensors for measuring soil suction. *Geotechnical Testing Journal*, **GTJODJ**, **12**(3): 188–194.
- Hoekstra, P. 1969. The physics and chemistry of frozen soils: Effects of temperature and heat on engineering behaviour of soils. *In Highway Research Board, Special Report 103*, pp. 78–90.
- Ingersoll, J., and Berg, R. 1981. Simulating frost action by using an instrumental soil column. *In Frost Action and Risk Assessment in Soil Mechanics*, Transportation Research Record 809, pp. 34–42.
- Johansen, O. 1975. Thermal conductivity of soils. Ph.D. thesis, (CRREL Draft Translation 637, 1977), Trondheim, Norway.
- Konrad, J. M. 1990. Segregation potential - pressure - salinity relationships, near thermal steady state for a clayey silt. *Canadian Geotechnical Journal*, **27**(2): 203–215.
- Lee, R.K.C. 1983. Measurement of soil suction using the MCS 6000 sensor. M.Sc. thesis, University of Saskatchewan, Saskatoon, SK, Canada.
- Low, P.F., Anderson, D.M., and Hoekstra, P. 1968. Some thermodynamic relationships for soils at or below the freezing point: 1. Freezing Point Depression and Heat Capacity. *Water Resources Research*, **4**(2): 379–394.
- van der Raadt, P. 1988. Field measurement of soil suction using thermal conductivity matric potential sensors. M.Sc. thesis, University of Saskatchewan, Saskatoon, SK, Canada.
- van Haveren, B.P. 1972. Measurement of relative vapour pressure in snow with thermocouple psychrometers. *In Psychrometry in Water Relations Research. Proceedings, Symposium on Thermocouple Psychrometers. Edited by R.W. Brown, and B.P. van Haveren.*, Utah State University, pp. 178–185.
- van Haveren, B.P., and Brown, R.W. 1972. The properties and behaviour of water in the soil-plant-atmosphere continuum. *In Psychrometry in Water Relations Research. Proceedings, Symposium on Thermocouple Psychrometers. Edited by R.W. Brown, and B.P. van Haveren.*, Utah State University, pp. 1–27.
- van Nijk, W.R. 1963. *Physics of Plant Environment*, North Holland Publishing. Co., 2nd edition.
- Williams, P.J. 1967. Properties and behaviour of freezing soils. *Norwegian Geotechnical Institute Publication*, Vol. 72.
- Williams, P.J. 1982. *The surface of the earth: An introduction to geotechnical science*. Longman, New York.

Direct measurement of high soil suction

Y. Guan and D.G. Fredlund

Abstract: A tensiometer-type suction probe was developed to directly measure soil suctions greater than 100 kPa. Cavitation was prohibited by cyclically pre-pressurising the water in the suction probe to high pressures of 12,000 kPa. Tests using the axis-translation technique showed that the suction probe was accurate and rapid in response to changes in negative pore-water pressures as low as -500 kPa. Measurements performed on various types of soils indicated that the suction probe was able to measure matric suction up to 1000 kPa with satisfactory accuracy. Variations were observed between the measurements of matric suction on a compacted glacial till, using the suction probe, filter paper method, null-pressure plate, and thermal conductivity sensor. The suction probe appeared to be the most accurate of all these techniques. Difficulties were encountered in measuring soils with a degree of saturation less than 40%, however.

Key words: tensiometer, suction probe, high pressure, negative pore-water pressure, matric suction, thermal conductivity.

Introduction

Measurements of soil suction are necessary for the solution of various geotechnical problems involving unsaturated soils. Typical engineering problems are those associated with slope stability, soil swelling and shrinking, soil collapsing, seepage, lateral earth pressures, and soil compaction. Analyses of these so called "problematic" soils (i.e., swelling soils, collapsing soils, residual soils, and soft clays) are dependent upon the appropriate assessment of soil suction.

Water is normally thought to have little tensile strength and will cavitate at a negative pressure of about -100 kPa. Consequently conventional tensiometers are limited to a direct measurement of soil suction less than 100 kPa. Under some conditions, however, the tensile strength of water has been measured by physicists to be greater than several atmospheres (Knapp et al. 1970, Trevena 1987). Applications of the tensile strength of water have been quite scarce. This paper reports direct measurement of high soil suction using the tensile strength of the water in a tensiometer-type suction probe. The suction probe was used to measure matric suctions in various types of soils. The measurements using the suction probe were compared with the measurements using filter paper method, null-pressure plate technique, and thermal conductivity sensor.

Background

The tensile strength of water is the tensile stress at which the liquid water cavitates or ruptures. The tensile stress in ordinary liquid water is generally thought of as being equal to the vapour pressure minus hydrostatic pressure. Historical tests on the tensile strength of water may be classified into several distinct approaches used for applying a tensile stress to liquid water (Guan 1996). These approaches include thermal contraction methods, superheating methods, hydrostatic methods, and dynamic methods. Thermal tests conducted by Jones et al. (1981) measured tensions greater than 500 kPa using a transducer. Tensions up to 1,450 kPa were also directly measured by Sedgewick and Trevena (1976) using piezoelectric transducers in a dynamic stressing test.

The mechanism of cavitation is generally explained using a gas-trapping model (Harvey et al. 1947). According to this model, pre-pressurisation of a water-container system can effectively remove a significant portion of the potential cavitation nuclei and increase the ability of the system to resist cavitation (Apfel 1970, Winterton 1977).

Little attention has been given to how long the tensile strength of water can be sustained. Vincent (1941) and Winterton (1977) measured high tensions that were sustained for only a few minutes. Henderson and Speedy (1980) reported a tension of 10,000 kPa that was sustained for over a week. Methods used by physicists for measuring high tensions in water, on the other hand, are not adaptable for the measurement of soil suction. Gilbert (1960) attempted to measure high tensions in sucrose solutions in a triaxial cell, based on a primitive concept of the tensile strength of water. Ridley (1993) pre-pressurised a small volume of water in a tensiometer-type device and measured matric suctions up to 1,500 kPa. More recent studies have shown that the tensile strength of the water in a small chamber can be significantly increased and is fundamentally useful for the direct measurement of high soil suction (Guan 1996).

Y. Guan. Graduate Student, Department of Civil Engineering, University of Saskatchewan, 57 Campus Drive, Saskatoon, SK, Canada S7N 5A9.

D.G. Fredlund. Professor, Department of Civil Engineering, University of Saskatchewan, 57 Campus Drive, Saskatoon, SK, Canada S7N 5A9.

Reproduced with permission from the *Proceedings, 3rd Brazilian Symposium on Unsaturated Soils, NSAT'97*, Rio de Janeiro, April 21–25, 1997, Vol. 2.

Equipment and methods

The developed suction probe consisted of a high pressure transducer and a stainless steel shroud which was precisely machined to envelope the transducer (Fig. 1). The sensing area was a smooth, circular surface with a diameter of 7.0 mm. A 15 bar ceramic disk was fitted into the shroud. A small volume of water was contained between the ceramic disk and the transducer diaphragm.

A pressurisation system was built to pre-pressurise the water in the suction probe. An early study indicated that 6 cycles of pressurisation produced the maximum sustainable tension (Guan 1996). Each cycle includes the application of a positive pressure of 12,000 kPa for 1 hour, followed by a negative pressure of -85 kPa for 1 hour. The sustainable tension appeared to be related to the characteristics of the used ceramic disk. The highest tension measured using the probe was about 1250 kPa.

Accuracy and response time of the probe

The accuracy and response time of the suction probe subjected to high tensions were tested in a modified pressure plate, using the axis-translation technique. The experimental set-up is illustrated in Fig. 2. A soil specimen was placed onto the 5 bar ceramic disk at the bottom of the pressure cell. The suction probe was placed on the soil. A brass block was placed over the probe to ensure good contact between the probe and the soil and to maintain a constant humidity within the cell. Air pressure was applied to the cell to force the water in the soil to flow out through the 5 bar ceramic disk. When equilibrium was attained, a matric suction equal to the applied air pressure should exist in the soil. If the air pressure was released to zero (i.e., atmospheric pressure), a negative pore-water pressure, which is numerically equal to the pre-applied air pressure, should be simultaneously established in the soil water, and should be measured by the suction probe. Air pressures equal to 200, 300, 400, and 500 kPa were subsequently used.

Measurement of soils with pre-applied matric suctions

Matric suctions ranging from 150 up to 550 kPa were applied to soil specimens in a pressure plate. The probe was used to measure the matric suction in the specimens. Aluminum foil and electric tape were used to cover the specimen to reduce moisture loss due to evaporation.

Comparison with other conventional methods

A comparison study was made of suction measurements using the suction probe, filter paper method, null-pressure plate method, and thermal conductivity sensor.

Schleicher and Schuell No. 589 White Ribbon filter paper was used following the ASTM procedure (D5298 - 92). A set of three filter papers were placed between two soil specimens which were compacted at the same water content and the same dry density. Matric suction of the soil specimen was obtained from the water content of the middle filter paper, based on the calibration curve recommended by ASTM (D5298 - 92) for Schleicher and

Fig. 1. The construction of the suction probe.

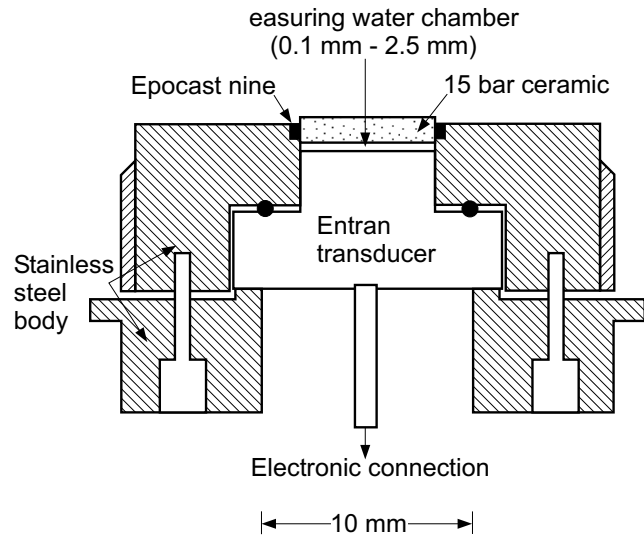
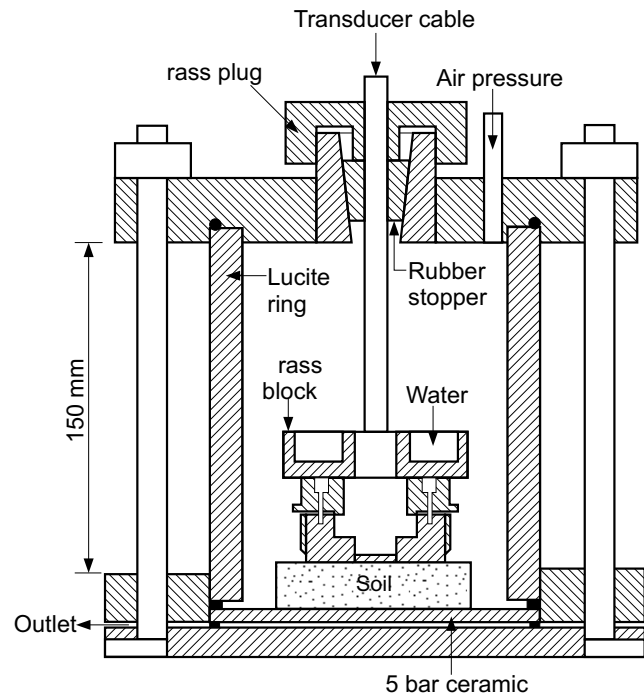


Fig. 2. The modified pressure plate for testing the suction probe for negative pressures.



Schuell No. 589 White Ribbon filter paper. Measurements were repeated on a number of soil specimens.

Following the filter paper measurement, each soil specimen was placed over a saturated 5 bar ceramic disk in a pressure plate cell. "Null flow" condition was obtained by adjusting the magnitude of the applied air pressure. Matric suction in the specimen was assumed to be equal to the applied air pressure at equilibrium.

Matric suction of each specimen was next measured using the new suction probe. A small amount of wet clay

paste was applied between the soil and the suction probe to improve soil-ceramic contact.

The thermal conductivity sensors used in this study were 28 mm long and 20 mm in diameter. The sensors had a rigid structure and a stable response. Variations in thermal conductivity among the sensors were relatively small. The sensors, however, had a poor sensitivity for matric suctions above 150 kPa.

Soil materials

Reconstituted specimens of a plastic clay and a fine silt were used to evaluate the performance of the suction probe for measuring soil suction. The clay specimen remains saturated at a suction less than 700 kPa. The prepared silt specimen de-saturates at a matric suction of less than 10 kPa and reaches the residual water content at a suction of about 300 kPa.

A compacted glacial till was used for the comparative study between measurements using the suction probe and several other conventional techniques. Five compaction densities and water contents were selected for preparing glacial till (Table 1). All five water contents were near or on the dry side of optimum. The soil was statically compacted in three layers to form specimens of 101 mm in diameter and 20 mm in height. Matric suction of each specimen was determined using filter paper, null-pressure plate, and the new suction probe in sequence. Matric suction measurements using the thermal conductivity sensor required a separate soil specimen which must be at least 40 mm long.

Results and discussions

Testing the suction probe for negative pressures

Figure 3 shows the changes in water pressure with time, from a test on a clay specimen, using the suction probe. When an air pressure of 200 kPa was applied to the pressure chamber, the probe recorded an instantaneous increase in water pressure from 0 to 195 kPa. The water pressure gradually reduced to about 25 kPa after 42 hours. The pressure registered by the probe did not return to zero pressure. This was likely due to the slow rate of soil water flow out of the pressure chamber under a small pressure gradient reducing the air pressure from 200 kPa to 0 kPa caused the water pressure to immediately fall below zero and a reading of -158 kPa was obtained. The reduction in air pressure (i.e., -200 kPa) was approximately equal to the reduction in water pressure (i.e., -183 kPa). The water pressure registered by the probe gradually increased because the water below the 5 bar ceramic disk of the pressure plate slowly flowed into the soil. When the water pressure reached -151 kPa, an increase in air pressure to 300 kPa produced an instantaneous jump of water pressure to about 145 kPa, an increase of 296 kPa.

Further tests also showed that a change in air pressure in the pressure chamber instantaneously produced an approximately equal amount of change in water pressure in the suction probe. The difference between the change in

Table 1. Densities and water contents for glacial till.

Water content (%)	Dry density (Mg/m ³)	Degree of saturation (%)
16.3 (optimum)	1.80	86.5
15.0	1.78	77.2
13.0	1.73	61.3
11.5	1.66	48.7
11.0	1.61	43.1

air pressure in the pressure chamber and the change in water pressure in the suction probe was generally less than 5%. When the air pressure in the pressure chamber was reduced from 500 kPa to zero, the water pressure in the suction probe immediately from 44 kPa to -443 kPa, a change of 487 kPa. The clay remained saturated during the test period.

Similar results were also obtained from the test on a silt specimen (Fig. 4). These tests indicate that the suction probe is accurate and the response time to a change in the external tension is only a few seconds. The quick response of the suction probe is attributed to the high degree of saturation and the rigidity of the measuring chamber of the probe.

The above results also justify the extrapolation of calibration of the transducer from positive to negative pressures. The principle of the axis-translation technique has been proven to be valid for negative pressures as low as -500 kPa.

Measurement of pre-applied matric suctions

Figure 5 shows the results of measurements of matric suction in a clay specimen using the new suction probe. The pre-applied matric suctions varied from 150 to 550 kPa in increments of 50 kPa. The recorded curves were in good agreement with the pre-applied matric suctions up to 450 kPa. The recorded negative pressures for pre-applied matric suctions of 500 and 550 kPa developed much slower. This could be due to the occurrence of a tension crack in the central part of the clay specimen when the pre-applied matric suction exceeded 450 kPa. The presence of the crack, however did not appear to influence the matric suction reading at equilibrium.

Figure 6 gives the results of measurements of matric suction on silt specimens. There was an apparent drift in the recorded tension when the pre-applied matric suction exceeded 300 kPa. A matric suction of 300 kPa corresponds to a degree of saturation of about 38% for the silt specimen. The drift was attributed to moisture loss due to evaporation from both the soil and the suction probe during measurement over which a tension can be sustained in the suction probe did not appear to be dependent on the magnitude of the tension.

Figure 7 shows three measurements of matric suction on reconstituted silt and Regina clay specimens. Pre-applied matric suctions of 300 kPa, 350 kPa, and 550 kPa were used. The results show that tensions in the probe can be sustained for at least 72 hours. The duration over which a tension can be sustained in the suction probe did

Fig. 3. Testing the probe for negative pressure in clay using the axis-translation.

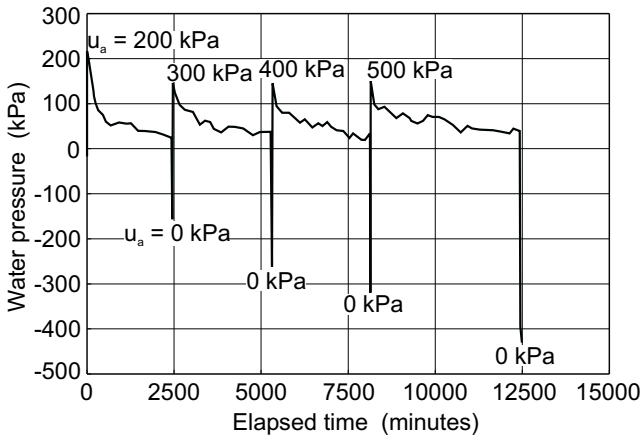
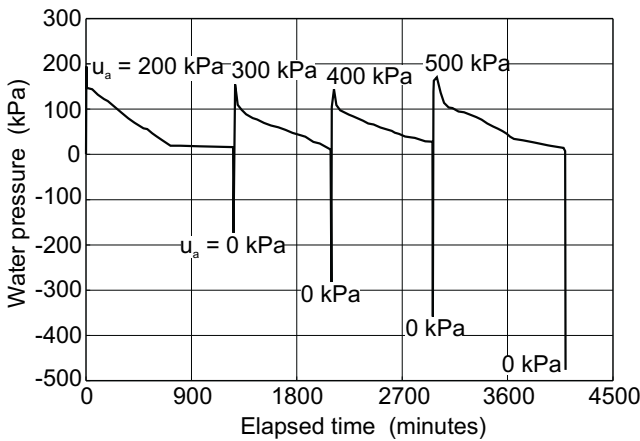


Fig. 4. Testing the probe for negative pressure in silt using the axis-translation.



not appear to be dependent on the magnitude of the tension.

Comparison with other methods

Figure 8 shows measurements obtained using the suction probe and filter paper method. Each data point for the suction probe method is the mean value of measurements on two specimens at the same water content. The determination of equilibrium was difficult for the till specimens prepared at 43.7% saturation. Figure 9 shows the measurements obtained using the suction probe, null-pressure plate, and thermal conductivity sensor. The results indicated that the measurements of matric suction were reproducible except for the filter paper method.

The filter paper method gave measurements close to the values obtained using the suction probe for matric suctions less than 200 kPa. As the soil became drier, the filter paper generally gave lower and more widely scattered values. Similar conclusions were also obtained by Ridley (1993). The low values from the filter paper method probably are a result of equilibrium not being achieved in seven days, particularly for soils at low degrees of saturation. Deka et al. (1995) suggested that

Fig. 5. Matric suction measurements on clay.

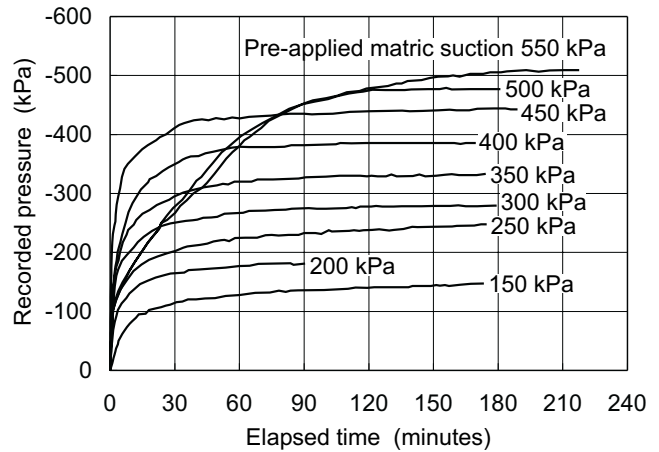


Fig. 6. Matric suction measurements on silt.

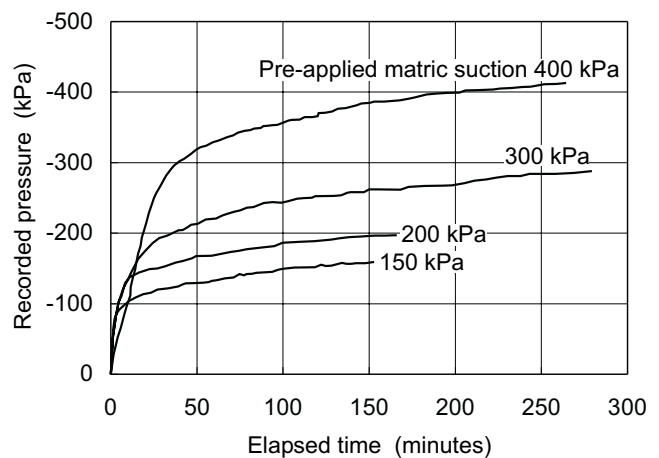
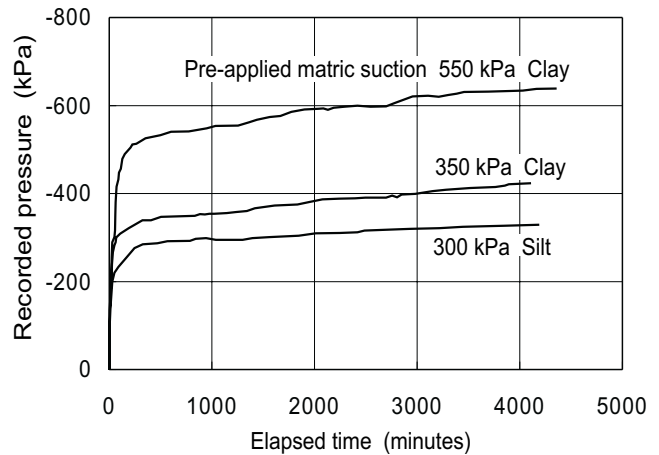


Fig. 7. Matric suction measurements on silt and clay.



equalisation periods longer than seven days are required for dry soils when using the filter paper method.

The thermal conductivity sensor produced measurements which are relatively close to the suction probe measurements for matric suctions less than 100 kPa. The

Fig. 8. Matric suction measurements on glacial till using the probe and filter paper.

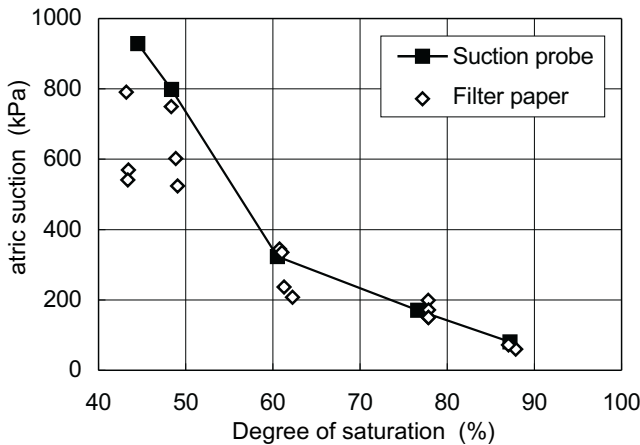
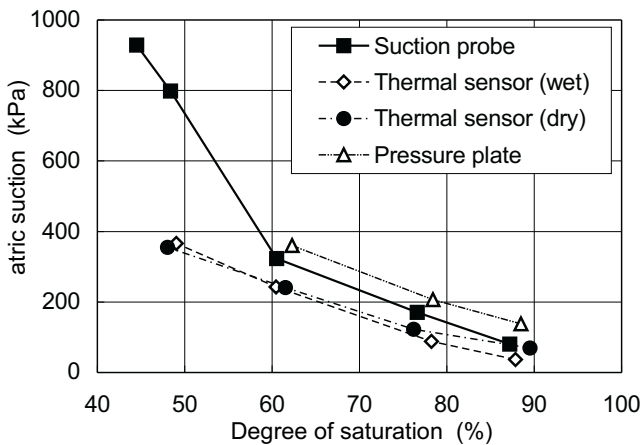


Fig. 9. Matric suction measurements on glacial till using the probe, pressure plate and thermal conductivity sensor.



thermal conductivity sensor, either initially dry or wet, appeared to under-estimate the matric suction at values exceeding 100 kPa.

The null-pressure plate gave higher values of matric suction than the suction probe, particularly for soils with a degree of saturation higher than 75%. The difference, however, became less significant when the degree of saturation was less than 60%. The higher matric suction measured using the pressure plate method, particularly for soils with a high degree of saturation, was also found by Madsen et al. (1986), and Campbell (1988). The primary reason for the higher matric suction measurements using the null-pressure plate may be due to occluded air bubbles in the soil water. Theoretical analysis made by Bocking and Fredlund (1980) indicated that occluded air bubbles in a soil can result in an over-estimation of matric suction when using the null-pressure plate technique. Soils near or above the optimum water content (i.e., degree of saturation above 80%) usually contain occluded air bubbles and the axis-translation may produce significant errors in the suction measurement.

Conclusions

The newly developed suction probe is suitable for measuring matric suctions up to 1000 kPa in both saturated and unsaturated soils with satisfactory accuracy. The principle of the axis-translation technique was proved to be correct for negative pore-water pressures as low as -500 kPa.

The suction probe is most suited to soils for which evaporation from the probe is less pronounced during the measurement process. These soils include wet clayey-type soils, and other soils with a relatively high degree of saturation. Difficulties were encountered in measuring soils with a degree of saturation less than 40%.

Reasonable agreements were observed between measurements using the suction probe, and those using the filter paper method and the thermal conductivity sensor for soils with a relatively high degree of saturation of the soil. The discrepancies in the measurements using the suction probe, the filter paper and the thermal conductivity sensor became more pronounced with decreasing degree of saturation. The null-pressure plate gave higher values of matric suction than the suction probe for soils near or above the optimum water content. The discrepancies in the measurement using the suction probe and the null-pressure probe became relatively smaller as the degree of saturation of the soil was reduced.

A soil-water system provides an excellent system for studying the behaviour of water subjected to high tensions. It appears that a tension in water can be sustained for a relatively long period of time.

References

- Apfel, R.E. 1970. The role of impurities in cavitation-threshold determination. *The Journal of the Acoustical Society of America*, **48**: 1179–1186.
- ASTM 1992. Standard test method for measurement of soil potential (suction) using filter paper (D5298–92). *In Annual book of ASTM standards*, Vol. 15.09, ASTM, Philadelphia, PA, pp. 1312–1316.
- Bocking, K.A. and Fredlund, D.G. 1980. Limitations of the axis-translation technique. *Proceedings, 4th International Conference on Expansive Soils*, Denver, CO, pp. 117–135.
- Campbell, G.S. 1988. Soil water potential measurement: an overview. *Irrigation Science*, **9**: 265–273.
- Deka, R.N., Wairiu, M., Mtakwa, P.W., Mullins, C.E., Veenendaal, E.M., and Townend, J. 1995. Use and accuracy of the filter paper technique for measurement of soil matric potential. *European Journal of Soil Science*, **46**: 233–238.
- Gilbert, O.H. 1960. A device for measuring tensions in water. *Highway Research Board Bulletin* 245, pp. 1–9.
- Guan, Y. 1996. The measurement of soil suction. Ph.D. thesis, University of Saskatchewan, Saskatoon, SK, Canada.
- Harvey, E.N., McElroy, W.D., and Whiteley, A.H. 1947. On cavity formation in water. *Journal of Applied Physics*, **18**: 162–172.
- Henderson, S.J., and Speedy, R.J. 1980. A Berthelot-Bourdon tube method for studying water under tension. *Journal of Physics E: Scientific Instrumentation*, **13**: 778–782.
- Jones, W. M., Overton, G.D.N., and Trevena, D.H. 1981. Tensile strength experiments with water using a new type of

- Berthelot tube. *Journal of Physics D: Applied Physics*, **14**: 1283–1291.
- Knapp, R.T., Daily, J.W., and Hammitt, F. 1970. Cavitation. McGraw-Hill Book Company.
- Madsen, H.B., Jensen, C.R., and Boysen, R. 1986. A comparison of the thermocouple psychrometer and the pressure plate methods for determination of soil water characteristic curves. *Journal of Soil Science*, **37**: 357–362.
- Ridley, A.M. 1993. The measurement of soil moisture suction. Ph.D. thesis, Imperial College, London, UK.
- Sedgewick, S.A., and Trevena, D.H. 1976. Limiting negative pressure of water under dynamic stressing. *Journal of Physics D: Applied Physics*, **9**: 1983–1990.
- Trevena, D.H. 1987. Cavitation and Tension in Liquids. Adam Hilser.
- Vincent, R.S. 1941. Measurement of tension in liquids by means of a metal bellows. *Proceedings of the Physics Society*, **53**: 126-140.
- Winterton, R.H.S. 1977. Nucleation of boiling and cavitation. *Journal of Physics D: Applied Physics*, **10**: 2041–2056.

Suction measurements on a Saskatchewan soil using a direct measurement, high suction sensor

D.G. Fredlund, J.K-M. Gan, Y. Guan, and N. Richardson

Abstract: A tensiometric-type suction sensor capable of direct measurement of matric suctions greater than 100 kPa has recently been developed. The sensor has been used to measure matric suctions up to 1250 kPa with an accuracy in the order of ± 20 kPa. The sensor makes use of the tensile strength of water for measurement. Cavitation of water in conventional tensiometers occurs at a negative pressure approaching 1 atmosphere due to the presence of cavitation nuclei. In the absence of cavitation nuclei, the tensile strength of water can be in the order of several atmospheres. The sensor has a relatively fast response time when used in soils with matric suctions below 200 kPa.

The direct measurement, high suction sensor has been used for the measurement of matric suction on borehole samples obtained during a soils investigation at a bridge site near the town of Outlook in Saskatchewan, Canada. The method has proven to be fast and simple to use. Matric suction measurements for the samples from the Outlook bridge site are presented, along with an interpretation of the laboratory data.

Key words: matric suction, direct measurement, high suction sensor, tensile strength of water.

Introduction

Direct matric suction measurements using a tensiometer have generally been limited to a matric suction of about 90 kPa. When measuring matric suctions greater than one atmosphere one had to resort to indirect means, such as thermal conductivity sensors or the filter paper method. The indirect methods usually require tedious calibration.

Research literature, particularly in the physical sciences, has shown that water under special conditions can have substantial tensile strength. Research at Imperial College, UK, found that a transducer which was used to measure the pore-water pressure of a saturated clay during undrained-unloading tests in a cell recorded tensions of -365 kPa for a period of about two hours. The recorded tension eventually bounced back to -100 kPa. The observation was attributed to the tensile strength of water

and led to the development of a tensiometer-type high suction probe (Ridley 1993).

Further research into the tensile strength of water was conducted at the University of Saskatchewan. As a result of research into the tensile strength of water, a direct measurement, high suction sensor, making use of the tensile strength of water, was developed at the University of Saskatchewan (Guan 1996).

An existing bridge located near Outlook, in Saskatchewan, is in the process of being upgraded by Saskatchewan Highways and Transportation. Stability analyses of existing conditions indicated that matric suction may be playing a significant role in the stability of the west bank of the river. Samples were retrieved from three boreholes at the Outlook Bridge site for matric suction measurements at the University of Saskatchewan, Saskatoon, using the direct measurement, high suction sensor.

Direct measurement, high suction sensor

Cavitation in a conventional tensiometer occurs as gas or vapour bubbles begin to form in the water measuring system. The bubbles are triggered at gaseous or other hydrophobic surfaces which are commonly called potential cavitation nuclei. In the absence of cavitation nuclei, water can sustain a high tension without cavitation. Tensile strengths of several atmospheres have been recorded (Vincent 1941; Temperley 1946; Temperley 1947; Harvey et al. 1947; and Fisher 1948) for water without cavitation nuclei.

Gaseous or other hydrophobic surfaces which may be present in the water or on the surfaces of a water container, can be suppressed by high pressure. Research has

D.G. Fredlund. Professor, Department of Civil Engineering, 57 Campus Drive, University of Saskatchewan, Saskatoon, SK, Canada S7N 5A9.
J.K-M. Gan. Research Engineer, Department of Civil Engineering, 57 Campus Drive, University of Saskatchewan, Saskatoon, SK, Canada S7N 5A9.
Y. Guan. Graduate Student, Department of Civil Engineering, 57 Campus Drive, University of Saskatchewan, Saskatoon, SK, Canada S7N 5A9.
N. Richardson. Saskatchewan Highways and Transportation, 3130-8th Street East, Saskatoon, SK, Canada S7K 2H6.

Reproduced with permission from *Session on Measurement of Soil Suction in the Laboratory and in the Field*, Transportation Research Board, 76th Annual Meeting, Washington, DC, 1997.

shown that in a system with a small volume of water, the potential cavitation nuclei in the system can be effectively eliminated by using five to six cycles of pressurization and depressurization to about +12,000 kPa and -80 kPa, respectively (Guan 1996).

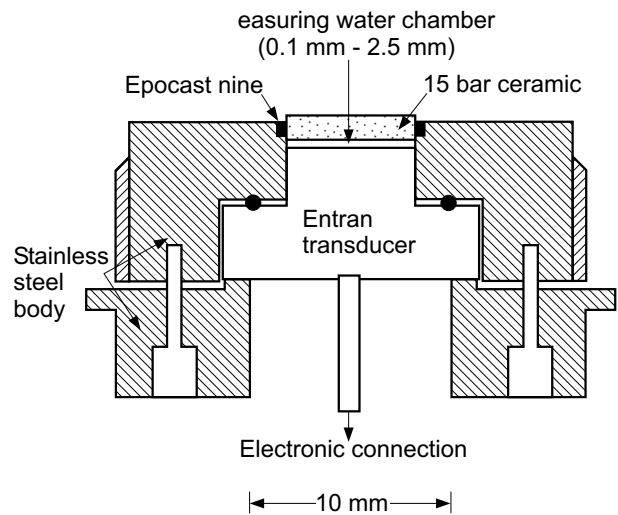
A schematic diagram of the direct measurement, high suction sensor that was developed at the University of Saskatchewan (Guan 1996) is shown in Fig. 1. The main components of the sensor are the high air-entry ceramic disk, stainless steel body and high pressure transducer. The surfaces of the stainless steel body were polished to a high finish in order to reduce potential cavitation nuclei sites.

A simple manual pressurization system was constructed for conditioning the water for the sensor. The pressurization system can provide pressures ranging from -85 kPa to 15,000 kPa. The water in the sensor was conditioned by using five to six cycles of pressurization and depressurization. Each cycle consisted of the application of a positive pressure of 12,000 kPa for one hour, followed by a negative pressure of 85 kPa for one hour. Studies have shown that the ability of the system to prevent cavitation does not significantly improve after more than six cycles of pressurization and depressurization (Guan 1996).

The direct measurement, high suction sensor has been tested for response time and accuracy using the pressure plate. The sensor was found to respond rapidly to pressure changes in the pressure plate. The measured pressure changes were essentially equal to the applied pressure changes. The time for the sensor to attain equilibrium suction with the soil is a function of the soil type and the degree of saturation of the soil. The time for the sensor to attain equilibrium increased with the plasticity of the soil and with the decrease in degree of saturation.

Readings obtained using the direct measurement, high suction sensor have also been compared with readings obtained using the filter paper method, null pressure plate method and thermal conductivity sensor (Guan 1996). The filter paper method gave results close to the direct measurement, high suction sensor readings for suction below 200 kPa. At suctions greater than 200 kPa, the filter paper method gave lower, as well as more widely scattered, values. The thermal conductivity sensor produced measurements which were close to the direct measurement, high suction sensor measurements for suction below 100 kPa. The thermal conductivity sensor produced lower values than the direct measurement, high suction sensor for suction values greater than 100 kPa. The null-pressure plate method produced readings higher than the direct measurement, high suction sensor for soils with a degree of saturation higher than 75%. The difference between the null plate value and the direct measurement, high suction sensor value decreases when the degree of saturation is less than 60%. The higher readings obtained when using the null-pressure plate method is believed to be due to the presence of occluded air bubbles in soils with degrees of saturation nearing total saturation.

Fig. 1. Direct measurement, high suction sensor.



The direct measurement, high suction sensor has been used to measure suctions up to 1250 kPa with an accuracy of ± 20 kPa, which is the order of accuracy of the transducer. The overall range of the pressure transducer is $\pm 15,000$ kPa. The high capacity of the transducer was required to withstand the high pressure (of 12,000 kPa) during pressurization for conditioning the water in the sensor system.

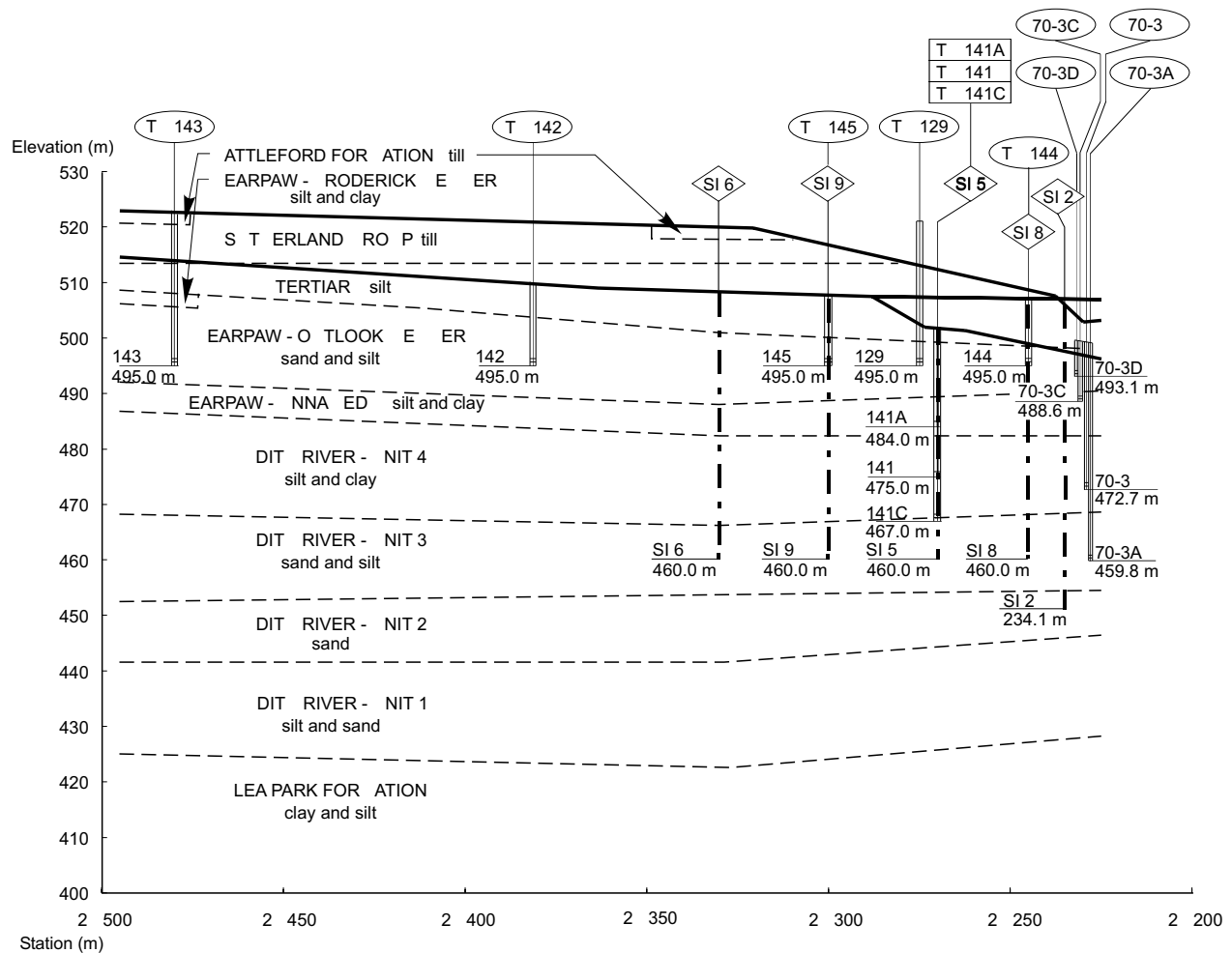
The sensor has been found to work well in clayey-type soils, and also in other types of soils that have a relatively high degree of saturation. Some difficulties have been encountered in measuring matric suctions with the direct measurement, high suction sensor in salty and sandy soils with degrees of saturation below 40%. The main difficulty is believed to be caused by minute amounts of evaporation from the ceramic disk in the sensor at low degrees of saturation of the soil.

The new Outlook Bridge, Saskatchewan

Saskatchewan Highways and Transportation is preparing to replace the existing steel truss bridge crossing Highway Number 15, near the town of Outlook in Saskatchewan, with a modern multi-span, steel and concrete structure. The new bridge will permit unrestricted passage of current-day load dimensions. The proposed bridge alignment is adjacent to the existing structure, but will require grading of new bridge approaches on both the east and west sides of the South Saskatchewan River.

The total valley relief at the proposed crossing is approximately 30 meters. The west river bank at the proposed site includes approximately 20 meters of near vertical slopes developed in glacial and pre-glacial silt soils. Relict landslides exist in the west bank, both immediately upstream and downstream from the proposed site.

The site investigation of the west bank (Fig. 2) included several stratigraphic boreholes involving undisturbed sampling, geophysical logging, piezometers and inclinometer installations to document the hydrogeologic

Fig. 2. Cross-section of west bank, Outlook Bridge site, Saskatchewan, Canada.

environment and existing river bank stability. After significant study it was concluded that there is no apparent geographic or geologic reason why the site of the proposed west bridge abutment and approach is stable while the adjacent areas are unstable. In other words, there is no obvious reason to account for the apparent strength of the silt materials.

Stability analyses of the existing west bank led to unrealistically high strength parameters for the strata involved. It was concluded that a significant matric suction component must be mobilised to enhance the apparent cohesion of the silt strata in the west river bank. Core sampling and testing were undertaken to determine the *in situ* matric suction values of the silt strata. The *in situ* matric suction values are to be used in the stability analyses for the site in order to refine the design of the bridge, the west bridge abutment and west approach configurations.

Soil samples from boreholes located at the west bank of the Outlook Bridge site in Saskatchewan were retrieved for matric suction measurements using the direct measurement, high suction sensors. The samples were extruded at the Materials Laboratory of the Saskatchewan

Highways and Transportation in Regina, Saskatchewan, Canada. Each sample was wrapped with aluminum foil and waxed before delivery to the Geotechnical Laboratory at the University of Saskatchewan in Saskatoon.

Laboratory test procedure for measuring matric suction

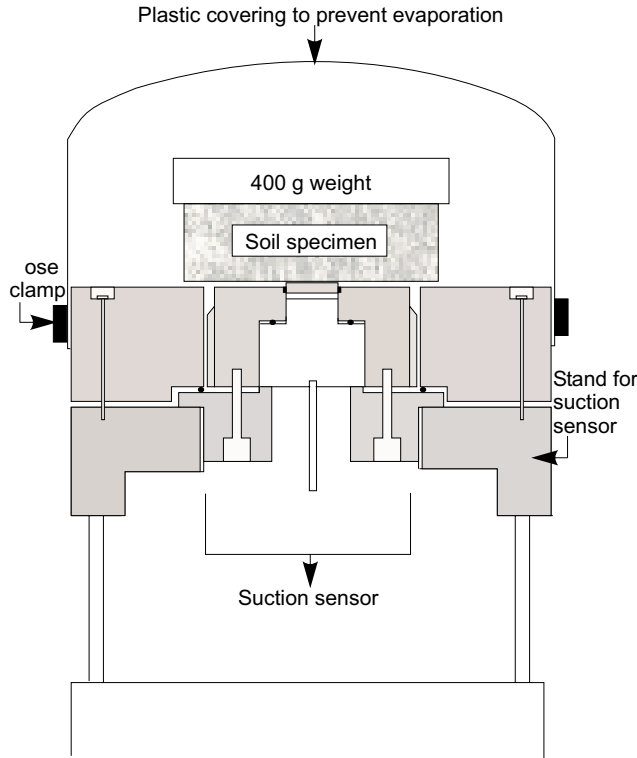
Prior to suction measurement in the laboratory using the direct measurement, high suction sensor, each soil specimen was removed from storage in the humidity-controlled cold room. The specimen was kept in the laboratory overnight for the specimen temperature to equilibrate with the laboratory room temperature. It has been found that steep temperature gradients (i.e., between soil and sensor) during measurement had an influence on the matric suction measurement and interfered with matric suction equilibration.

The water system of the direct measurement, high suction sensor was pre-conditioned by using five to six cycles of pressurization and depressurization to about +12,000 kPa and about -80 kPa, respectively. The conditioned sensor was mounted onto the sensor stand (Fig. 3).

The face of the ceramic disk in the sensor was kept moist at all times.

A thin layer of fine silt powder was applied to the face of the ceramic disk to help achieve good contact between

Fig. 3. Set-up of direct measurement high suction sensor for matric suction reading.



the soil and the sensor. One face of the soil specimen was trimmed flat. The soil trimmings were used for an initial water content determination. The flat face of the specimen was placed directly onto the sensor (Fig. 3). A 1 kg mass is placed on the specimen to help maintain good contact between the soil and the sensor. The entire set-up was then enclosed in a plastic bag to prevent any moisture loss during measurement.

Suction sensor readings with time were recorded using a data acquisition system. Readings were taken until equilibrium suction values were obtained. At the end of each suction measurement, a soil specimen was taken from the face of the soil in contact with the sensor for a final water content determination.

Laboratory test results

Direct measurement, high suction sensor readings with time for 11 specimens from borehole SI5, 9 specimens from borehole SI6, and 10 specimens from borehole SI9 are presented in Figs. 4, 5 and 6, respectively. The matric suction values for the specimens of borehole SI5, SI6 and SI9 are summarized in Tables 1, 2 and 3, respectively. The water contents corresponding to each matric suction measurement, along with degree of saturation measurements, are shown in Tables 1, 2 and 3.

Measurements were also conducted to determine the effect of specimen temperature on the matric suction values measured using the direct measurement, high suction sensor. Two sets of matric suction readings for specimen LS6-741 are presented in Fig. 7. One set of readings was taken immediately after the specimen was removed from the humidity-controlled cold room. The other set of read-

Fig. 4. Direct measurement high suction sensor reading versus time for specimens from borehole SI5.

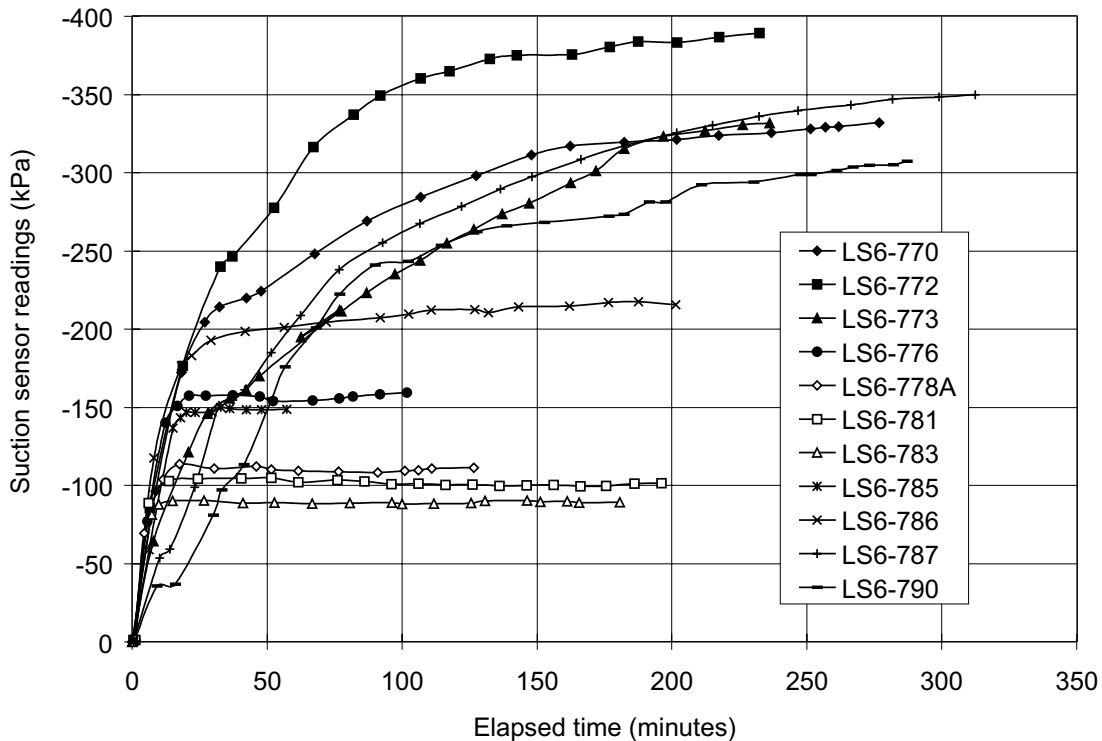


Fig. 5. Direct measurement high suction sensor reading versus time for specimens from borehole SI6.

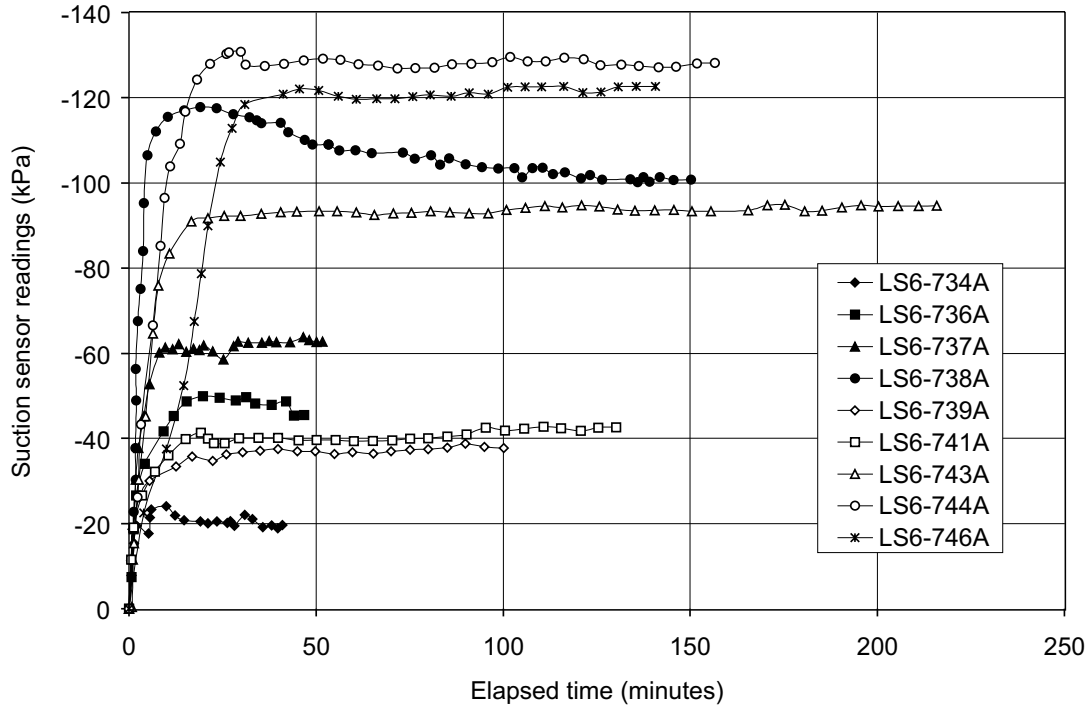
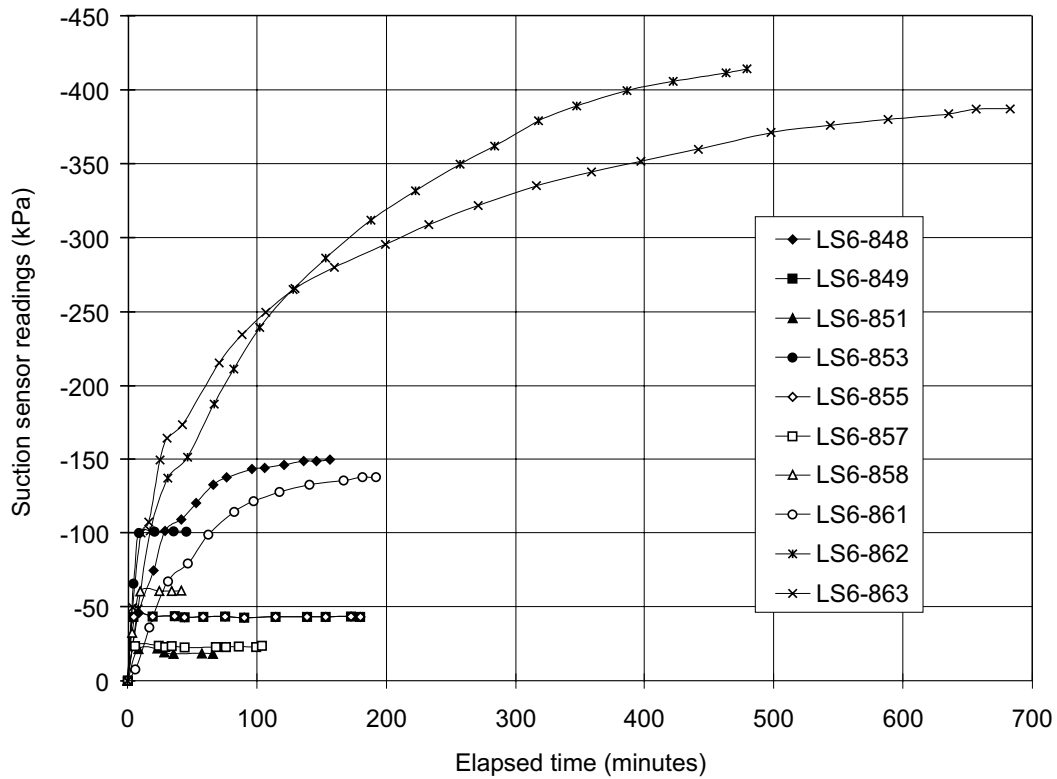


Fig. 6. Direct measurement high suction sensor reading versus time for specimens from borehole SI9.



ings was taken 12 hours after removal from the humidity-controlled cold room.

The matric suction, water content and degree of saturation measurements presented in Tables 1, 2, and 3 were

used for plotting matric suction, water content and degree of saturation profiles, respectively. The matric suction, water content and degree of saturation profiles at locations corresponding to boreholes SI5, SI6, and SI9 are

Table 1. Matric suction, water content and degree of saturation measurements for specimens from borehole SI5.

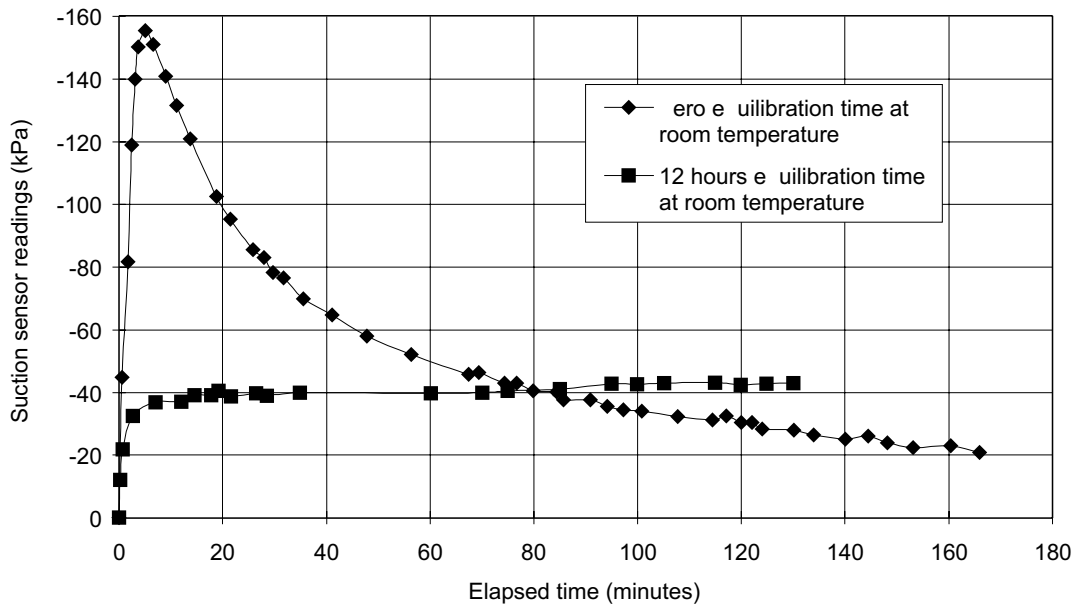
Specimen No.	Elevation (m)	Soil description	Initial water content (%)	Final water content (%)	Matric suction (kPa)	Degree of saturation (%)
LS6-770	510.31	uniform, brownish gray silt	11.70	11.41	328	61.0
LS6-772	508.76	uniform, light gray silt	15.42	15.00	385	
LS6-773	508.01	uniform, light gray silt	11.95	11.61	330	72.8
LS6-776	507.71	uniform, light gray silt	13.38	13.23	158	
LS6-778A	503.46	uniform, olive yellow silt	19.41	18.90	112	95.2
LS6-781A	499.96	olive yellow silt with iron stains	25.53	25.23	101	
LS6-783	496.91	yellowish gray silt with iron stains	25.37	24.15	88	86.0
LS6-785A	494.46	yellowish gray silt with iron stains	26.00	24.96	148	
LS6-786A	492.91	light gray silt, clay laminations with iron stains	22.60	22.33	216	95.6
LS6-787	491.41	dark gray clayey silt	25.16	24.49	348	
LS6-790	486.81	dark gray clayey silt	23.97	23.70	303	93.4

Table 2. Matric suction, water content and degree of saturation measurements for specimens from borehole SI6.

Specimen No.	Elevation (m)	Soil description	Initial water content (%)	Final water content (%)	Matric suction (kPa)	Degree of saturation (%)
LS6-734A	513.34	uniform, brownish gray silt	14.57	14.69	20	92.6
LS6-736A	510.29	uniform, brownish gray silt	18.41	18.80	47	
LS6-737A	508.74	uniform, brownish gray silt	14.67	15.22	63	76.3
LS6-738A	507.24	uniform, light yellowish brown silt	15.09	15.44	101	
LS6-739A	505.74	uniform, light yellowish brown silt	18.54	18.69	37	84.6
LS6-741A	502.69	uniform, light yellowish brown silt	19.61	19.62	43	
LS6-743A	499.64	olive yellow silt with grayish brown zones	27.96	28.33	94	94.7
LS6-744A	498.09	silt, sand, clay laminations with iron stains	25.70	25.24	128	
LS6-746A	495.09	silt, sand, clay laminations with iron stains	24.41	25.15	123	94.4

Table 3. Matric suction, water content and degree of saturation measurements for specimens from borehole SI9.

Specimen No.	Elevation (m)	Soil description	Initial water content (%)	Final water content (%)	Matric suction (kPa)	Degree of saturation (%)
LS6-848A	508.58	yellowish brown clayey silt	15.54	15.39	151	91.0
LS6-849A	505.83	yellowish brown uniform silt	15.60	15.80	44	
LS6-851A	502.83		19.71	19.48	20	94.3
LS6-853A	500.38	yellowish brown uniform	26.84	26.52	102	
LS6-855A	497.33	silt	28.27	28.03	44	93.9
LS6-857A	494.28	clayey silt with iron stains	24.87	24.51	24	
LS6-858A	492.73	silty sand with iron stains sand with iron stains	23.98	23.33	61	93.7
LS6-861A	489.73	sand, silt, clay laminations	25.76	25.81	138	
LS6-862A	486.68	with iron stains	22.06	22.28	412	96.9
LS6-863A	485.13	dark gray shale dark gray shale dark gray shale	23.09	23.23	383	89.8

Fig. 7. Effect of temperature on direct measurement, high suction sensor readings for specimen LS6-741.

presented in Figs. 4, 5, and 6, respectively. Plasticity index and liquid limit data for samples obtained from approximately the same locations are also presented in Figs. 4, 5 and 6. The plasticity index and liquid limit data were provided by Saskatchewan Highways and Transportation, Saskatoon.

Discussion

Suction sensor readings versus time curves for the soil specimens from boreholes SI5, SI6 and SI9 in Figs. 4, 5 and 6, respectively, show that the time to attain suction equilibrium increased with the matric suction of the soil. The time to attain equilibrium suction reading was rapid for matric suctions below 200 kPa. At higher matric suction values of about 300 to 400 kPa, equilibration became gradual and the time to attain suction equilibrium was rather long. The time to attain equilibrium suction was in the order of 10 to 30 minutes for the soil with matric suctions below 200 kPa. For the soil specimens with matric suctions in the order of 300 to 400 kPa, the time for the sensor reading to attain equilibrium with the soil matric suction was in the order of 150 minutes (Fig. 4), and can occasionally be as high as 500 to 600 minutes (Fig. 6).

Suction sensor reading versus time curves for specimens LS6-741 (Fig. 7), show the dramatic effect of soil specimen temperature on suction sensor reading. When the sensor reading was conducted immediately after the soil was removed from the humidity-controlled cold room, sensor readings increased rapidly (within about 5 minutes) to a value of 156 kPa, which is about 8 times the matric suction of the soil.

Upon removal from the humidity-controlled cold room, the soil specimen LS6-741 had an initial temperature of

approximately 12°C (i.e., temperature of the humidity-controlled cold room), which was approximately 10°C lower than the laboratory room temperature of 22°C. The cooler temperature of the soil specimen resulted in higher sensor reading. The sensor eventually reduced to a lower equilibrium value as the temperature of the soil specimen came to equilibrium with the room temperature. Experimental results showed that a temperature equilibration time of about four hours in the laboratory was adequate for the soil specimen to come to equilibrium with the laboratory temperature.

The matric suction profiles presented in Figs. 8 and 10 show that matric suction was highest near the ground surface. The matric suction values decreased with depth from the ground surface and reached a low of between 20 and 100 kPa at an elevation of about 500 to 510 m. With increasing depth, the suctions measured in the laboratory again increased.

The measured negative pore-water pressure (i.e., negative value of the suction) for the borehole samples is affected by the release of the *in situ* overburden pressure. The influence of unloading associated with the overburden pressure, on the measured suction value of the soil, is dependent upon the degree of saturation and the stiffness of the soil.

The B pore-pressure coefficient for a saturated soil is 1.0. The B pore-pressure coefficient decreases when the degree of saturation decreases. For example, results on a Peorian loess (Fig. 11) and a Champaign till (Fig. 12) showed that the B pore-pressure coefficient reduced dramatically when the degree of saturation dropped below approximately 80 to 90% for both soils (Campbell 1973). Above the water table, the B pore-pressure coefficient would decrease with elevation as a result of a decrease in the degree of saturation of the soil. The B pore-pressure

Fig. 8. Matric suction, water content, degree of saturation, plasticity index and liquid limit profiles at location of borehole SI5.

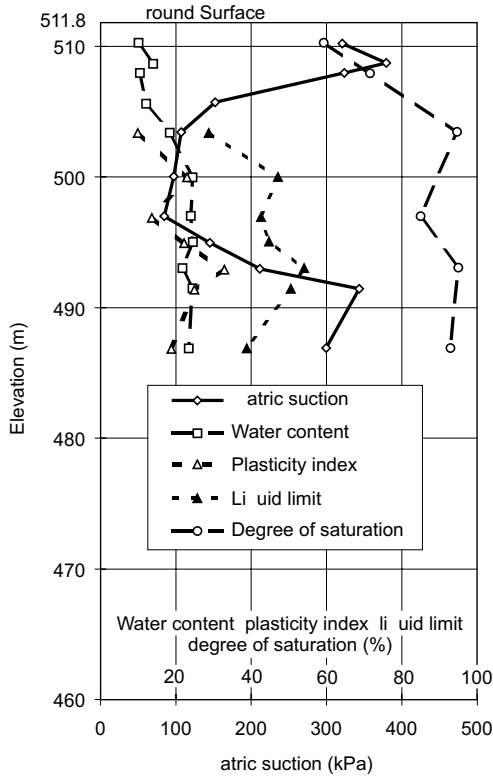


Fig. 9. Matric suction, water content, degree of saturation, plasticity index and liquid limit profiles at location of borehole SI6.

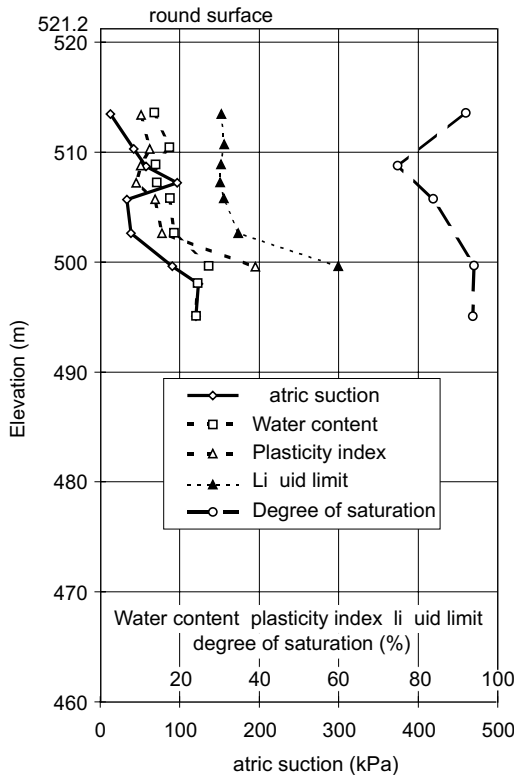
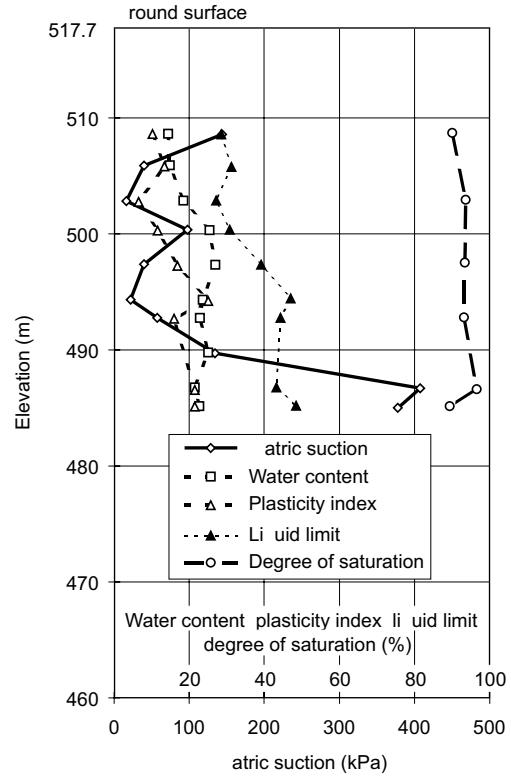


Fig. 10. Matric suction, water content, degree of saturation, plasticity index and liquid limit profiles at location of borehole SI9.



coefficient would be quite low (in the order of 0.1) near the ground surface and would increase to a value of 1.0 in the capillary zone above the water table.

The degree of saturation profiles in Figs. 8, 9, and 10 show that the soils have degrees of saturation ranging between 80 and 90%. The B pore-pressure coefficient was therefore estimated to be of the order of 0.1 to 0.3, based on degree of saturation and the stiffness of the soils at the Outlook Bridge site. The direct measurement high suction sensor suction values, along with the matric suction values corrected for B pore-pressure coefficients of 0.1 and 0.3 are shown in Figs. 13, 14, and 15. These results show that the soils at borehole location SI5, SI6, and SI9, possessed significant matric suctions. Matric suction values were estimated to range from 20 to about 400 kPa.

Conclusions

The direct measurement, high suction sensor has been used to obtain matric suction measurements up to 400 kPa for a Saskatchewan soil. The time for soil and sensor to reach equilibrium matric suction conditions increased with the matric suction of the soil.

The measurement results show that the soils at the west bank of the Outlook Bridge site possessed significant matric suctions. The matric suction in the soil must be taken into account during a back-analysis of the slope, in order to obtain realistic *in situ* shear strength parameters.

Fig. 11. B pore-pressure coefficient as a function of degree of saturation for Peorian loess (from Campbell 1973).

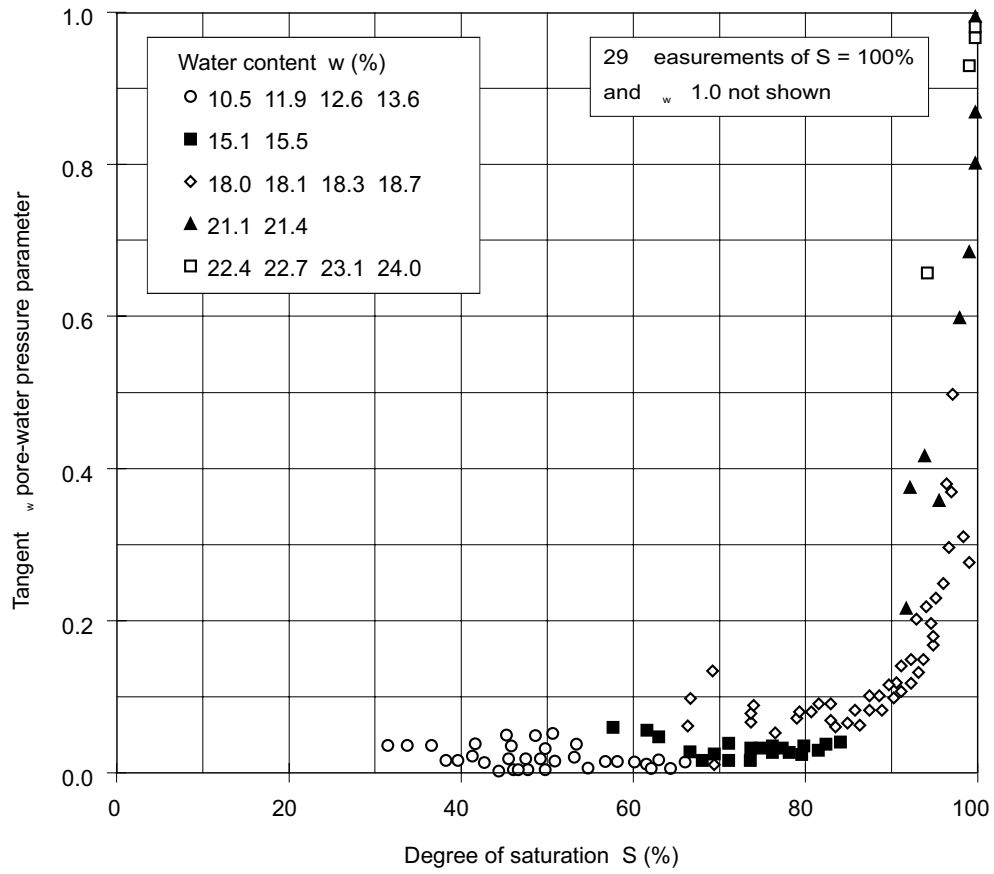


Fig. 12. B pore-pressure coefficient as a function of degree of saturation for Champaign till (from Campbell 1973)

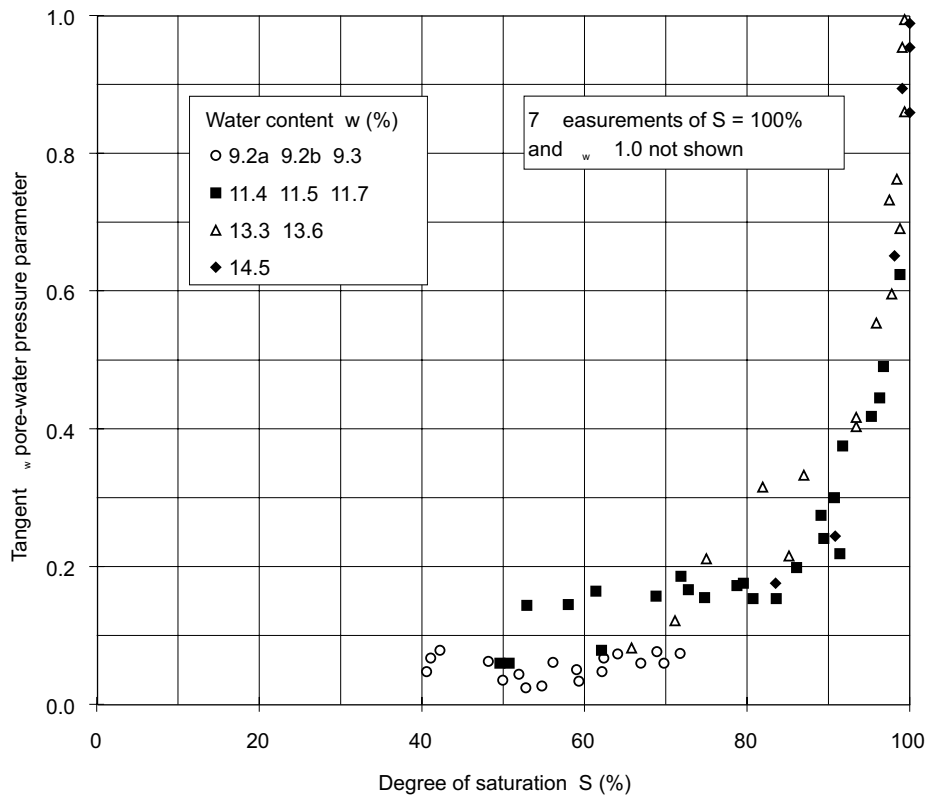


Fig. 13. Pore-water pressure profiles corresponding to various values of B pore-pressure coefficient at location of borehole SI5.

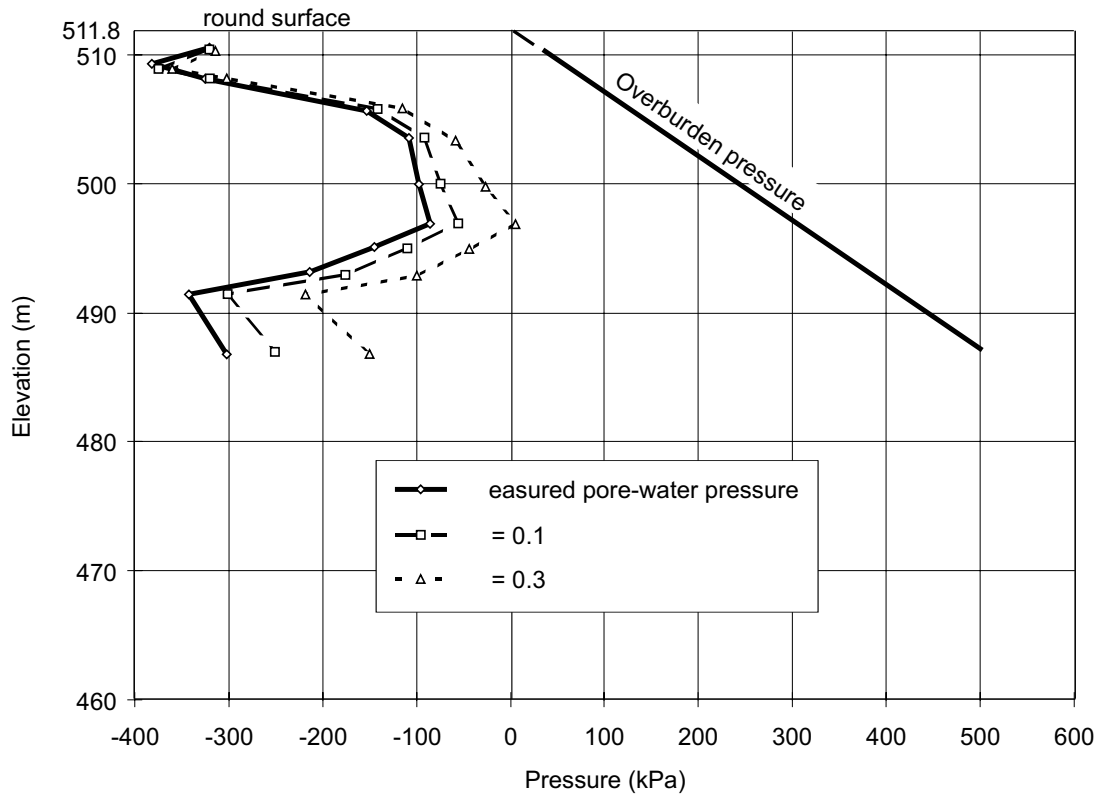


Fig. 14. Pore-water pressure profiles corresponding to various values of B pore-pressure coefficient at location of borehole SI6.

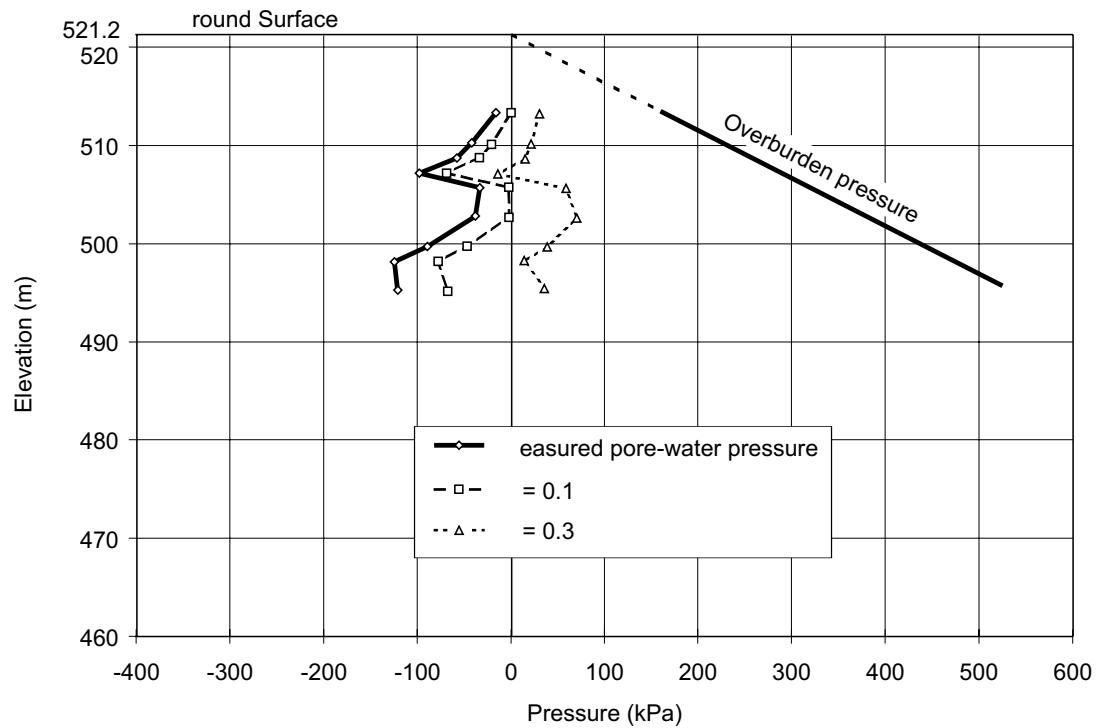
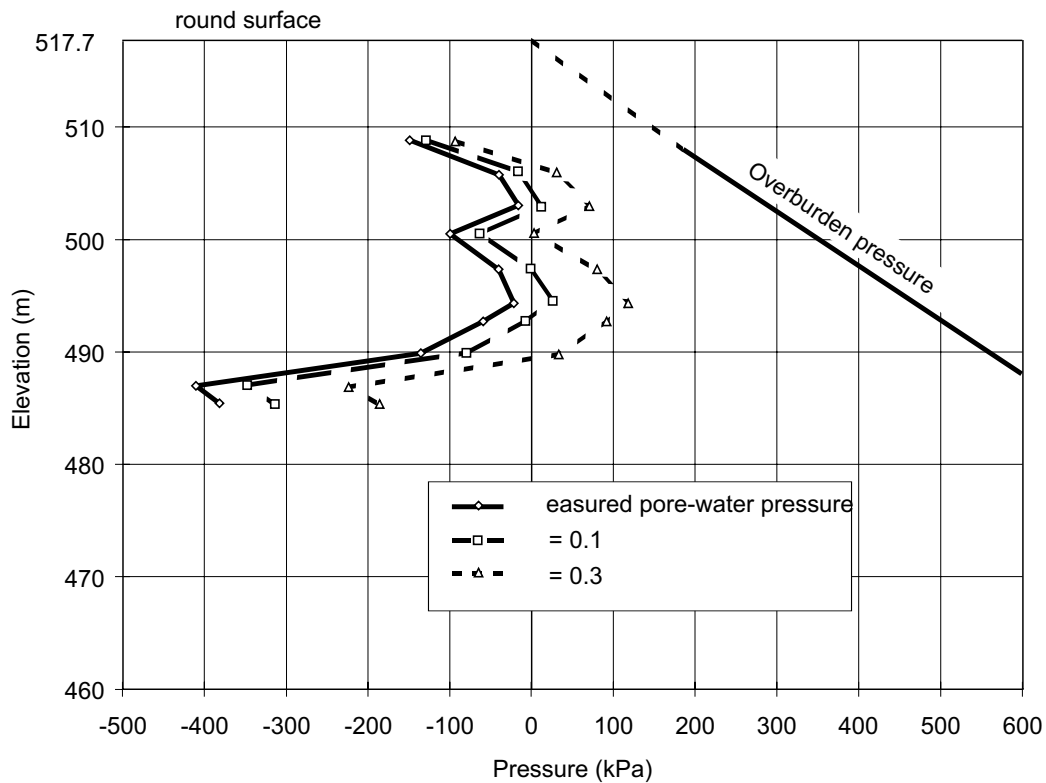


Fig. 15. Pore-water pressure profiles corresponding to various values of B pore-pressure coefficient at location of borehole SI9.

References

- Campbell, J.D. 1973. Pore pressures and volume changes in unsaturated soils. Ph.D. thesis, University of Illinois at Urbana-Champaign, Urbana-Champaign, ILL.
- Fisher, J.C. 1948 The fracture of liquids. *Journal of Applied Physics*, **19**: 1062–1067.
- Guan, Y. 1996 The measurement of soil suction. Ph.D. thesis, University of Saskatchewan, Saskatoon, SK, Canada.
- Harvey, E.N., McLeroy, W.D., and Whiteley, A.H. 1947. On cavity formation in water. *Journal of Applied Physics*, **18**: 162–172.
- Ridley, A.M., 1993. The measurement of soil moisture suction. Ph.D. thesis, Imperial College, London, UK.
- Temperley, H.N.V. 1946. The behaviour of water under hydrostatic tension: II. *Proceedings of the Physics Society*, **58**: 436–443.
- Temperley, H.N.V. 1947. The behaviour of water under hydrostatic tension: III. *Proceedings of the Physics Society*, **59**: 199–208.
- Vincent, R.S. 1941. Measurement of tensions in liquids by means of a metal bellows. *Proceedings of the Physics Society*, **53**: I26–I40.

Suction measurements on compacted till specimens and indirect filter paper calibration technique

D.G. Fredlund, J.K.-M. Gan, and P. Gallen

Abstract: Standard AASHTO compacted specimens were used to provide a constant-suction environment for an indirect calibration of filter paper sensors. The suctions of the compacted till specimens were measured with tensiometers, thermal conductivity matric suction sensors, and psychrometers. The compacted specimens had essentially constant degrees of saturation at water contents greater than optimum. The matric suction of specimens compacted greater than optimum was observed to vary linearly with the water content and the void ratio (i.e., matric suction varies directly with dry density and inversely with water content). Filter paper sensors in good contact with specimens compacted greater than optimum were found to yield a more consistent calibration curve than filter paper sensors that were not in contact with the soil. Calibration curves obtained showed that the transition from dominant liquid flow to dominant vapour flow occurred at approximately 20 to 90 kPa.

Key words: soil suction, total suction, filter paper, compacted soil.

Introduction

The behaviour of both saturated and unsaturated soils is affected by the pore-water pressures in the soil. Both positive and negative pore-water pressures have a major effect on the shear strength and volume change behaviour of a soil. The effect of negative pore-water pressures on the hydraulic conductivity behaviour of unsaturated soils has become increasingly important in analysing geo-environmental problems.

The measurement of positive pore-water pressures has become routine for engineering works such as embankments and dams. The measurement of negative pore-water pressures, however, has remained a research endeavour. The measurement of negative pore-water pressures over a wide range of values has proved to be difficult. Negative water pressures can range from 0 to 1 million kPa. The direct measurement of negative pore-water pressure is limited by the problem of cavitation. Water will cavitate when the vapour pressure is reached on an absolute pressure scale. As a result, the direct

measurement of negative pore-water pressures by a tensiometer is now limited to pressures of less than 1 atm. Research at Imperial College, London, has involved the use of thin water films in a tensiometer to reduce the problem of cavitation. It is hoped that this research will provide a means of extending the range of negative pore-water pressure measurements beyond the present 1 atm constraint.

Various indirect methods of assessing the negative pore-water pressure in soils have been used for a number of years. These methods include moisture blocks, thermal conductivity sensors, blotting papers, filter papers, and psychrometers. All these methods have their own set of limitations. All methods, except the psychrometer method, rely on the absorbency properties of a sensor material and thus suffer from non-linearity and hysteresis in the water-retention characteristics of the sensor medium. In the high suction range, the sensor materials generally display small water content changes at large suction changes.

Nevertheless, the filter paper method has some attractive features. It has been found to be applicable over a wide range of suctions. Filter paper provides an inexpensive sensor, and the methodology associated with its use is simple. The filter paper method, however, suffers from some procedural difficulties. Although the method is applicable to a wide range of suctions, the degree of accuracy is often inadequate. The filter paper method does not lend itself to automation processes, particularly in the area of data acquisition. The method is considered a destructive method in that the filter papers are not reusable.

The filter paper method is a technique that can be readily incorporated into routine site investigations. There has been considerable interest in the use of the filter paper method in several disciplines. Literature from early

D.G. Fredlund. Professor, Department of Civil Engineering, University of Saskatchewan, 57 Campus Drive, Saskatoon, SK, Canada S7N 5A9.

J.K.-M. Gan. Research Engineer, Department of Civil Engineering, University of Saskatchewan, 57 Campus Drive, Saskatoon, SK, Canada S7N 5A9.

P. Gallen. Graduate Student, Department of Civil Engineering, University of Saskatchewan, 57 Campus Drive, Saskatoon, SK, Canada S7N 5A9.

Reproduced with permission from *Transportation Research Record* 1481, Transportation Research Board, Committee on Environmental Research Factors Except Frost, 1995, pp. 3-9.

research (Fawcett et al. 1967; McQueen and Miller 1968; Al-Khafaf and Hanks 1974; Sneath and Johnson 1980; Hamblin 1981) and from more recent research (Chandler and Gutierrez 1986; Sibley et al. 1990; Sibley and Williams 1990; Chandler et al. 1992; Houston et al. 1994; McKeen 1985) studying the filter paper method is listed in the References section. Recent experiences with studies related to airport pavement subgrades (McKeen 1985) and the movement of foundations of light structures (Chandler et al. 1967) have indicated that the method deserves further consideration.

The objectives of this paper are (a) to determine the suction of compacted till specimens by using various suction measurement devices and (b) to evaluate an indirect method of calibrating filter paper sensors by using compacted soil specimens to provide constant suction environments. At present, the filter paper method has not gained wide acceptance in geotechnical engineering. The issues of whether the filter paper should be in contact with the soil or not in contact with the soil and of what suctions are measured in each case have been much debated. It is hoped that this study will assist in further resolving these questions related to the filter paper method.

Program for the laboratory study

The laboratory program involved (a) the measurements of suction in a set of standard AASHTO compacted till specimens and (b) using these compacted specimens to provide constant-suction environments for an indirect calibration of filter paper sensors.

Suction measurement devices

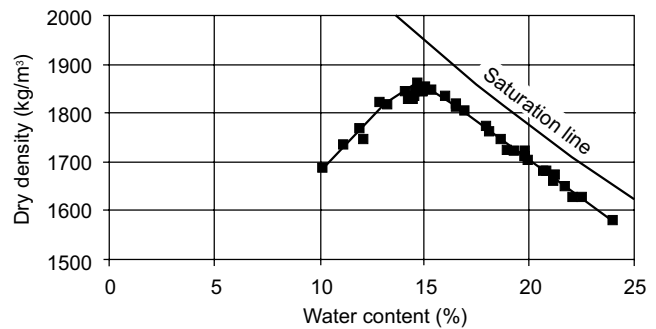
Suctions in the compacted till specimens were measured with the following suction measurement devices: jet-fill tensiometers, quick-draw tensiometers, MCS-6000 thermal conductivity matric suction sensors, and psychrometers.

Tensiometers are limited to a matric suction value of approximately 90 kPa. The MCS-6000 thermal conductivity matric suction sensors are reliable in the range from 0 to 300 kPa. Psychrometers start to become reliable at a suction near 100 kPa and measurements can be made up to 8000 kPa. Suctions of interest in geotechnical engineering generally range from 0 to 1500 kPa.

Soil selected for the study

The soil used in the laboratory tests program was a till from the Qu'Appelle Moraine east of the city of Regina in Saskatchewan, Canada. The grain size distributions of the till show 37% sand, 34% silt, and 29% clay. The till has a liquid limit of 38% and a plastic limit of 16%. Distilled water was added to the till to yield a set of samples with water contents ranging from 8% to 25%. Standard AASHTO compacted specimens were prepared from these samples for the testing. The compaction characteristics of the soil are presented in Fig. 1. The till has a maximum dry density of approximately 1.86 Mg/m^3 and a

Fig. 1. Compaction characteristics of till.



corresponding optimum water content of approximately 15%.

Different suction values were obtained by compacting the till at various water contents. In other words, the suctions in the compacted specimens were not directly induced or controlled as in a pressure plate device. The matric suction or the total suction values, or both, in each specimen were measured with one or more of the following devices: jet-fill tensiometer, quick-draw tensiometer, MCS 6000 sensor, or psychrometer.

Filter paper selected for the study

Schleicher and Schuell No. 589 white ribbon filter paper was used in the laboratory tests. The filter papers had a diameter of 55 mm. The filter papers were pre-treated by being dipped in a fungicide, drip dried, and over dried overnight. The fungicide was a mixture of 3.5 g technical-grade pentachlorophenol (i.e., 86% by weight of pentachlorophenol) in 100 g of ethyl alcohol, yielding a 3% "penta" solution.

A scanning electron micrograph of a Schleicher and Schuell No. 589 white ribbon filter paper is shown in Fig. 2. For comparison, a scanning electron micrograph of a Whatman filter paper is also shown in Fig. 2. The two types of filter paper appear similar in the scanning electron micrographs. The similarity of the filter papers has great implications with respect to the calibration of filter papers for suction measurements.

Installation procedures for filter paper sensors

The jet-fill tensiometers, quick-draw tensiometers, or MCS-6000 thermal conductivity matric suction sensors were snugly fitted into a hole drilled into the compacted specimens (Figs. 3–5). The psychrometers were installed in sets of three (Fig. 6). These sensors (i.e., jet-fill tensiometers, quick-draw tensiometers, MCS-6000 sensors, and psychrometers) are subsequently referred to as reference sensors.

Installation of good-contact filter papers in standard AASHTO compacted specimens

Two installation procedures were used. In the first procedure a vertical cut was made in the compacted specimen at a distance of approximately 3 cm on either side of the reference sensor (Fig. 3). In the second procedure, a single horizontal cut was made at a distance of approxi-

Fig. 2. Scanning electron micrographs: *left*, Schleicher and Schuell No. 589 filter paper; *right*, Whatman filter paper.

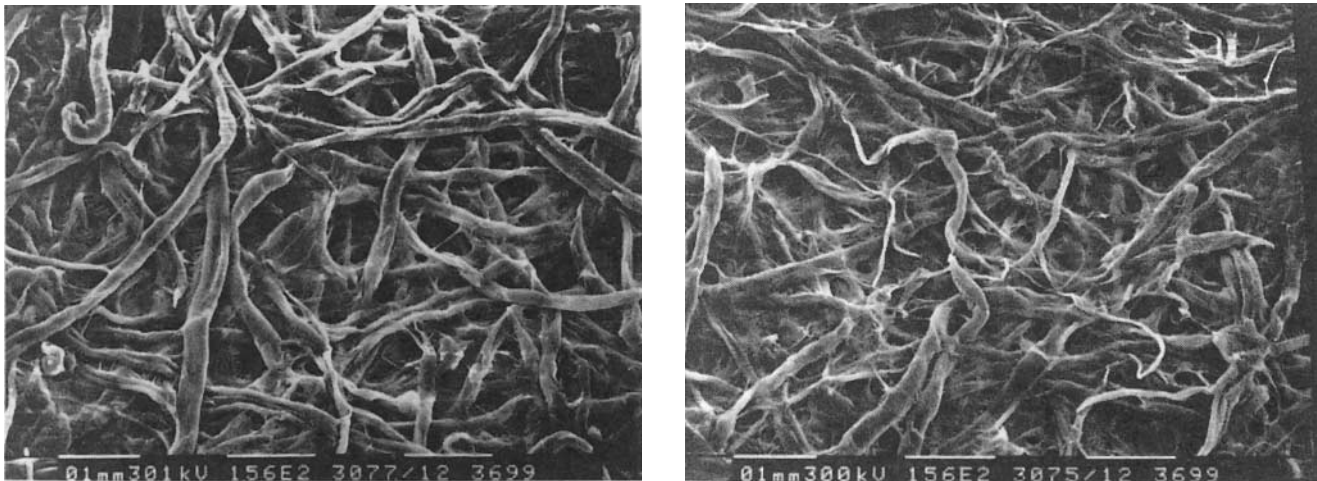


Fig. 3. Set-up 1 for calibration of good-contact filter paper sensors in standard Proctor specimens.

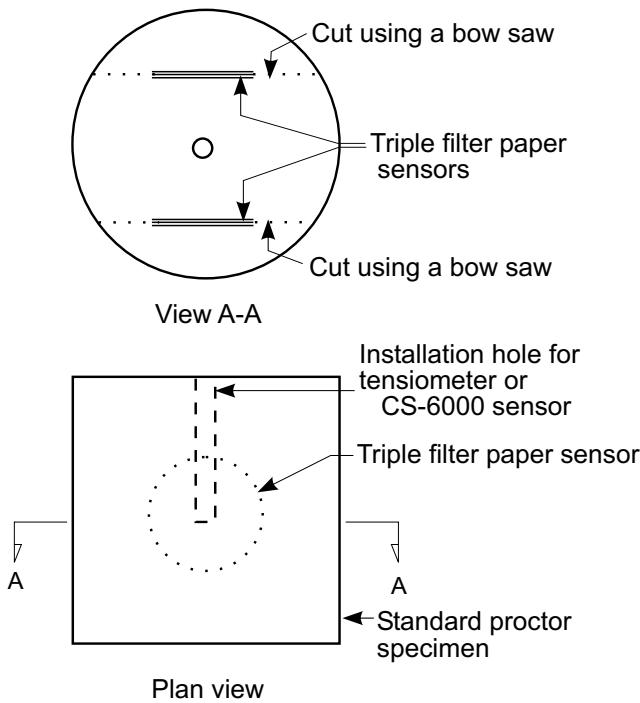
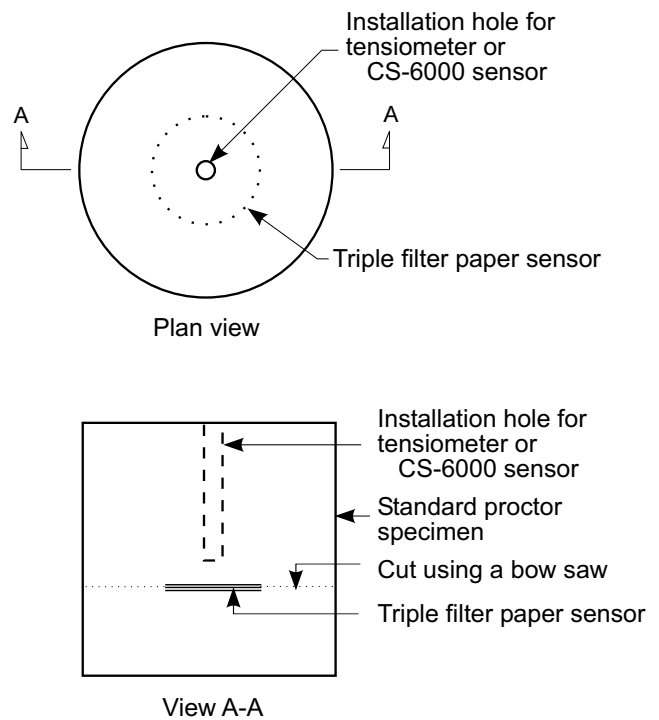


Fig. 4. Set-up 2 for calibration of good-contact filter paper sensors in standard Proctor specimens.



mately 2 cm below the tip of the sensor (Fig. 4). The cut was made either with a bow saw equipped with a piano wire for moist specimens or with a hacksaw blade for drier specimens.

A triple sandwich filter paper sensor was installed in each cut. The specimen was held together with masking tape, then wrapped with Saran wrap and aluminum foil followed by an outer layer of masking tape. The specimen was then placed in a Styrofoam chest packed with Styrofoam chips and left to equilibrate with time.

Installation of non-contact filter papers in standard AASHTO specimens

Three vertical holes surrounding the reference sensor were drilled into one end of a compacted specimen by a 22.23-mm (7/8-in.) drill bit. A plastic hair roller was installed in each hole (Fig. 5). A single filter paper sensor was curled with tweezers to fit inside each hair roller. The specimen was then wrapped in Saran wrap and alu-

Fig. 5. Set-up for calibration of non-contact filter paper sensors in standard Proctor specimens.

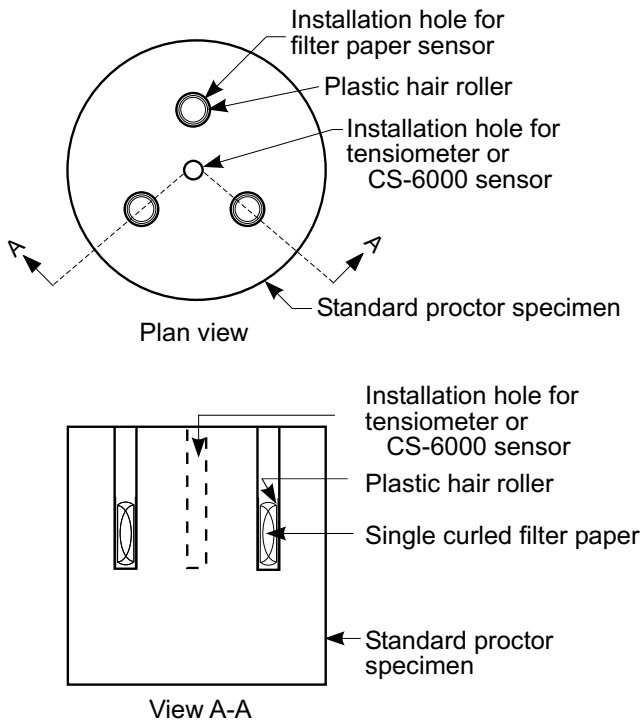
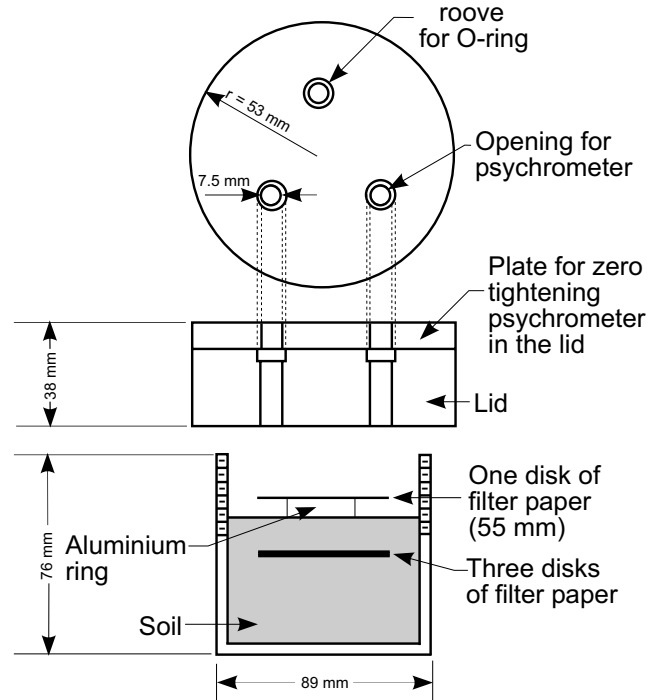


Fig. 6. Lucite container for filter paper calibration when psychrometers are used as reference sensors.



minum foil and tightly bound with masking tape. The specimen was left to equilibrate in a Styrofoam chest filled with Styrofoam chips.

Installation of good-contact and non-contact filter paper for calibration using psychrometers

Two slices of soil cut from a standard AASHTO compacted specimen were trimmed to fit into a Lucite container. Each slice was approximately 3 cm thick. A triple sandwich, good-contact filter paper sensor was placed between the slices. The two slices of soil were pressed tightly together inside the Lucite container. This procedure ensured good contact between the filter paper sensor and the soil. A single non-contact filter paper sensor was also installed by placing the filter paper on an aluminum ring placed on the surface of the soil. The set-up is shown in Fig. 6.

The Lucite container was fitted with three psychrometers and placed in a steel beaker immersed in a water bath for equilibration (Fig. 7). The temperature of the water bath was maintained at 24°C.

Presentation of results

The suction versus compaction water content relationship for the standard AASHTO compacted till specimens is presented in Fig. 8. The curve in Fig. 8 is not a soil-water characteristic curve because the relationship was obtained from a set of non-identical specimens. Also shown in Fig. 8 are the total suction and matric suction

curves obtained from another study on a similar till (Krahn and Fredlund 1972).

Calibration data obtained from the triple sandwich, good-contact filter paper sensors is presented in Fig. 9. The water content data for all three filter papers in each of the triple sandwich sensors were similar.

Calibration data from the non-contact single filter paper sensor is presented in Fig. 10. The calibration was conducted from low suction values of less than 10 kPa to suction values of approximately 1000 kPa. In retrospect, the calibration by the sorption procedure (i.e., non-contact filter paper) would be more meaningful if it were restricted to high suction values.

Discussion of results

Results of suction measurements on the compacted till are discussed, followed by a discussion of the results of the calibration of the filter paper sensors. The filter paper calibration curves obtained from this study are compared with currently available calibration curves. The merits or demerits of the indirect calibration procedure are discussed.

Suction measurements on the compacted till

The suction versus compaction water content data (Fig. 8) show that the suctions measured in the compacted till specimens have values comparable with those obtained from previous tests on a similar till (Krahn and Fredlund 1972). The psychrometer readings appear to

Fig. 7. Water bath for calibration with psychrometers (after Krahn and Fredlund 1972).

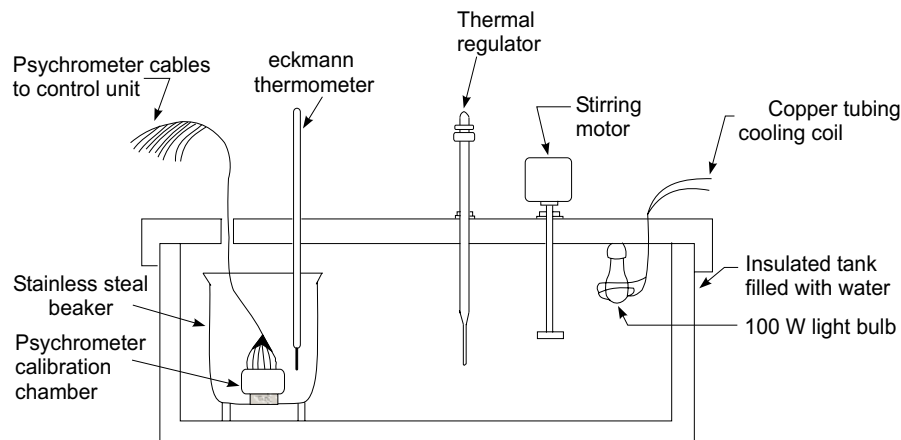
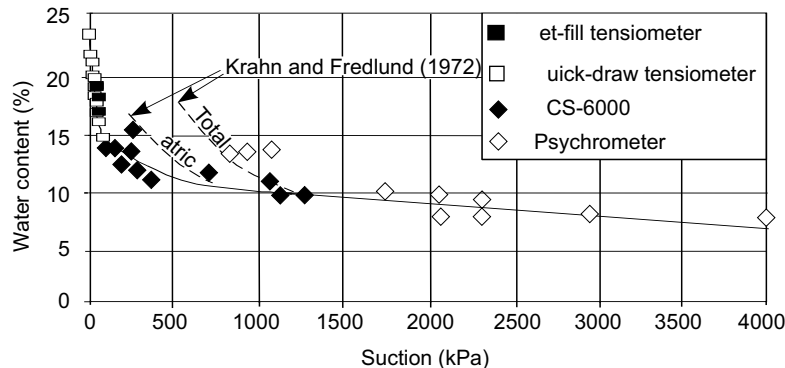


Fig. 8. Water-content - suction relationship for compacted till.



correspond well to the total suction curve from the previous study (Krahn and Fredlund 1972).

The suction versus compaction water content data, along with the void ratio and the degree of saturation versus compaction water content relationships, are shown side by side in Fig. 11 for comparison. The void ratios and degree of saturation values were calculated from the compaction data in Fig. 1.

Figures 8 and 11 show that the matric suction of the compacted specimens varied inversely linearly with compaction water content up to the optimum water content of 15%. At compaction water contents less than the optimum water content the matric suction values increased rapidly with a decrease in water content. The matric suction value at the optimum water content was approximately 80 kPa.

Results of calibration for filter paper sensors

The calibration curve for the good-contact filter paper sensor can be fitted by a bilinear curve (Fig. 9). There appears to be significant scatter near the break in the calibration curve. The calibration data for the non-contact filter paper sensors also appear to fit a bilinear curve (Fig. 10). The data from the non-contact filter paper sensors appear to be more scattered than the data for the good-contact filter paper sensor.

The water contents of the filter papers in good contact with the soil (Fig. 9) were in better agreement with the suction values measured by the reference sensors than the water contents of the filter papers not in contact with the soil (Fig. 10) for suction values of the compacted till below 100 kPa (i.e., above the optimum water content of the till).

Above the optimum water content of the till, there appear to be a direct transfer of water via the liquid phase. In other words, conductive flow is more efficient and reliable in the equilibration process at water content above the optimum.

Below the optimum water content the results obtained for the non-contact filter paper sensors do not appear to be inferior to the results obtained for the good-contact filter paper sensors. Below optimum water content the water is tightly bound to the soil particles. Liquid flow is small in comparison with the vapour flow. Consequently the variations in the water content as a result of liquid flow are small. The small liquid flow may be one reason for the seemingly smaller scatter, regardless of whether the filter paper is good contact with the soil. The differences may also be exaggerated because of the use of a logarithmic scale for suctions.

The greatest scatter in the calibration data for the filter paper sensors occurs near the break in the bilinear curve. This is more obvious for the non-contact filter paper sen-

Fig. 9. Data from calibrations of good-contact filter paper sensors, considering data from all three filter papers of each triple sandwich sensor.

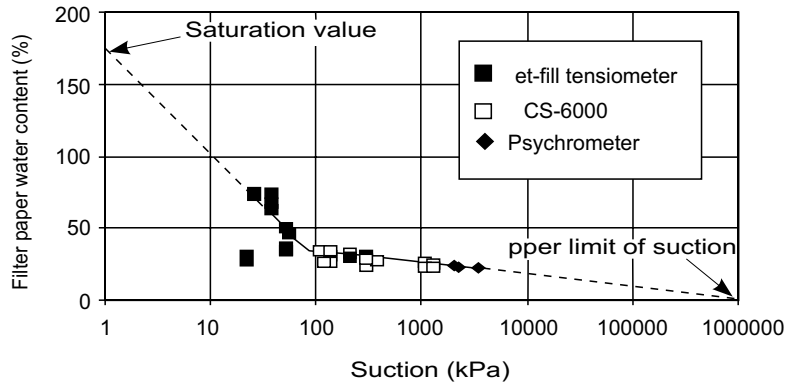


Fig. 10. Data from calibrations of non-contact filter paper.

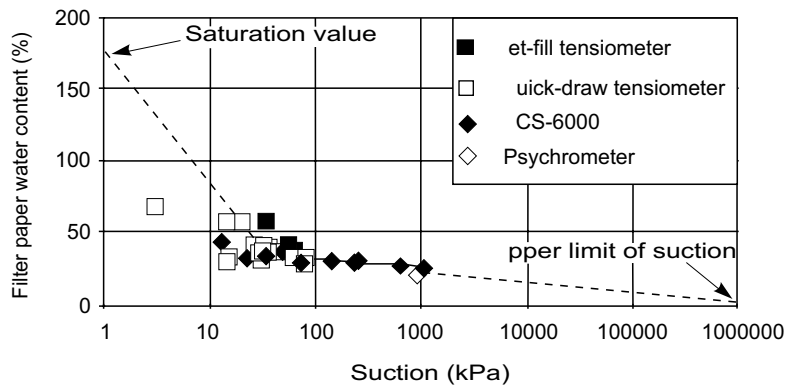
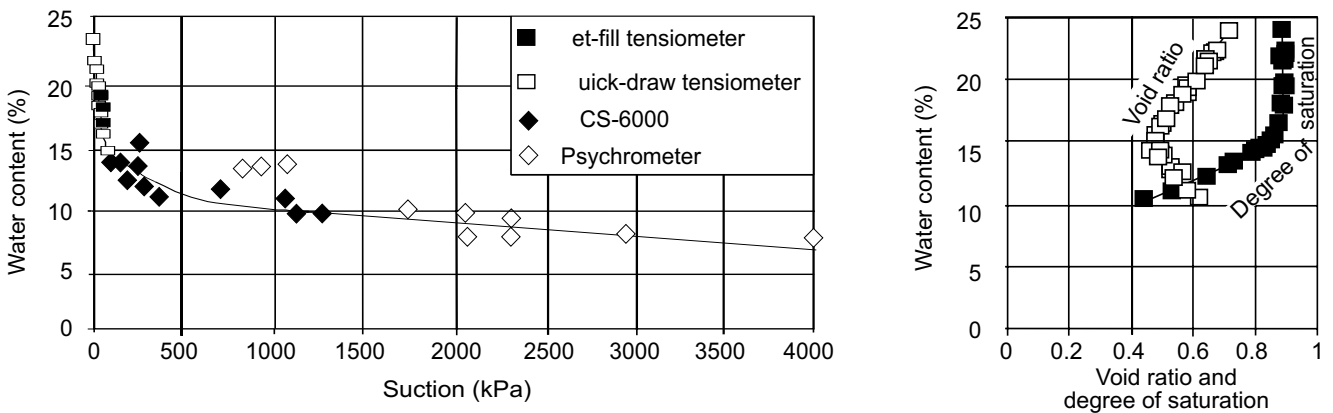


Fig. 11. Relationships between: *left*, water content – suction and *right*, water content – degree of saturation and void ratio for compacted till.



sors (Fig. 10). For the non-contact filter paper sensor it would appear to be more meaningful to restrict the calibration for suctions greater than 100 kPa.

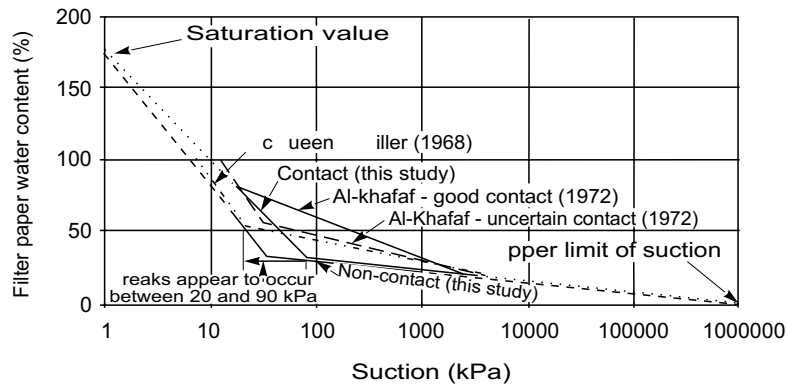
Comparison of filter paper calibration curves

The calibration curves obtained for the good-contact filter paper sensors and the non-contact filter paper sensors are shown in Fig. 12 along with some calibration curves previously obtained by others (McQueen and

Miller 1968, Al-Khafaf 1972) for the same brand of filter paper.

There appear to be considerable variations in the calibration curves in Fig. 12. There could be several reasons for the variations. First, the calibrations covered a time span from 1968 to the present. The characteristics of the Schleicher and Schuell filter papers could vary over this time period. Second, the pre-treatments given to the filter papers were not the same, although the same fungicide

Fig. 12. Comparison of calibration curves for Schleicher and Schuell No. 589 filter paper sensors.



was used in each case. In the present study the treated filter papers were oven dried. The filter papers in the other calibrations (McQueen and Miller 1968, Al-Khafaf 1972) were air dried. The oven drying was supposed to assist in suppressing the hysteresis effects. Third, the contact of the filter paper with the soil in each case varied widely. In one case (McQueen and Miller 1968), only one calibration curve was presented, presumably applicable to both good-contact and non-contact situations. In another case (Al-Khafaf 1972) a filter paper was placed at the bottom of the soil specimen, separated from the soil by a paper towel, and a second filter paper was laid on the surface of the soil. The filter paper at the bottom of the soil was deemed to have good contact with the soil, and the filter paper laid on the soil surface was considered to be in uncertain contact with the soil.

It appears that the breaks in all the calibration curves fall between 20 and 90 kPa. This suggests that the transition from liquid flow being dominant to vapour flow being dominant occurs near 20 kPa to 90 kPa.

The low suction portion of the calibration curve for the non-contact filter paper (Figs. 10 and 12) may not be meaningful, as the calibrations were obtained by a sorption process. The sorption process is more appropriate for high suction values.

Validity of the calibration curves from this study

The calibration curve in Fig. 9 for the good-contact filter paper sensors is applicable for assessing both matric suctions and total suctions in any soil. This is because the water contents of the good-contact filter paper in Fig. 9, which correspond to matric suction values, were equated to matric suctions of the compacted till specimens.

The calibration curve for the non-contact filter paper sensors in Fig. 10 is strictly valid only for the measurement of changes in matric suction and preferably only in the same soil used in the calibration (i.e., till). The water contents of the filter paper in Fig. 10 correspond to the total suctions of the soil. The suction values in Fig. 10, on the other hand, were matric suction values of the soil, measured with tensiometers or MCS-6000 thermal conductivity sensors. The water contents of the filter paper sensor corresponding to the total suctions of the soil were thus equated with the matric suctions of the soil. This

procedure is inconsistent and a separate evaluation of the osmotic suctions is required.

Consequently, psychrometers should be used only for the calibration of non-contact filter paper sensors. If filter paper in contact with the soil was calibrated by use of a psychrometer for assessing the suction in the soil, the water content corresponding to unknown matric suctions in the filter paper would be equated with the total suctions of the soil unless, of course, a separate evaluation of the osmotic suction was also conducted. At low water contents the extent of the contact between the soil and the filter may not be significant because the water flow will be restricted to the vapour phase.

Conclusions

The suction values were found to vary inversely linearly with compaction water contents in till specimens compacted at water contents wetter than optimum. The matric suction value at optimum water content was approximately 80 kPa for the till.

Compacted soil specimens at constant suction can be used for the calibration of filter paper sensors. The calibration, however, should be conducted in such a manner that the water contents of the filter paper sensors corresponding to matric suction values are referenced to matric suction values of the compacted soil specimens. Similarly, the water contents of the filter paper sensors corresponding to total suction values should be referenced to total suction values of the compacted soil specimens. The filter paper sensors, when calibrated appropriately, can be used for both matric suction and total suction measurement within the appropriate range of calibration values.

Calibration results for the filter paper sensors appear to have less scatter when the filter paper sensors are in good contact with the soil than when the filter papers are not in contact with the soil. The transition from dominant liquid flow to dominant vapour flow occurred at approximately 20 to 90 kPa.

References

- Al-Khafaf, S. 1972. Evaluation of the filter paper method for estimating soil water potential. M. Sc. thesis, Utah State University, Logan, Utah.

- Al-Khafaf, S., and Hanks, R.J. 1974. Evaluation of the filter paper method for estimating soil water potential. *Soil Science*, **117**(4): 194–199.
- Chandler, R.J., and Gutierrez, C.I. 1986. The filter paper method of suction measurement. *Géotechnique*, **36**: 265–268.
- Chandler, R.J., Crilly, M.S., and Montgomery-Smith, G. 1992. A low-cost method of assessing clay desiccation for low-rise buildings. Proceedings, Institution of Civil Engineers, Civil Engineering, Vol. 92, pp. 82–89.
- Fawcett, R.G., and Collis-George, N. 1967. A filter paper method for determining the moisture characteristics of soil. *Australian Journal of Experimental Agriculture and Animal Husbandry*, **7**:162–167.
- Hamblin, A.P. 1981. Filter-paper method for routine measurement of field water potential. *Journal of Hydrology*, **53**: 355–360.
- Houston, S.L., Houston, W.N., and Wagner, A.M. 1994. Laboratory Filter Paper Suction Measurements. *Geotechnical Testing Journal*, **17**: 185–194.
- Krahn, J., and Fredlund, D.G. 1972. On total, matric, and osmotic suction. *Journal of Soil Science*, **114**(5): 339–348.
- McKeen, R.G. 1985. Suction studies: filter paper method. Design of Airport Pavements for Expansive Soils. Final Report DOT/FAA/RD-81/25. FAA, U.S. Department of Transportation.
- McQueen, I.S., and Miller, R.F. 1968. Calibration of a wide-range gravimetric method for measuring moisture stress. *Soil Science*, **106**(3): 225–231.
- Sibley, J.W., and Williams, D.J. 1990. A new filter material for measuring soil suction. *Geotechnical Testing Journal*, **13**(4): 381–384.
- Sibley, J. W., G.K. Smyth, and Williams, D.J. 1990. Suction-moisture content calibration of filter papers from different boxes. *Geotechnical Testing Journal*, **13**(3): 257–262.
- Snethen, D.R. and Johnson, L.D. 1980. Evaluation of soil suction from filter paper. Miscellaneous Paper GL-80-4. Geotechnical Laboratory, US Army Engineer Waterways Experiment Station, Vicksburg, Mississippi.

Part III

Theoretical Framework for Unsaturated Soil Mechanics



Dr. A. Wayne Clifton
President, Clifton Associates Ltd.
Regina, Saskatchewan, Canada

Introduction and Overview

Effective stress is universally accepted as the foundation of classical soil mechanics, and $\sigma - u_w$ is recognized as the stress variable that controls the shear strength and volume change of saturated soils. Shear strength is defined by the parameter c' (effective cohesion) and ϕ' (effective angle of internal friction), while volume change is defined by effective stress changes and the moduli a_v (coefficient of compressibility), m_v (coefficient of volume change), and C_c (compressive index). The movement of fluids through porous media is governed by Darcy's Law and the coefficient of permeability is the soil property that allowed seepage to be analyzed. While many other phenomena have been studied, flow through porous media (seepage), volume change (settlement), and the shear strength of soils formed the basics of classical soil mechanics.

The theoretical framework for classical soil mechanics was sufficiently developed to have been a focus of the First International Conference of Soil Mechanics and Foundation Engineering in 1936. The concepts were well accepted by researchers and practitioners, and by the time of the Boulder Conference (ASCE Research Conference on Shear Strength of Cohesive Soils, University of Colorado at Boulder, 1960), the theoretical basis of classical soil mechanics was well defined and an appropriate technology had been developed and disseminated to design and deliver complex geotechnical projects.

While classical (saturated) soil mechanics prospered during the 1950s and 1960s, little progress was made in furthering the understanding of unsaturated soils during that era. Although it was a time of rapid engineering growth worldwide and most geotechnical projects used or were supported by unsaturated soils, their behaviour continued to be estimated using empirical methods. In other words, no comprehensive, rational theoretical scientific basis existed to support the practitioner in a manner comparable with saturated soil mechanics technology.

As a result of a lack of fundamental understanding of the mechanics of unsaturated soil behaviour, engineering practice and design methods for unsaturated soils were inconsistent and produced unreliable results. There was no universally accepted methodology for investigation, analysis, design, and monitoring of soils in the unsaturated state. A principal shortcoming was the inability to define the state of stress in the vadose zone. As a result, typical concerns included phenomena such as:

- “Dry” slopes becoming unstable even with a computed factor of safety generally accepted as safe, and often greater than 2.0.
- Unrealistic and unreliable predictions of soil heave.
- “Softening” of stiff clay soils, resulting in slope failures many years after construction.
- Ignoring fluid flow through the vadose zone; the upper boundary of fluid flow was usually taken to be the permanent groundwater table.

During this era, piezometers were generally installed to measure positive water pressures only, and soils with no free water were generally considered to be “dry”. Little attention was paid to the state of stress in the groundwater system or its influence on soil behaviour.

Much of the research during this period focused on problems associated with a particular class of soil. A typical example was the series of conferences dealing with swelling soils. These conferences focused on an exchange of information on soil behaviour and interchanged engineering experiences, but never progressed to providing a theoretical framework appropriate to all unsaturated soil problems.

D.G. Fredlund began his research into the behaviour of unsaturated soils in 1962, initially exploring the relationship of soil suction and volume change for an unsaturated soil. At that time, saturated and unsaturated soils were defined as two- and three-phase (air, water, solids) systems respectively. In the latter part of the 1970s, D.G. Fredlund postulated that unsaturated soils were, in fact, a four-phase system, adding the contractile water skin as a separate phase. This was justified in that it had differing properties from pore-water, had definable boundary surfaces, and was distinctive in its ability to exert tensile forces. While the volume of the contractile skin was insufficient to influence classical mass–volume calculations, its ability to transmit forces had a major influence on unsaturated soil behaviour.

In this unsaturated soil model, two of the phases (solids and contractile skin) moved to equilibrium under the applied stress gradients, while the fluid phases (air and water) flowed under the influence of stress gradients. The classical soil mechanics subjects (seepage, shear strength, and volume change) were studied by D.G. Fredlund and other researchers, and unsaturated soils constitutive relationships and theories were developed and shown to be an extension of classical soil mechanics theories. Two independent stress state variables ($\sigma - u_a$) and $(u_a - u_w)$, independent of physical soil properties, were used to describe shear strength and volume change of unsaturated soils. A smooth transition from unsaturated to saturated behaviour was demonstrated when the pore-air pressure became equal to the pore-water pressure.

A rheological model has been developed to assist in visualizing soil behaviour. The model consisted of two linear rheological models connected in series. One of the models simulated flow and compression of the air phase, while the other simulated flow and compression of the water phase.

It was necessary to have two sets of constitutive relations to define the phase changes that can occur in an unsaturated soil. The water phase relationship was used along with the relationship defining overall volume change (i.e., change in void ratio). The soil–water characteristic curve was part of the second relationship and was to become an important relationship in predicting properties of unsaturated soils.

The constitutive relationships enables mathematical formulation of practical engineering problems. Darcy's Law governs fluid flow, but the permeability function is dependent on soil suction and hence is a variable in unsaturated soils. Seepage and volume change formulations are combined to form a theory of consolidation (or swelling) for unsaturated soils. Once again, the transition from unsaturated to the saturated state is smooth, with the saturated state being a special case of the general unsaturated soil formulation.

The application of these formulations to engineering practice has been demonstrated and validated by field experience. The analysis of slope instability in Hong Kong (1985) was important in demonstrating the applicability of unsaturated soil mechanics theory to shear strength problems. Similar case histories have been presented by D.G. Fredlund and others in the areas of volume change (i.e., settlement, swelling, and collapse), bearing capacity, seepage, and contaminant transport.

Understanding and defining boundary conditions is paramount in the successful application of unsaturated soil mechanics theories. The particular importance of the influence of flux at the soil surface boundary was demonstrated by G.W. Wilson in 1990. D.G. Fredlund concurs that surface boundary flux has evolved as a very significant factor controlling the behaviour of unsaturated soils.

The properties of saturated soils were either assumed to be linear (e.g., coefficient of permeability) or were linearized (e.g., compressive index), for analysis purposes. Unsaturated soil research has revealed that soil properties are non-linear functions, resulting in non-linear theoretical formulations. In general, the cost of measuring non-linear soil property functions in the laboratory was several times the cost of measuring similar saturated soil properties. This high cost was a limitation in advancing unsaturated soil mechanics to a practical engineering science.

Research has shown that the soil–water characteristic curve can be used to predict or estimate the non-linear unsaturated soil property functions. The cost of measuring one branch of the soil–water characteristic curve was, in general, less than the cost of a one-dimensional consolidation test. Soil property functions determined from the soil–water characteristic curve appeared to be satisfactory for many geotechnical engineering applications. For example, it has become accepted practice to use the coefficient of permeability function estimated from the soil–water characteristic curve when performing saturated–unsaturated seepage analyses.

Recent research has also demonstrated that knowledge-based systems operating on large databases can be of great value in estimating the soil–water characteristic curve. The grain size curve has been used to assist in estimating a suitable soil–water characteristic curve for a particular soil. Some of these estimation procedures may at first appear to be quite approximate; however, their usage can be of great assistance to the geotechnical engineer in setting reasonable bounds on the properties of an unsaturated soil.

The theories for unsaturated soil mechanics were proposed as, and have been shown to be, relatively simple extensions of saturated soil mechanics theories. In reality, extensive research in the last three decades, and emerging practice have demonstrated that a generalized soil mechanics theory has emerged. This generalized theory allows comprehensive, rational consideration of the geosphere as a continuum extending from the atmosphere-soil interface to the deepest subsurface, uninterrupted by discontinuities or artificial analytical boundaries. The economical assessment of unsaturated soil property functions has enabled the application of that technology. As a result, a comprehensive theoretical framework is now available for the engineering application of both saturated and unsaturated soil mechanics.

Part III

Theoretical Framework for Unsaturated Soil Mechanics

- Fredlund, D.G. 1979. Second Canadian geotechnical colloquium: Appropriate concepts and technology for unsaturated soils. *Canadian Geotechnical Journal*, **16**(1): 121–139 . . . 111
- Fredlund, D.G., and Rahardjo, H. 1985. Theoretical context for understanding unsaturated residual soil behavior. *Proceedings of the First International Conference on Geomechanics in Tropical Lateritic and Saprolitic Soils, Brazilia, Brazil*, pp. 295–306 . 127
- Fredlund, D.G. 1985. Soil mechanics principles that embrace unsaturated soils. *Proceedings, 11th International Society for Soil Mechanics and Foundation Engineering, San Francisco, USA., Vol. 2*, pp. 465–473 133
- Fredlund, D.G. 1995. The scope of unsaturated soils mechanics: An overview. *Proceedings, 1st International Conference on Unsaturated Soils, Paris, France, Vol. 3*, pp. 1155–1177 . . . 140
- Wulfsohn, D., Adams, B.A., and Fredlund, D.G. 1996. Application of unsaturated soil mechanics for agricultural conditions. *Canadian Agricultural Engineering*, **38**(3): 173–181. . 157
- Fredlund, D.G. 1997. From theory to the practice of unsaturated soil mechanics. *Proceedings, 3rd Brazilian Symposium on Unsaturated Soils, Rio de Janeiro, Brazil* 166
- Fredlund, D.G., and Xing, A. 1994. Equations for the soil-water characteristic curve. *Canadian Geotechnical Journal*, **31**(3): 521–532 181
- Fredlund, D.G. 1964. Comparison of soil suction and one-dimensional consolidation characteristics of a highly plastic clay. *National Research Council of Canada, Division of Building Research, Technical Report No. 245, Ottawa, Ontario*. 193
- Fredlund, M.D., Fredlund, D.G. and Wilson, G.W. 1997. Prediction of the soil-water characteristic curve from grain-size distribution and volume-mass properties. *Proceedings, Third Brazilian Symposium on Unsaturated Soils, NSAT'97, Rio de Janeiro, Brazil, April 22–25, Vol. 1*, pp. 13–23 202
- Fredlund, M.D., Sillers, W.S., Fredlund, D.G. and Wilson, G.W. 1996. Design of a knowledge-based system for unsaturated soil properties. *Proceedings, Third Canadian Conference on Computing in Civil and Building Engineering, Aug. 26–28*, pp. 659–677. . . 207

Appropriate concepts and technology for unsaturated soils

D.G. Fredlund

Abstract: A practical science has not been fully developed for unsaturated soils for two main reasons. First, there has been the lack of an appropriate science with a theoretical base. Second, there has been the lack of an appropriate technology to render engineering practice financially viable.

This paper presents concepts that can be used to develop an appropriate engineering practice for unsaturated soils. The nature of an unsaturated soil is first described along with the accompanying stress conditions. The basic equations related to mechanical properties are then proposed. These are applied to practical problems such as earth pressure, limiting equilibrium, and volume change.

An attempt is made to demonstrate the manner in which saturated soil mechanics must be extended when a soil is unsaturated. Two variables are required to describe the stress state of an unsaturated soil (e.g., $(\sigma - u_a)$ and $(u_a - u_w)$). There is a smooth transition from the unsaturated case to the saturated case since the pore-air pressure becomes equal to the pore-water pressure as the degree of saturation approaches 100%. Therefore, the matric suction (i.e., $(u_a - u_w)$) goes to zero, and the pore-water pressure can be substituted for the pore-air pressure (i.e., $(\sigma - u_w)$).

The complete volumetric deformation of an unsaturated soil requires two three-dimensional constitutive surfaces. These converge to one two-dimensional relationship for a saturated soil. The shear strength for an unsaturated soil is a three-dimensional surface that reduces to the conventional Mohr-Coulomb envelope for a saturated soil.

The manner of applying the volumetric deformation equations and the shear strength equation to practical problems is demonstrated. For earth pressure and limiting equilibrium problems, the unsaturated soil can be viewed as a saturated soil with an increased cohesion. The increase in cohesion is proportional to the matric suction of the soil. For volume change problems it is necessary to have an indication of the relationship between the various soil moduli.

There is a need for further experimental studies and case histories to substantiate the proposed concepts and theories.

Key words: unsaturated soil mechanics, stress state variables, volume change, shear strength, earth pressure, slope stability.

Introduction

The success of the practice of soil mechanics can be traced largely to the ability of engineers to relate observed soil behaviour to stress conditions. This ability had led to the transmissibility of the science and a relatively consistent engineering practice. Although this has been true for saturated soils, such has not been the case for unsaturated soils.

The general field of soil mechanics can be subdivided into that portion dealing with saturated soils and that portion dealing with unsaturated soils (Fig. 1). This differentiation is necessary because of their basic difference in nature and behaviour. Whereas a saturated soil is a two-

phase system, an unsaturated soil with a continuous air phase is a four-phase system (Fredlund and Morgenstern 1977) (Fig. 2). The air phase generally becomes continuous when the degree of saturation is less than approximately 85–90%. The four phases of an unsaturated soil are (i) solids, (ii) water, (iii) air, and (iv) contractile skin (or air-water interface). Soils commonly falling into this category are the natural, desiccated soils and compacted soils. The pore-water pressures of these soils are generally negative and the most prevalent problems are related to their expansion and shrinkage.

There has been difficulty in extending soil mechanics to embrace unsaturated soils. This has been borne out by the empirical nature of most research associated with unsaturated soils.

The question can be asked: "Why hasn't a practical science developed and flourished for unsaturated soils?" A cursory examination may suggest there is not a need for such a science. However, this is not the case when the problems associated with expansive soils are considered. Jones and Holtz (1973) reported that in the United States alone: "Each year, shrinking and swelling soils inflict at

D.G. Fredlund. Professor, Department of Civil Engineering, University of Saskatchewan, 57 Campus Drive, Saskatoon, SK, Canada S7N 5A9.

Reproduced with permission from the *Canadian Geotechnical Journal*, Second Geotechnical Colloquium, 31st Canadian Geotechnical Conference, Winnipeg, Manitoba, Canada, October, 1978, **16**(1): 121–139.

Fig. 1. Categories of soil mechanics. * Dry sands are two-phase systems. ** Soils with occluded air bubbles are two-phase systems with a compressible pore fluid. *** Either swelling or collapsing soils.

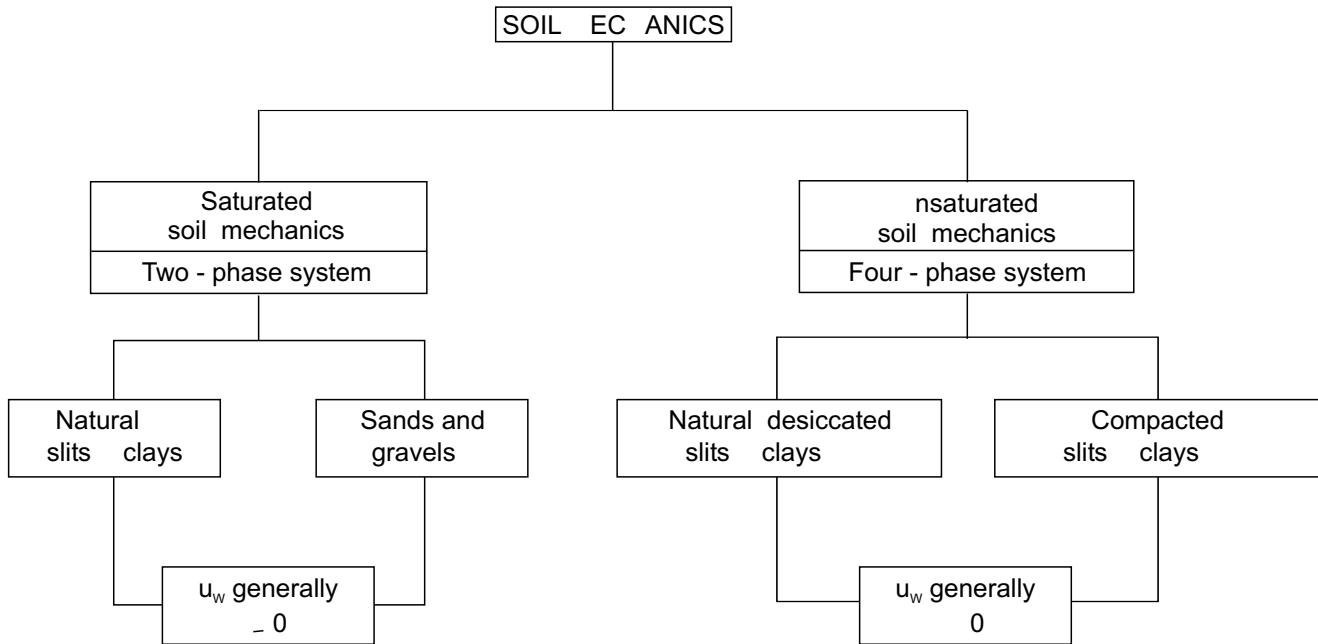
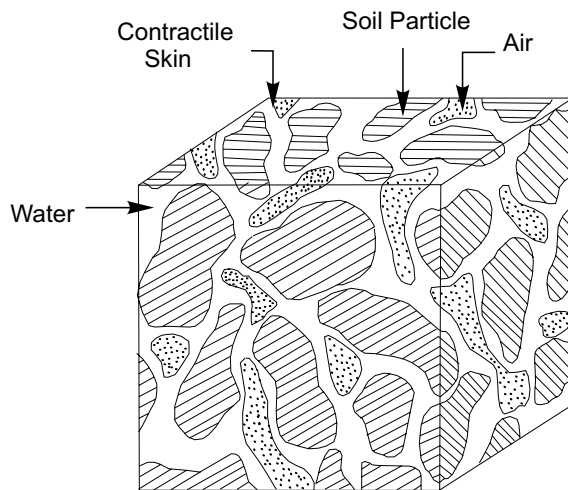


Fig. 2. An element of unsaturated soil (continuous air phase).



least \$2.3 billion in damages to houses, buildings, roads and pipelines more than twice the damage from floods, hurricanes, tornadoes and earthquakes!" They also reported that 60% of the new houses built in the United States will experience minor damage during their useful lives, that 10% will experience significant damage some beyond repair. In addition there is the need for reliable engineering design associated with the use of compacted soils.

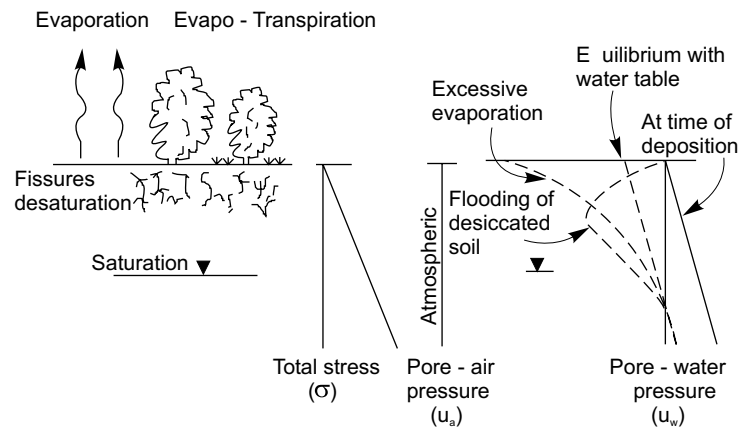
There appears to be two main reasons why a practical science has not developed for unsaturated soils (Holtz et al. 1974). First, there has been the lack of an appropriate science with a theoretical base. This commences with a lack of appreciation of the engineering problems and an inability to place the solution within a theoretical context.

The stress conditions and mechanisms involved as well as the soil properties that must be measured have not been fully understood. The boundary conditions for an analysis are generally related to the environment and are difficult to predict. Research work has largely remained empirical in nature with little coherence. As a result there is poor communication amongst engineers and design procedures are not widely accepted and adhered to.

Second, there is the lack of a system for financial recovery for services rendered by the engineer. In the case of expansive soils problems, the possible liability to the engineer is often too great relative to the financial remuneration. Other areas of practice are far more profitable to consultants. The owner often reasons that the cost outweighs the risk. The hazard to life and injury is largely absent and for this reason little attention has been given to the problem by government agencies. Although the problem basically remains with the owner, it is the engineer who has the greatest potential for circumventing possible problems.

This paper will address the need for an appropriate technology for unsaturated soil behaviour. Such a technology must: (i) be practical, (ii) not be too costly to employ, (iii) have a sound theoretical basis, and (iv) run parallel in concept to conventional saturated soil mechanics.

A macroscopic, phenomenological approach to unsaturated soil behaviour holds the greatest potential for satisfying the above conditions. In other words, the science is developed around observable phenomena while adhering to multiphase continuum mechanics principles. This has proven to be the most successful approach for saturated soils and should be retained for unsaturated soils. There-

Fig. 3. Stress distribution during desiccation of a soil.

fore, unsaturated soil behaviour can be viewed as an extension of saturated soil mechanics and retain a smooth transition in rationale between the two cases.

This paper will propose the basis of an appropriate technology for unsaturated soil behaviour. First, the nature of an unsaturated soil is described along with its stress conditions. Then the basic equations related to the mechanical properties are proposed. Finally, these are applied to earth pressure, limiting equilibrium, and volume change problems. An attempt will be made to demonstrate the extension of the theory for saturated soil conditions to that for unsaturated soils. Due to the broad scope of the paper, each aspect will be dealt with in a cursory manner.

Nature of unsaturated soils

Most soil deposits are originally saturated. Lacustrine deposits, for example, are deposited at water contents above the liquid limit and then are consolidated by the weight of the overlying sediments (Fig. 3). The drying up of the lake and subsequent evaporation of water commence desiccation of the sediments. The water table is drawn below the ground surface. The total stress on the sediments remains essentially constant while the pore-water pressure is reduced. The pore-water pressure becomes negative with respect to atmospheric pressure above the water table giving rise to consolidation and eventually desaturation of the sediments. Grasses, trees, and other plants start to grow on the surface, further drying out the soil by applying a tension to the water phase through evapotranspiration. Most plants are capable of applying 1 to 2 MPa (10 to 20 atm) of tension to the water phase prior to reaching their wilting point. Evapotranspiration results in further consolidation and desaturation of the soil.

The tension in the water phase acts in all directions and can readily exceed the lateral confining pressure in the soil mass. At this point, a secondary mode of desaturation commences (i.e., cracking). When a soil is remolded in the compaction process, desaturation is also the result of artificially subjecting the soil structure to tensile stresses.

Year after year the deposit is subjected to varying and changing environmental conditions. These produce changes in the pore-water pressure distribution, which in turn results in shrinking and swelling of the soil deposit. As a result of environmental changes, the pore-water pressure distribution can take on a wide variety of shapes (Fig. 3).

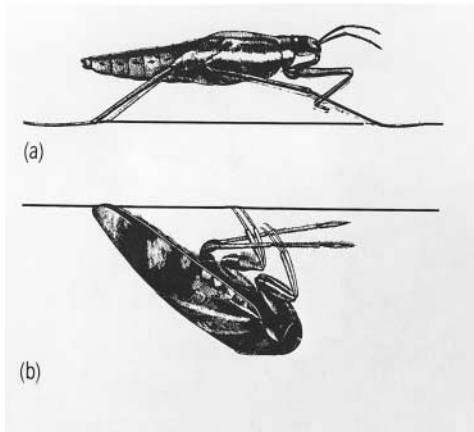
Generally, an unsaturated soil is considered to be a three-phase system. However, on the basis of the definition of a phase, the air-water interface should be considered as a fourth and independent phase. The air-water interface, commonly referred to as the 'contractile skin', qualifies as a phase since it has (i) differing properties from that of the contiguous materials and (ii) definite bounding surfaces.

The most distinctive property of the contractile skin is its ability to exert a tensile pull. It behaves like an elastic membrane under tension interwoven throughout the soil structure. It appears that most properties of the contractile skin are different from those of the contiguous water phase (Davies and Rideal 1963). For example, its density is reduced, its heat conductance is increased, and its birefringence data are similar to those of ice. The transition from the liquid water to the contractile skin has been shown to be distinct or jumpwise (Derjaguin 1965). It is interesting to note that insects such as the 'water strider' walk on top of the contractile skin and those such as the 'backswimmer' walk on the bottom of the contractile skin (Milne and Milne 1978). The water strider would sink into the water were it not for the contractile skin whereas the backswimmer would pop out of the water (Fig. 4).

It is imperative to recognize an unsaturated soil as a four-phase system when performing a stress analysis on an element (Fredlund and Morgenstern 1977). From a behavioural standpoint, an unsaturated soil can be visualised as a mixture with two phases that come to equilibrium under applied stress gradients (i.e., soil particles and contractile skin) and two phases that flow under applied stress gradients (i.e., air and water).

From the standpoint of the volume-weight relations for an unsaturated soil, it is possible to consider the soil as a three-phase system since the volume of the contractile skin is small and its weight can be considered as part of

Fig. 4. Insects living above and below the contractible skin (from Milne and Milne 1978): a) water strider; b) backswimmer.



the weight of water. All the commonly used volume-weight relations (for a selected specific gravity of solids) are shown in Fig. 5. The three most basic volume-weight variables are the void ratio, water content, and degree of saturation.

Although relations between these basic variables are fixed for saturated soils, such is not the case for unsaturated soils. For an unsaturated soil, a change in volume-weight conditions can involve changes anywhere below the 100% saturation line. It now becomes necessary to know any two of the basic volume-weight variables to describe all volume-weight relations. This also applies for changes in one or two of the volume-weight variables. Therefore, two constitutive relations are required to describe the volume change associated with all phases of an unsaturated soil whereas only one is required for a saturated soil. This can also be expressed in terms of the volumetric continuity requirement for a referential element of unsaturated soil.

$$[1] \quad \Delta V / V = \Delta V_w / V + \Delta V_a / V$$

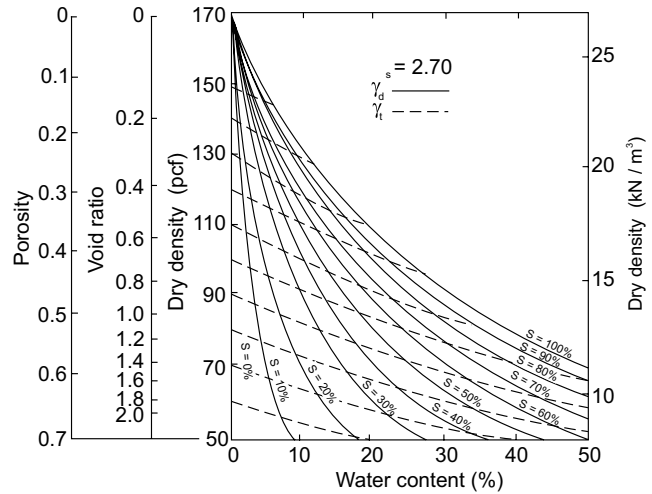
where:

- V = total volume of the element of soil,
- V_w = volume of water, and
- V_a = volume of air.

Stress state

Numerous so-called “effective stress” equations have been proposed for unsaturated soils (Bishop 1959; Croney et al. 1958; Lambe 1960; Aitchison 1961; Jennings 1961; Richards 1966). Common to all proposed equations is the incorporation of a soil parameter to couple together more than one stress variable. However, the description of the stress state should consist of independent stress variables, the number being dependent on the number of phases of the material. For example, the stress tensor for a one phase solid such as steel is the same as for “Jello”. Likewise the effective stress variable for a

Fig. 5. Volume-weight relations for unsaturated soils.



saturated soil is independent of the physical properties of the soil.

Recently, two independent stress tensors have been proposed for unsaturated soils (Fredlund and Morgenstern 1977). These can be supported by a stress analysis consistent with that used in multiphase continuum mechanics. The assumptions in the stress analysis are that the solids are incompressible and the soil is chemically inert. These assumptions are comparable to those associated with the stress state description for a saturated soil.

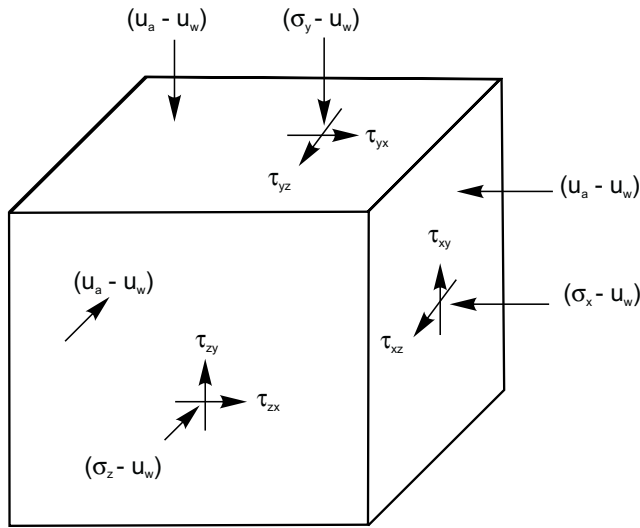
The stress analysis shows that any two of three possible stress variables can be used to describe the stress state of an unsaturated soil. Possible combinations are: (1) $(\sigma - u_a)$ and $(u_a - u_w)$, (2) $(\sigma - u_w)$ and $(u_a - u_w)$, and (3) $(\sigma - u_a)$ and $(\sigma - u_w)$, where σ = total stress, u_a = pore-air pressure, and u_w = pore-water pressure. After attempts to apply the stress state variables to earth pressure problems, shear strength problems, and volume change problems, the author has concluded that the $(\sigma - u_a)$ and $(u_a - u_w)$ combination is the most satisfactory. This combination is advantageous since the effects of total stress changes and pore-water pressure changes can be separated. This is beneficial both from a conceptual and analytical standpoint. (The air pressure for most practical problems is atmospheric.)

The complete stress state at a point is shown in Fig. 6. Only the $(\sigma - u_a)$ and $(u_a - u_w)$ combination will be used in the remainder of this paper. The $(\sigma - u_a)$ term is called the net total stress¹ and the $(u_a - u_w)$ term is called the matric suction.

The two independent stress tensors are represented by

$$[2] \quad \begin{bmatrix} \sigma_x - u_a & \tau_{xy} & \tau_{xz} \\ \tau_{yx} & \sigma_y - u_a & \tau_{yz} \\ \tau_{zx} & \tau_{zy} & \sigma_z - u_a \end{bmatrix}$$

¹The term “total stress” is used to represent σ relative to u_a .

Fig. 6. Stress state variables for an unsaturated soil.

for the first stress tensor and by

$$[3] \quad \begin{bmatrix} u_a - u_w & 0 & 0 \\ 0 & u_a - u_w & 0 \\ 0 & 0 & u_a - u_w \end{bmatrix}$$

for the second stress tensor.

The first stress invariants of the first and second stress tensors, respectively, are:

$$[4] \quad \begin{aligned} I_{11} &= \sigma_1 + \sigma_2 + \sigma_3 - 3u_a \\ I_{12} &= 3(u_a - u_w) \end{aligned}$$

The second stress invariants of the first and second stress tensors, respectively, are:

$$[5] \quad \begin{aligned} I_{21} &= (\sigma_1 - u_a)(\sigma_2 - u_a) + (\sigma_2 - u_a)(\sigma_3 - u_a) \\ &\quad + (\sigma_3 - u_a)(\sigma_1 - u_a) \\ I_{22} &= 3(u_a - u_w)^2 \end{aligned}$$

The third stress invariants of the first and second stress tensors, respectively, are:

$$[6] \quad \begin{aligned} I_{31} &= (\sigma_1 - u_a)(\sigma_2 - u_a)(\sigma_3 - u_a) \\ I_{32} &= (u_a - u_w)^3 \end{aligned}$$

where σ_1 = major principal stress, σ_2 = intermediate principal stress, and σ_3 = minor principal stress. Since the stress invariants of the second stress tensor are related, only one invariant is required. Therefore, the three-dimensional stress state can be described in terms of four stress invariants for an unsaturated soil as opposed to three stress invariants for a saturated soil.

The above stress state variables also provide a smooth transition in stress description when going from the unsaturated to the saturated soil case. As the degree of satu-

ration approaches 100%, the pore-air pressure approaches the pore-water pressure. Therefore, the matric suction term goes to 0 and the pore-air term in the first stress tensor becomes the pore-water pressure.

The state of stress for an unsaturated soil can be plotted on an extended Mohr type of diagram where the third orthogonal axis has been added to represent the matric suction (Fig. 7).

From thermodynamic or total energy considerations of the pore water, its total suction, h , can be subdivided into a matric suction component and an osmotic component, π (Aitchison and Richards 1965),

$$[7] \quad h = (u_a - u_w) + \pi$$

The relationship has been experimentally verified (Fig. 8) and changes in the osmotic component with water content are relatively small (Krahn and Fredlund 1972). It is possible to use total suction as a substitute for the matric suction variable. In this case either the changes in osmotic suction must be assumed to be small or else simulated between the field and the laboratory.

It is difficult to measure matric suction in the field due to cavitation of the measuring system at pore-water stresses approaching 100 kPa (1 atm) negative. In the laboratory these difficulties are circumvented using the axis-translation technique.

Recently psychrometers, which measure total suction, have received increased usage in evaluating the suction of a soil in the laboratory and the field (Fig. 9). The low cost of the psychrometers and the measuring equipment makes them attractive for engineering usage.² However, their use is restricted to soils with a suction greater than 100 kPa (1 atm).

Physical properties

Various types of constitutive relations are required in soil mechanics. Each equation requires soil properties that must be experimentally evaluated. Some of the constitutive relations required for an understanding of unsaturated soil behavior are listed in Table 1. The details of the derivations associated with each type of constitutive relation are presented in the references shown in Table 1.

Stress state variables versus volume-weight relations

The most basic and important constitutive equations are those relating the stress state variables and the volume-weight properties. Equations are required for each of two phases of an unsaturated soil. The soil structure (or overall element) and the water phase are selected for presenting the constitutive relations. The soil is first assumed to behave as an isotropic, linear elastic material. The constitutive relations can be developed in a semi-empirical manner as an extension of the elasticity formulation used for saturated soils as follows.

Soil structure:

²Manufacturers of psychrometers are: Wescor, Inc., 459 South Main Street, Logan, UT 84321; and Emco, P.O. Box 34, Angola, IN 46703.

Fig. 7. Extended Mohr diagram for unsaturated soils.

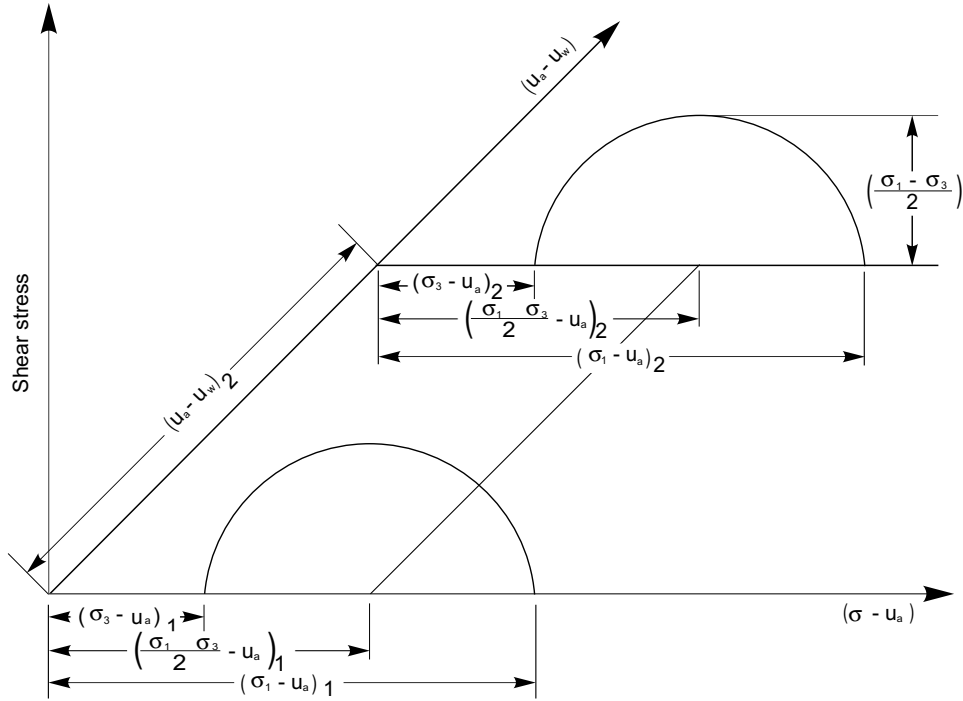
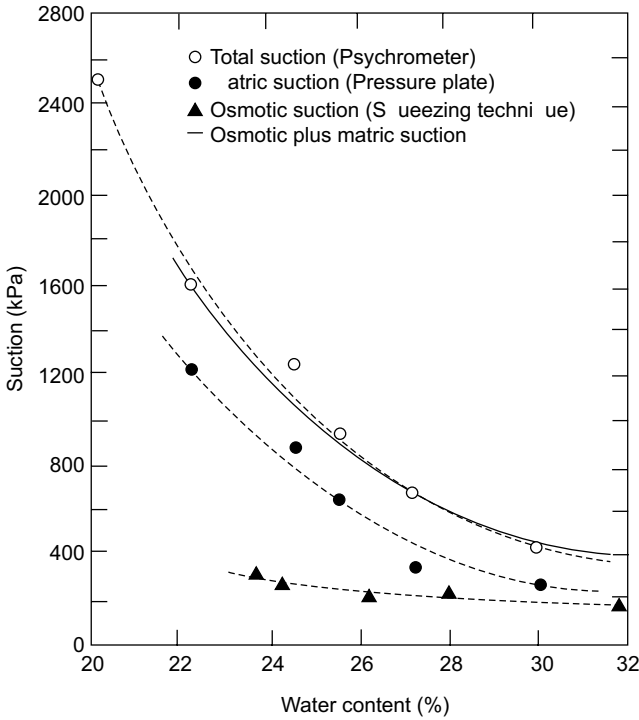


Fig. 8. Total, matric, and osmotic suction for Regina clay.



$$\epsilon_x = \frac{(\sigma_x - u_a)}{E_1} - \frac{\mu_1}{E_1}(\sigma_y + \sigma_z - 2u_a) + \frac{(u_a - u_w)}{H_1}$$

$$[8] \quad \epsilon_y = \frac{(\sigma_y - u_a)}{E_1} - \frac{\mu_1}{E_1}(\sigma_x + \sigma_z - 2u_a) + \frac{(u_a - u_w)}{H_1}$$

$$\epsilon_z = \frac{(\sigma_z - u_a)}{E_1} - \frac{\mu_1}{E_1}(\sigma_y + \sigma_x - 2u_a) + \frac{(u_a - u_w)}{H_1}$$

where:

- $\epsilon_x, \epsilon_y, \epsilon_z$ = strain in the $x, y,$ and z directions,
- E_1 = Young's modulus with respect to $(\sigma - u_a)$,
- μ_1 = Poisson's ratio, and
- H_1 = elastic modulus with respect to $(u_a - u_w)$.

Water phase:

$$[9] \quad \theta_w = \frac{(\sigma_x + \sigma_y + \sigma_z + 3u_a)}{3H_1'} + \frac{(u_a - u_w)}{R_1}$$

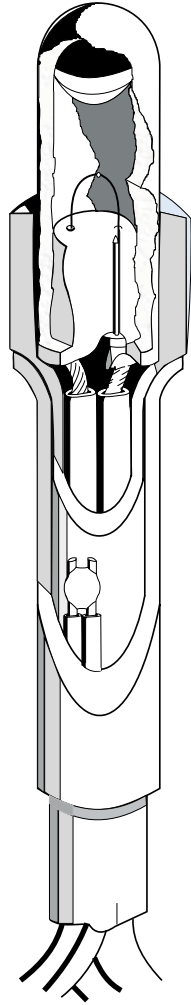
where:

- θ_w = change of volume of water in element (i.e., $\Delta V_w / V$,
- H_1' = water phase modulus with respect to $(\sigma - u_a)$, and
- R_1 = water phase modulus with respect to $(u_a - u_w)$.

In order to retain consistency with saturated soil mechanics, the void ratio change will be used to represent the strain in the soil structure. Also, the matric suction will be plotted in the same units as the total stress.³

³For engineering purposes this procedure is superior to the pF representation of soil suction commonly used in soil science.

Fig. 9. Soil psychrometer; scale: 4:1 (compliments of Wescor, Inc.).



For one-dimensional or K_0 loading conditions, the arithmetic plot of void ratio versus stress state variables can be presented as a three-dimensional surface (Fig. 10). Generally, the surface will be non-linear; however, coefficients of compressibility can be defined for small stress increments. The slopes of particular interest are those associated with each of the stress state variables. Let the

coefficient of compressibility with respect to the total stress be,

$$[10] \quad a_t = -de / d(\sigma - u_a)$$

and the coefficient of compressibility with respect to matric suction be,

$$[11] \quad a_m = -de / d(u_a - u_w)$$

For corresponding stress ranges, a_t will approximately equal a_m when the degree of saturation is near 100%. There will be a slight difference in the coefficients of compressibility since a_t is related to K_0 loading whereas a_m is related to isotropic loading. As the degree of saturation decreases it has been found that a_t will become greater than a_m . This shows that a change in $(\sigma - u_a)$ is more effective in changing void ratio than a change in $(u_a - u_w)$. In the plane of zero matric suction (i.e., the saturation plane), the pore-air pressure becomes equal to the pore-water pressure and the coefficient of compressibility with respect to total stress is equal to the coefficient of compressibility when the soil is saturated (i.e., a_v). Coefficients of compressibility corresponding to rebound portions of the surface can be further subscripted with an s (i.e., a_{ts} and a_{ms}). The proposed constitutive surface has been experimentally tested for uniqueness near a point (Fredlund and Morgenstern 1976) and for uniqueness when larger stress increments are used (Matyas and Radhakrishna 1968; Barden et al. 1969). The results indicate uniqueness as long as the deformation conditions are monotonic.

The constitutive surface can be linearized over a wider range of stress changes using the logarithm of the stress state variables (Fig. 11). The soil properties of interest are the compressive index with respect to the total stress, C_t , and the compressive index with respect to matric suction, C_m . The void ratio under any set of stress conditions can be written in terms of an extended form of the equation commonly used for saturated soils:

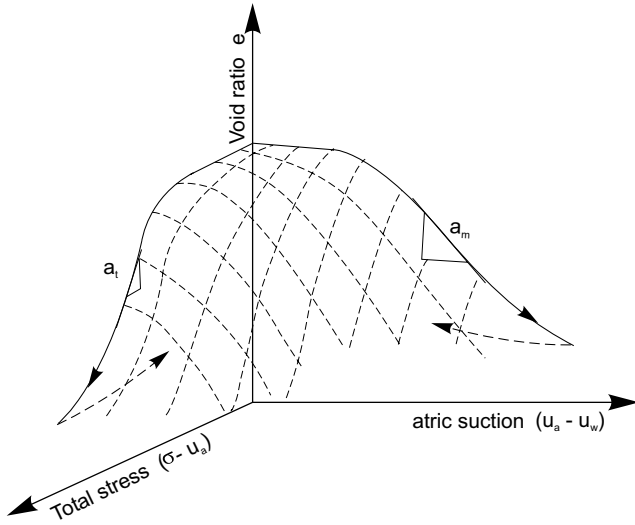
$$[12] \quad e = e_0 - C_t \log \frac{(\sigma - u_a)_f}{(\sigma - u_a)_0} - C_m \log \frac{(u_a - u_w)_f}{(u_a - u_w)_0}$$

where the f subscript represents final stress state and 0 represents the initial stress state. The range of applicability of the equation may be somewhat controlled by stress

Table 1. Types of constitutive relations

Type	Description	Reference
Stress vs. volume-weight	(1) Relates the stress state variables to strains, deformations, and volume-weight properties such as void ratio, water content, and degree of saturation	Fredlund and Morgenstern (1976)
	(2) Density equations for air-water mixtures	Fredlund (1976)
	(3) Compressibility equations for air-water mixtures	Fredlund (1976)
Stress vs. stress	(1) Pore pressure parameters relating the normal stress components for undrained loading conditions	Hasan and Fredlund (1977)
	(2) Strength equations relating shear strength to stress state variables	Fredlund et al. (1978)
Stress gradient vs. velocity	(1) Flow laws for the pore-air and pore-water	Hasan and Fredlund (1977)

Fig. 10. Arithmetic representation of stress state variables versus void ratio.



history. Once again, C_t is approximately equal to C_m when the degree of saturation approaches 100% and C_t becomes equal to the conventional compressive index, C_c (Fig. 12). At lower degrees of saturation, C_t will be greater than C_m . The quantitative relationship between the compressive indices must be evaluated experimentally. Unfortunately, the literature contains little if any complete data on compressive indices for soils with low degrees of saturation.

A similar constitutive surface exists for the water phase. Once again the non-linear arithmetic plot of water content versus the stress state variables can be linearized on a logarithm of stress plot (Fig. 13). Let us define the coefficient of water content with respect to the total stress as:

$$[13] \quad b_t = -dw / d(\sigma - u_a)$$

and the coefficient of water content with respect to matric suction as:

$$[14] \quad b_m = -dw / d(u_a - u_w)$$

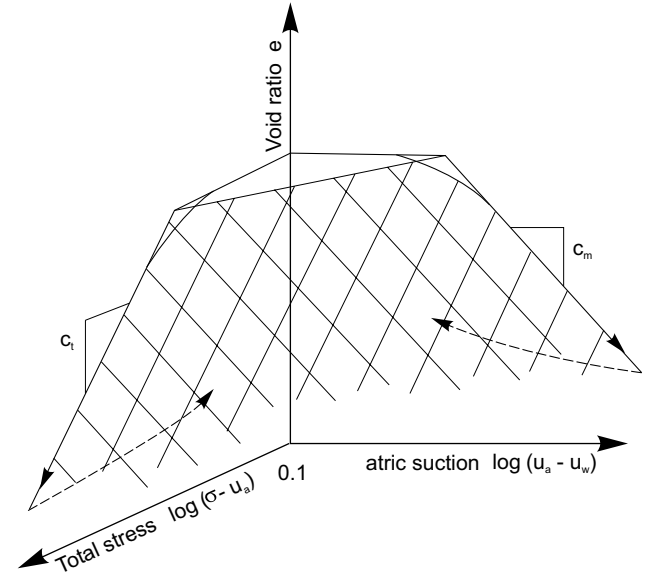
At 100% saturation, b_t approaches b_m . At lower degrees of saturation, b_m will generally be greater than b_t since stress applied directly to the water phase will be more effective in removing water from the sample. When b_t is measured on the saturation plane, it becomes equal to a_t or a_v provided b_t is multiplied by the specific gravity of the soil solids, G_s . On a logarithm of stress plot, the water content under any set of stresses can be written as:

$$[15] \quad w = w_0 - D_t \log \frac{(\sigma - u_a)_f}{(\sigma - u_a)_0} - D_m \log \frac{(u_a - u_w)_f}{(u_a - u_w)_0}$$

where:

- w_0 = initial water content,
- D_t = water content index with respect to total stress, and

Fig. 11. Logarithm of stress state variables versus void ratio.



D_m = water content index with respect to matric suction.

Relationship between moduli

Four compressibilities or indices have been defined to completely describe the volume-weight versus stress state variables for an unsaturated soil. The moduli are also different for increases and decreases of the stress state variables. All moduli tend towards one value for a saturated soil. For an unsaturated soil, four moduli are too much to evaluate on a routine basis for engineering purposes. Therefore a knowledge of the relationship of one modulus to another is highly advantageous.

First, the testing of a soil in the total stress plane (i.e., matric suction equal to zero) can be accomplished in the conventional triaxial or one-dimensional consolidation apparatus (Fig. 14). The two moduli on the total stress plane are approximately equal (i.e., a_t and b_t). Note that the modulus with respect to water content must be multiplied by the specific gravity of the solids, G_s , in order for it to equal the modulus with respect to void ratio. This reduces the four unknown moduli to three.

Second, at all degrees of saturation, there is a relationship between the volume-weight properties as defined by the two constitutive surfaces.

$$[16] \quad Se = wG_s$$

Changes in any one of the variables can produce changes in the other two variables. The change in water content can be written in terms of a change in degree of saturation and void ratio.

$$[17] \quad \Delta w = S_f \Delta e / G_s + e_0 \Delta S / G_s$$

Likewise, a change in void ratio can be written as:

$$[18] \quad \Delta e = G_s \Delta w / S_f - e_0 \Delta S / S_f$$

Fig. 12. Comparison of recompression curves for matric suction and total stress loading of initially saturated Regina clay (after Fredlund 1964).

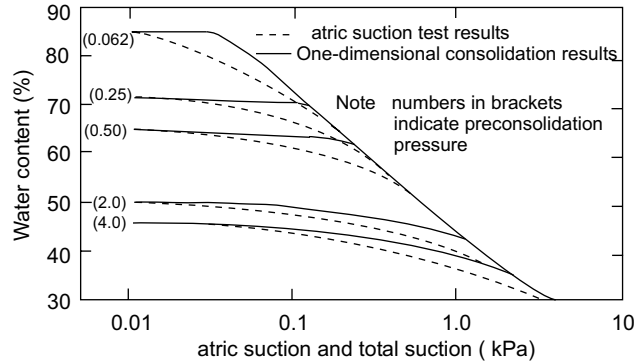
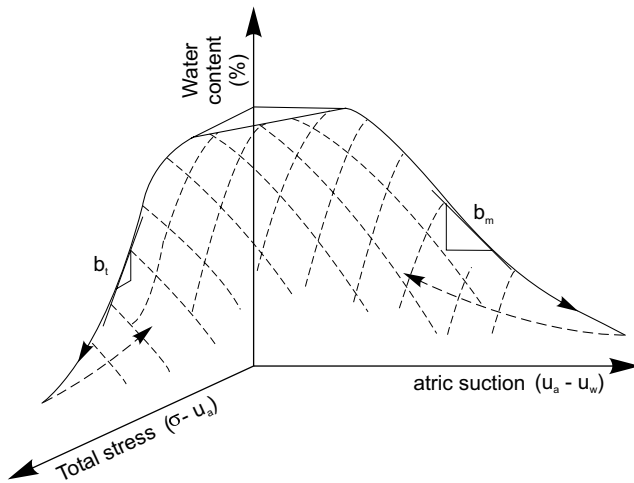


Fig. 13. Arithmetic representation of stress state variables versus water content.



If the change in degree of saturation is known or can be estimated, there is a fixed relationship between the modulus with respect to void ratio and water content. This, in essence reduces the number of unknown moduli to two. For problems such as the prediction of heave, the final degree of saturation will be close to 100%. Therefore, an analysis for the prediction of heave can be done in terms of a change in water content and the corresponding change in void ratio can be computed. In other words, there is a relationship between the moduli with respect to water content and void ratio.

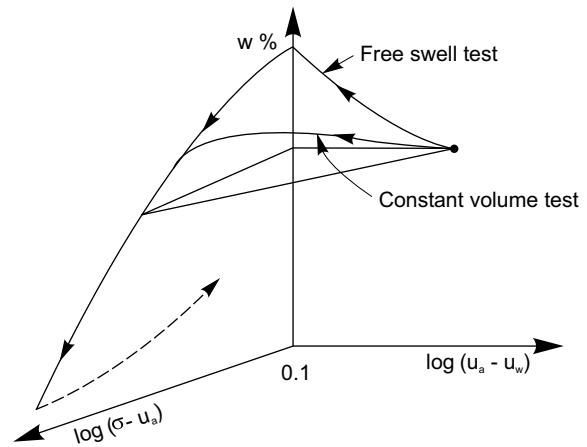
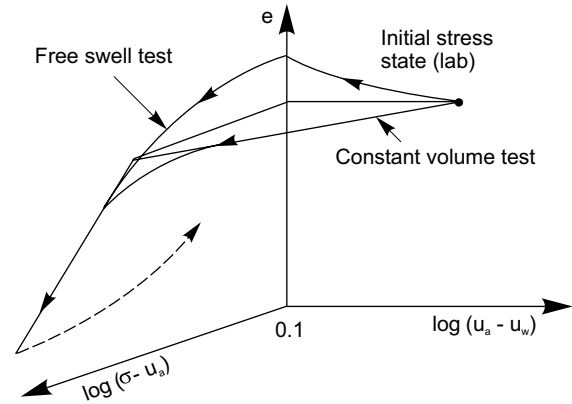
For the case where the change in water content is predicted, let the ratio of the void ratio modulus with respect to the water content modulus, ξ_w , be defined as follows:

$$[19] \quad \xi_w = \frac{a}{bG_s} = \frac{100}{S_f} \left(1 - \frac{e_0 \Delta S}{G_s \Delta w} \right)$$

where:

b = any coefficient of compressibility on the water content versus stress state variable plot, and

Fig. 14. Conventional consolidation test on an unsaturated soil.



a = the corresponding coefficient of compressibility on the void ratio versus stress state variable plot.

Equation [19] is presented graphically in Fig. 15.

For the case where the change in void ratio is predicted, let the ratio of the water content modulus with respect to the void ratio modulus, ξ_e , be defined as follows:

$$[20] \quad \xi_e = \frac{bG_s}{a} = \frac{S_f}{100} \left(1 + \frac{e_0 \Delta S}{100 \Delta e} \right)$$

A shrinkage limit type of test also gives the relationship between the void ratio and water content constitutive surfaces for the special case of changes in matric suction when the external loads are zero (Fig. 16). The specific bulk volume is the inverse of the dry density and is a measure of the void ratio. The slope of the shrinkage curve can be related to the ratio of the void ratio coefficient to the water content coefficient of compressibility.

Third, information is required on the relationship between the relative effects of a change in total stress and matric suction. If this were known, the number of unknowns would be reduced to one. However, little or no information is available on the relative effects of the two stress state variables. This is an area of much needed research.

Fig. 15. Compressibility ratios versus volume-weight properties.

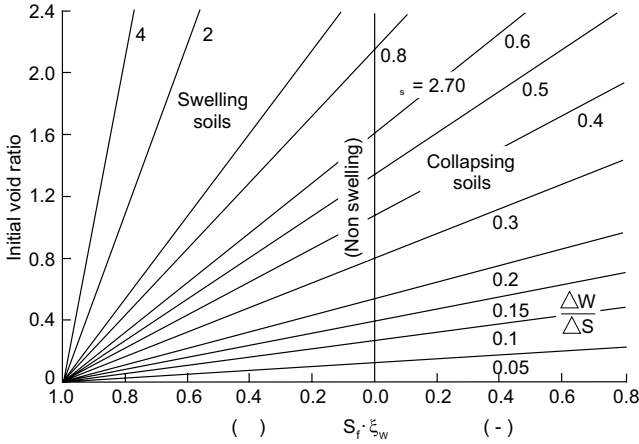
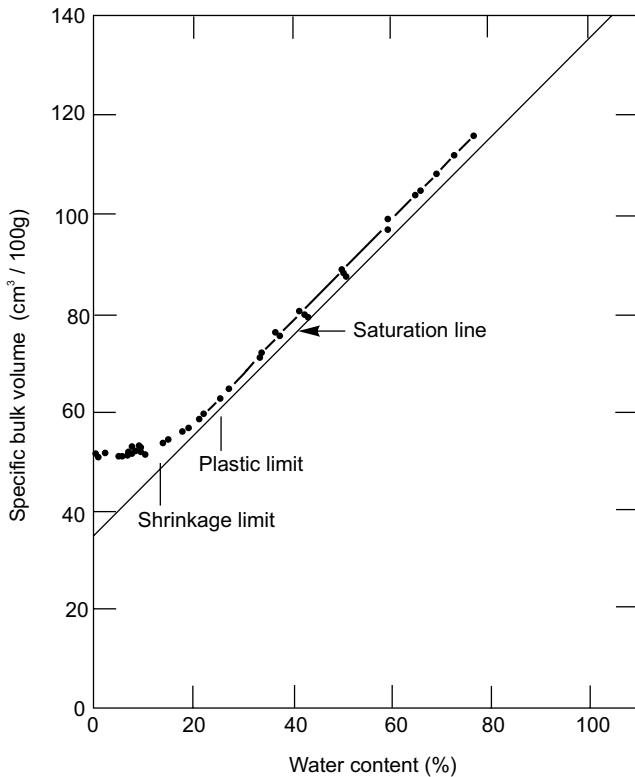


Fig. 16. Specific bulk volume versus water content for Regina clay.



Shear strength

The shear strength of an unsaturated soil can be written in an extended form of the Mohr-Coulomb diagram for a saturated soil (Fredlund et al. 1978).

$$[21] \quad \tau = c' + (\sigma - u_a) \tan \phi' + (u_a - u_w) \tan \phi^b$$

where:

- c' = cohesion intercept when the two stress variables are zero,
- ϕ' = the friction angle with respect to changes in the $(\sigma - u_a)$ stress variable, and
- ϕ^b = the friction angle with respect to changes in the $(u_a - u_w)$ stress variable.

Conceptually the equation can be visualised as a three-dimensional plot with matric suction plotted on the third axis (Fig. 17). As the soil approaches 100% saturation, u_a approaches u_w and the matric suction component becomes 0, leaving the remainder of the equation equivalent to that for a saturated soil. The c' and ϕ' parameters can be evaluated in the conventional manner used for saturated soils.

The ϕ^b can be computed by first plotting the difference between the strength of the unsaturated and saturated soil (under similar net total confining pressures) versus matric suction (Fredlund et al. 1978). This can be done using a stress point type of analysis where the change in the strength, $\Delta\tau_d$ (corrected to a distance perpendicular to the failure plane), is plotted against matric suction (Fig. 18). The equation of the resulting line is

$$[22] \quad \tan \alpha = (\Delta\tau_d \cos \psi') / (u_a - u_w)$$

where:

- ψ' = an angle similar to ϕ' but defined using the stress point procedure (i.e., $\sin \phi' = \tan \psi'$), and
- α = the angle between the change in shear strength and matric suction (using the stress point method of analysis).

The angle α can be first converted to a corresponding angle on the extended Mohr-Coulomb failure envelope and then to the friction angle with respect to matric suction, ϕ^b .

$$[23] \quad \tan \phi^b = \tan \phi' \left(1 - \frac{\tan \alpha}{\sin \psi'} \right)$$

The angle, ϕ^b , can be determined for a soil when the shear strength (and matric suction) is known at a matric suction greater than zero. Few sets of data are available that allow a complete analysis for unsaturated soils. Typical results are presented in Table 2 from data obtained by Bishop et al. (1960).

The shear strength parameters indicate that a decrease in pore-water pressure in an unsaturated soil is not as effective in increasing shear strength as an increase in the total confining stress.

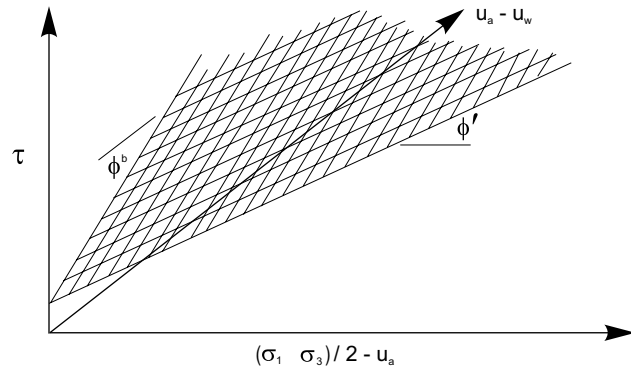
It is possible to envisage the three-dimensional shear strength diagram as a series of two-dimensional Mohr-Coulomb type diagrams, one for each matric suction (see Fig. 19). Therefore, the cohesion intercept is changed for each matric suction while the friction angle remains equal to that on the saturation plane.

$$[24] \quad c = c' + (u_a - u_w) \tan \phi^b$$

where:

Table 2. Typical shear strength parameters for unsaturated soils

Soil description	c'	ϕ'	ϕ^b	Initial water content (%)
Compacted shale	2.3	24.8	20.9	18.6
Boulder clay	1.4	27.3	24.0	11.6

Fig. 17. Shear strength envelope for unsaturated soils.

$c =$ the cohesion intercept at a particular matric suction.

Conceptually, an unsaturated soil has the same internal angle of friction as a saturated soil. At increasing matric suction values, the cohesion (or internal isotropic confining pressure) is increased. This treatment of the shear strength of unsaturated soils is particularly useful when considering *in situ* stress conditions and when performing limit equilibrium types of analysis.

Theoretical unsaturated soil mechanics

In this paper it is not possible to discuss all the constitutive relationships useful for describing the behavior of unsaturated soils. Therefore, an attempt has been made to describe those constitutive relations of greatest interest. These relations will now be applied to earth pressure, limit equilibrium, and volume change problems in unsaturated soils. Their treatment will be mainly dealt with from a conceptual standpoint.

Earth pressures

Some of the earliest work in saturated soil mechanics dealt with earth pressures on retaining walls. However, there is little information on the earth pressures exerted on engineering structures by unsaturated soils. Swelling pressures exerted by expansive soils have been of concern but there has been lacking a general earth pressure theory for these soils.

The total vertical stress in a large, level mass of soil is computed in the same manner for both a saturated and unsaturated soil. The pore-air pressure is generally in equilibrium with atmospheric pressure. The pore-water pressure must be measured unless the water table is within the height of capillary rise.

The horizontal pressure can be written as a ratio of the vertical pressure. Let the coefficient of earth pressure at rest, K_0 , be defined as

$$[25] \quad K_0 = (\sigma_h - u_a) / (\sigma_v - u_a)$$

The earth pressure at-rest can be estimated assuming the soil is in a state of elastic equilibrium. Using the elasticity form of the constitutive relations for an unsaturated soil (eq. [8]) and assuming the soil is laterally confined, the lateral pressure can be written as a ratio of the vertical stress:

$$[26] \quad \frac{(\sigma_h - u_a)}{(\sigma_v - u_a)} = \frac{\mu}{1 - \mu} - K_m \frac{(u_a - u_w)}{(\sigma_v - u_a)}$$

where:

$$K_m = E_1 / (1 - \mu)H_1$$

At saturation, the pore-air pressure approaches the pore-water pressure and the equation reverts to that for a saturated soil. When the matric suction becomes positive, the horizontal stress is reduced and is a function of depth. At shallow depths, the horizontal stresses will go to zero and attempt to go negative. This will result in cracking of the soil commencing at ground surface.

The active and passive earth pressures of an unsaturated soil can be determined assuming the soil is in a state of plastic equilibrium. The active earth pressure of an unsaturated soil is reduced from that of a saturated soil while the passive earth pressure is increased. The amount of the change in pressures can be visualised on a three-dimensional Mohr-Coulomb type of diagram (Fig. 19). The active earth pressure coefficient for any matric suction can be written in a form similar to that for a saturated soil exhibiting both friction and cohesion:

$$[27] \quad K_a = \frac{(\sigma_h - u_a)}{(\sigma_v - u_a)} \\ = (\sigma_v - u_a) \tan^2 \left(45 - \frac{\phi'}{2} \right) - 2c \tan \left(45 - \frac{\phi'}{2} \right)$$

where:

$$c = c' + (u_a - u_w) \tan \phi^b$$

The passive earth pressure coefficient can be written as

$$[28] \quad K_p = \frac{(\sigma_v - u_a)}{(\sigma_h - u_a)} \\ = (\sigma_v - u_a) \tan^2 \left(45 + \frac{\phi'}{2} \right) - 2c \tan \left(45 + \frac{\phi'}{2} \right)$$

In other words, the matric suction affects the active and passive earth pressure diagrams in the same manner as a soil having an increased cohesion (Fig. 20).

When the soil behind a retaining wall becomes moistened, the matric suction is reduced and the pressure

Fig. 18. Change in shear strength due to matric suction.

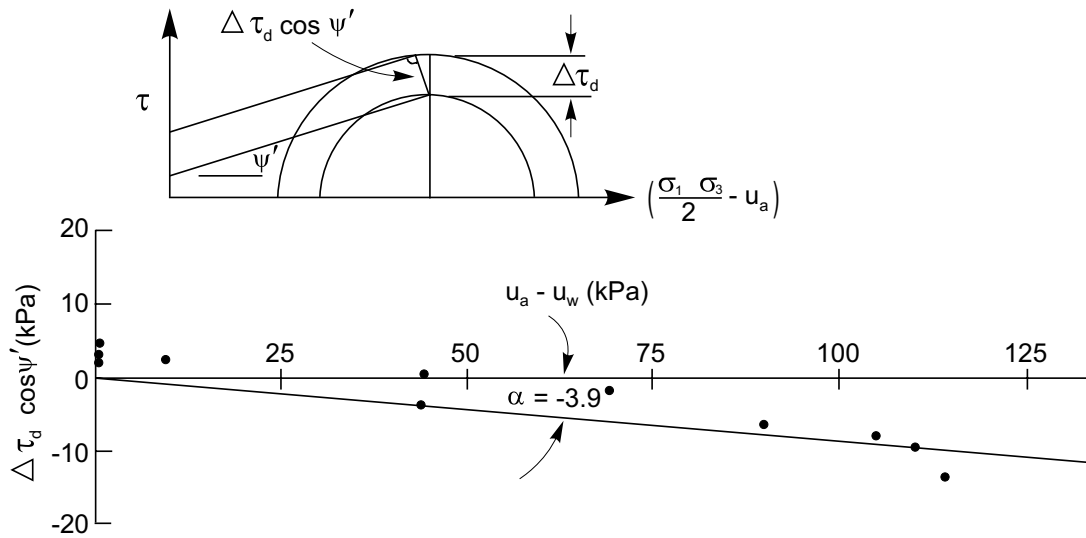
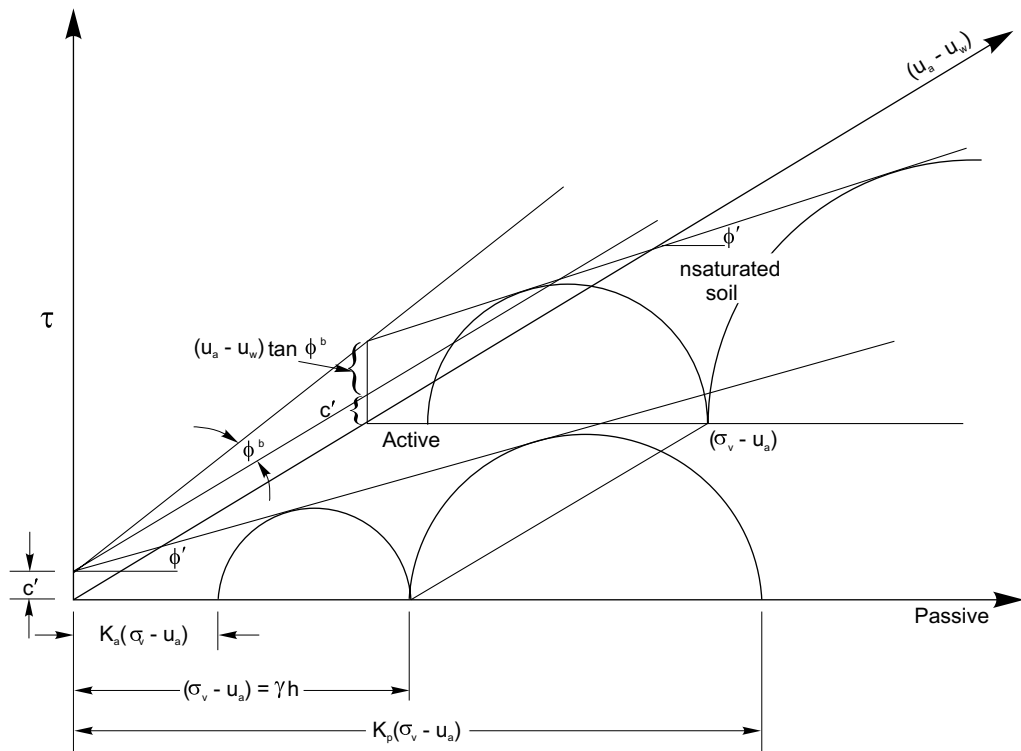


Fig. 19. Active and passive earth pressures for unsaturated soils.



against the wall is increased. If the wall is allowed to move laterally, the final pressure upon saturation would correspond to that dictated by the saturation plane of the Mohr-Coulomb diagram. If no movement of the wall is allowed, the pressure against the wall would increase; however, it would not exceed the passive pressure state on the saturation plane. Other cases of deformation would have to be considered as a soil structure interaction problem.

Limiting equilibrium

Two common problems handled using limit equilibrium analysis are slope stability and bearing capacity. In a slope stability analysis, the factor of safety is a measure of the reduction in shear strength required to produce a state of limiting equilibrium. For bearing capacity problems, the factor of safety is specified and the allowable bearing capacity is computed. In both of these cases, an unsaturated soil can be treated as a frictional soil with an

increased cohesion intercept (eq. [24]). Figure 21 demonstrates the increase in factor of safety for a soil with an increasing matric suction.

From a theoretical standpoint, the conventional slope stability and bearing capacity charts can be used for unsaturated soils. At present, there is need for both experimental results and case histories to substantiate the theoretical conclusions.

Volume change

The most common volume change problem associated with unsaturated soils is the heave of light engineering structures. Often such structures are placed on a desiccated soil. Subsequent to construction, moisture accumulates beneath the structure resulting in a decrease in matric suction and related heave. The engineer desires to sample the soil at various depths prior to construction and to be able to predict the amount of heave likely to occur under various loading conditions. Figure 22 shows how the soil sampling can occur anywhere along a drying or wetting portion of the matric suction plane. In the laboratory, the engineer would like to be able to re-establish the field state of stress and also obtain the moduli required for a heave analysis.

An analysis for the prediction of total heave has three aspects (Fredlund 1975b). First, the initial stress boundary conditions must be evaluated (Fig. 23a). The main variable of interest is the variation of pore-water pressure at various depths. The initial pore-water pressure can be evaluated by means of psychrometric measurements, axis-translation matric suction tests or oedometer tests on undisturbed samples. The psychrometer is generally used in the laboratory; however, it can also be used *in situ* where suctions are greater than 100 kPa (1 atm) and tem-

perature variations are small. The psychrometer measures total suction, which must be compensated for the osmotic suction component. When laboratory measurements are used, the suction must be divided into that portion due to overburden removal and that due to the *in situ* suction. This involves consideration of the pore pressure parameters that are outside the scope of this paper. The matric suction measurement using the axis-translation technique on a high air-entry disk must also be corrected for that portion due to overburden unloading.

Two types of oedometer tests are commonly performed on expansive soils. These are referred to as the Free Swell and Constant Volume consolidation tests (Fredlund 1969). In either of these tests, filter paper should not be placed on each side of the sample and the test results should be corrected for the compressibility of the apparatus. As well, the effects of sample disturbance should be taken into account. This correction is not as significant for the free swell test as for the Constant Volume test. However, the Constant Volume test with a sample disturbance correction appears to better represent *in situ* stress conditions (Fredlund 1975a). A Casagrande type of construction (Terzaghi and Peck 1948) appears to be satisfactory for compacted soils (Fig. 24); however, a detailed study has not been done on the best procedure to compensate for sample disturbance in undisturbed, natural samples.

When a correction for sample disturbance is applied to the consolidation test results, the horizontal distance out to the constructed point of volume decrease is a measure of the overburden pressure plus the matric suction. However, the matric suction measured in the laboratory will be smaller than the *in situ* matric suction since it is measured on the total stress plane. The laboratory measurement of matric suction will be satisfactory for analysis

Fig. 20. Active and passive earth pressures versus depth.

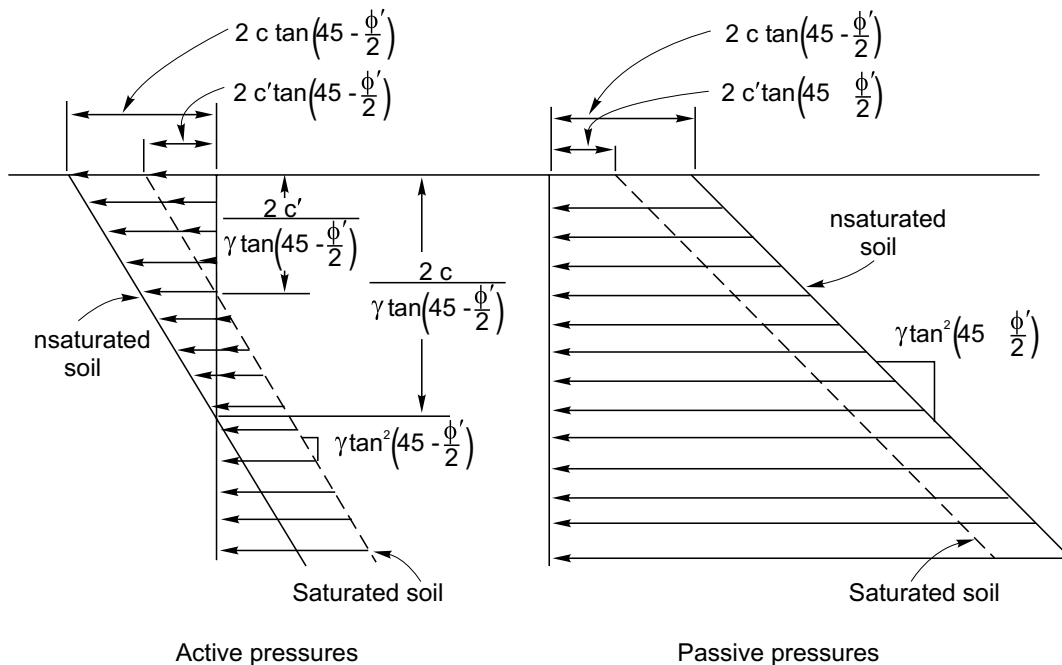
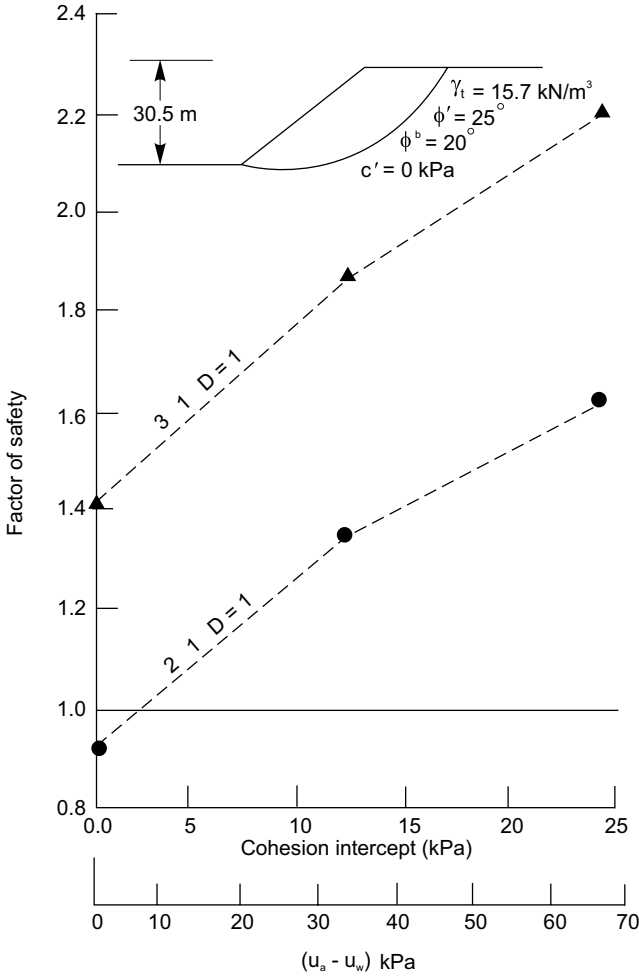


Fig. 21. Factor of safety of a simple slope versus matric suction.

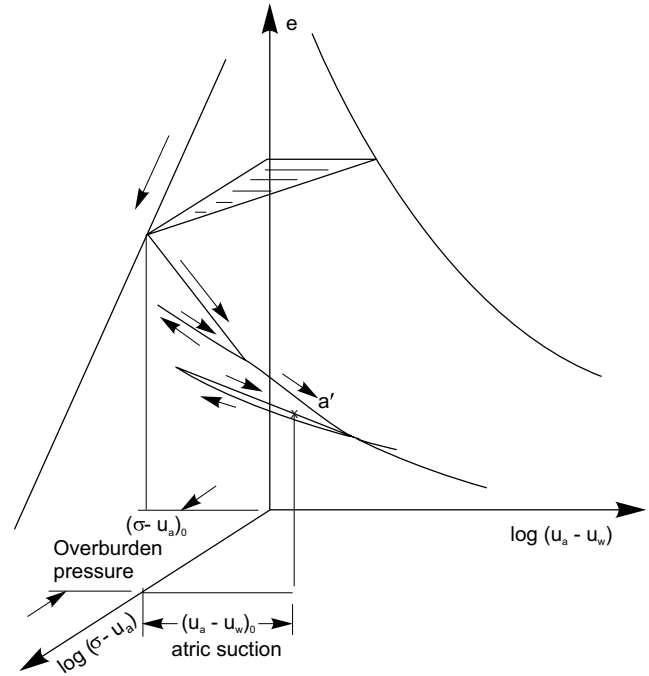


purposes if the deformation moduli are also measured on the total stress plane.

Second, the final stress boundary conditions must be estimated. The final or equilibrium pore-water pressure is mainly dependent on the geographical and climatic environment. Generally, one of three assumptions is made regarding the final pore-water pressures (Fig. 23b).

- (i) It could be assumed that moisture will accumulate beneath the structure and eventually the water table will rise to some elevation near the surface. Therefore, the final pore-water pressure distribution is hydrostatic. This assumption will result in the largest predicted heave.
- (ii) It could be assumed that the pore-water pressure is zero with depth. Although this is an unsteady state final boundary condition, it may be applicable when considerable moisture has been made available from the surface of the soil.
- (iii) It could be assumed that the final pore-water boundary condition is a state of slight tension in the water phase. The value of the pore-water tension is related

Fig. 22. Initial stress state when soil has undergone a drying and wetting history.



to the soil type and climatic conditions (Aitchison and Richards 1965; Carpenter et al. 1974).

Third, suitable constitutive relations are necessary to relate the initial and final stress boundary conditions. Since it is the amount of heave that is to be predicted, the main constitutive relationship of interest is the void ratio equation. The void ratio change can be summed for increments of depth to get the total heave, Δh .

$$[29] \quad \Delta h = \sum_{i=n}^{i=1} h_i \frac{\Delta e_i}{(1 + e_i)}$$

where:

- i = soil layer numbers ranging from layer 1 to layer n ,
- h_i = thickness of the soil layer, and
- e_i = void ratio for the layer.

The change in void ratio, Δe_i , can be written as:

$$[30] \quad \Delta e_i = C_t \log \frac{(\sigma - u_a)_f}{(\sigma - u_a)_0} + C_m \log \frac{(u_a - u_w)_f}{(u_a - u_w)_0}$$

Using the interpretation of the oedometer test previously suggested, the stresses become additive since the two moduli are the same.

$$[31] \quad \Delta e_i = C_t \log \frac{[(\sigma - u_a)_f + (u_a - u_w)_f]}{[(\sigma - u_a)_0 + (u_a - u_w)_0]}$$

The soil properties must be compatible with the load-increase or decrease being considered. A detailed recommended procedure for a heave analysis will not be

Fig. 23. Initial and final boundary conditions for heave analysis; a) initial boundary conditions, b) final boundary conditions.

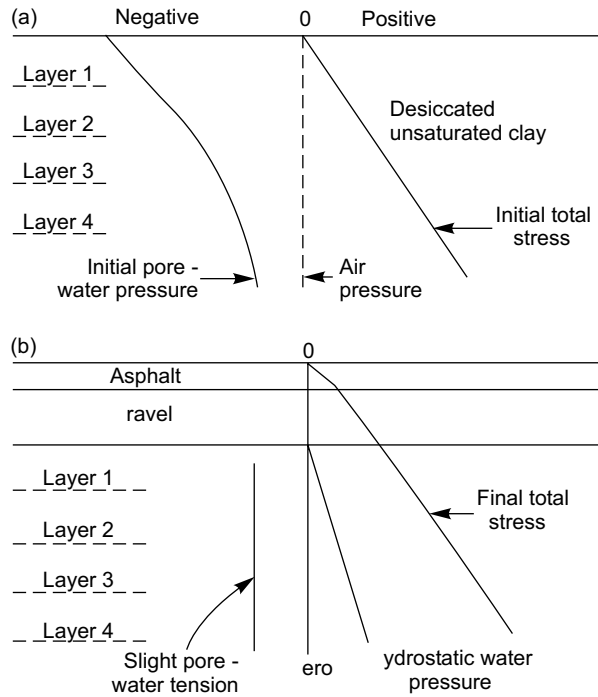
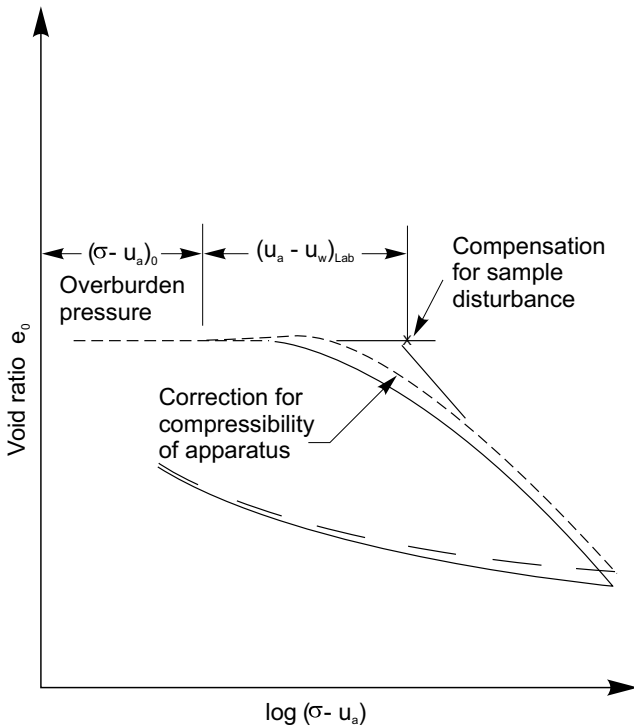


Fig. 24. Interpretation of the constant volume oedometer test.



presented; however, any procedure for heave should be consistent with the general theoretical content presented.

If the change in water content is also of interest, the water content constitutive relationship can be used. It is also possible to predict the change in water content by

some analysis and then relate this to a change in void ratio (Johnson 1977). For the heave analysis, the degree of saturation generally changes from some initial value up to approximately 100%. Therefore, there is a fixed relationship between the change in void ratio and the change in water content (Fig. 15).

Summary

The paper has presented some of the basic concepts and technology required to place engineering practice associated with unsaturated soils on a science base similar to that available for saturated soils. The unsaturated soil is recognized as a four-phase system with two phases that come to equilibrium under the application of a stress gradient (i.e., soil particles and contractile skin) and two phases that flow under the application of a stress gradient (i.e., air and water). The necessary stress variables for describing the stress state are presented, followed by proposed volume change and shear strength constitutive relations. These relations are applied to earth pressure, limit equilibrium, and volume change problems. In all cases, unsaturated soil mechanics is viewed as an extension of saturated soil mechanics while still retaining a smooth transition between the two cases. Further research is required to expand the proposed concepts to other problems associated with unsaturated soils.

References

Aitchison, G.D. 1961. Relationship of moisture stress and effective stress functions in unsaturated soils. *In* Pore Pressure and Suction in Soils Conference. British National Society of the International Society of Soil Mechanics and Foundation Engineering at the Institution of Civil Engineering. Butterworths, London, England. pp. 47–52.

Aitchison, G.D., and Richards, B.G. 1965. A broad scale study of moisture conditions in pavement subgrades throughout Australia, Part 4. *In* Moisture equilibria and moisture changes in soils beneath covered areas. A Symposium in Print. Edited by G.D. Aitchison, Butterworth, Sydney, Australia., pp. 226–236.

Barden, L., Madedor, A.O., and Sides, G.R. 1969. Volume change characteristics of unsaturated clay. *ASCE Journal of the Soil Mechanics and Foundation Division*, **95**(SM1): 33–52.

Bishop, A.W. 1959. The principle of effective stress. Lecture delivered in Oslo, Norway, 1955; *Technisk Ukeblad*, **106**(39): 859–863.

Bishop, A.W., Alpan, I., Blight, G.E., and Donald, I.B. 1960. Factors controlling the shear strength of partly saturated cohesive soils. *ASCE Research Conference on Shear Strength of Cohesive Soils*, University of Colorado, Boulder, CO., pp. 503–532.

Carpenter, S.H., Lytton, R.L., and Epps, J.A. 1974. Environmental factors relevant to pavement cracking in west Texas. Texas Transportation Institute, Texas A & M, College Station, TX, Research Report No. 18–1.

Croney, D., Coleman, J.D., and Black, W.P.M. 1958. The movement and distribution of water in soil in relation to highway design and performance. *In* Water and its Conduction in

- Soils, Highway Research Board Special Report No. 40, Washington, D.C., pp. 226–252.
- Davies, J.T., and Rideal, E.K. 1963. *Interfacial phenomena*. 2nd Edition. Academic Press, New York, NY.
- Derjaguin, B.V. 1965. Recent research into the properties of water in thin films and in micro-capillaries. *Proceedings, Society for Experimental Biology Symposia, XIX. The State and Movement of Water in Living Organisms*. Cambridge University Press, London, England.
- Fredlund, D.G. 1964. Comparison of soil suction and one-dimensional consolidation characteristics of a highly plastic clay. National Research Council of Canada, Division of Building Research, Technical Report 245.v, Ottawa, ON, Canada.
- Fredlund, D.G. 1969. Consolidometer test procedural factors affecting swell properties. *Proceedings, 2nd. International Conference on Expansive Soils, Texas A & M, College Station, TX.*, pp. 435–456.
- Fredlund, D.G. 1975a. Engineering properties of expansive clays. *Proceedings, Seminar on Shallow Foundations on Expansive Clays: Design, Construction and Performance*, Regina, SK, Oct. 27–28, pp. 3–64.
- Fredlund, D.G. 1975b. Prediction of heave in unsaturated soils. *Proceedings, Fifth Asian Regional Conference, Bangalore, India, Dec. 19–22.*, pp. 19–22.
- Fredlund, D.G. 1976. Density and compressibility characteristics of air-water mixtures. *Canadian Geotechnical Journal*, **13**(4): 386–396.
- Fredlund, D.G., and Morgenstern, N.R. 1976. Constitutive relations for volume change in unsaturated soils. *Canadian Geotechnical Journal*, **13**(3): 261–276.
- Fredlund, D.G., and Morgenstern, N.R. 1977. Stress state variables for unsaturated soils. *ASCE Journal of the Geotechnical Engineering Division*, **103**(GT5): 447–466.
- Fredlund, D.G., Morgenstern, N.R., and Widger, R.A. 1978. Shear strength of unsaturated soils. *Canadian Geotechnical Journal*, **15**(3): 313–321.
- Hasan, J., and Fredlund, D.G. 1977. Consolidation theory for unsaturated soils. *Symposium on Water Movement and Equilibrium in Swelling Soils, Committee on Water in the Unsaturated Zone, Section of Hydrology of the American Geophysical Union, San Francisco, CA.*
- Holtz, W.G., Day, D.A., and Richard, O.D. 1974. University-industry workshop on behavior of expansive earth materials. Final Report, National Science Foundation, Washington, DC.
- Jennings, J.E.B. 1961. A revised effective stress law for use in the prediction of the behavior of unsaturated soils. *In Pore Pressure and Suction in Soils Conference. British National Society of the International Society of Soil Mechanics and Foundation Engineering at the Institution of Civil Engineering*. Butterworths, London, England. pp. 26–30.
- Johnson, L.D. 1977. Evaluation of laboratory suction tests for prediction of heave in foundation soils. U.S. Army Engineer Waterways Experimental Station, P.O. Box 631, Vicksburg, MS, Technical Report S-77-7.
- Jones, D.E., and Holtz, W.G. 1973. Expansive soils — the hidden disaster. *ASCE, Civil Engineering*, **43**(8): 49–51.
- Krahn, J., and Fredlund, D.G. 1972. On total, matric and osmotic suction. *Soil Science*, **114**(5): 339–348.
- Lambe, T.W. 1960. A mechanistic picture of shear strength in clay. *Proceedings, ASCE Research Conference on Shear Strength of Cohesive Soils, University of Colorado, Boulder, CO*, pp. 555–580.
- Matyas, E.L., and Radhakrishna, H.S. 1968. Volume change characteristics of partially saturated soils. *Géotechnique*, **18**(4): 432–448.
- Milne, L.J., and Milne, M. 1978. Insects of the water surface. *Scientific American*, April, pp. 134–142.
- Richards, B.G. 1966. The significance of moisture flow and equilibria in unsaturated soils in relation to the design of engineering structures built on shallow foundations in Australia. *Symposium on Permeability and Capillarity, American Society for Testing and Materials, Atlantic City, NJ.*
- Terzaghi, K., and Peck, R.B. 1948. *Soil mechanics in engineering practice*. John Wiley & Sons Inc., New York, NY.

Theoretical context for understanding unsaturated residual soil behavior

D.G. Fredlund and H. Rahardjo

Abstract: The basic concepts for understanding the behavior of unsaturated residual soils are outlined. The available theory for fluid flow, shear strength and volume change of unsaturated soils are described. The application of the theory and technology in resolving shear strength problems of unsaturated residual soils is presented using case histories. The results of *in situ* measurements, laboratory tests and theoretical analyses have proven satisfactory in analysing problems involving unsaturated residual soils.

Key words: residual soils, unsaturated soil behavior, soil suction, shear strength.

Introduction

A large portion of the earth's surface is covered with residual soils which can be either saturated or unsaturated. The theory and technology for the saturated soils have been well developed and applied in engineering practice for over 5 decades. However, weathering processes have left over eighty percent of earth surface desiccated. As a result, cracks start to develop, and the soil becomes unsaturated. Many geotechnical problems have been encountered involving unsaturated soils, but our understanding of the behavior of these soils is far behind our knowledge of saturated soils. Most of the engineering problems involving heave, consolidation, collapse and dramatic changes in shear strength are directly related to the behavior of unsaturated soils. Cyclic variations in environmental conditions increase the complexity of the problems.

The objective of this paper is to summarize the theoretically based principles, and mathematical equations necessary for establishing a practical science and technology for unsaturated soils. The theory is consistent with multiphase continuum mechanics and has been directed towards resolving observable phenomena in unsaturated soils. Equations are presented for fluid flow, shear strength and volume change behavior of unsaturated soils. The equations for unsaturated soil behavior are extensions of the equations commonly used for saturated soils. The unsaturated soil theory is also applied to the slope stability problem in Hong Kong residual soils. The

application involves *in situ* measurements of soil suction, laboratory tests for shear strength and theoretical slope stability analyses.

Stress state variables

An unsaturated soil can be considered as a four phase system (Fredlund and Morgenstern 1977). The solid phases (i.e., soil particles and contractile skin) will reach an equilibrium under applied stress gradients, whereas the fluid phases (i.e., water and air) flow under applied stress gradients. The theoretical analysis of this four phase system using the multiphase continuum mechanics yields several combinations of independent stress state variables. However, the combination of $(\sigma - u_a)$ and $(u_a - u_w)$ as stress state variables are superior for practical applications because the effects of changes in total stress and pore-water pressure can be separated. The term $(u_a - u_w)$ is referred to as matric suction where u_a is the pore-air pressure; u_w is the pore-water pressure; and σ is the total stress. The stress state variables can be extended to a matrix form when multi-directional analyses are being attempted.

As a soil approaches saturation, the pore-water pressure approaches the pore-air pressure. Therefore, the matric suction term goes to zero, and there is a smooth transition to the saturated soil stress state variable, $(\sigma - u_w)$.

Flow laws and seepage

Darcy's Law can be used to describe the flow of water through an unsaturated soil (Childs and Collis-George 1950; Freeze and Cherry 1979),

$$[1] \quad v_w = -k_w \frac{\partial h_w}{\partial y}$$

where:

v_w = the velocity of water,

k_w = the coefficient of permeability with respect to the water phase,

h_w = the total head in the water phase, and

D.G. Fredlund. Professor, Civil Engineering Department, University of Saskatchewan, 57 Campus Drive, Saskatoon, SK, Canada S7N 5A9.

H. Rahardjo. Research Engineer, Civil Engineering Department, University of Saskatchewan, 57 Campus Drive, Saskatoon, SK, Canada S7N 5A9.

Reproduced with permission from the *Proceedings of the First International Conference on Geomechanics in Tropical Lateritic and Saprolitic Soils*, February 11–14, 1985, Brazilia, Brazil, A.A. Balkema, Rotterdam, The Netherlands, pp. 295–306.

y = the coordinate direction.

The coefficient of permeability, k_w , is highly variable and can be written as a function of negative pore-water pressure head (Gardner 1958).

$$[2] \quad k_w = \frac{k_s}{1 + a \left(\frac{u_a - u_w}{\rho_w g} \right)^n}$$

where:

- k_s = the saturated coefficient of permeability,
- ρ_w = density of water,
- g = the gravitational acceleration, and
- a, n = material properties.

The flow of air through an unsaturated soil may be required in the analysis of certain problems. In this case the flow of air can be described using Fick's Law (Blight 1971),

$$[3] \quad v_a = -D^* \frac{\partial u_a}{\partial y}$$

where:

- v_a = the mass rate of air flow, and
- D^* = the transmission constant of proportionality for the air phase.

The steady seepage equation for the water phase in an unsaturated soil becomes an expansion of the common La Placian equation,

$$[4] \quad k_w \frac{\partial^2 h}{\partial x^2} + \frac{\partial k_w}{\partial x} \frac{\partial h}{\partial x} + k_w \frac{\partial^2 h}{\partial y^2} + \frac{\partial k_w}{\partial y} \frac{\partial h}{\partial y} + \frac{\partial k_w}{\partial y} = 0$$

The second and fourth terms in eq. [4] account for the variation of the coefficient of permeability of water with respect to space. The fifth term is called the gravity term. As a soil approaches saturation, the spatial variations in permeability go to zero, resulting in a smooth transition to the saturated soil case.

Shear strength

The shear strength equation for an unsaturated soil can be written in terms of the $(\sigma - u_a)$ and $(u_a - u_w)$ stress state variables (Fredlund et al. 1978).

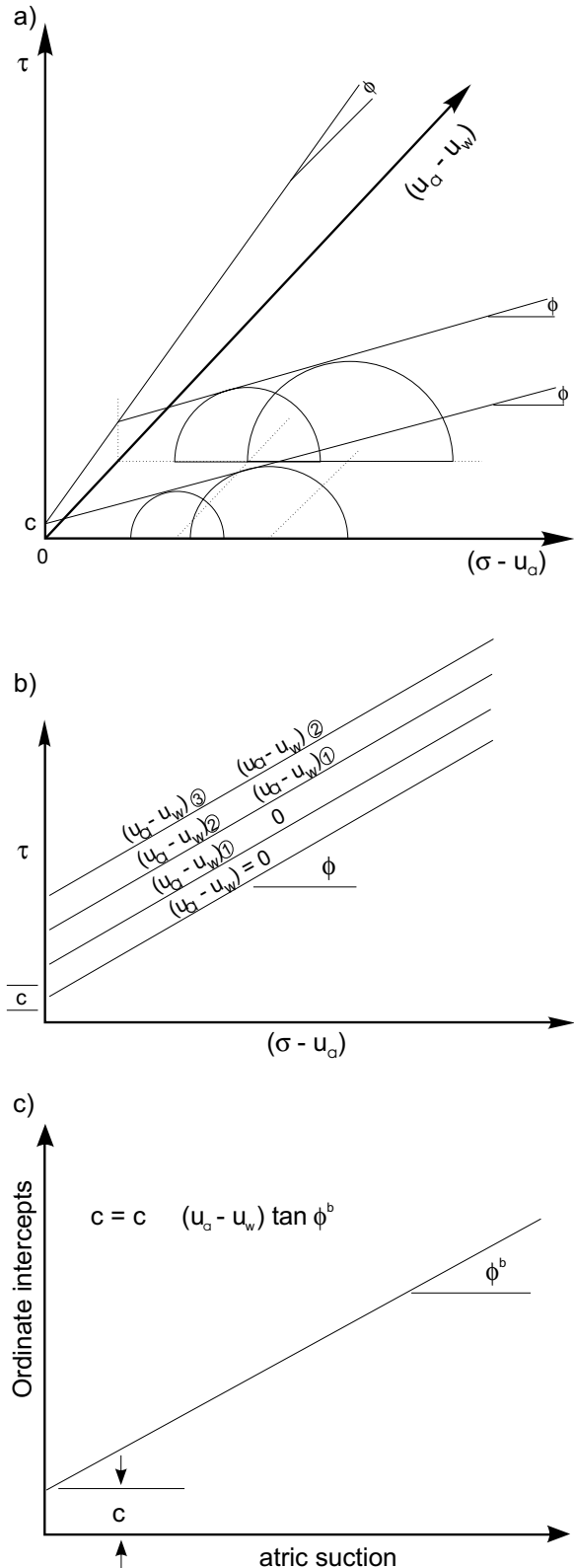
$$[5] \quad \tau = c' + (u_a - u_w) \tan \phi^b + (\sigma_n - u_a) \tan \phi$$

where:

- τ = the shear strength,
- c' = the effective cohesion intercept,
- ϕ^b = the angle of shear strength increase with an increase in $(u_a - u_w)$,
- σ_n = the total normal stress, and
- ϕ' = the effective angle of internal friction.

Equation [5] is an extension of the conventional Mohr-Coulomb failure criteria, and can be plotted in a three-dimensional form using $(\sigma - u_a)$ and $(u_a - u_w)$ as abscissas (Fig. 1a). The equation can also be visualized as a two-

Fig. 1. a) Three-dimensional failure surface for unsaturated soils; b) Projection of failure surface on the τ and $(\sigma - u_a)$ plane by looking parallel to the $(u_a - u_w)$ axis; c) The ordinate intercepts on the τ and $(u_a - u_w)$ plane for various matric suction contours.



dimensional graph with matric suction contoured as the third variable (Fig. 1b). A plot of the ordinate intercepts of the various matric suction contours on a τ versus $(u_a - u_w)$ graph gives the friction angle, ϕ^b (Fig. 1c).

The unsaturated soil is therefore visualized as having two components of cohesion (Figs. 1b and 1c).

$$[6] \quad c = c' + (u_a - u_w) \tan \phi^b$$

The second term in eq. [6] accounts for the increase in shear strength due to suction (Fredlund 1979). Once again, as a soil approaches saturation, the second component goes to zero and the shear strength equation takes the form commonly used for saturated soils.

Volume change relations

The volume change constitutive relations for an unsaturated soil can be represented using the $(\sigma - u_a)$ and $(u_a - u_w)$ stress state variables and the volume - mass soil properties. Volumetric continuity requires that two independent constitutive relations be written. One constitutive equation describes the deformation of the soil structure in terms of the change in void ratio, de .

$$[7] \quad de = a_t d(\sigma - u_a) + a_m d(u_a - u_w)$$

where:

e = the void ratio,

a_t = the coefficient of compressibility with respect to a change in $(\sigma - u_a)$, and

a_m = the coefficient of compressibility with respect to a change in $(u_a - u_w)$.

A second constitutive relation describes the change in water content, dw ,

$$[8] \quad dw = b_t d(\sigma - u_a) + b_m d(u_a - u_w)$$

where:

w = the water content,

b_t = the coefficient of water content change with respect to a change in $(\sigma - u_a)$, and

b_m = the coefficient of water content change with respect to a change in $(u_a - u_w)$.

Changes in the volume of air in the soil can be obtained by computing the difference between the change in void ratio and the change in water content.

The uniqueness of the proposed constitutive relations has been verified by several researchers (Matyas and Radhakrishna 1968; Barden et al. 1969; Fredlund and Morgenstern 1976). The volume change constitutive relations are particularly useful for heave predictions in swelling soils (Fredlund et al. 1980; Yoshida et al. 1983). Transient flow problems such as consolidation can also be formulated utilizing the volume change equations together with the flow laws (Fredlund and Hasan 1979; Fredlund 1982; Dakshanamurthy et al. 1984).

Heave or swelling is a problem encountered with some residual soils. However, equally as common is the seldom addressed problem of soil collapse in residual soils. Although little research has been conducted in this area, it is

the authors' opinion that the soil collapse phenomenon can best be understood in terms of changes in the stress state variables.

Application of unsaturated soil theory to slope stability analysis

The following portion of this paper demonstrates the application of the unsaturated soil theory to the analysis of slope stability problems in residual soils in Hong Kong.

Hong Kong case histories

The surficial soils in Hong Kong are unsaturated, residual soils mainly consisting of decomposed granite and decomposed volcanic rock (rhyolite). The residual soils extend to a considerable depth due to active weathering processes. The water table is located far below ground surface (e.g., 20 metres).

The stability of numerous steep slopes in residual soils has been a major problem in Hong Kong. Stability analyses performed on steep slopes, assuming saturated conditions, often resulted in a factor of safety less than 1. However, the slopes may not show signs of distress. The soil suction throughout a considerable depth of the soil profile has been shown to be the significant factor in maintaining the stability of these slopes (Sweeney and Robertson 1979; Ho and Fredlund 1982; Ching et al. 1984). Nevertheless, slope failures have frequently occurred during or after periods of heavy and prolonged rainfall. This can be attributed to the reduction in soil strength as a result of a loss of suction due to infiltration (Lumb 1975).

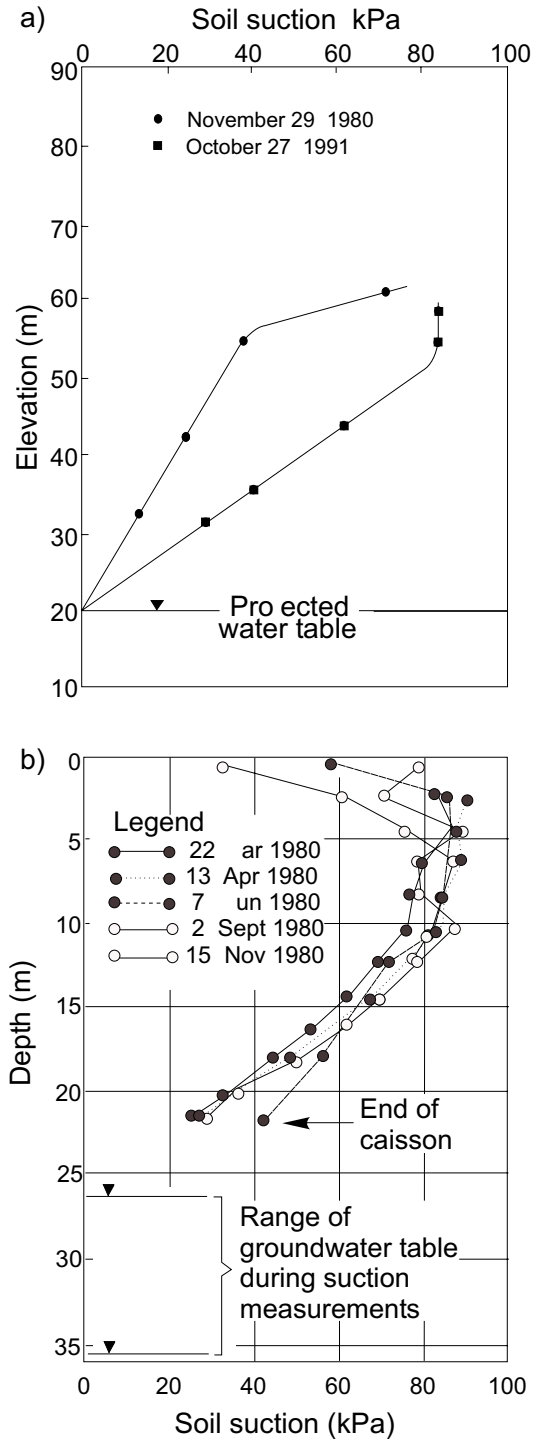
In situ measurements

The *in situ* measurement of soil suction was performed at two sites in Hong Kong in order to better understand the range in the magnitude of the soil suction and its variation with respect to time and environment. Sweeney (1982) reported the measurement of *in situ* soil suctions using tensiometers at three cut slopes in Hong Kong.

Exploratory concrete-lined shafts were made in order to measure suction at different depths at the Thorpe Manor site. Suction measurements were made in small holes perpendicular to the slope at the Fung Fai Terrace site. The matric suction measurement using a tensiometer is obtained from equilibrium across a high air entry porous medium. Two types of tensiometers (i.e., "Quick Draw" Soilmoisture Probe and Soilmoisture Probe (No. 2100) with a flexible tube) were used in the measurement of soil suction. Figures 2a and 2b show the matric suction profiles obtained from Fung Fai Terrace and Thorpe Manor sites, respectively. The suction values reached magnitudes of approximately 80 to 100 kPa which is the limit of the tensiometer. In general, the position of the water table and rainfall variations determined the characteristic of the measured suction profiles.

The measured suctions at the Thorpe Manor site were relatively constant throughout the seasons, with variations

Fig. 2. a) Suction measurements on Fung Fai Terrace; b) Suction measurements on Thorpe Manor.



occurring primarily in the extreme upper portion of the profile and at the water table. This observation may not be applicable to all cases.

Laboratory tests

Laboratory tests were performed on undisturbed samples to measure the effect of suction on shear strength. In

other words, the shear strength parameter, ϕ^b , as shown in Fig. 1c was quantified for the two Hong Kong residual soils.

Multi-stage triaxial tests were conducted on ten decomposed granites, and seven decomposed volcanics by Ho and Fredlund (1982). The tests were performed by controlling the pore-air and pore-water pressures so as to maintain a constant suction in the sample during each stage of the test. The axis-translation technique was used in order to apply suctions higher than one atmosphere.

The results showed that the increase in shear strength due to an increase in soil suction was in accordance with eq. [6]. The average angle of ϕ^b was found to be 15.3° for the decomposed granite, and 13.8° for the decomposed volcanic rock.

Slope stability analysis

The effect of soil suction on the computed factor of safety for the two slopes in Hong Kong, (i.e., Fung Fai Terrace and Thorpe Manor), was demonstrated by Ching et al. (1984). There is no need to reformulate the factor of safety equations when dealing with unsaturated soils, since the matric suction term can be considered as part of the cohesion of the soil.

Values of c' and ϕ' for the Hong Kong residual soils have been reported by Lumb (1962, 1965), and ϕ^b values measured by Ho and Fredlund (1982) were used in the analysis.

A cross section of the Fung Fai Terrace is shown in Fig. 3a, and the strength properties of each soil stratum are listed in Table 1. Several slope stability analyses were performed for various percentages of the negative hydrostatic profile. The analyses (Fig. 4) show an increase in the factor of safety as the matric suction value increases. For the saturated case the factor of safety computed was 0.86, which indicated instability of the slope. The slope, however, had remained stable, likely due to matric suction.

Several slope stability analyses were also performed based on the *in situ* suction measurements (Fig. 2a). The factor of safety was 1.07 based on the suction measurements on November 29, 1980, and 0.98 based on the suction measurements on October 27, 1981.

Figure 3b shows a cross-section of Thorpe Manor, and Table 2 gives the strength properties of each soil stratum. The results of the analyses are presented in Fig. 4, and indicate the increase in factor of safety with respect to an increase in matric suction. The analysis, using a saturated soil parameters resulted in a factor of safety of 1.05. When the *in situ* matric suction values are used (Fig. 2b), the factor of safety increased to 1.25.

Conclusions

The theory of unsaturated soil behavior provides a general conceptual framework for analyzing practical problems involving residual soils. It takes the form of an extension of saturated soil concepts with a smooth transition between the two cases.

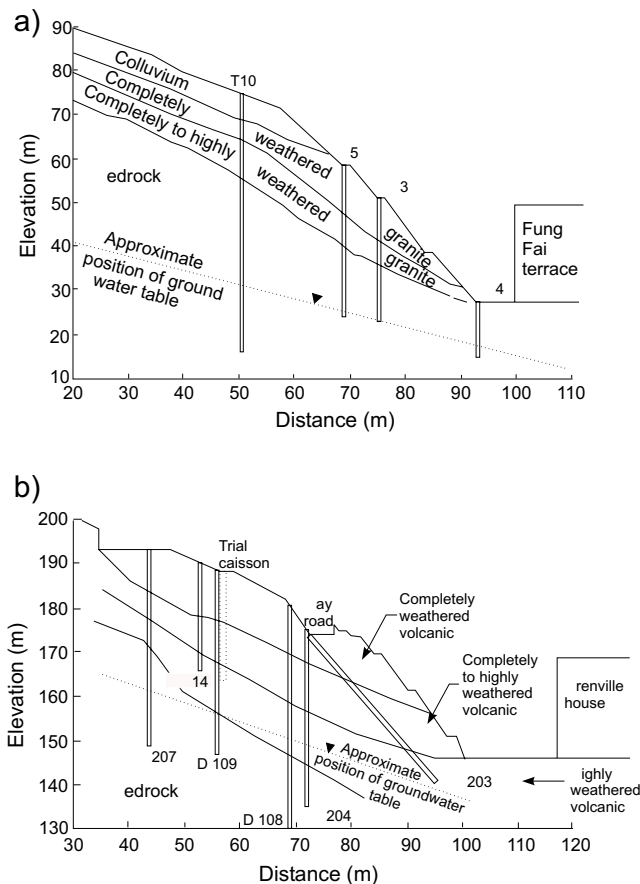
Table 1. Strength properties of soils at Fung Fai Terrace.

Soil type	Unit weight (kN/m ³)	c' (kPa)	φ' (degrees)	φ ^b (degrees)
Colluvium	19.6	10.0	35.0	15.0
Completely weathered granite	19.6	15.1	35.2	15
Completely to highly weathered granite	19.6	23.5	41.5	15.0

Table 2. Strength properties of soils at Thorpe Manor.

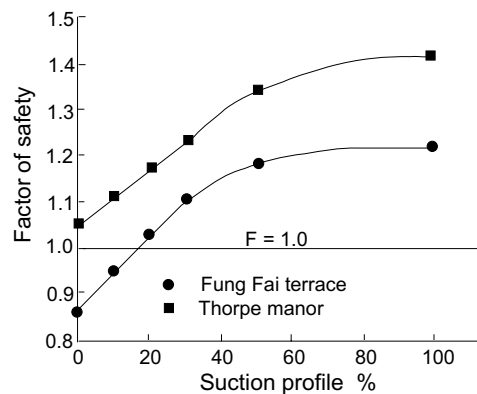
Soil type	Unit weight (kN/m ³)	c' (kPa)	φ' (degrees)	φ ^b (degrees)
Completely weathered rhyolite	18.4	10.1	42.6	12.0
Completely to highly weathered rhyolite	21.4	12.0	43.9	12.0

Fig. 3. a) Fung Fai Terrace cross section; b) Thorpe Manor cross section.



The application of the proposed theory in solving geotechnical problems in unsaturated, residual soils has been limited but has proven to be extremely useful. The influence of soil suction on shear strength can be quantified and applied to the slope stability problem. More case

Fig. 4. Factor of safety versus suction profile for two Hong Kong slopes.



histories are required to further verify the proposed theory in practice. In addition, there is a great need to improve our ability to measure negative pore-water pressures.

Acknowledgements

The authors wish to acknowledge the financial support from Fugro Hong Kong for the research program on residual soils at the University of Saskatchewan, Saskatoon, Saskatchewan, Canada. Much of the data presented in the paper was collected under the supervision of D. Sweeney, past managing director of Fugro Hong Kong. His assistance, as well as the support of R. Pope is gratefully acknowledged.

References

Barden, L., Madedor, A.O., and Sides, G.R. 1969. Volume change characteristics of unsaturated clay. ASCE, Journal of Soil Mechanics and Foundation Division, 95(SM1): 33–52.
 Blight, G.E. 1971. Flow of air through soils. ASCE, Journal of Soil Mechanics and Foundation Division, 97: 607–624.

- Childs, E.C., and Collis-George, N. 1950. The permeability of porous materials. *Proceedings of the Royal Society of London, Series A*, **201**: 392–405.
- Ching, R.K.H., Sweeney, D.J., and Fredlund, D.G. 1984. Increase in factor of safety due to soil suction for two Hong Kong slopes. *Proceedings, Fourth International Symposium on Landslides, Toronto, Canada, Vol. 1*, pp. 617–623.
- Dakshanamurthy, V., Fredlund, D.G., and Rahardjo, H. 1984. Coupled three-dimensional consolidation theory of unsaturated porous media. *Proceedings, Fifth International Conference on Expansive Soils, Adelaide, South Australia, Institute of Engineers, Australia*, pp. 99–103.
- Fredlund, D.G. 1979. Second Canadian Geotechnical Colloquium: Appropriate concepts and technology for unsaturated soils. *Canadian Geotechnical Journal*, **16**(1): 121–139.
- Fredlund, D.G. 1982. Consolidation of unsaturated porous media. *Proceedings, Symposium on the Mechanics of Fluid in Porous Media—New Approaches in Research, NATO Advance Study Institute, University of Delaware, Newark, DL*.
- Fredlund, D.G., and Hasan, J.U. 1979. One-dimensional consolidation theory: Unsaturated soils. *Canadian Geotechnical Journal*, **16**(3): 521–531.
- Fredlund, D.G., and Morgenstern, N.R. 1976. Constitutive relations for volume change in unsaturated soils. *Canadian Geotechnical Journal*, **13**(3): 261–276.
- Fredlund, D.G., and Morgenstern, N.R. 1977. Stress state variables for unsaturated soils. *ASCE, Journal of Geotechnical Engineering Division*, **103**(GT5): 447–466.
- Fredlund, D.G., Hasan, J.U., and Filson, H. 1980. The prediction of total heave. *Proceedings, 4th International Conference on Expansive Soils, Denver, CO, Vol. 1*, pp. 1–17.
- Fredlund, D.G., Morgenstern, N.R., and Widger, R.A. 1978. The shear strength of unsaturated soils. *Canadian Geotechnical Journal*, **15**(3): 313–321.
- Freeze, R.A., and Cherry, J.A. 1979. *Groundwater*. Prentice-Hall Inc., Englewood Cliffs, NJ.
- Gardner, W.R. 1958. Some steady state solutions of the unsaturated moisture flow equations with application to evaporation from a water-table. *Soil Science*, **85**(4):228–232.
- Ho, D.Y.F., and Fredlund, D.G. 1982. A multi-stage triaxial test for unsaturated soils. *ASTM Geotechnical Testing Journal*, **5**(1/2): 18–25.
- Lumb, P. 1962. The properties of decomposed granite. *Géotechnique*, **12**: 226–243.
- Lumb, P. 1965. The residual soils of Hong Kong. *Géotechnique*, **15**: 180–194.
- Lumb, P. 1975. Slope failures in Hong Kong. *Quarterly Journal of Engineering Geology*, **8**: 31–65.
- Matyas, E.L., and Radhakrishna, H.S. 1968. Volume change characteristics of partially saturated soils. *Géotechnique*, **18**(4): 432–448.
- Sweeney, D.J. 1982. Some *in situ* soil suction measurements in Hong Kong's residual soil slopes. *Proceedings, 7th Southeast Asia Geotechnical Conference, Hong Kong, Vol. 1*, pp. 91–106.
- Sweeney, D.J., and Robertson, P. 1979. A fundamental approach to slope stability in Hong Kong. *Hong Kong Engineering*, pp. 35–44.
- Yoshida, R., Fredlund, D.G., and Hamilton, J.J. 1983. The prediction of total heave of a slap-on-ground floor on Reginal clay. *Canadian Geotechnical Journal*, **20**(1): 69–81.

Soil mechanics principles that embrace unsaturated soils

D.G. Fredlund

Abstract: The classic saturated soil mechanics principles and equations have been extended to embrace the behavior of unsaturated soils. Equations are presented for fluid flow, shear strength and volume change. These equations are applied to practical problems such as steady state seepage, the consolidation process and slope stability analysis. In each case the accepted equations for saturated soils become a special case of the more general unsaturated soil mechanics equations.

Key words: unsaturated soils, stress state, coefficient of permeability, constitutive relations, shear strength, consolidation theory.

Introduction

An understanding of the behavior of unsaturated soils is important in dealing with numerous problems encountered in geotechnical engineering. For example, the heave associated with unsaturated, expansive soils sustains an enormous economic drain on society (Krohn and Slosson 1980). For another example, the shear strength of unsaturated, residual soils is important in understanding slope stability problems related to changes in soil suction. There are numerous other applications related to compacted soils in highways, airport runways, railroads and other earth structures.

In retrospect, the first International Society for Soil Mechanics and Foundation Engineering conference in 1936 provided a forum for the establishment of principles and equations relevant to saturated soil mechanics. These principles and equations have remained pivotal throughout subsequent decades of research. This same conference was also a forum for numerous research papers on unsaturated soil behavior. Unfortunately a parallel set of principles and equations did not immediately emerge for unsaturated soils. As a result, a science and technology for unsaturated soils has been slow to develop (Fredlund 1979). Not until the research at Imperial College in the late 1950's did a science for unsaturated soils begin to appear (Bishop 1959).

Saturated soil mechanics theory and technology have developed around a few classic equations. These can be summarized as: (i) the flow equation, (ii) the shear strength equation, and (iii) the volume change constitutive equation. The shear strength and volume change

equations are written in terms of a stress variable controlling the behavior of the soil structure. This stress variable, $(\sigma - u_w)$, is referred to as the effective stress of the soil where σ is the total stress and u_w represents the pore-water pressure. Uniqueness has been demonstrated for both the shear strength and volume change equations relative to specific stress paths. The flow equation was written in terms of the total head in the water phase.

This paper summarizes a set of classic equations for unsaturated soils which are a logical extension of those accepted for saturated soils. The research confirming each of the equations has been presented elsewhere and this paper synthesizes the results in terms of a limited number of equations. The objective of this paper is to provide a consistent set of classic equations for unsaturated soil behavior which can be widely accepted.

Relating soil behavior to stress variables

The shear strength and volume change behavior of saturated soils has been related to the $(\sigma - u_w)$ stress variable. The complete description of the stress state takes the form of a matrix.

$$[1] \quad \begin{bmatrix} (\sigma_x - u_w) & \tau_{xy} & \tau_{xz} \\ \tau_{yx} & (\sigma_y - u_w) & \tau_{yz} \\ \tau_{zx} & \tau_{zy} & (\sigma_z - u_w) \end{bmatrix}$$

σ_x , σ_y , σ_z , are the total stress in the x , y and z directions, respectively and τ_{xy} , τ_{yx} , τ_{xz} , τ_{zx} , τ_{zy} , τ_{yz} are shear stresses. In practice, it is not necessary to relate mechanical behavior of the saturated soil to all components of the stress state when specific stress paths are selected. Theoretically, the first, second and third stress invariants form a more fundamental basis for describing mechanical behavior.

The shear strength and volume change behavior of an unsaturated soil can best be described in terms of two independent stress variables; namely, $(\sigma - u_a)$ and $(u_a - u_w)$.

D.G. Fredlund. Professor, Department of Civil Engineering, University of Saskatchewan, 57 Campus Drive, Saskatoon, SK, Canada S7N 5A9.

Reproduced with permission from the *Proceedings, 11th International Society for Soil Mechanics and Foundation Engineering*, San Francisco, CA, USA, August 11–15, 1985. A.A. Balkema, Rotterdam, The Netherlands, Vol. 2, pp. 465–473.

The term $(u_a - u_w)$ is referred to as matric suction where u_a is the pore-air pressure (Fredlund and Morgenstern 1977). The complete description of the stress state takes the form of two matrices.

$$[2] \begin{bmatrix} (\sigma_x - u_a) & \tau_{xy} & \tau_{xz} \\ \tau_{yx} & (\sigma_y - u_a) & \tau_{yz} \\ \tau_{zx} & \tau_{zy} & (\sigma_z - u_a) \end{bmatrix}$$

and

$$[3] \begin{bmatrix} (u_a - u_w) & 0 & 0 \\ 0 & (u_a - u_w) & 0 \\ 0 & 0 & (u_a - u_w) \end{bmatrix}$$

The first, second and third stress invariants can be written for each matrix. However, in practice it is not necessary to relate mechanical behavior to all the stress variables provided a selected stress path is used for both the analysis and for measuring the soil parameters.

The above stress variables for an unsaturated soil also yield a smooth transition to the saturated case. As the degree of saturation approaches 100 percent, the pore-air pressure approaches the pore-water pressure. Therefore, the matric suction term goes to zero and the pore-air pressure term in the first stress matrix becomes the pore-water pressure.

Flow laws and steady state seepage

The driving potential for flow of the water phase in a saturated soil is the hydraulic head (i.e., elevation head plus pressure head). This is also true for an unsaturated soil.

Flow of water in a saturated soil is commonly described using Darcy's law.

$$[4] \quad v_w = -k_w \frac{\partial h_w}{\partial y}$$

where:

- v_w = velocity,
- k_w = coefficient of permeability for water, and
- y = coordinate direction.

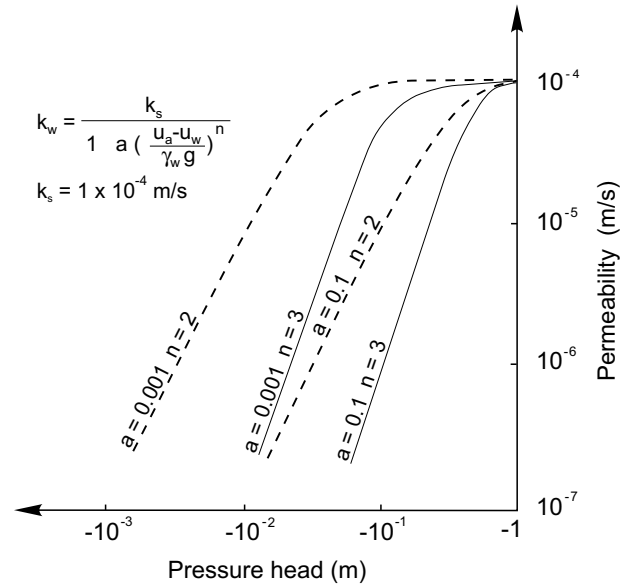
Darcy's law can also be used for unsaturated soils. However, the coefficient of permeability varies significantly with negative pore-water pressure head and must be assumed to be a variable in formulations. The most common form for the variation of permeability with negative pressure head is that proposed by Gardner (1958) (Fig. 1).

$$[5] \quad k_w = \frac{k_s}{1 + a \left(\frac{u_a - u_w}{\rho_w g} \right)^n}$$

where:

- k_s = saturated coefficient of permeability,

Fig. 1. Permeability related to negative pore-water head after Gardner (1958).



- ρ_w = density of water,
- g = gravity acceleration, and
- a and n = material parameters.

Equation [5] can be indirectly computed from the results of a suction versus water content test and a saturated permeability test. The form of the equation is particularly useful for sands and silts. More research is required on clayey soils which tend to crack and form a secondary structure as suction increases.

For some problems it may be necessary to describe the flow of air through an unsaturated soil. This requires an additional flow law; namely, Fick's law.

$$[6] \quad v_a = -D^* \frac{\partial u_a}{\partial y}$$

where:

- v_a = mass rate of air flow, and
- D^* = constant of proportionality.

The classic, two-dimensional, steady state seepage equation for an isotropic saturated soil is called the Laplace equation.

$$[7] \quad \frac{\partial^2 h}{\partial x^2} + \frac{\partial^2 h}{\partial y^2} = 0$$

For an unsaturated soil, the variation in permeability with negative head results in an expansion of the above equation.

$$[8] \quad k_w \frac{\partial^2 h}{\partial x^2} + \frac{\partial k_w}{\partial x} \frac{\partial h}{\partial x} + k_w \frac{\partial^2 h}{\partial y^2} + \frac{\partial k_w}{\partial y} \frac{\partial h}{\partial y} + \frac{\partial k_w}{\partial y} = 0$$

The second and fourth terms in eq. [8] account for the spatial variation in permeability while the fifth term is referred to as a gravity term. Equation [8] is a non-linear

partial differential equation which must also satisfy the permeability equation (e.g., eq. [5]).

Shear strength and slope stability analysis

The classic shear strength equation for a saturated soil is written in terms of the effective normal stress and takes the form of a Mohr-Coulomb failure criteria.

$$[9] \quad \tau = c' + (\sigma_n - u_w) \tan \phi'$$

where:

- τ = shear strength,
- c' = effective cohesion intercept,
- σ_n = total normal stress, and
- ϕ' = effective angle of internal friction.

For an unsaturated soil, the shear strength saturation takes the form of a three-dimensional extension of the Mohr-Coulomb failure criteria (Fig. 2).

$$[10] \quad \tau = c' + (u_a - u_w) \tan \phi^b + (\sigma_n - u_a) \tan \phi'$$

where:

- ϕ^b = angle of shear strength increase with an increase in $(u_a - u_w)$.

The angle, ϕ^b , has been measured on numerous soils from various countries of the world. Table 1 summarizes some of the experimental results.

The value for ϕ^b is consistently less than ϕ' and appears to commonly be in the range of 15°. Various laboratory testing procedures have been used but further research is still required.

The unsaturated soil can be visualized as having two components of cohesion

$$[11] \quad c = c' + (u_a - u_w) \tan \phi^b$$

When the matric suction goes to zero, eq. [10] reverts to eq. [9] for a saturated soil.

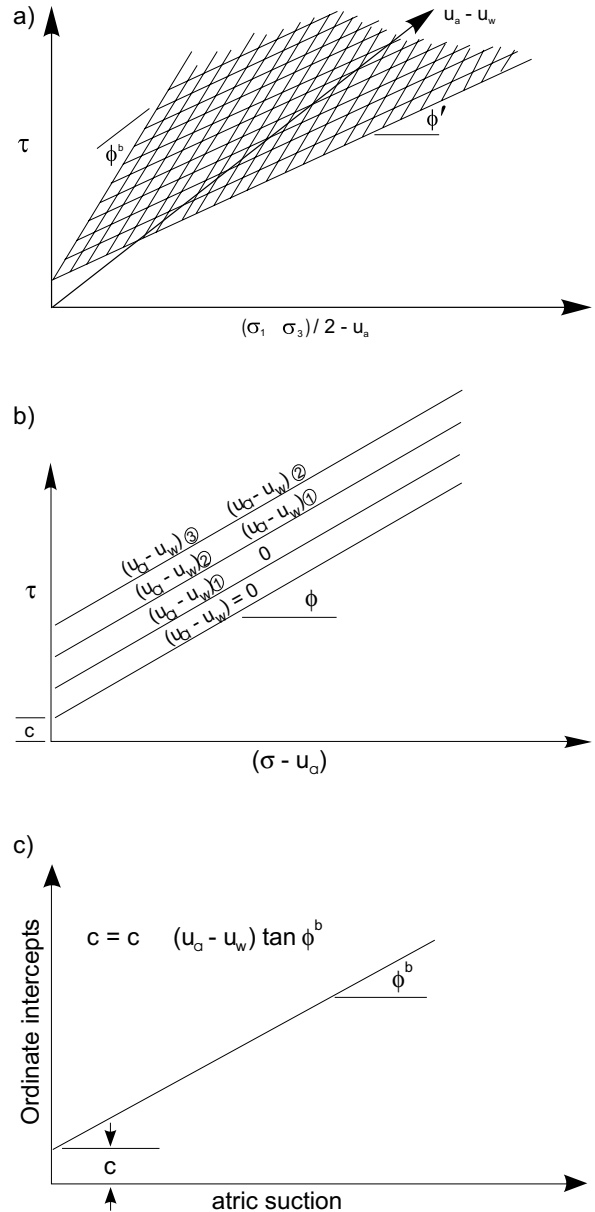
Not only is there a smooth transition between the saturated and unsaturated soil cases; the shear strength equation takes on the same form in both cases. This means that the same factor of safety equations used for a saturated soil can also be used for an unsaturated soil. It is merely necessary to make the cohesion of the soil a function of the negative pore-water pressure. Such analysis have already been applied to unsaturated soil slopes in Hong Kong (Ching et al. 1984) and other regions (Fontoura et al. 1984).

The results have shown that a relatively small magnitude of $(u_a - u_w)$ can produce a substantial increase in the computed factor of safety.

Constitutive relations

The classic volume change constitutive relations for saturated soils can be presented in one of several forms; namely the elasticity form, the compressibility form and the soil mechanics terminology forms. The elasticity form for saturated soils defines the linear strain of the soil

Fig. 2. Extended Mohr-Coulomb failure criteria for an unsaturated soil. a) Three-dimensional extended Mohr-Coulomb envelope surface; b) Effect of matric suction contoured on failure envelope; c) Increase in shear strength due to suction.



structure in three orthogonal directions for a linear, elastic material.

$$[12] \quad \begin{aligned} \epsilon_x &= \frac{(\sigma_x - u_w)}{E} - \frac{\mu}{E} (\sigma_y + \sigma_z - 2u_w) \\ \epsilon_y &= \frac{(\sigma_y - u_w)}{E} - \frac{\mu}{E} (\sigma_x + \sigma_z - 2u_w) \\ \epsilon_z &= \frac{(\sigma_z - u_w)}{E} - \frac{\mu}{E} (\sigma_x + \sigma_y - 2u_w) \end{aligned}$$

where:

Table 1. Experimental values for ϕ^b .

Soil type	ϕ^b (degrees)	Test procedure	Reference
Compacted shale; $w = 18.6\%$	18.1	Constant water content Triaxial	Bishop et al. (1960)
Boulder clay; $w = 22.2\%$	21.7	Constant water content Triaxial	Bishop et al. (1960)
Dhanauri clay; $w = 22.2\%$, $\gamma_d = 15.5 \text{ kN/m}^3$	16.2	Consolidated drained Triaxial	Satija (1978)
Dhanauri clay; $w = 22.2\%$, $\gamma_d = 14.5 \text{ kN/m}^3$	12.6	Consolidated drained Triaxial	Satija (1978)
Dhanauri clay; $w = 22.2\%$, $\gamma_d = 15.5 \text{ kN/m}^3$	22.6	Constant water content Triaxial	Satija (1978)
Dhanauri clay; $w = 22.2\%$, $\gamma_d = 14.5 \text{ kN/m}^3$	16.5	Constant water content Triaxial	Satija (1978)
Madrid Gray clay; $w = 29\%$, $\gamma_d = 13.1 \text{ kN/m}^3$	16.1	Consolidated drained Direct shear	Escario (1980)
Undisturbed decomposed granite; Hong Kong	15.3	Consolidated drained Multi-stage triaxial	Ho and Fredlund (1982)
Undisturbed decomposed rhyolite; Hong Kong	13.8	Consolidated drained Multi-stage triaxial	Ho and Fredlund (1982)
Cranbrook silt	16.5	Consolidated drained Multi-stage triaxial	Fredlund (unpublished)

$\epsilon_x, \epsilon_y, \epsilon_z$ = strain in the x, y and z directions,
 E = Young's modulus, and
 μ = Poisson's ratio.

The compressibility form for a saturated soil is as follows:

$$[13] \quad \epsilon = m_v d(\sigma - u_w)$$

where:

m_v = coefficient of volume compressibility and
 ϵ = volumetric strain, equal to $\epsilon_x + \epsilon_y + \epsilon_z$.

The compressibility modulus, m_v , can be written in terms of the elastic parameters, E and μ , for K_o and other loading conditions.

Using soil mechanics terminology, the volume change for a saturated soil is written as:

$$[14] \quad de = a_v d(\sigma_y - u_w)$$

where:

e = void ratio,
 a_v = coefficient of compressibility.

Constitutive relations for unsaturated soils have been written which are extensions of those presented above. It is also necessary to use more than one constitutive relation for an unsaturated soil because of the volumetric continuity requirement for a referential type element.

$$[15] \quad \epsilon = \theta_w + \theta_a$$

where:

θ_w = net inflow or outflow of water for an element, and
 θ_a = change in volume of air due to flow or compression.

The elasticity form for linear strain in the soil structure of an unsaturated soil can be written as a linear combination of the effects of each stress variable.

$$[16] \quad \begin{aligned} \epsilon_x &= \frac{(\sigma_x - u_a)}{E} - \frac{\mu}{E}(\sigma_y + \sigma_z - 2u_a) + \frac{(u_a - u_w)}{H} \\ \epsilon_y &= \frac{(\sigma_y - u_a)}{E} - \frac{\mu}{E}(\sigma_x + \sigma_z - 2u_a) + \frac{(u_a - u_w)}{H} \\ \epsilon_z &= \frac{(\sigma_z - u_a)}{E} - \frac{\mu}{E}(\sigma_x + \sigma_y - 2u_a) + \frac{(u_a - u_w)}{H} \end{aligned}$$

where:

H = elastic modulus with respect to $(u_a - u_w)$.

The E modulus must now be restricted to a change in the $(\sigma - u_a)$ stress variable.

A second independent, elasticity form of the constitutive equation can be written for the water phase.

$$[17] \quad \theta_w = \frac{(\sigma_x + \sigma_y + \sigma_z - 3u_a)}{3H'} + \frac{(u_a - u_w)}{R}$$

where:

H' = water phase (elasticity type) parameter with respect to $(\sigma_y - u_a)$, and
 R = water phase (elasticity type) parameter with respect to $(u_a - u_w)$.

The form of the above equation is the same as that first presented by Biot (1941) and Coleman (1962) and later by Fredlund and Morgenstern (1976).

The compressibility form of the constitutive equation for an unsaturated soil can be written as follows.

$$[18] \quad \epsilon = m_1^s d(\sigma - u_a) + m_2^s d(u_a - u_w)$$

where:

- m_1^s = compressibility of the soil structure with respect to a change in $(\sigma - u_a)$, and
 m_2^s = compressibility of the soil structure with respect to a change in $(u_a - u_w)$.

A second compressibility form of the constitutive equation can be written for the water phase.

$$[19] \quad \theta_w = m_1^w d(\sigma_y - u_a) + m_2^w d(u_a - u_w)$$

where:

- m_1^w = slope of the $(\sigma_y - u_a)$ versus θ_w plot, and
 m_2^w = slope of the $(u_a - u_w)$ versus θ_w plot.

A compressibility form of constitutive equation for the air phase can be written as the difference between the soil structure and water phase constitutive equations.

Using soil mechanics terminology, the change in void ratio, de , of an unsaturated soil can be written:

$$[20] \quad de = a_t d(\sigma_y - u_a) + a_m d(u_a - u_w)$$

where:

- a_t = coefficient of compressibility with respect to a change in $(\sigma_y - u_a)$, and
 a_m = coefficient of compressibility with respect to a change in $(u_a - u_w)$.

A second equation describing the change in water content, dw , of the soil can be written as:

$$[21] \quad dw = b_t d(\sigma_y - u_a) + b_m d(u_a - u_w)$$

where:

- b_t = coefficient of water content change with respect to $(\sigma_y - u_a)$, and
 b_m = coefficient of water content change with respect to $(u_a - u_w)$.

The above constitutive equations can be visualized as three-dimensional plots with each abscissa representing a stress variable and the ordinate representing the soil property (Fig. 3). These can also be reduced to two-dimensional plots which readily show the relationship between the various moduli (Fig. 3). It is also possible to plot both two-dimensional plots on one plot by using the variables Se and wG_s as ordinate variables where S is the degree of saturation and e the void ratio; w represents the water content and G_s is the specific gravity. The void ratio and water content constitutive relations can be largely linearized by plotting the logarithm of the stress variables.

The loading curve for $(\sigma_y - u_a)$ versus void ratio can readily be measured using conventional soil testing equipment (i.e., a_t or m_1^s). Equipment commonly used in soil science can be used to measure the relationship between water content and $(u_a - u_w)$ (i.e., b_m or m_2^w). Some research has been done on the remaining two relationships (i.e., $(a_m$ or $m_2^s)$ and $(b_t$ or $m_1^w)$), (Fredlund 1979). Sufficient research has already been done to verify the uniqueness of the proposed forms for the constitutive

equations (Matyas and Radhakrishna 1968; Barden et al. 1969; Fredlund and Morgenstern 1976).

Consolidation theory

The flow laws and constitutive equations provide the necessary physical relations for the formulation of transient flow problems. The one-dimensional formulation is presented to demonstrate the extension of the saturated soil case to that for an unsaturated soil. The Terzaghi equation for a saturated soil is derived by equating the time differential of the constitutive equation to the divergence of velocity.

$$[22] \quad \frac{\partial u_w}{\partial t} = c_v \frac{\partial^2 u_w}{\partial y^2}$$

where:

- t = time, and
 c_v = coefficient of consolidation.

For an unsaturated soil there is the possibility of flow in both the water and air phases. Two partial differential equations can be derived considering the continuity of the water and air phases respectively (Fredlund and Hasan 1979; Fredlund 1982). The water phase partial differential equation is as follows:

$$[23] \quad \frac{\partial u_w}{\partial t} = c_v^w \frac{\partial^2 u_w}{\partial y^2} - C_w \frac{\partial u_a}{\partial t} + \frac{c_v^w}{k_w} \frac{\partial k_w}{\partial y} \frac{\partial u_w}{\partial y} + c_g \frac{\partial k_w}{\partial y}$$

where:

- c_v^w = coefficient of consolidation with respect to the water phase,
 C_w = interactive constant associated with the water phase equation, and
 c_g = gravity term constant.

The second term to the right of the equal sign arises because of an interaction between simultaneous air and water flow from the soil. The third term to the right of the equal sign must be retained since the permeability can vary significantly with space during the consolidation process.

A smooth, mathematical transition to the saturated case occurs when the coefficient of permeability becomes a constant and the gradient in the air phase disappears.

The air phase partial differential equation is as follows:

$$[24] \quad \frac{\partial u_a}{\partial t} = c_v^a \frac{\partial^2 u_a}{\partial y^2} - C_a \frac{\partial u_w}{\partial t} + \frac{c_v^a}{D^*} \frac{\partial u_a}{\partial y}$$

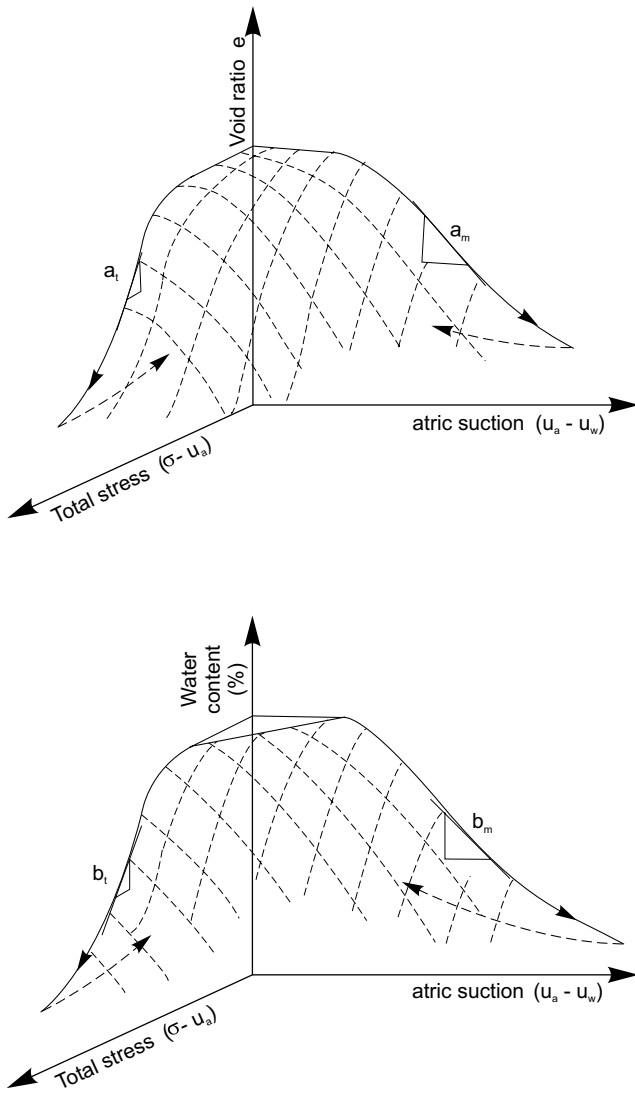
where:

- c_v^a = coefficient of consolidation with respect to the air phase, and
 C_a = interactive constant associated with the air phase equation.

The pore-water and pore-air pressures can be solved simultaneously for all depths and elapsed times. In many practical cases, the gradient in the air phase can be as-

Fig. 3. Constitutive surfaces for an unsaturated soil.

Fig. 3a. Three-dimensional void ratio and water content constitutive surfaces.



sumed to be insignificant in which case only the water phase partial differential equation needs to be solved.

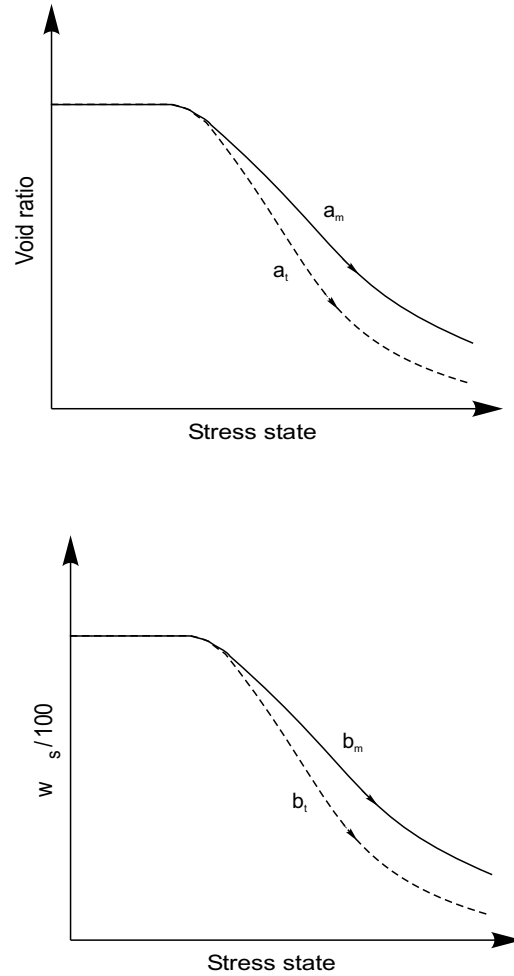
Pore pressure parameters

The A- and B-pore pressure parameters are used to predict excess pore pressures induced during the undrained loading of a soil. For an unsaturated soil, pore pressure parameters are required for both the water and air phases (Hasan and Fredlund 1980). The general form of these equations is the same as for a saturated soil (Skempton 1954; Bishop and Henkel 1962).

$$[25] \quad \Delta u_w = B_w [\Delta \sigma_3 + A_w (\Delta \sigma_1 - \Delta \sigma_3)]$$

$$[26] \quad \Delta u_a = B_a [\Delta \sigma_3 + A_a (\Delta \sigma_1 - \Delta \sigma_3)]$$

Fig. 3b. Two-dimensional comparison of compressibility moduli.



The B-pore pressure parameter can be written in terms of the constitutive equations and the density and compressibility equations for air-water mixtures (Fredlund 1976). These, in turn, make use of Boyle's and Henry's gas laws. The effect of Henry's law may or may not be included depending on whether the undrained loading is short or long term.

The B_w and B_a parameters can be solved simultaneously when eqs. [25] and [26] are written in terms of the compressibility of the soil and air-water mixtures. Earlier equations published by Hilf (1948) and Bishop (1959) are simplifications of the more rigorous formulation by Hasan and Fredlund (1980). Once again, the more rigorous equations show a smooth transition to the case of a saturated soil.

Measurement of pore-water pressure

A technology cannot survive and grow simply on sound theoretical equations. It must also be possible to

measure the necessary stress variables and soil properties in an economically viable manner. This has been possible in the case of saturated soils.

For unsaturated soils, the pore-water pressure is negative and its measurement has remained the primary stumbling block in advancing a suitable technology. However, in recent years significant advances have been made in the measurement of negative pore-water pressures. A detailed review of the research in this area is outside the scope of this paper. However, the author would encourage that review and research be conducted on this subject.

Recent research on the thermal conductivity type gauges has shown promise for geotechnical engineering (Picornell et al. 1983; Lee and Fredlund 1984). Further studies, however, are required prior to its endorsement.

The axis-translation technique (Hilf 1948) has proven to be satisfactory for numerous laboratory studies. The technique, however, cannot be used for *in situ* measurements. The measurement of the (corrected) swelling pressure of soils has also been used as an indirect measurement of matric suction (Fredlund et al. 1980).

Conclusion

A suitable science for unsaturated soils is presently available. It can be visualized as a logical extension of classic saturated soil mechanics principles and equations. The greatest need in the ensuing decade is to improve our ability to measure negative pore-water pressure. Also requiring further studies are the procedures for the measurement of relevant soil parameters. These stress and soil parameter measurements, combined with the summarized equations can form the basis for much needed case histories concerning all aspects of unsaturated soil behavior.

References

- Barden, L., Madedor, A.D., and Sides, G.R. 1969. Volume change characteristics of unsaturated clay. *ASCE, Journal of the Soil Mechanics and Foundation Division*, **95**(SM1): 33–52.
- Biot, M.A. 1941. General theory of three-dimensional consolidation. *Journal of Applied Physics*, **12**(2): 155–164.
- Bishop, A.W. 1959. The principle of effective stress. Lecture delivered in Oslo, Norway, 1955; *Technisk Ukeblad*, **106**(39): 859–863.
- Bishop, A.W., Alpan, I., Blight, G.E., and Donald, I.B. 1960. Factors controlling the strength of partly saturated cohesive soils. *Proceedings, ASCE Research Conference on Shear Strength of Cohesive Soils*, Boulder, CO, pp. 503–532.
- Bishop, A.W., and Henkel, D.J. 1962. *The measurement of soil properties in the triaxial test*. Edward Arnold Ltd., London, England, 2nd Edition, pp. 180–211.
- Ching, R.K.H., Sweeney, D.J., and Fredlund D.G. 1984. Increase in factor of safety due to soil suction for two Hong Kong slopes. *Proceedings, IV International Symposium on Landslides*, Toronto, Canada, Vol. 1, pp. 617–623.
- Coleman, J.D. 1962. Stress/strain relations for partly saturated soils. *Correspondence in Géotechnique*, **12**(4): 348–350.
- Escario, V. 1980. Suction controlled penetration and shear tests. *Proceedings, 4th International Conference on Expansive Soils*, Denver, CO, American Society of Civil Engineers, Vol. 2, pp. 781–797.
- Fontoura, A.B., De Compos, L.E., and Costa Filho, L.M. 1984. A reanalysis of some slides in gneissic residual soils. *Proceedings, 4th International Symposium on Landslides*, Toronto, Canada.
- Fredlund, D.G. 1976. Density and compressibility characteristics of air-water mixtures. *Canadian Geotechnical Journal*, **13**(4): 386–396.
- Fredlund, D.G. 1979. Appropriate concepts and technology for unsaturated soils. *Second Canadian Geotechnical Colloquium*, *Canadian Geotechnical Journal*, **16**(1): 121–139.
- Fredlund, D.G. 1982. Consolidation of unsaturated porous media. *Proceedings, Symposium on the Mechanics of Fluid in Porous Media-New Approaches in Research*, NATO Advance Study Institute, University of Delaware, Newark, DL.
- Fredlund, D.G., and Hasan, J.U. 1979. One-dimensional consolidation theory: unsaturated soils. *Canadian Geotechnical Journal*, **1**(3): 521–531.
- Fredlund, D.G., and Morgenstern, N.R. 1976. Constitutive relations for volume change in unsaturated soils. *Canadian Geotechnical Journal*, **13**(3): 261–276.
- Fredlund, D.G., and Morgenstern, N.R. 1977. Stress state variables for unsaturated soils. *ASCE, Journal of the Geotechnical Engineering Division*, **103**(GT5): 447–466.
- Fredlund, D.G., Hasan, J.U., and Filson, H.L. 1980. The prediction of total heave. *Proceedings, 4th International Conference on Expansive Soils*, Denver, CO, pp. 1–17.
- Gardner, W.R. 1958. Laboratory studies of evaporation from soil columns in the presence of water table. *Soil Science of America*, **85**: 244.
- Hasan, J.U., and Fredlund, D.G. 1980. Pore pressure parameters for unsaturated soils. *Canadian Geotechnical Journal*, **17**(3): pp. 395–404.
- Hilf, J.W. 1948. Estimating construction pore pressures in rolled earth dams. *Proceedings, 2nd International Conference on Soil Mechanics and Foundation Engineering*, Rotterdam, Vol. 3, pp. 234–240.
- Ho, D.Y.F., and Fredlund, D.G. 1982. Increase in shear strength due to suction for two Hong Kong soils. *Proceedings, Conference on Engineering and Construction in Tropical and Residual Soils*, ASCE, Honolulu, Hawaii, January 11–15, pp. 263–295.
- Krohn, J.P., and Slosson, J.E. 1980. Assessment of expansive soils in the United States. *Proceedings, 4th International Conference on Expansive Soils*, Denver, CO, pp. 596–608.
- Lee, R.K.C., and Fredlund, D.G. 1984. Measurement of soil suction using the MCS 6000 sensor. *Proceedings, 5th International Conference on Expansive Soils*, Adelaide, South Australia, May 21–23, pp. 50–54.
- Matyas, E.L., and Radhakrishna, H.S. 1968. Volume change characteristics of partially saturated soils. *Géotechnique*, **18**(4): 432–448.
- Picornell, M., Lytton, R.L., and Steinberg, M. 1983. Matrix suction instrumentation of a vertical moisture barrier. *Transport Research Records*, **954**: 16–21.
- Satija, D.J. 1978. Shear behaviour of partially saturated soils. Ph.D. thesis, Indian Institute of Technology, New Delhi, India.
- Skempton, A.W. 1954. The pore pressure coefficients, A and B. *Géotechnique*, **4**(4): 143–147.

The scope of unsaturated soil mechanics: An overview

D.G. Fredlund

Abstract: Theories and formulations developed for the behavior of unsaturated soils are shown to include the behavior of saturated soils as a special case, leading to a generalization of the mechanics for soils. The scope of a generalized soil mechanics is illustrated through a series of visualization aids and diagrams.

Man lives in direct contact with the vadose zone (i.e., the unsaturated zone). The upper boundary of the vadose zone (i.e., the ground surface) is subjected to a flux type boundary condition for many of the problems faced by geotechnical engineers. The atmosphere, down through the vadose zone to the soil below the groundwater table should be viewed as a continuum. A generalized mechanics for soils which is applicable for both saturated soils and unsaturated soils is necessary for dealing with the soil of the subterranean zone in a consistent manner (i.e., the saturated zone and the unsaturated zone should not be treated in isolation). There is also a need to treat the atmosphere and the soils as a unit. The soil-water characteristic curve has been shown to be a key soil function which can be used to approximate the behavior of unsaturated soils.

Key words: soil mechanics, unsaturated soils, unsaturated soil property functions, continuum, soil-water characteristic curve, soil suction, stress state variables, flow, shear strength, volume change.

Introduction

In the past, theoretical soil mechanics has dealt mainly with saturated soil below the groundwater table. The soil above the groundwater table was mostly dealt with using empirical formulations. A rational, scientific basis was lacking in dealing with the mechanics of the unsaturated soil media. A scientific basis is essential for problems to be properly understood and for the problems to be handled in a rational and consistent manner. In saturated soil mechanics, the principle of effective stress provided the key element for understanding the behavior of the saturated soil. The effective stress, $(\sigma - u_w)$, has been proven to be an adequate variable to define the stress state of the saturated soil. There is a need to use a state variable approach in the understanding of the behavior of unsaturated soils. It will be shown that there can be one generalized theory of soil mechanics whose concepts are applicable to both saturated and unsaturated soils.

In this paper, a more all encompassing representation of the discipline of a generalized soil mechanics is illustrated through a series of visualization aids. An attempt is made to use simplicity in describing concepts and explaining example situations. The visualization aids may not be drawn to scale and may appear to be exaggerated situations.

D.G. Fredlund. Professor, Department of Civil Engineering, University of Saskatchewan, 57 Campus Drive, Saskatoon, SK, Canada S7N 5A9.

Reproduced with permission from the *Keynote Address, 1st International Conference on Unsaturated Soils*, Paris, France. Edited by Alonso, E.E., and Delage, P., September 6–8, 1995, A.A. Balkema Publishers, Rotterdam, The Netherlands. Vol. 3, pp. 1155–1177.

Generalized soil mechanics

The term, “generalized soil mechanics”, is used in the sense that the theories and formulations apply to the high majority of soil conditions encountered in engineering practice. Generalized soil mechanics applies to soils near the ground surface as well as those at greater depths. It applies to soils above the water table as well as those below the water table. It applies to unsaturated soils and saturated soils alike using the same general theories and formulations. It can be shown that theories and formulations which embrace the unsaturated portion of a soil profile have saturated soil behavior as a special case (i.e., there is one unified theory for soil mechanics).

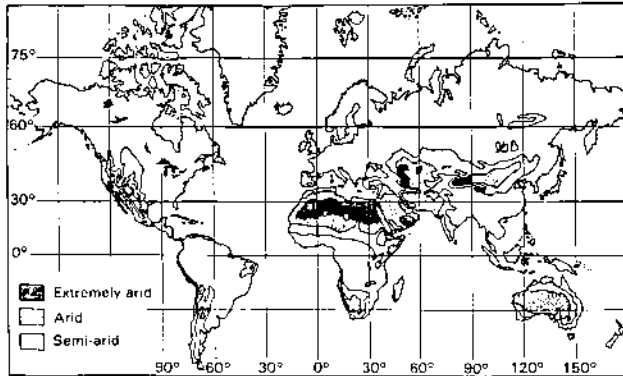
In this paper, the terms generalized soil mechanics or generalized soil elements will be used when referring to soils which can be either saturated or unsaturated.

Need for a generalized mechanics of soils

A large portion of the world population is found in the arid regions of the world where the groundwater table is deep. There appears to be a strong correlation between the arid regions and the population density (Fig. 1). The 10–40 window of the world is defined by +10° and +40° latitude north, and 10° and 40° longitude. This window is inhabited by approximately 3.1 billion people or 60% of the world population, and also contains 60% of the countries of the world.

The drier climatic regions have become increasingly aware of the uniqueness of their regional soil mechanics problems. In recent years there has also been a shift in emphasis in the developed regions from the behavior of engineered structures to the impacts of developments on

Fig. 1. World map showing extremely arid, arid and semi-arid regions of the world.



the natural world. This shift in emphasis resulted in greater need to deal with the vadose zone. There has been an ongoing desire to expand the science dealing with soil mechanics such that it will also embrace the behavior of unsaturated soils. An all encompassing generalized soil mechanics has emerged in the developed countries and is today receiving acceptance on a global scale.

There is a need to deal with the behavior of unsaturated soil beyond the utilization of empirical formulations. Empiricism generates methods of handling specific problems but does not provide proper theoretical explanations for the problems. A rational, scientific basis is also needed to teach and transfer technology such that the theories can become a part of world-wide geotechnical engineering. The effective stress variable is the key that has led to the rapid transfer of geotechnology of saturated soils around the world. Similarly, the stress state variable approach is the means of transferring unsaturated soil behavior (and generalized soil behavior) from one country to another.

Events which spur the emergence of unsaturated soil mechanics

The development of a rational approach to the behavior of unsaturated soils can be traced to three main events.

- (1) In arid countries around the world there have been problems associated with volume changes of unsaturated soils in response to changes in the water content of the soil. The great economic consequences associated with damages to structures (particularly homes) due to these volume changes has provided the initiative to conduct research on the behavior of unsaturated, expansive soils.
- (2) There is an increasing concern for the environment in developed countries. Today the geotechnical engineer is called upon to predict chemical pollutant concentrations in the ground with respect to time and space. The diffusion of a chemical is superimposed on the conductive movement within the water phase. In other words, an additional diffusive analysis has been added to the seepage of water through a soil. The hy-

draulic conductivity (or coefficient of permeability) of soil has often been regarded as one of the most difficult soil properties to evaluate. Now, this property is the central focus of many analyses and much research has been directed towards its quantification. Many of the processes of concern to the environment and to the water resources occur in the upper portion of the soil profile; in the vadose zone where the pore-water pressures are negative. In this zone, the hydraulic conductivity is a function of the negative pore-water pressure, resulting in non-linear flow formulations. The groundwater table is no longer the upper boundary of concern. Rather, the ground surface geometry becomes the boundary for the problem and movements through the unsaturated zone become of vital importance.

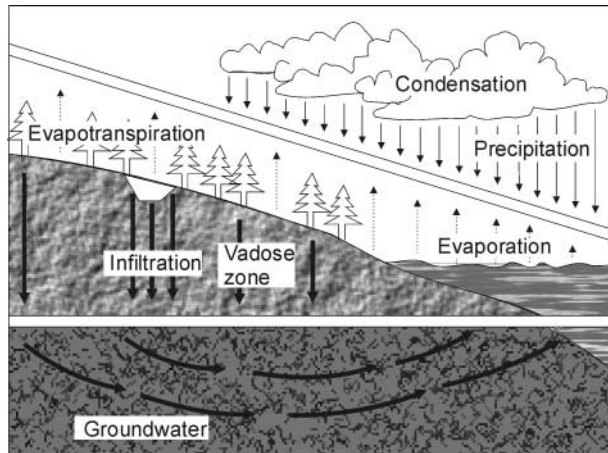
- (3) The rapid development in the computer industry has provided the engineer with the means to handle complex geotechnical problems associated with unsaturated soils behavior. Software related to coupled, transient problems is becoming increasingly used on a routine basis in engineering offices. The software is often used in a parametric or sensitivity manner in order to embrace a range of possible field conditions.

Illustrations of the scope of geotechnical problems involving generalized soil mechanics

The geotechnical engineering works of man always start at the ground surface. While some projects extend well below the groundwater table, many projects remain in the zone above the groundwater table. For example, engineers place building foundations in the zone above the groundwater table for ease of construction. Whenever possible, the geotechnical engineer will attempt to do the design such that construction can remain in the unsaturated zone. In addition to shallow foundations, retaining walls and cuts in slopes are generally designed such that they remain above the water table. Over the past decades, much of the engineering design associated with soils above the water table has remained relatively empirical. At the same time, engineering designs involving soil below the water table have utilized the effective stress analyses in advancing practical designs.

Geotechnical engineers have been slow to realize the close link which exists between the area of surface hydrology and the flux boundary condition for their problems. A visualization of the hydrologic cycle quickly brings an awareness that the ground surface is a flux boundary and that water moving to the groundwater table must first pass through the unsaturated, vadose zone. Fig. 2 illustrates the artificial separation which is often placed between the hydrologic components, the vadose zone and the groundwater. In reality, the movement cycle of water is a continuous process from the atmosphere to the groundwater table. The near surface phenomena can be dynamic and extreme. Changes in the boundary conditions affect the pore-water pressures in the soil.

Fig. 2. Schematic showing the artificially imposed boundaries between the atmosphere and the groundwater (from OSU 1994).



The building of the infrastructure for society has largely involved soils above the groundwater table. Infrastructure developments have also given rise to extensive environmental concerns (Fig. 3). Many of the environmental problems originate on or near ground surface. Contaminants must move through the unsaturated vadose zone and may eventually end up in the groundwater. An understanding of the movement of contaminants through the unsaturated, vadose zone becomes necessary when predicting the transport of chemicals from their source to their destination in the aqueous environment. Theoretical models must embrace convective flow and diffusion within the unsaturated, vadose zone.

Many geotechnical engineering projects are involved with the use of remolded, compacted soils. Dams and highway embankments are two examples of engineered structures which involve large volume of compacted soils. Problems related to compacted soils requires the application of unsaturated soil mechanics.

Visualization aids for generalized soil mechanics

The “geotechnical world” is presented as an ellipse with a mid-level horizontal line representing the groundwater table (Fig. 4). The situations in temperate, humid regions and in arid regions of the world can be visualized as shown in Figs. 5 and 6, respectively. In temperate, humid regions, the groundwater table may be close to the ground surface (Fig. 5). In arid regions, the groundwater table can be very deep (Fig. 6).

Below the water table, the pore-water pressures will be positive and the soils will, in general be saturated. Above the water table, the pore-water pressures will, in general, be negative. Immediately above the water table is a zone called the capillary fringe where the degree of saturation approaches 100 percent. This zone may range from less than one metre to approximately 10 metres in thickness,

depending upon the soil type. The entire zone above the water table is called the vadose zone.

The negative pore-water pressures above the water table are generally referenced to the pore-air pressure (i.e., $(u_a - u_w)$). The difference between the pore-air pressure and the pore-water pressure is called the matric suction. The term originated in Soil Science and was later shown to be one of two stress state variables required to describe the behavior of an unsaturated soil.

Definition of soil suction

Suction in an unsaturated soil is made up of two components; namely, matric suction and osmotic suction. The sum of the two components is called total suction. Matric suction is defined as the difference between the pore-air pressure, u_a , and the pore-water pressure, u_w (i.e., matric suction = $u_a - u_w$). The osmotic suction is a function of the amount of dissolved salts in the pore fluid, and is written in terms of a pressure. The matric suction is of primary interest because it is the stress state variable which is strongly influenced by environmental changes.

The terminology, saturated soil mechanics and unsaturated soil mechanics, would suggest that it is the degree of saturation which provides the distinction between these two categories (Fig. 7). While this is true, it is difficult to measure the degree of saturation and to use the degree of saturation in the analysis of unsaturated soil behavior. It is rather the state of stress in the water phase which has become the primary indicator for classification purposes. Any soil with a negative pore-water pressure is considered to be part of unsaturated soil mechanics. It is recognized that soils with negative pore-water pressures can be saturated or contain air bubbles in an occluded form. Figure 8 shows a soil classification based on the continuity of the air and water phases.

The physics and engineering principles involved with dry soils are essentially the same as those involved with saturated soils. The difference between a completely dry and a completely saturated soil is related to the compressibility of the pore fluid. The water in a saturated soil is essentially incompressible. The water becomes compressible as air bubbles appear in the water. Most attention in research has been given to the case where air and water are continuous throughout the voids. It appears to be the case most relevant to engineering practice.

Categorization of generalized soil mechanics

Generalized soil mechanics can be categorized in a manner consistent with the traditional classic areas of soil mechanics. There are three main categories; namely, seepage, shear strength and volume change. This subdivision, along with the basic equations associated with each category, are shown in Fig. 9. This categorization shows that the same types of problems are of interest for both saturated and unsaturated soils. It also shows that the behavior of an unsaturated soil is a function of the stress states. The stress state categorization provides the basis

Fig. 3. Illustration of the geo-environmental impact of man's activities (redrawn from Miller 1993)

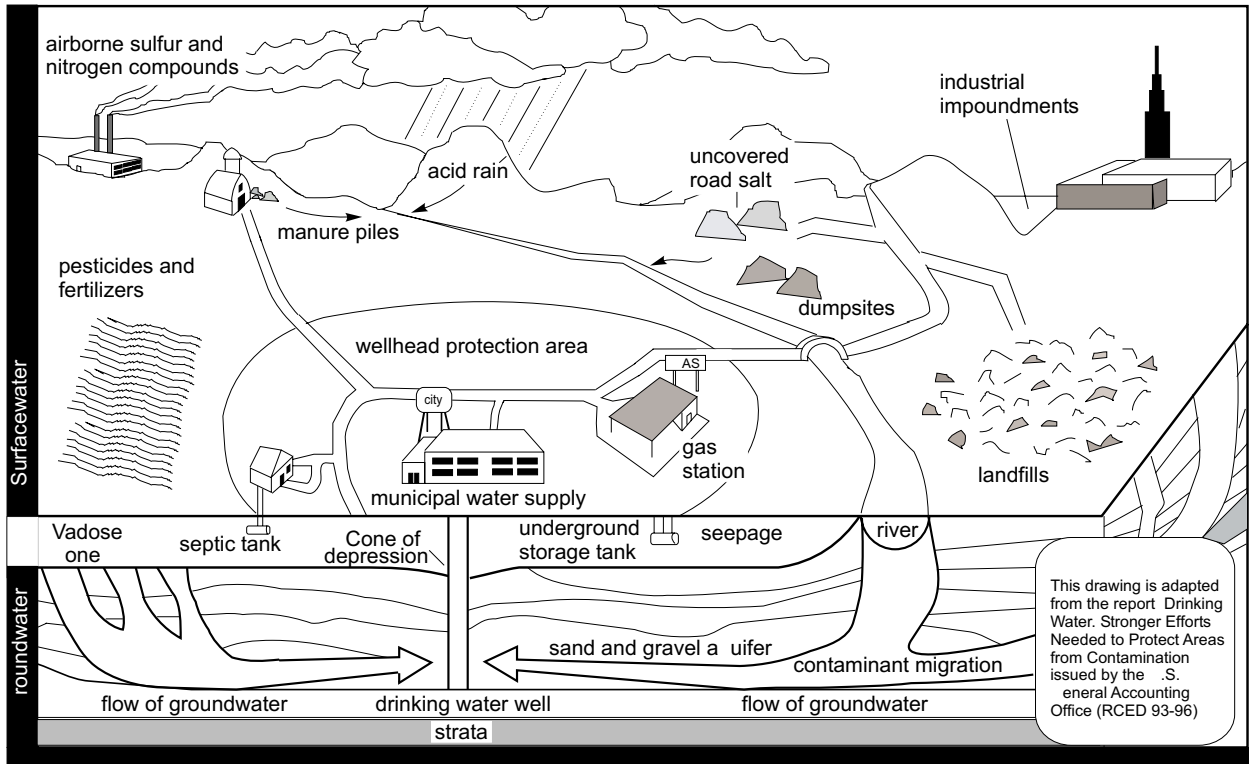


Fig. 4. Visualization aid for the generalized world of soil mechanics.

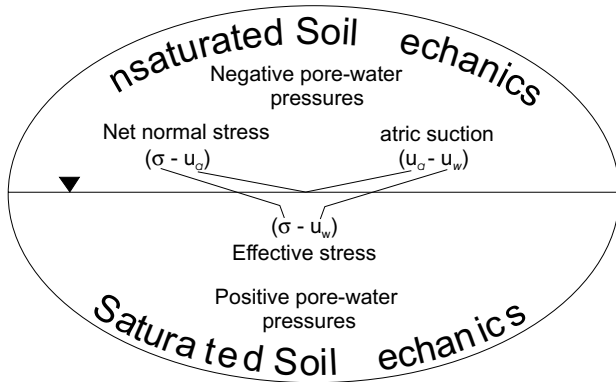


Fig. 5. Visualization aid for the temperate, humid regions.

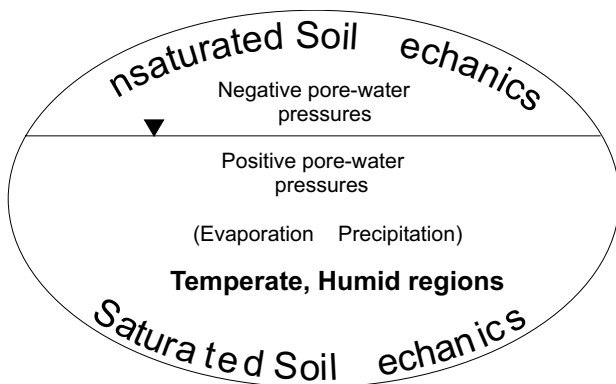
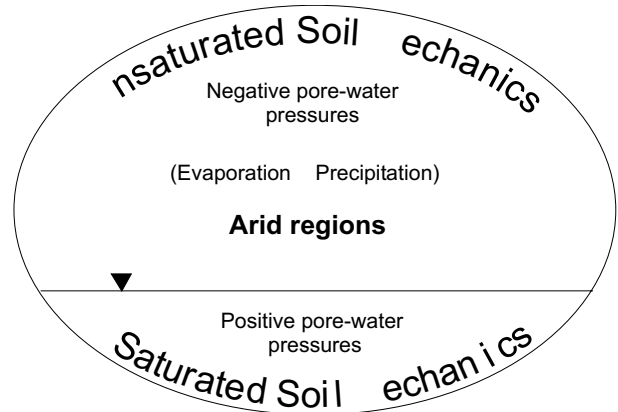


Fig. 6. Visualization aid for the arid regions.



for a science which is transferable the world over. An unsaturated soil may either increase or decrease in overall volume when subjected to wetting (i.e., a decrease in matric suction). If the volume increases upon wetting, the soil has a swelling nature and if the volume decreases upon wetting, the soil has a collapsing nature. The difference in behavior is associated with the structure of the soil. The swelling soil has a "stable-structure" and the collapsing soil has a "meta-stable-structure". This categorization also applies to both remolded (i.e., compacted) and natural soils. The awareness of these types of behavior is important since the constitutive relationships (i.e., volume change behavior in particular) are different for each case. The case for swelling of a stable-structured

Fig. 7. Categorization of soil above the water table based on the variation in degree of saturation.

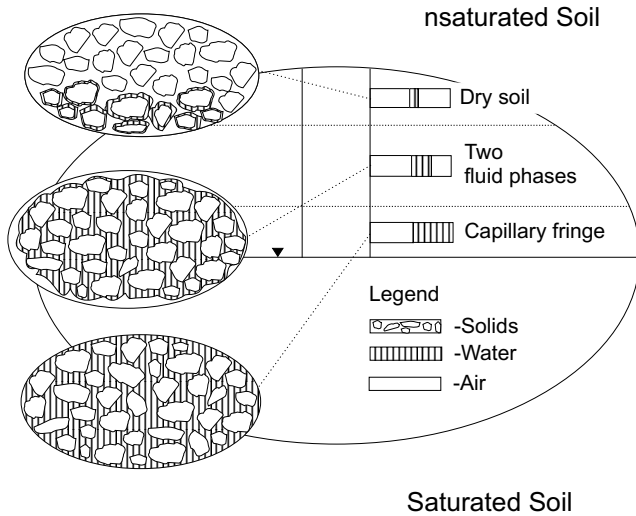
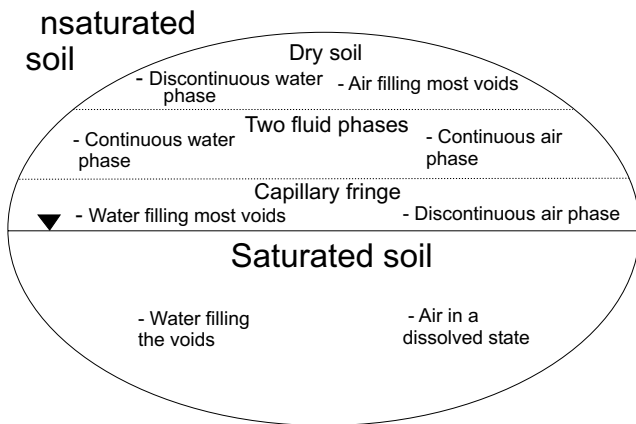


Fig. 8. Visualization of generalized soil mechanics based on the nature of the fluid phases.



soil is illustrated in Fig. 10. The soil suction is shown to generally increase as ground surface is approached. Likewise, the potential for swelling increases exponentially. This is applicable to soils with high plasticity.

The character of the non-linear coefficient of permeability function is illustrated in Fig. 11. Once the air entry value of the soil is exceeded, the coefficient of permeability decreases from its saturated value. The decrease in coefficient of permeability bears a linear log-log correspondence to soil suction. Various mathematical forms have been proposed for the coefficient of permeability function. Figure 11 shows the mathematical form known as the equation by Gardner (1958).

It is apparent from Fig. 9 that the basic constitutive relations for each category of problem are more complex for unsaturated soils than for saturated soils. At the same time, each of the equations specializes from the unsaturated case to the saturated case as the matric suction term goes to zero. A second soil parameter, ϕ^b , is required when describing the shear strength of an unsaturated soil.

Fig. 9. Categorization of soil mechanics based on the type of engineering problem.

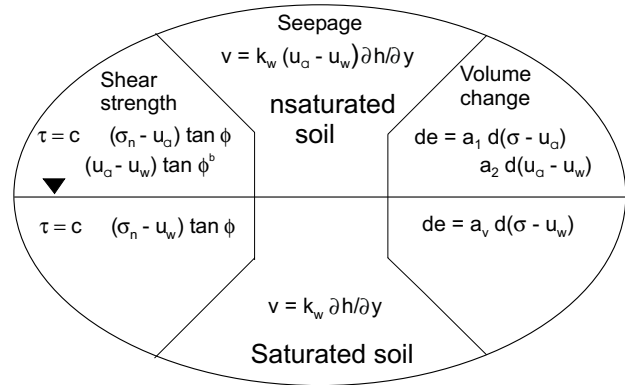
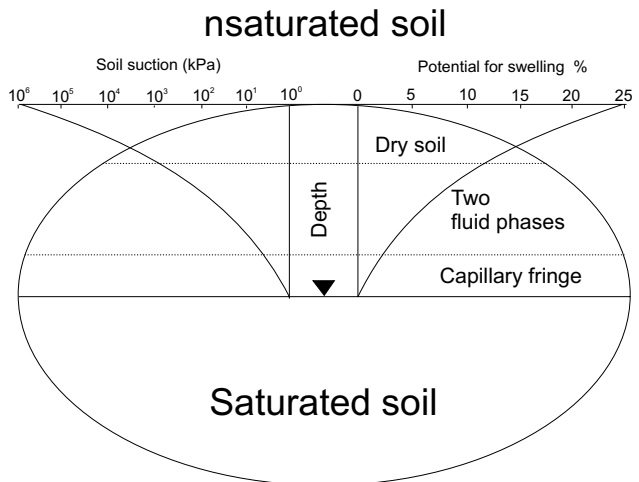


Fig. 10. Illustration of the potential for swelling versus depth and soil suction.



The coefficient of permeability becomes a non-linear function for the analysis of seepage problems. Two independent coefficients of compressibility are required to define void ratio changes for an unsaturated soil. As well, changes in water content must be predicted using an independent constitutive relation when analysing unsaturated volume-mass changes.

In addition to the above, soils can also be categorized genetically. The geologic genesis of a deposit has certain characteristics which indicate the nature of engineering properties likely to be encountered. Some of the common genetic categories can be listed as follows: lacustrine soils, bedrock soils, aeolian soils, alluvial soils, residual soils and others (Fig. 12). From the standpoint of a theoretical framework, this categorization has little to offer in describing the behavior of soils. In other words, essentially the same theories can be shown to apply for all types of soil.

There are also textural and plasticity categories of soils (i.e., sands, silts and clays).

Regardless of the various soil categorizations, similar engineering problems can be encountered.

Fig. 11. Visualization of the coefficient of permeability function in the unsaturated soil zone.

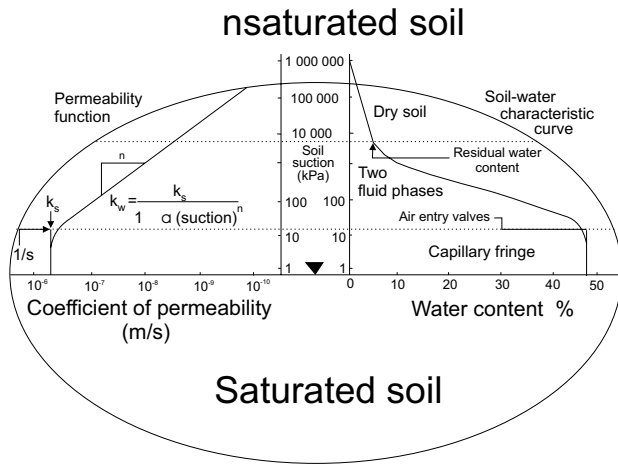
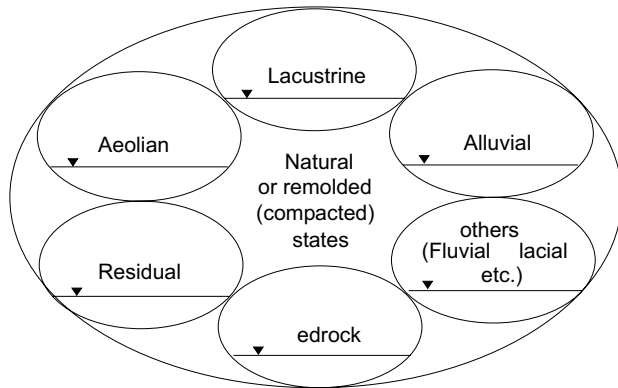


Fig. 12. Categorization of soil mechanics based on the geological origins.



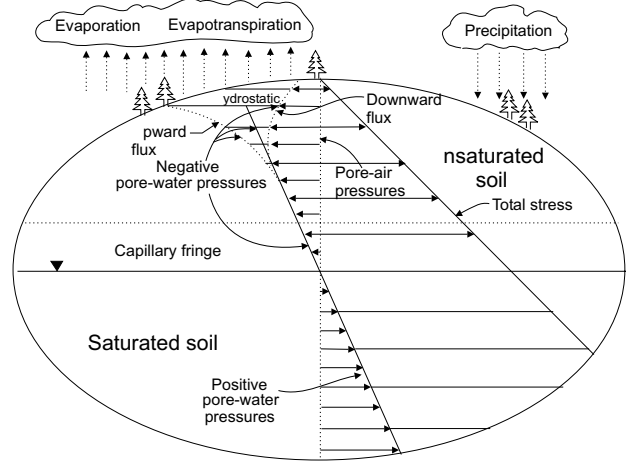
Climate and the vadose zone

The location of the groundwater table (i.e., separation between negative and positive pore-water pressures) is strongly influenced by the long term climatic conditions in a region (Figs. 5 and 6). If the region is arid or semi-arid, the groundwater table is slowly lowered with time (i.e., geologic time scale), (Fig. 6). If the climate is temperate or humid, the groundwater table may remain quite close to the ground surface (Fig. 5). It is the difference between the downward flux (i.e., precipitation) and the upward flux (i.e., evaporation and evapotranspiration) on a long term basis, which determines the location of the groundwater table (Fig. 13).

The portion of the soil profile above the groundwater table, called the vadose zone, can be readily subdivided into two portions. The portion immediately above the water table, called the capillary fringe, remains saturated even though the pore-water pressures are negative. The portion above the capillary fringe is unsaturated.

Regardless of the degree of saturation of the soil, the pore-water pressure profile in Fig. 13 will come to equilibrium at a hydrostatic condition when there is zero flux

Fig. 13. Visualization of soil mechanics showing the role of the surface flux boundary condition.



from the ground surface. If moisture is extracted from the ground surface (e.g., evaporation), the pore-water pressure profile will be drawn to the left. If moisture enters at the groundwater surface (e.g., infiltration), the pore-water profile will be drawn to the right.

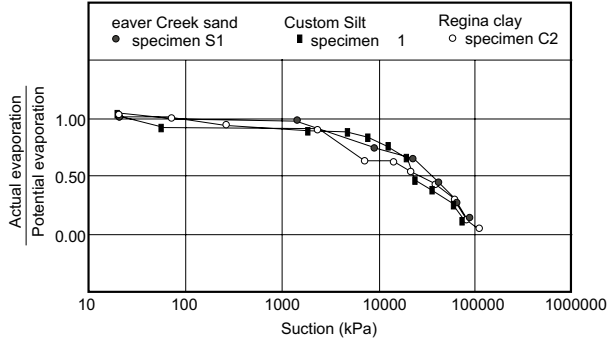
The precipitation conditions at a site are often known from past records and are available for design purposes. The evaporative flux, on the other hand, must be computed through the use of one of several models. Some of the most approximate estimates for geotechnical problems have been associated with the assessment of evaporative flux. Only recently have engineers begun to include the role of soil suction in computing the rate of evaporation from the ground surface (Wilson 1990). Figure 14 shows that the rate of release of water to the atmosphere, from a sand, silt or clay, is related to the suction in the soil. The computation of the evaporative flux has become an area of research which is of great value to engineers dealing with geo-environmental problems.

There are many complexities associated with the vadose zone because of its fissured and fractured nature. The tendency in geotechnical engineering has been to avoid the analysis of this zone, if possible. However, in many cases it is an understanding of this zone which holds the key to the performance of an engineered structure.

Historically, classical seepage problems involved saturated soils where the boundary conditions consisted of either a designated head or zero flux. However, the real world for the engineer often involved a ground surface, where there may be a positive or negative flux condition. Geo-environmental type problems have done much to force the engineer to give consideration of saturated/unsaturated seepage analyses with flux boundary conditions. The improved computing capability available to the engineer has assisted in accommodating these changes.

Most of the manmade structures are placed on the surface of the earth (Fig. 15) and as such will have an environmental flux boundary condition. Consider, for example, a highway where the soil in the embankment

Fig. 14. Relationship between the ratio of actual evaporation to potential evaporation, and soil suction for three soils (from Wilson 1990).



and subgrade have an initial set of conditions or stress states. These conditions will change with time primarily because of environmental (or surface moisture flux) changes. The foundations for light structures are likewise generally placed well above the groundwater table where the pore-water pressures are negative. In fact, most of the light engineered structures of the world are placed within the vadose zone.

One of the characteristics of the upper portion of the vadose zone is its ability to slowly release water vapor to the atmosphere at a rate dependent upon the permeability of the intact portions of soil. At the same time, downward flow of water can occur through the fissures under a gradient of unity. There appears to be no impedance to the inflow of water until the soil swells and the mass becomes intact, or until the fissures and cracks are filled with water.

A common misconception is that water can always enter the soil at the ground surface. However, if the soil is intact, the maximum flux of water at the ground surface is equal to the saturated coefficient of permeability of the soil. This value may be extremely low. If the ground surface is sloping, the surface layer can become saturated and have a higher coefficient of permeability than the underlying soil. As a result, water runs down the top layers of soil on the slope, and may not enter the underlying soil.

Stress state of a soil

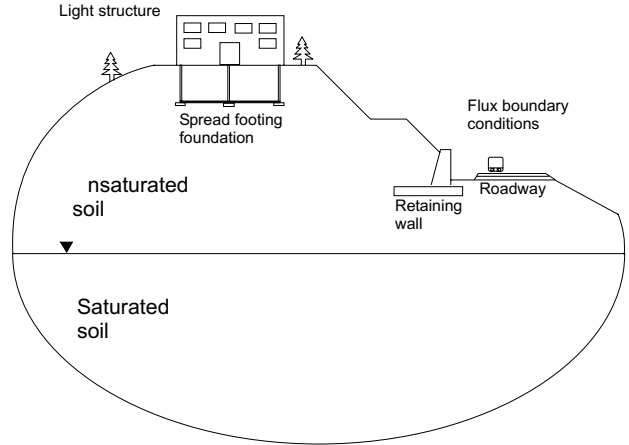
The stress state of a saturated soil is completely defined by effective stress variables,

$$[1] \begin{bmatrix} (\sigma_x - u_w) & \tau_{yx} & \tau_{zx} \\ \tau_{xy} & (\sigma_y - u_w) & \tau_{zy} \\ \tau_{xz} & \tau_{yz} & (\sigma_z - u_w) \end{bmatrix}$$

where:

- $\sigma_x, \sigma_y, \sigma_z$ = total stresses in x, y, z directions, respectively,
- τ = shear stress, and
- u_w = pore-water pressure.

Fig. 15. Examples of engineered structures commonly placed above the water table.



Using a similar stress state approach, it was established that the stress state of an unsaturated soil is defined by two sets of independent stress state variables (Fredlund and Morgenstern 1977). There are three sets of possible stress state variables, of which only two of the three sets are independent.

The stress tensors associated with the three sets of independent stress state variables are:

Stress state set No. 1:

$$[2a] \begin{bmatrix} (\sigma_x - u_a) & \tau_{yx} & \tau_{zx} \\ \tau_{xy} & (\sigma_y - u_a) & \tau_{zy} \\ \tau_{xz} & \tau_{yz} & (\sigma_z - u_a) \end{bmatrix}$$

Stress state set No. 2:

$$[2b] \begin{bmatrix} (\sigma_x - u_w) & \tau_{yx} & \tau_{zx} \\ \tau_{xy} & (\sigma_y - u_w) & \tau_{zy} \\ \tau_{xz} & \tau_{yz} & (\sigma_z - u_w) \end{bmatrix}$$

and

Stress state set No. 3:

$$[2c] \begin{bmatrix} (u_a - u_w) & 0 & 0 \\ 0 & (u_a - u_w) & 0 \\ 0 & 0 & (u_a - u_w) \end{bmatrix}$$

In the special case of a saturated soil, the pore-air pressure, u_a , is equal to the pore-water pressure, u_w , and the three stress tensors reduce to one single stress tensor (i.e., eq. [1]).

The stress state variables most often used for unsaturated soils are the following two stress state variables:

$$[3a] \begin{bmatrix} (\sigma_x - u_a) & \tau_{yx} & \tau_{zx} \\ \tau_{xy} & (\sigma_y - u_a) & \tau_{zy} \\ \tau_{xz} & \tau_{yz} & (\sigma_z - u_a) \end{bmatrix}$$

and

$$[3b] \begin{bmatrix} (u_a - u_w) & 0 & 0 \\ 0 & (u_a - u_w) & 0 \\ 0 & 0 & (u_a - u_w) \end{bmatrix}$$

The stress state at a point in an unsaturated soil element, in terms of the above two sets of stress state variables are shown in Fig. 16.

Stress invariants

The three principal stresses on three mutually orthogonal planes for a generalized soil element are $(\sigma_1 - u_a)$, $(\sigma_2 - u_a)$ and $(\sigma_3 - u_a)$ respectively. In addition, the matric suction, $(u_a - u_w)$, also acts equally on all three planes.

There are three stress invariants that can be derived from each of the two independent stress tensors corresponding to the stress state variables, $(\sigma - u_a)$ and $(u_a - u_w)$ for an unsaturated soil. The first stress invariants of the stress tensors associated with the stress state variables, $(\sigma - u_a)$ and $(u_a - u_w)$ are:

$$[4a] \quad I_{11} = \sigma_1 + \sigma_2 + \sigma_3 - 3u_a$$

and

$$[4b] \quad I_{12} = 3(u_a - u_w)$$

where:

I_{11} = first stress invariant of the first tensor, and
 I_{12} = first stress invariant of the second tensor.

The second stress invariants of the same set of stress tensors are:

$$[5a] \quad I_{21} = (\sigma_1 - u_a)(\sigma_2 - u_a) + (\sigma_2 - u_a)(\sigma_3 - u_a) + (\sigma_3 - u_a)(\sigma_1 - u_a)$$

and

$$[5b] \quad I_{22} = 3(u_a - u_w)^2$$

where:

I_{21} = second stress invariant of the first tensor, and
 I_{22} = second stress invariant of the second tensor.

The third stress invariants of the same set of stress tensors are:

$$[6a] \quad I_{31} = (\sigma_1 - u_a)(\sigma_2 - u_a)(\sigma_3 - u_a)$$

and

$$[6b] \quad I_{32} = (u_a - u_w)^3$$

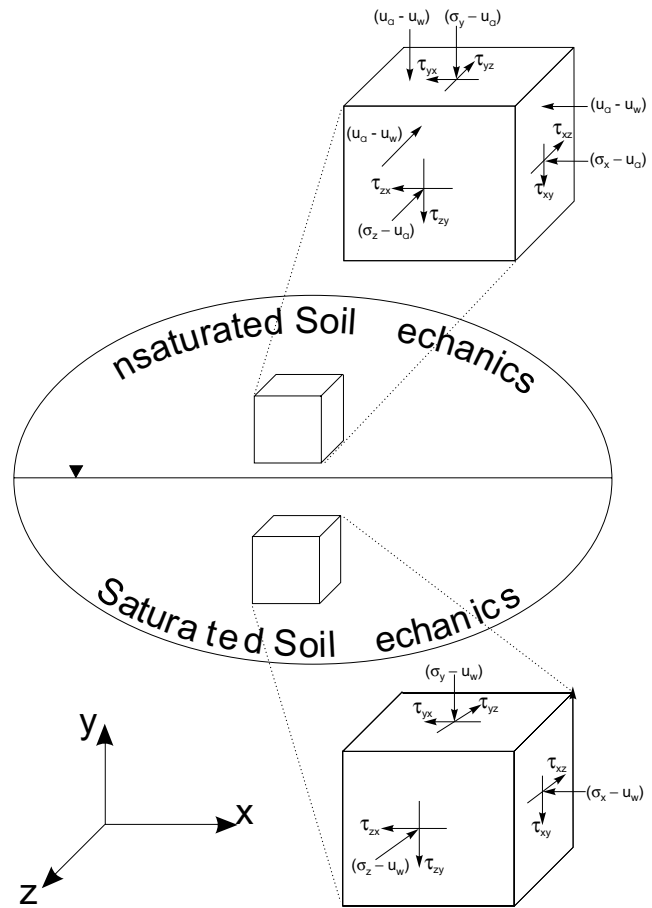
where:

I_{31} = third stress invariant of the first tensor, and
 I_{32} = third stress invariant of the second tensor.

The stress invariants of the second tensor, I_{12} , I_{22} and I_{32} are related. Therefore, only one stress invariant is required to represent the second tensor associated with the stress state variable (i.e., $(u_a - u_w)$).

A total of four stress invariants (i.e., three for the first stress tensor corresponding to the state variable $(\sigma - u_a)$, and one for the stress tensor corresponding to the state

Fig. 16. Elements showing the stress state at a point in a saturated soil and in an unsaturated soil.



variable, $(u_a - u_w)$ are therefore required to characterize the stress state of a generalized soil element. When the soil is saturated, u_a is equal to u_w , and the stress invariants corresponding to the state variable, $(u_a - u_w)$, of the second tensor is zero. The remaining three stress invariants corresponding the state variable, $(\sigma - u_a)$, revert to the same form as that require to characterize the stress state of a saturated soil.

Stress point designations

Some researchers have found that it is more convenient to deal with stress points, defined by p and q , rather than with principal stresses, σ_1 , σ_2 and σ_3 , or with the stress invariants. Two different systems of stress point designations have been defined. These are the MIT designation (Lambe and Whitman 1969) and the critical state soil mechanics designation (Wheeler and Sivakumar 1992). Similar designations for the stress points, p , q and r , for a generalized soil element can also be written (Fredlund and Rahardjo 1993).

MIT designation for stress point parameters

The MIT designation for stress point, p and q , for a saturated soil are defined as:

$$[7a] \quad p = \left(\frac{\sigma_1 + \sigma_3}{2} \right) - u_w$$

and

$$[7b] \quad q = \frac{\sigma_1 - \sigma_3}{2}$$

In an unsaturated soil, the corresponding stress point are denoted by p , q and r , have been defined (Fredlund and Rahardjo 1993):

$$[8a] \quad p = \frac{(\sigma_1 - u_a) + (\sigma_3 - u_a)}{2}$$

$$\text{or} \quad p = \left(\frac{\sigma_1 + \sigma_3}{2} \right) - u_a$$

$$[8b] \quad q = \frac{\sigma_1 - \sigma_3}{2}$$

and

$$[8c] \quad r = (u_a - u_w)$$

The stress points, p and q , using the MIT designation were originally obtained by considering only the state of stress in the plane that contains the major and the minor principal stresses, σ_1 and σ_3 . It should be noted that the p and q parameters so defined should appropriately be applied only to stresses on a failure plane. These parameters would not be totally appropriate for describing general stress state conditions prior to failure.

Critical state soil mechanics designation for stress point parameters

The critical state soil mechanics designation (Wheeler 1992), for a saturated soil, defined in terms of the stress points, p and q , for triaxial conditions are as follows:

$$[9a] \quad p = \left(\frac{\sigma_1 + 2\sigma_3}{3} \right) - u_w$$

and

$$[9b] \quad q = \sigma_1 - \sigma_3$$

The corresponding stress points, p , q and r for an unsaturated soil are:

$$[10a] \quad p = \left(\frac{\sigma_1 + 2\sigma_3}{3} \right) - u_a$$

$$[10b] \quad q = \sigma_1 - \sigma_3$$

and

$$[10c] \quad r = (u_a - u_w)$$

For general three-dimensional stress state conditions in a saturated soil, the stress points denoted by p and q can be written as:

$$[11a] \quad p = \left(\frac{\sigma_1 + \sigma_2 + \sigma_3}{3} \right) - u_w$$

$$[11b] \quad q = \sqrt{\frac{1}{2} [(\sigma_2 - \sigma_3)^2 + (\sigma_3 - \sigma_1)^2 + (\sigma_1 - \sigma_2)^2]}$$

The corresponding stress point, p , q and r , for the general stress state in an unsaturated soil are respectively:

$$[12a] \quad p = \left(\frac{\sigma_1 + \sigma_2 + \sigma_3}{3} \right) - u_a$$

$$[12b] \quad q = \sqrt{\frac{1}{2} [(\sigma_2 - \sigma_3)^2 + (\sigma_3 - \sigma_1)^2 + (\sigma_1 - \sigma_2)^2]}$$

and

$$[12c] \quad r = (u_a - u_w)$$

The stress points according to the Critical State Soil Mechanics designation are applicable under working load conditions as well as under failure conditions.

Plotting of stress points for an unsaturated soil

Since there are three parameters, p , q and r , associated with each stress point for an unsaturated soil, the stress states for an unsaturated soil are plotted in three dimensions with q as the ordinate and p and r as the abscissas.

Theoretical formulations for a generalized mechanics of soils

The formulations for volume change, shear strength and flow in a generalized soil element are briefly summarized in this section.

Volume change moduli

The volume change constitutive behavior of an unsaturated soil can be written in several possible forms. Only the classical soil mechanics form involving void ratio, e , water content, w and/or degree of saturation, S , is shown in this paper. The independent stress state variables can be used to formulate the constitutive relations for an unsaturated (or generalized) soil element. The volume change constitutive equation for isotropic loading, $(\sigma_c - u_a)$, written in terms of void ratio, e , is,

$$[13] \quad de = a_t d(\sigma_c - u_a) + a_m d(u_a - u_w)$$

where:

$$a_t = \frac{\partial e}{\partial(\sigma_c - u_a)}$$

and

$$a_m = \frac{\partial e}{\partial(u_a - u_w)}$$

The void ratio change can be independent of the water content change for an unsaturated soil element. For a complete volume-mass characterization, a second constitutive relationship is required. The water content constitutive relationship is generally used and can be written as follows for the case of isotropic loading,

$$[14] \quad dw = b_t d(\sigma_c - u_a) + b_m d(u_a - u_w)$$

where:

$$b_t = \frac{\partial w}{\partial(\sigma_c - u_a)}$$

and

$$b_m = \frac{\partial w}{\partial(u_a - u_w)}$$

Similar sets of constitutive equations can also be written for non-isotropic loading conditions.

A similar approach can be applied in the critical state framework as proposed by Wheeler and Sivakumar (1992), which use three parameters, p , q , r , along with two additional state parameters (i.e., water content, w , and specific volume, v). The specific volume, v , and void ratio, e , are related as follows:

$$[15] \quad v = 1 + e$$

The void ratio and water content constitutive surfaces corresponding to eqs. [13] and [14] can be represented graphically as shown in Fig. 17, where the water content, w , or void ratio, e , are plotted against the ordinates, $(\sigma - u_a)$ and $(u_a - u_w)$.

The void ratio constitutive surfaces for the loading and unloading of a stable-structured soil are shown in Fig. 18. The void ratio constitutive surfaces of a meta-stable-structured soil are shown in Fig. 19.

Shear strength

The shear strength equation for an unsaturated (or generalized) soil can be formulated as a linear combination of the stress state variables, [i.e., $(\sigma_n - u_a)$ and $(u_a - u_w)$]:

$$[16] \quad \tau = c' + (\sigma_n - u_a) \tan \phi' + (u_a - u_w) \tan \phi^b$$

where:

c' = effective cohesion,

ϕ' = effective angle of internal friction,

ϕ^b = friction angle associated with the matric suction stress state variable, $(u_a - u_w)$, and

$(\sigma_n - u_a)$ = net normal stress on failure plane.

Three-dimensional representations of eq. [16] are presented in Fig. 20. It has been found that the shear strength relationship involving suction can be either linear or non-linear. In general it is possible to linearize the non-linear shear strength versus suction relationship over a selected range of soil suction.

Flow

Darcy's flow law which states that the velocity of flow is proportional to the hydraulic head gradient, is applica-

ble to both saturated and unsaturated soil media. For a saturated or unsaturated soil, Darcy's flow equation can be written as follows:

$$[17] \quad v_w = -k_w(u_a - u_w) \frac{\partial h}{\partial y}$$

where:

v_w = flow rate of water

$k_w(u_a - u_w)$ = coefficient of permeability with respect to the water phase, as a function of matric suction, $(u_a - u_w)$.

$\partial h_w / \partial y$ = hydraulic head gradient in the y -direction.

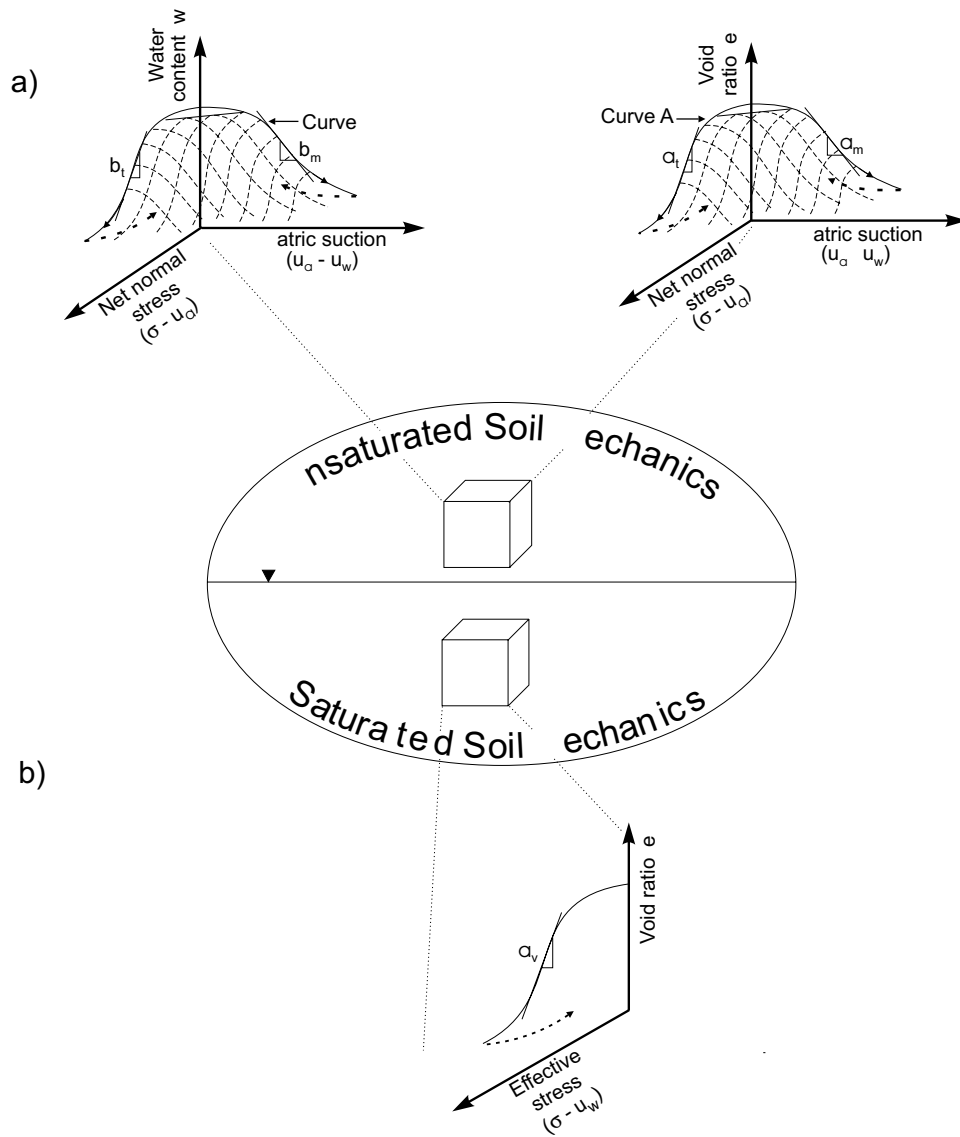
In a saturated soil, the coefficient of permeability (or hydraulic conductivity) is a constant. The constant coefficient of permeability for a saturated soil is due to a constant value for the water content. The water content is related to the porosity available for water flow. The water content, on the other hand, decreases as a soil desaturates. The dependence of the coefficient of permeability on the water content is based on the assumption that water can only flow through the wetted portion of the soil as shown in Fig. 21. An integration along the soil-water characteristic curve provides a measure of the quantity of water in the soil. The permeability function represented by Gardner (1958) have been found to fit the computed values obtained from the soil-water characteristic curve (Fig. 22).

Relationship between soil-water characteristic curves and behavior of generalized soils

The soil-water characteristic curve of a soil has been shown to be closely related to unsaturated soil property functions (Fredlund 1993). Laboratory tests have indicated that there is unique relationship between the behavior of a soil and the soil-water characteristic curve of the soil. The soil-water characteristic curve defines the relationship between the volume of water content in the soil and the matric suction of a soil.

Figure 23 shows a typical plot of a soil-water characteristic curve for a silty soil. The key features of a soil-water characteristic curve are identified in Fig. 23. The soil-water characteristic curve shows the phenomena of hysteresis under drying and wetting conditions. It is usually sufficient to only consider the desorption curve. The air entry value is the matric suction at which air commences to enter the soil, beginning with the largest pores at the exterior of the soil. The residual water content is the water content value at which a large increase in suction is required to remove additional water from the soil. An indication of the air entry value and the residual water content is shown in Fig. 23. Thermodynamic considerations show that the total suction corresponding to zero water content is approximately 1 million kPa.

Fig. 17. Void ratio and water content constitutive surfaces for: a) unsaturated soil; b) saturated soil.



Equation for soil-water characteristic curves

Numerous equations have been proposed to characterize the soil-water characteristic curve. Fredlund and Xing (1994) proposed the following general equation for the soil-water characteristic curve,

$$[18] \quad \theta_w = \theta_s \left[\frac{1}{\ln[e + ((u_a - u_w) / a)^n]} \right]^m$$

where:

- θ_w = volumetric water content,
- θ_s = volumetric water content at saturation,
- $e = 2.718$.
- $(u_a - u_w)$ = matric suction,
- a = approximately the air entry value,
- n = soil parameter related to the rate of desaturation, and
- m = soil parameter related to the residual water content.

The upper limit of suction of 1 million kPa at zero water content can be incorporated into the above equation to give the following equation:

$$[19] \quad \theta_w((u_a - u_w), a, n, m) = C(u_a - u_w) \frac{\theta_s}{\{\ln[e + ((u_a - u_w) / a)^n]\}^m}$$

where:

$$C(u_a - u_w) = 1 - \frac{\ln(1 + (u_a - u_w) / (u_a - u_w)_r)}{\ln[1 + (1000000 / (u_a - u_w)_r)]}$$

Equation [19] along with the appropriate values for the relevant parameters, a , n and m , has been found to fit essentially all experimentally obtained soil-water characteristic curves.

In the following sections, it is shown how eq. [19] can be used to obtain the shear strength function, the permeability function and the storage coefficient for unsaturated soils.

Fig. 18. Loading and unloading constitutive surfaces for a stable structured, unsaturated soil.

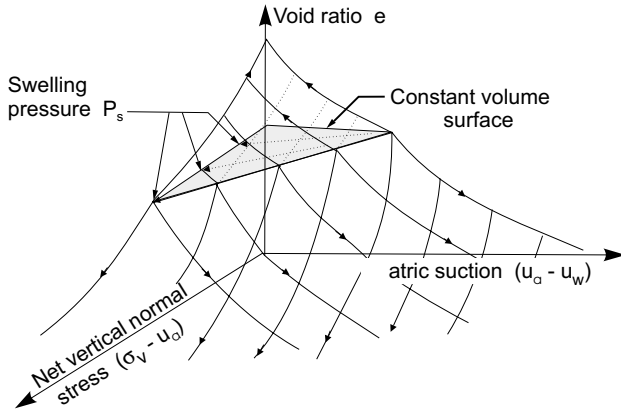
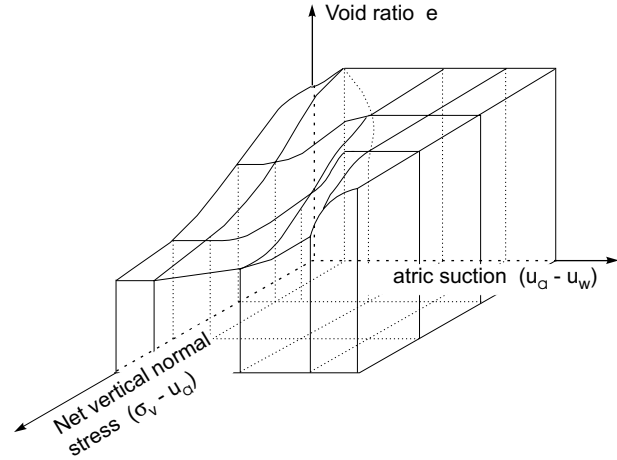


Fig. 19. Loading and unloading constitutive surfaces for a meta-stable structured, unsaturated soil.



Relationship between soil-water characteristic curve and shear strength

The slope (i.e., slope of the shear strength versus matric suction curve), ϕ^b , plotted against the matric suction bears a similar shape to the soil-water characteristic curve (Gan et al. 1988). Figure 24 shows that the ϕ^b angle begins to deviate from the effective angle of internal friction, ϕ , as the soil desaturates at suctions greater than the air entry value of the soil. As the matric suction reaches a value corresponding to the residual water content, the ϕ^b angle appears to approach an angle near zero degrees or it may even be negative.

The shear strength function can be obtained by considering the soil-water characteristic curve. The soil-water characteristic curve can be represented by eq. [19].

The following shear strength expression (eq. [20]) as a function of matric suction and the effective angle of internal friction is obtained by Fredlund et al. (1995).

$$[20]^1 \quad \tau(u_a - u_w) = c' + (\sigma_n - u_a) \tan \phi' + \tan \phi [\Theta(u_a - u_w)]^p (u_a - u_w)$$

where:

$\Theta(u_a - u_w) = \theta_w / \theta_s$, the dimensionless water content, and

$\theta_w(u_a - u_w)$ = the volumetric water content at any suction, which can be represented by eq. [19], and

p = soil fitting parameter.

Relationship between soil-water characteristic curve and permeability

The effective water conductive porosity for a given soil is a function of its water content. The water content of a given soil is in turn a function of the stress state of the soil. Therefore, there is a relationship between the hydraulic conductivity and the soil-water characteristic curve. This relationship was shown in Fig. 21.

Fredlund et al. (1994) derived the following expression for the permeability function of an unsaturated soil, when using the soil-water characteristic curve with matric suction on a logarithmic scale.

$$[21] \quad k(u_a - u_w) = k_s \left[\frac{\int_{\ln(u_a - u_w)}^b \frac{\theta_w(e^{\ln(u_a - u_w)} - \theta_w(u_a - u_w))}{e^{\ln(u_a - u_w)}} \frac{\partial \theta_w}{\partial \ln(u_a - u_w)} (e^{\ln(u_a - u_w)}) d \ln(u_a - u_w)}{\int_{\ln(u_a - u_w)_{aev}}^b \frac{\theta(e^{\ln(u_a - u_w)} - \theta_s)}{e^{\ln(u_a - u_w)}} \frac{\partial \theta_w}{\partial \ln(u_a - u_w)} (e^{\ln(u_a - u_w)}) d \ln(u_a - u_w)} \right]$$

where:

k_s = saturated coefficient of permeability,

$b = \ln(1,000,000) = 13.8155$,

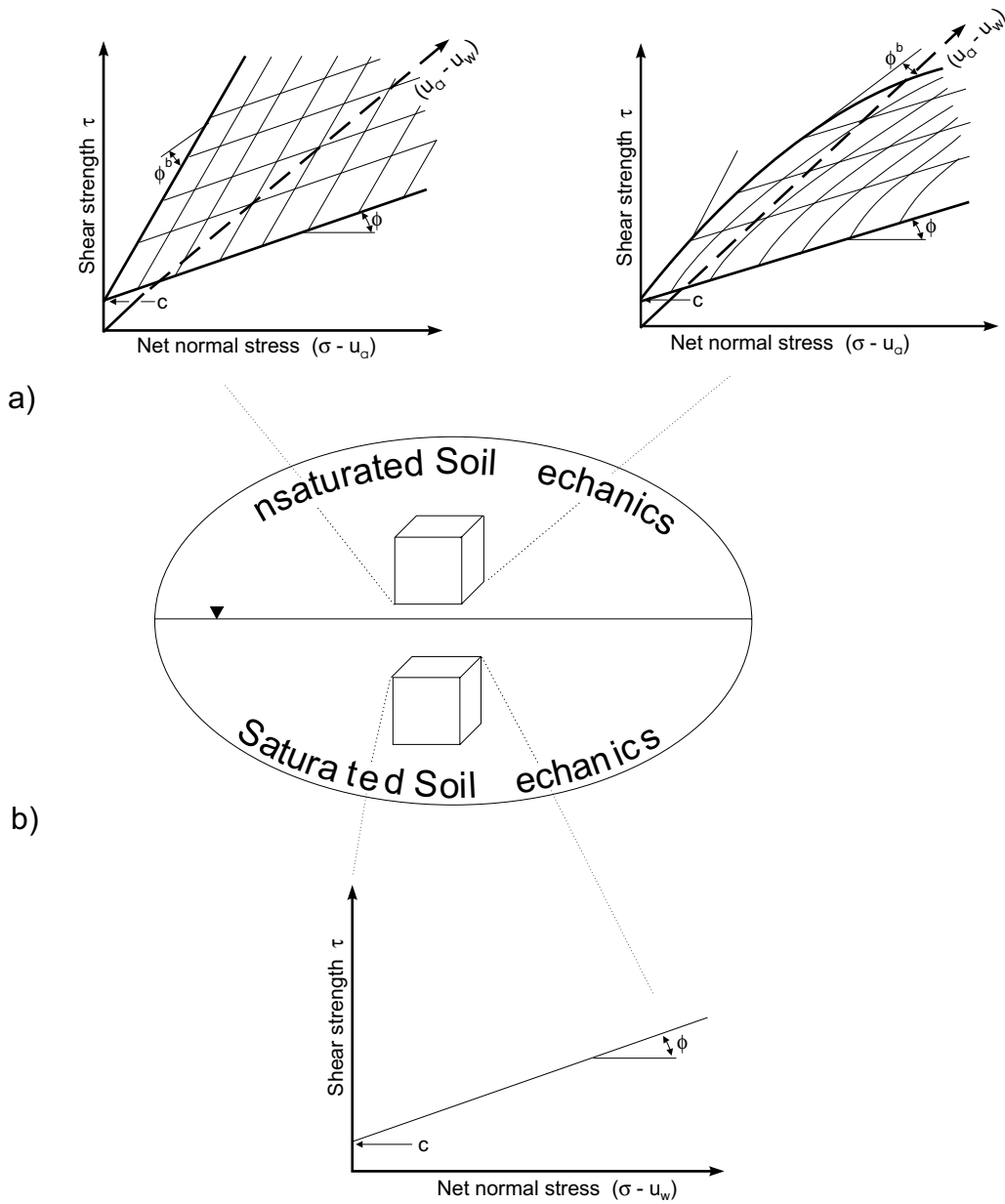
$e = 2.718\dots$, and

$(u_a - u_w)_{aev}$ = air entry matric suction value.

The equation for the volumetric water content, θ , as a function of matric suction, $(u_a - u_w)$, is given by eq. [19].

¹Note: An error occurred in the original print of eq. [20]: $\tau(u_a - u_w) = c' + (\sigma_n - u_a) \tan \phi' + \int_0^{u_a - u_w} [\Theta(u_a - u_w) d(u_a - u_w)]$.

Fig. 20. Mohr-Coulomb shear strength envelopes for: a) unsaturated soil; b) saturated soil.



Relationship between soil-water characteristic curve and storage coefficient

The storage coefficient, also known as the coefficient of water volume change with respect to change in matric suction, m_2^w , is the slope of the soil-water characteristic curve (Fig. 21). The storage coefficient, m_2^w , is obtained by differentiating the soil-water characteristic curve.

The equation for m_2^w is:

$$[22] \quad m_2^w = \frac{\partial V_w}{\partial(u_a - u_w)}$$

If the volume of the soil remains a constant, the storage coefficient m_2^w , can be expressed as:

$$[23] \quad m_2^w = \frac{\partial \theta_w}{\partial(u_a - u_w)}$$

since $\theta_w = \frac{V_w}{V}$,

where:

V_w = volume of water, and
 V = total volume of soil.

The soil-water characteristic curve (i.e., the relationship between the volumetric water content, θ_w , and matric suction, $(u_a - u_w)$) represented by eq. [19], can be differentiated with respect to matric suction, $(u_a - u_w)$ to give the storage coefficient, m_2^w ,

Fig. 21. Relationship between soil-water characteristic curve and the permeability for a sand and a clayey silt.

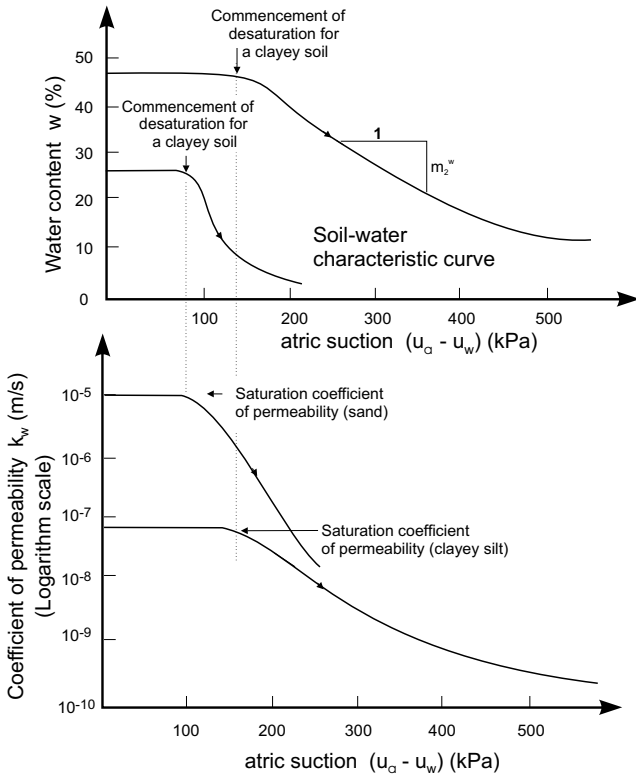


Fig. 22. Typical Gardner empirical permeability functions shown for a sand and a clayey silt.

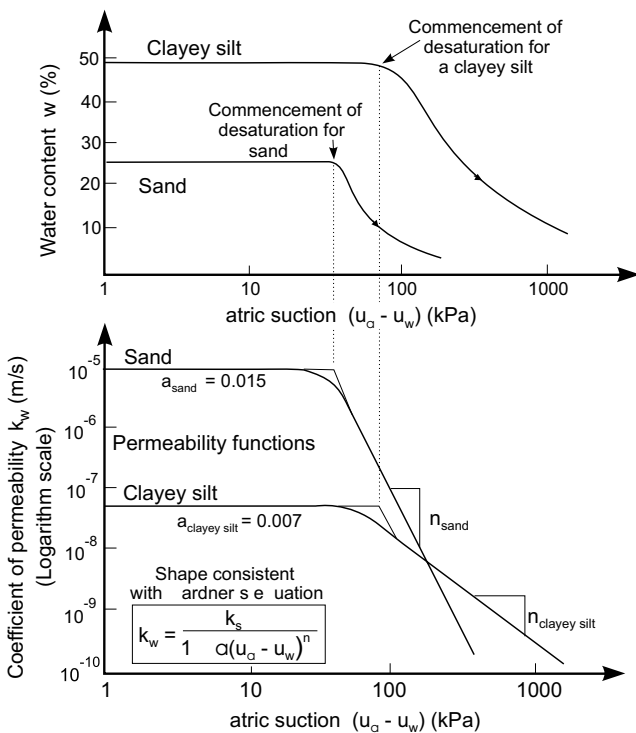


Fig. 23. Typical soil-water characteristic curve for a silty soil.

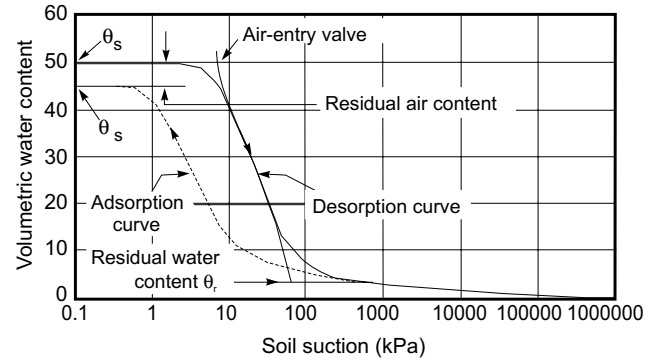
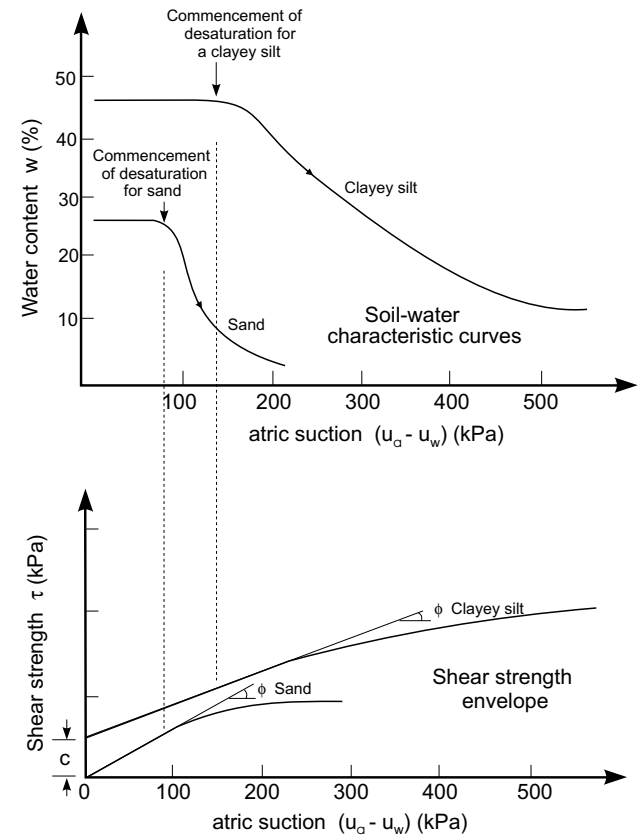


Fig. 24. Relationship between soil-water characteristic curve and shear strength for a sand and a clayey silt.



$$\begin{aligned}
 [24] \quad m_2^w &= \frac{\partial \theta_w}{\partial (u_a - u_w)} \\
 &= C' (u_a - u_w) \frac{\theta_s}{\left[\ln \left(e + \left(\frac{u_a - u_w}{a} \right)^n \right) \right]^m} + C(u_a - u_w) D(u_a - u_w)
 \end{aligned}$$

where:
 $e = 2.718$,
 $\theta_s =$ saturated volumetric water content,

$$C'(u_a - u_w) = \frac{\left(\frac{1}{(u_a - u_w) + (u_a - u_w)_r} \right)}{\ln(1 + 1000000 / (u_a - u_w)_r)}$$

and

$$D(u_a - u_w) = \frac{-mn \theta_s (u_a - u_w)^{n-1}}{\left[\ln \left(e + \left(\frac{u_a - u_w}{a} \right)^n \right) \right]^{m+1} e a^n + (u_a - u_w)^n}$$

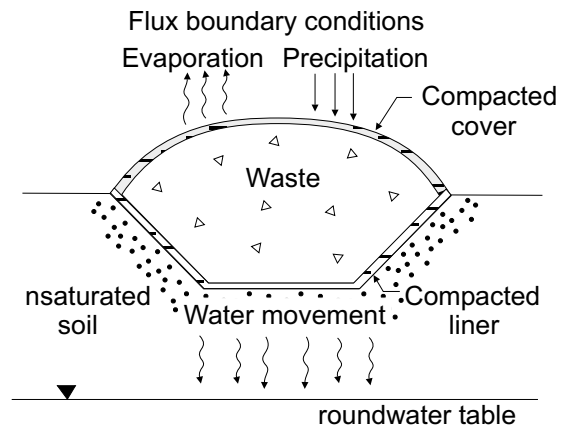
Generalized soil mechanics approach in geotechnical engineering

In many routine problems, a generalized soil mechanics approach along with a consideration of the surface flux boundary conditions is found to be essential to the evaluation of the problem. A few examples are described in this section, under the general soil mechanics categories of (i) seepage, (ii) shear strength and (iii) volume change, respectively.

Seepage problems

- (1) Contamination of groundwater from chemical spills is now of serious concern. The movement of the contaminants from the ground surface to the groundwater table is a process which has to be analyzed, taking into the consideration the continuum consisting of the atmosphere, the vadose zone and the saturated zone below the groundwater table. The vadose zone is the buffer providing protection to the groundwater. The movement of the contaminants through the vadose zone is controlled by the permeability and storage characteristics of the soils in the vadose zone. In addition to bulk flow under gravity in the case of liquid contaminants, a conveyance or transport agent is required. The transport agent is usually water. The flux condition at the ground surface is therefore of importance in terms of the water that will be available for transport. The stress state of the soil in the vadose zone is affected by the flux occurring at the surface. The stress state (i.e., matric suction) affects the hydraulic conductivity of the soils.
- (2) Compacted clay covers have become a common solution to control water flow through waste management facilities (Fig. 25). The performance of the cover is largely controlled by the hydraulic conductivity and storage characteristics of the cover along with the surface flux to which the cover is subjected.
- (3) The movement of moisture in the entire region surrounding a waste containment area is often closely related to the hydraulic conductivity of the vadose zone. The mounding of the groundwater table below a waste containment area occurs in response to flow through unsaturated soils (Fig. 25). Although the soil below the waste containment may maintain negative pore-water pressures, there still will be flow in re-

Fig. 25. Example of the movement of water through a cover and flow in the unsaturated zone below a liner.



sponse to a hydraulic gradient, commensurate with a lower unsaturated hydraulic conductivity.

- (4) During the construction phase, much of the earth dam consists of compacted unsaturated soil. As the reservoir is filled, there will be water flow through the dam both in the negative and positive pore-water pressure regions. The permeability function which is a function of the negative pore-water pressure must be used in modelling the flow of water through the unsaturated zone. Once the reservoir is filled, a steady state condition is achieved and most of the flow is through the saturated soil. However, one of the conditions which can trigger instability arises from the extended infiltration on the surface of the dam. In this case, water will infiltrate through the unsaturated zone above the phreatic line.
- (5) Expansive soils often cause distress to light structures as a result of the ingress of water into the soil. As the pore-water pressures increase, the soil expands. The flow may be through the fissures and cracks in the soil. This becomes a difficult unsaturated soil problem to analyze.
- (6) Long-term predictions with respect to wastes resulting from mining operations are strongly controlled by the assessment of the surface flux boundary conditions. This is particularly true for the case of "closure" or decommissioning of a mine.

Shear strength problems

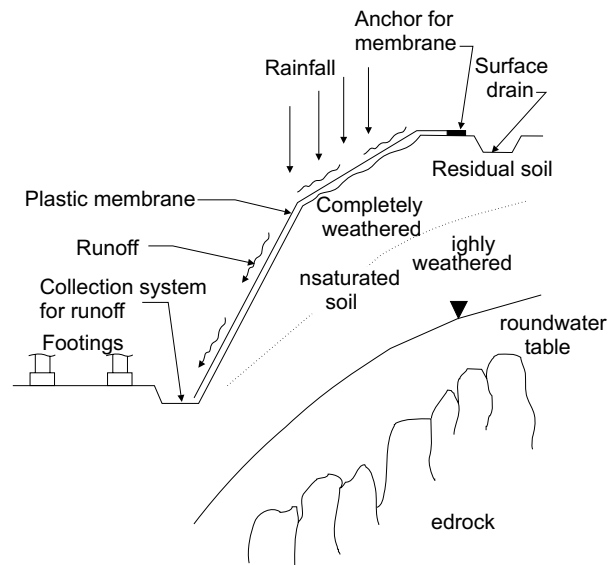
- (1) Natural slopes generally fail at some time following a high level of precipitation over a prolonged period of time. While the mechanics leading up to failure is well known, few attempts have been made to model the problem. The main reason appears to be related to the difficulties in modelling the flux boundary condition and the flow through the unsaturated zone.
- (2) The stability of loosely compacted fills can result in high velocity mass movements upon approaching saturation. The soil structure may experience collapse with the result that the load is transferred onto the water phase.

- (3) The stability of cuts or trenches for laying pipelines involves unsaturated soils. The costs associated with temporary bracing are high. Each year lives are lost due to collapse of the bracing arising from loss of shear strength of the unsaturated soil from wetting.
- (4) The assessment of stability of temporary excavations around construction sites is a difficult task. It is often left to the contractor to handle the problem. It has been observed in Southeast Asia that it is quite common practice for contractors to place a plastic membrane over a newly excavated slope (Fig. 26). The slope may be part of an excavation for a foundation or part of a remediation (or landscaping). The plastic membrane ensures that a major portion of the rainfall will be shed to the bottom of the slope. In other words, the use of a plastic membrane is an attempt to maintain the negative pore-water pressures in the backslope. The practice of using plastic membranes in this manner has potential usage in other parts of the world.
- (5) The backfill material for an earth retaining structure should be a cohesionless material. However, many retaining structures are backfilled with cohesive materials which change volume and shear strength in response to the intake of water. The lateral pressures against the wall are a function of the shear strength of the unsaturated soil and the extent of wetting.
- (6) The bearing capacity of shallow footings is commonly based on the compressive strength of the soil. These strength measurements are often performed on soil specimens from above the groundwater table where the soil has negative pore-water pressures and may be fissured and unsaturated. The assumption is then made for design purposes that conditions in the future will remain similar. This may not be a realistic assumption.

Volume change problems

- (1) Volume changes in the soil below shallow footings generally take place in response to a moisture flux around the perimeter of the structure. While the mechanism involved is well understood, there is still a need for two- or three-dimensional numerical models to simulate these conditions.
- (2) In some countries, the shrinkage of high volume change soils under drying conditions poses a more serious problem than swelling. Shrinkage is the reverse of swelling in term of the stress state. However, the analyses and solutions for the two problems can be quite different.
- (3) The collapse of meta-stable-structured soils such as loess or poorly compacted silts and sand is a problem involving a volume decrease resulting from a decrease in suction. There is a need to have the analysis of collapsing soils within a generalized mechanics for soils.
- (4) The prediction of the depth of cracking is related to the volume change behavior of the soil. The depth of cracking influences earth pressure and slope stability

Fig. 26. Example of the control of infiltration through the use of geomembranes.



solutions. An increase in suction increases the depth of cracking. A complete analysis of the problem is still not available.

- (5) There needs to be an analysis for the volume change of compacted fills such as dams and embankments. The changes in volume of the unsaturated soil may be due to total stress or matric suction changes.
- (6) The cracking of covers for waste containment areas is an example of a geo-environmental problem for which a volume change analysis is required.

Conclusions

Many problems in geotechnical engineering involve unsaturated soils. In fact many engineering problems require the consideration of the continuum consisting of the ground surface through the vadose zone to the zone below the water table. It is important that engineers begin to analyze soils problems within one consistent theoretical context. There is a great need for seminars and workshops on unsaturated soil mechanics in order to transfer technology into the hands of practicing engineers. There is also a need for simplistic visual aids which would assist in the visualization of the complex concepts associated with unsaturated soil behavior. Some visual aids have been suggested to bring unsaturated soil behavior within the scope of generalized soil mechanics.

Problems involving unsaturated soils often have the appearances of being extremely complex. It is the hope of this paper to allay much of this fear. The paper has shown by way of a generalized soil mechanics approach that essentially the same theories and formulations established in classical soil mechanics are applicable to problems involving unsaturated soils through appropriate extensions to the established theory on saturated soil mechanics. The numerical computation involving unsaturated soils are generally more complex. However, the concepts are

equivalents to those required for the understanding of classical soil mechanics.

One soil property which is recurrent in dealing with unsaturated soils is the soil-water characteristic curve. The soil-water characteristic curve has emerged to be a key relationship which is of value in characterizing the behavior of unsaturated soil.

Acknowledgement

The author acknowledges the assistance of Julian K.-M. Gan in writing this paper.

References

- Bishop, A.W., Alpan, I., Blight, G.E., and Donald, I.B. 1960. Factors controlling the shear strength of partly saturated cohesive soils. *In* ASCE Research Conference Shear Strength of Cohesive Soils, University of Colorado, Boulder, CO, pp. 503–532.
- Fredlund D.G., and Xing, A. 1994. Equations for the soil-water characteristic curve. *Canadian Geotechnical Journal*, **31**: 521–532.
- Fredlund, D.G. 1979. Second Canadian geotechnical colloquium: Appropriate concepts and technology for unsaturated soils. *Canadian Geotechnical Journal*, **16**(1): 121–139.
- Fredlund, D.G., A. Xing, and Huang, S. 1994. Predicting the permeability function for unsaturated soils using the soil-water characteristic curve. *Canadian Geotechnical Journal*, **31**: 533–546.
- Fredlund, D.G., and Morgenstern, N.R. 1977. Stress state variables for unsaturated soils. *ASCE Journal of Geotechnical Engineering Division*, **103**(DT5): 447–466.
- Fredlund, D.G., and Rahardjo, H. 1987. Soil mechanics principles for highway engineering in arid regions. *Transportation Research Record* 1137, pp. 1–11.
- Fredlund, D.G., and Rahardjo, H. 1988. State of development in the measurement of suction. *Proceedings, International Conference on Engineering Problems on Regional Soils*, Beijing, China, August 11–15, pp. 582–588.
- Fredlund, D.G., and Rahardjo, H. 1993. An overview of unsaturated soil behavior. *ASCE 1993 Annual Convention, Session 3L on Unsaturated Soil Behavior in Engineering Practice*, Dallas, TX, October 24–28, pp. 1–31.
- Fredlund, D.G., and Rahardjo, H. 1993. *Soil mechanics for unsaturated soils*. John Wiley & Sons, New York.
- Fredlund, D.G., Vanapalli, S.K., Xing, A., and Pufahl, D.E. 1995. Predicting the shear strength function for unsaturated soils using the soil-water characteristic curve. *Proceedings, First International Conference on Unsaturated Soils*. Paris, France, September 6–8. *Edited by* E.E. Alonso and P. Delage. A.A. Baklema, Rotterdam, The Netherlands, Vol. 1, pp. 63–70.
- Gan, J.K.-M., Fredlund, D.G., and H. Rahardjo 1988. Determination of the shear strength parameters of an unsaturated soil using the direct shear. *Canadian Geotechnical Journal*, **25**(3): 500–510.
- Gardner, W.R. 1958. Some steady state solutions of the unsaturated moisture flow-equation with applications to evaporation from a water-table. *Soil Science*, **85**(4): 228–232.
- Lambe, T.W., and Whitman, R.V. 1969. *Soil Mechanics*, John Wiley & Sons, New York.
- Manahan, S.E. 1991. *Environmental chemistry*. Fifth Edition, Lewis Publishers, Chelsea, Michigan, (Figure on page 430).
- Miller, P. 1993. Managing our watersheds: a systems approach to maintaining water quality. *Small Flows*, **7**(4): 1–9.
- OSU. 1994. Practical approaches to groundwater hydrology and contamination. A 6-week course, presented by Oklahoma State University, School of Geology and Arts & Science Extension, Stillwater, ON
- Wheeler, S.J. 1991. Alternative framework for unsaturated soil behavior. *Géotechnique*, **41**(2): 257–261.
- Wheeler, S.J., and Sivakumar, V. 1992. Critical state concepts for unsaturated soil. *Proceedings, of the 7th International Conference on Expansive Soils*, August 3–5, Dallas, Texas, U.S.A., Vol. 1, pp. 167–172.
- Wilson, G.W. 1990. Soil evaporative fluxes for geotechnical engineering problems. Ph.D. thesis, University of Saskatchewan, Saskatoon, SK, Canada.

Application of unsaturated soil mechanics for agricultural conditions

D. Wulfsohn, B.A. Adams, and D.G. Fredlund

Abstract: Agricultural engineers often draw upon the classical theories of soil mechanics in their study of agricultural soil behaviour. These theories are largely based on the assumption that the soil is saturated. In an emerging theoretical framework, an unsaturated soil is considered to have four phases: solid, air, water, and contractile skin (the air-water interface). The contractile skin acts like a rubber membrane as it induces a matric suction in the soil pores. Suction has been shown to affect both strength and volume change characteristics of unsaturated soils. The relationship between water content and matric suction (the soil-water characteristic) becomes an important component of the unsaturated soil mechanics framework. In this paper, concepts and implications of these developments for some agricultural shear strength-based models are discussed. Experimental data highlighting these relationships are also presented.

Key words: soil suction, soil-water characteristic, shear strength.

Introduction

Over the years, agricultural engineers have adapted theories of classical soil mechanics as necessary to produce solutions relevant to agricultural soil conditions. The classical theories were originally developed for saturated soil. In view of the unsaturated nature of surficial soils, the extent to which desaturation affects soil behaviour needs to be understood. While similarities exist between the behaviour of saturated and unsaturated soil, there are also significant differences. These differences have been found to be related to the role of matric suction as a stress variable when dealing with unsaturated soils. This paper discusses the influence of soil suction on unsaturated soil behaviour and explores the manner in which some accepted strength-based agricultural soil mechanics models can be extended for varying moisture conditions. Some typical formulations are used to illustrate the incorporation of unsaturated soil mechanics principles.

Unsaturated soil and matric suction

Apart from the three independent phases, namely solid, water, and air, usually ascribed to soil, a fourth phase has

been postulated as being of importance in understanding the behaviour of an unsaturated soil. This additional phase is described as the air-water interface (i.e., contractile skin) and provides a normal stress due to the pore-water pressure (Fredlund and Rahardjo 1993a). While a saturated soil possesses positive pore-water pressure, an unsaturated soil is characterized by negative pore-water pressures which exerts a tensile pull at all air-water interfaces in the soil profile (Fig. 1). The surface tension on the contractile skin pulls the particles together providing additional strength to an unsaturated soil compared to a saturated soil where, in contrast, the positive pore-water pressure reduces the strength. At the air-water interface of an unsaturated soil, the pore-air pressure, u_a , is greater than the pore-water pressure, u_w . The difference in these two independent pressures, $(u_a - u_w)$, is referred to as the soil matric suction. There is increasing acceptance for applying matric suction as an independent stress state variable in describing the behaviour of an unsaturated soil.

Soil stress state variables

The soil stress state is influenced by the number of phases present. The effective stress for a saturated soil, $(\sigma - u_w)$, can be reinterpreted as a stress state variable for saturated soil behaviour rather than a physical law (Fredlund and Rahardjo 1993a). Because of the presence of an additional phase (the contractile skin), two independent stress variables are needed to describe unsaturated soil behaviour. Three possible combinations of stress state variables have been identified. These are:

$$(\sigma - u_a) \text{ and } (u_a - u_w)$$

$$(\sigma - u_w) \text{ and } (u_a - u_w)$$

$$(\sigma - u_a) \text{ and } (\sigma - u_w)$$

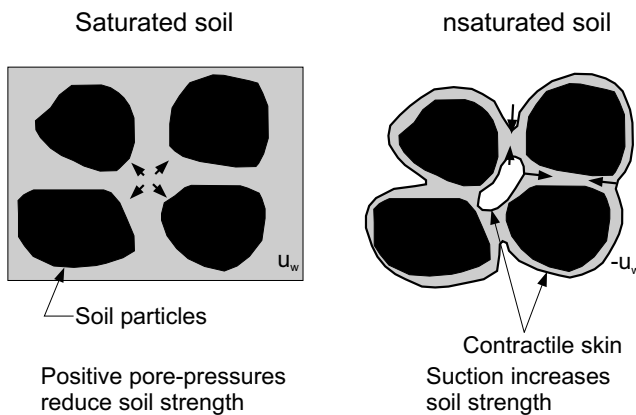
The first pair is generally used in practical engineering problems since it separates the effect due to changes in

D. Wulfsohn. Professor, Agricultural & Bioresource Engineering Department, University of Saskatchewan, 57 Campus Drive, Saskatoon, SK, Canada S7N 5A9.

B.A. Adams. Graduate Student, Agricultural & Bioresource Engineering Department, University of Saskatchewan, 57 Campus Drive, Saskatoon, SK, Canada S7N 5A9.

D.G. Fredlund. Professor, Civil Engineering Department, University of Saskatchewan, 57 Campus Drive, Saskatoon, SK, Canada S7N 5A9.

Reproduced with permission from *Canadian Agricultural Engineering*, 38(3): 173-181, 1996.

Fig. 1. Effect of pore pressure on soil strength.

normal total stress from the effect due to changes in pore-water pressure. In this framework, the matric suction becomes an essential parameter in describing the state of a soil. It is more common to determine the soil water content; however, there is an important relationship between soil suction and water content which can be determined.

Experimental nature of soil water content versus matric suction

Two forms of the relationship between soil suction and water content have been identified. The first form is obtained from soil specimens compacted at different densities and water contents (i.e., these specimens are unidentical in the sense that they may have different soil structures and are thus “different soils”). Studies by Croney and Coleman (1954) and Olson and Langfelder (1965) showed a distinct relationship between soil suction and water content for soils compacted at various water contents. However, static and kneading methods of compaction yield different soil suction versus water content relationships as observed by Mou and Chu (1981) for an expansive clay and Mojilaj et al. (1992) for a clay loam. In other words, different methods of compaction (i.e., impact, kneading, vibratory, or static compaction) result in significantly different fabrics in both sands and clays (Mitchell 1993).

The second form of the relationship between soil suction and water content is called the soil-water characteristic curve. This curve is obtained by testing one soil specimen or several “identical” soil specimens (e.g., using pressure plate apparatus or Tempe cells). The distinction between these two kinds of soil suction versus water content relationships becomes important since the soil-water characteristic curve characterizes a particular soil of the same structure. A variation in suction in this case is induced by wetting or drying. It is important to note that there may be considerable hysteresis in the soil-water characteristic curve. Thus, if the stress history of the soil is not known, knowledge of the water content only (i.e., a deformation state variable) may not be sufficient for determining the matric suction (i.e., a stress state variable).

The difference between the soil suction versus water content relationship (as compacted) and the soil-water characteristic for a glacial till is shown in Fig. 2. The “as-compacted” points indicate the states for specimens which have been compacted by static compaction at different water contents and densities. The soil-water characteristic curve on the other hand shows the progressive decrease in water content as a single specimen (or several identical ones) dries, as evident by the increasing matric suction.

There are benefits in using the soil-water characteristics in unsaturated soil research. It is generally easier, faster, and cheaper to determine the water content of the soil than its suction, although recent advances in time-domain reflectometry and other technologies (e.g., Woodburn et al. 1993; Whalley et al. 1994) are beginning to eliminate such constraints. The relationship between soil suction and water content was originally used by soil scientists in predicting the soil water available for plant growth. It is also extensively used to empirically estimate the hydraulic conductivity function. Similarly, it has been proposed that the unsaturated shear strength may be estimated using the soil-water characteristic curve (Fredlund and Rahardjo 1993b).

The agricultural soil failure criterion

Agricultural engineers and soil scientists have long recognized that soil suction contributes toward soil strength in both shear and tensile (e.g., Greacen 1960; Chancellor and Vomocil 1970; Williams and Shaykewich 1970; Koolen and Kuipers 1983; Mullins and Panayiotopoulos 1984; Mullins et al. 1990; McKyes et al. 1994); however, there has not been a rigorous theoretical framework quantifying the contribution of soil suction. In the following sections we will consider failure conditions for a soil in light of the stress state variables and implications for some practical problems.

Shear strength failure criterion

A common shear strength failure criterion for a saturated soil is called the Mohr-Coulomb equation which is expressed as:

$$[1] \quad \tau_f = c' + (\sigma_n - u_w) \tan \phi'$$

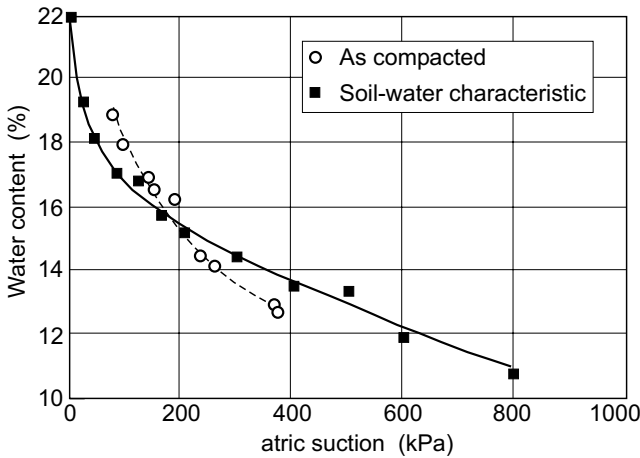
where:

- τ_f = shear strength,
- c' = effective cohesion,
- ϕ' = effective angle of internal friction,
- σ_n = total normal stress on the failure plane, and
- u_w = pore-water pressure.

Equation [1] has proven to be satisfactory for applications where the soil is saturated and the pore-water pressures are positive. A modified Mohr-Coulomb failure criterion has been proposed by Fredlund et al. (1978) for an unsaturated soil:

$$[2] \quad \tau_f = c' + (\sigma_n - u_a) \tan \phi' + (u_a - u_w) \tan \phi^b$$

Fig. 2. Soil water content versus matric suction for a glacial till (data from Vanapalli 1994).



where:

- u_a = pore-air pressure,
- $(\sigma_n - u_a)$ = net normal stress,
- $(u_a - u_w)$ = matric suction,
- ϕ' = angle of internal friction relating change in shear strength to net normal stress, and
- ϕ^b = angle relating change in shear strength with respect to a change in matric suction.

The modified Mohr-Coulomb failure criterion introduces a new shear strength parameter, namely ϕ^b and the stress state variables $(\sigma - u_a)$ and $(u_a - u_w)$. The proposed failure envelope in stress space is shown in Fig. 3. While the effective angle of internal friction, ϕ' , is a property related to the friction between the soil particles, ϕ^b is indirectly related to friction through the stresses in the pore fluids. Equation [2] suggests a linear relationship between shear strength and matric suction but the experimental research by Gan et al. (1988), shown in Fig. 4, shows that this relationship is linear only up to some value of suction (i.e., estimated as the air entry value of the soil), while beyond this value, the relationship becomes non-linear. At low matric suctions, the change in shear strength is controlled by ϕ' , while ϕ^b governs the change in shear strength at high matric suctions.

Fredlund et al. (1978) found that the angle ϕ' in eq. [2] is essentially equal to the effective angle of internal friction. Various researchers, testing a range of soil textures, have found small increases of the angle ϕ' with increasing matric suction (Escario 1980; Escario and Sáez 1986; Drumright 1989). However, Drumright (1989) showed that when variations in net applied stress were accounted for, the differences in ϕ' with respect to suction were reduced. The angle ϕ^b has been shown to be consistently equal to or less than ϕ' (Fredlund and Rahardjo 1993a).

A failure equation traditionally used by agricultural engineers is:

$$[3] \quad \tau_f = c + \sigma_n \tan \phi$$

where:

Fig. 3. Extended Mohr-Coulomb failure envelope for unsaturated soil.

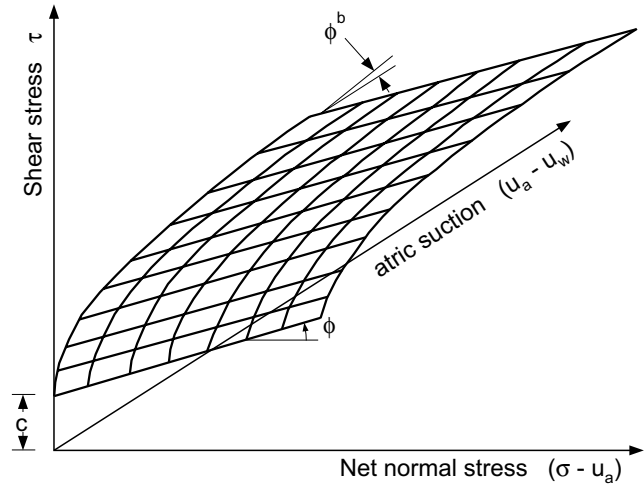
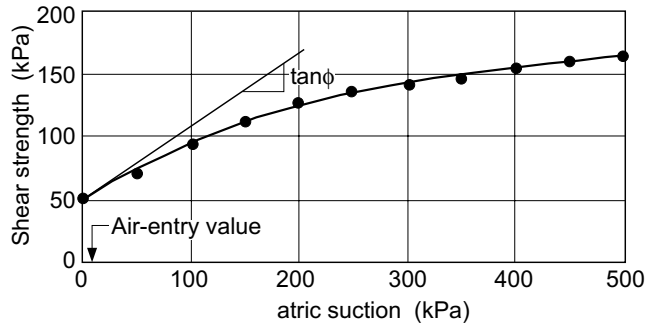


Fig. 4. Shear strength versus matric suction relationship for glacial till (from Gan et al. 1988). The slope, $\tan \phi^b$, is equal to $\tan \phi'$ up to the air-entry value, beyond which ϕ^b decreases with increasing suction.



- c = total cohesion, and
- ϕ = angle of internal friction.

For agricultural conditions the pore-air pressure is approximately atmospheric (i.e., $u_a = 0$ gauge). If indeed the angle of internal friction in eq. [3] may be equated to the effective angle of internal friction (i.e., $\phi = \phi'$), then eqs. [2] and [3] are identical provided the cohesion can be written as:

$$[4] \quad c = c' + (u_a - u_w) \tan \phi^b$$

Equation [4] proposes that the total cohesion depends on an apparent cohesion generated due to matric suction, $[(u_a - u_w) \tan \phi^b]$, and effective cohesion, c' . The latter is dependent on many factors, such as chemical cementation and mineral and organic interparticle attractions (Koolen and Kuipers 1983; Mitchell 1993). The total cohesion, c , includes the effect of suction and can be considered to be a variable function of suction. The failure criterion given by eq. [3] is therefore applicable only for the relevant soil suction conditions. A failure criterion of the form of eq. [2] is useful when considering varying field suction (or moisture) conditions.

Prediction of shear strength for varying suction conditions

Several models have been proposed to relate the shear strength of a soil to the matric suction (e.g., Greacen 1960; Vomocil and Chancellor 1967; Fredlund et al. 1978, McKyes et al. 1994; Fredlund et al. 1996). Most of these models are based on the assumption that the contribution of suction towards the strength of the soil is related to the area of contact of water in the soil pores. Curvature of the shear strength versus matric suction envelope arises as the net area reduces with drainage (Gan 1986).

Fredlund et al. (1996), using eq. [2] as the basis of a strength versus suction relationship, proposed a model relating ($\tan \phi^b$) to the degree of saturation (or normalized water content). The relationship between the instantaneous angles of friction can be written as:

$$[5] \quad \frac{\tan \phi^b}{\tan \phi'} \approx S^p$$

where:

- S = degree of saturation (i.e., w/w_s),
- w = any gravimetric water content of the soil,
- w_s = water content at saturation, and
- p = a soil parameter related to the soil texture, and thus, to the effective area of water in the soil for a given water content.

By substituting eq. [5] into eq. [2], a prediction equation for the shear strength of an unsaturated soil is obtained as:

$$[6] \quad \tau \approx c' + (\sigma - u_a) \tan \phi' + (u_a - u_w) S^p \tan \phi'$$

Equation [6] provides an estimate of the shear strength of an unsaturated soil for a given matric suction and water content using the soil-water characteristic curve [i.e., $S = S(u_a - u_w)$] and the effective strength parameters c' and ϕ' . At this time there are limited published data to support this relationship. Fredlund et al. (1996) tested the prediction model using a Hong Kong soil for matric suction values up to 200 kPa and found excellent agreement with measured data. A value of p equal to 1 appears to give acceptable results for sandy soils and the parameter generally increases with the plasticity of the soil and lies between $2 \leq p \leq 6$ for clay soils. The shapes of soil-water characteristic curves in the lower ranges of matric suction (i.e., where S is on the order of 100%) would suggest that a value of p equal to 1 should be acceptable for finer-textured soils as well, as long as predictions are limited to the lower values of suction.

Cui and Delage (1993) found that at a high suction (i.e., 1500 kPa) the general shape of shear stress and volumetric strain versus axial strain curves was quite different than those at lower suctions (i.e., 50 to 800 kPa). Their findings show that suction has an important effect on stiffness and maximum shear strength. This emphasizes the need for precise models for the soil-water characteristic curve if the shear strength characteristics are to

be estimated at elevated suctions (i.e., low water contents in fine-textured soils) with any confidence, using prediction equations such as eq. [6].

Verification of shear strength equation for an agricultural soil

Data are presented for a sandy clay loam having the properties given in Table 1. Specimens were statically compacted to the same bulk density (i.e., 1.2 Mg/m³) at several water contents, four dry of optimum and one wet of optimum (Table 2). Under these conditions, the "dry of optimum" specimens are expected to all have similar structures and the 'wet of optimum' specimen to have a somewhat different structure. Soil-water characteristic curves were determined using a pressure cell (University of Saskatchewan design) for specimens statically compacted at 16.0% and 20.4% to represent specimens dry and wet of optimum, respectively (Fig. 5).

Unsaturated shear strength parameters for the soil were determined using direct shear box tests. Net normal stresses, $(\sigma - u_a)$, from 25 kPa to 150 kPa in 25 kPa intervals were used for the specimens at each water content. The specimens were sheared at a rate of 0.9 mm/min. In addition, the effective strength parameters were obtained from triaxial tests on saturated specimens, using the apparatus described by Wulfsohn et al. (1994). Results of the strength tests are presented in Table 2. The results verify that, for this soil, the unsaturated internal friction angle ϕ can be taken as equal to the effective internal angle of friction ϕ' . The total cohesion, c , shows no trend with water content.

With c' and ϕ' and the soil-water characteristic curves known, the unsaturated shear strength was then calculated using eq. [6]. The predicted shear strength envelope is plotted versus matric suction and versus net normal stress in Figs. 6 and 7, respectively. The value of p used in these predictions was 2.6. The shear strength of the soil did not increase much with reduced water content (increasing suction) in the experiments and this trend was predicted by the model (Fig. 6).

Samples at all water contents developed similar strengths (also see Table 2). Figure 7 supports the conjecture that all samples compacted dry of optimum were of similar structure. The data also indicate that the sample wet of optimum had a similar structure. If the soil-water

Table 1. Index properties of the soil used in the test program.

Parameters	Values	
Texture:	Sand (%)	48.1
	Silt (%)	23.6
	Clay (%)	28.3
Specific gravity		2.65
Liquid limit (%)		32.9
Plastic limit (%)		18.8
Plasticity index (%)		14.1
Optimum water content (%)		18.0
Maximum dry bulk density (Mg/m ³)		1.65

Table 2. Properties of sandy clay loam soil specimens prepared by static compaction to 1.2 Mg/m³ bulk density.

As-compacted conditions				Unsaturated strength parameters ^c	
Water content (%)	Void ratio	Degree of saturation (%)	Matric suction (kPa)	<i>c</i> (kPa)	ϕ (degrees)
dry of optimum					
3.5	1.29	7.2	— ^a	6.5	35.8
9.2	1.41	17.3	— ^a	5.3	37.4
14.6	1.53	25.3	595	8.3	35.8
16.9	1.58	28.3	195	6.2	36.8
wet of optimum					
21.1	1.67	33.4	35 ^b	1.3 ^d	35.8 ^d
			saturated strength parameters ^e		
			0	~0	36.5

^aLies outside range of suction for which experimental data falls.

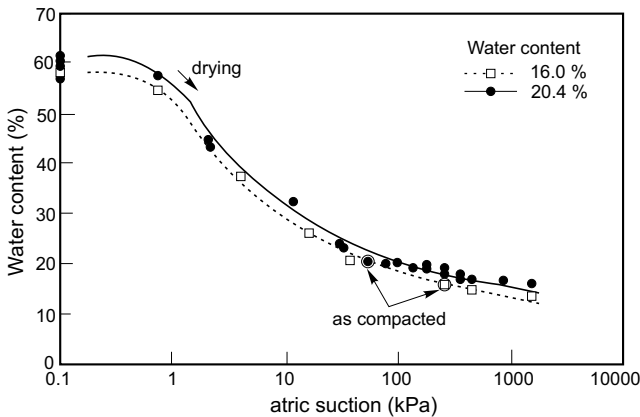
^bFrom null pressure plate test.

^cParameters of eq. [3], determined from shear box test data.

^dBased on linear regression through 3 data points at low normal stresses (see Fig. 7).

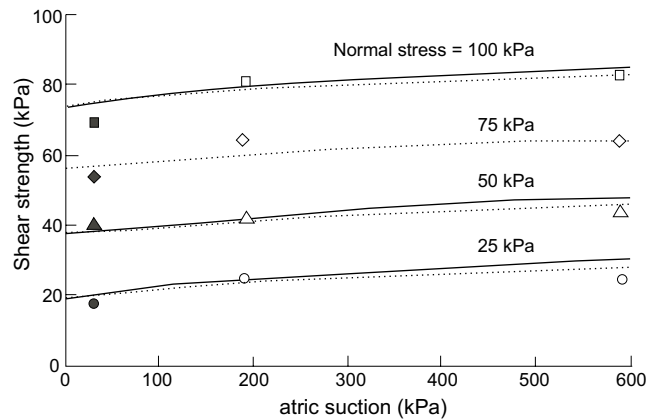
^eFrom triaxial test data for specimens compacted at 20.4% water content show $c' = 0$ and $\phi' = 36.5^\circ$.

Fig. 5. Water content versus matric suction relationship for specimens compacted at water contents dry of optimum and wet of optimum, to a bulk density of 1.2 Mg/m³.



characteristic curves (Fig. 5) are replotted with degree of saturation on the vertical axis, the curves almost overlap. Nevertheless, the strength of the wet of optimum specimen (i.e., $w = 21.1\%$) dropped off significantly at higher net stress levels. This type of behaviour was also observed by Greacen (1960). It is suggested that the strength decreases when normal loads exceeding some critical value greater than the soil suction are applied (see Croney and Coleman 1953; Larson and Gupta 1980). Above this value the tension in the soil water will rapidly decrease, and the pore-water pressure increases as the “contractile skin” is distorted. Thus, a reduction in strength is observed for the wet of optimum specimen ($u_a - u_w = 38$ kPa) but not for the drier specimens which all had suction values well exceeding the range of normal loads applied in the shear box tests.

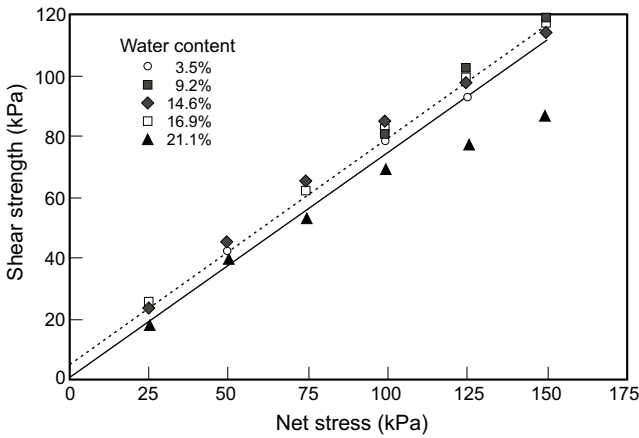
Fig. 6. Predicted and measured shear strength versus matric suction for a sandy clay loam soil. Predicted relationships are based on eq. [6] and soil-water characteristic curves for (---) dry of optimum and (—) wet of optimum specimens (Fig. 5). Open symbols are for specimens compacted at water contents dry of optimum ($w = 9.2, 14.6,$ and 16.9%), filled symbols represent specimens wet of optimum ($w = 21.1\%$).



Application to some agricultural strength related models

The strength of soil is of fundamental importance in agricultural soil-engaging processes. The shear strength prediction equation presented above is based on parameters (i.e., effective shear strength parameters and the soil-water characteristic curve) that need only be determined once for a given soil structure, providing a means to simulate the behaviour of strength dependent processes under different moisture conditions. Two examples will be presented here.

Fig. 7. Predicted and measured shear strength versus normal stress for a sandy clay loam soil. Predicted relationships are based on eq. [6] and soil-water characteristic curves for (---) dry of optimum and (—) wet of optimum specimens (Fig. 5).



Example Problem No. 1: Estimation of traction

To illustrate the role of unsaturated soil strength, a simplified model of traction is used in the estimation of traction to illustrate the role of unsaturated soil strength. From a consideration of equilibrium, the net traction developed by a tire (or track) on a deformable soil surface is given by the sum of all horizontal components of stress in the direction of travel acting over the tire-soil interface (Fig. 8):

$$[7] \quad NT = \int_A [\tau \cos \theta - \sigma \sin \theta] dA$$

where:

- NT = net traction,
- τ = shear stress,
- σ = normal stress,
- θ = angle between surface normal and the vertical at any point on the contact surface, and
- A = contact surface.

The major contribution to net traction comes from the shear stress distribution. Therefore the maximum net traction is limited by the shear strength of the soil. Maximum tractive effort is not practically realized due to slip between tire and soil. A soil shear stress-displacement relationship is usually employed to account for this. Bekker (1957) proposed using a shear stress-displacement relation of the form:

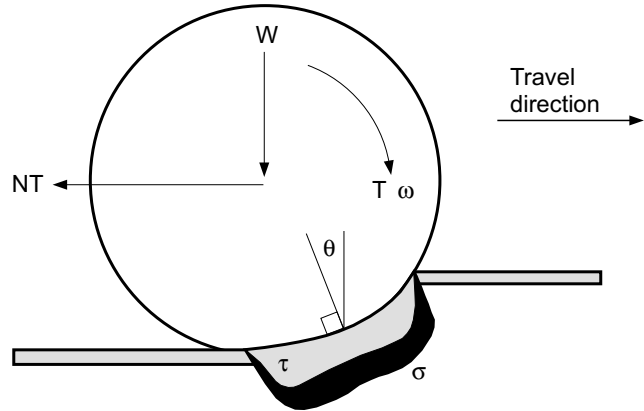
$$[8] \quad \tau = \tau_f (1 - e^{-j/K})$$

where:

- τ = shear stress [F/L^2]
- τ_f = shear strength [F/L^2]
- j = soil shear deformation [L], and
- K = shear deformation modulus [L].

To obtain an expression for net traction for varying field moisture conditions, eq. [6] may be used as the expression for shear strength along with the soil-water char-

Fig. 8. Traction model for the interaction between tire and soil.



acteristic curve to relate suction to water content; however, the variation of prediction shear modulus K with varying suction is not known. The shear modulus, K , is itself a composite (i.e., it is not a fundamental soil property) which depends on the distribution of shear deformation with depth beneath a traction device. There have been relatively few studies on strain in the ground beneath traction devices. A more complete analysis would require the investigation of the effect of suction on soil deformation characteristics.

Figure 9 shows the effect of water content on traction coefficient, NT/W , where W is the dynamic axle load, for the sandy clay loam soil for a normal stress of 135 kPa, $L/K = 8$ and two slip levels. The experimental data shown were obtained from Grouser plate tests with two plate sizes in the Department of Agricultural and Bioresource Engineering soil bin. The soil was prepared by compacting it at 20% water content using a sheep-foot roller followed by a smooth roller, and then allowed to dry out to various water contents. Under these conditions similar soil structures are expected to those for which soil-water characteristic curves were determined. For rigid Grouser plates $j = iL$ was substituted in eq. [6], where i presents the slip and L is the plate length. Predicted and measured data agree fairly well.

Example Problem No. 2: A tillage tool force prediction model

A commonly used model for tillage tool force prediction is based on the Universal Earth Moving Equation proposed by Reece (1965). The model was originally developed for wide tools cutting the soil in a passive type failure (Fig. 10) (Hettiaratchi et al. 1966). The approach has since been extended by others to narrow tools (Hettiaratchi and Reece 1967; Godwin and Spoor 1977; McKeyes and Ali 1977; Perumpral et al. 1983). The force on the tool is related to soil properties, tool parameters, and several dimensionless factors by:

$$[9] \quad F = (\gamma h^2 N_\gamma + ch N_c + qh N_q + c_\alpha h N_{c\alpha}) b$$

where:

Fig. 9. Variation of traction coefficient, NT/W , with soil water content for two levels of slip, $L/K = 8$, $\sigma_n = 135$ kPa, in a sandy clay loam soil.

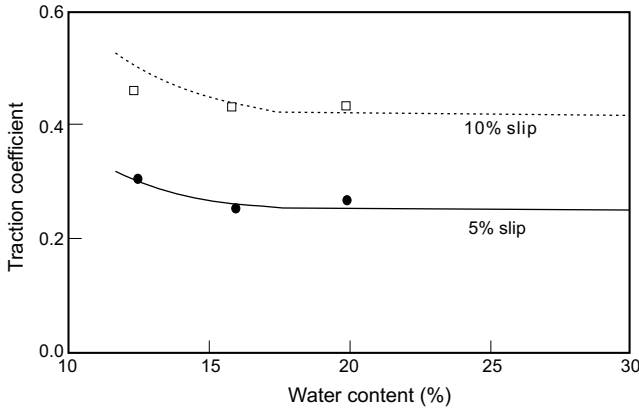
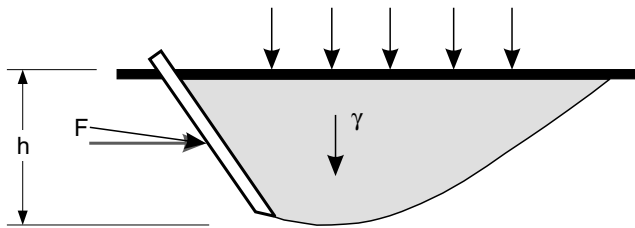


Fig. 10. Tillage tool and soil failure pattern.



- F = soil force $[F]$,
- γ = total unit weight of the soil $[F/L^3]$,
- h = tool depth into the soil $[L]$,
- c = soil cohesion $[F/L^2]$,
- c_{α} = soil-tool adhesion $[F/L^2]$,
- b = tool width $[L]$, and
- q = soil surcharge $[F/L^2]$.

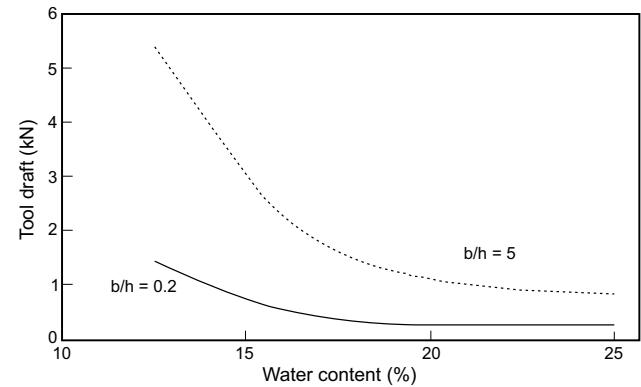
The dimensionless factors, N_{γ} , N_c , $N_{c\alpha}$, and N_q relate the tool geometry to the internal friction angle and the soil-tool friction angle, and can be obtained from established charts.

For a given surcharge, the largest contributions to draft are from the cohesion and weight terms. Soil-tool adhesion arises almost entirely from soil suction (Fountainne 1954, and others) and may vary considerably with soil moisture. However, it has a relatively small contribution to the overall draft (i.e., $N_{c\alpha}$ is small compared with N_c and N_{γ}). By introducing the total cohesion form for an unsaturated soil (i.e., eq. [4]) and eq. [5] to relate ϕ^b and degree of saturation, this model can be appropriated to predict the variation in tillage tool force for variable moisture conditions, as:

$$[10] \quad F = \{ \gamma h^2 N_{\gamma} + [c' + (u_a - u_w)(S)^p \tan \phi'] h N_c + q h N_q \} b$$

where the adhesion component has been neglected. The variation in soil unit weight with water content can also be computed using the basic volume-mass relationship:

Fig. 11. Predicted variation of draft, H , with water content for a wide ($b/h = 5$) and a narrow ($b/h = 0.2$) tool operating at 150 mm depth, 40° rake angle in a sandy clay loam soil (1.04 Mg/m³ dry bulk density).



$$[11] \quad Se = wG_s$$

where:

- e = void ratio,
- w = gravimetric water content, and
- G_s = specific gravity of soil solids.

Equation [10] was used to predict the variation of draft with water content in the sandy clay loam soil for two tool configurations: (1) wide blade, $b = 750$ mm; (2) narrow blade, $b = 30$ mm, both operating at a depth $h = 150$ mm and a 40° rake angle, and having a soil-tool friction angle of 24° (Fig. 11). Values of the N-factors were obtained from charts in McKyes (1985). In these predictions, the cohesive term accounted for over 90% of the draft for water contents up to 14%. The contribution of the weight term gradually increased with increasing water content, so that at a water content of 25% the weight term accounted for 52% and 48% of the draft for the wide and narrow tools, respectively.

Conclusions

The above examples illustrate how the principles discussed in this paper can be used with some elementary strength-based models. The experimental data obtained for a sandy clay loam soil supported the use of the soil-water characteristic curve combined with saturated strength parameters to estimate shear strength over a wide range of suctions. The modified forms of prediction relationships for traction and tool draft should be valid for all water contents for a given soil. Their particular advantage is that they provide a means to estimate tractive ability and tillage forces in a given soil without having to determine *in situ* strength parameters for every water content encountered in the field. However, the use of the soil-water characteristic curve to relate matric suction and water content or degree of saturation to soil strength is only valid for the soil structure for which the soil-water characteristic curve was obtained. Variable factors in soil structure such as aggregate size distribution, cracks,

macropores, fabric anisotropy, bulk density, and moisture status influence soil strength and volume change tendencies. If the structure alters significantly under wetting or drying or due to mechanical disturbance, the saturated strength parameters, as well as the soil-water characteristic curve will all change. Predicting these structural changes requires an understanding of the effect of the stress variables on the soil deformation characteristics and the soil-water characteristic curve. Most real agricultural problems, however, engage the shear and compressive strengths and deformation responses of soil simultaneously. For the full effectiveness of the unsaturated framework to be realized it will be necessary to adapt unified models of soil behaviour by incorporating matric suction and the soil-water characteristic curve.

Acknowledgements

The data presented in Figs. 2 and 4 are courtesy of Dr. Sai Vanapalli (Postdoctoral Fellow) and Julian Gan (Research Engineer), respectively, Department of Civil Engineering, University of Saskatchewan. The authors are also grateful to Dr. E. McKyes, Professor of Agricultural and Biosystems Engineering, McGill University, Ste. Anne de Bellevue, QC, for his valuable comments and suggestions with regard to the manuscript. This work was financially supported by NSERC.

References

- Bekker, M.G. 1957. The theory of land locomotion - The mechanics of vehicle mobility. University of Michigan Press, Ann Arbor, MI.
- Chancellor, W.J., and Vomocil, J.A. 1970. Relation of moisture content to failure strengths of seven agricultural soils. Transactions of the ASAE, **13**: 9-13, 17.
- Croney, D., and Coleman, J.D. 1953. Soil moisture suction properties and their bearing on the moisture distribution in soils. Proceedings, 3rd International Conference on Soil Mechanics and Foundation Engineering, Vol. 1, pp. 13-18.
- Croney, D., and Coleman, J.D. 1954. Soil structure in relation to soil suction (pF). Journal of Soil Science, **5**: 75-85.
- Cui, Y.J., and Delage, P. 1993. On the elasto-plastic behaviour of an unsaturated silt. In Unsaturated Soils. Edited by S.L. Houston and W.K. Wray, New York, NY, American Society of Civil Engineers, pp. 115-126.
- Drumright, E.E. 1989. The contribution of matric suction to the shear strength of unsaturated soils. Ph.D. thesis. Colorado State University, Fort Collins, CO.
- Escario, V. 1980. Suction controlled penetration and shear tests. Proceedings, 4th International Conference on Expansive Soils, Denver, CO, American Society of Civil Engineers, Vol. 2, pp. 781-797.
- Escario, V., and Sáez, J. 1986. The shear strength of partly saturated soils. Géotechnique, **36**(3): 453-456.
- Fontaine, E.R. 1954. Investigation into the mechanism of soil adhesion. Journal of Soil Science, **5**(2): 251-263.
- Fredlund, D.G., Morgenstern, N.R., and Widger, R.A. 1978. The shear strength of unsaturated soils. Canadian Geotechnical Journal, **15**: 313-321.
- Fredlund, D.G., and Rahardjo, H. 1993a. Soil mechanics for unsaturated soils. John Wiley & Sons New York, NY.
- Fredlund, D.G., and Rahardjo, H. 1993b. An overview of unsaturated soil behaviour. In Unsaturated Soils. Edited by S. L. Houston and W.K. Wray, New York, NY. pp. 1-31.
- Fredlund, D.G., Xing, A., Fredlund, M.D., and Barbour, S.L. 1996. The relationship of the unsaturated soil shear strength to the soil-water characteristic curve. Canadian Geotechnical Journal, **33**: 440-448.
- Gan, J.K.-M. 1986. Direct shear strength testing of unsaturated soils. M.Sc. thesis, University of Saskatchewan, Saskatoon, SK.
- Gan, J.K.-M., Fredlund, D.G., and Rahardjo, H. 1988. Determination of the shear strength parameters of an unsaturated soil using the direct shear test. Canadian Geotechnical Journal, **25**(3): 500-510.
- Godwin, R.J., and Spoor, G. 1977. Soil failure with narrow tines. Journal of Agricultural Engineering Research, **22**(4): 213-228.
- Greacen, E.L. 1960. Water content and soil strength. Journal of Soil Science, **11**: 313-333.
- Hettiaratchi, D.R.P., and Reece, A.R. 1967. Symmetrical three-dimensional soil failure. Journal of Terramechanics, **4**(3): 45-67.
- Hettiaratchi, D.R.P., Witney, B.D., and Reece, A.R. 1966. The calculation of passive pressure in two dimensional soil failure. Journal of Agricultural Engineering Research, **11**(2): 89-107.
- Koolen, A.J., and Kuipers, H. 1983. Agricultural soil mechanics. Advanced Series in Agricultural Sciences 13. Berlin, Germany, Springer Verlag.
- Larson, W.E., and Gupta, S.C. 1980. Estimating critical stress in unsaturated soils from changes in pore-water pressure during confined compression. Soil Science Society of America Journal, **44**(6): 1127-1132.
- McKyes, E. 1985. Soil Cutting and Tillage. Developments in Agricultural Engineering 7. Elsevier Science Publishers, Amsterdam, The Netherlands.
- McKyes, E., and Ali, O.S. 1977. The cutting of soil by narrow blades. Journal of Terramechanics, **14**(2): 43-58.
- McKyes, E., Nyamugafata, P., and Nyamapfene, K.W. 1994. Characterization of cohesion, friction and sensitivity of two hardsetting soils from Zimbabwe. Soil and Tillage Research, **29**: 357-366.
- Mitchell, J. K. 1993. Fundamentals of Soil Behaviour. Second edition, John Wiley & Sons New York, NY.
- Mojlaj, E.G., Wulfsohn, D., and Adams, B.A. 1992. Analysis of soil cutting tool using critical state soil mechanics. ASAE Paper No. 92-1501. St. Joseph, MI.
- Mou, C.H., and Chu, T.Y. 1981. Soil suction approach for swelling potential evaluation. Transportation Research Record 790, Washington, DC: US Government Printing, pp. 54-60.
- Mullins, C.E., MacLeod, D.A., Northcote, K.H., Tisdall, J.M., and Young, I.M. 1990. Hardsetting soils: behaviour, occurrence and management. Advances in Soil Science, **11**: 37-108.
- Mullins, C.E., and Panayiotopoulos, K.P. 1984. The strength of unsaturated mixtures of sand and kaolin and the concept of effective stress. Journal of Soil Science, **35**: 459-468.
- Olson, R.E., and Langfelder, L.J. 1965. Pore-water pressures in unsaturated soils. ASCE, Journal of Soil Mechanics and Foundation Division, **91**(SM4): 127-160.

- Perumpral, J.V., Grisso, R.D., and Desai, C.S. 1983. A soil-tool model based on limit equilibrium analysis. *Transactions of the ASAE*, **26**(4): 991–995.
- Reece, A.R. 1965. The fundamental equation of earth moving mechanics. *In* Symposium of Earth Moving Machinery, The Institute of Mechanical Engineers, 179, Part 3F. London, England.
- Vanapalli, S.K. 1994. Simple test procedures and their interpretation in evaluating the shear strength of an unsaturated soil. Ph.D. thesis. University of Saskatchewan, Saskatoon, SK, Canada.
- Vomocil, J.A., and Chancellor, W.J. 1967. Compressive and tensile failure strengths of three agricultural soils. *Transactions of the ASAE*, **10**(6): 771–774, 779.
- Whalley, W.R., Leeds-Harrison, P.B., Joy, P., and Hoefsloot, P. 1994. Time domain reflectometry and tensiometry combined in an integrated soil water monitoring system. *Journal of Agricultural Engineering Research*, **59**: 141–144.
- Williams, J., and Shaykewich, C.F. 1970. The influence of soil water matric potential on the strength properties of unsaturated soil. *Soil Science Society of America Proceedings*, **34**(6): 835–840.
- Woodburn, J.A., Holden, J.C., and Peter, P. 1993. The transistor psychrometer. A new instrument for measuring soil suction. *In* *Unsaturated Soils*. Edited by S.L. Houston and W.K. Wray, New York, NY. pp. 91–102.
- Wulfsohn, D., Adams, B.A., and Fredlund, D.G. 1994. Triaxial testing of unsaturated agricultural soils. ASAE Paper No. 94–1036. St. Joseph, MI.

From theory to the practice of unsaturated soil mechanics

D.G. Fredlund

Abstract: The implementation of unsaturated soil mechanics into engineering practice comes at a time when the geotechnical engineer is accepting a new soil mechanics paradigm. Computers and numerical modelling play a dominant role in responding to “What if — ?” scenarios to engineering problems. For many problems involving unsaturated soils, it is necessary to be able to input approximate unsaturated soil property functions into the numerical model. In most cases, these functions can be approximated from either a knowledge of the soil-water characteristic curve or the grain distribution of the soils involved. Knowledge-based systems become an important part of determining the necessary input soil property functions. This implementation procedure deviates somewhat from historical classical soil mechanics procedures but has proven to provide acceptable procedures for engineering practice.

Key words: unsaturated soil mechanics, unsaturated soil property functions, soil-water characteristic curve, grain size distribution, computers.

Introduction

There is a long “road” from the formulation of theories and the discovery of a sound scientific basis, to the development of a viable technology for engineering practice. Even after the physics and the theories related to a particular geotechnical problem have been resolved, the “road ahead” for implementation to become a reality, can be quite lengthy. Tardiness associated with the implementation of a new engineering science is usually due, in part, to an unwillingness of the profession to accept new engineering practices; however, more likely it is due to procedural “gaps” related to the detailing of viable engineering practice procedures. The intent of this paper is to address factors associated with the implementation of unsaturated soil mechanics into engineering practice.

The characterization of shear strength and volume change in terms of two independent stress state variables appears to be generally accepted as evidenced from the proceedings of the First International Conference on Unsaturated Soils, Paris, France, 1995. Figure 1 uses a visualization aid to illustrate the smooth transition in stress state when going from saturated soil conditions to unsaturated soil conditions (Fredlund and Morgenstern 1977). Theories have been formulated for the classic areas of: i) seepage, ii) shear strength, and iii) volume change, for unsaturated soils (Fredlund 1979). Figure 2 illustrates the constitutive relationships associated with the classic areas of soil mechanics for saturated and unsaturated soils. Not shown on Fig. 2 is the relationship between the water

content and soil suction for an unsaturated soil. This relationship, known as the soil-water characteristic curve, has become of great value in estimating unsaturated soil property functions. The characterization of seepage, for example, in terms of a hydraulic head gradient and a coefficient of permeability function appears to be generally accepted (Fredlund 1995). Figure 3 illustrates the relationship between the soil-water characteristic curve and the coefficient of permeability function for the unsaturated portion of the soil profile. The use of nonlinear soil property functions for analyzing unsaturated soils problems appears to be gaining general acceptance.

The best theories, and even the most accepted theories, do not necessarily translate into a widespread use of the related formulations in engineering practice. There needs to be greater diligence given towards clearly defining the implementation steps in order for the theories to be a part of “problems solving” in geotechnical engineering. All too often it is easiest to learn about the theory and then revert to past experience and “rule of thumb” procedures, in order to arrive at an expedient and low cost solution. The breakdown in implementation often centers around our inability to measure or assess the physical soil properties (or soil property functions) for input to an analysis. The assessment of suitable boundary conditions for the problem-at-hand may also pose a serious problem. However, many of the required analyses are available for usage with little time required for inputting the problem into the computer. Figure 4 illustrates the meaning of the word, “implementation”, as it relates to a saturated/unsaturated seepage problem.

The uppermost part of Fig. 4 shows the basic constitutive relations (i.e., flow laws) which apply to the saturated and unsaturated soil portions of the profile. The water coefficient of permeability, shown as a constant in the saturated zone, becomes increasingly smaller in a nonlinear manner in the unsaturated zone. Giving consid-

D.G. Fredlund. Professor, Department of Civil Engineering, University of Saskatchewan, 57 Campus Drive, Saskatoon, SK, Canada S7N 5A9.

Reproduced with permission from *Proceedings, 3rd Brazilian Symposium on Unsaturated Soils*, Rio de Janeiro, Brazil, April 22–26, 1997. Freitas Bastos Editora.

Fig. 1. A visualization aid for the world of saturated/unsaturated soil mechanics.

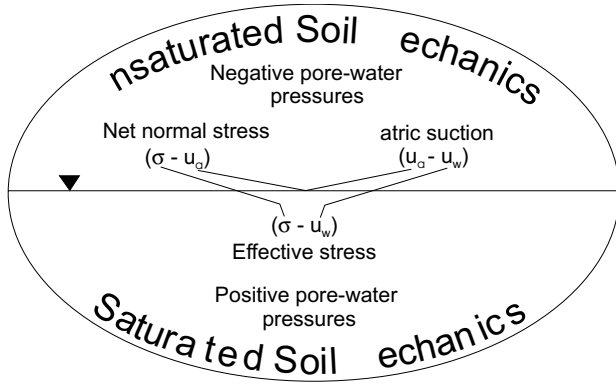


Fig. 2. Constitutive relationships for the classic areas of soil mechanics.

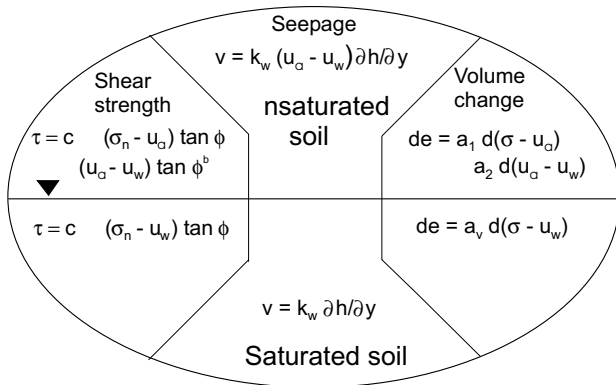
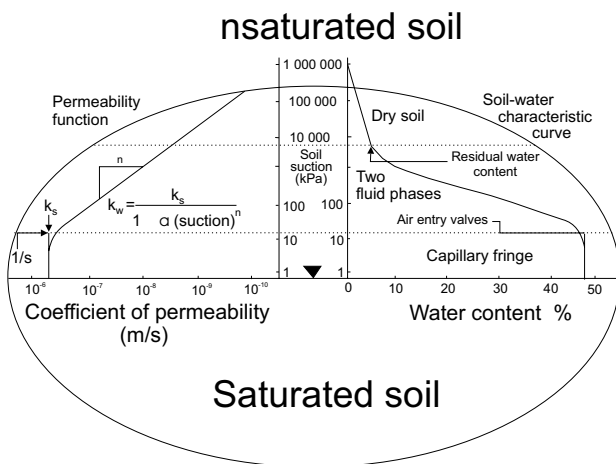
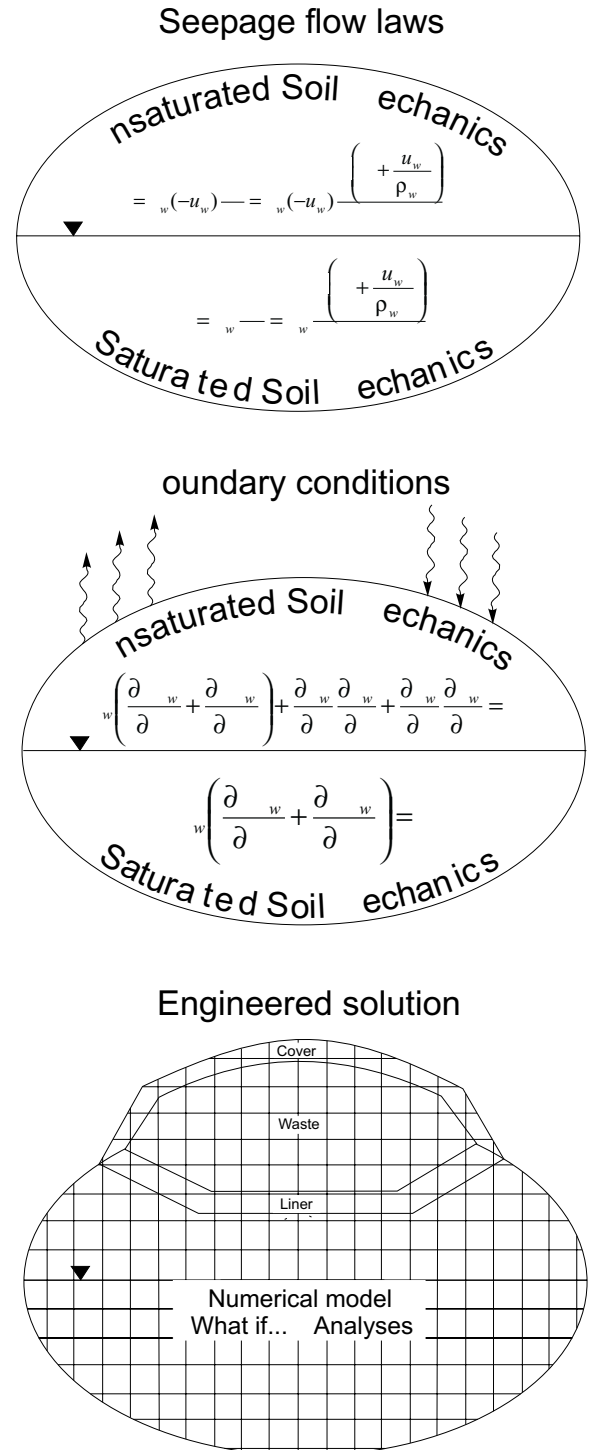


Fig. 3. Visualization of the relationship between the coefficient of permeability function and the soil-water characteristic curve.



eration to the conservation of mass constraints gives rise to a saturated/unsaturated seepage formulation which applies to every element in the soil mass. These formulations can then be converted to linear and nonlinear numerical models. The modeller then requires two additional pieces of information in order to commence per-

Fig. 4. Steps involved in implementing an engineered solution.



forming analyses. These two pieces of information are: (1) the soil properties and the unsaturated soil property functions, and (2) the boundary conditions for the problem. The primary boundary condition being referred to is the ground surface moisture flux which is related to environmental conditions. The use of knowledge-based sys-

tems can be of great benefit in providing the information required to encourage greater implementation of saturated/unsaturated soil models.

Easy-to-use computer software programs (e.g., finite element, saturated/unsaturated seepage software) are now readily available to engineers. Whether or not an appropriate analysis is done often depends upon costs related to the measurement or the assessment of soil properties and soil property functions. More extensive implementation of numerical models for saturated/unsaturated soils problems can be brought about through a better understanding of how to assess the unsaturated soil property functions.

The objective of this paper is to assist geotechnical engineers in bridging the gap between unsaturated soils theories and unsaturated soils engineering practice. The paper will attempt to dispel some of the myths related to numerical modelling and will then concentrate on the assessment of unsaturated soil property functions for engineering practice.

Basic needs in the practice of unsaturated soil mechanics

The engineer must be able to visualize the problem at hand in terms of the types of analyses which could prove to be beneficial in arriving at a solution. The engineer is most strategically positioned to verbalize the nature of the problem and then translate the problem into analytical (mathematically based), predictive procedures which can be performed. Without the use of analytical, predictive procedures, engineering practice remains more of an art than a science. The intent is to increase the use of predictive technology in the practice of unsaturated soil mechanics.

Another basic need in the practice of unsaturated soil mechanics is related to the assessment of unsaturated soil property functions. These functions must be either measured, indirectly computed or estimated in a cost effective manner which still yields sufficient accuracy to address the questions and concerns at hand.

A third basic need arises in being able to answer the following question; namely: "What will happen at some time in the future if certain conditions are changed?" Some examples will help to illustrate the three needs mentioned.

One example involves the influence of rainfall on the stability of a slope. Figure 5 shows a typical slope along with reference to the information required in order to perform analytical studies. The question of concern can be verbalized as follows. Under what rainfall conditions (i.e., intensity and duration) could the slope fail? The problem can be reduced to a seepage problem and a soil-atmosphere interactive problem, combined with a limit equilibrium slope stability analysis. The seepage problem requires the characterization of two soil property functions in order for the analysis to be solved; namely, the coefficient of water storage function and the coefficient of permeability function. The slope stability analysis requires a function for the shear strength of the soil. It

might also be suggested that a function is required for the unit weight of the soil; however, it could be argued that this is a secondary effect.

Let us assume that the stratigraphy and the saturated soil parameters associated with the problem at hand, are known or can be measured. This being the case, the greatest need of the engineer will be for unsaturated soil property functions and the assessment of appropriate boundary conditions for the problem. The engineer needs to know: i) how to estimate, compute or measure the soil property functions, and ii) what degree of accuracy is required for the soil property functions.

Even if laboratory facilities were available to measure unsaturated soil properties, it would quickly become obvious that the costs associated with measuring all unsaturated soil property functions in the laboratory is prohibitive. The tendency at this point is to scrap the analytical aspects of the study and revert to the use of past experience and empirical information. Rather, the engineer needs to know if it is possible to estimate or compute the necessary unsaturated soil property functions. An important question to ask at this point is: "What degree of accuracy does the engineer require in order to perform the necessary analyses?" First, the question of accuracy as it relates to the functions required in order to envelope the soil conditions will be addressed.

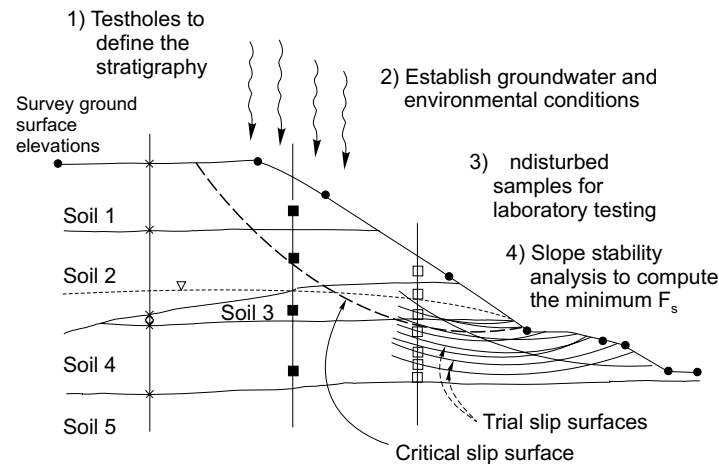
How accurate should the unsaturated soil property functions be?

The properties of all soils involved in a "boundary value" type problem must be defined in order to obtain a solution to the problem. The accuracy of the computed results will depend on the accuracy of the input soil properties. However, the accuracy with which the soil properties (and the soil property functions in the case of unsaturated soils) need to be defined depends upon the independent variable being computed. It is important to ascertain the accuracy with which the soil properties (and soil property functions) need to be defined in light of the question to be answered from the analysis.

Example No. 1: Stress analysis

Consider the case of a stress analysis where a load is applied to a steel plate placed on a homogeneous soil mass. The input soil parameters for a simple, linear elastic analysis are Young's modulus, E , and Poisson's Ratio, μ . If the purpose of the analysis is to predict the normal stresses in the soil mass, the soil parameters do not need to be nearly as well defined as when displacements are being predicted. Stated another way, almost any value for Young's modulus will give a reasonable estimate of the vertical stresses. The horizontal stresses will require that a reasonably correct value for Poisson's Ratio be used in the analysis. However, the accuracy of the predicted displacements are directly related to the accuracy with which Young's modulus has been defined.

The above example illustrates that different degrees of accuracy are required for the input soil parameters de-

Fig. 5. Example problem illustrating the use of seepage and slope stability analyses.

pending upon the objective of the analysis. Simply stated, it is much easier to predict stresses than it is to predict displacements. In other words, the soil properties need to be defined more accurately for the prediction of displacements than for the prediction of stresses. The above example was for the case of a homogeneous soil mass. When two or more soils are involved, the above scenario does not rigidly apply, but the general observations are still applicable.

Example No. 2: Seepage analysis

Consider a second example involving the steady state seepage of water through the saturated and unsaturated portions of a homogeneous, compacted earthfill dam (Fig. 6). The input soil parameter for the saturated soil is the coefficient of permeability. For the unsaturated portion of the soil the coefficient of permeability function, $k_w(u_w)$, must also be input into the analysis. (For a transient analysis, a coefficient of water volume change, m_2^w , would also need to be input into the analysis.) If the purpose of the analysis is to predict the pore-water heads (or the pore-water pressures), the soil parameters do not need to be nearly as well defined as when the amount of seepage (i.e., water fluxes) are being predicted. Almost any coefficient of permeability (and coefficient of permeability function), and storage function will give a reasonable estimate of the pore-water pressure heads, both above and below the phreatic line. However, the predicted quantity of water flowing through the dam will be directly related to the accuracy of the coefficient of permeability (and the permeability function).

The above seepage example again illustrates that different degrees of accuracy are required for the input soil parameters, depending on the objective of the analysis. Geotechnical engineers have long known that flow net solutions for homogeneous soil masses are independent of the coefficient of permeability of the soil. This rationale can also be extended to the use of soil property functions for unsaturated soils. Essentially any coefficient of permeability function can be used for the unsaturated portion of the soil and the predicted pore-water heads will remain essentially constant. This means that an approxi-

mate soil property function is sufficient when performing a saturated/unsaturated seepage analysis for the prediction of pore-water heads. The predicted pore-water heads can be used in a slope stability analysis. In other words, a means of approximating the unsaturated soil property functions is all that is required for certain types of geotechnical analyses.

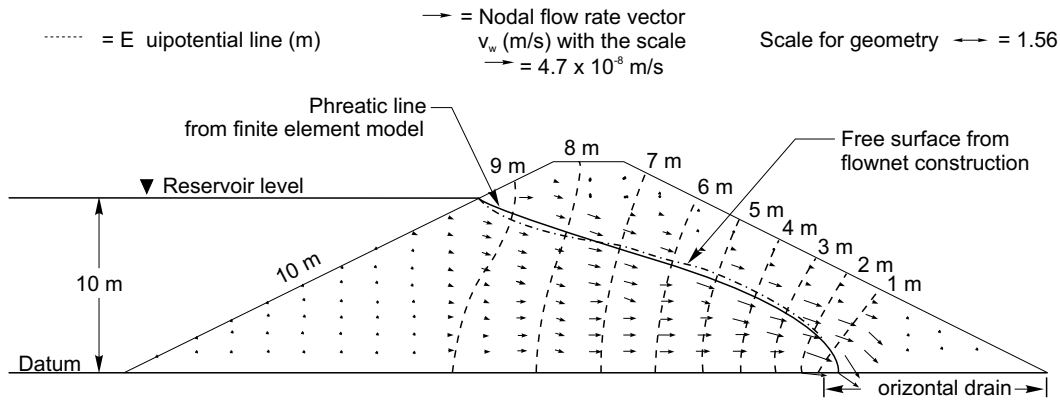
Conclusions from the above examples

A means of estimating or indirectly computing unsaturated soil property functions will be sufficient for modelling many saturated/unsaturated soils problems. This provides the basis for justifying the usage of the soil-water characteristic curve of a soil for the prediction of unsaturated soil property functions. There is a theoretical basis justifying the usage of approximate unsaturated soil property functions for analytical purposes. This provides the basis for an economical means of implementing unsaturated soil mechanics into engineering practice. It is important that the proposed procedures for the estimation of unsaturated soil property functions not be considered as being sufficient and satisfactory for all modelling situations. The engineer must take into consideration the nature of the independent variable being computed.

The engineer commonly suggests that the “observational procedure” (Peck 1969) be used on projects of some significance. The observation of behaviour becomes the verification on the many approximations and estimations which have been made during the design. For many problems, the estimation of the unsaturated soil property functions allows the engineer to make more realistic assumptions as part of the design phase of the project.

The use of parametric type studies, or the application of probability theory, also play an important role in the modelling of geotechnical problems. The engineer should always consider possible variations (or potential ranges) in the input soil properties and thereby attempt to envelope all possible conditions for design purposes. The above examples show that approximate values for the unsaturated soil property function will allow the engineer to envelope the pattern of behaviour for most problems.

Fig. 6. Steady state seepage through an earthfill dam illustrating the independence of the equipotential lines on the permeability properties.



The soil-water characteristic curve

The behaviour of unsaturated soils (i.e., unsaturated soil property functions) are strongly related to the pore size geometry and the pore size distribution. As a result, the soil-water characteristic curve becomes a dominant relationship for understanding unsaturated soil behaviour. The soil-water characteristic curve defines the degree of saturation corresponding to a particular suction in the soil. Therefore, the soil-water characteristic curve becomes a measure of the pore size distribution of the soil. Figure 7 shows the general features of the soil-water characteristic curve. A number of equations have been proposed to empirically best-fit the soil-water characteristic curve. Following is the equation proposed by Fredlund and Xing (1994) along with a definition of the soil properties required to define the equation as a closed-form function.

$$[1] \quad \theta_w((u_a - u_w), a_s, n_s, m_s) = C(u_a - u_w) \frac{\theta_s}{\{\ln[e + ((u_a - u_w) / a_s)^{n_s}]\}^{m_s}}$$

where:

- θ_w = volumetric water content,
- θ_s = volumetric water content at saturation
- $e = 2.718,$
- $(u_a - u_w)$ = soil suction,
- a_s = soil parameter approximating the air entry of the soil,
- n_s = soil parameter related to the rate of desaturation,
- m_s = soil parameter related to residual water content conditions, and

$C(u_a - u_w)$ = correction factor to ensure that the function goes through 1 000 000 kPa of suction at zero water content.

The soil parameters defining the soil-water characteristic curve are also shown on Fig. 7. The soil-water characteristic curve can then be used to compute approximate soil property functions for unsaturated soils. Examples are the coefficient of permeability function, the coeffi-

cient of water volume change function and the shear strength function (Fredlund 1995).

While it is relatively easy to measure the soil-water characteristic curve in the laboratory, it is still quite costly, and the test has not found its way into most conventional soils laboratories. For this reason, an examination should be made of the possibility of using grain size distribution classification test data for the prediction of the soil-water characteristic curve. Once again, this procedure will give rise to an approximation and this must be taken into consideration when using this technique. With further research it should be possible to gain increasing confidence in using the grain size distribution curve to predict the soil-water characteristic curve.

Determination of unsaturated soil property functions

There are several approaches that can be taken for the determination of unsaturated soil properties. Each approach has its advantages and its disadvantages. The disadvantages and advantages can usually be expressed in terms of the cost to perform the test and the accuracy of the results. For example, it would generally be conceded that *in situ* testing to determine a particular soil property may provide the most representative measurement of a particular soil property. However, the difficulty and cost of performing such a test would likely make the measurement of the soil property prohibitive in most cases. Therefore, the laboratory testing of undisturbed soil samples provides a compromising measurement.

Figure 8 shows that several approaches are possible when performing a laboratory testing program for the determination of unsaturated soil property functions. The term, unsaturated soil property functions, refers to such relationships as: (1) the coefficient of permeability versus soil suction, (2) the water storage variable versus soil suction, and (3) the shear strength versus soil suction.

The first class of laboratory tests involves the direct measurement of the required unsaturated soil property. For example, it may be a (modified) direct shear test to measure the relationship between matric suction and

Fig. 7. Definition of variables associated with the soil-water characteristic curve.

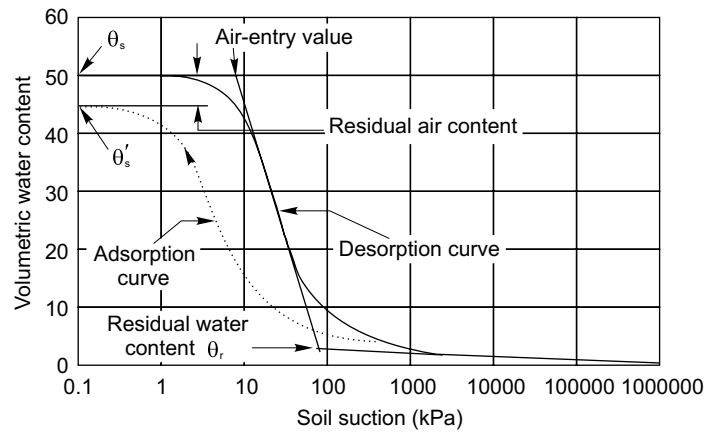
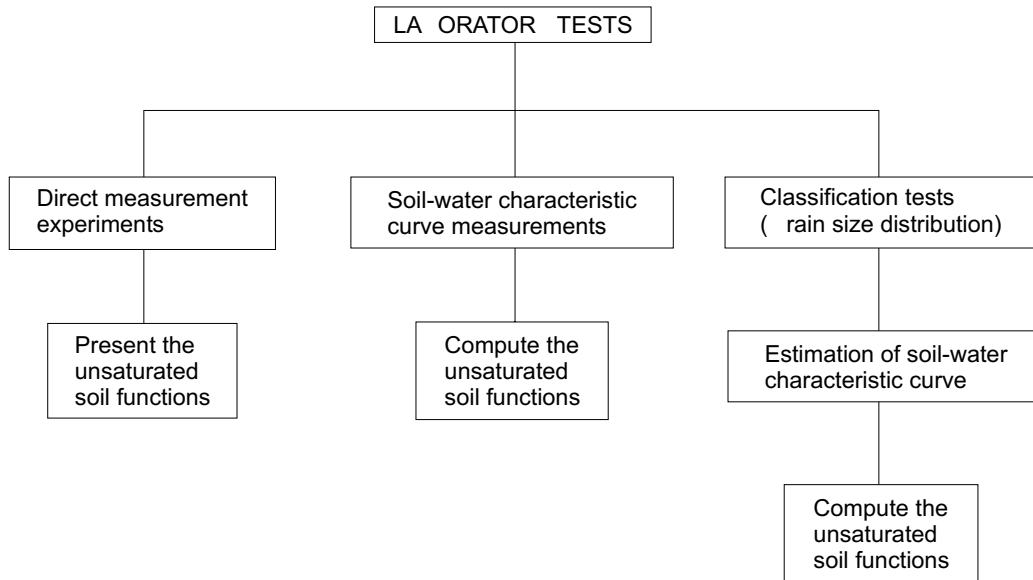


Fig. 8. Approaches that can be used in the laboratory to determine the unsaturated soil properties.



shear strength (Fig. 9). These tests can be costly and the necessary equipment may not be available. Therefore, it may be sufficient to revert to a second class of laboratory tests involving the measurement of the soil-water characteristic curve (SWCC) for the soil (Fig. 10). The soil-water characteristic curve can then be used in conjunction with the saturated shear strength properties of the soil, to predict the relationship between shear strength and matric suction (Fig. 11). Some accuracy will likely be lost in reverting to this approach; however, the trade-off between accuracy and cost may be acceptable. In this case, the desired unsaturated soil property function has been indirectly determined from a physical property measurement.

Figure 8 shows a third class of laboratory test which can be used to provide a determination for the desired unsaturated soil property function. In this case, a classification test such as a grain size analysis (Fig. 12) is used to estimate the soil-water characteristic curve (Fig. 13) which in turn is used to determine the unsaturated soil property function (Fig. 14). Once again, the cost of the

testing program is reduced but at the same time, the accuracy of the final prediction is also reduced. While there is a reduction in the accuracy of the predicted unsaturated soil property function, the engineer must assess whether or not the approximated soil function is satisfactory for the analyses which must be performed. In general, it would appear that it is better to perform the necessary analyses using approximate determinations of the unsaturated soil property functions, than not to perform engineering analyses.

The use of the grain size distribution curve for the prediction of the soil-water characteristic curve would appear to be more acceptable for coarse-grained soils than for clayey soils. Secondary structure, in particular, may render predictions of the soil-water characteristic curves unreliable.

Figure 15 illustrates how one of several approaches can be used to determine the unsaturated soil property functions when using the classification and/or soil-water characteristic curve to compute the unsaturated soil property

Fig. 9. Experimental measurement of the shear strength versus suction relationship for a compacted glacial till; implementing procedure 1 (after Vanapalli 1994).

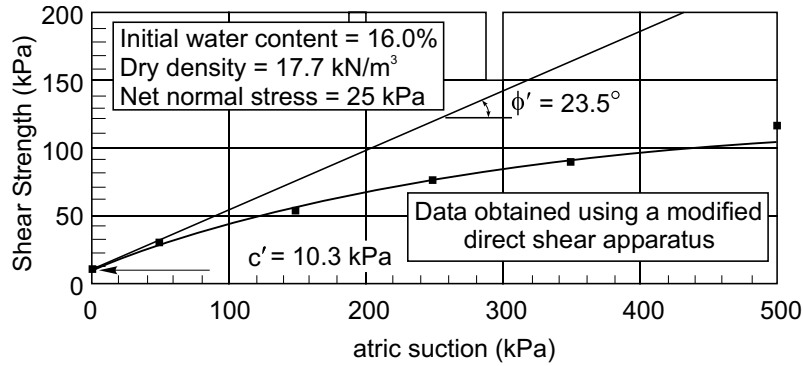


Fig. 10. Experimental measurement of the soil-water characteristic curve for a compacted glacial till; implementing procedure 2 (after Vanapalli 1994).

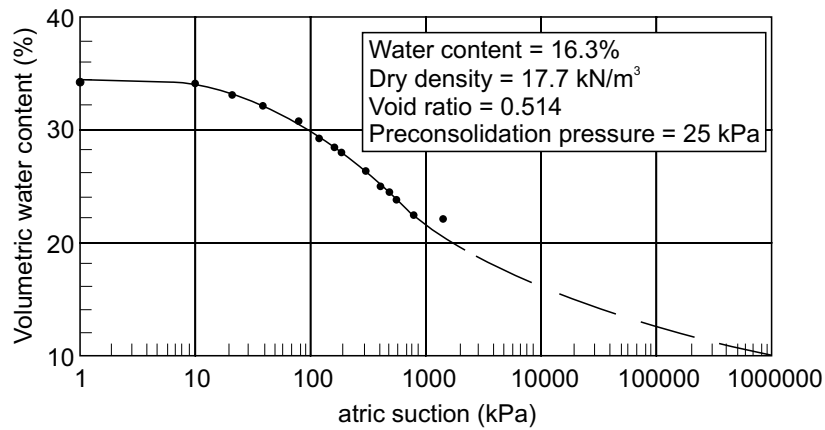


Fig. 11. Prediction of the unsaturated shear strength function from the soil-water characteristic curve; implementing procedure 2 (after Vanapalli 1996).

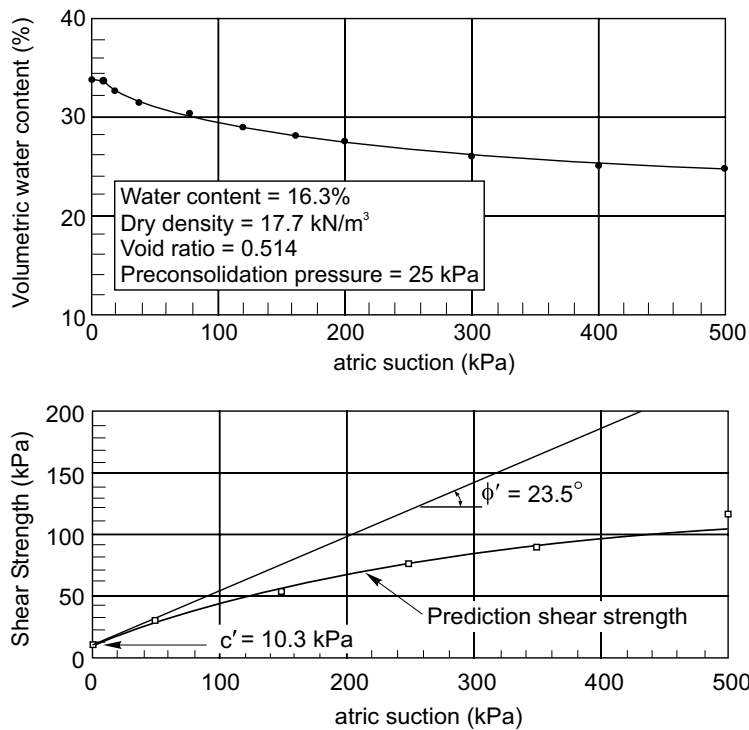


Fig. 12. Selection of series of soils from a database belonging to a particular soil classification; implementing procedure 3.

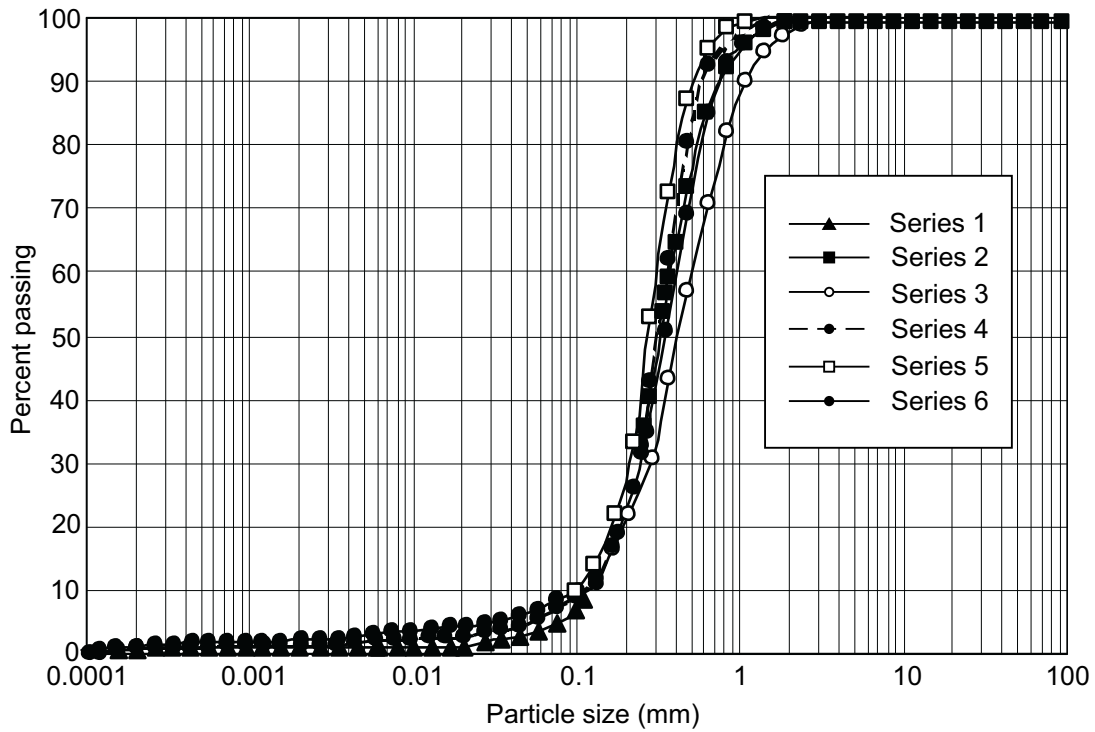
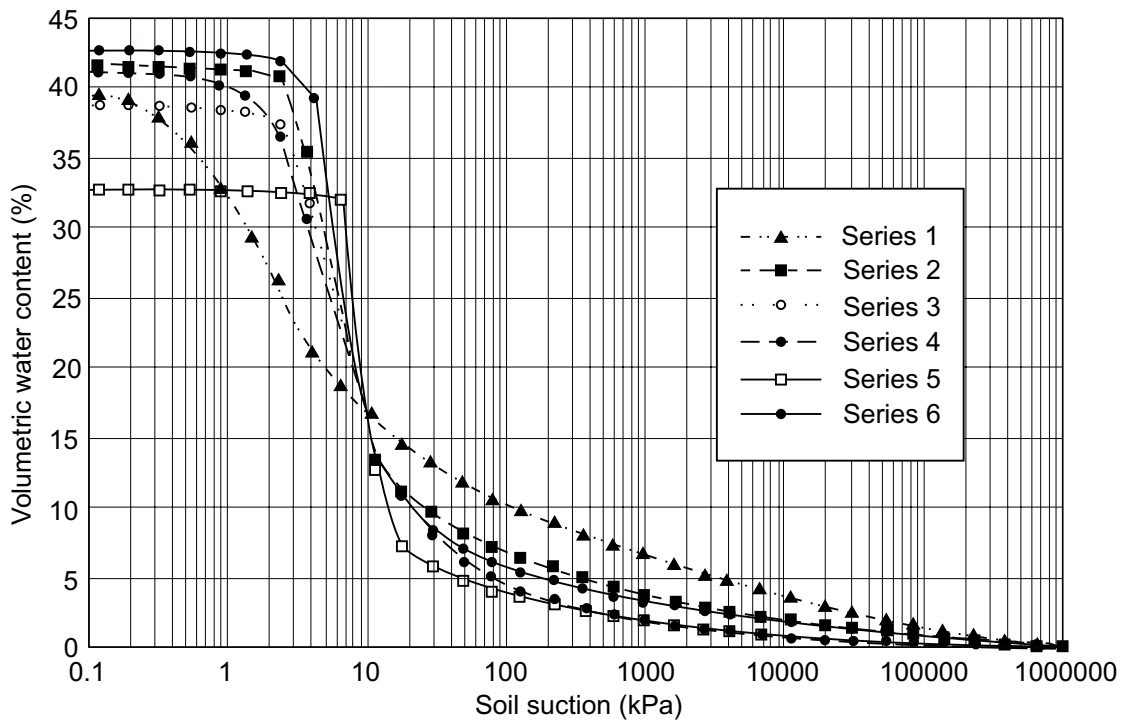


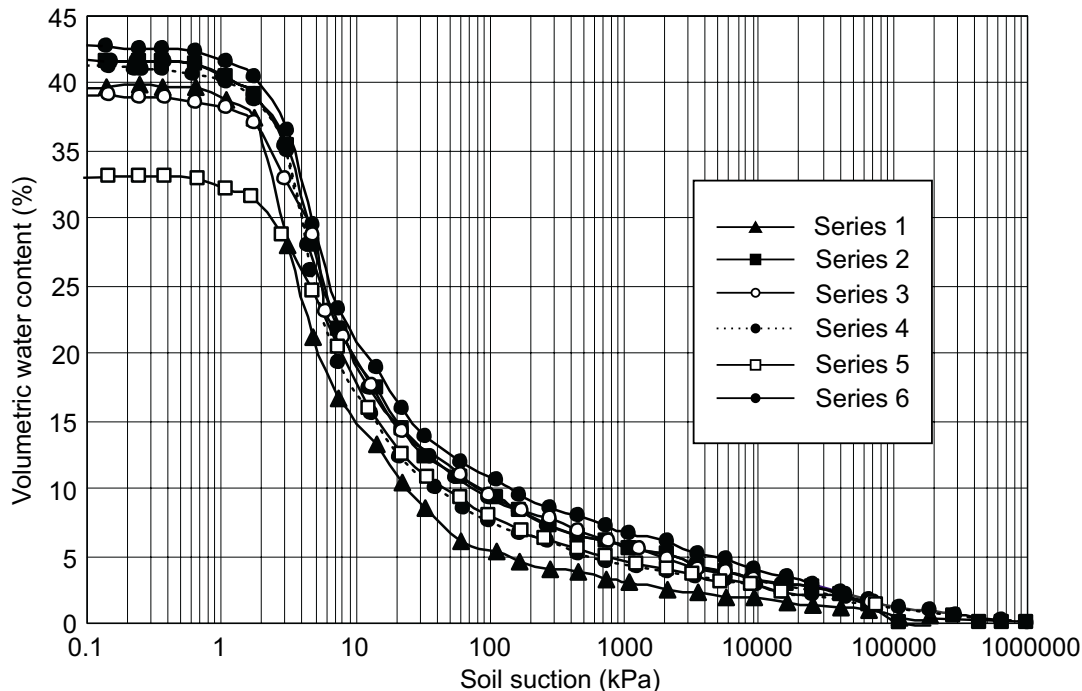
Fig. 13. Selection of soil-water characteristic curve from a database, corresponding to the selected grain size curves; implementing procedure 3.



functions. Plausible procedures can best be viewed within the context of a knowledge-based system. In this way, ongoing use is made of data accumulated from other laboratory studies. The first suggested procedure involves

matching measured soil-water characteristic curves with soil-water characteristic curves already in the data base. The measured soil-water characteristic curves can be either used to compute unsaturated soil property functions

Fig. 14. Predicted soil-water characteristic curves corresponding to the selected grain size distribution curves; implementing procedure 3.



or used to select unsaturated soil property functions already in the data base. It is also possible to use both the computed and the selected soil property functions in arriving at suitable functions for analysis purposes.

The second suggested procedure involves matching measured classification properties (i.e., grain size distribution curves) with classification properties already in the data base. Once one or more soils have been found, corresponding soil-water characteristic curves can be retrieved from the data base. These SWCC data can be used to compute suitable unsaturated soil property functions or existing unsaturated soil property functions can be retrieved from the data base.

The third suggested procedure involves working directly with the measured grain size distribution curve. There may also be some value in comparing the grain size distribution curve to grain size distribution curves in the data base. Soil-water characteristic curves are then computed and compared to soil-water characteristic curves in the data base. A decision is made regarding a reasonable soil-water characteristic curve and then the unsaturated soil property functions are computed.

Each of the above suggested procedures becomes increasingly less precise. The procedure used in each case will depend to a degree upon the nature of the study being undertaken. The above suggested procedures may at first appear to simply involve a series of approximations. However, the approach being suggested can also be viewed as being totally consistent with developments in the use of knowledge-based systems, operations research and the use of critical state soil mechanics. Critical state soil mechanics is a more recent approach to soil mechanics problems which involves a series of assumptions

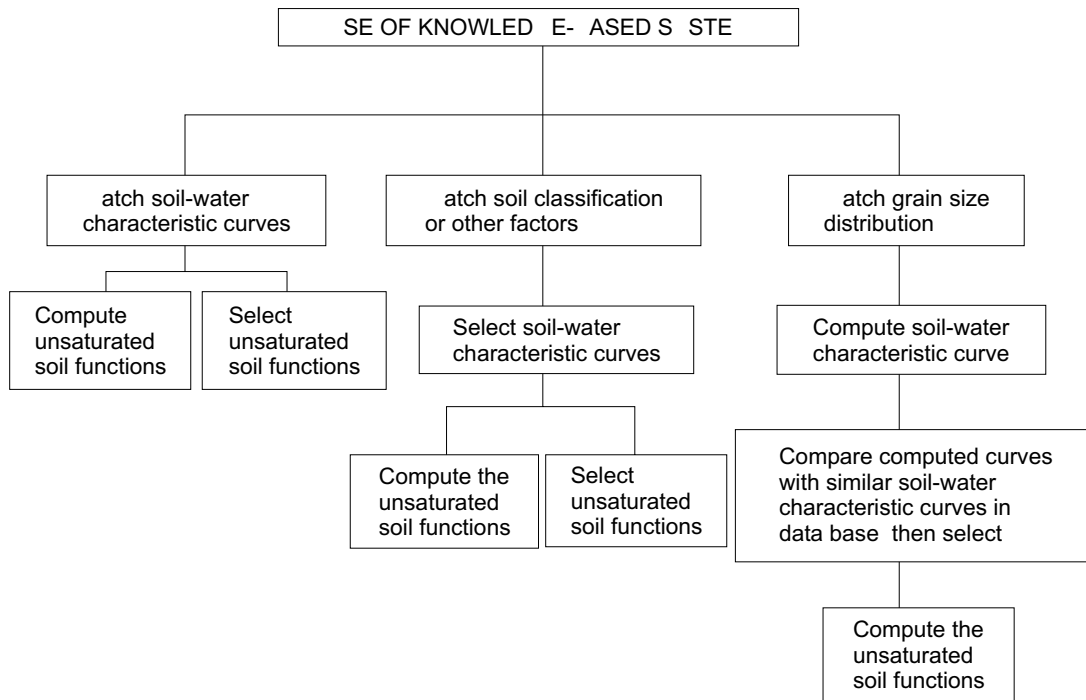
which are approximations (Wood 1990). And while critical state soil mechanics is generally applied as an approximate model, it still forms a very useful model for soil mechanics analyses.

Relationship between unsaturated soil mechanics analyses and microcomputers

Saturated soil mechanics developed as a science subsequent to 1936 when the stress state for a saturated soil was defused by Terzaghi. A science for unsaturated soils began to emerge around 1960 (Bishop et al. 1960). The complete formulations for the classic areas of soil mechanics were assembled and published primarily in the 1970's (Fredlund 1979). The stress state variables for an unsaturated soil were theoretically and experimentally tested by the mid 1970's. The volume change constitutive relations were also verified experimentally by the mid 1970's while the shear strength constitutive relationship was confirmed by the late 1970's. These constitutive relations proved, in general, to be nonlinear.

The nonlinear formulations for unsaturated soil mechanics problems result in the need to use an iterative procedure when solving numerical problems. Nonlinear numerical models for steady state and transient seepage problems involving unsaturated soil became common place in the mid 1980's. It was not possible to provide the engineer with simple equations and closed form solutions. In general, it was necessary to use a digital computer to obtain solutions. In other words, it was not possible to provide the engineer with solutions to boundary value type problems until the computer was readily available.

Fig. 15. Approaches that can be used to determine the unsaturated soil property functions when using classification tests and a database.



Many of the unsaturated soils problems also require a knowledge of the ground surface moisture flux boundary conditions. In particular, it was necessary to be able to determine the evaporative flux from the soil surface. The evaporative flux could be approximated by simultaneously solving the heat and mass transfer partial differential equations for near ground surface conditions. This solution was computationally intensive and became available around 1990. Analytical procedures became available for the estimation of unsaturated soil property function in the early 1990's. The rapid development of the fundamental theories for unsaturated soil behaviour relied heavily upon the application of the computer. The relationship between the development of unsaturated soils engineering and the increase in computing power is shown in Fig. 16.

Mainframe computers became available in most universities in the 1960's. By the late 1960's, there were a number of computer programs written for geotechnical problems. It was not until the late 1970's that personal computers were introduced into the marketplace. But it was in the 1980's that it became practical to use microcomputers to solve large nonlinear geotechnical problems. Figure 16 shows the rate at which computing power has grown over the past few decades (Gates 1995).

This brief review of the development of unsaturated soil mechanics and the development of computers, shows that both areas developed at essentially the same time. This is rather fortuitous since powerful microcomputers are necessary in order to obtain solutions to unsaturated soil mechanics problems. Today, the computing power available to geotechnical engineers is fully adequate for the solution of large, saturated/unsaturated numerical

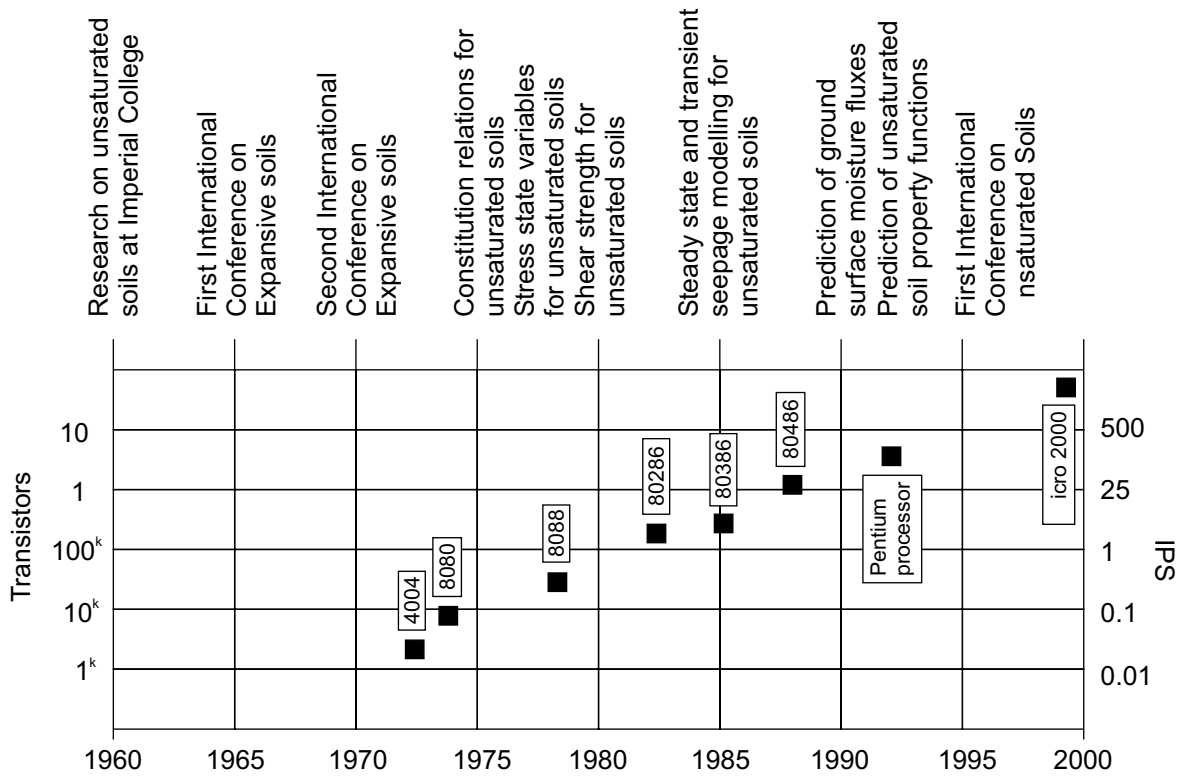
models. The engineer can no longer complain of inadequate computing capabilities as a reason for not implementing unsaturated soil mechanics into engineering practice. Now, the more pressing concern of the engineer is related to the assessment of suitable input soil properties and soil property functions.

The practice of soil mechanics paradigm shift

The old soil mechanics paradigm developed between the 1930's and the 1970's. Under the old soil mechanics paradigm, a typical slope stability problem would be approached as follows. A field subsurface investigation program would be undertaken in an attempt to define the stratigraphy, obtain disturbed and undisturbed soil samples for laboratory testing, and necessary steps would be taken to define the hydrogeologic conditions. The laboratory tests on the disturbed samples were for classification of the soil. The laboratory tests on the undisturbed samples were used to define physical soil parameters such as cohesion and the angle of internal friction. The emphasis was on measuring the soil mechanics parameters as accurately as possible with an attempt to be more and more meticulous in their definition. A characteristic of the old paradigm was the emphasis on the measurement of the soil properties; whether in the laboratory or *in situ*.

A slope stability analysis would then be performed assuming that the region above the groundwater table had no influence on the analytical study. In other words, the unsaturated soil region was assumed to be saturated with zero pore-water pressures. The influence of the climate,

Fig. 16. Correspondence of the development of unsaturated soil mechanics to computing power.



and infiltration into the soil, would in general, not be taken into consideration.

The advent of powerful microcomputers gave rise to a new approach to most soil mechanics problems. However, the new soil mechanics paradigm is not simply related to the ability to solve more complex problems using increasingly sophisticated constitutive models. The primary new characteristic identifying the new soil mechanics paradigm is the place where emphasis is placed by the engineer. The computer has brought with it the ability to move towards studying many possible scenarios and many possible and varied stress conditions. The engineer now asks himself a series of: "What if — ?" types of questions and studies their influence on the solutions and design considerations. The engineering approach has moved, consciously or unconsciously, from a mainly deterministic approach to soil mechanics problems to a more probabilistic (or parametric) approach.

The new soil mechanics paradigm can quickly study the effects of a wide range of possible conditions. The cost of performing sophisticated laboratory tests has become prohibitive in many cases and the emphasis has moved towards determining acceptable estimation techniques that will embrace possible soil conditions. In so doing, the engineering design will reflect a spectrum of possible soil property and boundary conditions. In other words, the microcomputer has changed the entire approach to solving geotechnical problems.

Another important characteristic of the new soil mechanics paradigm is the emphasis on simultaneously modelling both the saturated and the unsaturated portions

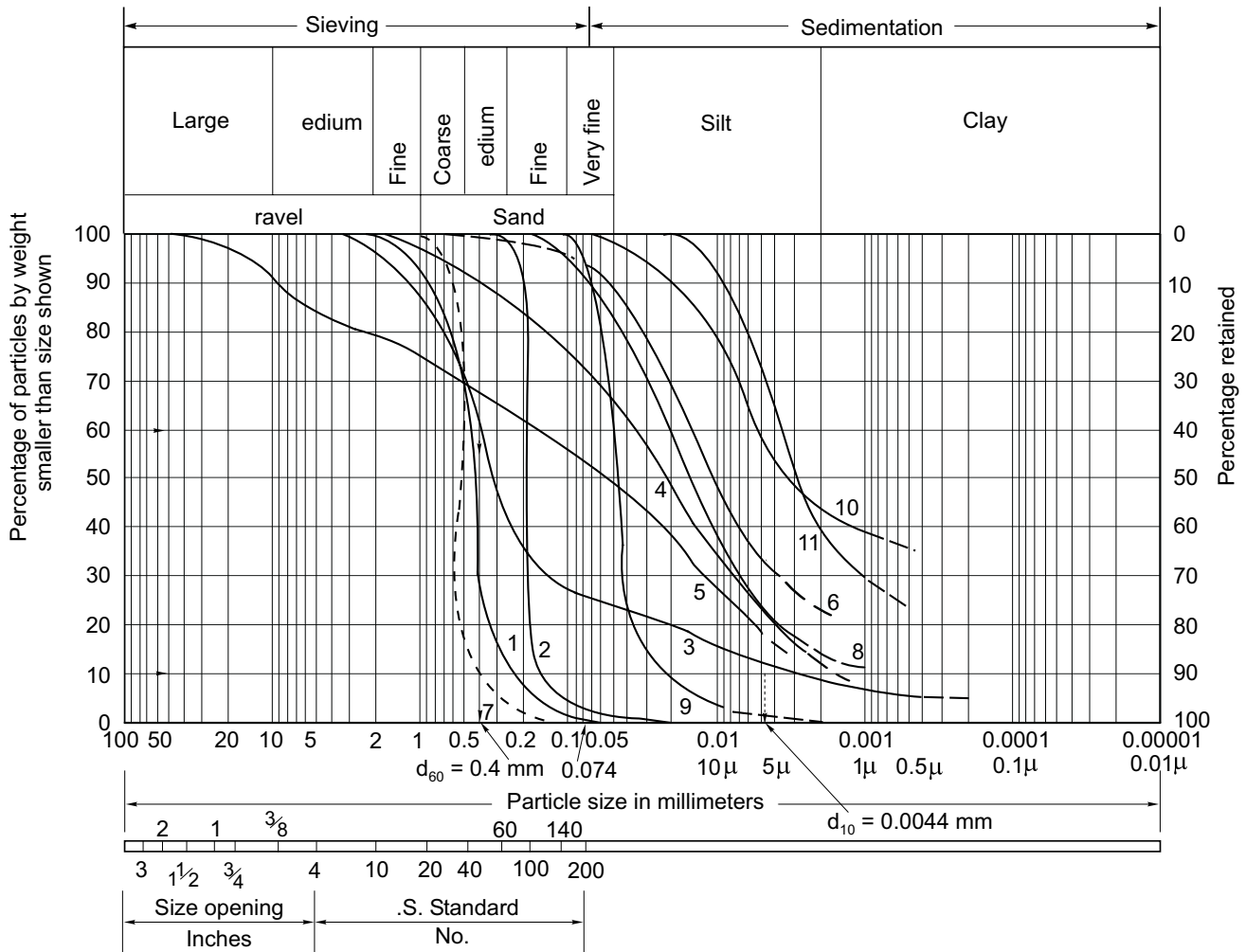
of the soil profile. The computer is playing an increasing role in the estimation of suitable soil property functions for unsaturated soils. The use of knowledge-based software systems has an important role to play in implementing unsaturated soil mechanics into the new soil mechanics paradigm.

Back to soil classification (grain size distribution curve)

The most widely accepted soil classification system in geotechnical engineering is the Unified Soil Classification System. The system is based on the plasticity and the grain size distribution of a soil. The plasticity and grain size distribution are both considered to be important; however, grain size distribution takes on an increased importance when dealing with unsaturated soils. The grain classification test provides information on the particle size distribution of the soil solids. Of greater importance to the engineer, however, is the pore size distribution which can be visualized as the inverse of the solids distribution.

The grain size distribution curve has been partitioned according to particle sizes (i.e., % clay size <0.002 mm, % silt sizes, % sand sizes). In addition to knowing the particle size divisions there is value in fitting a mathematical equation through the grain distribution points. The grain size distribution curve generally possesses a characteristic S-shape but may deviate from this shape when the soil is gap graded.

Fig. 17. Typical grain size curves for several soils (after Jumikis 1967).



- | | |
|---|---------------------------------|
| 1. Cape May N.J. sand | 7. Lewis beach Del. sand |
| 2. Daytona beach Florida sand | 8. Neissic rock flour N.P. N.L. |
| 3. Dunellen N.J. silty sand | 9. Fine silty sand N.J. |
| 4. Montalto N.J. sandy silt | 10. Raritan clay N.J. |
| 5. Pennsylvania Pike Del. silty gravelly sand | 11. Varved clay N.J. |
| 6. Delaware Memorial ridge Del. sand from bridge approach | |

The mathematical equation forms that have been used for describing the soil-water characteristic curve are also suitable for fitting the grain size distribution curve. One of several equation forms could be used; however, reference will only be made to the above mentioned eq. [1] proposed by Fredlund and Xing (1994). The advantage of eq. [1] lies in its ability to characterize the two extremes of the function independently. As such, the portion describing the coarse fraction can be different in character from that describing the fine fraction.

The Fredlund and Xing (1994) equation (i.e., eq. [1]) uses three parameters and a correction factor to define a mathematical function. The meaning of the parameters has been described in relation to the soil-water character-

istic curve but these parameters need to be redefined with respect to the grain size distribution curve.

$$[2] \quad P(d, a_s, n_s, m_s) = C(d) \frac{100}{\{\ln[e + (d/a_s)^{n_s}]\}^{m_s}}$$

where:

- P = percent passing
- 100 = represents 100 percent passing
- $e = 2.718...$
- d = diameter of the particles, mm
- a_s = parameter approximating the large particle in the distribution

Table 1. Summary of soil parameters for some typical soils.

Sample No.	Description	Gravel	Sand	Clay	a_s	n_s	m_s
1	Sand, Cape May, NJ	7	93	0	0	0.461	2.13
2	Sand, Dayton Beach, FL	0	99	1	0	0.158	2.92
3	Sand silt, Dunellen, NJ	13	63	17	7	0.609	0.943
4	Sandy, slit, Montalto, NJ	3	29	56	12	0.0166	2.91
5	Silty, gravelly sand, DW	25	28	38	9	0.037	3.23
6	Sand, Delaware Mem.	0	8	70	22	0.021	1.07
7	Sand, Lewis Beach, DW	1	99	0	0	0.469	6.24
8	Gneiss Rock Flour, NL	0	13	74	13	0.0246	1.31
9	Fine silty sand, NJ	0	65	34	1	0.0468	1.38
10	Raritan clay, NJ	0	2	55	43	0.0122	0.566
11	Varved clay, NJ	0	0	62	38	0.0055	0.781

n_s = parameter related to the uniformity of the particle size distribution, (note the similarity to the uniformity coefficient C_u).

m_s = parameter related to the residual particle portion, and

$C(d_f)$ = correction factor to ensure that the function intercepts a lower limit particle diameter of 0.00001 mm.

Correlations for the various soil parameters defining the grain size curve, (i.e., a_s , n_s , and m_s) can be obtained by performing best-fit studies on existing databases. Figure 17 shows a series of typical grain size distribution curves for soil ranging from fine to coarse and from well-graded to poorly graded. Each of the grain size distribution curves was best-fit with eq. [2]. The parameters for each soil are listed in Table 1 along with the particle size percentages.

Figure 18 shows the best-fit particle size equation for soil No. 6 (Delaware sand). The solid line represents the best-fit equation results while the symbols are the experimental data points. It is possible to obtain close agreement between the data points and the best-fit equation as long as the particle size distribution is not gap graded. The best-fit equations for all 11 soils are shown in Fig. 19. The best-fit parameters, listed in Table 1, show that there are relationships between the character of the grain size distribution curve and the best-fit parameters. For example, a uniform soil has a high n_s parameter. Soil No. 2. is extremely uniform and yields an n_s value in excess of 30. Soil No. 5 is well-graded and yields an n_s value of 0.46. The a_s values range from 0.61 mm to 0.0055 mm and represent the largest particle size in the soil particle distribution. The m_s values range from 0.56 to 6.2 and are related to the finer particle sizes of a particular grain size distribution. There is need for further studies in order to gain a better understanding of the meaning of the new parameters for the grain size distribution curve. These parameters are useful when attempting to perform a search for similar soils in an existing data base. The soil parameters allow the grain size distribution of a soil to be represented as a continuous mathematical function for further analysis.

The grain size curve can provide valuable information on the pore size distribution of the soil. This is true only to a degree, and the volume-mass properties must also be taken into consideration in the form of a “packing factor”.

Mathematically characterizing the grain size curve provides a more definite way of defining the particle size distribution. It provides a mathematical function and thereby forms the basis for a theory to estimate the pore-size distribution. Several attempts have been made to characterize the pore-size distribution from the grain size distribution (Gupta and Larson 1979; Ghosh 1980; Arya and Paris 1981; Ahuja et al. 1985; Haverkain and Parlange 1986). Information on the pore size distribution in turn, allows for the estimation of the soil-water characteristic curve of a soil.

The decision: To use or not to use unsaturated soil mechanics analyses

Taking unsaturated soil mechanics from the realm of theory and formulations into the realm of engineering practice rests upon our ability to provide economically viable means of determining unsaturated soil property functions. If the unsaturated soil property functions can be estimated or computed from tests which are not too costly, unsaturated soil mechanics should enjoy a much greater degree of acceptance in practice.

There is need for further teaching and training in the methods of determining unsaturated soil property functions. There is need for the development of knowledge-based software which will allow use to be made of past test results on soils. There is need for engineers to realize that the practice of soil mechanics (and particularly unsaturated soil mechanics) is going through a paradigm shift; a change in which the computer and numerical modelling are playing an important role. The decision rests with the engineering profession and centers around whether or not engineers will make even greater use of soil mechanics analyses when making engineering decisions.

Fig. 18. Experimental and theoretically fitted grain size curve for soil No. 6 from Jumikis (1967).

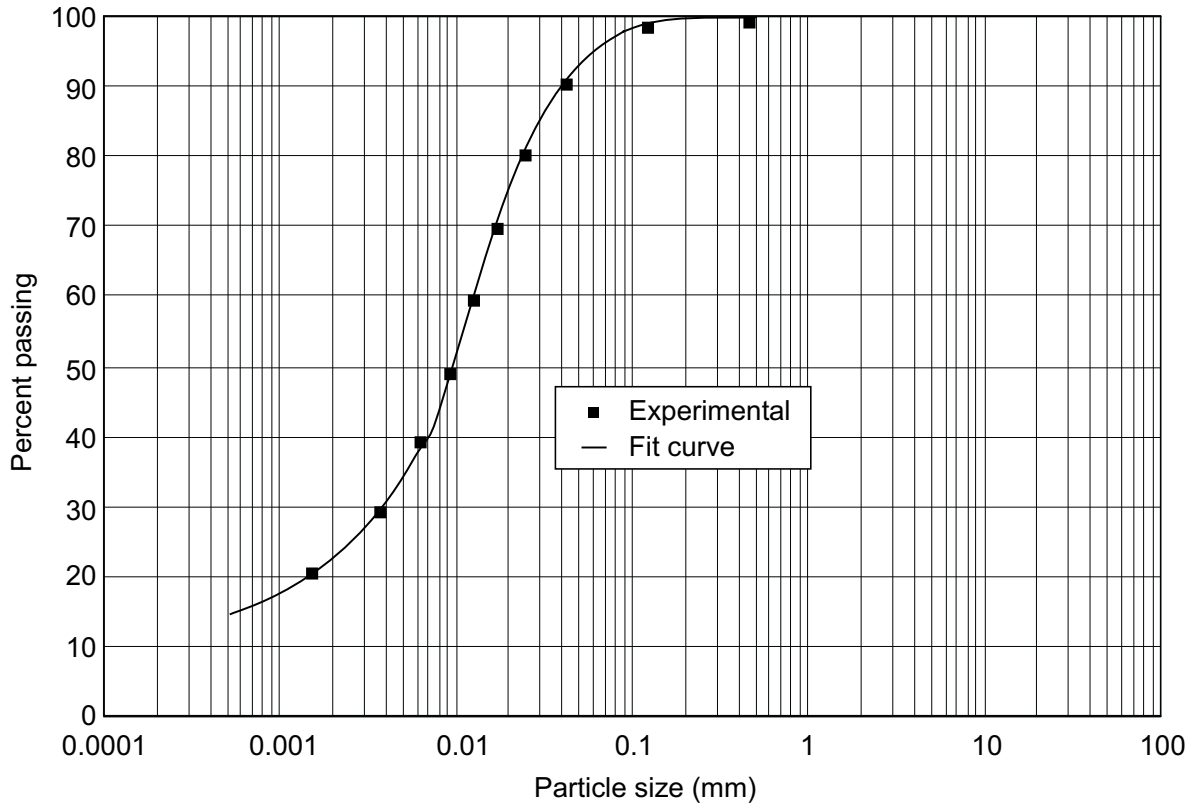
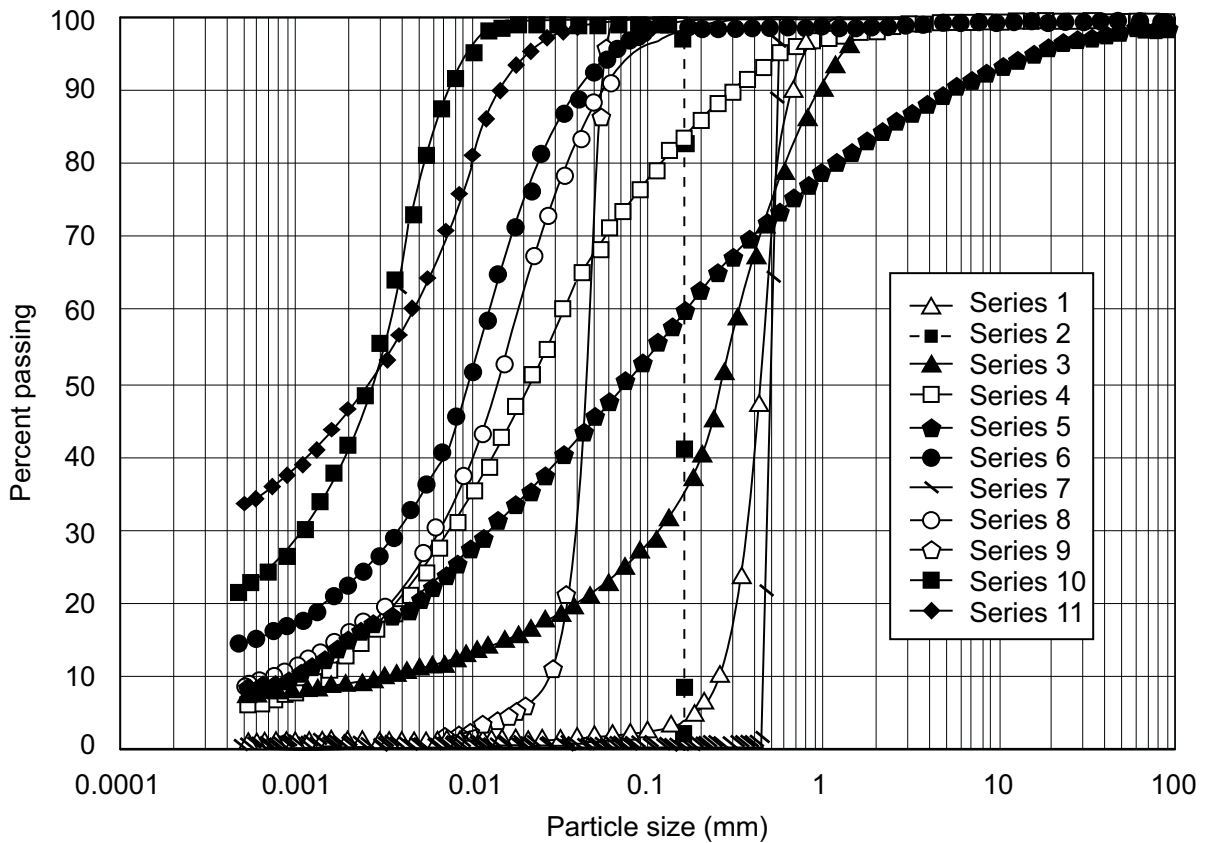


Fig. 19. Theoretically fitted grain size curves for the soils from Jumikis (1967).



References

- Ahuja, L.R., Naney, L.W., and Williams, R.D. 1985. Estimating soil-water characteristics from simpler properties and limited data. *Soil Science of America Journal*, **49**: 1100–1105.
- Arya, L.M., and Paris, J.F. 1981. A physicoempirical model to predict the soil moisture characteristic from particle size distribution and bulk density data. *Soil Science Society of America Journal*, **45**: 1023–1030.
- Bishop, A.W., Alpan, T., Blight G.E., and Donald, T.B. 1960. Factors controlling the shear strength of partly saturated cohesive soils. Proceedings, ASCE Research Conference on Shear Strength of Cohesive Soils, University of Colorado, Boulder, pp. 503–532.
- Fredlund, D.G. 1979. Appropriate concepts and technology for unsaturated soils. Second Canadian Geotechnical Colloquium, *Canadian Geotechnical Journal*, **16**(1): 121–139.
- Fredlund, D.G. 1995. The scope of unsaturated soils problems. Proceedings, 1st International Conference on Unsaturated Soils, Paris, September 6–8, Vol. 3, pp.1155–1177.
- Fredlund, D.G. 1996. Microcomputers and saturated/unsaturated continuum modelling in geotechnical engineering. Symposium on Computers in Geotechnical Engineering, INFOGEO '96, Sao Paulo, Brazil, August 28–30, Vol. 2, pp. 29–50.
- Fredlund, D.G., and Morgenstern, N.R. 1977. Stress state variables for unsaturated soils. *ASCE Journal of Geotechnical Engineering Division*, **103**(GT5): 447–466.
- Fredlund, D.G., and Rahardjo, H. 1993. *Soil mechanics for unsaturated soils*. John Wiley & Sons, New York.
- Fredlund, D.G., and Xing, A. 1994. Equations for the soil-water characteristic curve. *Canadian Geotechnical Journal*, **31**: 521–532.
- Fredlund, M.D., Sillers, W., Fredlund, D.G., and Wilson, G.W. 1996. Design of a knowledge-based system for unsaturated soil properties. Proceedings, 3rd Canadian Conference on Computing in Civil Engineering, August 26–28, Montreal, Quebec, pp. 659–677.
- Gates, W.H. 1995. *The road ahead*. Quebor Printing/Faiffield Inc., Allentown, PA. 286p.
- Ghosh, R.K. 1980. Estimation of soil moisture characteristics from mechanical properties of soils. *Soil Science Journal*, **130**(2): 60–63.
- Ghosh, S.C., and Larson, W.E. 1979. Estimating soil water retention characteristics from particle size distribution, organic matter percent, and bulk density. *Water Resources Research Journal*, **15**(6): 1633–1635.
- Gupta, S.C., and Larson, W.E. 1979. Estimating soil water retention characteristics from particle size distribution, organic matter percent, and bulk density. *Water Resources Research Journal*, **15**(6): 1633–1635.
- Haverkamp, R., and Parlange, J.Y. 1986. Predicting the water-retention curve from particle-size distribution: 1. Sandy soils without organic matter. *Soil Science Journal*, **142**(6): 325–339.
- Jumikis A.R. 1967. *Introduction to soil mechanics*. D. Van Nostrand Co. Inc., Princeton, N.J., 436p.
- Peck, R.B. 1969. Advantages and limitations of the observational method in applied soil mechanics. *Géotechnique*, **19**(2): 171–187.
- Vanapalli, S.K. 1994. Simple test procedures and their interpretation in evaluating the shear strength of unsaturated soils. Ph.D. thesis, University of Saskatchewan, Saskatoon, SK, Canada.
- Vanapalli, S.K. 1996. Model for the prediction of shear strength with respect to soil suction. *Canadian Geotechnical Journal*, **33**: 379–392.
- Wood, D. M. 1990. *Soil behaviour and critical state soil mechanics*. Cambridge University Press, Cambridge.

Equations for the soil-water characteristic curve

D.G. Fredlund and A. Xing

Abstract: The soil-water characteristic curve can be used to estimate various parameters used to describe unsaturated soil behaviour. A general equation for the soil-water characteristic curve is proposed. A non-linear, least-squares computer program is used to determine the best-fit parameters for experimental data presented in the literature. The equation is based on the assumption that the shape of the soil-water characteristic curve is dependent upon the pore-size distribution of the soil (i.e., the desaturation is a function of the pore-size distribution). The equation has the form of an integrated frequency distribution curve. The equation provides a good fit for sand, silt, and clay soils over the entire suction range from 0 to 10^6 kPa.

Key words: soil-water characteristic curve, pore-size distribution, non-linear curve fitting, soil suction, water content.

Introduction

A theoretical framework for unsaturated soil mechanics has been established over the past two decades. The constitutive equations for volume change, shear strength, and flow through unsaturated soil have become generally accepted in geotechnical engineering (Fredlund and Rahardjo 1993a). The measurement of soil parameters for the unsaturated soil constitutive models, however, remains a demanding laboratory process. For most practical problems, it has been found that approximate soil properties are adequate for analysis (Papagiannakis and Fredlund 1984). Hence, empirical procedures to estimate unsaturated soil-parameters would be valuable.

Laboratory studies have shown that there is a relationship between the soil-water characteristic curve for a particular soil and the properties of the unsaturated soil (Fredlund and Rahardjo 1993b). For example, it has become an acceptable procedure to predict empirically the permeability function for an unsaturated soil by using the saturated coefficient of permeability and the soil-water characteristic curve (Marshall 1958; Mualem 1986; University of Saskatchewan 1984). Similar procedures have been suggested for the shear strength properties of an unsaturated soil (Fredlund and Rahardjo 1993b). Since the soil-water characteristic curve is used as the basis for the prediction of other unsaturated soil parameters, such as the permeability and shear-strength functions, it is impor-

tant to have a reasonably accurate characterization of the soil-water characteristic curve.

This paper reviews the forms of mathematical equations that have been suggested to characterize the soil-water characteristic curve. It appears that none of the suggested equations accurately fit laboratory data over the entire suction range. This paper proposes a new equation that can be used to fit laboratory data over the entire soil suction range. A mathematical basis for the equation is described and a best-fit procedure is outlined to obtain the parameters for the equation.

Definitions¹

The soil-water characteristic curve for a soil is defined as the relationship between water content and suction for the soil (Williams 1982). The water content defines the amount of water contained within the pores of the soil. In soil science, volumetric water content, θ , is most commonly used. In geotechnical engineering practice, gravimetric water content, w , which is the ratio of the mass of water to the mass of solids, is most commonly used. The degree of saturation, S , is another term commonly used to indicate the percentage of the voids that are filled with water. The above variables have also been used in a normalized form where the water contents are referenced to a residual water content (or to zero water content).

D.G. Fredlund. Professor, Department of Civil Engineering, University of Saskatchewan, 57 Campus Drive, Saskatoon, SK, Canada S7N 5A9.

A. Xing. Research Associate, Department of Civil Engineering, University of Saskatchewan, 57 Campus Drive, Saskatoon, SK, Canada S7N 5A9.

Reproduced with permission from the *Canadian Geotechnical Journal*, **31**(3): 521–532, 1994.

¹There are several soil terms that are used interchangeably in the literature. The terminology used in the paper is most consistent with that found in the geotechnical literature. Other terms are used in the geo-environmental, petroleum, and some of the soil science disciplines. Some of these equivalences are as follows: matric suction \equiv capillary pressure, air-entry value \equiv displacement pressure, and soil-water characteristic curve \equiv suction volumetric water content curve.

The suction may be either the matric suction (also known as capillary pressure) of the soil (i.e., $u_a - u_w$, where u_a is the pore-air pressure and u_w is the pore-water pressure) or total suction (i.e., matric plus osmotic suction). At high suctions (i.e., greater than about 1500 kPa), matric suction and total suction can generally be assumed to be equivalent.

As a result of the different terminologies used, the soil-water characteristic curves have taken on numerous forms. It is suggested that the term soil-water characteristic curve be used to represent the relationship between volumetric water content, θ , and matric suction. Volumetric water content test results in the low suction range are often presented using an arithmetic scale. Soil-water characteristic curves over the entire suction range are often plotted using a logarithmic scale.

Figure 1 shows a typical plot of a soil-water characteristic curve for a silty soil, along with some of its key characteristics. The air-entry value of the soil (i.e., bubbling pressure) is the matric suction where air starts to enter the largest pores in the soil. The residual water content is the water content where a large suction change is required to remove additional water from the soil. This definition is vague and an empirical procedure for its quantification would be useful. A consistent way to define the residual water content is shown in Fig. 1. A tangent line is drawn from the inflection point. The curve in the high-suction range can be approximated by another line. The residual water content θ_r , can be approximated as the ordinate of the point at which the two lines intersect (Fig. 1). The total suction corresponding to zero water content appears to be essentially the same for all types of soils. A value slightly below 10^6 kPa has been experimentally supported for a variety of soils (Croney and Coleman 1961). This value is also supported by thermodynamic considerations (Richards 1965). In other words, there is a maximum total suction value corresponding to a zero relative humidity in any porous medium.

The main curve shown in Fig. 1 is a desorption curve. The adsorption curve differs from the desorption curve as a result of hysteresis. The end point of the adsorption curve may differ from the starting point of the desorption curve because of air entrapment in the soil. Both curves have a similar form; however, this paper primarily considers the desorption curve.

Typical soil-water characteristic curves (i.e., desorption curves) for different soils are shown in Fig. 2. The saturated water content, θ_s , and the air-entry value or bubbling pressure, $(u_a - u_w)_b$, generally increase with the plasticity of the soil. Other factors such as stress history also affect the shape of the soil-water characteristic curves.

Literature review

Numerous empirical equations have been proposed to simulate the soil-water characteristic curve. Among the earliest is an equation proposed by Brooks and Corey (1964). It is in the form of a power-law relationship:

Fig.1. Typical soil-water characteristic curve for a silty soil.

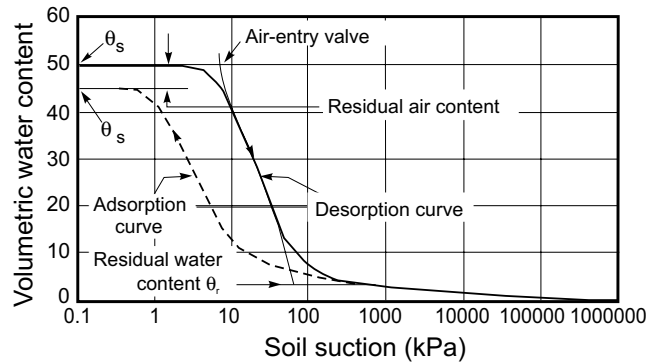
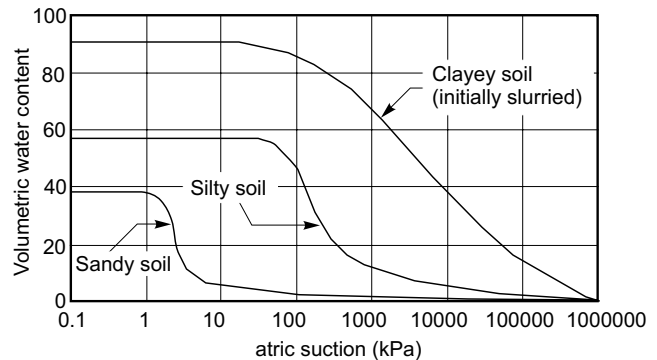


Fig. 2. Soil-water characteristic curves for a sandy soil, a silty soil, and a clayey soil.



$$[1] \quad \Theta = \left(\frac{\Psi_b}{\Psi} \right)^\lambda$$

where:

Θ = normalized (or dimensionless) water content (i.e., $\Theta = (\theta - \theta_r) / (\theta_s - \theta_r)$, where θ_s and θ_r are the saturated and residual volumetric water contents, respectively),

Ψ = suction,

Ψ_b = air-entry value, and

λ = pore-size distribution index.

The degree of saturation, S , has also been used in place of the normalized water content. Equation [1] has been verified through several studies (Campbell 1974; Clapp and Hornberger 1978, Gardner et al. 1970a, 1970b; Rogowski 1971; Williams et al. 1983; McCuen et al. 1981).

The following linear relationship between the logarithm of volumetric water content and the logarithm of suction was used by Williams et al. (1983) to describe the soil-water characteristic curve of many soils in Australia.

$$[2] \quad \ln \psi = a_1 + b_1 \ln \theta$$

where:

a_1 and b_1 = curve-fitting parameters.

McKee and Bumb (1984) suggested an exponential function for the relationship between the normalized water content and suction. This has been referred to as the Boltzmann distribution:

$$[3] \quad \Theta = e^{-(\Psi - a_2)/b_2}$$

where:

a_2 and b_2 = curve-fitting parameters.

Equations [1] and [3] have been found to be valid for suction values greater than the air-entry value of the soil. The equations are not valid near maximum desaturation or under fully saturated conditions. To remedy this condition, McKee and Bumb (1987) and Bumb (1987) suggested the following relationship:

$$[4] \quad \Theta = \frac{1}{1 + e^{(\Psi - a_3)/b_3}}$$

where:

a_3 and b_3 = curve-fitting parameters.

This equation gives a better approximation in the low suction range. The equation is not suitable in the high suction range, since the curve drops exponentially to zero at high suction values.

Equation [1] implies that there is a sharp discontinuity in suction near saturation. Although some coarse-grained sands may have a rapid change in suction at low suctions, most soils, particularly medium and fine textured soils, show a gradual curvature in the air-entry region near saturation. A modification of eq. [1] was suggested by Roger and Hornberger (1978) to account for gradual air entry. In the case where the volumetric water content is referenced to zero water content and the normalized volumetric water content, Θ , (i.e., θ / θ_s), is plotted as the abscissa, the general soil-water characteristic plot has an inflection point where the slope, $d\Psi / d\Theta$, changes from an increasing value to a decreasing value as Θ decreases. The inflection point is assigned the coordinates (Θ_i, Ψ_i) , and the interval $\Theta_i \leq \Theta \leq 1$ can be described by a parabola:

$$[5] \quad \Psi = -a_4(\Theta - b_4)(\Theta - 1)$$

where:

a_4 and b_4 = curve-fitting parameters.

The parameters a_4 and b_4 are obtained by forcing eq. [5] through the two points (Θ_i, Ψ_i) and $(1, 0)$. The slopes of both eq. [1] and eq. [5] are equal at the inflection point.

Another frequently used form for the relationship between suction and the normalized water content was given by van Genuchten (1980):

$$[6] \quad \Theta = \left[\frac{1}{1 + (p\Psi)^n} \right]^m$$

where:

p , n , and m = three different soil parameters.

This form of the equation gives more flexibility than the previous equations described. In an attempt to obtain a closed-form expression for hydraulic conductivity, van Genuchten (1980) related m and n through the equation $m = (1 - 1/n)$. This, however, reduces the flexibility of eq. [6]. More accurate results can be obtained by leaving m and n parameters with no fixed relationship.

Gardner (1958) proposed an equation for the permeability function. The equation emulates the soil-water characteristic curve and can be visualized as a special case of eq. [6]:

$$[7] \quad \Theta = \frac{1}{1 + q\Psi^n}$$

where:

q = curve-fitting parameter related to the air-entry value of the soil, and

n = curve-fitting parameter related to the slope at the inflection point on the soil-water characteristic curve.

Theoretical basis for the shape of the soil-water characteristic curve

The equations proposed in the research literature are empirical in nature. Each equation appears to apply for a particular group of soils. There are other equations of slightly differing forms that could be tested to assess their fit with experimental data. For example, the soil-water characteristic curve appears to have the form of the right-hand side of a normal-distribution curve. Therefore, the following equation can be used to approximate the soil-water characteristic curve:

$$[8] \quad \Theta = a_5 e^{-(b_5\Psi)^m}$$

where:

a_5 , b_5 , and m = curve-fitting parameters.

Equation [8] is not suitable as a general form, although it might apply for some soils over a limited range of suction values.

To establish a theoretical basis for the soil-water characteristic curve, let us consider the pore-size distribution curve for the soil. The soil may be regarded as a set of interconnected pores that are randomly distributed. The pores are characterized by a pore radius, r , and described by a function $f(r)$, where $f(r) dr$ is the relative volume of pores of radius r to $(r + dr)$. In other words, $f(r)$ is the density of pore volume corresponding to radius r . Since $f(r) dr$ is the contribution of the pores of radius r to $(r + dr)$ that are filled with water, the volumetric water content can be expressed as:

$$[9] \quad \theta(R) = \int_{R_{\min}}^R f(r) dr$$

where:

$\theta(R)$ = volumetric water content when all the pores with radius less than or equal to R are filled with water, and

R_{\min} = minimum pore radius in the soil.

Let R_{\max} denote the maximum pore radius. Then, for the saturated case:

$$[10] \quad \theta(R_{\max}) = \theta_s$$

The capillary law states that there is an inverse relationship between matric suction and the radius of curvature of the air-water interface. In other words, the air-water interface bears an inverse relationship to the pore size being desaturated at a particular suction:

$$[11] \quad r = \frac{C}{\psi}$$

where:

$C = (2T \cos \omega)$, a constant,

T = surface tension of water, and

ω = angle of contact between water and soil.

Two particular suction conditions can be defined as follows:

$$[12] \quad \psi_{\max} = \frac{C}{R_{\min}}$$

and

$$[13] \quad \psi_{\text{aev}} = \frac{C}{R_{\max}}$$

where:

ψ_{\max} = the suction value corresponding to the minimum pore radius, and

ψ_{aev} = the air-entry suction value of the soil.

Using the capillary law, eq. [9] can be expressed in terms of suction:

$$[14] \quad \theta(\psi) = \int_{\psi_{\max}}^{\psi} f\left(\frac{C}{h}\right) d\left(\frac{C}{h}\right) = \int_{\psi_{\max}}^{\psi} f\left(\frac{C}{h}\right) \frac{C}{h^2} dh$$

where:

h = variable of integration, representing suction.

Equation [14] is the general form describing the relationship between volumetric water content and suction. If the pore-size distribution, $f(r)$, of a soil is known, the soil-water characteristic curve can be uniquely determined by eq. [14]. Several special cases are as follows:

(1) Case of a constant pore size function

The pore sizes are uniformly distributed, that is, $f(r) = A$, where A is a constant. It follows, from eq. [14] that:

$$[15] \quad \theta(\psi) = \int_{\psi}^{\psi_{\max}} \frac{AC}{h^2} dh = AC \left(\frac{1}{\psi} - \frac{1}{\psi_{\max}} \right) = \frac{B}{\psi} - D$$

where:

$B = AC$, a constant, and

$D = AC / \psi_{\max}$, a constant.

(2) Case where pore-size function varies inversely as r^2

For the case of $f(r) = A / r^2$, the relationship between volumetric water content and suction is:

$$[16] \quad \theta(\psi) = \int_{\psi}^{\psi_{\max}} \frac{Ah^2}{C^2} \frac{C}{h^2} dh = B - D\psi$$

where:

$B = A\psi_{\max} / C$, a constant, and

$D = A / C$, a constant.

Equation [16] represents a linear variation in the pore sizes. In other words, there is a linear relationship between volumetric water content and suction.

(3) Case where pore-size function varies inversely as $r^{(m+1)}$

For the case of $f(r) = A / r^{(m+1)}$, where m is an integer, the relationship between volumetric water content and suction is:

$$[17] \quad \theta(\psi) = \int_{\psi}^{\psi_{\max}} \frac{Ah^{m+1}}{C^{m+1}} \frac{C}{h^2} dh = B - D\psi^m$$

where:

$B = A(\psi_{\max})^m / (mC^m)$, a constant, and

$D = A / (mC^m)$, a constant.

The power-law relationship (i.e., eq. [1]) proposed by Brooks and Corey (1964) is simply a special case of eq. [17]. In other words, the Brooks and Corey (1964) power-law relationship is valid only when the pore-size distribution is close to the distribution $f(r) = A / r^{m+1}$.

To describe the soil-water characteristic curve over the entire suction range from 0 to 10 sup 6 kPa, volumetric water content is referenced to zero water content (otherwise, the normalized water content becomes negative if θ is less than θ_s). In this case, the normalized water content Θ becomes θ / θ_s . Equation [14] suggests that the following integration form can be used as a general form to approximate the soil-water characteristic curve:

$$[18] \quad \theta(\psi) = \theta_s \int_{\psi}^{\infty} f(h) dh$$

where:

$f(h)$ = pore-size distribution as a function of suction.

Equation [18] will generally produce a non-symmetrical S-shaped curve. Several special cases are as follows.

(1) Case of a normal distribution

Let us assume that $f(h)$ is a normal distribution. That is:

$$[19] \quad f(h) = \frac{1}{\sqrt{2\pi}\sigma} e^{-(h-\mu)^2/2\sigma^2}$$

where:

μ = mean value of the distribution of $f(h)$, and
 σ = standard deviation of the distribution of $f(h)$.

The soil-water characteristic curve defined by eq. [18] can be expressed as follows:

$$[20] \quad \theta(\psi) = \theta_s \int_{\psi}^{\infty} f(h) dh = \frac{\theta_s}{2} \frac{2}{\sqrt{\pi}} \int_{(\psi-\mu)/\sqrt{2}\sigma}^{\infty} e^{-y^2} dy$$

$$= \frac{\theta_s}{2} \operatorname{erfc}\left(\frac{\psi-\mu}{\sqrt{2}\sigma}\right)$$

where:

$\operatorname{erfc}(x)$ = complement of the error function $\operatorname{erf}(x)$.

$$\operatorname{erf}(x) = \frac{2}{\sqrt{\pi}} \int_0^x e^{-y^2} dy$$

$$\int_x^{\infty} e^{-y^2} dy = 1 - \operatorname{erf}(x)$$

$$(x) = 1 - \frac{2}{\sqrt{\pi}} \int_0^x e^{-y^2} dy$$

Equation [20] describes a symmetrical S-shaped curve. Therefore, if the pore-size distribution of a soil can be approximated by a normal distribution, the soil-water characteristic curve of the soil will be close to a symmetrical S-shaped curve, and eq. [20] can be used as a model to describe this relationship.

The two fitting parameters (i.e., the mean value, μ , and the standard deviation, σ in eq. [20]) are related to the air-entry value of the soil and the slope at the inflection point on the soil-water characteristic curve. If the slope at the inflection point is s and the air-entry value is ψ_{aev} , then the standard deviation, σ , can be written as:

$$[21] \quad \sigma = \frac{\theta_s}{\sqrt{2\pi}s}$$

and the mean value, μ , can be calculated as:

$$[22] \quad \mu = \psi_{aev} + \frac{\theta_s}{2s}$$

(2) Case of a gamma distribution

Consider the case of a gamma-type distribution for the function $f(r)$. That is, $f(h)$ takes the following form:

$$[23] \quad f(h) = \begin{cases} \frac{h^{\alpha-1} e^{-h/\beta}}{\beta^{\alpha} \Gamma(\alpha)}, & \alpha, \beta > 0, \quad 0 \leq h \leq \infty \\ 0, & \text{elsewhere} \end{cases}$$

where:

$$\Gamma(\alpha) = \int_0^{\infty} h^{\alpha-1} e^{-h} dh$$

In this case, the soil-water characteristic curve defined by eq. [18] has a smaller air-entry value, a steeper slope near

saturation, and a gentler slope near the residual water content. In the special case when α is an integer, the soil-water characteristic curve defined by eq. [18] becomes:

$$[24] \quad \theta(\psi) = \theta_s \int_{\psi}^{\infty} \frac{h^{\alpha-1} e^{-h/\beta}}{\beta^{\alpha} \Gamma(\alpha)} dh$$

$$= \frac{\theta_s}{\Gamma(\alpha)} \int_{\psi}^{\infty} h^{\alpha-1} e^{-h} dh = \theta_s \sum_{i=0}^{\alpha-1} \frac{\psi^i e^{-\psi/\beta}}{i! \beta^i}$$

For $\alpha = 1$, the gamma distribution becomes an exponential distribution:

$$[25] \quad f(h) = \begin{cases} \frac{1}{\beta} e^{-h/\beta}, & \beta > 0, \quad 0 \leq h \leq \infty \\ 0, & \text{elsewhere} \end{cases}$$

and the soil-water characteristic curve defined by eq. [18] can be written as:

$$[26] \quad \theta(\psi) = \theta_s e^{-\psi/\beta}$$

Note that eq. [26] has the same form as eq. [3], which was used by McKee and Bumb (1984) to describe the soil-water characteristic curve. Therefore, eq. [3] gives the best results if the pore-size distribution of the soil is close to a gamma distribution.

(3) Case of a beta distribution

Consider the case of a beta distribution for the function $f(r)$:

$$[27] \quad f(h) = \begin{cases} \frac{h^{\alpha-1} (1-h)^{\beta-1}}{B(\alpha, \beta)}, & \alpha, \beta > 0, \quad 0 \leq h \leq 1 \\ 0, & \text{elsewhere} \end{cases}$$

where:

$$B(\alpha, \beta) = \int_0^1 h^{\alpha-1} (1-h)^{\beta-1} dh = \frac{\Gamma(\alpha)\Gamma(\beta)}{\Gamma(\alpha+\beta)}$$

In this case, the soil-water characteristic curve given by eq. [18] has greater flexibility. For α equal to β , eq. [18] generates a symmetrical S-shaped curve. For α greater than β , the curve is non-symmetrical and has a higher air-entry value, a gentler slope near saturation, and a steeper slope near the residual water content. For α less than β , the curve has a smaller air-entry value, a steeper slope near saturation, and a gentler slope near the residual water content. In the case when α and β are integers, the soil-water characteristic curve defined by eq. [18] and eq. [27] is related to the binomial probability function as follows (Mendenhall et al. 1981):

$$[28] \quad \theta(\psi) = \theta_s \int_{\psi}^1 \frac{h^{\alpha-1} (1-h)^{\beta-1}}{B(\alpha, \beta)} dh$$

$$= \theta_s - \theta_s \sum_{i=\alpha}^{\alpha+\beta-1} \binom{\alpha+\beta-1}{i} \psi^i (1-\psi)^{\alpha+\beta-1-i}$$

Equation [28] has a form similar to that of eq. [5] suggested by Roger and Homberger (1978), which was used to account for a gradual air entry. Note, that defining r over the interval (0, 1) does not restrict its use. The beta density function can be applied to any interval by translation and a change in the scale.

Proposal for a new equation

The pore-size distribution of eq. [6] can be written as follows:

$$[29] \quad f(\psi) = \frac{mnp(p\psi)^{n-1}}{[1 + (p\psi)^n]^{m+1}}$$

Figure 3 shows a sample probability distribution for eq. [29] along with its integration (i.e., eq. [6]). It can be seen that the integration drops to zero over a narrow suction range. Therefore, eq. [6] is not suitable in the high suction region. Experimental data show that after the residual water content, the plot should decrease linearly to a value of about 10 sup 6 kPa (Croney and Coleman 1961). To describe the soil-water characteristic curve more accurately, the following distribution is suggested:

$$[30] \quad f(\psi) = \frac{mn(\psi/a)^{n-1}}{a[e + (\psi/a)^n]\{\log[e + (\psi/a)^n]\}^{m+1}}$$

Equation [30] and its integration form are shown in Fig. 4 for the same set of parameters (i.e., $a = 1/p, n, m$). This distribution function drops more slowly than eq. [29] as ψ increases and, therefore, eq. [30] produces a non-symmetrical curve that is closer to the experimental data.

Integrating eq. [30] using eq. [18] gives the following relationship between volumetric water content and suction:

$$[31] \quad \theta = \theta_s \left[\frac{1}{\ln[e + (\psi/a)^n]} \right]^m$$

Figures 5 to 7 show the effect of varying the three parameters $a, n,$ and m on the shape of the soil-water characteristic curve. From Fig. 5 it can be seen that when n and m are fixed, the parameter a (with a unit of kPa) is closely related to the air-entry value. In general, the value for the parameter a would be higher than the air-entry value. However, for small values of m , the air-entry value can be used for parameter a .

Figure 6 indicates that parameter n controls the slope of the soil-water characteristic curve. The distribution given by eq. [30] attains its maximum value approximately at the value of a . Therefore, the point $(a, \theta(a))$ can be used to approximate the inflection point. Using this information, a graphical estimation for the three parameters can be obtained from the soil-water characteristic curve. First, locate the inflection point (ψ_i, θ_i) on the soil-water characteristic plot and draw a tangent line through this point (Fig. 8). Let s denote the slope of the tangent line. Then, the three parameters $a, n,$ and m are determined as follows:

Fig. 3. A sample distribution using eq. [29] and its integration (eq. [6]).

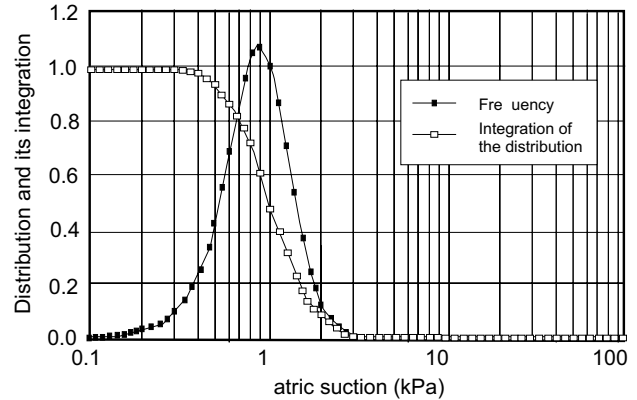


Fig. 4. A sample distribution using eq. [30] and its integration.

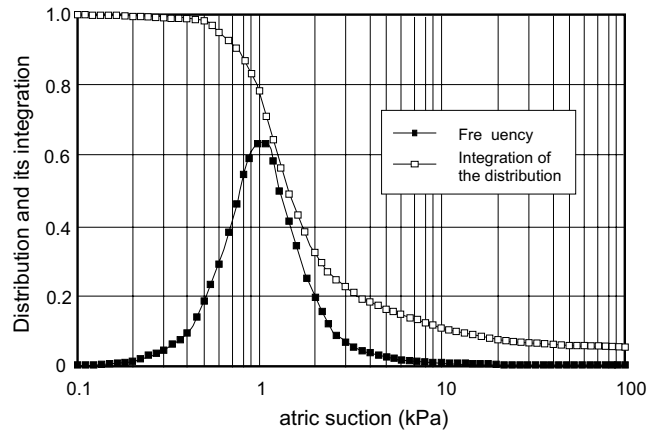
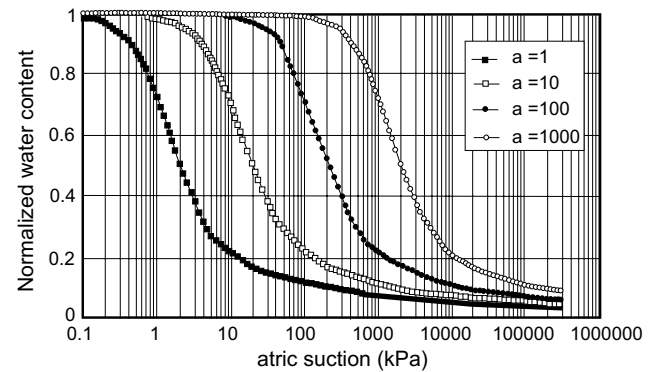


Fig. 5. Sample plots of eq. [31] with $n = 2$ and $m = 1$ (a varies).



$$[32] \quad a = \psi_i$$

$$[33] \quad m = 3.67 \ln \left(\frac{\theta_s}{\theta_i} \right)$$

$$[34] \quad n = \frac{1.31^{m+1}}{m\theta_s} 3.72s\psi_i$$

The slope, s , of the tangent line can be calculated as:

Fig. 6. Sample plots of eq. [31] with $a = 100$ and $m = 1$ (n varies).

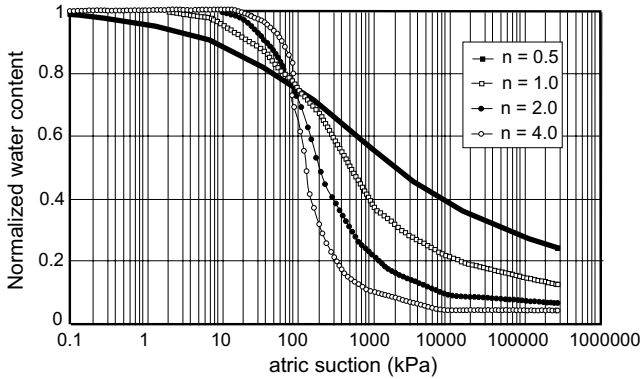


Fig. 7. Sample plots of eq. [31] with $a = 100$ and $m = 2$ (n varies).

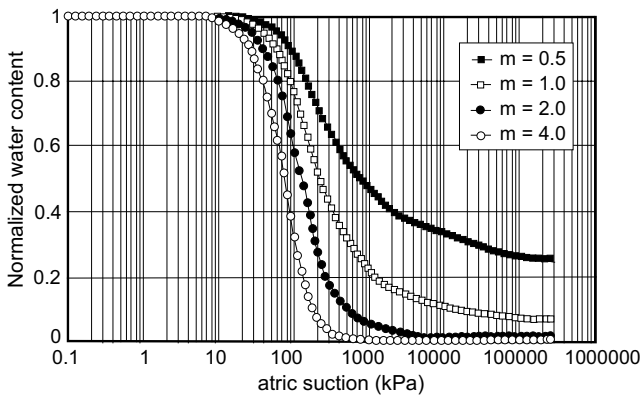
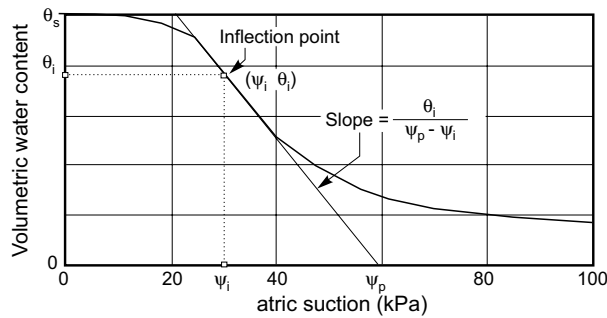


Fig. 8. A sample plot for the graphical solution of the three parameters (a , n , and m) in eq. [31].



$$[35] \quad s = \frac{\theta_i}{\psi_p - \psi_i}$$

where:

ψ_p = intercept of the tangent line and the matric suction axis (Fig. 8).

Small values of m result in a moderate slope in the high-suction range, and large values of n produce a sharp corner near the air-entry value (see Fig. 9). Another example of a best-fit curve to the experimental data for a

Fig. 9. A best-fit curve to the experimental data of a till (S. Vanapalli, personal communication, 1993).

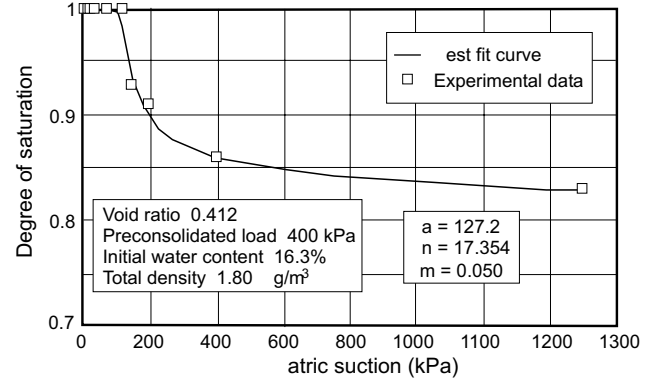


Fig. 10. A best-fit curve to the experimental data of a silty loam (data from Brooks and Corey 1964).

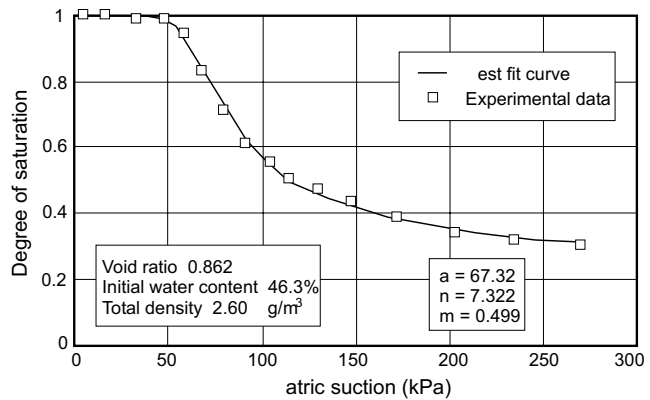
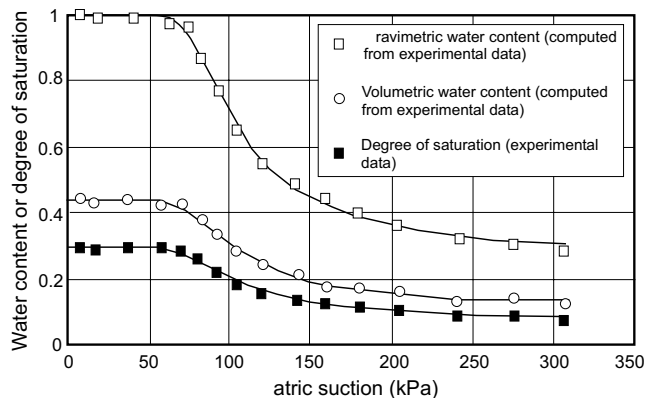


Fig. 11. Best-fit curves to the experimental data of a silty loam using three different representations of the water content, (i.e., degree of saturation, volumetric water content, and gravimetric water content; data from Brooks and Corey 1964).



silty loam from Brooks and Corey (1964) is shown in Fig. 10.

In eq. [31], θ becomes equal to θ_s when the suction is zero, and θ becomes zero when the suction goes to infinity. It is also possible to use the degree of saturation for curve fitting, since the degree of saturation varies from 0

to 1. Gravimetric water content can be similarly normalized for curve-fitting purpose. Three plots are shown for the same soil (i.e., silty loam) in Fig. 11, using different ways of representing the water content of the soil (i.e., degree of saturation, volumetric water content, and gravimetric water content).

Experimental data have previously shown that the suction of a soil reaches a maximum value of approximately 10^6 kPa at zero water content. This upper limit can be built into eq. [31] as follows:

$$[36] \quad \theta(\psi, a, n, m) = C(\psi) \frac{\theta_s}{\{\ln[e + (\psi / a)^n]\}^m}$$

where:

$C(\psi)$ is a correction function defined as:

$$C(\psi) = \frac{-\ln(1 + \psi / \psi_r)}{\ln[1 + (1,000,000 / \psi_r)]} + 1$$

where:

ψ_r = suction corresponding to the residual water content, θ_r .

It can be seen that $C(1,000,000)$ is equal to zero. Therefore, at the limiting point where ψ is equal to 10^6 kPa, the water content, θ , calculated from eq. [36] is zero. A sample plot for eq. [36] is shown in Fig. 12. The curve at the low-suction range is not significantly affected, since the correction function $C(\psi)$ is approximately equal to 1 at low suctions.

Figure 13 shows a best-fit curve to the experimental data obtained for a glacial till, using eq. [31]. A best-fit curve to the same experimental data using eq. [36] is shown in Fig. 14. It can be seen that the modified equation (i.e., eq. [36]) fits the data better than eq. [31]. The main difference is that the curve is forced by $C(\psi)$ to zero at a suction of 10^6 kPa.

A graphical estimation of the four parameters a , n , m , and ψ_r , in eq. [36] can be obtained from a semilog plot of the soil-water characteristic curve. First, determine the suction corresponding to the residual water content ψ_r by locating a point where the curve starts to drop linearly in the high suction range (Fig. 15). Numerical results show that, in most cases, eq. [36] gives a satisfactory approximation for $\psi_r > 1500$ kPa. Its magnitude will generally be in the range of 1500 to 3000 kPa. Figure 15 uses ψ_r equal to 3000 kPa for illustration purposes. Next, locate the inflection point (ψ_i, θ_i) on the semilog plot and draw a tangent line through this point (Fig. 15). Let s denote the slope of the tangent line on the semilog plot. Then, the fitting parameters a , n , and m can be determined as follows:

$$[37] \quad a = \psi_i$$

$$[38] \quad m = 3.67 \ln \left[\frac{\theta_s C(\psi_i)}{\theta_i} \right]$$

$$[39] \quad n = \frac{1.31^{m+1}}{mC(\psi_i)} 3.72s^*$$

Fig. 12. A sample plot of eq. [36].

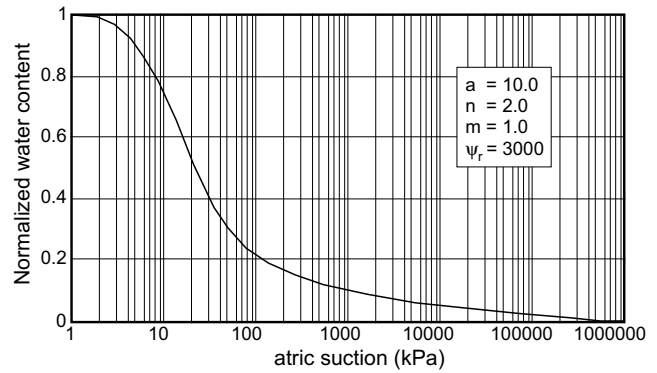


Fig. 13. A best-fit curve to the experimental data of a till using eq. [31] (S. Vanapalli, personal communication, 1993).

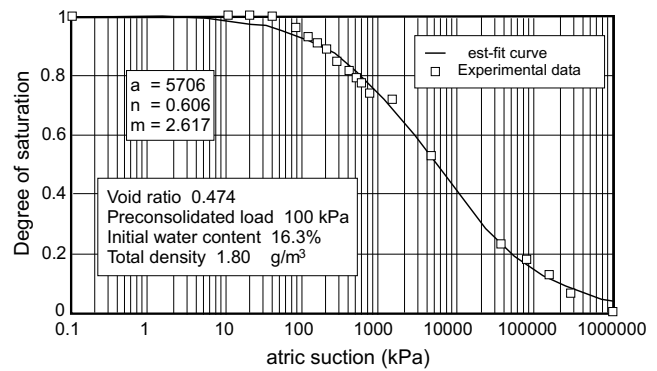
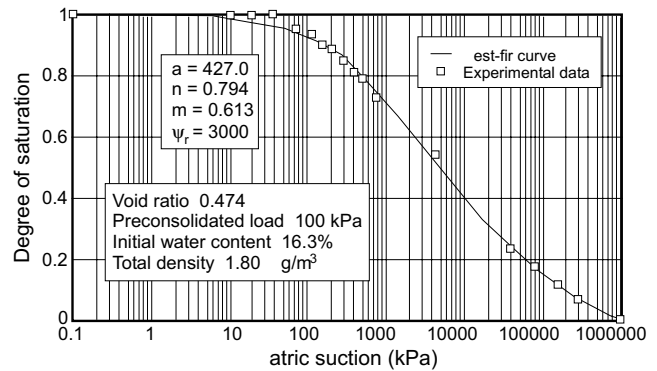


Fig. 14. A best-fit curve to the experimental data in Fig. 13 using eq. [36].



where:

$$s^* = \frac{s}{\theta_s} - \frac{\psi_i}{1.31^m(\psi_i + \psi_r) \ln[1 + (1,000,000 / \psi_r)]}$$

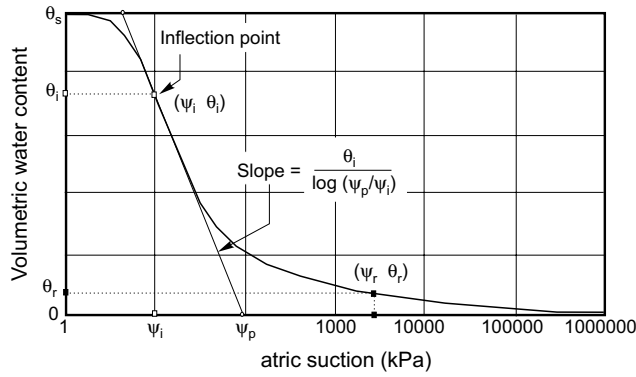
The slope, s , of the tangent line can be calculated as follows:

$$[40] \quad s = \frac{\theta_i}{\ln(\psi_p / \psi_i)}$$

where:

ψ_p = intercept of the tangent line on the semilog plot and the matric suction axis (Fig. 15).

Fig. 15. A sample plot for the graphical solution of the four parameters (a , n , m , and ψ_r in eq. [36]).



A graphical estimation only gives approximate values for the parameters. To obtain a closer fit to experimental data, the three parameters (a , n , and m) in eq. [36] can be determined using a least squares method, if the measured data for θ and ψ are available. The idea is to choose the three parameters such that the calculated values from eq. [36] are as close as possible to the measured values. Therefore, the following objective function (i.e., sum of the squared deviations of the measured data from the calculated data) is minimized with respect to the three parameters a , n , and m .

$$[41] \quad O(a, m, n) = \sum_{i=1}^M [\theta_i - \theta(\psi_i, a, m, n)]^2$$

where:

- $O(a, m, n)$ = objective function,
- M = total number of measurements, and
- θ_i and ψ_i = measured values.

This is a non-linear minimization problem. A curve-fitting utility CFVIEW was coded based on eq. [36] and eq. [41] using a quasi-Newton method. The detailed non-linear curve-fitting algorithm is presented in the Appendix. Best-fit curves for a tailings sand, a silt, and a clay are shown in Figs. 16 to 23. An arithmetic scale has been used when the experimental data in the high suction range are not available. It can be seen, from these results, that eq. [36] can be used to fit the experimental data reasonably well over the entire suction range of 0 to 10^6 kPa.

Some applications require an estimation of the residual water content. The following slightly different form of eq. [31] can be used to estimate the residual water content θ_r :

$$[42] \quad \theta = \theta_r + \frac{\theta_s - \theta_r}{\{\ln[e + (\psi/a)^n]\}^m}$$

Here, θ_r and θ_s are treated as two additional parameters. The five parameters a , n , m , θ_r , and θ_s , in eq. [42] can be systematically identified through a best-fit analysis on experimental data.

Fig. 16. A best-fit curve to the experimental data of a sand (data from Moore 1939).

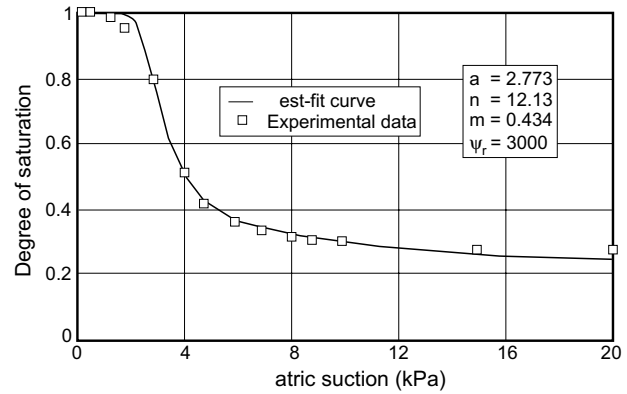


Fig. 17. A best-fit curve to the experimental data of a sand (Soil Laboratory data, University of Saskatchewan).

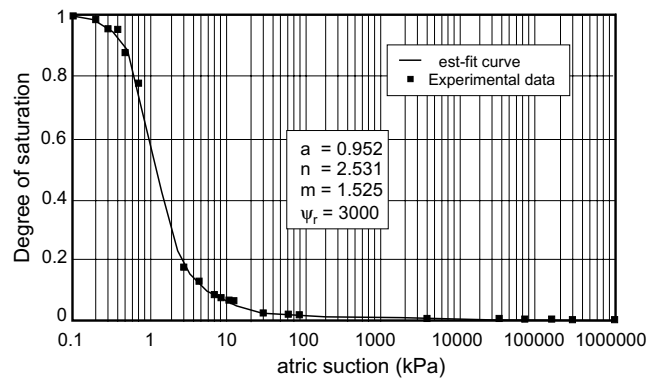
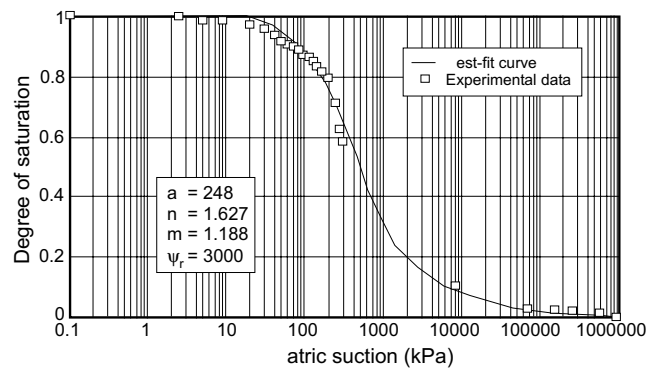


Fig. 18. A best-fit curve to the experimental data of Kidd Creek tailings (N. Yang, personal communication, 1992).



Conclusions

General empirical equations have been proposed to describe the soil-water characteristic curve. Each equation has its own limitations. A general form of the relationship between water content and suction was developed based on the pore-size distribution of the soil. If the pore-size distribution of a soil can be obtained or predicted, then

Fig. 19. A best-fit curve to the experimental data of a sand (Soil Laboratory data, University of Saskatchewan).

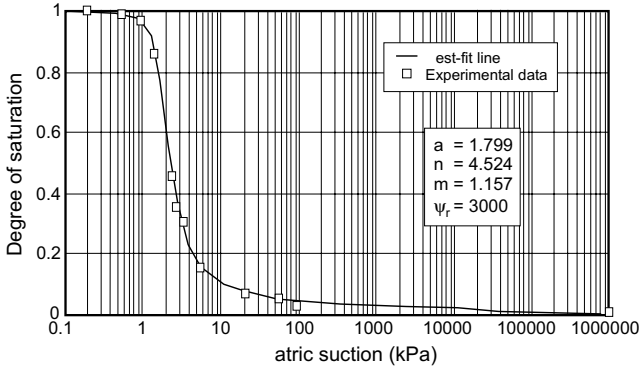


Fig. 22. A best-fit curve to the experimental data of a silt (Soil Laboratory data, University of Saskatchewan).

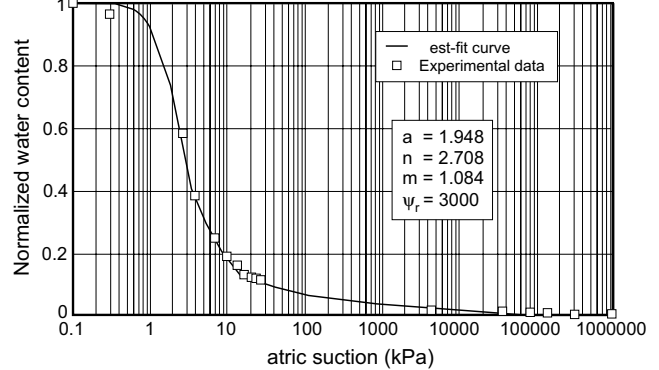


Fig. 20. A best-fit curve to the experimental data of a sand (University of Toronto data: University of Saskatchewan 1984).

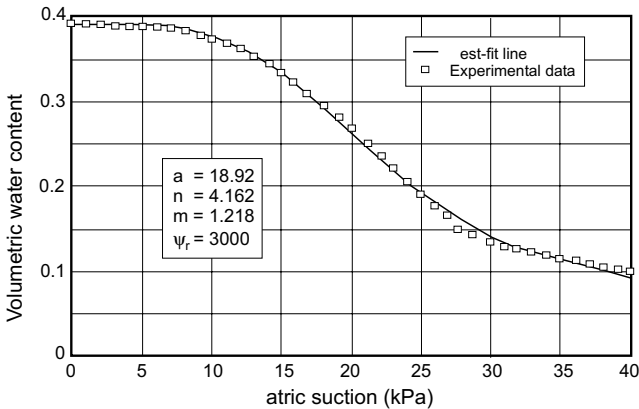


Fig. 23. A best-fit curve to the experimental data of an initially slurried Regina clay (data from Fredlund 1964).

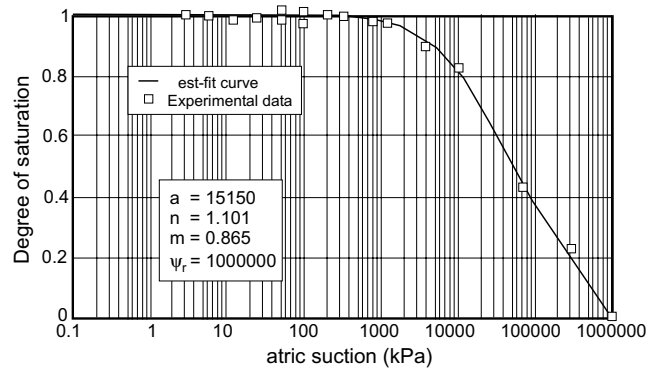
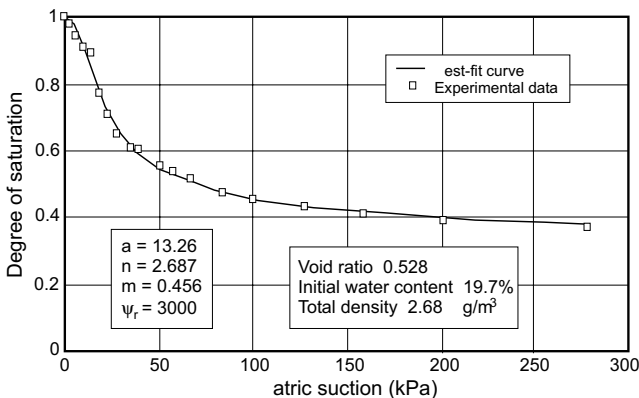


Fig. 21. A best-fit curve to the experimental data of a silt (S. Huang, personal communication 1993).



found that the equation fits experimental data reasonably well over the entire suction range from 0 to 10^6 kPa.

Acknowledgement

The authors would like to thank Sai Vanapalli for supplying experimental data and for helpful suggestions for the curve-fitting program.

References

Brooks, R.H., and Corey, A.T. 1964. Hydraulic properties of porous medium. Colorado State University (Fort Collins), Hydrology Paper, Nr. 3, March.

Bumb, A.C. 1987. Unsteady-state flow of methane and water in coalbeds. Ph.D. thesis, Department of Chemical Engineering, University of Wyoming, Laramie.

Campbell, G.S. 1974. A simple method for determining unsaturated conductivity from moisture retention data. *Soil Science*, **117**: 311–314.

Clapp, R.B., and Hornberger, G.M. 1978. Empirical equations for some soil hydraulic properties. *Water Resources Research*, **14**: 601–604.

Croney, D., and Coleman, J.D. 1961. Pore pressure and suction in soils. *Proceedings, Conference on Pore Pressure and Suction in Soils*. Butterworths, London. pp. 31–37.

the soil-water characteristic curve is uniquely determined from the proposed general equation.

The analysis in this paper provides not only a theoretical basis for most of the empirical equations but also proposes a new, more general equation to describe the soil-water characteristic curve. Based on the proposed equation, a curve-fitting utility, CFVIEW, was coded. It was

- Fredlund, D.G. 1964. Comparison of soil suction and one-dimensional consolidation characteristics of a highly plastic clay. M.Sc. thesis, Department of Civil Engineering, University of Alberta, Edmonton, AB, Canada.
- Fredlund, D.G., and Rahardjo, H. 1993a. Soil mechanics for unsaturated soils. John Wiley & Sons, Inc., New York.
- Fredlund, D.G., and Rahardjo, H. 1993b. An overview of unsaturated soil behaviour. Proceedings, ASCE Specialty Series on Unsaturated Soil Properties, Dallas, TX., October 24–28, pp. 1–33.
- Gardner, W.R. 1958. Some steady state solutions of the unsaturated moisture flow equation with application to evaporation from a water-table. *Soil Science*, **85**: 228–232.
- Gardner, W.R., Hillel D., and Benyamini, Y. 1970a. Post irrigation movement of soil water. I. Redistribution. *Water Resources Research*, **6**: 851–861.
- Gardner, W.R., Hillel D., and Benyamini, Y. 1970b. Post irrigation movement of soil water. II. Simultaneous redistribution and evaporation. *Water Resources Research*, **6**: 1148–1153.
- Marshall, T.J. 1958. A relation between permeability and size distribution of pores. *Journal of Soil Science*, **9**: 1–8.
- McCuen, R.H., Rawls, W.J., and Brakensiek, D.L. 1981. Statistical analyses of the Brook-Corey and the Green-Ampt parameters across soil textures. *Water Resources Research*, **17**: 1005–1013.
- McKee, C.R., and Bumb, A.C. 1984. The importance of unsaturated flow parameters in designing a monitoring system for hazardous wastes and environmental emergencies. Proceedings, Hazardous Materials Control Research Institute National Conference, Houston, TX, March 1984. pp. 50–58.
- McKee, C.R., and Bumb, A.C. 1987. Flow-testing coalbed methane production wells in the presence of water and gas. *In* SPE Formation Evaluation, December, pp. 599–608.
- Mendenhall, W., Scheaffer, R.L., and Wackerly, D.D. 1981. *Mathematical statistics with applications*. 2nd Edition. Duxbury Press, Boston.
- Moore, R.E. 1939. Water conduction from shallow water tables. *Hilgardia*, **12**: 383–426.
- Mualem, Y. 1986. Hydraulic conductivity of unsaturated soils: prediction and formulas. *In* Methods of soil analysis. Part I Physical and mineralogical methods. 2nd Edition. Agronomy. Edited by A. Klute. American Society of Agronomy, Inc. and Soil Society of America, Inc., Madison, Wis., U.S.A., pp. 799–823.
- Papagiannakis, A.T., and Fredlund, D.G. 1984. A steady state model for flow in saturated-unsaturated soils. *Canadian Geotechnical Journal*, **21**: 419–430.
- Richards. B.G. 1965. Measurement of the free energy of soil moisture by the psychrometric technique using thermistors. In *Moisture equilibria and moisture changes in soils beneath covered areas*. Edited by G.D. Aitchison. Butterworth & Co. Ltd., Sydney, Australia, pp. 39–46.
- Roger, B.C., and Hornberger. G.M. 1978. Empirical equations for some soil hydraulic properties. *Water Resources Research*, **14**:601–604.
- Rogowski, A.S. 1971. Watershed physics: model of the soil moisture characteristic. *Water Resources Research*, **7**: 1575–1582.
- Sadler, D.R. 1975. Numerical methods for nonlinear regression. University of Queensland Press, St. Lucia, Queensland, Australia.
- University of Saskatchewan. 1984. KCAL User's manual. A computer program for calculating unsaturated permeability. Department of Civil Engineering, University of Saskatchewan. Saskatoon.
- van Genuchten, M.T. 1980. A closed-form equation for predicting the hydraulic conductivity of unsaturated soils. *Soil Science Society of America Journal*, **44**: 892–898.
- Williams, P.J. 1982. The surface of the Earth, an introduction to geotechnical science. Longman Inc., New York.
- Williams, J., Prebble, R.E., Williams, W.T., and Hignett, C.T. 1983. The influence of texture, structure and clay mineralogy on the soil moisture characteristic. *Australian Journal of Soil Research*, **21**: 15–32.

Appendix: Non-linear curve-fitting algorithms for the soil-water characteristic curve

The proposed equation for the soil-water characteristic curve is:

$$[A1] \quad \theta(\psi, a, n, m) = C(\psi) \frac{\theta_s}{\{\ln[e + (\psi/a)^n]\}^m}$$

Let $p = (a, n, m)$ denote the unknown vector of the three parameters a , n , and m and suppose that measured data (θ_i, ψ_i) ($i = 1, 2, \dots, M$) are available, where M is the number of measurements. The least squares estimate of p is the vector p^* , which minimizes the following objective function (i.e., sum of the squared deviations of the measured data from the calculated data).

$$[A2] \quad O(p) = O(a, n, m) = \sum_{i=1}^M [\theta_i - \theta(\psi_i, a, n, m)]^2$$

In other words, the least squares method determines the three parameters such that the calculated values from eq. [A1] are as close as possible to the measured values.

A standard requirement of iterative minimization algorithms is that the value of the objective function decreases monotonically from iteration to iteration. Let p_i be the estimate of p at the beginning of the i th iteration (p_0 is the initial guess and, theoretically, it is arbitrary). The new estimate p_{i+1} is chosen such that $O(p_{i+1}) < O(p_i)$. The steepest descent method is one of the easiest methods for minimizing a general non-linear function of several variables. It exploits the fact that from a given starting point a function decreases most rapidly in the direction of the negative gradient vector evaluated at the starting point. Let g denote the gradient of $O(p)$ at p_i . That is:

$$[A3] \quad g = \left[\begin{array}{c} \frac{\partial O(p)}{\partial a} \\ \frac{\partial O(p)}{\partial n} \\ \frac{\partial O(p)}{\partial m} \end{array} \right]_{p=p_i}$$

The steepest descent iteration is defined by

$$[A4] \quad p_{i+1} = p_i - \alpha g$$

where:

α = scalar that determines the length of the step taken in the direction of $-g$.

From eq. [A2] it follows that:

$$[A5] \quad \frac{\partial O(p)}{\partial a} = -2 \sum_{i=1}^M [\theta_i - \theta(\psi, a, n, m)] \frac{\partial \theta(\psi_i, a, n, m)}{\partial a}$$

Similarly,

$$[A6] \quad \frac{\partial O(p)}{\partial n} = -2 \sum_{i=1}^M [\theta_i - \theta(\psi, a, n, m)] \frac{\partial \theta(\psi_i, a, n, m)}{\partial n}$$

$$[A7] \quad \frac{\partial O(p)}{\partial m} = -2 \sum_{i=1}^M [\theta_i - \theta(\psi, a, n, m)] \frac{\partial \theta(\psi_i, a, n, m)}{\partial m}$$

From eq. [A1], the partial derivatives in eqs. [A5] to [A7] can be obtained as follows:

$$[A8] \quad \frac{\partial \theta(\psi_i, a, n, m)}{\partial a} = mC(\psi_i) \theta_s \{ \ln[e + (\psi_i / a)^n] \}^{-m-1} \times \frac{n(\psi_i / a)^{n-1} (\psi_i / a^2)}{e + (\psi_i / a)^n}$$

$$[A9] \quad \frac{\partial \theta(\psi_i, a, n, m)}{\partial n} = -mC(\psi_i) \theta_s \{ \ln[e + (\psi_i / a)^n] \}^{-m-1} \times \frac{(\psi_i / a)^n \ln(\psi_i / a)}{e + (\psi_i / a)^n}$$

$$[A10] \quad \frac{\partial \theta(\psi_i, a, n, m)}{\partial m} = -C(\psi_i) \theta_s \{ \ln[e + (\psi_i / a)^n] \}^{-m} \times \ln \{ \ln [e + (\psi_i / a)^n] \}$$

The steepest descent method is not efficient for practical use, since the rate of convergence is slow, especially near the stationary point. The following quasi-Newton

method (Sadler 1975) was used for the curve-fitting program:

$$[A11] \quad p_{i+1} = p_i - A_i g_i$$

where:

g_i = gradient of the objective function evaluated at p_i , and

A_i = operative matrix at the i -th iteration.

Equation [A11] becomes the steepest descent method if A_i is the identity matrix multiplied by a step length (a scalar). Denote $p_{i-1} - p_i$ by d_i and $g_{i+1} - g_i$ by q_i . Then A_i is updated using the following formula:

$$[A12] \quad A_{i+1} = A_i + \frac{(d_i - A_i q_i)(d_i - A_i q_i)^T}{(d_i - A_i q_i)^T q_i}$$

where:

the superscript T denotes the transpose of a vector matrix.

A suitable choice for A_0 is the diagonal matrix defined by:

$$[A13] \quad a_{ij} = \begin{cases} \frac{\alpha_i}{2\beta_i} & \text{if } i = j \\ 0 & \text{if } i \neq j \end{cases}$$

where:

α_i = i -th element of the starting vector p_0 ,

β_i = i -th element of the gradient g sub o evaluated at the starting vector.

The quasi-Newton method does not require matrix inversion or equivalent, since the sequence A_i ($i = 0, 1, 2, \dots$) converges to the inverse Hessian. In practice, the objective function is often approximately quadratic near the minimum, so a second-order convergence can be eventually expected. However, there is no guarantee that A_i remain positive definite, even for a quadratic function. The product $g_i^T d_i$ should be checked and d_i replaced by its negative, if $g_i^T d_i > 0$. Numerical difficulties may also arise when the scalar product $(d_i - A_i q_i)^T q_i$ is very small, resulting in unduly large elements in A_{i+1} . One of several possible strategies is to reinitialize A_{i+1} if the cosine of the angle between $(d_i - A_i q_i)$ and q_i is less than 0.0001. For a non-quadratic objective function it is reasonable to adjust the step length so that the objective function is reduced at each iteration.

Comparison of soil suction and one-dimensional consolidation characteristics of a highly plastic clay

D.G. Fredlund

Preface, by Dr. Robert F. Legget, Director, NRC: As fine-grained soils above the water table are dried through processes of evaporation or plant transpiration, pore-water pressures become increasingly negative with respect to atmospheric conditions. Soils of high clay content exhibit large volume change with change in moisture stress. In subhumid to semi-arid climates, negative pore-water stresses cause effective stresses on the soil solid phase that may be much larger than the stresses imposed by engineering structures. Changes in these stresses arising from the soil climate are then of overriding importance in the long-term performance of foundations placed on such soils.

The purpose of this study was to compare the effects of one-dimensional consolidation caused by the application of load to the solid phase, with the shrinkage caused by a reduction of stress in the fluid phase. This report summarizes results presented in a M.Sc. thesis by Fredlund (1964), entitled "Comparison of Soil Suction and One-dimensional Consolidation Characteristics of a Highly Plastic Clay", presented to the Faculty of Graduate Studies, University of Alberta in May 1964). Much of the field and laboratory work associated with this study was carried out by the author while employed as a summer assistant with the Division of the NRC Prairie Regional Station in Saskatoon during the summers of 1962 and 1963, and forms part of a broad divisional study of problems affecting building foundations on volume changing clay subsoils.

Abstract: Investigation of the shrinking and swelling action of highly plastic clays in the Prairie Provinces has been carried out for several years by the Division of Building Research, National Research Council, DBR/NRC. The problem facing engineers associated with the building industry is the lack of an analysis whereby the probable amount of vertical movement of a light structure can be predicted. A literature review of research work in England, South Africa, Australia, Israel and the United States was conducted and a study made of two analyses that have been developed; one by Croney et al. (1952) and the other by Jennings and Knight (1957).

A testing program was conducted which involved the determination of moisture-suction characteristics of Regina Clay and a comparison of these results with the moisture-pressure relationships obtained by the conventional consolidation test. It was found that virgin pressure-void ratio curves are essentially the same for both consolidation and suction tests at close to full saturation. The curvatures of the recompression branches of the pressure-void ratio curves for the two test techniques, however, are quite different.

In recent years increasing interest has been shown in the behaviour of highly swelling soil. Vertical movements of engineering structures placed on the highly plastic lacustrine clays in Western Canada pose a serious problem (Baracos and Marantz 1952; Baracos and Bozozuk 1957; Hamilton 1963). The basic problem confronting foundation designers appears to be the lack of a method of predicting the probable heave.

A considerable amount of research on this problem has been conducted in various countries of the world. A literature survey revealed two analyses that appear promising. One was developed in England (Croney et al. 1952) and is based on the results from a suction test and a shrinkage test. The other, developed in South Africa (Jennings and Knight 1957), is based on the results of one-dimensional consolidation tests.

This paper discusses the stresses associated with the swelling problem in the field and an assimilation of these stresses in the laboratory. The major point of investigation comprises a comparison of the soil suction test and the one-dimensional consolidation test since it is these test results which have been used by other investigators to predict probable heave.

Key words: one-dimensional consolidation, pressure plate tests, pressure membrane tests, soil suction, prediction of heave.

D.G. Fredlund, Professor, Department of Civil Engineering, University of Saskatchewan, 57 Campus Drive, Saskatoon, SK, Canada S7N 5A9.

Reproduced with permission from Technical Report No. 245, Division of Building Research, National Research Council, Ottawa, Ontario, July 1967.

Stresses associated with the swelling problem

Upward vertical movements often occur in light structures as a result of the disturbance of the moisture regime existing prior to construction. The amount of movement depends upon the difference between the initial and final equilibrium water regimes. The moisture regimes are related to the relative importance of factors such as transpiration, evaporation, and infiltration. In areas where the climate is humid and the soil profile relatively wet, settlement of a structure may occur due to a cut-off in the amount of infiltration (Aitchison 1960). In Western Canada where the climate is generally semi-arid, transpiration and evaporation give rise to a moisture-deficient soil profile. Evaporation and transpiration place a tensile stress on the water phase and thus increase the effective stress in the soil. Construction of a building, however, inhibits transpiration and evaporation and the net upward movement of water results in a moisture gain. The moisture gain decreases the pore-water tension and results in a volume increase.

The distribution of stresses in the soil profile and the changes that can occur due to transpiration, evaporation, and infiltration have been clearly outlined by Jennings and Kerrich (1962) (Fig. 1). Let us assume the case of a soil mass which is initially saturated, with a water table at a certain distance below the ground surface. For the condition of no water flow (Fig. 1a), the pore-water stress is negative, linear, and directly related to its height above the water table.

The term "soil suction" to designate the stress in the water phase is defined as "the difference between the pressure of the pore-water and atmospheric pressure and is a measure of the surface forces retaining water in the soil structure" (Croney et al. 1952).

Figure 1b shows the new equilibrium pore-water pressure conditions if a constant evaporation is imposed which is not large enough to cause the entry of air into the soil mass. The pore-water pressure versus depth relationship is still linear, but lies to the left of the previous pore-water pressure line. The increase in effective stress causes consolidation and thus a settlement of the ground surface.

As further evaporation and transpiration by plants add to the tensile stress in the pore-water, the effective stress is greatly increased and the high tensile stress may cause the soil to crack (Fig. 1c). Placing a light structure on this soil mass increases the total stress. The prevention of evaporation and transpiration, however, and the infiltration of rain water results in a gradual decrease of pore-water tension, a reduction in the effective stress, and a volume increase. The volume change or the amount of heave depends upon the magnitude of the initial and final effective stress conditions in the soil mass.

Two procedures for the prediction of heave

One analysis for the prediction of total heave was developed by Croney et al. (1952) and is based on the re-

sults of a suction test and a shrinkage test. This analysis has been used for several years in Great Britain, India and other countries to estimate the probable amount of heave beneath asphalt and concrete roadways and airport runways (Russam 1962).

The initial soil conditions are measured in terms of a water content profile. The final conditions are in terms of an equilibrium water content profile based on an estimated pore-water stress profile which is below atmospheric pressure and a function of the distance above the water table. (The final equilibrium water conditions are estimated from the soil suction versus water content results.) The shrinkage test results are used to relate water contents to the specific bulk volume of the soil.

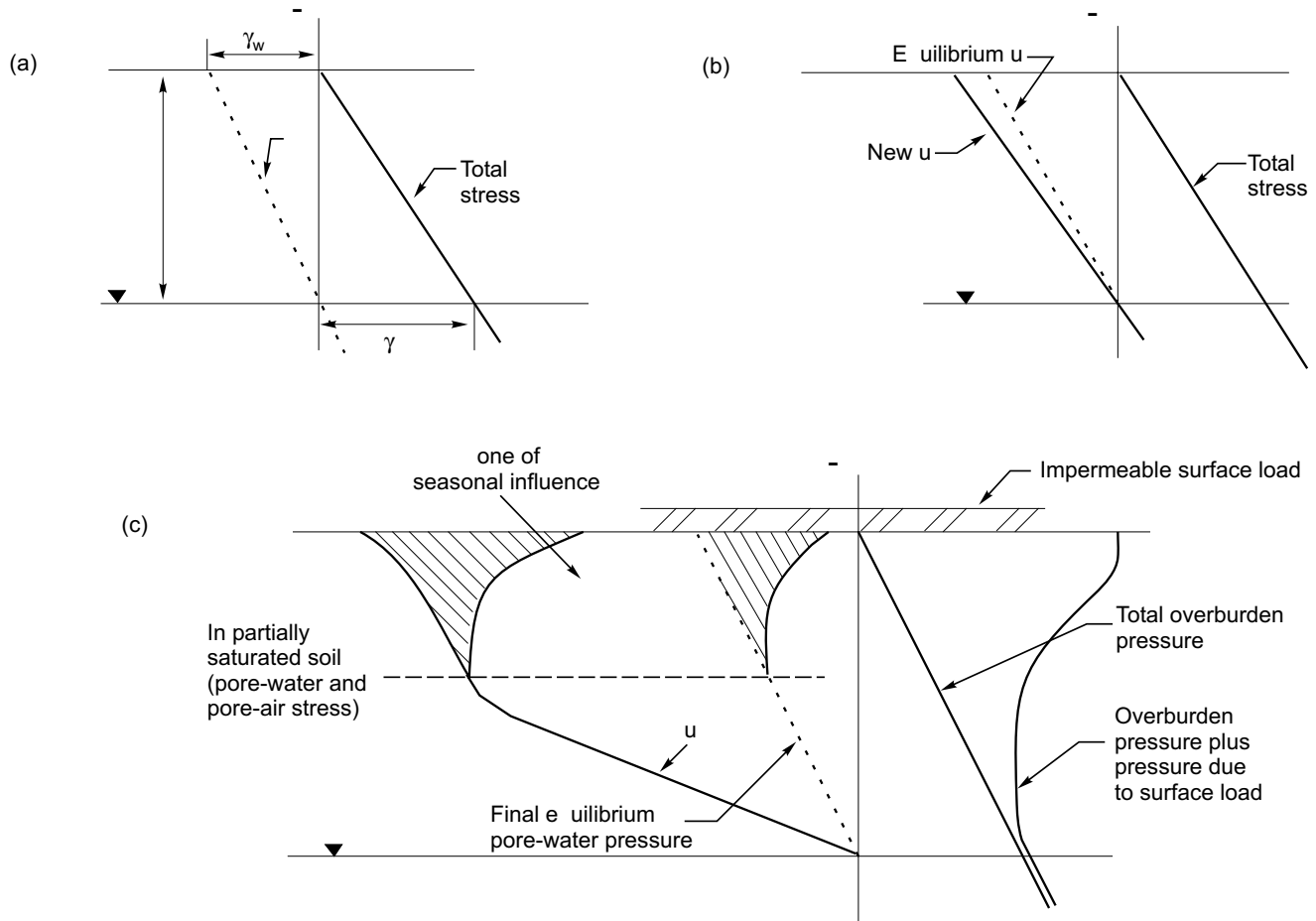
Another analysis was developed by Jennings and Knight (1957) and is based on the results of a "field or natural water content" consolidation test and a "free-swell" consolidation test. The "natural water content" consolidation test is used to represent field conditions where load is applied to the soil without any other external influence to change the moisture regime. The "free-swell" test is used to estimate the final equilibrium water content conditions under the applied load which acts as an impermeable covering over the soil. The amount of heave is predicted by determining the change in void ratio which occurs between the initial and final stress conditions in the field. Further research and modification of this procedure has been reported by Burland (1962).

Theory

Since the two main procedures that have been used to predict heave are based on two different tests, it was decided to study the relationship between the tests on a typical volume-changing clay soil from Regina, Saskatchewan. There appears to be a definite lack of literature which deals specifically with this relationship. There is also the question of whether the suction test or the one-dimensional consolidation test more closely parallels the conditions to which a soil is subjected in the field such as transpiration, evaporation, infiltration, as well as changes in physical loading.

For clarity, the suction test theory is outlined in considerable detail since it is not found in present soil mechanics textbooks. The process of consolidation has been explained by Taylor (1948) and others by reference to a mechanical analogy using a piston and spring. A modification of their analogy is now proposed to represent the process of consolidation due to suction stresses in the pore-water instead of loads applied directly to the solid phase. The modified piston and spring analogy is shown in Fig. 2. Consider two frictionless, tightly fitting pistons, one placed in the chamber and the other in the cylinder as shown. The piston in the chamber has a hole which represents a pore at the surface of a soil mass. Initially, the stopcock at the bottom of the chamber is closed to prevent the escape of water and a load is placed on the pan connected to the bottom piston. The instant the stopcock is opened, water starts to move from the chamber into the cylinder and as both pistons sink, the load is taken up by

Fig. 1. Stresses accompanying the drying and covering of a soil mass: *a*) No evaporation from surface; *b*) With evaporation small enough that no air entry or cracking of the soil occurs; *c*) Evaporation large enough to cause air entry and cracking of the soil (after Jennings and Kerrich 1962).



the spring. The length of time required for the spring to take up the applied load depends upon the rate at which water escapes through the stopcock. When the piston stops moving, the load on the spring is equivalent to the stress in the water phase. It should be noted that the water meniscus that forms as part of the top piston has a radius of curvature, which is a function of the tension applied to the water phase. The maximum tension that the water phase can develop is equal to the air entry value of the opening. Considering the case of a clay soil, the maximum air entry value may be in excess of one atmosphere or greater.

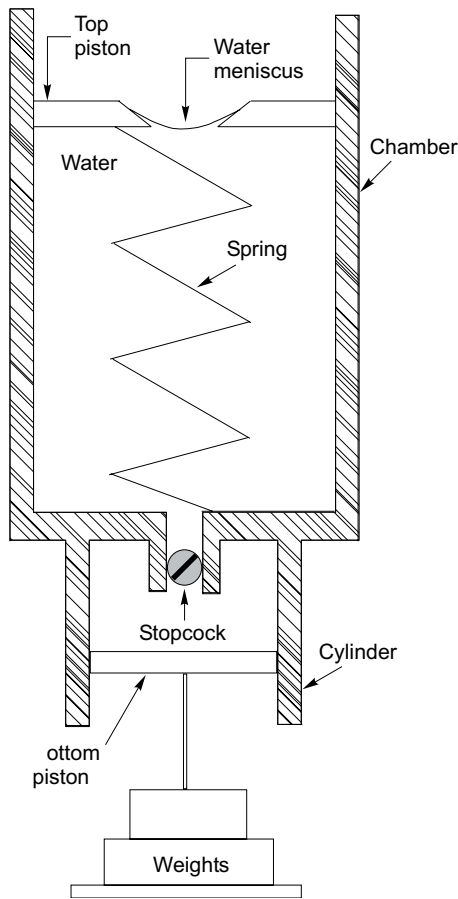
The changes in neutral and effective stresses during the "consolidation process" in a suction test are shown in Fig. 3. Let us consider an undisturbed soil sample, the sample is placed on the porous plate in the suction apparatus and allowed access to water until it comes to equilibrium under an applied suction. The total neutral and effective stresses are then known and are as shown in Fig. 3a. Application of a new suction increment does not alter the stresses throughout the sample, except at the drainage surface where the neutral stress goes to $-P_2$ and the effective stress to $+P_2$ (Fig. 3b). As consolidation pro-

ceeds, the effective stress increases and the tension in the pore-water increases a corresponding amount (Fig. 3c). When the pore-water tension throughout the sample is equal to P_2 , the effective stress is also equal to P_2 and the consolidation is complete. Several points about the suction test are noteworthy: the total stress is atmospheric pressure throughout the consolidation process; after consolidation the water is in a state of tension; volume changes are always of a three-dimensional nature.

It should be noted that the laboratory testing program was carried out on a pressure plate and pressure membrane apparatus rather than on a true suction apparatus. The theoretical difference between a true suction test and a pressure test is related to the change in pressure datum. Lowering the stress in the water and leaving the surrounding atmospheric pressure constant (as is done in a suction test) is the same as raising the water surrounding air pressure in the cell and keeping the water stress at atmospheric (as is done in a pressure test).

Considering the pressure plate test, Fig. 3 would remain essentially unchanged. In either test the important factors to remember in drawing stress diagrams are that stress is being applied to the water phase only, and that

Fig. 2. Suction test-piston and spring analogy.



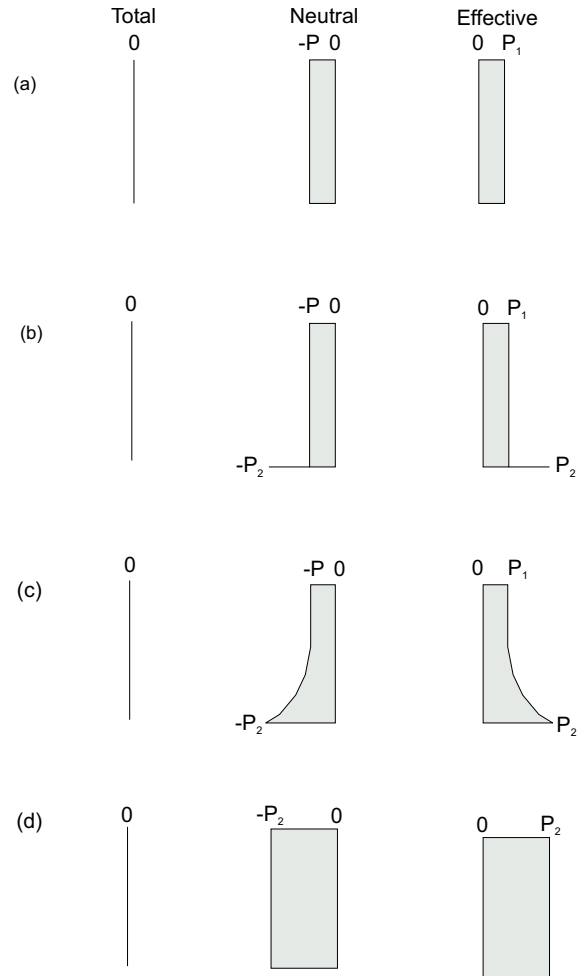
the flow gradient must initially be at the “stopcock” or point of drainage. The above explanation refers only to a saturated soil mass.

Soil and testing program

The soil used for this testing program was clay of high plasticity from the glacial Lake Regina sediment. It was obtained at elevation 1866.1 ft. (569.2 m), i.e., 15.6 ft (4.8 m) below the original ground surface of 1881.75 ft. (573.9 m), from a test pit in the basement excavation for the new Saskatchewan Government Telephones Building on the north-west corner of College Avenue and Albert St., in Regina, Saskatchewan. A summary of the classification tests is shown in Table 1.

A pressure plate extractor (Fig. 4) and a pressure membrane extractor (Fig. 5) were used to obtain results in a pressure range comparable to that of the standard consolidation test. The pressure plate extractor had an operating range of 0 to 1 kg/cm² (0 to 100 kPa). The specimens are placed on a porous stone of high air-entry. Air pressure is applied from above; the water beneath the stone is at atmospheric pressure (Richards and Fireman 1943). The pressure membrane extractor extends the operating range by means of a cellulose membrane which has a very high air-entry value (Croney et al. 1958).

Fig. 3. Stress changes during the consolidation process in a suction test: a) Just prior to the application of a new pressure; b) The instant after the application of a pressure increment; c) After partial consolidation; d) After complete consolidation. Note: Drainage at bottom of sample only.



As part of this study, a new pressure plate apparatus was built which allows the measurement of the rate of consolidation (Fig. 6). The permeability of the porous stone is more than 100 times greater than that of the soil and does not cause significant error in the determination of rate of consolidation.

The testing program involved the determination of the soil suction versus water content relationship, and a comparison of these results with those obtained from the standard one-dimensional consolidation test. Specific bulk volume was determined during the suction test as well as during evaporation after the samples were removed from the suction test apparatus. All testing was performed on soil which was initially remoulded at a water content near the liquid limit. The suction test samples were prepared by consolidating slurry in a one-dimensional consolidometer to various pressures after which they were rebounded to a token pressure. Varying the consolidation pressures resulted in the various initial water contents. Thus the stress conditions associated with the preparation

Table 1. Summary of classification tests on Regina clay

Test	Result
Specific Gravity	2.83
Atterberg Limits	
Liquid Limit	75.5%
Plastic Limit	24.9%
Shrinkage Limit	13.1%
Plastic Index	50.6%
Grain Size Distribution*	
Sand Sizes	8%
Silt Sizes	41%
Clay Sizes	51%
Mineralogical Composition of material	
less than 2 microns**	
Montmorillonite	77%
Illite	15%
Kaolinite	8%
Exchange Capacity***	
(milliequivalents per 100 grams dry weight of soil)	31.7 meq/100 g
Exchangeable Cations	
Magnesium	15.3 meq/100 g
Calcium	54.4 meq/100 g
Potassium	0.59 meq/100 g
Sodium	1.77 meq/100 g

* M. I. T. Grain-size Scale.

**X-ray Analysis performed by Alberta Research Council.

***Exchange capacity analyses performed by the Soil Science Department (University of Alberta).

Note: Specific gravity, Atterberg limits, and grain size are the average of three sets of tests; X-ray analysis and exchange capacity were performed on one average sample.

of the suction and one-dimensional consolidation test specimens were the same.

Discussion of test results

The results of tests carried out in the pressure plate and pressure membrane apparatus are referred to as soil suction values. These tests, however, do not reduce the pore-water stress below atmospheric pressure, but rather increase the surrounding air pressure and leave the pore-water stress at atmospheric pressure. The difference is essentially one of technique and does not appreciably alter the test results (Penner 1959).

Figure 7 shows the relationship between water content and logarithm of soil suction for all suction tests performed on both the pressure plate and pressure membrane extractors. The one-dimensional consolidation results are shown in Fig. 8 which is a plot of water content versus logarithm effective pressure. In comparing the test results, it should be first noted that the one-dimensional consolidation test induces anisotropic consolidation of the sample while the suction test causes isotropic consolidation. Comparisons of the two processes of consolidation (Aboshi and Monden 1961; Bishop and Henkel 1962)

have shown that more water is forced out of the soil during isotropic consolidation. The difference in the amount of consolidation occurring is explained in terms of changes in the soil structure resulting from anisotropic and isotropic consolidation. The shear stress between the soil particles is lower in isotropic consolidation and permits more consolidation of the soil mass. In the field, evaporation and transpiration are conducive to isotropic consolidation.

Comparison of the suction and one-dimensional consolidation test results shows their virgin compression branches to be very similar (Fig. 9). When the consolidation curve was corrected for the compressibility of the filter paper and side friction in the consolidation ring, the curve appeared to fall directly on top of the suction curve for pressures up to 10 kg/cm².

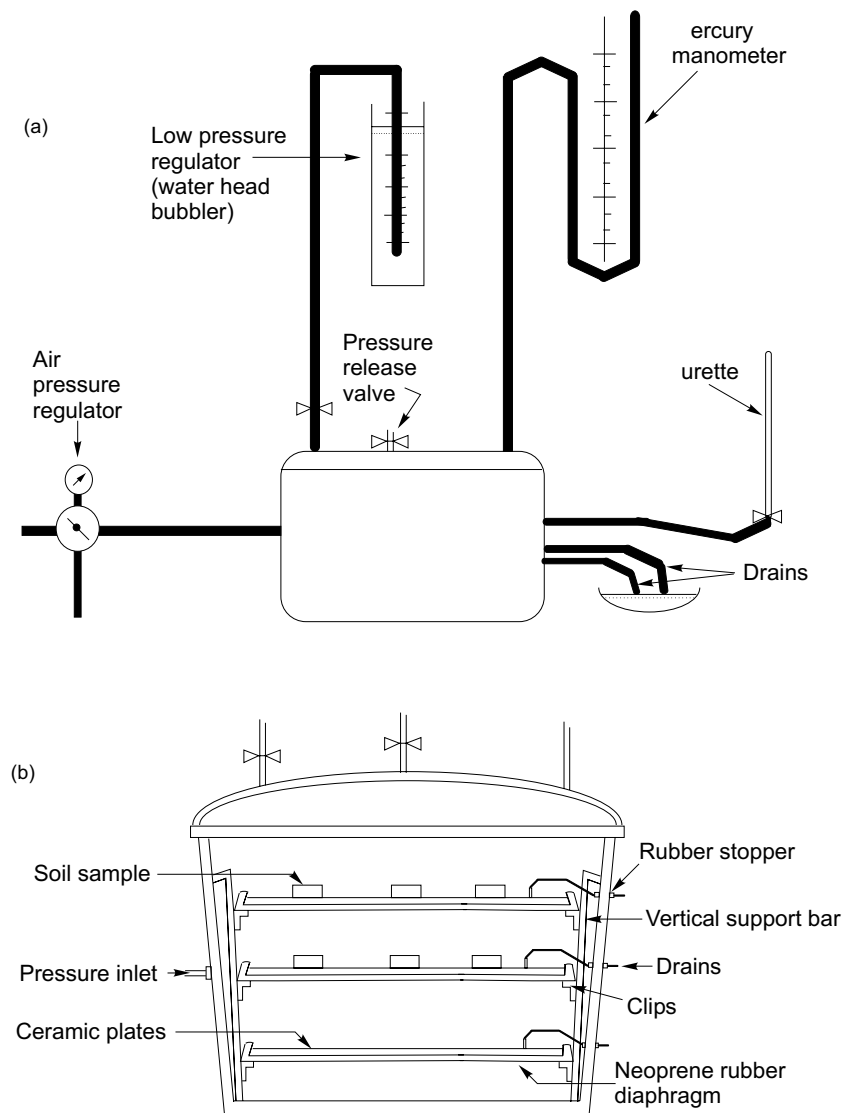
There appears to be a difference in the recompression branches of the two curves (Fig. 9). The suction test shows a smoother curve with no distinct break in curvature at the point where the preconsolidation pressure is exceeded. In addition, the suction results have lower water contents than the one-dimensional consolidation results on the recompression branch. The difference in the two curves is probably related either to the structural resistances and shearing stresses associated with isotropic and anisotropic consolidation or to the effect of side friction in the consolidation rings.

Jennings (1960) and Aitchison (1960) proposed that a point would be reached on the virgin compression branch where the suction and consolidation results separate. This point was believed to coincide with the commencement of air entry into the specimen. Figure 10 shows the relationship between specific bulk volume and water content as specimens of Regina clay were dried, first in the pressure plate extractor and later by evaporation. Specific bulk volume is herein defined as the volume in cubic centimetres occupied by one hundred grams of moist soil. Figure 11 shows the degree of saturation versus water content for the same specimens. On the basis of the test results, it can be predicted that the curves should begin to diverge at a water content of approximately 25 per cent, with the one-dimensional consolidation curve going below the suction curve. The classification tests showed the plastic limit to be 25 per cent. The soil suction at this point would be approximately 16 kg/cm² (1600 kPa). The conventional effective stress equation for a two-phase system will not hold below this water content as the soil then constitutes a three-phase system.

In the analyses previously reviewed for the prediction of heave, the suction and the free swell test were used to estimate the final equilibrium conditions. Since the test results appear to be essentially the same, either analysis should give the same equilibrium conditions up to the air entry value of the soil. The main discrepancy would occur in the recompression range of the curves.

The rate of consolidation for Regina clay in the suction tests and in the one-dimensional consolidation test are also compared. Figure 12 shows the coefficient of consolidation versus soil suction and effective pressure for the

Fig. 4. a) Assembly of Pressure Plate extractor; b) Pressure Plate extractor.



suction tests and the one-dimensional consolidation tests. In all cases, the load increment ratio was approximately 1. Since several of the factors affecting the coefficient of consolidation are equal in both tests, it is advantageous for the sake of clarity to plot pressure versus time to 50 per cent consolidation for a corrected length of drainage path. Figure 13 shows the plot of time to 50 per cent consolidation versus effective pressure for a corrected drainage length of 1 cm. The results show that at very low effective pressures (approximately 0.1 kg/cm^2 (10 kPa)) the time to reach 50 per cent consolidation for both types of tests is similar. At higher effective pressures the suction test requires much longer time for 50 per cent consolidation.

Conclusions

The following conclusions have been reached in this investigation:

- (1) The virgin compression branch of the suction and the one-dimensional consolidation test results are essentially the same in the pressure range tested.
- (2) The recompression branch of the suction test shows no distinct break in curvature at the preconsolidation pressure. At a given stress within the recompression range the equilibrium moisture content in the suction test is lower than in the conventional consolidation test. This difference is believed to be a result of structural resistance to recompression due to shearing stresses and/or side friction in the consolidation ring.
- (3) When Regina clay is dried from a slurried condition, the soil remains saturated to a water content near the plastic limit which corresponds to a soil suction of approximately 16 kg/cm^2 (1600 kPa). At water contents lower than the plastic limit, air invasion takes place resulting in partial saturation. At this and lower water contents the suction and the one-dimensional tests are not comparable.

Fig. 5. Pressure Membrane extractor: a) Assembly of Pressure Membrane extractor; b) Section view of extraction process.

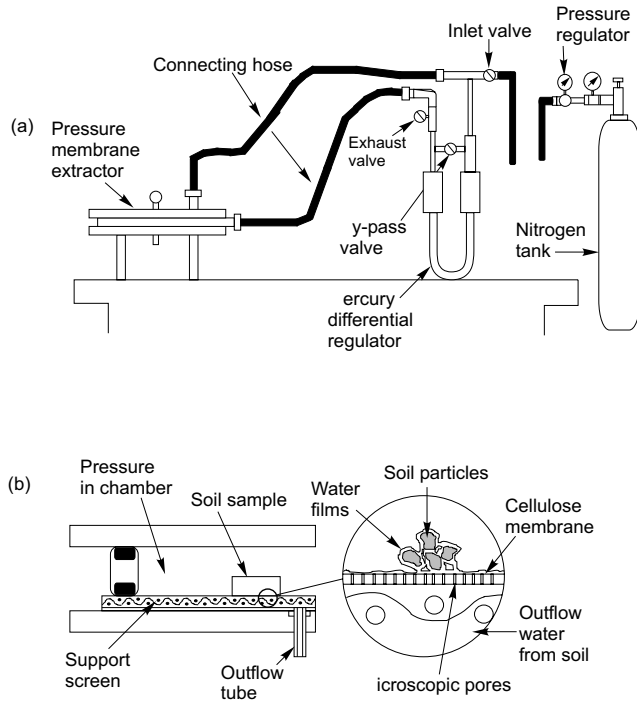
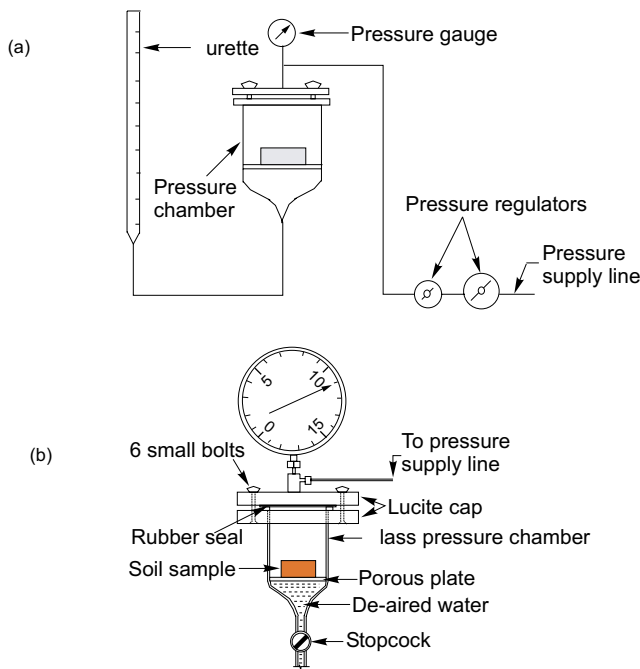


Fig. 6. a) Assembly of new Porous Plate apparatus; b) New Pressure Plate apparatus.



(4) The rate of consolidation appears to be different in the suction test than in the one-dimensional consolidation test. At low levels of effective stress (i.e., below 0.15 kg/cm^2 or 15 kPa) the rate in the former is

Fig. 7. Soil suction versus water content for remolded Regina clay.

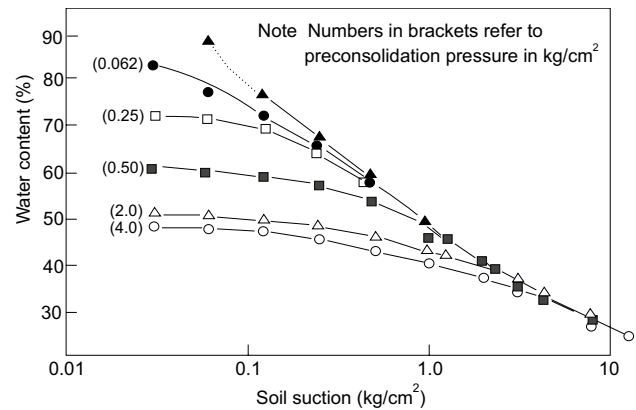


Fig. 8. Effective pressure versus water content for remolded Regina clay derived from one-dimensional consolidation tests.

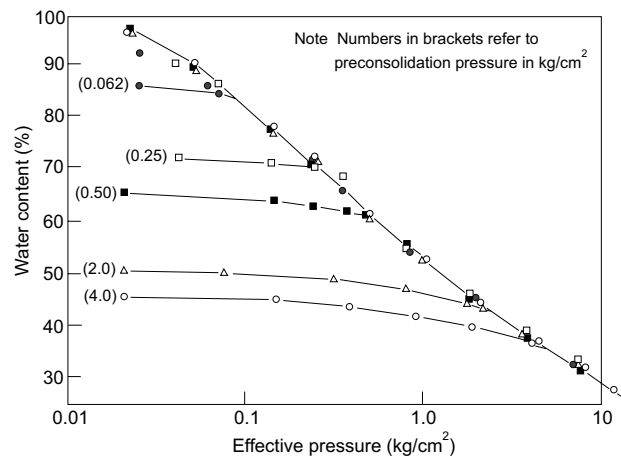
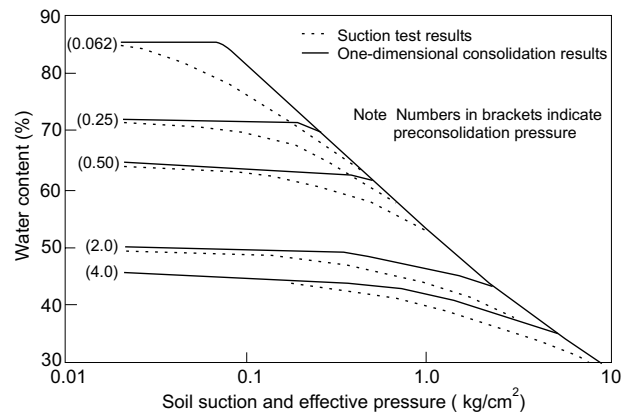


Fig. 9. Comparison of recompression branches for suction and one-dimensional consolidation tests for Regina clay.



greater than in the latter. At higher stress levels the reverse is true with the difference in rate increasing at higher effective stress levels. The plot of consolidation time to 50 per cent consolidation versus effective

Fig. 10. Specific bulk volume-water content for Regina clay.

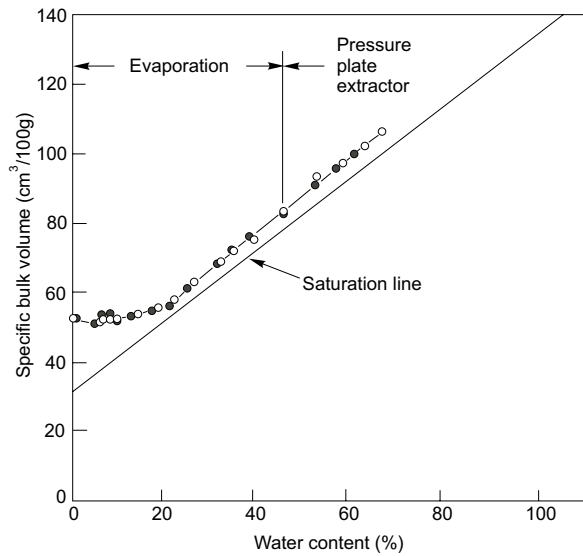
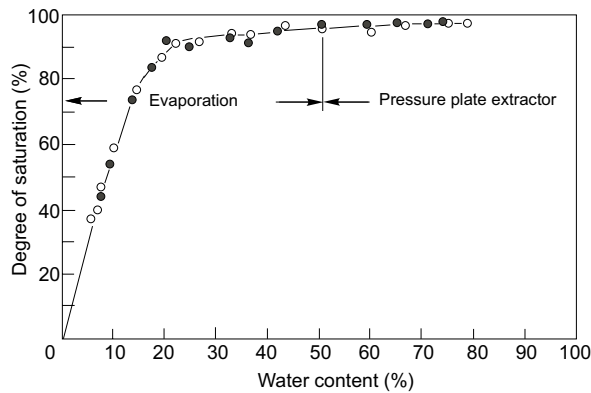


Fig. 11. Degree of saturation-water content relationship of Regina clay.



tive pressure shows the time to be longer in the suction test with a greater difference with increasing pressure. The low effective pressure range should, therefore, be further investigated.

Acknowledgements

The author's interest in the shrinking and swelling behaviour of highly plastic clay soils was stimulated during summer employment with the National Research Council of Canada at the Prairie Regional Laboratory in Saskatoon, Saskatchewan.

He wishes to acknowledge the guidance and assistance given during the study and in the preparation of this report by Mr. J. J. Hamilton of the Division of Building Research and Dr. S. Thomson of the Civil Engineering Department, University of Alberta.

References

Aboshi, H., and Monden, H. 1961. Three dimensional consolidation of saturated clays. Proceedings, 5th International Con-

Fig. 12. Coefficient of consolidation in the one-dimensional consolidation and suction tests versus effective pressure.

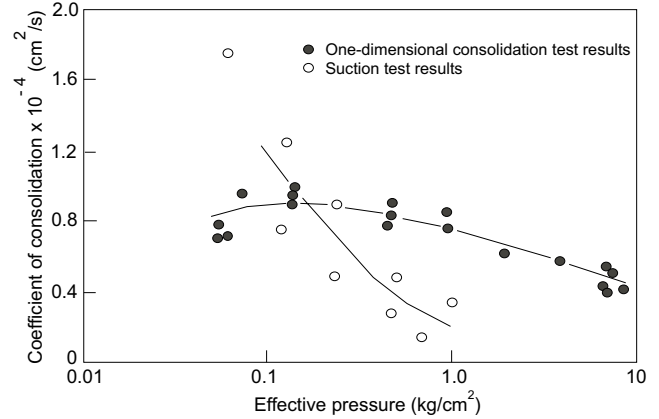
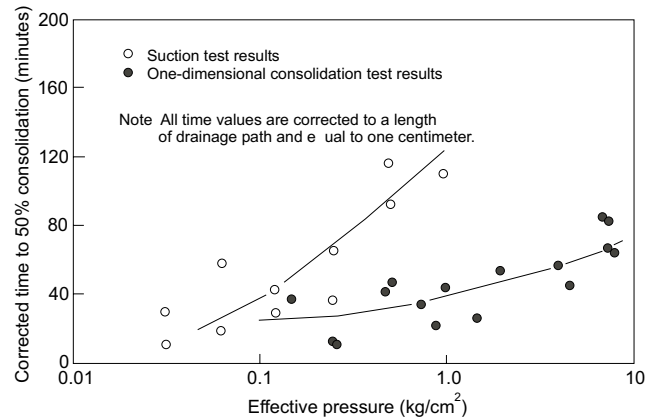


Fig. 13. Corrected time to 50% consolidation in the one-dimensional consolidation and suction tests versus effective pressure.



ference of Soil Mechanics and Foundation Engineering, Paris, France, Vol. 1, pp. 559-562.

Aitchison, G.D. 1960. Relationship of moisture stress and effective stress functions in unsaturated soils. *In Pore Pressure and Suction in Soils Conference*, London, Butterworths, pp. 47-52.

Aitchison, G.D., and Holmes, J.W. 1961. Suction profiles in soils beneath covered and uncovered areas. Proceedings, 5th International Conference on Soil Mechanics and Foundation Engineering, Paris, France, Vol. 2, pp. 187-191.

Baracos, A., and Marantz, O. 1952. Vertical ground movements. Proceedings, 6th Canadian Soil Mechanics Conference of the Associate Committee on Soil and Snow Mechanics, National Research Council Tech. Memo. Vol. 27, pp. 29-36.

Baracos, A., and Bozozuk, M. 1957. Seasonal movement in some Canadian clays. Proceedings, 4th International Conference on Soil Mechanics and Foundation Engineering, London, Vol. 3, pp. 264-268.

Bishop, A.W., and Henkel, D.J. 1962. The measurement of soil properties in the triaxial test. Second Edition. Edward Arnold (Publishers) Ltd.

- Burland, J.B. 1962. The estimation of field effective stress and the prediction of total heave using a revised method of analyzing the double oedometer test. *Die Sivielle Ingenieur in Suid-Afrika*, July.
- Croney, D., Coleman, J.D., and Bridge, P.M. 1952. The suction of moisture held in soil and other porous materials. Road Research Technical Paper No. 24, H. M. Stationary Office, London.
- Croney, D., Coleman, J.D., and Black, W.P.M. 1958. Movement and distribution of water in soil in relation to highway design and performance. Water and its conduction in soils. Highway Research Board, Special Report No. 40, pp. 226–252.
- Fredlund, D.G. 1964. Comparison of soil suction and one-dimensional consolidation characteristics of a highly plastic clay. M.Sc. thesis, University of Alberta, Edmonton, AB, Canada.
- Hamilton, J.J. 1963. Volume changes in undisturbed clay profiles in Western Canada. *Canadian Geotechnical Journal*, **1**(1): 27–42.
- Jennings, J.E.B. 1960. A revised effective stress law for use in the prediction of the behaviour of unsaturated soils. Proceedings, Conference on Pore Pressure and Suction in Soils, Butterworths, London, pp. 26–30.
- Jennings, J.E.B., and Knight, K. 1957. Discussion by G. W. Donaldson and G. M. A. de Bruijn of “The prediction of total heave from the double oedometer test”. Symposium on Expansive Soils, Transactions of the South African Institution of Civil Engineers, **7**(9):13–19.
- Jennings, J.E.B., and Kerrich, J.E. 1962. The heaving of buildings and the associated economic consequences, with particular reference to the Orange Free State goldfields. *Die Sivielle Ingenieur in Suid-Afrika*.
- Penner, E. 1959. Soil moisture suction - its importance and measurement. National Research Council, Ottawa, Technical Paper No. 76.
- Richards, L.A., and Fireman, M. 1943. Pressure plate apparatus for measuring moisture sorption and transmission by soils. *Soil Science*, **56**: 395–404
- Russam, K. 1962. The distribution of moisture in soils at overseas airfields. Road Research Technical Paper No. 58, London, England.
- Taylor, D.W. 1948. Fundamentals of soil mechanics. John Wiley and Son, New York, NY.

Prediction of the soil-water characteristic curve from grain-size distribution and volume-mass properties

M.D. Fredlund, G.W. Wilson, and D.G. Fredlund

Abstract: This paper presents a method of estimating the soil-water characteristic curve from the grain-size distribution curve and volume-mass properties. The grain-size distribution is divided into small groups of uniformly-sized particles. A packing porosity and soil-water characteristic curve is assumed for each group of particles. The incremental soil-water characteristic curves are then summed to produce a final soil-water characteristic curve. Prediction of the soil-water characteristic curve from grain-size distribution allows for a inexpensive description of the behavior of unsaturated soils. The soil-water characteristic curve forms the basis for computer modelling of processes in unsaturated soils.

Key words: Grain size curve, soil-water characteristic curve, curve fitting, particle size distribution.

Introduction

This paper presents a model for the prediction of the soil-water characteristic curve, (SWCC), based on the particle-size distribution, dry density, void ratio, and specific gravity of a soil. The model first fits a modification of the Fredlund and Xing (1994) equation to the grain-size distribution curve (Fig. 1). The grain-size distribution curve is then analysed as an incremental series of particle sizes from the smallest to the largest in order to build an overall soil-water characteristic curve. Small increments of uniform-sized particles are transposed to obtain a soil-water characteristic curve representing the average particle size. Once the entire grain-size distribution curve is incrementally analysed, the individual soil-water characteristic curves are superimposed to give the soil-water characteristic curve for the entire soil.

In order to build the general soil-water characteristic curve, it must be assumed that the soil-water characteristic curve for each uniform particle size is relatively unique. Typical soil-water characteristic curves and grain-size distribution curves for a mixture of sand, silt, and clay were obtained from SoilVision (Fredlund et al. 1996), which contains data on over 6000 soils. The soil-water characteristic curves were then fitted with the Fredlund and Xing (1994) equation. This provided an approximation for the curve fitting parameters in the Fredlund and Xing (1994) equation classified according

to dominant particle size. Parameters used in the Fredlund and Xing (1994) equation for soils composed entirely of sand or entirely of clay are easy to obtain. Uniform soils containing only mid-range particle sizes are more difficult to obtain and as a result some estimation is required.

During development of the algorithm to predict the soil-water characteristic curve, it was decided that provision must be made for the storage of grain-size information. If grain-size information was to be stored, a method of mathematically representing each grain-size curve should be found. The benefits of a mathematical fit would be two-fold. A grain-size curve fit with a mathematical equation would then allow further computations to be performed on the curve. It was reasoned that a prediction of the soil-water characteristic curve would be possible if the grain-size distribution could be fit with an equation. This idea was then implemented in the form of a least-squares curve-fitting algorithm which allowed for fitting of the grain-size distribution data.

The second benefit of mathematically representing each grain-size curve was that it would provide coefficients of indices by which grain-size curves could be classified. This provides the ability to search the database for soils with grain-size curves within a specified band. This technique has proven invaluable in performing sensitivity analyses on soil parameters.

Theory for mathematically representing the grain-size distribution curve

Previous research work to fit the grain-size curves was reviewed. Wagner (1994) presented several lognormal distributions capable of fitting the grain-size curve. Providing a meaningful representation of the grain-size data in the extremes proved difficult for a lognormal distribution.

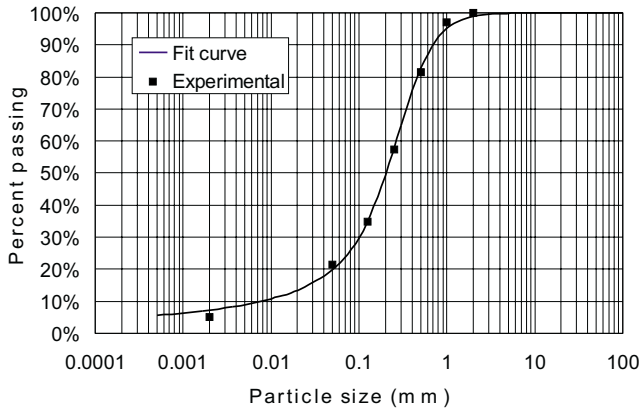
Due to similarity between the shape of the grain-size distribution and the shape of the soil-water characteristic

M.D. Fredlund, Graduate Student, Department of Civil Engineering, University of Saskatchewan, 57 Campus Drive Saskatoon SK, Canada S7N 5A9.

G.W. Wilson and D.G. Fredlund, Professors, Department of Civil Engineering, University of Saskatchewan, 57 Campus Drive Saskatoon SK, Canada S7N 5A9.

Reproduced with permission from the *Proceedings, 3rd Brazilian Symposium on Unsaturated Soils*, Rio de Janeiro, Brazil, April 22–25, 1997. A.A. Balkema, Rotterdam. Vol. 1, pp. 13–23.

Fig. 1. Fit grain-size curve using a modified Fredlund and Xing (1994) equation (# 10741).



curve, a different approach was taken. The Fredlund and Xing (1994) equation, which had previously been used to fit soil-water characteristic curve data, provided a flexible and continuous equation that could be fit by the non-linear regression using three parameters. The equation was modified to permit the fitting of grain-size curves. The modified equation, eq. [1], allows for a continuous fit and proper definition of the extremes of the curve.

$$[1] \quad P_p(d) =$$

$$\frac{1}{\ln \left[\exp(1) + \left(\frac{g_a}{d} \right)^{g_n} \right]^{g_m}} \left[1 - \frac{\left[\ln \left(1 + \frac{d_r}{d} \right) \right]^7}{\left[\ln \left(1 + \frac{d_r}{d_m} \right) \right]^7} \right]$$

where:

- $P_p(d)$ = percent passing a particular grain-size, d ,
- g_a = fitting parameter corresponding to the initial break in the grain-size curve,
- g_n = fitting parameter corresponding to the maximum slope of grain-size curve,
- g_m = fitting parameter corresponding to the curvature of the grain-size curve,
- d = particle diameter (mm),
- d_r = residual particle diameter (mm), and
- d_m = minimum particle diameter (mm).

Theory of predicting the soil-water characteristic curve from the grain-size distribution

The mathematical fit of the grain-size distribution led to the development of an algorithm capable of predicting the soil-water characteristic curve. A review of current research showed that one of two approaches have typically been taken in the prediction of the soil-water characteristic curve from grain-size. The first approach entails a statistical estimation of properties describing the soil-water characteristic curve from grain-size and volume-mass properties (Gupta 1979; Ahuja 1985; Ghosh 1980; Aberg

1996) It appeared that a theoretical approach to the problem would hopefully provide superior predictions.

The second approach was theoretical and involved converting the grain-size distribution to a pore-size distribution which was then developed into a soil-water characteristic curve (Arya 1981). This research was duplicated and compared to experimental data. Difficulty was encountered in generating a reasonable soil-water characteristic curve along the entire range. Predicted soil-water characteristic curves typically showed abnormal “humps” and fell to zero volumetric water content long before the experimental data was completely desaturated (Fig. 2).

A new approach is proposed for predicting the soil-water characteristic curve from the grain-size distribution curve. It was assumed that a soil composed entirely of a uniform, homogeneous particle size would have a unique soil-water characteristic curve. The shape of the soil-water characteristic curve for pure sands, pure silts and pure clays was known. Using a best-fit analysis with the Fredlund and Xing (1994) equation, three parameters were computed for each soil type. It was then assumed that these parameters could be associated with a dominant particle size on the grain-size plot. The uniqueness of the soil parameters was confirmed by querying the SoilVision database for plots of the n and m parameters versus the percent sand, silt, and clay of a soil. It was hypothesized that as a soil tended towards uniformity, the n and m parameters would show a trend towards a particular value. The particle sizes falling between pure clays, pure silts and pure sands were then approximated. This resulted in the production of two plots, one for the n parameter, and one for the m parameter. These plots described the variation in the n and m parameters with grain-size and allowed n and m parameters to be estimated for any soil composed of uniform diameter particles.

The grain-size distribution curve can be divided up into small divisions of uniform soil particles. Starting at the smallest diameter size, a packing porosity was estimated (Harr 1977) for each division and a soil-water characteristic curve estimated as shown in Fig. 3. The divisional soil-water characteristic curves were then summed starting with the smallest particle size and continuing until the volume of pore space is equal to that of the entire heterogeneous soil. The result is a theoretically predicted soil-water characteristic curve.

Implementation of the soil-water characteristic curve prediction into SoilVision

Information relevant to describing the grain-size distribution is organized in a single form in the SoilVision knowledge-based system. Figure 4 shows the grain-size form for the knowledge-based system. Two pages are required to present the information. The first page contains parameters controlling the fit of grain-size, the smallest particle diameter, the error between the fit data and experimental data, the error between predicted soil-water

Fig. 2. Illustration of abnormalities associated with prediction of soil-water characteristic curve from pore-size distribution.

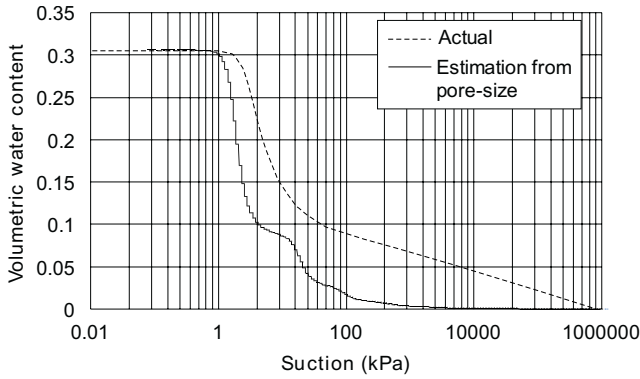


Fig. 3. Small divisions of particle size used to build complete soil-water characteristic curve.

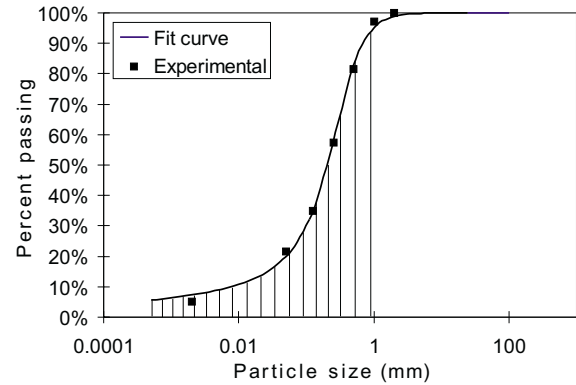


Fig. 4. Page one of the grain-size distribution form.

The screenshot shows a software window titled 'Soils'. It contains several input fields and a table. The 'Project_ID' is 'P1003' and 'Soil_Counter' is '1'. The 'Texture' is 'Clay' and 'Soil Group' is empty. The 'Structure grade' is 'Strong'. The 'Mineralogy' table lists minerals and their percentages. The 'Soil Name' is 'Frank' and the 'Soil Description' is 'This is a trial soil obtained from Xing's Actual.dat file'. The 'Notes' field contains a disclaimer: 'Note: this soil is NOT A REAL SOIL but was created during the testing and development of the database system.' The 'Contact' is 'Murray Fredlund' and the 'Rating' is '8'.

Mineral:	Percentage of Mineral:
Smectite	20.00%
Fe-Mg chlorite	30.00%
K-Feldspar	13.00%
Quartz	4.00%
Kaolinite	6.00%

characteristic curve and experimental data predicted and experimental data, and counters which Access® uses to identify individual records. *Page one* also contains the packing porosity field which controls the prediction of the soil-water characteristic curve. *Page two* displays the equation used to fit the experimental data as well as experimental data points and generated data points on the best fit curve. Figure 5 shows the second page of the grain-size distribution form.

The header on the form allows for a number of helpful functions and algorithms. If soil data consists of % Coarse, % Sand, % Silt, % Clay or D10, D20, D30, D50, or D60 data on *page two* of the main soil form, pressing a button will convert this data into experimental points along the grain-size distribution graph. Once ex-

perimental data is obtained, pressing Fit Curve! will initiate the linear regression algorithm that will best-fit the equation to experimental data. The results of the fit can be viewed by pressing the Graph! button and a soil-water characteristic curve can be predicted by pressing the Predict SWCC button.

Conclusions

The readapted Fredlund and Xing (1994) equation produces a satisfactory fit of the grain-size distribution. Figure 3 shows that the experimental data can be fit with a minimal error. A good curve fit of the grain-size curve is essential for the prediction of a reasonable soil-water characteristic curve. The minimum particle size was also

Fig. 5. Page two of the grain-size distribution form.

Fig. 6. Grain-size distribution fit for a sand (# 10720).

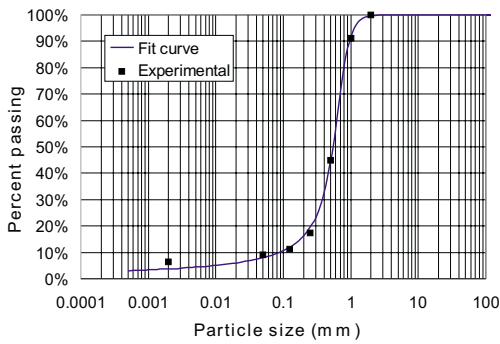


Fig. 7. Comparison between experimental and predicted curves for a sand (# 10720).

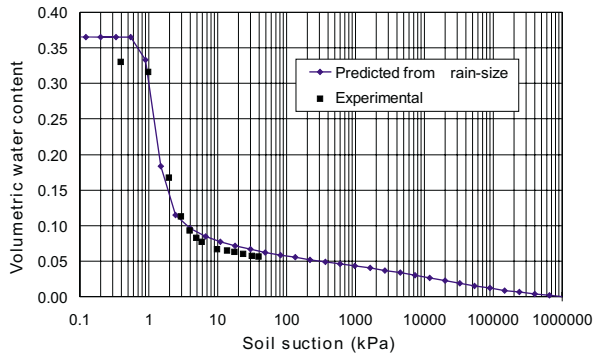


Fig. 8. Grain-size distribution fit for a loamy sand (# 10741).

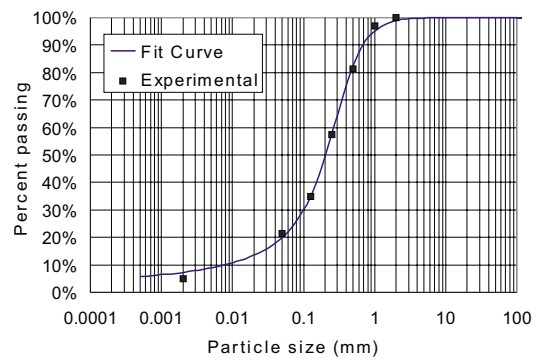


Fig. 9. Comparison between experimental and predicted curves for a loamy sand (# 10741).

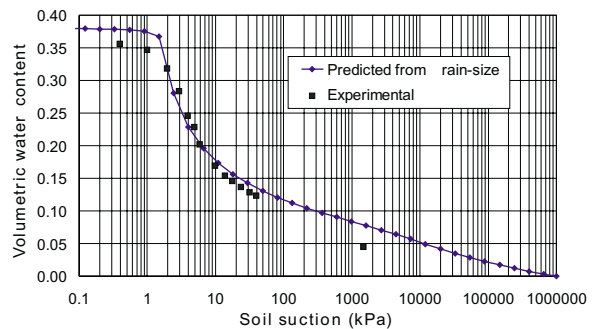
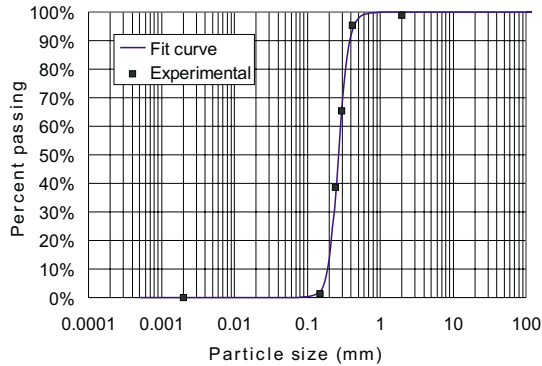
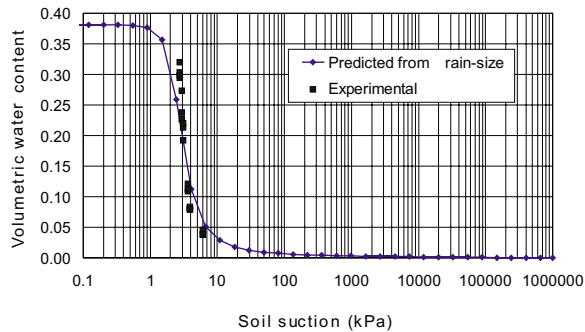


Fig. 10. Grain-size distribution for a sand (# 350).**Fig. 11.** Comparison between experimental and predicted data for a sand (# 350).

found to have an influence on the prediction of the soil-water characteristic curve prediction. If the minimum particle size variable was too low, the overabundance of clay size particles would dominate the prediction. If the minimum particle size was too high, an absence of smaller particles would result in the soil drying out prematurely.

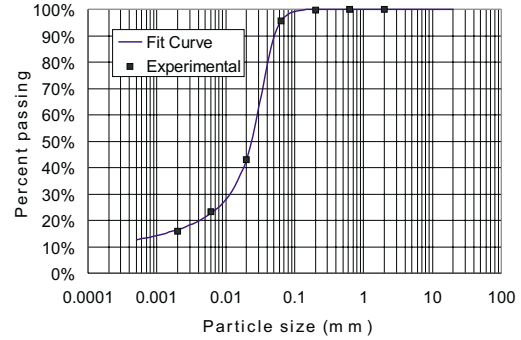
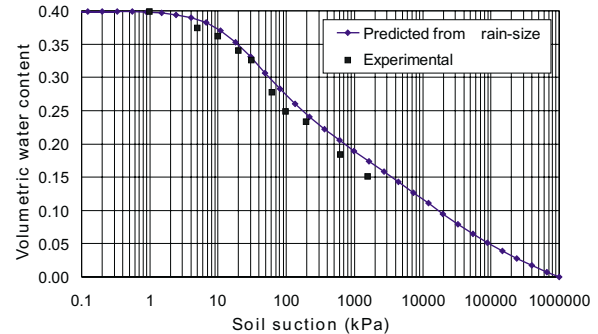
The prediction of soil-water characteristic curve from the grain-size distribution was found to be particularly accurate for sands, and reasonably accurate for silts. Clays, tills and loams were more difficult to predict although the accuracy of the prediction algorithm appears to be reasonable. Results tended to be sensitive to the packing porosity and more research is required in this regard. Soils with experimental data for both the grain-size curve and the soil-water characteristic curve were extracted from the database. The results of comparisons between experimental and predicted data can be seen in Figs. 6 to 13.

Acknowledgements

The authors wish to acknowledge the help received from Dr. Sai Vanapalli.

References

Aberg, B. 1996. Void sizes in granular soils. *Journal of Geotechnical Engineering*, **122**(3): 236–239.

Fig. 12. Grain-size distribution for a silt loam (# 10861).**Fig. 13.** Comparison between experimental and predicted data for a silt loam (# 10861).

Ahuja, L.R., Naney, J.W., and Williams, R.D. 1985. Estimating soil-water characteristics from simpler properties or limited data. *Soil Science Society of America Journal*, **49**: 1100–1105.

Arya, L.M., and Paris J.F. 1981. A physicoempirical model to predict the soil moisture characteristic from particle-size distribution and bulk density data, *Soil Science Society of America Journal*, **45**: 1023–1030.

Fredlund D.G., and Xing, A. 1994. Equations for the soil-water characteristic curve. *Canadian Geotechnical Journal*, **31**(3):521–532.

Fredlund, M.D., Sillers, W., Fredlund, D.G., and Wilson, G.W. 1996. Design of a knowledge-based system for unsaturated soil properties. *Proceedings, 3rd Canadian Conference on Computing in Civil Engineering*, August 26–28, Montreal, Quebec, pp. 659–677.

Ghosh, R.K. 1980. Estimation of soil-moisture characteristics from mechanical properties of soils. *Soil Science Journal*, **130**(2): 60–63.

Gupta, S.C., and Larson, W.E. 1979. Estimating soil-water retention characteristics from particle size distribution, organic matter percent, and bulk density. *Water Resources Research Journal*, **15**(6): 633–1635.

Harr, M.E. 1977. *Mechanics of particulate media*. McGraw-Hill International Book Company, New York.

Wagner, L.E., and Ding, D. 1994. Representing aggregate size distributions as modified lognormal distributions. *American Society of Agricultural Engineers*, **37**(3): 815–821.

Design of a knowledge-based system for unsaturated soil properties

M.D. Fredlund, W.S. Sillers, D.G. Fredlund, and G.W. Wilson

Abstract: The soil-water characteristic curve (SWCC) is an important soil function relating the water content in a soil to soil suction. Many soil properties (or functions) can be related to the water content versus suction relationship of a soil. Hydraulic conductivity, shear strength, chemical diffusivity, chemical adsorption, storage, unfrozen volumetric water content, specific heat, thermal conductivity and volume change are all functions of the soil-water characteristic curve. Considerable judgement is required to develop the relationship between soil property functions. The judgement rules can be enforced by a knowledge-based system based on observations and empirical relationships. A knowledge-based system was developed using a relational database management system (RDBMS) known as Microsoft's Access® database program. Access® provided a suitable environment for combining the user interface, knowledge base, database, and query system. This system provides an estimate of the soil-water characteristic curve as well as the other unsaturated soil property functions using basic soil classification data such as grain-size distribution, density and specific gravity. The system allows estimation for many complex soil properties while reducing both time and cost requirements.

Key words: unsaturated soil property functions, soil-water characteristic curve, knowledge-based system, database, classification properties.

Introduction

Theory governing the behaviour of unsaturated soils has been available for several years and has shown that the soil-water characteristic curve is the central relationship describing how a soil behaves as it desaturates. Research has shown that empirical relationships can be used to describe property functions related to the soil-water characteristic curve. These empirical relationships can then be used to predict how the permeability, shear strength, thermal properties, diffusion and adsorption will behave as a soil desaturates. The principles of how an unsaturated soil behaves are encoded into the knowledge-based system. The process for predicting the behaviour of unsaturated soils is then greatly simplified. General soil properties are stored in a primary knowledge frame. Subsidiary properties are stored in frames with links respective to the main soil frame. Knowledge was acquired by interviewing experts in the field as well as researching current publications. Soils information for the soils database was acquired from several different sources with a total of approximately 6000 soils represented in the database.

D.G. Fredlund and G.W. Wilson. Professors, Department of Civil Engineering, University of Saskatchewan, 57 Campus Drive, Saskatoon, SK, Canada S7N 5A9
M.D. Fredlund, W.S. Sillers. Graduate Students, Department of Civil Engineering, University of Saskatchewan, 57 Campus Drive, Saskatoon, SK, Canada S7N 5A9

Reproduced with permission from the *Proceedings, Third Canadian Conference on Computing in Civil and Building Engineering*, Montreal, Que., Canada, April 26–28, 1996. Canadian Society for Civil Engineering. pp. 659–677.

Problem definition

Classical soil mechanics has emphasized specific types of soils (e.g., saturated sands, silts, and clays and dry sands). Textbooks cover these types of soils in a completely dry or a completely saturated condition. Recently, it has been shown that attention must be given to soils that do not fall into common categories. A large portion of these soils can be classified as unsaturated soils. Unsaturated soils have typically been avoided due to the complexity of their behaviour. An unsaturated soil consists of more than two phases and therefore the natural laws governing its behaviour are changed. Central to the behaviour of an unsaturated soil is the relationship between water and air as the soil desaturates. This relationship is described as the soil-water characteristic curve (SWCC). Laboratory studies have shown that there is a relationship between the soil-water characteristic curve and unsaturated soil properties (Fredlund and Rahardjo 1993). Properties such as hydraulic conductivity, shear strength, storage, unfrozen water content, specific heat, thermal conductivity, diffusion and adsorption can all be related to the soil-water characteristic curve. Until present, however, a method of combining unsaturated soil property functions into a single system has not existed. The knowledge system provides a way to link complex property functions together to describe the behaviour of an unsaturated soil.

The soil-water characteristic curve (SWCC)

The soil-water characteristic curve, typically the desaturation or moisture retention curve, is a continuous sigmoidal function representing the water storage capacity of a soil as it is subjected to increasing soil suction. It

is the relationship between volumetric water content, θ , and stress state, $(u_a - u_w)$. The soil-water characteristic curve can be used as a means of deriving and linking soil behaviours such as permeability, shear strength and volume change. It is the centre or base of the engineering behaviour of an unsaturated soil. The soil-water characteristic curve provides a means of relating the fundamental soil properties to each other and controlling the state at which each engineering behaviour is calculated. This is important for modelling more than one aspect of soil behaviour in a single analysis. The soil-water characteristic curve contains three important pieces of information: pore size distribution, amount of water contained in the pores at any suction and the stress state of the soil and soil water. The soil-water characteristic curve has three stages which describe the process of desaturation of a soil (i.e., increasing suction). These are outlined below starting at saturation of the soil.

- (1) The Capillary Saturation Zone, where the pore-water is in tension but the soil remains saturated due to capillary forces. This stage ends at the air entry value $(u_a - u_w)_b$, where the applied suction overcomes the capillary water forces in the soil and air enters the soil pores.
- (2) The Desaturation Zone, where water is displaced by air within the pores. Liquid water drains from the pores and is displaced by air. This stage ends at the residual water content, θ_r , where pore-water becomes occluded and the permeability is greatly reduced.
- (3) The Residual Saturation Zone, where the water is tightly adsorbed onto the soil particles and flow occurs in the form of vapour. In this stage the term suction loses its physical significance. Instead it can be regarded as a term for energy required to withdraw a unit of water from a mass of soil. This stage is terminated at oven dryness. When the soil is heated to 105°C, corresponding to a suction of approximately 1×10^6 kPa, and is assumed to have zero water content. This point is a benchmark for all soils, any water not driven off is chemically bonded to the soil and is not important with respect to engineering behaviour.

The soil-water characteristic curve is a measured soil property that is used to derive other soil functions and provides a common reference to stress state at which other properties are calculated. In other words, it ensures that each soil property is calculated at the same state.

Methods of obtaining soil-water characteristic curve

There are several methods available in the knowledge-based system for obtaining a soil-water characteristic curve for a particular soil. The method used should be determined by the application for which the soil-water characteristic curve will be used and its desired accuracy. The most accurate way to determine a soil-water characteristic curve is through laboratory experimentation. Because of the high cost of lab equipment and the time required to run this test, alternate methods are often desirable. The knowledge-based system provides three alternative meth-

ods of determining a soil-water characteristic curve. The first method involves searching the database for a soil with similar properties as the current soil being analyzed and assuming a similar soil-water characteristic curve. Secondly, the knowledge-based system will “look up and suggest” reasonable fitting parameters based on the current soil properties. To accommodate recent research, a third method was also provided in the system. It has been found that correlations exist between the grain-size distribution and the soil-water characteristic curve (Arya and Paris 1981). A method was therefore developed that allowed the prediction of the soil-water characteristic curve from the grain-size distribution. The final method selected to obtain a soil-water characteristic curve will depend on a users confidence in each of the three prediction methods.

Prediction of unsaturated soil properties based on soil-water characteristic curve

Laboratory studies have shown that there is a relationship between the soil-water characteristic curve and unsaturated soil properties (Fredlund and Rahardjo 1993). To confirm this belief, a literature review was performed to determine the best prediction methods currently available. It was found that extensive research has been performed in predicting various unsaturated soil property functions. The predictions adopted for the knowledge-based system were then selected based on the following criteria. Firstly, the prediction method should have a correct theoretical basis. Statistical predictions were avoided and prediction methods were accepted if they were founded in theory governing soil behaviour. Secondly, it was attempted to find the most accurate prediction methods. The amount of error between experimental and predicted results was noted in the selection process. The prediction methods finally selected appear to be the best available in current literature.

Knowledge acquisition

The most important process in a knowledge-based system is knowledge acquisition. How the knowledge is obtained and where it is obtained determines the usefulness of the system. The knowledge-based system described in this paper compiles information from three primary sources. Experts in the field of unsaturated soils were interviewed to obtain methods and heuristics common to the field of unsaturated soils. A search of current and past research was performed to determine the framework of the system. Experimental soil data containing at the minimum a soil-water characteristic curve was required for the database system. Lastly, current computer modelling software in the field of unsaturated soils was reviewed to determine what input properties were most significant. The information was then compiled to create a system to describe the property functions for unsaturated soils.

Interviewing Experts

Much knowledge in the field of unsaturated soils can only be found by probing the minds of people currently

involved in research. Documentation of the newer techniques is not extensive, making it necessary to rely on the experience of current experts. Members of the Unsaturated Soils Group, USG, at the University of Saskatchewan provided insight and guidance into the design of the system. Mention must also be given to Walter Rawls from the USDA who provided input in determining what methods to use in the prediction of saturated hydraulic conductivity. Advice from the aforementioned experts provided the foundation for the design of the system as well as the heuristic rules used in the field of unsaturated soils.

Search of current literature

An extensive literature review was performed to determine the best prediction methods to use in the knowledge system. The prediction methods used by the knowledge system are summarized in Table 1.

Acquisition of existing databases

Existing experimental data was used as the starting point in the development of the knowledge based system. Once a database of soil information is acquired, statistical calculations can be performed to check the validity of theoretical predictions as well as providing an estimation of the reasonableness of current soil properties. Soil data is continually being added to the system but original data was collected from four main sources. Hundreds of research publications containing soil-water characteristic curves were reviewed and compiled by the co-author into a database of over 200 soils (Sillers 1997). Williams et al. (1992) from the USDA contributed soils information from his personal database of approximately 650 soils all with a well-defined soil-water characteristic curve. Rawls and Brakensiek (1989) also from the USDA contributed 4200 soils with experimentally measured soil-water characteristic curves. Finally, soils information for approximately 770 soils containing experimental grain-size, hydraulic conductivity, and soil-water characteristic curve information was contributed by Feike Leij from the USDA. In summary, this provided a database with information on approximately 6000 soils from all over the world.

Review of current computer modelling procedures

The input functions required in the five programs listed in Table 2 are used as an indication of the soil functions that are most widely used in unsaturated soils modelling.

Seepage modelling programs for unsaturated soils typically require a soil-water characteristic curve and a hydraulic conductivity curve. Either of these curves can be obtained in two main ways from the knowledge system. The curves can be theoretically predicted or the database can be searched for experimental data representing a similar soil.

TEMP/W performs uncoupled thermal analysis of soils and therefore requires property functions describing thermal conductivity and specific heat capacity. SoilCover is a fully coupled, one-dimensional finite element program

to model the flux boundary conditions at the surface of unsaturated soils. As such it requires property curves describing volumetric water content, hydraulic conductivity, thermal conductivity, specific heat capacity and unfrozen water content. To satisfy the needs of these programs, the knowledge system is capable of providing functions representing volumetric water content versus suction (soil-water characteristic curve), hydraulic conductivity versus suction, thermal conductivity versus suction, volumetric specific heat versus suction, and unfrozen volumetric water content versus degrees below freezing.

The program SIGMA/W allows for uncoupled modelling of the stress state of an unsaturated soil. To properly model this phenomenon, a function describing the relationship between the volume change of an unsaturated soil and suction and net normal stress is required. The knowledge-based system provides a method of predicting this function. For fully coupled programs modelling volume changes in soils, the system is also capable of providing property functions describing the change in void ratio versus both suction and net normal stress.

CTRAN/W allows uncoupled modelling of contaminant transport in unsaturated soils. To do modelling of contaminant transport, property functions describing how the coefficient of diffusion and the coefficient of adsorption vary according to different levels of saturation is needed. An estimate of each of these curves can be obtained by the knowledge-based system.

The knowledge-based system provides property functions to allow for coupled or uncoupled modelling in the areas of seepage, thermal, contaminant transport, and volume change.

Knowledge Representation

The area of knowledge-based systems has blossomed over the past decade from merely an academic interest into a useful technology. Carrico et al. (1989) describes knowledge systems as follows:

Knowledge systems are software systems that have structured knowledge about a field of expertise. They are able to solve some problems within their domain by using knowledge derived from experts in the field.

Development of the methods for knowledge representation followed the knowledge acquisition phase. With a suitable amount of knowledge gathered, the structure and representation method for the knowledge system can be described. The knowledge representation is shown in Fig. 1. Information was represented in frames. Each frame consisted of a database of experimental data, a database of theoretical data, a knowledge base consisting of rules and algorithms applicable to the current frame, and the user interface which allowed the information to be viewed in forms, tables, or charts. Examples of frames in the system are the main soil information frame which contains soil texture, description, volume-mass relations, soil origin, etc. or the permeability frame which stores information related to the hydraulic conductivity of a soil as well as algorithms and rules applicable to this frame.

Table 1. Summary of prediction methods used in knowledge-based system.

Description	Reference
Prediction of SWCC from grain-size curve	Fredlund (1996)
Prediction of adsorption curve from SWCC	Lim (1995)
Prediction of unfrozen volumetric water content curve from SWCC	Lim et al. (1998)
Prediction of unfrozen volumetric water content from the SWCC	Black and Tice (1989)
Prediction of specific heat capacity from the SWCC	Frouki (1986)
Prediction of thermal conductivity from the SWCC	Johansen (1975)
Prediction of quartz content	Tatnawski and Wagner (1993)
Prediction of shear strength envelope from the SWCC	Fredlund et al. (1996)
Prediction of saturated hydraulic conductivity using D_{10}	Holtz and Kovacs (1981)
Prediction of saturated hydraulic conductivity using an effective porosity, n_e	Ahuja et al. (1989)

Table 2. Software programs to model unsaturated soil properties.

Company	Product Name	Description
Geo-Slope	SEEP/W	Modelling of unsaturated soil water flow
Geo-Slope	TEMP/W	Modelling of thermal fluxes in unsaturated soils
Geo-Slope	SIGMA/W	Modelling of stress/deformation of unsaturated soils
Geo-Slope	CTTRAN/W	Modelling of contaminant processes in unsaturated soils
U. of Saskatchewan	SoilCover	Modelling of boundary fluxes in unsaturated soils

Fig. 1. Representation of knowledge in the system.

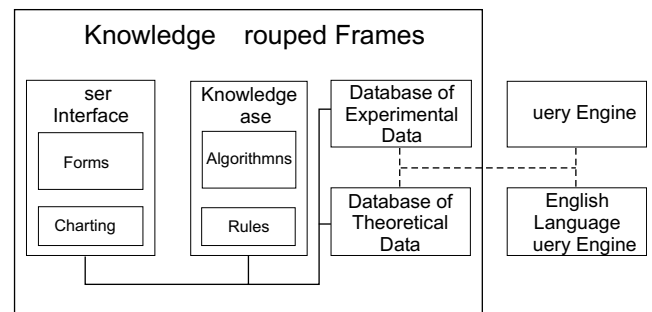


Fig. 2. Knowledge frames included in the system.

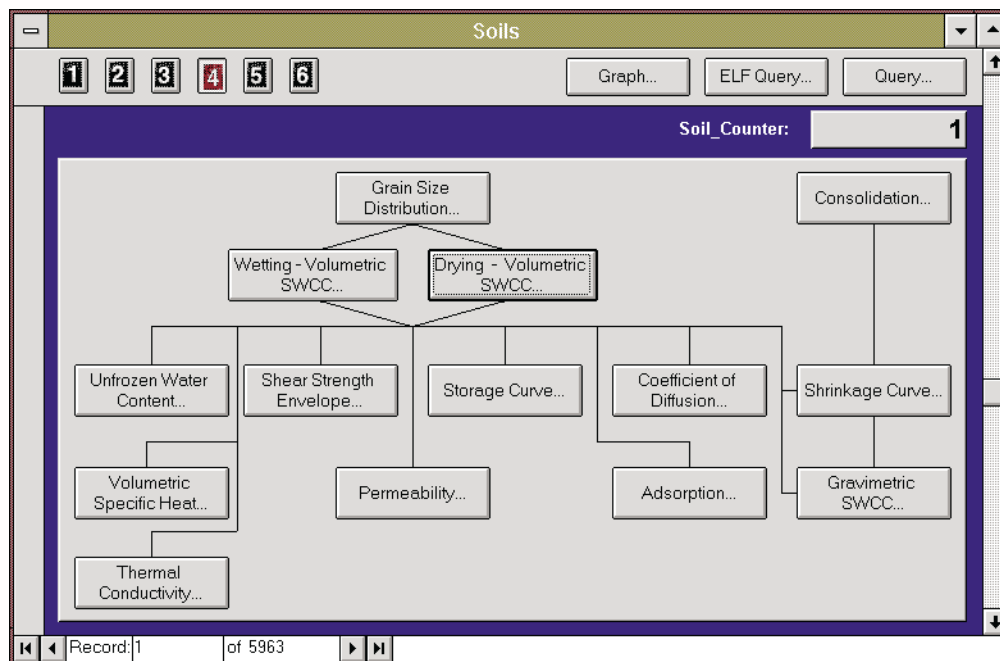
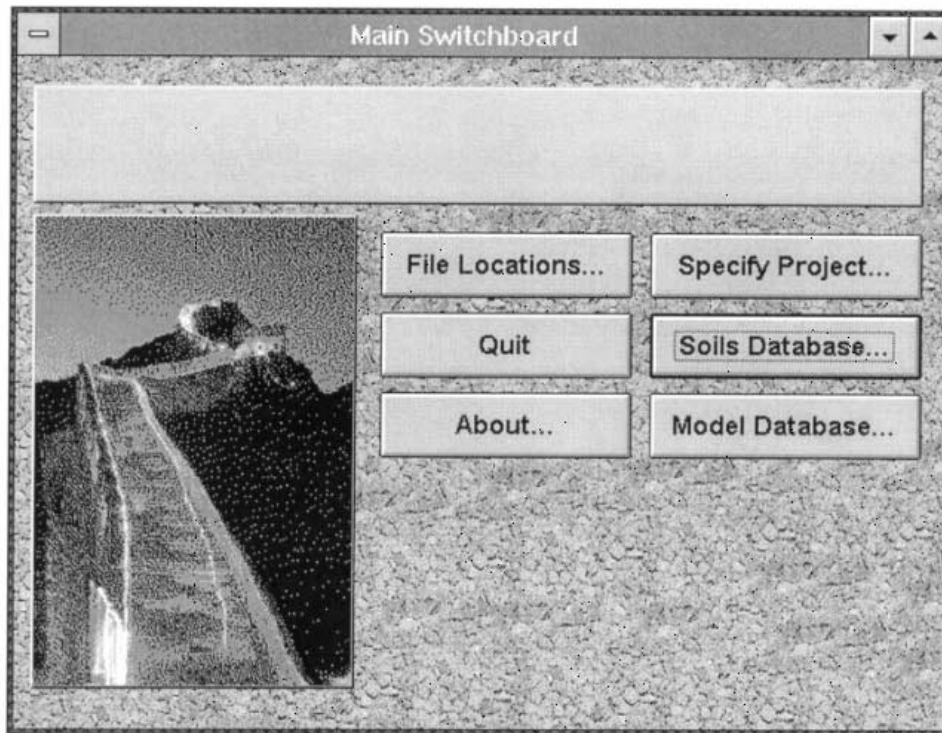


Fig. 3. Main switchboard for knowledge-based system.

Independent of the knowledge frames are two query engines which allow for access to pertinent information. The main query engine builds a query by stepping the user through a series of forms while the English language engine allows querying the database with common statements like: “Show me soils with porosities between 0.25 and 0.30.”.

The soil properties are organized into separate frames or subcategories which are linked to the main soil information frame. The manner in which this is done is shown in Fig. 2. While Fig. 1 shows the theoretical structure of the knowledge-based system (KBS), Fig. 2 displays the physical implementation of the system in Access®.

Knowledge system shell

Once the structure of the knowledge-based system was determined, a shell or programming environment was needed to build the system. The relational database shell provided by Microsoft’s Access® relational database management system (RDMS) was selected as an environment. The database system handled the manipulation of large amounts of data while allowing time to be focused on the coding of the knowledge system. The system requires at least a 486 class personal computer with 8 megabytes of RAM while a suggested system would be a Pentium class machine with 16 megabytes of RAM for operation of the system. Approximately 20 megabytes of hard disk storage are required for installation of the application. A picture of the main switchboard for the system can be seen in Fig. 3.

Knowledge-based systems typically contain an inference engine allowing for a decision-tree type of dialogue between the system and the user. The size of the unsaturated soil mechanics field and uncertainty regarding the application the system dictated several decisions. A parameter-driven inference engine was selected to lessen ambiguity. Also, the inference engine has been limited to handling the statistical estimation of soil parameters should a gap be found in the current data.

Main Soil Information Frame

The fields used for classification of the soil were adopted from current USDA soil databases for the sake of familiarity. Figure 4 shows the main text descriptors used in the classification of soils. The volume-mass and grain-size properties have also typically been used for soil classification and are shown in Fig. 5. Other soil properties that are stored are Atterberg limits, water chemistry, soil origin properties, publication information, and the geographical location of the soil (Country, State, County, Site). Soil origin fields store information such as horizon depth, horizon type, family, and soil series.

The main soil information form also provides links to the forms describing soil properties such as soil-water characteristic curve, permeability, shear strength, etc. Typical forms linked to the main soil form are described in the following sections. For the sake of brevity, not all the forms linked to the main soil form are shown.

Other frames linked to main frame

Complimentary to data stored in the main soil frame is information stored in other frames which are linked to the

Fig. 4. Page one of the main soil form showing classification properties.

Soils

1 2 3 4 5 6

Graph... ELF Query... Query...

Project_ID: F100 Soil_Counter: 1

Texture: Clay Soil_Group:

Texture Modifier:

Structure grade: Strong

Structure size:

Structure type:

Soil Name: Frank

Soil Description: This is a trial soil obtained from Xing's Actual.dat file

Notes: Note: this soil is NOT A REAL SOIL but was created during the testing and development of the database system.

Contact: Murray Fredlund

Rating: 8 1 to 10 with 10 the best

Mineral:	Percentage of Mineral:
Smectite	20.00%
Fe-Mg chlorite	30.00%
K-Feldspar	13.00%
Quartz	4.00%
Kaolinite	6.00%

Record: 1 of 5

Record: 1 of 5963

Fig. 5. Page two of the main soil form showing volume-mass classification properties.

Soils

1 2 3 4 5 6

Graph... ELF Query... Query...

Experimentally Determined:

Note... Saturation: 87.96% Predict

Vol. Water Content: 0.317

Porosity, n: 36.06%

Void Ratio, e: 0.564

Water Content, w: 18.72%

Dry Density: 1694.4 kg/m³

Total Density: 2011.6 kg/m³

Total Unit Weight: 19.734 kN/m³

Specific Gravity, G_s: 2.65

Density of Water: 1000.0 kg/m³

Accel of Gravity, g: 9.810 m/s²

Soil_Counter: 1

% Clay: 3.50% < 0.002 mm

% Silt: 5.59% 0.05 - 0.002 mm

% Sand: 44.58% 2.0 - 0.05 mm

% Coarse: 45.71% > 2.0 mm

% Organic: 5.00%

D10: 0.0659 mm

D20: 0.3368 mm

D30: 0.7082 mm

D50: 1.7435 mm

D60: 2.5241 mm

Cu: 38.304

Cc: 3.015

CALCULATE

Note: check boxes indicates lacked properties.

Record: 1 of 5963

Table 3. Properties or frames linked to the main soil frame.

Adsorption	Shear strength	Consolidation
Shrinkage	Diffusion	Specific heat
Unfrozen volumetric water content	Water storage modulus	Grain-size distribution
Volumetric soil-water characteristic curve	Gravimetric soil-water characteristic curve	Thermal conductivity
Permeability		

Fig. 6. Page one of form describing soil-water characteristic curve information.

Soil-Water Characteristic Curve (SWCC)

1 2 3 Fit All... Fit Curve! Calculate! Graph! Graph Wet/Dry! Graph Compare!

Param_ID: 451 SWCC Soil_Counter: 1

SWCC Curve Type: **Drying**

SWCC Description: Unknown Test Method

SWCC Fit Type: Fredlund & Xing (Type 1)

SWCC Fit?: Yes

Saturated Vol. Water Content: 0.317

Iteration: 624.3897

Fit Data Source: Experimental Predicted

n: 0.8039 m: 0.7339 hr: 3000.0000

SWCC Squared Residual: 0.001805

Residual VWC: 0.179

Suction Units: kPa

Record: 4 of 8

Fig. 7. Page two of form describing soil-water characteristic curve information.

Soil-Water Characteristic Curve (SWCC)

1 2 3 Fit All... Fit Curve! Calculate! Graph! Graph Wet/Dry! Graph Compare!

SWCC Equation: $\Theta_{w} = \Theta_{sat} * (1 - \ln(1 + h/3000.0000) / \ln(1 + 10^6/3000.0000)) * (1 / (\ln(\exp(1) + (h/624.3897)^{0.8039}))^{0.7339})$

Experimental Data:

Suction:	Vol. Water Content:
2.00E+01	0.317
3.00E+01	0.313
4.00E+01	0.311
5.00E+01	0.308
6.00E+01	0.305
8.00E+01	0.300
1.00E+02	0.296
1.20E+02	0.293
1.40E+02	0.289
1.60E+02	0.286
1.80E+02	0.284
2.00E+02	0.284
2.20E+02	0.279

Record: 1 of 21

Fit Data:

Suction:	Vol. Water Content:
1.00E-02	3.17E-01
1.65E-02	3.17E-01
2.72E-02	3.17E-01
4.48E-02	3.17E-01

Record: 1 of 38

Predicted from grain-size distribution:

Suction:	Vol. Water Content:
1.00E-02	0.317
1.65E-02	0.317
2.72E-02	0.317
4.48E-02	0.317

Record: 1 of 38

Record: 4 of 8

main frame. Information was organized in frames for storage efficiency reasons as well as to provide a good conceptual view of the different soil properties. The properties or frames linked to the main soil frame are listed in Table 3.

Page one of the soil-water characteristic curve frame can be seen in Fig. 6. This frame stores pertinent information relating to the soil-water characteristic curve as well as experimental and fitted points on the curve. The equation describing the curve shown in Fig. 7 is stored in the database once experimental data is fit with a curve. A focus of the knowledge-based system was to allow mathematical representation of soil property functions wher-

ever possible. This then allows the equations to be entered into finite element modelling packages for modelling of unsaturated soil behaviour. To provide a starting point for mathematical representation, the soil-water characteristic curve, grain-size distribution, and consolidation curves must be fit with a mathematical equation. A single equation was selected to fit each of the grain-size and consolidation curves. For the soil-water characteristic curve, however, a number of different equations have been previously used. To accommodate this variability, 28 different equations are available for use in the system. For each equation, a routine allowing the equation to be fit to experimental data must be provided.

Fig. 8. Page one of the shear strength frame.

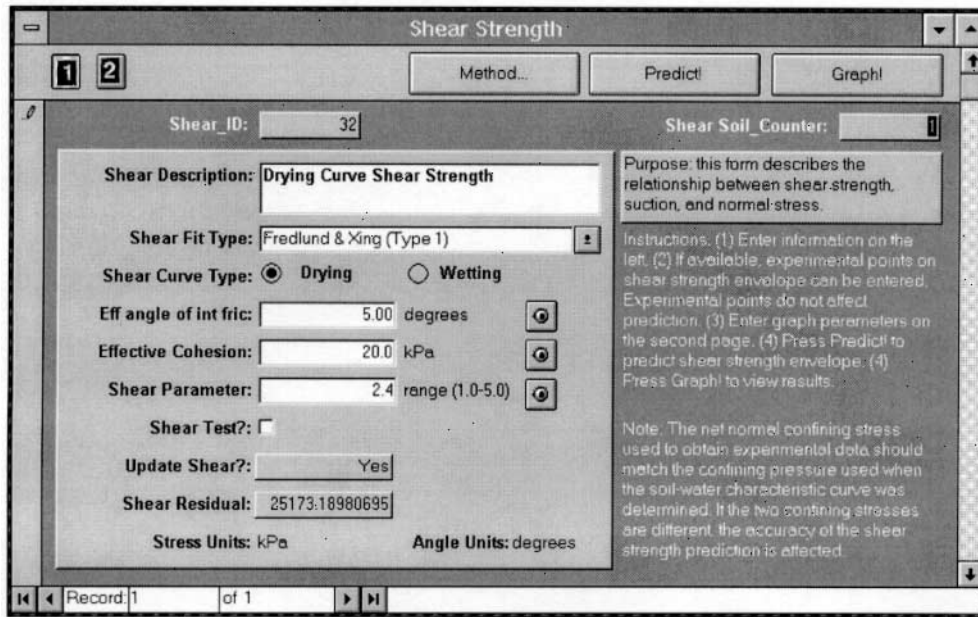
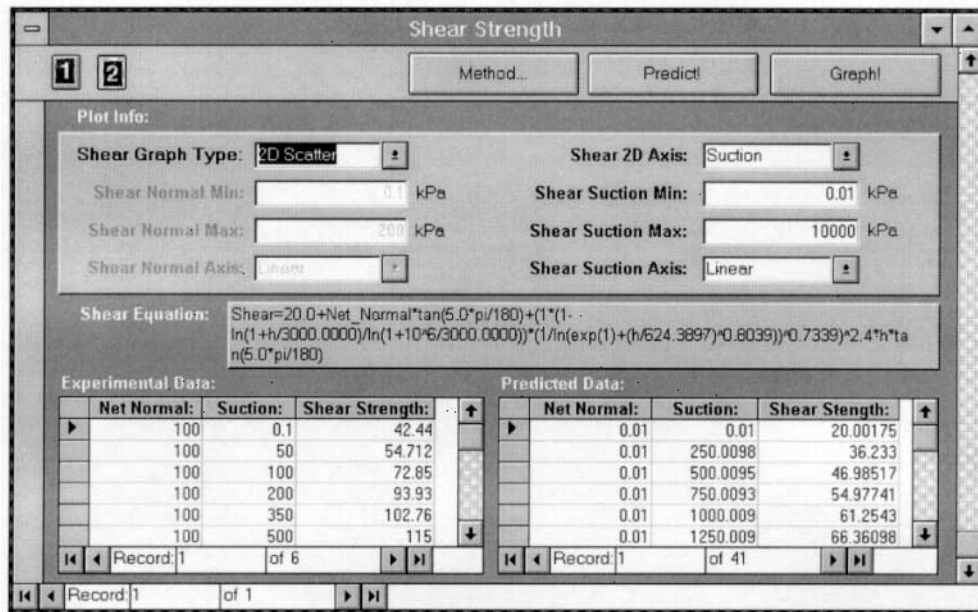


Fig. 9. Page two of the shear strength frame.



Therefore, a number of curve fitting algorithms were implemented. Once an equation is fit to experimental data, the resulting equation can be used in the calculation of other soil properties.

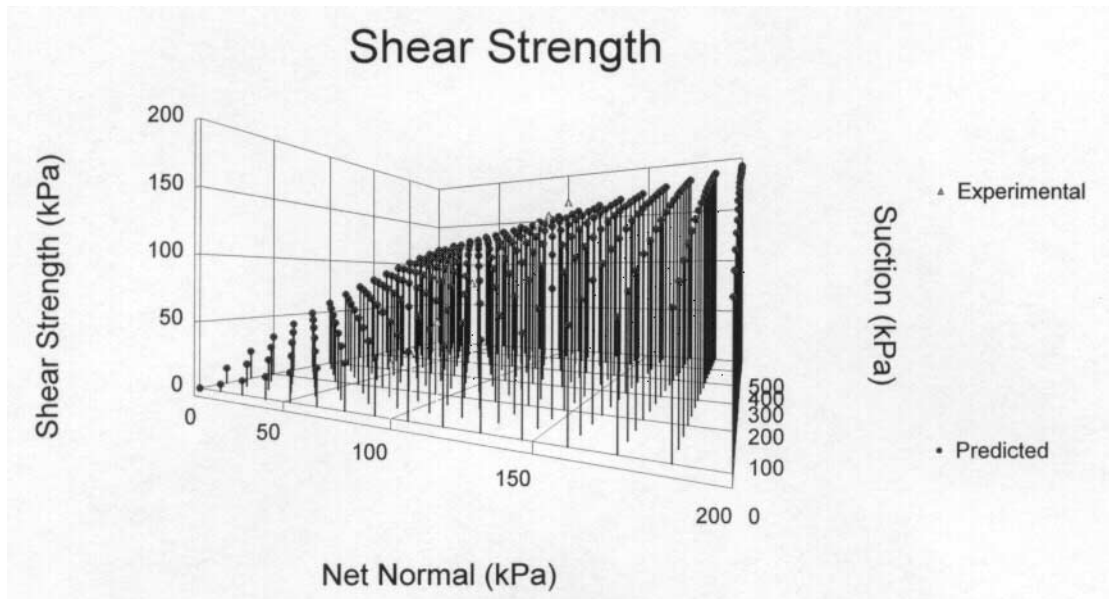
Shear strength frame

The shear strength frame provides an example of a frame linked to the main soil information frame. *Page one*, which can be seen in Fig. 8, stores soil parameters relating to the shear strength of the current soil. Knowing the effective angle of internal friction and the effective cohesion, the prediction method references the soil-water

characteristic curve to predict the shear strength of the soil will behave at different levels of saturation.

Summary

Theory governing the behaviour of unsaturated soils has been available for several years and has shown that the soil-water characteristic curve is the central relationship describing how a soil behaves as it desaturates. Research has shown that empirical relationships can be used to describe property functions related to the soil-water characteristic curve. These empirical relationships can then be used to predict how the permeability, shear

Fig. 10. Plot of predicted shear strength envelope and experimental points.

strength, thermal properties, diffusion and adsorption will behave as a soil desaturates. The complexity of unsaturated soil physics requires a knowledge-based system to provide tools for describing unsaturated soil behaviour. Knowledge was accumulated from experts in the field of unsaturated soil mechanics, published research, and current databases. The system was described within the relational database shell provided by Microsoft's Access® relational database management system (RDMS). The database system handled the manipulation of large amounts of data while allowing time to be focused on the coding of the knowledge system. Information was stored in frames consisting of a main soil frame with links established to alternate soil property frames. The current database consists of information on over 6000 soils. The knowledge-based system manipulates 13 separate property frames and allows prediction of 10 different soil property functions. The system then allows for the estimation of unsaturated soil properties when experimental data is limited or too costly to obtain. The unsaturated property functions can be used in finite element modelling among other applications to give an estimate of engineering design limits.

Concluding Remarks

The current system allows for expansion in a number of ways. The most pressing interest appears to be to combine the soil knowledge-based system with a modelling program so that unsaturated soil processes can be more accurately studied. Property functions are currently defined in terms of suction. Describing property functions in terms of net normal stress may be a possible area of development. A complete inference engine covering the field of unsaturated soil mechanics would also enhance the system. However, the availability of personal computers will allow extensive benefit from the current system when applied to numerous situations.

References

- Ahuja, L.R., Cassel, D.K., Bruce, R.R., and Barnes B.B. 1989. Evaluation of spacial distribution of hydraulic conductivity using effective porosity data. *Soil Science Journal*, **148**(6): 404–411.
- Arya, L.M., and Paris, J.F. 1981. A physicoempirical model to predict the soil moisture characteristic from particle-size distribution and bulk density data. *Soil Science Society of America Journal*, **45**: 1023–1030.
- Black, P.B., and Tice, A.R. 1989. Comparison of soil freezing curve and soil water curve data for Windsor sandy loam. *Water Resources Research*, **25**: 2205–2210.
- Carrico, M.A., Girard, J.E., and Jones, J.P. 1989. Building knowledge systems. McGraw-Hill Book Company, New York.
- Fredlund, D.G., and Rahardjo, H. 1993. *Soil mechanics for unsaturated soils*. John Wiley & Sons Inc., New York.
- Fredlund, D.G., Xing, A., Fredlund, M.D., and Barbour, S.L. 1996. The relationship of the unsaturated soil shear strength functions to the soil-water characteristic curve. *Canadian Geotechnical Journal*, **33**(3): 440–448.
- Fredlund, M.D. 1996. Design of a knowledge-based system for unsaturated soils. M.Sc. thesis, University of Saskatchewan, Saskatoon, SK, Canada.
- Frouki, O.T. 1986. Thermal properties of soils. Trans. Technical. Publications, Clausthal-Zellerfeld, Germany.
- Holtz, R.D., and Kovacs, W.D. 1981. *An introduction to geotechnical engineering*. Prentice-Hall, Inc., Englewood Cliff, New Jersey.
- Johansen, O. 1975. Thermal conductivity of soils. Ph.D. thesis, (CRREL Draft Translation 637, 1977), Trondheim, Norway.
- Lim, P.C. 1995. Characterization and prediction of the functional for the coefficients of diffusion and adsorption for inorganic chemicals in unsaturated soils. Ph.D. thesis, University of Saskatchewan, Saskatoon, SK, Canada.
- Lim, P.C., Barbour, S.L., and Fredlund, D.G. 1998. Diffusion and adsorption processes in unsaturated soils II: The influ-

- ence of the degree of saturation on the coefficient of adsorption. *Canadian Geotechnical Journal*, submitted for publication.
- Rawls W.J., and Brakensiek, D.L. 1989. Estimation of soil water retention and hydraulic properties. *In Unsaturated Flow in Hydrologic Modeling: Theory and Practice. Edited by H.J. Morel-Seytoux*, Kluwer Academic Publishers, Beltsville, MD, pp. 275–300.
- Sillers, W. S. 1997. The mathematical representation of the soil-water characteristic curve. M.Sc. thesis, University of Saskatchewan, Saskatoon, SK, Canada.
- Tatnawski, V.R., and Wagner B. 1993. Thermal and hydraulic properties of soils. Saint Mary's University, Division of Engineering, Halifax, Nova Scotia.
- Williams, R.D., Ahuja, L.R., and Naney, J.W. 1992. Comparison of methods to estimate soil water characteristics from texture, bulk density, and limited data., *Soil Science*, **153**: 172–184.

Part IV

Shear Strength of Unsaturated Soils and its Application



Dr. Harianto Rahardjo
Geotechnical Research Centre
School of Civil and Structural Engineering
Nanyang Technological University
Singapore

Introduction and Overview

The shear strength equations for an unsaturated soil have proven to be relatively easy to formulate, verify, and apply in engineering practice. The equations have taken the form of an extension of the shear strength equations for a saturated soil.

The Mohr-Coulomb shear strength equation for a saturated soil can be written in terms of effective shear strength parameters: c' = effective cohesion and ϕ' = effective angle of internal friction.

$$[1] \quad \tau = c' + (\sigma_n - u_w) \tan \phi'$$

The shear strength equation for an unsaturated (or saturated/unsaturated) soil can be formulated as a linear combination of two independent stress state variables, (i.e., $(\sigma_n - u_a)$ and $(u_a - u_w)$):

$$[2] \quad \tau = c' + (\sigma_n - u_w) \tan \phi' + (u_a - u_w) \tan \phi^b$$

Equation [2] can be plotted to form a three-dimensional surface. It has been found that the shear strength relationship involving suction can be either linear or non-linear. In general, it is possible to linearize the non-linear shear strength versus suction relationship over a selected range of soil suctions.

At low suctions, a change in the negative pore-water pressure produces the same change in shear strength as a change in total stress (under drained conditions), as long as the soil remains saturated. The ϕ^b angle corresponding to suctions below the air-entry value of the soil, is equal to ϕ' . As the soil desaturates, the ϕ^b angle decreases because water no longer covers the entire void space on the failure plane.

The laboratory measurement of the shear strength of a soil versus soil suction can be performed using either a modified triaxial apparatus or a modified direct shear apparatus. In each case, the equipment must be modified to allow for the independent measurement (or control) of the pore-air and pore-water pressures. The pore-air pressure can be applied through a coarse or extremely low air entry value ceramic disk. The pore-water pressure can be measured or controlled below a high air entry disk that is sealed around the edges with epoxy to the lower base platen.

The direct shear apparatus has proven to be superior to the triaxial apparatus for testing unsaturated soils because the reduced length of drainage path provides for more rapid equalization of the pore-water pressures. Even so, testing clayey soils in the direct shear apparatus will often require two to four days for equalization under the applied stress state and then one day to apply the shear stress to failure under drained loading conditions. Since the shear strength relationship is non-linear, several specimens are required, or multi-stage testing must be carried out. Triaxial testing can require considerably more time than direct shear testing. The end result is that unsaturated soil testing is time consuming and the testing procedures require that great care be exercised.

As discussed earlier, the ϕ^b angle for an unsaturated soil will decrease when there is an increase in soil suction and this results in a non-linear variation of shear strength. The non-linear variation can be related to the volumetric water content of the soil. However, this relationship does not have to be directly proportional to the volumetric water content. The relationship between the shear strength of an unsaturated soil and soil suction is referred to as the shear strength function. This relationship can be predicted with sufficient accuracy for many engineering problems through a knowledge of the saturated shear strength parameters and the soil-water characteristic curve. It is possible to represent the non-linear form of the unsaturated shear strength envelope in a mathematical form.

Two procedures have been suggested for predicting the shear strength function. One procedure involves the use of the entire soil-water characteristic curve and applies a κ variable as an exponent to the dimensionless volumetric water content, Θ .

$$[3] \quad \tau(u_a - u_w) = c' + (\sigma_n - u_a) \tan \phi' + [\Theta(u_a - u_w)]^\kappa (u_a - u_w) \tan \phi'$$

The dimensionless volumetric water content, Θ , in eq. [3] is defined as θ / θ_s , where θ is the volumetric water content and θ_s is the saturated volumetric water content.

The second procedure involves the use of a residual volumetric water content, θ_r , that can be estimated from the soil-water characteristic curve. In this case, the shear strength equation for an unsaturated soil can be written as follows.

$$[4] \quad \tau(u_a - u_w) = c' + (\sigma_n - u_a) \tan \phi' + \left(\frac{\theta - \theta_r}{\theta_s - \theta_r} \right) (u_a - u_w) \tan \phi'$$

The first procedure appears to give a better fit between the predicted and experimental data through the use of the κ factor than does the second procedure which involves the use of an estimate of the residual volumetric water content, θ_r . The difference may be related to the estimation of a precise value for the residual volumetric water content, θ_r , particularly for fine-grained clayey soils. Comparisons between the measured and predicted shear strength function for a glacial till have been shown to be satisfactory using both methods.

On some engineering projects, it may be feasible to measure the unsaturated soil shear strength properties in the laboratory. However, in many situations, it is also satisfactory to predict or estimate the unsaturated shear strength function from the soil-water characteristic curve. The soil-water characteristic curve can be measured in the laboratory, or it can be either estimated from a grain size curve or through use of a knowledge-based database.

In some of the early publications the form of the shear strength equation for an unsaturated soils is shown with an “integration” symbol. Corrections have been applied and noted in two of the papers included in the shear strength section of Part IV.

Part IV

Shear Strength of Unsaturated Soils and its Application

- Fredlund, D.G., Morgenstern, N.R., and Widger, R.A. 1978. The shear strength of unsaturated soils. *Canadian Geotechnical Journal*, **15**(3): 313–321 223
- Fredlund, D.G., Rahardjo, H., and Gan, J.K.-M. 1987. Non-linearity of strength envelope for unsaturated soils. Proceedings, 6th International Conference on Expansive Soils, New Delhi, India, pp. 49–54 231
- Ho., D.Y.F. and Fredlund, D.G. 1982. A multistage triaxial tests for unsaturated soils. *ASTM, Geotechnical Testing Journal*, **5**(1/2): 18–25 237
- Gan, J.K.-M., Fredlund, D.G., and Rahardjo, H. 1988. Determination of the shear strength parameters of an unsaturated soil using the direct shear test. *Canadian Geotechnical Journal*, **25**(8): 500–510 244
- Gan, J.K.-M., and Fredlund, D.G. 1996. Shear strength characteristics of two saprolitic soils. *Canadian Geotechnical Journal*, **33**: 595–609 255
- Oloo, S.Y., and Fredlund, D.G. 1996. A method for the determination of ϕ^b for statically compacted soils. *Canadian Geotechnical Journal*, **33**(2): 272–280 269
- Fredlund, D.G., Xing, A., Fredlund, M.D., and Barbour, S.L. 1996. The relationship of the unsaturated shear strength to the soil-water characteristic curve. *Canadian Geotechnical Journal*, **33**(3): 440–448 277
- Vanapalli, S.K., Fredlund, D.G., Pufahl, D.E., and Clifton, A.W. 1996. Model for the prediction of shear strength with respect to soil suction. *Canadian Geotechnical Journal*, **33**(3): 379–392 286
- Ho, D.Y.F., and Fredlund, D.G. 1982. Increase in shear strength due to soil suction for two Hong Kong soils. Proceedings, ASCE, Geotechnical Conference on Engineering and Construction in Tropical and Residual Soils, Honolulu, Hawaii, pp. 263–295 300
- Ching, R.K.H., Sweeney, D.J., and Fredlund, D.G. 1984. Increase in factor of safety due to soil suction for two Hong Kong slopes. Proceedings, Fourth International Symposium on Landslides, Toronto, Canada, pp. 617–623 313
- Fredlund, D.G. 1989. Negative pore-water pressures in slope stability. Proceedings, South American Symposium on Slope Stability, Paipa, Colombia 320
- Fredlund, D.G. 1995. The stability of slopes with negative pore-water pressures. *In The Ian Boyd Donald Symposium on Modern Developments in Geomechanics. Edited by C.M. Haberfield, Monash University, Department of Civil Engineering, Clayton, Australia*, pp. 99–116 333
- Hasan, J.U., and Fredlund, D.G. 1980. Pore pressure parameters for unsaturated soils. *Canadian Geotechnical Journal*, **17**(3): 395–404 344
- Fredlund, D.G., Rahardjo, H., and Ng, T. 1993. Effect of pore-air and negative pore-water pressures on stability at the end-of-construction. Proceedings, International Conference on Dam Engineering, Johor Bahru, Malaysia, pp. 43–51 352
- Pufahl, D.E., Fredlund, D.G., and Rahardjo, H. 1983. Lateral earth pressures in expansive clay soils. *Canadian Geotechnical Journal*, **20**(2): 228–241 360
- Oloo, S.Y., Fredlund, D.G., and Gan, J.K.-M. 1997. Bearing capacity of unpaved roads. *Canadian Geotechnical Journal*, **34**(3): 398–407 373

The shear strength of unsaturated soils

D.G. Fredlund, N.R. Morgenstern, and R.A. Widger

Abstract: The shear strength of an unsaturated soil is written in terms of two independent stress state variables. One form of the shear strength equation is:

$$\tau = c' + (\sigma - u_w) \tan \phi' + (u_a - u_w) \tan \phi''$$

The transition from a saturated soil to an unsaturated soil is readily visible. A second form of the shear strength equation is:

$$\tau = c' + (\sigma - u_a) \tan \phi' + (u_a - u_w) \tan \phi^b$$

Here the independent roles of changes in total stress, σ , and changes in pore-water pressure, u_w , are easily visualized.

Published research literature provides limited data. However, the data substantiate that the shear strength can be described by a planar surface of the forms proposed. A procedure is also outlined to evaluate the pertinent shear strength parameters from laboratory test results.

Key words: unsaturated soils, shear strength parameters, stress state variables, ϕ^b , triaxial tests.

Introduction

During the past two decades there has been an increasing use of two independent stress variables to describe the behaviour of unsaturated soils (Coleman 1962; Bishop and Blight 1963; Burland 1965; Aitchison 1967; Matyas and Radhakrishna 1968; Barden et al. 1969; Brackley 1971; Fredlund 1974; Fredlund and Morgenstern 1976, 1977). Most consideration has been given to describing the volume change behaviour (and suitable constitutive relations) for unsaturated soils. Several investigations have been made into the shear strength characterization of unsaturated soils (Bishop et al. 1967; MIT (Massachusetts Institute of Technology) 1963; Sridharan 1968; Maranha Das Neves 1971); however, none has proven completely successful.

Fredlund and Morgenstern (1977) showed from a stress field analysis that any two of three possible stress variables can be used to define the stress state in an unsaturated soil. Possible combinations are: (1) $(\sigma - u_a)$ and $(u_a - u_w)$, (2) $(\sigma - u_w)$ and $(u_a - u_w)$, and (3) $(\sigma - u_a)$ and $(\sigma - u_w)$, where, σ is the total normal stress, u_a is the pore-air pressure, and u_w is the pore-water pressure. Null experiments (i.e., $\Delta\sigma = \Delta u_a = \Delta u_w$) supported the proposed theoretical stress state variables.

The objective of this paper is to present the shear strength of an unsaturated soil in terms of two independent stress state variables. The shear strength, using two possible combinations of stress state variables, is presented and the relationship between the two cases is shown. The first stress state variables used are $(\sigma - u_w)$ and $(u_a - u_w)$. The advantage of this combination of variables is that it provides a readily visualized transition from the unsaturated to the saturated case. The disadvantage arises in that, when the pore-water pressure is changed, two stress state variables are being affected. The relative significance of each variable must be borne in mind when considering the shear strength. (This is also the disadvantage associated with utilizing the $(\sigma - u_a)$ and $(\sigma - u_w)$ combination of stress state variables.)

The second combination of stress state variables used is $(\sigma - u_a)$ and $(u_a - u_w)$. The advantage of this combination is that only one stress variable is affected when the pore-water pressure is changed. Regardless of the combination of stress variables used to define the shear strength, the value of shear strength obtained for a particular soil with certain values of σ , u_a and u_w must be the same.

Research data from the testing program of other workers are used to demonstrate the use of the proposed shear strength equations for unsaturated soils.

Theory

For a saturated soil, a stress circle corresponding to failure conditions is plotted on a two-dimensional plot of effective normal stress versus shear strength. A series of tests gives a line of failure (i.e., a Mohr-Coulomb failure envelope).

In the case of an unsaturated soil, the stress circle corresponding to the failure conditions must be plotted on a

D.G. Fredlund. Professor, Department of Civil Engineering, University of Saskatchewan, 57 Campus Drive Saskatoon, SK, Canada S7N 5A9.

N.R. Morgenstern. Professor, Department of Civil Engineering, University of Alberta, Edmonton AB., Canada T6G 2G7.

R.A. Widger. Department of Highways, Prince Albert, SK, Canada S6V 5S4.

Reproduced with permission from the *Canadian Geotechnical Journal*, 15(3): 313-321, 1978.

three-dimensional diagram. The axes in the horizontal plane are the stress state variables and the ordinate is the shear strength. A series of tests gives a surface defining failure conditions.

(a) Shear strength in terms of the $(\sigma - u_w)$ and $(u_a - u_w)$ stress state variables

The vertical plane of $(\sigma - u_w)$ versus shear strength, with $(u_a - u_w)$ equal to zero, corresponds to the case where the soil is saturated. If the soil has a positive matric suction, (i.e., $(u_a - u_w)$ is greater than zero), a third dimension is required to plot the stress circle. It is initially assumed that the surface defined by a series of tests, on unsaturated soil samples, is planar. Therefore, the equation defining the surface of failure can be written as an extension of the conventional saturated soil case:

$$[1] \quad \tau = c' + (\sigma - u_w) \tan \phi' + (u_a - u_w) \tan \phi''$$

where:

- c' = effective cohesion parameter,
- ϕ' = friction angle with respect to changes in $(\sigma - u_w)$ when $(u_a - u_w)$ is held constant, and
- ϕ'' = friction angle with respect to changes in $(u_a - u_w)$ when $(\sigma - u_w)$ is held constant.

A three-dimensional plot of the stress state variables versus shear strength is difficult to analyze. Therefore, a procedure is outlined to assist in obtaining the desired shear strength parameters. For convenience in handling the strength data from triaxial tests, the stress point at the top of each stress circle can be used, (i.e., $[(1/2)(\sigma_1 - \sigma_3) - u_w]$ and $(u_a - u_w)$). The equation for the plane through the stress points is:

$$[2] \quad (1/2)(\sigma_1 - \sigma_3) = d' + [(1/2)(\sigma_1 + \sigma_3) - u_w] \tan \psi' + (u_a - u_w) \tan \psi''$$

where:

- d' = intercept when the two stress points are zero,
- ψ' = angle between stress point plane and the $[(1/2)(\sigma_1 + \sigma_3) - u_w]$ axis when $(u_a - u_w)$ is held constant, and
- ψ'' = angle between stress point plane and the $(u_a - u_w)$ axis when $[(1/2)(\sigma_1 - \sigma_3) - u_w]$ is held constant.

The relationship between a plane through the stress points and the failure surface is shown in the Appendix along with the corresponding soil parameters. It is necessary to plot the data in a special manner in order to obtain the ϕ'' friction parameter.

(b) Shear strength in terms of the $(\sigma - u_a)$ and $(u_a - u_w)$ stress state variables

The equation for the failure surface when $(\sigma - u_a)$ and $(u_a - u_w)$ are used as stress variables is:

$$[3] \quad \tau = c'' + (\sigma - u_a) \tan \phi^a + (u_a - u_w) \tan \phi^b$$

where:

- c'' = cohesion intercept when the two stress variables are zero,

- ϕ^a = friction angle with respect to changes in $(\sigma - u_a)$ when $(u_a - u_w)$ is held constant, and
- ϕ^b = friction angle with respect to changes in $(u_a - u_w)$ when $(\sigma - u_a)$ is held constant.

The number of parameters, however, can be reduced. When the matric suction is zero, the $(\sigma - u_a)$ plane will have the same friction angle parameter as the $(\sigma - u_w)$ plane when using the previous combination, (a), of stress state variables. Therefore, ϕ^a is the same as ϕ' . Also, c'' is the same as c' . The shear strength equation is now:

$$[4] \quad \tau = c' + (\sigma - u_a) \tan \phi' + (u_a - u_w) \tan \phi^b$$

Equation [1] or [4] will give the same value for shear strength. Therefore, it is possible to equate them and obtain the relationship between the various angles of friction.

$$[5] \quad \tan \phi' = \tan \phi^b - \tan \phi''$$

Test data

Published research literature reveals that few tests have been performed where the principal stresses and the pore-air and pore-water pressures have been measured as the specimen is loaded. Three sets of data are presented below.

(a) Compacted shale (Bishop et al. 1960)

Triaxial tests were performed on a shale compacted at a water content of 18.6%. The clay content was 22%. All specimens were sheared at a constant water content. The failure envelope for tests on saturated specimens gave ϕ' equal to 24.8° and c' equal to 15.8 kPa (2.3 psi) (Fig. 1). The data for the tests on unsaturated test specimens are plotted in Fig. 1 and summarized in Table 1. Figure 2 shows a plot of $[(1/2)(\sigma_1 + \sigma_3) - u_w]$ and $(u_a - u_w)$ versus $(1/2)(\sigma_1 - \sigma_3)$. It is obvious that this type of plot is not very useful since it is impossible to visualize the plane on which the points fall. As proposed in the Appendix, $(\Delta\tau_d \cos \psi')$ is plotted versus $(u_a - u_w)$ in order to obtain α (Fig. 3). The graphically obtained angle, α , for the compacted shale is equal to -3.9° . This corresponds to a ψ'' value of -4.2° and a ϕ'' value of -4.6° . One form of the shear strength equation would be:

$$[6] \quad \tau = 2.3 + (\sigma - u_w) \tan 24.8^\circ - (u_a - u_w) \tan 4.6^\circ$$

The ϕ'' angle is negative since the pore-water pressure variable appears in both stress variables. The physical significance can be stated as follows:

A decrease in pore-water pressure, u_w , is not as efficient in increasing the $(\sigma - u_w) \tan \phi'$ component of strength as is a corresponding increase in total stress. Rather, decreasing the pore-water pressure increases the frictional resistance of the soil by $(\tan 24.8^\circ - \tan 4.6^\circ)$, which is equal to $(\tan 20.9^\circ)$. On the basis of eq. [5] the 20.9° angle is equal to ϕ^b . Therefore, another form of the shear strength equation is:

$$[7] \quad \tau = 2.3 + (\sigma - u_a) \tan 24.8^\circ + (u_a - u_w) \tan 20.9^\circ$$

Fig. 1. Triaxial tests on a compacted shale (clay fraction 22%) compacted at a water content of 18.6% and sheared at constant water content (from Bishop et al. 1960).

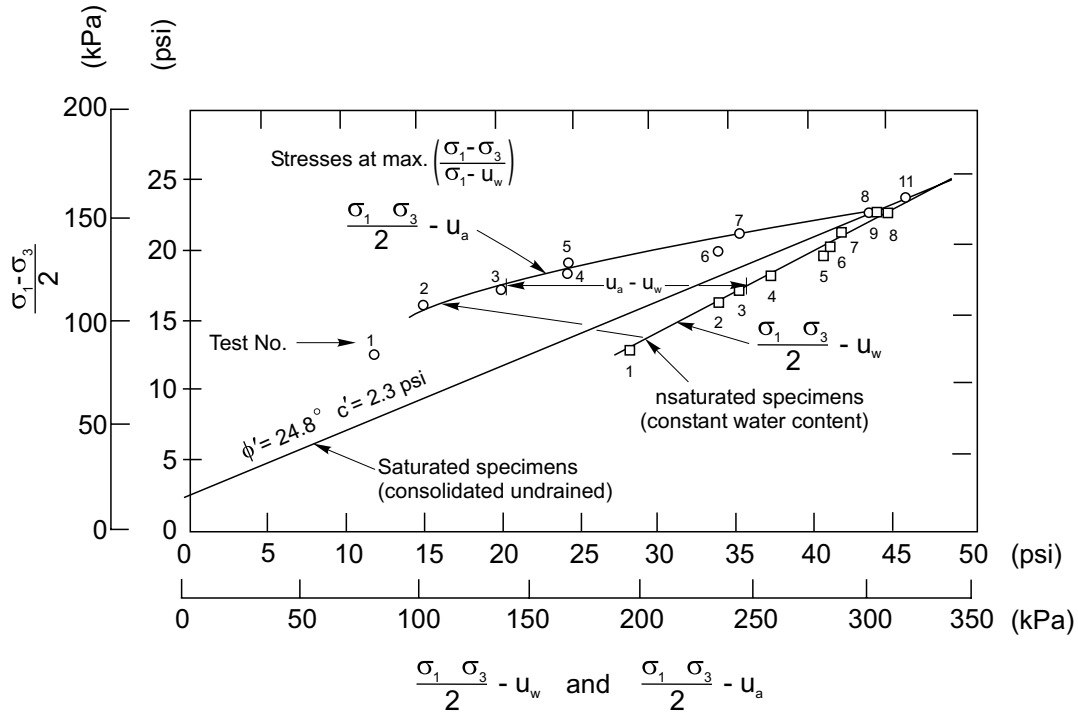
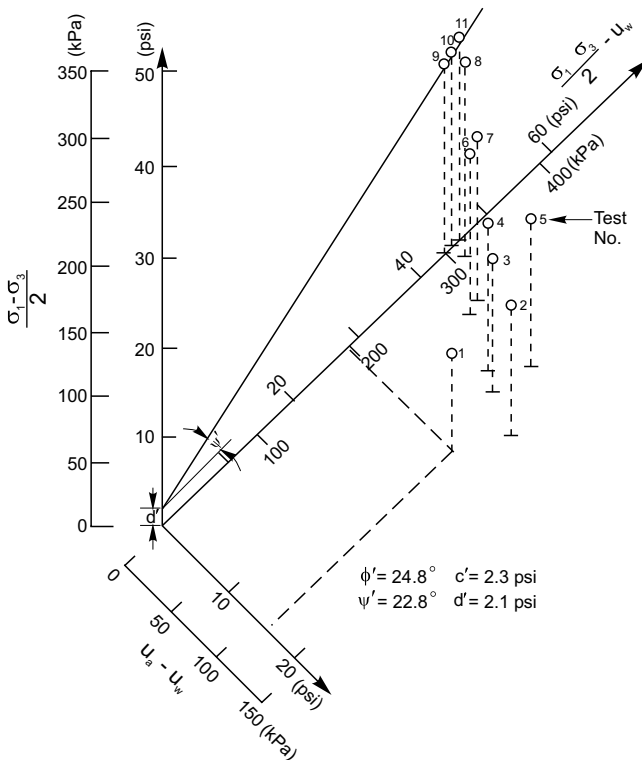


Fig. 2. Three-dimensional strength envelope for compacted shale.



From this equation, the relative shear strength contributions of the total stress and the pore-water pressures are readily inspected.

(b) Boulder clay (Bishop et al. 1960)

These triaxial tests were performed on specimens compacted at a water content of 11.6% and sheared at a constant water content. The clay fraction was 18%. The data are shown in Fig. 4 and summarized in Table 2. The saturated specimens gave a ϕ' angle equal to 27.3° and an effective cohesion c' equal to 9.6 kPa (1.4 psi). Figure 5 shows the $(\Delta\tau_d \cos \psi')$ versus $(u_a - u_w)$ plot. The best fit line gives an angle α equal to -3.3°. The corresponding angle ψ'' is equal to -3.6° and ϕ'' is equal to -4.1°. The ϕ^b angle is 24.0°. The forms of the shear strength equation for the Boulder clay are:

$$[8] \quad \tau = 1.4 + (\sigma - u_w) \tan 27.3^\circ - (u_a - u_w) \tan 4.1^\circ$$

$$[9] \quad \tau = 1.4 + (\sigma - u_w) \tan 27.3^\circ + (u_a - u_w) \tan 24.0^\circ$$

The interpretation of eqs. [8] and [9] is the same as for eqs. [6] and [7].

(c) Potters flint and Peerless clay (MIT 1963)

A series of triaxial tests was run on an artificial mixture (by weight) of 80% Potters flint and 20% Peerless clay, at MIT (Massachusetts Institute of Technology). The samples were compacted at a water content of 17.5%, 3% dry of optimum. The dry density was 1.6 Mg/m³ (100 lb/ft³). The specimens were failed at a constant water content. The saturated specimens gave an effective angle of internal friction ϕ' equal to 35.6° and an effective cohesion c' equal to 0.0 kPa. The results are summarized in Table 3. Figure 6 shows a plot of $(\Delta\tau_d \cos \psi')$ versus $(u_a - u_w)$, yielding an angle α equal to 2.4°. The corresponding angle ψ'' is equal to 2.8° and ϕ'' is equal to 3.4°.

Table 1. Results for compacted shale (from Bishop et al. 1960).

$\frac{1}{2}(\sigma + \sigma) - u_a$		$(\sigma + \sigma) - u_w$		$(\sigma - \sigma)$		$u_a - u_w$		$(\sigma - \sigma)$		$\Delta\tau$		$\Delta\tau$	ψ'
(kPa)	(psi)	(kPa)	(psi)	(kPa)	(psi)	(kPa)	(psi)	(kPa)	(psi)	(kPa)	(psi)	(kPa)	(psi)
81	11.8	196	28.4	82	11.9	114	16.6	97	14.0	-14	-2.1	-13	-1.9
104	15.1	236	34.2	103	15.0	132	19.1	113	16.4	-9.7	-1.4	-9.0	-1.3
139	20.1	243	35.3	110	16.0	105	15.2	117	16.9	-6.2	-0.9	-5.5	-0.8
168	24.4	258	37.4	117	17.0	90	13.0	123	17.8	-5.5	-0.8	-4.8	-0.7
168	24.4	280	40.6	123	17.9	112	16.2	132	19.1	-8.3	-1.2	-7.6	-1.1
236	34.2	281	40.7	128	18.6	45	6.5	132	19.2	-4.1	-0.6	-3.4	-0.5
243	35.3	289	41.9	137	19.8	46	6.6	136	19.7	0.7	0.1	0.7	0.1
301	43.6	310	45.0	147	21.3	9.7	1.4	145	21.0	2.1	0.3	2.1	0.3
302	43.8	302	43.8	145	21.1	0.0	0.0	141	20.4	4.8	0.7	4.1	0.6
305	44.3	305	44.3	145	21.1	0.0	0.0	143	20.7	2.8	0.4	2.1	0.3
316	45.9	316	45.9	153	22.2	0.0	0.0	148	21.4	5.5	0.8	5.5	0.8

* The calculated value refers to the shear stress on the saturated failure envelope.

Table 2. Results of compacted Boulder clay (from Bishop et al. 1960).

$\frac{1}{2}(\sigma_1 + \sigma_3) - u_a$		$\frac{1}{2}(\sigma_1 + \sigma_3) - u_w$		$\frac{1}{2}(\sigma_1 - \sigma_3)$		$u_a - u_w$		Calculated*		$\Delta\tau_d$		$\Delta\tau_d \cos \psi'$	
(kPa)	(psi)	(kPa)	(psi)	(kPa)	(psi)	(kPa)	(psi)	(kPa)	(psi)	(kPa)	(psi)	(kPa)	(psi)
129	18.7	300	43.5	126	18.3	171	24.8	146	21.2	-14	-2.9	-18	-2.6
137	19.8	316	45.8	134	19.5	179	26.0	154	22.3	-14	-2.8	-17	-2.5
274	39.7	417	60.5	197	28.6	143	20.8	200	29.0	-2.8	-0.4	-2.1	-0.3
310	45.0	460	66.7	214	31.0	150	21.7	219	31.8	-5.5	-0.8	-4.8	-0.7
396	57.5	530	76.8	243	35.2	133	19.3	252	36.5	-9.0	-1.3	-7.6	-1.1
536	77.8	632	91.7	286	41.5	96	13.9	299	43.3	-12	-1.8	-11	-1.6
574	83.3	633	91.8	291	42.2	59	8.5	292	42.4	-1.4	-0.2	-1.4	-0.2
629	91.3	662	96.0	316	45.8	32	4.7	315	45.7	0.7	0.1	0.7	0.1
722	104.7	722	104.7	341	49.5	0.0	0.0	340	49.3	1.4	0.2	1.4	0.2

* The calculated value refers to the shear stress on the saturated failure envelope.

Fig. 3. Change in shear strength from saturated strength plane for compacted shale.

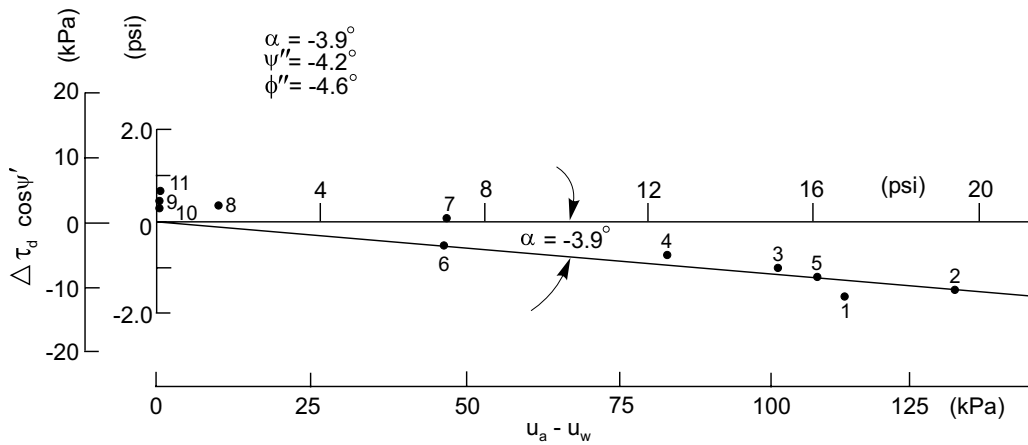


Fig. 4. Triaxial tests on a compacted Boulder clay (clay fraction 18%) compacted at a water content of 11.6% and sheared at constant water content (from Bishop et al. 1960).

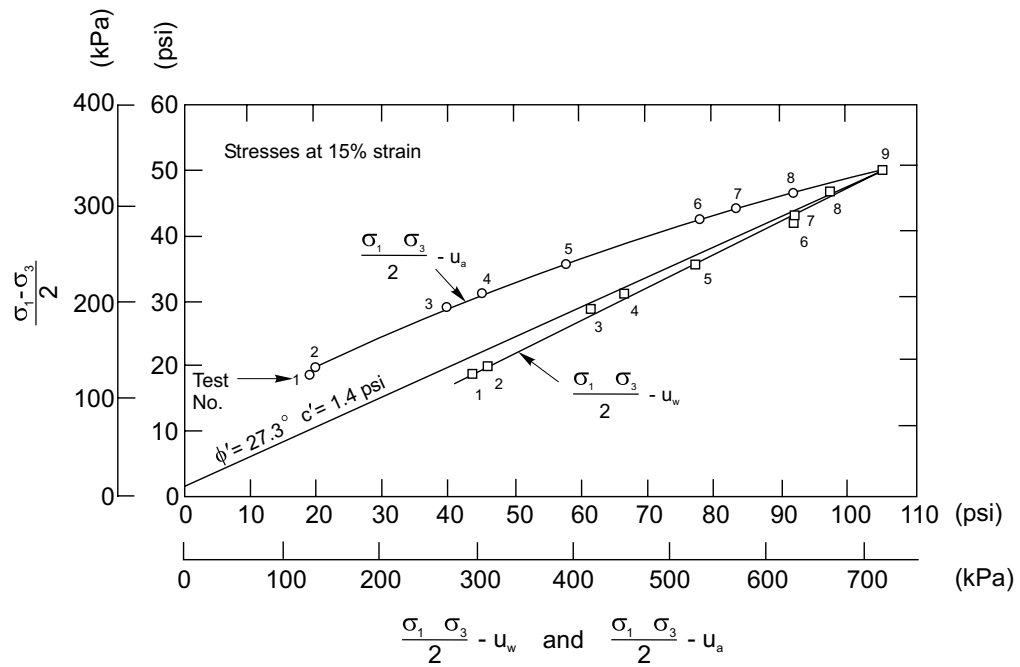


Fig. 5. Change in shear strength from saturated strength plane for Boulder clay.

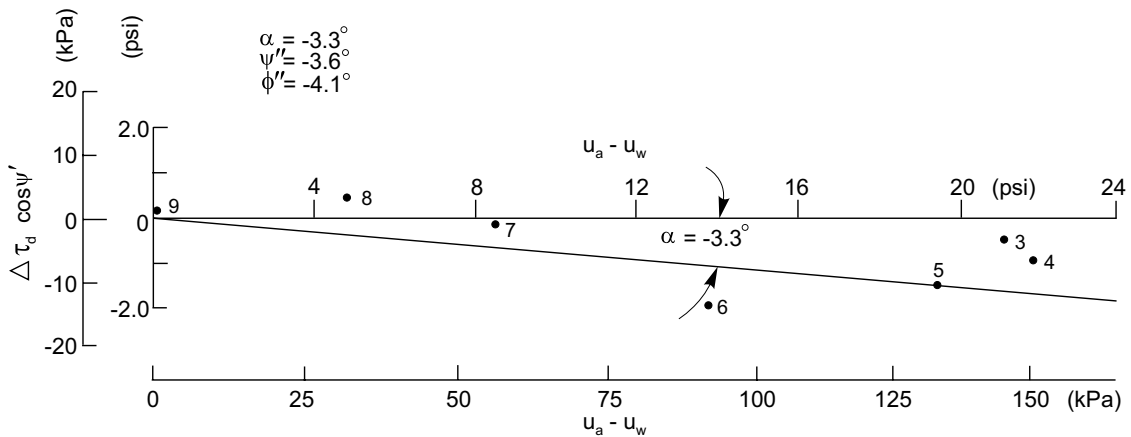


Fig. 6. Change in shear strength from saturated strength plane for Potters flint and Peerless clay.

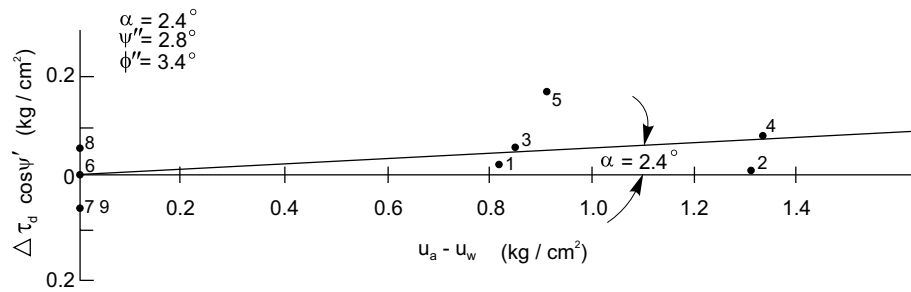
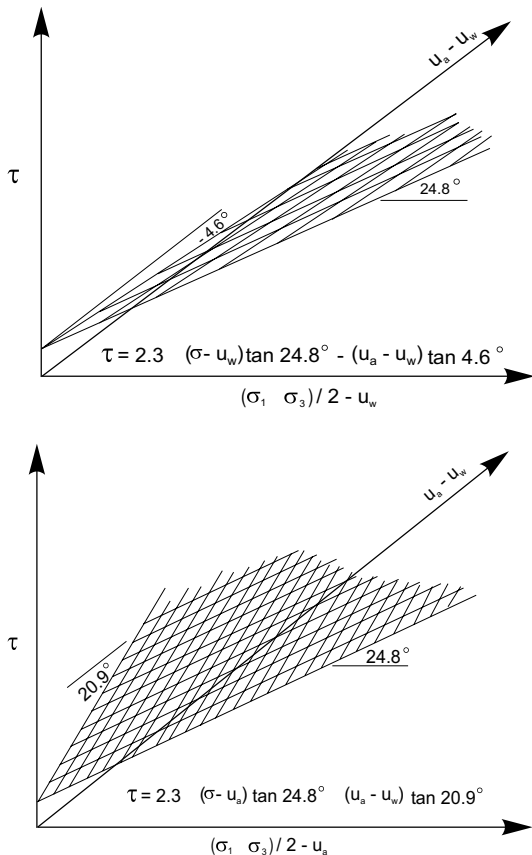


Table 3. MIT results for Potters flint and Peerless clay (MIT 1963).

Sample	$\frac{1}{2}(\sigma_1 - \sigma_3)$ ()	$\frac{1}{2}(\sigma'_1 + \sigma'_3)$ ()	$\sigma - u_a$ ()	$u_a - u_w$ ()	Calculated $(\sigma_1 + \sigma_3) - u_w$ ()	Calculated* $\frac{1}{2}(\sigma_1 - \sigma_3)$ (kg/cm)	$\Delta\tau_d$ ()	$\Delta\tau_d \cos \psi'$ (kg/cm)
SB-1	1.41		0.14	0.82	2.37	1.380	0.030	0.026
SB-2	2.05		0.14	1.31	3.50	2.037	0.013	0.011
SD-1	1.54		0.14	0.85	2.53	1.472	0.067	0.058
SB-4	2.26		0.14	1.33	3.73	2.171	0.089	0.077
SD-2	2.60		0.63	0.91	4.14	2.410	0.190	0.165
<i>a u a</i>								
SA-1	2.325	4.000				2.320	0.005	0.004
SA-2	3.100	6.425				3.150	-0.050	-0.043
SA-3	3.950	6.700				3.890	0.060	0.052
SA-4	4.050	7.050				4.100	-0.050	-0.043

Fig. 7. Graphical form of eqs. [1] and [4] for compacted shale data.



The ϕ^b angle is 37.8° . These results show the opposite behaviour to that reported in parts (a) and (b). All samples were tested at low confining pressures. There is considerable scatter in the data (Fig. 6) and the authors are not definite as to its interpretation. The results would indicate that a decrease in pore-water pressure increases the frictional resistance of the soil more than a corresponding increase in confining pressure.

Summary

The three sets of data are considered to be analyzed in terms of two independent sets of stress variables. Two possible forms for the shear strength equation are given by eqs. [1] and [4]. The graphical form of eqs. [1] and [4] are shown in Fig. 7 using data on the compacted shale from Bishop et al. (1960). The authors suggest that the second form (i.e., eq. [4]) will prove to be the most useful form in engineering practice. Further testing using other soils will improve our understanding of the shear strength of unsaturated soils.

Acknowledgements

The authors wish to acknowledge the Department of Highways, Government of Saskatchewan, for their financial support of the research work presented in this paper.

References

Aitchison, G.D. 1967. Separate roles of site investigation, quantification of soil properties, and selection of operational envi-

ronment in the determination of foundation design on expansive soils. Proceedings, 3rd Asian Regional Conference on Soil Mechanics and Foundation Engineering, Haifa, Israel, Vol. 2, pp. 72–77.

- Barden, L., Madedor, A.O., and Sides, G.R. 1969. Volume change characteristics of unsaturated clay. ASCE, Journal of the Soil Mechanics and Foundation Division, **95** (SM1): 33–51.
- Bishop, A.W., and Blight, G.E. 1963. Some aspects of effective stress in saturated and unsaturated soils. *Géotechnique*, **13**: 177–197.
- Bishop, A.W., Alpan, I., Blight, G.E., and Donald, I.B. 1960. Factors controlling the shear strength of partly saturated cohesive soils. Proceedings, ASCE Research Conference on Shear Strength of Cohesive Soils, University of Colorado, Boulder, CO., pp. 503–532.
- Brackley, I.J.A. 1971. Partial collapse in saturated expansive clay. Proceedings, 5th Regional Conference on Soil Mechanics and Foundation Engineering, Luanda, South Africa, Vol. 1, pp. 23–30.
- Burland, J.B. 1965. Some aspects of the mechanical behavior of partly saturated soils. *In* Moisture equilibrium and moisture changes in soils beneath covered areas. A symposium in print. Edited by G.D. Aitchison, Butterworth and Company (Australia) Ltd., Sydney, Australia, pp. 270–278.
- Coleman, J.D. 1962. Stress/strain relations for partly saturated soil. Correspondence, *Géotechnique*, **12**(4): 348–350.
- Fredlund, D.G. 1974. Engineering approach to soil continua. Proceedings, 2nd Symposium on the Applications of Solid Mechanics, Hamilton, Ont., Vol. 1, pp. 46–59.
- Fredlund, D.G., and Morgenstern, N.R. 1967. Constitutive relations for volume change in unsaturated soils. *Canadian Geotechnical Journal*, **13**: 261–276.
- Fredlund, D.G., and Morgenstern, N.R. 1977. Stress state variables for unsaturated soils. ASCE, Journal of the Geotechnical Engineering Division, **107**(GT5): 447–466.
- Maranha Das Neves, E. 1971. The influence of negative pore-water pressures on the strength characteristic of compacted soils. Publication No. 386, National Laboratory of Civil Engineering, Lisbon, Portugal. (In Portuguese).
- MIT. 1963. Engineering behaviour of partially saturated soils. Phase Report No. 1. to U.S. Army Engineers Waterways Experimental Station, Vicksburg, Mississippi. The Soil Engineering Division, Department of Civil Engineering, Massachusetts Institute of Technology, Contract No. DA-22-079-eng-288.
- Matyas, E.L., and Radhakrishna, H.S. 1968. Volume change characteristics of partially saturated soils. *Géotechnique*, **18**(4): 432–448.
- Sridharan, A. 1968. Some studies on the strength of partly saturated clays. Ph.D. thesis, Purdue University, Lafayette, IN.
- Widger, R.A. 1976. Slope stability in unsaturated soils. M.Sc. thesis, University of Saskatchewan, Saskatoon, SK. Canada.

Appendix – Stress Ppoint method to obtain the shear strength parameters

This appendix derives the mathematical relationship between the stress points at the top of a stress circle and the failure surface for an unsaturated soil (Widger 1976). The stress variables are $[(1/2)(\sigma_1 + \sigma_3) - u_w]$ and $(u_a - u_w)$. Figure A1 views the strength data parallel to the $(u_a - u_w)$ axis. The conversions for the zero matric suction plane (Bishop et al. 1960) are:

$$[A1] \quad \sin \phi' = \tan \psi'$$

and

$$[A2] \quad c' = d' / \cos \phi'$$

where:

ψ' = angle of the line through the stress point at the top of the stress circles, and
 d' = the intercept formed by the line through the stress points.

It is also necessary to convert the angle ϕ'' for the unsaturated case. From the definition of ϕ'' :

$$[A3] \quad \tan \phi'' = \Delta\tau_c / (u_a - u_w)$$

and

$$[A4] \quad \tan \phi'' = \Delta\tau_d / (u_a - u_w)$$

where:

ψ'' = angle between the line through the stress points and the $(u_a - u_w)$ axis,
 $\Delta\tau_c$ = change in shear strength between the saturated soil failure envelope and the failure envelope corresponding to a particular $(u_a - u_w)$ value, and
 $\Delta\tau_d$ = change in shear strength between the saturated soil envelope through the stress points and the envelope through the stress points at a particular $(u_a - u_w)$ value.

The matric suction is the same value in eqs. [A3] and [A4] and therefore:

$$[A5] \quad (\tan \phi'') / \Delta\tau_c = (\tan \psi'') / \Delta\tau_d$$

Considering the shear strength axis gives:

$$[A6] \quad \Delta\tau_d = c_s' - c'$$

and

$$[A7] \quad \Delta\tau_d = d_s' - d'$$

where:

c_s' = cohesion intercept of the failure envelope at a matric suction $(u_a - u_w)$, and
 d_s' = cohesion intercept at a matric suction $(u_a - u_w)$ using the stress point method.

Since ϕ' is constant for all matric suction values:

$$[A8] \quad \Delta\tau_d = (c_s' - c') \cos \phi'.$$

Substituting eqs. [A6] and [A8] into eq. [A5] gives:

$$[A9] \quad \tan \phi'' = \frac{\tan \psi''}{\cos \phi'}$$

In order to compute ϕ'' , it is necessary to obtain ψ'' . The procedure that appears most convenient involves the use of the stress point method failure surface (Fig. A2). Imagine viewing along the failure envelope for a saturated soil (plane ABFE); if the matric suction variable does not affect the shear strength, the three-dimensional failure surface as viewed along the matric suction axis appears as a

Fig. A1. Failure circles looking parallel to $(u_a - u_w)$ axis to compare failure envelopes.

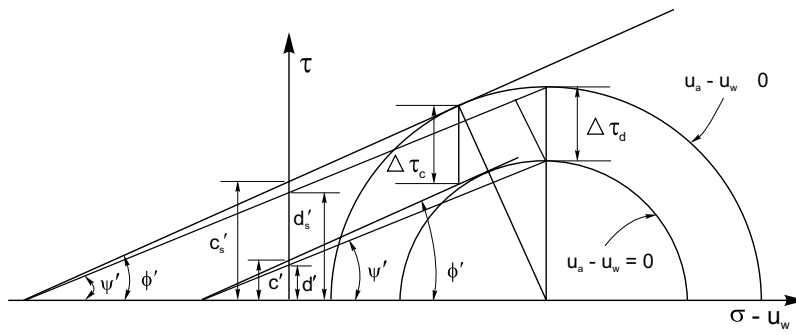


Fig. A2. Three-dimensional failure surface using the stress point method.

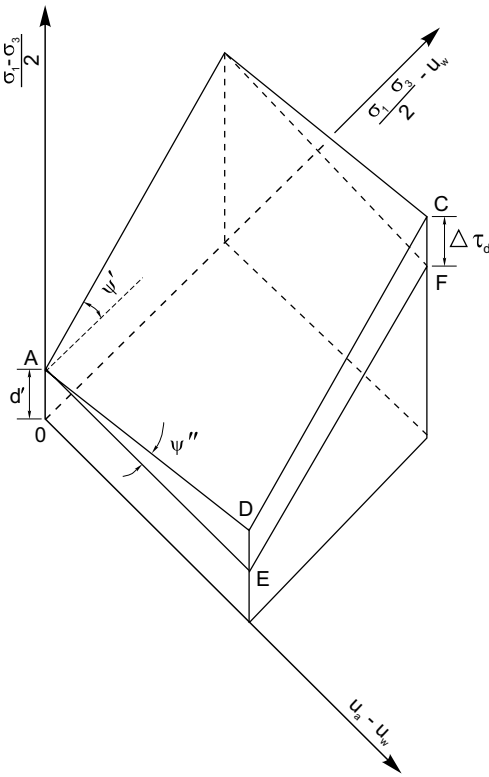
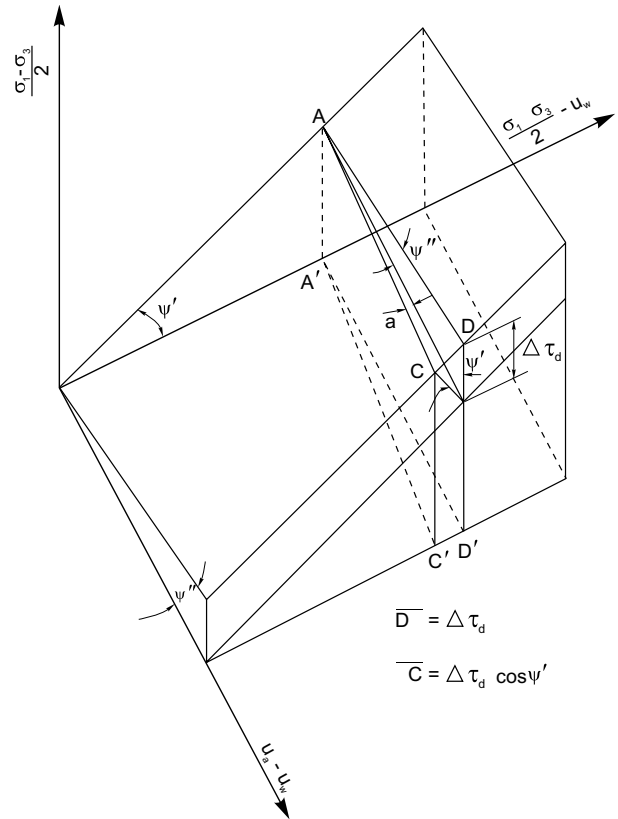


Fig. A3. Failure surface showing projection of shear strength onto the saturated strength plane.



line. However, the change in shear strength ($\Delta\tau_d$) must be multiplied by $\cos \psi'$ in order to transform it into a line perpendicular to the saturation failure plane (Fig. A3). Let the slope of the plot of $(\Delta\tau_d \cos \psi')$ versus matric suction be $\tan \alpha$.

$$[A10] \quad \tan \alpha = \frac{\Delta\tau_d \cos \psi'}{u_a - u_w}$$

Substituting eq. [A4] into eq. [A11] gives:

$$[A11] \quad \tan \psi'' = \frac{\tan \alpha}{\cos \psi'}$$

The value of $\tan \phi''$ can now be computed from eq. [A9].

Non-linearity of strength envelope for unsaturated soils

D.G. Fredlund, H. Rahardjo, and J.K.-M. Gan

Abstract: A literature review on the theory and measurements of shear strength in unsaturated soils is presented. Recent experimental data exhibiting non-linearity in the failure envelope are reported and discussed. The results of direct shear tests on compacted glacial till specimens are presented. Various procedures for handling the non-linear failure envelope are proposed in this paper.

Key words: shear strength, matric suction, direct shear test, non-linearity.

Introduction

The shear strength theory for unsaturated soils has received increased attention during the past three decades. Measurements of relevant shear strength parameters have been made in many parts of the world. The shear strength behaviour of an expansive soil is similar to that of an unsaturated soil due to the presence of negative pore-water pressures. This paper first presents a brief review of relevant literature on the shear strength behaviour of unsaturated soils and traces the gradual evolution of our understanding.

Research during the past few years has revealed that there may be significant non-linearity in the shear strength envelope for unsaturated soils. The nature of this non-linearity is addressed along with a description of possible ways to accommodate it in practice. The manner in which the proposed shear strength equation can be used to describe the non-linear failure envelope is discussed later in this paper. This paper also attempts to address the question of whether all testing procedures will yield unique shear strength parameters.

Review of theory and relevant laboratory data

In 1978, a shear strength equation for an unsaturated soil was proposed using the independent stress state variables (Fredlund et al. 1978). The two stress state variables are the net normal stress, $(\sigma - u_a)$, and the matric

suction, $(u_a - u_w)$, where σ is the total normal stress; u_a is the pore-air pressure; and u_w is the pore-water pressure. The uniqueness of the proposed equation was justified using the analysis of triaxial tests results on unsaturated soils published by other researchers.

Several triaxial test techniques for measuring the shear strength of an unsaturated soil were proposed by Bishop et al. (1960). Bishop and Donald (1961) tested an unsaturated loose silt using a consolidated drained test. The axis-translation technique proposed by Hilf (1956) is commonly used for testing unsaturated soils at matric suctions higher than 101 kPa. The high air entry disk must have an air entry value greater than the matric suction of the soil. The acceptability of the axis-translation technique was verified by Bishop and Blight (1963).

Two sets of shear strength test data were reported by Bishop et al. (1960). These tests were on a compacted shale and a compacted boulder clay. The data were later used in the examination of the shear strength equation proposed for an unsaturated soil by Fredlund et al. (1978). The data were re-analyzed in terms of the two independent stress state variables. The results indicated essentially a planar failure envelope when the shear stress, τ , was plotted with respect to the $(\sigma - u_a)$ and $(u_a - u_w)$ variables.

The results of consolidated drained and constant water content tests on unsaturated Dhanauri clay were presented by Satija (1978) and Gulhati and Satija (1981). The re-analysis of these results appears to support a planar type of failure envelope (Ho and Fredlund 1982; Fredlund and Rahardjo 1987).

A series of consolidated drained direct shear and triaxial tests on unsaturated Madrid gray clay were reported by Escario (1980). These data were further studied by Ho and Fredlund (1982) and showed that a planar failure envelope adequately defined failure conditions. Ho and Fredlund (1982) published the results of multistage, consolidated drained triaxial tests on undisturbed specimens of a decomposed rhyolite and a decomposed granite. The plotted test results showed some non-linearity, but this was interpreted as being related to the nature of the multistage test.

D.G. Fredlund. Professor, Department of Civil Engineering, University of Saskatchewan, 57 Campus Drive, Saskatoon, SK, Canada S7N 5A9.

H. Rahardjo. Research Engineer, Department of Civil Engineering, University of Saskatchewan, 57 Campus Drive, Saskatoon, SK, Canada S7N 5A9.

J.K.-M. Gan, Geotechnical Engineer, Minconsult Sdn. Bhd., 14 Jalan 20/16A, Paramount Carder, 46300 Petaling Jaya Selangor, Malaysia.

Reproduced with permission from the *Proceedings, 6th International Conference on Expansive Soils*, New Delhi, India, December 1-4, 1987. pp. 49-54.

Experimental data analysed in accordance with the shear strength equation proposed by Fredlund et al. (1978) have been shown to indicate essentially a planar failure envelope. However, recent direct shear tests on an unsaturated glacial till has shown a significant non-linearity (i.e., curvature) in the failure envelope with respect to the $(u_a - u_w)$ axis (Gan 1986). Escario and Sáez (1986) also reported a non-linearity in the shear stress, τ , versus matric suction, $(u_a - u_w)$, relationship. Their results were obtained using direct shear tests on three soils.

Theory of shear strength

The proposed shear strength equation (Fredlund et al. 1978) for an unsaturated soil has the following form:

$$[1] \quad \tau_{ff} = c' + (\sigma_{ff} - u_{af}) \tan \phi' + (u_a - u_w)_f \tan \phi^b$$

where:

- τ_{ff} = shear stress on the failure plane at failure,
- c' = intercept of the “extended” Mohr-Coulomb failure envelope on the shear stress axis when the net normal stress and the matric suction at failure are equal to zero. It is also referred to as the “effective cohesion”,

$(\sigma_{ff} - u_{af})$ = net normal stress on the failure plane at failure,

σ_{ff} = total normal stress on the failure plane at failure,

u_{af} = pore-air pressure at failure,

ϕ' = angle of internal friction associated with the net normal stress state variable $(\sigma_{ff} - u_{af})$,

$(u_a - u_w)_f$ = matric suction at failure,

u_{wf} = pore-water pressure at failure, and

ϕ^b = angle indicating the rate of change in shear strength relative to changes in matric suction, $(u_a - u_w)_f$.

Equation [1] describes a planar surface which is called the extended Mohr-Coulomb failure envelope as illustrated in Fig. 1. The surface is tangent to the Mohr circles at failure. The shear strength of an unsaturated soil is considered to consist of an effective cohesion, c' , and the independent contributions from net normal stress, $(\sigma - u_a)$, and matric suction $(u_a - u_w)$. The shear strength contribution from net normal stress and matric suction are characterized by ϕ' and ϕ^b angles, respectively.

Experimental evidence indicating non-linearity of the failure envelope

The planar failure envelope as shown in Fig. 1 has been used to describe the shear strength of an unsaturated soil. For a planar failure envelope, the slope angles, ϕ' and ϕ^b , are assumed to be constants. As an example consider the triaxial test results on two compacted soils presented in Fig. 2. The results are plotted on the τ versus $(u_a - u_w)$ plane corresponding to a zero net normal stress at failure (i.e., $(\sigma_{ff} - u_{af})$ is equal to 0). The failure envelopes drawn through the plotted data indicate essentially planar

Fig. 1. Extended Mohr-Coulomb failure envelope.

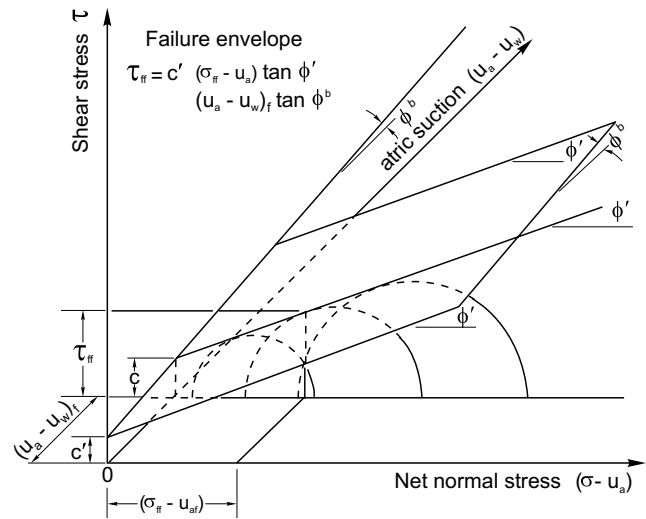
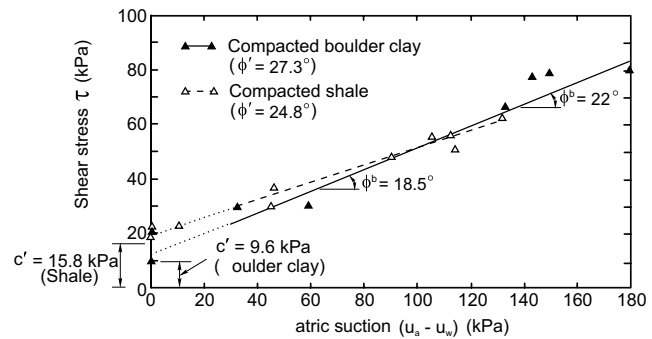


Fig. 2. Planar failure envelopes on the τ versus $(u_a - u_w)$ plane for two compacted soils (data from Bishop et al. 1960).



surfaces with respect to the $(u_a - u_w)$ axis. In other words, the ϕ^b angles are constant within the matric suction range used in the experiments (i.e., 0 to 200 kPa).

Recent experimental evidence using a higher range of matric suction (i.e., 0 to 500 kPa) indicates a significant non-linearity in the failure envelope with respect to the matric suction axis. The results of several multistage direct shear tests on a glacial till (Gan 1986) exhibit non-linear failure envelopes (Fig. 3). The failure envelopes are plotted on the τ versus $(u_a - u_w)$ plane corresponding to an average net normal stress at failure of 72.2 kPa. The results fall within a band of failure envelopes as indicated in Fig. 3. The spread in the failure envelopes appears to be due to slight differences in the initial void ratios or initial densities of the soil specimens.

The slopes of the failure envelopes with respect to the $(u_a - u_w)$ axis (i.e., ϕ^b angle) commence at an angle equal to ϕ' (i.e., 25.5°) near saturation and significantly decrease at matric suctions in the range or 50 kPa to 100 kPa. The ϕ^b angles reach a fairly constant value ranging from 5° to 10° when the matric suction exceeds 250 kPa. Figure 4

Fig. 3. Curved failure envelopes on the τ versus $(u_a - u_w)$ plane for a glacial till (from Gan 1986).

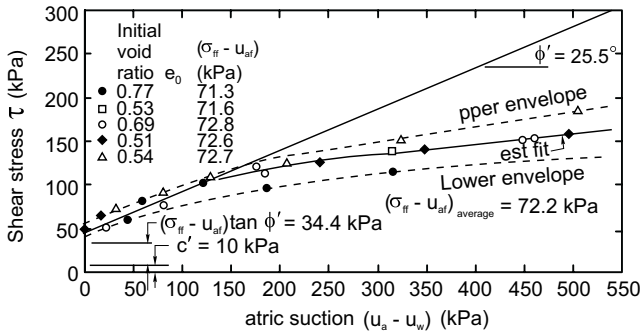


Fig. 4. ϕ^b values corresponding to the three curved failure envelopes (from Gan 1986).

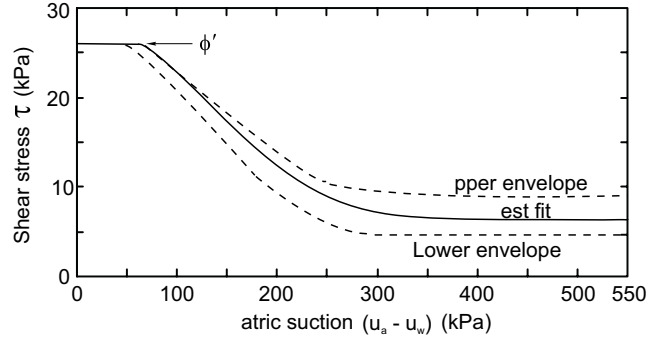


Table 1. Triaxial tests on compacted Dhanauri clay (data from Satija 1978).

Soils	CU tests on <i>saturated</i> specimens		Analysis of tests results on <i>unsaturated</i> specimens performed by Ho and Fredlund (1982)		
	c' (kPa)	ϕ' (°)	Types of tests	c' (kPa)	ϕ^b (°)
Low density, $\rho_d = 1478 \text{ kg/m}^3$, $w = 22.2\%$	7.8	29	CD	20.3	12.6
			CW	11.3	16.5
High density, $\rho_d = 1580 \text{ kg/m}^3$, $w = 22.2\%$	7.8	28.5	CD	37.3	16.2
			CW	15.5	22.6

Note: ρ_d = dry density; w = water content; CU = consolidated undrained; CD = consolidated drained; CW = constant water content.

shows the variation in the ϕ^b angle with respect to matric suction for the three failure envelopes.

An analysis of the triaxial test results on compacted Dhanauri clay also reveals some non-linearity in the failure envelope. The original shear strength parameters along with the parameters computed by Ho and Fredlund (1982), using a planar failure envelope are summarized in Table 1. The linear interpretation of the failure envelope results in different c' and ϕ^b values for the same soil tested under two different types of tests (i.e., consolidated drained and constant water content tests). This means that different types of tests on the same soil yield different shear strength parameters.

In other words, the use of a planar failure envelope in analyzing these data causes a problem of non-uniqueness in the resulting shear strength parameters. In addition, the c' values obtained from the analysis do not agree with values obtained from triaxial tests on saturated specimens (Table 1).

The problem of non-uniqueness in the failure envelope necessitates a re-evaluation of the shear strength data presented by Satija (1978). The reanalysis of these data was performed by assuming a curved failure envelope with respect to the $(u_a - u_w)$ axis. The results are plotted on the τ versus $(u_a - u_w)$ plane corresponding to a zero net normal stress at failure (i.e., $(\sigma_{ff} - u_{df})$ equal to 0). Figures 5 and 6 present the results for compacted Dhanauri clay at low and high densities, respectively. The shear strength parameters, c' and ϕ' obtained from the consolidated undrained tests on the saturated specimens (Table 1) were

used in this reanalysis. The curved failure envelopes have a cohesion intercept of c' and a slope angle, ϕ^b , equal to ϕ' starting at zero matric suction. The ϕ^b angles start to decrease significantly at matric suctions less than 50 kPa for the low density specimens and at matric suctions of 75 kPa to 100 kPa for the high density specimens. For the low density specimens, the ϕ^b angles reach a constant value of 11° when the matric suction exceeds 150 kPa (Fig. 5b). The ϕ^b angles for the high density specimens reach a constant value of 9° when the matric suction exceeds 300 kPa (Fig. 6b).

There is now good agreement between the failure envelopes through the consolidated drained and constant water content test results when using the curved failure envelopes depicted in Figs. 5 and 6. In other words, the application of a curved failure envelope to these data leads to an essentially unique failure envelope for the same soil tested under different stress paths or procedures. The uniqueness of the curved failure envelope is also demonstrated at two densities as shown in Figs. 5 and 6. The soil prepared at each initial density should be considered as an independent soil.

Procedures for accommodating the non-linear failure envelope

A typical non-linear failure envelope with respect to the $(u_a - u_w)$ axis is shown in Fig. 7. The envelope has a cohesion of intercept of c' plus the term $((\sigma_{ff} - u_{df}) \tan \phi')$ which is due to the applied net normal stress at failure

Fig. 5. Non-linearity in the failure envelope with respect to the $(u_a - u_w)$ axis: a) curved failure envelopes for compacted Dhanauri clay at low density (data from Satija 1978); b) corresponding ϕ^b values.

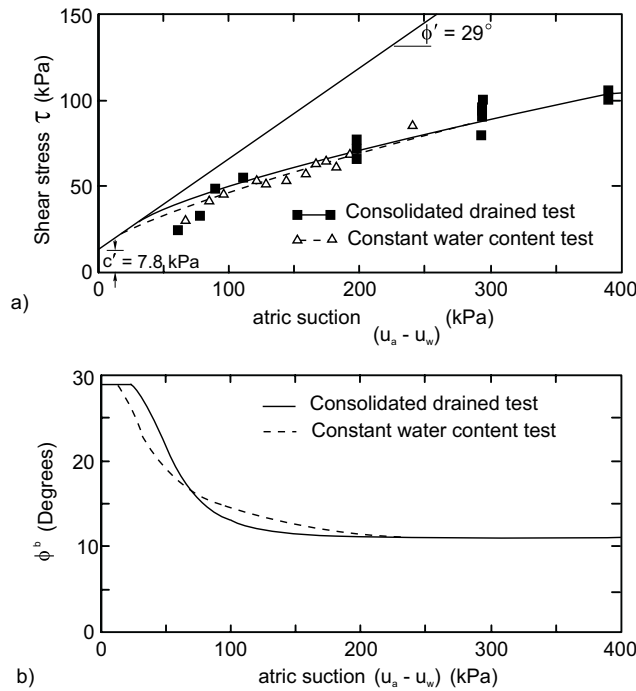
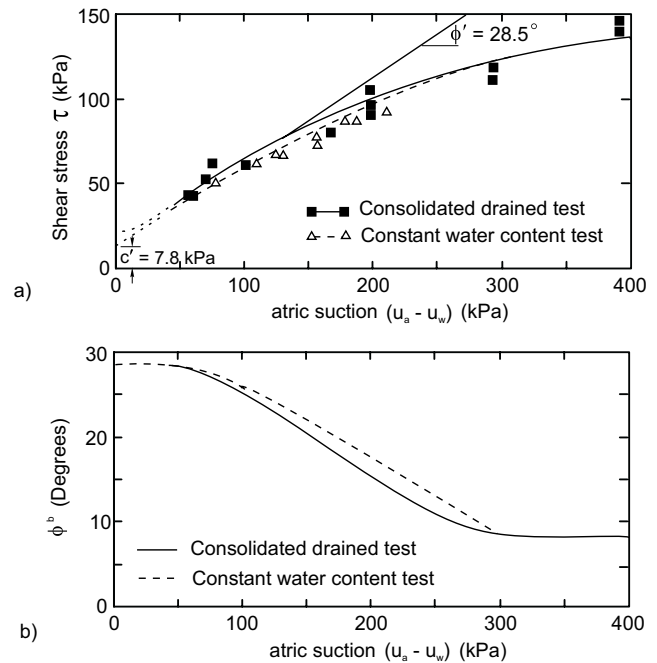


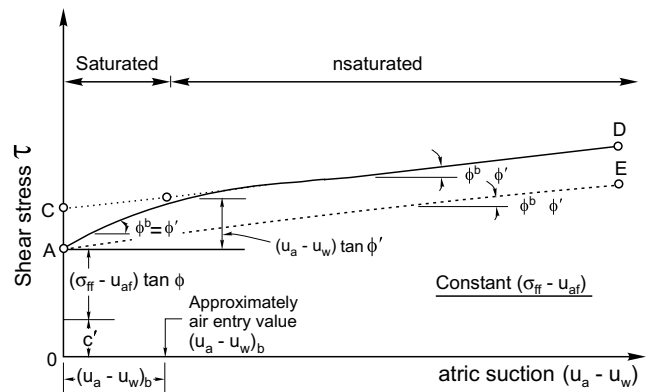
Fig. 6. Non-linearity in the failure envelope with respect to the $(u_a - u_w)$ axis: a) curved failure envelopes for compacted Dhanauri clay at high density (data from Satija 1978); b) corresponding ϕ^b values.



(i.e., point A). The ϕ^b angle is equal to ϕ' at low matric suction (i.e., AB) and decreases to a lower value at high matric suctions (i.e., BD). The variation in the ϕ^b angle with respect to matric suction can be better understood by considering the pore-volume on which the pore-water pressures act. At low matric suctions, the soil specimen remains saturated and the entire pore-volume is filled with the pore-water. At saturation, the pore-water pressure and the total normal stress are referenced to the external air pressure. In this case, the effects of pore-water pressure and total normal stress on the shear strength are characterized by the same friction angle, ϕ' . Therefore, an increase in matric suction produces the same increase in shear strength as does an increase in the net normal stress. In other words, the ϕ^b angle is equal to ϕ' . Substituting ϕ' for ϕ^b in eq. [1] reduces the equation to that used for a saturated soil. This means that the shear strength equation for saturated soils is applicable when the pore-water pressures are negative, provided the soil remains saturated (Aitchison and Donald 1956).

As matric suction is increased, water is drawn out from the pores of the soil. When the air entry value of the soil, $(u_a - u_w)_b$, is reached, air displaces water in the pores (i.e., desaturation begins). For an unsaturated soil, the pore-water pressure and the total normal stress are referenced to the pore-air pressure as illustrated by the $(u_a - u_w)$ and $(\sigma - u_a)$ variables. The pore-water now occupies only a portion of the soil pores. A further increase in matric suction proves not as effective as an increase in net normal stress in increasing the shear strength of the soil. Figure 7

Fig. 7. Non-linearity in the failure envelope on the τ versus $(u_a - u_w)$ plane.



indicates a decrease in the ϕ^b angle to a value lower than ϕ' as matric suction is increased beyond point B. The matric suction corresponding to point B appears to be correlative with the air entry value of the soil. The air entry value depends largely on the grain size distribution but may depend to some extent upon the net confining pressure. The effects of normal stress and pore-water pressure on the shear strength of an unsaturated soil are best independently evaluated with reference to the $(\sigma - u_a)$ and $(u_a - u_w)$ stress state variables (i.e., eq. [1]).

Experimental results to date indicate that the soil has a fairly constant value for the ϕ^b angle beyond the breaking point B (Fig. 7). Some results appear to exhibit essentially no non-linearity in the failure envelope with respect

to the matric suction (see Fig. 2). Non-linearity in the failure envelope can be handled in one of several ways. First the non-linearity illustrated in Fig. 7 can be accommodated using two linear envelopes, \overline{AB} and \overline{BD} . The \overline{AB} envelope corresponds to matric suctions less than the soil air entry value, while the \overline{BD} envelope can be used for matric suctions greater than the air entry value. The \overline{AB} and \overline{BD} envelopes have a slope angle of ϕ and ϕ^b respectively. The cohesion intercept of the \overline{AB} and \overline{BD} envelopes are indicated by points A and C, respectively in Fig. 7. A second procedure is to use only one linear envelope with a slope angle equal to ϕ^b starting from the condition of zero matric suction. This case is illustrated by line \overline{AE} in Fig. 7. The shear strength predicted using the \overline{AE} failure envelope will be lower than the actual strength. A third procedure is to discretize the failure envelope into several linear segments with varying ϕ^b angles. This may be necessary in the case of a highly non-linear envelope.

A fourth procedure is to linearize the failure envelope using the method illustrated in Fig. 8. As noted previously, the matric suction along line \overline{AB} in Fig. 7 produces the same increase in shear strength as does the net normal stress. This means that the effect of their changes can be characterized by the same friction angle, ϕ' . Therefore, the line \overline{AB} portion of the failure envelope can be translated onto the τ versus $(u_a - u_w)$ plane (Fig. 8). As the matric suction increases beyond the air entry value or the soil, $(u_a - u_w)_b$, the soil begins to desaturate. At this point the matric suction axis can be used to separate the different effects of normal stress and matric suction on the shear strength. This causes line \overline{BD} to be drawn on the shear stress versus matric suction plane (Figs. 8 and 9). In other words, the curved failure envelope can be linearized if the $(u_a - u_w)$ axis is drawn starting from the air entry value, $(u_a - u_w)_b$, (Figs. 8 and 9), as opposed to starting from zero matric suction (Fig. 7). It is assumed that the air entry value remains constant at various net confining pressures.

Conclusions

The following conclusions can be made:

- (1) The relationship between shear strength and matric suction may be somewhat non-linear.
- (2) At low matric suctions when the soil remains saturated, the ϕ^b angle is approximately equal to the ϕ angle. As the matric suction exceeds the air entry value of the soil, desaturation commences and the ϕ^b angle appears to reduce to a relatively constant value. On the basis of existing data, the curved failure envelope can be approximated by a bi-linear envelope.
- (3) Various other procedures can be used to accommodate the non-linearity of the failure envelope with respect to matric suction. These procedures are outlined in the text. It is also possible to linearize the failure envelope by translating the portion of the failure envelope corresponding to lower matric suctions, to the τ versus $(\sigma - u_a)$ plane. This procedure elimi-

Fig. 8. Linearized extended Mohr-Coulomb failure envelope.

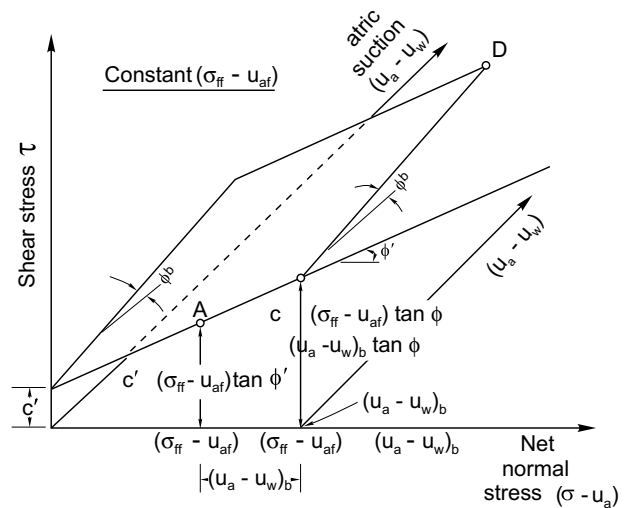
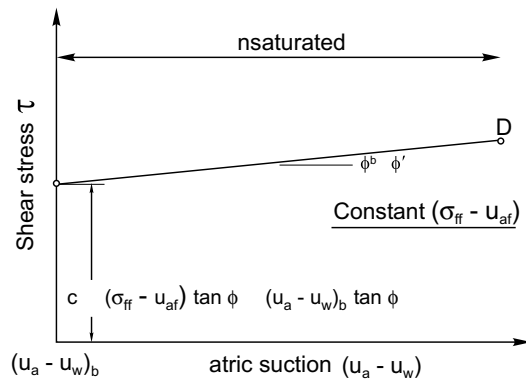


Fig. 9. Linearized failure envelope on the τ versus $(u_a - u_w)$ plane.



ates the need for using different shear strength equations for different matric suctions.

References

Aitchison, G.D., and Donald, I.B. 1956. Effective stresses in unsaturated soils. Proceedings, 2nd Australia – New Zealand Conference on Soil Mechanics, pp. 192–199.

Bishop, A.W., Alpan, I., Blight, G.E., and Donald, I.B. 1960. Factors controlling the shear strength of partly saturated cohesive soils. Proceedings, ASCE Research Conference on Shear Strength of Cohesive Soils, University of Colorado, Boulder, CO, pp. 503–532.

Bishop, A.W., and Donald, I.B. 1961. The experimental study of partly saturated soil in the triaxial apparatus. Proceedings, 5th International Conference on Soil Mechanics and Foundation Engineering, Paris, France, Vol. 1, pp. 13–21.

Bishop, A.W., and Blight, G.E. 1963. Some aspects of effective stress in saturated and unsaturated soils. Géotechnique, 13(3): 177–197.

Escario, V. 1980. Suction controlled penetration and shear tests. Proceedings, 4th International Conference on Expansive Soils, Denver, CO, American Society of Civil Engineers, Vol. 2, pp. 781–797.

- Escario, V., and Sáez, J. 1986. The shear strength of partly saturated soils. *Géotechnique*, **36**(3): 453–456.
- Fredlund, D.G., Morgenstern, H.R., and Widger R.A. 1978. The shear strength of unsaturated Soils. *Canadian Geotechnical Journal*, **15**(3): 313–321.
- Fredlund, D.G., and Rahardjo, H. 1987. Soil mechanics principles for highway engineering in arid regions. *Transportation Research Record* 1137, Washington, D.C., pp. 1–11.
- Gan, J. K.-M. 1986. Direct shear strength testing of unsaturated soils. M.Sc. thesis, University of Saskatchewan, Saskatoon, SK, Canada.
- Gulhati, S.K., and Satija, B.S. 1981. Shear strength of partially saturated soils. *Proceedings, 10th International Conference on Soil Mechanics and Foundation Engineering*, Stockholm, Sweden, Vol. 1, pp. 609–612.
- Hilf, J.W. 1956. An Investigation of pore pressures in compacted cohesive soils. *Technical Memorandum 654*, U.S. Department of Interior, Bureau of Reclamation, Denver, CO, USA.
- Ho, D.Y.F., and Fredlund, D.G. 1982. The increase in shear strength due to soil suction for two Hong Kong soils. *Proceedings, ASCE Geotechnical Conference on Engineering and Construction in Tropical and Residual Soils*, Honolulu, Hawaii, USA.
- Satija, B.S. 1978. Shear behavior of partly saturated soils. Ph.D. thesis, Indian Institute of Technology, New Delhi, India.

A multistage triaxial test for unsaturated soils

D.Y.F. Ho and D.G. Fredlund

Abstract: A triaxial testing procedure is presented for measuring the increase in shear strength resulting from soil suction in an unsaturated soil. Necessary modifications on a conventional triaxial cell are described. A simple graphical method is presented to interpret the test data in accordance with the shear strength equation for unsaturated soils.

Key words: soil tests, shear strength, triaxial tests, capillary pressures, pore-air pressures, high air entry disk, diffused air, multi-stage triaxial test.

Triaxial testing is commonly used to quantify the shear strength of a soil, and procedures for such testing of saturated soils are well established (Bishop and Henkel 1962). However, triaxial testing procedures are needed to quantify the significance soil suction with respect to an increase in shear strength for an unsaturated soil. The procedure outlined in this paper is applicable to relatively permeable unsaturated soils. If the procedure is applied to soils with low permeability, the length of time required to run the test may become excessive.

The proposed procedure can obtain a maximum amount of information from a limited number of tests and can eliminate the effect of variability in the soil from one test to the next. The test results can be readily applied to slope stability and earth pressure problems involving unsaturated soils (Fredlund 1979).

The unsaturated soil shear strength theory (Fredlund et al. 1978) is used as a basis for the interpretation of the test data. The shear strength, τ , is written in terms of the stress state variables for an unsaturated soil and is an extension of the form of equation used for saturated soils.

$$[1] \quad \tau = c' + (\sigma - u_a) \tan \phi' + (u_a - u_w) \tan \phi^b$$

where:

- c' = effective cohesive,
- σ = total stress,
- u_a = pore-air pressure,
- ϕ' = effective angle of friction,
- u_w = pore-water pressure,
- $(u_a - u_w)$ = matric suction, and
- ϕ^b = friction angle with respect to changes in $(u_a - u_w)$ when $(\sigma - u_a)$ is held constant.

Graphically, the equation can be visualized on a three-dimensional plot (a modified Mohr-Coulomb envelope) by using the stress state variables as abscissas (Fig. 1).

D.Y.F. Ho. Geotechnical Engineer, Fugro (Hong Kong) Ltd., 1 Hennessy Rd., 105 Asian House, Hong Kong.

D.G. Fredlund. Professor, Department of Civil Engineering, University of Saskatchewan, 57 Campus Drive Saskatoon, SK, Canada S7N 5A9.

Reproduced with permission from the ASTM, *Geotechnical Testing Journal*, 5(1/2): 18-25, 1982.

The equation can also be visualized as a two-dimensional graph with matric suction contoured as the third variable (Fig. 1).

Two unsaturated Hong Kong residual soils were tested to verify the proposed testing procedure. A couple of typical test results are presented in the discussion.

Apparatus

The laboratory testing program involved two conventional triaxial cells modified for unsaturated soil testing (Fig. 2). The plumbing layout for the triaxial apparatus control board is shown in Fig. 3. The modifications on the triaxial cells are as follows.

Pore-water pressure control

Some means to measure or control the pore-air and pore-water pressures are necessary when unsaturated soils are tested. A porous, ceramic disk that allows the passage of water but prevents the flow of free air was sealed onto the base pedestal (Fig. 2) of each triaxial cell. The disk has small pores to allow the slow passage of water but resist air flow. Such a disk placed underneath the soil serves to separate the pore-air and pore-water pressures. So long as the difference between the pore-air and pore-water pressure does not exceed the "air entry value" (Fredlund 1973) of the disk, there is a continuous column of water from the specimen to the pore-water pressure transducer below the porous disk and the pore-water pressure can then be independently controlled (or measured). The ceramic disks used in the study blocked the entry of air at pressures below 505 kPa (5 bars) and were 0.635 cm (1/4 in.) thick.

Pore-air pressure control

The addition of a controlled pore-air pressure line to a conventional triaxial cell is essential to control the pore-air pressure in the specimen. The air pressure line was connected to a port on the loading cap (Fig. 2). Between the loading cap and the specimen, a 0.32 cm (1/8 in.) thick, coarse corundum stone was used as the drainage element for air.

Fig. 1. Graphical representations of the shear strength of an unsaturated soil.

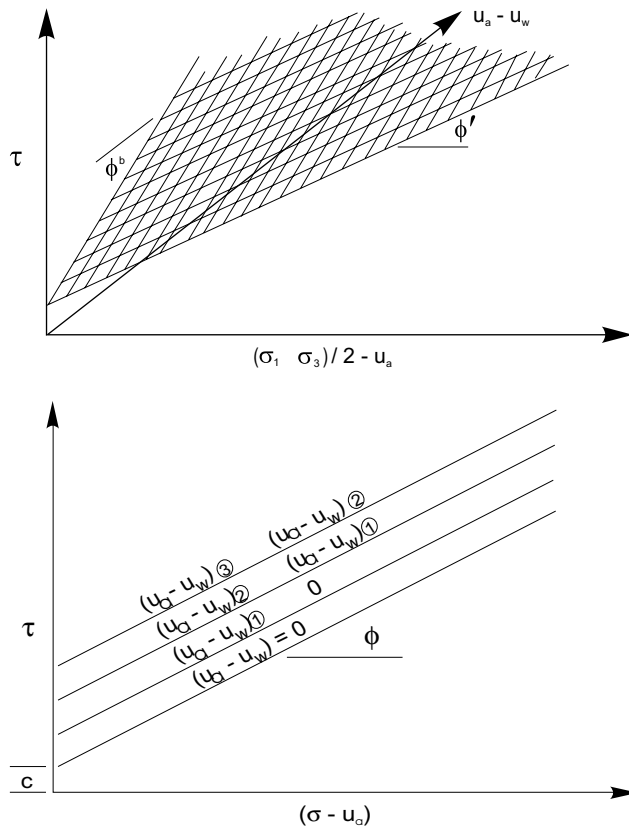


Fig. 2. Modified triaxial cell for testing unsaturated soils (1 in. = 24.5 mm).

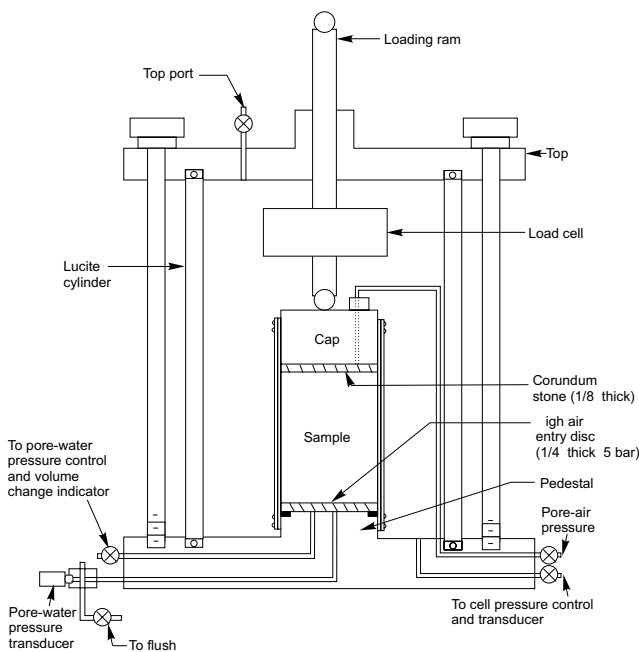
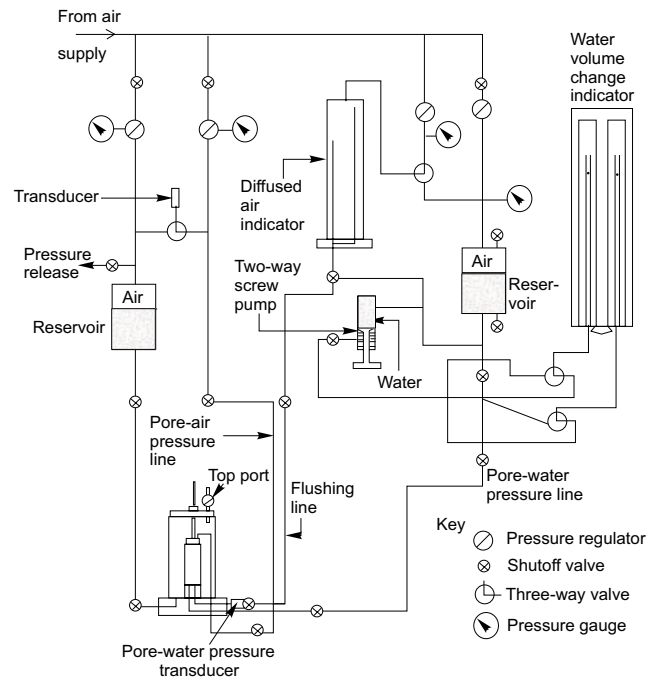


Fig. 3. Schematic diagram of plumbing layout for triaxial apparatus control board.



Flushing system

Although the ceramic disk did not allow the passage of free air, dissolved air could have diffused through the water in the disk and collect as free air bubbles at the base of the disk. The free air bubbles in an open system (Bishop and Henkel 1962) will block the passage of water into the specimen when the specimen dilates or swells and in a closed system will cause misleading measurements of the pore-water pressure and total water volume change.

To cope with the diffused air problem, a flushing system was used. An extra pore-water drainage line with a control valve was connected to the base of the triaxial apparatus (Fig. 2). By closing the valve on the pore-water drainage line leading to the pore-water pressure control and opening the valve on the added drainage line, diffused air accumulated below the disk could be flushed. For testing in a closed system, the volume of the diffused air can be measured with a diffused air indicator (Fredlund 1975) (Fig. 3).

Testing Procedure

The testing procedure involved the control of the air and water pressures during the entire test rather than their measurement in a closed system (Bishop and Henkel 1962). Suction in the specimen was maintained constant during the application of the deviator stress. Maintaining the pore-air and pore-water pressure is similar to performing a "slow" or drained test on a saturated soil. The axis-translation technique (Bocking and Fredlund 1980)

was used to impose suctions greater than 100 kPa (1 atm).

To obtain maximum information from a limited number of tests and to eliminate the effect of soil variability, a multistage testing procedure was attempted (Kenny and Watson 1961, Lumb 1964). The test procedure used is outlined as follows.

Reduction of matric suction

After the trimmed specimen was mounted in the triaxial cell (Fig. 2), two rubber membranes were placed around the specimen. O-rings were placed over the membrane on the bottom pedestal. A spacer (two pieces of 3.2 mm [1/8 in.] plastic tubing) was placed between the membranes and the upper loading cap so that air within the specimen could escape while water was added to the specimen to reduce the suction.

The object of this part of the testing procedure was to relax the suction to a low value before Stage 1 of loading. The following procedure (Ho 1981) was adopted for reducing the initial suction of the soil. First, the Lucite® cylinder was put in place around the specimen and water was added in the cylinder up to a level about 0.5 cm (0.2 in.) below the top of the specimen. The water provided support to the specimen while additional water was subsequently added slowly to the specimen through the air pressure line connected to the top loading cap. During this stage, the air pressure line was connected to a water reservoir to pass water into the top of the specimen. Water could not readily be added to the bottom of the specimen because of the low permeability of the ceramic disk and the danger of cracking the disk by upward pressure. The specimen was then left for several hours to allow the water to distribute throughout the specimen. The saturation process was continued until air could no longer be seen escaping from around the top of the specimen (that is, from between the membrane and the top loading cap).

To use this procedure the Lucite® cylinder must be in place around the specimen while the “top” of the triaxial cell is detached (see Fig. 1). It is then possible to remove the spacer between the membranes and the upper loading cap, once the water has been added to the specimen. At this point, the line connected to the top loading cap is disconnected from the water reservoir and connected directly to the air pressure line.

Several other procedures (Ho 1981) were tried to reduce the initial suction in the specimen but were inferior to the described procedure.

Application of stresses

Once the specimen had imbibed water, the top O-rings were placed around the loading cap. The stresses associated with the first stage of testing were applied and the specimen was allowed to consolidate. A typical set of stresses for Stages 1, 2, 3 are given in Table 1. The associated stress state variables are given in Table 2.

The consolidation process after Stage 2 is similar to that experienced by a specimen placed in a pressure plate apparatus (Bocking and Fredlund 1980). Once no further

Table 1. Typical set of stresses for Stages 1, 2, and 3.

Stage	σ_3^* kPa	u_a kPa	u_w kPa
1	250	100	50
2	350	200	50
3	500	350	50

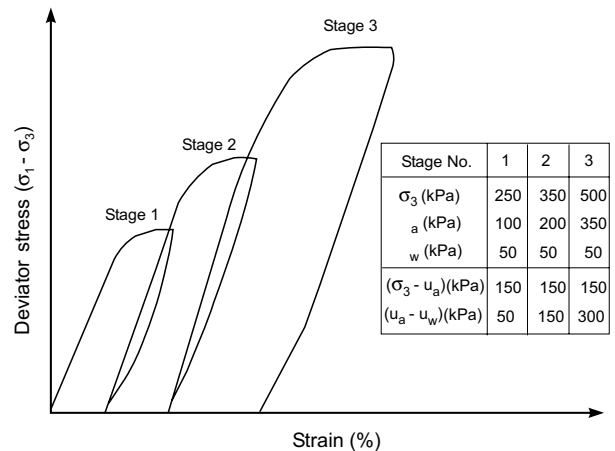
* Where σ_3 is a minor principal stress.

Table 2. Associated stress state variables.

Stage	$(\sigma_3 - u_a)^*$ kPa	$(u_a - u_w)$ kPa
1	150	50
2	150	150
3	150	300

* Where σ_3 is a minor principal stress.

Fig. 4. Ideal stress versus strain curves for a multistage test using the cyclic loading procedure (σ_1 = major principal stress and σ_3 = minor principal stress).



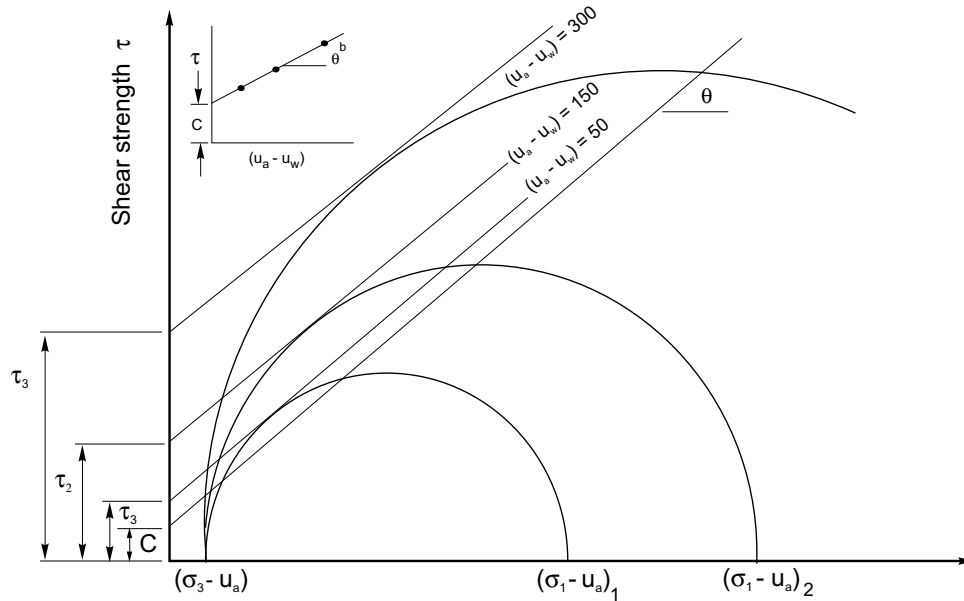
water volume change can be detected from the specimen, the specimen is in equilibrium with the applied stresses.

Loading

After consolidation is complete, the stresses are maintained while the specimen is loaded at a constant strain rate. The choice of strain rate was based on the coefficient of consolidation observed during the consolidation of the specimen (Ho 1981). A 95% degree of dissipation of the induced pore pressures in the specimen was the prime criterion in determining the appropriate strain rates. A typical loading rate was 0.001% strain per minute.

A “cyclic loading” procedure was adopted in testing the specimen. The deviator stress was applied until it was apparent that the stress was reaching a peak value. At this point, the vertical load was “backed-off” the specimen (Fig. 4). A new set of stresses for Stage 2 was applied to the specimen, consolidation was again allowed, and the loading process was repeated as before. The procedure was further repeated for Stage 3.

Fig. 5. Interpretation of a multistage triaxial test to get the angle of friction with respect to matric suction (σ_1 = major principal stress and σ_3 = minor principal stress).



An alternate loading process, the “sustained loading” procedure, was attempted. The applied vertical load was sustained when the deviator stress reached a peak value. This procedure was later found to be inferior to “cyclic loading” because of problems of accumulated strain. Details will be presented later in this paper.

Data interpretation

Test data can be readily interpreted in accordance with the unsaturated soil shear strength equation (Fredlund et al. 1979) with a graphical method. The stress circles corresponding to the failure conditions can be plotted on a two-dimensional graph with matric suction contoured as the third variable.

To interpret the data it is necessary to know the effective angle of friction ϕ' . Conventional triaxial tests were performed by Fugro (Hong Kong), Ltd., on saturated specimens to obtain ϕ' . The angle of friction for the decomposed granite is 33.4°, and 35.3° for the decomposed rhyolite. The details of these tests are presented in unpublished site investigation reports in the files of Fugro (Hong Kong), Ltd.

The ordinate intercepts (when $[\sigma - u_a]$ is equal to zero) of the various matric suction contours can be plotted versus matric suction to give the friction angle ϕ^b (Fig. 5). Details of a similar but analytical method can be found in other publications (Fredlund et al. 1979; Ho 1981).

The justification for the linear form of the unsaturated soil shear strength equation has been verified by experimental laboratory tests (Ho and Fredlund 1982; Fredlund 1981). The results of the re-analyses on published test data showed that the unsaturated soil shear strength the-

ory (Fredlund et al. 1979) is satisfactory for engineering purposes.

Typical test results and their interpretation

The two most commonly found Hong Kong residual soils are decomposed granite and rhyolite. Seventeen 6.35 cm (5 in.) long undisturbed samples were tested, ten of the samples being decomposed granite and seven being decomposed rhyolite. Samples 11B and 11C were decomposed rhyolite from the proposed Thorpe Manor site in Hong Kong. Samples 5, 22, and 16 were decomposed granite from two other sites in Hong Kong. Further details of the soils at these sites can be found in Ho (1981) and Fredlund (1981).

Deviator stress versus strain curves for two decomposed granite and two decomposed rhyolite samples are shown in Figs. 6 and 7. Further test data can be found in Ho (1981) and Ho and Fredlund (1982).

In general, the deviator stress on most of the specimens dropped off significantly immediately after peaking in Stage 3. The specimens seemed to show signs of structural breakdown or collapse in the third stage of loading. The drop in strength in Stage 3 appeared to be related to the amount of strain accumulated while the specimen was failing. Problems associated with excessive deformation in multistage triaxial tests have been noted by other researchers (Kenny and Watson 1961; Wong 1978). It is suggested that the specimen should not be deformed excessively during the earlier stage of loading (that is, past its peak strength). When the specimen is overly strained it will tend to develop a shear failure plane and undergo a strength decrease. The measured strength will then tend

Fig. 6. Stress versus strain curves for decomposed granite: (a) Sample 5 and (b) Sample 22 ($\sigma_3 =$ minor principal stress).

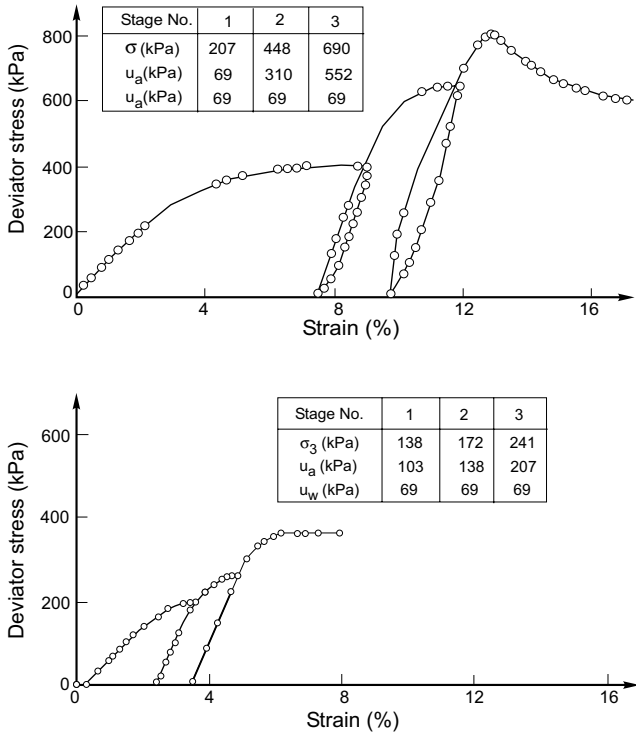
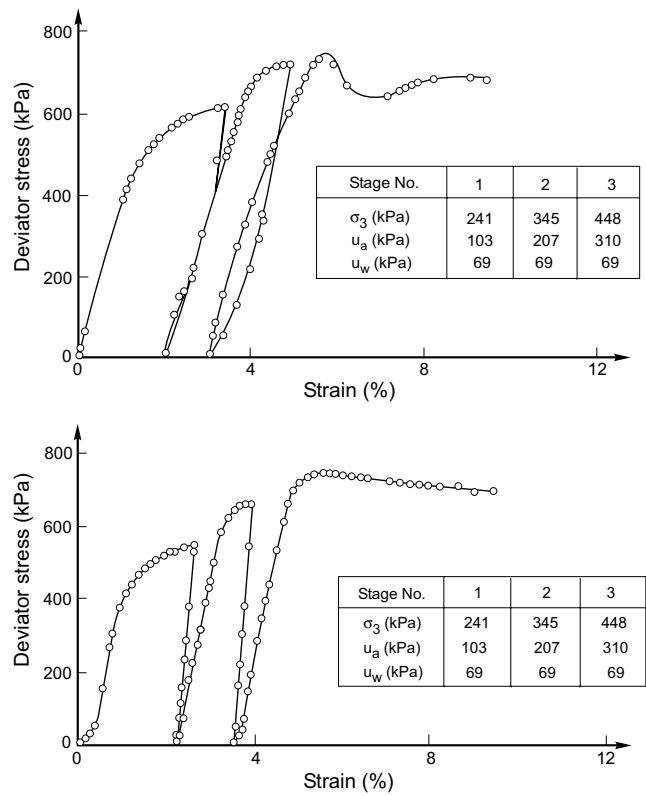


Fig. 7. Stress versus strain curves for decomposed rhyolite: (a) Sample 11B and (b) Sample 11C ($\sigma_3 =$ minor principal stress).

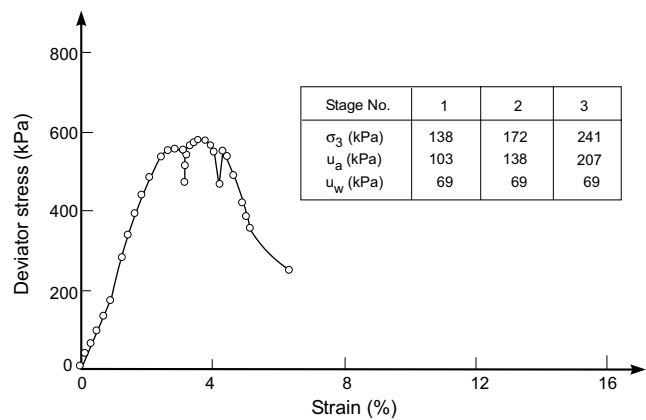


towards a lower ultimate shear strength. Different soils will have varying sensitivity to the accumulated strain.

The “cyclic loading” procedure is believed to be preferable to “sustained loading” in reducing the amount of strain accumulated in the specimen. There are several advantages associated with releasing the applied deviator stress between stages of the test. It prevents further creep of the soil structure, which would occur under sustained loading. Part of the accumulated strain can be restored through elastic recovery (Figs. 6a to 7b). It has also been found that rapid unloading of the specimen provides better strain recovery than slow unloading does (Ho 1981). If the load on the specimen is sustained between stages, the specimen may continue to deform by creep (Fig. 8). Although a time scale is not shown in Fig. 8, the creep phenomenon is reflected by a drop in deviator stress between the stages of loading.

The test data were analyzed in accordance with the unsaturated soil shear strength theory to establish the relationship between soil suction and shear strength. The unsaturated soil shear strength parameter ϕ^b is used to quantify the effect of soil suction on shear strength. Graphs were used to analyze the data. Plots showing the stress conditions at failure for each stage, as well as the interpretation of data for four of the specimens tested, are shown in Figs. 9a to 10b. The relationship between matric suction and shear strength for each specimen is also shown on each figure. The average friction angles ϕ^b based on data from all three stages of testing are indicated.

Fig. 8. Stress versus strain curves for decomposed granite: Sample 16 ($\sigma_3 =$ minor principal stress).



In theory, the ordinate intercepts of the various matric suction contours should fall in a straight line when plotted versus matric suction (Fig. 5). However, as a multistage test progresses, the soil structure of a specimen will be disturbed to a certain degree. As a result, the mea-

Fig. 9. Graphical analysis for decomposed granite: (a) Sample 5 and (b) Sample 22.

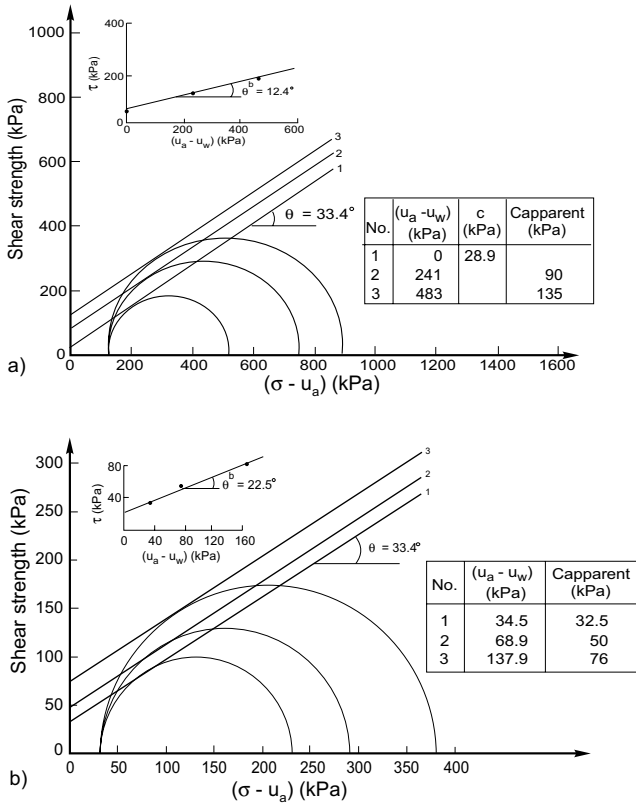
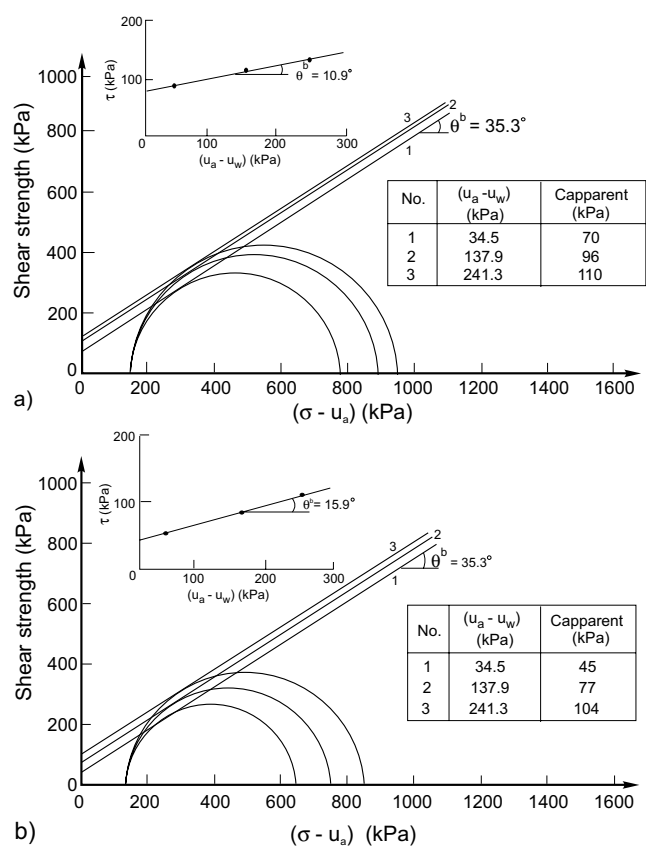


Fig. 10. Graphical analysis for decomposed rhyolite: (a) Sample 11B and (b) Sample 11C.



sured peak strength for Stage 3 may actually be smaller than the peak strength for the specimen under the same stress conditions in a single stage test. The loss in strength in the specimen resulting from structural disturbance appears to be evident when the predicted Stage 3 strength is compared with the measured Stage 3 strength (Fig. 11). As a result, a change in the friction angle ϕ^b from Stage 1 to Stage 3 can be observed (Fig. 12). An average friction angle ϕ^b based on results from all three stages of testing should give a conservative estimate of the significance of soil suction to the shear strength of an unsaturated soil. The value of the friction angle ϕ^b used in practice should be left to the discretion of the engineer.

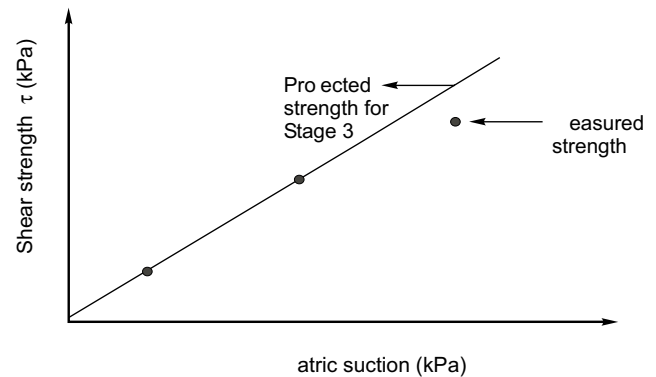
Conclusion

A proposed triaxial testing procedure has been presented to quantify the effect of matric suction on the shear strength of an unsaturated soil. The proposed multi-stage triaxial testing procedure can be used to evaluate the friction angle ϕ^b from a single test.

The matric suction term in the shear strength equation for an unsaturated soil can be considered as contributing to the cohesion of the soil (Fredlund 1979):

$$c = c' + (u_a - u_w) \tan \phi^b$$

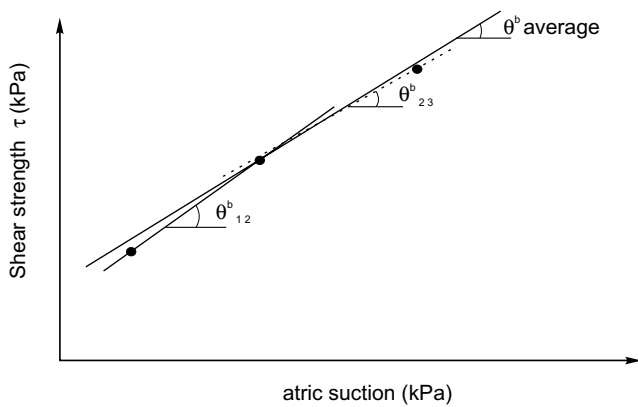
Fig. 11. Comparison between the projected and measured strength for Stage 3 testing.



where:

c = the total or apparent cohesion of an unsaturated soil.

In other words, the suction in an unsaturated soil increases the cohesion of an unsaturated soil. In this way, conventional saturated soil shear strength concepts can be applied to practical problems involving unsaturated soils.

Fig. 12. The change in ϕ^b in a multistage shear test.

Acknowledgements

This research was initiated and funded by the Fugro (Hong Kong), Ltd. Their financial support to the University of Saskatchewan, Saskatoon, Canada, is gratefully acknowledged.

References

- Bishop, A.W., and Henkel D.J. 1962. The measurement of soil properties in triaxial test. Second edition. Edward Arnold, Ltd., London, England, pp. 180–211.
- Bocking, K.A., and Fredlund, D.G. 1980. Limitations of the axis-translation technique. Proceedings, 4th International Conference on Expansive Soils, Denver CO, American Society of Civil Engineers, New York, pp. 117–135.
- Fredlund, D.G. 1973. Volume change behaviour of unsaturated soils. Ph. D. thesis, University of Alberta, Edmonton, AB., Canada.
- Fredlund, D.G. 1975. A diffused air volume indicator for unsaturated soils. Canadian Geotechnical Journal, **12**(4): 533–539.
- Fredlund, D.G. 1979. Appropriate concepts and technology for unsaturated soils. Second Canadian Geotechnical Colloquium. Canadian Geotechnical Journal, **16**(1): 121–139.
- Fredlund, D.G. 1981. The shear strength of unsaturated soils and its relationship to slope stability problems in Hong Kong. The Hong Kong Engineer. **9**(4): 37–45.
- Fredlund, D.G., and Morgenstern, N.R., and Widger, A. 1978. Shear strength of unsaturated soils. Canadian Geotechnical Journal, **15**(3): 313–321.
- Ho, D.Y.F., and Fredlund, D.G. 1982. The increase in shear strength due to soil suction for two Hong Kong soils. Proceedings, ASCE Geotechnical Conference on Engineering and Construction in Tropical and Residual Soils, Honolulu, HI, January 11–15, pp. 263–295.
- Kenny, T.C., and Watson, G.H. 1961. Multiple-stage triaxial test for determining c' and ϕ' of saturated soils. Proceedings, 5th International Conference on Soil Mechanics and Foundation Engineering, Paris, France, pp. 191–195.
- Lumb, P. 1964. The multi-stage triaxial test on undisturbed soils. Civil Engineering Public Works Review, p. 59.
- Wong, H.Y. 1978. Soil strength parameter determination. The Hong Kong Engineer, Journal of the Hong Kong Institution of Engineers, March, pp. 33–39.

Determination of the shear strength parameters of an unsaturated soil using the direct shear test

J.K.-M. Gan, D.G. Fredlund, and H. Rahardjo

Abstract: Multistage direct shear tests have been performed on saturated and unsaturated specimens of a compacted glacial till. A conventional direct shear apparatus was modified in order to use the axis-translation technique for direct shear tests on unsaturated soils. The soil can be subjected to a wide range of matric suctions. The testing procedure and some typical results are presented. Non-linearity in the failure envelope with respect to matric suction was observed. Suggestions are made as to how best to handle the non-linearity from a practical engineering standpoint.

Key words: shear strength, unsaturated soils, negative pore-water pressures, soil suction, direct shear.

Introduction

Most man-made earth structures involve the use of compacted soils. The compaction process produces a soil with a degree of saturation usually in the range of 75–90%. Earthfill dams, embankments, and highways are typical examples of earth structures made of compacted, unsaturated soils. The theory and measurement of shear strength of unsaturated soils have gained increasing attention during the past three decades. A brief review on the development of our understanding of the shear strength behavior of unsaturated soils is presented in this paper.

This paper presents the results of a series of direct shear tests on an unsaturated soil. Direct shear testing of unsaturated soils is desirable since less time is required to fail the soil specimen than when using the triaxial test. The time to failure in the direct shear test is greatly reduced because the specimen is relatively thin. The lengthy testing period for unsaturated soils is due to the low coefficient of permeability of the soil and the high air entry disk in contact with the specimen.

A conventional direct shear apparatus was modified to accommodate a wide range of applied matric suctions (Gan 1986). A multistage test procedure was used. A description of the modified direct shear box and testing procedure is presented. The soil used in this investigation is a compacted glacial till from Indian Head, Saskatchewan.

A series of single-stage and multistage direct shear tests on saturated specimens is analyzed to provide the saturated shear strength parameters of the soil (i.e., c' and ϕ). The possibility of non-linearity with respect to matric suction is also addressed.

Literature review and theory

Donald (1956) conducted a series of direct shear tests on fine sands and coarse silts subjected to a negative pore-water pressure. The soil specimens were exposed to the atmosphere to maintain a pore-air pressure, u_a , of zero gauge pressure. The negative gauge pore-water pressure, u_w , was controlled by applying a constant negative head to the water phase through a membrane at the base of the specimen. This apparatus limited the applied matric suction, $(u_a - u_w)$, to 101 kPa (1 atm) because water cavitates in the measuring system at a negative gauge pressure approaching 101 kPa. The results showed an increase in shear strength as matric suction was increased.

Hilf (1956) suggested that pore-air and pore-water pressures could both be raised to positive pressures in order to apply matric suctions higher than 101 kPa without cavitation in the measuring system. The proposed procedure is referred to as the axis-translation technique. This technique is performed with the use of a high air entry disk that allows the passage of water but prevents the passage of air. As a result, the pore-air and pore-water pressures can be controlled or measured independently as long as the matric suction of the soil does not exceed the air entry value of the ceramic disk.

Bishop et al. (1960) proposed several techniques for measuring the shear strength of an unsaturated soil using triaxial equipment. Results obtained from several different tests were presented. Bishop and Donald (1961) performed a consolidated drained test on an unsaturated loose silt. The acceptability of the axis-translation technique for the shear strength testing of unsaturated soils was verified by Bishop and Blight (1963).

J.K.-M. Gan. Minconsult Sdn. Bhd., 14 Jalan 20/16A, Paramount Garden, 46300 Petaling Jaya, Selangor, Malaysia.

D.G. Fredlund. Professor, Department of Civil Engineering, University of Saskatchewan, Saskatoon, SK, Canada S7N 5A9.

H. Rahardjo. Research Engineer, Department of Civil Engineering, University of Saskatchewan, Saskatoon, SK, Canada S7N 5A9.

Reproduced with permission from the *Canadian Geotechnical Journal*, 25(8): 500–510, 1988.

A shear strength equation for an unsaturated soil in which two independent stress state variables are used was proposed by Fredlund et al. (1978). The two stress state variables most commonly used are the net normal stress, $(\sigma - u_a)$, and the matric suction, $(u_a - u_w)$, where σ is total normal stress, u_a is pore-air pressure, and u_w is pore-water pressure. The proposed shear strength equation has the following form:

$$[1] \quad \tau_{ff} = c' + (\sigma_f - u_a)_f \tan \phi' + (u_a - u_w)_f \tan \phi^b$$

where:

τ_{ff} = shear stress on the failure plane at failure,
 c' = intercept of the "extended" Mohr-Coulomb failure envelope on the shear stress axis when the net normal stress and the matric suction at failure are equal to zero; it is also referred to as the "effective cohesion,"

$(\sigma_f - u_a)_f$ = net normal stress on the failure plane at failure,

σ_{ff} = total normal stress on the failure plane at failure,

u_{af} = pore-air pressure at failure,

ϕ' = angle of internal friction associated with the net normal stress state variable, $(\sigma_f - u_a)_f$,

$(u_a - u_w)_f$ = matric suction at failure,

u_{wf} = pore-water pressure at failure,

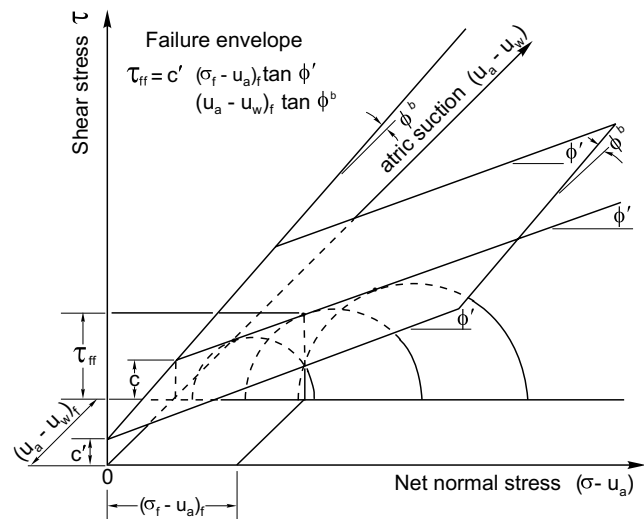
ϕ^b = angle indicating the rate of change in shear strength relative to changes in matric suction.

Equation [1] defines a planar surface, which is called the extended Mohr-Coulomb failure envelope (Fig. 1). The envelope is tangent to the Mohr circles representing failure conditions. The shear strength of an unsaturated soil consists of an effective cohesion intercept, c' , and the independent contributions to shear strength from net normal stress, $(\sigma - u_a)$, and matric suction, $(u_a - u_w)$. The shear strength contributions from net normal stress and matric suction are characterized by ϕ' and ϕ^b angles, respectively. The failure envelope on the frontal plane (i.e., τ versus $(\sigma - u_a)$ plane) is the same as the Mohr-Coulomb failure envelope for saturated conditions.

Two sets of shear strength data reported by Bishop et al. (1960) were analyzed by Fredlund et al. (1978) using the proposed shear strength equation. The results indicated essentially a planar failure envelope when the shear stress, τ , was plotted with respect to the independent stress state variables.

Several sets of triaxial test results on unsaturated Dhanauri clay were presented by Satija (1978). The tests performed were consolidated drained and constant water content tests. These data were analyzed by Ho and Fredlund (1982) assuming that the failure surface was planar with respect to the independent stress state variables. Escario (1980) conducted a series of consolidated drained shear and triaxial tests on unsaturated Madrid gray clay. The tests were performed under controlled matric suction conditions using the axis-translation technique. A modified direct shear box, enclosed in a pressure

Fig. 1. Extended Mohr-Coulomb failure envelope.



chamber, was used to apply a controlled air pressure to the soil specimen. The specimen was placed on a high air entry disk in contact with water at atmospheric pressure. This arrangement is similar to the pressure plate system where the matric suction is controlled by varying the pore-air pressure while the pore-water pressure is maintained constant. The results exhibited an increase in the shear strength as the matric suction was increased.

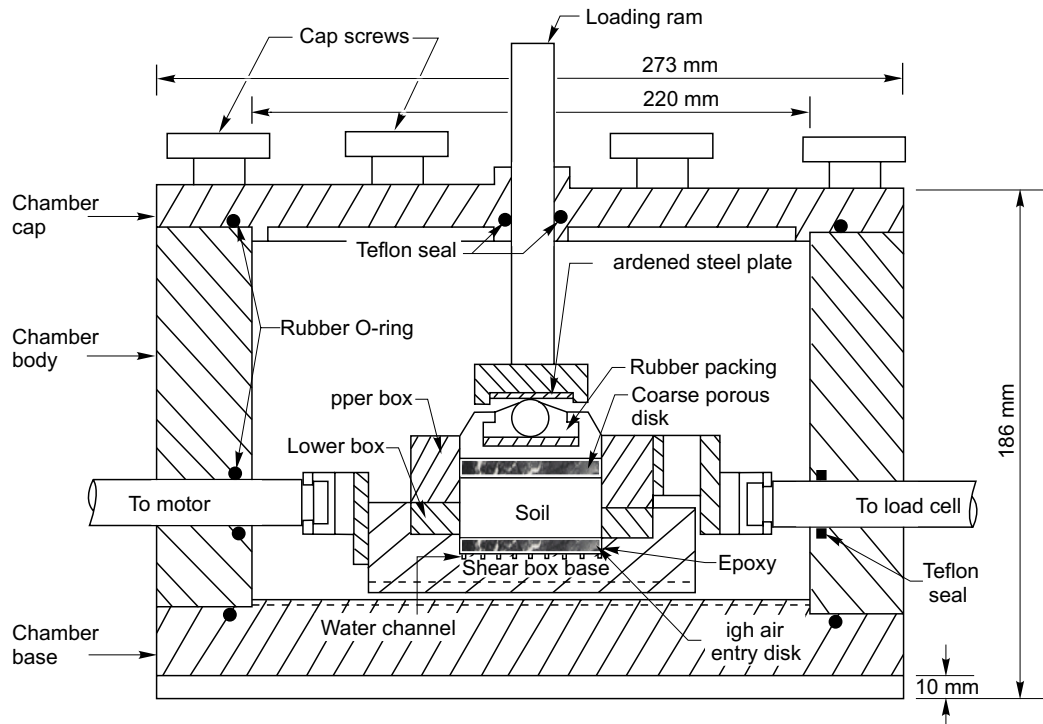
A series of multistage triaxial tests on unsaturated, residual soils from Hong Kong was carried out by Ho and Fredlund (1982). The tests were consolidated drained tests with the pore-air and pore-water pressures controlled during shear. The assumption that the failure surface was essentially planar was made in the analysis of the test data.

Recent experimental evidence using a higher range of matric suctions has shown some non-linearity in the failure envelope with respect to the matric suction axis. Escario and Sáez (1986) performed direct shear tests on three soils using a modified direct shear box and the procedure described by Escario (1980). The results exhibit curvature in the relationship between shear stress and matric suction. Similarly, a reanalysis of the triaxial test results of Satija (1978) also reveals some non-linearity in the shear stress versus matric suction failure envelope (Fredlund et al. 1987).

Description of equipment

A conventional direct shear apparatus has been modified to control the pore-air and pore-water pressures applied to the soil specimen. The direct shear box is placed in an air pressure chamber as shown in Fig. 2. The soil specimen has a coarse porous disk placed at its top and a high air entry disk at its bottom. The pore-air pressure, u_a , in the soil specimen is controlled by pressurizing the air in the chamber. The air pressure in the chamber has direct contact with the coarse disk on top of the specimen through the gap between the loading cap and the upper

Fig. 2. Modified direct shear apparatus.



box. The pore-water pressure, u_w , is controlled through the high air entry disk at the base of the specimen. The flow of water through the disk ensures a continuous column of water between the soil specimen and the water below the disk. However, with time, pore-air may diffuse through the water in the high air entry disk and appear as air bubbles in the water compartment below the disk. Therefore, the water compartment is made to allow for the flushing of diffused air bubbles on a periodic basis. The total normal stress, σ , is applied vertically to the specimen through a loading ram. The uplift pressure of the air on the loading ram is taken into account.

The lower part of the direct shear box is seated on rollers that run in grooved tracks on the chamber base (Fig. 2). The lower box is connected to a motor, through a gear box, for the application of the horizontal shear load to the specimen. The upper part of the box is connected to a load cell in order to measure the applied horizontal shear load.

A water movement indicator was used to measure the movement of water into and out from the soil specimen. The measured volume change of water in the specimen must be corrected for the volume of diffused air (Fredlund 1975). The vertical deflection and horizontal displacement of the soil specimen were measured using linear voltage displacement transducers (LVDT's).

Soil and test program

The soil used in this investigation is a glacial till from the Indian Head area of Saskatchewan. Only material passing the No. 10 sieve was used. The index properties of the soil are summarized in Table 1. Prior to testing, the

soil was compacted in accordance with the American Association of State Highway and Transportation Officials (AASHTO) standard. The maximum dry density and optimum water content are listed in Table 1. The clay fraction is predominately a calcium montmorillonite.

The testing program consisted of (1) a pilot test program of direct shear tests to determine the displacement rate required to ensure drained conditions during shear, (2) consolidated, drained direct shear tests on saturated specimens, and (3) consolidated drained direct shear tests on unsaturated specimens.

The pilot test program consisted of four single-stage direct shear tests on unsaturated specimens. The tests were performed at four different displacement rates using the modified direct shear equipment. The effect of displacement rate on the shear strength was investigated by using a constant net normal stress and matric suction within the specimens for the four tests.

The second part of the testing program consisted of several single-stage and multistage direct shear tests performed on saturated specimens using the conventional direct shear apparatus and procedure. The purpose of this testing program was to obtain the shear strength parameters c' and ϕ' , and to assess the applicability of the multistage direct shear procedure for Indian Head glacial till. The results of multistage direct shear tests on saturated specimens were studied to obtain a suitable failure criterion for the multistage direct shear testing. The selected failure criterion was used in the analysis of the multistage test results for unsaturated specimens.

The third part of the testing program consisted of a series of five multistage direct shear tests on unsaturated specimens. The tests were performed to obtain the shear

Table 1. Index properties for the glacial till from the Indian Head area of Saskatchewan.

Property	Value
Liquid limit	35.5%
Plastic limit	16.8%
Plasticity index	18.7%
Percent sand sizes	28%
Percent silt sizes	42%
Percent clay sizes	30%
Specific gravity of soil solids	2.734
AASHTO standard compaction	
Maximum dry density	1815 kg/m ³
Optimum water content	16%

strength parameter, ϕ^b . The initial volume mass properties of the five specimens are tabulated in Table 2. Each specimen had three to seven stages of shearing. The tests were performed by maintaining a constant net normal stress, $(\sigma - u_a)$, of approximately 72.6 kPa and varying the matric suction, $(u_a - u_w)$ between stages (Table 2). The matric suctions ranged from 0 to 500 kPa. As a result, the shear stress versus matric suction failure envelope was obtained and the ϕ^b parameter was computed.

The multistage direct shear tests on unsaturated specimens were conducted using the modified direct shear apparatus (Fig. 2). Each test was commenced by saturating the high air entry disk with de-aired water. The soil specimen was then mounted in the shear box and initially allowed access to water through the top coarse porous disk. The predetermined total normal stress, σ , pore-air pressure, u_a , and pore-water pressure, u_w , were then applied to the specimen, in this order.

The soil specimen was allowed to come to equilibrium under the applied net normal stress, $(\sigma - u_a)$, and matric suction, $(u_a - u_w)$. During the equalization process, the vertical deflection and the water movement from the soil specimen were measured. Equilibrium was assumed to have been achieved when there was no further flow of water from the specimen. Upon attaining equilibrium, the soil specimen was sheared under a constant rate of displacement. Water movement from the specimen was observed during shear. Part of the observed movement is due to water flow and part is due to the flow of diffused air. No attempt was made to separate these two quantities. However, the diffused air was flushed from below the high air entry disk on a daily basis. The shearing process was stopped when the peak shear stress of the soil was imminent. The horizontal shear load was then released from the specimen. The next stage was performed by applying a new matric suction to the specimen and repeating the above procedure. Details on the test procedure are given by Gan (1986).

Presentation of test results

The results of the pilot test program indicate that the peak shear stress remained essentially constant when the

displacement rate was less than 2.2×10^{-4} mm/s. On the basis of these results, a displacement rate of 1.7×10^{-1} mm/s was selected for the entire direct shear testing program.

The analysis of the multistage direct shear test results on saturated specimens shows that a shear displacement of 1.2 mm was sufficient to mobilize the peak shear stress. Figure 3 shows typical data from a multistage direct shear test on a saturated glacial till specimen. A shear displacement of 1.2 mm on specimen size of 50 mm by 50 mm was selected as the failure criterion for all multistage direct shear tests.

A plot of shear stress versus net normal stress corresponding to failure is shown in Fig. 4 for the saturated specimens. The data were obtained from both single-stage and multistage direct shear tests on saturated specimens. The peak shear stress was used as the shear stress at failure for the single-stage tests. On the other hand, the shear stress corresponding to 1.2 mm of shear displacement was assumed to be the shear stress at failure for the multistage tests. The lines plotted through the data points in Fig. 4 form Mohr-Coulomb failure envelopes for the saturated specimens (i.e., the frontal plane of Fig. 1). The authors have no explanation as to why the test results from specimen GT-15-N3 produce a negative cohesion intercept.

A few typical results of the multistage direct shear tests on unsaturated specimens are presented in this paper. Figure 5 shows a typical plot of water volume change and consolidation for specimen GT-16-N4 at the beginning of its second stage. These volume changes occurred during matric suction equilibration. A negative volume change refers to a decrease in volume, whereas a positive volume change indicates a volume increase. Matric suction equilibration was generally attained in about 1 day (Fig. 5a). Some tests were allowed to equilibrate for more than 10,000 min to ensure that equilibrium was indeed attained.

Results from one of the multistage direct shear tests on unsaturated specimens are illustrated in Fig. 6 (specimen GT-16-N4). The vertical deflection versus horizontal displacement curves (Fig. 6b) generally show that the soil dilated during shear, except for initial stages at low matric suctions. As the matric suction increases the curves show an increase in the specimen height with increasing horizontal displacement (Fig. 6b).

The shear stress normalized with respect to matric suction is plotted versus horizontal displacement in Fig. 6c. The curves indicate a decrease in the normalized peak stress with increasing matric suction. These peak values appear to approach a relatively low, constant value at high matric suctions.

Specimens GT-16-N1 – GT-16-N4 were tested at the selected displacement rate of 1.76×10^{-4} mm/s. Specimen GT-16-N5 was tested at a displacement rate equal to approximately one-half the above rate (i.e., 0.833×10^{-4} mm/s). Midway through the last stage of test on GT-16-N5, the displacement rate was further reduced to 0.194×10^{-4} mm/s. The reduced displacement rates were

Table 2. Multistage direct shear tests on unsaturated glacial till specimens.

Initial properties	Specimen number									
	GT-16-N1	GT-16-N2	GT-16-N3	GT-16-N4	GT-16-N5					
Void ratio, e_o	0.77	0.53	0.69	0.51	0.54					
Degree of saturation S_o (%)	42	59	48	65	61					
Water content, w_o (%)	11.83	11.50	12.27	12.23	12.08					
Stage No.	Stress state at each stage (kPa)									
	$(\sigma - u_a)$	$(u_a - u_w)$	$(\sigma - u_a)$	$(u_a - u_w)$	$(\sigma - u_a)$	$(u_a - u_w)$	$(\sigma - u_a)$	$(u_a - u_w)$	$(\sigma - u_a)$	$(u_a - u_w)$
1	70.94	37.86	71.28	176.95	72.83	23.45	72.55	16.62	73.73	0.85
2	71.29	176.89	71.58	314.7	72.84	79.04	72.61	60.69	72.58	33.89
3	71.58	315.25	71.99	453.53	72.68	448.05	72.59	120.3	72.59	78.07
4					72.68	448.05	72.56	239.83	72.57	126.2
5							72.58	347.7	72.55	204.53
6							72.53	494.5	72.57	321.89
7									72.20	504.34

Fig. 3. Multistage direct shear test data on saturated glacial till specimen GT-15-N2: a) shear stress versus horizontal displacement; b) vertical deflection versus horizontal displacement; c) τ / σ versus horizontal displacement.

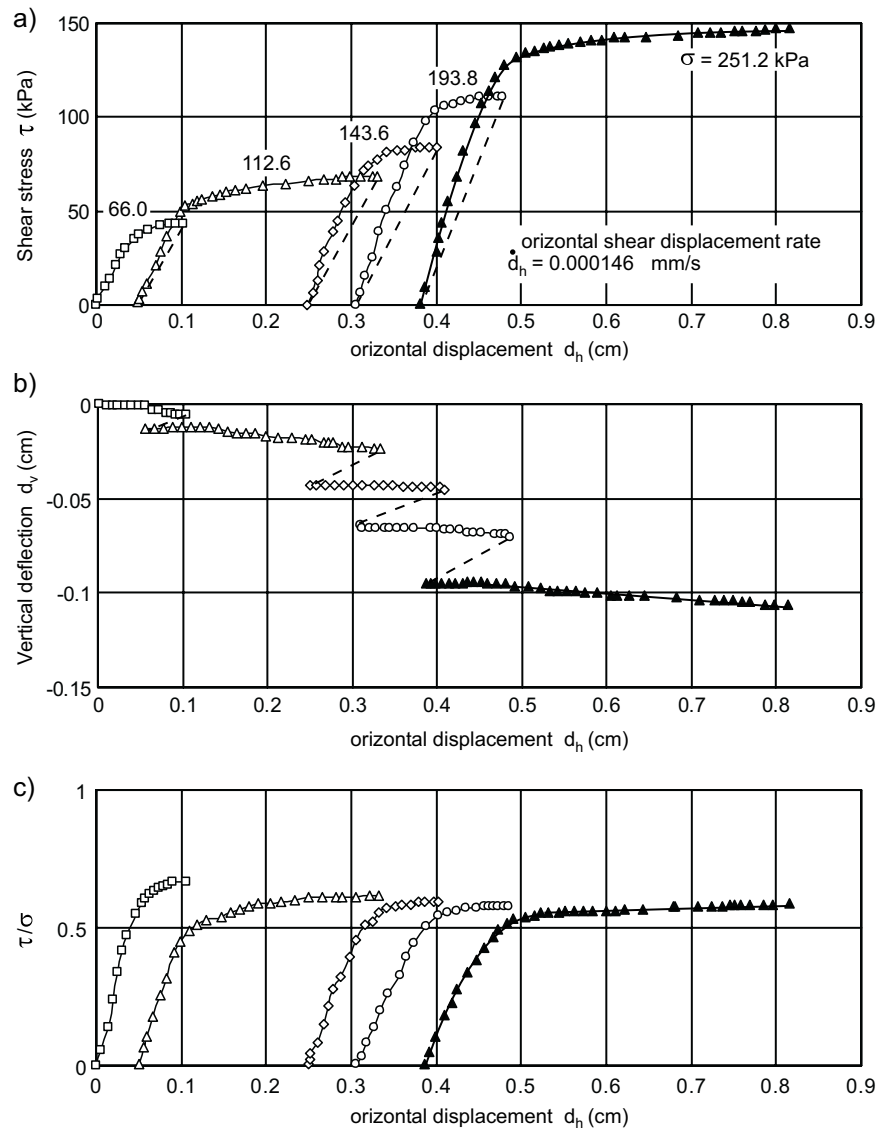


Fig. 4. Mohr-Coulomb failure envelopes for direct shear tests on saturated glacial till.

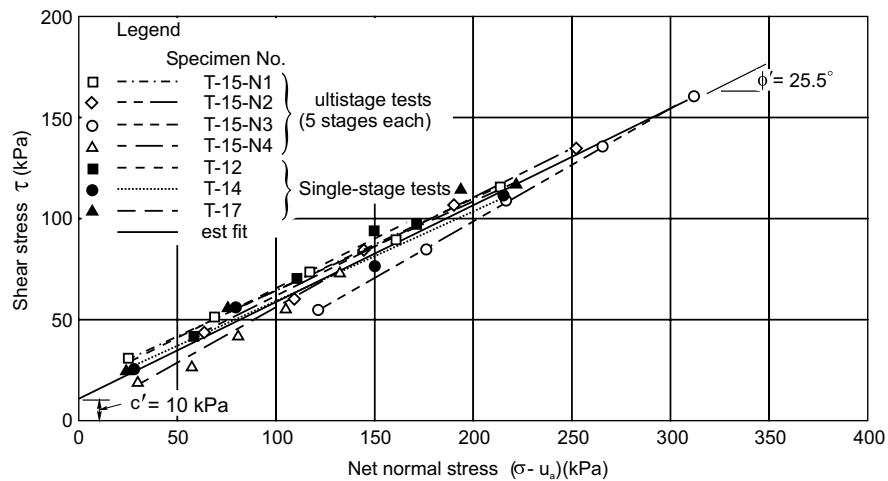
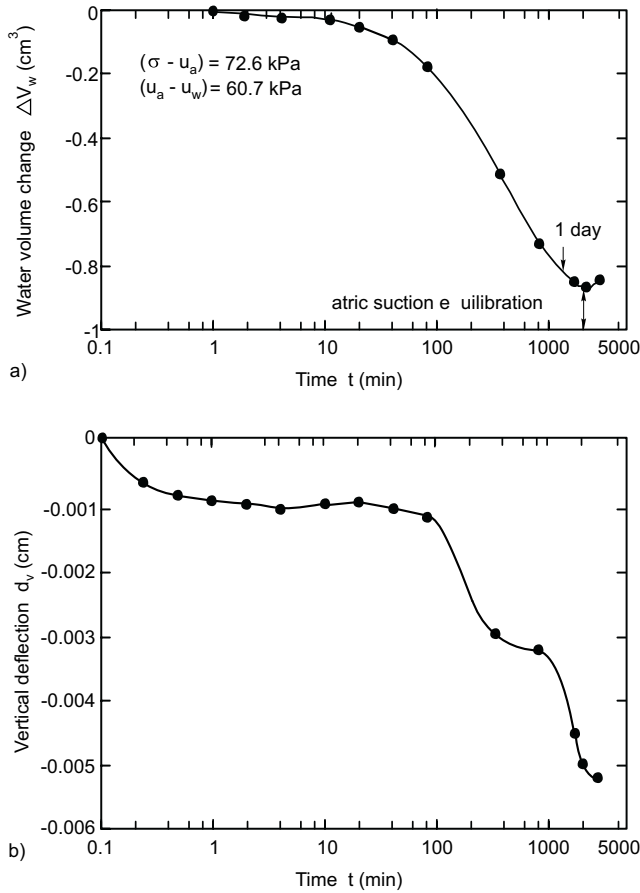


Fig. 5. Water volume change and consolidation of specimen GT-16-N4 (stage 2) during matric suction equilibration: a) water volume equilibration; b) consolidation.



used to demonstrate that the selected displacement rate of 1.76×10^{-4} mm/s was indeed adequate to ensure drained conditions during shear. The test results obtained from specimen GT-16-N5 tested at the reduced displacement rate (Fig. 7) exhibit similar behavior to that observed from the results obtained on other specimens (Fig. 6). In the last stage, the shear stress versus horizontal displacement curve continues monotonically regardless of the further reduction in the displacement rate (i.e., 0.194×10^{-1} mm/s), (Fig. 7a). The small drop observed was believed to be due to the “slack” in the gear system when changing from one gear ratio to another.

The shear stresses corresponding to a shear displacement of 1.2 mm are plotted against matric suction in Fig. 8a for specimen GT-16-N4. The line joining the data points forms the shear stress versus matric suction failure envelope (i.e., the third dimension of Fig. 1). The shear stress versus matric suction plane in Fig. 8a corresponds to an average net normal stress at failure, $(\sigma_{ff} - u_{af})$, of 72.6 kPa. The slope of the failure envelope gives the ϕ^b angle. The ϕ^b angles are plotted with respect to matric suction in Fig. 8b.

Figure 9a presents a summary of the results obtained from five unsaturated specimens tested using the multi-

stage direct shear test (see Table 2). The results fall within a band, forming the failure envelopes shown in Fig. 9a. The ϕ^b angles corresponding to the failure envelopes are plotted in Fig. 9b with respect to matric suction. No single-stage direct shear tests were performed on the unsaturated soil specimens.

Discussion of test results

The direct shear test results on saturated glacial till specimens exhibit essentially linear failure envelopes with respect to the net normal stress axis (Fig. 4). The failure envelopes also show close agreement between the single-stage and multistage direct shear test results. This would indicate an acceptability of the multistage direct shear test technique for Indian Head glacial till. It should be emphasized that the multistage test technique may not be acceptable for all types of unsaturated soils. The use of 1.2 mm of shear displacement, as the failure criterion, was verified for testing of the glacial till. A best-fit envelope drawn through the data points in Fig. 4 results in shear strength parameters c' and ϕ' of 10 kPa and 25.5° , respectively. The scatter in the cohesion intercept was about ± 7 kPa.

The direct shear test results on the unsaturated specimens exhibit significant non-linearity for the failure envelope with respect to the matric suction (Figs. 8 and 9). The ϕ^b angles commence at a value equal to ϕ' (i.e., 25.5°) at matric suctions close to zero and decrease significantly at matric suctions in the range of 50 to 100 kPa. The ϕ^b angles reach a fairly constant value ranging from 5° to 10° when the matric suction exceeds 250 kPa (Fig. 9b). The scatter in the failure envelopes (Figs. 4 and 9) appears to be due to variations in the initial void ratios of the soil specimens. There also appears to be some change in the thickness of each specimen during shear. However, it is difficult to quantify the change in void ratio of the soil near the failure zone.

Figures 8a and 9a show that there is a slight discrepancy in the intercepts where the saturated strength envelope intersects with the strength envelope obtained while the matric suction is controlled. For example, when the strength equation is applied to Fig. 8a, the following equality should be satisfied:

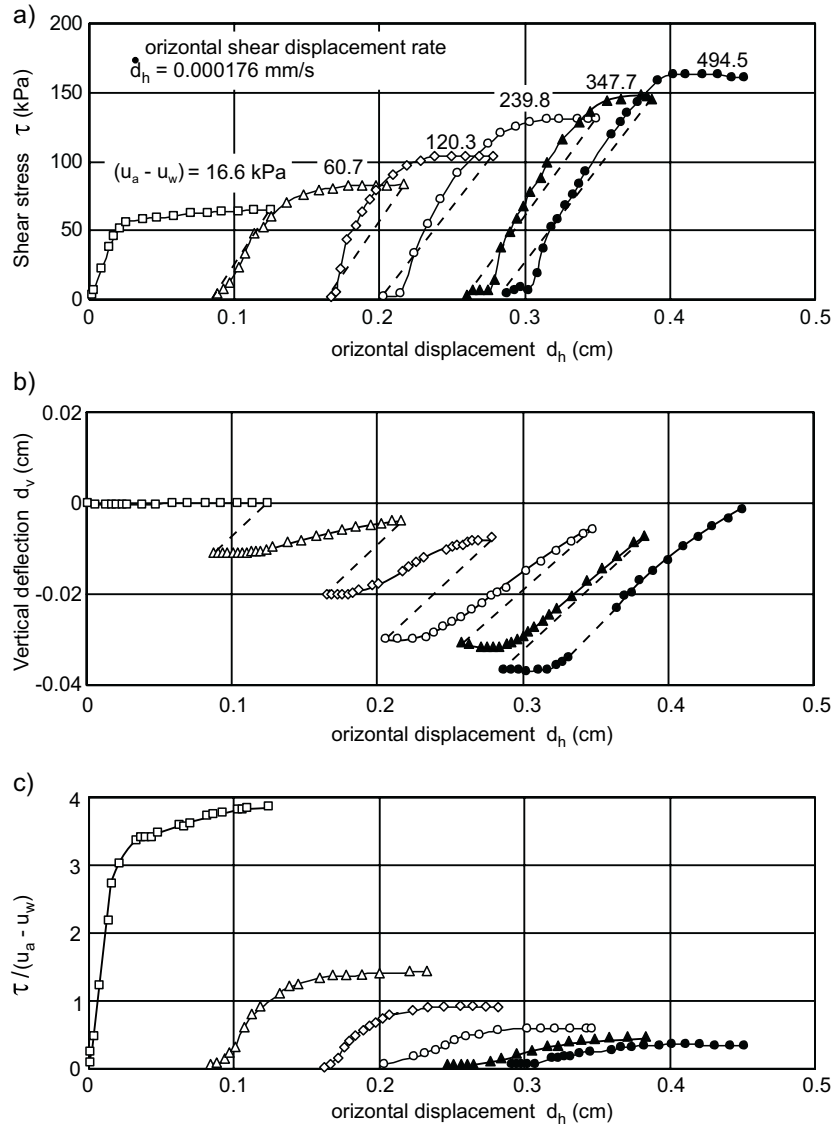
$$[2] \quad \tau_{ff} = c' + (\sigma_f - u_a)_f \tan \phi' + (u_a - u_w)_f \tan \phi^b$$

$$[3] \quad 55 \neq 10.0 + (72.6) \tan 25.5$$

The difference in eq. [3] is 10.4 kPa. The authors feel that this difference can be explained in terms of (1) variation in the initial void ratios of the specimen used for the saturated and unsaturated tests and (2) the fact that two different direct shear machines were used: namely, the conventional apparatus for testing the saturated specimens and the modified apparatus for the unsaturated specimens. The variation in the initial void ratios produces scatter in the intercepts obtained for both the saturated and unsaturated specimens.

The angle ϕ^b can be viewed in terms of being either part of the frictional component of shear strength or part

Fig. 6. Multistage direct shear test results on unsaturated glacial till specimen GT-16-N4: a) shear stress versus horizontal displacement; b) vertical deflection versus horizontal displacement; c) $\tau / (u_a - u_w)$ versus horizontal displacement.



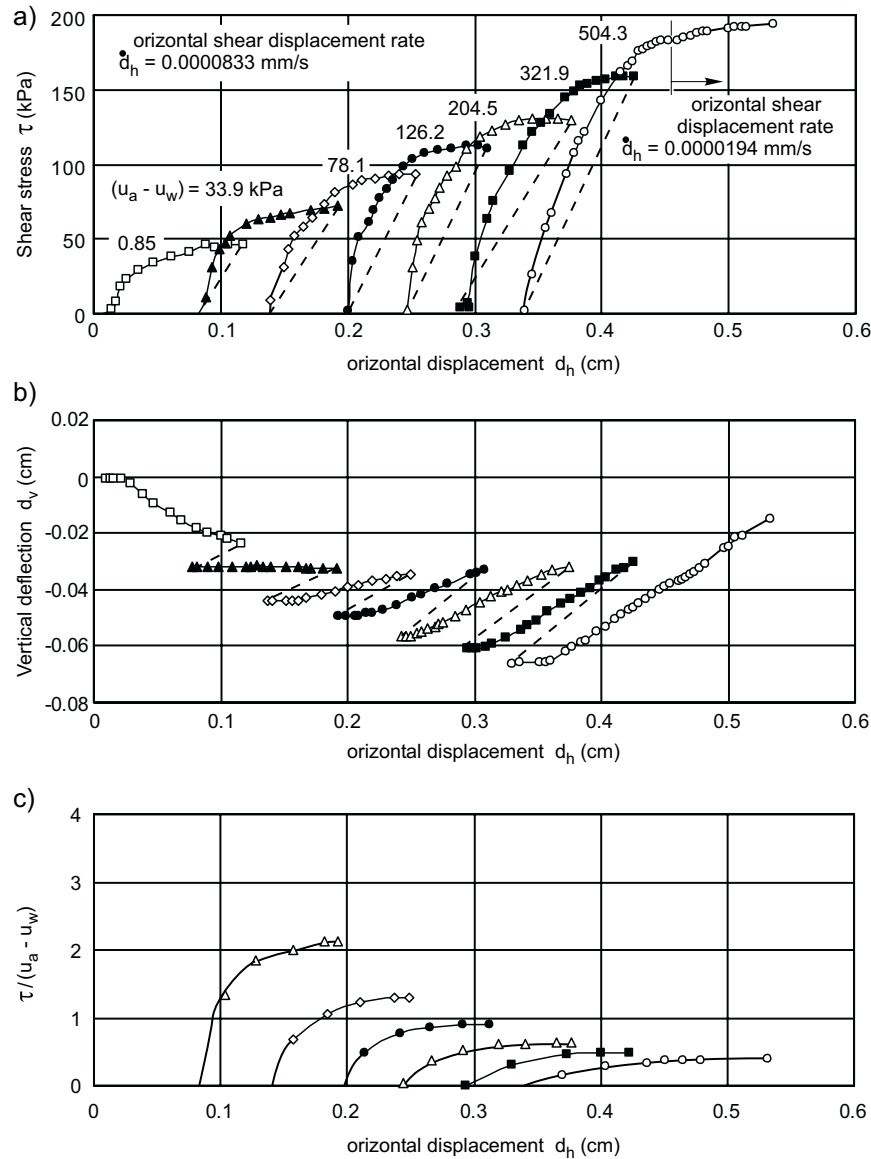
of the cohesive component of shear strength. As part of the frictional component, its maximum value can be assumed to be equal to ϕ^b . As the soil becomes unsaturated the cross-sectional area through which the water phase acts is decreased, and as such, an increase in the matric suction is not as effective in increasing the shear strength as is an increase in the normal stress. As part of the cohesive component, the angle ϕ^b is simply used as a mathematical convenience for defining the increase in strength as matric suction is increased. It would appear preferable to view the soil as having one angle of internal friction, namely, ϕ .

The direct shear tests on the unsaturated specimens have been conducted at a constant net normal stress of 72.2 kPa. Therefore, comments regarding the non-linearity in the failure envelope strictly apply to a net normal stress of 72.2 kPa. Further testing at different net

normal stresses is recommended to more fully characterize the entire failure envelope.

The non-linearity of the failure envelope with respect to matric suction has been addressed and discussed in detail by Fredlund et al. (1987). Triaxial test results on compacted Dhanauri clay were re-analyzed using the assumption of a curved failure envelope. The consolidated drained and constant water content test failure envelopes exhibited close agreement, indicating uniqueness in the strength designation. In other words, both the consolidated drained and constant water content test data yielded the same non-linear shear strength surface. It should be noted however, that this was not the case when the same data were analyzed using a planar failure envelope (Ho and Fredlund 1982). In summary, the non-linear interpretation of the shear strength test data for unsaturated soils appears to provide a unique failure envelope.

Fig. 7. Multistage direct shear test results on unsaturated glacial till specimen GT-16-N5: a) shear stress versus horizontal displacement; b) vertical deflection versus horizontal displacement; c) $\tau / (u_a - u_w)$ versus horizontal displacement.



In some cases, however, it may not be necessary to use a non-linear interpretation.

Procedures for accommodating the non-linearity of the shear strength envelope

Several procedures for handling the non-linearity of failure envelope have been proposed by Fredlund et al. (1987). These are illustrated in Fig. 10. The failure envelope shown in Fig. 10 has a cohesion intercept of c' plus the term $((\sigma_f - u_a)_f \tan \phi^b)$, which is due to the applied net normal stress at failure (i.e., point A). The ϕ^b angle along the AB portion is equal to ϕ' and decreases to a value lower than ϕ' as matric suction is increased beyond point B. The matric suction at point B appears to be correlative with the air entry value of the soil, $(u_a - u_w)_b$. The ϕ^b an-

gle is equal to ϕ' when the soil remains saturated (i.e., \overline{AB}) and the ϕ^b angle decreases to a lower value when the soil has become unsaturated.

The first procedure suggested for handling the non-linearity in the failure envelope is to use two linear envelopes, AB and BD , for the two ranges of matric suction (Fig. 10). The second procedure is to use a lower limit failure envelope (i.e., AE) along with the lower ϕ^b angle for the entire range of matric suction. This procedure is simpler, but gives a lower shear strength than the actual shear strength. The third procedure is to discretize the failure envelope into several linear segments if the envelope is highly non-linear. Fourthly, the \overline{AB} portion can be translated onto the shear stress versus $(\sigma - u_a)$ plane, since the ϕ^b angle is equal to ϕ' . As a result, the failure envelope on the shear stress versus matric suction plane constitutes

Fig. 8. Failure envelope obtained from unsaturated glacial till specimen GT-16-N4: a) failure envelope on τ versus $(u_a - u_w)$ plane, b) corresponding ϕ^b values.

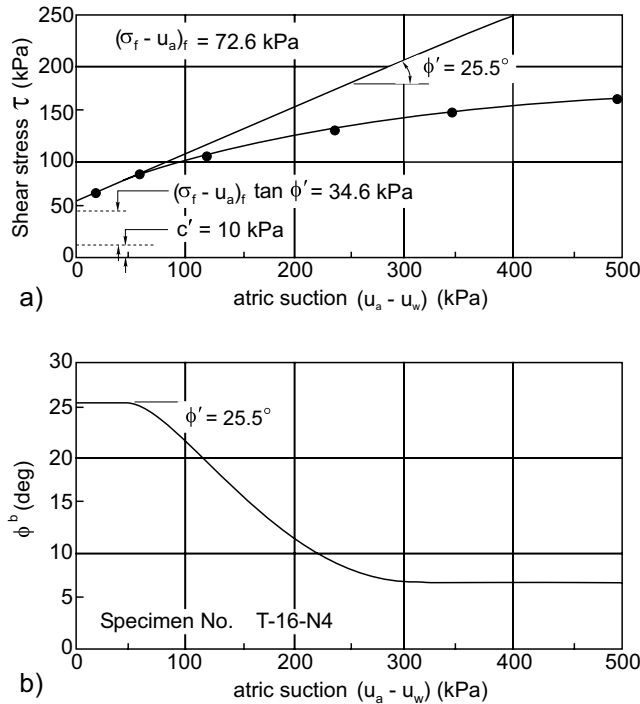


Fig. 9. Failure envelope obtained from unsaturated glacial till specimens: a) failure envelope on τ versus $(u_a - u_w)$ plane, b) ϕ^b values corresponding to the three failure envelopes.

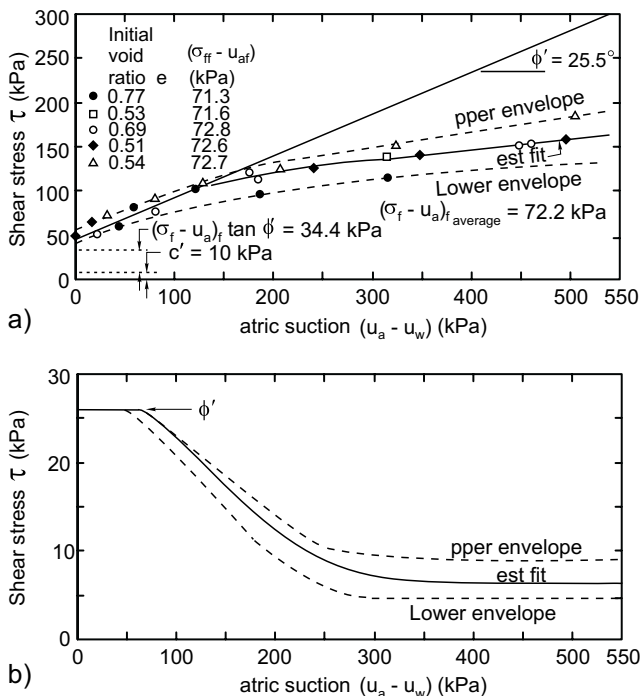
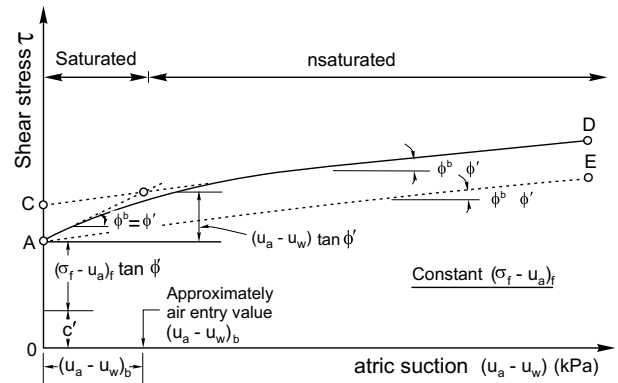


Fig. 10. Several procedures for handling the non-linearity of the failure envelope.



the \overline{BD} portion of Fig. 10. In this case, the non-linear failure envelope is linearized by commencing the matric suction axis at the air entry value of the soil, $(u_a - u_w)_b$.

Conclusions

The shear strength parameters of an unsaturated soil can be obtained using a direct shear apparatus, modified in order to apply matric suctions greater than 101 kPa (1 atm) to the soil specimen. The direct shear test uses a relatively thin specimen, in comparison with the triaxial test, and can significantly reduce the time required for testing unsaturated soils of low permeability.

The multistage direct shear test on Indian Head glacial till yields consistent results. It appears that the failure envelope for an unsaturated soil may be somewhat non-linear with respect to the matric suction axis. When the soil remains saturated, the ϕ^b angle is approximately equal to the ϕ angle. As the soil desaturates at higher matric suctions, the ϕ^b angle appears to decrease to a relatively constant value. The non-linearity in the failure envelope becomes noticeable when the soil is tested over a wide range of matric suctions (e.g., 0 to 500 kPa).

References

Bishop, A.W., and Blight, G.E. 1963. Some aspects of effective stress in saturated and unsaturated soils. *Géotechnique*, **13**(3): 177–197.

Bishop, A.W., and Donald, I.B. 1961. The experimental study of partly saturated soil in the triaxial apparatus. *Proceedings, 5th International Conference on Soil Mechanics and Foundation Engineering, Paris, France, Vol. 1, pp. 13–21.*

Bishop, A.W., Alpan, I., Blight, G.E., and Donald, I.B. 1960. Factors controlling the shear strength of partly saturated cohesive soils. *Proceedings, ASCE Research Conference on Shear Strength of Cohesive Soils, University of Colorado, Boulder, CO, pp. 503 - 532.*

Donald, I.B. 1956. Shear strength measurements in unsaturated, non-cohesive soils with negative pore pressure. *Proceedings, 2nd Australia – New Zealand Conference on Soil Mechanics and Foundation Engineering, pp. 200–205.*

- Escario, V. 1980. Suction controlled penetration and shear tests. Proceedings, 4th International Conference on Expansive Soils, Denver, CO. American Society of Civil Engineers, Vol. 2, pp. 781–797.
- Escario, I., and Saez, J. 1986. The shear strength of partly saturated soils. *Géotechnique*, **36**: 453–456.
- Fredlund, D.G. 1975. A diffused air volume indicator for unsaturated soils. *Canadian Geotechnical Journal*, **12**: 533–539.
- Fredlund, D.G., Morgenstern, N.R., and Widger, R.A. 1978. The shear strength of unsaturated soils. *Canadian Geotechnical Journal*, **12**: 313–321.
- Fredlund, D.G., Rahardjo, H., and Gan, J.K.-M. 1987. Non-linearity of strength envelope for unsaturated soils. Proceedings, 6th International Conference on Expansive Soils, New Delhi, India, pp. 49–54.
- Gan J.K.-M. 1986. Direct shear strength testing of unsaturated soils. M.Sc. thesis, University of Saskatchewan, Saskatoon, SK, Canada.
- Hilf, J.W. 1956. An investigation of pore-water pressure in compacted cohesive soils. Ph.D. thesis, Technical Memorandum No. 654, United States Department of the Interior Bureau of Reclamation, Design and Construction Division, Denver, Colorado, U.S.A.
- Ho, D.Y.F., and Fredlund, D.G. 1982. The increase in shear strength due to soil suction for two Hong Kong soils. Proceedings, ASCE Geotechnical Conference on Engineering and Construction in Tropical and Residual Soils, Honolulu, HI, pp. 263–295.
- Satija, B.S. 1978. Shear behavior of partly saturated soils. Ph.D. thesis, Indian Institute of Technology, New Delhi, India.

Shear strength characteristics of two saprolitic soils

J.K.-M. Gan and D.G. Fredlund

Abstract: The saturated and unsaturated shear strength behavior of an undisturbed, completely decomposed fine ash tuff and an undisturbed, completely decomposed granite from Hong Kong were studied using direct shear and triaxial tests. The completely decomposed fine ash tuff is a fine- to medium-grained saprolite. The completely decomposed granite is a coarse-grained saprolite. Results show that the matric suction increases the shear strength of both soils. The extent of the increase in the shear strength with matric suction is related to the soil-water characteristic curve for the soil and to the amount of dilation during shear. The effect of matric suction on the shear strength was more pronounced for the fine- to medium-grained completely decomposed fine ash tuff than for the coarse-grained completely decomposed granite. These studies on the saprolitic soils provide insight into the understanding of the shear strength of unsaturated, coarse-grained soils.

Key words: saprolitic soil, shear strength, matric suction, triaxial tests, direct shear tests, soil-water characteristic curve.

Introduction

Saprolitic soils, commonly found in tropical regions of the world, are derived from *in situ* rock weathering where the original rock texture, fabric, and structure are retained (Massey and Pang 1988). The behavior of saprolitic soils is complex because of their variability and heterogeneity. Saprolitic soils are often found in an unsaturated state in nature.

Considerable research has been done on the behaviour of unsaturated, fine-grained soils; however, little research has been done on sands and other coarse-grained soils. The soils previously tested have generally been clays of low to high plasticity (Escario 1980; Escario and Saez 1986; Satija 1978; Gan et al. 1988; Toll 1990). Donald (1956) performed some direct shear tests on sands and noted that the shear strength reached a plateau (and even decreased) when the degree of saturation decreased considerably.

Matric suction is an important variable related to the stability of natural slopes. Slopes in Hong Kong are generally steep and the groundwater table is located at some depth. Rainwater generally sheds quickly from the steep slopes in Hong Kong. Under prolonged rainfall, considerable wetting may occur, reducing the *in situ* matric suction to low or zero values, often with catastrophic results.

The characterization of coarse-grained soils as the degree of saturation decreased is revisited in this paper. The

effects of decreased saturation (i.e., translated in matric suction) on the shear strength of two undisturbed saprolitic soils from Hong Kong are presented. The saprolitic soils tested in this study are a completely decomposed fine ash tuff and a completely decomposed granite (Figs. 1 and 2, respectively). The decomposed fine ash tuff is fine- to medium-grained soil (Fig. 3) and the decomposed granite is a coarse-grained soil (Fig. 4). The geology of both soils has been described in detail by Irfan (1989, 1991). Both of these saprolitic soils possessed intergranular bonding, relict joints, and are unsaturated in their natural state. The tasks of sampling, testing, and the characterization of the shear strength of these saprolitic soils are challenging.

Shear strength of unsaturated soils

This section briefly reviews the non-linear shear strength versus matric suction shear strength envelope and the relationship of the non-linear envelope to the soil-water characteristic curve.

Shear strength equation for unsaturated soils

The shear strength of unsaturated soils has been formulated in terms of two independent stress state variables (i.e., $(\sigma - u_a)$ and $(u_a - u_w)$) (Fredlund et al. 1978). The equation for the shear strength of unsaturated soils is commonly expressed as follows:

$$[1] \quad \tau_{ff} = c' + (\sigma_n - u_a)_f \tan \phi' + (u_a - u_w)_f \tan \phi^b$$

where:

τ_{ff} = shear stress on the failure plane at failure,
 c' = intercept of the "extended" Mohr-Coulomb failure envelope on the shear stress axis where the net normal stress and the matric suction are equal to zero,

J.K.-M. Gan. Research Engineer, Department of Civil Engineering, University of Saskatchewan, Saskatoon, SK, Canada S7N 5A9.

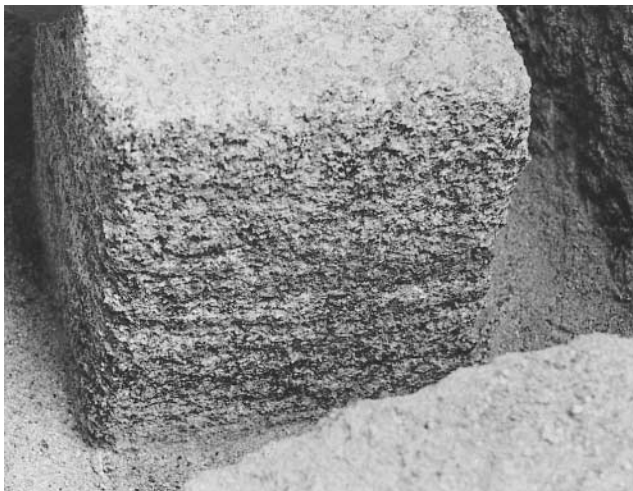
D.G. Fredlund. Professor, Department of Civil Engineering, University of Saskatchewan, Saskatoon, SK, Canada S7N 5A9.

Reproduced with permission from the *Canadian Geotechnical Journal*, 33: 595-609, 1996.

Fig. 1. Photograph of a bulk sample of completely decomposed fine ash tuff (Irfan 1989).



Fig. 2. Photograph of a bulk sample of completely decomposed granite (Irfan 1991).



$(\sigma_n - u_a)_f$ = net normal stress state variable on the failure plane at failure,
 ϕ' = angle of internal friction associated with the net normal stress state variable, $(\sigma_n - u_a)_f$,
 $(u_a - u_w)_f$ = matric suction on the failure plane at failure, and

Fig. 3. Grain size distribution for the completely decomposed fine ash tuff.

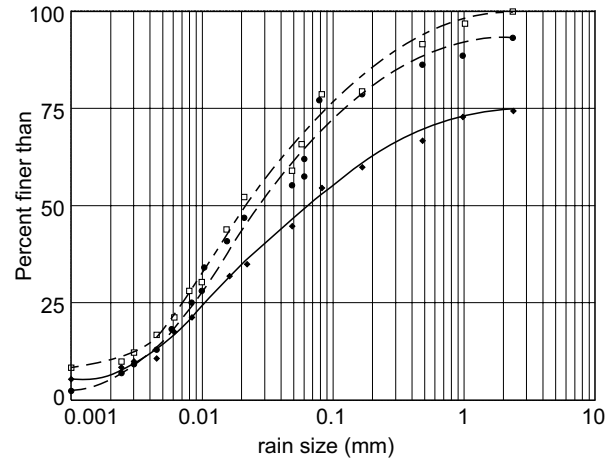
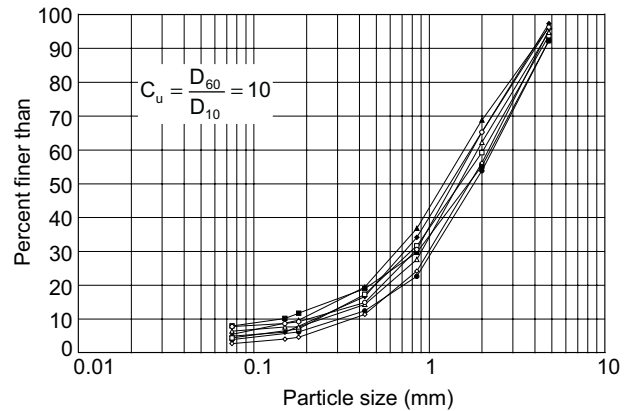


Fig. 4. Grain size distribution for the completely decomposed granite.



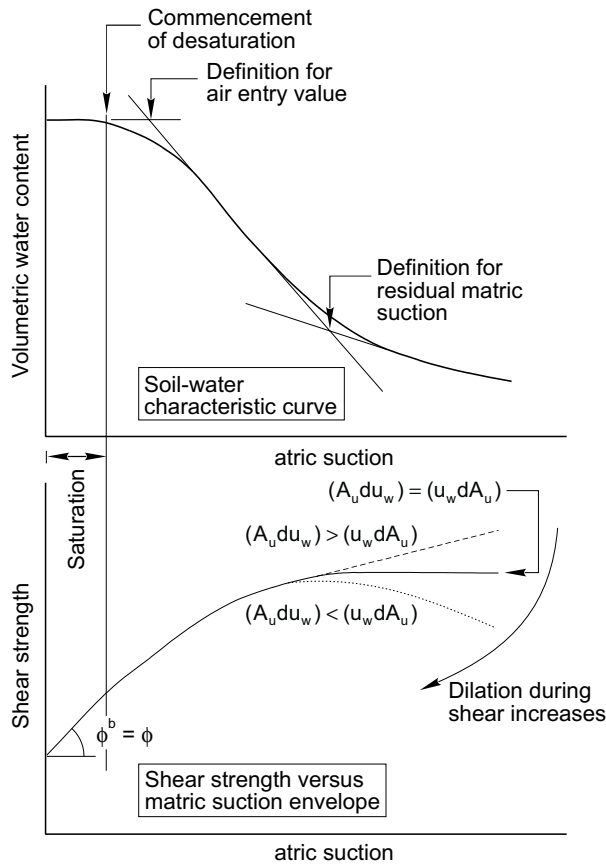
ϕ^b = angle indicating rate of increase in shear strength relative to the matric suction, $(u_a - u_w)$.

The shear strength of unsaturated soils can be determined in the laboratory using modified versions of triaxial (Ho and Fredlund 1982) and direct shear equipment (Gan and Fredlund 1988; Escario 1980).

Non-linear shear strength envelope and relationship to soil-water characteristic curve

The shear strength versus matric suction envelope has been found to be non-linear (Gan et al. 1988; Escario and Saez 1986). The slope of the shear strength versus matric suction envelope can also be negative (Donald 1956). The non-linearity of the shear strength versus matric suction envelope is related to the soil-water characteristic curve of the soil (i.e., to the effects of desaturation due to an applied matric suction) (Fig. 5). At saturation, the slope of the shear strength versus matric suction envelope, ϕ^b , is equal to the effective friction angle, ϕ' . The value of the ϕ^b angle decreases when the soil begins to desaturate. The relationship between the angle ϕ^b and the effective fric-

Fig. 5. Relationship between soil-water characteristic curve and shear strength versus matric suction envelope. Illustrating the effect of desaturation and dilation during shear on the slope of the envelope.



tion angle, ϕ' , can be illustrated by considering, on a particulate level, a two-grain soil element (Fig. 6).

In the absence of any externally applied total net normal force, N , the frictional resistance, R , for the saturated soil and for the unsaturated soil can be written as follows:

$$[2] \quad R = \mu F_w \equiv (\tan \phi')(A_0 u_{w1}) \quad \text{for a saturated soil}$$

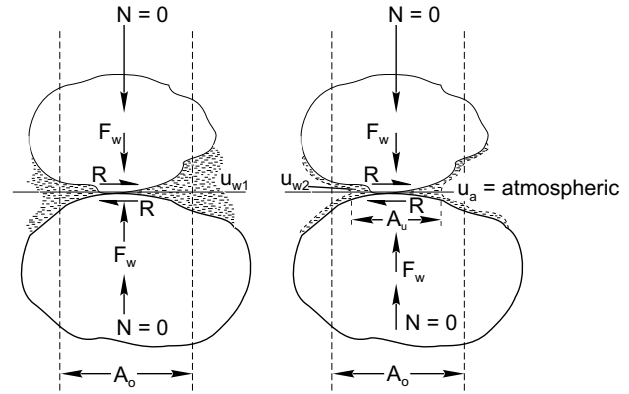
$$\equiv (\tan \phi')(A_u u_{w2}) \quad \text{for an unsaturated soil}$$

where:

- F_w = normal force due to the negative pore-water pressure (i.e., matric suction),
- A_0 = total area contribution from soil and water in the saturated soil,
- u_{w1} = negative pore-water pressure (i.e., matric suction) in the saturated soil,
- A_u = total area contribution from soil and water in the unsaturated soil, and
- u_{w2} = negative pore-water pressure (i.e., matric suction) in the unsaturated soil.

The frictional resistance forces can be normalized to the entire cross-sectional area, A_0 , as follows:

Fig. 6. Effect of desaturation on the shear strength behaviour of a two-grain soil element.



$$[3] \quad \tau = \frac{R}{A_0} \equiv (\tan \phi')(u_{w1}) \quad \text{for a saturated soil}$$

$$\equiv (\tan \phi') \left(\frac{A_u}{A_0} \right) u_{w2} \quad \text{for an unsaturated soil}$$

where:

τ = frictional resistance stress.

Since $A_u \leq A_0$, therefore,

$$[4] \quad \left(\frac{A_u}{A_0} \tan \phi' = \tan \phi^b \right) \leq \tan \phi'$$

The value of A_u is dependent on the degree of saturation of the soil and is a function of the soil-water characteristic curve of the soil. The value of A_u is also affected by dilation during shear.

The area, A_u , is equal to A_0 (i.e., soil is saturated) for matric suction values below the air entry value of the soil. For matric suction values exceeding the air entry value, the shear strength, τ , also becomes a function of the area A_u (see eq. [3]). From eq. [3], the shear strength for an unsaturated soil can be written as a function of the area, A_u , and the negative pore-water pressure, u_{w2} , as follows:

$$[5] \quad \tau = \frac{\tan \phi'}{A_0} (A_u u_{w2})$$

where:

$$\frac{\tan \phi'}{A_0} = \text{constant.}$$

Differentiating eq. [5], the change in shear strength, $d\tau$, can be expressed as:

$$[6] \quad d\tau = \frac{\tan \phi'}{A_0} (A_u du_{w2} + u_{w2} dA_u)$$

In eq. [6], the area, A_u , and the matric suction (i.e., negative pore-water pressure), u_{w2} , are both positive. The term dA_u is negative, while the term du_{w2} is positive when the matric suction, u_{w2} , increases (i.e., the soil desaturates).

and the value of A_u decreases as matric suction increases). The term $(A_u du_{w2})$ is positive, while the term $(u_{w2} dA_u)$ is negative. The value of $d\tau$ (i.e., $(A_u du_{w2} + u_{w2} dA_u)$) will decrease when A_u is small or when dA_u is decreasing faster than du_{w2} is increasing. When this occurs, the normal force between particles decreases with matric suction (i.e., the pressure u_{w2} is high but the area A_u is small) and the soil has a greater tendency to dilate during shear. If the magnitude of A_u is small while dA_u is large, the value of $d\tau$ in eq. [6] may become negative (Fig. 5).

When dilation during shear occurs, the local density decreases and the area, A_u , would decrease further, leading eventually to a disruption of the water phase. Disruption of the water phase reduces the effectiveness of matric suction in generating normal force between particles and the shear resistance will decrease. On the one hand, dilation increases shear strength because of interlocking effects; on the other hand, dilation during shear tends to decrease the contribution of matric suction to shear strength because of a disruption of the water phase (Fig. 5).

Testing program

The testing program for the completely decomposed fine ash tuff is presented in Table 1. Both saturated and unsaturated, direct shear tests were conducted on undisturbed specimens of the completely decomposed fine ash tuff. The applied stresses used in the saturated direct shear and the unsaturated direct shear tests are presented in Tables 2 and 3, respectively.

The testing program for the completely decomposed granite is presented in Table 4. Direct shear tests and triaxial tests were used. The tests were conducted on both saturated and unsaturated specimens of undisturbed soils. Two remolded, saturated specimens were also tested using direct shear tests. The applied stresses used in the saturated direct shear and unsaturated direct shear tests are presented in Tables 5 and 6, respectively. The applied stresses used in the saturated triaxial and unsaturated triaxial tests are presented in Tables 7 and 8, respectively.

Single-stage as well as multistage shearing were used in the triaxial and direct shear tests. Multistage shear tests have some advantages over single-stage shear tests because of the highly heterogeneous nature of both soils. However, the cemented nature of both soils along with the presence of relict joints and discontinuities are sensitive to the disturbances inherent in multistage shear testing.

Further details on the testing of the decomposed fine ash tuff and the decomposed granite can be found in Gan and Fredlund (1992) and Gan and Fredlund (1994), respectively.

Experimental results and interpretation

The results for the completely decomposed fine ash tuff are presented first, followed by the results for the completely decomposed granite.

Completely decomposed fine ash tuff

The peak strength and the ultimate strength envelopes are presented in Fig. 7. The ultimate shear strength envelope is linear, with a slope of 33° and an intercept of 10 kPa. The peak strength envelope is composed of two segments, a curvilinear segment, followed by a linear segment. The linear segment has a slope of 40° . The transition from the curvilinear segment to the linear segment of the peak strength envelope occurs at a normal stress of about 105 kPa.

The shear strengths from the first and second series of multistage, unsaturated direct shear tests are presented in Fig. 8. Shear strength versus matric suction envelopes were constructed for each of the specimens. The envelopes have a slope of 40° (i.e., equal to ϕ' of 40°) for matric suction up to about 40 kPa. The slope of the envelopes decreases when matric suction exceeds about 40 kPa. For specimens in the first series, the slope of the envelopes appears to decrease to a negative value. The first series was conducted at a constant net normal stress of 20 kPa. The slope of the envelopes for the specimens of the second series appear to decrease to a limit of zero. The second series was conducted at a constant net normal stress of 100 kPa.

Completely decomposed granite

The shear strength envelope for remolded, saturated specimens is presented in Fig. 9. The remolded specimens were statically compacted to a dry density of 1.50 Mg/m^3 , which is comparable to the dry density of the undisturbed specimens used in the saturated direct shear tests (Table 5). The results in Fig. 9 show that the remolded, unbonded soil has an effective angle of internal friction of 35.5° .

The peak strength results are presented in Fig. 10. The best-fit envelope for the entire normal stress range of up to 600 kPa has a slope of 31° . A value of 31° for the effective angle of internal friction appears low when compared with the effective angle of internal friction for the remolded, unbonded soil (Fig. 9). Considering only normal stresses up to 200 kPa, a bi-segment envelope composed of a curvilinear segment followed by a linear segment provides a more reasonable value for the effective friction angle. The linear segment has a slope of 38° . The transition from the curvilinear segment to the linear segment of the bi-segment envelope occurs at a net normal stress of about 120 kPa.

The shear strength versus matric suction results from the first and second series of unsaturated, two-stage direct shear tests are presented in Figs. 11 and 12, respectively. In the first series, each specimen was subjected to the same first stage matric suction value of 10 kPa. For the second stage, four out of ten specimens were subjected to a matric suction value of 10 kPa. For the second stage, four out of ten specimens were subjected to a matric suction value of 20 kPa. These four specimens at a matric suction value of 20 kPa produced approximately the same shear strength value of about 32 kPa. In the second series of unsaturated direct shear tests, each specimen was subjected to a matric suction increase of 50 kPa, from the

Table 1. Testing program for completely decomposed fine ash tuff.

Type of shear test	Specimen size	Drainage condition	Specimen type	No. of shear stages	No. of specimens tested
Saturated direct shear	50 mm × 50 mm × 21 mm height	Drained	Undisturbed	Single and multistage (1–5 stages per specimen)	10
Unsaturated direct shear	50 mm × 50 mm × 21 mm height	Air phase — drained Air phase — drained	Undisturbed	Single and multistage (1–5 stages per specimen)	11

Table 2. Saturated direct shear tests on completely decomposed fine ash tuff.

Specimen No.	Initial void ratio, e	Applied net normal stress, σ_n (kPa)				
		Stage 1	Stage 2	Stage 3	Stage 4	Stage 5
P2	0.987	49.8	100.1	201.2		
P3	0.936	9.4	29.7	50.2	100.5	201.7
P4	1.095	207.1	107.4	55.9	29.7	9.4
P5	1.121	101.5	202.7			
P6	1.013	30.0	50.3	100.9	202.0	
P7	1.056	201.0	99.8	54.2	30.5	16.2
P8	1.000	50.4	101.1	202.1		
P9	0.961	28.8	54.1	104.6	211.7	
P10		20.0				
P11		12.4				

Table 3. Unsaturated direct shear tests on completely decomposed fine ash tuff.

Specimen No.	Net normal stress, ($\sigma_n - u_a$) (kPa)	Stage 1		Stage 2		Stage 3		Stage 4		Stage 5	
		u_a (kPa)	u_w (kPa)	u_a (kPa)	u_w (kPa)	u_a (kPa)	u_w (kPa)	u_a (kPa)	u_w (kPa)	u_a (kPa)	u_w (kPa)
First Series											
US-3	20	83.0	39.8	128.0	40.8	223.0	40.9	372.0	40.7		
US-4	20	55.0	44.6	66.0	45.1	89.0	44.6	134.0	45.4	234.0	45.0
US-6	20	127.0	47.6	207.0	47.1	368.0	48.8				
US-9	20	50.0	31.7	90.0	31.8	195.0	30.0				
US-12	20	200.0	41.1								
US-14	20	200.0	39.0								
Second Series											
US-1	100	110.0	103.4	121.0	103.9	144.0	102.9	170.0	101.7	257.0	104.0
US-5	100	69.0	51.7	90.0	50.1	135.0	52.5	235.0	52.2	359.0	53.0
US-10	100	108.0	29.3	192.0	30.4						
US-11	100	70.0	31.3	115.0	33.5	214.0	33.1				
US-13	100	214.0	55.3								

first stage to the second stage of shear. Results from both series of unsaturated, two-stage direct shear tests show there is a slight increase in shear strength with matric suction.

The results of consolidated, undrained, saturated triaxial tests for two decomposed granite specimens subjected to a consolidation pressure of 20 and 100 kPa are presented in Figs. 13 and 14, respectively. The shear strength data from consolidated, undrained triaxial tests on all nine saturated specimens are presented in Fig. 15 as a p' versus q' plot. The K_f line has a slope of 32° and

an intercept of 22 kPa. The equivalent effective friction angle and cohesion are 38.5° and 28 kPa, respectively.

The shear strength versus net principal stress plots for the first and second stage of the unsaturated triaxial tests are presented in Figs. 16 and 17, respectively. The shear strength values at zero net normal stress corresponding to each applied matric suction value are obtained from the intercepts of the Mohr envelopes in Figs. 16 and 17. The Mohr envelopes were constructed using an effective angle of internal friction, ϕ' , of 38.5° . The shear strength at zero net normal stress versus matric suction plot is pre-

Table 4. Testing program for completely decomposed granite.

Specimen size	Drainage condition	Specimen type	No. of shear stages	No. of specimens tested
100 mm × 100 mm ×	Drained	Undisturbed	Single stage	11
		Remolded	Multistage (4 and 7 stages on two specimens respectively)	2
100 mm ×	Air phase — drained Water phase — drained	Undisturbed	Single and multi-stage (1–5 stages per specimen)	19
71 mm diameter ×	Consolidated undrained	Undisturbed	Single stage	9
80 mm diameter × 150 mm height	Air phase — drained Water phase — drained	Undisturbed	Two stage	8

Table 5. Saturated direct shear tests on completely decomposed granite.

Specimen No.	Initial dry density, γ_d (Mg/m ³)	Initial void ratio, e	Applied net normal stress, σ_n (kPa)
HK-31	1.434	0.827	600
HK-32	1.417	0.849	400
HK-33	1.366	0.918	400
HK-34	1.479	0.771	200
HK-35	1.453	0.803	100
HK-25	1.447	0.811	100
HK-26	1.534	0.708	10
HK-27	1.497	0.750	75
HK-28	1.318	0.989	50
HK-29	1.392	0.822	50
HK-30	1.459	0.796	10

sented in Fig. 18. The shear strength versus matric suction envelopes in Fig. 18 show that there is a slight increase in shear strength with matric suction.

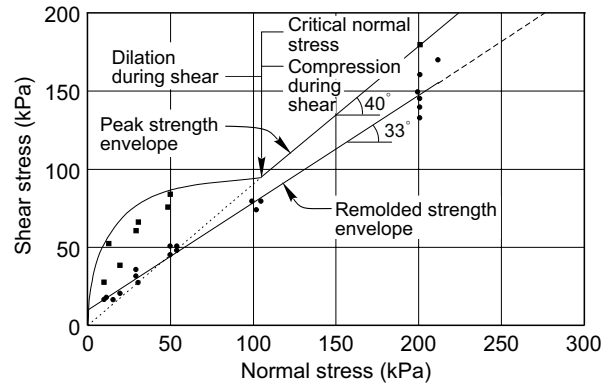
Discussion

Saturated shear strength results are discussed first, followed by a discussion of the unsaturated shear strength results.

Saturated shear strength results

Peak shear strength envelopes for both the completely decomposed fine ash tuff and the completely decomposed granite have the characteristic bi-segment form. These bi-segment envelopes are similar to the peak strength envelopes usually obtained for overconsolidated soils. The decomposed fine ash tuff and the decomposed granite are not overconsolidated in the conventional sense. The *in situ* densities of both soils are below the expected densi-

Fig. 7. Bi-segment Mohr-Coulomb failure envelope and remolded strength envelope for the completely decomposed fine ash tuff.



ties corresponding to the *in situ* stress conditions. The decomposed fine ash tuff and the decomposed granite have natural void ratios of about 1.0 and 0.85, respectively.

Similar bi-segment peak shear strength envelopes for saprolitic soils from Hong Kong were reported by Irfan (1988). Massey et al. (1989), Pun and Shen (1993), and Cheung et al. (1988). The normal stress delineating the curvilinear segment from the linear segment has been termed the “critical normal stress.” Research at the Geotechnical Engineering Office, Government of Hong Kong in Hong Kong has found that the soil dilates during shear below the critical normal stress and compresses during shear above the critical normal stress. Irfan (1988) attributed the compressive behavior during shear above the critical normal stress to the destruction of the primary relic structures, the destruction of the secondary bonding, and the collapse of weak fabric elements.

Dilation below the critical net normal stress and compression above the critical net normal stress were observed in the saturated direct shear tests on decomposed fine ash tuff. For the decomposed granite, dilation was in-

Table 6. Unsaturated direct shear tests on completely decomposed granite.

Specimen No.	Applied net normal stress, $(\sigma_n - u_a)$ (kPa)	First stage, Matric suction $(u_a - u_w)_1$ (kPa)	Second stage, Matric suction $(u_a - u_w)_2$ (kPa)	$[(u_a - u_w)_2 - (u_a - u_w)_1]$ (kPa)
First Series				
HK-12, HK-19, HK-22, HK-23	20	10	20	10
HK-13	20	10	40	30
HK-14, HK-20	20	10	60	50
HK-16	20	10	80	70
HK-17, HK-21	20	10	100	90
Second Series				
HK-8, HK-11	20	10	60	50
HK-7	20	20	70	50
HK-6, HK-10	20	30	80	50
HK-5	20	40	90	50
HK-4, HK-9, HK-24	20	50	100	50

Table 7. Consolidated, undrained, saturated triaxial tests on completely decomposed granite.

Specimen No.	Initial dry density, γ_d (Mg/m ³)	Initial void ratio, e	Back pressure (kPa)	Confining pressure (kPa)
TRI-1	1.447	0.811	210	310
TRI-2	1.571	0.667	210	260
TRI-5	1.377	0.903	210	410
TRI-6	1.397	0.876	210	285
TRI-7	1.372	0.909	210	230
TRI-8	1.436	0.825	210	220
TRI-9	1.398	0.874	210	260
TRI-10	1.450	0.807	210	310
TRI-11	1.442	0.817	210	220

Table 8. Unsaturated, consolidated, drained triaxial tests on completely decomposed granite.

Specimen No.	Initial dry density, γ_d (Mg/m ³)	Initial void ratio, e	First stage			Second stage		
			Confining pressure, σ_c (kPa)	Air pressure, u_a (kPa)	Water pressure, u_w (kPa)	Confining pressure, σ_c (kPa)	Air pressure, u_a (kPa)	Water pressure, u_w (kPa)
UT-1	1.409	0.859	33	13	3	83	63	3
UT-2	1.465	0.789	33	13	3	83	63	3
UT-3	1.339	0.957	43	23	3	93	73	3
UT-4	1.416	0.850	53	33	3	103	83	3
UT-5	1.394	0.879	53	33	3	103	83	3
UT-6	1.409	0.859	63	43	3	113	93	3
UT-7	1.373	0.908	73	53	3	123	103	3
UT-8	1.411	0.857	73	53	3	123	103	3

variably observed except for one test specimen. The amount of dilation, however, decreases with the net normal stress. The critical net normal stress for the decomposed granite was found to be approximately equal to the “apparent” preconsolidation pressures. “Apparent” preconsolidation pressure ranging from 95 to 150 kPa were obtained for the decomposed granite. The critical net normal stress for the decomposed fine ash tuff and the de-

composed granite were approximately 105 kPa (Fig. 7) and 120 kPa (Fig. 10), respectively.

From the results of consolidated, undrained, saturated triaxial tests, bonding appears to be a significant component of the shear strength of the undisturbed, completely decomposed granite at low consolidation and confining pressures. This is evident from the small axial strains required to mobilize the peak stress ratio condition at low

Fig. 8. Peak shear stress versus matric suction envelope for the completely decomposed fine ash tuff.

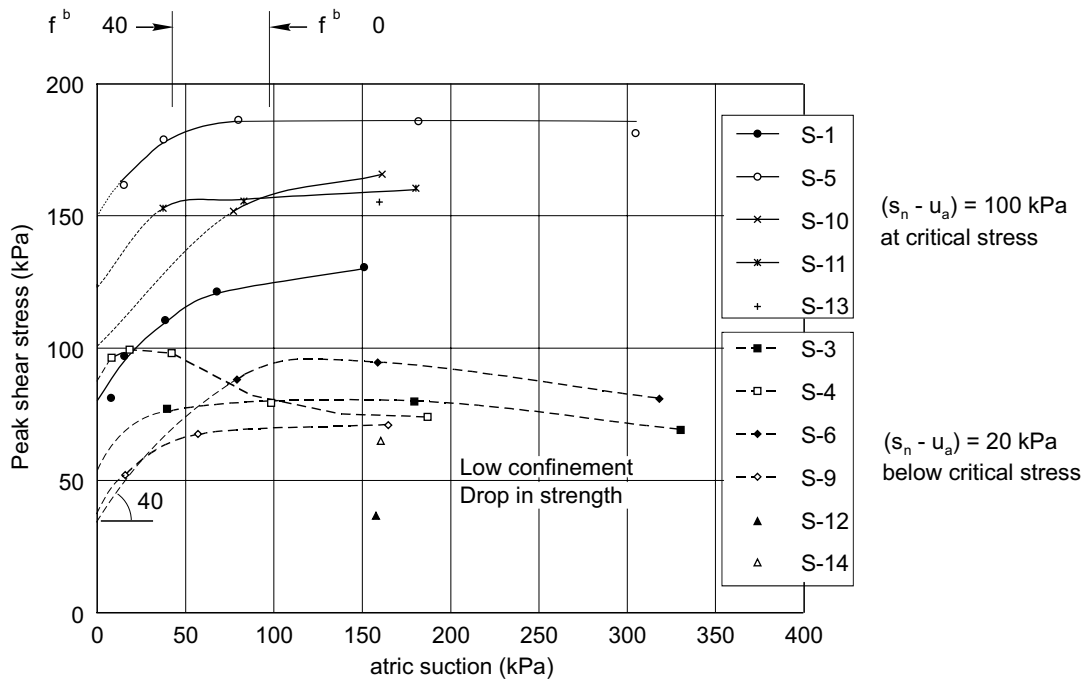


Fig. 9. Ultimate direct shear strength envelope for the completely remolded, completely decomposed granite.

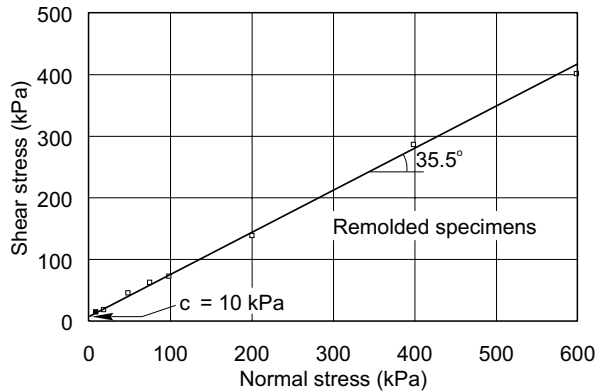
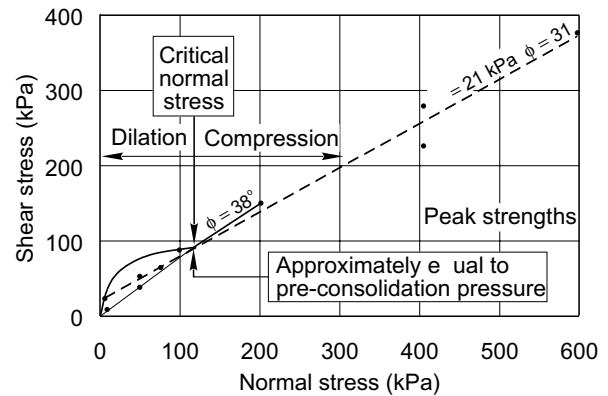


Fig. 10. Peak shear stress envelopes for the completely decomposed granite in direct shear.



consolidation pressures (Fig. 13). The axial strains required to mobilize the peak stress ratio condition increases with consolidation and confining pressures (Fig. 14). The axial strains required to mobilize the peak stress ratio and peak deviator stress as a function of the consolidation pressure are shown in Fig. 19. At low consolidation pressure, the peak stress ratio condition is mobilized long before the peak deviator stress condition. As the consolidation pressure increases, the axial strain required to mobilize the peak stress ratio increases while the axial strain required to mobilize the peak deviator stress condition decreases. The maximum angle of obliquity at a consolidation pressure of 10 kPa was as high as 58° (Fig. 20). The maximum angle of obliquity decreases with consolidation pressure. This behavior is indicative of the bonded nature of the soil. The bonding strength is of significance at low consolidation pressures and at small strains (Figs. 19 and 20).

Axial strains of between 10 and 14% were required for specimens subjected to consolidation pressures of 10 to 20 kPa to attain a peak deviator stress condition (Fig. 19). At higher consolidation pressures, the axial strains required to attain maximum deviator stress decreased to between 7 and 10% strains. At peak deviator stress condition, frictional shear resistance remains the predominant component in the shear strength. Shear resistance due to cementation bonds is either small or non-existent. It appears that the shear displacement to achieve the required degree of particle rearrangement for full mobilization of the frictional resistance of the decomposed granite decreases with the confining stresses.

Unsaturated shear strength results

The shear strength results for the unsaturated decomposed fine ash tuff and the unsaturated decomposed granite show considerable scatter. The scatter is due to (1) soil

Fig. 11. Shear stress versus matric suction data from the first series of unsaturated, direct shear test on completely decomposed granite.

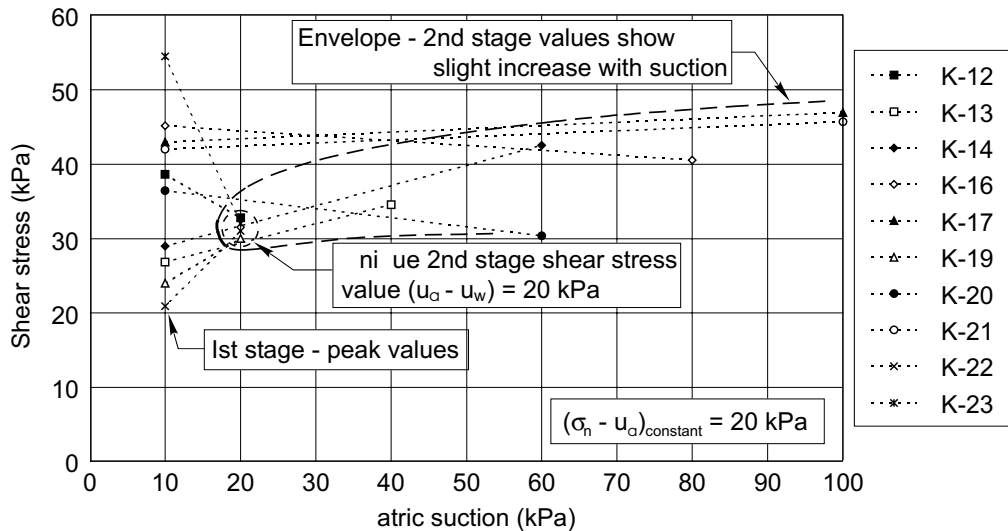
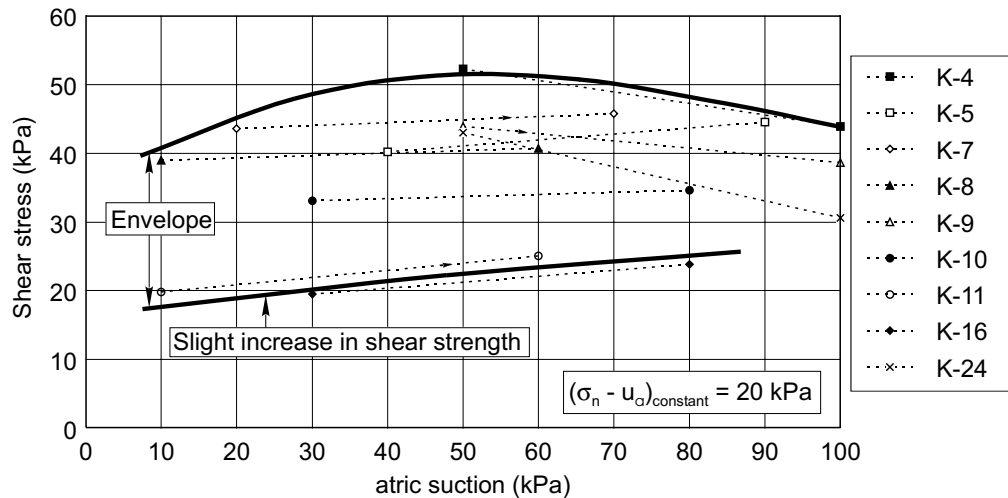


Fig. 12. Shear stress versus matric suction data from the second series of unsaturated, direct shear test on completely decomposed granite.



variability (even within the same undisturbed block sample) of the highly heterogeneous nature of both soils, and (2) variable degree of disturbance to the soil specimens during sampling and testing. For each individual specimen of the decomposed fine ash tuff, the results from multistage shear tests appear to follow a consistent trend (Fig. 8).

Decomposed fine ash tuff

The non-linearity of the shear strength versus matric suction envelopes for the decomposed fine ash tuff (Fig. 8) can be explained using the soil-water characteristic curve of the soil and the critical net normal stress concept. The soil-water characteristic curve for the decomposed fine ash tuff is given in Fig. 21. The shear strength versus matric suction envelopes (Fig. 8) have an initial slope of 40°, which is the value of ϕ' . The slope of the envelopes begin to decrease between matric suction values of 20 to 40 kPa, which is approximately the air en-

try value of the soil (Fig. 21). Below the air entry value, the soil remains saturated and the value of ϕ^b is equal to the value of ϕ' . At matric suctions exceeding the air entry value, the soil desaturates, and the value of ϕ^b decreases. At a matric suction greater than about 100 kPa, the slope of the envelopes decreases to a limit of zero degrees for specimens tested at a net normal stress of 100 kPa or to a negative value for specimens tested at a net normal stress of 20 kPa.

At a matric suction exceeding 100 kPa (residual matric suction), the amount of water remaining in the soil is small. The magnitude of the area, A_w , in eq. [5] is small, and the normal force between particles due to matric suction is correspondingly small. At the residual matric suction condition, the water phase is also easily disrupted when there is dilation during shearing, particularly with coarse soils. Dilation is more likely to occur under a net normal stress of 20 kPa than under a net normal stress of 100 kPa.

Fig. 13. Consolidated, undrained, saturated, triaxial test on an undisturbed, completely decomposed granite specimen No. TR1-1, consolidated at 20 kPa.

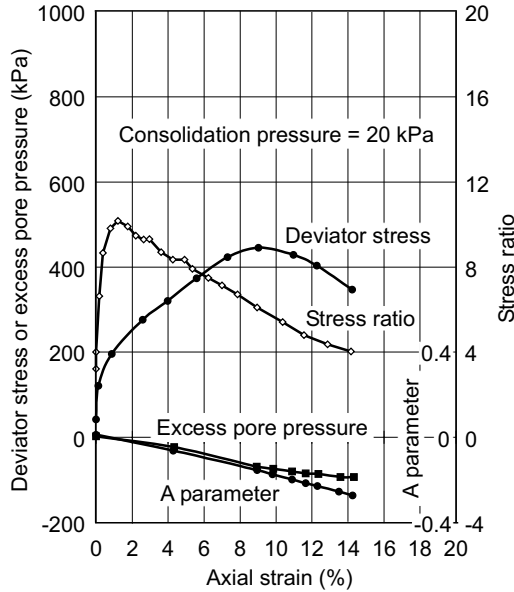
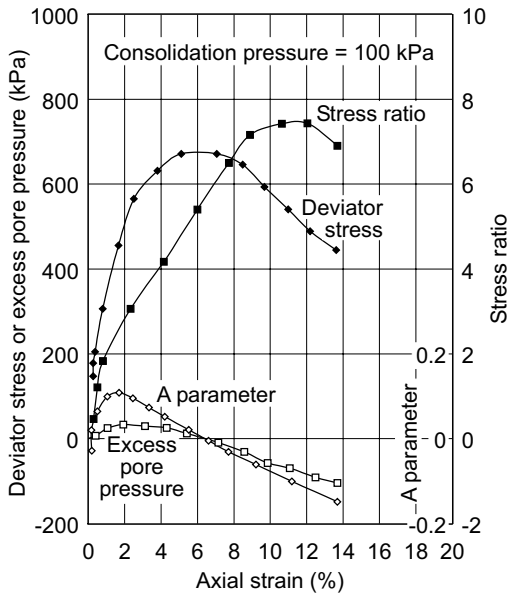


Fig. 14. Consolidated, undrained, saturated, triaxial test on an undisturbed, completely decomposed granite specimen No. TR1-7, consolidated at 100 kPa.



A net normal stress of 100 kPa is approximately equal to the critical net normal stress (Fig. 7) for the decomposed fine ash tuff. Specimens tested under a net normal stress of 100 kPa showed little dilation during shear (Fig. 22). Specimens tested at a net normal stress of 20 kPa showed pronounced dilation during shear (Fig. 23). Disruption of the water phase due to dilation during shear further reduces the area, A_u , in eq. [5]. As a result, the shearing resistance, τ , due to matric suction decreases due to the low value of A_u .

Fig. 15. Plot of p' versus q' values corresponding to peak deviator stress and peak stress ratio conditions in the saturated, consolidated, undrained, triaxial tests on the completely decomposed granite.

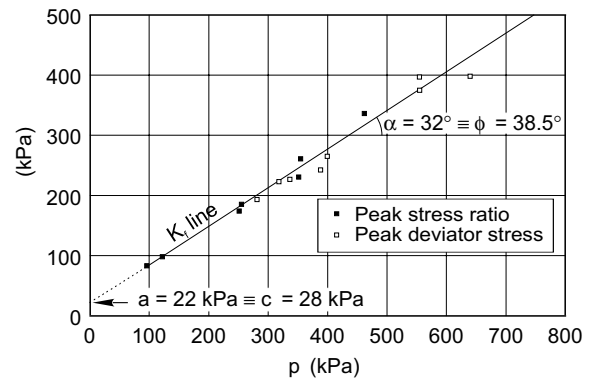


Fig. 16. Shear stress versus principal stress plot of data from the first stage of shear in the unsaturated, drained triaxial test on the completely decomposed granite.

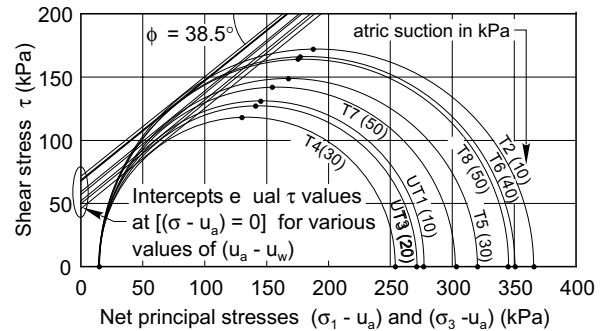
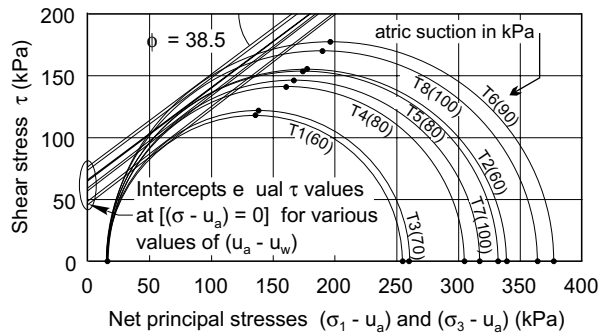


Fig. 17. Shear stress versus principal stress plot of data from the second stage of shear in the unsaturated, drained triaxial test on the completely decomposed granite.



Decomposed granite

The highly scattered shear strength versus matric suction data presented in Figs. 11 and 12 for the decomposed granite appear complex. Interpretation of the results in Figs. 11 and 12 is complicated by the variable contribution of bonding to the shear strength of the decomposed granite. The contribution of bonding to shear strength varies due to the varying degree of disturbance from sampling and testing. In general, the effect of bonding is more significant for the first stage of shear than for latter

Fig. 18. Shear strength at zero net normal stress versus matric suction relationships from the results of unsaturated, two-stage, triaxial tests on the undisturbed, completely decomposed granite.

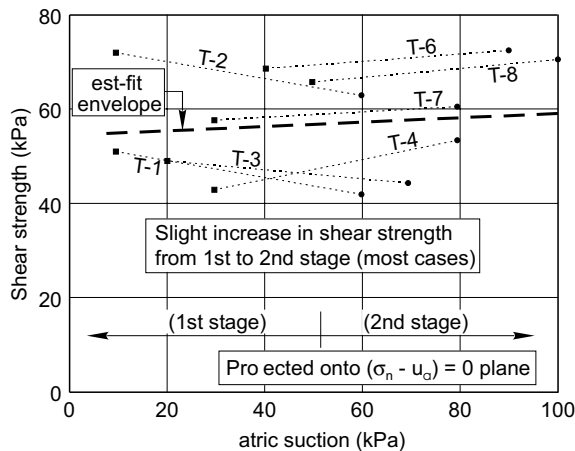
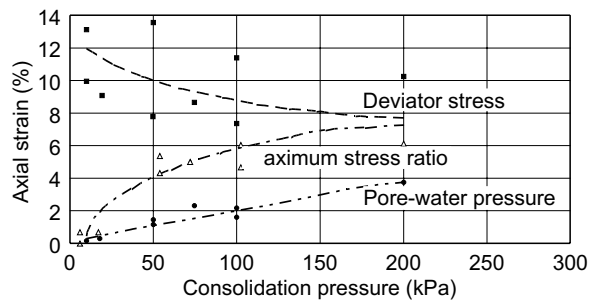


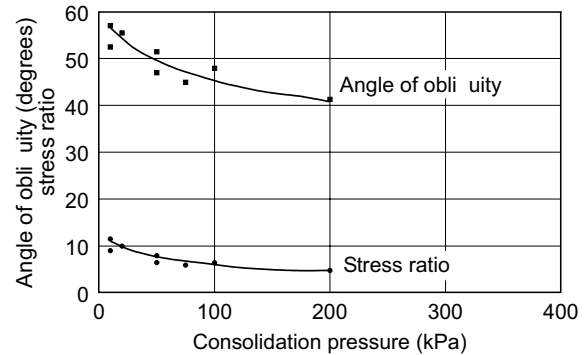
Fig. 19. Axial strains to mobilize peak deviator stress conditions, peak stress ratio condition and maximum pore-water pressure in the consolidated, undrained triaxial tests, as a function of consolidation pressure.



stages of shear. This is evident in Fig. 11 where the shear strength data from the first stage of shear for 10 specimens under a net normal stress of 20 kPa and a matric suction of 10 kPa show a scatter ranging from 20 to 55 kPa. Under a low net normal stress and low matric suction, shear resistance due to friction is small and the bonding strength becomes significant in comparison to the shear resistance of the soil due to friction. Interpretation of the unsaturated shear strength data for the decomposed granite in Figs. 11 and 12 can be simplified if the effect of bonding can be ignored.

The effect of bonding could be totally obliterated by the axial strains required for full frictional resistance to be mobilized in the second stage of shear. The effect of bonding on shear strength in the second stage of shear could be considered small or negligible, and the changes in shear strength with matric suction can be attributed to the effect of matric suction and dilation during shear (Fig. 24). Specimens that dilate during the first stage of shear (Fig. 25) tend to decrease in shear strength with matric suction in the second stage of shear. Specimens which exhibit little or no dilation during the first stage of shear tend to increase in shear strength with matric suc-

Fig. 20. Stress ratio and equivalent angle of obliquity as a function of the consolidation pressure in the consolidated, undrained triaxial tests on the completely decomposed granite.



tion in the second stage of shear (Fig. 26). Depending on the extent of dilation during shear, various shear strength versus matric suction envelopes could be obtained (Fig. 24).

The effective angle of internal friction for the decomposed granite was established on the basis of saturated direct shear tests to be 38°. The total cohesion, c , corresponding to a net normal stress of 20 kPa, an effective cohesion, c' , equal to zero, and an effective friction angle, ϕ , of 38° is 15.6 kPa. An envelope with a cohesion intercept of 15.6 kPa and a slope of 38° passes through the unique shear strength value of about 32 kPa obtained for four specimens at a matric suction of 20 kPa (Fig. 24) in the second stage of shear. Shear strength values in excess of 15.6 kPa could be directly attributed to the contribution of matric suction to the shear strength of the unsaturated decomposed granite.

The extent of the contribution of matric suction to shear strength is a function of the soil-water characteristic curve and the amount of dilation during shear. The soil-water characteristic curve for the decomposed granite is presented in Fig. 27. There were insufficient data to establish the air entry value for the decomposed granite. It could only be concluded that the air entry value for the decomposed granite is less than 20 kPa. The soil-water characteristic curve in Fig. 27 shows that for matric suction exceeding about 20 kPa to a matric suction of 100 kPa, the soil maintains a fairly constant water content of about 12 to 14%. The grain size distribution (Fig. 4) shows that the decomposed granite contains about 5% clay-sized particles. At a water content higher than about 12 to 14%, the small amount of clay-sized particles will likely remain at a high degree of saturation. Though the overall degree of saturation of the specimen is low when the air entry value is exceeded, the local degree of saturation of the fines remains high and the soil is able to maintain a value of ϕ^b equal to ϕ for matric suction up to about 20 to 30 kPa (Fig. 24). At higher matric suction values, the amount of water contributing to the cross-sectional area, A_w , is reduced. The normal force between particles due to matric suction (eq. [5]) is consequently small, and the soil will have a greater tendency to dilate during shear. Dilation during shear leads to disruptions in

Fig. 21. Soil-water characteristic curve for the completely decomposed fine ash tuff.

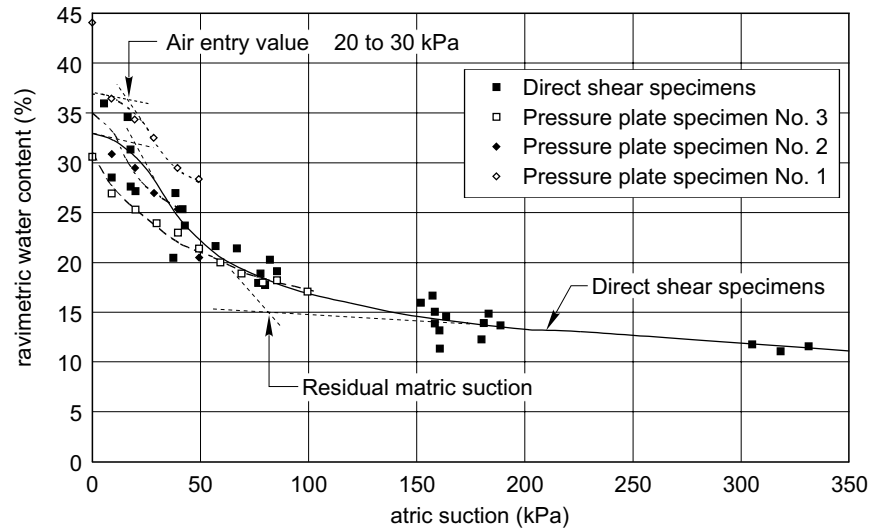
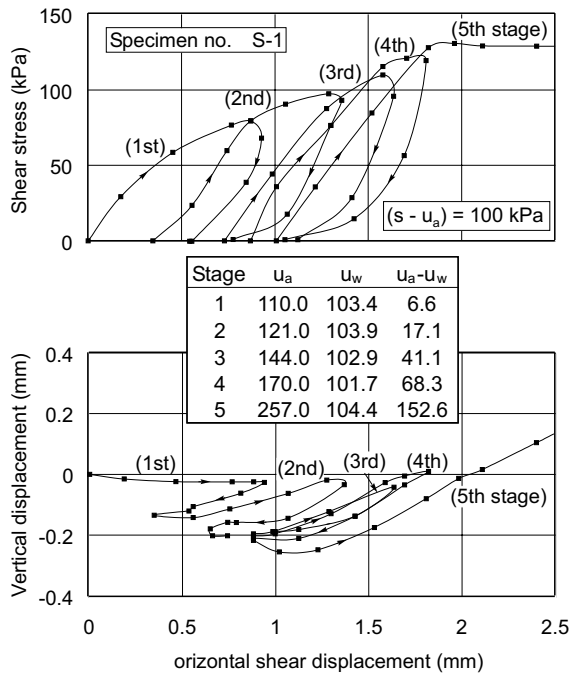


Fig. 22. Multistage, unsaturated direct shear test on decomposed fine ash tuff specimen No. US-1, under a net normal stress of 100 kPa, illustrating the effect of small dilation during first stage shear on shear strength of second stage shear.

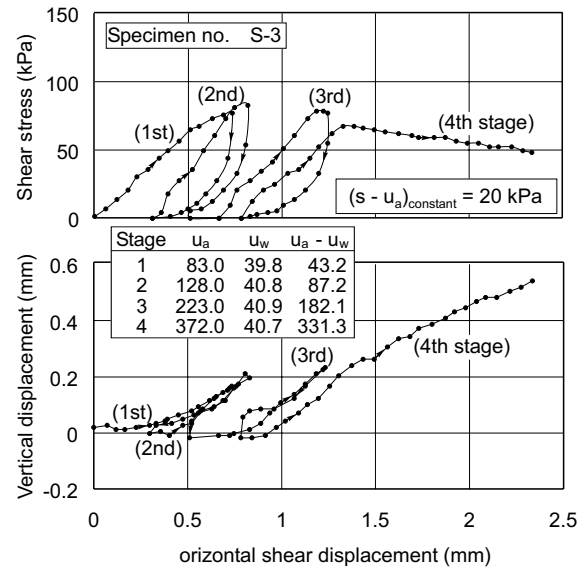


the water phase, causing a further decrease in A_w . As a result, the shear strength component due to matric suction decreases (Fig. 24).

Conclusions

Testing of two saprolitic soils from Hong Kong has provided insight into the understanding of the shear strength behavior of coarse-grained, unsaturated soils. More specifically, the conclusions are as follows:

Fig. 23. Multistage, unsaturated direct shear test on decomposed fine ash tuff specimen No. US-3, under a net normal stress of 20 kPa, illustrating the effect of large dilation during first stage shear on shear strength of second stage shear.



- (1) Matric suction increased the shear strength of the completely decomposed fine ash tuff and the completely decomposed granite.
- (2) The effect of matric suction on shear strength is more clearly defined for the fine- to medium-grained, completely decomposed fine ash tuff than for the coarse-grained, completely decomposed granite.
- (3) The non-linear character of the shear strength versus matric suction relationship is related to the soil-water characteristic curve of the soil and to the amount of dilation during shear. The ϕ^b value is equal to the ϕ' value when the soil is saturated. The value of ϕ^b decrease, when the soil desaturates. At high matric suc-

Fig. 24. “Unbonded” shear strength data from second stage shear of the first and second series of unsaturated, two-stage shear, direct shear tests on decomposed granite.

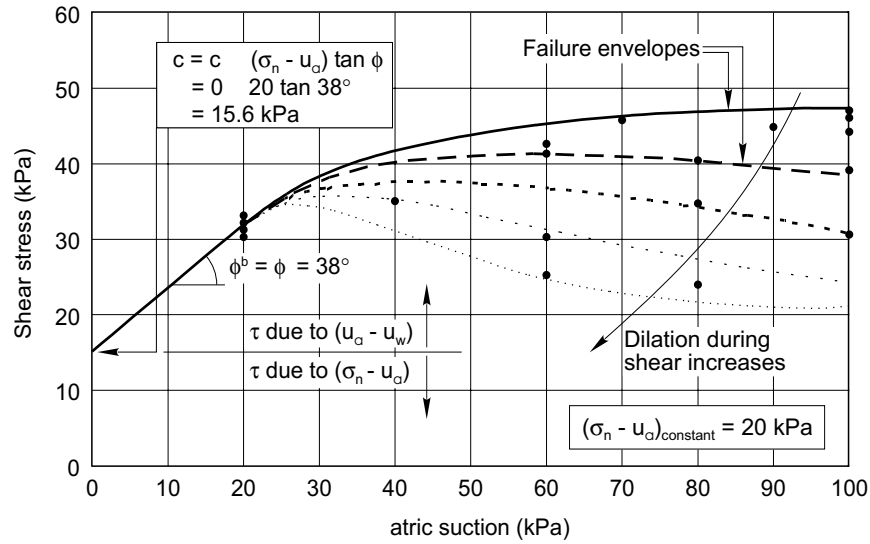


Fig. 25. Unsaturated, two-stage shear, direct shear test on a completely decomposed granite specimen No. HK-23, illustrating the loss of shear strength with matric suction in the second stage shear due to dilation during shear in the first stage.

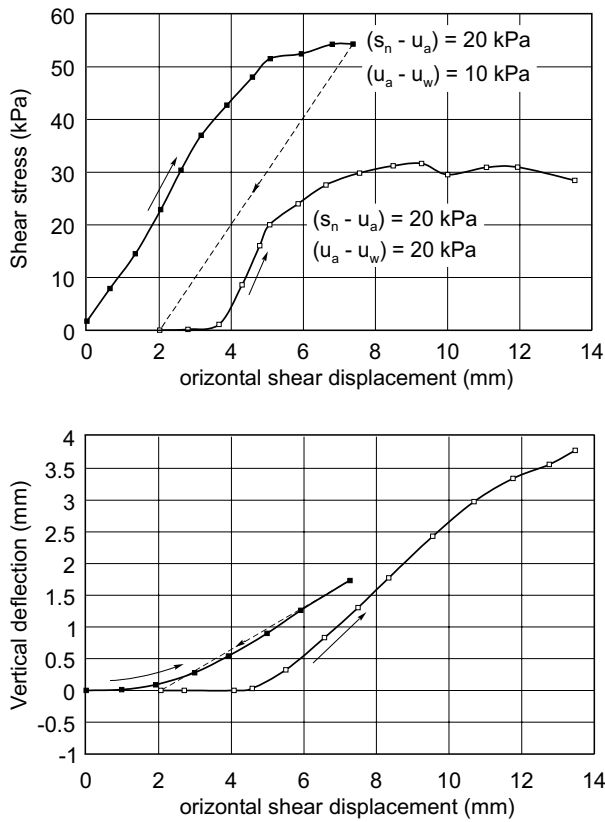
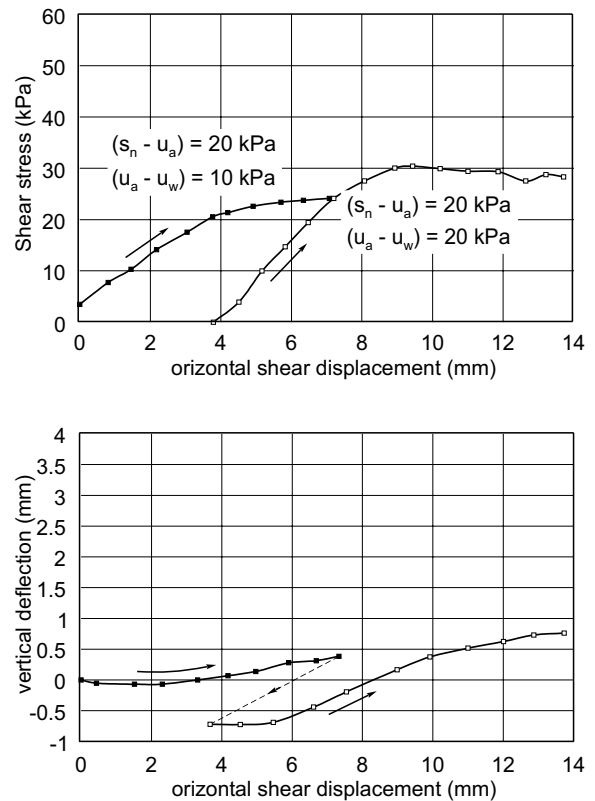


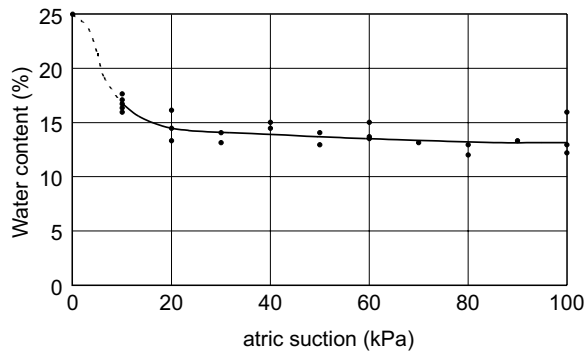
Fig. 26. Unsaturated, two-stage shear, direct shear test on a completely decomposed granite specimen No. HK-19, showing the positive contribution of matric suction to shear strength when dilation during shear in the first stage is small.



tion values, the values of ϕ^b may be positive or negative depending on the rate of desaturation with matric suction and on the amount of dilation during shear.

(4) Saturated direct shear tests show that dilation during shear decreases with applied net normal stress. Unsaturated direct shear tests show that dilation during shear tends to increase with matric suction.

Fig. 27. Soil-water characteristic curve for the completely decomposed granite.



- (5) The contribution of cementation to the shear strength of the completely decomposed fine ash tuff and the completely decomposed granite is difficult to quantify. The bond strength due to cementation is significant at low normal stress values and at small strain values. At higher normal stresses and strain values, the shearing resistance due to the frictional component of shear strength would govern.
- (6) Multistage shear has some desirable aspects from a testing standpoint because of the highly heterogeneous nature of the soil. Great care, however, is required in the interpretation of the data when multistage shear tests are used for saprolitic soils. This is due to the presence of cementation bonds, the sensitivity of the cementation bond to disturbance, the presence of relict structures, and the presence of discontinuities.

Acknowledgements

The authors are grateful to the Geotechnical Engineering Office, Government of Hong Kong, for financial support of the projects. This paper is published with the approval of the Director of Civil Engineering of the Hong Kong Government. The interpretation of the results and the conclusions presented are the sole responsibilities of the authors and in no way reflect on the policy of the Geotechnical Engineering Office, Hong Kong. The authors would like to acknowledge their colleague Dr. S.L. Barbour for his contributions during the preparation of the paper.

References

Cheung, C.K., Greenway, D.R., and Massey, J.B. 1988. Direct shear testing of a completely decomposed granite. Proceedings, 2nd International Conference on Geomechanics in Tropical Soils, Singapore, December 12–14, Vol. 1, pp. 109–118.

Donald, I.B. 1956. Shear strength measurements in unsaturated non-cohesive soils with negative pore pressure. Proceedings, 2nd Australia and New Zealand Conference on Soil Me-

chanics and Foundation Engineering, Christchurch, New Zealand, pp. 200–205.

Escario, V. 1980. Suction controlled penetration and shear tests. Proceedings, 4th International Conference on Expansive Soils, Denver, CO, American Society of Civil Engineers, Vol. 2, pp. 781–797.

Escario, V., and Saez, J. 1986. The shear strength of partly saturated soils. *Géotechnique*, **36**: 453–456.

Fredlund, D.G., Morgenstern, N.R., and Widger, R.A. 1978. The shear strength of unsaturated soils. *Canadian Geotechnical Journal*, **15**: 313–321.

Gan, J.K.M., and Fredlund, D.G. 1988. Multistage direct shear testing of unsaturated soils. *Geotechnical Testing Journal*, ASTM, **11**(2): 132–138.

Gan, J.K.-M., and Fredlund, D.G. 1992. Direct shear testing of a Hong Kong soil under various applied matric suctions. Geotechnical Engineering Office, Civil Engineering Department, Government of Hong Kong, Hong Kong, GEO Report No. I 1.

Gan, J.K.-M., and Fredlund, D.G. 1994. A comparative study of direct shear and triaxial testing of a Hong Kong soil under saturated and unsaturated conditions. Research Report submitted to the Geotechnical Engineering Office, Civil Engineering Department, Government of Hong Kong, Hong Kong.

Gan, J.K.-M., Fredlund, D.G., and Rahardjo, H. 1988. Determination of the shear strength parameters of an unsaturated soil using the direct shear test. *Canadian Geotechnical Journal*, **25**: 500–510.

Ho, D.Y.F., and Fredlund, D.G. 1982. Multistage triaxial tests for unsaturated soils. *Geotechnical Testing Journal*, ASTM, **5**: 18–25.

Irfan, T.Y. 1988. Fabric variability and index testing of a granitic saprolite. Proceedings, 2nd International Conference on Geomechanics in Tropical Soils, Singapore, December 12–14, Vol. 1, pp. 25–35.

Irfan, T.Y. 1989. Tuff sampling rite and description of samples. Geotechnical Control Office Report, Civil Engineering Department, Government of Hong Kong, Hong Kong.

Irfan, T.Y. 1991. Description of sampling site and block samples — Shouson Hill, Hong Kong Island. Geotechnical Control Office Report, Civil Engineering Department, Government of Hong Kong, Hong Kong.

Massey, J.B., and Pang, P.L.R. 1988. Stability of slopes and excavations in tropical soils. Proceedings, 2nd International Conference on Geomechanics in Tropical Soils, Singapore, December 12–14, Vol. 2, pp. 551–570.

Massey, J.B., Irfan, T.Y., and Cipullo, A. 1989. The characterization of granitic saprolitic soils. Proceedings, 12th International Conference on Soil Mechanics and Foundation Engineering, Rio de Janeiro, Vol. 1, pp. 533–542.

Pun, W.K., and Shen, J.M. 1993. Laboratory investigation of skin friction of remolded saprolitic soils. Geotechnical Engineering Office, Civil Engineering Department, Government of Hong Kong, Hong Kong, Special Project Report SPR 6/93.

Satija, B.S. 1978. Shear behavior of partly saturated soils. Ph.D. thesis, Indian Institute of Technology, New Delhi, India.

Toll, D.G. 1990. A framework for unsaturated soil behavior. *Géotechnique*, **40**(1): 31–44.

A method for determination of ϕ^b for statically compacted soils

S.Y. Oloo and D.G. Fredlund

Abstract: The unsaturated shear strength parameter, ϕ^b , is usually determined using triaxial or direct shear apparatus that have been modified to allow for the control and (or) measurement of pore-air and pore-water pressures. A fairly high level of expertise is required for the characterization of ϕ^b using these modified apparatuses. A simple procedure for determining ϕ^b for statically compacted soils at different water contents is presented along with a method of analysis. The tests can be performed on a conventional direct shear apparatus. The unsaturated shear strength parameter, ϕ^b , obtained using the proposed procedure is shown to be comparable to that obtained using the modified direct shear test. Since the proposed procedure utilizes standard laboratory direct shear equipment and takes a relatively short time to complete, it offers an easy and convenient alternative for the determination of ϕ^b for statically compacted soils.

Key words : shear strength, matric suction, unsaturated soils, statically compacted soils, direct shear test.

Introduction

Compacted soils are used extensively in dams, embankments, and the substructure of pavements. A value for the shear strength of compacted soils is required in the evaluation of the stability of these structures. When the soil is saturated, the shear strength can be characterized in terms of the effective shear strength parameters, c' and ϕ . Compacted soils are unsaturated, and it is necessary to use two independent stress state variables to characterize the shear strength. Each compaction water content represents a different state of stress, and the shear strength can be defined in terms of changes in two independent stress state variables (Fredlund and Morgenstern 1977; Fredlund 1979; Fredlund and Rahardjo 1987).

The shear strength of an unsaturated soil can be expressed in terms of the net normal stress ($\sigma_n - u_a$) and the matric suction ($u_a - u_w$) (Fredlund et al. 1978, 1987) as follows:

$$[1] \quad \tau = c' + (\sigma_n - u_a) \tan \phi' + (u_a - u_w) \tan \phi^b$$

where:

τ = shear strength,
 c' = effective cohesion,
 ϕ = effective angle of internal friction,
 ϕ^b = rate of increase in shear strength with matric suction, and

$(\sigma_n - u_a)$ = net normal stress at failure on the failure plane.

Background on shear strength testing of unsaturated soils

The shear strength of unsaturated soils has been measured using triaxial equipment modified to allow for the control and measurement of pore-air and pore-water pressures (Gibbs et al. 1960; Bishop et al. 1960; Satija 1978; Escario 1980; Ho and Fredlund 1982; Peterson 1988; Toll 1990). Other researchers have used a modified direct shear apparatus with pore-air and pore-water measurements (Donald 1956; Escario 1980; Gan 1986). However, the equipment and level of expertise required for the characterization of ϕ^b using these tests are beyond the capabilities of most geotechnical laboratories. Furthermore, the time required to perform the tests runs into weeks or even months depending on the coefficient of permeability of the soil being tested.

A simple method of testing soils compacted at different water contents in the direct shear apparatus is presented and a method of analysis is proposed in this paper. The unsaturated shear strength parameter, obtained using the proposed procedure is compared with that obtained using a modified direct shear test.

Experimental procedure

Two soil types, a Botkin Pit silt and an Indian Head till, were tested to evaluate the saturated shear strength parameters (i.e., c' and ϕ as well as the compacted shear strengths (i.e., undrained shear strength, s_u) and the unsaturated shear strength parameter, ϕ^b). Classification properties of the two soil types are given in Table 1. The soil-water characteristic curves for both soils are shown in Fig. 1. The soil-water characteristic curves were obtained using pressure plate tests.

S.Y. Oloo, Department of Civil Engineering, University of Nairobi, Nairobi, Kenya.

D.G. Fredlund, Professor, Department of Civil Engineering, University of Saskatchewan, 57 Campus Drive, Saskatoon, SK, Canada S7N 5A9.

Reproduced with permission from the *Canadian Geotechnical Journal*, 33: 272-280, 1996.

Table 1. Index properties of the soils used in the test program.

Property	Botkin Pit silt	Indian Head till
Liquid limit	22	36
Plastic limit	16	17
Plasticity index	6	19
% clay	10	30
% silt	37.5	42
% sand	52.5	28
Optimum water content (%)	14.2	16.3
Maximum dry unit weight (kN/m ³)	18.4	17.7
Specific gravity	2.68	2.73

Direct shear tests on saturated specimens

The saturated shear strength parameters, c' and ϕ' , for the silt were obtained from consolidated-drained direct shear tests. Specimens of silt were statically compacted to a dry unit weight of 17.5 kN/m³ at water contents ranging from 15% to 19%. The compacted specimens were extruded into the shear box, flooded with water, and left to saturate. After saturation, each direct shear specimen was allowed to consolidate. Each specimen was subjected to three stages of shearing under normal stresses of 50, 100, and 150 kPa.

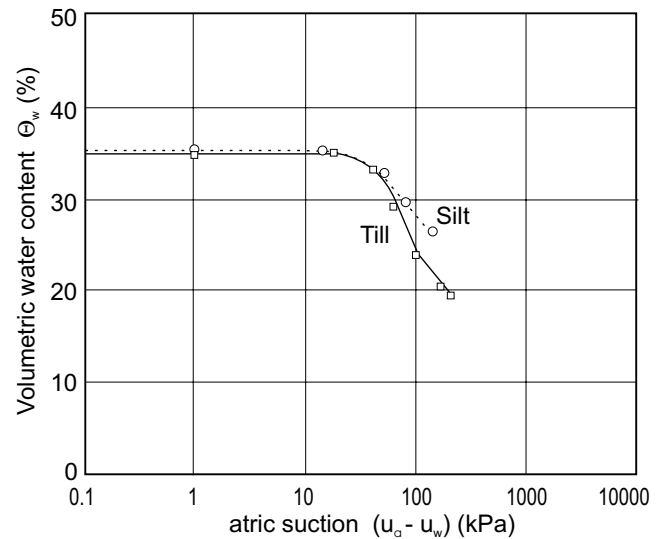
After consolidation at each stage was complete, the specimens were sheared at a constant shear rate of 0.05 mm/min until peak shear strength was attained. The measured effective cohesion, c' , and the effective angle of internal friction, ϕ' , for the silt were 2.5 kPa and 28°, respectively.

Saturated shear strength parameters for the till were obtained by Vanapalli (1994) for specimens statically compacted to a dry unit weight of 17.0 kN/m³. The effective cohesion and the effective angle of internal friction for the till were 17 kPa and 22°, respectively.

As-compacted shear strength of the silt and till

Specimens of the silt and till were statically compacted over a range of water contents while keeping the dry unit weights constant as shown in Figs. 2 and 3, respectively. The compacted specimens were sealed and stored in a temperature- and moisture-controlled environment for a period of 1 week to facilitate matric suction equilibration. At the end of this period, the specimens were placed in the shear box.

The sides of the shear box were sealed with vacuum grease to prevent the evaporation of water during the shear test. The specimens were consolidated at constant water content under selected net normal stresses. Net normal stress levels of 50, 100, and 150 kPa were used for each compaction water content.

Fig. 1. Soil-water characteristic curves for the silt and till specimens.

The specimens were sheared at a fast rate of 1 mm/min to ensure minimal changes in water content during the shearing process. Failure usually occurred within 6 min of shearing. The specimens were not allowed access to water during consolidation and shearing.

Unsaturated shear strength tests on the silt and till

Unsaturated shear strength parameters for the compacted silt specimens were determined in the modified direct shear apparatus. A discussion of construction aspects and details of operation of the modified direct shear apparatus have been presented by Gan (1986) and Gan and Fredlund (1988).

Specimens of the silt for the modified direct shear test were statically compacted at a water content of 18.0% to a dry unit weight of 17.5 kN/m³. The specimens were allowed to cure for 1 week in a moisture-controlled environment.

Unsaturated shear strength parameters for the compacted till were obtained from Vanapalli (1994). The shear strength parameters were determined in the modified direct shear apparatus on samples compacted to a dry density of 17.0 kN/m³. The same testing procedure as described for the silt samples was used.

The high air entry disk at the base of the direct shear apparatus was saturated by flooding the base with de-aired water and pressuring the air chamber to force water out through the porous disk. Diffused air was removed from the water chamber below the high air entry disk by flushing de-aired water through the system. After removing all air bubbles, the two halves of the shear box were assembled and sealed with vacuum grease to prevent water leakage. Excess water was removed from the disk and the specimen was mounted in the shear box. The shear box was filled with water and the specimen was allowed to soak for at least 12 h. Excess water was removed, the

Fig. 2. Compaction curve and compaction path for direct shear tests on silt specimens.

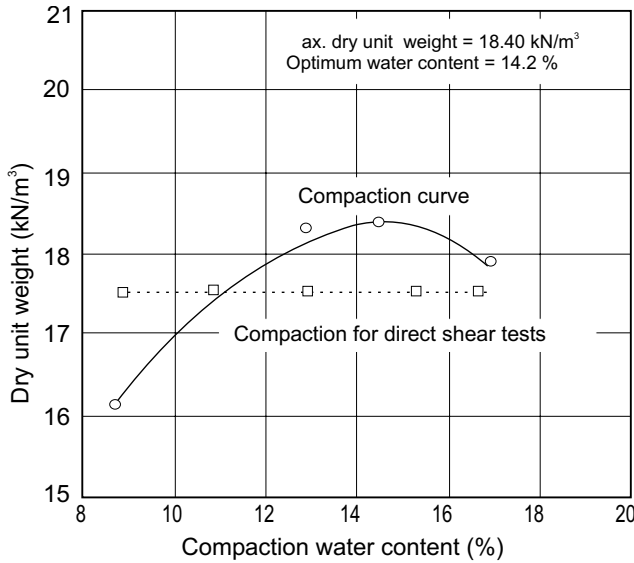
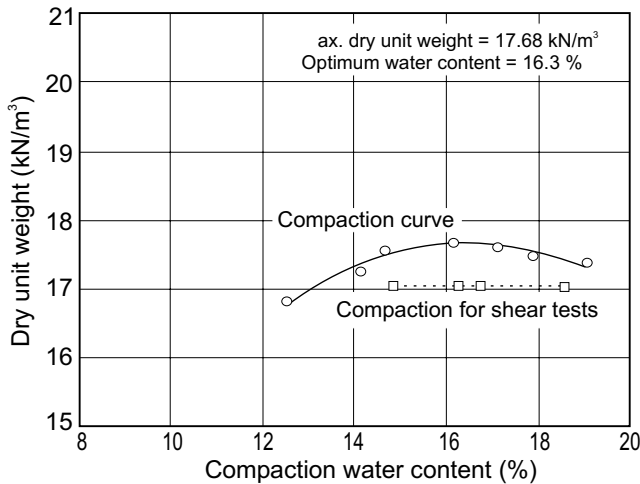


Fig. 3. Compaction curve and compaction path for direct shear tests on till specimens.



loading cap and then the chamber cap were fitted in place.

The required normal load and the chamber air pressure were applied. The specimen was allowed to consolidate until matric suction equilibrium was attained. Equilibrium was considered to have been attained when the flow of water from the specimen ceased. The specimen was then sheared at a constant shear displacement rate of 0.0186 mm/min. This shear displacement rate was sufficiently slow to ensure fully drained conditions during shearing.

As-compacted shear strength test results

The variation of shear strength with compaction water content for three levels of net normal stress is shown in

Fig. 4. Shear strength versus compaction water content for specimens of silt.

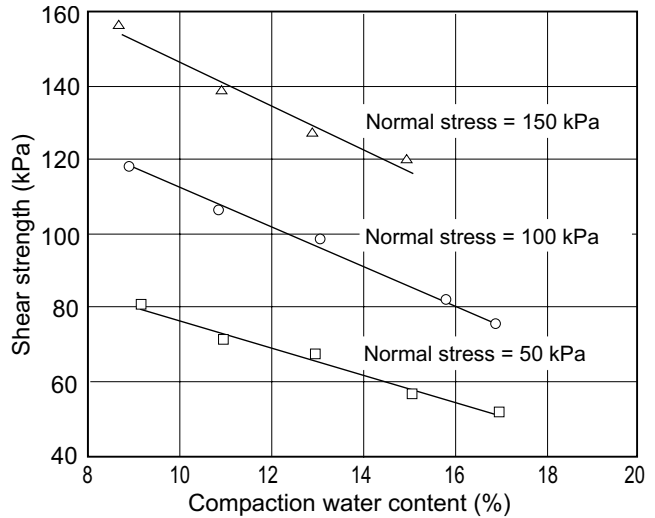


Fig. 5. Shear strength versus compaction water content for specimens of till.

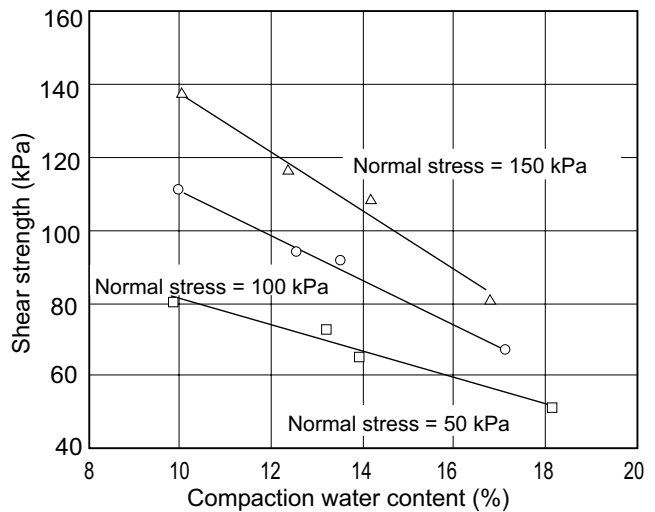


Fig. 4 for the silt and Fig. 5 for the till. The variation of shear strength with compaction water content is approximately linear over the range tested, with the shear strength decreasing as the compaction water content increases. The results can also be plotted with respect to the net normal stress (Figs. 6 and 7). The water contents shown are the mean values for three specimens from each batch prepared at similar water content values. The specimens in each batch were tested at net normal stresses of 50, 100, and 150 kPa. The relationship between shear strength and net normal stress is also linear for constant initial compaction water contents. The linearity between shear strength and normal stress is an indication of the existence of an apparent cohesion and friction angle in terms of total stresses.

The apparent cohesion values for both silt and till specimens were determined from Figs. 6 and 7. The apparent cohesion values are plotted against compaction water

Fig. 6. Shear strength versus normal stress at different initial compaction water contents, w , for specimens of silt.

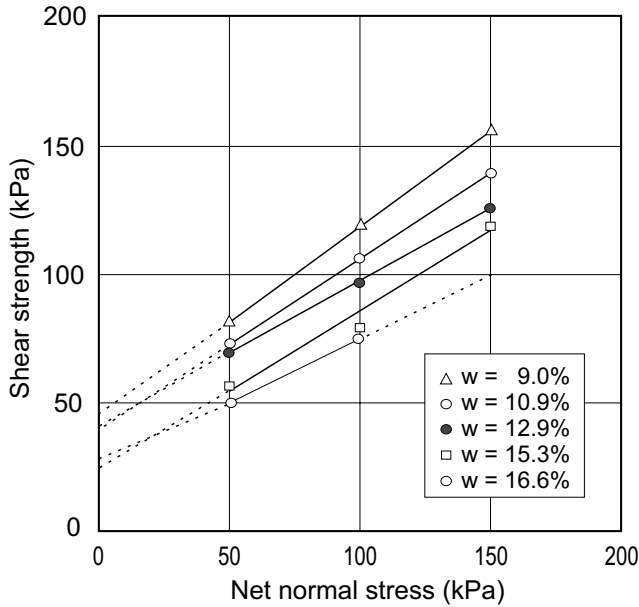
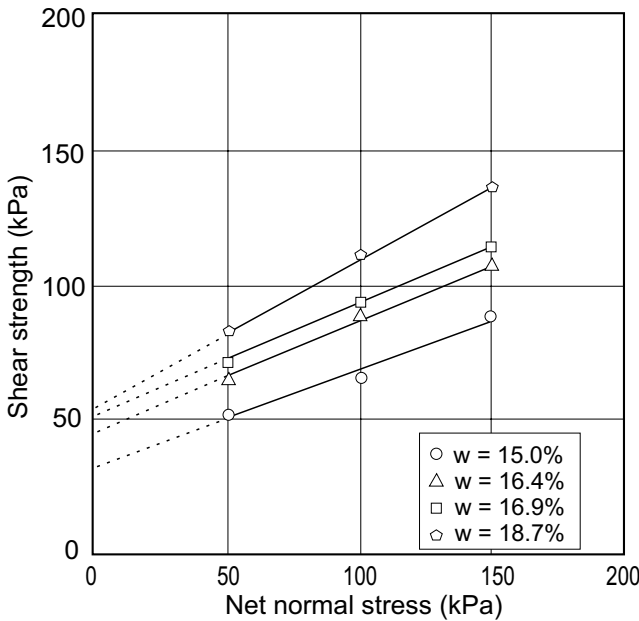


Fig. 7. Shear strength versus normal stress at different initial compaction water contents, w , for specimens of till.



content in Fig. 8. The general tendency is for the apparent cohesion to decrease with increasing compaction water content. The till specimens tend to exhibit higher apparent cohesions because of their higher clay content and plasticity. The apparent friction angles were also determined and are shown in Fig. 9 for both types of soil. The apparent friction angle also decreases with increasing compaction water content. The silt, being a coarse material, exhibits higher apparent friction angles than is observed for the till.

Fig. 8. Apparent cohesion versus compaction water content for compacted silt and till specimens.

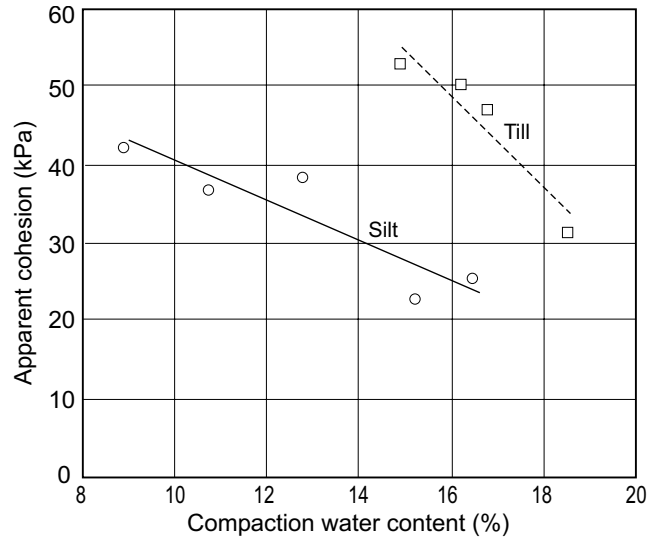
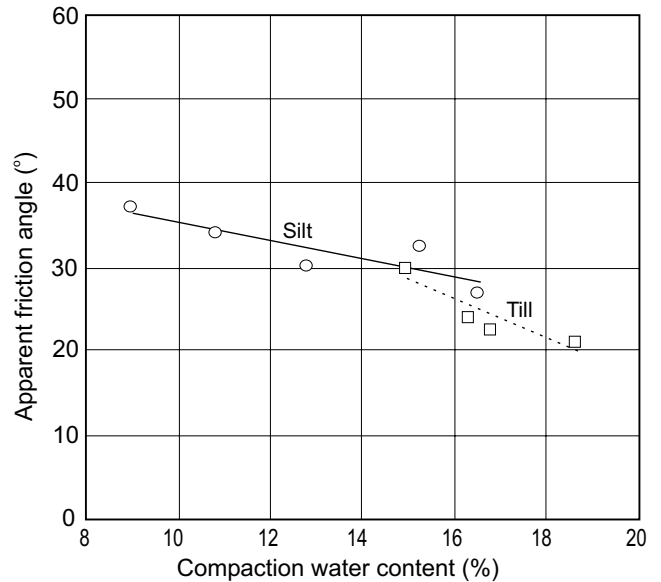


Fig. 9. Apparent friction angle versus compaction water content for compacted silt and till specimens.



The characterization of ϕ^b , as given by eq. [1], requires the definition of the stress state variables, $(\sigma_n - u_a)$ and $(u_a - u_w)$, at failure. These parameters were not measured during the direct shear tests on as-compacted samples, but information on the c' and ϕ' parameters along with theoretical considerations of the stress paths involved were used to compute ϕ^b .

The initial matric suction of the compacted specimens can be obtained from experimental measurements relating compaction water content and matric suction. The next step in the analysis involves estimating changes in pore-water pressures arising from total stress changes. It is proposed that the change in matric suction occurring during the consolidation stage of the direct shear tests be estimated using a modification of the analysis proposed by

Hilf (1948). It is assumed that a relatively fast rate of shearing results in a small change in matric suction during the shearing stage. The matric suction at failure will then be essentially equal to the matric suction at the end of the consolidation stage. If it is further assumed that at failure the pore-air pressure is atmospheric, the net normal stress, $(\sigma_n - u_a)$, at failure will be equal to the total normal stress, σ_n . The net normal stress and matric suction at failure can then be defined, and eq. [1] can be used in conjunction with the saturated shear strength parameters, c' and ϕ , to determine ϕ^b .

Determination of the initial matric suction

The matric suctions of compacted specimens of silt and till were measured in a pressure plate apparatus using the axis-translation technique described in Krahn and Fredlund (1972). The variation of matric suction with compaction water content (at a constant unit weight) for specimens of silt and till are shown in Fig. 10. The relationship between compaction water content and matric suction is essentially linear on the semi-logarithmic plots. The relationships between matric suction and compaction water content were used to estimate the matric suction of the compacted specimens at the beginning of the normal loading stage of the direct shear tests on as-compacted specimens.

Matric suction at the end of consolidation

The change in matric suction resulting from the application of the vertical normal stress was estimated using the analysis proposed by Hilf (1948). It was assumed that the volume change of an unsaturated soil due to a total stress increase was due to the compression of air in the voids and the dissolution of air in the water. By considering the change in soil volume due to the application of the total stress, and applying Boyle's and Henry's laws, the following equation can be derived for any air pressure increase under undrained conditions (Hilf 1948):

$$[2a] \quad \Delta \bar{u}_a = \frac{\Delta n \bar{u}_{a0}}{(1 - S_0)n_0 h S_0 - \Delta n}$$

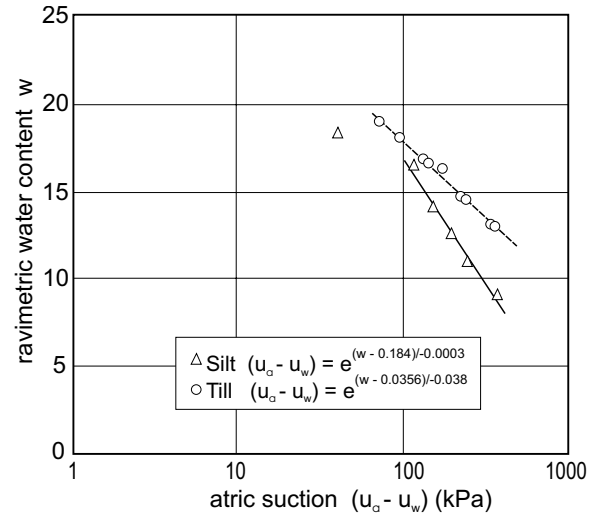
where:

- $\Delta \bar{u}_a$ = change in air pressure,
- Δn = change in porosity,
- S_0 = initial degree of saturation,
- n_0 = initial porosity,
- h = volumetric coefficient of solubility, and
- \bar{u}_{a0} = initial absolute air pressure.

Equation [2a] was used to calculate the change in air pressure during the consolidation stage of the direct shear tests. Hilf (1948) assumed that the change in pore-water pressure was equal to the change in pore-air pressure. The change in pore-water pressure is then also given by eq. [2a]:

$$[2b] \quad \Delta u_w = \Delta \bar{u}_a = \frac{\Delta n \bar{u}_{a0}}{(1 - S_0)n_0 h S_0 - \Delta n}$$

Fig. 10. Compaction water content versus matric suction relationships for silt and till specimens.



In the series of direct shear tests carried out on compacted specimens, an attempt was made to maintain undrained conditions with respect to the air and water phases. Vacuum grease was applied between the upper and lower portions of the shear box, as well as around the loading cap. While this procedure was effective in preventing evaporation and ensuring undrained conditions in the water phase, fully undrained conditions in the air phase could not be maintained over long periods of time. It was also assumed that the pore-air pressure generated by the application of the normal stress dissipated quickly and only the pore-water pressure could be relied upon to contribute to the matric suction in the soil. The difficulty of ensuring undrained conditions with respect to the air phase has been recognized by other researchers (Blight 1961; Bishop et al. 1960).

By assuming that the change in pore-air pressure drops to zero, the change in matric suction can be set equal to the change in pore-water pressure and the net normal stress becomes equal to the total normal stress. This application of the analysis by Hilf (1948) enables the simulation of the change in matric suction in response to changes in total stress.

The change in height during the consolidation of each direct shear specimen was determined from the consolidation curve. A typical consolidation curve for the as-compacted specimens and the definition of change in height are shown in Fig. 11. The change in porosity corresponding to the change in height was calculated for the K_0 -loading conditions in the shear box and substituted into eq. [2b] to obtain the change in matric suction. The change in matric suction arising from a change in the net normal stress can be expressed in terms of the α parameter (Croney 1952; Croney and Coleman 1961; Bishop 1961; Bishop and Henkel 1962) as follows:

$$[3] \quad \alpha = \frac{\Delta(u_a - u_w)}{\Delta(\sigma - u_a)}$$

Fig. 11. Typical consolidation curve for as-compacted specimens.

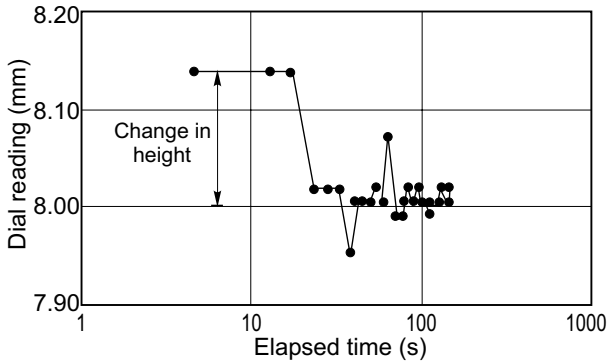


Fig. 12. The α parameter versus the net normal stress for compacted specimens of silt as a function of the degree of saturation, S .

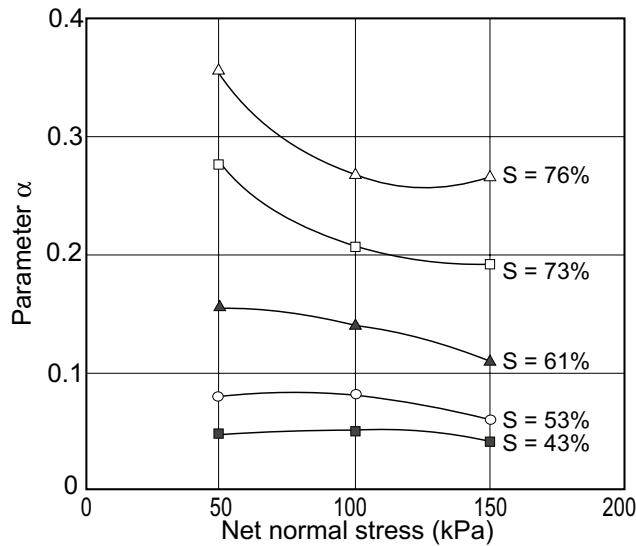


Fig. 13. The α parameter versus the net normal stress for compacted specimens of till as a function of the degree of saturation, S .

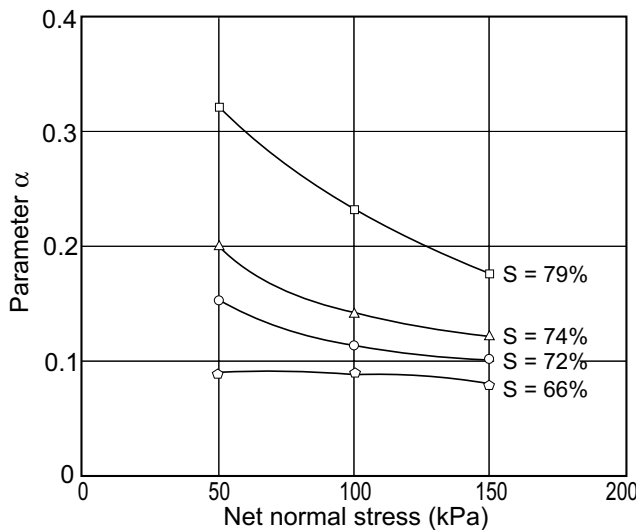


Fig. 14. Shear strength versus matric suction for as-compacted specimens of silt.

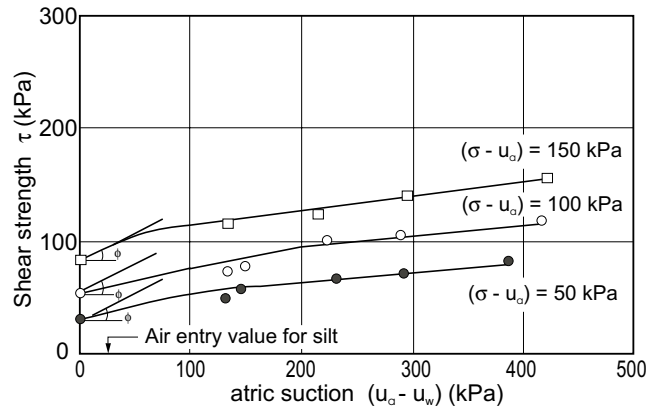
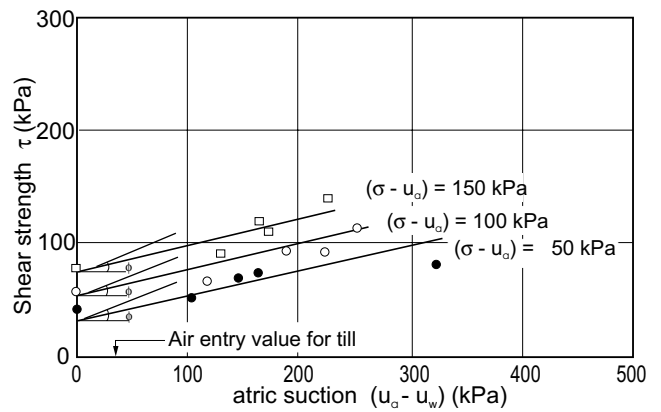


Fig. 15. Shear strength versus matric suction for as-compacted specimens of till.



The α parameter was originally proposed by Croney (1952) and Croney and Coleman (1961) for the estimation of matric suction changes due to total stress changes during constant water content tests. The air phase is fully drained in a constant water content test resulting in the net normal stress being equal to the total stress.

The α parameter during the deformation due to consolidation loading at the start of the direct shear test was calculated for the compacted specimens of silt and till and plotted against the net normal stress in Figs. 12 and 13 for different initial degrees of saturation.

Determination of ϕ^b

The values of the shear stress at failure in the as-compacted direct shear test are plotted against the matric suction in Figs. 14 and 15 for the silt and till specimens, respectively. The slope of the shear strength versus matric suction curve gives the value of $(\tan \phi^b)$ in eq. [1]. It is apparent from Figs. 14 and 15 that consistent relationships exist between the shear strength and the matric suction of the compacted specimens. The best-fit curves have similar slopes for different levels of net normal stress, confirming the form of the variation of $(\tan \phi^b)$ for a given soil.

The shear strength envelopes for the silt in Fig. 14 and for the till in Fig. 15 are markedly non-linear. The non-linearity of the shear strength envelopes with respect to matric suction is a result of the diminishing contribution of matric suction to shear strength as the water content of soil approaches residual water content (i.e., residual water content is the water content at the limit of liquid water extraction). This behavior has been observed by a number of researchers including Gan et al. (1988), Escario and Saez (1986), and Escario and Juca (1989).

The consistent variations depicted in Figs. 14 and 15 confirm the viability of the proposed method of testing and analysis of the as-compacted specimens in predicting ϕ^b . The reliability of the ϕ^b predicted in this manner can be observed by comparing the computed results to the results from the modified direct shear tests.

Comparison between as-compacted and the modified direct shear test results

The modified direct shear test is an accepted method of determining unsaturated shear strength parameters. The value of $(\tan \phi^b)$ is obtained from the slope of the shear strength versus matric suction curves. The results of the modified direct shear tests are compared with the results of the as-compacted direct shear tests in Figs. 16 and 17 for the silt and till specimens, respectively. It is apparent from these plots that the variation of shear strength with matric suction is similar for specimens tested in the modified direct shear and in the as-compacted state. The modified direct shear results in the low matric suction ranges are close to the curves generated from the as-compacted tests for both soils.

The as-compacted and modified direct shear tests on till were carried out at similar levels of matric suction. The relationships in Fig. 17 show the similarity in results between the two methods of testing, since the tests were conducted over the same ranges of matric suction. The two methods of testing yielded similar a relationship between shear strength and matric suction (i.e., $\tan \phi^b$).

Rationale for the proposed procedure of analysis

Soils compacted at different water contents are assumed to be different soils since the structures of the soils are different (Fredlund 1989). In other words, soil compacted with the same compactive effort but prepared at different water contents will have different shear strength parameters, c' and ϕ . In this paper, although the water contents are varied, the soils are statically compacted to the same density to minimize differences in soil structure. For statically compacted soils, the soil structure remains approximately the same when compacted to the same density.

The proposed procedure of analysis is therefore suitable for statically compacted soils that retain approximately the same soil structure when compacted to the same density at different water contents. It is important to

Fig. 16. Comparison between modified direct shear and as-compacted shear results for compacted specimens of silt.

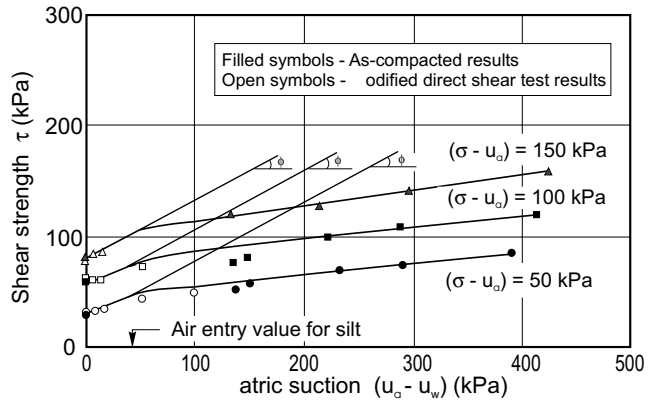
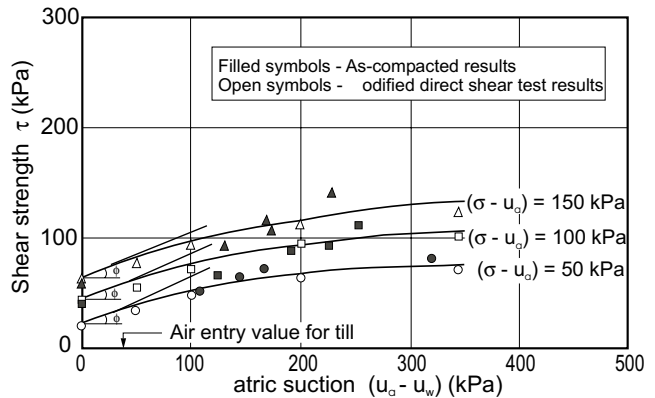


Fig. 17. Comparison between modified direct shear and as-compacted shear results for compacted specimens of till.



ensure that these conditions are met when attempting to use the proposed procedure for obtaining ϕ^b .

Conclusions

The values of ϕ^b determined using direct shear testing of soils in their as-compacted states are comparable to those measured using the more sophisticated modified direct shear test for the two soils considered. The proposed procedure utilizes standard laboratory direct shear equipment and takes much less time to complete. It therefore offers an easy and convenient alternative procedure for the characterization of ϕ^b in compacted soils, which can be conducted in most geotechnical laboratories. Further tests should be performed on different soil types to assess the general applicability of the proposed procedure.

Acknowledgements

The study reported herein was carried out with financial aid from the International Development Research Centre (IDRC), Ottawa, Canada. The authors extend appreciation to IDRC for providing the financial support. The authors wish to acknowledge Mr. Julian K.-M. Gan for his critique on the manuscript and for his editorial assistance.

References

- Bishop, A.W. 1961. Discussion on general principles and laboratory measurements. Proceedings, Conference on Pore Pressures and Suction in Soils, London. Butterworths, pp. 63–66.
- Bishop, A.W., and Henkel, D.J. 1962. The measurement of soil properties in the triaxial test. Second Edition, Edward Arnold Ltd., London.
- Bishop, A.W., Alpan, I., Blight, G.E., and Donald, I.B. 1960. Factors controlling the shear strength of partly saturated cohesive soils. Proceedings, American Society of Civil Engineers Conference on Shear Strength of Cohesive Soils, Boulder, CO, pp. 503–532.
- Blight, G.E. 1961. Strength and consolidation characteristics of compacted soils. Ph.D. thesis, University of London, London, England.
- Croney, D. 1952. The movement and distribution of water in soils. *Géotechnique*, **3**: 1–16.
- Croney, D., and Coleman, J.D. 1961. Pore pressure and suction in soil. Proceedings, Conference on Pore Pressure and Suction in Soils, Butterworth, London. pp. 31–37.
- Donald, I.B. 1956. Shear strength measurements in unsaturated non-cohesive soils with negative pore pressures. Proceedings, 2nd Australian and New Zealand Conference on Soil Mechanics and Foundation Engineering, pp. 200–205.
- Escario, V. 1980. Suction controlled penetration and shear tests. Proceedings, 4th International Conference on Expansive Soils, Denver, CO, Vol. 2, pp. 781–797.
- Escario, V., and Juca, J.F.T. 1989. Strength and deformation of partly saturated soils. Proceedings, 12th International Conference on Soil Mechanics and Foundation Engineering, Rio de Janeiro, Vol. 2, pp. 43–46.
- Escario, V., and Saez, J. 1986. The strength of partly saturated soils. *Géotechnique*, **36**(3): 453–456.
- Fredlund, D.G. 1979. Second Canadian Geotechnical Colloquium: Appropriate concepts and technology for unsaturated soils. *Canadian Geotechnical Journal*, **16**: 121–139.
- Fredlund, D.G. 1989. The character of the shear strength envelope for unsaturated soils. Proceedings, The Victor de Mello Volume, 12th International Conference on Soil Mechanics and Foundation Engineering, Rio de Janeiro, Brazil, pp. 142–149.
- Fredlund, D.G., and Morgenstern, N.R. 1977. Stress state variable for unsaturated soils. *Journal of the Geotechnical Engineering Division, ASCE*, **103**(GTS): 447–466.
- Fredlund, D.G., and Rahardjo, H. 1987. Soil mechanics principles for highway engineering in arid regions. *Transportation Research Record*, No. 1137, pp. 1–11.
- Fredlund, D.G., Morgenstern, N.R., and Widger, R.A. 1978. The shear strength of unsaturated soils. *Canadian Geotechnical Journal*, **15**: 313–321.
- Fredlund, D.G., Rahardjo, H., and Gan, J.K.-M. 1987. Nonlinearity of shear strength envelope of unsaturated soils. Proceedings, 6th International Conference on Expansive Soils, New Delhi, India, Vol. 1, pp. 49–54.
- Gan, J.K.-M. 1986. Direct shear strength testing of unsaturated soils. M.Sc. thesis, University of Saskatchewan, Saskatoon, SK, Canada.
- Gan, J.K.M., and Fredlund, D.G. 1988. Multistage direct shear testing of unsaturated soils. *Geotechnical Testing Journal, ASTM*, **11**(2): 132–138.
- Gan, J.K.-M., Fredlund, D.G., and Rahardjo, H. 1988. Determination of shear strength parameters of an unsaturated soil using the direct shear test. *Canadian Geotechnical Journal*, **25**(3): 500–510.
- Gibbs, H.J., Hilf, J.W., Holtz, W.G., and Walker, F.C. 1960. Shear strength of saturated soils. Proceedings, American Society of Civil Engineers Conference on Shear Strength of Cohesive Soils, Boulder, CO, pp. 33–162.
- Hilf, J.W. 1948. Estimating construction pore pressures in rolled earth dams. Proceedings, 2nd International Conference on Soil Mechanics and Foundation Engineering, Rotterdam, Vol. 3, pp. 234–240.
- Ho, D.Y.F., and Fredlund, D.G. 1982. Multi-stage triaxial tests for unsaturated soils. *Geotechnical Testing Journal, ASTM*, **5**: 18–25.
- Krahn, J., and Fredlund, D.G. 1972. On total and osmotic suction. *Journal of Soil Science*, **114**(5): 339–348.
- Peterson, R.F.W. 1988. Interpretation of triaxial compression test results on partially saturated soils. *In* Advanced triaxial testing of soil and rock. American Society for Testing and Materials, Philadelphia, Special Technical Publication No. 977, pp. 512–538.
- Satija, B.S. 1978. Shear behavior of partly saturated soils. Ph.D. thesis, Indian Institute of Technology, New Delhi, India.
- Toll, D.G. 1990. A framework for unsaturated soil behavior. *Géotechnique*, **40**(1): 31–44.
- Vanapalli, S.K. 1994. Simple test procedures and their interpretation in evaluating the shear strength of an unsaturated soil. Ph.D. thesis, University of Saskatchewan, Saskatoon, SK, Canada.

The relationship of the unsaturated soil shear strength to the soil-water characteristic curve

D.G. Fredlund, A. Xing, M.D. Fredlund, and S.L. Barbour

Abstract: The measurement of soil parameters, such as the permeability and shear strength functions, used to describe unsaturated soil behaviour can be expensive, difficult, and often impractical to obtain. This paper proposes a model for predicting the shear strength (versus matric suction) function of unsaturated soils. The prediction model uses the soil-water characteristic curve and the shear strength parameters of the saturated soil (i.e., effective cohesion and effective angle of internal friction). Once a reasonable estimate of the soil-water characteristic curve is obtained, satisfactory predictions of the shear strength function can be made for the unsaturated soil. Closed-form solutions for the shear strength function of unsaturated soils are obtained for cases where a simple soil-water characteristic equation is used in the prediction model.

Key words: soil suction, soil-water characteristic curve, shear strength function, unsaturated soil.

Introduction

A theoretical framework for unsaturated soil mechanics has been firmly established over the past couple of decades. The constitutive equations for volume change, shear strength, and flow for unsaturated soil have become generally accepted in geotechnical engineering (Fredlund and Rahardjo 1993a). The measurement of soil parameters for the unsaturated soil constitutive models, however, remains a demanding laboratory process. For most practical problems, it has been found that approximate soil properties are adequate for most analyses (Fredlund 1995). Hence, empirical procedures to estimate unsaturated soil functions are adequate.

Laboratory studies have shown that there is a relationship between the soil-water characteristic curve and the unsaturated soil properties (Fredlund and Rahardjo 1993b). Several models have been proposed to empirically predict the permeability function for an unsaturated soil from the soil-water characteristic curve by using the saturated coefficient of permeability as the starting value (Fredlund et al. 1994). This paper provides engineers with a means of estimating the shear strength function for an unsaturated soil of the soil-water characteristic curve by using the saturated shear strength parameters as the starting values.

Literature review

The shear strength of a soil is required for numerous analysis, such as the prediction of the stability of slopes, the design of foundations, and earth retaining structures. The effective stress variable proposed by Terzaghi (1936)

has been used in the Mohr-Coulomb theory for predicting the shear strength of saturated soils. The shear strength equation for saturated soils is expressed as a linear function of effective stress and is given as follows:

$$[1] \quad \tau = c' + (\sigma_n - u_w) \tan \phi'$$

where:

- τ = shear strength,
- c' = effective cohesion,
- ϕ' = effective angle of internal friction,
- σ_n = total normal stress on the plane of failure,
- $(\sigma_n - u_w)$ = effective normal stress on the plane of failure, and
- u_w = pore-water pressure.

Many practical problems involve assessing the shear strength of unsaturated soils. Fredlund and Morgenstern (1977) showed that the shear strength of unsaturated soils can be described by any two of three stress state variables, namely $(\sigma - u_a)$, $(\sigma - u_w)$, and $(u_a - u_w)$, where u_a is the pore-air pressure. Fredlund et al. (1978) proposed the following equation for the shear strength of unsaturated soils:

$$[2] \quad \tau = c' + (\sigma_n - u_a) \tan \phi' + (u_a - u_w) \tan \phi^b$$

where:

- ϕ^b = angle indicating the rate of increase in shear strength relative to a change in matric suction, $(u_a - u_w)$, when using $(\sigma_n - u_a)$ and $(u_a - u_w)$ as the two state variables, and

D.G. Fredlund and S.L. Barbour. Professors, Department of Civil Engineering, University of Saskatchewan, 57 Campus Drive, Saskatoon, SK, Canada S7N 5A9.

A. Xing and M.D. Fredlund. Grad. Students, Department of Civil Engineering, University of Saskatchewan, 57 Campus Drive, Saskatoon, SK, Canada S7N 5A9.

Reprinted with permission from the *Canadian Geotechnical Journal*, 33: 440-448, 1996.

ϕ' = angle indicating the rate of increase in shear strength with respect to net normal stress, $(\sigma_n - u_w)$, when using $(\sigma_n - u_w)$ and $(u_a - u_w)$ as the two state variables.

The effects of changes in total stress and pore-water pressure are handled in an independent manner in eq. [2]. Equation [2] can be rewritten in the following form:

$$[3] \quad \tau = c' + (\sigma_n - u_a) \tan \phi' + (u_a - u_w) \beta \tan \phi'$$

where:

$$\beta = \tan \phi^b / \tan \phi'$$

β represents the decrease in effective stress resistance as matric suction increases. As such, β varies from 1 at saturation to a low value at low water contents. This means that the angle ϕ^b is equal to ϕ' at saturation and then reduces with suction.

Lamborn (1986) proposed a shear strength equation for unsaturated soils by extending a micromechanics model based on principles of irreversible thermodynamics to the energy versus volume relationship in a multiphase material (i.e., solids, fluids, and voids). The equation is as follows:

$$[4] \quad \tau = c' + (\sigma - u_a) \tan \phi' + (u_a - u_w) \theta_w \tan \phi'$$

where:

θ_w = volumetric water content, which is defined as the ratio of the volume of water to the total volume of the soil.

The volumetric water content, θ_w , decreases as matric suction increases, and it is a non-linear function of matric suction. However, it should be noted that the friction angle associated with matric suction does not become equal to ϕ' at saturation unless the volumetric water content is equal to one.

For soils having a degree of saturation less than 85%, Peterson (1988) proposed the following shear strength equation:

$$[5] \quad \tau = c' + (\sigma - u_a) \tan \phi' + C_\psi$$

where:

C_ψ = the apparent cohesion due to suction.

The influence of soil suction on shear strength in eq. [5] is considered as an increase in the cohesion of the soil. The apparent cohesion due to suction, C_ψ , is dependent on the water content of the soil. Equation [5] is equivalent to eq. [2] when the apparent cohesion, C_ψ , is expressed as being equal to $[(u_a - u_w) \tan \phi^b]$.

Equations for shear strength were also proposed by Satija (1978), Karube (1988), and Toll (1990). Most of the shear strength equations for unsaturated soils in the literature are either linear or bilinear approximations. A non-linear model is more realistic and should provide a better approximation. While numerous forms have been proposed for the unsaturated shear strength equation, there has been little verification of the equations with experimental data.

Soil-water characteristic curve

The soil-water characteristic curve for a soil is defined as the relationship between water content and suction. The water content variable (i.e., volumetric water content, gravimetric water content, or degree of saturation) defines the amount of water contained in the pores of the soil. The variable has often been used in a dimensionless form where the water content is referenced to a residual or zero water content.

$$[6] \quad \Theta = \frac{\theta - \theta_r}{\theta_s - \theta_r}$$

where:

θ = volumetric water content at any suction (or $\theta(u_a - u_w)$),

θ_s = volumetric water content at saturation,

θ_r = volumetric water content at residual conditions, and

Θ = normalized volumetric water content. When the reference volumetric water content, θ_r , is taken as being zero, $\Theta = \theta / \theta_s$.

The suction may be either the matric suction (i.e., $(u_a - u_w)$) or total suction (i.e., matric plus osmotic suction) of the soil. At high suctions (e.g., >3000 kPa), matric suction and total suction are generally assumed to be essentially the same.

The total suction corresponding to zero water content appears to be essentially the same for all type of soils. A value slightly below 1,000,000 kPa has been experimentally supported for a variety of soils (Croney and Coleman 1961; Russam and Coleman 1961; Fredlund 1964). The value is also supported by thermodynamic considerations (Richards 1965). In other words, there is a maximum total suction value corresponding to a zero relative humidity in any porous medium. A general equation describing the soil-water characteristic curve over the entire suction range (i.e., 0 to 1,000,000 kPa) is given by Fredlund and Xing (1994):

$$[7] \quad \theta = \theta_s \left[1 - \frac{\ln \left(1 + \frac{\Psi}{\Psi_r} \right)}{\ln \left(1 + \frac{1000000}{\Psi_r} \right)} \right] \left[\frac{1}{\ln \left[e + \left(\frac{\Psi}{a} \right)^n \right]} \right]^m$$

where:

Ψ = total soil suction (kPa),

e = natural number, 2.71828...

Ψ_r = total suction (kPa) corresponding to the residual water content, θ_r ,

a = a soil parameter that is related to the air entry value of the soil (kPa),

n = a soil parameter that controls the slope at the inflection point in the soil-water characteristic curve, and

m = a soil parameter that is related to the residual water content of the soil.

The parameters, a , n , and m , in eq. [7] can be determined using a non-linear regression procedure outlined by Fredlund and Xing (1994). The residual water content, θ_r , is assumed to be zero. The normalized (volumetric or gravimetric) water content when referenced to zero water content is equal to the degree of saturation, S , provided the total volume change is negligible (Fredlund et al. 1994).

The shear strength of a soil is a function of matric suction, as it goes from the saturated condition to an unsaturated condition. In turn, the water content is a function of matric suction. Equation [7] can be expressed in terms of the matric suction of the soil:

$$[8] \quad \theta = \theta_s \left\{ 1 - \frac{\ln \left[1 + \frac{(u_a - u_w)}{(u_a - u_w)_r} \right]}{\ln \left[1 + \frac{1000000}{(u_a - u_w)_r} \right]} \right\} \times \left\{ \frac{1}{\ln \left[e + \left(\frac{(u_a - u_w)}{a} \right)^n \right]} \right\}^m$$

where:

$(u_a - u_w)_r$ = matric suction corresponding to the residual water content, θ_r .

A model for the shear strength function for unsaturated soils

The contribution of matric suction to the shear strength of an unsaturated soil can be assumed to be proportional to the product of matric suction, $(u_a - u_w)$, and the normalized area of water, a_w , at a particular stress state (Fredlund et al. 1995):

$$[9] \quad \tau = a_w(u_a - u_w) \tan \phi'$$

where:

$$a_w = A_{dw} / A_{tw},$$

A_{dw} = area of water corresponding to any degree of saturation, and

A_{tw} = total area of water at saturation.

The normalized area of water, a_w , decreases as the matric suction increases. The chain rule of differentiation on eq. [9] shows that there are two components of shear strength change associated with a change in matric suction.

$$[10] \quad d\tau = \tan \phi' [a_w d(u_a - u_w) + (u_a - u_w) da_w]$$

The normalized area of water in the soil, a_w , may be assumed to be proportional to the normalized volumetric water content at a particular suction value by applying Green's theorem (Fung 1977) (i.e., $\Theta(u_a - u_w)$, which is equal to $\theta(u_a - u_w) / \theta_s$). The normalized area of water can be defined by the following equation:

$$[11] \quad a_w = [\Theta(u_a - u_w)]^\kappa$$

where:

$\Theta(u_a - u_w)$ = normalized water content as a function of matric suction, and

κ = a soil parameter dependent upon the soil type.

Then, substituting eq. [11] into eq. [10] gives:¹

$$[12] \quad d\tau = \tan \phi' \{ [\Theta(u_a - u_w)]^\kappa + \kappa (u_a - u_w) \times [\Theta(u_a - u_w)]^{\kappa-1} d\Theta(u_a - u_w) \} d(u_a - u_w)$$

The normalized volumetric water content, $\Theta(u_a - u_w)$, is defined by the soil-water characteristic function and can be obtained from eq. [8]. In other words, eq. [9] can be used to predict the shear strength function of an unsaturated soil using the soil-water characteristic curve and the saturated shear strength parameters.

Equation [2] can be written in a different form as follows:

$$[13] \quad \tau = c' + (\sigma_n - u_a) \tan \phi' + (u_a - u_w) [\Theta(u_a - u_w)]^\kappa \tan \phi'$$

This equation is found by substituting eq. [11] into eqs. [9] and [2]. The simple form of eq. [13] now allows for the easy substitution of a normalized soil-water characteristic curve.

Comparison of theory to example data

Consider two different soils, soil 1 and soil 2, shown in Fig. 1. The soil-water characteristic curves are typical of a medium- and fine-grained sand, respectively. Soil 1 has an effective cohesion of 0 kPa, an effective angle of internal friction of 32.0°, and an air entry value of 20 kPa. Soil 2 has an effective cohesion of 0 kPa, an effective angle of internal friction of 25.0°, and an air entry value of 60 kPa. The predicted shear strength curves for soil 1 and soil 2 using eq. [16] are shown in Fig. 2. It can be seen that the shear strength of both soils increases linearly at the rate of $(\tan \phi')$ up to the air entry values of the soils. Beyond the air entry values, the rate of change of shear strength with matric suction decreases. The change in shear strength with respect to suction is in accordance with eq. [12].

The shapes of the shear strength curves with respect to matric suction are similar to those measured by Donald (1956). Donald's test results for several sands are shown in Fig. 3. In each case the shear strength increases with suction and then drops off to a lower value. A similar be-

¹Equation [12] was erroneously integrated in the original text and the integration has been omitted in this reprinting.

Fig. 1. Two sample soil-water characteristic curves from eq. [7].

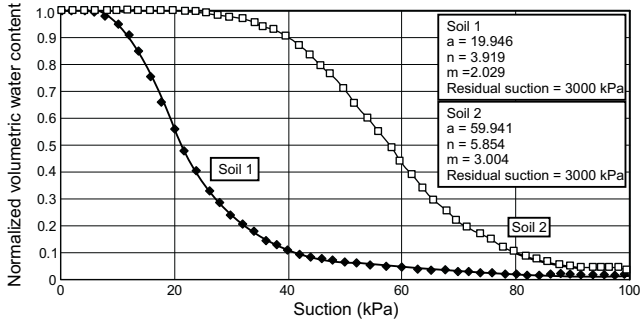


Fig. 2. Predicted shear strength curves using eq. [16] and the soil-water characteristic curves in Fig. 1.

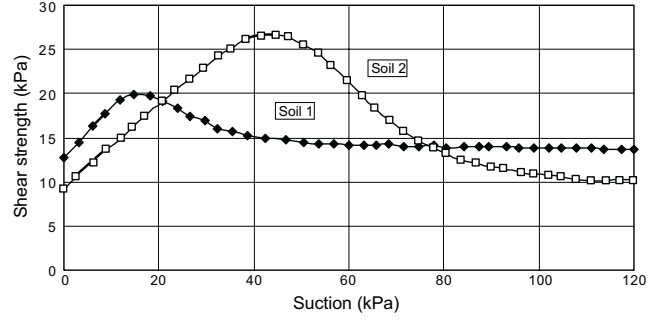


Fig. 3. Results of direct shear tests on sands under low matric suctions (modified from Donald 1956).

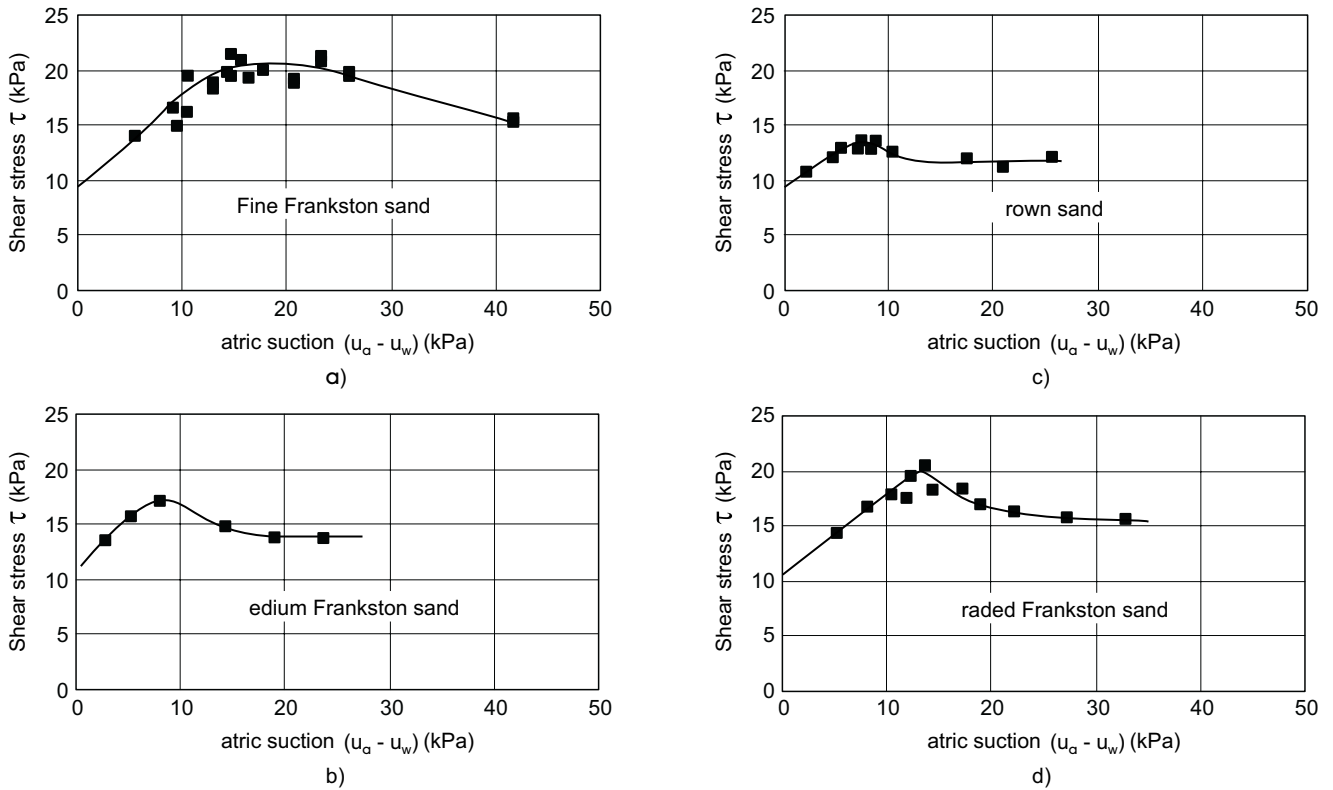
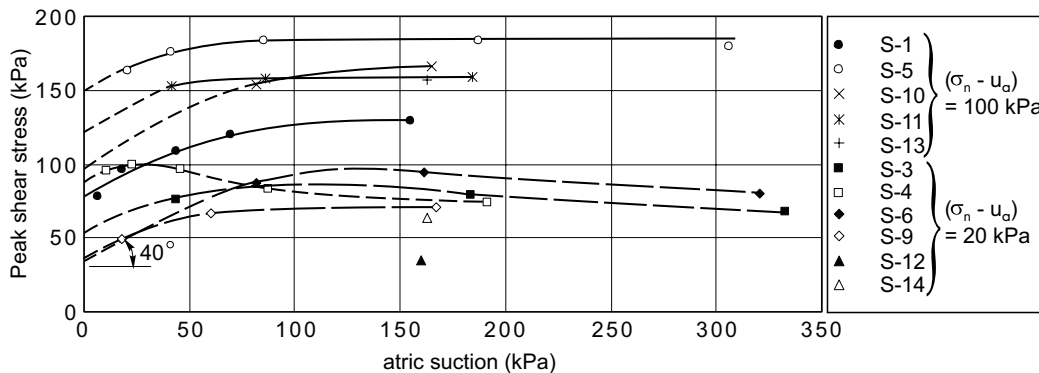


Fig. 4. Peak shear stress versus matric suction envelope for the completely decomposed fine ash tuff (from Gan and Fredlund 1996).



havior was observed in the testing of a fine- to medium-grained decomposed tuff from Hong Kong (Fig. 4). The results indicate that at low confining pressures the shear strength may rise and then start to fall with increasing suction. At higher confining pressures the shear strength shows a continual rise in strength with increasing suction. These results also illustrate the importance of applying an appropriate confining pressure to the soil when measuring the soil-water characteristic curve.

$$[14] \quad \tan \phi^b = \frac{d\tau}{d(u_a - u_w)}$$

$$= \{[\Theta(u_a - u_w)]^\kappa + \kappa(u_a - u_w)\} \\ \times [\Theta(u_a - u_w)]^{\kappa-1} d\Theta(u_a - u_w) \tan \phi'$$

The ratio between the two friction angles (i.e., ϕ' and ϕ^b) can be shown as a function of the normalized water content.

$$[15] \quad \beta = \frac{\tan \phi^b}{\tan \phi'} = [\Theta(u_a - u_w)]^\kappa \\ + \kappa(u_a - u_w)[\Theta(u_a - u_w)]^{\kappa-1} d\Theta(u_a - u_w)$$

Equations [14] and [15] show that the angle ϕ^b is equal to the effective angle of internal friction, ϕ' , up to the air entry value of the soil (i.e., $\Theta(u_a - u_w)$ equal to 1). Beyond the air entry value, ϕ^b decreases as the matric suction increases (Fig. 2). This is in agreement with experimental observations (Gan et al. 1988).

Equation [13] has been tested using experimental data from a completely decomposed tuff from Hong Kong (Gan and Fredlund 1992). A best-fit soil-water characteristic curve using eq. [8] is found by using a curve-fitting program to match the measured water contents at various matric suction values (Fig. 5). The shear strength function is calculated from eq. [13]. The predicted shear strength values, along with the measured shear strength values are shown in Fig. 6. The parameters used in the model are listed in Table 1. The value of the soil parameter, κ , was set to 1 for the prediction. The model with κ equal to 1, appears to give satisfactory predictions for sandy soils. The value of κ generally increases with the plasticity of the soil and can be greater than 1.0.

The value of κ affects the rate at which the angle decreases as the matric suction exceeds the air entry value of the soil. The effect of κ on the shear strength function of a soil with a soil-water characteristic curve defined in Figs. 7 and 8 is shown in Fig. 9. The values of κ range from 1.0 to 3.0. The influence of κ on the shape of the shear strength function occurs once the air entry value of the soil is exceeded. In the example shown, a value of κ equal to 2.0 shows that the shear strength envelope becomes essentially horizontal shortly after the air entry value is exceeded. The variable κ can be visualized as an indication of the relationship between the volumetric representation of water in the voids and the area representation of water in the voids, as represented by an unbiased plane passed through the soil mass.

Closed-form solutions

Closed-form solutions for shear strength functions are developed for two cases, using the empirical equations proposed by McKee and Bumb (1984) and Brooks and Corey (1964), respectively.

The following exponential relationship for the soil-water characteristic curve is suggested by McKee and Bumb (1984) for the case where the suction is greater than the air entry value (i.e., $(u_a - u_w) > (u_a - u_w)_b$). A sample plot of the equation proposed by McKee and Bumb (1984) can be seen in Fig. 10.

$$[16] \quad \Theta = e^{-[(u_a - u_w) - (u_a - u_w)_b] / f}$$

where:

$(u_a - u_w)_b$ = air entry value (also known as the bubbling pressure), and
 f = fitting parameter.

Equation [16] describes the soil-water characteristic curve for suction values greater than the air entry value. The normalized volumetric water content, Θ , is assumed to be constant in the range from zero soil suction to the air entry value of the soil. For simplicity, the soil parameter, κ , was assumed to be equal to 1. Substituting eq. [16] into eq. [13] gives the closed-form equation:

$$[17] \quad \tau = c' + (\sigma - u_a) \tan \phi' \\ + (e^{-[(u_a - u_w) - (u_a - u_w)_b] / f})^\kappa (u_a - u_w) \tan \phi'$$

Sample plots of eq. [17] showing the effect of varying the air entry value and f parameter are shown in Figs. 11 and 12, respectively.

The soil-water characteristic curve given by Brooks and Corey (1964) can be expressed in the following form for the case where the suction is greater than the air entry value (i.e., $(u_a - u_w) > (u_a - u_w)_{AEV}$). A sample plot of eq. [18] can be seen in Fig. 13.

$$[18] \quad \Theta = \left[\frac{(u_a - u_w)_{AEV}}{(u_a - u_w)} \right]^{f'}$$

where:

$(u_a - u_w)_{AEV}$ = air entry value, and
 f' = fitting parameter.

Equation [18] is valid for matric suctions greater than the air entry value (i.e., the value of Θ is assumed to be a constant up to the air entry value). Substituting eq. [18] into eq. [13] gives:

$$[19] \quad \tau = c' + (\sigma_n - u_a) \tan \phi' \\ + \left[\frac{(u_a - u_w)_{AEV}}{(u_a - u_w)} \right]^{f'} (u_a - u_w) \tan \phi'$$

Sample plots using eq. [19] with varying f' and air entry values are shown in Figs. 14 and 15, respectively. The parameters f and f' appear to have similar effects on the shear strength function (Figs. 12, 15) as the parameter κ (Fig. 9). The parameters f and f' can therefore be ex-

Table 1. Soil properties and fitting parameters for the Hong Kong soil US-1.

Equation [13]			Equation [7]			
$\tan \phi'$	c' (kPa)	κ	a (kPa)	n	m	ψ_r (kPa)
0.8012	0	1	110.48	2.015	10.618	3000

Fig. 5. Soil-water characteristic curve for a completely decomposed tuff (specimen US-1) from Hong Kong; experimental values (from Gan and Fredlund 1992) and calculations using eq. [7].

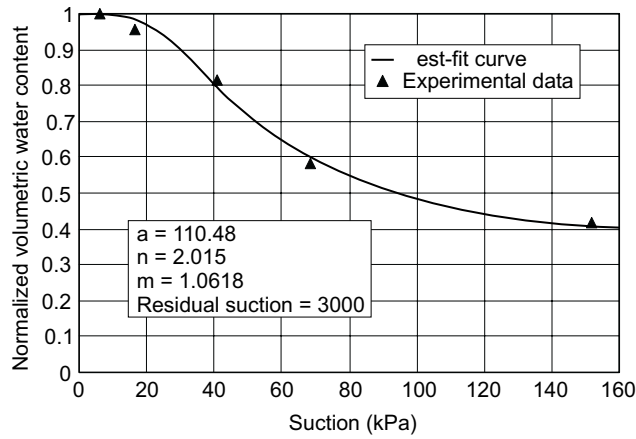


Fig. 6. Comparison of the predicted shear strength curve with the experimental shear strength data for the completely decomposed tuff (specimen US-1) from Hong Kong (from Gan and Fredlund 1992).

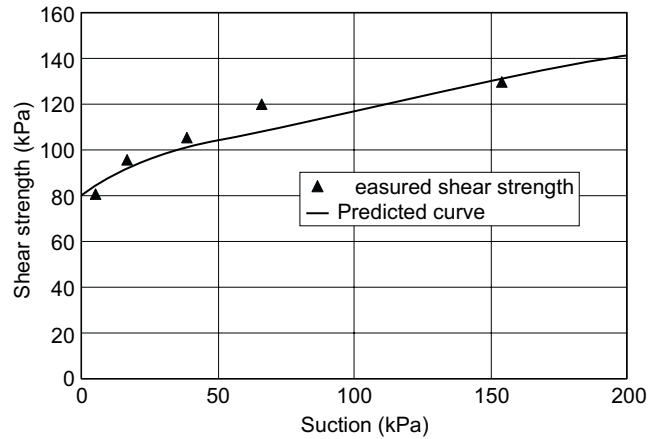


Fig. 7. The normalized soil-water characteristic curve over the entire range of suction values.

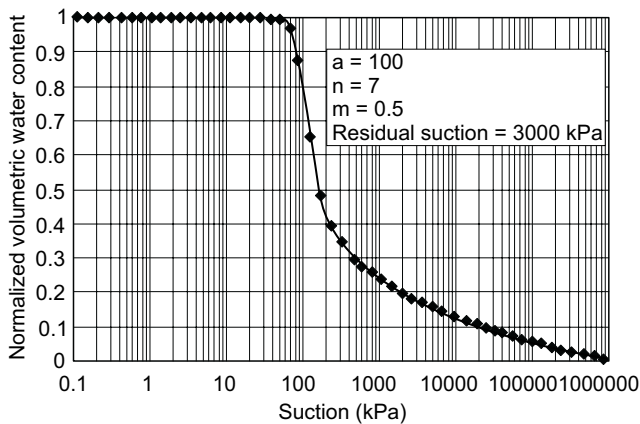
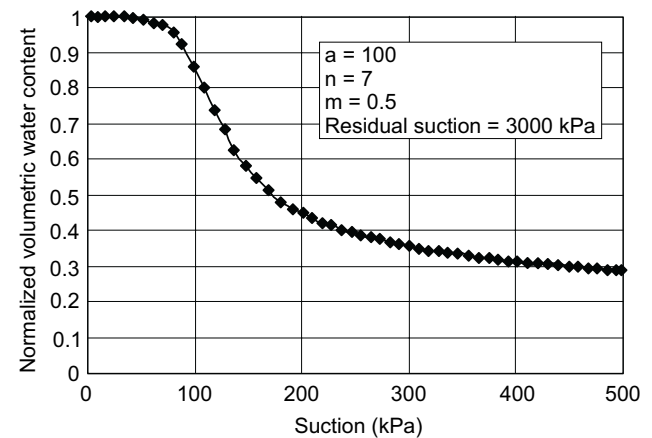


Fig. 8. Effect of the parameter, κ , on the shear strength function of a soil; the soil-water characteristic curve of the soil.



pressed in terms of the parameter κ , thus eliminating one additional parameter from eqs. [17] and [19].

Alternate solution to the general shear strength equation for an unsaturated soil

The experimental data used to illustrate the use of eq. [13] was from a sandy soil (i.e., a decomposed tuff from Hong Kong). The data set showed a good fit with the parameter κ set equal to 1. However, for highly plas-

tic soils, the parameter κ is greater than 1. At present, its magnitude is an unknown variable.

Attempts to best-fit other data sets have shown that it is possible to always leave the variable κ at 1.0 but change the upper limit of integration to reflect the soil suction near residual conditions. Unfortunately, the best-fit of the shear strength data often occurs when the residual conditions vary from those used in the best-fit of the soil-water characteristic curve. In other words, there may not be a common residual suction value for both the soil-water characteristic data and the shear strength data.

Fig. 9. Effect of the parameter, κ , on the shear strength function of a soil; the shear strength function showing the effect of varying κ .

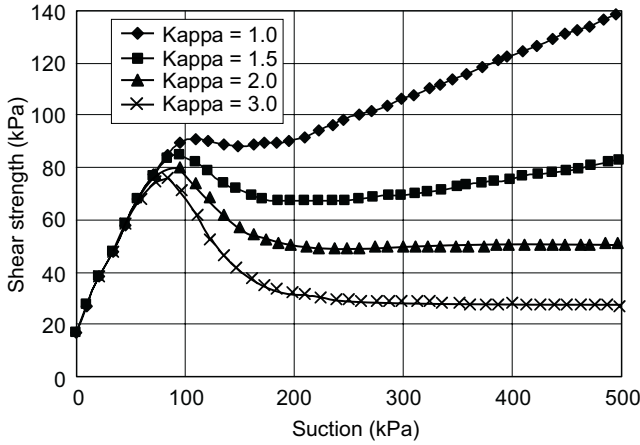


Fig. 10. A sample plot of the McKee and Bumb equation (1984).

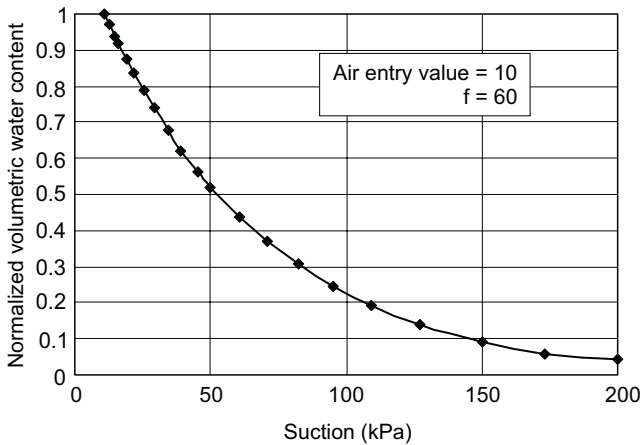


Fig. 11. Shear strength function predicted using the McKee and Bumb equation (1984); illustrating the effect of varying the air-entry value.

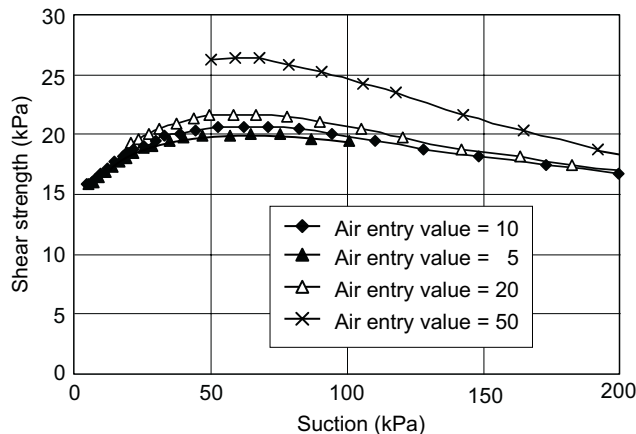


Fig. 12. Shear strength function predicted using the McKee and Bumb equation (1984); illustrating the effect of varying the f parameter.

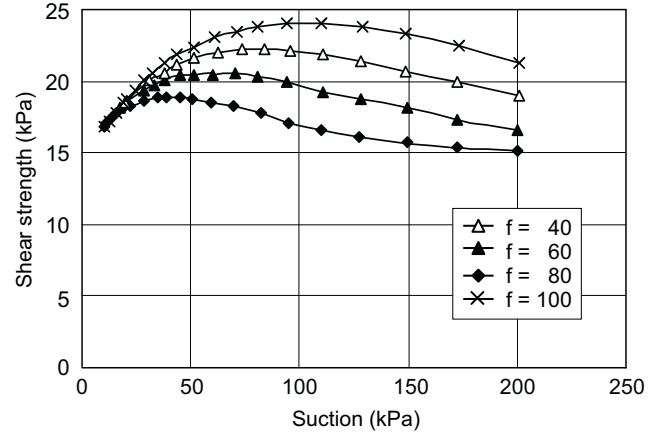


Fig. 13. A sample soil-water characteristic curve using the Brooks and Corey equation (1964).

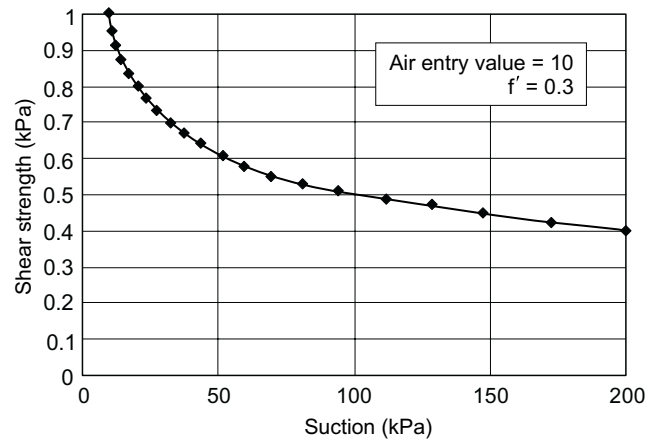


Fig. 14. Shear strength equation using the Brooks and Corey equation (1964) for the soil-water characteristic curve and illustrating the effects of varying the air-entry value.

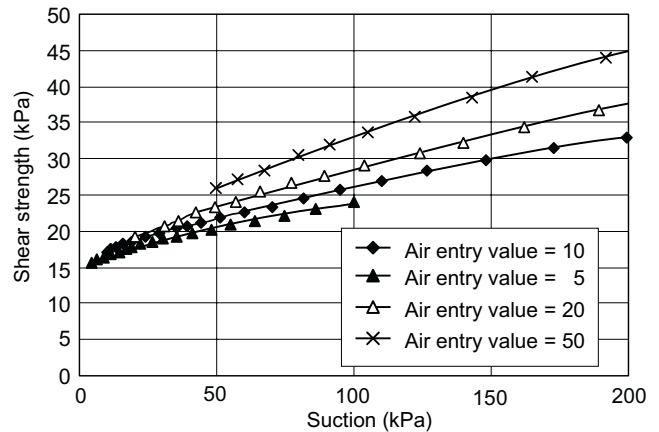
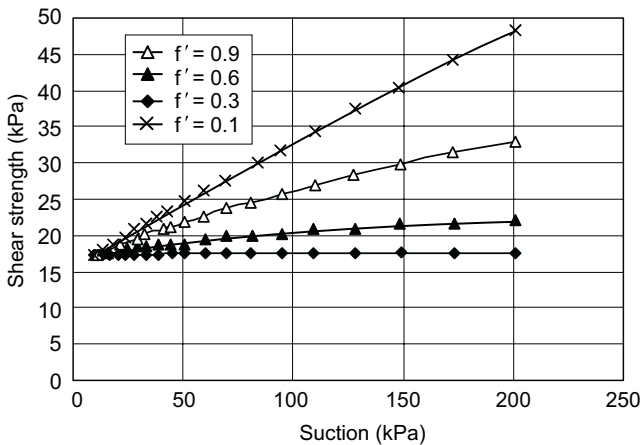


Fig. 15. Shear strength equation developed using the Brooks and Corey equation (1964) for the soil-water characteristic equation and illustrating the effects of varying the f' parameter.



More data sets are required, along with further best-fit regression analyses, in order to better understand how best to predict the shear strength of an unsaturated soil.

Conclusions

A model is proposed for the prediction of the shear strength of an unsaturated soil. The model makes use of the soil-water characteristic curve and the saturated shear strength properties of the soil to predict the shear strength. The use of the model is illustrated using experimental data for a decomposed tuff soil from Hong Kong. The predicted shear strength curve shows good agreement with measured data; however, there is an additional soil parameter, κ , which becomes greater than 1 as the plasticity of the soil increases.

Acknowledgements

The authors would like to acknowledge the assistance of Mr. Julian K.-M. Gan, Research Engineer at the University of Saskatchewan, Saskatoon, in critiquing this manuscript, as well as performing the laboratory tests on the decomposed tuff from Hong Kong. The authors also wish to acknowledge the assistance of Dr. Sai Vanapalli in developing the theoretical concepts for the shear strength of unsaturated soils.

References

- Brooks, R.H., and Corey, A.T. 1964. Hydraulic properties of porous media. Colorado State University Hydrology Paper, Fort Collins, Nr. 3, Vol. 27, March.
- Crony, D., and Coleman, J.D. 1961. Pore pressure and suction in soils. Proceedings, Conference on Pore Pressure and Suction in Soils. Butterworths, London, pp. 31–37.
- Donald, I.B. 1956. Shear strength measurements in unsaturated non-cohesive soils with negative pore pressures. Proceedings, 2nd Australia – New Zealand Conference on Soil Me-

chanics and Foundation Engineering, Christchurch, New Zealand, pp. 200–205.

- Fredlund, D.G. 1964. Comparison of soil suction and one-dimensional consolidation characteristics on a highly plastic clay. National Research Council Canada, Division of Building Research, Ottawa, ON, Technical Report No. 245.
- Fredlund, D.G. 1995. The stability of slopes with negative pore-water pressures. The Ian Boyd Donald Symposium on Modern Developments in Geomechanics. Edited by C.M. Haberfield. Monash University, Department of Civil Engineering, Clayton, Victoria 3168, Australia, pp. 99–116.
- Fredlund, D.G., and Morgenstern, N.R. 1977. Stress state variables for unsaturated soils. ASCE, Journal of the Geotechnical Engineering Division, **103**(GTS): 447–466.
- Fredlund, D.G., and Rahardjo, H. 1993a. Soil mechanics for unsaturated soils. John Wiley & Sons, New York.
- Fredlund, D.G., and Rahardjo, H. 1993b. An overview of unsaturated soil behaviour. Proceedings, American Society of Civil Engineers, Speciality Series on Unsaturated Soil Properties, Dallas, TX, Oct. 24–28, pp. 1–31.
- Fredlund, D.G., and Xing, A. 1994. Equations for the soil-water characteristic curve. Canadian Geotechnical Journal, **31**: 521–532.
- Fredlund, D.G., Morgenstern, N.R., and Widger, R.A. 1978. The shear strength of unsaturated soils. Canadian Geotechnical Journal, **15**(3): 313–321.
- Fredlund, D.G., Xing, A., and Huang, S. 1994. Predicting the permeability function for unsaturated soils using the soil-water characteristic curve. Canadian Geotechnical Journal, **31**: 533–546.
- Fredlund, D.G., Vanapalli, S., Xing, A., and Pufahl, D.E. 1995. Predicting the shear strength function for unsaturated soils using the soil-water characteristic curve. Proceedings, 1st International Conference on Unsaturated Soils, Paris, France, pp. 63–69.
- Fung, Y.C. 1977. A first course in continuum mechanics. Prentice-Hall Inc., Englewood Cliffs, N.J.
- Gan, J.K.-M., and Fredlund, D.G. 1992. Direct shear testing of a Hong Kong soil under various applied matric suctions. Geotechnical Engineering Office, Civil Engineering Department, Hong Kong, GEO Report No. 11.
- Gan, J.K.-M., and Fredlund, D.G. 1996. Shear strength characteristics of two saprolitic soils. Canadian Geotechnical Journal, **33**(4): 595–606.
- Gan, J.K.-M., Fredlund, D.G., and Rahardjo, H. 1988. Determination of the shear strength parameters of an unsaturated soil using the direct shear test. Canadian Geotechnical Journal, **25**: 500–510.
- Karube, D. 1988. New concept of effective stress in unsaturated soil and its proving test. In Advanced triaxial testing of soil and rock. American Society for Testing and Materials, Philadelphia, ASTM STP 977, pp. 539–552.
- Lamborn, M.J. 1986. A micromechanical approach to modeling partly saturated soils. M.Sc. thesis, Texas A & M University, College Station, TX.
- McKee, C.R., and Bumb, A.C. 1984. The importance of unsaturated flow parameters in designing a monitoring system for hazardous wastes and environmental emergencies. Hazardous Materials Control Research Institute National Conference, Houston, TX., March, pp. 50–58.
- Peterson, R.F.W. 1988. Interpretation of triaxial compression test results on partially saturated soils. In Advanced triaxial

- testing of soil and rock. American Society for Testing and Materials, Philadelphia, ASTM STP 977, pp. 512–538.
- Richards, B.G. 1965. Measurement of the free energy of soil moisture by the psychrometric technique using thermistors. *In* Moisture equilibria and moisture changes in soils beneath covered areas. Butterworth, Australia, pp. 39–46.
- Russam, K., and Coleman, C.D. 1961. The effect of climatic factors on subgrade moisture conditions. *Géotechnique*, **11**(1): 22–28.
- Satija, B.S. 1978. Shear behaviour of partly saturated soils. Ph.D. thesis, Indian Institute of Technology, Delhi, India.
- Terzaghi, K. 1936. The shear resistance of saturated soils. Proceedings, 1st International Conference on Soil Mechanics and Foundation Engineering, Cambridge, Vol. 1., pp. 54–56.
- Toll, D.G. 1990. A framework for unsaturated soil behaviour. *Géotechnique*, **40**(1): 31–44.

Model for the prediction of shear strength with respect to soil suction

S.K. Vanapalli, D.G. Fredlund, D.E. Pufahl, and A.W. Clifton

Abstract: Experimental studies on unsaturated soils are generally costly, time-consuming, and difficult to conduct. Shear strength data from the research literature suggests that there is a non-linear increase in strength as the soil desaturates as a result of an increase in matric suction. Since the shear strength of an unsaturated soil is strongly related to the amount of water in the voids of the soil, and therefore to matric suction, it is postulated that the shear strength of an unsaturated soil should also bear a relationship to the soil-water characteristic curve. This paper describes the relationship between the soil-water characteristic curve and the shear strength of an unsaturated soil with respect to matric suction. An empirical, analytical model is developed to predict the shear strength in terms of soil suction. The formulation makes use of the soil-water characteristic curve and the saturated shear strength parameters. The results of the model developed for predicting the shear strength are compared with experimental results from a glacial till. The shear strength of statically compacted glacial till specimens as measured using a modified direct shear apparatus. Specimens were prepared at three different water contents and densities (i.e., corresponding to dry of optimum, at optimum, and wet of optimum conditions). Various net normal stresses and matric suctions were applied to the specimens. There is a good correlation between the predicted and measured values of shear strength for the unsaturated soil.

Key words: soil-water characteristic curve, shear strength, unsaturated soil, soil suction, matric suction.

Introduction

A value for the shear strength of a soil is required in the prediction of the stability of slopes and embankments, the bearing capacity of foundations, and pressures against earth retaining structures. The Mohr-Coulomb theory, using the effective stress state, is commonly used for predicting the shear strength of saturated soils. Even though soils encountered in engineering practice are often unsaturated, slope stability analyses are usually based on the saturated shear strength parameters. Similar design approaches have been adopted for retaining structures, pavements, and other earth structures. These approaches are conservative to varying degrees in that the influence of soil suction is ignored. However, even low suctions can be responsible for maintaining the stability of slopes (Walle and Hachich 1989).

The concept of stress state variables to describe the behavior of unsaturated soils was introduced by Fredlund

and Morgenstern (1977). The shear strength of an unsaturated soil, in terms of these stress state variables, was proposed by Fredlund et al. (1978). Elastic-plastic, critical state soil mechanics theories have also been proposed using the concept of stress state variables (Karube 1988; Toll 1990; Wheeler and Sivakumar 1995).

Using a phenomenological approach consistent with continuum mechanics, the shear strength behavior of an unsaturated soil can be written in terms of $(\sigma - u_a)$ and $(u_a - u_w)$, with independent soil properties. This approach has been thoroughly studied in laboratory investigations by various researchers (Gan et al. 1988; Abramento and Carvalho 1989; Escario and Juca 1989; Vanapalli 1994).

Although shear strength theories of an unsaturated soil have been formulated and found to be consistent with observed experimental behavior, experimental measurements of shear strength are time-consuming and require costly laboratory facilities. This has to some degree limited the application of the shear strength theories for unsaturated soils to research and academic areas. To-date, there has been only limited practical application of the unsaturated soils shear strength theory in practice. The success of any theory depends on how readily and successfully it can be applied in engineering practice. It is therefore important to develop a simpler approach for predicting the shear strength of an unsaturated soil for various engineering applications. This would encourage the use of unsaturated shear strength theories in engineering practice.

Some attempts have been made to predict the shear strength of an unsaturated soil using empirical procedures. Escario and Juca (1989), for their experimental data on different soils have found that an ellipse with a

S.K. Vanapalli. Research Associate, Department of Civil Engineering, University of Saskatchewan, Saskatoon, SK, Canada S7N 5A9.

D.G. Fredlund. Professor, Department of Civil Engineering, University of Saskatchewan, Saskatoon, SK, Canada S7N 5A9.

D.E. Pufahl. Professor, Department of Civil Engineering, University of Saskatchewan, Saskatoon, SK, Canada S7N 5A9.

A.W. Clifton. Clifton Associates, Regina, SK, Canada S4N 5Y5.

Reproduced with permission from the *Canadian Geotechnical Journal*, 33(3): 379-392, 1996.

2.5° angle, reproduced the variation of shear strength with respect to suction reasonably well. Abramento and Carvalho (1989) used a curve-fitting technique for their experimental data using an exponential function that retains the form of the shear strength equation proposed by Fredlund et al. (1978), treating $(\tan \phi^b)$ as a variable with respect to suction. These empirical procedures may or may not be suitable for all types of soils. This paper concentrates on developing an equation for the shear strength of an unsaturated soil using the soil-water characteristic curve and the shear strength parameters of the saturated soil.

Use of the soil-water characteristic curve in predicting the shear strength of an unsaturated soil

Features of a typical soil-water characteristic curve

The soil-water characteristic curve defines the relationship between the amount of water in the soil and soil suction. The amount of water can be a gravimetric water content, w , a volumetric water content, θ , or degree of saturation, S . Typical soil-water characteristic features for the drying and wetting of a soil are shown in Fig. 1.

Volumetric water content, θ , is defined as the ratio of volume of water to the total volume of soil. Relationships can be written between the various volume-mass designations for water content. The relationship between volumetric water content and other variables can be written as:

$$[1] \quad \theta = \frac{Se}{1+e} = Sn$$

where:

- S = degree of saturation,
- e = void ratio, and
- n = porosity.

The relationship between volumetric water content, θ , and gravimetric water content, w , can be written:

$$[2] \quad \theta = w\rho_d$$

where:

- ρ_d = dry density of the soil, and
- w = gravimetric water content.

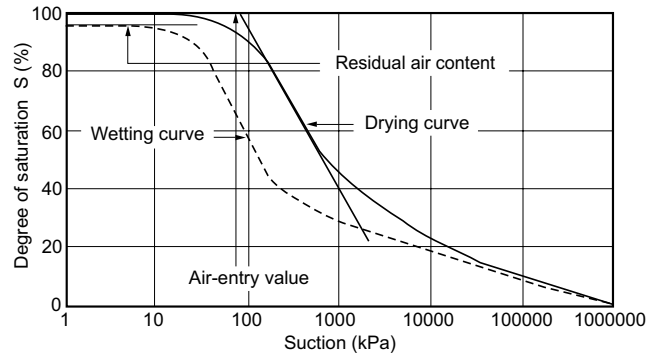
Some soils undergo significant void ratio changes (i.e., overall volume changes) as a result of changes in soil suction. An equation can also be written for the relationship between changes in the various volume-mass variables (Fredlund and Rahardjo 1993).

$$[3] \quad \Delta e = \frac{G_s \Delta w - e_i \Delta S}{S_f}$$

where:

- Δw = change in water content,
- e_i = initial void ratio,
- ΔS = change in degree of saturation, and
- S_f = final degree of change in saturation.

Fig. 1. Typical soil-water characteristic curve features for the drying and wetting of a soil.



The changes in void ratio that occur due to soil suction changes can be taken into consideration by substituting eq. [3] into eq. [1], if the variables in eq. [3] are known. Therefore, it is possible to incorporate the effect of changes in void ratio into the study of the soil-water characteristic curve.

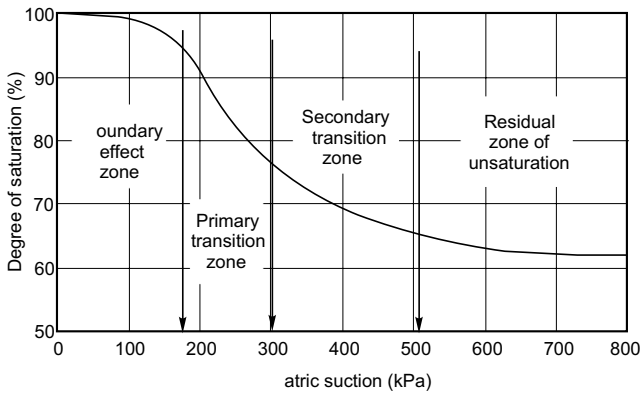
Total suction, ψ , is comprised of both matric and osmotic suction. However, it is primarily the matric suction component, $(u_a - u_w)$, which governs the engineering behavior of unsaturated soils in the lower suction range encountered in most field situations. Laboratory data has indicated that a change in total suction is essentially equivalent to a change in the matric suction in an unsaturated soil where the water contents are less than the residual value (Krahn and Fredlund 1972).

A physical model for explaining the unsaturated shear strength behavior

Different saturation stages can be identified as the desaturation process of a soil takes place. White et al. (1970) have provided the original concepts for the different stages of desaturation, and the authors have modified these ideas somewhat. The results are shown in Fig. 2. There are three identifiable stages of desaturation: the boundary effect stage, the transition stage (i.e., primary and secondary transition stages), and the residual stage of unsaturation.

Figure 3 illustrates the variation of area of water with desaturation for different stages of the soil-water characteristic curve (Vanapalli 1994). In the boundary effect stage all the soil pores are filled with water (i.e., the water menisci in contact with the soil particles or aggregates are continuous in this stage) (see Fig. 3a). The soil is essentially saturated at this stage, and there is no reduction in the area of water in this stage. Under these conditions, the single stress state, $(\sigma - u_w)$, describes the behavior of the soil. The first point of importance on the soil-water characteristic curve is the air-entry value, $(u_a - u_w)_b$. This value of suction identifies the point at which air enters the largest pores of the soil. The soil starts to desaturate in the transition stage. The water content in the soil reduces significantly with increasing suction in this stage. The amount of water at the soil particle or aggregate contacts reduces as desaturation continues (i.e., the water

Fig. 2. Degree of saturation – soil suction curve for a hypothetical porous medium.

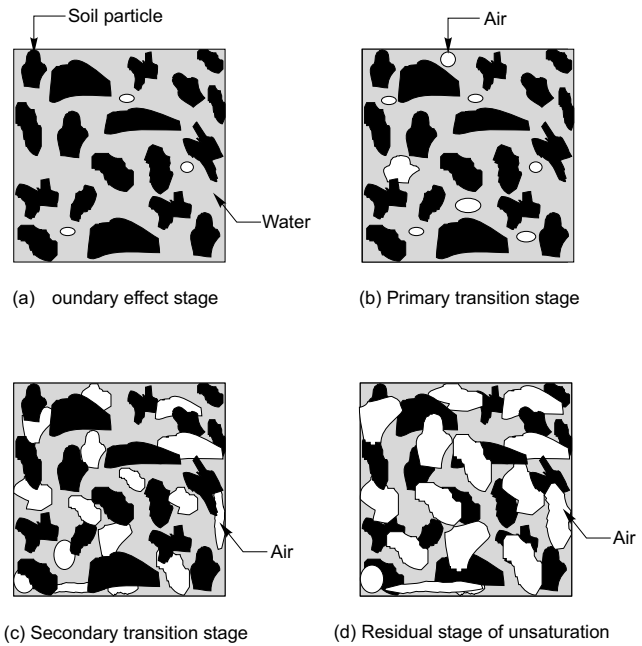


menisci area in contact with the soil particles or aggregates is not continuous and starts reducing in this stage (Figs. 3b and 3c). Eventually large increases in suction lead to a relatively small change in water content (or degree of saturation). This stage is referred as the residual stage of unsaturation (Fig. 3d). The water content in the soil at the commencement of this stage is generally referred to as the residual water content. The amount of water is small in this stage. (i.e., the water menisci area is small).

The rate at which shear strength changes in unsaturated conditions appears to be related to the area of water (i.e., the water menisci area in contact with the soil particles or aggregates) (see Fig. 3d). Thus, it is apparent that there should be a relationship between the soil-water characteristic curve and the shear strength of an unsaturated soil. The physical model described in Fig. 3 along with the corresponding desaturation stages shown in Fig. 2 assist in understanding the shear strength behavior of an unsaturated soil.

The typical relationship between the shear strength and the soil-water characteristic curve can be seen by comparing Figs. 4a and 4b. There is a linear increase in shear strength up to the air-entry value. The rate of desaturation with respect to an increase in matric suction, (i.e., $dS / d(u_a - u_w)$) is greatest between the air-entry value and the suction corresponding to residual water content conditions. There is a non-linear increase in shear strength in this region. However, beyond the residual suction conditions, the shear strength of an unsaturated soil may increase, decrease, or remain relatively constant during further desaturation. In some cases, particularly in soils that desaturate relatively fast (e.g., sands and silts), it can be expected that the shear strength will decrease. Generally, it can be expected that there is little water left in soil pores when the soil reaches the residual state. The water content in sands and silts at residual suction conditions can be quite low and may not transmit suction effectively to the soil particle or aggregate contact points. Thus, even large increases in suction will not result in a significant increase in shear strength.

Fig. 3. Probable variation of water area in different stages of a soil-water characteristic curve.

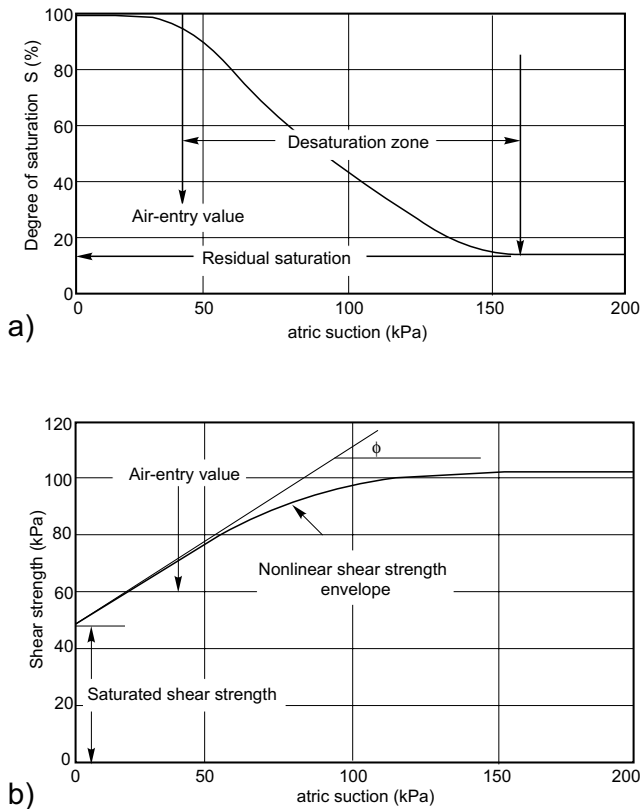


In contrast, clays may not have a well-defined residual state. Even at high values of suction there could still be considerable water (i.e., in the form of adsorbed water) available to transmit suction along the soil particle or aggregate contacts, which contributes towards increases in the shear strength. This phenomenon can occur for a large range of suction values for clays. This subject is further discussed later in this paper.

The residual state occurs at a relatively low suction value for gravels, sands, silts, and their mixtures (i.e., generally between 0 and 200 kPa suction range) and is well defined. The residual state conditions of such soils can be reasonably well predicted from the soil-water characteristic curve plotted on an arithmetic scale. For clays with low plasticity, the residual state will generally be in the range of 500–1500 kPa. However, for intermediate to highly plastic soils, the residual state can be greater than 1500 kPa. In some cases, (e.g., highly plastic, intact clays) it is difficult to define the residual break in the curve.

The residual water content and its corresponding value of soil suction have been defined in a number of ways in the literature; however, the accepted use of these terms is not always in agreement. Some investigators suggest that a water content corresponding to a suction of about 1500 kPa can be used as the residual water content (van Genuchten 1980). This magnitude of suction, corresponding to residual conditions, is similar to the wilting point of many plants. Water in the liquid phase drains from most of the soil pores when the suction has attained a value of about 1500 kPa. Desaturation beyond residual conditions occurs primarily as a result of vapor movement up to the point where the soil water content is in equilibrium with the vapor pressure of its surroundings.

Fig. 4. a) A typical soil-water characteristic curve. b) Shear strength behavior of soil as it relates to the soil-water characteristic curve.



Terminal suction and the soil-water characteristic curve

There appears to be a common value of total suction (i.e., the sum of matric suction and osmotic suction) where all types of soils approach zero water content (see Fig. 1). This suction value corresponds to approximately 1 000 000 kPa. The experimental results of Russam (1958), Crony et al. (1958), Fredlund (1964), Fleureau et al. (1993), and Vanapalli (1994) on various soils experimentally supports this value. This observed behavior is also supported using thermodynamic principles (Richards 1965). Engineers are generally concerned with the performance of geotechnical structures in the relatively low suction range of 0 to 500 kPa. Suction values approaching 1 000 000 kPa and the corresponding low water contents are, however, useful when defining flux boundary conditions, and, therefore, it is of value to mathematically define the entire soil-water characteristic curve.

Mathematical representation of the soil-water characteristic curve

There are several empirical equations proposed in the literature to represent the soil-water characteristic curve (Brooks and Corey 1964; McKee and Bumb 1987; van Genuchten 1980). These equations, while suitable for the

data at hand, have often been restricted to certain types of soils or to soil-water characteristic curves of a particular shape or to a limited range of suction values.

Fredlund and Xing (1994) provided an analytical basis for mathematically defining the entire soil-water characteristic curve. The equation applies over the entire range of suctions from 0 to 1 000 000 kPa. This relationship is empirical, but is derived based on the pore size distribution, assuming that the soil consists of a set of interconnected pores that are randomly distributed. The equation is most commonly written in terms of volumetric water content, θ .

$$[4] \quad \theta = C(\psi) \left\{ \frac{\theta_s}{\ln[e + (\psi/a)^n]} \right\}^m$$

where:

- θ = volumetric water content,
- θ_s = saturated volumetric water content,
- a = suction related to the air-entry value of the soil,
- n = soil parameter related to the slope at the inflection point on the soil-water characteristic curve,
- ψ = soil suction,
- m = soil parameter related to the residual water content,
- θ_r = volumetric water content at residual conditions,
- e = natural number, 2.71828..., and
- $C(\psi)$ = correction function that forces the soil-water characteristic curve through a suction of 1 000 000 kPa and zero water content.

The correction factor is defined as:

$$[5] \quad C(\psi) = \left[1 - \frac{\ln \left(1 + \frac{\psi}{\psi_r} \right)}{\ln \left(1 + \frac{1000000}{\psi_r} \right)} \right]$$

where:

- ψ_r = the suction value corresponding to residual water content, θ_r .

Equation [4] can be written in a normalized form by dividing both sides of the equation by the volumetric water content at saturation:

$$[6] \quad \Theta = [C(\psi)] \left[\frac{1}{\ln(e + (\psi/a)^n)} \right]^m$$

The normalized volumetric water content, Θ , is defined as:

$$[7] \quad \Theta = \frac{\theta}{\theta_s}$$

where:

θ = volumetric water content, and
 θ_s = volumetric water content at saturation.

The degree of saturation, S , however, is also equal to the normalized volumetric water content.

$$[8] \quad \Theta = S$$

Equation [4] or [6] can be used to best-fit soil-water characteristic curve data of any soil for the entire range of suctions. The fitting parameters (i.e., a , n , and m values) must be determined using a non-linear regression procedure (Fredlund and Xing 1994). An empirical, analytical model is developed both in terms of volumetric water content, θ , and degree of saturation, S , and the saturated shear strength parameters, effective cohesion, c' , and effective angle of shearing resistance, ϕ' , to predict the variation of shear strength with respect to suction.

The analytical relationship between the soil-water characteristic curve and the shear strength

Linear shear relationship

A linear shear strength equation for an unsaturated soil was proposed by Fredlund et al. (1978):

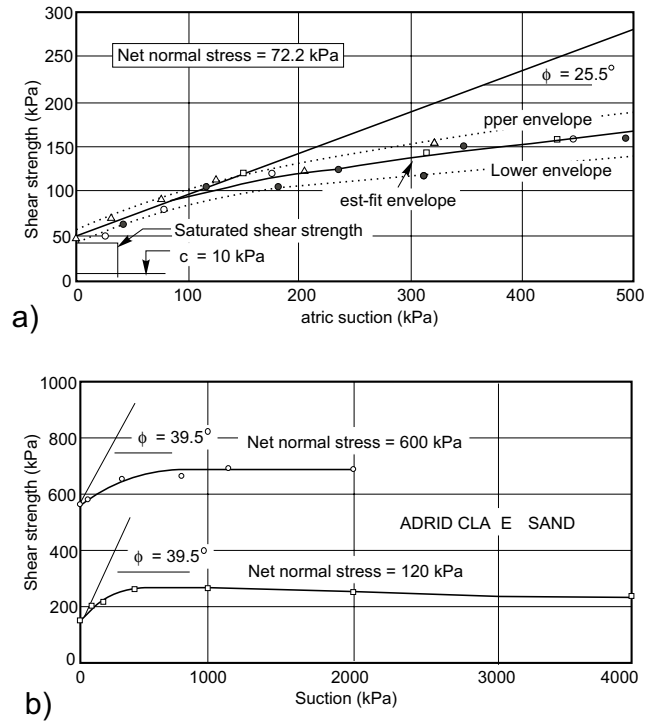
$$[9] \quad \tau_f = c' + (\sigma_n - u_a) \tan \phi' + (u_a - u_w) \tan \phi^b$$

where:

- τ_f = shear strength of an unsaturated soil,
- c' = effective cohesion of saturated soil,
- ϕ' = effective angle of shearing resistance for a saturated soil,
- ϕ^b = angle of shearing resistance with respect to matric suction,
- $(\sigma_n - u_a)$ = net normal stress on the plane of failure at failure, and
- $(u_a - u_w)$ = matric suction of the soil on the plane of failure.

Some experimental results showing the variation in shear strength with respect to matric suction are shown in Fig. 5 (Gan et al. 1988; Escario and Juca 1989). The effective angle of shearing resistance, ϕ' , of glacial till tested by Gan et al. (1988) is 25.5°, and that of clayey sand tested by Escario and Juca (1989) is 39.5°. The experimental results show non-linear shear strength behavior when tests are performed over a wide range of suctions (Fig. 5). Soils that are resistant to desaturation, such as highly plastic clays, for example, can exhibit essentially a linear shear strength behavior over a relatively large range of soil suctions. Rahardjo et al. (1995) reported essentially linear shear strength behavior for a suction range of 0 to 500 kPa for a residual clay in Singapore. Equation [4] can be used to describe the shear strength behavior with respect to soil suction provided the suction range is specified. The angle of shearing resistance with respect to soil suction, ϕ^b , is a variable for soils that exhibit non-linear shear strength behavior.

Fig. 5. a) Variation of shear strength with matric suction (modified after Gan et al. 1988). b) Variation of shear strength with matric suction (modified after Escario and Juca 1989).



Role of area of water

At lower values of matric suction (i.e., at high degrees of saturation) the pore-water pressure acts directly to increase the effective stress in contributing to the shear strength. This condition applies until the soil begins to desaturate under an applied matric suction. The rate at which suction contributes towards shear strength can be related to the normalized area of water, a_w . The normalized area of water is assumed to be in direct proportion to the water volume in the soil by applying Greens theorem (Fung 1977). The normalized area of water, a_w , is defined as:

$$[10] \quad a_w = \frac{A_{dw}}{A_{tw}}$$

where:

- A_{tw} = total area of water at 100% saturation, and
- A_{dw} = area of water corresponding to any degree of saturation.

The normalized area of water, a_w , is a dimensionless number. This number can be visualized as representing the amount of water in the soil. The value of a_w varies from unity at saturation, to a small value under residual state conditions, and zero when the soil is dry. The normalized volumetric water content, Θ , of the soil also varies in a manner similar to the area of water, a_w , for a large range of suction values.

Due to the similarity in the normalized area of water, a_w , and the normalized volumetric water content, Θ , the following relationship can be written:

$$[11] \quad a_w = (\Theta^\kappa)$$

where:

$$\kappa = \text{fitting parameter.}$$

The significance of the fitting parameter, κ , will be discussed later.

The shear strength contribution due to suction, τ_{us} , in terms normalized area of water, a_w , can be mathematically expressed as:

$$[12] \quad \tau_{us} = (u_a - u_w)(a_w \tan \phi')$$

Substituting eq. [11] in eq. [12] results in eq. [13]:

$$[13] \quad \tau_{us} = (u_a - u_w)[(\Theta^\kappa)(\tan \phi')]$$

The incremental shear strength contribution due to suction, $d\tau$, can be obtained by differentiating eq. [13] with respect to suction, $(u_a - u_w)$. The result is:

$$[14] \quad d\tau = d(u_a - u_w)[(\Theta^\kappa)(\tan \phi')] \\ + (u_a - u_w)[d(\Theta^\kappa)(\tan \phi')]$$

The value of $(\tan \phi^b)$ at any suction is:

$$[15] \quad \tan \phi^b = \frac{d\tau}{d(u_a - u_w)} \\ = \left[(\Theta^\kappa) + (u_a - u_w) \frac{d(\Theta^\kappa)}{d(u_a - u_w)} \right] \tan \phi'$$

Up to the air-entry value of the soil, Θ is equal to unity and there is no change in the normalized area of contact, a_w . The rate of change Θ (i.e., $[d(\Theta^\kappa)]/[d(u_a - u_w)]$) equals zero up to the air-entry value of soil. In other words, the value of a_w is unity in the boundary effect stage, as the soil is in a saturated state (Figs. 2 and 3). Up to the air entry value, the ϕ^b angle is equal to the effective angle of shearing resistance, ϕ' , in eq. [4]. Figure 6a shows the variation of shear strength with respect to suction in this stage with reference to the soil-water characteristic curve in Fig. 2.

The rate of change of Θ , (i.e., $[d(\Theta^\kappa)]/[d(u_a - u_w)]$) is always a negative value for increments of suction beyond the air-entry value (i.e., in the primary and secondary transition stage and residual stage). However, the net shear strength contribution due to suction, $d\tau$, in eq. [15] is positive. This occurs because the shear strength contribution due to a suction change is more effective than the reduction in a_w in this stage. In other words, even though a_w decreases as a result of an increase in suction, the net contribution due to suction is positive, and, hence, there is an increase in the shear strength. Figures 6b and 6c show the variation of shear strength with respect to suction in the transition stage with reference to the soil-water characteristic curve in Fig. 2.

At high values of suction (i.e., in the residual stage of unsaturation) Θ is extremely small and the value of

$[d(\Theta^\kappa)]/[d(u_a - u_w)]$ in this stage is negative. The net summation of:

$$\left[(\Theta^\kappa) + (u_a - u_w) \frac{d(\Theta^\kappa)}{d(u_a - u_w)} \right] \tan \phi'$$

in eq. [15] may approach negative values. In other words, the net contribution of suction in the residual stage of unsaturation causes a reduction in the shear strength.

Equation [15] satisfies the conceptual behavior of the shear strength of unsaturated soils and provides a theoretical basis for the use of the soil-water characteristic curve to develop a shear strength function.

Shear strength equation and the soil-water characteristic curve

It is proposed that the shear strength of an unsaturated soil at any given value of suction be written as follows:

$$[16] \quad \tau = [c' + (\sigma_n - u_a) \tan \phi'] + (u_a - u_w)[(\Theta^\kappa)(\tan \phi')]$$

The first part of the equation is the saturated shear strength, when the pore-air pressure, u_a , is equal to the pore-water pressure, u_w . This part of the equation is a function of normal stress, as the shear strength parameters c' and ϕ' are constant for a saturated soil. For a particular net normal stress, this value is a constant. The second part of the equation is the shear strength contribution due to suction, which can be predicted using the soil-water characteristic curve.

To obtain a better correlation between predictions and experimental shear strength data, a fitting parameter such as κ is useful. This is similar to the matching factor used by Green and Corey (1971) to match experimental and calculated values for the coefficient of permeability function. The analyses carried out using eq. [16] are referred to as the "first approach" in the paper.

Extending the same philosophical concepts, another equation is proposed in this paper for predicting the shear strength without using the fitting parameter, κ . The equation is given below:

$$[17] \quad \tau = c' + (\sigma_n - u_a) \tan \phi' \\ + (u_a - u_w) \left[(\tan \phi') \left(\frac{\theta - \theta_r}{\theta_s - \theta_r} \right) \right]$$

where:

$$\theta_r = \text{residual volumetric water content.}$$

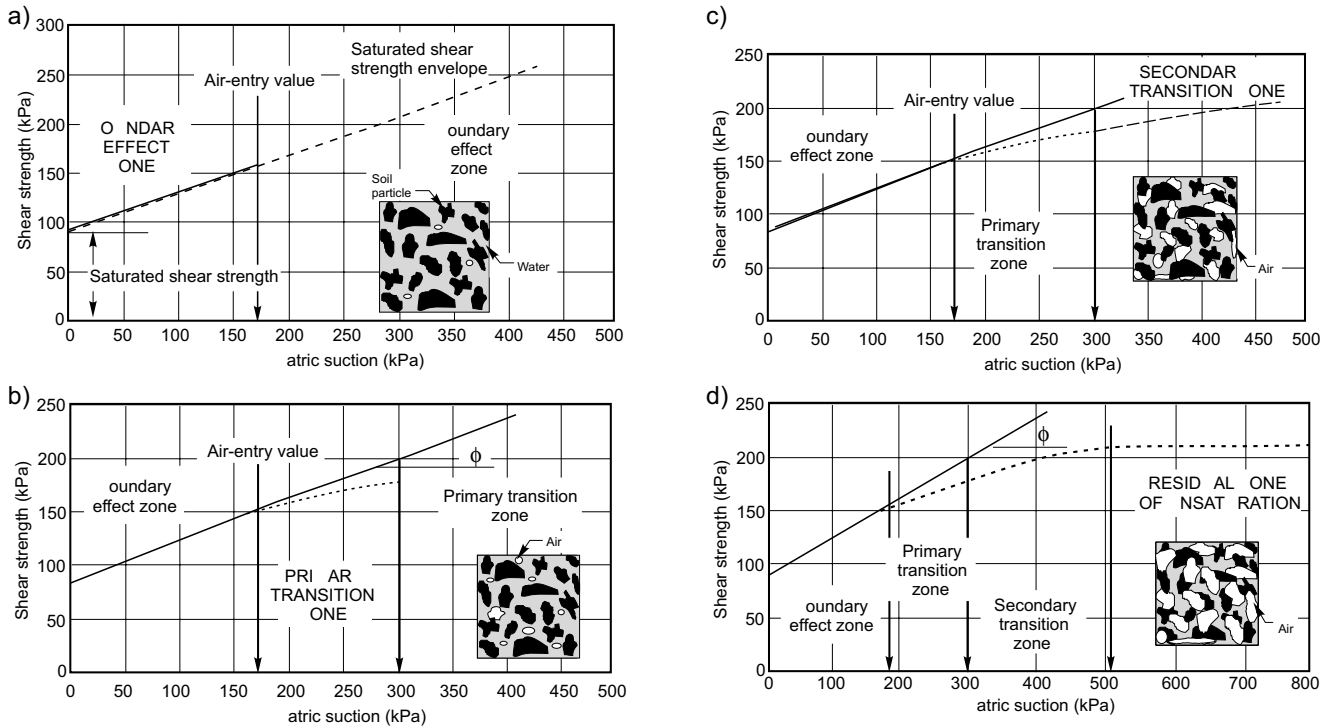
Equation [17] can also be written directly in terms of the degree of saturation:

$$[18] \quad \tau = c' + (\sigma_n - u_a) \tan \phi' \\ + (u_a - u_w) \left[(\tan \phi') \left(\frac{S - S_r}{100 - S_r} \right) \right]$$

where:

$$S_r = \text{residual degree of saturation.}$$

Fig. 6. a) Variation of shear strength with matric suction in the boundary effect stage. b) Variation of shear strength with matric suction in the primary transition stage. c) Variation of shear strength with matric suction in the secondary transition stage. d) Variation of shear strength with matric suction in the residual zone of unsaturation.



The residual volumetric content, θ_r , or the residual degree of saturation, S_r , can be determined from the soil-water characteristic curve. The results analyzed using eq. [17] are referred to as the “second approach” in the rest of the paper. Sensitivity analyses will be presented for the proposed shear strength equations (i.e., eq. [16] and eq. [17]). The advantages and disadvantages of each equation are discussed later while presenting the results.

Procedure for predicting the shear strength of unsaturated soils

The procedure for predicting the shear strength of unsaturated soils is as follows:

- (1) The three fitting parameters for the soil-water characteristic curve (i.e., a , n , and m) apply for the entire suction range from 0 to 1 000 000 kPa. Therefore, eq. [4] or eq. [6] can be estimated using a non-linear minimization technique. The initial values used in non-linear regression analysis for all the soil-water characteristic curves were as follows: $a = 10$, $n = 1$, and $m = 1$. The objective is to obtain three soil parameters that produce a curve that closely matches the measured values on the soil-water characteristic curve.
- (2) The residual state of the soil (i.e., S_r and ψ_r) is estimated from the soil-water characteristic curve.

- (3) The required input parameters for obtaining the shear strength function are the strength parameters, c' and ϕ' , and the soil-water characteristic curve. The shear strength function can generally be predicted using either eq. [16] or eq. [17] for the suction range of interest (i.e., up to 1 000 kPa).

Shear strength behavior of soils beyond the residual state

The non-linear increase in shear strength occurs from the air entry value of the soil to its residual condition. The shear strength of soils such as sands and silts and certain clays drops beyond a particular value of suction. This drop in shear strength may be assumed to start near the residual value of suction. Similarly, some soils can exhibit a relatively constant shear strength for a large range of suction values. The general nature of the soil-water characteristic curve gives some indication of the behavior of shear strength after the residual state.

The shear strength of an unsaturated soil may remain relatively constant, increase or decrease beyond the residual state. Presently, there are no data available to show the soil-water characteristic curves and experimental shear strength data to support and explain the shear strength behavior beyond the residual state. However, there is experimental evidence available in the literature to show that the shear strength decreases (Donald 1956; Escario and Juca 1989). A decrease in shear strength is

possible at low suction values for soils such as sands and gravels that desaturate quite rapidly. Donald (1956) showed results that indicated a drop in shear strength after a suction value of 10 to 15 kPa for four different sands tested. For soils that have the highest percentage of fines, the shear strength drops only at larger values of suction. Escario and Juca (1989) have observed increases in shear strength up to suction values of 1000 kPa for a clayey sand. However, for suctions from 1000 to 4000 kPa, a drop in shear strength was observed (see Fig. 5b).

For certain soils like highly plastic clays, there may be no defined residual stage of unsaturation. Such soils show increase in shear strength even at relatively high values of suction. Escario and Juca (1989) report increased shear strength for a Guadalix red clay at suction values as high as 10 000 kPa. The residual state for highly plastic soils seems to occur only as the water content in the soil approaches zero. It may be assumed that the shear strength for such soils increases up to the point where the degree of saturation approaches a zero value or an extremely high suction. For example, the dry strength of highly plastic clays is high and continues to rise to a dry condition (e.g., adobe bricks).

Parameters influencing the shear strength behavior of unsaturated soils

The soil structure and stress history that may occur in the field should be reasonably simulated in the laboratory while developing the soil-water characteristic curve. Conventional, soil-water characteristic curves are developed using a pressure plate apparatus without any loading applied to the specimen. A method for developing soil-water characteristic curves under differing stress conditions for fine-grained soils using the pressure plate apparatus is provided by Vanapalli (1994). This procedure is briefly explained later in the paper.

Another parameter that has to be considered in the shear strength prediction is the influence of suction on the angle of shearing resistance, ϕ . Vanapalli (1994) showed results where ϕ was independent of suction for a glacial till tested at various densities and initial water contents for a range of suctions from 0 to 500 kPa. Karube (1988) reported similar results for a kaolinite. Drumright (1989) has reported that ϕ was slightly influenced by suction. Escario and Juca (1989), however, have found that ϕ was independent of suction for Madrid clayey sand (i.e., soil having a w_L of 32%, I_p of 15%, with clay, silt, and sand contents of 17%, 31%, and 46%, respectively) but not for Guadalix red clay (i.e., soil having a w_L of 33%, I_p of 13.6%, with clay, silt, and sand contents of 86%, 11%, and 3%, respectively) when tested for a large range of suction values (0 to 10 000 kPa). For all practical purposes, it would appear that ϕ can be assumed to be constant for a suction range of 0 to 500 kPa. This is generally the range of practical interest for geotechnical and geo-environmental engineers.

Comparison of predicted unsaturated shear strength of a glacial till with the experimental results

The unsaturated shear strength behavior of a statically compacted glacial till was studied at three different water contents and densities. These conditions represented the optimum, dry and wet of optimum conditions. Varying net normal stresses and varying matric suction values were applied to the specimens and the strength behavior was experimentally studied using a modified direct shear apparatus.

Soil-water characteristic curves were developed for the suction range of 0 to 300 000 kPa using a pressure plate apparatus and osmotic desiccators with specimens pre-consolidated to an equivalent net normal stresses used in the experimental program. The experimental results of unsaturated shear strength are compared with the predicted shear strengths.

Soil and the testing program

A glacial till obtained from Indian Head, Saskatchewan, was used for the study. The soil used for the entire testing program was obtained in a single batch to ensure uniformity of the specimens. The soil was air dried for several days, pulverized using a rubber mallet, and passed through a 2 mm sieve. The Atterberg limits of the soil showed a liquid limit, w_L , of 35.5% and the plastic limit, w_p , of 16.8%. The fractions of sand, silt, and clay were 28%, 42%, and 30%, respectively. The AASHTO (American Association of State Highway and Transportation Officials) standard compacted density was 1.80 Mg/m³, which corresponded to an optimum water content of 16.3%.

Precalculated amounts of distilled water were sprayed on to several layers of the soil and left overnight in covered plastic bags and stored in a humidity controlled room. The soil was then thoroughly hand mixed. To avoid soil-water clods the mixed soil was again passed through 2 mm sieve. This soil-water mixture was then placed in plastic bags and kept in a moist room for at least 48 hours.

A comprehensive experimental program was conducted, using statically compacted specimens of the prepared soil. Three initial water contents were selected representing dry of optimum conditions (i.e., initial water content 13%, and a dry density, γ_d , of 1.73 Mg/m³), optimum conditions (i.e., initial water content 16.3%, and a dry density, γ_d , of 1.80 Mg/m³), and wet of optimum conditions (i.e., initial water content 19.2%, and a dry density, γ_d of 1.77 Mg/m³). The densities and water contents used in the research program were selected from the soil compaction curve.

Statically compacted specimens 100 mm diameter and 21 mm height were prepared using a constant volume mold at the prescribed densities and water contents. The specimens used for the direct shear tests and for develop-

ing the soil-water characteristic curves were obtained from the 100 mm diameter specimens.

Saturated shear strength tests in direct shear

Effective shear strength parameters were determined both under single stage and multistage testing with the soil in a saturated state. The residual shear strength of the soil was also studied. Single stage and residual shear strength testing was conducted using a conventional direct shear apparatus. Multistage testing was conducted using a modified direct shear apparatus. The same apparatus was used for unsaturated shear strength testing. All tests were conducted using a conventional testing procedure for direct shear tests.

Unsaturated shear strength tests using modified direct shear equipment

The unsaturated shear strength of the statically compacted specimens was determined by using modified direct shear equipment designed by Gan and Fredlund (1988) for multistage testing. Multistage testing overcomes two main problems generally encountered in testing unsaturated soils. Firstly, the time required for testing is reduced making it feasible to test unsaturated soils of a low coefficient of permeability in a reasonable time. Secondly, the same specimen can be tested under a relatively large range of matric suctions. This procedure helps avoid the variability caused by non-uniformity of different specimens and results in using fewer specimens for testing purposes. Design details of modified direct shear equipment and the procedure of testing using multistage loading are detailed by Gan and Fredlund (1988).

A matric suction range of 0 to 500 kPa was selected for testing based on the air-entry value of the ceramic in the modified direct shear testing apparatus. The glacial till used in this study desaturates reasonably well from a degree of saturation of 100% to around 60% over the matric suction range of 0 to 500 kPa. Since the non-linear variation of shear strength is dependent on desaturation, there should be a wide variation in shear strength over the testing range used in this study.

Soil-water characteristic curves

Soil-water characteristic curves cannot be measured while applying an external load when using a conventional pressure plate apparatus. An indirect method was used to allow a known level of stress to be applied to the specimens. First, a series of consolidation and swelling curves were measured for the soil using conventional one-dimensional consolidation test procedures. The consolidation and swelling characteristics of the soil (i.e., compression index, C_c , and the swelling index, C_s) were then used to estimate the initial stress state and void ratio of the soil to be used in the pressure plate tests. More details on preparing "precompressed" specimens used for developing soil-water characteristic curves are available in Vanapalli (1994).

Soil-water characteristic curves were developed using a pressure plate apparatus on specimens, which had been

precompressed to the net normal stresses used in the direct shear test for determining the unsaturated shear strength. The precompressed specimens were placed in a consolidation ring 63.5 mm in diameter. The ring plus the soil were placed on the ceramic disk of the pressure plate with a 5 N surcharge load to ensure a good contact between the specimen and the ceramic disk. The airtight chamber of the pressure plate apparatus was then pressurized to a desired matric suction.

The initial volume and mass of the precompressed specimens were measured. As the suction was applied, water drained from the specimen. The mass of the specimen was calculated after the specimen attained equilibrium conditions under the applied matric suction. Equilibrium was assumed to have been attained when water no longer discharged from the pressure plate. Approximately 5 to 7 days were required to attain equilibration under each applied matric suction. After equilibration was attained, the test assembly was dismantled and the specimens were weighed. This procedure was repeated at every desired matric suction.

Soil-water characteristic curves were determined for matric suction ranging from 0 to 1500 kPa. Approximately half the specimen was used for the measurements of the water content. The water contents at various matric suctions were determined from back-calculations. Calculations for the degree of saturation in this study were made from the initial void ratio of the specimen using the volume-mass relationships. Since statically compacted specimens are relatively stiff and resistant to shrinkage, the change in void ratio with increasing suction was not considered to be significant. The suggested procedure facilitates testing of several specimens simultaneously in the conventional pressure plate apparatus.

To attain the suction versus water content relationship beyond 1500 kPa (i.e., 4500 to 300 000 kPa), an osmotic desiccator was used. Small pieces of a specimen (i.e., about 5 g) obtained from a larger specimen after the completion of the pressure plate tests were used to complete the soil-water characteristic curves by placing them in glass desiccators containing salt solutions. The salt solutions in the glass desiccators controlled the relative humidity (or vapor pressure) in the specimen. Five aqueous solutions were selected that covered the range of suction values from 4500 to 300 000 kPa.

Test results

Saturated shear strength results

The saturated shear strength parameters were calculated for all three different initial conditions (i.e., an initial water content of 13% and a dry density, γ_d , of 1.73 Mg/m³, an initial water content of 16.3% and a dry density, γ_d , of 1.80 Mg/m³, and an initial water content of 19.2% and a dry density, γ_d , of 1.77 Mg/m³). The saturated shear strength parameters were approximately the same for all the tests conducted regardless of different initial conditions. Lee and Haley (1958) and Gibbs and Hilf (1954) reported similar results when testing soils

with different initial conditions (i.e., water content and dry densities).

A series of residual strength tests was conducted on the saturated specimens at optimum conditions (i.e., initial water content equal to 16.3% and the dry density, γ_d , equal to 1.80 Mg/m³). Only one series of the tests was conducted because the analysis of the single-stage tests showed that different initial conditions of the soil did not significantly influence the saturated shear strength parameters. The results obtained from the residual shear testing show that there is essentially no drop in strength once the soil has attained a peak strength. Under continued reversals there was still no significant loss of strength. As a result, the soil can be said to be suitable for multistage testing.

A series of multistage tests were conducted on saturated specimens at optimum condition (i.e., initial water content of 16.3% and a dry density, γ_d , of 1.80 Mg/m³). These tests were conducted using modified direct shear equipment. A strain rate of 2.7 mm/day was used for shearing. A similar strain rate was used for testing the unsaturated specimens using the modified direct shear equipment.

Shear strength envelopes obtained from the three different types of tests are shown in Fig. 7. The shear strength parameters along with the strain rates are summarized in Table 1. The three types of tests conducted show that there is no significant variation in the angle of shearing resistance, ϕ , when using the three different types of tests. The variation in cohesion from 15 kPa in single-stage testing to 4 kPa in multistage testing may be due to the variation in strain rate, different pieces of direct shear equipment used, type of testing procedures, and the possible variation in soil properties.

The test that produced the lowest effective cohesion value under drained shearing conditions is assumed to be most accurate (i.e., 4 kPa). Ruddock (1966) postulated that for multistage testing, failure to achieve complete dissipation of pore pressure will be reflected in an increase in the measured cohesion. However, the angle of shearing resistance, ϕ , would not be significantly affected. It is possible that by the time the frictional component of strength is fully mobilized, the actual cohesion present in the measured sheared strength may be small. Gan (1986) tested the same till used for this study and showed that at peak shear strength mobilized, the cohesion component was negligible.

As the unsaturated shear strength tests of the present study were conducted using multistage testing adopting a strain rate of 2.7 mm/day, an effective angle of internal friction, ϕ , equal to 23° and an effective cohesion, c' , equal to 0 kPa would be most reasonable.

Pressure plate and desiccator test results

Figures 8 and 9 show typical soil-water characteristic curves developed for the specimens with precompression normal stresses of 0, 25, 100, and 200 kPa. These soil-water characteristic curves were developed on specimens

Fig. 7. Results of saturated shear strength tests under different procedures.

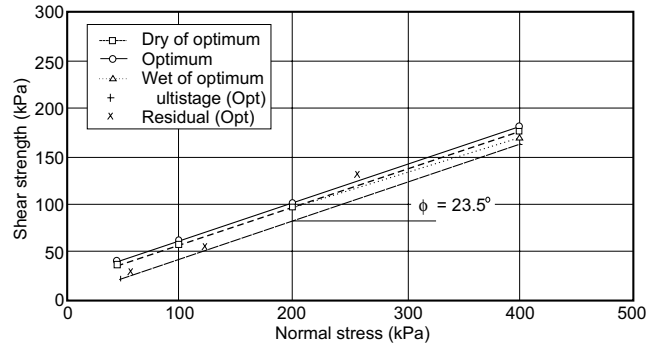


Table 1. Strength parameters of saturated till from different types of direct shear tests.

Type of direct shear test	c' (kPa)	ϕ' (°)	Strain rate (mm/day)
Single stage	15	22.5	18
Residual	8	23	18
Multistage	4	23	2.7

Fig. 8. Soil-water characteristic curves of precompressed specimens using pressure plate.

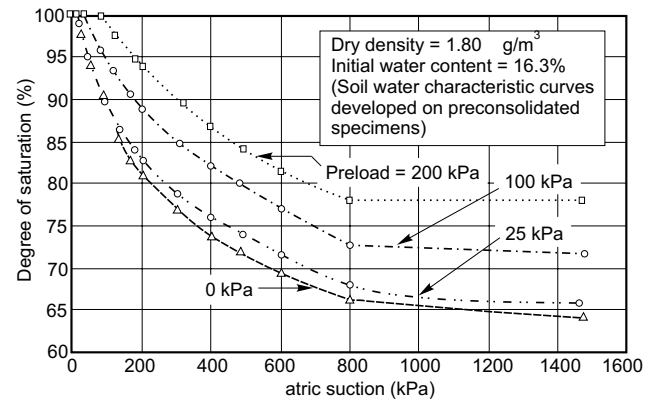
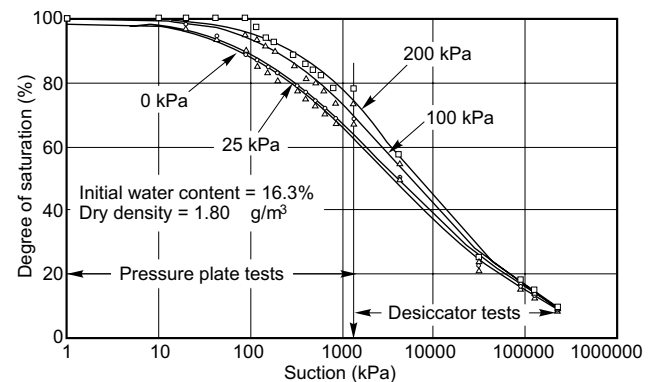


Fig. 9. Soil-water characteristic curves of precompressed specimens using pressure plate and desiccators.



with an initial water content of 16.3% and a dry density of 1.80 Mg/m³, reflecting the optimum conditions.

The soil-water characteristic curves are plotted on a linear scale in Fig. 8 with degree of saturation as the ordinate and matric suction as the abscissa. The soil-water characteristic curves for the same precompressed specimens for the range of 0 to 300 000 kPa suction are shown on a semilogarithmic scale in Fig. 9. It can be seen that the degree of saturation continues to reduce up to a suction of 300 000 kPa.

Similar trends were observed for the specimens at wet and dry of optimum conditions. However, the specimens that were prepared dry of optimum desaturated considerably faster.

The soil-water characteristic curve data can be defined as a mathematical expression using eq. [4] or eq. [6] for suctions ranging from 0 to 1 000 000 kPa. The constants a , n , and m were computed using the program CFVIEW developed by Xing (1993). The soil-water characteristic curve data obtained from the pressure plate apparatus and the desiccator tests are summarized in Table 2.

Prediction of shear strength for unsaturated soils using the soil-water characteristic curve and the saturated shear strength parameters

The test results for dry of optimum specimens (series D, as defined in Table 3) tested with a net normal stress of 25 kPa are analyzed and discussed using eq. [16] (i.e., first approach) and eq. [17] (i.e., second approach). The saturated shear strength parameters are c' equal to zero and ϕ' equal to 23°. Soil-water characteristic curve data measured using the pressure plate apparatus and desiccators were best-fit for the entire suction range of 0 to 1 000 000 kPa using eq. [4] or eq. [6]. The constants a , n , and m for the data from the non-linear regression analysis were 34.1, 0.80, and 0.57, respectively.

The variation of shear strength with respect to suction using eq. [16] for different values of κ (i.e., 1, 2, 2.2, and 3) are shown along with the experimental results in Fig. 10. It can be seen that there is a good correlation between the experimental values for the range of suction tested (i.e., 0 to 500 kPa) and the predicted shear strength when using a value of κ equal to 2.2.

In the second approach (i.e., using eq. [17]), a fitting parameter, κ , is not required. However, residual conditions have to be identified from the soil-water characteristic curve data. Figure 11 shows the variation of volumetric water content with respect to suction. As discussed earlier it is difficult to clearly define the residual conditions for fine-grained soils. The shear strength predicted using eq. [17] for various selected residual suction values (i.e., 1500, 3000, and 5000 kPa) is shown in Fig. 12. Experimental results are also shown in this figure. There is good agreement between the experimental results and the predicted shear strength values for a selected residual suction value of 3000 kPa. The specimens prepared at dry of optimum conditions are more sensitive

Table 2. Input parameters to predict the shear strength of unsaturated till.

Preload stress (kPa)	a	n	m	κ	Ψ_r
Dry of optimum initial conditions					
25	34.1	0.80	0.57	2.2	3000
100	71.4	0.66	0.54	2.5	3000
200	125.2	0.81	0.45	2.8	3000
Optimum initial conditions					
25	140.3	0.77	0.57	2.4	3000
100	406.7	0.81	0.60	2.5	3000
200	812.7	0.84	0.61	4.8	3000
Wet of optimum initial conditions					
25	482.8	0.88	0.71	2.4	3000
100	473.1	0.91	0.59	2.4	3000
200	239.5	1.15	0.40	2.4	3000

to suction values towards desaturation in comparison to specimens with optimum and wet of optimum conditions. It was observed that 3000 kPa was a reasonable value for residual suction in the prediction shear strength using eq. [17] for all series of tests conducted in this research program. For many soils, the residual suction value can be estimated reasonably well, and good predictions are possible using the second approach.

The limitation of this approach is that the shear strength drops to zero when suction values approach the residual suction value. There are no experimental results available to confirm by way of experimental data the shear strength at higher suction values for the soil tested. However, both the approaches predict the unsaturated shear strength for the suction range tested (i.e., 0 to 500 kPa) (see series D results in Fig. 14). The analysis of the remainder of the test results was conducted such that both of the approaches (i.e., first and second) give the same results and are close to the experimental shear strength values.

Unsaturated shear strength results

The unsaturated shear strength behavior of the till specimens prepared at different initial conditions are shown in Table 3.

The variation of shear stress with matric suction for the specimens tested with the initial conditions representing optimum water contents under a net normal stresses of 25, 75, and 200 kPa (i.e., results of series C, A1 and A2, and B) are shown in Fig. 13. All the experimental points are shown with symbols. The continuous curves in Fig. 13 are the predicted shear strength envelopes using the soil-water characteristic curve and the effective shear strength parameters using both the approaches. The κ value used for the first approach and the residual suction value used for the second approach for all the series of tests are summarized in Table 2. There is good correlation between the experimental data on shear strength and the predicted values.

Table 3. Multistage unsaturated shear strengths in direct shear.

Sample No.	Series	Water content relative to optimum	Initial water content (%)	Dry density, γ_d (Mg/m ³)	($\sigma - u_a$) (kPa)	Final water content (%)
1	Series A1	Optimum	16.6	1.79	75	13.69
2	Series A2	Optimum	16.3	1.80	75	13.41
3	Series B	Optimum	16.3	1.81	200	13.39
4	Series C	Optimum	16.0	1.78	25	13.51
5	Series D	Dry of optimum	13.0	1.73	25	13.60
6	Series E	Dry of optimum	13.3	1.73	100	14.05
7	Series F1	Dry of optimum	12.8	1.74	200	14.05
8	Series F2	Dry of optimum	13.0	1.73	200	14.60
9	Series G	Wet of optimum	18.8	1.77	25	17.07
10	Series H	Wet of optimum	19.1	1.76	100	14.72
11	Series I	Wet of optimum	19.2	1.78	200	13.67

Fig. 10. Variation of shear strength with matric suction using various values of κ .

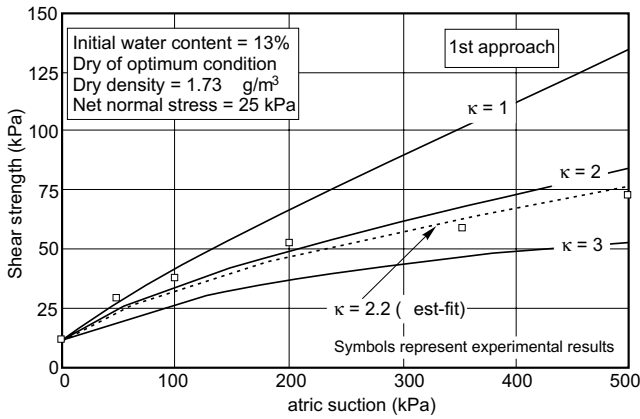
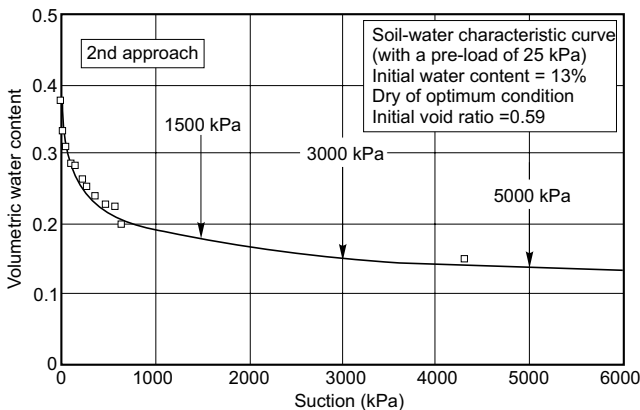
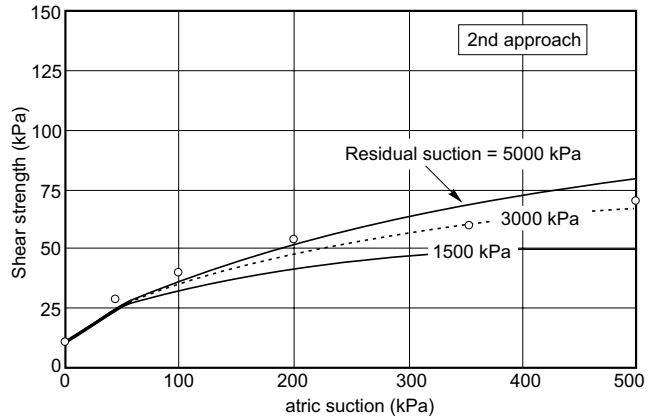


Fig. 11. Variation of volumetric water content versus suction for specimen at dry of optimum conditions.



The non-linear behavior can be observed from all the strength envelopes. Shear strength envelopes representing the adopted value of ϕ' equal to 23°, starting at a zero matric suction value are plotted. The ordinate values represent the saturated shear strength values for the respective net normal stresses (i.e., 25, 75, and 200 kPa). The shear strength envelopes obtained from the results of series D, E, F1, and F2 representing the dry of optimum

Fig. 12. Variations of shear strength with respect to suction using different residual suction values.



conditions are shown in Fig. 14. Similarly, the results of series G, H, and I representing the wet of optimum initial conditions are shown in Fig. 15. There is a good correlation between the predicted and measured shear strength values.

Limitations of the proposed method

Obtaining a reliable soil-water characteristic curve is important when using the proposed method. The pressure plate apparatuses presently available can be used to measure the soil-water characteristic curves without a confining pressure being applied to the soil specimen. From an engineering point of view, the soil always has *in situ* confining stress. As such, a soil-water characteristic curve should be measured simulating the field loading condition. Pressure plates should be designed such that soil-water characteristic curves can be measured with specified loading conditions on the specimens. Unfortunately the special advantage of conducting tests simultaneously on several specimens using a single pressure plate would be lost. For each loading condition, a separate pressure plate would have to be used. To overcome this problem, an indirect method was proposed for determining the soil-water characteristic curves for different loading condi-

Fig. 13. Variations of shear strength with suction under different net normal stresses for specimens at optimum water content conditions.

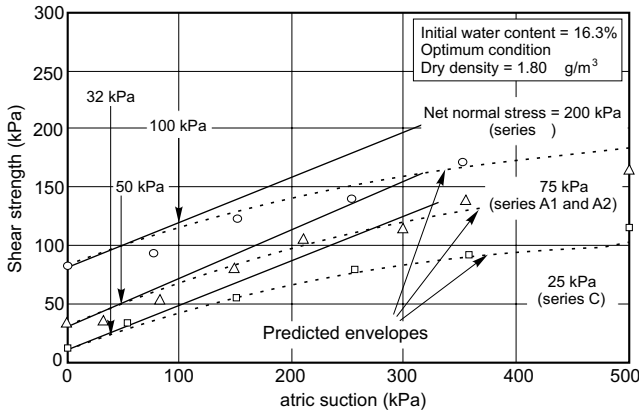
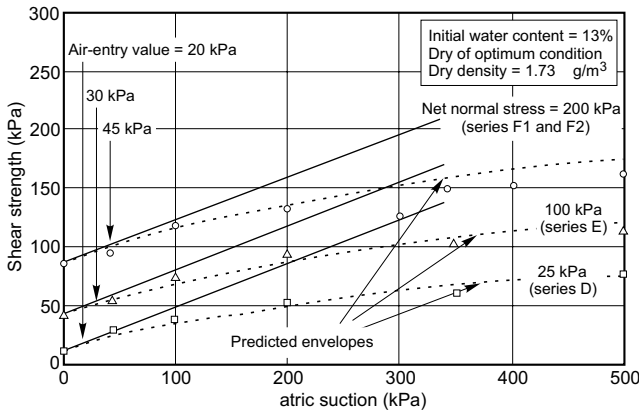


Fig. 14. Variations of shear strength with matric suction under different net normal stresses for specimens at dry of optimum water content condition.



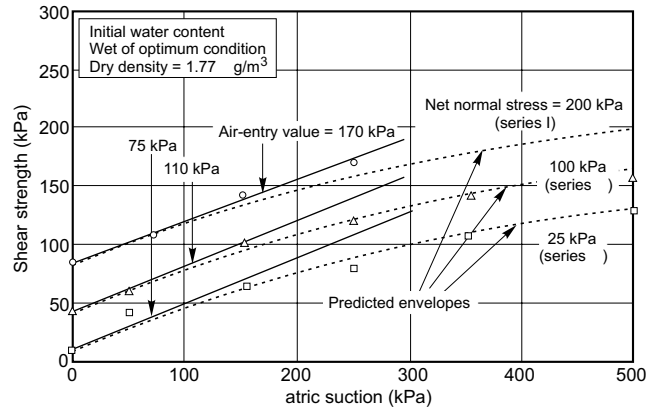
tions. More details of this procedure are available in Vanapaili (1994). The proposed method should be suitable for soils such as tills and clays.

Summary

An empirical, analytical model is developed and two approaches are provided for predicting the shear strength of an unsaturated soil. This model extends the theory proposed by Fredlund et al. (1978). The models use the soil-water characteristic curve and the effective shear strength parameters of a soil. The soil-water characteristic curve is defined in terms of the soil constants a , n , and m using eq. [4] or eq. [6] for the entire range of suction (i.e., from 0 to 1 000 000 kPa). The shear strength variation with respect to suction can be predicted using the first approach (i.e., using eq. [16]) or the second approach (i.e., using eq. [17]).

The shear strength prediction is dependent the fitting parameter κ using the first approach. For the second approach, the residual conditions can be estimated from the soil-water characteristic curve. The fitting parameters for κ varied between 2.2 and 2.8 for the soil tested under dif-

Fig. 15. Variations of shear strength with matric suction under different net normal stresses for specimens at wet of optimum water content condition.



ferent net normal stresses and initial water content conditions. A fitting parameter, κ equal to 2.5 is suggested for the Indian Head till tested for this research program. The authors had to use κ equal to 4.8 to obtain a good correlation between the experimental results and predict the values of shear strength for one series of results (i.e., series B). There is good comparison between the experimental results and predicted values using a residual suction of 3000 kPa for all the series of tests (i.e., for the range 0 to 500 kPa matric suction) for the glacial till tested.

Acknowledgements

The authors wish to thank the Natural Sciences and Engineering Research Council of Canada for providing the financial support for conducting this research. The helpful suggestions provided by S.L. Barbour, M. Fredlund, and A. Xing are also acknowledged.

References

Abramento, M., and Carvalho, C.S. 1989. Geotechnical parameters for the study of natural slopes instabilization at Serra do Mar-Brazilian Southeast. Proceedings, 12th International Conference on Soil Mechanics and Foundation Engineering, Rio de Janeiro, Vol. 3, pp. 1599–1602.

Brooks, R.H., and Corey, A.T. 1964. Hydraulic properties of porous media. Colorado State University Hydrology Paper, Fort Collins, Nr. 3, Vol. 27, March.

Croney, D., Coleman, J.D., and Black, W.P.M. 1958. The movement and distribution of water in soil in relation to highway design and performance. Road Research Laboratory, Research Note 3209, pp. 1–14.

Donald, I.B. 1956. Shear strength measurements in unsaturated non-cohesive soils with negative pore pressures. Proceedings, 2nd Australia - New Zealand Conference on Soil Mechanics and Foundation Engineering, pp. 200–204.

Drumright, E.E. 1989. The contribution of matric suction to the shear strength of unsaturated soils. Ph.D. thesis, Colorado State University, Fort Collins, USA.

- Escario, V., and Juca, J. 1989. Strength and deformation of partly saturated soils. Proceedings, 12th International Conference on Soil Mechanics and Foundation Engineering, Rio de Janeiro, Vol. 3, pp. 43–46.
- Fleureau, J.-M., Kheirbek-Saoud, S., Soemitro, R., and Taibi, S. 1993. Behavior of clayey soils in drying-wetting paths. Canadian Geotechnical Journal, **30**: 287–296.
- Fredlund, D.G. 1964. Comparison of soil suction and one-dimensional consolidation characteristics of a highly plastic clay. M.Sc. thesis, Department of Civil Engineering, University of Alberta, Edmonton.
- Fredlund, D.G., and Morgenstern, N.R. 1977. Stress state variables for unsaturated soils. Journal of the Geotechnical Engineering Division, ASCE, **103**(GT5): 447–466.
- Fredlund, D.G., and Rahardjo, H. 1993. Soil mechanics for unsaturated soils. Wiley Publications, New York.
- Fredlund, D.G., and Xing, A. 1994. Equations for the soil-water characteristic curve. Canadian Geotechnical Journal, **31**: 521–532.
- Fredlund, D.G., Morgenstern, N.R., and Widger, R.A. 1978. The shear strength of unsaturated soils. Canadian Geotechnical Journal, **15**: 313–321.
- Fung, Y.C. 1977. A first course in continuum mechanics. Prentice-Hall, Inc., Englewood Cliffs, N.J.
- Gan, J.K.M. 1986. Direct shear strength testing of unsaturated soils. M.Sc. thesis, Department of Civil Engineering, University of Saskatchewan, Saskatoon, Canada.
- Gan, J.K.M., and Fredlund, D.G. 1988. Multistage direct shear testing of unsaturated soils. Geotechnical Testing Journal, ASTM, **11**(2): 132–138.
- Gan, J.K.M., Fredlund, D.G., and Rahardjo, H. 1988. Determination of the shear strength parameters of an unsaturated soil using the direct shear test. Canadian Geotechnical Journal, **25**: 500–510.
- Gibbs, H.J., and Hilf, J.W. 1954. Discussion on: Leonards, G.A. (1953), Strength characteristics of compacted clays, Proceedings, American Society of Civil Engineers, Volume 79, Separate No. 360, pp. 360-1 – 360-45. Proceedings, American Society of Civil Engineers, Volume 80, Separate No. 518, pp. 518-9 – 518-34.
- Green, R.E., and Corey, J.C. 1971. Calculation of hydraulic conductivity: A further evaluation of some predicted methods. Soil Science Society of America Proceedings, **35**: 3–8.
- Karube, D. 1988. New concept of effective stress in unsaturated soil and its proving test. In Advanced Triaxial Testing of Soil and Rock. American Society for Testing and Materials: Philadelphia, Special Technical Publication No. 977, pp. 539–552.
- Krahn, J., and Fredlund, D.G. 1972. On total, matric and osmotic suction. Journal of Soil Science, **114**: 339–348.
- Lee, K.L., and Haley, S.C. 1968. Strength of compacted clay at high pressure. Journal of the Soil Mechanics and Foundations Engineering Division, ASCE, **94**(SM6): 1303–1329.
- McKee, C.R., and Bumb, A.C. 1987. Flow-testing coalbed methane production wells in the presence of water and gas. SPE Formation Evaluation, Dec, pp. 599–608.
- Rahardjo, H., Lim, T.T., Chang, M.F., and Fredlund, D.G. 1995. Shear strength characteristics of a residual soil. Canadian Geotechnical Journal, **32**: 60–77.
- Richards, B.G. 1965. Measurement of the free energy of soil moisture by the psychometric technique using thermistors. In Moisture Equilibria and Moisture Changes in Soils Beneath Covered Areas. A Symposium in print, Sydney, Australia. Edited by G.D. Aitchison. Butterworths & Co. Ltd., pp. 35–46.
- Ruddock, E.C. 1966. Correspondence: The engineering properties of residual soils. Géotechnique, **16**(1): 78–81.
- Russam, K. 1958. An investigation into the soil moisture conditions under roads in Trinidad, B.W.I. Géotechnique, **8**: 55–71.
- Toll, D.G. 1990. A framework for unsaturated soils behavior. Géotechnique, **40**(1): 31–44.
- Vanapalli, S.K. 1994. Simple test procedures and their interpretation in evaluating the shear strength of unsaturated soils. Ph.D. thesis, University of Saskatchewan, Saskatoon, SK, Canada.
- van Genuchten, M.Th. 1980. A closed-form equation of predicting the hydraulic conductivity of unsaturated soils. Soil Science Society of American Journal, **44**: 892–898.
- Walle, C.M., and Hachich, W. 1989. Rain-induced landslides in south eastern Brazil. Proceedings, 12th International Conference on Soil Mechanics and Foundation Engineering, Rio de Janeiro, Vol. 3, pp. 1639–1642.
- Wheele, S.J., and Sivakumar, V. 1995. An elastic-plastic critical state framework for unsaturated soil. Géotechnique, **45**: 35–53.
- White, N.F., Duke, H.R., Sunada, D.K., and Corey, A.T. 1970. Physics of desaturation in porous materials. Journal of the Irrigation and Drainage Division, ASCE, **96**(IR2): 165–191.
- Xing, A. 1993. CFVIEW — A curve fitting utility designed to fit soil-water characteristic curve data. Civil Engineering Department, University of Saskatchewan, Saskatoon, Canada.

Increase in strength due to suction for two Hong Kong soils

D.Y.F. Ho and D.G. Fredlund

Abstract: The surficial, residual soils of Hong Kong are unsaturated *in situ*, having negative pore-water pressures which contribute to their strength. The major geotechnical problem in Hong Kong is the stability of natural slopes of decomposed granite and decomposed volcanics (rhyolite). For many years, the stability of these extremely steep slopes has been attributed to matric suction (i.e., the negative pore-water pressure in the soil); however, the significance of suction has never been quantified.

The paper presents the results of the measurement of the shear strength parameters of the two mentioned Hong Kong residual soils and quantitatively interprets their significance in the light of the slope stability problem. More specifically, the paper deals with the relationship between soil suction and shear strength for the Hong Kong soils.

The testing program involved multi-stage triaxial tests. This procedure was chosen to eliminate the effect of the variability of residual soils. Seventeen 2 1/2 inch diameter, undisturbed samples were tested, including ten decomposed granites and seven decomposed volcanics (rhyolite). During the test, air and water pressures were controlled to maintain constant suction in the soil specimen throughout any stage of the test. With a 5 bar, high air entry disk installed at the bottom of a modified triaxial cell, the axis-translation technique was used to control the matric suction in the specimen.

The unsaturated soil shear strength theory of Fredlund et al. (1978) was used as basis for the interpretation of data.

The paper concludes that the increase in strength due to suction, $(u_a - u_w)$, can be evaluated from a single triaxial test using the multistage procedure. The most convenient form for expressing the increase in shear strength due to suction is as an increase in the cohesion:

$$c = c' + (u_a - u_w) \tan \phi^b$$

where:

$$c = \text{total cohesion of the soil.}$$

In other words, the suction in an unsaturated soil increases the cohesion of the soil. Accordingly, the shear strength parameters used in a slope stability analysis should be modified to reflect the *in situ* soil suction conditions.

Key words: unsaturated soil, matric suction, cohesion, shear strength, Hong Kong soils, triaxial test, slope stability, axis translation technique.

Introduction

Slope failures are common in Hong Kong. In general, most of the natural slopes in Hong Kong have soils that are desiccated to a considerable depth and the water table is far below ground surface. These steep slopes stand well in dry seasons but collapse when there is continuing precipitation. Traditionally, Janbu's et al. (1956) simplified method and saturated soil shear strength parameters, (i.e.,

the effective cohesion, c' , and the effective friction angle, ϕ'), are used in slope stability analyses.

The computed factor of safety often gives values that are less than 1.0, even for stable slopes. In other words, either there is a deficiency in the method of analysis or else there is a deficiency in the procedure used to evaluate the shear strength parameters.

Through a parametric study of various methods of slope stability analyses, Ching (1981) demonstrated that the quantitative difference between factors of safety computed using different methods appears to be of secondary significance for the Hong Kong conditions. However, an increase in the input cohesion parameter in a stability analysis significantly increases the computed factor of safety. Fredlund (1979) suggested that the suction of a soil could be considered as an increase in cohesion. This suggests that soil suction may be a significant factor in the stability of slopes in Hong Kong (Fredlund 1981). In other words, the slopes are stable because of the exist-

D.Y.F. Ho. Geotechnical Engineer, Fugro (Hong Kong) Ltd., 105 Asian House, 1 Hennessy Road, Hong Kong.

D.G. Fredlund. Professor, Department of Civil Engineering, University of Saskatchewan, 57 Campus Drive, Saskatoon, SK, S7N 5A9 Canada.

Reproduced with permission from the *Proceedings, ASCE Geotechnical Conference on Engineering and Construction in Tropical and Residual Soils*, Honolulu, Hawaii, 1982. pp. 263–295.

ence of suction and become unstable if soil suction is negated.

This paper presents the results of the measurement of the shear strength parameters of two commonly found Hong Kong residual soils and interprets their significance in view of the slope stability problem. More specifically, the paper deals with the relationship between soil suction and shear strength for the Hong Kong residual soils.

The shear strength theory for unsaturated soils

Fredlund et al. (1978) proposed a shear strength equation for unsaturated soils which was an extension of the commonly used Mohr-Coulomb equation (Terzaghi 1936) for saturated soils. In the extended form of the Mohr-Coulomb equation, the effect of matric suction, $(u_a - u_w)$, is assumed to yield a linear increase in shear strength. When $(\sigma - u_a)$ and $(u_a - u_w)$ are used as the stress state variables, the proposed unsaturated soil shear strength equation is as follows:

$$[1] \quad \tau = c' + (\sigma - u_a) \tan \phi' + (u_a - u_w) \tan \phi^b$$

The friction angle, ϕ^b , is equal to the slope of the plot of matric suction, $(u_a - u_w)$, versus shear strength, when $(\sigma - u_a)$ is held constant. The form of the equation describes a plane on a three-dimensional plot (Fig. 1). The stress circles corresponding to the failure conditions can be plotted on a three-dimensional diagram with the two stress state variables plotted on the horizontal axes and the shear strength as the ordinate (Fig. 2). Test data can be interpreted by either a mathematical (Fredlund et al. 1978) or a graphical method (Fredlund 1981; Ho 1981). The interpretation of the data is easier to visualize using the graphical method and for this reason will be used throughout this paper.

Using the graphical method, the equation can be visualized as a two-dimensional graph with matric suction contoured as the third variable (Fig. 3a). Consequently, the ordinate intercepts of the various matric suction contours (i.e., when $(\sigma - u_a)$ is equal to zero) can be plotted versus matric suction to give the friction angle, ϕ^b (Fig. 3b).

There is a smooth transition from Fredlund et al. (1978) unsaturated soil shear strength equation to the conventional shear strength equation for saturated soils (Terzaghi 1936). As saturation is approached, the pore-air pressure, u_a , becomes equal to the pore-water pressure, u_w . At this condition, the proposed equation reverts to the conventional shear strength equation for a saturated soil.

Verification of the shear strength theory for unsaturated soils

The justification for the linear form of the unsaturated soil shear strength equation must be verified by experimental laboratory test data.

Bishop et al. (1960) presented several sets of triaxial test data for unsaturated soils. Two sets of data were from

Fig. 1. Graphical representation of the shear strength equation for unsaturated soils.

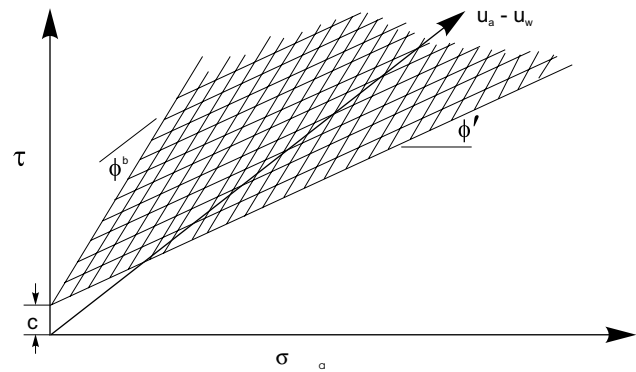
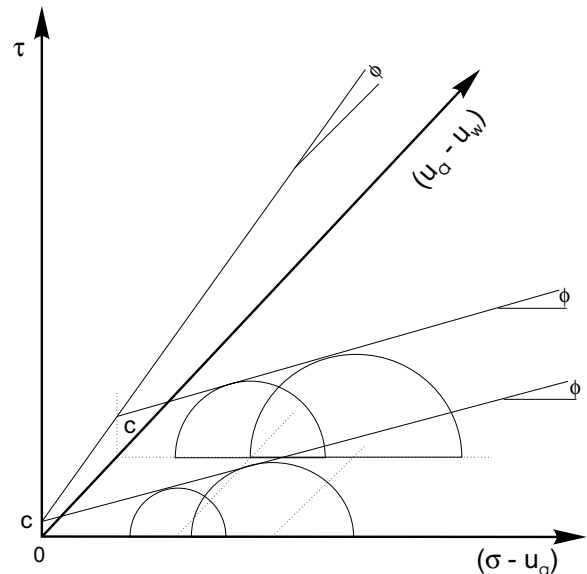


Fig. 2. Three-dimensional failure surface using stress variables $(\sigma - u_a)$ and $(u_a - u_w)$.



constant water content tests with pore-air and pore-water pressure measurements. The soils tested were compacted shale and a Boulder clay. The data have been reanalysed using the mathematical and graphical methods (Fredlund et al. 1978; Ho 1981). The results are summarized in Table 1.

It can be seen that the correlation coefficients for the ordinate intercepts versus matric suction plots are high (i.e., between 0.97 and 0.98). If the surface describing stress combinations at failure were ideally planar, the ordinate intercepts versus matric suction plot should be a straight line having a correlation coefficient of 1.0.

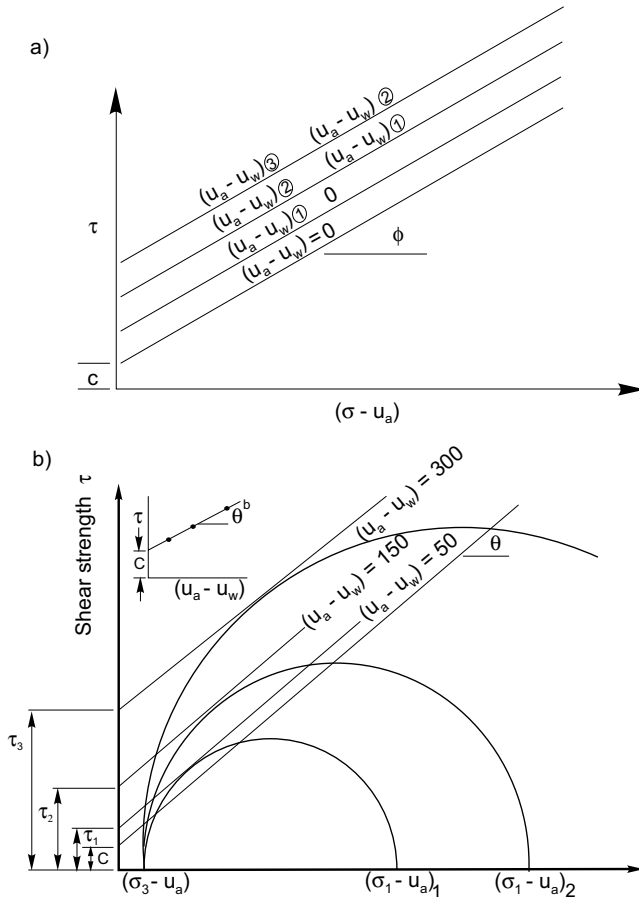
Satija (1978) initiated an extensive laboratory testing program on statically compacted Dhanauri clay. Four series of constant water content (CW) and consolidated drained (CD) tests were conducted with pore-air and pore-water pressure measurements. The soil was compacted at two densities but with the same initial water contents. Both the constant water content and consolidated drained tests were performed at each of the com-

Table 1. Triaxial tests on unsaturated soils (Bishop et al. 1960).

Soil type	c' (kPa)	ϕ' (degrees)	ϕ^b (degrees)	Correlation coefficients*
Compacted shale $w = 18.6\%$	15.8	24.8	18.1	0.970
Boulder clay $w = 11.6\%$	9.6	27.3	21.7	0.974

* Correlation coefficient is for the computation of ϕ^b .

Fig. 3. a) Failure surface of an unsaturated soil looking parallel to the $(u_a - u_w)$ axis; b) Interpretation of a multi-stage triaxial test to get the angle of friction with respect to matric suction.



paction conditions. Although the specimens for a particular series of tests were compacted at the same density and water content, they were allowed to equalize to various initial stress states to form an equally spaced grid of tests on a three-dimensional surface. The original data have been reanalysed using the graphical method (Ho 1981). Figure 4a shows the failure stress circles for one series of the constant water content tests performed on specimens with a high initial density. The shear strength versus matric suction plot for all the constant water content tests on the high initial density specimens is shown in Fig. 4b. The results are summarized in Table 2. The correlation coefficients for all the ordinate intercepts versus matric suction plots are high and reveal no tendency

for warping of the failure surface except at low suctions, less than 100 kPa.

Escario (1980) performed direct shear tests with pore pressure controls on compacted Madrid Gray clay. The tests results are shown in Fig. 5a. The results have been reanalysed using the graphical method (Ho 1981) and show a ϕ^b angle of 16.1 degrees (Fig. 5b). The correlation coefficient is high and there is no indication of warping of the surface describing the stress combinations at failure (Fig. 5b).

To date, the published test data demonstrates that the surface describing the stress combination of failure for an unsaturated soil is essentially planar. Although the failure surface could possibly be somewhat curved, especially at low suction, it appears to be sufficiently close to being planar that the unsaturated soil shear strength theory as per Fredlund et al. (1978) is satisfactory for engineering purposes.

Test Program

The two most commonly found Hong Kong residual soils, decomposed granite and rhyolite, were tested in the laboratory program. The mineral compositions of these two residual soils are essentially the same, including quartz, orthoclase, plagioclase and biotite. The main difference between the two soils is their grain size distribution. In general, the decomposed granite has a sand size texture, whereas the decomposed rhyolite has a medium to fine silt size texture. Both residual soils are brittle and highly variable (Lumb 1962, 1965). Undisturbed specimens were obtained from test drilling (using the Fugro sampler) or open cuts (using block samples) at various sites on the Hong Kong island (Table 3).

The test program consisted of triaxial shear tests on both decomposed granite and rhyolite. Seventeen, 2½ inch (6.35 cm) diameter, undisturbed specimens were tested with ten of the specimens being decomposed granite and seven of the specimens being decomposed rhyolite. The test procedure involved the control of the air and water pressures during the entire test rather than their measurements in a closed system (Bishop and Henkel 1962). Since the decomposed granite and rhyolite are comparatively coarse-grained with high coefficients of permeability (Lumb 1965), it is possible to maintain the pore-air and pore-water pressures constant during the application of the deviator stress. The testing procedure is similar to performing a “slow” or drained test on a saturated soil. A 5 bar (i.e., 505 kPa) high air entry disk was sealed into the bottom pedestal of a modified conventional triaxial cell (Fig. 6) in order to separately control

Table 2. Triaxial tests on unsaturated Dhanauri Clay (Satija 1978).

Soil type	c' (kPa)	ϕ' (degrees)	ϕ^b (degrees)	Correlation coefficients*
CD test $\gamma_d = 15.5 \text{ kN/m}^3$ $w = 22.2\%$	37.3	28.5	16.2	0.974
CD test $\gamma_d = 14.5 \text{ kN/m}^3$ $w = 22.2\%$	20.3	29.0	12.6	0.963
CW test $\gamma_d = 15.5 \text{ kN/m}^3$ $w = 22.2\%$	15.5	28.5	22.6	0.992
CW test $\gamma_d = 14.5 \text{ kN/m}^3$ $w = 22.2\%$	11.3	29.0	16.5	0.971

*Refers to the best-fit line for ϕ^b .

Fig. 4. a) Mohr failure circles for Dhanauri Clay with high as-compacted density from CW tests, Series 3; b) Shear strength versus matric suction for Dhanauri Clay with high as-compacted density from CW tests (from Satija 1978).

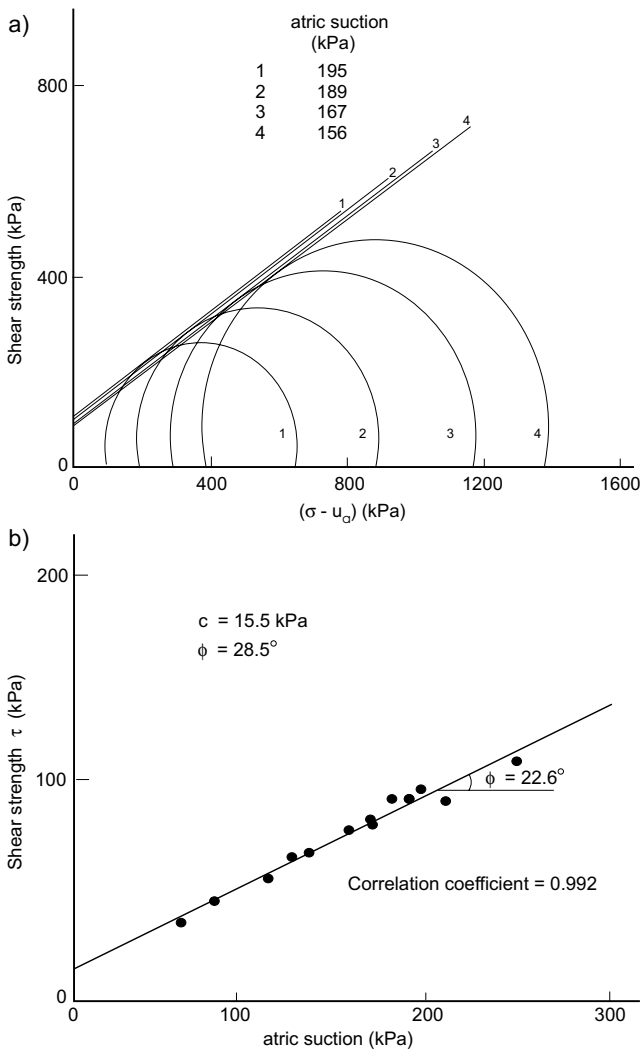


Fig. 5. a) Shear strength of Madrid Grey Clay at various suction levels; b) Shear strength versus matric suction of Madrid Grey Clay (after Escario 1980).

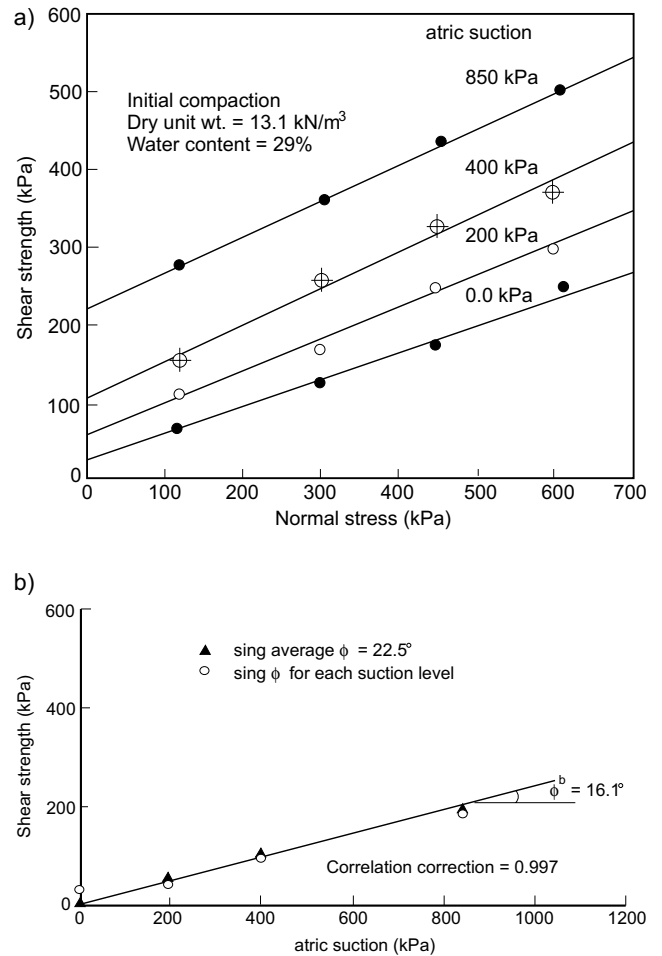


Table 3. Summary of undisturbed specimens used in the test program.

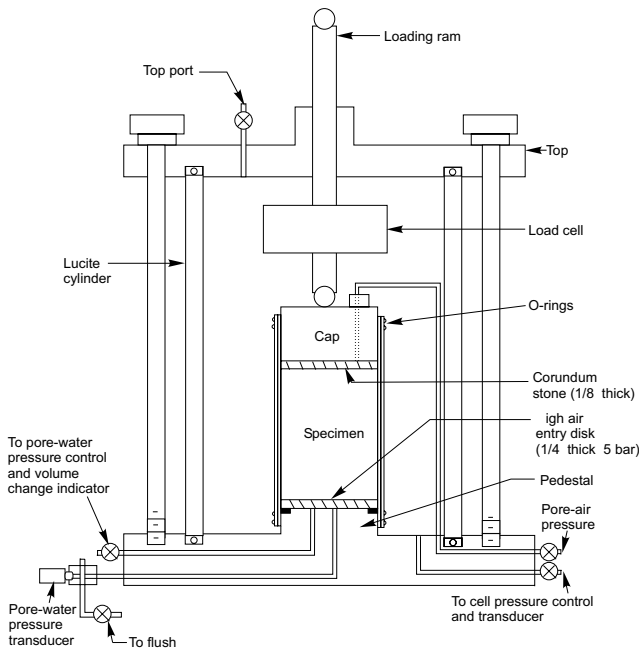
Sample No.	Location	Fugro sampler blowcount	Description of soil sample
5	Hong Kong Hospital and Sanatorium, Happy Valley (depth = 10.15 m)	27	Brownish pink, dense, slightly clayey, sandy silt with some fine gravel. (Completely weathered granite)
6	Hong Kong Hospital and Sanatorium, Happy Valley (depth = 4.65 m)	42	Pink with grey spots, dense to very dense, silt and sand with some fine gravel. (Completely to highly weathered granite)
8	Hong Kong Hospital and Sanatorium, Happy Valley (depth = 14.15 m)	63	Pink with grey spots, dense, sandy silt with some fine gravel. (Completely weathered granite)
10	Hong Kong Hospital and Sanatorium, Happy Valley (depth = 4.15 m)	12	Brownish pink, medium dense, slightly clayey, sandy silt with some fine gravel. (Completely weathered granite)
11A 11B 11C 11D	Thorpe Manor Site, Hong Kong (depth = 10.15 m to 10.38 m)	Block Sample	Brownish, medium to fine, slightly clayey, sandy silt. (Decomposed volcanic rock)
12	9 Brewin Path, Hong Kong (depth = 15.0 m to 15.3 m)	65	Light yellowish grey with some white, dense (slightly clayey), silt and fine sand (with some medium and coarse sand). (Completely weathered volcanic rock)
14	9 Brewin Path, Hong Kong (depth = 16.5 m to 16.8 m)	74	Light yellowish grey with some white, dense (slightly clayey), silt and fine sand (with some medium and coarse sand). (Completely weathered volcanic rock)
16	Chun Fai Road, Jardine's Lookout, Hong Kong (depth = 7.5 m to 7.95 m)	87	Yellowish brown, dense silty sand with some fine gravel. (Completely weathered granite)
17	Chun Fai Road, Jardine's Lookout, Hong Kong (depth = 6.0 m to 6.45 m)	23	Orange brown, medium dense sandy silt. (Completely weathered granite)
20	97 Robinson Road, Hong Kong (depth = 22.0 m to 22.3 m)	35	Reddish brown, silty sand with patches of white, plastic, fine clay. (Completely weathered granite)
21	97 Robinson Road, Hong Kong (depth = 14.0 m to 14.3 m)	53	Reddish brown, silty sand with patches of white, plastic, fine clay. (Granitic residual soil)
22	97 Robinson Road, Hong Kong (depth = 4.0 m to 4.3 m)	16	Reddish brown with dark green and white specks, sandy silt with some fine gravel and patches of plastic clay. (Granite residual soil)
23	Chun Fai Road, Jardine's Lookout, Hong Kong (depth = 10.5 m to 10.95 m)	49	Yellowish brown with dark green specks, dense sandy silt. (Completely weathered granite)

the pore-air and pore-water pressures. The axis-translation technique (Bocking and Fredlund 1980) was used to impose suctions higher than one atmosphere in the specimen. During the test, the air and water pressures were controlled so as to maintain constant suction in the specimen throughout each stage of the test.

In order to obtain the maximum amount of information from a limited number of tests and eliminate the effect of variability in residual soils, a multi-stage type of test procedures was used (Kenny and Watson 1961; Lumb 1964; Wong 1978). The test procedure was as follows:

- (1) The specimen was trimmed for testing. The specimens were 2½ inches (6.35 cm) in diameter and approximately 5½ inches (14.0 cm) long.
- (2) The specimen was mounted in the triaxial cell (Fig. 6) and two rubber membranes were placed around the specimen.
- (3) O-rings were placed over the membranes on the bottom pedestal and a spacer was placed between the membranes and the loading cap in order that air within the specimen could escape during the saturation process.
- (4) To ensure that the suction applied to the specimen for Stage 1 testing was greater than the initial soil suction, the specimens were saturated by allowing the intake of water. De-aired water was added to the specimen through the air pressure line connected to the loading cap.

Fig. 6. Modified triaxial cell for testing unsaturated soils.



- (5) Once the specimens had fully imbibed water, the top O-rings were placed around the loading cap.
- (6) The stress associated with the first stage of testing (i.e., Stage 1) were applied and the specimen was allowed to consolidate. A typical set of stresses for Stage 1, 2 and 3 is as follows:

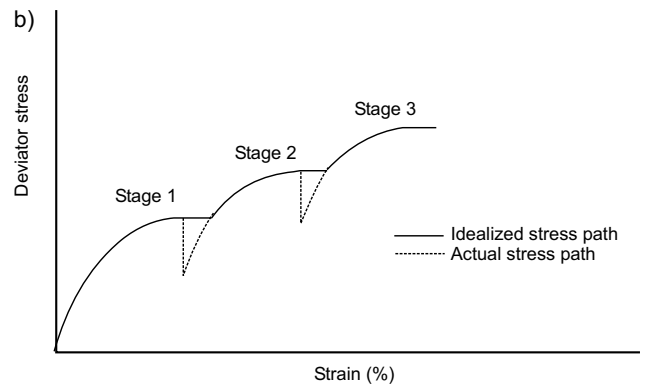
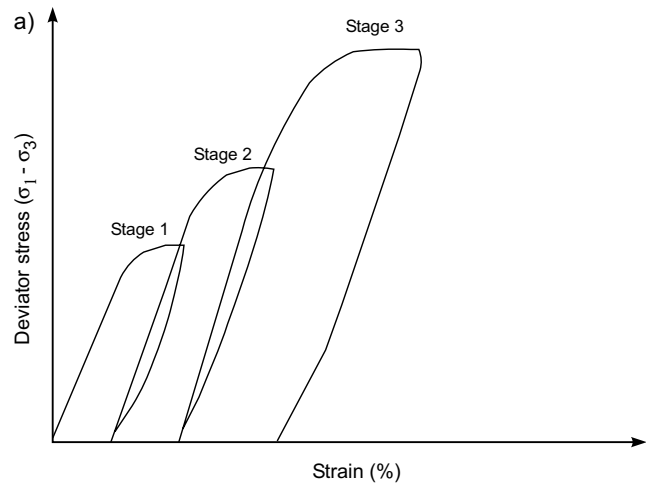
Stage No.	σ_a (kPa)	u_a (kPa)	u_w (kPa)
1	250	100	50
2	350	200	50
3	500	350	50

The associated stress state variables are:

Stage No.	$(\sigma_3 - u_a)$ (kPa)	$(u_a - u_w)$ (kPa)
1	150	50
2	150	150
3	150	300

- (7) After consolidation was complete, the stresses were maintained while the specimen was loaded at a constant strain rate. A typical loading rate was 0.001 per cent strain per minute (Ho 1981).
- (8) Two kinds of loading procedure (i.e., the cyclic and sustained loading) were used. Once the deviator stress reached a peak value, the applied vertical load was either released (i.e., cyclic loading) or sustained (i.e., sustained loading), (Fig. 7a and 7b), (Ho 1981).

Fig. 7. a) Ideal stress versus strain curves for a multi-stage test using the cyclic loading procedure; b) Ideal stress versus strain curves for a multi-stage test using the saturated loading procedure.



- (9) A new set of stresses for Stage 2 was applied to the specimen, consolidation was again allowed and the loading process was repeated as before.
- (10) The above procedure was further applied to Stage 3.

Presentation of Data

Stress measurements made in the multi-stage triaxial tests are summarized in Table 4. The stress σ_1 was computed from the measured load and calculated cross-sectional area. Deviator stress versus strain plots for six decomposed granite and six decomposed rhyolite specimens are presented in Figs. 8a to 13b.

In general, the deviator stress of most of the specimens dropped off significantly immediately after peaking in Stage 3. The specimens seemed to show signs of structural breakdown or collapse in the third stage of loading. The amount of strength “drop-off” in Stage 3 appeared to be related to the amount of accumulated strain. Problems associated with excessive deformation in multi-stage triaxial tests have been noted by other researchers (Kenny

Table 4. Stress measurements made in the multi-stage triaxial tests.

	σ ()	u_a ()	u_w (kPa)	σ ()	$(\sigma_3 - u_a)$ ()	$(\sigma_1 - u_a)$ ()	$\frac{(\sigma_1 - \sigma_3)}{2}$ (kPa)	$(u_a - u_w)$ ()	$\frac{(\sigma_1 + \sigma_3)}{2} - u_a$ (kPa)
1	206.9	68.9	68.95	613.7	137.9	544.7	203.4	0.0	341.3
2	448.2	310.3	68.95	1102.0	137.9	791.2	326.7	214.3	464.6
3	689.5	551.6	68.95	1496.0	137.9	944.6	403.4	482.2	541.3
1	241.3	103.4	68.95	794.8	137.9	691.4	276.8	34.5	414.7
2	344.8	206.9	68.95	1019.0	137.9	811.8	336.9	137.9	474.9
3	517.1	310.3	68.95	1636.0	137.9	1325.0	599.3	241.3	766.2
1	241.3	103.4	68.95	976.9	137.9	873.5	367.8	34.5	505.7
2	344.8	206.9	68.95	1179.0	137.9	972.1	417.1	137.9	554.9
3	517.1	310.3	68.95	1639.0	137.9	1328.0	560.8	241.3	767.6
1	241.3	103.4	68.95	725.4	137.9	621.9	242.0	34.5	379.9
2	344.8	206.9	68.95	952.3	137.9	745.5	303.8	137.9	441.2
3	448.2	310.3	68.95	1143.0	137.9	833.1	347.6	241.3	485.5
1	241.3	103.4	68.95	747.8	137.9	644.4	253.3	34.5	391.2
2	344.8	206.9	68.95	946.9	137.9	740.0	301.0	137.9	438.9
3	448.2	310.3	68.95	1120.0	137.9	809.4	335.8	241.3	473.7
1	241.3	103.4	68.95	875.0	137.9	771.6	316.9	34.5	454.8
2	344.8	206.9	68.95	1083.0	137.9	875.6	368.9	137.9	506.8
3	448.2	310.3	68.95	1221.0	137.9	910.9	386.5	241.3	524.4
1	241.3	103.4	68.95	790.9	137.9	687.5	274.8	34.5	412.7
2	344.8	206.9	68.95	1020.0	137.9	813.5	337.8	137.9	475.7
3	448.2	310.3	68.95	1210.0	137.9	899.4	380.8	241.3	518.7
1	241.3	103.4	68.95	855.7	137.9	752.3	307.2	34.5	445.1
2	344.8	206.9	68.95	1080.0	137.9	873.3	367.7	137.9	505.6
3	448.2	310.3	68.95	1298.0	137.9	987.9	425.0	241.3	562.9
1	137.9	103.4	68.95	288.9	34.48	185.5	75.5	34.5	109.9
2	241.3	206.9	68.95	530.2	34.48	323.4	144.5	137.9	178.9
3	344.8	310.3	68.95	680.8	34.48	370.5	168.0	241.3	202.5
1	137.9	103.4	68.95	313.3	34.48	209.9	87.7	34.5	122.2
2	241.3	206.9	68.95	542.6	34.48	335.8	150.6	137.9	185.1
3	344.8	310.3	68.95	681.5	34.48	371.2	168.4	241.3	202.8
1	137.9	103.4	68.95	292.4	34.48	188.9	77.3	34.5	111.7
2	241.3	206.9	68.95	607.1	34.48	400.3	182.9	137.9	217.4
3	344.8	310.3	68.95	754.8	34.48	444.5	205.0	241.3	239.5
1	137.9	103.4	68.95	694.0	34.48	590.6	278.1	34.5	312.5
2	172.4	206.9	68.95	753.8	34.48	615.9	290.7	137.9	325.2
3	241.3	310.3	68.95	786.3	34.48	579.5	272.5	241.3	306.9
1	137.9	103.4	68.95	449.9	34.48	346.5	156.0	34.5	190.5
2	172.4	206.9	68.95	494.4	34.48	356.5	161.0	137.9	195.5
3	241.3	310.3	68.95	543.3	34.48	335.5	151.0	241.3	185.5
1	137.9	103.4	68.95	426.2	34.48	322.8	144.2	34.5	178.6
2	172.4	206.9	68.95	507.8	34.48	369.9	167.7	137.9	202.2
3	241.3	310.3	68.95	620.1	34.48	413.3	189.4	241.3	223.9
1	137.9	103.4	68.95	437.9	34.48	334.5	150.0	34.5	184.5
2	172.4	206.9	68.95	492.4	34.48	354.5	160.0	137.9	184.5
3	241.3	310.3	68.95	626.4	34.48	419.5	192.6	241.3	227.0
1	137.9	103.4	68.95	343.9	34.48	240.5	103.0	34.5	137.5
2	172.4	206.9	68.95	441.1	34.48	303.2	134.4	137.9	168.8
3	241.3	310.3	68.95	608.0	34.48	401.2	183.2	241.3	217.8
1	137.9	103.4	68.95	747.4	34.48	643.9	304.8	34.5	339.2
2	172.4	206.9	68.95	805.6	34.48	667.7	316.6	137.9	351.1
3	241.3	310.3	68.95	905.8	34.48	698.0	332.3	241.3	366.7

Fig. 8. *a)* Stress versus strain curves for decomposed granite (Sample No. 5); *b)* Stress versus strain curves for decomposed granite (Sample No. 10).

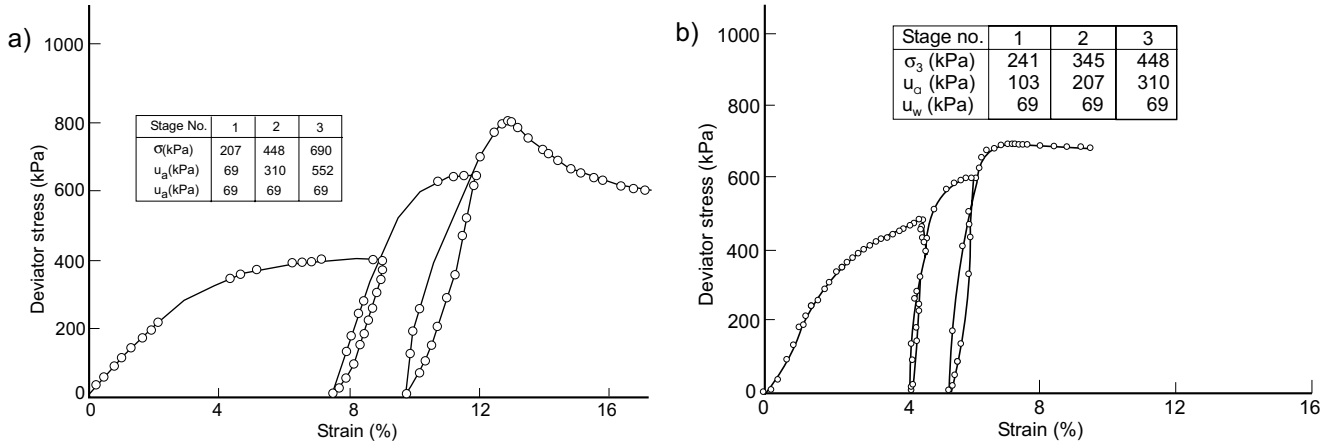


Fig. 9. *a)* Stress versus strain curves for decomposed granite (Sample No. 16); *b)* Stress versus strain curves for decomposed granite (Sample No. 20).

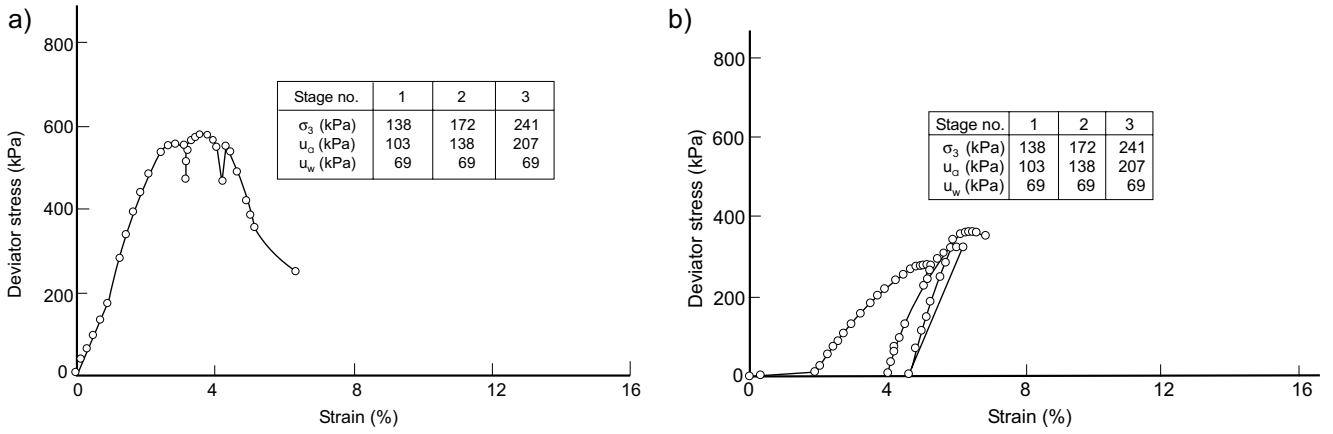
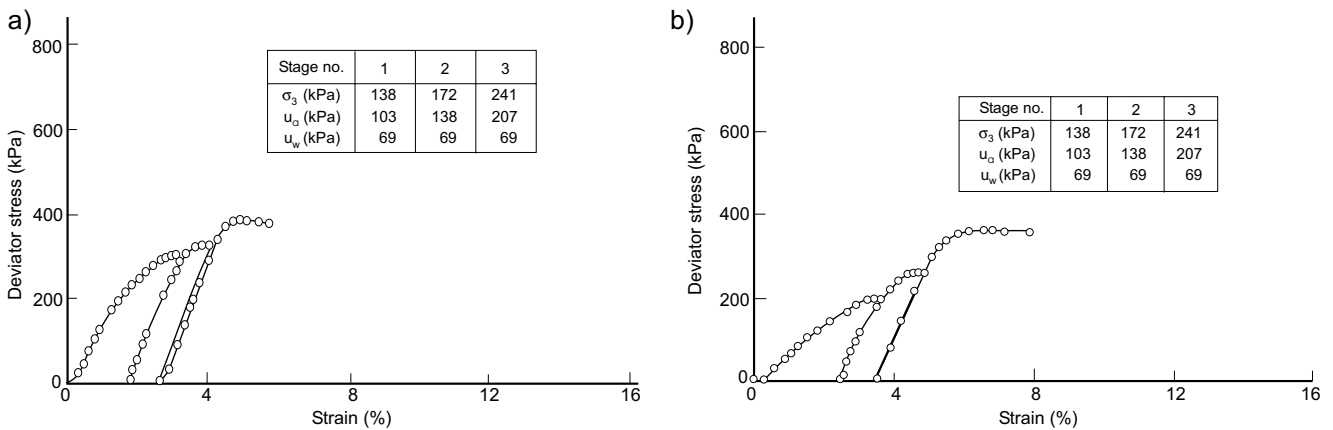


Fig. 10. *a)* Stress versus strain curves for decomposed granite (Sample No. 21); *b)* Stress versus strain curves for decomposed granite (Sample No. 22).



and Watson 1961; Wong 1978). It is suggested that the specimen should not be deformed excessively during the earlier stage of loading. When the specimen is overstrained, the specimen will tend to develop a shear failure

plane and undergo a strength decrease. The measured strength will then tend towards the ultimate shear strength. Therefore strain accumulation can be a problem to multi-stage testing.

Fig. 11. *a)* Stress versus strain curves for decomposed rheolite (Sample No. 11A); *b)* Stress versus strain curves for decomposed rheolite (Sample No. 11B).

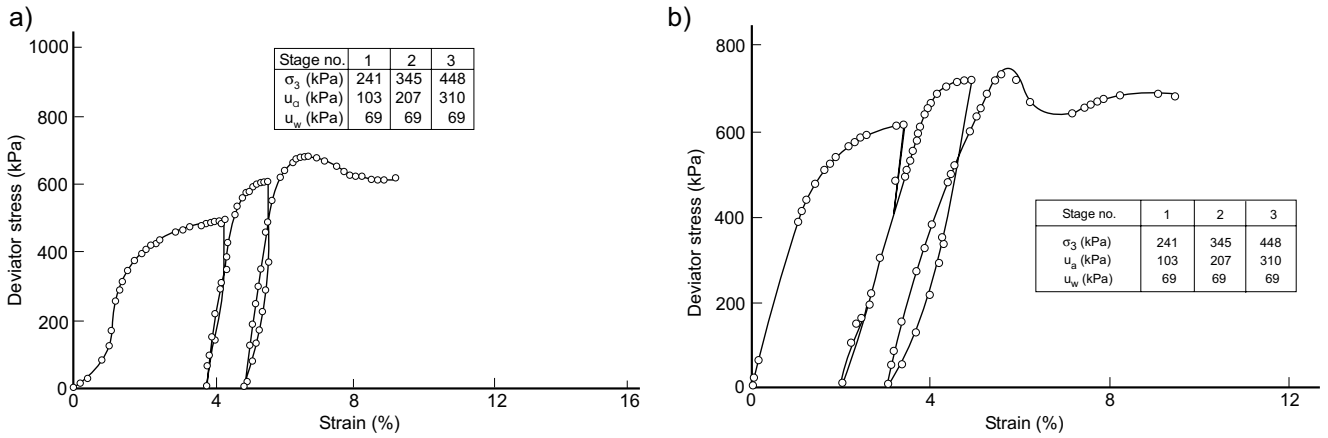


Fig. 12. *a)* Stress versus strain curves for decomposed rheolite (Sample No. 11C); *b)* Stress versus strain curves for decomposed rheolite (Sample No. 11D).

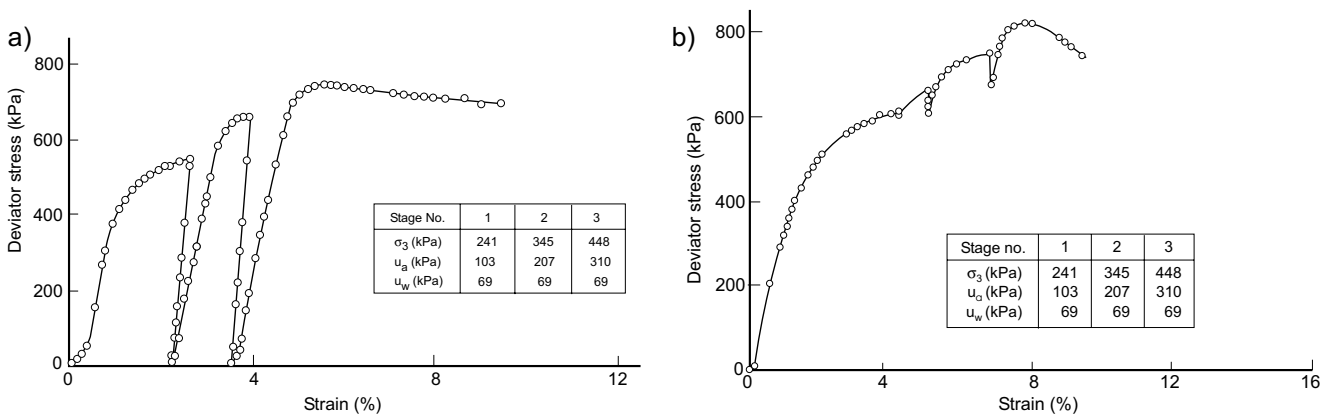
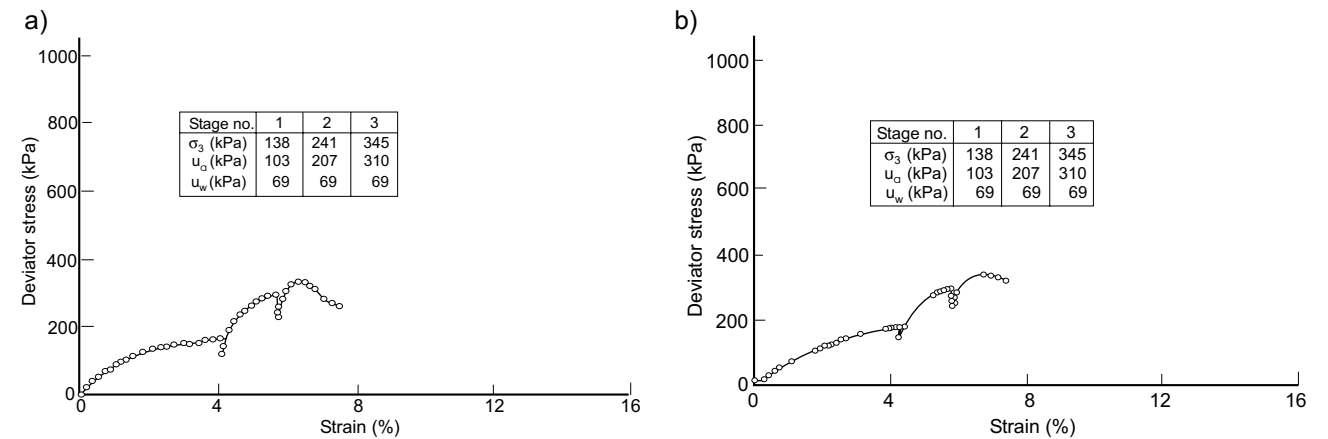


Fig. 13. *a)* Stress versus strain curves for decomposed rheolite (Sample No. 12); *b)* Stress versus strain curves for decomposed rheolite (Sample No. 14).



The cyclic loading procedure is preferable to the sustained loading procedure in reducing accumulated strain in the specimen. The advantages associated with releasing the applied deviator stress between stages are as fol-

lows. First, it prevents further straining of the soil structure under sustained loading. Second, part of the accumulated strain can be restored through elastic recovery (Figs. 8a, 8b and 9b to 12a). If the load on the speci-

Table 5a. Summary of the unsaturated shear strength parameters for the decomposed granite samples (by the graphical method).

Sample No.	5	6	8	10	16	17	20	21	22	23
ϕ^b (degrees)	12.4	27.4	14.6	16.2	11.5	4.2	12.5	12.6	22.5	8.0

* Outlier (ignored).

** ϕ' (input) = 33.4° (Fugro data)***; c' (input) = 28.9 kPa (Fugro data)***.

***Fugro (Hong Kong) Limited, Unpublished Site Investigation Report for 14–23 Fung Fai Terrace, Hong Kong, 1979.

Table 5b. Summary of the unsaturated shear strength parameters for the decomposed rhyolite samples (by the graphical method).

Sample No.	11A	11B	11C	11D	12	14	15
ϕ^b (degrees)	11.7	10.9	15.9	15.4	13.3	11.7	17.7

* ϕ' (input) = 35.3° (Fugro data)**; c' (input) = 7.35 kPa (Fugro data)**.

** Fugro(Hong Kong) Limited, Unpublished Site Investigation Report for 9 Brewin Path, Hong Kong, 1979.

men is sustained between stages, the specimen may continue to deform by creep (Fig. 9a).

Analysis of Results

The test data were analyzed in accordance with the unsaturated soil shear strength theory to establish the relationship between soil suction and shear strength. The unsaturated soil shear strength parameter, ϕ^b , is used as a means to quantify the effect of soil suction to the shear strength of the two Hong Kong residual soils. The graphical method was used to analyse the data. Plots showing the stress conditions of failure for each stage, as well as the interpretation of data for twelve of the specimens tested are shown in Figs. 14a to 19b. The relationship between matric suction and shear strength for each specimen is also shown on each figure. The results of all seventeen multi-stage triaxial tests are summarized in Tables 5a and 5b.

The average angle of friction with respect to matric suction, ϕ^b , is 15.3 degrees with a range from 8.0 degrees to 27.4 degrees and a standard deviation of ± 5.7 degrees for the decomposed granite. The average angle of friction with respect to matric suction is 13.8 degrees with a range from 10.9 degrees to 17.7 degrees and standard deviation of ± 2.4 degrees for the decomposed rhyolite. Much of the dispersion associated with the measured angles of friction, ϕ^b , are related to the learning associated with the new testing procedure. It is also recognized that some of the specimens were subjected to excessive strains in the last stage of testing.

As a multi-stage test progresses, the soil structure of a specimen is disturbed to some degree. The change in strength with increasing strain is demonstrated by observing the change in ϕ^b angle from Stage 1 to Stage 3. From the matric suction ($u_a - u_w$), versus shear strength plots, the angles of friction, ϕ^b , based on the Stage 2 and 3 data are summarized in Tables 6a and 6b.

Table 6a shows that there was an average ϕ^b reduction of 2.1 degrees for the decomposed granite. The comparable ϕ^b reduction for the decomposed rhyolite was 7.5 degrees. It is evident that there is a significant strength reduction in a specimen during the multi-stage shear test.

Based on the limited test data, it appears the rhyolite is more susceptible to the structural disturbance caused by multi-stage testing than the decomposed granite.

Conclusion

There is a definite relation between soil suction and shear strength for the Hong Kong residual soils. An increase in soil suction increases strength in accordance with the ϕ^b angle of friction. The proposed multistage triaxial testing procedure can be used to evaluate the increase in strength due to soil suction from a single test.

The average angle of friction with respect to matric suction, ϕ^b , is found to be 15.3 degrees with a standard deviation of ± 5.7 degrees for the decomposed granite. The average angle of friction with respect to matric suction, ϕ^b , is found to be 13.8 degrees with a standard deviation of ± 2.4 degrees for the decomposed rhyolite. When only the Stage 1 and 2 test results are considered, the average ϕ^b angle is 15.5 degrees with a standard deviation of ± 5.3 degrees for the decomposed granite. Similarly, the average ϕ^b angle is 17.6 degrees with a standard deviation of ± 4.9 degrees for the decomposed rhyolite.

In order to assess the *in situ* conditions of the Hong Kong residual soils, the effect of soil suction should be included in the evaluation of the shear strength. The effect of soil suction is of particular interest in the analysis of slope stability problems. The matric suction term in the shear strength equation for an unsaturated soil can be considered as contributing to the cohesion of the soil.

$$c = c' + (u_a - u_w) \tan \phi^b$$

where:

$$c = \text{total or apparent cohesion of the soil.}$$

In other words, the suction in an unsaturated soil increases the cohesion of an unsaturated soil. In this case, conventional soil shear strength concepts can be applied to practical slope stability problems.

Fig. 14. *a)* Graphical analysis for decomposed granite (Sample No. 5); *b)* Graphical analysis for decomposed granite (Sample No. 10).

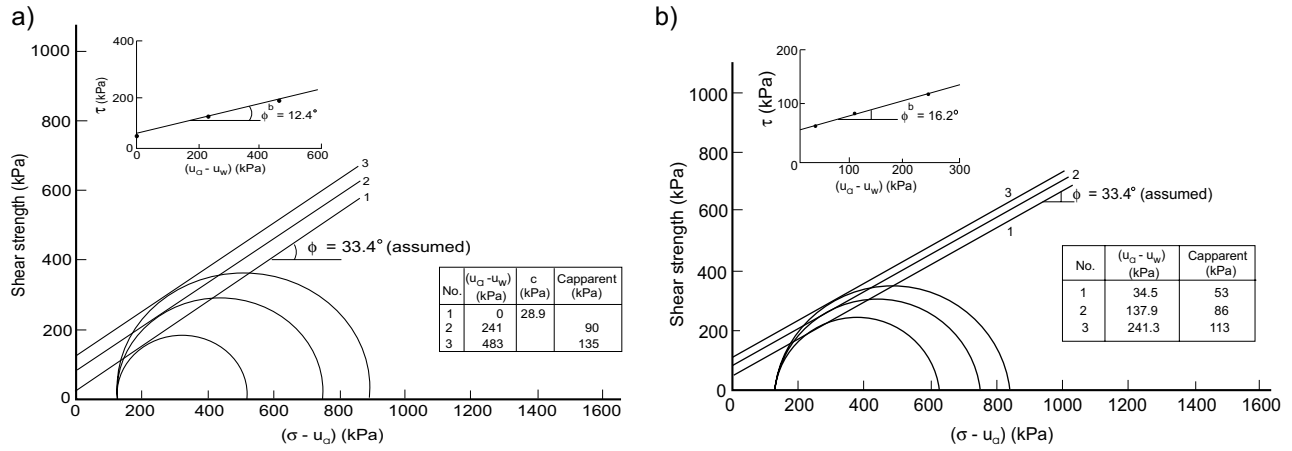


Fig. 15. *a)* Graphical analysis for decomposed granite (Sample No. 16); *b)* Graphical analysis for decomposed granite (Sample No. 20).

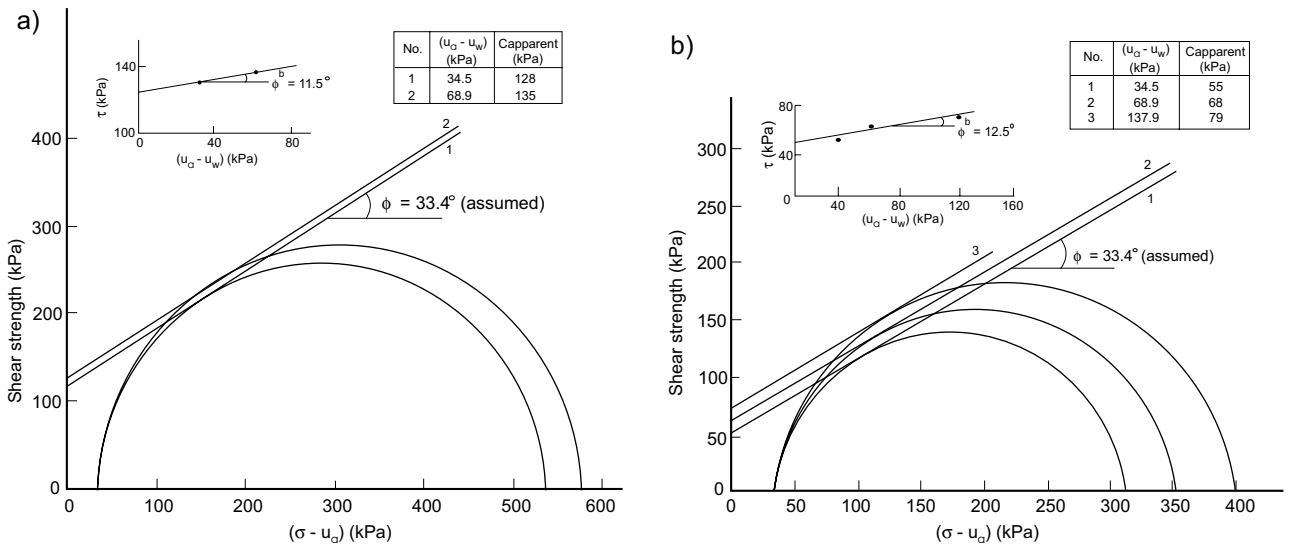


Fig. 16. *a)* Graphical analysis for decomposed granite (Sample No. 21); *b)* Graphical analysis for decomposed granite (Sample No. 22).

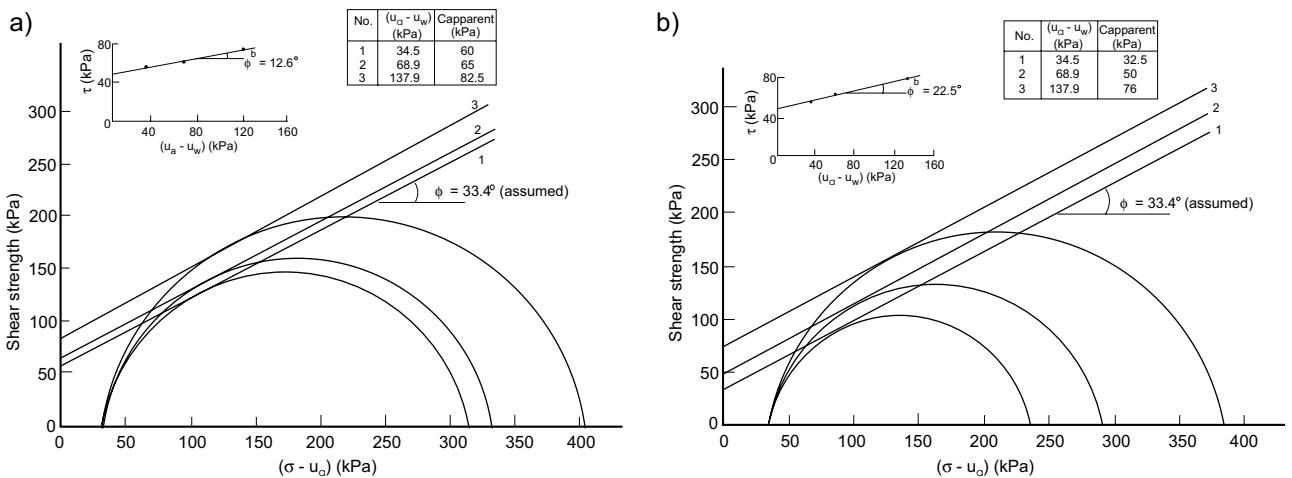


Fig. 17. *a)* Graphical analysis for decomposed rhyolite (Sample No. 11A); *b)* Graphical analysis for decomposed rhyolite (Sample No. 11B).

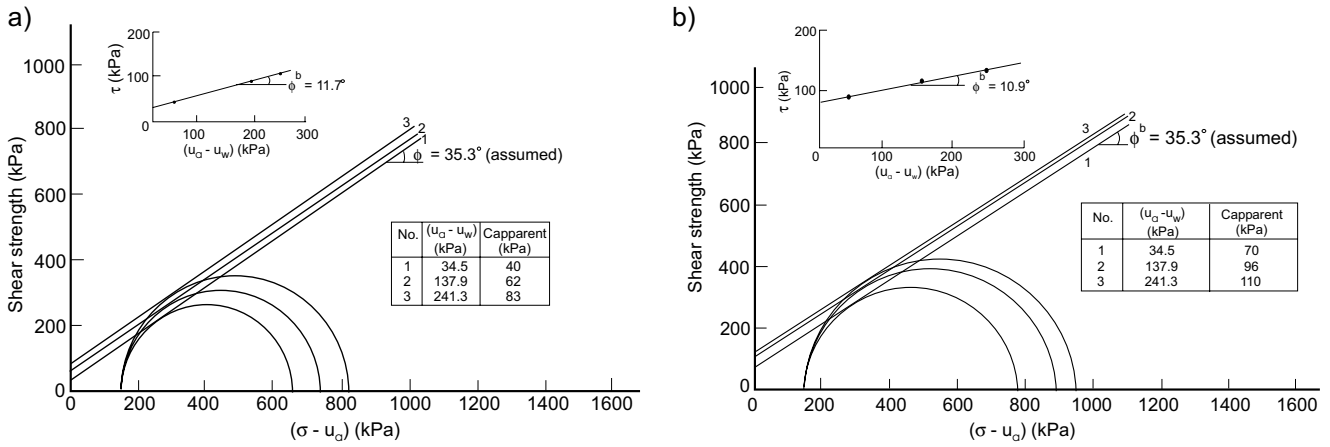


Fig. 18. *a)* Graphical analysis for decomposed rhyolite (Sample No. 11C); *b)* Graphical analysis for decomposed rhyolite (Sample No. 11D).

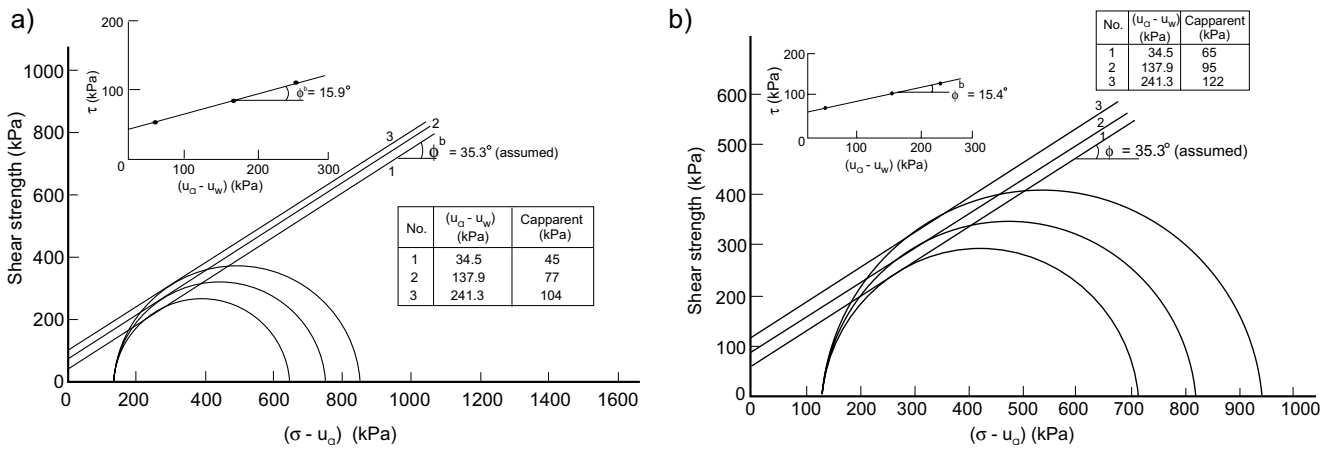


Fig. 19. *a)* Graphical analysis for decomposed rhyolite (Sample No. 12); *b)* Graphical analysis for decomposed rhyolite (Sample No. 14).

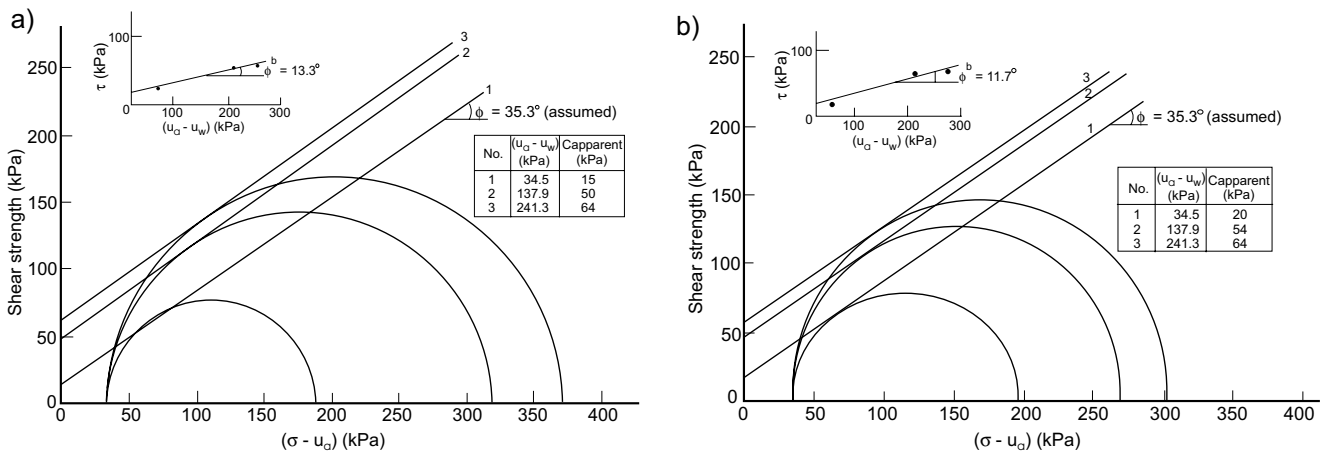


Table 6a. Comparison between ϕ^b values obtained using Stage 1 and 2 and Stage 2 and 3 data (for decomposed granite).

Sample No.	5	6	8	10	16	17	20	21	22	23	Ave.
$\phi_{1,2}^b$ (degrees)	15.0	15.5	13.0	18.5	11.5	4.5*	20.5	8.0	26.5	11.0	15.5 \pm 5.3**
$\phi_{2,3}^b$ (degrees)	10.0	37.0*	16.5	15.5	—	—	9.5	14.5	21.0	7.0	13.4 \pm 4.5**

* Outlier (ignored).

** Standard deviation.

Table 6b. Comparison between ϕ^b values obtained using Stage 1 and 2 and Stage 2 and 3 data (for decomposed rhyolite).

Sample No.	11A	11B	11C	11D	12	14	15	Ave.
$\phi_{1,2}^b$ (degrees)	11.0	14.0	18.0	15.5	18.5	18.0	28.0	17.6 \pm 4.9*
$\phi_{2,3}^b$ (degrees)	12.0	8.0	14.0	15.5	8.5	6.0	7.0	10.1 \pm 3.4

** Standard deviation.

Acknowledgements

The authors wish to thank the Fugro (Hong Kong) Ltd. for funding the described research work. The establishment of a research scholarship at the University of Saskatchewan has provided opportunity to be involved in a most interesting and challenging problem.

References

- Bishop, A.W., Alpan, I., Blight, G. E. and Donald, I. B. 1960. Factors controlling the strength of partly saturated cohesive soils. Proceedings, ASCE Research Conference on Shear Strength of Cohesive Soils, Boulder, Colorado, U.S.A., pp. 503–532.
- Bishop, A. W. and Henkel, D. J. 1962. The measurement of soil properties in the triaxial test. Second edition, Edward Arnold Ltd., London, England, 1962.
- Bocking, K.A., and Fredlund, D.G. 1980. Limitations of the axis-translation technique. Proceedings, 4th International Conference on Expansive Soils, ASCE, Denver, Colorado, U.S.A., pp. 117–135.
- Ching, R. 1981. A theoretical examination and practical applications of the limit equilibrium methods to slope stability problems. M.Sc. thesis, University of Saskatchewan, Saskatoon, SK, Canada.
- Escario, V. 1980. Suction controlled penetration and shear tests. Proceedings, 4th International Conference on Expansive Soils, ASCE, Denver, Colorado, U.S.A., Vol. 2, pp. 781–797.
- Fredlund, D. G. 1979. Second Canadian geotechnical colloquium: Appropriate concepts and technology for unsaturated soils. Canadian Geotechnical Journal, **16**(1): 121–139.
- Fredlund, D. G. 1981. The shear strength of unsaturated soils and its relationship to slope stability problems in Hong Kong. The Hong Kong Engineer, Journal of the Hong Kong Institution of Engineers, **9**(4): 37–45.
- Fredlund, D.G., Morgenstern, N.R., and Widger, A. 1978. Shear strength of unsaturated soils. Canadian Geotechnical Journal, **15**(3): 313–321.
- Ho, D.Y.F. 1981. The shear strength of unsaturated Hong Kong soils. M.Sc. thesis, University of Saskatchewan, Saskatoon, SK, Canada.
- Janubu, N., Bjerrum, L., and Kjaernsli, B. 1956. Stabilitetsberegning for fyllinger skjaeringer og naturlige skraninger. Norwegian Geotechnical Publication No. 16, Oslo, Norway.
- Kenney, T.C., and Watson, G.H. 1961. Multi-stage triaxial test for determining c' and ϕ' of saturated soils. Proceedings, 5th International Conference on Soil Mechanics and Foundation Engineering, Paris, France, Vol. 1, pp. 191–195.
- Lumb, P. 1962. General nature of the soils of Hong Kong. Symposium on Hong Kong Soils, pp. 19–32.
- Lumb, P. 1964. Multi-stage triaxial test on undisturbed soils. Civil Engineering and Public Works Review, **59**: 591–595.
- Lumb, P. 1965. The residual soils of Hong Kong. Géotechnique, **15**: 180–194.
- Satija, D.J. 1978. Shear behaviour of partially saturated soils. Ph.D. thesis, Indian Institute of Technology, New Delhi, India.
- Terzaghi, K. 1936. The shearing resistance of saturated soils. Proceedings, 1st International Conference on Soil Mechanics and Foundation Engineering, Cambridge, MA, Vol. 1, pp. 54–56.
- Wong, H.Y. 1978. Soil strength parameter determination. The Hong Kong Engineer, Journal of the Hong Kong Institution of Engineers, March, pp. 33–39.

Appendix

The following symbols are used in this paper:

- c = total or apparent cohesion
- c' = effective cohesion
- u_a = pore-air pressure
- u_w = pore-water pressure
- $(u_a - u_w)$ = matric suction
- w = water content of the soil
- τ = shear strength
- γ_d = dry unit weight
- σ = total stress
- σ_1 = total major principal stress
- σ_3 = total minor principal stress (i.e., total confining stress)
- ϕ' = effective friction angle
- ϕ^b = friction angle with respect to changes in $(u_a - u_w)$ when $(\sigma - u_a)$ is held constant
- $\phi_{1,2}^b$ = angle of friction, ϕ^b , based on the Stage 1 and 2 data
- $\phi_{2,3}^b$ = angle of friction, ϕ^b , based on the Stage 2 and 3 data

Increase in factor of safety due to soil suction for two Hong Kong slopes

R.K.H. Ching, D.J. Sweeney, and D.G. Fredlund

Abstract: Stability analyses for two cut slopes are presented to show the effects of soil suction on the computed factors of safety. The increase in soil strength due to suction is included in terms of an increased cohesion. The effect of suction on the location of the critical slip surface is also presented.

Key words: slope stability analysis, negative pore-water pressure, soil suction, unsaturated soil, factor of safety, General Limit Equilibrium method.

Introduction

The effect of negative pore-water pressure on the soil strength has usually not been considered in the stability analysis of slopes. Rather, it has generally been assumed that the negative pore-water pressure will eventually dissipate, resulting in a reduction in soil strength and a decrease in the stability of the slope with time (Widger and Fredlund 1979). Therefore, stability analyses are usually performed using saturated parameters although the soil in the slope may remain unsaturated. This may lead to a discrepancy between the analytical results and actual conditions.

Intense urban developments in Hong Kong have inevitably spread to the nearby hillsides despite encountering perilous conditions. These developments often involve cuts that are designed on the basis of precedent experiences with similar sites. Allowable slopes are relatively steep, often exceeding 45 degrees.

It has been observed that many steep slopes, both natural and cut, are unsaturated. Soil suctions are measurable from the surface to a considerable depth. Slope failures have been common and have frequently occurred during or after periods of heavy and prolonged rainfall. This rainfall causes infiltration and a reduction in soil strength as a result of a loss of suction in the slopes (Lumb 1975). Back analysis of steep slopes assuming saturated conditions has often shown their factor of safety to be less than 1.0 (e.g., 0.8). Sweeney and Robertson (1979) concluded that soil suction is a significant factor contributing to the shear strength of the Hong Kong slopes.

In this paper, two cut slopes in Hong Kong are studied to demonstrate the effect of soil suction on their stability. The increase in strength due to soil suction is included in terms of an increase in the cohesion of the soil. The analyses are performed using the General Limit Equilibrium (GLE) method of slices.

Theoretical aspects

Fredlund et al. (1978) presented the shear strength equation for unsaturated soils written in terms of two stress state variables ($\sigma - u_a$) and $(u_a - u_w)$.

$$[1] \quad \tau = c' + (\sigma - u_a) \tan \phi' + (u_a - u_w) \tan \phi^b$$

where:

τ = shear strength of an unsaturated soil,

c' = effective cohesion,

σ = total normal stress,

u_a = pore-air pressure in the soil,

u_w = pore-water pressure in the soil,

ϕ' = angle of internal friction with respect to changes in $(\sigma - u_a)$,

ϕ^b = angle of internal friction with respect to changes in $(u_a - u_w)$.

$(\sigma - u_a)$ = total stress, and

$(u_a - u_w)$ = matric suction.

The shear strength equation for an unsaturated soil can be incorporated in a slope stability analysis in a manner similar to that used for a saturated soil. The net result can be presented in either of the following ways.

- (1) First, the limit equilibrium equations for factor of safety can be re-derived. Equation [1] can be used to represent the soil strength from which the factor of safety can be computed. This approach can readily be applied to the General Limit Equilibrium (GLE) method of slices (Fredlund et al. 1981). The equations associated with this modified method of analysis are similar to those for a conventional slope stability analysis. The differences are that the modified equations contain the matric suction term, $(u_a - u_w)$, and that the pore-water pressure, u_w , is substituted by the pore-air pressure, u_a .

D.G. Fredlund. Professor, Department of Civil Engineering, University of Saskatchewan, 57 Campus Drive, Saskatoon, SK, Canada S7N 5A9.

R.K.H. Ching. Graduate Student, Department of Civil Engineering, University of Saskatchewan, 57 Campus Drive, Saskatoon, SK, Canada S7N 5A9.

D.J. Sweeney. Fugro Inter Inc., Houston, TX, USA.

Reproduced with permission from the *Proceedings, Fourth International Symposium on Landslides*, Toronto, Canada, September 16–21, pp. 617–623.

- (2) Second, the influence of matric suction can be considered as an increase in the cohesion of the soil (Fredlund 1979). This procedure makes it unnecessary to reformulate the factor of safety equations, thus it was adopted in this study. The total cohesion, c , therefore, is equal to the sum of the effective cohesion, c' , and the increase in cohesion due to the matric suction (eq. [2]).

$$[2] \quad c = c' + (u_a - u_w) \tan \phi^b$$

where:

c = total cohesion for an unsaturated soil.

Description of soil materials and *in situ* soil suction measurements

The principal surficial materials of Hong Kong are residual soils derived from the igneous rocks, mainly granite and rhyolite. Active weathering processes have resulted in residual soils to a considerable depth in most places. These soils are highly variable owing to the differential weathering processes and the differences in the mineralogy of the parent rocks (Lumb 1962, 1965).

The strength properties of the Hong Kong residual soils have been previously investigated (Lumb 1962, 1965). For coarse to medium-grained granitic soils, the angle of internal friction, ϕ , varied from 35 to 40 degrees whereas it ranged from 20 to 40 degrees for the fine-grained soils. The friction angle, ϕ , for the rhyolitic soils ranged from 30 to 35 degrees. The friction angle tended to increase with the soil density and granularity for both soil types. The cohesive component of strength for both residual soils was variable and was primarily dependent on the degree of saturation. The variation in the cohesion is believed to be more directly related to the effect of soil suction (Fredlund 1979).

Ho (1981) measured the unsaturated shear strength parameters for both Hong Kong soils using a multi-stage triaxial test. The multistage test was used in order to minimize the effect of soil variability. The axis-translation technique was used to maintain various suction values in the soil. The average friction angle with respect to matric suction, ϕ^b , for the weathered granite ranged from 10 to 20 degrees and 11 to 16 degrees for the weathered rhyolite.

In order to include the effect of increased strength due to suction, the matric suction profile for the soil in the field must be known. The matric suction profile can be determined directly by field measurements. *In situ* soil suction measurements have been carried out at several sites in Hong Kong (Sweeney 1982). The measured matric suction profiles have been observed to vary almost linearly with respect to the distance above the water table. The suction values reached an upper limit of approximately 80 to 100 kPa, which is the ultimate capacity of the tensiometer. The suction increased at a rate of 1 to 3 kPa per metre above the water table. This corresponds to approximately 10 to 30 percent of the negative hydrostatic pressure.

Figure 1 illustrates the relationship between the matric suction above the water table and the increase in the cohesion of the soil. A ϕ^b angle of 15 degrees has been used in Fig. 1. Various percentages of the negative hydrostatic profile are later used for the analysis, while maintaining a maximum suction value of 100 kPa.

Stability analyses for two study sites

Study Site 1: Fung Fai Terrace

Fung Fai Terrace is located in the north central part of Hong Kong Island. The site consists of a row of residential buildings as shown in Fig. 2. At the back of these buildings is a steep cut slope with an average inclination of 60 degrees to the horizontal and a maximum height of 35 metres. The cutting has been protected from infiltration of surface water by a layer of soil cement and lime plaster (i.e., locally referred to as chunam plaster), and has been in place for more than 40 years. Small, but dangerous failures have occurred periodically at the crest of the cut slope and the low calculated factor of safety causes some concern. These circumstances prompted a detailed investigation.

Three cross-sections A, B and C are shown in Figs. 3 to 5. The stratigraphy consists primarily of weathered granite. There is a layer of granitic colluvium of 4 to 5 metres thick present at the top of slope. Beneath the colluvium is a layer of completely weathered granite varying from 10 to 20 metres in thickness which is underlain by a layer of completely to highly weathered granite of about 10 metres thick. Bedrock is situated 20 to 30 metres below the surface. The water table is located well into the bedrock. It is estimated that the water table may rise under the influence of heavy rains with return periods of 10 and 1000 years by 5 and 8 metres, respectively. The groundwater level does not directly affect the stability analyses.

Undisturbed core samples were tested to establish the pertinent strength parameters. Results are given in Table 1. The average ϕ^b angle for the soils was taken as 15 degrees (Ho 1981).

Soil suctions were measured at this site using a tensiometer inserted through small openings made into the face of the slope. Figure 6 shows two typical suction profiles obtained from a location near section A-A. The suctions varied considerably since the measurements were influenced by the proximity of the slope face. Measurements on the upper part of the profile could not be accurately taken because the capacity of the tensiometer was exceeded.

Stability analysis at Fung Fai Terrace

Limit equilibrium stability analyses were performed on the three cross-sections shown in Figs. 3 to 5. The GLE method was used with the assumption that the resultant interslice forces were horizontal. Since numerical difficulties were often encountered in the analyses of steeply inclined slopes using a method involving the force equilibrium, a method satisfying only the moment equilibrium was used to solve for the factor of safety. The computa-

Fig. 1. Variation in soil suction and equivalent increase in cohesion.

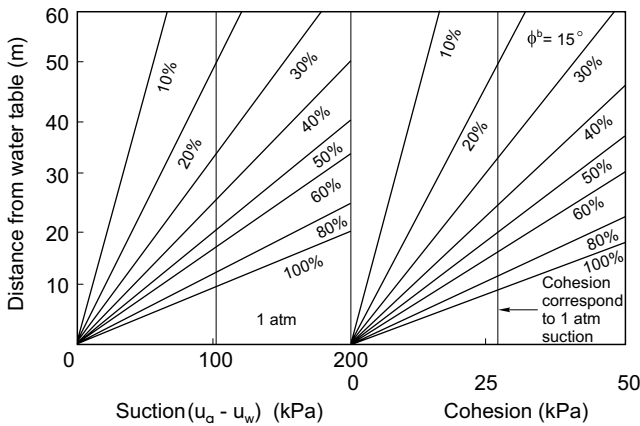
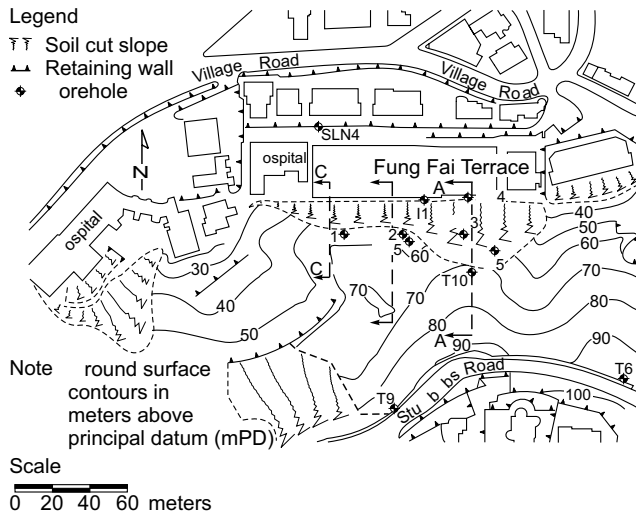


Fig. 2. Site plan of Fung Fai Terrace.



tions were performed using the SLOPE-II computer program (Fredlund 1981). Circular surfaces were analyzed to determine the critical surface corresponding to a minimum factor of safety. All critical surfaces passed through the toe of the slope. Table 2 summarizes the stability results without the effect of soil suction.

The most critical factor of safety is 0.86. The results indicate that the slope would be unstable if all conditions were representative. The fact that this slope has remained stable implies that the analysis is not completely representative of the field conditions. An additional strength is available, possibly due to soil suction.

The cross-sections were re-analyzed including the effect of soil suction. Each of the cross-sections was further divided into sub-strata drawn parallel to the water table in order to account for the varying suction. Sub-strata were 5 metres thick. Figure 7 shows the subdivision for cross-section A. Each of the sub-strata was assumed to have a different total cohesion, c , as described by eq. [2]. The equivalent increase in cohesion for a substratum was interpreted from the respective matric suction profile.

Fig. 3. Section A-A at Fung Fai Terrace.

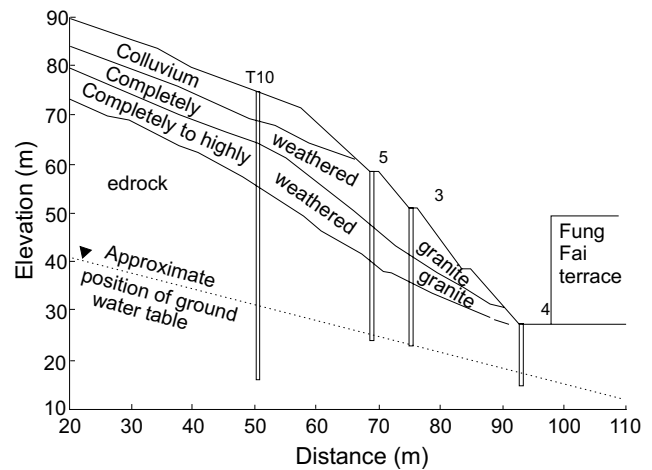


Fig. 4. Section B-B at Fung Fai Terrace.

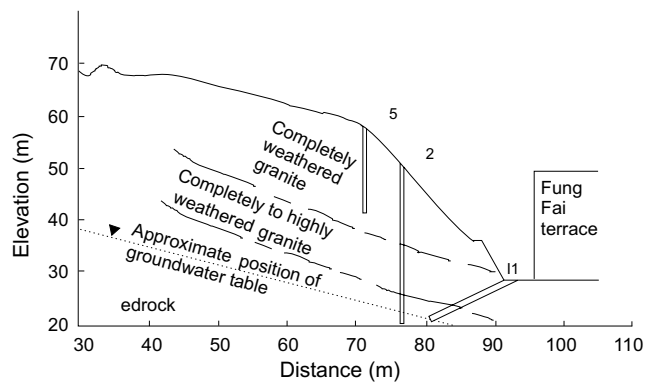
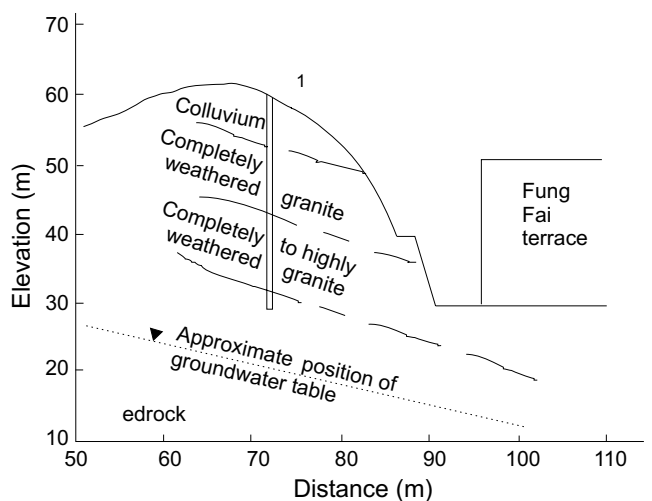


Fig. 5. Section C-C at Fung Fai Terrace.



A parametric study was conducted to demonstrate changes in the factor of safety in response to variations in the matric suction. Suction profiles as shown in Fig. 1 were assumed. Results for the parametric study are summarized in Table 3 and plotted in Fig. 8. Figure 8 shows that a suction profile of 10 to 20 percent negative hydrostatic pressure is required to render a factor of safety of

Table 1. Strength properties for soils at Fung Fai Terrace.

Soil type	Unit weight (kN/m ³)	c' (kPa)	φ' (degree)
Colluvium	19.6	10.0	35.0
Completely weathered granite	19.6	15.1	35.2
Completely to highly weathered granite	19.6	23.5	41.5

Fig. 6. Suction measurements obtained from Fung Fai Terrace.

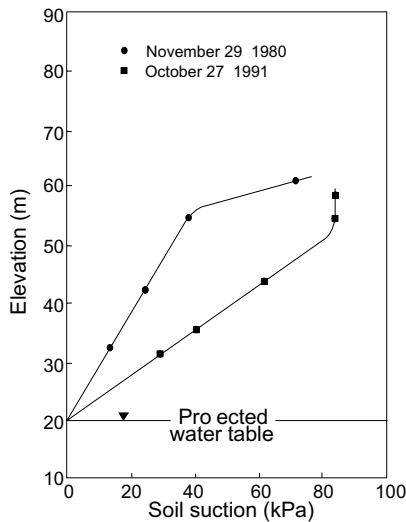


Table 2. Stability results for Fung Fai Terrace without the effect of suction.

Section	Center of rotation (m)*			Factor of safety
	X	Y	R	
A-A	232.5	190.0	216.0	0.864
B-B	143.8	120.0	89.5	0.910
C-C	171.6	118.1	120.8	0.881

*Critical centre of rotation.

1.0. The factor of safety for various sections is increased by 10 to 40 percent for matric suction profiles corresponding to 10 to 100 percent of negative hydrostatic pressure, respectively. Figure 9 shows the variations in the position for the critical centre for section A-A. The critical slip surface tends to penetrate deeper into the slope as the cohesion increases.

Stability calculations were also performed using the actual matric suction values obtained from the field (Fig. 6) to assess the actual stability of the slope. The average increase in cohesion for each soil sub-stratum was calculated from the actual matric suction profile up to the corresponding maximum value (Fig. 6). The results are presented in Table 4. The overall factor of safety is approximately 1.10 based on the suction profile measured on November 29, 1980, whereas it is about 1.01 based on the suction profile measured on October 27, 1981.

Study Site 2: Thorpe Manor

Thorpe Manor is a site located in the Mid Levels district of Hong Kong Island. It has been proposed for a

Fig. 7. Soil subdivision for section A-A at Fung Fai Terrace.

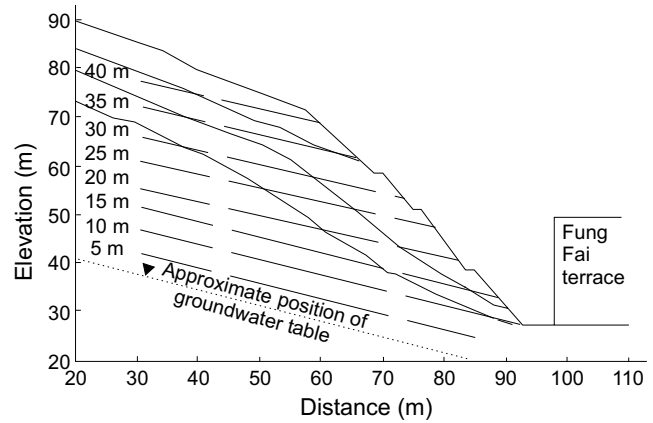
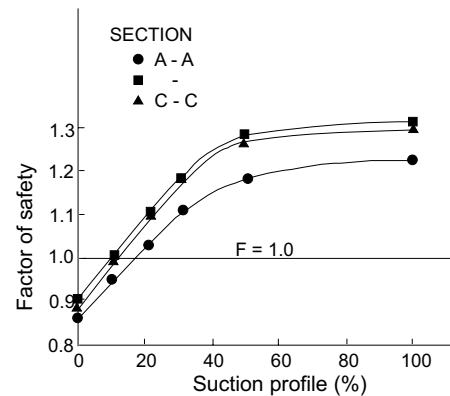


Fig. 8. Results of parametric stability analysis for Fung Fai Terrace.



high-rise residential building. An unusually steep and high cut slope exists below the site, accommodating an existing residential building. This led to a detailed investigation to access the long-term stability of the site taking into account the imposed loads from the new building and induced changes in surface and subsurface drainage.

Figure 10 shows the site plan of Thorpe Manor, which is topographically situated at the front of a spur which is protruding from the main hillside. The cut slope under consideration is below a major access road (i.e., May Road) and its critical cross-section, A, is shown in Fig. 11. The slope is inclined at 60 degrees to the horizontal and has an average height of 30 metres. The stratification consists entirely of weathered rhyolite. The surficial material is a completely weathered rhyolite of 5 to 10 metres in thickness. The second stratum is a layer of completely to highly weathered rhyolite varying from 5 to 10 metres in thickness. Underlying is another layer

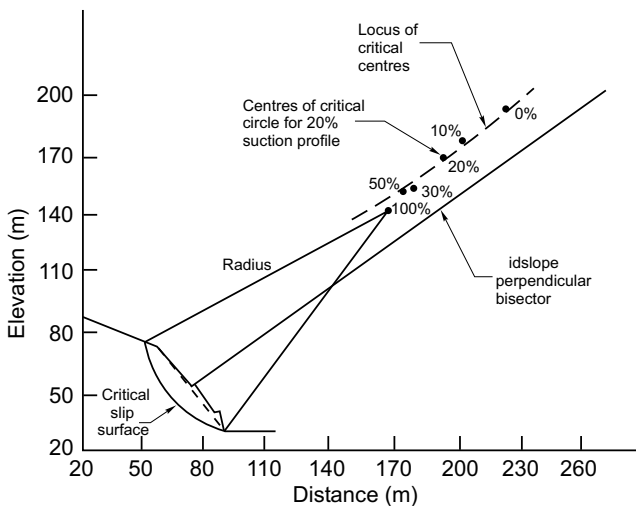
Table 3. Stability results for parametric study for Fung Fai Terrace.

Hydrostatic suction %	Centre of rotation (m)			Factor of safety
	X	Y	R	
A. Section A-A				
10	210.0	175.0	190.0	0.948
20	200.0	167.0	178.0	1.030
30	185.0	150.0	155.0	1.108
50	180.0	150.0	151.0	1.179
100	173.3	139.0	139.0	1.226
B. Section B-B				
10	130.6	112.5	78.8	1.011
20	130.6	112.5	78.8	1.097
30	133.1	117.5	81.4	1.184
50	130.0	117.5	79.8	1.274
100	143.8	132.5	99.7	1.308
C. Section C-C				
10	151.3	102.5	95.7	0.991
20	138.8	96.3	83.1	1.088
30	134.1	93.1	77.8	1.179
50	138.8	96.3	83.1	1.267
100	138.8	96.3	83.1	1.296

Table 4. Stability results with the effect of suction for Fung Fai Terrace.

Section	Centre of rotation (m)			Factor of safety
	X	Y	R	
A. Suction profile (November 29, 1980)				
A-A	176.3	141.9	143.0	1.072
B-B	133.1	117.5	81.4	1.143
C-C	138.8	96.3	83.1	1.132
B. Suction profile (October 27, 1981)				
A-A	201.3	167.5	178.6	0.984
B-B	165.0	125.0	122.2	1.046
C-C	156.9	108.8	104.1	1.014

Fig. 9. Critical centres for section A-A.



of slightly weathered rhyolite. Bedrock is located approximately 20 to 30 metres below the surface. The water table lies well below the ground surface. It is estimated that the water table will rise under the influence of heavy rain with return periods of 10 and 1000 years to less than 5 and 8 metres, respectively. Therefore, the water table does not directly influence the stability analysis.

Undisturbed core samples were tested to obtain the shear strength parameters. The ϕ^b angle for the soils was independently evaluated. Table 5 gives a summary for the soil properties.

In situ soil suction measurements were made from an exploratory caisson shaft installed near the cut slope (Fig. 10). Suction profiles obtained during the rainy season of 1980 are plotted in Fig. 12. These profiles are relatively uniform, except that variations occurred as a result of infiltration and fluctuation in the position of the water table.

Table 5. Properties for soils at Thorpe Manor.

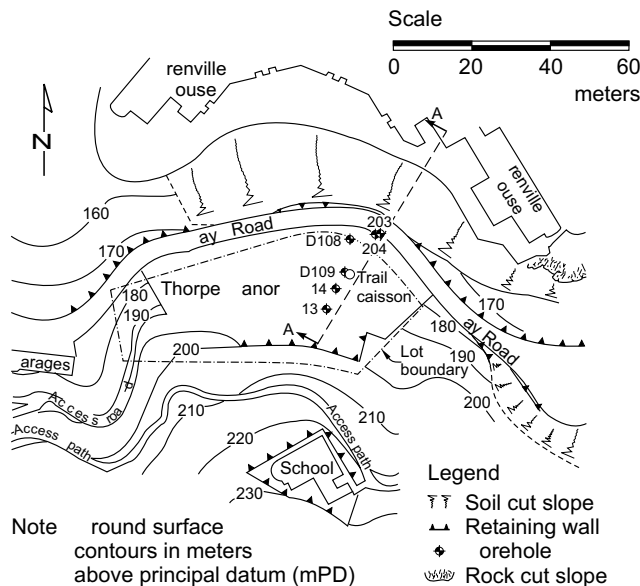
Soil Type	Unit weight (kN/m ³)	c' (kPa)	φ' (degree)	φ ^b (degree)
Completely weathered rhyolite	18.4	10.1	42.6	12.0
Completely to highly weathered rhyolite	21.4	12.0	43.9	12.0

Table 6. Stability results for Thorpe Manor.

Suction profile (%)	Centre of rotation (m)			Factor of safety
	X	Y	R	
A. Approximate water table				
0	148.8	205.0	76.1	1.046
10	141.3	202.5	69.6	1.114
20	139.7	202.5	68.6	1.181
30	138.1	202.5	67.7	1.242
50	135.0	202.5	66.0	1.342
100	135.0	202.5	66.0	1.428
Actual *	126.9	192.5	55.3	1.254
B. Water table corresponding to 1:10 year rain				
10	145.0	205.0	73.8	1.091
20	141.3	202.5	69.6	1.139
30	150.0	212.5	82.8	1.191
50	141.9	207.5	74.0	1.270
100	136.9	202.5	67.1	1.370
C. Water table corresponding to 1:1000 year rain				
10	145.0	205.0	73.8	1.078
20	141.3	202.5	69.6	1.114
30	160.0	220.0	94.9	1.159
50	141.9	207.5	74.0	1.216
100	148.1	212.5	81.7	1.320

* Suction profile of September 2, 1980.

Fig. 10. Site plan of Thorpe Manor.

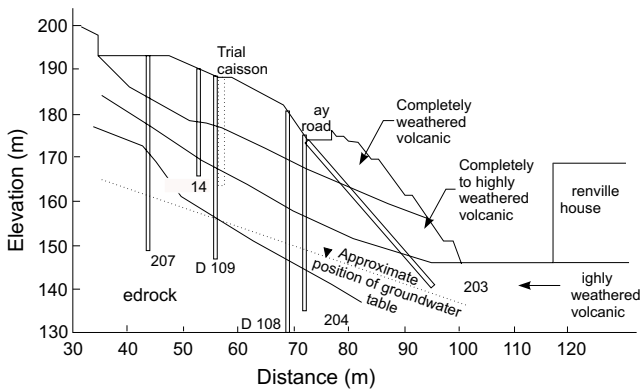
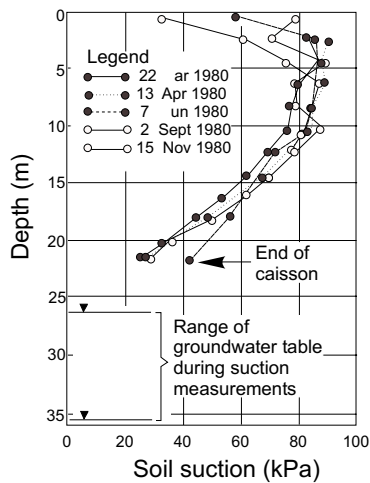


Stability analysis for Thorpe Manor

Stability analyses using circular slip surfaces were performed on section A-A. The computations were first made assuming saturated conditions. A parametric study was included in order to evaluate the effect of the changes in the soil suction profile and the water table on the computed factor of safety. Various suction profiles were assumed. Water tables corresponding to heavy rains with return periods of 10 and 1000 years, respectively, were used. Results for the stability analyses are summarized in Table 6.

The critical factor of safety for the cut slope without the effect of soil suction is approximately 1.05, suggesting that this slope is in a nearly unstable condition although no distress is observed. Its value is increased to 1.25 when the actual soil suctions are included. In other words, matric suction contributes approximately 20% towards an increased factor of safety.

Results from the parametric study show that factor of safety computations are sensitive to changes in the suction profile but less sensitive to the position of the water table. The computed factor of safety is 1.43 when using a matric suction profile equivalent to 100 percent of nega-

Fig. 11. Section A-A of Thorpe Manor.**Fig. 12.** Suction measurements obtained from Thorpe Manor.

tive hydrostatic pressure. For water table positions corresponding to heavy rains with return periods of 10 and 1000 years, the respective factors of safety are 1.37 and 1.32.

Discussion

The increase in soil strength due to matric suction is generally ignored in the stability analysis of slopes. This is mainly because of the uncertainties regarding the long term reliability of the soil suctions. In general, it has been assumed that there will be a complete loss of soil suction due to an ingress of water. This conventional approach, in many cases, will give conservative factors of safety. Analyses using this approach for the Hong Kong residual soil slopes underestimate the actual factor of safety and may adversely influence the use of wise engineering judgements in designs. It is postulated that long term soil suction profiles play a significant role in the stability of many steep natural and cut slopes.

Stability studies on the two cut slopes in Hong Kong provide valuable case histories on the quantification of the influence of soil suction on stability. The computed factors of safety appear to be unrealistically low when saturated conditions are assumed. When the effect of soil

suction is included, the stability results become more reasonable in the sense that they better represent the actual observed stability conditions.

The computed factors of safety for the cut slopes at Fung Fai Terrace and Thorpe Manor are approximately 0.86 and 1.05, respectively, when neglecting the effect of soil suction. The factors of safety are increased to 1.01 and 1.25 when taking into consideration the actual soil suctions. It is concluded that the soil suction does make a substantial contribution to the stability for the two slopes.

Suctions may vary with time. However, measurements have indicated that significant soil suctions in the two slopes are maintained throughout the wet and dry seasons. In both cases, the soil in the cut slopes is protected from infiltration by chunam plaster while infiltration above the chunam cover is inhibited by the steepness of the ground and thick vegetation.

Acknowledgements

Financial assistance for this study was provided by Fugro (H.K.) Ltd. This support is gratefully acknowledged. Much of the data in this paper has been collected by Fugro (H.K.) Ltd. and was made available for the publication of this paper.

References

- Fredlund, D.G., Morgenstern, N.R., and Widger, R.A. 1978. The shear strength of unsaturated soils. *Canadian Geotechnical Journal*, **15**: 313–321.
- Fredlund, D.G. 1979. Second Canadian geotechnical colloquium: Appropriate concepts and technology for unsaturated soils. *Canadian Geotechnical Journal*, **16**: 121–139.
- Fredlund, D.G. 1981. SLOPE-II computer program user's manual S-10. Geo-Slope Programming Ltd., Calgary, Alberta, Canada.
- Fredlund, D.G., Krahn, J., and Pufahl, D.E., 1981. The relationship between limit equilibrium slope stability methods. *Proceedings, 10th International Conference on Soil Mechanics and Foundation Engineering*, Stockholm, Sweden, Vol. 3, pp. 409–416.
- Ho, D.Y.F. 1981. The shear strength of unsaturated Hong Kong soils. M.Sc. thesis. University of Saskatchewan, Saskatoon, Canada.
- Lumb, P. 1962. The properties of decomposed granite. *Géotechnique*, **12**: 226–243.
- Lumb, P. 1965. The residual soils of Hong Kong. *Géotechnique*, **15**: 180–194.
- Lumb, P. 1975. Slope failures in Hong Kong. *Quarterly Journal of Engineering Geology*, **8**: 31–65.
- Sweeney, D.J., and Robertson, P.K. 1979. A fundamental approach to slope stability problems in Hong Kong. *Hong Kong Institute of Engineering Journal*, **7**(10): 35–44.
- Sweeney, D.J. 1982. Some *in situ* soil suction measurements in Hong Kong's residual soil slopes. *Proceedings, 7th South-East Asian Geotechnical Conference*, Hong Kong, Vol. 1, pp. 91–106.
- Widger, R.A., and Fredlund, D.G. 1979. Stability of swelling clay embankments. *Canadian Geotechnical Journal*, **16**: 140–151.

Negative pore-water pressures in slope stability

D.G. Fredlund

Abstract: There are numerous aspects to a conventional slope stability study. In most situations the factor of safety is predicted on a slope where the pore-water pressures are positive. However, there are many situations where the pore-water pressures are negative and there is still concern about instability. In order for the geotechnical engineer to perform such studies, he must be able to extend the concepts of saturated soil mechanics into the range of unsaturated soil mechanics (i.e., soils with negative pore-water pressures). There must be extensions made to the limit equilibrium theory used to compute the factor of safety. There must be extensions made to the shear strength theory and to the experimental procedures used to measure the shear strength. There must be extensions made to the flow theory in order to accommodate flow modeling in the unsaturated soil zone. In addition, there must be techniques available to measure highly negative pore-water pressures in the field.

All of the above components of theory must be understood when performing a stability study on soils with negative pore-water pressures. This paper outlines the essence of each of the above aspects and attempts to illustrate how each can be integrated into a stability study.

Key words: slope stability, shear strength, factor of safety, site investigation, instrumentation, negative pore-water pressure, matric suction, unsaturated soil.

Introduction

Slope stability analyses have become a common analytical tool to assess the factor of safety of natural and man-made slopes. Saturated shear strength parameters are generally used in such an analysis. The portion of the soil profile above the groundwater table where the pore-water pressures are negative is usually ignored. This is a reasonable assumption for many situations where the major portion of the slip surface is below the groundwater table. However, for situations where the groundwater table is deep or where the concern is over the possibility of a shallow failure surface, there is need to understand how to perform a slope stability analysis where the soil has negative pore-water pressures. The main objective of this paper is to discuss recent developments which allow the effects of negative pore-water pressures to be taken into consideration in a slope stability analysis.

Several aspects of a slope stability study remain the same for soils with positive pore-water pressures (e.g., saturated soils) and soils with negative pore-water pressures (e.g., unsaturated soils). For example, the nature of the site investigation, identification of the strata and the measurement of total unit weight remain the same in both situations. On the other hand, extensions to conventional procedures are required with respect to the characteriza-

tion of the shear strength and permeability properties of the soil. The analytical tools used to quantify pore-water pressures and calculate the factor of safety also need to be extended.

The following scenario will be used to create a typical problem involving a slope stability analysis for a soil with negative pore-water pressures. Let us assume that numerous houses have recently been built at the toe of a steep slope and now there is concern regarding the stability of the slope. A failure of the slope would cause serious destruction of property and possible loss of life. This is typical of situations reported in Hong Kong, South America and other parts of the world (Brand 1984; Fontura de Campos and Costa Filno 1984). Let us suppose that a geotechnical consulting firm is commissioned to proceed with a site investigation and an assessment of the stability of the slope. The commission also asks the engineer to study the likelihood of a failure at some time in the future under possible rainfall conditions.

During the site investigation, the engineer discovers that the water table is approximately 20 metres below the ground surface and the soil in the upper portion of the slope is unsaturated. The slope appears presently to be stable but the engineer must still quantitatively justify his conclusions. Those issuing the commission have requested answers to the following questions:

- i) What is the present factor of safety of the slope?
- ii) Where would be the location of a potential slip surface?
- iii) What effect does the housing development have on the factor of safety?
- iv) How would a heavy rainfall over an extended period of time affect the stability of the slope?

D.G. Fredlund. Professor, Department of Civil Engineering, University of Saskatchewan, 57 Campus Drive, Saskatoon, SK, Canada S7N 5A9.

Reproduced with permission from the *Proceedings, Simposio Suramericano de Deslizamientos*, Paipa, Columbia, 1989.

These and many other questions could be asked and the engineer would like to have analytical procedures for their study. It does not really matter whether the soil is of a residual or a transported nature. The main difficulties arise because the pore-water pressures in the soil are negative. This fact alone will strongly influence both the assessment of relevant soil properties and the manner in which the analyses are performed. Another important aspect is the assessment of the microclimate at the site which gives rise to a flux boundary condition.

This paper emphasizes recent developments in the testing of unsaturated soils which are relevant to the problem at hand as well as extensions to unsaturated soil mechanics theories which must be understood.

Theories, analytical tools, and testing procedures required

Let us assume that the engineer desires to perform his stability studies in a manner parallel in concept to those conventionally used for an effective stress analysis in saturated soil mechanics. The engineer must know how to obtain the shear strength parameters and the permeability characteristics of the soil.

Let us refer to the soil with negative pore-water pressures as an unsaturated soil. However, the zone immediately above a groundwater table may remain essentially saturated while the pore-water pressures are slightly negative. At a further distance above the groundwater table, the pore-water pressures become more negative and the degree of saturation of the soil decreases. The pore-water pressure can become highly negative and difficult to measure. This is one of the primary reasons why engineers have generally elected to ignore the strength in the unsaturated soil zone. This may be reflected in the use of highly conservative and sometimes unreasonable assumptions regarding the zone above the groundwater table.

Recent developments in several devices now make the measurement of negative pore-water pressures possible. Some of the more promising techniques are mentioned in this paper. In order to perform a slope stability analysis it is necessary to know how the shear strength of the soil changes with respect to the negative pore-water pressure. Since its shear strength will not have the same rate of strength change with respect to total stress and pore-water pressure, it is necessary to have an additional soil property when defining shear strength. This additional soil property is called ϕ^b and is defined as the increase in shear strength with respect to a change in matric suction.

Modeling the hydrologic conditions at a site can provide information on possible changes in the stability of a slope with respect to time. The input data for such modeling involves the characterization of the permeabilities of the soil strata. Initially it may appear to be an overwhelming task to consider the permeability characterization of the numerous strata involved since their variation can be extensive. Even so, hydrological modeling of sites has made tremendous strides in recent years.

Finite element modeling of flow problems has been extended from saturated soils to unsaturated soil conditions

(Papagianakis and Fredlund 1984). Computer studies have shown that it is difficult to predict quantities of flow in unsaturated soils. At the same time, studies have shown that the prediction of pore-water pressure heads are relatively insensitive to the changes in the permeabilities in the unsaturated zone. This is welcomed information for slope stability studies since it is the pore-water pressure which must be used in a slope stability analysis.

As the pore-water pressures in a soil become increasingly negative, the soil becomes unsaturated and its coefficient of permeability decreases. The decrease can be significant, involving several orders of magnitude. The relationship between negative pore-water pressures (or matric suctions) and the coefficient of permeability is referred to as the permeability function. When matric suction is equal to zero, the permeability is equal to the saturated coefficient of permeability for the soil. As a result of the insensitivity of the computed pore-water pressure heads to the changes in the unsaturated coefficient of permeability, it is possible to use somewhat approximate and empirical procedures to quantify the permeability functions.

The surface flux boundary conditions for hydrological modeling should be based on the regional climatic conditions. Reasonable flux boundary conditions are assumed for the example considered later.

Shear strength theory for unsaturated soils

Fredlund and Morgenstern (1977) described the use of independent stress state variables for an unsaturated soil. The proposed independent stress state variables for analysing practical problems were the net total stress, $(\sigma - u_a)$, and matric suction, $(u_a - u_w)$, with u_a representing the pore-air pressure and u_w representing the pore-water pressure.

This led to the formulation of an extended Mohr-Coulomb failure criterion for unsaturated soils (Fredlund et al. 1978). It is logical to extend the two-dimensional failure envelope for a saturated soil to a three-dimensional failure envelope for an unsaturated soil (Fig. 1). If the envelope is assumed to be planar, the unsaturated shear strength, τ , can be written as follows:

$$[1] \quad \tau = c' + (\sigma_n - u_a) \tan \phi' + (u_a - u_w) \tan \phi^b$$

where:

c' = effective cohesion intercept,

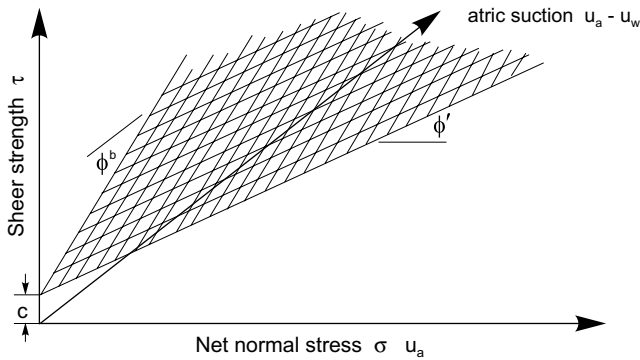
ϕ' = effective angle of internal friction,

ϕ^b = rate of increase in shear strength with respect to matric suction, and

σ_n = total normal stress on the failure plane.

The friction angle, ϕ^b , is equal to the slope of shear strength versus matric suction when the net normal stress is held constant. The effective angle of internal friction is the same for all suction values since the failure envelope is assumed to have no 'warp'. The stress circles corresponding to failure conditions can be plotted on a three-

Fig. 1. Planar surface representing the shear strength equation for unsaturated soil.



dimensional diagram with the two stress state variables plotted on the horizontal axes and the shear strength as the ordinate (Fig. 2). Test data can be interpreted using the graphical procedure proposed by Fredlund (1981).

The shear strength equation can be visualized as a two-dimensional graph with matric suction contoured as the third variable (Fig. 3). Consequently, the ordinate intercepts (i.e., when $(\sigma_n - u_a)$ is equal to zero) of the various matric suction contours can be used to obtain the friction angle, ϕ^b , (Fig. 4).

The angle, ϕ^b , can either be visualized as a friction angle or as a component of cohesion. If it is considered as a component of cohesion, the total cohesion of the soil, c , has two components.

$$[2] \quad c = c' + (u_a - u_w) \tan \phi^b$$

The shear strength equation for an unsaturated soil can then be reduced to the same form of equation as that used for a saturated soil.

$$[3] \quad \tau = c + (\sigma_n - u_a) \tan \phi'$$

There is a smooth transition from the unsaturated soil shear strength equation to the conventional shear strength equation for saturated soils. As saturation is approached, the pore-air pressure, u_a , becomes equal to the pore-water pressure, u_w , and eq. [1] reverts to the conventional shear strength equation for a saturated soil.

The justification for the linear form of the unsaturated soil shear strength equation must be substantiated by experimental laboratory test data. Numerous researchers have presented data which can be used to obtain the ϕ^b angle. Some of the data are summarized in Table 1.

Until recently, the published test data indicated that the failure surface for an unsaturated soil was essentially planar. Some recent studies with the matric suction changing over a wide range, indicate some non-linearity in the shear strength versus matric suction relationship. Such is the case for data published by Satija (1978) and Gan et al. (1988). Procedures for handling this non-linearity have been described by Fredlund et al. (1987).

Gan and Fredlund (1988) tested numerous specimens of compacted glacial till using a multistage procedure in a modified direct shear apparatus. Figure 5 shows a summary of several tests. The shear strength versus matric

Fig. 2. Mohr circles at failure for an unsaturated soil.

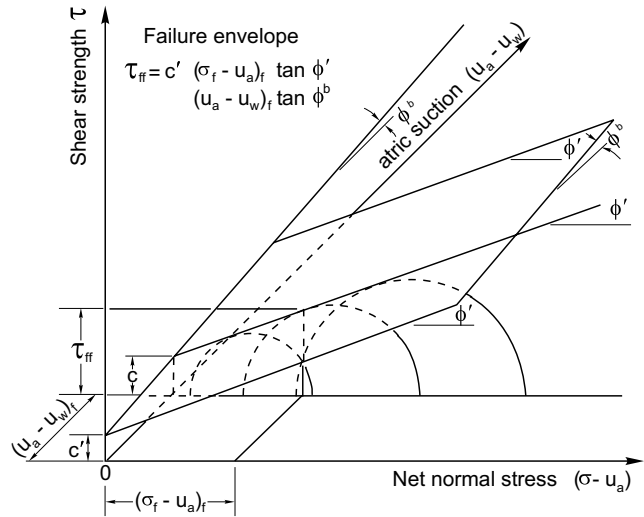


Fig. 3. Failure surfaces for an unsaturated soil viewed parallel to the $(u_a - u_w)$ axis.

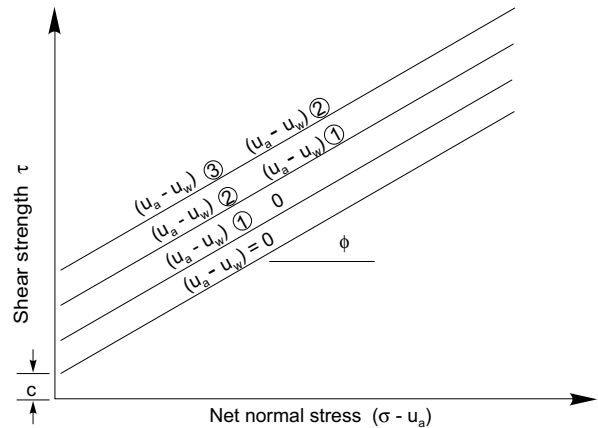
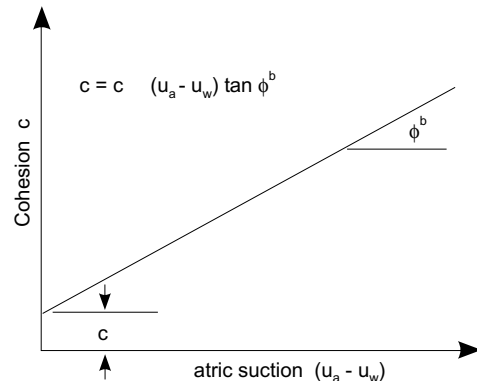


Fig. 4. The increase in shear strength (cohesion) with matric suction when $(\sigma - u_a)$ is zero.

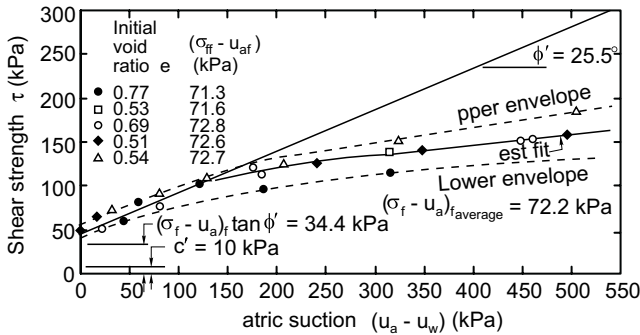


suction curves become distinctively non-linear over the range from 0 to 500 kPa. However, it should be noted that such results do not annul the use of the linear form of the extended Mohr Coulomb equation. Rather, it is important in a stability analysis, to use a ϕ^b value appropriate to the matric suction range involved.

Table 1. Shear strength data on unsaturated soils.

Soil type	c' (kPa)	ϕ' (deg.)	ϕ^b (deg.)	References
Compacted shale $w = 18.6\%$	15.8	24.8	18.1	Bishop et al. (1960)
Boulder Clay $w = 11.6\%$	9.6	27.3	21.7	Bishop et al. (1960)
Madrid grey clay	25.0	22.5	16.1	Escario (1980)
Decomposed granite	28.9	33.4	15.3	Ho and Fredlund (1982a)
Decomposed rhyolite	7.4	35.3	13.8	Ho and Fredlund (1982a)

Fig. 5. Failure envelopes on τ versus $(u_a - u_w)$ plane obtained from unsaturated glacial till specimens.



Equipment and procedures for measuring ϕ^b

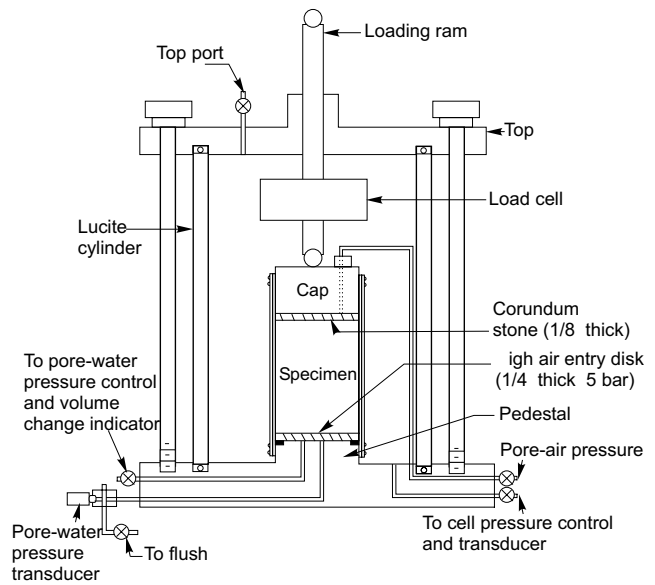
A conventional triaxial cell for testing saturated soils (Bishop and Henkel 1962) can be modified to accommodate the testing of unsaturated soils. The testing can be performed either in a multistage mode (i.e., on one specimen) or as single stress versus strain tests on several specimens at similar initial stress and volume-weight conditions (Ho and Fredlund 1982b).

The major modification to a conventional triaxial cell involves the sealing of a high air entry disk onto the base pedestal of the triaxial cell (Fig. 6). The high air entry disk allows the measurement of the pore-water pressure independent of the pore-air pressure. The air entry value of the disk must be higher than the maximum matric suction that will be applied to the sample. Generally, a 9.53 mm (3/8 inch) thick, 5 bar (505 kPa) ceramic disk is most satisfactory. A coarse or low air entry disk can be placed on the top of the specimen to control the air pressure.

The testing procedure usually involves the control of the air and water pressures during the entire test. A suction is maintained constant on a specimen during the application of the deviator stress. The procedure used to impose suctions greater than 100 kPa (1 atm) is known as the axis-translation technique (Hilf 1956; Bocking and Fredlund 1980).

The main limitation associated with the use of triaxial equipment is the length of time required for pore pressure equalization. The coefficient of permeability of an unsaturated soil becomes low and the equalization time varies as the square of the length of the drainage path. As a re-

Fig. 6. Modified triaxial cell for testing unsaturated soils.

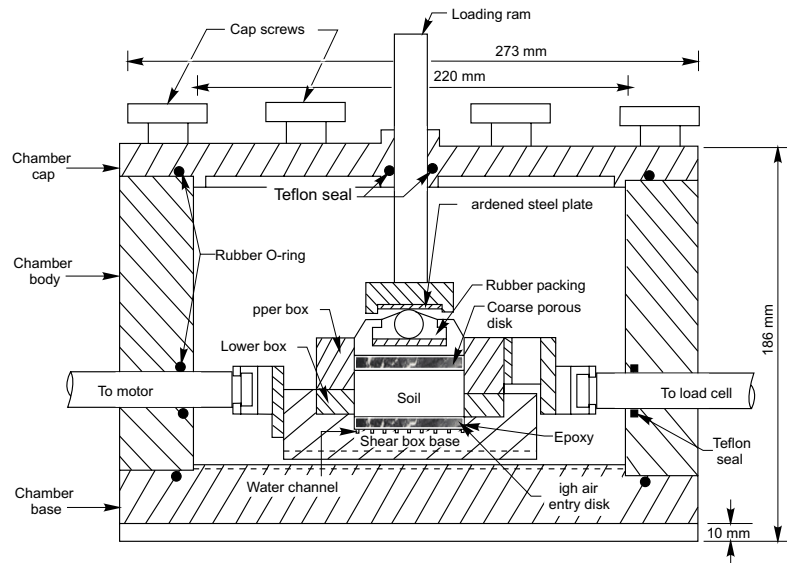


sult, unsaturated soils must be sheared at an extremely slow rate (Ho and Fredlund 1982c). The use of a modified direct shear apparatus has a distinct advantage in that the length of the drainage path is relatively small (Fig. 7).

A conventional direct shear apparatus can be modified to control the pore-air and pore-water pressures applied to the soil specimen. The direct shear box is placed in an air pressure chamber. The soil specimen has a coarse porous disk placed at its top and a high air entry disk at its bottom. The air pressure in the chamber has direct contact with the coarse disk on top of the specimen. The pore-water pressure is controlled through the high air entry disk at the base of the specimen.

Figure 8 shows the results of a multistage, direct shear test on a glacial till. The liquid limit of the soil is 35.5%, the plastic limit is 16.8% and the percent clay sizes is 30.0%. The specimens were tested at a net confining pressure (i.e., $(\sigma_n - u_a)$) of 72.6 kPa. The matric suction was applied to the specimen and allowed to equilibrate for about 1 day. A horizontal shear force was then applied until the shear stress versus displacement curve began to plateau. The shear force was then reduced and a higher suction was applied. The above procedure was repeated about six times. It was then possible to plot the shear

Fig. 7. Modified direct shear apparatus (after Gan et al. 1988).



strength versus matric suction for each of the stages (Fig. 9). For the glacial till, the relationship between shear strength and matric suction was somewhat non-linear, giving rise to a variable ϕ^b angle. The ϕ^b angle approached the ϕ' angle at low values of matric suction and reduced as matric suction increased. Fredlund et al. (1987) provide procedures for the use of the non-linear data in slope stability studies.

Slope stability analysis involving unsaturated soils

Any one of a number of commonly used limit equilibrium methods of slices can be used to demonstrate the effect of negative pore-water pressures on the slope stability analysis. The General Limit Equilibrium (GLE) method proposed by Fredlund et al. (1981) will be used since it satisfies both force and moment equilibrium and allows the visualization of other methods as special cases.

The aspect of a slope stability analysis which changes when considering an unsaturated soil is the description of the shear strength. One of two approaches can be used for the factor of safety derivations (Fredlund 1981).

First, it is possible to consider the matric suction term as part of the cohesion of the soil. In other words, the matric suction increases the cohesion of the soil. Therefore, the factor of safety equations do not need to be re-derived. Rather, the cohesion of the soil, c , simply has two components in accordance with eq. [2]. The mobilized shear force at the base of a slice, S_m , can be written:

$$[4] \quad S_m = \frac{\beta}{F} (c + (\sigma_n - u_a) \tan \phi')$$

where:

- F = factor by which the shear strength of the soil must be reduced to bring the soil mass into state of limiting equilibrium, and
- β = length across the base of a slice.

This approach has the advantage that the shear strength equation retains its conventional form. Therefore, it is possible to utilize a computer program written for saturated soils to solve unsaturated soils problems. In this case, the soil in the negative pore-water pressure region must be subdivided into several discrete layers with each layer having a constant cohesion. The pore-air and pore-water pressures must be set to zero. This approach has the disadvantage that the cohesion is not a continuous function and the cohesions must be manually computed.

Second, it is possible to rederive the factor of safety equations using the shear strength equation for the unsaturated soil (eq. [1]). The mobilized shear force at the base of a slice can be written as:

$$[5] \quad S_m = \frac{\beta}{F} (c' + (\sigma_n - u_a) \tan \phi' + (u_a - u_w) \tan \phi^b)$$

The forces acting on a slice within a sliding soil mass are shown in Fig. 10, and can be defined as follows:

- W = total weight of a slice of width b and height h ,
- N = total normal force acting on the base of a slice; equal to $\sigma_n \beta$ where σ_n is the normal stress acting over the sloping distance, β ,
- E_L, E_R = horizontal interslice normal force on the left and right sides of a slice, respectively,
- X_L, X_R = vertical interslice shear force on the left and right sides of a slice, respectively,
- R = radius or moment arm associated with resistance, S_m , and
- α = angle between the base of the slice and the horizontal.

The normal force at the base of a slice, N , is derived by summing forces in the vertical direction. For most analyses the pore-air pressure can be set to zero and the normal force equation becomes:

Fig. 8. Shear stress versus horizontal displacement from a multistage direct shear test on glacial till (specimen GT-16-N4).

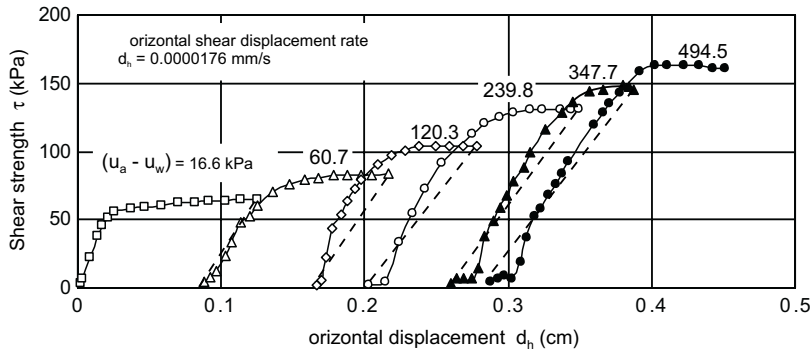
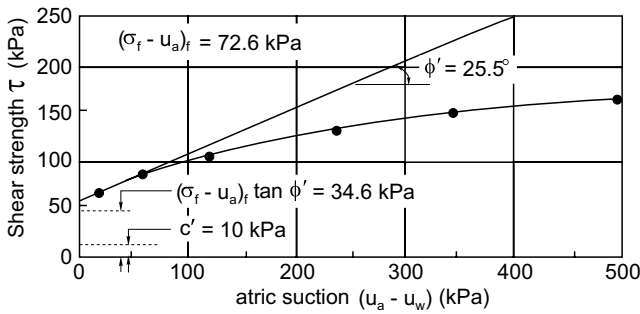


Fig. 9. Failure envelope showing shear strength versus matric suction for the glacial till (specimen GT-16-N4).



$$[6] \quad N = \frac{W - (X_R - X_L) - \frac{c' \beta \sin \alpha}{F} + u_w \frac{\beta \sin \alpha \tan \phi^b}{F}}{\cos \alpha + \frac{\sin \alpha \tan \phi'}{F}}$$

When the soil becomes saturated, ϕ^b can be set to ϕ and therefore the same equation can be used for both saturated and unsaturated soils. Computer coding can be written such that ϕ^b is used whenever the pore-water pressure is negative and ϕ is used when the pore-water pressure is positive.

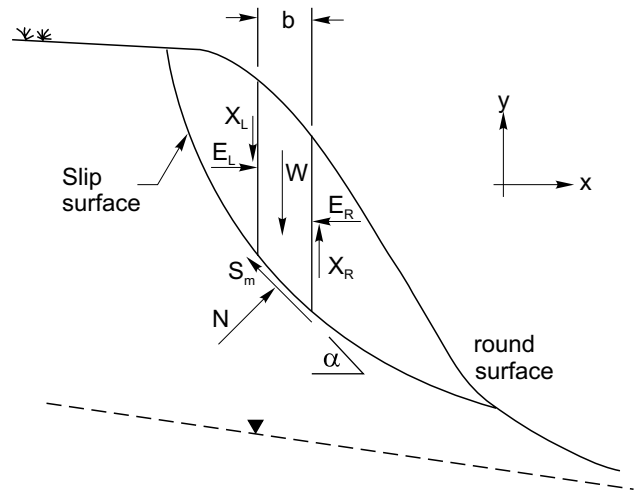
Two independent factor of safety equations can be derived; one with respect to moment equilibrium and the other with respect to horizontal force equilibrium. Moment equilibrium can be satisfied with respect to an arbitrary point above the central portion of the slip surface. Let us assume that the pore-air pressures are zero (or atmospheric). The moment equilibrium factor of safety, F_m , can be written:

$$[7] \quad F_m = \frac{\sum \left\{ c' \beta R + \left(N - u_w \beta \frac{\tan \phi^b}{\tan \phi'} \right) R \tan \phi' \right\}}{\sum Wx - \sum NF}$$

where:

- X = horizontal distance from the centre of each slice to the centre of moments, and
- F = offset distance from the normal force to the centre of moments.

Fig. 10. Forces acting on each slice for a slope stability analysis.



The factor of safety with respect to force equilibrium, F_f , can be derived by summing the forces in the horizontal direction for all slices.

$$[8] \quad F_f = \frac{\sum \left\{ c' \beta \cos \alpha + \left(N - u_w \beta \frac{\tan \phi^b}{\tan \phi'} \right) \tan \phi' \cos \alpha \right\}}{\sum N \sin \alpha}$$

The above formulations apply for both saturated and unsaturated soils, as long as the pore-air pressure is zero. When the soil is saturated, the ϕ^b term must be set equal to ϕ . The computer software PC-SLOPE, distributed by Geo-Slope Programming Ltd., Calgary, Alberta, Canada, performs the stability analysis of unsaturated soils in accordance with the above equations.

Measurements of negative pore-water pressures

The measurement of *in situ* pore-water pressures are relevant both with respect to performing slope stability analyses as well as performing saturated-unsaturated flow modeling. In order to predict the factor of safety of a

slope at a specific time, it is necessary to know the pore-water pressures in the slope. On the other hand, a knowledge of the *in situ* pore-water pressure conditions can be used as an initial boundary condition for saturated-unsaturated flow modeling. While numerous devices have long been available for measuring positive pore-water pressures, it is more recent that it has become possible to measure highly negative pore-water pressures.

The total suction of a soil is composed of two components; namely, matric suction, $(u_a - u_w)$ and osmotic suction, ψ_0 . Devices and procedures have been developed for measuring each of the components of suction. But, it is the matric suction component which is of greatest value with respect to slope stability analyses and flow modeling related to unsaturated soils. More correctly, a knowledge of the matric suction is required for the shear strength and permeability characterization of an unsaturated soil. There may, however, be situations where it is more appropriate to measure total suction and osmotic suction and then compute the matric suction.

The readers are referred to a paper by Fredlund and Rahardjo (1988) for a thorough review of the state-of-development of devices to measure suction. This paper only briefly mentions two methods available to measure matric suction. One method uses tensiometer type devices and the other method uses thermal conductivity matric suction sensors.

The Quickdraw tensiometer manufactured by Soil-moisture Corporation, Santa Barbara, California (Fig. 11) has proven to function in a superior manner to a conventional tensiometer. Subsequent to servicing the Quickdraw tensiometer, it can be used to measure pore-water pressures approaching -100 kPa since the tension is applied to the water in the measuring device for only a short period of time.

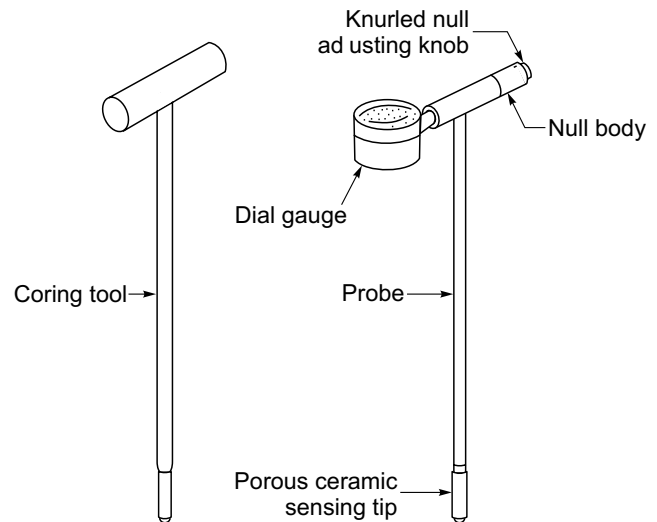
Thermal conductivity matric suction sensors have a range well beyond 100 kPa of suction. The sensors can be used on undisturbed samples in the laboratory but are particularly well suited for long term *in situ* monitoring using a data acquisition system. Thermal conductivity sensors called AGWA-II, are presently manufactured and distributed by Agwatronics Incorporated, Merced, California, U.S.A.

It is important to realize that devices are presently available for measuring negative pore-water pressures. Geotechnical engineers should avail themselves of these devices, thereby obtaining experience and building up case histories on their performance.

Saturated – unsaturated flow modeling

Upon first observation it would appear to be a formidable task to predict the changes in pore-water pressures in a slope occurring as a result of changing surface flux boundary conditions. The surface flux boundary conditions consist of infiltration due to precipitation and exfiltration due to evaporation and evapotranspiration. The problem at hand is one where the pore-water pressure heads (and subsequently the pore-water pressures) are predicted, as opposed to the prediction of flow quanti-

Fig. 11. Quickdraw tensiometer from Soil-Moisture Corporation, Santa Barbara, California.



ties. The pore-water pressure heads are primarily a function of the relative permeabilities of the soils involved as opposed to their absolute magnitudes. As a result, it is possible to perform valuable simulations of realistic situations encountered in geotechnical engineering.

In recent years, several numerical computer models have been developed to perform saturated-unsaturated transient flow analyses. These models, generally in the finite element form, can be used to predict the pore-water pressures which may exist in a slope as a result of changes in the microclimate. The changing negative and positive pore-water pressures can then be used in a limit equilibrium slope stability analysis to compute the factor of safety with respect to time. These models have few restrictions with respect to non-homogeneity and anisotropy of the soil.

The pore-air pressure in a natural slope can be assumed to be equal to atmospheric conditions. As a result, only water flow needs to be modelled. Water flow occurs in response to variations in hydraulic head and is governed by Darcy's law for both saturated and unsaturated conditions (Childs and Collis-George 1950). However, there is one difference. The coefficient of permeability for a saturated soil can usually be assumed to be a constant. For unsaturated soils, the coefficient of permeability must be written as a function of either matric suction, pore-water pressure head, pore-water pressure or water content. In this paper, it is assumed that the coefficient of permeability, k , is a function of matric suction (i.e., $k = k(u_a - u_w)$).

Since pore-air pressure is a constant, the coefficient of permeability can be written as a function of the negative pore-water pressure (i.e., $k(-u_w)$). Water flows from a point of high hydraulic head to a point of low hydraulic head. The hydraulic head, h , is comprised of an elevation head, Y , and a pore-water pressure head (i.e., $u_w / \rho_w g$, where ρ_w is the density of water and g is the gravity acceleration).

The flow in and out of a two-dimensional, referential element can be expressed in terms of Darcy's law and equated to the rate of change of water volume (i.e., $\partial(V_w / V_0) / \partial t$).

$$[9] \quad \frac{\partial(V_w / V_0)}{\partial t} = -\frac{\partial}{\partial x} \left(k_x \frac{\partial h}{\partial x} \right) - \frac{\partial}{\partial y} \left(k_y \frac{\partial h}{\partial y} \right)$$

where:

V_w = volume of water in the element, and
 V_0 = total initial volume of the element.

Fredlund and Morgenstern (1976) proposed the following water phase constitutive relationship for an unsaturated soil.

$$[10] \quad \frac{\Delta V_w}{V_0} = m_1^w d(\sigma - u_a) + m_2^w d(u_a - u_w)$$

where:

m_1^w = slope of the water volume versus $(\sigma - u_a)$ relationship when $d(u_a - u_w)$ is zero, and
 m_2^w = slope of the water volume versus $(u_a - u_w)$ relationship when $d(\sigma - u_a)$ is zero (i.e., storage parameter).

Assuming that total stress remains constant and the pore-air pressure is atmospheric, eq. [10] can be substituted into eq. [9] to give,

$$[11] \quad \frac{\partial}{\partial x} \left(k_x \frac{\partial h}{\partial x} \right) + \frac{\partial}{\partial y} \left(k_y \frac{\partial h}{\partial y} \right) = \rho_w g m_2^w \frac{\partial h}{\partial t}$$

Equation [11] has been programmed in the PC-SEEP computer software, marketed by Geo-Slope Programming Ltd., Calgary, Alberta, Canada, and was used in the study presented herein.

Example to illustrate seepage/slope stability studies

A typical cross-section of a steep slope is used to illustrate the types of seepage/slope stability studies which can be conducted. The ground surface of the section is subjected to a flux to simulate a severe rainfall condition. The factor of safety will be computed at various elapsed times after the commencement of rainfall.

The example presented is that of a steep slope (typical of conditions in Hong Kong) in a residual soil, subjected to a particular environmental condition. The first part of the analysis involves the prediction of pore-water pressures as a result of a specified rainfall condition. The analysis is performed using the computer software, PC-SEEP. The second part of the analysis uses the computer software, PC-SLOPE, to determine the most critical, limit equilibrium factor of safety of the slope at various elapsed times. The effect of various ϕ^b values (presented as a ratio, ϕ^b / ϕ'), is also studied.

General layout of problem and material properties

The cut slope has an inclination of approximately 55 degrees to the horizontal. Its height is about 38 metres. The cross-section, along with the stratigraphy, is shown in Fig. 12.

The slope consists primarily of the residual soil, decomposed granite. The upper 5 meters consist of a layer of colluvium overlying a layer of completely decomposed granite. Below this is a layer of completely to highly decomposed granite. A thick layer of highly decomposed granite lies at the bottom of these strata. The face of the slope is covered by a thin layer of low permeability, cement-lime stabilized, decomposed granite called "chunam".

Several soil properties related to permeability and shear strength are required for the analyses. The saturated coefficients of permeability are presented in Table 2.

The unsaturated coefficient of permeability functions can be computed from a knowledge of the saturated coefficient of permeability and the suction versus water content relationships. The suction versus water content data for the colluvium and completely decomposed granite used in the example problem are shown in Fig. 13.

These data were used as input to a computer program which computed the relationship between suction and unsaturated coefficient of permeability (Lam 1984). The computed relationship can be fitted to the form of the permeability function proposed by Gardner (1958).

$$[12] \quad k = k_s / \left[1 + a \left(\frac{u_w}{\rho_w g} \right)^n \right]$$

where:

k = unsaturated coefficient of permeability (m/s),
 k_s = saturated coefficient of permeability (m/s),
 a = constant depending on the units of permeability and the pore-water pressure head at which the soil begins to desaturate, and
 n = positive dimensionless constant.

The values for a and n for the colluvium and decomposed granite were computed to be approximately 1.0 and 3.0, respectively. The storage parameter, m_2^w , for the colluvium and the decomposed granite was assumed to be 0.03 1/m for unsaturated soils. The shear strength properties and unit weights for the soils involved are summarized in Table 3.

The ϕ^b angle for each material are assumed to be varying percentages of the effective angle of internal friction (i.e., 0%, 25%, 50%, 75% and 100% of ϕ).

Initial conditions for the seepage analysis

The finite element mesh of the steep slope, along with the initial boundary conditions, are shown in Fig. 14. It is assumed that when the applied flux is in excess of the amount of water that can be taken in by the soil, water will not be allowed to pond at the boundaries. It is possible that a seepage face will develop from the base of the slope along the boundary EF , with time.

Fig. 12. Cross section of a cut slope in residual soil in Hong Kong.

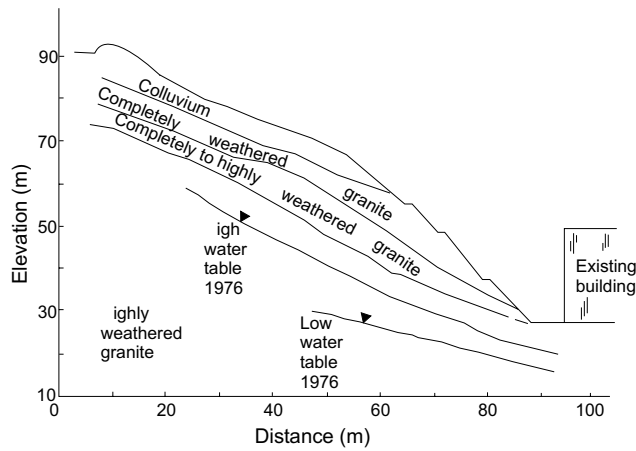


Table 2. Summary of saturated coefficients of permeability for the soils in the example.

Soil type	Saturated permeability (m/s)
Colluvium	3×10^{-5}
Completely decomposed granite	7×10^{-6}
Completely to highly decomposed granite	6×10^{-6}
Highly decomposed granite	5×10^{-6}

The initial boundary conditions are established by assuming the following condition. An average recharge flux of 2080 mm/year is applied to the system through the surface boundaries. The “chunam” portion is assumed to allow only 10% intake of the applied flux. Figure 15 shows the position of the initial groundwater table and the pore-water pressure head contours.

Seepage and slope stability results under rainfall conditions

One rainfall condition is selected for simulation using the transient seepage analysis. A rainfall intensity of 3.3×10^{-5} m/s is assumed. The rainfall is assumed to continue until steady state conditions are established. The analyses were performed using the PC-SEEP software. Figures 16 to 18 show the position of the groundwater tables and pore-water pressure head contours at several elapsed times as the analysis goes towards steady state conditions. Steady state conditions appear to be achieved in about one day. Figure 19 shows the change in pore-water pressure conditions along the vertical section, X-X, at various elapsed times.

The PC-SLOPE then used the output from the analysis performed using the PC-SEEP seepage program. Figure 20 shows the factors of safety with respect to various ϕ^b / ϕ ratios, for various elapsed times. Figure 21 illustrates the change in factor of safety with elapsed time for various ϕ^b / ϕ ratios. These are simply two ways of presenting the same information.

Fig. 13. Suction versus volumetric water content curves for completely decomposed granite and colluvium.

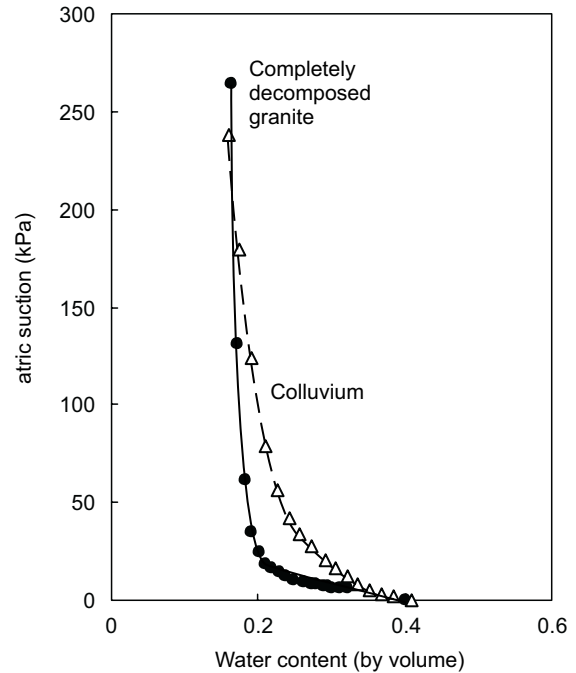


Fig. 14. Finite element mesh of the steep cut slope and the initial boundary conditions.

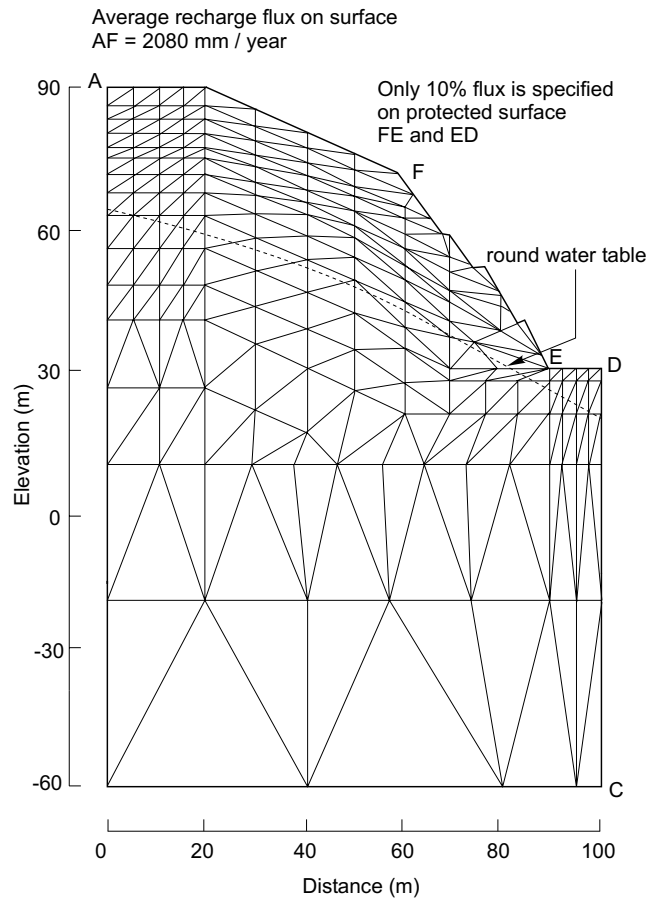


Table 3. Summary of shear strength parameters and total unit weights for the soils in the example.

Soil type	Cohesion, c' (kPa)	Effective angle of internal friction, ϕ' (degrees)	Total unit weight, γ_t (kN/m ³)
Colluvium	10	35	19.6
Completely decomposed granite	10	38	19.6
Completely to highly decomposed granite	29	33	19.6
Highly decomposed granite	24	41.5	19.6

Fig. 15. Initial groundwater condition and pore-water pressure head contour lines.

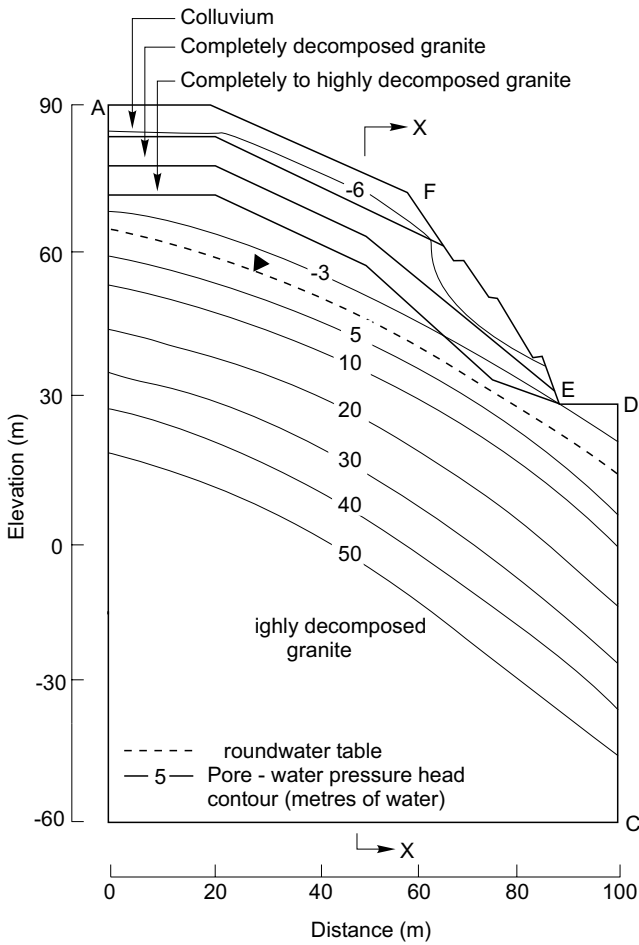
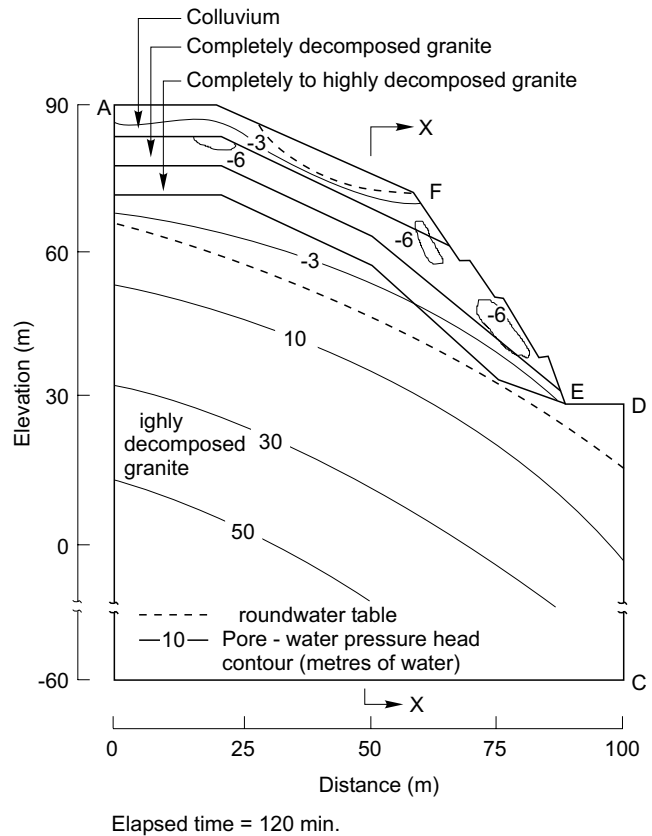


Fig. 16. Positions of groundwater table and pore-water pressure head contour lines at time = 120 min.



Analysis of the seepage/slope stability results

The seepage analysis shows that the groundwater table starts to mound beneath the toe of the slope at about 420 minutes. The wetting band below ground surface, AF, continues its downward development and connects with the groundwater table at about 960 minutes. Finally, when steady state conditions are achieved at 1410 minutes, the entire slope is essentially saturated.

Figures 20 and 21 show the effect of the negative pore-water pressure on the computed factor of safety. Under initial conditions, a considerable portion of the slope has negative pore-water pressures. The computed factor of

safety is 0.9 when the negative pore-water pressures are excluded from the slope stability analysis (i.e., $\phi^b / \phi' = 0.0$). The initial factors of safety ranged from 1.0 to 1.4 when the ϕ^b / ϕ' ratios ranged from 0.25 to 1.0, respectively. In other words, the negative pore-water pressures can have a significant effect on the stability of the slope.

During the rainfall, the factors of safety drop. Even when the ϕ^b / ϕ' ratio is equal to zero, the factors of safety drop because of the increase in positive pore-water pressures. In the other cases, the factor of safety drops primarily as a result of the diminishing negative pore-water pressures. After 600 minutes, the factors of safety for all cases are less than unity. Under steady state conditions the factor of safety goes to 0.81.

This is simply one example to illustrate:

Fig. 17. Positions of groundwater table and pore-water pressure head contour lines at time = 480 min.

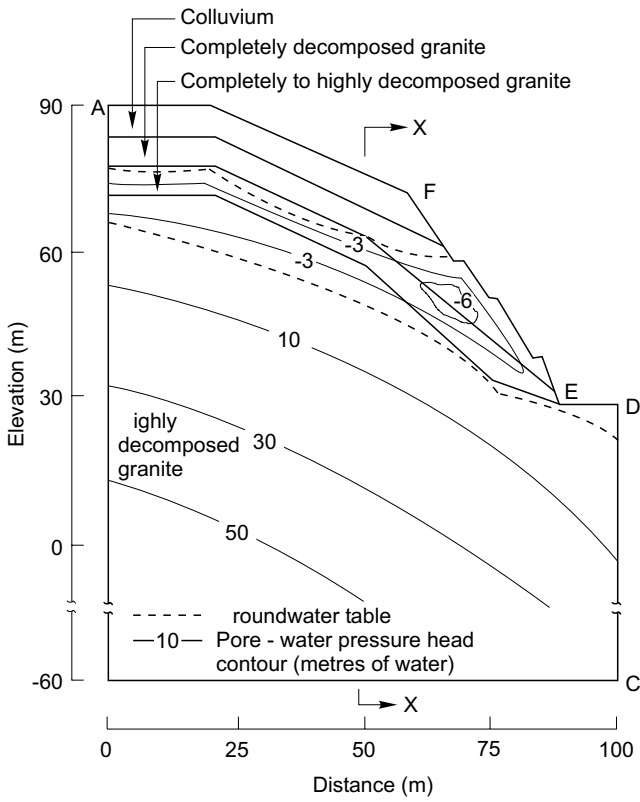


Fig. 18. Positions of groundwater table and pore-water pressure head contour lines at time = 1410 min.

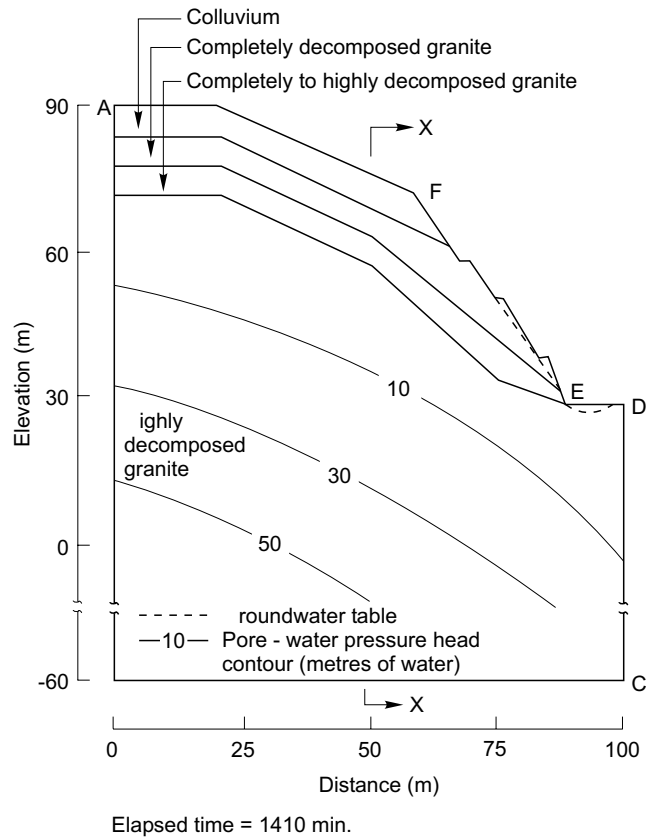


Fig. 19. Suction profiles for section X-X at various elapsed times.

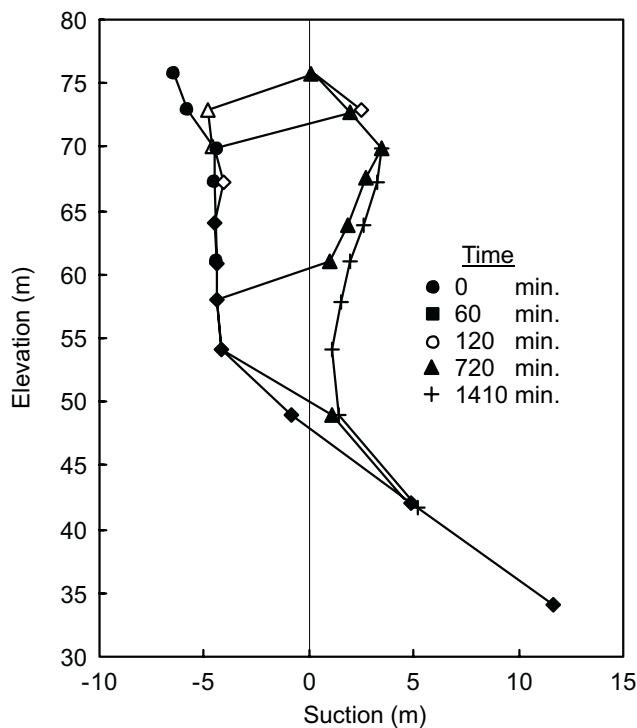


Fig. 20. Factor of safety with respect to ϕ^b / ϕ' .

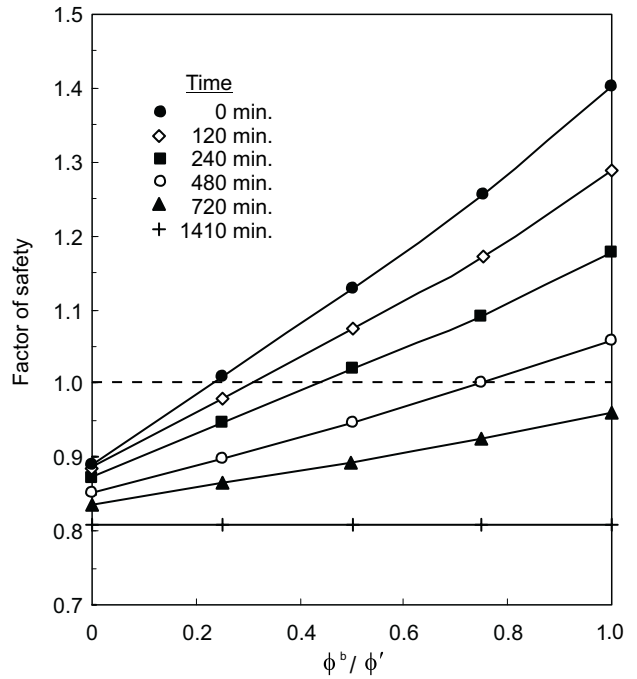
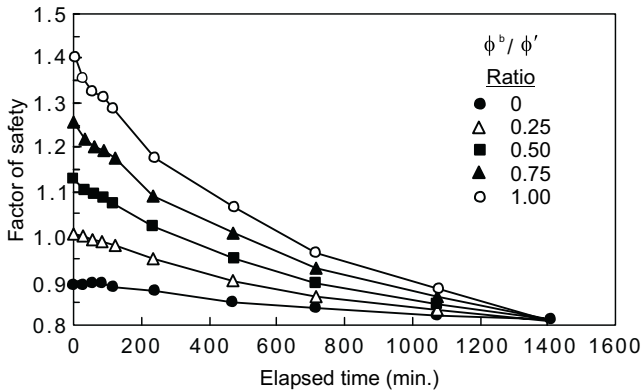


Fig. 21. Factor of safety with respect to elapsed times from the beginning of the rainfall.



- i) the manner in which saturated-unsaturated flow modeling can be combined with limit equilibrium slope stability analysis in order to study the effect of various microclimatic conditions, and
- ii) the role that negative pore-water pressures play in the computation of the factor of safety. It is beyond the scope of this paper to consider other examples.

Conclusion

In summary, the theory, experimental, and analytical tools are available for performing studies on the unsaturated portion of soil profiles. The strength contribution due to matric suction is significant in many cases and must be taken into consideration in order to perform meaningful analyses.

The present need is for case histories where:

- i) the *in situ* negative pore-water pressures are measured,
- ii) shear strength tests are performed to obtain the ϕ^b parameter in addition to the c' and ϕ' parameters,
- iii) the coefficients of permeability is measured and the unsaturated permeability function is determined, and
- iv) seepage/slope stability analyses are done to simulate the conditions of relevance.

As these type of case histories are conducted, a greater confidence will be obtained for analysing slope stability problems involving unsaturated soils.

References

- Bishop, A.W., Alpan, I., Blight, G.E., and Donald, I.B. 1960. Factors controlling the shear strength of partly saturated cohesive soils. Proceedings, ASCE Research Conference on Shear Strength of Cohesive Soils, University of Colorado, Boulder, CO, pp. 503–532.
- Bishop, A.W., and Henkel, D.J. 1962. The measurement of soil properties in the triaxial test. Second edition. Edward Arnold (Publisher) Ltd., London.
- Bocking, K.A., and Fredlund, D.G. 1980. Limitations of the axis-translation technique. Proceedings, 4th International Conference on Expansive Soils, Denver, CO, U.S.A., Vol. 1, pp. 117–135.
- Brand, E.W. 1984. Landslides in southeast Asia: A state of-art report. Proceedings, 4th International Symposium on Landslides, Toronto, Canada, September, 16–21, Vol. 1, pp. 17–59.
- Childs, E.C., and Collis-George, N. 1950. The permeability of porous materials. Proceedings of the Royal Society of London, Series A, **201**: 392–405.
- Escario, V. 1980. Suction controlled penetration and shear tests. Proceedings, 4th International Conference on Expansive Soils, Denver, CO, U.S.A., Vol. 2, pp. 781–797.
- Fontura, S.A.B., de Campos, L.E.P., and Costa Filno, L.M. 1984. A reanalysis of some slides in gneissic residual soils. Proceedings, 4th International Symposium on Landslides, Toronto, Canada, Vol. 1, pp. 625–630.
- Fredlund, D.G. 1981. The shear strength of unsaturated soils and its relationship to slope stability problems in Hong Kong. The Hong Kong Engineer, **9**(4): 37–45.
- Fredlund, D.G., and Morgenstern, N.R. 1976. Constitutive relations for volume change in unsaturated soils. Canadian Geotechnical Journal, **13**(3): 261–276.
- Fredlund, D.G., and Morgenstern, N.R. 1977. Stress state variables for unsaturated soils. ASCE, Journal of the Geotechnical Engineering Division, **103**(GT5): 447–466.
- Fredlund, D.G., and Rahardjo, H. 1988. State-of-development in the measurement of soil suction. Proceedings, 1st International Conference on Engineering Problems on Regional Soils, August 11–15, Beijing, China, pp. 582–588.
- Fredlund, D.G., Krahn, J., and Pufahl, D.E., 1981. The relationship between limit equilibrium slope stability methods. Proceedings, 10th International Conference on Soil Mechanics and Foundation Engineering, Stockholm, Sweden, Vol. 3, pp. 409–416.
- Fredlund, D.G., Morgenstern, N.R., and Widger, R.A. 1978. Shear strength of unsaturated soils. Canadian Geotechnical Journal, **15**(3): 313–321.
- Fredlund, D.G., Rahardjo, H., and Gan, J.K. 1987. Non-linearity of strength envelope for unsaturated soils. Proceedings, 6th International Conference on Expansive Soils, New Delhi, India, pp. 49–54.
- Gan, J.K., and Fredlund, D.G. 1988. Multistage direct shear testing of unsaturated soils. Geotechnical Testing Journal, **GTJODJ**, **11**(2): 132–138.
- Gan, J.K., Fredlund, D.G., and Rahardjo, H. 1988. Determination of the shear strength parameters of an unsaturated soil using the direct shear test. Canadian Geotechnical Journal, **25**(8): 500–510.
- Gardner, W.R. 1958. Some steady state solutions of unsaturated moisture flow equation with application to evaporation from a water table. Soil Science, **85**: 228–232.
- Hilf, J.W. 1956. An investigation of pore-water pressure in compacted cohesive soils. Ph.D. thesis, Technical Memorandum No. 654, United States Department of the Interior Bureau of Reclamation, Design and Construction Division, Denver, Colorado, U.S.A.
- Ho, D.Y.F., and Fredlund, D.G. 1982a. The increase in shear strength due to soil suction for two Hong Kong soils. Proceedings, ASCE Geotechnical Conference on Engineering and Construction in Tropical and Residual Soils, Honolulu, Hawaii, January, pp. 263–295.

- Ho, D.Y.F., and Fredlund, D.G. 1982*b*. Multi-stage triaxial tests for unsaturated soils. *Geotechnical Testing Journal*, **5**(1/2): 18–25.
- Ho, D.Y.F., and Fredlund, D.G. 1982*c*. Strain rates for unsaturated soils shear strength testing. *Proceedings, 7th Southeast Asian Geotechnical Conference*, November 22–26, Hong Kong, pp. 787–803.
- Lam, L. 1984. KCAL — A computer program for calculating unsaturated permeability. User's manual CD-19. Transportation and Geotechnical Group, Department of Civil Engineering, University of Saskatchewan, Saskatoon, SK, Canada.
- Papagianakis, A.T., and Fredlund, D.G. 1984. A steady state model for flow in saturated-unsaturated soils. *Canadian Geotechnical Journal*, **21**(3): 419–430.
- Satiya B.S. 1978. Shear behavior of partially saturated soils. Ph.D. thesis, Indian Institute of Technology, New Delhi, India.

The stability of slopes with negative pore-water pressures

D.G. Fredlund

Abstract: It is quite common engineering practice when analyzing the stability of a slope, to ignore the negative pore-water pressures above the groundwater table. This assumption however, may not be realistic and can affect both the computed factor of safety and the location of the critical slip surface.

This paper presents the derivation of the moment and force equilibrium factor of safety equations for an unsaturated soil and illustrates how its strength can be characterized. In addition to experimentally measuring the unsaturated shear strength properties of a soil, it is also possible to estimate these properties with sufficient accuracy from the soil-water characteristic curve.

Two example problems are analyzed to illustrate the manner in which the inclusion of the unsaturated soil strength affects a slope stability analysis. The unsaturated soil can have a significant affect on the computed results, particularly when the slope is steep and the water table is quite deep. The inclusion of the unsaturated soil strength has the effect of increasing the cohesion of the soil and results in a deepening of the critical slip surface.

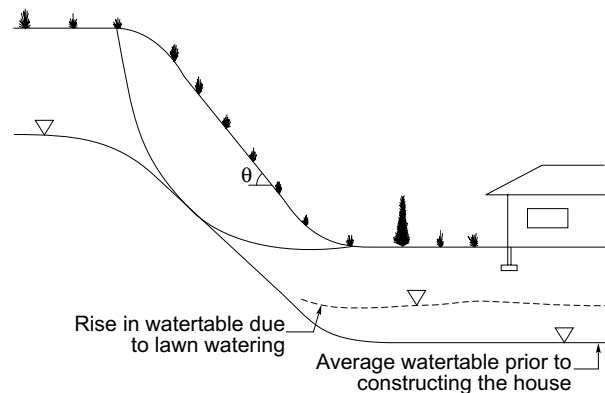
Key words: slope stability, negative pore-water pressure, unsaturated shear strength, factor of safety, critical slip surface.

Introduction

The practice of soil mechanics has, to a large extent been a discipline which has addressed problems where the pore-water pressures are positive. Situations where the pore-water pressures are negative have usually been dealt with by an all-encompassing assumption. The assumption may be to ignore the negative pore-water pressures by setting them to zero or to rely on the pore-water pressures remaining constant with time. These two extremes can be illustrated through the slope stability and bearing capacity example shown in Fig. 1.

When dealing with slope stability problems, the geotechnical engineer has often rationalized that negative pore-water pressures should be ignored because they cannot be relied upon in the longterm. In other words, it is envisaged that a heavy rainfall will result in the elimination of all the negative pore-water pressures. While at first this sounds plausible, it must be remembered that an unsaturated soil has both a low coefficient of permeability and a large water storage capacity. There can be conditions where a wetting front moves downward through a soil profile, essentially eliminating the negative pore-water pressures, however this may be more the exception than the rule. In order for this to occur, the ground sur-

Fig. 1. Illustration showing a slope stability and bearing capacity problem.



face infiltration must be sustained and high, approaching the saturated coefficient of permeability of the soil.

When dealing with the bearing capacity of spread footings and other types of foundations for structures, the geotechnical engineer has often followed the practice of performing unconfined compression tests and using these values to assist in computing a bearing capacity. The strength obtained from the unconfined compression test is to a large degree directly related to the negative pore-water pressure which is holding the specimen together. In using this practice, the engineer is assuming that the pore-water pressures will remain constant with time. At the same time, the owner of the building may regularly water his lawn, supplying more water to the soil than is received from precipitation. In some semi-arid regions it has been estimated that the water sprinkled onto lawns

D.G. Fredlund. Professor, Department of Civil Engineering, University of Saskatchewan, 57 Campus Drive, Saskatoon, SK, Canada S7N 5A9.

Reproduced with permission from the *Proceedings, Ian Boyd Donald Symposium on Modern Developments in Geomechanics*, Monash University, Melbourne, Australia, June 7, 1995. pp. 99–116.

may be as much as three times that of natural precipitation.

The above example is used to illustrate an inconsistency in the rationale on the part of the engineer. In the case of slope stability problems, it has been found to be expedient to ignore all negative pore-water pressures. In the case of bearing capacity problems, it has been found to be expedient to assume that the pore-water pressures will not change with time. The real reason behind these procedures has been related to a lack of understanding of unsaturated soil behavior and the inability to economically model flux boundary condition problems. Geotechnical engineers have preferred to analyze head boundary condition and zero flux boundary condition problems. The incorporation of the actual microclimatic conditions into analyses has proven difficult.

The objective of this paper is to illustrate the influence that negative pore-water pressures can have on the stability of a slope. Both planar and curvilinear shear strength envelopes for an unsaturated soil will be analysed. Examples involving steep slopes and flat slopes will be illustrated.

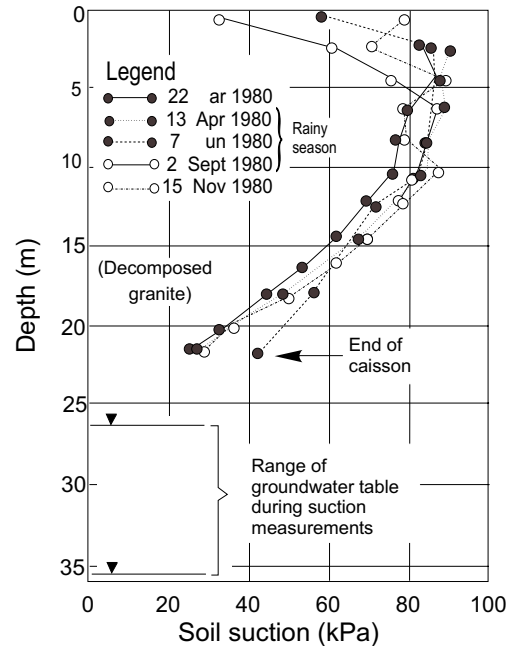
The permanency of negative pore-water pressures

Negative pore-water pressures cannot always be assumed to remain relatively constant with time. On the other hand, negative pore-water pressures cannot be assumed to disappear following each rainstorm. The negative pore-water pressure profile is dynamic, changing with time and is dependent upon many factors. Some of these factors are: 1.) the duration and intensity of the rainstorm, 2.) the saturated and unsaturated coefficient of permeability function for the soil, and 3.) the storage characteristics of the unsaturated soil.

Example situations have been published which illustrate both of the above mentioned conditions. The first example is from a slope instrumented with tensiometers in Hong Kong (Sweeney 1982). The slope is inclined at 60 degrees to the horizontal and has an average height of 30 metres. The stratigraphy consists entirely of weathered rhyolite. The surficial material is a completely weathered rhyolite 5 to 10 metres in thickness. The next stratum is a layer of completely to highly weathered rhyolite varying from 5 to 10 metres in thickness. The underlying stratum is a slightly weathered rhyolite followed by bedrock at 20 to 30 metres.

In situ suction measurements were made from an exploratory caisson shaft installed on the slope. Suction measurements were made on a periodic basis throughout the year, 1980, using a QuickDraw tensiometer. The measurements which extended through the rainy season of 1980 are shown in Fig. 2. Several noteworthy observations can be made from Fig. 2. First, the suction values over a depth of approximately 5 to 17 metres remained relatively constant throughout the year. Second, suctions in the upper 5 metres showed a gradual reduction during the rainy season. Third, the water table rose and fell about 9 metres throughout the season. In general, these

Fig. 2. Suction measurements in a weathered rhyolite in Hong Kong (after Sweeney 1982).



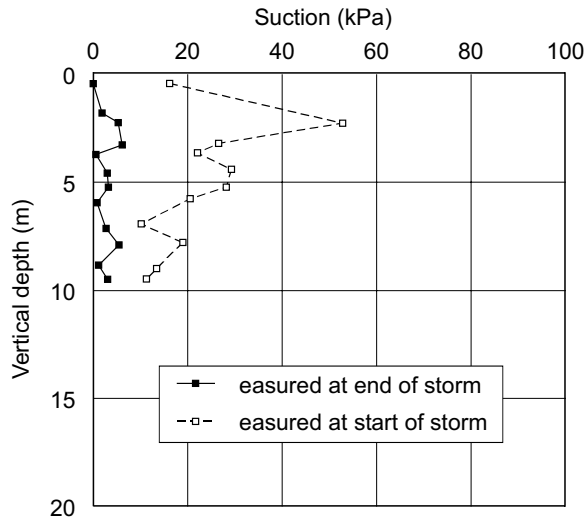
results illustrate the extreme buffering capabilities of the soil, provided the ground surface flux conditions and the soil permeability conditions bear the right relationship. Water continued to flow downward through the soil profile throughout the rainy season but the suctions remained almost constant. On the other hand, the groundwater table rose significantly because the soil in the capillary fringe is essentially saturated and requires only a small quantity of water to raise its elevation.

The second example involves a slope consisting of colluvium material in Hong Kong (Fig. 3). Once again, an exploratory caisson was advanced from which suction measurements were made (Anderson 1983). The weathered colluvial material which has accumulated on the slope is texturally more coarse than the soil mentioned in the first example. The saturated coefficient of permeability for the colluvium is approximately 3×10^{-5} m/s.

The *in situ* suction measurements proved to be relatively low. Also, during a rainstorm, the suctions essentially disappeared as a wetting front moved downward through the soil. In other words, a wetting front can move downward through the soil profile only under certain situations. The soil must be able to take the water in at a sufficiently high rate or the rainfall must continue over a long period of time.

The computer simulation of slopes consisting of various soil types, subjected to varying rainfall conditions, has supported the above observations (Fredlund 1989; Rulon and Freeze 1985). Further research is required in order to better understand the conditions under which suction can be relied upon in the long term. Figure 4 shows the relationship of water content and the coefficient of permeability to the suction in the soil. The water content versus matric suction relationship provides information on the water storage capability of the soil. The co-

Fig. 3. Suction measurements in a colluvium in Hong Kong (after Anderson 1983).



efficient of permeability versus matric suction relationship provides information on the ease with which water can move through the soil profile. This information along with the characteristics of the rainstorm are the primary factors influencing the long-term matric suction in the soil.

Derivation of force and moment equilibrium factor of safety equations

The General Limit Equilibrium method (GLE) proposed by Fredlund et al. (1981) is used to compare the changes to the limit equilibrium theory as different failure criteria are used. Essentially all other methods of slices using the limit equilibrium theory can be visualized as special cases of the GLE method (Fredlund and Krahn 1977). Figure 5 shows a typical steep slope divided into slices with the force and dimension variables defined. The definition of all the variables shown remains the same regardless of whether the soil is saturated or unsaturated. The factor of safety equations will be derived such that they are applicable for both the circular and non-circular slip surfaces.

Shear force mobilized at the base of a slice

The only variables affected in going from the saturated condition to the unsaturated condition is the shear force mobilized at the base of each slice, S_m . The shear force mobilized at the base of the slice can be written in terms of the shear strength of the soil:

$$[1] \quad S_m = \frac{\tau\beta}{F_s}$$

where:

F_s = factor of safety; more specifically, the factor by which the shear strength of the soil must be reduced to bring the soil mass into a state of limiting equilibrium,

Fig. 4. Illustration of the relationships between water content, soil suction and coefficient of permeability.

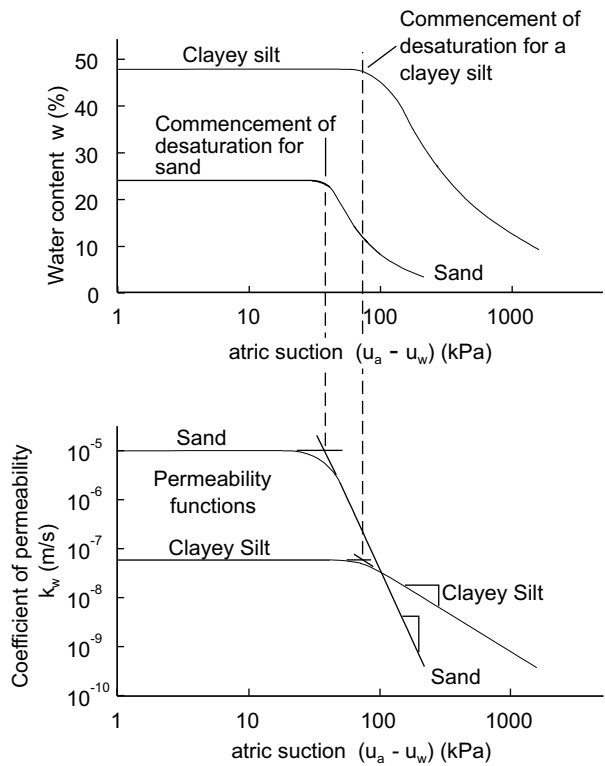
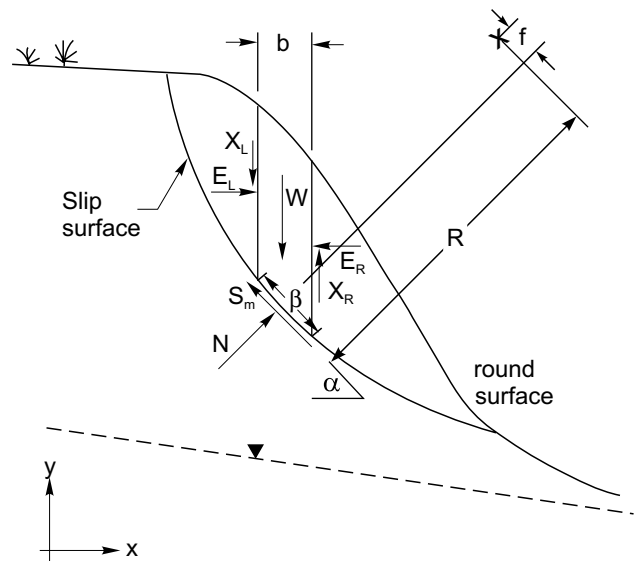


Fig. 5. Forces acting on each slice for a slope stability analysis.



τ = the shear strength of the saturated or unsaturated soil, and
 β = length across the base of a slice

It is therefore possible to derive moment and force equilibrium factor of safety equations which apply equally for both saturated and unsaturated conditions.

Normal force at the base of a slice

For either the force or moment equilibrium factor of safety equations, it is necessary to write the normal force at the base of a slice in terms of the other forces acting on the slice. The normal force, N , is derived by summing forces in the vertical direction.

$$[2] \quad N = \frac{W - (X_R - X_L) - S_m \sin \alpha}{\cos \alpha}$$

where:

N = total normal force acting on the base of a slice, equal to $\sigma_n \beta$ where σ_n is the normal stress acting over the sloping distance, β ,

W = total weight of a slice of width b and height h ,

X_R, X_L = vertical interslice shear force on the left and right sides of a slice, respectively, and

α = angle between the base of the slice and the horizontal.

Force equilibrium factor of safety equation

The factor of safety equation with respect to force equilibrium is derived by summing forces in the horizontal direction for all slices.

$$[3] \quad F_F = \frac{\sum \tau \beta}{\sum N \sin \alpha}$$

where:

F_F = factor of safety with respect to force equilibrium.

Moment equilibrium factor of safety equation

The factor of safety with respect to moment equilibrium can be derived by summing moments relative to an arbitrary point above the central portion of the slip surface. The point about which moments are summed is not of relevance provided both force and moment conditions are satisfied (Fredlund et al. 1992). However, the point should be in the general region above the slip surface to prevent possible problems with numerical instability. When only moment equilibrium is satisfied, the computed factor of safety varies slightly with respect to the point selected for the summation of moments.

$$[4] \quad F_M = \frac{\sum \tau \beta R}{\sum Wx - \sum Nf}$$

where:

R = radius or moment arm associated with the shear strength mobilized at the base of each slice,

x = horizontal distance from the centre of each slice to the centre of moments,

f = offset distance from the normal force on the base of a slice to the centre of moments, and

F_M = factor of safety with respect to moment equilibrium.

Other forces required to solve for the factor of safety

The objective of the stability analysis is to compute a factor of safety, F , which satisfies both force and moment equilibrium conditions. However, to do this, it is necessary to compute some other forces. For example, while all the interslice shear and normal forces cancel when computing the force and moment equilibrium factors of safety, such is not the case when computing the normal forces on each slice. The summation of horizontal forces on each slice can be used to compute the total interslice normal force, E .

$$[5] \quad (E_R - E_L) = [W - (X_R - X_L)] \tan \alpha - \frac{\tau \beta}{F \cos \alpha}$$

Since the factor of safety appears in the equation to compute the interslice normal force, it is necessary to first assume these forces are zero until an estimate of the factor of safety is computed. Then, through an iterative process it is possible to solve for interslice normal forces which satisfy the overall factor of safety.

A further difficulty arises in that the interslice shear forces are also unknown. In fact, the overall solution for the factor of safety is indeterminate. The indeterminacy has been most commonly accommodated by assuming that a functional relationship exists between the interslice shear and normal forces (Morgenstern and Price 1965).

$$[6] \quad X = \lambda f(x)E$$

where:

$f(x)$ = a functional relationship which describes the manner in which the magnitude of X/E varies across the slip surface, and

λ = a scaling constant which represents the percentage of the function, $f(x)$, used for solving the factor of safety equations.

Equation [6] applies for both the right side and the left side of the slice and is usually considered to be in terms of total stresses. The computed magnitudes for the interslice shear forces must lag one iteration behind the computation of the normal force at the base of each slice, along with the computation of the interslice normal forces.

Originally, the interslice force functions, $f(x)$, were arbitrarily selected. Fan et al. (1983) performed finite element analyses where the gravity forces were 'switched-on' and the magnitudes of the interslice force functions were computed. This analysis was performed for hundreds of trial slip surfaces on many different geometric configurations. The results yielded an empirical interslice force relationship which has the form of an extended error function.

$$[7] \quad f(x) = \frac{Ke^{(-c^n \omega^n)}}{2}$$

where:

e = base of the natural logarithm (i.e., 2.71828),

- K = magnitude of the interslice force function at midslope (i.e., maximum value for the function). This value can be set to 1.0 if desired and its effect will be taken into account in the solution through a change in the computed λ value,
- C = variable to define the inflection points of the function, $f(x)$,
- n = variable to specify the flatness or sharpness of curvature of the function, and
- ω = dimensionless x -position relative to the mid-point of the slope.

The constants C and n are a function of the slope inclination (Fredlund 1984). It is possible to write unique mathematical equations which best-fit these functions. As a result, the interslice force function can be computed solely based on a knowledge of the inclination of the slope, δ . Proposed empirical equations for C and n are shown below.

[8] $C = 0.039 \delta$ when $\delta \leq 45^\circ$
 $C = 0.091 \delta$ when $\delta > 45^\circ$

[9] $n = 18.31 - 4.29 \ln(\delta)$ when $\delta \leq 45^\circ$
 $n = 2.0$ when $\delta > 45^\circ$

where:

δ = average angle of inclination of the slope, measured from the horizontal (in degrees).

Shear strength theory

The difference between performing slope stability analyses on saturated and unsaturated soils lies in the equation used to define shear strength.

Saturated soil shear strength envelope

The shear strength of a saturated soil is controlled by one stress state variable, namely, the effective stress, $(\sigma_n - u_w)$. The corresponding Mohr-Coulomb failure envelope is a straight line defined by an intercept, c' (i.e., effective cohesion) and a slope, $\tan \phi'$ (i.e., tangent of the effective angle of internal friction) as shown in Fig. 6. The saturated shear strength equation is written as follows:

[10] $\tau = c' + (\sigma_n - u_w) \tan \phi'$

where:

σ_n = total normal stress on the slip surface.

Unsaturated soil with a planar modified Mohr-Coulomb envelope

An unsaturated soil requires two independent stress state variables which must be given consideration in defining the failure envelope. The Mohr-Coulomb type formulation for a saturated soil has been extended to a formulation for unsaturated soils by Fredlund et al. (1978). In so doing, the two-dimensional failure line for saturated soils becomes a three-dimensional failure sur-

Fig. 6. Mohr-Coulomb failure envelope for a saturated soil.

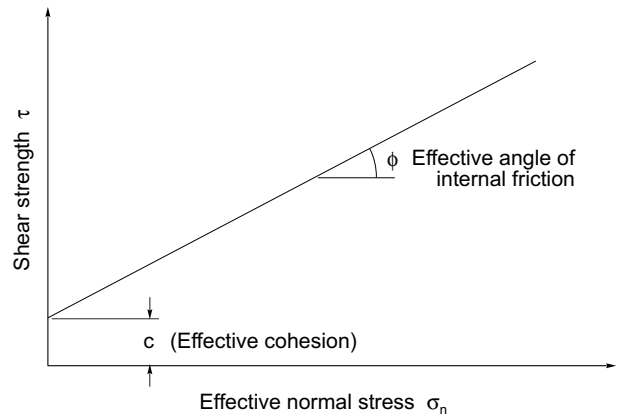
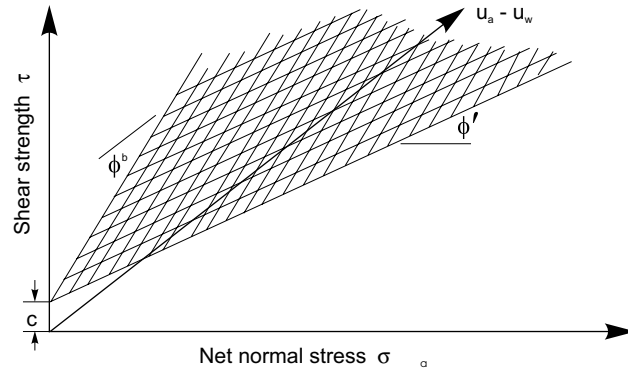


Fig. 7. Planar modified Mohr-Coulomb failure envelope as a planar surface for an unsaturated soil.



face for an unsaturated soil (Fig. 7). If the surface is assumed to be planar, the equation for the unsaturated shear strength can be written as follows:

[11] $\tau = c' + (\sigma_n - u_a) \tan \phi' + (u_a - u_w) \tan \phi^b$

where:

ϕ^b = the slope of the shear strength versus matric suction, $(u_a - u_w)$, relationship when $(\sigma_n - u_a)$ is held constant, and

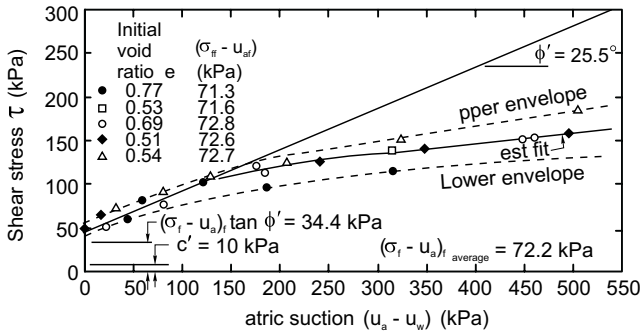
u_a = pore-air pressure in the soil which in many cases will be, equal to atmospheric conditions.

The effective angle of internal friction is assumed to be the same for all suction values. In other words, the planar surface has no 'warp'.

Unsaturated soil with a curved matric suction envelope

As unsaturated soils have been tested over an increasingly larger range of suction values, it has become clear that the failure envelope with respect to suction is non-linear. Several researchers have published data which clearly shows the non-linearity. One example is the laboratory data on a compacted glacial till presented by Gan et al. (1988) (Fig. 8). The tests were performed in a modified direct shear box with matric suctions ranging from 0

Fig. 8. Shear strength versus matric suction for a compacted glacial till with a net normal stress of 72.2 kPa (after Gan et al. 1988).



to 500 kPa. At matric suctions below the air entry value (i.e., 120 kPa) the ϕ^b value is equal to the ϕ' value. At matric suctions greater than the air entry value, the ϕ^b value decreases with matric suction.

Similar results showing the non-linearity of the failure envelope were obtained by Donald (1956) on tests performed on several sands (Fig. 9). The sands, being coarser in texture, desaturate at relatively low suction values. Unfortunately, the value of these data went largely unheeded by the research community.

When a non-linear shear strength versus suction relationship is incorporated into the Mohr-Coulomb failure envelope, a warped surface is obtained (Fig. 10). It is assumed that the non-linearity in the matric suction direction is the same at all net normal stresses. This may not be rigorously correct but represents a first approximation of the non-linearity with respect to matric suction.

Use of the soil-water characteristic curve to estimate the shear strength versus matric suction relationship

Experimental studies to measure the unsaturated shear strength parameters are generally costly, time consuming and difficult to conduct. It would be of value to be able to approximate the shear strength versus matric suction relationship through the use of a relatively simple laboratory test. Fredlund and Rahardjo (1993) suggested that the soil-water characteristic curve can be used to obtain approximations for shear strength versus matric suction relationship.

The soil-water characteristic curve is defined as the variation of water storage capacity of a soil with respect to suction. The soil-water characteristic curve is generally plotted as the variation of volumetric water content, θ , or gravimetric water content, w , or degree of saturation, S , with respect to suction. The suction may be either the matric suction (i.e., $(u_a - u_w)$), or the total suction (i.e., the matric plus osmotic suction) of the soil. At high suctions (i.e., greater than about 2,500 kPa), matric suction and total suction are generally assumed to be similar.

Figure 11(a) shows a typical soil-water characteristic curve plotted as the degree of saturation versus matric suction. The air-entry value of the soil, $(u_a - u_w)_b$, and the residual degree of saturation, S_r , are shown on the figure.

Fig. 9. Results of direct shear tests on sands under low matric suctions (modified after Donald 1956).

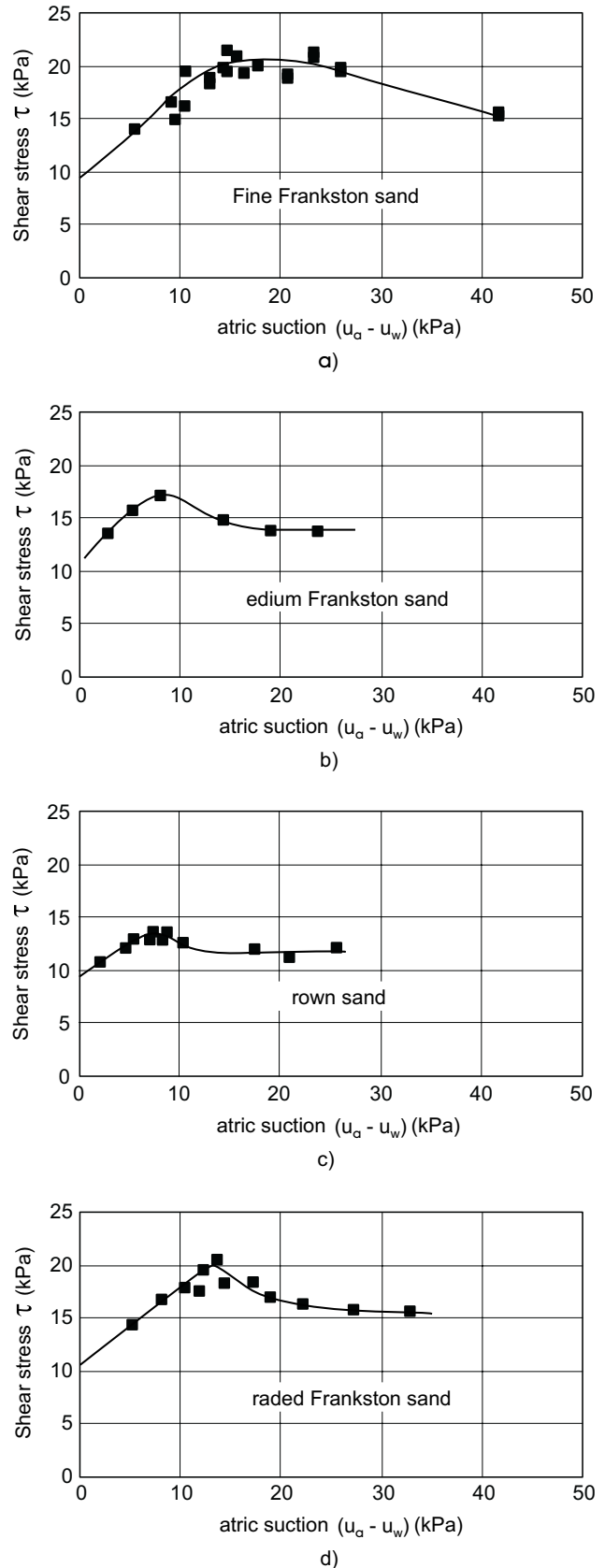
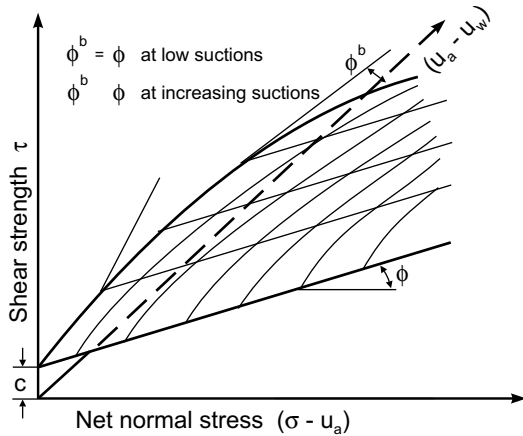


Fig. 10. Non-planar Mohr-Coulomb failure envelope with respect to matric suction for an unsaturated soil.



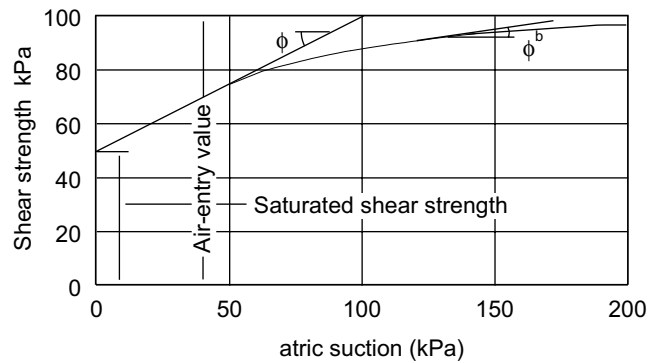
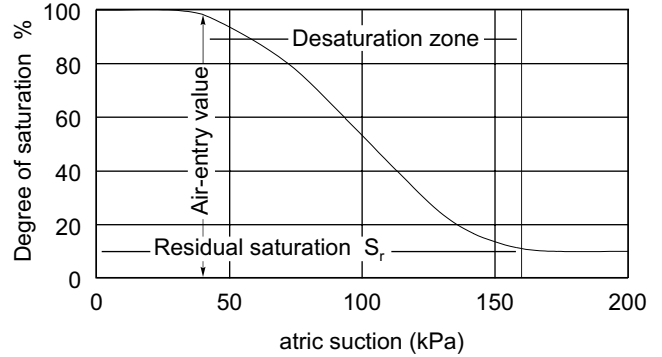
The air-entry value, $(u_a - u_w)_b$, of the soil is the matric suction at which the specimen starts to desaturate. Desaturation continues as matric suction is increased until eventually an increase in suction produces little decrease in the degree of saturation. The degree of saturation at this value of suction is called the residual degree of saturation, S_r .

Figure 11b shows a typical shear strength soil suction relationship. Figure 11a and Figure 11b show the relationship between the shear strength and the soil-water characteristic curves. The rate of desaturation with respect to an increase in matric suction, (i.e., $dS / d(u_a - u_w)$) is greatest between the air-entry value and the suction value corresponding to residual conditions. There is little or no desaturation of the soil up to the air-entry value, $(u_a - u_w)_b$ (i.e., the soil acts essentially as a fully saturated soil up to its air-entry value and ϕ^b is equal to ϕ). At suctions above the air entry value, the contribution of shear strength due to suction decreases with the desaturation of the soil. This results in a non-linear variation of shear strength with respect to suction. Thus, there is a strong correlation between the shear strength behavior of an unsaturated soil and the soil-water characteristic curve.

Several investigators have made contributions towards the prediction of the unsaturated coefficient of permeability of soils through the use of soil-water characteristic curve along with the saturated coefficient of permeability of the soil (Marshall 1958; van Genuchten 1980; Fredlund et al. 1994). A similar type of formulation can also be used to predict the unsaturated shear strength of soils. An equation describing the soil-water characteristic curve for entire suction range of (i.e., 0 to 1,000,000 kPa) is given by Fredlund and Xing (1994), as:

$$[12] \quad \theta = \theta_s \left[1 - \frac{\ln \left(1 + \frac{\Psi}{\Psi_r} \right)}{\ln \left(1 + \frac{1000000}{\Psi_r} \right)} \right] \left[\frac{1}{\ln \left(e + \left(\frac{\Psi}{a} \right)^n \right)} \right]^m$$

Fig. 11. General behavioral relationship between soil-water characteristic curve and shear strength (modified from Vanapalli 1994).



In terms of degree of saturation versus suction, eq. [12] takes the form:

$$[13] \quad S = \left[1 - \frac{\ln \left(1 + \frac{\Psi}{\Psi_r} \right)}{\ln \left(1 + \frac{1000000}{\Psi_r} \right)} \right] \left[\frac{1}{\ln \left(e + \left(\frac{\Psi}{a} \right)^n \right)} \right]^m$$

where:

- θ = volumetric water content,
- θ_s = saturated volumetric water content or porosity,
- S = degree of saturation defined as the ratio of volume of voids to total volume,
- e = base of the natural logarithm, 2.71828,
- Ψ = soil suction,
- Ψ_r = suction corresponding the residual water content, θ_r or residual saturation, S_r ,
- a = an approximation of the air-entry value,
- n = parameter controlling the slope at the inflection point in the soil-water characteristic curve, and
- m = parameter related to the residual water content.

The fitting parameters in eq. [12] or eq. [13] (i.e., a , n , and m) using the soil-water characteristic curve data can be determined using a non-linear regression procedure

outlined by Fredlund and Xing (1994). The soil-water characteristic curve data of any soil can be defined as a mathematical function. Numerical results show that eq. [12] or eq. [13] describe the soil-water characteristic curve reasonably well for most soils over the entire suction range (i.e., 0 to 1,000,000 kPa). A general predictive model for shear strength using the rigorous form of the soil-water characteristic curve eq. [13] is given by Vanapalli (1994) :

$$[14] \quad \tau = c' + (\sigma_n - u_a) \tan \phi' + \tan \phi' \left[\frac{(S - S_r)}{100 - S_r} \right] (u_a - u_w)^*$$

where:

S in eq. [14] is defined by eq. [13].

The residual degree of saturation, S_r , and its corresponding suction value is approximated from the soil-water characteristic curve data.

Test data and analysis to illustrate prediction of shear strength versus suction

An experimental program was conducted for determining the shear strength characteristics of specimens of a statically compacted glacial till at different water contents (i.e., representing dry, optimum and wet of optimum conditions) and densities under consolidated drained conditions using multistage direct shear tests. The tests were conducted under different levels of net normal stress and matric suction. The soil-water characteristic curves were developed using a pressure plate apparatus and desiccators with specimens pre-consolidated to the equivalent net normal stresses used in the experimental program. The experimental test results were compared with the predictive model. There is a good correlation between the experimental results and the predicted values of shear strength (Vanapalli 1994).

In this paper only a typical set of experimental results conducted on a specimen loaded to a net normal stress of 25 kPa are presented. The initial water content of the specimen was 16% and the dry density, γ_d , was 1.78 Mg/m³. The saturated shear strength parameters are as follows: effective cohesion, c' is equal to zero and angle of internal friction, ϕ' is 23.5 degrees. The soil-water characteristic curve for the entire range of suctions from 0 to 1 000 000 kPa is shown in Fig. 12.

The fitting parameters obtained using non-linear regression analysis for defining the soil-water characteristic curve were : a is equal to 117.3, n is equal to 0.77 and m is equal to 0.49 using eq. [20]. The residual degree of saturation and suction was 65% and the corresponding matric suction was 1,500 kPa. The residual degree of saturation at 1,500 kPa is not very distinct for this soil (Fig. 12). At this value of suction the rate of desaturation has dropped considerably, and only small changes in degree of saturation result for large increments of suction.

The variation of shear strength with suction using the model and experimental results are shown in Fig. 13. The

Fig. 12. Soil-water characteristic curve for a compacted glacial till specimen with 25 kPa net normal stress.

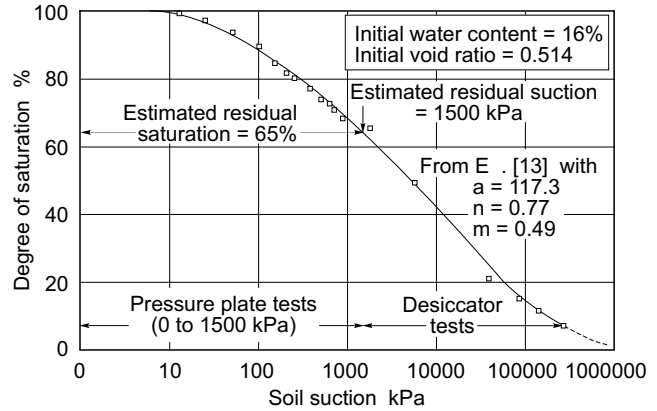
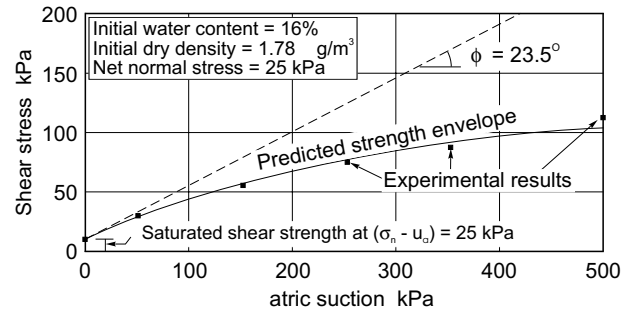


Fig. 13. Comparison of experimental and predicted variation of shear strength with matric suction.



experimental results are shown by symbols and the continuous line is the predicted variation of shear strength with suction. There is good correlation between the experimental results and the predicted values of shear strength using eq. [14].

The effect of matric suction on the shear strength of the soil is reduced as the soil desaturates (or as the volumetric water content decreases). Since the soil-water characteristic curve provides the relationship between degree of saturation and suction, it is possible to use this relationship to predict changes in shear strength with respect to matric suction.

Influence of negative pore-water pressures on the factor of safety

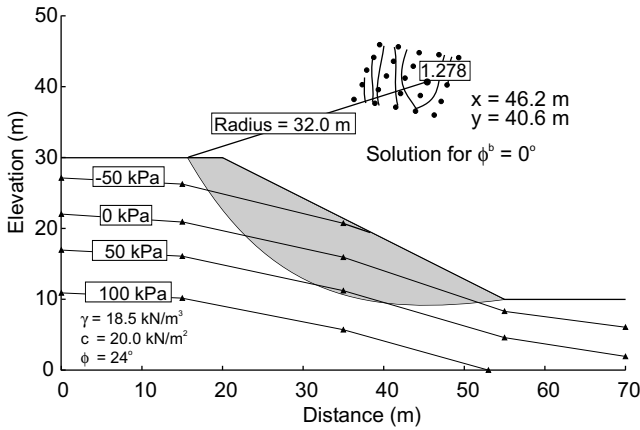
Two example problems have been selected to illustrate the effect of taking negative pore-water pressures into account in a slope stability analysis. One slope is relatively flat with a high water table while the other is steep with a deeper water table. Each slope is analysed using a planar, modified Mohr-Coulomb failure envelope for the unsaturated soil. The angle with respect to matric suction, ϕ^b , is varied from 0 degrees to 25 degrees.

Case of a relatively flat slope

The relatively flat slope is 20 metres high at a slope angle of 30 degrees (Fig. 14). Approximately two-thirds

*Note: An error occurred in the original print of Eq. [14]: $\tau = c' + (\sigma - u_a) \tan \phi' + \tan \phi' \int_0^{\psi} \left[\frac{(S - S_r)}{1 - S_r} \right] d(u_a - u_w)$.

Fig. 14. The critical slip surface for a relatively flat slope when negative pore-water pressures are not taken into account.



of the slip surface passes below the water table. The unit weight of the soil is 18.5 kN/m³. The cohesion is 20 kN/m² and the effective angle of internal friction is 24 degrees. The factor of safety values are computed using the GLE method.

Figure 14 also shows the general layout of the example along with the solution for the case where the negative pore-water pressures are not taken into account. The minimum factor of safety is 1.278. At each grid center a series of radii were analysed to ensure that a minimum value had been obtained. The factor of safety versus radius for all of the grid centers is shown in Fig. 15. It can be seen that while the shorter radius slip surface indicates an increased factor of safety, the increase is relatively small. In some cases it has been noted that the minimum slip surface turns out to be the most shallow surface when the negative pore-water pressures are ignored.

Figure 16 shows the results using a ϕ^b angle of 15 degrees. The factor of safety has increased to 1.319 (i.e., only about 2.9%) but the location of the critical slip surface is on average 1.5 metres deeper than previous. The location of the corresponding grid center stayed almost the same but there appears to be a slight rise and movement towards the left. In other words, negative pore-water along with their associated strength cause the slip surface to deepen. The factor of safety versus radius for all of the grid centers is shown in Fig. 17. The character of the results has changed dramatically from those in Fig. 15. All of the shallow slip surfaces now show factors of safety going beyond a magnitude of 4.0. There is now no tendency for a shallow slip surface to be computed as the critical slip surface.

When the ϕ^b angle was increased to 25 degrees, the factor of safety increased to 1.353 (i.e., about 5.3% over the case when ignoring negative pore-water pressures). The critical slip surface also deepened.

Taking the negative pore-water pressure into account appears to be beneficial in the case of only a relatively small portion of the slip surface raising above the water

Fig. 15. Factor of safety versus radius for all grid centres for a relatively flat slope when negative pore-water pressures are ignored.

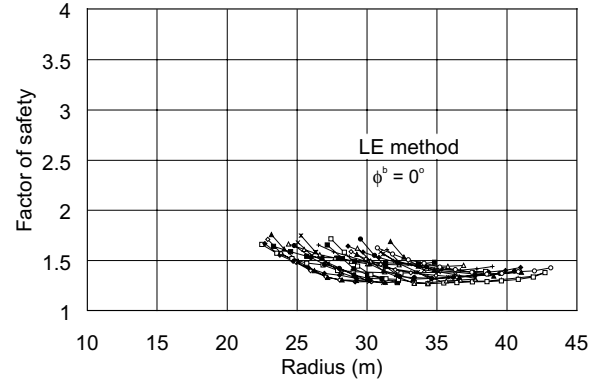


Fig. 16. The critical slip surface for a relatively flat slope when negative pore-water pressures are taken into consideration.

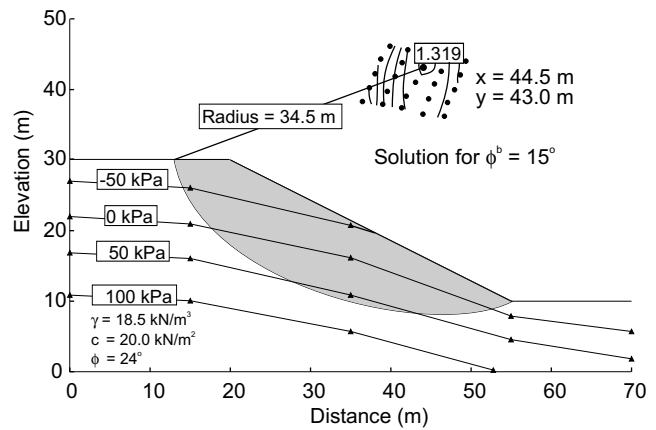


Fig. 17. Factor of safety versus radius for all grid centres for a relatively flat slope when negative pore-water pressures are taken into consideration.

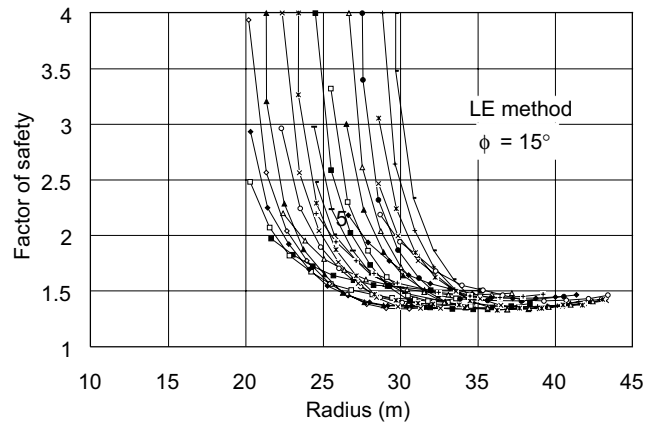


table. The problem will generally be modelled in a more realistic manner and the location of the critical slip surface should be more meaningful.

Fig. 18. The critical slip surface for a steep slope when negative pore-water pressures are ignored.

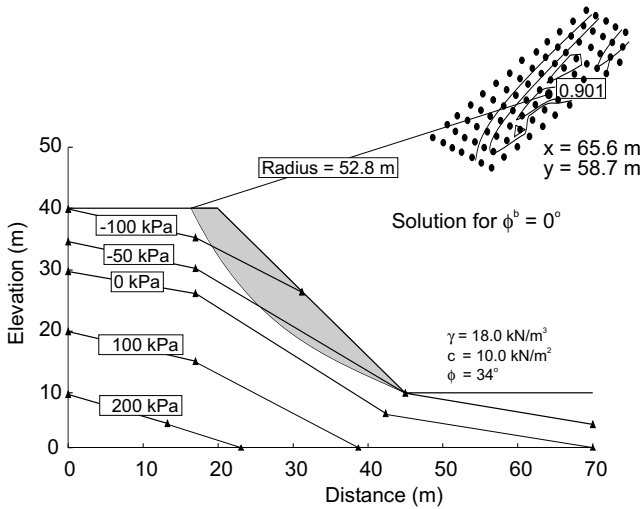
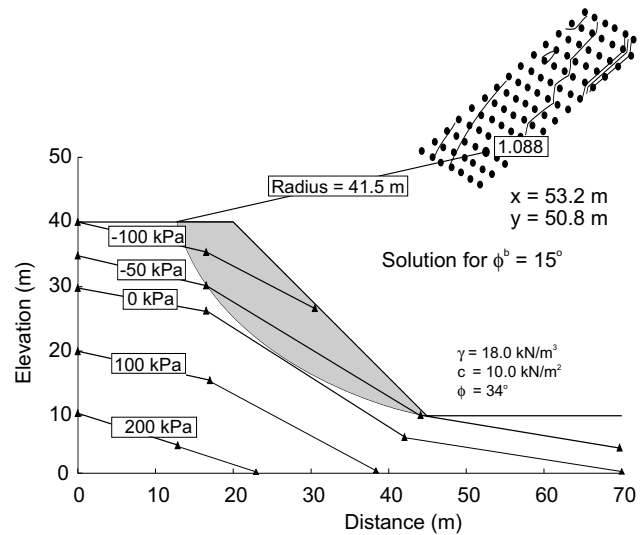


Fig. 19. The critical slip surface for a steep slope when negative pore-water pressures are taken into account.



Case of a steep slope

The steeper slope example has an angle of 50 degrees to the horizontal. Most of the slip surface will pass above the water table which is on average 8 metres below the surface of the slope. The unit weight of the soil is 18.0 kN/m³. The cohesion is 10.0 kN/m² and the effective angle of internal friction is 34 degrees.

Figure 18 shows the geometry of the example along with the solution when negative pore-water pressures are ignored. The computed factor of safety for the critical slip surface is 0.901. Figure 19 shows the results when the ϕ^b angle is 15 degrees and negative pore-water pressures are taken into account. The factor of safety on the critical slip surface is now 1.088 or an increase of 20.3%. The critical slip surface went considerably deeper and the corresponding grid centre moved towards the slope.

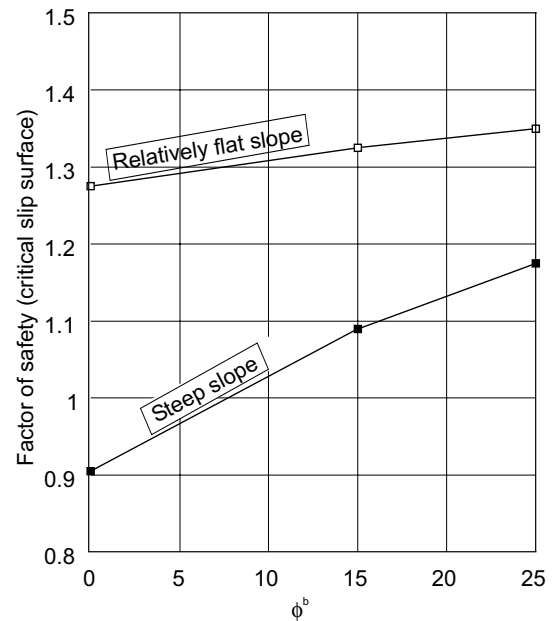
Increasing the ϕ^b angle to 25 degrees, the factor of safety increased to 1.170 (i.e., about 29.6% increase over the case where negative pore-water pressures were ignored). The critical slip surface also deepened.

Figure 20 shows the factors of safety for the above two examples plotted versus the ϕ^b angle. The factors of safety are shown to increase with suction. The examples selected are by no means extreme cases. For example, it is possible for *in situ* negative pore-water pressures to be considerably higher than shown in the examples. At the same time it must be realized that the soils near the ground surface may have a significant decrease in suction at certain times of the year.

Summary

The conventional moment and force methods of slices can readily be extended to accommodate unsaturated soil behavior. Either a planar or non-planar designation of the shear strength with respect to matric suction can be used in the analysis. The non-planar surface can either be mea-

Fig. 20. The increase in factor of safety versus the ϕ^b angle for the relatively flat and steep slope.



sured in the laboratory or estimated from the saturated shear strength parameters and the soil-water characteristic curve.

The effect of negative pore-water pressures should be taken into consideration when analysing both relatively flat slopes with high water tables and steep slopes with much deeper water tables. Taking negative pore-water pressure into account on a relatively flat slope does not significantly change the computed factor of safety. It sometimes, however, prevents the analyst from concluding that a relatively shallow slip surface is the most critical slip surface.

The location of the critical slip surface is changed somewhat when negative pore-water pressures are taken into account. The negative pore-water pressures and the associated ϕ^b angle can be taken into account in an appropriate manner.

For steep slopes with a relatively deep water table, the effect of negative pore-water pressures can be quite significant. The location of the critical slip surface can change significantly when negative pore-water pressures are taken into account. The same is true for the computed factors of safety.

Acknowledgements

The author would like to acknowledge the assistance of D. Cook, J.K-M. Gan and S.K. Vanapalli in the preparation of this manuscript.

References

- Anderson, M.G. 1983. Prediction of soil suction for slopes in Hong Kong. Geotechnical Control Office Publication No. 1184, Special Projects Division, Engineering Development Department, Hong Kong, pp. 243.
- Donald, I.B. 1956. Shear strength measurements in unsaturated non-cohesive soils with negative pore pressures. Proceedings, 2nd Australia-New Zealand Conference on Soil Mechanics and Foundation Engineering, Christchurch, New Zealand, pp. 200–205.
- Fan, K., Fredlund, D.G., and Wilson, G.W. 1986. An interslice force function for limit equilibrium slope stability analysis. Canadian Geotechnical Journal, **23**(3): 287–296.
- Gan, J.K-M., Fredlund, D.G., and Rahardjo, H. 1988. Determination of the shear strength parameters of an unsaturated soil using the direct shear test. Canadian Geotechnical Journal, **25**(8): 500–510.
- Fredlund, D.G. 1984. Analytical methods for slope stability analysis: State-of-the art. Proceedings, 4th International Symposium on Landslides, Toronto, Canada, Vol. 1, pp. 229–250.
- Fredlund, D.G. 1989. Negative pore-water pressures in slope stability. Proceedings, Simposio Suramericano de Deslizamientos, Paipa, Colombia, pp. 429–439.
- Fredlund, D.G., and Krahn, J. 1977. Comparison of slope stability methods of analysis. Canadian Geotechnical Journal, **14**: 429–439.
- Fredlund, D.G. and Rahardjo, H. 1993. The role of unsaturated soil behavior in geotechnical engineering practice. Proceedings, 11th Southeast Asian Geotechnical Conference, Singapore, pp. 37–49.
- Fredlund, D.G., and Xing, A. 1994. Equations for the soil-water characteristic curve. Canadian Geotechnical Journal, **31**: 521–532.
- Fredlund, D.G., and Morgenstern, N.R., and Widger, A. 1978. Shear strength of unsaturated soils. Canadian Geotechnical Journal, **15**(3): 313–321.
- Fredlund, D.G., Krahn, J., and Pufahl, D.E. 1981. The relationship between limit equilibrium slope stability methods. Proceedings, 10th International Conference on Soil Mechanics and Foundation Engineering, Stockholm, Sweden, Vol. 3, pp. 409–416.
- Fredlund, D.G., Zhang, Z., and Lam, L. 1992. Effect of the axis of moment equilibrium in slope stability analysis. Canadian Geotechnical Journal, **29**: 456–465.
- Fredlund, D.G., Xing, A., and Huang, S. 1994. Predicting the permeability function for unsaturated soils using the soil-water characteristic curve. Canadian Geotechnical Journal, **31**: 533–546.
- Morgenstern, N.R., and Price, V.E. 1965. The analysis of the stability of general slip surfaces. Géotechnique, **15**(1): 79–93.
- Marshall, T.J. 1958. A relation between permeability and size distribution of pores. Journal of Soil Science, **9**: 1–8.
- Rulon, J.J., and Freeze, R.A. 1985. Multiple seepage faces on layered slopes and their implications for slope-stability analysis. Canadian Geotechnical Journal, **22**: 347–356.
- Sweeney, D.J. 1982. Some *in situ* soil suction measurements in Hong Kong's residual soil slopes. Proceedings, 7th Southeast Asian Regional Conference, Vol. 1, pp. 91–106.
- Vanapalli, S.K. 1994. Simple test procedures and their interpretation in evaluating the shear strength of an unsaturated soil. Ph.D. thesis, University of Saskatchewan, Saskatoon, SK, Canada.
- van Genuchten, M-Th. 1980. A closed-form equation of predicting the hydraulic conductivity of unsaturated soils. Soil Science Society of America Journal, **44**: 892–898.

Pore pressure parameters for unsaturated soils

D.G. Fredlund and J.U. Hasan

Abstract: The concept of pore pressure parameters has been found convenient to visualize the pore pressure response of saturated soils for various applied stress changes. This paper derives pore pressure parameters that can be utilized in determining the pore pressure response of unsaturated soils. The expressions derived for the estimation of pore-air and pore-water pressures under undrained, isotropic loading are called the B_a and B_w pore pressure parameters. Measured pore pressures are compared with predicted values. Various factors influencing the proposed pore pressure parameters are discussed.

Pore pressure parameter expressions are also derived for the pore-air and pore-water pressures induced as a result of deviator stress changes during undrained loading (i.e., A_a and A_w).

Key words: pore pressure parameter, unsaturated soil, isotropic loading, matric suction.

Introduction

The behavior of an unsaturated soil tested under undrained loading conditions depends on the magnitudes of the pore-air and pore-water pressure developed. The concept of pore pressure parameters has been found to be convenient (Skempton 1954; Bishop 1954) to obtain a visualization of how the pore pressures respond to various applied stress changes. Examples of their application are shear strength problems (Fredlund et al. 1978), volume change problems (Fredlund and Morgenstern 1976), and transient flow problems (Hasan and Fredlund 1977; Fredlund and Hasan 1979).

Hilf (1948) formulated an equation for the pore-air pressure developed in an unsaturated soil as a result of total stress changes under undrained conditions. Hilf (1948) utilized Boyle's and Henry's laws and assumed that the change in the pore-air pressure was equal to the change in the pore-water pressure. Skempton (1954) and Bishop (1954) presented the concept of pore pressure coefficients. Bishop and Henkel (1962) proposed two pore pressure coefficients, B_a and B_w , to represent the induced pore-air and pore-water pressures, respectively, due to a change in applied load. Similar types of pore pressure parameters have recently been proposed for the tar sands (Harris and Sobkowicz 1978; Dusseault 1979).

In this paper, the B pore pressure parameters (i.e., B_a and B_w) are derived utilizing the stress state variables for an unsaturated soil (Fredlund and Morgenstern 1977) and recently proposed constitutive relations (Fredlund and

Morgenstern 1976; Fredlund 1976). The proposed B_a and B_w pore pressure parameters have been previously suggested for the boundary conditions associated with the theory of consolidation for an unsaturated soil (Fredlund and Hasan 1979). Data from the research literature are used to substantiate the derived equations. Expressions are also derived for the A pore pressure parameters (i.e., A_a and A_w).

Derivation of the B pore pressure parameters (isotropic loading)

The physical basis for the B pore pressure parameter is readily understood by considering a simple elastic model in which the soil skeleton and the pore-fluid phases are represented by compressible springs. Skempton (1954) and Bishop (1954) derived the following equation for the B pore pressure parameter:

$$[1] \quad B = \frac{\Delta u_w}{\Delta \sigma_3} = \frac{1}{1 + \frac{nC_w}{C_c}}$$

where:

- Δu_w = change in pore-water pressure,
- $\Delta \sigma_3$ = isotropic change in total stress,
- n = porosity,
- C_w = compressibility of water, and
- C_c = compressibility of the soil skeleton.

In a saturated soil, the compressibility of the water is small relative to the soil skeleton compressibility and, therefore, the B pore pressure parameter approaches 1. The B parameter decreases with a decrease in the degree of saturation since air renders the pore fluid highly compressible. The Skempton (1954) and Bishop (1954) analysis did not take into account surface tension effects, which result in different pressures in the air and water phases.

D.G. Fredlund. Professor, Department of Civil Engineering, University of Saskatchewan, 57 Campus Drive, Saskatoon, SK Canada S7N 5A9.

J.U. Hasan. Graduate Student, Department of Civil Engineering, University of Saskatchewan, 57 Campus Drive, Saskatoon, SK Canada S7N 5A9.

Reproduced with permission from the *Canadian Geotechnical Journal*, 17(3): 395-404, 1980.

For an unsaturated soil, it is possible to derive two pore pressure parameters to predict changes in the pore-air and pore-water pressures as a result of an isotropic total stress change. The two pore pressure parameters are defined as:

$$[2] \quad B_a = \Delta u_a / \Delta \sigma_3 \quad \text{and} \quad B_w = \Delta u_w / \Delta \sigma_3$$

where:

$$\Delta u_a = \text{change in pore-air pressure.}$$

Let us consider the piston and spring analogy shown in Fig. 1 in order to understand the mechanism of pore pressure generation in an unsaturated soil. The top loading cap will move downward upon loading by an amount dependent upon the compressibilities of the various phases and the applied load. The overall compression of a soil element and the corresponding induced pore-air and pore-water pressures are dependent on the compressibility of the pore-air, pore-water, and soil skeleton. In addition, the contractile skin (i.e., the air-water interface) has an effect on the relative magnitude of the pore-air and pore-water pressures. This interfacial effect is taken into account by using two independent stress variables to describe the stress state of the unsaturated soil and using these stress variables to write independent deformation equations for the air and water phases (Fredlund and Morgenstern 1976). Let us assume that the air pressure is uniform throughout the air phase and the escape of pore-air and pore-water is not permitted when the soil is loaded. The continuity requirement for an unsaturated soil element is:

$$[3] \quad \Delta V / V = (\Delta V_w / V) + (\Delta V_a / V)$$

where:

V = volume of the overall element (i.e., soil skeleton),

V_w = volume of water in the element, and

V_a = volume of air in the element.

The overall volume change of the air-water mixture can be written in terms of the compressibility of the pore fluid and the change in pore fluid pressure:

$$[4] \quad (\Delta V_w + \Delta V_a) / V = \beta_m n \Delta u_f$$

where:

β_m = compressibility of an air-water mixture,

n = porosity of the soil, and

Δu_f = change in the fluid pressure.

Fredlund (1976) derived the compressibility of an air-water mixture as:

$$[5] \quad \beta_m = S\beta_w + B_{aw} \left[\frac{(1-S) + HS}{(u_a + u_{atm})} \right]$$

where:

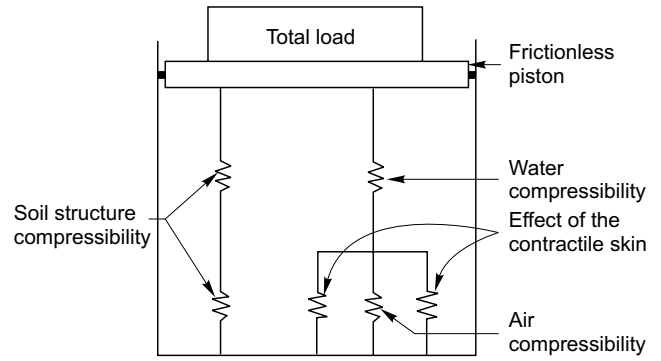
S = degree of saturation,

β_w = compressibility of water,

B_{aw} = change in pore-air pressure relative to a change in pore-water pressure,

u_a = gauge pore-air pressure,

Fig. 1. Mechanical model for pore pressure generation.



u_{atm} = atmospheric air pressure (i.e., standard pressure), and

H = Henry's solubility coefficient.

The fluid pressure has been referenced to the water phase in eq. [5]. Substituting eq. [5] into eq. [4] and referencing the pore-fluid pressure to the water phase gives:

$$[6] \quad \frac{\Delta V_w + \Delta V_a}{V} = S n \beta_w \Delta u_w + \left[\frac{(1-S)n + HS n}{(u_a + u_{atm})} \right] \Delta u_a$$

The volume change must be equal to that dictated by the constitutive relation for the soil skeleton (Fredlund and Morgenstern 1977). Equating [6] to the constitutive relation for the soil skeleton gives:

$$[7] \quad m_1^s \Delta(\sigma_3 - u_a) + m_2^s \Delta(u_a - u_w) = S n \beta_w \Delta u_w + \left[\frac{(1-S)n + HS n}{(u_a + u_{atm})} \right] \Delta u_a$$

where:

m_1^s = compressibility of the soil structure when $\Delta(u_a - u_w)$ is zero, and

m_2^s = compressibility of the soil structure when $\Delta(\sigma_3 - u_a)$ is zero.

Letting R_s be equal to m_2^s / m_1^s , eq. [7] can be solved for the change in pore-water pressure:

$$[8] \quad \Delta u_w = \left[\frac{(R_s - 1) - \frac{(1-S)n + HS n}{(u_a + u_{atm})} m_1^s}{R_s + S n \beta_w / m_1^s} \right] \Delta u_a + \left[\frac{1}{R_s + S n \beta_w / m_1^s} \right] \Delta \sigma_3$$

Equation [8] has two unknowns (i.e., u_w and u_a) and, therefore, a second independent equation is required. A second equation can be derived by considering the continuity of the air phase. Volume change due to the compression of the air must equal the volume change described by the constitutive relation for the air phase.

The volume change of the air phase due to compression can be written as:

$$[9] \quad \frac{\Delta V_a}{V} = \left[\frac{(1-S)n + HS n}{(u_a + u_{am})} \right] \Delta u_a$$

Equation [9] is equated to the constitutive relation for the air phase (Fredlund and Morgenstern 1976):

$$[10] \quad m_1^a \Delta(\sigma_3 - u_a) + m_2^a \Delta(u_a - u_w) = \left[\frac{(1-S)n + HS n}{(u_a + u_{am})} \right] \Delta u_a$$

where:

m_1^a = air phase volume change modulus when $\Delta(u_a - u_w)$ is zero, and

m_2^a = air phase volume change modulus when $\Delta(\sigma_3 - u_a)$ is zero.

Letting R_a be equal to m_2^a / m_1^a , eq. [10] can be solved for the change in pore-air pressure:

$$[11] \quad \Delta u_a = \left[\frac{R_a}{(R_a - 1) - \frac{(1-S)n + HS n}{(u_a + u_{am})m_1^a}} \right] \Delta u_a - \left[\frac{1}{(R_a - 1) - \frac{(1-S)n + HS n}{(u_a + u_{am})m_1^a}} \right] \Delta \sigma_3$$

Equations [8] and [11] must be solved simultaneously for the change in pore-water and pore-air pressures resulting from a change in the applied isotropic stress. These equations can be simplified by defining the following variables:

$$[12] \quad R_1 = \frac{(R_s - 1) - \frac{(1-S)n + HS n}{(u_a + u_{am})m_1^s}}{R_s + S n \beta_w / m_1^s}$$

$$[13] \quad R_2 = \frac{1}{(R_s + S n \beta_w / m_1^s)}$$

$$[14] \quad R_3 = \frac{R_a}{(R_a - 1) - \frac{(1-S)n + HS n}{(u_a + u_{am})m_1^a}}$$

and

$$[15] \quad R_4 = \frac{1}{(R_a - 1) - \frac{(1-S)n + HS n}{(u_a + u_{am})m_1^a}}$$

Equations [8] and [11] then reduce to:

$$[16] \quad \Delta u_w = R_1 \Delta u_a + R_2 \Delta \sigma_3$$

$$[17] \quad \Delta u_a = R_3 \Delta u_w + R_4 \Delta \sigma_3$$

Equations [16] and [17] are combined and solved to give two pore pressure parameters for unsaturated soils:

$$[18] \quad B_w = \frac{\Delta u_w}{\Delta \sigma_3} = \frac{R_2 - R_1 R_4}{1 - R_1 R_3}$$

$$[19] \quad B_a = \frac{\Delta u_a}{\Delta \sigma_3} = \frac{R_2 R_3 - R_4}{1 - R_1 R_3}$$

Both eqs. [18] and [19] are non-linear due to an absolute pore-air pressure term on the right side of the expressions. Therefore, the following iterative technique is used for the solution of these equations. Since the induced pore-air pressure is always less than the induced pore-water pressure, the value for the gauge air pressure, u_a , is initially assumed equal to zero in the computation of R_1, R_3 , and R_4 . These values are used in the initial calculation of the change in pore-air and pore-water pressures. For the second iteration, the pore-air pressure values are assumed to be equal to the previously computed pore-air pressures and are used in the calculation of the new R_1, R_3 , and R_4 values. The procedure is continued until there is convergence between the assumed and computed pore-air pressures.

Derivation of the pore pressure parameters (three-dimensional loading)

The B_a pore pressure parameter

The volumetric deformation for the air phase is written assuming the soil behaves as an isotropic, homogeneous, elastic soil (Fredlund and Morgenstern 1976):

$$[20] \quad \frac{\Delta V_a}{V} = \frac{1}{3} [m_1^a (\Delta \sigma_1 + \Delta \sigma_2 + \Delta \sigma_3 - 3 \Delta u_a) + m_2^a 3 \Delta(u_a - u_w)]$$

If triaxial loading conditions are assumed where σ_2 is equal to σ_3 , eq. [20] then becomes:

$$[21] \quad \frac{\Delta V_a}{V} = \frac{1}{3} [m_1^a \Delta(\sigma_1 + 2\sigma_3 - 3u_a) + m_2^a 3\Delta(u_a - u_w)]$$

The compression of the air phase (i.e., eq. [9]) can be substituted into the air phase constitutive relation (i.e., eq. [21]):

$$[22] \quad m_1^a \Delta(\sigma_1 + 2\sigma_3 - 3u_a) + m_2^a 3\Delta(u_a - u_w) = 3 \left[\frac{(1-S)n + HS n}{(u_a + u_{am})} \right] \Delta u_a$$

Re-arranging eq. [22], the change in pore-air pressure can be written as:

$$[23] \quad \Delta u_a = \frac{1}{(R_a - 1) - \frac{(1-S)n + HS n}{(u_a + u_{am})m_1^a}} \times [R_a \Delta u_w - \Delta \sigma_3 - (1/3)\Delta(\sigma_1 - \sigma_3)]$$

For isotropic loading, the change in $(\sigma_1 - \sigma_3)$ is zero and eq. [23] can be written as:

$$[24] \quad \Delta u_a = \left[\frac{1}{(R_a - 1) - \frac{(1-S)n + HS n}{(u_a + u_{am})m_1^a}} \right] [R_a \Delta u_w - \Delta \sigma_3]$$

Dividing both sides of eq. [24] by $\Delta \sigma_3$ gives:

$$[25] \quad \frac{\Delta u_a}{\Delta \sigma_3} = B_a = \left[\frac{R_a}{(R_a - 1) - \frac{(1-S)n + HS n}{(u_a + u_{am})m_1^a}} \right] B_w - \frac{1}{(R_a - 1) - \frac{(1-S)n + HS n}{(u_a + u_{am})m_1^a}}$$

Equation [25] is the general equation for the pore-air pressure parameter, B_a . If we assume that R_a is equal to zero, the modulus m_2^g becomes equal to zero and the constitutive relationship reduces to:

$$[26] \quad \Delta V / V = m_1^a \Delta(\sigma_3 - u_a)$$

In this case, the B_a pore pressure parameter reduces to the form proposed by Hilf (1948). When the soil is completely saturated, the percent volume of free air [i.e., $(1-S)n$] is zero, and B_a approaches 1.

The A_a pore pressure parameter

Substituting eq. [25] into eq. [23] and re-arranging gives:

$$[27] \quad \Delta u_a = B_a \Delta \sigma_3 - 3 \left[\frac{1}{(R_a - 1) - \frac{(1-S)n + HS n}{(u_a + u_{am})m_1^a}} \right] \Delta(\sigma_1 - \sigma_3)$$

Equation [27] can be reduced to:

$$[28] \quad \Delta u_a = B_a \Delta \sigma_3 + A_a \Delta(\sigma_1 - \sigma_3)$$

When the soil is fully saturated, B_a , becomes equal to unity, and A_a for an ideal, elastic soil is equal to 1/3. The form of eq. [28] is the same as that proposed by Skempton (1954) for a saturated soil.

The B_w pore pressure parameter

The constitutive relation for the soil structure in triaxial loading can be equated to the compressibility of the pore fluid (i.e., eq. [6]):

$$[29] \quad m_1^s \Delta(\sigma_1 + 2\sigma_3 - 3u_a) + m_2^s \Delta(u_a - u_w) = S\beta_w n \Delta u_w + \left[\frac{(1-S)n + HS n}{(u_a + u_{am})} \right] \Delta u_a$$

Equation [29] can be re-arranged as follows for isotropic loading:

$$[30] \quad \frac{\Delta u_w}{\Delta \sigma_3} = B_w = \left[\frac{(R_s - 1) - \frac{(1-S)n + HS n}{(u_a + u_{am})m_1^s}}{R_s + Sn\beta_w / m_1^s} \right] B_a$$

$$+ \frac{1}{R_s + Sn\beta_w / m_1^s}$$

When the soil becomes fully saturated, R_a equals 1.0, and B_a equals 1.0; therefore, eq. [30] takes the form of the expression proposed by Skempton (1954) for the B pore pressure parameter:

$$[31] \quad B_w = \frac{1}{1 + n\beta_w / m_1^s}$$

The A_w pore pressure parameter

Equation [29] can be rewritten in the following form:

$$[32] \quad \Delta u_w = \left[\frac{(R_s - 1) - \frac{(1-S)n + HS n}{(u_a + u_{am})m_1^s}}{R_s + Sn\beta_w / m_1^s} \right] \Delta u_a + \left[\frac{1}{R_s + Sn\beta_w / m_1^s} \right] \Delta \sigma_3 + 3 \left[\frac{1}{R_s + Sn\beta_w / m_1^s} \right] \Delta(\sigma_1 - \sigma_3)$$

Substituting eq. [30] into eq. [32] gives

$$[33] \quad \Delta u_w = B_w \Delta \sigma_3 + \frac{1}{3(R_s + Sn\beta_w / m_1^s)} \Delta(\sigma_1 - \sigma_3)$$

Equation [33] can be written as:

$$[34] \quad \Delta u_w = B_w \Delta \sigma_3 + A_w \Delta(\sigma_1 - \sigma_3)$$

When the soil becomes fully saturated, B_w equals 1.0 and A_w equals 1/3 for an ideal, elastic soil and eq. [35] has a similar form to that proposed by Skempton (1954) for saturated soils:

$$[35] \quad \Delta u_w = \Delta \sigma_3 + A \Delta(\sigma_1 - \sigma_3)$$

Relationship of the B pore pressure parameters to the equation proposed by Hilf (1948)

Hilf (1948) presented the following equation for the estimation of the change in pore-air pressure in an unsaturated soil:

$$[36] \quad \Delta u_a = \frac{u_{ai} \Delta V / V}{(1-S)n + HS n - \Delta V / V}$$

where:

$$u_{ai} = \text{initial pore-air pressure (absolute),}$$

$$(1-S)n = \text{volume of free air in the soil,}$$

HSn = volume of dissolved air in the soil, and
 $\Delta V / V$ = volume change from a one-dimensional oedometer test.

Equation [36] can be rearranged and written as follows:

$$[37] \quad \Delta V / V = \frac{\Delta u_a}{(u_{ai} + \Delta u_a)} [(1 - S)n + HSn]$$

Hilf (1948) assumed that the interfacial tension between the fluid phases was negligible and that the change in pore-air pressure was equal to the change in pore-water pressure. Hilf (1948) also assumed that the volume change of a soil skeleton could be expressed as:

$$[38] \quad \Delta V / V = m_v \Delta(\sigma_1 - u_a)$$

where:

m_v = coefficient of compressibility for one-dimensional loading.

The modulus, m_v , was measured on the saturation plane where the pore-air pressure was equal to the pore-water pressure. Equations [38] and [37] can be equated and solved for the B_a pore pressure parameter:

$$[39] \quad B_a = \frac{1}{1 + \frac{(1 - S)n + HSn}{m_v(u_{ai} + \Delta u_a)}}$$

Also inherent in this formulation is the assumption that $\Delta\sigma_1$ from one-dimensional loading is equal to $\Delta\sigma_3$. Let us define C as equal to $(u_{ai} + \Delta u_a)m_v / n$ and substitute it into eq. [29]:

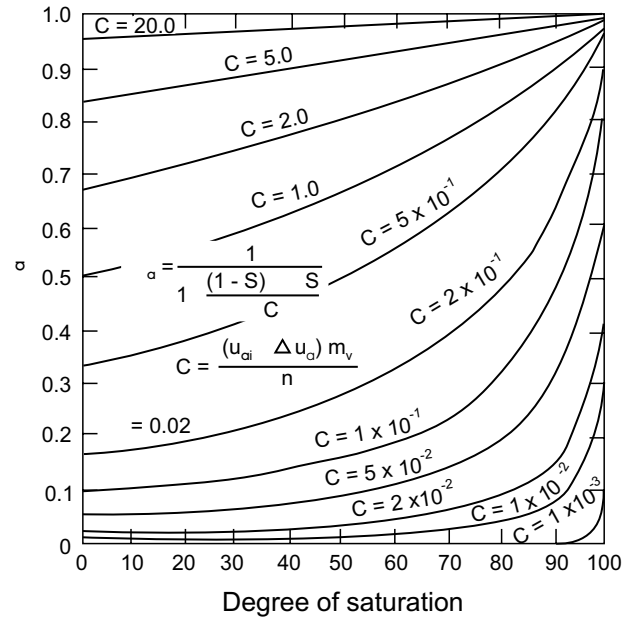
$$[40] \quad B_a = \frac{1}{1 + \frac{(1 - S) + HS}{C}}$$

Equation [40] gives the pore-air pressure parameter for an unsaturated soil where the interfacial tension between the pore fluids is neglected and the stress-volume change behavior of the soil skeleton is described using a one-dimensional oedometer test. Figure 2 presents the solution of eq. [40], proposed by Hilf (1948) for various values of the degree of saturation, porosity, pore-air pressure, and compressibility of the soil. Since Hilf (1948) assumed that the change in pore-air pressure, the B_a pore pressure parameter is equal to B_w . In other words, the difference between a change in pore-water pressure and pore-air pressure could not be separated using the analysis by Hilf (1948).

Solution of the B_a and B_w pore pressure parameter equations

A computer programme, which utilizes an iterative technique, has been used to evaluate the B_a and B_w pore pressure parameter, (i.e., eq. [18] and eq. [19]) for various initial conditions. Figures 3 and 4 show the B_w pore pressure for two soil skeleton compressibilities. (Only two soil skeleton compressibilities have been arbitrarily selected to demonstrate the pore pressure parameter behav-

Fig. 2. Graphical solution of the equation by Hilf (1948).



ior.) All calculations are performed assuming there is sufficient time for free air to be dissolved in water. The magnitudes of B_a and B_w are significantly affected by the compressibility of the soil skeleton. As the compressibility of the soil skeleton increases, the pore pressure response increases and vice versa. The initial degree of saturation also has a marked influence on the amount of pore-air and pore-water pressures generated in an unsaturated soil. When the ratio of the soil skeleton modulus to the air phase modulus (i.e., m_1^s / m_1^a) is equal to unity, both B_a and B_w are equal for all compressibilities of the soil skeleton and initial degrees of saturation. The values of B_a and B_w are the same as predicted by Hilf (1948) when m_1^s / m_1^a is equal to unity.

Figures 7 and 8 indicate the development of the B_a and B_w become essentially equal. As saturation is approached, B_a and B_w tend towards unity. The equations for B_a and B_w become discontinuous when the volume of free air is zero. At this point there is no air to be driven into solution and, therefore, the term (HSn) must be dropped from the equations to obtain B_a and B_w equal to 1 at complete saturation. Figures 7 and 8 show that the shape of the B_a and B_w pore pressure response curves are strongly influenced by the compressibilities of the soil.

Experimental results

Experimental data with respect to pore-air and pore-water pressures have been published by numerous researchers (Hilf 1948; Bishop and Henkel 1962; Gibbs 1963; Penman 1978; Hakimi et al. 1973). An attempt is made herein to compare the theoretical estimates of pore-air and pore-water pressures with some of the measured values. Hilf (1948) published the results of piezometer measurements made in the compacted cores of several earth dams. The piezometers had coarse porous tips and

Fig. 3. B_w pore pressure parameter versus m_1^s / m_1^a ($m_1^s = 1.45 \times 10^{-4}$ kPa⁻¹).

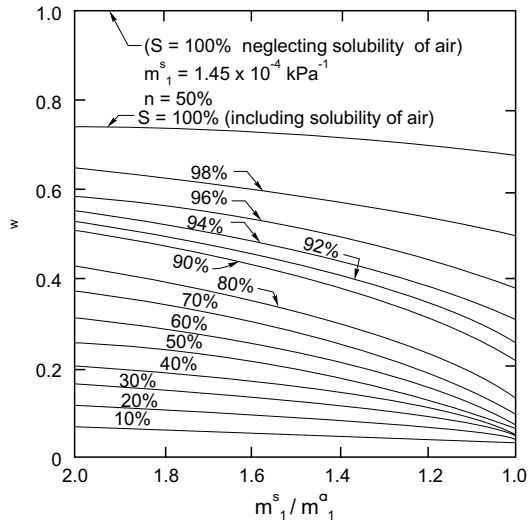


Fig. 4. B_w pore pressure parameter versus m_1^s / m_1^a ($m_1^s = 1.45 \times 10^{-3}$ kPa⁻¹).

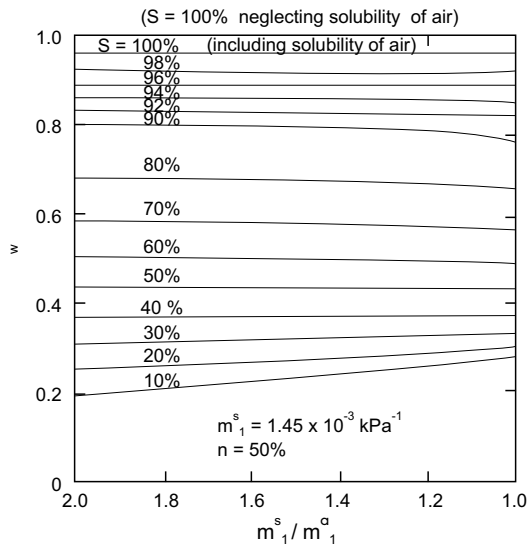


Fig. 5. B_a pore pressure parameter versus m_1^s / m_1^a ($m_1^s = 1.45 \times 10^{-4}$ kPa⁻¹).

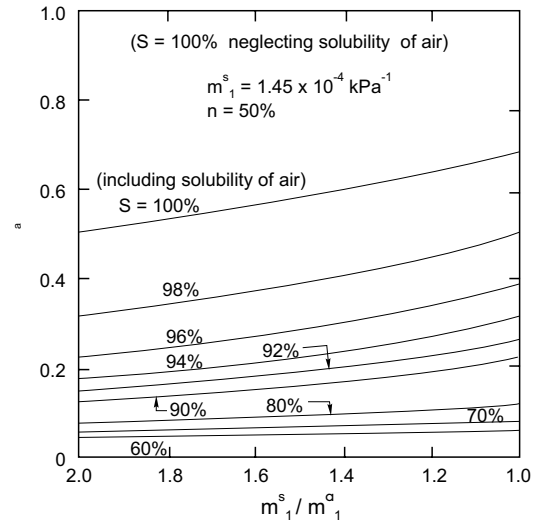
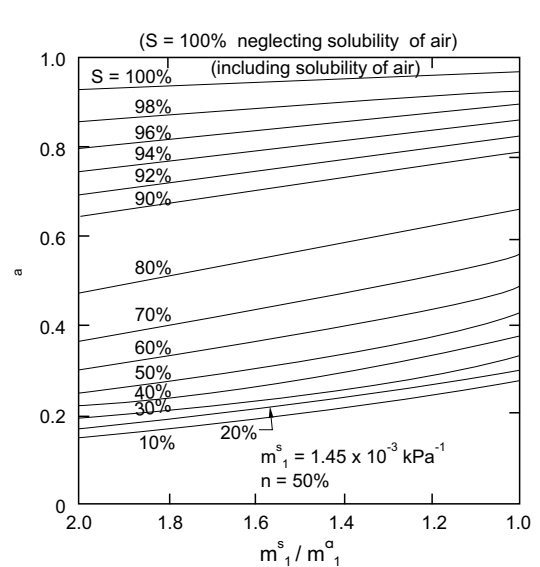


Fig. 6. B_a pore pressure parameter versus m_1^s / m_1^a ($m_1^s = 1.45 \times 10^{-3}$ kPa⁻¹).



measured the pore-water pressure. Figure 9 shows the readings from two piezometers installed in the Anderson Ranch dam. The published coefficient of permeability of the core material was 5.8×10^{-8} cm/s. The average soil skeleton compressibility modulus was 2.3×10^{-5} kPa⁻¹. A pore-air and (or) pore-water pressure versus total stress line is drawn using the method of analysis proposed by Hilf (1948). Equations [18] and [19] for the B_a and B_w pore pressure parameters give the same results as applying the analysis proposed by Hilf (1948) since the m_1^s / m_1^a ratio is assumed equal to unity. When the m_1^s / m_1^a ratio is assumed equal to 1.4, the pore-air and pore-water pressures are no longer the same and the pore-air pressure line lies above the solution by Hilf (1948).

Figure 10 shows pore-water pressures measured in an unsaturated soil by Gibbs (1963). A comparison of mea-

sured and predicted pore-water pressures is shown. It was necessary to assume soil modulus values in order to solve the B_a and B_w pore pressure parameter equations. The deviation between the measured and predicted values is due to a changing compressibility of the soil with increased loading. In the calculations, a constant soil skeleton compressibility was used throughout the range of loading. By decreasing the soil skeleton compressibility with increased loading it is possible to match the measured pore-water pressures.

Figure 11 shows pore-air and pore-water pressures measured by Bishop and Henkel (1962) in a triaxial cell, for two unsaturated soil samples. There is close agreement between the measured and predicted pore pressures. In this case, the compressibility of the soil was decreased at higher confining pressures to improve the agreement

Fig. 7. Total vertical stress versus pore pressure parameters ($m_1^s = 1.45 \times 10^{-4} \text{ kPa}^{-1}$).

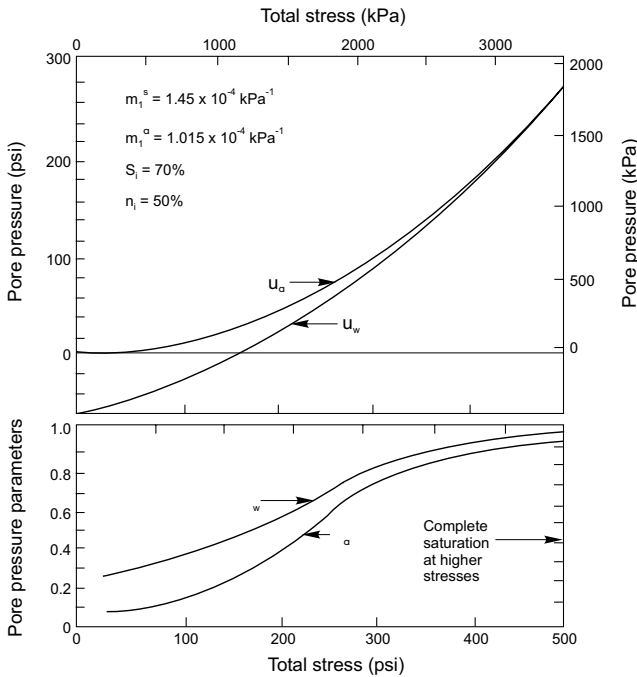
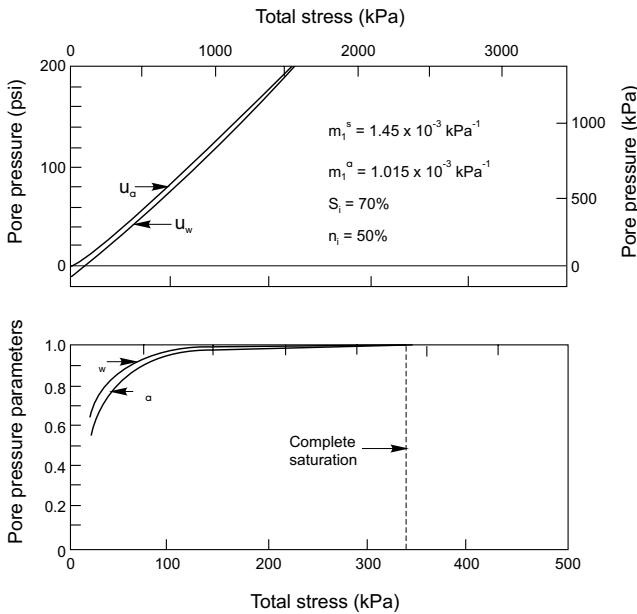


Fig. 8. Total vertical stress versus pore pressure parameters ($m_1^s = 1.45 \times 10^{-3} \text{ kPa}^{-1}$).



between the laboratory measurements and the theoretically evaluated results.

Discussion

The difference between the method of analysis presented by Hilf (1948) and that proposed in this paper is

Fig. 9. Measured and predicted pore pressures (after Hilf 1948).

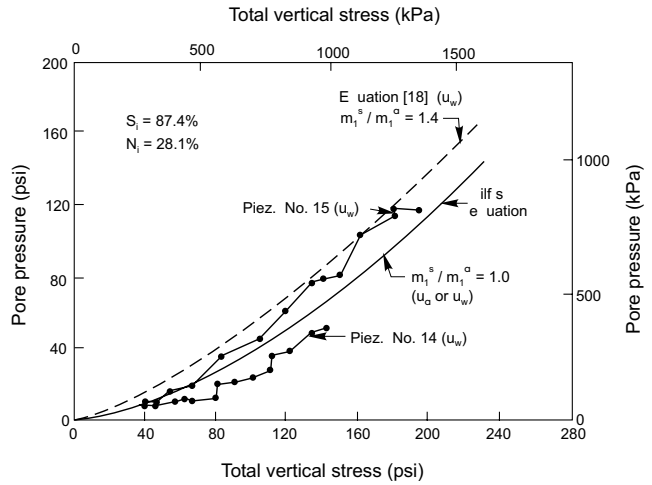
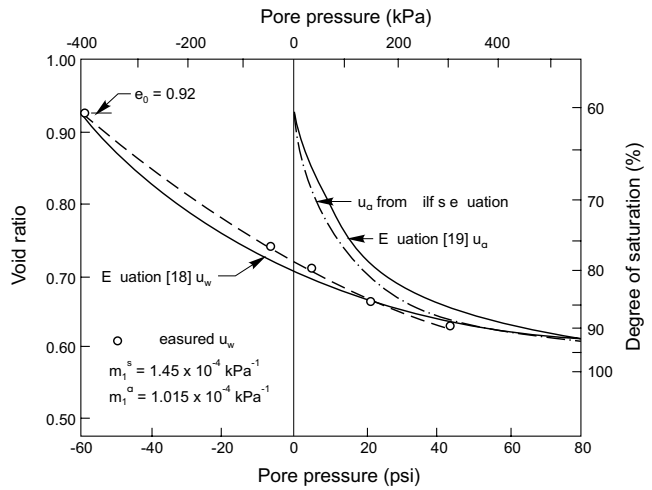


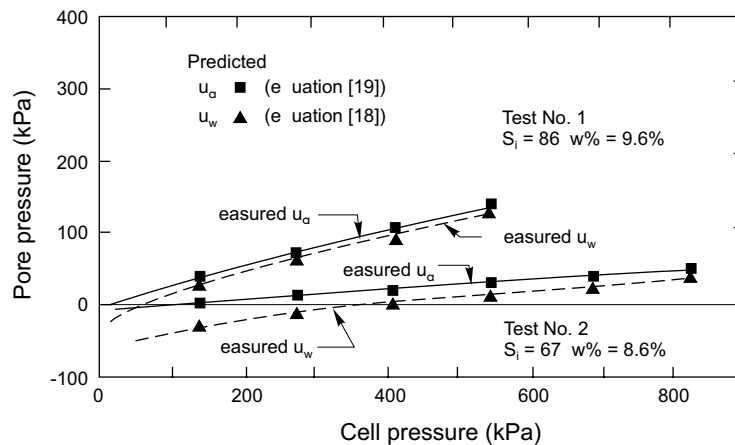
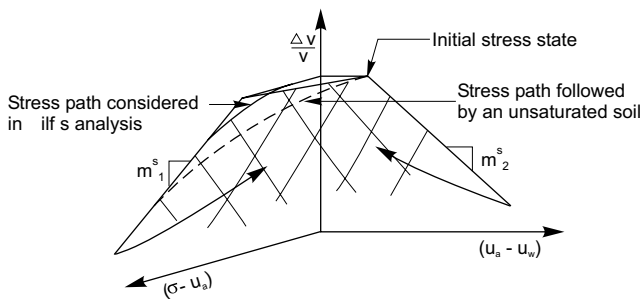
Fig. 10. Measured and predicted pore pressures (after Gibbs 1963).



demonstrated in Fig. 12. In a cohesive soil, the effect of matric suction must be taken into account. In this case, the stress deformation relationship is controlled by two compressibility moduli. The relative magnitudes of the pore-air and pore-water pressures depend primarily upon the pore fluids and the soil skeleton. In cases where the soil has a highly rigid structure and the matric suction is low, a reasonably good estimate of pore pressure would be anticipated using the equation proposed by Hilf (1948). When the soil has greater compressibility and the initial matric suction is significant, it is suggested that the proposed equations (i.e., eq. [18] and eq. [19]) be used to estimate the independent pore-air and pore-water pressures in response to applied loads.

Summary

- (1) The equations for two pore pressure parameters, B_a and B_w are derived for the pore-air and pore-water

Fig. 11. Measured and predicted pore pressures (after Bishop and Henkel 1962).**Fig. 12.** Stress paths using the analysis by Hilf (1948) and the proposed pore pressure equations.

pressures in unsaturated soils resulting from undrained, isotropic loading.

- (2) Two additional pore pressure parameters, A_a and A_w , are derived to account for pore pressure changes resulting from changes in deviator stresses applied during undrained loading of unsaturated soils.
- (3) Predicted pore-air and pore-water pressures compare well with measured values. (It was necessary to estimate the soil compressibility moduli in some cases.)
- (4) The pore pressure response of unsaturated soils is dependent upon the degree of saturation, porosity, total stress, and the relative magnitudes of the compressibility moduli of the various phases.

References

- Bishop, A.W. 1954. The use of pore-pressure coefficients in practice. *Géotechnique*, **4**(4): 148–152.
- Bishop, A.W., and Henkel, D.J. 1962. The measurement of soil properties in the triaxial test. Second edition, Edward Arnold (Publisher) Ltd., London, England.
- Dusseault, M.B. 1979. Undrained volume and stress change behavior of unsaturated very dense sands. *Canadian Geotechnical Journal*, **16**: 627–640.
- Fredlund, D.G. 1976. Density and compressibility characteristics of air-water mixtures. *Canadian Geotechnical Journal*, **13**: 386–396.
- Fredlund, D.G., and Hasan, J.U. 1979. One-dimensional consolidation theory: unsaturated soils. *Canadian Geotechnical Journal*, **16**: 521–531.
- Fredlund, D.G., and Morgenstern, N.R. 1976. Constitutive relations for volume change in unsaturated soils. *Canadian Geotechnical Journal*, **13**: 261–276.
- Fredlund, D.G., and Morgenstern, N.R. 1977. Stress state variables for unsaturated soils. *ASCE, Journal of the Geotechnical Engineering Division*, **103**(GT5): 447–466.
- Fredlund, D.G., Morgenstern, N.R., and Widger, R.A. 1978. The shear strength of unsaturated soils. *Canadian Geotechnical Journal*, **15**: 313–321.
- Gibbs, H.J. 1963. Pore-pressure control and evaluations for triaxial compressions. American Society for Testing and Materials, Special Technical Publication No. 361, pp. 212–221.
- Hakimi, Marchand, and Orliac. 1973. Pore pressure in partly saturated soils: Prediction, laboratory test and *in situ* measurements. Proceedings, 8th International Conference on Soil Mechanics and Foundation Engineering, Moscow, Vol. 1, Part 1–2, pp. 163–170.
- Harris, M.C., and Sobkowicz, J.C. 1978. Engineering behavior of oil sand. In *The oil sands of Canada-Venezuela*. Edited by D.A. Redford and A.G. Winestock. Canadian Institute of Mining and Metallurgy, Special Vol. 17, pp. 270–281.
- Hasan, J.U., and Fredlund, D.G. 1977. One-dimensional consolidation theory for unsaturated soils. Proceedings, Symposium on water movement and equilibrium in swelling soils, Committee on water in the unsaturated zone, Section of Hydrology of the American Geophysical Union, San Francisco, CA.
- Hilf, J.W. 1948. Estimating construction pore pressures in rolled earth dams. Proceedings, 2nd International Conference on Soil Mechanics and Foundation Engineering, Rotterdam, Vol. 3, pp. 234–240.
- Penman, D.M. 1978. Construction pore pressures in two earth dams. Building Research Establishment, Watford, UK, CP 82/78.
- Skempton, A.W. 1954. The pore pressure coefficients, A and B . *Géotechnique*, **4**(4): 143–147.

Effect of pore-air and negative pore-water pressures on stability at the end-of-construction

D.G. Fredlund, H. Rahardjo, and T. Ng

Abstract: An analytical method for predicting the pore pressure change under undrained loading conditions was proposed by the United States Bureau of Reclamation around 1950 (i.e., the USBR method). The same analytical method was later proposed by Bishop (1957). This method was developed by computing pore-air pressure changes during undrained loading using Boyle's and Henry's laws along with the results from one-dimensional consolidation tests. It was then assumed that changes in the pore-air pressure were equal to changes in the pore-water pressure. Subsequently, in practice, the pore-air pressure plot versus total stress has often been used to predict the pore-water pressure in a compacted fill. Such an assumption can become quite conservative in terms of the computed factor of safety.

This paper presents an analytical procedure that serves as an extension to the USBR method. In the proposed procedure, the development of the pore-air and pore-water pressures during an undrained loading are not assumed to be equal. The development of pore-water pressure is predicted in an empirical manner, using the initial negative pore-water pressure, (i.e., the matric suction of the soil in an unloaded state), the theoretical saturation pressure and the pore-pressure parameters at saturation. In other words, both the pore-air and pore-water pressures are predicted as independent values for the construction process. The predicted pore-water pressures are consistent with measured results.

A typical example problem is given in the paper to illustrate the use of this method in analyzing the end-of-construction stability for an earth dam. The significance of considering, or omitting the pore-air pressure generation on the stability of the dam is also demonstrated. The difference between including and omitting the pore-air pressure is shown to be significant.

Analytical comparisons are made for various values of the friction angle with respect to matric suction, and for various combinations of pore-air and pore-water pressures at the end-of-construction. The extended method of pore pressure prediction can be used to more accurately compute the factor of safety of a compacted fill at the end-of-construction.

Key words: pore pressure, undrained loading, earthfill dam construction, matric suction, stability analysis, factor of safety, computer analysis.

Introduction

The construction of compacted earthfill dams and embankment results in changes in the pore pressures within the compacted soil. In a compacted soil, the pore-air pressure will be either atmospheric or will have a positive magnitude above atmospheric conditions while the pore-water pressure is generally negative with respect to the atmospheric pressure. Pore pressure changes during con-

struction are commonly assumed to take place under undrained conditions during a relatively rapid construction period. As the embankment is constructed, the lower layers are compressed by the placement of the overlying layers. The pore-air and pore-water pressures change within each compacted layer during the period of construction.

The objective of this paper is to present an extended method to more closely simulate the pore-air and pore-water pressures generated in a compacted fill. The effect of various assumptions regarding the magnitude of the pore pressures is studied in terms of factor of safety.

Literature review

Hilf (1948) presented his analytical procedure for predicting the pore-air pressure developed in an unsaturated, compacted fill as a result of total stress changes under undrained conditions. The analysis as used by the United States Bureau of Reclamation and it became known as the USBR method. The same analytical procedure was again proposed by Bishop (1957).

D.G. Fredlund. Professor, Department of Civil Engineering, University of Saskatchewan, 57 Campus Drive, Saskatoon, SK, Canada S7N 5A9.

H. Rahardjo. Senior Lecturer, School of Civil and Structural Engineering, Nanyang Technological University, Singapore 2261.

T. Ng. Geotechnical Engineer, Manitoba Highways and Transportation, Government of Manitoba, Winnipeg, MB, Canada.

Reproduced with permission from the *Proceedings, International Conference on Dam Engineering*, Johor Bahru, Malaysia, January 12–13, 1993. pp. 43–51.

The pore pressure prediction was based upon Boyle's and Henry's gas laws, along with the results from a one-dimensional oedometer test. The relationship between the change in pore-air pressure and the volume change of the soil under undrained conditions was derived. The change in pore-air pressure was then assumed to be equal to the change in pore-water pressure. This assumption may be reasonable for some low plasticity soils. However, as the plasticity of the soil in the compacted fill increases, likewise the difference between the pore-air and pore-water pressures increases. At the time of compaction, the difference between the pore-air and pore-water pressures can be several atmospheres for a clayey soil.

Skempton (1954) and Bishop (1954) introduced the concept of A and B pore pressure parameters for saturated and unsaturated soils. Their derivations introduced the theory of elasticity, incorporating elastic parameters into the formulation of the pore pressure parameters. Hasan and Fredlund (1980) extended the pore pressure parameter derivations to include the constitutive relations for unsaturated soils (Fredlund and Morgenstern 1976). The A and B pore pressure parameters appear to have experienced limited usage on engineering practice for the prediction of pore pressures at the end-of-construction.

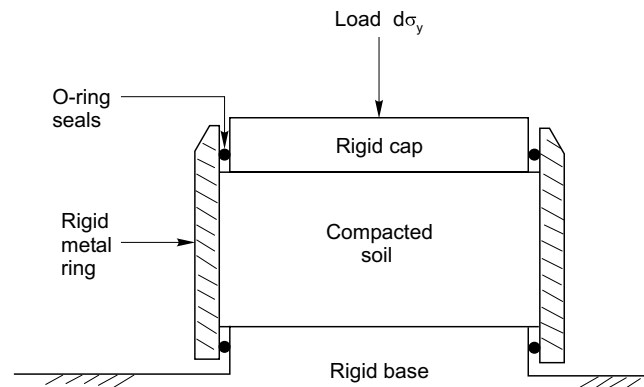
The main reason that predictions of pore pressures at the end-of-construction have not been used in practice, is that until recently there has not been a slope stability formulation which took both pore-air and pore-water pressures into account. The shear strength equation for a compacted soil, which took both pore-air and pore-water pressures into account was proposed by Fredlund et al. (1978). The equation was later applied to a limit equilibrium slope stability analysis (Fredlund 1984). However, research has not been carried out to study the effect of both pore-air and pore-water pressures on the computed factors of safety. The latter is one of the objectives of this study.

Theory related to the analysis by Hilf (1948)

Hilf (1948) simulated the undrained loading of a compacted soil using a one-dimensional loading of the soil with a frictionless piston sealed against a cylinder. Each applied load resulted in a volume change. The volume change was due to the compression of air and the dissolving of air in water (Fig. 1). With known initial and final volumes of air, the final pressure associated with the air phase is computable. The assumptions associated with using the analysis by Hilf (1948) are as follows:

- (1) Only vertical strain takes place during loading (i.e., K_0 -loading),
- (2) the relationship between the effective stress and strain can be measured by performing a conventional, one-dimensional oedometer test on a compacted specimen immersed in water.
- (3) the initial pore-water pressure can be assumed to be atmospheric (i.e., 101.3 kPa absolute),
- (4) strain is due to the compression of air and the solution of air in water,

Fig. 1. Frictionless piston analogy of the compression of an unsaturated soil.



- (5) there is no dissipation of pore-air (or pore-water) pressure with time,
- (6) the effects of vapour pressure and temperature are negligible, and
- (7) the change in pore-water pressure can be assumed to be equal to the computed change in pore-air pressure.

It is this last assumption which is more fully addressed in an extension to the theory.

The initial volume of free and dissolved air in a compacted soil can be written,

$$[1] \quad V_{a0} = [(1 - S_0)n_0 + hS_0n_0]V_0$$

where:

V_{a0} = initial volume of free and dissolved air,

S_0 = initial degree of saturation,

n_0 = initial porosity,

V_0 = initial volume of the soil, and

h = Henry's coefficient of solubility by volume which is approximately 0.02 at typical ambient temperatures.

The volume of free air is equal to $(1 - S_0)n_0$ and the volume of dissolved air is equal to (hS_0n_0) . The initial pore-air pressure, u_{a0} , is assumed to be atmospheric.

After a load is applied, the final volume of air, V_{af} , can be expressed as:

$$[2] \quad V_{af} = [(1 - S_0)n_0 + hS_0n_0 - \Delta n]V_0$$

where:

V_{af} = final volume of free and dissolved air, and

Δn = change (i.e., decrease) in porosity.

The initial and final volume conditions are shown in the phase diagram in Fig. 2. The final pore-air pressure, u_{af} , can be expressed:

$$[3] \quad \bar{u}_{af} = \bar{u}_{a0} + \Delta u_a$$

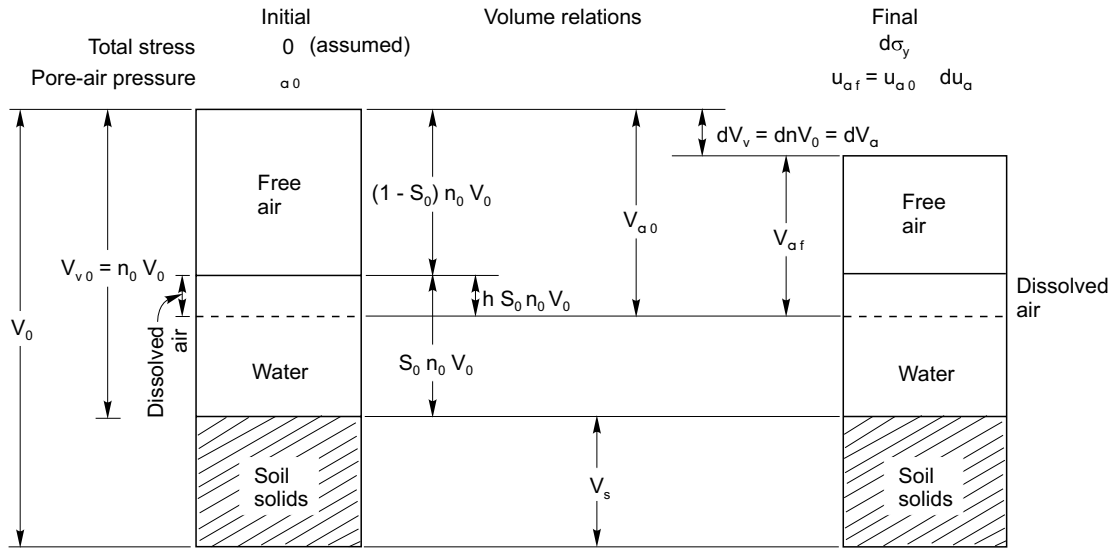
where:

\bar{u}_{a0} = initial pore-air pressure (absolute),

\bar{u}_{af} = final pore-air pressure (absolute), and

Δu_a = change (i.e., increase) in absolute pore-air pressure.

Fig. 2. Initial and final volume relations for before and after loading conditions of the unsaturated soil.



Boyle's law can be applied to the sum of the free and dissolved air volumes.

$$[4] \quad \bar{u}_{a0} V_{a0} = \bar{u}_{af} V_{af}$$

The initial and final stress and volume conditions can be substituted into eq. [4]:

$$[5] \quad \bar{u}_{a0} [(1 - S_0)n_0 + hS_0 n_0] V_0 = (\bar{u}_{a0} + \Delta u_a) [(1 - S_0)n_0 + hS_0 n_0 - \Delta n] V_0$$

The change in pore-air pressure can be solved from eq. [5].

$$[6] \quad \Delta u_a = \left\{ \frac{\Delta n}{[(1 - S_0)n_0 + hS_0 n_0 - \Delta n]} \right\} \bar{u}_{a0}$$

Equation [5] provides a relationship between the change in volume, Δn , and the change in pore-air pressure. At this point, it has generally been assumed that changes in the pore-air pressure are equal to changes in the pore-water pressure (i.e., $\Delta u_a = \Delta u_w$). The justification and effect of this assumption are later discussed.

The relationship between effective stress and volume change is obtained from the results of a one-dimensional oedometer test. Usually the results are plotted as void ratio versus the logarithm of effective stress. However, for the problem at hand, the void ratio can be converted to a change in volume (i.e., $\Delta n = \Delta e / (1 + e_0)$) and the effective stress is plotted on an arithmetic scale.

The change in volume can be plotted versus effective stress and pore pressure (Figure 3). The principle of effective stress (i.e., $\sigma = \sigma' + u$) is now used to compute the total stress versus the change in volume.

It is possible to plot the total stress and pore-water pressure as shown in Fig. 4. The slope of the resulting curve is quite flat at low total stresses and gradually increases to 45 degrees at saturation. At this point, changes in the total stress are equal to changes in the pore-water pressure. The above analysis appears to be consistent with experimental results associated with the pore-water phase as long as the soil is of low plasticity and has a

Fig. 3. Stress components versus volume change.

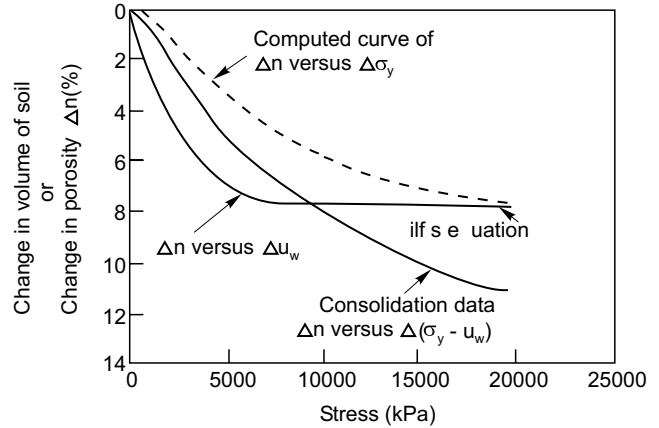
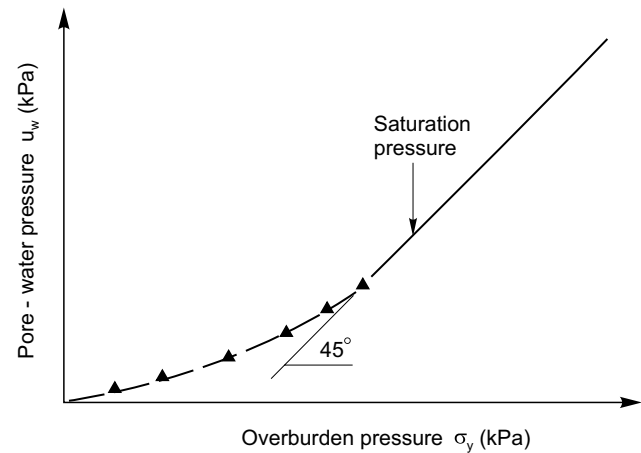
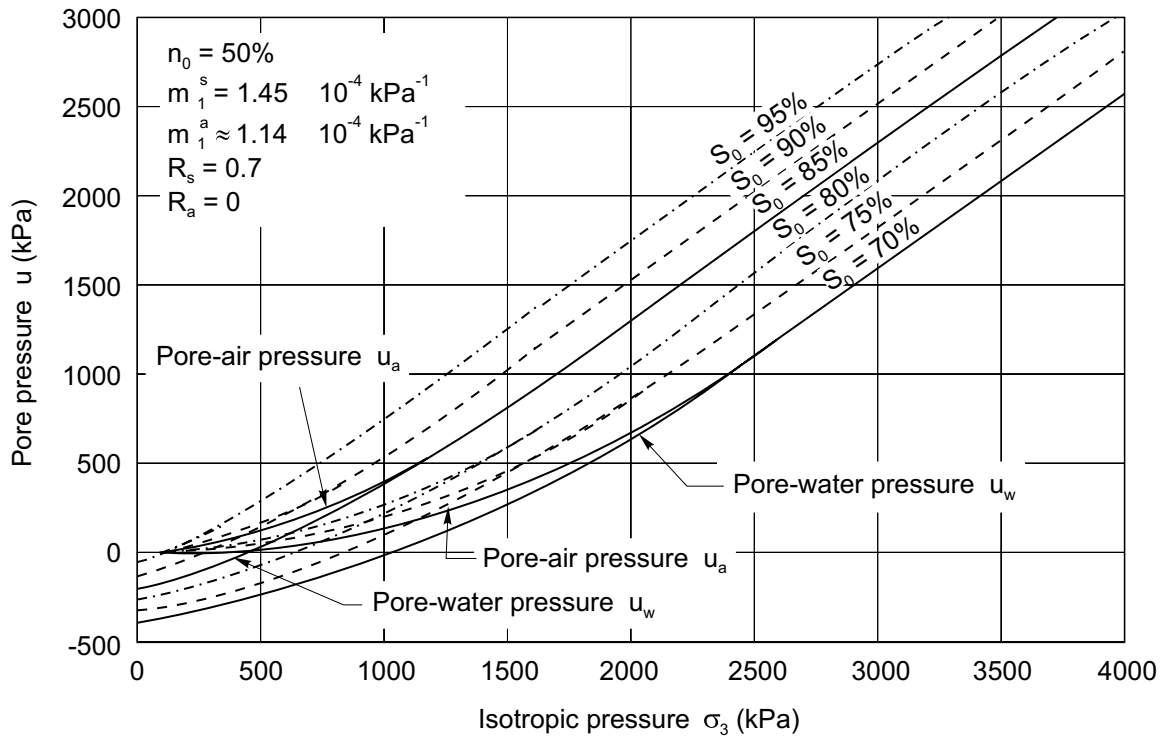


Fig. 4. Non-linear pore pressure versus total stress relationship.



small initial matric suction (Hasan and Fredlund 1980). The authors feel that more correctly, the analysis by Hilf (1948) applies to the pore-air phase as long as conditions are undrained.

Fig. 5. Shape and character of pore pressure versus total stress.

There is a limiting condition to which the equation by Hilf (1948) can be applied. When the soil becomes saturated, the total change in volume will be equal to the initial volume of free air.

$$[7] \quad \Delta n = (1 - S_0)n_0$$

Beyond this point, no further volume change is possible. Substituting the volume of free air into Eq. [6] gives the pore-air pressure change required for saturation.

$$[8] \quad \Delta u_{as} = (1 - S_0)\bar{u}_{a0} / (S_0 h)$$

where:

Δu_{as} = pore-air pressure change (i.e., increase) required for saturation.

The relationship between the equation by Hilf (1948) and the pore pressure parameter (i.e., $B_{ah}' = \Delta u_a / \Delta \sigma_y$) is as follows.

$$[9] \quad B_{ah}' = 1 / [1 + (1 - S_0 + hS_0)n_0 / (\bar{u}_{a0} + \Delta u_a)m_v]$$

where:

$\Delta \sigma_y$ = change in vertical stress,
 m_v = coefficient of volume change, and
 B_{ah}' = secant pore-air pressure parameter (i.e., $\Delta u_a / \Delta \sigma_y$) for K_0 -undrained loading in accordance with the analysis by Hilf (1948).

Equation [9] applies as long as a single value can be ascribed to the coefficient of volume change.

Extensions to the analysis by Hilf (1948)

Some extensions can be made to the above analysis in order to independently predict the pore-air and pore-water pressure under undrained loading conditions. The analysis by Hilf (1948) is now used to provide the relationship between total stress and pore-air pressure. The shape and character of the pore-water pressure versus total stress relationship have been studied and can be empirically predicted. Typical shape and character of pore pressure and total stress relationships are shown in Figure 5.

The following assumptions can be made regarding the pore-water pressure versus total stress curve:

- (1) the pore-water pressure curve is parabolic in shape,
- (2) when the soil approaches saturation, changes in total stress, pore-air pressure and pore-water pressure become equal. This means that at saturation the slope of the total stress versus pore pressure becomes 1.0.

If the pore-water pressure versus total stress curve is parabolic, it will adhere to the following general form:

$$[10] \quad u_w = A\sigma^2 + B\sigma + C$$

where:

A, B, C = constants to be evaluated by considering appropriate boundary conditions

When the total stress is zero, the constant C , is equal to the initial pore-water pressure (or the matric suction when $u_a = 0$; where u_a = gauge air pressure). This is equivalent to the matric suction of the soil measured in an unconfined condition on a Pressure Plate apparatus.

$$[11] \quad C = (u_a - u_w)_0$$

When the soil approaches saturation, the applied total stress can be written as σ_s , and the pore-water pressure can be written as u_{ws} . At saturation u_{as} is equal to u_{ws} , and the pore pressure can be designated as u_s . For the point of saturation, eq. [10] can be written:

$$[12] \quad u_s = A\sigma_s^2 + B\sigma_s + (u_a - u_w)_0$$

The slope of the pore-water pressure versus total stress curve at saturation is equal to 1 (i.e., $du_w / d\sigma = 1$).

$$[13] \quad du_s / d\sigma = 2A\sigma_s + B = 1$$

or,

$$[14] \quad B = 1 - 2A\sigma_s$$

The A constant can be computed after substituting the B constant into eq. [12].

$$[15] \quad A = [\sigma_s - u_s + (u_a - u_w)_0] / \sigma_s^2$$

Equation [14] can now be used to calculate the B constant:

$$[16] \quad B = 1 - 2[(\sigma_s - u_s + (u_a - u_w)_0) / \sigma_s]$$

The expressions for A , B , C can be substituted into eq. [10] to give a general expression for the pore-water pressure curve.

$$[17] \quad u_w = \{[\sigma_s - u_s + (u_a - u_w)_0] / \sigma_s^2\} \sigma^2 + \{1 - 2[(\sigma_s - u_s + (u_a - u_w)_0) / \sigma_s]\} \sigma + (u_a - u_w)_0$$

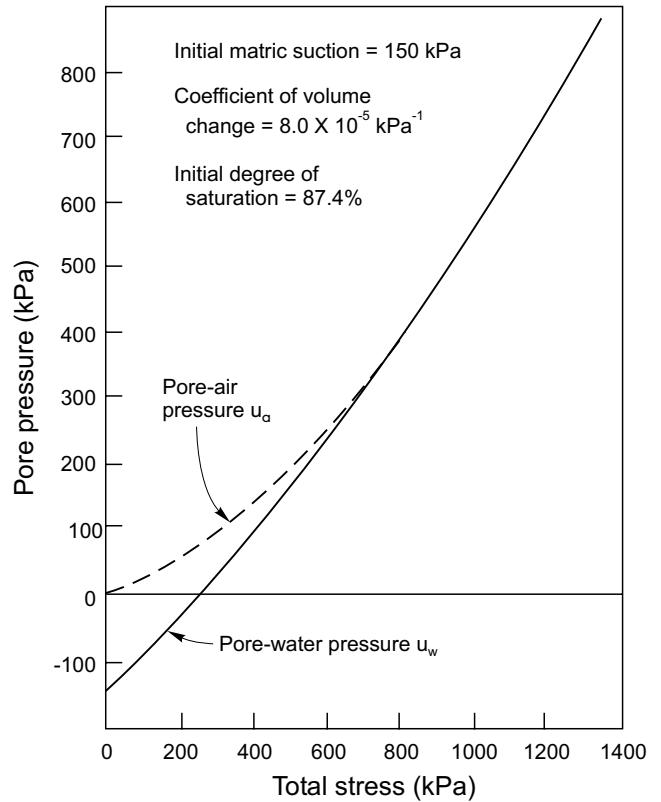
The saturation pore-water pressure, u_s , is computed using eq. [8] (i.e., $u_s = \Delta u_{as} + \bar{u}_{a0}$). The total stress associated with saturation, σ_s , can be obtained when the equation by Hilf (1948) is combined with the results of an oedometer test (Fig. 3).

The relationship between total stress and pore-water pressure can be plotted along with the relationship between total stress and pore-air pressure. The end result is an independent, empirical pore-water pressure curve (Fig. 5) which is consistent in character and magnitude to measured results.

Description of the example problem of a dam

An earthfill dam, 30 meters high and 130 meters wide, with 1:2 side-slopes on the upstream and downstream faces, is used for an example problem. The dam consists of one soil type with a total unit weight of 20.5 kN/m³. The effective angle of internal friction, ϕ , is assumed to be 30 degrees and the effective cohesion, c' , is 20 kPa. The initial degree of saturation of the compacted soil, S , is 87.4% and the initial matric suction, $(u_a - u_w)_0$, is 150 kPa. The coefficient of volume change, m_v , is 8.0×10^{-5} 1/kPa. These properties are used to compute the total stress versus pore-air and pore-water pressures (Fig. 6).

Fig. 6. Relationships between pore-air pressure, pore-water pressure and total stress used for the example problem.

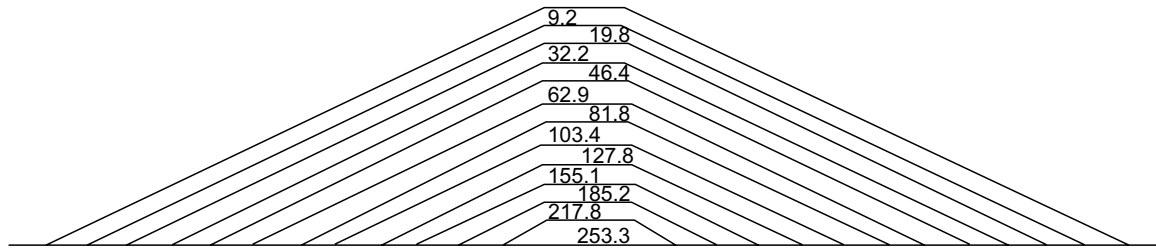


The earthfill dam is divided into 12 layers, with each layer being 2.5 m thick, for the end-of-construction slope stability analyses. The pore-water pressures are input as a series of constant pressure contours while the pore-air pressures are input as independent variables for each soil layer¹ (Fig. 7). Different angles of friction with respect to matric suction, ϕ^b , were selected within the range from 0 degrees to 30 degrees.

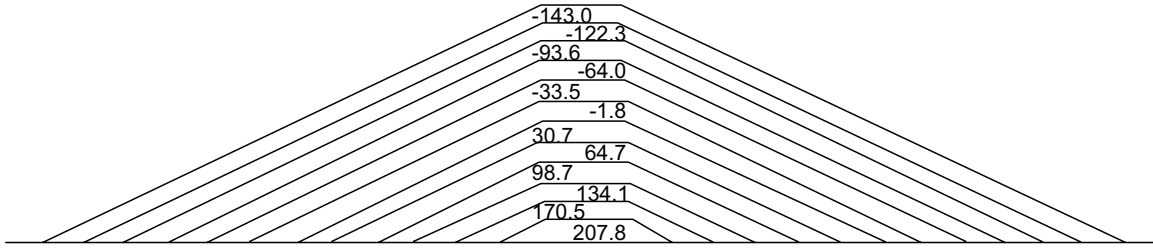
Assumptions concerning the pore-air and pore-water pressures

Two separate assumptions were used concerning the pore-air pressures in the analyses. The first assumption was that the pore-air pressures were equal to the values determined using the analysis by Hilf (1948). The second assumption was that the pore-air pressures dissipated and were equal to zero. In both cases, the pore-water pressures were assumed to be equal to those predicted from eq. [17].

These assumptions, together with various ϕ^b values, affect the shear strength equation for unsaturated soils and as a result, affect the computed factors of safety.

Fig. 7. Pore-air and pore-water pressures of the dam for the end-of-construction case.

a.) Pore-air pressures at various depths in the dam (kPa)



b.) Pore-water pressures at various depths in the dam (kPa)

Effect of pore pressure assumptions on shear strength

The general shear strength equation for an unsaturated soil can be written as follows (Fredlund et al. 1978):

$$[18] \quad \tau = c' + (\sigma_n - u_a) \tan \phi' + (u_a - u_w) \tan \phi^b$$

There are several specializations of eq. [18] for various pore-air pressure assumptions and ϕ^b conditions. When the pore-air pressures are equal to values computed using the equation by Hilf (1948), and:

(1) the ϕ^b value is zero, eq. [18] becomes,

$$[19] \quad \tau = c' + (\sigma_n - u_a) \tan \phi'$$

(2) the ϕ^b angle has a value between zero and ϕ' , eq. [18] can be written,

$$[20] \quad \tau = c' + \sigma_n \tan \phi' - u_a (\tan \phi' - \tan \phi^b) - u_w \tan \phi^b$$

(3) the ϕ^b angle is equal to ϕ , and eq. [18] becomes the same as that used for saturated soils.

$$[21] \quad \tau = c' + (\sigma_n - u_w) \tan \phi'$$

Let us now assume that the pore-air pressures dissipate rapidly while the pore-water pressure remains the same. When the pore-air pressures are set equal to zero, and,

(1) the ϕ^b value is zero, eq. [18] becomes,

$$[22] \quad \tau = c' + \sigma_n \tan \phi'$$

(2) the ϕ^b angle, has a value between zero and ϕ , eq. [18] can be written,

$$[23] \quad \tau = c' + \sigma_n \tan \phi' - u_w \tan \phi^b$$

(3) the ϕ^b angle is equal to ϕ , eq. [18] becomes the same as that used for a saturated soil.

$$[24] \quad \tau = c' + (\sigma_n - u_w) \tan \phi'$$

These equations affect the mobilized shear strength computed for the factor of safety calculations.

Results of the stability analyses

The pore-air pressure values computed applying the analysis by Hilf (1948), ranged from 9 kPa at the top layer to 253 kPa near the bottom centre of the dam. The generated pore-water pressures ranged from -143 kPa at the top of the dam to +208 kPa at the bottom centre of the dam.

The computed factors of safety for the above two assumptions regarding the pore-air pressure, are summarized in Table 1. These results are plotted in Fig. 8. The results indicate that with the pore-air pressure introduced into the analysis and the ϕ^b values equal to zero, the factor of safety drops from 1.70 to 1.27 (i.e., 25%). Once the angle of friction with respect to matric suction is increased, the factors of safety increase for both assumptions regarding the pore-air pressure.

When the angle of friction with respect to matric suction is equal to ϕ , the pore-air pressure no longer affects the shear strength. The computed factor of safety is 1.90. For the case of no pore-air pressures this represents an increase of 12%. For the case with pore-air pressures equal to those computed applying the analysis of Hilf (1948), the factor of safety is increased almost by 50%. These changes in factor of safety are substantial. Ignoring the influence of pore-air pressures could lead to a too low estimate of the factor of safety.

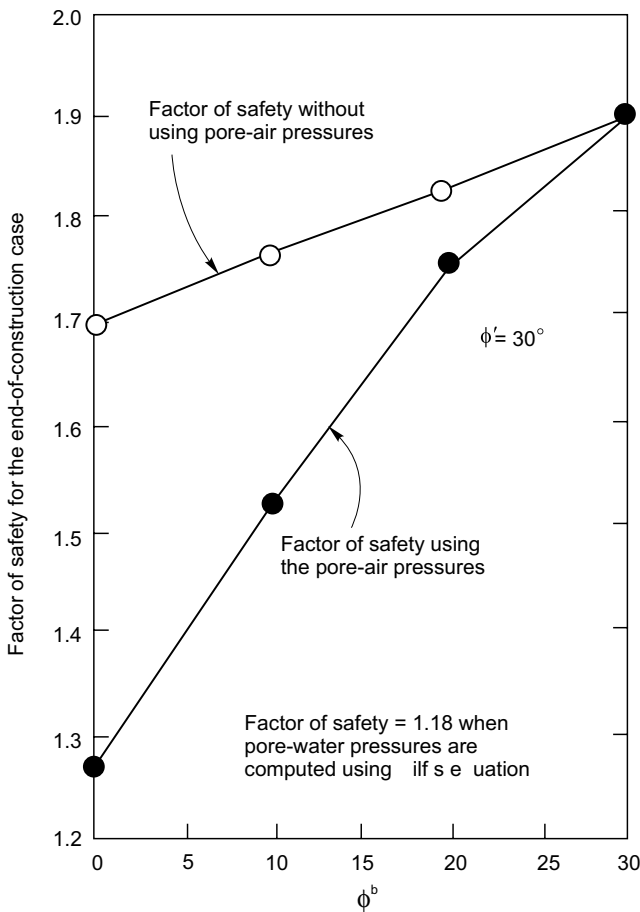
At first observation, it might appear that the computed factors of safety are the opposite to what one's intuition might suggest. For example, it could be reasoned that if the pore-air pressure is zero, then matric suction would

Table 1. Results for the end-of-construction case.

ϕ^b	Shear strength equation	Factor of safety
(a) The pore-air pressure values equal to the values determined applying the analysis of Hilf (1948)		
0	$\tau = c' + (\sigma_n - u_n) \tan \phi'$	1.27
10	$\tau = c' + \sigma_n \tan \phi' - u_a (\tan \phi' - \tan \phi^b) - u_w \tan \phi^b$	1.53
20	$\tau = c' + \sigma_n \tan \phi' - u_a (\tan \phi' - \tan \phi^b) - u_w \tan \phi^b$	1.75
30	$\tau = c' + (\sigma_n - u_w) \tan \phi'$	1.90
(b) The pore-air pressure values equal to zero		
0	$\tau = c' + \sigma_n \tan \phi'$	1.70
10	$\tau = c' + \sigma_n \tan \phi' - u_w \tan \phi^b$	1.76
20	$\tau = c' + \sigma_n \tan \phi' - u_w \tan \phi^b$	1.83
30	$\tau = c' + (\sigma_n - u_w) \tan \phi'$	1.90

Note: The pore-water pressures are the same for both cases.

Fig. 8. Factor of safety with respect to ϕ^b for the end-of-construction case.



be less and the factor of safety would be less. However, the opposite is true.

In reality, the pore-air pressure influences both the ϕ and ϕ^b components of shear strength. However, when the ϕ^b value is equal to zero, the pore-air pressure has a significant influence on the factor of safety because it operates on the ϕ term alone.

The difficulty in understanding the computed results appears to be related to the fact that the engineer usually visualizes shear strength either in terms of the effect of normal stress, σ_n , or in terms of the effect of matric suction, $(u_a - u_w)$. Since the pore-air pressure is involved, it is necessary to visualize shear strength behavior in terms of both $(\sigma_n - u_a)$ and $(u_a - u_w)$. The $(\sigma_n - u_a)$ term operates on $(\tan \phi')$. The $(u_a - u_w)$ term operates on $(\tan \phi^b)$. When the ϕ^b value is equal to zero, the effect of matric suction disappears but the effect of $(\sigma_n - u_a)$ does not disappear.

Another assumption is made regarding pore pressures at the end of construction. It is sometimes assumed that the pore-air pressure curve obtained with the analysis of Hilf (1948) should be used as a prediction of the pore-water pressure in the fill. At the same time, the pore-air pressures are ignored. The result is the computation of a reduced factor of safety because of the excessively high pore-water pressures used in the calculation. For the example problem, the computed factor of safety would be 1.18 if these pore pressures were used in the analysis.

Suggested procedure for computing factor of safety at end-of-construction

It is suggested that, while numerous assumptions can be used in a stability analysis concerning the pore pressures at the end-of-construction, it is important that the factor of safety also be computed using the most realistic conditions. These conditions would include:

- (1) The use of a realistic angle of friction with respect to matric suction for the compacted soil. This can be measured in the laboratory using modified shear strength testing equipment. It can also be estimated as being equal to approximately one half of the ϕ value.
- (2) The use of pore-water pressures in accordance with those predicted using the empirical equation proposed in this paper. The main new information required for such an analysis is a measure of the as-compacted matric suction of the soil.
- (3) The use of pore-air pressures set to zero in the analysis could lead to computed factors of safety that are

too low relative to an analysis performed using pore-air pressures equal to those predicted using the equation by Hilf (1948).

References

- Bishop, A.W. 1954. The use of pore-pressure coefficients in practice. *Géotechnique*, **4**(4): 148–152.
- Bishop, A.W. 1957. Some factors controlling the pore pressures set up during the construction of earth dams. Proceedings, 4th International Conference of Soil Mechanics and Foundation Engineering, Paris, France, Vol. 2, pp. 294–300.
- Fredlund, D.G. 1984. Slope stability analysis incorporating the effect of soil suction. *In Geotechnics and Geomorphology of Mass Movement. Edited by M.G. Anderson and K.S. Richards, J. Wiley and Son*, pp. 113–144.
- Fredlund, D.G., and Morgenstern, N.R. 1976. Constitutive relations for volume change in unsaturated soils. *Canadian Geotechnical Journal*, **13**(3): 261–276.
- Fredlund, D.G., Morgenstern, N.R., and Widger, R.A. 1978. The shear strength of unsaturated soils. *Canadian Geotechnical Journal*, **15**(3): 313–321.
- Hasan, J.U., and Fredlund, D.G. 1980. Pore pressure parameters for unsaturated soils. *Canadian Geotechnical Journal*, **17**(3): 395–404.
- Hilf, J. 1948. Estimating construction pore pressures in rolled earth dams. Proceedings, 2nd International Conference on Soil Mechanics and Foundation Engineering, Rotterdam, The Netherlands, Vol. 3, pp. 234–240.
- Skempton, A.W. 1954. The pore pressure coefficients *A* and *B*. *Géotechnique*, Vol. 4, pp. 143–147.

Lateral earth pressures in expansive clay soils

D.E. Pufahl, D.G. Fredlund, and H. Rahardjo

Abstract: Lateral earth pressures produced by saturated clays with negative pore-water pressures and unsaturated expansive clays with positive matric suctions are considered from a theoretical standpoint. Simple earth pressure equations are formulated in terms of total stresses using the Mohr-Coulomb failure criteria and the assumptions consistent with the Rankine earth pressure theory.

Conventional practice is to separate the pressure that the soil exerts on the wall into the pressure produced by the soil structure (effective stress) and that produced by the water (neutral stress). Since two stress state variables are required to describe the behavior of unsaturated soils, the expressions can no longer be separated into two distinct components.

The change in lateral pressures resulting from decreases in pore-water pressure or increases in matric suction are quantified by considering a 6 m high wall for the active and passive cases. Tension cracks are shown to have little effect on the conditions shown.

The magnitude of the lateral pressure generated due to changes in matric suction under conditions where walls are restrained from moving depends upon the ratio (K_T) of horizontal to vertical stress and the matric suction of the backfill at the time that it is placed behind the wall. When structural members are cast directly against undisturbed clays, similar criteria govern the magnitude of the lateral pressures that may be generated due to changes in matric suction. The maximum pressure that can be developed in some cases will be equal to the passive pressure of the soil when it is saturated.

An expression for the critical height of a vertical bank for the saturated and unsaturated cases is developed. The role of tension cracks is shown by computing the critical height of a vertical slope for a typical soil both in the absence and in the presence of tension cracks.

In many instances it is apparent that methods devised to sustain the matric suction at or near its original value may result in substantial savings in design or ensure adequate performance standards for existing facilities.

Key words: Lateral earth pressure, active pressure, passive pressure, soils, expansive soils, tension cracks, retaining walls, unsupported excavations.

Introduction

The use of cohesive backfill behind earth retaining structures is avoided as much as possible because of the uncertainties associated with the behavior of these materials. This uncertainty is frequently reflected in the observed performance of these structures. For example, Ireland (1964) showed that 68% of the unsatisfactory retaining walls considered in one study either used clay as a backfill or were founded upon clay.

Some of the problems encountered with these structures result from the tendency of the cohesive materials to creep under sustained shearing stress, others are often due to a lack of effective drainage. Additional questions arise if the backfill is an unsaturated expansive clay that undergoes substantial changes in volume with changes in water content. Nevertheless, there are numerous situations where cohesive soils are used as backfill or where struc-

tural members are cast in place against them. It is apparent that the ability to predict the behavior of these soils under many circumstances is not completely developed.

Unsupported trenches or excavations with vertical or nearly vertical walls are frequently made in cohesive soils. If the area of the excavation is comparatively large, a slope failure may not represent a serious hazard to men and equipment working at the base. On the other hand, when the excavation is narrow, as is the case for temporary trenches required for the installation of utilities, a failure often results in the death of workers in the trench. It has been estimated that in excess of 200 deaths per year in the United States alone result from the failure of these trenches (Thompson and Tanenbaum 1977).

The purpose of this paper is to provide a simplistic treatment of anticipated earth pressures in cohesive soils under different conditions of saturation as well as to pro-

D.E. Pufahl and D.G. Fredlund. Professors, Department of Civil Engineering, University of Saskatchewan, 57 Campus Drive, Saskatoon, SK, Canada S7N 5A9.

H. Rahardjo. Research Engineer, Department of Civil Engineering, University of Saskatchewan, 57 Campus Drive, Saskatoon, SK, Canada S7N 5A9.

Reproduced with permission from the *Canadian Geotechnical Journal*, 20(2): 228–241, 1983.

vide appropriate expressions for the critical height of vertical or nearly vertical cuts. The equations are formulated first for saturated conditions when the surface of the soil behind the wall is horizontal and where friction between the wall and the soil is negligible. In addition the groundwater conditions are considered to be static.

It is recognized that seepage patterns will develop that will influence the magnitude of the pressures on the wall and the height of the unsupported cuts that are computed from the equations provided. Moreover, these flow patterns will be influenced by the configuration and location of sand drains that form an integral part of retaining wall design. However, it is virtually impossible to consider all groundwater conditions and to provide expressions for the earth pressures associated with them.

Since vertical tension cracks are ubiquitous in unsaturated cohesive soils, it is of interest to assess their apparent effect on the pressure on walls and the critical height of vertical cuts. Since it is difficult to accurately estimate the depth of existing cracks based on present environmental and soil moisture conditions, the depth of crack can only be established from observations on previous excavations.

Finally, the importance of monitoring soil suction is considered and the increase in earth pressures and the decrease in critical height of a cut associated with decreases in suction are emphasized.

General formulation

Much of the theoretical treatment of lateral earth pressures in cohesive soils where maximum pressures or resistances are the dominant unknowns have used the Mohr-Coulomb failure criteria and concepts of plastic equilibrium. A variety of methods is available in the literature to calculate these pressures. The major differences in the pressures computed using these methods are due mainly to the assumptions made regarding the angle or development of wall friction, the shape of the failure surface, the amount or type of movement of the wall, and the application of earth statics (Morgenstern and Eisenstein 1970). When water pressures are involved, the resulting pressures on the wall are usually separated into two components: those created by the soil structure (effective stresses) and those created by the water (neutral stresses). If the soil has an apparent cohesion intercept on the Mohr-Coulomb failure envelope, the upper part of the "soil structure" in active failure conditions is apparently in tension. Frequently this portion of the effective pressure distribution is neglected when the total force on the wall is computed (Terzaghi and Peck 1967). This modification presupposes that the soil structure cannot adhere to the wall even though the total stress on the wall may be in compression.

Some difficulty arises when this same procedure is applied to unsaturated soils because a single effective stress equation cannot be used to describe the behavior of the soil structure (Fredlund and Morgenstern 1977). The two stress state variables that appear to be most satisfactory

for most soil mechanics problems are $(\sigma - u_a)$ and $(u_a - u_w)$, where σ is the total applied stress, u_a the pore-air pressure, and u_w the pore-water pressure.

The term $(\sigma - u_a)$ is called the net total stress and $(u_a - u_w)$ is called the matric suction. Under these conditions the pressures acting on the wall can be computed in terms of total stresses, pore-air pressures, and matric suction. Since the pore-air pressure will invariably be equal to zero relative to the atmosphere, its inclusion in the equations is somewhat academic and so it will usually disappear in the final result.

If a comparison is to be made between pressures exerted by the same soil when it is saturated and when it is unsaturated, the resulting pressure on the wall for all degrees of saturation must be formulated in terms of total pressure. In addition, it has been suggested that the effect of matric suction on a soil can be most easily visualized if it is considered as contributing to the apparent cohesion intercept on the Mohr-Coulomb failure envelope (Fredlund et al. 1978). In view of the latter proposal, the effect of pore-water pressure on saturated soils will be evaluated in the same manner so that a direct comparison can be made.

The failure plane is assumed to be planar, the surface of the backfill is horizontal, and wall friction is neglected; this set of conditions is in accordance with the classic Rankine earth pressure theory.

Finally all formulations will deal with drained loading. That is to say, pore-water pressures are due only to existing groundwater levels and environmental conditions, and not to changes in total applied stresses.

Total horizontal earth pressures

The shearing resistance of an unsaturated soil was given by Fredlund et al. (1978) as:

$$[1] \quad \tau = (\sigma - u_a) \tan \phi' + [c' + (u_a - u_w) \tan \phi^b]$$

where:

- ϕ' = the effective angle of shearing resistance of a saturated soil,
- ϕ^b = the angle of shearing resistance with respect to changes in matric suction, and
- c' = the effective cohesion intercept.

Although ϕ^b may not be constant over a range of extremely large suction values, present experimental evidence indicates that it will be essentially constant over the range of suction values that are commonly encountered in practice (Ho and Fredlund 1982).

Equation [1] is illustrated by Circle 1 in Fig. 1. Figure 1 is an extended Mohr-Coulomb failure envelope where $(\sigma_v - u_a)$ is the horizontal axis, $(\sigma_v - \sigma_h)/2$ is the vertical axis. The third axis indicates the matric suction, $(u_a - u_w)$, as soil moves into the plane of the paper, and a positive pore-water pressure as the soil moves out of the plane of the paper (e.g., Circle 3).

As the soil moves from Circle 1 (the unsaturated state) to Circle 2 (the saturated state), $\tan \phi^b$ approaches $\tan \phi'$ and eq. [1] reverts to:

$$[2] \quad \tau = (\sigma - u_w) \tan \phi' + c'$$

which is the classic equation for the shear strength of a saturated soil (Terzaghi 1943).

Circle 2 in Fig. 1 indicates a saturated soil with zero pore-water pressure (somewhat hypothetical). From the geometry of this circle, the total active pressure at any depth will be:

$$[3] \quad \sigma_h = \frac{\sigma_v}{N_\phi} - \frac{2c'}{\sqrt{N_\phi}}$$

where:

$$N_\phi = \frac{1 + \sin \phi'}{1 - \sin \phi'} = \tan^2(45 + \phi'/2)$$

and

$$\begin{aligned} \sigma_v &= \rho g z \text{ (total vertical stress),} \\ \sigma_h &= \text{total horizontal stress,} \\ \rho &= \text{total mass density of the soil (Mg/m}^3\text{),} \\ g &= \text{acceleration due to gravity (m/s}^2\text{), and} \\ z &= \text{distance measured positively downward from} \\ &\quad \text{the surface (m).} \end{aligned}$$

The pressure distribution in the soil during active failure is shown in Fig. 2.

$$[4] \quad Z_t = \frac{2\sqrt{N_\phi} c'}{\rho g}$$

The pressure distribution on the wall will be area *abc* if the tension zone is disregarded.

$$[5] \quad P_A = \left[\frac{\rho g H}{N_\phi} - \frac{2c'}{\sqrt{N_\phi}} \right] \frac{(H - z_t)}{2}$$

The total passive pressure at any depth will be,

$$[6] \quad \sigma_h = \sigma_v N_\phi + 2c' \sqrt{N_\phi}$$

The pressure distribution is shown in Fig. 3.

The total passive force will be:

$$[7] \quad P_p = \frac{\rho g H^2}{2} N_\phi + 2c' \sqrt{N_\phi} H$$

The same problem is considered with the water table at a depth, *D*, below the surface. The soil has a negative pore-water pressure above the water table, but is still saturated.

The total active horizontal pressure will be predicted by:

$$[8] \quad \sigma_h = \frac{\sigma_v}{N_\phi} - \frac{2}{\sqrt{N_\phi}} [c' - (z - D) \rho_w g \tan \phi']$$

where:

ρ_w = density of water.

The pressure distribution on the wall is shown in Fig. 4.

It is apparent from eq. [8] and Fig. 1 that the water pressure acts to increase the apparent cohesion intercept above the water table where the pore-water pressures are negative and decreases the apparent cohesion intercept where the pore-water pressures are positive (Circle 3, Fig. 1).

The depth, Z_{ts} , over which the soil is exerting an apparent tensile stress on the wall is:

$$[9] \quad Z_{ts} = \frac{2\sqrt{N_\phi} [c' + D\rho_w g \tan \phi']}{(\rho_s - \rho_w)g + \rho_w g N_\phi}$$

The denominator in eq. [9] can be rewritten as:

$$[10] \quad Z_{ts} = \frac{2\sqrt{N_\phi} [c' + D\rho_w g \tan \phi']}{\rho_s g + 2\rho_w g (\tan \phi') \sqrt{N_\phi}}$$

where:

ρ_s = saturated mass density of the soil.

The total active force on the wall, indicated by area *abc*, will be:

$$[11] \quad P_A = \left\{ \frac{\rho_s g H}{N_\phi} - \frac{2}{\sqrt{N_\phi}} [c' - (H - D) \rho_w g \tan \phi'] \right\} \times \left[\frac{(H - Z_{ts})}{2} \right]$$

It is apparent from eqs. [10] and [11] that lowering the water table has a significant effect in reducing the total force on the wall.

The total passive pressure at any depth as shown in Fig. 5 will be:

$$[12] \quad \sigma_h = \sigma_v N_\phi + 2\sqrt{N_\phi} [c' - (z - D) \rho_w g \tan \phi']$$

The total passive force is equal to area *abcd* and is given by:

$$[13] \quad P_p = \frac{\rho_s g H^2 N_\phi}{2} + 2\sqrt{N_\phi} H \left[c' - \left(\frac{H}{2} - D \right) \rho_w g \tan \phi' \right]$$

Unsaturated soil

From Circle 1 in Fig. 1 the total active pressure will be:

$$[14] \quad \sigma_h = \frac{\sigma_v}{N_\phi} - \frac{2}{\sqrt{N_\phi}} [c' + (u_a - u_w) \tan \phi^b - u_a \tan \phi']$$

A comparison of eq. [8] and eq. [14] indicates that the term $[(z - D) \rho_w g \tan \phi']$ in eq. [8] is equivalent to the

Fig. 1. Active and passive earth pressure for saturated and unsaturated soils.

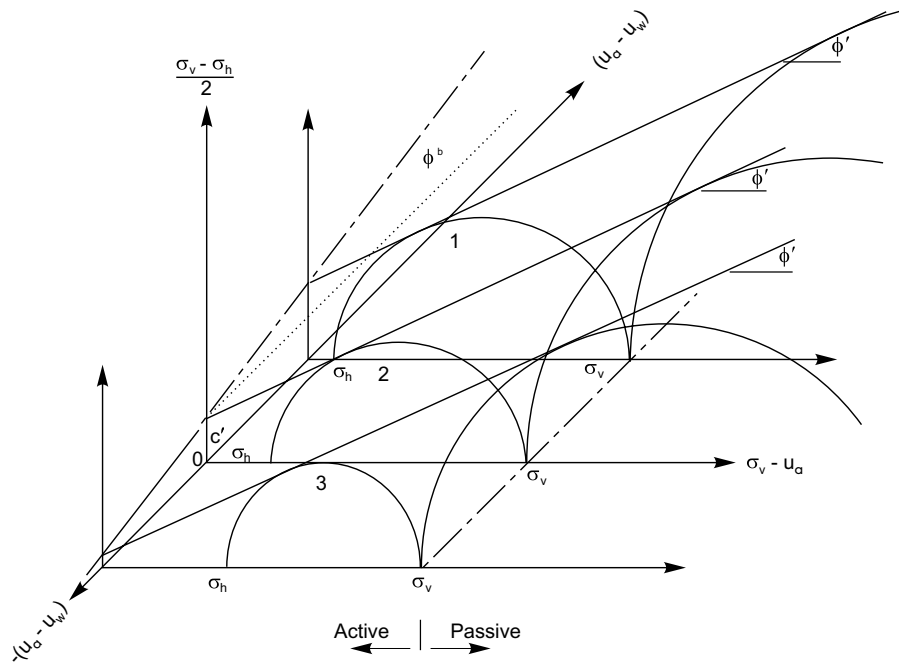


Fig. 2. Active earth pressure (saturated, pore-water pressure equal to 0).

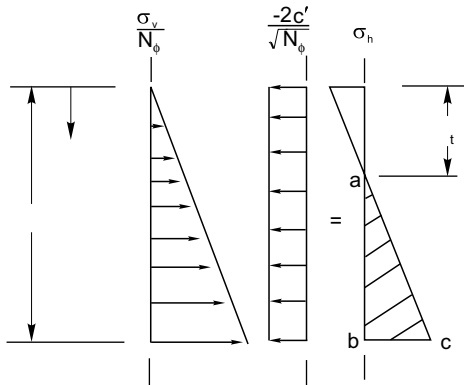


Fig. 3. Passive earth pressure (saturated, pore-water pressure equal to 0).

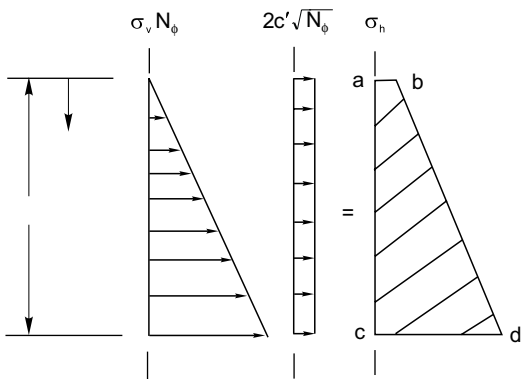


Fig. 4. Active earth pressure (saturated, water table below surface).

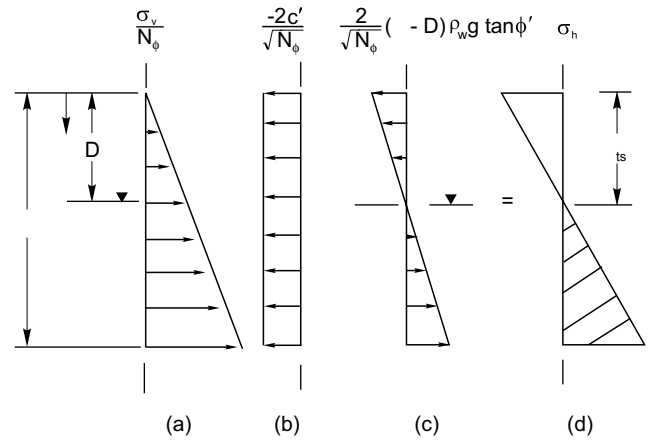
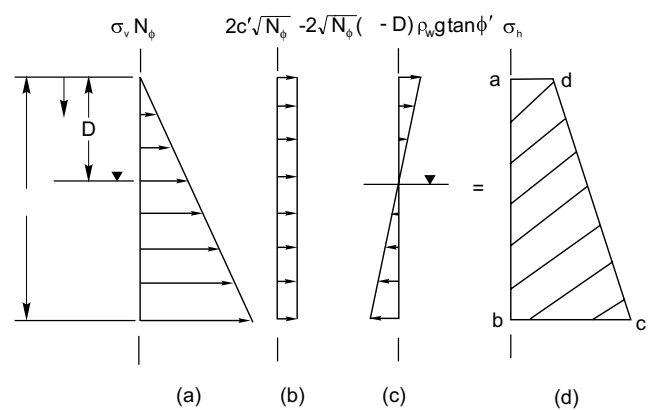


Fig. 5. Passive earth pressure (saturated, water table below surface).



term $[(u_a - u_w) \tan \phi^b]$ in Eq. [14]. A negative sign appears in eq. [8] where a positive sign appears in eq. [14]. However, this sign difference is resolved when appropriate substitutions of the variables are made into the respective equations. The pore-air pressure, u_a , in the unsaturated soil acts in the same way as a positive pore-water pressure in the saturated soil. In practice, u_a is equal to zero relative to the atmosphere and so its effect will not be important. It is included here so that a complete picture of the behavior of the material will be evident. As the soil in eq. [14] moves to the saturated state, $\tan \phi^b$ approaches $\tan \phi'$ and eq. [14] reverts to eq. [8], where u_w becomes $[(z - D)\rho_w g]$.

Equation [14] indicates that $(u_a - u_w)$, is constant with depth. Since $(u_a - u_w)$ will generally decrease with increasing depth, a suitable relationship should be used to account for this condition. Figure 6 shows a typical suction profile with depth, which is shown as the solid line between a and b ; abc represents the hydrostatic condition. A simple linear relationship may be used to adequately estimate the variation of suction with depth for the proposed profile. Then for $z \leq D$,

$$[15] \quad (u_a - u_w)_z = (u_a - u_w)_s \left(1 - \frac{z}{D}\right)$$

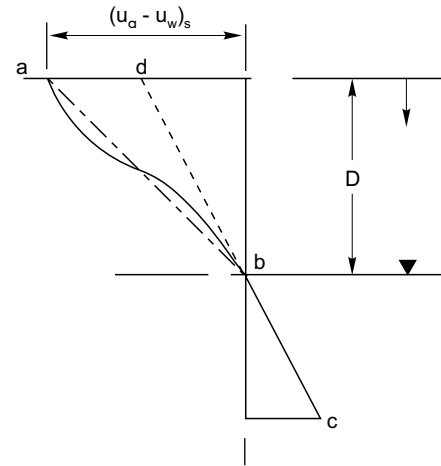
The total active pressure above D will be:

$$[16] \quad \sigma_h = \frac{\sigma_v}{N_\phi} - \frac{2}{\sqrt{N_\phi}} \left[c' + (u_a - u_w)_s \left(1 - \frac{z}{D}\right) \tan \phi^b \right]$$

The total active pressure below D will again be given by eq. [8].

The pressure diagrams resulting from eq. [16] and eq. [8] are shown in Fig. 7. The distance Z_{tu} over which

Fig. 6. Typical suction profile.



tension apparently exists between the soil and the wall is predicted by eq. [17]:

$$[17] \quad Z_{tu} = \frac{2\sqrt{N_\phi} [c' + (u_a - u_w)_s \tan \phi^b]}{\rho_u g + \frac{2\sqrt{N_\phi}}{D} (u_a - u_w)_s \tan \phi^b}; \quad Z_{tu} < D$$

where:

ρ_u = unsaturated mass density of the soil.

When $Z_{tu} > D$,

$$[18] \quad Z_{tu} = \frac{2\sqrt{N_\phi} [c' + D\rho_w g \tan \phi'] + (\rho_s - \rho_u)gD}{\rho_s g + 2\sqrt{N_\phi}\rho_w g \tan \phi'}$$

The total force on the wall will be due to area $cdef$. The exact expression for this area is unduly complex and so, for practical purposes, it may be expressed as:

$$[19] \quad P_A = \left\{ \frac{\rho_u g D}{N_\phi} + \frac{\rho_s g (H - D)}{N_\phi} - \frac{2}{\sqrt{N_\phi}} [c' - (H - D)\rho_w g \tan \phi'] \right\} \left(\frac{H - Z_{tu}}{2} \right)$$

This expression assumes that cfe is linear which is not rigorously correct; however, the error is not considered to be significant.

A comparison of eqs. [10] and [18] indicates that, because Z_{tu} is greater than Z_{ts} , the magnitude of P_A from eq. [19] will be less than that from eq. [11]. As soil moves from the unsaturated to the saturated state, $\tan \phi^b$ approaches $\tan \phi'$, eq. [17] reverts to eq. [10], and eq. [19] reverts to eq. [11].

The total passive pressure above depth D will be:

$$[20] \quad \sigma_h = \sigma_v N_\phi + 2\sqrt{N_\phi} \left[c' + (u_a - u_w)_s \left(1 - \frac{z}{D}\right) \tan \phi^b \right]$$

The total passive pressure below D will again be given by eq. [12]. The pressure distribution is shown in Fig. 8.

$$[21] \quad P_P = N_\phi \left[\frac{\rho_u g D^2}{2} + p_u g D (H - D) + \rho_s g (H - D)^2 \right] + 2\sqrt{N_\phi} \left[c' H + (u_a - u_w)_s (\tan \phi^b) \frac{D}{2} - \rho_w g \tan \phi' \frac{(H - D)^2}{2} \right]$$

Earth pressures and tension cracks

The foregoing expressions for lateral earth pressures have assumed that the soil is intact throughout its entire depth. This will rarely be the case and vertical tension cracks either exist or will develop in the soil behind the wall. The following section provides equations for active earth pressures when tension cracks are present in the soil.

Figure 9 shows a retaining wall of height H with tension cracks of depth Z_c and with the water table at a depth D below the surface. If the soil above the water table and below depth Z_c is assumed to be saturated, eq. [8] may be modified to provide a measure of the total pressure on the wall. The mass of the soil within depth Z_c can be considered as a surcharge load, q_s . The horizontal component of the surcharge on the wall below depth Z_c is (q_s / N_ϕ) , where q_s is equal to $(\rho_u g Z_c)$.

$$[22] \quad \sigma_h = \frac{\sigma_v}{N_\phi} - \frac{2}{\sqrt{N_\phi}} [c' - (z - D)\rho_w g \tan \phi'] + \frac{q_s}{N_\phi}$$

The pressure diagrams from eq. [22] are shown in Fig. 10.

The depth over which tension exists is Z_{tsc} , where:

$$[23] \quad Z_{tsc} = \frac{2\sqrt{N_\phi} [c' + (D - Z_c)\rho_w g \tan \phi'] - q_s}{(\rho_s - \rho_w)g + \rho_w g N_\phi}$$

The total active force, P_A , on the wall is expressed by eq. [24]:

$$[24] \quad P_A = \left\{ \frac{\rho_s g (H - Z_c)}{N_\phi} - \frac{2}{\sqrt{N_\phi}} [c' - (H - D)\rho_w g \tan \phi'] + \frac{q_s}{N_\phi} \right\} \left(\frac{H - Z_c - Z_{tsc}}{2} \right)$$

When the soil is unsaturated above the water table, eq. [16] can be modified to account for the effect of tension cracks.

$$[25] \quad \sigma_h = \frac{\sigma_v}{N_\phi} - \frac{2}{\sqrt{N_\phi}} \left[c' + (u_a - u_w)_s \left(1 - \frac{Z}{D - Z_c} \right) \tan \phi^b \right] + \frac{q_s}{N_\phi}$$

where:

$(u_a - u_w)_s$ = matric suction at depth Z_c below the surface.

The total horizontal active pressure below the water table will be given by eq. [22].

The pressure diagrams associated with eq. [25] are essentially the same as shown in Fig. 10, except for parts d and e . Figure 10 will be the same as Fig. 7c below depth Z_c . In this case the depth, Z_{tuc} , of tension is:

$$[26] \quad Z_{tuc} = \frac{2\sqrt{N_\phi} [c' + (u_a - u_w)_s \tan \phi^b] - q_s}{\rho_u g + 2 \frac{\sqrt{N_\phi}}{(D - Z_c)} (u_a - u_w)_s \tan \phi^b}; \quad Z_{tuc} < D - Z_c$$

When $Z_{tuc} > (D - Z_c)$,

$$[27] \quad Z_{tuc} = \frac{2\sqrt{N_\phi} [c' + (D - Z_c)\rho_w g \tan \phi'] + (\rho_s - \rho_w)g(D - Z_c) - q_s}{\rho_s g + 2\sqrt{N_\phi}\rho_w g \tan \phi'}$$

The total active force will be approximately equal to:

$$[28] \quad P_A = \left\{ \frac{\rho_u g (D - Z_c) + \rho_s g (H - D)}{N_\phi} - \frac{2}{\sqrt{N_\phi}} [c' - (H - D)\rho_w g \tan \phi'] + \frac{q_s}{N_\phi} \right\} \left(\frac{H - Z_c - Z_{tuc}}{2} \right)$$

Fig. 7. Active earth pressure (unsaturated).

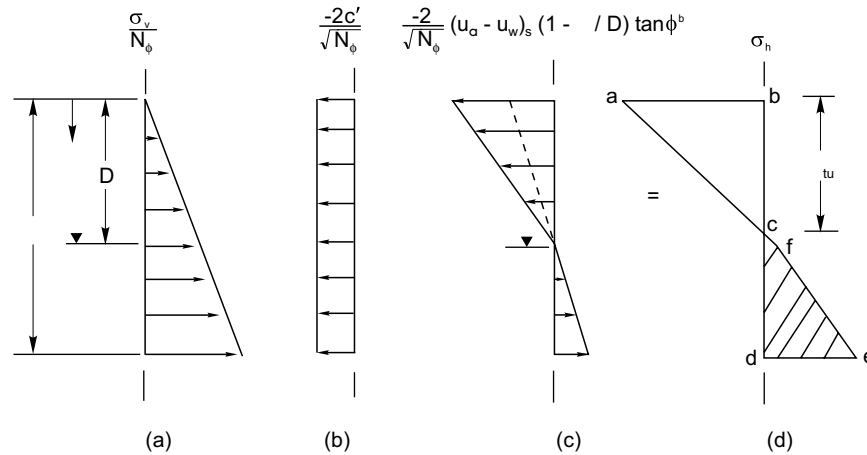


Fig. 8. Passive earth pressure (unsaturated).

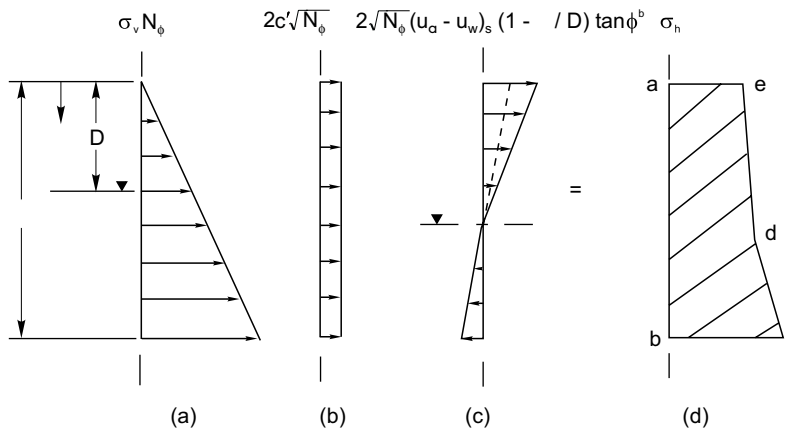
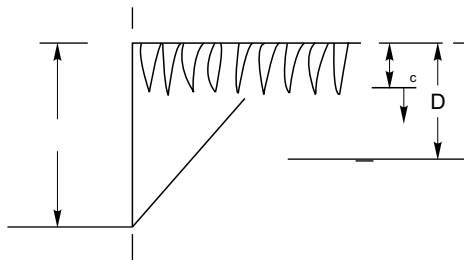


Fig. 9. Retaining wall with tension cracks in the backfill.



Changes in pressure due to changes in water table

Figure 11 provides a quantitative comparison of the lateral earth forces on a typical wall as the water table is lowered from the surface to the base of the wall. It also shows the change in pressure that occurs when the soil is unsaturated and the matric suction at the surface is 200 kPa. The water table is allowed to vary from 3 to 6 m while the matric suction at the surface is held constant. The average saturated density and the average unsaturated density of the soil are assumed to remain constant with decreases in pore-water pressure or increases in

matric suction. Details of calculations are shown in the Appendix.

The effect of tension cracks in the backfill behind the wall is also considered for the active case. In this circumstance the suction is measured at the base of the tension crack. In reality the unsaturated soil will always be cracked so that the term unsaturated intact is hypothetical and is used here for comparison purposes only. The presence of tension cracks is insignificant in affecting the total force on the wall. Since the upper portion of the wall that was apparently in tension has been neglected in computing the total force on the wall, placing additional tension cracks in the soil has little effect except to reduce the total mass density of the soil.

Figure 11 shows the maximum active force, consistent with the assumptions involved in the formulation, that can be developed against the wall provided the wall is free to move away from the fill. If the wall is subjected to some restraint the horizontal pressures behind the wall will increase well beyond those shown in the figure.

In general, the magnitude of the lateral pressure developed against a fixed wall will depend upon the ratio, K_T , of horizontal to vertical pressures and on the matric suction at the time of placement.

Fig. 10. Active earth pressure with tension cracks.

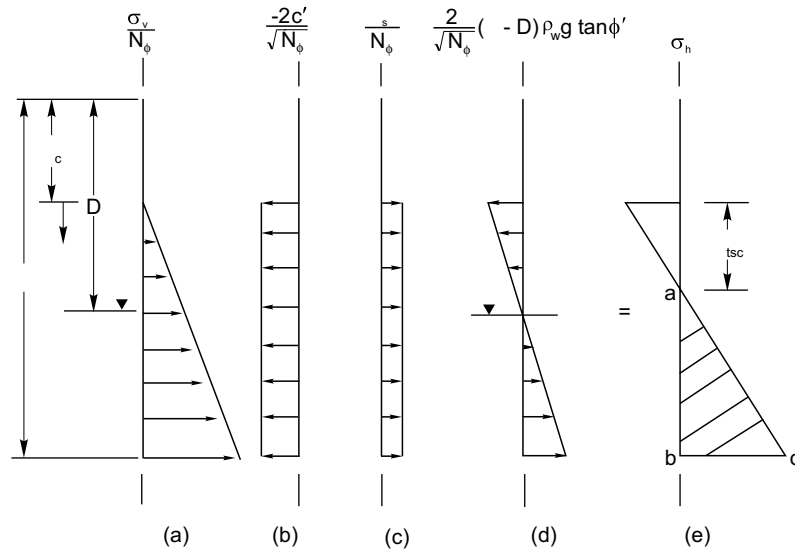
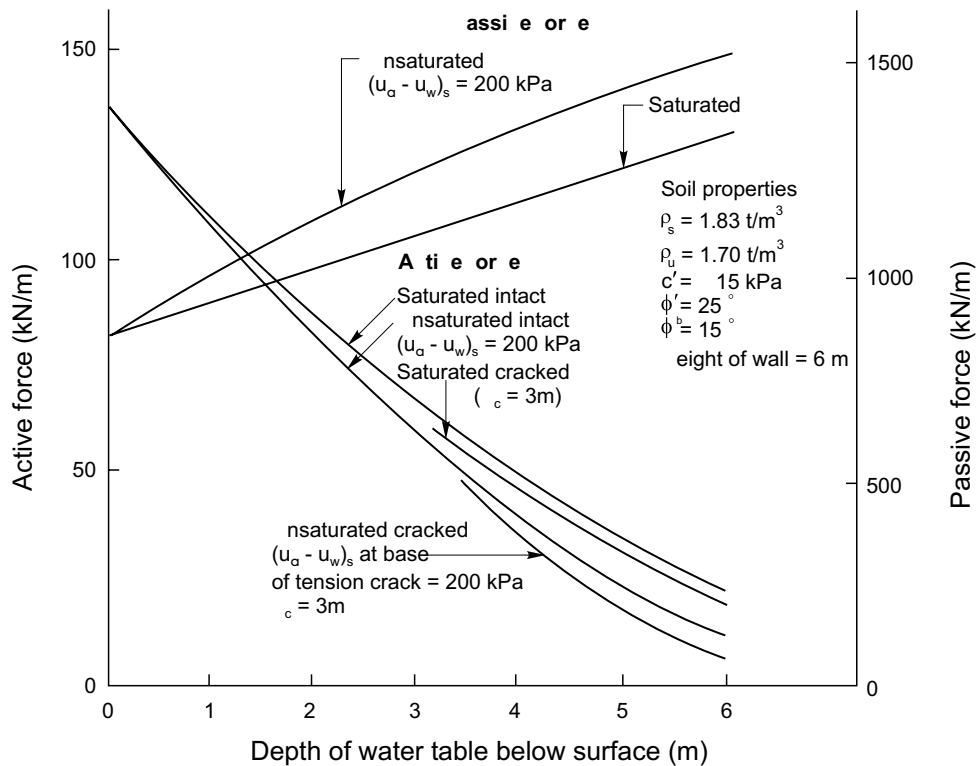


Fig. 11. Active and passive forces on a 6 m wall versus depth of water table (saturated and unsaturated).



Circle A in Fig. 12 denotes the total vertical and horizontal pressures at some depth z for fully active conditions. As the water content increases and the suction decreases under these unrestricted movements, the horizontal pressures will move along stress path a and the vertical pressures along path b to Circle A_1 . The magnitude of the pressure increase in the horizontal direction can be noted in Fig. 11.

On the other hand, if backfill is placed behind a fixed wall at the same matric suction as in A but at a stress ra-

tio K_T , as indicated in Circle C, the horizontal earth pressure change will result in stress path c and Circle C_1 will be the result. Similarly, if K_T is equal to 1, then stress path d is proposed. The exact paths would have to be established experimentally and those shown here are only qualitative in nature.

There will undoubtedly be conditions in practice where backfill is placed against rigid walls or occasions when heavy structural members are cast against undisturbed clays with K_T values of 1 or greater. In these circum-

Fig. 12. Lateral pressures on walls subjected to limited movement.

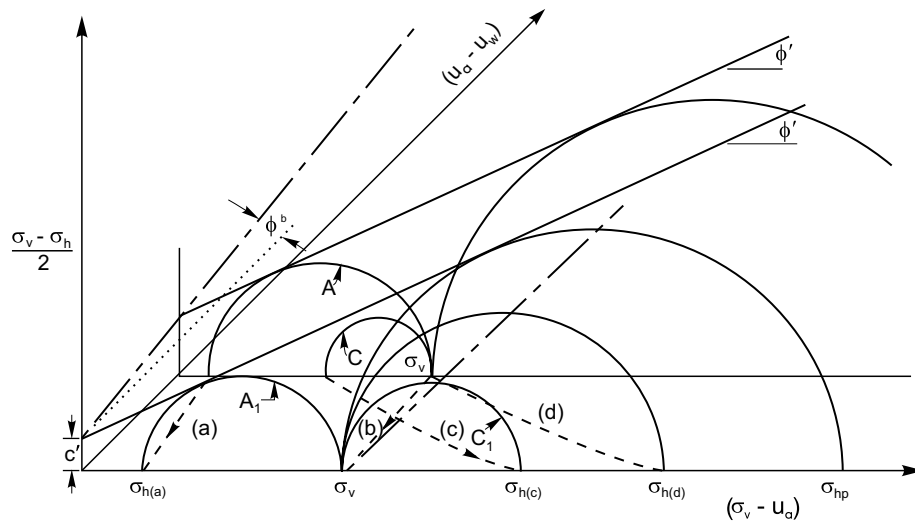
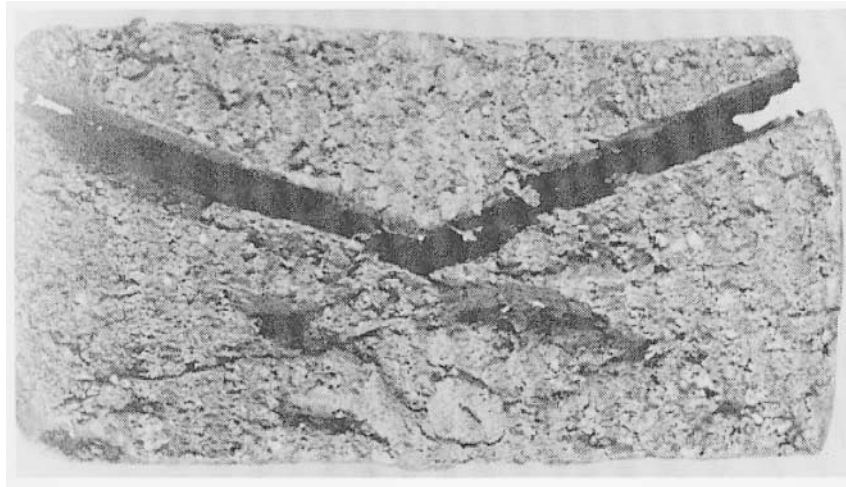


Fig. 13. Passive failure of compacted clay till due to one-dimensional swelling.



stances, the horizontal stresses will move to σ_{hp} , which is the passive resistance of the soil. In these situations either the structural member will fail or the soil will fail in shear.

Figure 13 is a photograph of a compacted clay till sample that was allowed to swell one-dimensionally while confined in a consolidation ring. It is evident that the soil has failed in the passive sense.

If a structural member is designed such that it is not free to move, and if it is expected to perform satisfactorily under the conditions outlined above, it must be designed to resist the full saturated passive earth pressure of the soil.

Unsupported excavations

Frequently the slopes of temporary cuts or excavations in cohesive soils are allowed to stand unsupported in the vertical or near vertical position. If the slope is assumed to fail along a planar surface, the critical height H_s can be

determined by considering a balance of forces on the sliding wedge shown in Fig. 14.

$$[29] \quad H_s = \frac{4\sqrt{N_\phi} (c' + D\rho_w g \tan \phi')}{\rho_s g + 2\rho_w g (\tan \phi') \sqrt{N_\phi}}$$

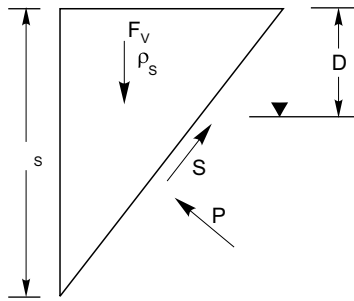
(Note that H_s is equal to $2Z_{ts}$ as computed from eq. [10]).

If the soil is unsaturated above the water table, the maximum unsupported height (H_u) may be obtained most readily by summing forces parallel and perpendicular to the failure plane shown in Fig. 15.

$$[30] \quad S_1 = c' l_1 + (P_1 - u_a l_1) \tan \phi' + \frac{(u_a - u_w)_s l_1}{2} \tan \phi^b$$

$$[31] \quad S_2 = c' l_2 + \left[P_2 - \frac{(H_u - D)}{2} \rho_w g l_2 \right] \tan \phi'$$

Fig. 14. Unsupported vertical slope (saturated, intact).



[32] $H_u =$

$$\frac{4\sqrt{N_\phi} \left[c' + \frac{m}{2} (u_a - u_w)_s \tan \phi^b \right]}{(1 - m^2)g[\rho_s + 2 \tan \phi' \sqrt{N_\phi} \rho_w] + m(2 - m)\rho_u g}$$

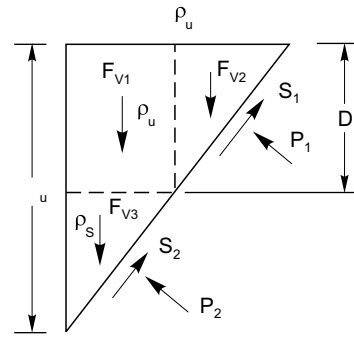
where:

$$m = D / H_u.$$

Equation [32] requires a trial and error solution because H_u appears on both sides of the equal sign.

Although this is not readily evident, eq. [32] reverts to eq. [29] as ρ_u approaches ρ_s and $\tan \phi^b$ approaches $\tan \phi'$.

Fig. 15. Unsupported vertical slope (unsaturated, intact).



Effect of tension cracks on the unsupported height

If the upper zone of soil has been weakened by tension cracks of depth Z_c , the expression for the maximum unsupported height of bank, H_{sc} (eq. [33]), when the soil is saturated upwards from the water table to the base of the crack and the water table is at a depth D below the surface, may be obtained by summing forces in Fig. 16:

[33] $H_{sc} = \frac{4\sqrt{N_\phi} [c' + D\rho_w g \tan \phi'] - Z_c[(\rho_u - \rho_s)g + (N_\phi - 1)\rho_w g]}{\rho_s g + 2\rho_w g \sqrt{N_\phi} \tan \phi'}$

If the soil is unsaturated above the water table, the expression for the critical height, H_{uc} , can be obtained by summation of forces shown in Fig. 17.

The expressions for S_1 and S_2 will again be given by eqs. [30] and [31]. However, P_1 and P_2 will be different. The end result is a rather complex expression for H_{uc} , as given in eq. [34]:

[34] $H_{uc} = \frac{4\sqrt{N_\phi} \left\{ \left[(1 - n)c' + \frac{(m - n)}{2} \tan \phi^b (u_a - u_w)_s \right] - 2Z_c \rho_u g \right\}}{(1 - m)^2 \rho_s g + [m(2 - m) + n(n - 2)]\rho_u g - 2n^2 \rho_u g + 2(1 - m)^2 \rho_w g (\tan \phi') \sqrt{N_\phi}}$

where:

$$m = D / H_{uc},$$

$$n = Z_c / H, \text{ and}$$

D = the distance from the water table to the surface.

H_{uc} appears on both sides of the equal sign, thus eq. [34] requires a trial and error solution. The complexity of the equation make hand calculations rather tedious. In addition, a variety of conditions can occur to reduce the critical height or the factor of safety for which the slope was designed. For example, if a sudden heavy rain-storm occurs and fills the cracks with water, ρ_u approaches ρ_s . A horizontal water force acting to the left

must be included. Moreover, the negative pore-water pressure (or positive suctions) will be reduced throughout the depth, $D - Z_c$. In view of the variety of factors that can influence the critical height of the slope, it is better to formulate the expression in terms of a factor of safety equation and to use a computer program for the solution. This will allow more flexibility in the boundary conditions, the geometry of the problem, and the suction profile.

Figure 18 indicates the relationship between the critical height of an unsupported vertical slope, depth of water table, and depth of tension cracks. It is readily apparent that negative pore-water pressures or positive matric suctions will increase the critical height substantially. On the other

Fig. 16. Unsupported vertical slope (saturated, cracked).

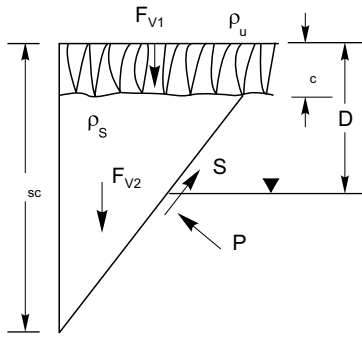


Fig. 17. Unsupported vertical slope (unsaturated, cracked).

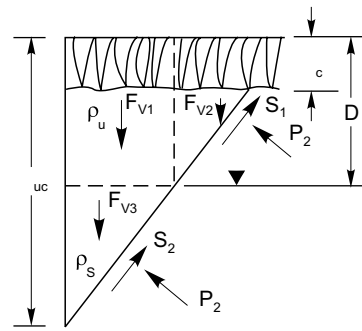
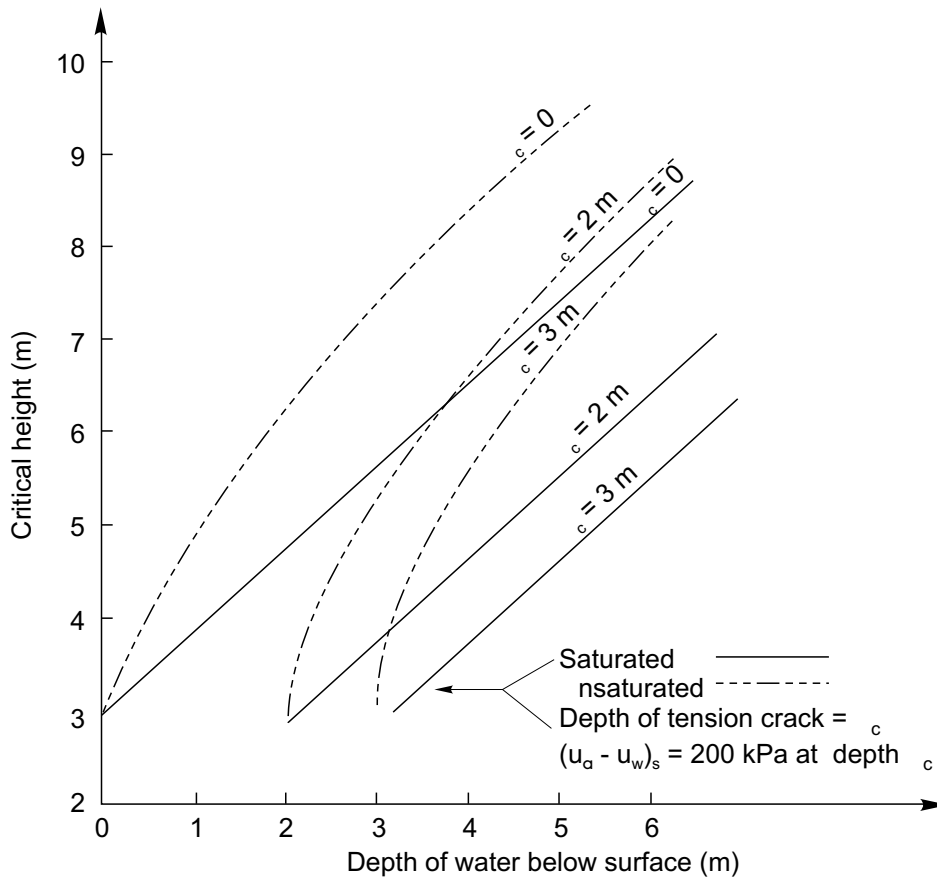


Fig. 18. Critical height of unsupported vertical slope with tension cracks versus depth of water table.



hand, tension cracks substantially reduce the critical height. It is evident that their presence must be considered when designing an open cut in cohesive soils.

Conclusions

Expressions for active and passive earth pressures have been formulated in terms of total stresses for both the saturated and unsaturated states using the Mohr-Coulomb failure criterion and plastic equilibrium. The assumptions regarding the shape of the failure surface, the lack of wall friction, and the horizontal surface of the backfill are in accordance with the classic Rankine earth pressure theory.

The approach that has been taken is that the total lateral stresses on the wall govern the design and no attempt has been made to separate the stresses in the soil structure (effective stresses) from those in the water phase (neutral stresses). Water pressure or matric suction is considered to affect the magnitude of the apparent cohesion intercept. This is an obvious departure from classic analyses of lateral earth pressures in saturated soils. However, it was adopted here so that direct comparisons could be made between the saturated and unsaturated states. When total active forces were computed, any portion of the wall in tension was neglected.

The results indicate (Fig. 11) that, for saturated soils, negative pore-water pressure or, for unsaturated soils,

matric suction acts to decrease the total active pressure on retaining walls or to increase the passive resistance on anchors or similar structures. It is apparent that for a given height of wall the total active force on the wall decreases slightly as the depth of tension crack increases.

The stress paths shown in Fig. 12 help to illustrate why walls with cohesive backfills may undergo large outward movements during the life of the wall. As the soil dries, a crack will open between the soil and the wall. Dust and debris will tend to collect in the opening, thus partially filling it with relatively incompressible material. As the matric suction decreases during wetter seasons the soil will swell, pushing out the wall until the resistance of the wall is in equilibrium with the total lateral force exerted by the soil. This cycle is repeated each time the soil experiences a decrease in water content and then an increase in water content.

It is also apparent that very large pressures, those approaching the passive condition, will develop when a wall or other structural member is restrained from moving. The pressures developed will depend, for backfill, upon the ratio, K_T , of the horizontal to vertical stresses at the time of placement or, for undisturbed soils, on the *in-situ* K_T ratio. If large lateral pressures are to be avoided because of volume changes in the soil, the backfill material should be placed at rather low densities and at water contents that are near optimum. This procedure will result in lower values of K_T and correspondingly lower values of pressure. When structural members are cast against undisturbed expansive clays, a compressible material placed between the structure and the soil will help to relieve some of the pressure generated during the lateral swelling of the clay.

The results in Fig. 18 indicate that the critical height of vertical slopes in cohesive soils will increase substantially as the water table is lowered or as the matric suction is increased. The effect of tension cracks is also displayed in this figure.

Since matric suction is so effective in increasing the critical height of a slope or increasing the safety factor of an existing slope, every attempt should be made to maintain the water content of these soils at a fairly constant value during the time that these excavations are expected to remain open.

Such obvious measures as covering the bank adjacent to the excavation with an impermeable membrane and diverting surface runoff during heavy rains would be beneficial. Tensiometers may be placed in the bank near the base of the tension cracks so that the magnitude of, or changes in the suction can be monitored. These changes in suction can then be directly correlated with changes in the factor of safety of the unsupported bank and at least provide a rational means of predicting the continued safety of the excavation.

References

Fredlund, D.G., and Morgenstern, N.R. 1977. Stress state variables for unsaturated soils. ASCE, Journal of the Geotechnical Engineering Division, **103**(GT5): 447–466.

Fredlund, D.G., Morgenstern, N. R., and Widger, R.A. 1978. The shear strength of unsaturated soils. Canadian Geotechnical Journal, **15**: 313–321.

Ho, D.Y.F., and Fredlund, D.G. 1982. Increase in strength due to suction for two Hong Kong soils. Proceedings, Conference on Engineering and Construction in Tropical and Residual Soils, ASCE, Honolulu, pp. 263–295.

Ireland, H.O. 1964. Design and construction of retaining walls. In Soil mechanics lecture series: design of structures to resist earth pressure. American Society of Civil Engineers, Chicago, ILL.

Morgenstern, N.R., and Eisenstein, Z. 1970. Methods of estimating lateral loads and deformations. Proceedings, Lateral Stresses and Earth-retaining Structures. Speciality Conference, ASCE, Cornell University, Ithaca, NY, pp. 51–102.

Terzaghi, K. 1943. Theoretical soil mechanics. John Wiley and Sons, New York, NY.

Terzaghi, K., and Peck, R.B. 1967. Soil mechanics in engineering practice. Second edition. John Wiley and Sons, New York, NY.

Thompson, L.J., and Tanenbaum, R.J. 1977. Survey of construction related trench caverns. ASCE, Journal of the Construction Division, **103**(CO3): 501–512.

Appendix

A.1 Retaining wall

A retaining wall problem is analyzed to describe the use of all equations formulated in this paper for the active and passive forces. A cohesive backfill against a vertical wall of 6 m height is analyzed as shown in Fig. A.1. The calculations presented in this Appendix are only for a depth of water table, D of 4.0 m. Conditions with various depths of water table have also been analyzed; the results are plotted in Fig. 11.

The active forces of an intact backfill can be computed according to eqs. [11] and [19] for the saturated and unsaturated conditions. The depth, Z_{ts} , of the tensile region in the saturated condition is obtained from eq. [9]; it is Z_{ts} equal to 3.24 m.

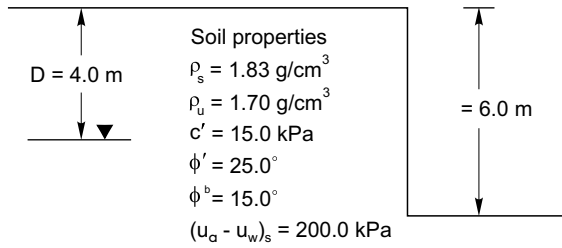
The active force, P_A , for the saturated condition is computed from eq. [11]. This gives P_A equal to 50.1 kN per metre of wall. The depth, Z_{tu} , of the tensile region in the unsaturated condition is computed from eq. [17]. This gives Z_{tu} equal to 3.67 m.

If the computed Z_{tu} is greater than D , then Z_{tu} should be calculated again according to eq. [18]. In this problem, Z_{tu} (i.e., 3.67 m) is less than D (i.e., 4.0 m). The active force, P_A , for the unsaturated condition is computed from eq. [19] and is P_A equal to 39.9 kN per metre of wall.

When tension cracks are present in the soil, the active earth forces are calculated using eqs. [24] and [28] for the saturated and unsaturated conditions, respectively. In this problem, the tension cracks are assumed to develop down to a depth of 3.0 m. The mass of the cracked soil is considered as a surcharge load, q_s , with a magnitude of $q_s = \rho_{tu}gZ_c$, which is equal to 50.02 kPa.

The depth, Z_{tsc} , over which tension exists for the saturated condition is obtained from eq. [23] and is Z_{tsc} equal to 0.35 m.

Fig. A.1. Retaining wall problem.



The active force of the cracked backfill for the saturated condition is calculated from eq. [24] to be P_A equal to 45.9 kN per metre of wall.

The depth of tension for the unsaturated condition can be computed according to eq. [26]. This gives Z_{tuc} equal to 0.89 m. Since Z_{tuc} (0.89 m) is less than $D - Z_c$ (3.0 m), Z_{tuc} can be substituted directly into eq. [28] to calculate the active force for the unsaturated condition, giving P_A equal to 36.0 kN per metre of wall.

Similar calculations can be performed for conditions with different depths, D , to the water table. The computed active forces can then be plotted against the depth of the water table as shown in Fig. 11.

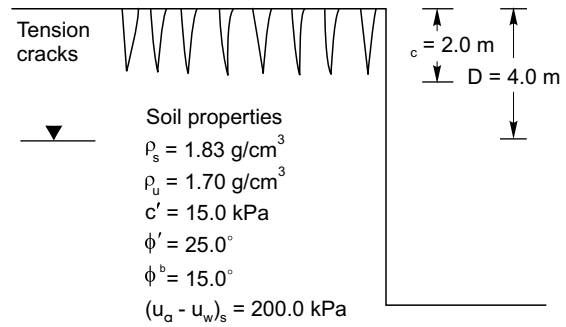
The passive force of an intact backfill is calculated from eq. [13] for the saturated condition; which gives P_p equal to 1164.6 kN per metre of wall.

For the unsaturated condition, the passive force can be obtained from eq. [21], and P_p is equal to 1438.6 kN per metre of wall. The passive forces are computed for various depths of water table and plotted against depth of water table in Fig. 11.

A.2 Unsupported vertical slope

An unsupported vertical slope as shown in Fig. A.2 is analyzed for the saturated and unsaturated conditions. In addition, the depths, Z_c , of the tension cracks are also varied from 0 to 3.0 m. The calculations presented in this Appendix are only for a depth of water table, D , of 4.0 m and depths of tension cracks of 0 and 2.0 m. The results of analyses with various depths of water table are shown in Fig. 18.

Fig. A.2. Unsupported vertical slope.



The critical height of an intact slope can be computed according to eqs. [29] and [32] for the saturated and unsaturated conditions. Substituting the soil properties and the depth of water table, D , into eq. [29] gives the critical height for the saturated condition, H equal to 6.47 m.

The critical height for the unsaturated condition is obtained from eq. [32]. Rearranging this non-linear equation and solving it as a quadratic equation give two values of H_u ; H_{u1} equal to 8.35 m and H_{u2} equal to -3.13 m. The value of the critical height of the intact backfill, which is unsaturated, is H_{u1} equal to 8.35 m.

When tension cracks are present down to a depth of 2.0 m, the critical heights are calculated from eqs. [33] and [34] for the saturated and unsaturated conditions, respectively. Substituting the properties of soil and the depth of water table into eq. [33] gives H_{sc} equal to 4.63 m.

The critical height for the unsaturated condition is given by eq. [34], where: $m = D / H_{uc}$, which is equal to $4.0 / H_{uc}$, and $n = Z_c / H$, which is equal to $2.0 / 6.0$, equal to $1/3$. Again this is a non-linear equation that can be solved as a quadratic equation to give H_{uc} equal to 6.62 m.

Similar calculations are carried out for various depths of water table and tension crack. The computed critical heights are plotted against depth of the water table in Fig. 18.

Bearing capacity of unpaved roads

S. Oloo, D.G. Fredlund, and J.K-M. Gan

Abstract: Elastic layer theories may be valid for relatively stiff pavement materials and pavements subjected to low traffic stresses; however, the assumption of linear elastic behavior is not suitable for thin pavements and unpaved roads consisting of untreated granular bases over cohesive subgrades. The behavior of such pavements, even at low traffic stresses, is markedly non-linear. Pavement design methods based on a bearing capacity theory are more applicable to roads with thin pavements. This paper outlines an ultimate strength method of designing low-volume roads. A procedure for determining the ultimate loads in layered systems, incorporating the effect of matric suction, is also presented. Existing empirical relationships which account for traffic loading are used in the proposed design procedure.

Key words: bearing capacity, unpaved roads, non-linear theory, ultimate strength.

Introduction

Elastic layer theories hypothesize that stresses and strains are only dependent on the elastic modulus and Poisson's ratio. The assumption of isotropic elastic behavior may be valid for relatively stiff pavement materials and pavements subjected to low traffic stresses. In thin pavements and unpaved roads consisting of untreated granular bases over cohesive subgrades, the assumption of linear elastic behavior is not suitable. The behavior of such pavements, even at low traffic stresses, is markedly non-linear.

In using ultimate strength methods, it is assumed that shear failure of the pavement structure occurs if traffic stresses are sufficiently high. Pavement material behavior is assumed to be plastic rather than elastic. The assumption of plastic response is more realistic for thin pavements and unpaved roads in which traffic stresses invariably exceed the elastic range of the pavement materials. The same may apply to thick pavements subjected to high traffic stresses.

The implementation of elastic layer theories in the pavement design process requires the quantification of the elastic modulus and the Poisson's ratio. Difficulties associated with the determination of these parameters for pavement materials are well known. Ultimate strength methods of pavement design are based on the shear strength parameters, c' and ϕ' (and also ϕ^b in the case of an unsaturated soil), which are more clearly defined.

Ultimate strength methods allow for the design of pavements with known factors of safety. The quantification of a factor of safety, which is lacking in elastic layer methods, allows for the assessment of pavement damage due to any loading condition. This flexibility is particularly useful in load zoning of light pavements and for the issuing of over-weight vehicle permits.

Ultimate strength approaches suffer from the disadvantage that deformations prior to pavement collapse cannot be quantified. Deformations during the life of the pavement determine its serviceability and must be controlled. Difficulties associated with the prediction of displacements during the service life of the pavement can be surmounted through the judicious selection of the factor of safety to limit deformations.

Literature review

The relative merits of ultimate strength methods have been recognised. There have been attempts by McLeod (1953, 1954), and Broms (1963, 1964) to extend traditional bearing capacity theory to the design of pavements. More recently Milligan et al. (1989), Bender and Barenberg (1978), and Giroud and Noiray (1981) have used bearing capacity theory to analyze the contribution of geotextiles to the load carrying capacity of unpaved roads. These methods represent a more rational idealization of pavement behavior but fall short of providing an adequate quantification of the subgrade portion of the pavement design problem. The shortcomings can be attributed to; (1) uncertainty in the prediction of the ultimate loads in layered pavements, (2) difficulties associated with the incorporation of environmental changes in the bearing capacity formulation, and (3) lack of a suitable method to deal with traffic loading.

This paper outlines an ultimate strength method of designing low-volume roads based on new procedures for determining ultimate loads in layered systems and for incorporating the effect of matric suction on bearing capacity. Existing empirical relationships are used to account for traffic loading in the proposed design procedure.

S. Oloo. Department of Civil Engineering, University of Nairobi, Nairobi, Kenya.

D.G. Fredlund. Professor, Department of Civil Engineering, University of Saskatchewan, 57 Campus Drive, Saskatoon, SK, Canada S7N 5A9.

J.K-M. Gan. Research Engineer, Department of Civil Engineering, University of Saskatchewan, 57 Campus Drive, Saskatoon, SK, Canada S7N 5A9.

Reproduced with permission from the *Canadian Geotechnical Journal*, 34(3): 398-407, 1997.

Idealization of pavement geometry

A typical unpaved road cross-section consists of an unbound base layer directly overlying the subgrade. A surfacing layer may or may not be present. Where a surfacing layer exists, it serves to protect the underlying layers from variations in the surface flux but makes little contribution to the bearing capacity of the pavement. If a subbase layer is present, it is assumed that its shear strength characteristics (i.e., c' , ϕ' and ϕ^b parameters) are not significantly different from those of the base. For the purpose of determining bearing capacity, the unpaved road can be idealized as consisting of the base and subgrade layers only (i.e., a two-layer system).

The wheel loads are assumed to be applied at sufficient distance from the pavement shoulders to avoid slope failure or other edge effects affecting the layout of the general shear failure mechanism. The process of pavement design becomes one of determining the depth of the base layer required to carry the design traffic.

Determination of contact area and pressure

The design of pavements based on bearing capacity theory is based on a fixed level of traffic approach. The fixed level of traffic approach involves the design of the pavement for a critical wheel load, usually the heaviest wheel load. The fixed level of traffic approach is used mainly in airport design. The traffic volume in unpaved roads is low and comparable to the frequency of landing of aircrafts on smaller airports.

The fixed level of traffic approach requires the determination of an equivalent single wheel load (ESWL) in cases where there is more than one wheel. Design methods based on elastic theory define the ESWL in terms of the relative influences of single and multiple wheel configurations on stresses or strains. In contrast, methods based on bearing capacity theory require the representation of the wheel configurations in terms of a contact pressure and the dimensions of the contact area.

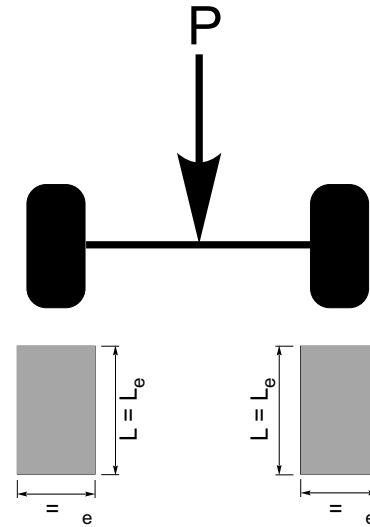
The contact area was assumed to be rectangular for rigid pavements by the Portland Cement Association (PCA 1984). Although the idealization by the PCA was intended for rigid pavements, it is frequently used for flexible pavements and is herein adopted for unpaved roads. The actual pressure and area to be used in the bearing capacity analysis depends on the configuration of axles and number of tires. The following cases were considered:

- (1) single axle with single tires, and,
- (2) single axle with dual tires.

Single axle with single tires

The arrangement of single tires on a single axle is shown in Fig. 1. The tire contact area is calculated from the axle load using the following equation:

Fig. 1. Idealization of the tire contact area for a single axle load with single tires.



$$[1] \quad A_c = \frac{P}{2P_t}$$

where:

- P = axle load,
 A_c = tire contact area, and
 P_t = tire inflation pressure.

The contact area can be approximated by a rectangular area as proposed by PCA (1984). The dimensions for the equivalent rectangle are given by:

$$[2] \quad L = 0.8712 \sqrt{\frac{A_c}{0.5227}}$$

and

$$[3] \quad B = 0.6 L$$

where:

- L and B = length and width of the equivalent rectangle, respectively.

The dimensions to be used in the determination of bearing capacity for a single axle with single tires are similar to the length and width of the equivalent rectangle and are given by:

$$[4] \quad L_e = L$$

and

$$[5] \quad B_e = B$$

where:

- L_e and B_e = dimensions of the equivalent contact area to be used in the bearing capacity analysis.

The equivalent contact pressure is given by the following equation:

$$[6] \quad P_e = \frac{P}{2L_e B_e}$$

Single axle with dual tires

The layout of dual tires on a single axle is shown in Fig. 2. The dual tires can be analyzed by assuming that the soil between the tires is mechanically associated with the tires. The two tires, therefore, behave as a single entity in distributing the axle load to the soil.

The contact area due to each tire is given by:

$$[7] \quad A_c = \frac{P}{4P_t}$$

The dimension of the equivalent rectangular area for each tire is given by eqs. [2] and [3]. The equivalent contact pressure of the dual tire assembly is assumed to be acting over the area enclosing both tires. The dimensions of the equivalent contact area for the single axle with dual tires configuration are given by:

$$[8] \quad B_e = (2B + d)$$

and

$$[9] \quad L_e = L$$

where:

d = clear distance between dual tires.

The clear distance between the dual tires, d , is given by the following equation:

$$[10] \quad d = S_d - B$$

where:

S_d = center to center spacing between the dual tires.

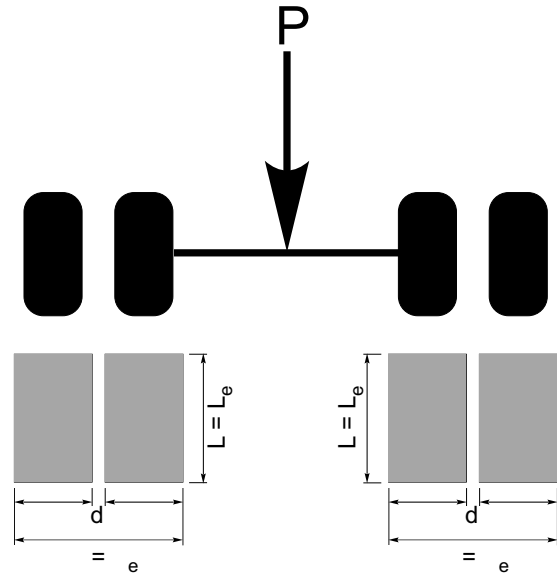
The equivalent contact pressure is given by eq. [6].

Determination of strength parameters

The determination of the bearing capacity of an unpaved road requires a knowledge of the effective shear strength parameters, c' and ϕ' for the materials comprising the base and subgrade. The shear strength parameter with respect to matric suction, ϕ^b , is also required in cases where the pavement soil layers are unsaturated. The shear strength parameters, c' , ϕ' and ϕ^b can be determined using triaxial or direct shear tests. The determination of ϕ^b in the test and in the direct shear test are described by Ho and Fredlund (1982) and Gan and Fredlund (1988), respectively.

Mixtures of coarse aggregates and fine-grained soil are the preferred materials for the base layer. Stability requirements demand the existence of a small fraction of fines in the base layer. The presence of fines in the aggregates often increases cohesion to an extent that the base layer cannot be treated as being purely frictional. Under these circumstances, design methods which ignore cohesion in the base can be unnecessarily conservative. The

Fig. 2. Idealization of the tire contact area for a single axle load with dual tires.



presence of fines also enhances the contribution of matric suction to the shear strength of the base layer. The characterization of shear strength should include the determination of ϕ^b to include the contribution of matric suction to shear strength.

Estimation of matric suction

Pavement designs are commonly based on the saturated shear strength parameters of the subgrade. In many cases, the water contents in the subgrade does not reach saturation and the assumption of saturation leads to over design.

Moisture conditions in the pavement layers are controlled by climatic and soil conditions. Russam (1965) proposed criteria for the determination of long-term equilibrium water contents depending on the depth of the water table and climatic conditions. The criteria recommended actual measurements of water contents in most cases and are widely used for design.

The distribution of moisture in a layered soil depends on the relative hydraulic conductivities and the water retention characteristics of the soil in each layer. Saturated-unsaturated flow modeling that takes into consideration the flux boundary conditions (Lytton et al. 1990; Barbour et al. 1992; Wallace 1977) are likely to give more insight into the moisture distribution within layered soils. The determination of the surface fluxes to be used in the modeling requires the characterization of climatic and ground surface conditions and the solution of a system of coupled heat and mass transfer equations. Lytton et al. (1990) presented a comprehensive model for the prediction of matric suction variations under pavements based on a finite difference solution of the coupled heat and mass transfer equations. The model also provides a means of characterizing climate. Solutions of the coupled heat and

mass transfer equations have also been presented by Wilson (1990) based on the finite difference method and by Joshi (1993) based on the finite element method.

The estimation of equilibrium water contents and/or matric suction profiles is prerequisite to the application of the bearing capacity theory to pavement design. Techniques are available for the prediction (Fredlund 1997) as well as the monitoring (Wilson et al. 1997) of matric suction in the field. It is assumed in this paper that equilibrium matric suction profiles in the pavement layers are known or can be estimated from soil and climatic information.

Determination of ultimate wheel loads

The bearing capacity based pavement design methods can be classified into two categories depending on the assumptions made with regard to the failure mechanism. The first method consider the base layer as an elastic material whose sole purpose is to distribute the load to the subgrade (Broms 1963, 1964; Bender and Barenberg 1978; Giroud and Noiray 1981; Milligan et al. 1989; Sattler et al. 1989; Szafron 1991). The second method assumes a general shear failure type of mechanism involving all pavement layers (McLeod 1953).

The mobilization of the ultimate strength of the subgrade requires large deformations. Since the pavement must continue to behave as a continuous system, large deformations of the subgrade invariably translate into equally large deformations of the overlying layers. The base layer is unlikely to continue behaving elastically over the large deformations required to mobilize the ultimate strength of the subgrade. Furthermore, observations of pavement failure modes (McLeod 1953; Hveem 1958) have confirmed the occurrence of failure mechanisms involving all the pavement layers.

The assumption of a general shear failure type of mechanism involving all pavement layers as adopted by McLeod (1953) is more realistic for pavements. However, the method of solution proposed by McLeod is tedious and difficult to extend to more complicated situations. The upper bound solution proposed by Purushothamaraj et al. (1974) based on a general shear failure mechanism is complex, rendering the incorporation of pore-water pressures and matric suction difficult. A solution that can accurately predict bearing capacity in a two-layer soil and still retain sufficient simplicity to allow for the incorporation of matric suction and positive pore-water pressures is required.

The limit equilibrium method has been used extensively in geotechnical engineering to provide solutions to bearing capacity, lateral earth pressure and slope stability problems. The simple formulation of the limit equilibrium method can easily handle such complex factors as soil layering and pore-water pressures. Furthermore, the suitability of limit equilibrium methods in providing reasonable solutions for bearing capacity in homogeneous soils (Terzaghi 1943; Meyerhof 1951) and layered soils (Button 1953; Raymond 1967; Meyerhof 1974; Meyerhof

and Hanna 1978) has been demonstrated. Consequently, the limit equilibrium method was selected as the tool for the development of solutions for bearing capacity in layered soils and for the incorporation of the effect of matric suction on bearing capacity.

Idealization of the problem

A two-layer soil with varying cohesion, angle of internal friction and unit weight as shown in Fig. 3 was considered. The effect of surcharge was neglected in the analysis since wheel loads are usually applied to the surface of the pavement (i.e., there is no depth or overburden factor). The bearing capacity of the layered system was assumed to be given by the following equation:

$$[11] \quad q_f = c_1' N_c + \frac{1}{2} B \gamma_1 N_\gamma$$

where:

- q_f = bearing capacity of pavement system,
- c_1' = cohesion of top soil layer (i.e., base layer),
- B = width of foundation,
- γ_1 = unit weight of top soil layer (base),
- N_c = cohesion bearing capacity factor, and
- N_γ = surcharge bearing capacity factor.

The cohesion bearing capacity factor, N_c , and the surcharge bearing capacity factors, N_γ , in eq. [11] are a function of the shear strength and unit weights of both soil layers (i.e., base layer and subgrade).

The following assumptions were made in the development of the solution for bearing capacity of a two-layer soil:

- (1) The Terzaghi general shear failure mechanism is valid for layered soils.
- (2) The length of the footing is large in comparison to its width so that plane strain conditions apply.
- (3) The footings are smooth and no shear stresses are developed between the soils and the footing.
- (4) The soil in each layer is homogeneous and isotropic.
- (5) Shear stresses at the interface between the soil layers are neglected.
- (6) The shape of the log spiral is controlled by the shear strength parameters of both soils and the relative depth of the top soil layer.
- (7) The principle of superposition is applicable to the individual components of bearing capacity.

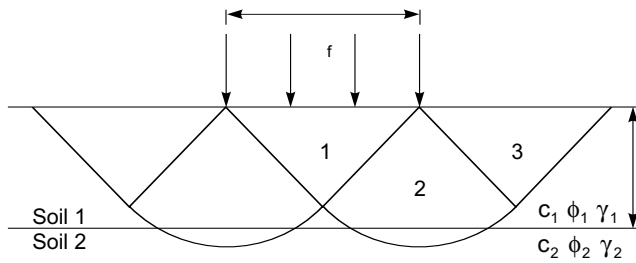
Assumptions No. 2 and 3 are not rigorously adhered to, but should be satisfactory for analytical purposes.

The bearing capacity of the soil was determined by considering the equilibrium of the passive and active soil wedges (Fig. 4) as proposed by Terzaghi (1943). Only the resultant forces for the two soils are shown in Fig. 4 for simplicity of presentation.

The passive pressure on the side of the passive wedge can be determined from lateral earth pressure theory as follows:

$$[12] \quad p_p = \gamma z K_p + 2c' \sqrt{K_p}$$

Fig. 3. General shear failure mechanism in a two-layer soil.



where:

- p_p = passive pressure at depth, z ,
- γ = unit weight of the soil,
- K_p = Passive pressure coefficient, which is equal to $[\tan^2(45^\circ + \phi'/2)]$,
- c' = effective cohesion of the soil, and
- ϕ' = effective friction angle of the soil.

The moment, M_c , due to cohesion along the log spiral is calculated from the length of the log spiral and the cohesion of the soil. The resultant force, P , can be calculated by taking moments about the center of the log spiral. The resultant normal force, F , at the base of the log spiral is inclined at an angle equal to the angle of internal friction of the soil and therefore acts through the center. Since the resultant normal force has no moment, its value need not be determined. To solve for the resultant force, P , assumptions have to be made with regard to the points of action of the weights and passive forces. Once the resultant force, P , has been determined, the bearing capacity of the footing can be calculated by considering the equilibrium of the active wedge in Fig. 4b.

A complete derivation for the bearing capacity of a two-layer soil based on the above procedure is given by Oloo (1994). Separate determinations were made for the components of bearing capacity due to cohesion and self weight. Superposition was assumed to be applicable to layered soils so that the total bearing capacity could be determined by the summation of the cohesion and self weight components of bearing capacity.

Results for the bearing capacity factor N_c

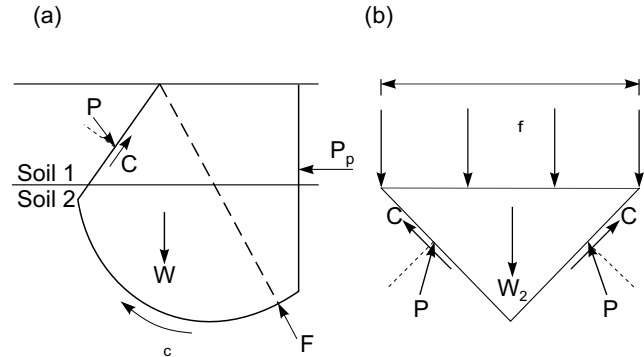
The bearing capacity factor, N_c , for the two-layer system was determined by considering the equilibrium of a weightless soils with cohesion and friction. The component containing the factor N_γ is eliminated from eq. [11] since the soil is assumed to have no weight.

The proposed solution gave values for the bearing capacity factor, N_c , which were equal to the Prandtl (1921) solutions for homogeneous soils. For a two-layered soil system, the proposed solution was found to give results consistent with the physical boundaries of the problem.

Typical results for a strong soil overlying a weak soil layer are given in Fig. 5. As the depth of the top layer, H_1 , increases, the bearing capacity factor approaches the value of a homogeneous top layer. The bearing capacity

Fig. 4. Equilibrium of the soil wedges for the general case.

- a) Equilibrium of radial shear zone and passive wedge;
- b) equilibrium of active wedge.



factor approaches the value of a homogeneous bottom layer as the depth of the top layer, H_1 , is decreased. The transition between the two extreme values of N_c is smooth.

Result for the bearing capacity factor, N_γ

There are no known suitable solutions in the literature for the bearing capacity factor, N_γ , in layered soils against which the proposed solution can be compared. Although the upper bound solution of Purushothamaraj et al. (1974) provides a solution for this class of problem, the complexity of the equations precludes the possibility of making a comparison.

The effect of changing the depth of the top soil layer, H_1 , is illustrated in Fig. 6 for a stronger soil overlying a weaker one. The bearing capacity factor approaches the value for the top soil layer as the depth increases. As the depth of the top soil layer approaches zero, the bearing capacity factor approaches the value for the bottom soil layer.

Overall bearing capacity

Independent derivations have been made for the components of bearing capacity due to cohesion and due to self weight. Assuming the principle of superposition to be valid, the overall bearing capacity of a surface footing on a two-layer soil system is given by eq. [11]. The variation of the overall bearing capacity for a two-layer soil with the depth of the top soil layer, H_1 , is shown in Fig. 7. The bearing capacity varies between a minimum value for zero depth of the top soil layer to a maximum corresponding to the bearing capacity of the top soil layer. In general the proposed method appears to give reasonable estimates of bearing capacity.

Effect of matric suction on bearing capacity

When a soil is subjected to a negative pore-water pressure beyond its air entry value, air enters the pores and

Fig. 5. Bearing capacity factor, N_c , versus ratio of depth of top layer, H_1 , to foundation width, B , where the top layer is stronger than the bottom layer.

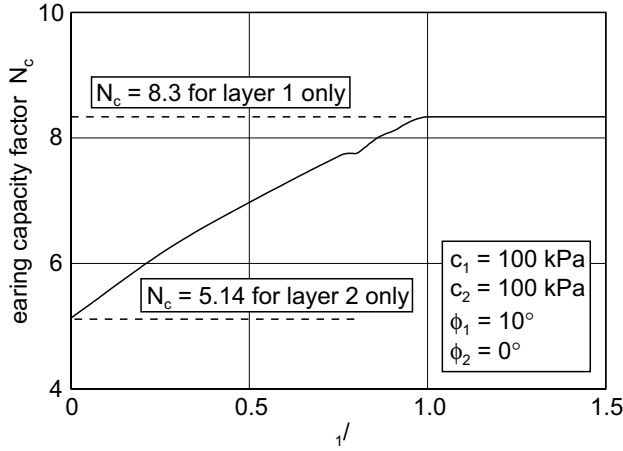
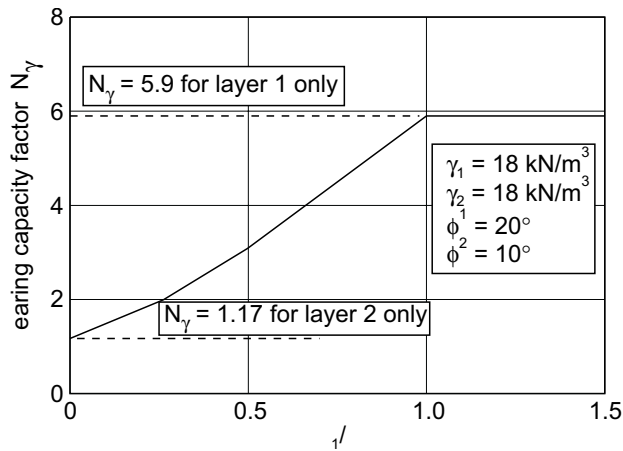


Fig. 6. Bearing capacity factor, N_γ , versus ratio of depth of top soil layer, H_1 , to foundation width, B , where the top layer is stronger than the bottom layer.



the soil becomes unsaturated. The equilibrium of the unsaturated soil structure must then be assessed in terms of two independent state stress variables. The stress state variables, $(\sigma - u_a)$ and $(u_a - u_w)$, appear to be the most satisfactory for use in engineering practice (Fredlund 1979; Fredlund and Rahardjo 1987). The term $(\sigma - u_a)$ is referred to as the net normal stress while $(u_a - u_w)$ is the matric suction. Both the net normal stress and the matric suction will determine the equilibrium of the soil wedges shown in Fig. 4. Since matric suction does not have a gravitational component, the influence of matric suction on the stability of the soil under the footing will arise from its contribution to the shear strength of the soil.

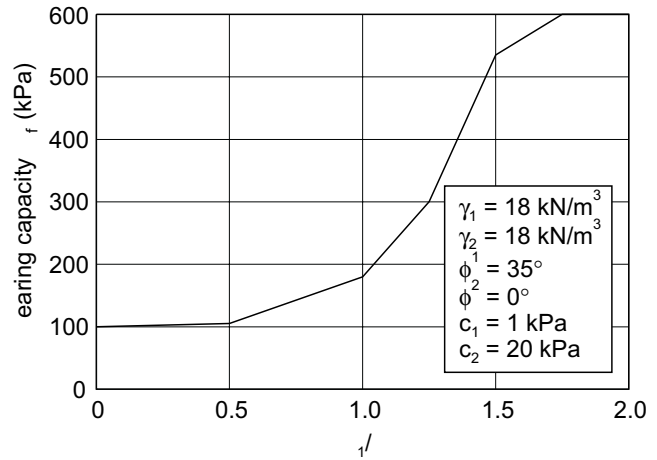
The shear strength of an unsaturated soil can be expressed as follows (Fredlund et al. 1978):

$$[13] \quad \tau = c' + (\sigma - u_a) \tan \phi' + (u_a - u_w) \tan \phi^b$$

where:

- ϕ' = effective friction angle of the soil,
- c' = effective cohesion, and

Fig. 7. Overall bearing capacity of a 2-layer soil versus the ratio of depth of top soil layer, H_1 , to foundation width.



ϕ^b = friction angle associated with the matric suction of the soil.

The effect of matric suction is to pull soil particles together. The contribution of matric suction to shear strength is due to the forces between the soil grains arising from this pull. Matric suction can be visualized as a contribution to the cohesion of the soil and the components of the equation for the shear strength of the unsaturated soil can be rearranged as follows:

$$[14] \quad \tau = [c' + (u_a - u_w) \tan \phi^b] + (\sigma - u_a) \tan \phi'$$

The behavior of ϕ^b is non-linear beyond the air entry value of the soil. The non-linear relationship between shear strength and matric suction can be approximated by a bi-linear envelope (Gan et al. 1988) as shown in Fig. 8.

The equation for shear strength of an unsaturated soil at zero net normal stress, based on a bi-linear envelope, is then given by:

$$[15] \quad \tau = c' + (u_a - u_w)_b \tan \phi' + [(u_a - u_w) - (u_a - u_w)_b] \tan \phi^b$$

where:

$$\phi^b = \phi' \text{ if } (u_a - u_w) \leq (u_a - u_w)_b,$$

and

$$(u_a - u_w)_b = \text{air entry value.}$$

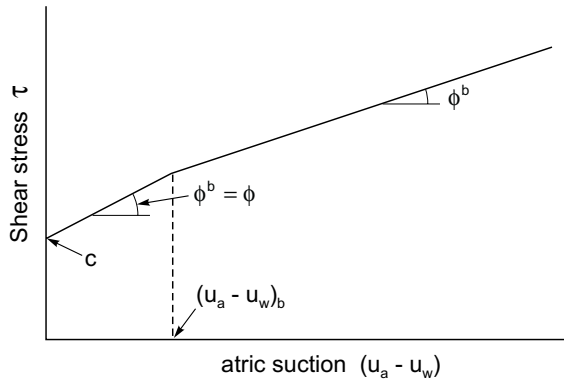
The entire shear strength, τ , at zero net normal stress given by eq. [15] is considered the total cohesion of the unsaturated soil.

If the net normal stress, $(\sigma - u_a)$, is greater than zero, the general equation for shear strength for an unsaturated soil based on a bi-linear envelope becomes:

$$[16] \quad \tau = \{c' + (u_a - u_w)_b \tan \phi' + [(u_a - u_w) - (u_a - u_w)_b] \tan \phi^b\} + (\sigma - u_a) \tan \phi'$$

The contribution of matric suction to bearing capacity can be determined using the limit equilibrium approach outlined for two-layer soils by considering the contribu-

Fig. 8. Bi-linear failure envelope for an unsaturated soil at zero net normal stress.



tion of matric suction to the passive force and to the shear resistance along the length of the log spiral.

The influence of matric suction on passive pressure is the same as that of cohesion. The bearing capacity factor associated with matric suction is also the same as that associated with cohesion. The total cohesion for the unsaturated soil is given by eq. [15]. If the matric suction is uniform for the soil layer, the expression for bearing capacity is given by:

$$[17] \quad q_f = \{c' + (u_a - u_w)_b \tan \phi'\} + [(u_a - u_w) - (u_a - u_w)_b] \tan \phi^b N_c + \frac{1}{2} B \gamma N_\gamma$$

Equation [17] further simplifies, if the air entry value of the soil approaches zero, as follows:

$$[18] \quad q_f = [c' + (u_a - u_w) \tan \phi^b] N_c + \frac{1}{2} B \gamma N_\gamma$$

Ultimate wheel loads

The ultimate wheel load a two-layer pavement system can sustain is determined by combining the solutions derived for bearing capacity in two-layer soils with the solution for the effect of matric suction on bearing capacity. The solution developed for the effect of matric suction on bearing capacity was restricted to a homogeneous soil. The influence of a non-uniform matric suction profile on the bearing capacity of layered soils is complicated and would require major modifications to the existing solutions. Difficulties associated with this limitation can be circumvented by approximating the matric suction profile in each layer with a constant value. The bearing capacity factor with respect to a constant matric suction is equivalent to that of cohesion, and the component of shear strength due to matric suction can be incorporated into the cohesion of the soil. Under these conditions, the form of the bearing capacity equation is retained for the layered soil.

The cohesion of the two soils is calculated using the following equations, and assuming the air-entry value for both soils approaches zero:

$$[19] \quad c_1 = c_1' + (u_a - u_w)_1 \tan \phi_1^b$$

$$[20] \quad c_2 = c_2' + (u_a - u_w)_2 \tan \phi_2^b$$

where:

- c_1 = total cohesion of the base,
- c_2 = total cohesion of the subgrade,
- c_1' = effective cohesion of the base,
- c_2' = effective cohesion of the subgrade,
- $(u_a - u_w)_1$ = matric suction in the base layer,
- $(u_a - u_w)_2$ = matric suction in the subgrade,
- $\tan \phi_1^b$ = friction angle associated with matric suction (base), and
- $\tan \phi_2^b$ = friction angle associated with matric suction (subgrade).

The ultimate bearing capacity of a typical unpaved pavement section consisting of a base layer over a subgrade can be calculated from the following modification of eq. [11]:

$$[21] \quad q_f = c_1 N_c + \frac{1}{2} B_e \gamma_1 N_\gamma$$

The bearing capacity factors, N_c and N_γ , are dependent upon the dimensions of the loaded area, the depth of the base layer, the unit weights and the shear strength parameters of both layers (i.e., shear strength parameters, c_1' , c_2' , ϕ_1' , ϕ_2' , ϕ_1^b and ϕ_2^b , where ϕ_1' and ϕ_2' are the effective angles of internal friction of the base and the subgrade, respectively). The determination of the bearing capacity factors and of the equivalent contact width, B_e , have been discussed.

The derivation of eq. [21] was based on the assumption of plane strain. Since the tire contact area is assumed to be rectangular, corrections have to be applied to account for the differences in shape. It is recommended that the shape factors proposed by De Beer (1970) be used.

The bearing capacity, q_f , is adjusted by changing the depth of the base layer, H_1 , until a value for q_f equal to the equivalent contact pressure given by eq. [6] is obtained. The depth of the base layer corresponding to this conditions is equivalent to the required base depth for the given loading condition.

Determination of design wheel loads

The ultimate wheel load determined from eq. [21] represents the failure condition. Wheel loads corresponding to the ultimate bearing capacity of the pavement would cause excessive deformation. It is necessary to apply a load factor to the ultimate bearing capacity to limit pavement deformations to acceptable levels.

The choice of a suitable load factor value to be applied to the ultimate wheel load presents major difficulties. Existing pavement design methods based on bearing capacity theory adopt a variety of recommendations for the factor of safety or load factor (Table 1).

Broms (1963) recommended the use of an overall factor of safety depending on the traffic volume while other authors recommended the use of partial factors of safety applied to the shear strength of the subgrade. Partial factors of safety applied to the shear strength account for un-

certainties in the method of analysis and in the determination of the shear strength parameters. The partial factors of safety can be increased sufficiently to limit deformations as well.

The response of a pavement to applied wheel loads depends on the relative stiffness of the pavement system. The stiffness of the pavement depends on the shear strength properties and deformation moduli of its components, as well as on the depth of the base layer. The value of the load factor to limit settlements will depend on pavement stiffness and the level of acceptable deformations of the pavement dictated by its design standard.

A tentative load factor of 2.5 based on consideration of the upper limit of deformations from finite element analysis of typical pavement sections is proposed.

Consideration of traffic volume

The procedure outlined for the determination of the pavement bearing capacity is based on static loading. Pavements are, however, subjected to wheel loads that are both transient and repetitive. A method of incorporating the effects of repetitive and transient loading in the design process is required.

A theoretical analysis of the effects of repeated loading on pavements is beyond the current state of knowledge. Most pavement design methods resort to empirically derived relationships to take repeated loading into consideration. The same approach is adopted for the design of unpaved roads, using the following relationship:

$$[22] \quad \left(\frac{N_S}{N} \right) = \left(\frac{P}{P_S} \right)^4$$

where:

N_S = number of repetitions of an axle load, P_S ,
and
 N = number of repetitions of the axle load, P .

An equation similar to eq. [22] was used by Giroud and Noiray (1981) for the design of unpaved roads. Equation [22] can be used to calculate the static axle load from a known number of repetitions of a transient axle load. Recognizing that the static load corresponds to a single pass, eq. [22] can be rearranged to give the equivalent static axle load as:

$$[23] \quad P_S = \frac{P}{\left(\frac{1}{N} \right)^{0.25}}$$

where:

P_S = equivalent static axle load,
 P = design axle load, and
 N = number of repetitions of axle load P .

Equation [23] implies an equivalent static axle load that is usually larger than the transient axle load. Design based on the equivalent static axle load results in a pavement whose thickness is proportional to the number of

Table 1. Recommendations for factors of safety used in the design of unpaved roads.

Source	Load factor	Remarks
Broms (1963)	2	Low traffic volume
Broms (1963)	3	High traffic volume
Bender and Barenburg (1978)	1.6	On shear strength of subgrade
Sellmeijer et al. (1982)	1.5	On shear strength of subgrade
Giroud and Noiray (1981)	1.6	On shear strength of subgrade

axle load repetitions. The tire pressure is assumed to remain constant.

Typical design results

The proposed method of analysis and design was applied to a pavement section consisting of materials whose properties are given in Table 2. The results are presented in this section to illustrate typical variations in design pavement thickness as a function of the axle load, tire inflation pressure, load factor and number of load applications.

The variation of design pavement thickness with tire pressure for different static axle loads is shown in Fig. 9. A load factor of one was used and the matric suction was assumed to be zero in both layers. The required thickness of the base layer was obtained by using eq. [21] to determine bearing capacity for the known material properties. The bearing capacity of the pavement was obtained by varying the depth of the base layer until the calculated bearing capacity became equal to the equivalent contact pressure given by eq. [6]. Single axle loading with single tires was assumed.

The required thickness of the base increases as the tire pressure and axle load increase. For each axle load, there is an upper limit of the tire inflation pressure that the pavement can sustain. This limit corresponds to the maximum bearing capacity of the pavement system where the failure mechanism is fully contained in the base layer. Most existing design methods for unpaved roads fail to recognize the existence of this limit (Broms 1963, 1964; Bender and Barenburg 1978; Giroud and Noiray 1981).

The contribution of matric suction to the bearing capacity of the pavement was investigated by assuming constant matric suction values in each of the pavement layers. The cohesion in each layer was increased by an amount equal to the product of $(\tan \phi^b)$ and the matric suction. The values of $(\tan \phi^b)$ given in Table 2 were deliberately chosen on the lower side to demonstrate the significant contribution of matric suction to bearing capacity.

The effect of increasing matric suction in the subgrade layer is illustrated in Fig. 10 for a static axle load of 150 kN. The thickness of the base layer required to support a given tire pressure decreases as the matric suction

Table 2. Material properties for the base and subgrade layers used for analysis.

Soil Property	Subgrade layer	Base layer
Cohesion (kPa)	1.0	1.0
Friction angle, ϕ'	20.0	40.0
Unit weight, γ (kN/m ³)	20.0	20.0
$\tan \phi^b$	0.15 ($\phi^b = 8.5^\circ$)	0.10 ($\phi^b = 5.7^\circ$)

Fig. 9. Required thickness of the base layer versus tire pressure and axle load.

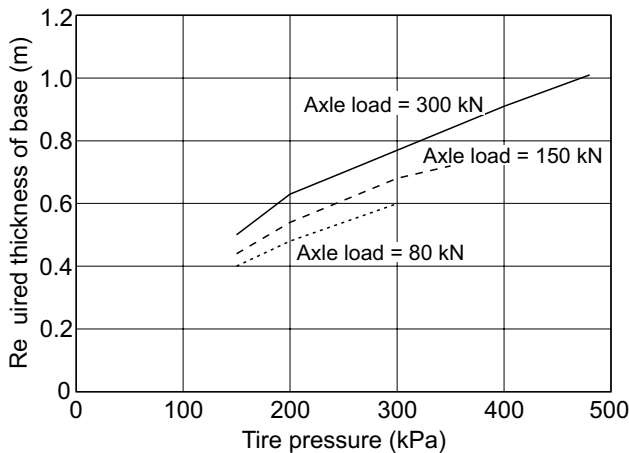
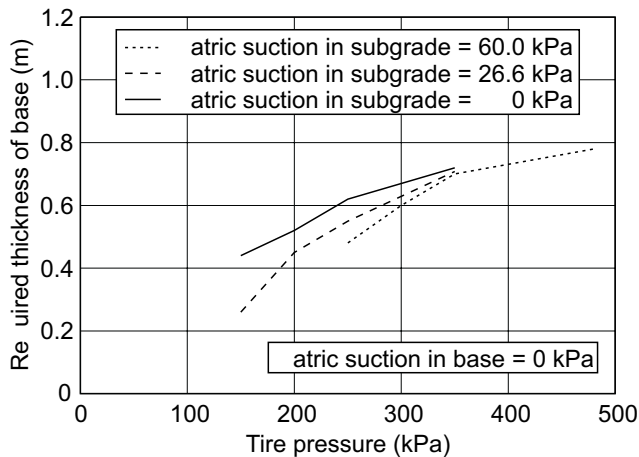


Fig. 10. Required thickness of the base layer versus the tire pressure for different levels of matric suction in the subgrade, for a static axle load of 150 kN.



increases. The decrease in thickness is particularly significant at low tire pressures.

Factors of safety have not been applied to the results reported in Figs. 9 and 10. The effect of applying a load factor is to increase the required base layer thickness. This effect is shown in Fig. 11 for an axle load of 300 kN. The value of the load factor depends, amongst other things, on the design standard of the road. Since the choice of the load factor has a significant effect on the design pavement thickness, every effort should be made to determine an appropriate value.

Fig. 11. Required thickness of the base layer versus tire pressure for different factors of safety, for a static axle load of 300 kN.

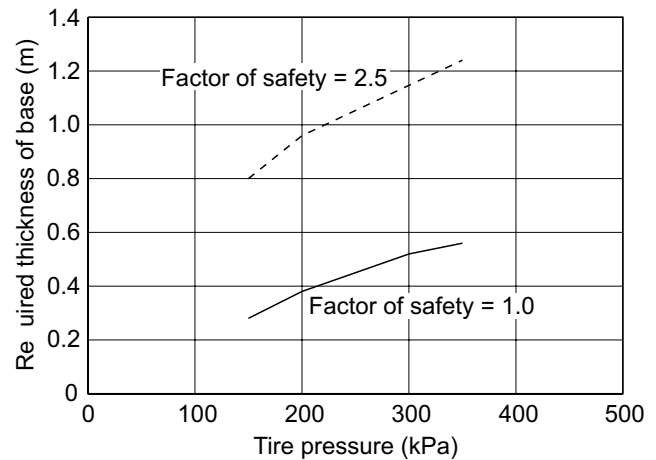
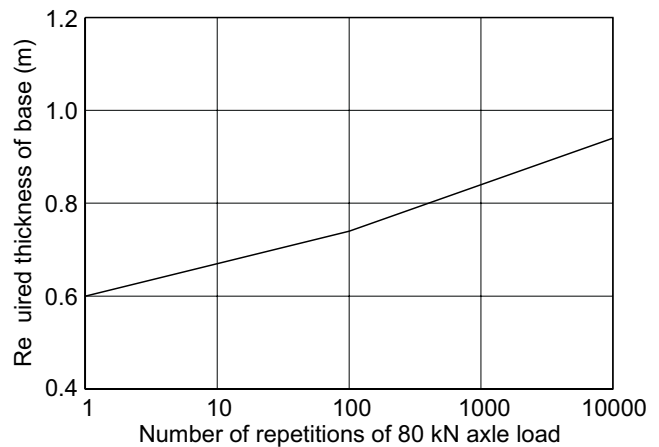


Fig. 12. Required thickness of the base layer versus the number of repetitions of the axle load, for a static axle load of 80 kN and a tire pressure of 300 kPa.



The effect of increasing the number of axle load repetitions is illustrated in Fig. 12 for an 80 kN axle load and a tire pressure of 300 kPa. The required depth of the base layer increases as the number of axle load repetitions increases. The increase is a reflection of the increase in the design static axle load as given by eq. [23].

Conclusions

A limit equilibrium method for bearing capacity in layered soils, incorporating the contribution of matric suction, has been presented for the design of unpaved roads. The following conclusions can be made from the preceding discussions on the design of unpaved roads using the solutions for the bearing capacity in two-layered soils.

The required thickness of the base layer depends on the shear strength and the unit weight of both the base layer and the subgrade of the unpaved road. An upper limit of traffic loading exists for a given set of base and subgrade properties. Beyond this upper limit of traffic loading, increases in the base layer thickness do not increase the bearing capacity of the given pavement system. Matric

suction can have a significant effect on the bearing capacity of pavement structures.

Acknowledgement

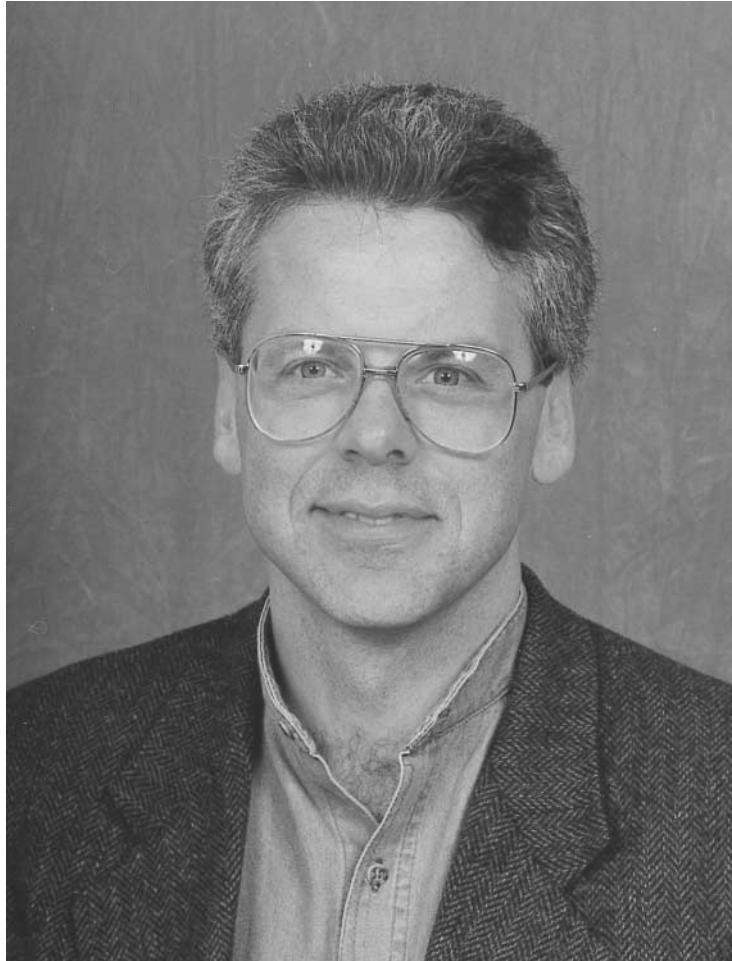
The author would like to extend his appreciation to the International Development Research Centre, Government of Canada, for their grant that made the research reported herein possible.

References

- Barbour, S.L., Fredlund, D.G., Gan, J.K.M., and Wilson, G.W. 1992. Prediction of moisture movements in highway subgrade soils. Proceedings, 45th Canadian Geotechnical Conference, Toronto, pp. 41A-1 – 41A-13.
- Bender, D.A., and Barenberg, E.J. 1978. Design and behavior of soil-fabric-aggregate systems. Transportation Research Record, 671, Transportation Research Board, Washington, pp. 64–75.
- Broms, B.B. 1963. The bearing capacity of pavements subjected to frost action. Highway Research Board, No. 39, pp. 66–180.
- Broms, B.B. 1964. The effect of degree of saturation on the bearing capacity of flexible pavements. Highway Research Record, No. 71, pp. 1–14.
- Button, S.L. 1953. The bearing capacity of footings on a 2-layer cohesive subsoil. Proceedings, 3rd International Conference on Soil Mechanics and Foundation Engineering, Vol. 1, pp. 332–335.
- Fredlund, D.G. 1979. Appropriate concepts and technology for unsaturated soils. Second Canadian Colloquium, Canadian Geotechnical Journal, **16**(1): 121–139.
- Fredlund, D.G. 1997. From theory to practice of unsaturated soil mechanics. Proceedings, NSAT '97, 3rd Brazilian Symposium on Unsaturated Soils, April 21–25, Rio de Janeiro, Brazil.
- Fredlund, D.G., and Rahardjo, H. 1987. Soil mechanics principles for highway engineering in arid regions. Transport Research Record, No. 1137, pp. 1–11.
- Fredlund, D.G., Morgenstern, N.R., and Wider, R.C.A. 1978. The shear strength of unsaturated soils. Canadian Geotechnical Journal, **15**(3): 316–321.
- Gan, J.K-M., Fredlund, D.G. 1988. Multistage direct shear testing of unsaturated soils. ASTM Geotechnical Testing Journal, **11**(2): 132–138.
- Gan, J.K-M., Fredlund, D.G., and Rahardjo, H. 1988. Determination of the shear strength parameters of an unsaturated soil using the direct shear test. Canadian Geotechnical Journal, **25**: 500–510.
- Giroud, J.P., and Noiray, L. 1981. Geotextile-reinforced unpaved road design. ASCE, Journal of Geotechnical Engineering Division, **107**(GT9), pp. 1233–1254.
- Ho, D.Y.F., and Fredlund, D.G. 1982. A multi-stage triaxial test for unsaturated soils. ASTM Geotechnical Testing Journal, **5**(1/2): 18–25.
- Hveem, F.N. 1958. Types and causes of failure in highway pavements. Highway Research Board Bulletin, **187**: 1–52.
- Joshi, B. 1993. A finite element model for the coupled flow of moisture and heat in soils. M.Sc. thesis, University of Saskatchewan, Saskatoon, SK, Canada.
- Lytton, R.L., Pufahl, D.E., Michalak, C.H., Liang, H.S., and Dempsey, B.J. 1990. An integrated model of the climatic effects on pavements. Final Report No. RF 7089. Texas Transportation Institute, Texas A&M University, TX.
- McLeod, N.W. 1954. The ultimate strength approach to flexible pavement design. Proceedings, The Association of Asphalt Paving Technologists, Vol. 23.
- McLeod, N.W. 1953. Some basic problems in flexible pavement design. Proceedings, Highway Research Board, No. 32, pp. 90–109.
- Meyerhof, G.G. 1951. The ultimate bearing capacity of foundations. *Géotechnique*, **2**: 301–332.
- Meyerhof, G.G. 1974. Ultimate bearing capacity of footings on sand layer overlying clay. Canadian Geotechnical Journal **11**(2): 223–229.
- Meyerhof, G.G. and Hanna, A.M. 1978. Ultimate bearing capacity of foundations on layered soils under inclined load. Canadian Geotechnical Journal, **15**: 565–572.
- Milligan, G.W.E., Jewell, R.A., Houlsby, G.T. and Burd, H.J. 1989. A new approach to the design of unpaved roads, Part 1. Ground Engineering, **22**(3): 25–29.
- Oloo, S.Y. 1994. A bearing capacity approach to the design of low-volume traffic roads. Ph.D. thesis, University of Saskatchewan, Saskatoon, SK, Canada.
- PCA 1984. Design thickness for concrete highway and street pavements. Portland Cement Association.
- Prandtl, L. 1921. Eindringungsfestigkeit und Festigkeit von Schneiden. *Zeitschrift Angewandte Mathematik und Mechanik*, **1**(4): 15–20.
- Purushothamaraj, P., Ramiah, B.K., and Venkatakrishna Rao, K.N. 1974. Bearing capacity of strip footings in two layered cohesive-friction soils. Canadian Geotechnical Journal, **11**(3): 32–45.
- Raymond, G.P. 1967. The bearing capacity of large footings and embankments on clays. *Géotechnique*, **17**:1–10.
- Russam, K. 1965. The prediction of subgrade moisture conditions for design purposes. *In* Moisture equilibria and moisture changes in soils beneath covered areas. Butterworth, Sydney, Australia, pp. 233–236.
- Sattler, P., Fredlund, D.G., Klassen, M.J., Jubien, W.B., and Rowan, W.G. 1989. Bearing capacity approach to railway design, using subgrade matric suction. Transportation Research Board, Transportation Research Record 1241, pp. 27–33.
- Sellmeijer, J.B., Kenter, C.J., and van den Berg, C. 1982. Calculations for fabric reinforced roads. Proceedings, 2nd International Conference on Geotextiles, Las Vegas, Industrial Fabric Association International, St. Paul, MIN., Vol. 2, pp. 393–398.
- Szafron, B.J. 1991. The influence of soil suction on bearing capacity failures of low volume roads. M.Sc. thesis, University of Saskatchewan, Saskatoon, Saskatchewan, SK, Canada.
- Terzaghi, K. 1943. Theoretical soil mechanics. John Wiley and Sons, New York.
- Wallace, K.B. 1977. Moisture transients at the pavement edge; analytical studies of the influence of materials and cross-section design. *Géotechnique*, **27**(4): 497–516.
- Wilson, G. W. 1990. Soil evaporative fluxes for geotechnical engineering. Ph.D. thesis, University of Saskatchewan, Saskatoon, Saskatchewan, SK, Canada.
- Wilson, G.W., Fredlund, D.G., Barbour, S.L. and Pufahl D.E. 1997. The use of ground surface flux boundary conditions in geotechnical engineering. Proceedings, 14th International Conference on Soil Mechanics and Foundation Engineering, Hamburg, Germany, Vol. 3, pp. 1861–1864.

Part V

Steady State and Transient Flow Through Unsaturated Soils



Dr. S. Lee Barbour
Department of Civil Engineering
University of Saskatchewan
Saskatoon, Saskatchewan, Canada

Introduction and Overview

The flow through saturated soils can be described by Darcy's flow law, which states that the discharge per unit area, q , is equal to the hydraulic conductivity (i.e., coefficient of permeability) multiplied by the hydraulic gradient. The hydraulic conductivity provides a measure of the ability of a soil to conduct water and consequently the value of hydraulic conductivity varies with effective pore size (represented by grain size), open area for flow (represented by void ratio), and the geometry of the flow path (represented by soil structure). For example, it would be expected that hydraulic conductivity would decrease if the grain-size was decreased, the soil was consolidated, or the soil was re-compacted wet of optimum versus dry of optimum. If there were no change in grain-size, void ratio, or soil structure, the hydraulic conductivity of a saturated soil can be considered to be a constant.

Darcy's law is equally as valid for unsaturated soils as it is for saturated soils; however, the hydraulic conductivity is not a constant but is a function of soil suction (or degree of saturation). The relationship between the degree of saturation and soil suction is described through the use of the soil-water characteristic curve. The capillary model illustrates how suction can be related to the effective radius of a fluid-filled pore. As suction is increased, the first pores to drain are the largest, followed by smaller and smaller pores. This conceptual model helps to explain why the relationship between hydraulic conductivity and suction is highly non-linear. As suction increases, the largest pores drain, decreasing the open area for flow (e.g., degree of saturation), decreasing the effective radius of fluid filled pores, and increasing the tortuosity or structure of the flow path.

The relationship between soil suction and the coefficient of permeability of an unsaturated soil is referred to as the permeability function. This function can be measured directly under either steady state or transient flow conditions. Steady state and unsteady state testing procedures have been successfully used to measure the coefficient of permeability of a soil under varying applied soil suctions and therefore varying degrees of saturation. Unsteady state testing procedures require the application of a transient flow analysis in the interpretation of the data. The steady state testing procedure is relatively easy to perform provided the applied suctions do not exceed one atmosphere of suction. Each specimen may require one or more weeks for testing at different applied suctions. Extending the apparatus beyond 100 kPa of suction requires the use of an axis-translation technique.

This permeability function can be also be predicted with sufficient accuracy for many engineering problems through a knowledge of the saturated coefficient of permeability and the soil-water characteristic curve. A variety of forms of the permeability function have been proposed. This allows engineers flexibility in estimating an appropriate permeability function based solely on a measured soil-water characteristic curve and a known value of the coefficient of permeability for a saturated soil. The type of permeability function to be used in a numerical solution for an unsaturated flow problem can be selected by the user.

The analysis of steady state flow in a saturated-unsaturated soil begins with writing Darcy's Law for the case where the Cartesian coordinates are the same as the direction of the major and minor coefficients of permeability:

$$[1] \quad v_x = k_x \frac{dh}{dx}; \quad v_y = k_y \frac{dh}{dy}$$

The subscripts x and y refer to the x - and y -Cartesian directions, v is the Darcy flux, k is the coefficient of permeability, h is hydraulic head, and $(u_a - u_w)$ represents the matric suction.

The partial differential flow equation for an unsaturated soil is formulated by satisfying conservation of mass for a representative elemental volume. The partial differential equation is non-linear because the flow law is non-linear. The pore-water pressure changes from point to point in the soil and these changes are reflected in the partial differential flow equation. Therefore, an unsaturated soil is similar to a heterogeneous soil with a constantly changing coefficient of permeability.

A modulus defining the amount of water stored in the soil is required when performing an unsteady state or transient seepage analysis on saturated-unsaturated soils. For a saturated soil, the water storage property is referred to as the coefficient of volume change, m_v (i.e., the relation-

ship between effective stress and volume change). For unsteady state seepage analysis in an unsaturated soil, it is the slope of the soil-water characteristic curve, m_s^w , that defines the relationship between a change in soil suction and a change in the volume of water stored in the soil. This relationship can be predicted with sufficient accuracy for many engineering problems through a knowledge of the saturated coefficient of volume change and the soil-water characteristic curve.

Numerical methods such as the finite element technique have become a necessary tool for solving saturated–unsaturated flow problems. Early attempts to solve saturated–unsaturated flow problems such as seepage through a dam were based on the erroneous assumption that flow only occurs through saturated soil. These solutions attempted to find a position for the phreatic surface, which also served as the uppermost flow line, with the result that these methods were numerically unstable. Current numerical methods analyze the entire soil cross-section to ground surface and use methods of repeated substitution to solve for the pore-water pressure and coefficient of permeability throughout the soil cross-section. There has been wide acceptance of saturated–unsaturated modeling in engineering practice since the 1980s and today there are several software packages available that provide great flexibility in solving seepage problems. D.G. Fredlund was also involved in providing such software to the geotechnical community through the company Geo-Slope International Ltd. Analyzing the entire soil cross-section to the ground surface also allows boundary conditions due to climate-soil interactions to be incorporated into the analyses.

Numerical analyses of seepage are the most common type of “flux” predictions made by geotechnical engineers. The two last papers in this section describe how similar techniques to those already described can also be used to predict the flow and transport of dissolved salts as a result of hydraulic and chemical gradients in both saturated and unsaturated soils.

Part V

Steady State and Transient Flow Through Unsaturated Soils

- Fredlund, D.G., Xing, A., and Huang, S.Y. 1994. Predicting the permeability function for unsaturated soils using the soil-water characteristic curve. *Canadian Geotechnical Journal*, **31**(4): 533–546 389
- Papagianakis, A.T., and Fredlund, D.G. 1984. A steady state model for flow in saturated-unsaturated soils. *Canadian Geotechnical Journal*, **21**(3): 419–430 399
- Lam, L., Fredlund, D.G., and Barbour, S.L. 1988. Transient seepage model for saturated-unsaturated systems: A geotechnical engineering approach. *Canadian Geotechnical Journal*, **24**(4): 565–580 411
- Lim, T.T., Rahardjo, H., Chang, M.F., and Fredlund, D.G. 1996. Effect of rainfall on matric suction in a residual soil slope. *Canadian Geotechnical Journal*, **33**(4): 618–628. . . . 426
- Fredlund, D.G., and Hasan, J. 1979. One-dimensional consolidation theory: unsaturated soils. *Canadian Geotechnical Journal*, **16**(2): 521–531. 436
- Fredlund, D.G., and Xing, A. 1997. The use of a rheological model for the visualization of unsaturated soils proceses. *Proceedings, 6th National Congress on Mechanics, Hanoi, Vietnam* 445
- Fredlund, D.G., and Rahardjo, H. 1985. Unsaturated soil consolidation theory and laboratory experimental data. *In Consolidation of Soils: Testing and Evaluation*, ASTM STP 892. 450
- Rahardjo, H., and Fredlund, D.G. 1996. Consolidation apparatus for testing unsaturated soil. *Geotechnical Testing Journal*, **19**(4): 341–353 457
- Rahardjo, H., and Fredlund, D.G. 1995. Experimental verification of the theory of consolidation for unsaturated soils. *Canadian Geotechnical Journal*, **32**(5): 749–766 468
- Barbour, S.L., and Fredlund, D.G. 1989. Mechanics of osmotic flow and volume change in clay soils. *Canadian Geotechnical Journal*, **26**: 551–562. 485
- Barbour, S.L., Lim, P.C. and Fredlund, D.G. 1996. A new technique for diffusion testing of unsaturated soils. *ASTM, Geotechnical Testing Journal*, **19**(3): 247–258 498

Predicting the permeability function for unsaturated soils using the soil–water characteristic curve

D.G. Fredlund, A. Xing, and S. Huang

Abstract: The coefficient of permeability for an unsaturated soil is primarily determined by the pore-size distribution of the soil and can be predicted from the soil–water characteristic curve. A general equation, which describes the soil–water characteristic curve over the entire suction range (i.e., from 0 to 10^6 kPa), was proposed by the first two authors in another paper. This equation is used to predict the coefficient of permeability for unsaturated soils. By using this equation, an evaluation of the residual water content is no longer required in the prediction of the coefficient of permeability. The proposed permeability function is an integration form of the suction versus water content relationship. The proposed equation has been best fit with example data from the literature where both the soil–water characteristic curve and the coefficient of permeability were measured. The fit between the data and the theory was excellent. It was found that the integration can be done from zero water content to the saturated water content. Therefore, it is possible to use the normalized water content (volumetric or gravimetric) or the degree of saturation data versus suction in the prediction of the permeability function.

Key words: coefficient of permeability, soil–water characteristic curve, unsaturated soil, water content, soil suction.

Introduction

There is no engineering soil property that can vary more widely than that of the coefficient of permeability. For saturated soils, the coefficient of permeability can vary more than 10 orders of magnitude when considering soils that range from a gravel to a clay. This wide range in coefficient of permeability has proven to be a major obstacle in analyzing seepage problems.

Soils that become desaturated are even more difficult to analyze. In this case it is possible for a single soil to have a coefficient of permeability that ranges over 10 orders of magnitude. Initial consideration of problems involving unsaturated soils might lead an engineer to conclude that no useful analyses are possible when the soil becomes unsaturated. However, experience has now shown that many important questions can be addressed using seepage analyses on unsaturated soils.

Generally an upper and lower bound can be established on the coefficient of permeability function for the soil. As a result, an upper and lower bound can also be established on other pertinent variables such as mass flows and pore-water pressures. Analyses have shown that the mass of water flowing through a soil is directly proportional to the coefficient of permeability. On the other hand, the

pore-water pressures and hydraulic heads are to a large extent independent of the absolute coefficient of permeability values. This observation is particularly of value as analyses are extended into the unsaturated soil zone.

For many geotechnical problems involving unsaturated soils, a knowledge of the pore-water pressures or hydraulic heads is of primary interest. These values are relatively insensitive to the saturated coefficient of permeability and the permeability function. This becomes particularly valuable when one considers the difficulties of the work involved in measuring the unsaturated coefficients of permeability for a soil.

The coefficient of permeability has been shown to be a relatively unique function of the water content of a soil during the desorption process and a subsequent sorption process. The function appears to be unique as long as the volume change of the soil structure is negligible or reversible. However, to use this procedure in a seepage analysis, it is necessary to know the relationship between water content and matric suction. This relationship is highly hysteretic with respect to the desorption and sorption processes (Fig. 1). As a result, it appears to be more reasonable to go directly to a permeability function related to matric suction.

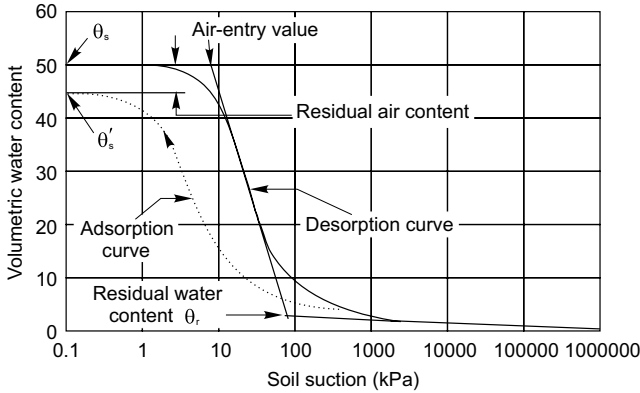
There is one permeability function for the desorption process and another function for the sorption process in an unsaturated soil. Both functions have a similar characteristic shape and as such can be fitted with a similar form of mathematical equation. Most engineering problems usually involve either a desorption process or a sorption process. Even in many cases where both desorption and sorption processes are involved, a single equation is appropriate for engineering purposes.

D.G. Fredlund. Professor, Department of Civil Engineering, University of Saskatchewan, 57 Campus Drive, Saskatoon, SK, Canada S7N 5A9.

A. Xing and S. Huang. Research Associates, Department of Civil Engineering, University of Saskatchewan, 57 Campus Drive, Saskatoon, SK, Canada S7N 5A9.

Reproduced with permission from the *Canadian Geotechnical Journal*, 31: 533–546, 1994.

Fig. 1. Typical desorption and adsorption curves for a silty soil. θ_s , saturated volumetric water content (desorption); θ'_s , saturated volumetric water content (adsorption).



Numerous attempts have been made to predict empirically the permeability function for an unsaturated soil. These procedures make use of the saturated coefficient of permeability and the soil–water characteristic curve for the soil. As more precise equations have been developed for the soil–water characteristic curve, likewise, more reliable predictions have been made for the coefficient of permeability function.

This paper reviews the background of the empirical prediction of the coefficient of permeability function. Using the present knowledge of a mathematical relationship for the soil–water characteristic curve, a new permeability function is predicted. The theoretical basis for the permeability function is shown. The function is based on the entire soil–water characteristic curve (i.e., from saturation down to a water content of zero or a suction of 10^6 kPa) and assumes that the ease of water flow through the soil is a function of the amount of water in the soil matrix.

Definitions

The coefficient of permeability k of an unsaturated soil is not a constant. The coefficient of permeability depends on the volumetric water content θ , which, in turn, depends upon the soil suction, ψ . The soil suction may be either the matric suction of the soil, (i.e., $u_a - u_w$, where u_a is pore-air pressure, and u_w is pore-water pressure), or the total suction (i.e., matric plus osmotic suctions). Soil suction is one of the two stress state variables that control the behaviour of unsaturated soils. Therefore, it is suggested that the term “permeability function for unsaturated soils” be used to represent the relationship between the coefficient of permeability and soil suction. When the coefficient of permeability at any soil suction, $k(\psi)$, is referenced to the saturated coefficient of permeability k_s , the relative coefficient of permeability, $k_r(\psi)$, can be written as follows:

$$[1] \quad k_r(\psi) = \frac{k(\psi)}{k_s}$$

The relative coefficient of permeability as a function of volumetric water content, $k_r(\theta)$, can be defined similarly. The relative coefficient of permeability, ($k_r(\psi)$ or $k_r(\theta)$), is a scalar function. The volumetric water content, θ , can be used in its normalized form, which is also referred to as the relative degree of saturation:

$$[2] \quad \Theta = \frac{\theta - \theta_r}{\theta_s - \theta_r}$$

where:

Θ = the normalized volumetric water content or relative degree of saturation,

θ_s = the saturated volumetric water content, and

θ_r = the residual volumetric water content.

Degree of saturation, S , which indicates the percentage of the voids filled with water, is often used in place of the normalized water content, Θ .

Literature review

There are two approaches to obtain the permeability function of an unsaturated soil: (i) empirical equations, and (ii) statistical models. Several measured permeability data are required to use an empirical equation. A statistical model can be used to predict the permeability function when the saturated coefficient of permeability, k_s , and the soil–water characteristic curve are available.

Empirical equations

Several empirical equations for the permeability function of unsaturated soils are listed in Tables 1 and 2. These equations can be used in engineering practice when measured data are available for the relationship between the coefficient of permeability and suction, $k(\psi)$, or for the relationship between the coefficient of permeability and the water content, $k(\theta)$. The smallest number of measured points required to use one of the permeability equations in Tables 1 and 2 is equal to the number of fitting parameters in the adopted equation. When the number of measurements exceeds the number of the fitting parameters, a curve-fitting procedure can be applied to determine the fitting parameters. This approach allows a closed-form analytical solution for unsaturated flow problems.

Statistical models

Statistical models have also been used to determine the permeability function for an unsaturated soil using the characteristics of the soil–water characteristic curve. This approach is based on the fact that both the permeability function and the soil–water characteristic curve are primarily determined by the pore-size distribution of the soil under consideration. Figure 2 shows a typical soil–water characteristic curve for a sandy loam and its permeability function. Based on the pore-size distribution, Burdine (1953) proposed the following equation for the relative coefficient of permeability:

Table 1. Empirical equations for the unsaturated coefficient of permeability $k(\theta)$.

Function	Reference
$k_r = \Theta^n$, where $\Theta = (\theta - \theta_r) / (\theta_s - \theta_r)$, and $n = 3.5$	Averjanov (1950)
$k = k_s (\theta / \theta_s)^n$	Campbell (1973)
$k = k_s \exp[\alpha(\theta - \theta_s)]$	Davidson et al. (1969)

Table 2. Empirical equations for the unsaturated coefficient of permeability $k(\psi)$.

Function	Reference
$k = k_s$, for $\psi \leq \psi_{aev}$	Brooks and Corey (1964)
$k_r = (\psi / \psi_{aev})^{-n}$ for $\psi \geq \psi_{aev}$	
$k_r = \exp(-\alpha\psi)$	Gardner (1958)
$k = k_s / (\alpha\psi^n + 1)$	
$k = a\psi + b$	Richards (1931)
$k = k$ for $\psi \leq \psi$	Rijtema (1965)
$k_r = \exp[-\alpha(\psi - \psi_{aev})]$ for $\psi_{aev} \leq \psi \leq \psi_1$	
$k = k_1 (\psi / \psi_1)^{-n}$ for $\psi > \psi_1$	
$k = \alpha\psi^{-n}$	Wind (1955)

Notes: ψ_1 is the residual soil suction (i.e., ψ_r), and k_1 is the coefficient of permeability at $\psi = \psi_1$.

$$[3] \quad k_r(\theta) = \frac{k(\theta)}{k_s} = \Theta^q \frac{\int_{\theta_r}^{\theta} \frac{d\theta}{\psi^2(\theta)}}{\int_{\theta_r}^{\theta_s} \frac{d\theta}{\psi^2(\theta)}}$$

where:

$$q = 2.$$

The square of the normalized water content was used to account for tortuosity. This model is significantly more accurate than the same equation without the correction factor, θ^q .

Childs and Collis-George (1950) proposed a model for predicting the coefficient of permeability based on the random variation of pore size. This model was improved by Marshall (1958) and further modified by Kunze et al. (1968). The calculations are performed by dividing the relation between volumetric water content and suction into n equal water-content increments (Fig. 3). The following permeability function has been slightly modified to use SI units and matric suction instead of pore-water pressure head:

$$[4] \quad k(\theta_i) = \frac{k_s}{k_{sc}} \frac{T_s^2 \rho_w g}{2\mu_w} \frac{\theta_s^p}{n^2} \sum_{j=1}^m [(2j+1-2i)\psi_j^{-2}];$$

$$i = 1, 2, \dots, m$$

where:

Fig. 2. Typical soil-water characteristic curve and permeability function for a silty soil.

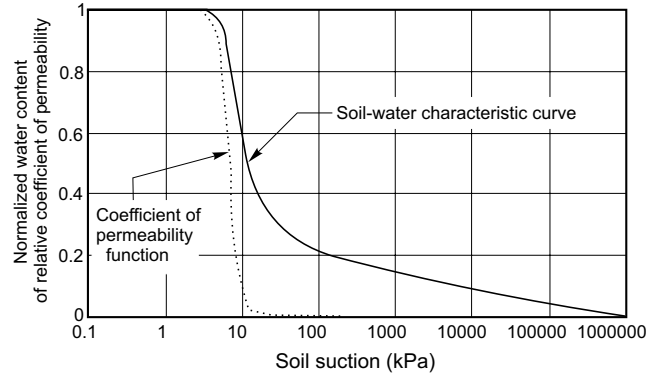
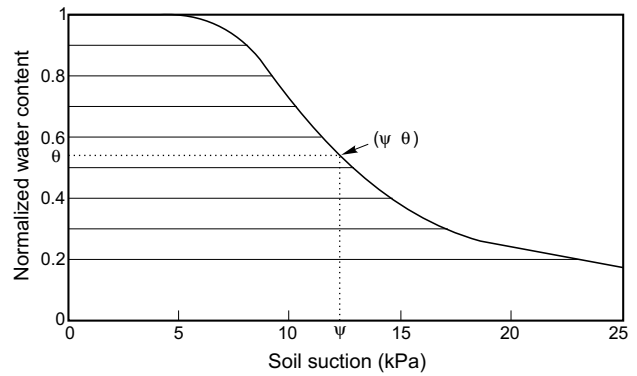


Fig. 3. Typical soil-water characteristic curve for predicting the permeability function. θ_j , midpoint of the j -th water content interval; ψ_j , suction corresponding to θ_j .



$k(\theta_i)$ = calculated coefficient of permeability for a specified volumetric water content θ_i , corresponding to the i -th interval,

i = interval number that increases with decreasing water content (for example, $i = 1$ identifies the first interval that closely corresponds to the saturated water content θ_s , and $i = m$ identifies the last interval corresponding to the lowest water content θ_L , on the experimental soil-water characteristic curve),

j = counter from i to m ,

k_{sc} = calculated saturated coefficient of permeability,

T_s = surface tension of water,

ρ_w = water density,

g = the gravitational acceleration,

μ_w = the absolute viscosity of water,

p = a constant that accounts for the interaction of pores of various sizes,

m = the total number of intervals between the saturated volumetric water content θ_s and the lowest water content θ_L on the experimental soil-water characteristic curve,

n = the total number of intervals computed between the saturated volumetric water content θ_s and zero volumetric water content (i.e.,

$\theta = 0$) (Note: $n = m [\theta_s / (\theta_s - \theta_L)]$, $m \leq n$ and $m = n$, when $\theta_L = 0$), and,
 ψ_j = the suction (kPa) corresponding to the midpoint of the j -th interval (Fig. 3).

The calculation of the coefficient of permeability, $k(\theta_i)$, at a specific volumetric water content, θ_i , involves the summation of the suction values that correspond to the water contents at and below θ_i . The matching factor, (k_s / k_{sc}), based on the saturated coefficient of permeability, is necessary to provide a more accurate fit for the unsaturated coefficient of permeability. The shape of the permeability function is determined by the terms inside the summation-sign portion of the equation which, in turn, are obtained from the soil-water characteristic curve.

Mualem (1976a) analyzed a conceptual model of a porous medium similar to that of the Childs and Collis-George (1950) model and derived the following equation for predicting the coefficient of permeability:

$$[5] \quad k_r(\theta) = \Theta^q \left[\frac{\int_{\theta_r}^{\theta} \frac{d\theta}{\psi(\theta)}}{\int_{\theta_r}^{\theta_s} \frac{d\theta}{\psi(\theta)}} \right]^2$$

where:

$$q = 0.5.$$

The value of q depends on the specific soil-fluid properties, and thus may vary considerably for different soils. Based on the permeability data of 45 soils, Mualem (1976a) found that the optimal value of q was 0.5.

When using a statistical model, soil suction has to be expressed as a function of volumetric water content. The integrations are performed along the volumetric water content axis and the permeability is expressed as a function of volumetric water content. Van Genuchten (1980) proposed an equation for the soil-water characteristic curve. By substituting his equation into the statistical models proposed by Burdine (1953) and Mualem (1976a) (i.e., eqs. [3] and [5]), van Genuchten (1980) derived closed-form expressions for the permeability function.

Theory and computational formula

Both eqs. [3] and [5] contain a correction factor, Θ^q , which depends upon the properties of the soil under consideration. This paper uses eq. [4] for the prediction of the coefficient of permeability of unsaturated soils, since it was proven to give satisfactory predictions. It is assumed, throughout this paper, that the volume change of the soil structure is negligible. Equation [4] can be expressed in the form of an integration as follows:

$$[6] \quad k(\theta) = \frac{k_s}{k_{sc}} \frac{T_s^2 \rho_w g \theta_s^p}{\mu_w} \int_{\theta_L}^{\theta} \frac{\theta - x}{\Psi^2(x)} dx$$

where:

ψ = soil suction which is given as a function of volumetric water content θ , and
 x = dummy variable of integration representing water content.

Equation [4] can also be expressed in the form of a relative coefficient of permeability, $k_r(\theta_i)$, as follows:

$$[7] \quad k_r(\theta_i) = \sum_{j=1}^m \frac{2(j-i) + 1}{\Psi_j^2} \bigg/ \sum_{j=1}^m \frac{2j-1}{\Psi_j^2}$$

The integration form of eq. [7] is as follows:

$$[8] \quad k_r(\theta) = \int_{\theta_L}^{\theta} \frac{\theta - x}{\Psi^2(x)} dx \bigg/ \int_{\theta_L}^{\theta_s} \frac{\theta_s - x}{\Psi^2(x)} dx$$

The residual volumetric water content, θ_r , is the water content below which a large increase in suction is required to remove additional water. The residual water content can generally be observed as a break in the soil-water characteristic curve. It is commonly assumed that the coefficient of permeability of a soil is essentially zero when its water content is below the residual water content. Kunze et al. (1968) investigated the effect of using a partial soil-water characteristic curve for the prediction of coefficient of permeability. It was concluded that the accuracy of the prediction is significantly improved when the complete soil-water characteristic curve is used namely when the condition,

$$[9] \quad \theta = \theta_r, \quad k_r = 0$$

is realistically prescribed. The integration in eq. [8], therefore, should be carried out in the interval θ_r to θ_s instead of the interval θ_L to θ_s :

$$[10] \quad k_r(\theta) = \int_{\theta_r}^{\theta} \frac{\theta - x}{\Psi^2(x)} dx \bigg/ \int_{\theta_r}^{\theta_s} \frac{\theta_s - x}{\Psi^2(x)} dx$$

Although all models for the relative coefficient of permeability k_r (i.e., eqs. [3], [5], and [10]) require a knowledge of the residual water content, soil-water characteristic curves are rarely measured over their entire range of water content. Brooks and Corey (1964), Mualem (1976a, b), and van Genuchten (1980) suggest different methods for the extrapolation of the measured soil-water characteristic data and the determination of the residual water content. The conventional procedure for the prediction of the coefficient of permeability using eq. [10] consists of two steps. First, the residual water content of the soil under consideration is estimated from the experimental data. Then, the measured soil-water characteristic data are fitted by a mathematical equation in the interval θ_r to θ_s , and the integrations are evaluated using the best-fit curve. A generally accepted procedure for determining the residual water content does not appear to exist. It would be an asset to predict the coefficient of permeability without having to estimate the residual water content.

The total suction corresponding to zero water content is essentially the same for all types of soils. This value is

about 10⁶ kPa and has been supported experimentally by results of tests on a variety of soils (Croney and Coleman 1961) and by thermodynamic considerations (Richards 1965). A general equation describing the soil-water characteristic curve over the entire suction range (i.e., 0 to 10⁶ kPa) was proposed by Fredlund and Xing (1994):

$$[11] \quad \theta = C(\psi) \frac{\theta_s}{\{\ln[e + (\psi / a)^n]\}^m}$$

where:

- e = natural number, 2.71828,
- a = approximately the air-entry value of the soil,
- n = parameter that controls the slope at the inflection point in the soil-water characteristic curve,
- m = parameter that is related to the residual water content, and
- C(ψ) = correcting function defined as

$$C(\psi) = 1 - \frac{\ln\left(1 + \frac{\psi}{C_r}\right)}{\ln(1 + 1000000 / C_r)}$$

where:

- C_r = constant related to the matric suction corresponding to the residual water content, θ_r (Fredlund and Xing 1994).

A typical value for residual suction is about 1500 kPa. Equation [11] fits the experimental data well in the entire suction range from 0 to 10⁶ kPa (Fredlund and Xing 1994).

To calculate the coefficient of permeability using eqs. [10] and [11], it is convenient to perform the integration along the soil suction axis. Equation [10] can be transformed into the following form:

$$[12] \quad k_r(\psi) = \int_{\psi}^{\psi_r} \frac{\theta(y) - \theta(\psi)}{y^2} \theta'(y) dy \bigg/ \int_{\psi_{aev}}^{\psi_r} \frac{\theta(y) - \theta_s}{y^2} \theta'(y) dy$$

where:

- ψ_{aev} = air-entry value of the soil under consideration (i.e., the suction where air starts to enter the largest pores in the soil),
- ψ_r = suction corresponding to the residual water content θ_r,
- y = a dummy variable of integration representing suction, and
- θ' = derivative of eq. [11].

Since eq. [11] fits the experimental data over the entire suction range, the integrations in eq. [12] can be performed from ψ_{aev} to 10⁶ for all types of soils. This greatly simplifies the prediction procedure for the coefficient of permeability, since the residual value (θ_r or ψ_r) does not have to be determined experimentally for each soil.

To avoid the numerical difficulties of performing the integration over the soil suction range from ψ_{aev} to 10⁶ kPa, it is more convenient to perform the integration on a logarithmic scale. Therefore, the following variation of eq. [12] is preferred:

$$[13] \quad k_r(\psi) = \frac{\int_{\ln(\psi)}^b \frac{\theta(e^y) - \theta(\psi)}{e^y} \theta'(e^y) dy}{\int_{\ln(\psi_{aev})}^b \frac{\theta(e^y) - \theta_s}{e^y} \theta'(e^y) dy}$$

where:

- b = ln(1000000), and
- y = dummy variable of integration representing the logarithm of integration.

When the soil-water characteristic curve is considered over the entire suction range, volumetric water content is referenced to zero water content (otherwise, the normalized water content becomes negative if θ is less than θ_r). In this case, the normalized volumetric water content is equivalent to the degree of saturation, provided that the volume change of the soil structure is negligible:

$$[14] \quad \Theta = \frac{\theta}{\theta_s} = \frac{V_w / V_t}{V_v / V_t} = \frac{V_w}{V_v} = S$$

where:

- V_w = volume of water in the soil specimen,
- V_v = volume of void in the soil specimen, and
- V_t = total volume of the soil specimen.

Similarly, if the gravimetric water content, w, is referenced to zero water content, the normalized gravimetric water content, W, can be written as follows:

$$[15] \quad W = \frac{w}{w_s} = \frac{W_w / W_p}{W_{ws} / W_p} = \frac{W_w}{W_{ws}} = \frac{V_w \gamma_w}{V_v \gamma_w} = \frac{V_w}{V_v} = S$$

where:

- w_s = saturated gravimetric water content,
- W_w = weight of water,
- W_p = weight of soil particles,
- W_{ws} = weight of water when the soil is at saturation, and
- γ_w = specific weight of water.

Equations [14] a [15] indicate that the normalized (gravimetric or volumetric) water content is identical to the degree of saturation when referenced to zero water content and the volume change of the soil structure is negligible. Therefore eq. [13] is valid for any of the three water-content variables, (i.e., volumetric water content, gravimetric water content, or degree of saturation) if the soil-water characteristic curve is described by Eq. [11].

Table 3. Soil properties and fitting parameters of eq. [11] for the example soils.

Soil type	θ_s	$k_s \times 10^{-6}$ (m/s)	a	n	m	C_r
Touchet silt loam (GE3)	0.43	—	8.34	9.90	0.44	30.0
Columbia sandy loam	0.458	—	6.01	11.86	0.36	30.0
Yolo light clay	0.375	0.123	2.70	2.05	0.36	100.0
Guelph loam						
drying	0.52	3.917	5.61	2.24	0.40	300.0
wetting	0.43	—	3.12	4.86	0.23	100.0
Superstition sand	—	18.3	2.77	11.20	0.45	300.0

Numerical results and comparisons with experimental data

Numerical integration using [13] has been incorporated into a curve-fitting program (written in C language) called CFVIEW. The program first determines the four parameters $a, n, m,$ and C_r in eq. [11] through use of a non-linear least squares routine. With the soil-water characteristic curve known, the program then calculates the permeability function using eq. [13]. The procedure of numerical integration for eq. [13] is listed in the Appendix. The best-fit analysis is done on the suction versus water-content data. None of the residual values $\theta_r,$ and C_r is explicitly required during the curve fitting procedure. The detailed non-linear curve-fitting algorithm was outlined by Fredlund and Xing (1994). Comparisons are given in this section of the paper between measured and predicted coefficient of permeability curves for five soils. The soil properties and values of the fitting parameters for eq. [11] for each soil are listed in Table 3.

Figure 4 shows a best-fit curve to the experimental data for Touchet silt loam (GE3) from Brooks and Corey (1964). The predicted coefficient of permeability based on the best fit curve in Fig. 4 is compared with the measured permeability data in Fig. 5. The predicted curve is close to the measured permeability data. Results obtained for Columbia sandy loam (Brooks and Corey 1964) are presented in Figs. 6 and 7. Good predictions of the relative coefficient of permeability are obtained.

A best-fit curve to the experimental data for Superstition sand (Richards 1952) is shown in Fig. 8. The relative coefficient of permeability predicted based on its soil-water characteristic curve is shown in Fig. 9. It can be seen that the prediction of the relative coefficient of permeability becomes less accurate as the soil suction increases. This poor prediction can be traced back to the poor fit to the experimental data as shown in Fig. 8. The poor fit to the experimental data is partially caused by the limitation of the curve-fitting program. A minor modification to the curve-fitting program gives a better fit of the experimental data. The improved best-fit curve to the experimental soil-water characteristic data for the Superstition sand is shown in Fig. 10. Compared with the results shown in Fig. 9, the prediction based on the improved best-fit curve is considerably more accurate, as shown in Fig. 11. Therefore, a good description of the experimental

Fig. 4. Best-fit curve to the experimental data for Touchet silt loam (GE3) (data from Brooks and Corey 1964).

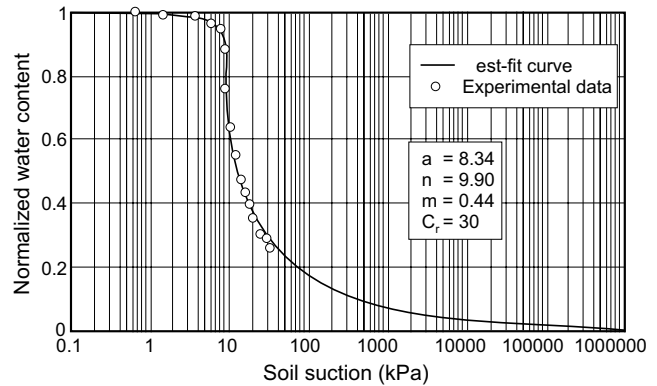
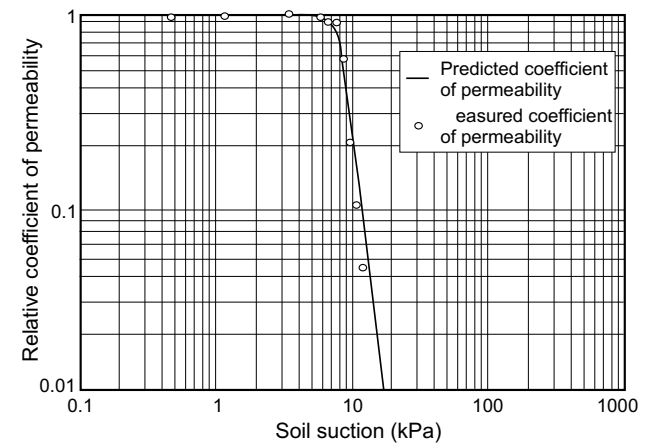


Fig. 5. Comparison of the predicted relative coefficient of permeability with the measured data for Touchet silt loam (GE3) (data from Brooks and Corey 1964).



soil-water characteristic data is essential to obtain an accurate prediction of the coefficient of permeability.

The results for Yolo light clay (Moore 1939) are presented in Figs. 12 and 13. The predicted permeability is close to the measured data when the soil suction is less than 4 kPa. It would appear that there may have been errors involved in the measured permeability data when the suction was greater than 4 kPa. The prediction of coefficient of permeability for clayey soils is generally less accurate than that for sandy soils.

Fig. 6. Best-fit curve to the experimental data for Columbia sandy loam (data from Brooks and Corey 1964).

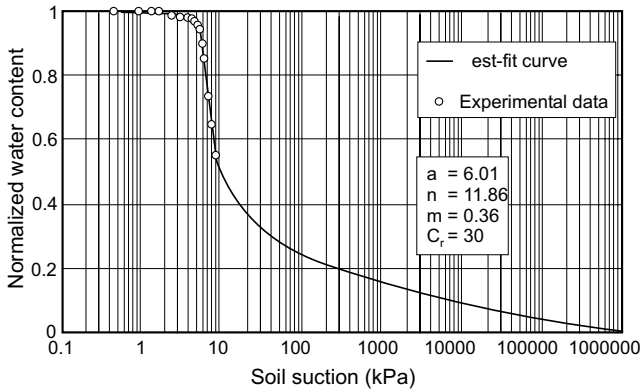


Fig. 7. Comparison of the predicted relative coefficient of permeability with the measured data for Columbia sandy loam (data from Brooks and Corey 1964).

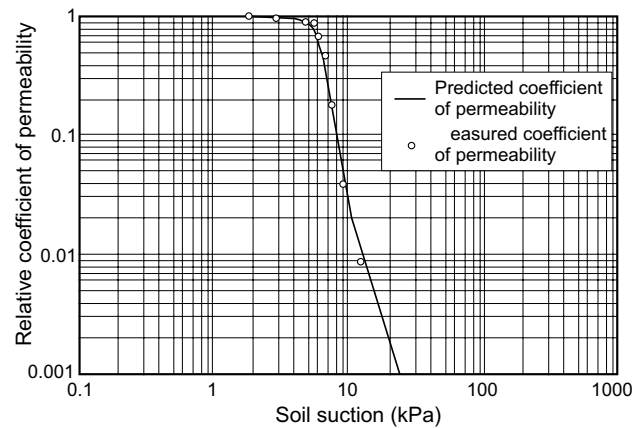
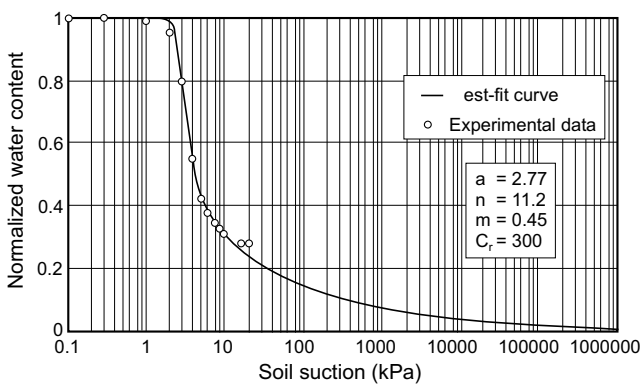


Fig. 8. Best-fit curve to the experimental data for Superstition sand (data from Richards 1952).



Results for Guelph loam (Elrick and Bowman 1964) are shown in Figs. 14 and 15. This is an example in which hysteresis is present in the soil-water characteristic curve. As shown by the results, although a considerable hysteresis loop is observed in the $\theta(\psi)$ plane, the $k(\theta)$ hysteresis is much less significant. Therefore, in most cases, only one branch (normally the drying branch) is used in the calculation of permeability.

Fig. 9. Comparison of the measured data with the predicted relative coefficient of permeability using the best-fit curve in Fig. 8 (data from Richards 1952).

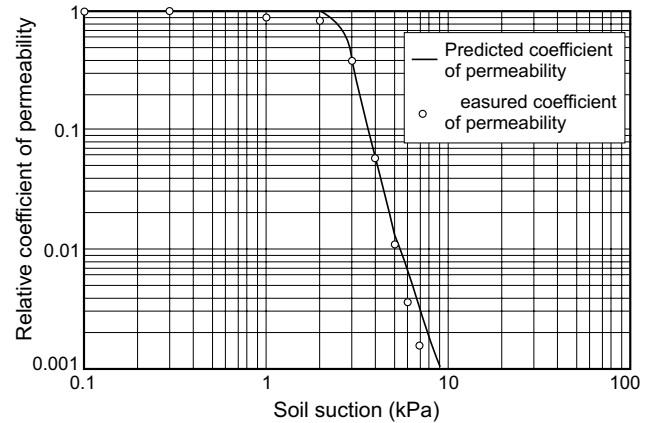


Fig. 10. Improved best-fit curve to the experimental data shown in Fig. 8.

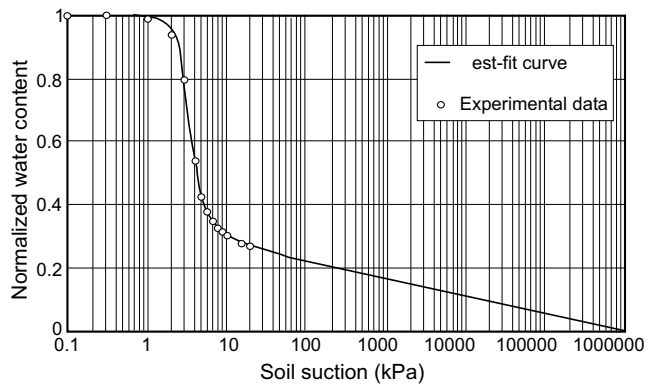
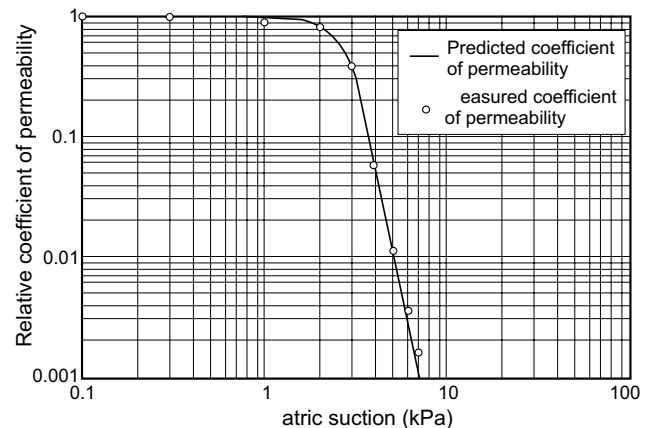


Fig. 11. Comparison of the measured data with the predicted relative coefficient of permeability using the improved best-fit curve in Fig. 10.



Summary of fit between theory and data

All the experimental soil-water characteristic data used in this paper are in the low suction range. Equation [11] is not only used to fit the experimental data in the low

Fig. 12. Best-fit curve to the experimental data for Yolo light clay (data from Moore 1939).

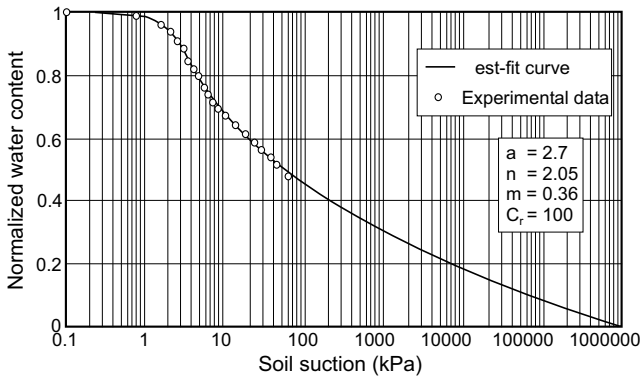
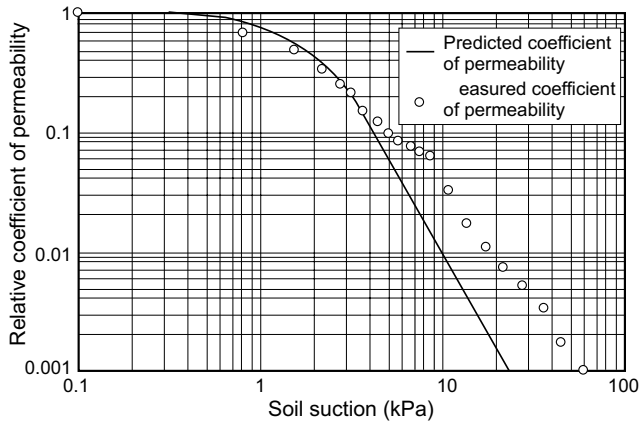


Fig. 13. Comparison of the predicted relative coefficient of permeability with the measured data for Yolo light clay (data from Moore 1939).



suction range, but also to estimate the soil–water characteristic behaviour in the high suction range. By so doing, it is no longer necessary to estimate the residual volumetric water content θ_r for each soil when predicting the coefficient of permeability. Since reasonable predictions of the coefficient of permeability are obtained in all the cases studied in this paper, eq. [11] gives a satisfactory description of the soil–water characteristic curve, which can then be used in the prediction of the coefficient of permeability. It is recommended, however, that the soil–water characteristic curve also be measured in the high suction range whenever possible, in order to increase the accuracy in the prediction of the coefficient of permeability.

The accuracy of the prediction of the coefficient of permeability depends not only on the closeness of the best-fit curve to the experimental soil–water characteristic data, but also on the precision of the model adopted. As concluded by Mualem (1986), there is no single model that fits every soil. The proposed models have been found to be most satisfactory for sandy soils, whereas agreement with experimental data is often unsatisfactory for fine-grained soils. The flexibility of eq. [13] can be increased by multiplying the equation by a correction factor, Θ^q . The correction factor takes into account the

Fig. 14. Best-fit curves to the experimental data for Guelph loam (data from Elrick and Bowmann 1964).

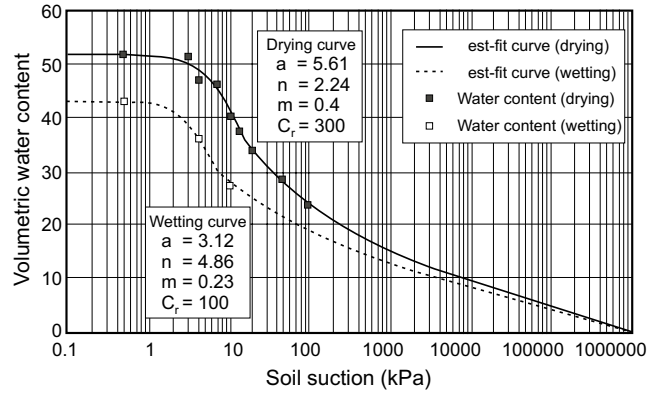
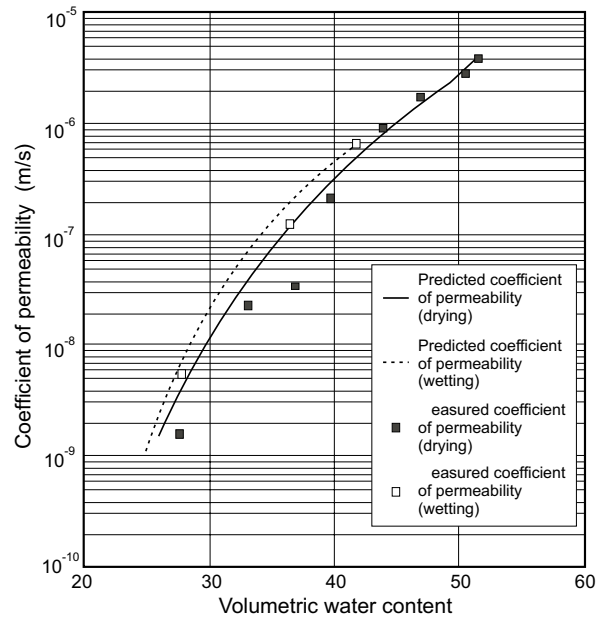


Fig. 15. Comparison of the predicted coefficient of permeability with the measured data for Guelph loam (data from Elrick and Bowmann 1964).



tortuosity (Mualem 1986). More accurate predictions can be obtained by using the following modification of eq. [13]:

$$[16] \quad k_r(\psi) = \frac{\Theta^q(\psi) \int_{\ln(\psi)}^b \frac{\theta(e^y) - \theta(\psi)}{e^y} \theta'(e^y) dy}{\int_{\ln(\psi_{ave})}^b \frac{\theta(e^y) - \theta_s}{e^y} \theta'(e^y) dy}$$

Based on the work by Kunze et al. (1968), the value of the power q is equal to 1.

Application in engineering practice

The flow of water through saturated-unsaturated soils is of primary significance in an increasing number of engineering problems. The design of earth dams or tailings

impoundments require flow models to describe the flow in the saturated-unsaturated zones under various boundary and soil conditions. Resource development and waste management are two examples where a rational approach to seepage analysis is needed. Recent developments in the area of unsaturated soils offer the appropriate concepts and technology for a detailed study of seepage through unsaturated soils. With the aid of digital computers, numerical methods, such as the finite-difference and finite-element methods, can be applied to solve the complex differential equations for saturated-unsaturated flow.

The fundamental equation that governs the flow of water in a saturated-unsaturated soil is as follows:

$$[17] \quad \frac{\partial}{\partial x} \left(k_x(\psi) \frac{\partial h}{\partial x} \right) + \frac{\partial}{\partial y} \left(k_y(\psi) \frac{\partial h}{\partial y} \right) + \frac{\partial}{\partial z} \left(k_z(\psi) \frac{\partial h}{\partial z} \right) + q = \frac{\partial \theta}{\partial t}$$

where:

- h = total fluid head,
- k_x, k_y, k_z = material properties (permeability) in the x , y , and z directions, respectively,
- q = applied external boundary flux,
- θ = volumetric water content, and
- t = time.

To model the flow of water in an unsaturated soil, it is necessary to define the relationship between the coefficient of permeability and soil suction. One method of defining this relationship is to use one of the empirical equations listed in Tables 1 and 2 (for example, the equation proposed by Gardner 1958). As pointed out earlier, this method requires measured data for the permeability function to determine the parameters in the permeability equation. Since establishing the soil-water characteristic curve is generally not as difficult nor demanding as measuring the coefficient of permeability at various suction levels, the task of defining the permeability function can be simplified by calculating the coefficient of permeability from the soil-water characteristic curve using the procedure proposed in this paper. In other words, the prediction procedure proposed in this paper has become part of the seepage modeling program.

Conclusions

The numerical results predicted using the procedure proposed in this paper show good agreement with the published data on measured coefficients of permeability for unsaturated soils. The equation for the soil-water characteristic curve proposed by Fredlund and Xing (1994) was found to be effective in the prediction of the coefficient of permeability for unsaturated soils. In the case where experimental soil-water characteristic data are not available in the high-suction range, this equation can be used to estimate the soil-water characteristic behaviour in this range.

The procedure proposed in this paper for predicting the unsaturated coefficient of permeability does not require a knowledge of the residual water content of the soil under consideration. Since the residual water content is assumed to be zero for all soils, the normalized water content is identical to the degree of saturation and, therefore, the proposed procedure for the prediction of the unsaturated coefficient of permeability is valid for all three variables describing water content in a soil (i.e., volumetric water content, gravimetric water content, and degree of saturation). The predicted curve for the coefficient of permeability is sensitive to the soil-water characteristic curve. Therefore, an accurate description of the soil-water characteristic behaviour is essential to the prediction of the coefficient of permeability. A modification of the procedure (i.e., eq. [16]) is suggested to increase the accuracy of the prediction of the coefficient of permeability. This modification combines eq. [13] and the empirical equation proposed by Averjanov (1950) in Table 1.

References

- Averjanov, S.F. 1950. About permeability of subsurface soils in case of incomplete saturation. *In* English Collection, Vol. 7. As quoted by P. Ya Palubarinova, 1962. The theory of ground water movement (English translation by I.M. Roger DeWiest. Princeton University Press, Princeton, NJ), pp. 19–21.
- Brooks, R.H., and Corey, A.T. 1964. Hydraulic properties of porous media. Colorado State University Hydrology Paper, Fort Collins, Nr. 3, Vol. 27, March.
- Burdine, N.T. 1953. Relative permeability calculation size distribution data. Transactions of the American Institute of Mining, Metallurgical, and Petroleum Engineers, **198**: 71–78.
- Campbell, J.D. 1973. Pore pressures and volume changes in unsaturated soils. Ph.D. thesis, University of Illinois at Urbana-Champaign, Urbana-Champaign, ILL.
- Childs, E.C., and Collis-George, G.N. 1950. The permeability of porous materials. Proceedings, Royal Society of London, Series A. **201**: 392–405.
- Croney, D., and Coleman, J.D. 1961. Pore pressure and suction in soils. Proceedings, Conference on Pore Pressure and Suction in Soils. Butterworths, London, pp. 31–37.
- Davidson, J.M., Stone, L.R., Nielsen, D.R., and Larue, M.E. 1969. Field measurement and use of soil-water properties. Water Resources Research, **5**: 1312–1321.
- Elrick, D.E., and Bowman, D.H. 1964. Note on an improved apparatus for soil moisture flow measurements. Soil Science Society of America Proceedings, **28**: 450–453.
- Fredlund, D.G., and Xing, A. 1994. Equations for the soil-water characteristic curve. Canadian Geotechnical Journal, **31**: 533–546.
- Gardner, W.R. 1958. Some steady state solutions of the unsaturated moisture flow equation with application to evaporation from a water table. Soil Science, **85**: 228–232.
- Kunze, R.J., Uehara, G., and Graham, K. 1968. Factors important in the calculation of hydraulic conductivity. Soil Science Society of America Proceedings, **32**: 760–765.
- Marshall, T.J. 1958. A relation between permeability and size distribution of pores. Journal of Soil Science, **9**: 1–8.
- Moore, R.E. 1939. Water conduction from shallow water tables. Hilgardia, **12**: 383–426.

Mualem, Y. 1976a. A new model for predicting the hydraulic conductivity of unsaturated porous media. *Water Resources Research*, **12**: 593–622.

Mualem, Y. 1976b. Hysteretical models for prediction of the hydraulic conductivity of unsaturated porous media. *Water Resources Research*, **12**: 1248–1254.

Mualem, Y. 1986. Hydraulic conductivity of unsaturated soils: prediction and formulas. *In Methods of soil analysis. Part 1. Physical and mineralogical methods. Second edition. Agronomy. Edited by A. Klute. American Society of Agronomy, Inc. and Soil Science Society of America, Inc. Madison, WI, USA, pp. 799–823.*

Richards, L.A. 1931. Capillary conduction of liquids through porous medium. *Physics*. **1**: 318–333.

Richards, L.A. 1952. Water conducting and retaining properties of soils in relation to irrigation. *Proceedings, International Symposium on Desert Research, Jerusalem*, pp. 523–546.

Richards, B.G. 1965. Measurement of the free energy of soil moisture by the psychrometric technique using thermistors. *In Moisture equilibria and moisture changes in soils beneath covered areas. Edited by G.D. Aitchison, Butterworths, Australia*, pp. 39–46.

Rijtema, P.E. 1965. An analysis of actual evapotranspiration. *Agricultural Research Reports (Wageningen)*, No. 659.

van Genuchten, M.T. 1980. A closed form equation for predicting the hydraulic conductivity of unsaturated soils. *Soil Science Society of America Journal*, **44**: 892–898.

Wind, G.P. 1955. Field experiment concerning capillary rise of moisture in heavy clay soil. *Netherlands Journal of Agricultural Science*, **3**: 60–69.

Appendix: Numerical integration of eq. [13] for the relative coefficient of permeability

The permeability function is expressed in the form of integrations that are performed on a logarithm scale (see eq. [13]). The two integrals in eq. [13] can be evaluated using the following numerical integration method.

Let a and b denote the lower and upper limits of the integration. Then,

$$[A1] \quad a = \ln(\psi_{aev}), \quad b = \ln(1000000)$$

Let us divide $[a, b]$ into N subintervals of the same size and let Δy denote the length of each subinterval. Then,

$$[A2] \quad a = y_1 < y_x < \dots < y_N < y_{N+1} = b, \quad \Delta y = \frac{b-a}{N}$$

The denominator of eq. [13] can be evaluated as follows:

$$[A3] \quad \int_{\ln(\psi_{aev})}^b \frac{\theta(e^y) - \theta_s}{e^y} \theta'(e^y) dy \approx \Delta y \sum_{i=1}^N \frac{\theta(e^{\bar{y}_i}) - \theta_s}{e^{\bar{y}_i}} \theta'(e^{\bar{y}_i})$$

where:

y_i = midpoint of the i -th interval, $[y_i, y_{i+1}]$, and θ' = derivative of eq. [11], which is given as follows:

$$[A4] \quad \theta'(\psi) = C'(\psi) \frac{\theta_s}{\{\ln[e + (\psi/a)^n]\}^m} - C(\psi) \frac{\theta_s}{\{\ln[e + (\psi/a)^n]\}^{m+1}} \frac{mn \left(\frac{\psi}{a}\right)^{n-1}}{a[e + (\psi/a)^n]}$$

where:

$$C'(\psi) = \frac{-1}{(C_r + \psi) \ln \left(1 + \frac{100000}{C_r} \right)}$$

For any suction value ψ in the range between the air-entry value ψ_{aev} and 10^6 , the value $\ln(\psi)$ is between a and b . Assume that $\ln(\psi)$ is in the j -th interval, $[y_j, y_{j+1}]$. Then, the numerator of eq. [13] can be evaluated as follows:

$$[A5] \quad \int_{\ln(\psi)}^b \frac{\theta(e^y) - \theta(\psi)}{e^y} \theta'(e^y) dy \approx \Delta y \sum_{i=j}^N \frac{\theta(e^{\bar{y}_i}) - \theta(\psi)}{e^{\bar{y}_i}} \theta'(e^{\bar{y}_i})$$

Therefore, the relative permeability $k_r(\psi)$ at suction ψ is:

$$[A6] \quad k_r(\psi) \approx \frac{\sum_{i=j}^N \frac{\theta(e^{\bar{y}_i}) - \theta(\psi)}{e^{\bar{y}_i}} \theta'(e^{\bar{y}_i})}{\sum_{i=1}^N \frac{\theta(e^{\bar{y}_i}) - \theta_s}{e^{\bar{y}_i}} \theta'(e^{\bar{y}_i})}$$

The lower limit of the integration given by eq. [13] corresponds to the saturated water content θ_s . Although the air-entry value is used as the lower limit of the integration, any other value between 0 and ψ_{aev} can be used. In other words, the air-entry value does not have to be known precisely. However, the value must be positive to perform the integration on a logarithm scale.

A steady state model for flow in saturated-unsaturated soils

A.T. Papagianakis and D.G. Fredlund

Abstract: A model is proposed describing continuous flow between saturated and unsaturated soil. The flow is assumed to be two-dimensional and under steady state conditions. In the unsaturated zone, the coefficient of permeability is treated as a function of pore-water pressure head. The non-linear differential equation governing the flow is solved using an iterative finite element scheme. The flow equation for an element is derived using the Galerkin weighed residuals method. Several example problems are solved and compared with flow net solutions. The proposed flow model is superior to traditional models, which consider flow only in the saturated zone. The results show that the zero pressure isobar is not an upper flow boundary. The finite element solution is shown to be relatively insensitive to the function used to express the relationship between the coefficient of permeability and the pore-water pressure head.

Key words: saturated-unsaturated soil, pore-water pressure, head, phreatic line, finite element, seepage.

Introduction

There is an increasing number of engineering problems involving flow through saturated-unsaturated soils. Such problems range from seepage pressure calculations in earth structures to estimates of contaminant migration in groundwater systems. The solution of these engineering problems awaits the development of rigorous flow models that will simulate these complex situations.

In seepage analysis, engineers have traditionally relied on graphical and numerical methods that consider only the saturated flow region. However, methods such as the flow net technique (Casagrande 1937) cannot adequately deal with problems involving flow through saturated-unsaturated soils.

The proposed model describes continuous flow between saturated-unsaturated soil. Flow is assumed to be two-dimensional and under steady state conditions. The coefficient of permeability is treated as a function of the pore-water pressure head. The non-linear differential equation governing the flow is solved using an iterative finite element scheme.

The theoretical formulation is implemented into a computer program called SEEP. SEEP, documented by Papagianakis (1983), can handle arbitrary degrees of anisotropy and heterogeneity and includes certain plotting capabilities for the graphical representation of the results.

Background

Some of the earliest theoretical work in the area of flow through unsaturated soils was presented by Richards

(1931). The term "capillary conduction" was used to describe the moisture movement through unsaturated soils. It was first recognized by Richards (1931) that "the essential difference between flow through a porous medium which is saturated and flow through medium which is unsaturated is that under the latter condition the pressure is described by capillary forces and the conductivity depends on the moisture content of the medium."

Casagrande (1937) proposed the flow net technique for the solution of seepage problems. According to this technique, flow problems were subdivided into "confined" and "unconfined" situations. In the case of "unconfined" flow, the upper boundary of the flow region, referred to as the line of seepage, was considered as the upper boundary of flow in the soil.

Research developments in the area of unsaturated soils have resulted in the development of relationships between the coefficient of permeability and the pore-water pressure head. Brooks and Corey (1966) derived a mathematical relationship between the coefficient of permeability and the "capillary pressure" (eq. [1]).

$$[1] \quad k = \begin{cases} k_0 & \text{for } P_c \leq P_b \\ \left(\frac{P_b}{P_c} \right)^n & \text{for } P_c \geq P_b \end{cases}$$

where:

P_c = capillary pressure (i.e., difference between pore-air and pore-water pressure), (dyne/cm²;
1 dyne = 10⁻⁵ N),

A.T. Papagianakis. Graduate Student, Department of Civil Engineering, University of Saskatchewan, 57 Campus Drive, Saskatoon, SK, Canada S7N 5A9.

D.G. Fredlund. Professor, Department of Civil Engineering, University of Saskatchewan, 57 Campus Drive, Saskatoon, SK, Canada S7N 5A9.

Reproduced with permission from the *Canadian Geotechnical Journal*, 21: 419-430, 1984.

- P_b = bubbling pressure (dyne/cm²), (i.e., minimum capillary pressure at which continuous air phase exists),
- k_0 = coefficient of permeability at saturation (cm²),
- k = coefficient of permeability at capillary pressure P_c , (cm²); and
- n = positive dimensionless constant.

Equation [1] represents two straight lines in a plot of the logarithm of the coefficient of permeability versus the logarithm of capillary pressure. Similar results were experimentally obtained by Laliberte and Corey (1967) (Fig. 1).

Taylor and Brown (1967) proposed a finite element model for seepage problems with a “free surface”. This model considered the flow of water in the saturated zone only and as a result, “the principal problem is locating the free surface that has both zero flow normal to it and prescribed pressure”. The proposed trial and error procedure for locating the free surface is cumbersome and often has convergence problems.

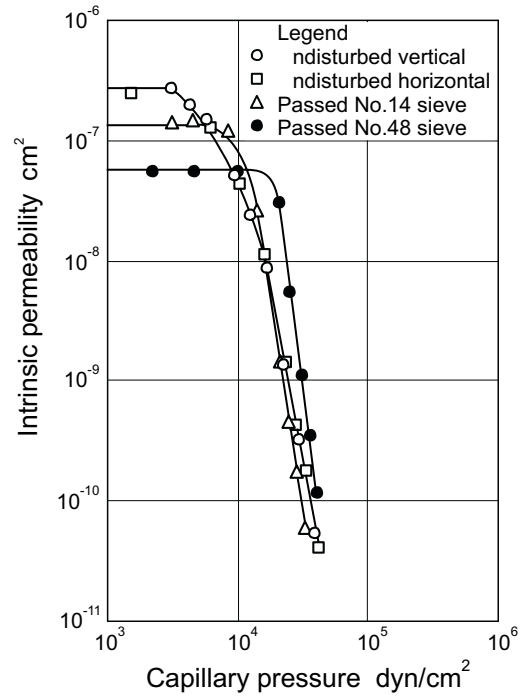
Flow models considering continuous flow between saturated–unsaturated soil were first introduced by hydrogeologists and soil scientists. Freeze (1971a) described a three-dimensional finite difference model for “saturated–unsaturated transient flow in non-homogeneous and anisotropic geologic basins”. The model “treats the complete subsurface region as a unified whole considering continuous flow between the saturated and unsaturated zones”. The differential equation governing the flow is expressed as a function of the pore-water pressure head and is similar to the equation proposed by Richards (1931). The solution is obtained using an iterative procedure and assuming a relationship between the coefficient of permeability and the pressure head.

Subsequently, Freeze (1971b) compared the traditional flow models that consider the flow only in the saturated zone with the saturated–unsaturated approach. Criticizing models dealing only with the flow in the saturated region, Freeze states that “boundary conditions that are satisfied on the free surface specify that the pressure head must be atmospheric and the surface must be a streamline. Whereas the first of these conditions is true, the second is not.” With respect to the continuous saturated–unsaturated flow approach, Freeze also states, “we can avoid the incorrect boundary conditions by solving the complete saturated–unsaturated boundary value problem”.

Neuman (1972) presented an iterative Galerkin finite element method for the solution of transient water flow problems in saturated–unsaturated porous media. However, the model considers the soil moisture content as the field variable, thus being rather unsuitable for engineering applications.

For the solution of steady state flow problems, engineers have traditionally relied on the flow net technique (Casagrande 1937). Flow models adopted later considered the flow of water only in the saturated zone (e.g., Taylor and Brown 1967). This “loyalty” to the concepts of “confined” and “unconfined” flow along with a lack of

Fig. 1. Relationship between capillary pressure and intrinsic permeability (after Laliberte and Corey 1967); 1 dyne = 10⁻⁵ N.



understanding associated with unsaturated soil behavior have discouraged the use of models considering continuous flow in saturated–unsaturated systems. Recent developments in the area of unsaturated soils (Fredlund and Morgenstern 1977; Dakshanamurthy and Fredlund 1980) offer the necessary background for using comprehensive flow models for saturated–unsaturated soils.

Theory

The differential equation governing flow is derived assuming that flow follows Darcy’s law regardless of the degree of saturation of the soil (Richards 1931). Assuming steady state flow conditions, the net flow quantity from an element of soil must be equal to zero. For the case where the direction of the maximum or minimum coefficient of permeability is parallel to either the x- or y-axis, the differential equation governing the flow can be written as follows:

$$[2] \quad \frac{\partial}{\partial x} \left(k_x(u_w) \frac{\partial h}{\partial x} \right) + \frac{\partial}{\partial y} \left(k_y(u_w) \frac{\partial h}{\partial y} \right) = 0$$

where:

- h = total head (m), (i.e., pressure head plus elevation head), and
- $k_x(u_w)$, and $k_y(u_w)$ = coefficient of permeability (m/s), in the x- and y-direction, respectively, depending upon the pore-water pressure head, u_w .

The non-linear differential equation (eq. [2]) is solved using an iterative finite element scheme. In each iteration, the coefficient of permeability is assumed to be constant in an element with a value depending upon the average pore-water pressure at its nodes.

The set of flow equations for an element is derived using a Galerkin weighted residual method (Zienkiewicz 1977), (eq. [3]).

$$[3] \quad \int_A \left\{ \begin{array}{c} \frac{\partial}{\partial x} \{L\} \\ \frac{\partial}{\partial y} \{L\} \end{array} \right\}^T \left\{ \begin{array}{cc} k_x(u_w) & 0 \\ 0 & k_y(u_w) \end{array} \right\} \left\{ \begin{array}{c} \frac{\partial}{\partial x} \{L\} \\ \frac{\partial}{\partial y} \{L\} \end{array} \right\} dA \{h^n\} - \int_S \{L\}^T q dS = 0$$

where:

$\{L\} = \{L_1, L_2, L_3\}$ = matrix of the area coordinates for an element,

$\{h^n\}$ = matrix of the nodal head values for an element,

A = area of an element,

S = perimeter of an element, and

q = flow across the sides of an element.

Assembling eq. [3] for all elements gives a set of global flow equations (eq. [4]).

$$[4] \quad \sum \{B\}^T \{k\} \{B\} A \{H^n\} - \int_S \{L\}^T q dS = 0$$

where:

$$\{B\} = \left\{ \begin{array}{c} \frac{\partial}{\partial x} \{L\} \\ \frac{\partial}{\partial y} \{L\} \end{array} \right\} = \frac{1}{2A} \left\{ \begin{array}{ccc} y_2 - y_3 & y_3 - y_1 & y_1 - y_2 \\ x_3 - x_2 & x_1 - x_3 & x_2 - x_1 \end{array} \right\}$$

$$\{k\} = \left\{ \begin{array}{cc} k_x(u_w) & 0 \\ 0 & k_y(u_w) \end{array} \right\}$$

x_i, y_i = Cartesian coordinates of the element nodes,

$\{H^n\}$ = column matrix including all the nodes of the discretized region.

The "summation" indicated in eq. [4] is performed routinely (Desai and Abel 1972), and the surface integral is taken over the external perimeter of the flow region (Zienkiewicz 1977). When the boundary flow is zero, the second term in eq. [4] drops to zero. When a flow value q is specified across a boundary, the surface integral in eq. [4] distributes the surface flow into nodal flow at the corresponding boundary nodes (Seegerlind 1976). The detailed finite element formulation is presented by Papagianakis (1982).

Computer implementation

The finite element formulation described above is implemented into the computer program SEEP. SEEP han-

dles up to eight different soil materials with arbitrary anisotropy. Flow regions can also be modeled where the direction of the major coefficient or permeability is at an angle to the horizontal. The boundary conditions, that can be specified are either head or flow values at the nodes of the discretized flow region. SEEP calculates element coefficients of permeability, water velocities, and gradients, and computes average nodal coefficients of permeability, average nodal water velocities, and average nodal gradients.

Two different functions are programmed into SEEP for the relationship between the coefficient of permeability and the pore-water pressure head. First, a linear relationship between the logarithm of the coefficient of permeability and the negative pressure head can be used (Fig. 2). Second, a linear relationship between the logarithm of the coefficient of permeability and the logarithm of pressure head, for pressure heads lower than -1.0 m, can be used (Fig. 3). Similar relationships were experimentally obtained by Richards (1931) and Laliberte and Corey (1967), respectively.

SEEP includes a method for determining the exit point of the phreatic line and adjusting the boundary conditions along free seepage boundaries. The method requires an initial guess for the exit point of the phreatic line. In subsequent iterations, the boundary conditions along the free surface are adjusted to satisfy the condition of negative pressure head for boundary nodes higher than the current exit point of the phreatic line.

Results

The solutions of several example problems are presented to demonstrate the capabilities of the proposed model (Figs. 4 to 15). In all cases, a total head value of 10.0 m is specified at all nodes along the wetted upstream face of the cross section of the dam. For the cases of dams with a horizontal drain (Figs. 4 to 13), a zero pressure head is specified at all nodes along the drain. For the cases shown in Figs. 4 to 11 and 14 to 15, the upper flow boundary is assumed to be subjected to zero flow. For the problems shown in Figs. 12 and 13, boundary flow values of 0.1×10^{-4} m³/s and 0.2×10^{-4} m³/s, respectively, are specified at the nodes along the upper flow boundary.

The problems shown in Figs. 14 and 15 demonstrate the ability of the computer program, SEEP, to deal with flow problems involving free boundary surfaces. In these cases, the lower boundary of the dam is assumed to be impervious and the exit point of the phreatic line is determined by the previously mentioned trial and error procedure.

For the example problems considered, a uniform grid with 195 nodal points and 336 elements was used. The number of iterations required for convergence ranges from 6 to 14, accepting a 1% tolerance (i.e., acceptable difference between corresponding nodal heads in two successive iterations). The dam geometry, the nodal head values, and the contours in Figs. 4 to 15 are drawn using the plotting capabilities of SEEP.

Fig. 2. Relationship between the coefficient of permeability and the pressure head (NOPT = 1).

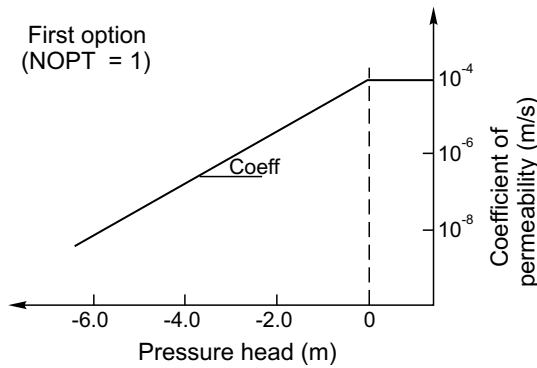
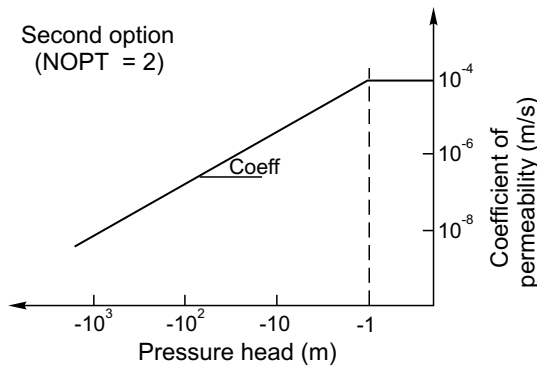


Fig. 3. Relationship between the coefficient of permeability and the pressure head (NOPT = 2).



Discussion

The solutions of the example problems presented are compared with flow net solutions by observing the requirements for the phreatic line and the equipotential lines (Casagrande 1937). For all problems with zero flow specified across the upper boundary (Figs. 4 and 6 to 9 and 14 and 15), the equipotential lines coincide with the phreatic line at right angles. Furthermore, the elevation of the point of intersection of any equipotential line with the phreatic line is equal to the total head represented by this equipotential line. These observations offer evidence that the phreatic line (i.e., zero pressure isobar) approximately coincides with the line of seepage, as defined by Casagrande (1937). This latter condition will be further examined by comparing quantities of flow through various vertical sections. The problems in Figs. 12 and 13 demonstrate that when flow is applied externally, the phreatic line departs from the streamline condition.

For the problems shown in Figs. 4 and 14, the quantities of flow obtained by summing element flow quantities are compared with the flow quantities calculated from flow net solutions. The methodology for calculating flow quantities was proposed by Papagianakis (1982). The results are summarized in Tables 1 and 2, where NOPT is the type of function used and COEFF is its slope in the unsaturated region (Figs. 2 and 3).

Tables 1 and 2 show that the quantity of seepage is becoming lower for increasing COEFF values. This can be explained by the reduction of the conductivity in the unsaturated zone. It can also be seen that the quantity of seepage for NOPT equal to 1 and high COEFF values (e.g., 3.0 or 4.0) agrees favourably with the quantity of seepage obtained from the flow net solution. This indicates a certain dependence of the solution on the coefficient of permeability function used and suggests the need for a more detailed study on this aspect.

Figure 5 shows the effect of anisotropy on the shape of the saturated zone. For higher ratios of horizontal to vertical coefficients of permeability, the saturated zone may coincide with the downstream face of the dam.

Figures 6 and 7 illustrate that the drop of the phreatic line is becoming sharper for decreasing coefficients of permeability for the core material. However, even for three orders of magnitude difference in the coefficients of permeability, there is still some head drop taking place outside the core.

Figures 8 and 9 illustrate the deflection angles of the phreatic line at the boundary of the two materials with different coefficients of permeability. Table 3 summarizes these angles and shows that the condition ($\beta = 270^\circ - \alpha - \omega$) (Casagrande 1937) is not exactly fulfilled. The difference between the angle β and the term ($270^\circ - \alpha - \omega$) raises doubts about the streamline condition of the zero pressure isobar.

Figures 10 and 11 illustrate the distorted shape of the phreatic line and equipotential lines in flow regions where the direction of the maximum coefficient of permeability is at an angle to the horizontal. In the cases where positive boundary flow is specified (Figs. 12 and 13), the location of the phreatic line is somewhat higher than in the case where zero flow is specified (Fig. 4).

Figures 14 and 15 illustrate the use of the previously mentioned procedure for revising the boundary conditions along an open flow surface. It can be seen that the presence of the downstream water causes the exit point of the phreatic line to rise. This shows that the exit point of the phreatic line in no case coincides with the free surface at the downstream water level.

The limitations of the traditional saturated-only flow models, in terms of computing effort and convergence difficulty, are well known (Taylor and Brown 1967). Furthermore, the assumption such models employ with respect to the line of seepage should be questioned. Is the zero pressure isobar (i.e., phreatic line) a streamline?

The concept of zero flow across the phreatic line is examined by comparing the quantities of flow across various vertical sections (Fig. 16a). Flow quantities across vertical sections are computed using two different methodologies, one proposed by Papagianakis (1982) and the other by Lam (1984). According to the first methodology, the flow quantity is calculated by summing the products of element horizontal velocities multiplied by the cross-sectional areas of these elements (Fig. 16b). According to the second methodology, the flow quantity is calculated by summing internodal flow quantities (Fig. 16c). For the

Fig. 4. Homogeneous dam with a horizontal drain.

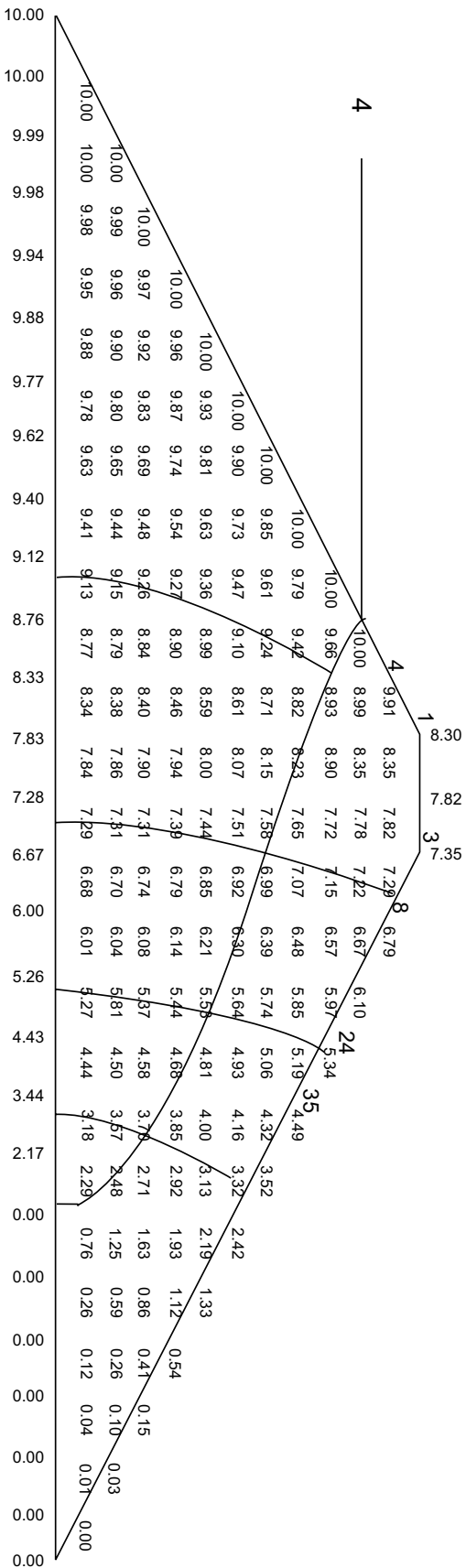


Fig. 5. Anisotropic dam with a horizontal drain, $k_x = 10k_y$.

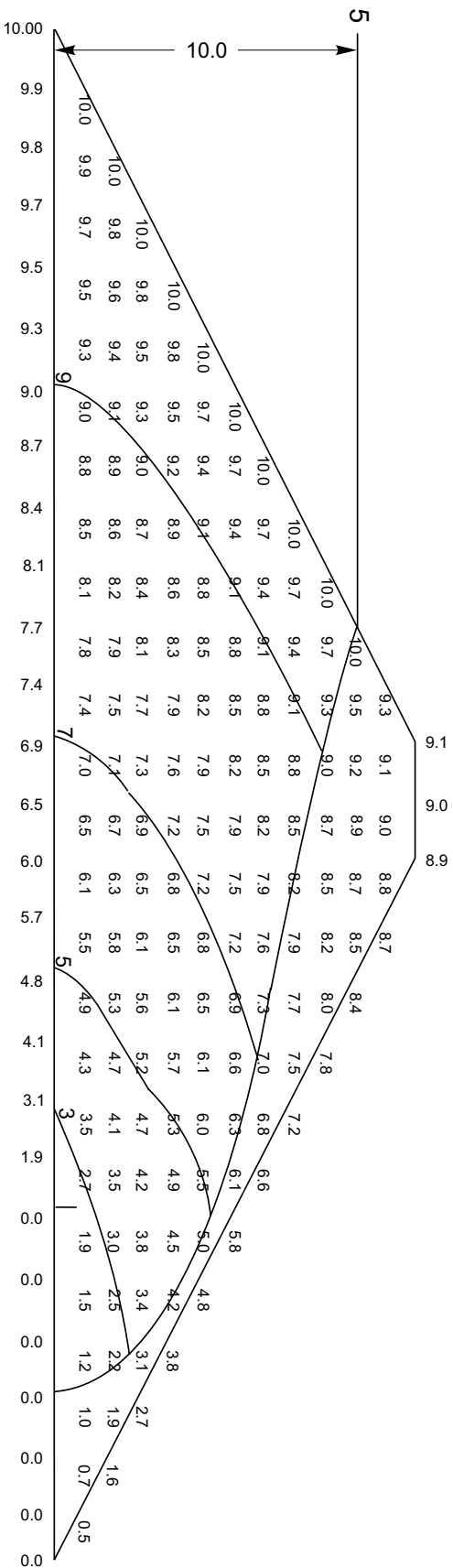


Fig. 8. Heterogeneous dam with a horizontal drain; permeabilities at saturation: $k_A = 10^{-4}$ m/s, $k_B = 10^{-5}$ m/s.

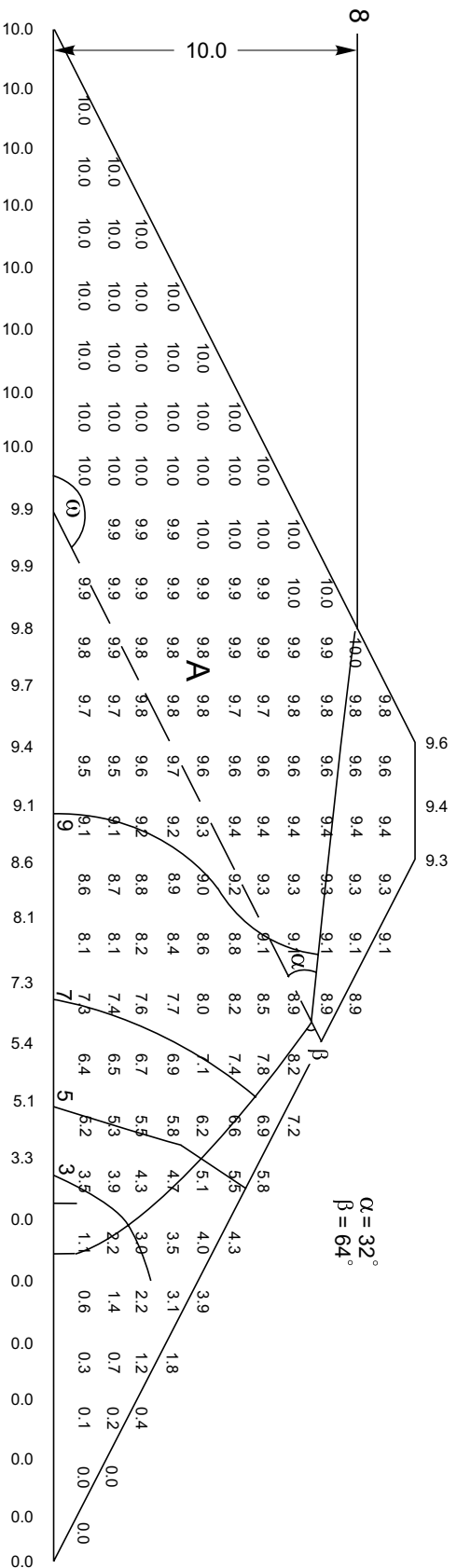


Fig. 9. Heterogeneous dam with a horizontal drain; permeabilities at saturation: $k_A = 10^{-5}$ m/s, $k_B = 10^{-4}$ m/s.

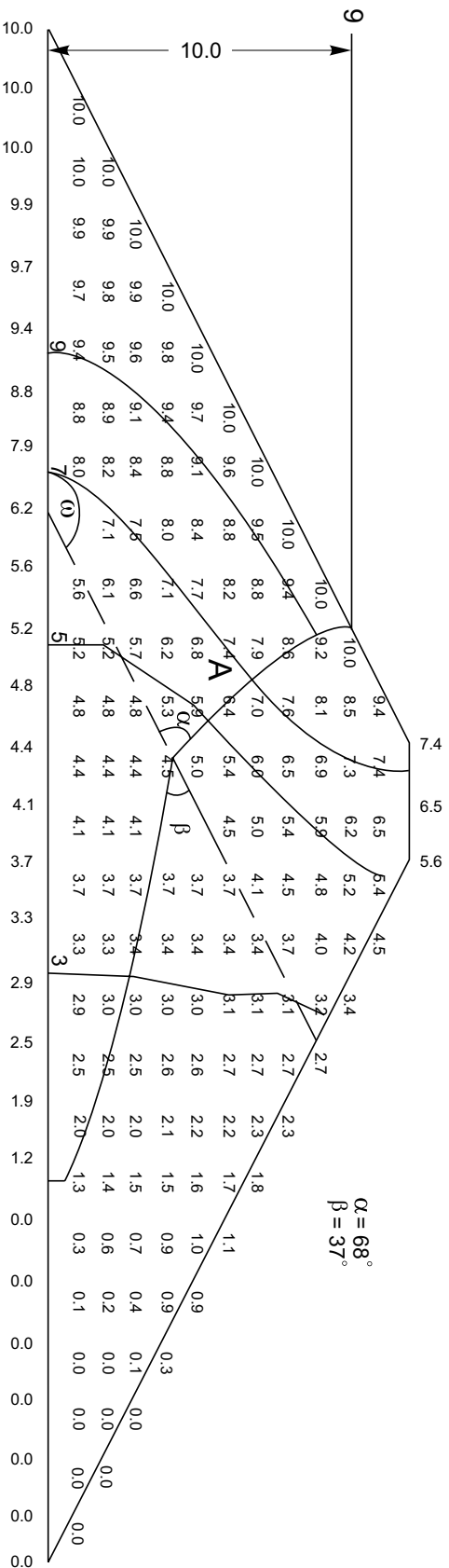


Fig. 10. Dam with a horizontal drain; the direction of the major coefficient of permeability is at an angle 0.5 rad to the horizontal.

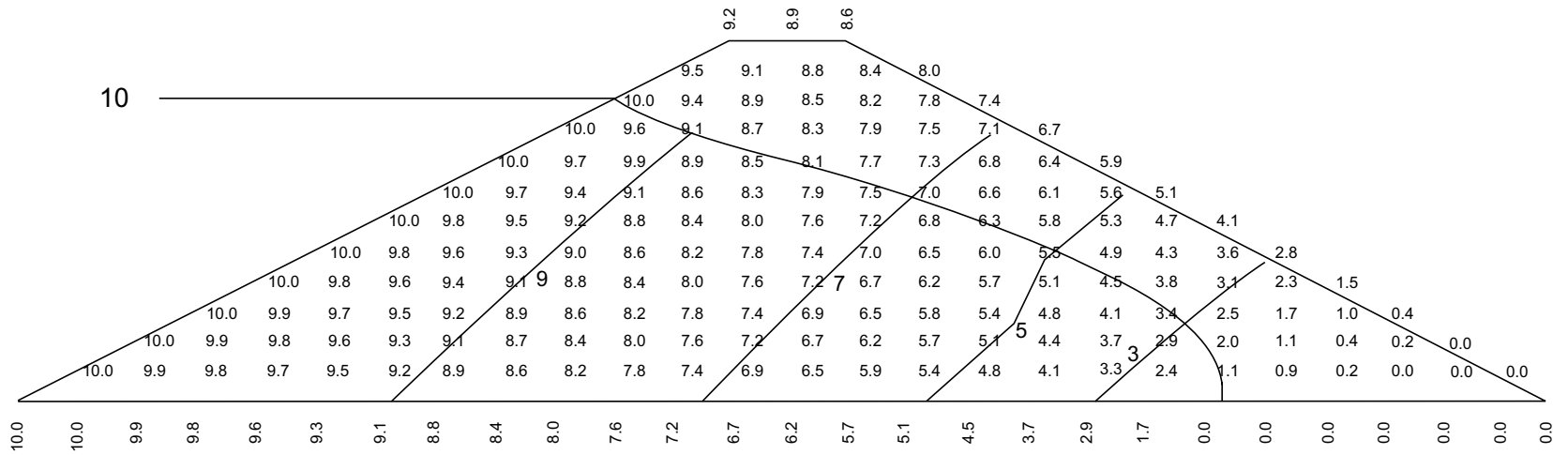


Fig. 11. Dam with a horizontal drain; the direction of the major coefficient of permeability is at an angle -0.5 rad to the horizontal.

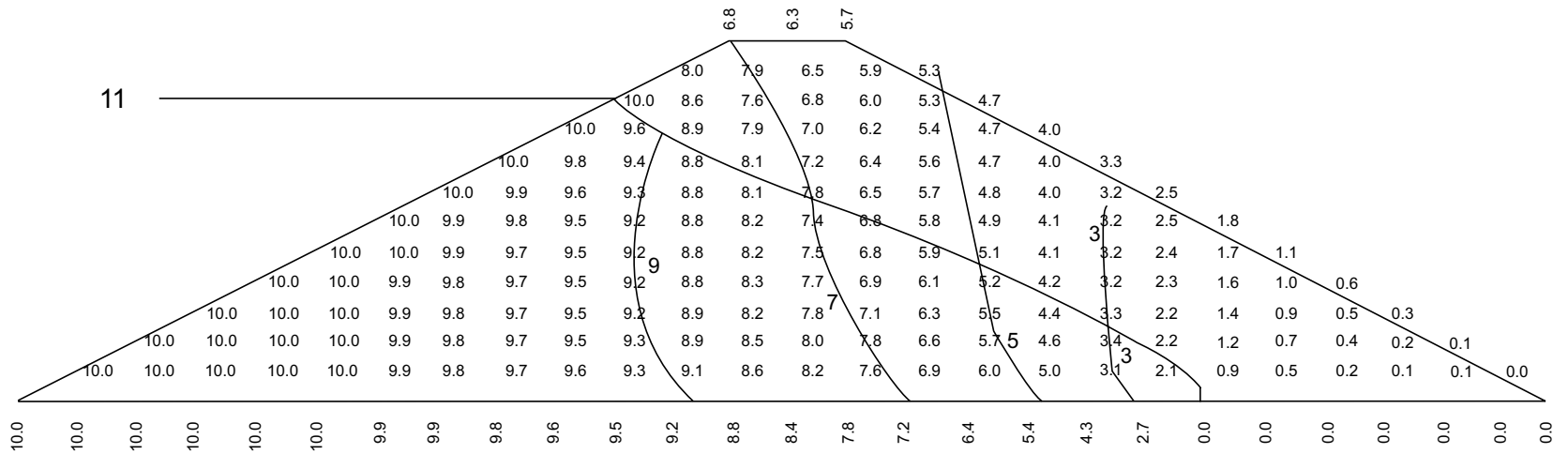


Fig. 12. Homogeneous dam under rainfall; boundary flow equal to 0.1×10^{-4} m/s.

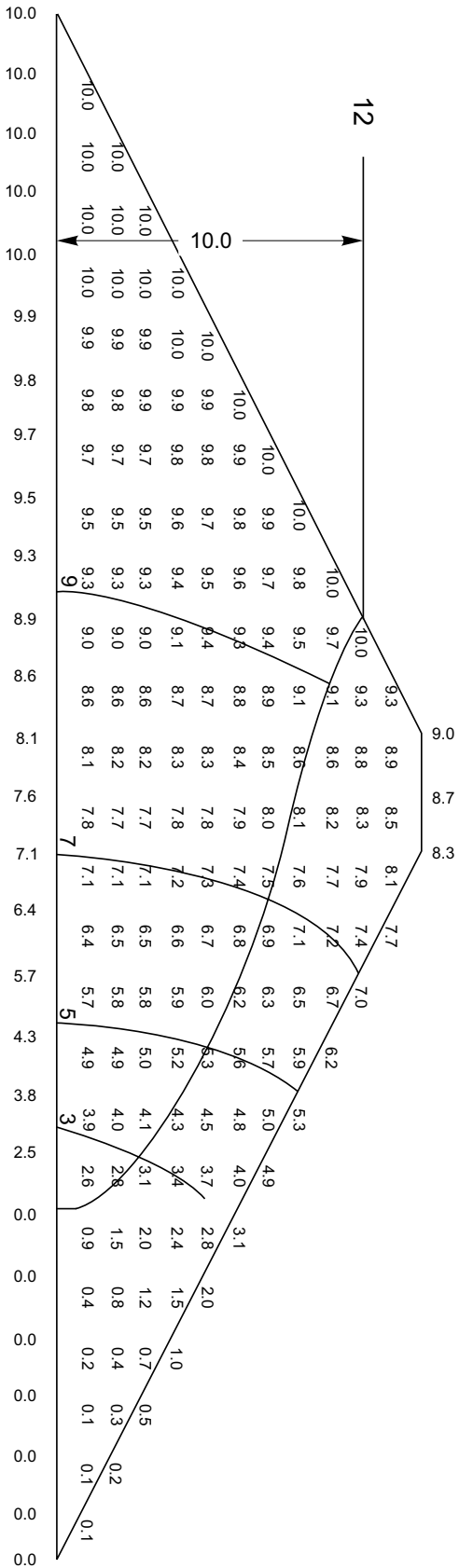


Fig. 13. Homogeneous dam under rainfall; boundary flow equal to 0.2×10^{-4} m/s.

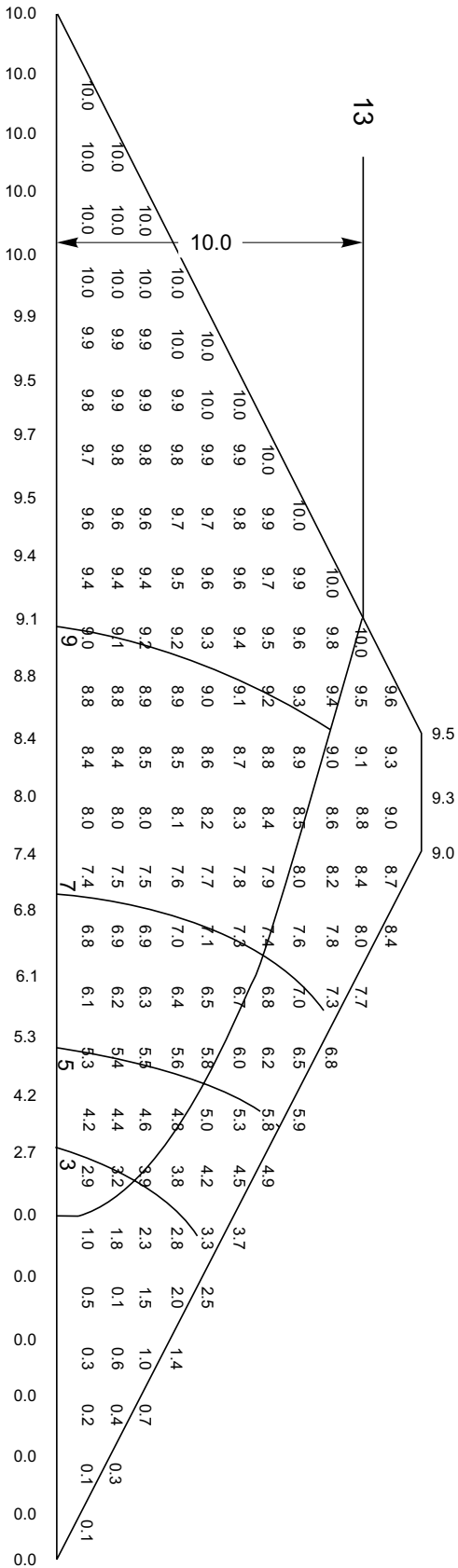


Fig. 14. Homogeneous dam with impervious lower boundary.

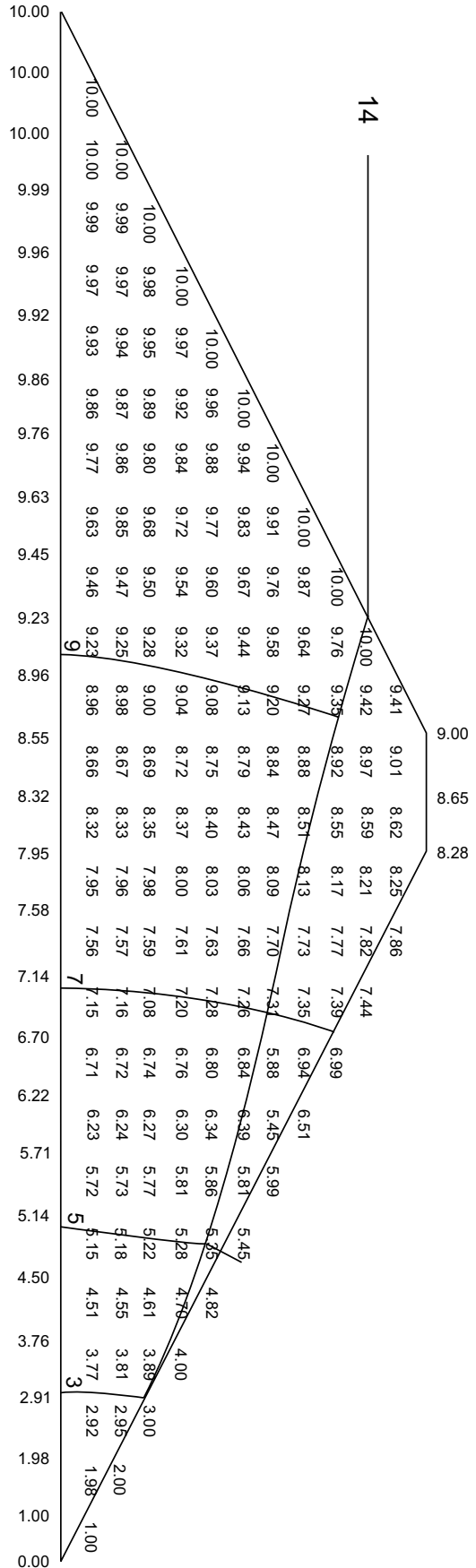


Fig. 15. Homogeneous dam with impervious lower boundary; 4.0 m of downstream water.

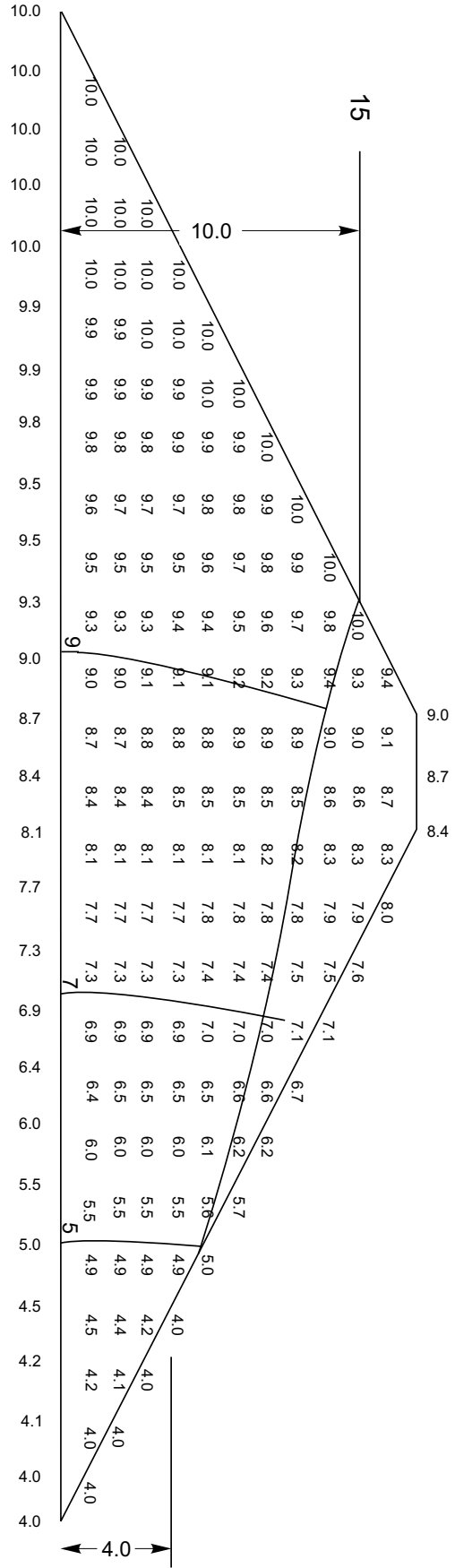


Table 1. Flow quantities (m³/s); problem in Fig. 4.

COEFF	NOPT = 1	NOPT = 2
0.2	2.645 × 10 ⁻⁴	—
0.6	2.283 × 10 ⁻⁴	—
1.0	2.230 × 10 ⁻⁴	2.932 × 10 ⁻⁴
2.0	2.175 × 10 ⁻⁴	2.731 × 10 ⁻⁴
3.0	—	2.636 × 10 ⁻⁴
4.0	2.129 × 10 ⁻⁴	2.580 × 10 ⁻⁴
From flow net solution = 2.08 × 10 ⁻⁴ to 2.43 × 10 ⁻⁴		

Note: NOPT = type of function (Figs. 2 or 3); COEFF = slope of function in the unsaturated zone.

Table 2. Flow quantities (m³/s), problem in Fig. 14.

COEFF	NOPT = 1	NOPT = 2
0.2	1.713 × 10 ⁻⁴	—
0.6	1.636 × 10 ⁻⁴	—
1.0	1.580 × 10 ⁻⁴	1.814 × 10 ⁻⁴
2.0	1.518 × 10 ⁻⁴	1.798 × 10 ⁻⁴
3.0	—	1.793 × 10 ⁻⁴
4.0	1.482 × 10 ⁻⁴	1.794 × 10 ⁻⁴
From flow net solution = 1.52 × 10 ⁻⁴ to 1.73 × 10 ⁻⁴		

Note: NOPT = type of function (Figs. 2 or 3); COEFF = slope of function in the unsaturated zone.

Table 3. Deflection angles (degrees) of the phreatic line for examining the condition $\beta = 270^\circ - \alpha - \omega$.

	α	β	$270^\circ - \alpha - \omega$
Fig. 8	32	64	84
Fig. 9	68	37	48

Note: $\omega = 135^\circ$ (Figs. 8 and 9).

example problem shown in Fig. 4, the results of the flow calculations for three vertical sections are tabulated in Tables 4 and 5. It can be seen that for both methodologies, the quantities of flow across the sections in the unsaturated zone are not equal. This implies that there is flow across the phreatic line, which as a result is not a streamline. Thus, the assumption of zero flow across the phreatic line is not only unnecessary, but it is also incorrect. This conclusion is in agreement with the work by Freeze (1971b). Considering that total flow quantities through various cross sections should be constant, it appears that the second methodology is more accurate.

The sensitivity of the finite element solution with respect to the function used to express the relationship between the coefficient of permeability and the pressure head was part of an extensive parametric study by Papagianakis (1982). The two problems shown in Figs. 4 and 14 were solved using various slopes of the two types of linear relationships in the unsaturated zone (Figs. 2 and 3). The solution in all cases converged in less than 20 iterations for a 1% tolerance. It was also observed that the number of iterations required for convergence increased for steeper functions. The calculated total head values and the location of the phreatic line were relatively

Fig. 16. Calculation of flow quantities: a) Comparison of flow quantities across vertical sections; b) methodology (after Papagianakis 1982); c) methodology (after Lam 1984).

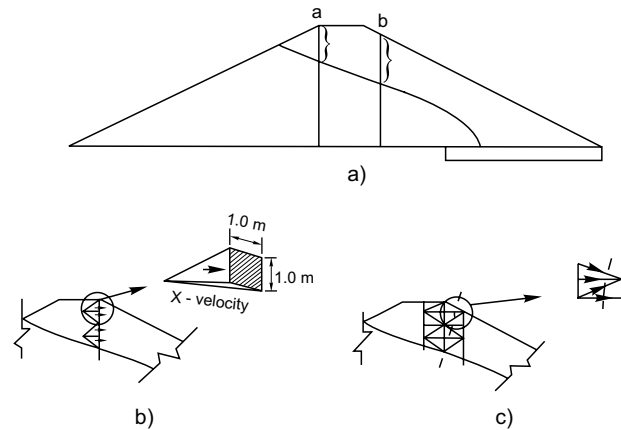


Table 4. Flow quantities (10⁻⁴ m³/s) across three vertical sections, methodology (after Papagianakis 1982).

	At node 3	At node 4	At node 35
Unsaturated zone	0.5585	0.3642	0.6961
Saturated zone	2.2560	2.3890	2.1728
Total	2.8145	2.7532	2.8689

Table 5. Flow quantities (10⁻⁴ m³/s) across three vertical sections, methodology (after Lam 1984).

	At node 1	At node 8	At node 24
Unsaturated zone	0.5252	0.6557	0.5913
Saturated zone	2.2368	2.1063	2.1707
Total	2.7620	2.7620	2.7620

unchanged under a wide range of functional relationships. The water conductivity of the unsaturated zone, however, decreased for increasing COEFF values. It is, therefore, concluded that the relative quantity of flow in the saturated and the unsaturated zone depends upon the function used. As expected, the solution obtained for a low conductivity in the unsaturated zone (i.e., high COEFF values) agrees favourably with the solutions of Casagrande (1937).

Conclusions

The proposed model appears to adequately describe two-dimensional steady state flow through saturated-unsaturated soils. The computer program SEEP was proven to be relatively flexible and suitable for modelling various soil and boundary conditions. The main conclusions are as follows:

- (1) There is no need to retain the arbitrary categorization of flow problems as “confined” and “unconfined” situations.
- (2) There is continuous flow between the saturated and the unsaturated zone.

- (3) It is incorrect to assume that the zero pressure isobar is the upper streamline and that no flow crosses it.

References

- Brooks, R.H., and Corey, A.T. 1966. Properties of porous media affecting fluid flow. *ASCE Journal of the Irrigation and Drainage Division*, **92**(IR2): 61–88.
- Casagrande, A. 1937. Seepage through dams. *New England Water Works*, **51**(2): 295–336.
- Dakshanamurthy, V., and Fredlund, D.G. 1980. Moisture and air flow in an unsaturated soil. *Proceedings, 4th International Conference on Expansive Soils*, Denver, CO, Vol. 1, pp. 514–532.
- Desai, C.S., and Abel, J.F. 1972. *Introduction to the finite element method for engineering analysis*. Van Nostrand Reinhold, New York.
- Fredlund, D.G., and Morgenstern, N.R. 1977. Stress state variables for unsaturated soils. *ASCE Journal of the Geotechnical Engineering Division*, **103**: 447–464.
- Freeze, R.A. 1971*a*. Three dimensional, transient, saturated–unsaturated flow in a groundwater basin. *Water Resources Research*, **7**(2): 347–366.
- Freeze, R.A. 1971*b*. Influence of the unsaturated flow domain on seepage through earth dams. *Water Resources Research*, **7**(4): 929–940.
- Laliberte, G.E., and Corey, A.T. 1967. Hydraulic properties of disturbed and undisturbed soils. *ASTM Special Technical Publication*, STP 417.
- Lam, L. 1984. Transient finite element seepage program (TRASEE). *Computer Documentation CD-18*, Transportation and Geotechnical Group, University of Saskatchewan, Saskatoon, SK, Canada.
- Neuman, S.P. 1972. Finite element computer programs for flow in saturated–unsaturated porous media. Report No. A10-SWC-77, Hydrodynamics and Hydraulics Laboratory, Technion, Haifa, Israel.
- Papagianakis, A.T. 1982. A steady state model for flow in saturated–unsaturated soils. M.Sc. thesis, University of Saskatchewan, Saskatoon, SK, Canada.
- Papagianakis, A.T. 1983. SEEP, a two-dimensional steady state finite element computer model for flow in saturated–unsaturated soils. *Computer Documentation CD-17*, Transportation and Geotechnical Group, University of Saskatchewan, Saskatoon, Saskatchewan, Canada.
- Richards, L.A. 1931. Capillary conduction of liquids through porous mediums. *Physics (New York)*, **1**: 318–333.
- Segerlind, L.J. 1976. *Applied finite element analysis*. John Wiley & Sons, New York.
- Taylor, R.L., and Brown, C.B. 1967. Darcy flow with a free surface. *ASCE Journal of the Hydraulics Division*, **93**(HY2): 25–33.
- Zienkiewicz, O.C. 1977. *The finite element method in engineering science*. McGraw-Hill, New York.

Transient seepage model for saturated-unsaturated soil systems: A geotechnical engineering approach

L. Lam, D.G. Fredlund, and S.L. Barbour

Abstract: A two-dimensional finite element model is proposed to simulate transient seepage for complex groundwater flow systems. The complete soil system is treated as a continuum encompassing flow in both saturated and unsaturated zones. In the unsaturated zone, the air phase is assumed to be continuous and open to atmospheric pressure. The coefficient of permeability of the unsaturated soil is assumed to be a function of pore-water pressure.

The governing differential equation is derived within a framework familiar to geotechnical engineers. The stress state variables and the constitutive relationships for an unsaturated soil are used in the derivation. The finite element solution to the governing differential equation is based on the Galerkin weighted-residual method. The non-linearity of the equation is solved by iterative procedures.

The finite element formulation is implemented into a computer model named TRASEE. The model can be applied to a wide variety of problems involving complex boundary conditions and geometries with arbitrary degrees of heterogeneity and anisotropy. Example problems are presented to demonstrate the capabilities of the model. The results indicate that the quantity of water flow in the unsaturated zone may be substantial, and that the phreatic line is not a flow line. It has been found that the traditional "saturated-only" flownet technique can be approximated as a special case to the proposed saturated-unsaturated model.

Key words: Unsaturated flow, finite element model, phreatic line, permeability function, transient seepage.

Introduction

In geotechnical engineering, seepage analysis may be of interest with respect to slope stability analysis, groundwater contamination control, and the design of hydraulic structures. Since Casagrande's (1937) classic paper "Seepage through dams," seepage problems in geotechnical engineering have been generally solved by sketching flownets. This method is based on the assumption that water flows only in the saturated zone. This method of solution is practical for simple steady state problems where the boundary of the flow region is clearly defined and the soil conditions are not too complex. However, many seepage problems of practical interest are complex, and a flownet solution is not feasible.

With the development of high-speed digital computers, numerical methods are increasingly used in solving seepage problems. Some of the first attempts at modeling seepage using the finite element method also considered water flow only in the saturated zone. An example is the

finite element flow model proposed by Taylor and Brown (1967). In this "saturated-only" approach, the phreatic line was assumed to be the upper boundary of the flow region for unconfined flow problems. In order to obtain the location of the phreatic line, a trial and error procedure is used to search for a surface that has both zero water pressure along it and zero flow across it. For each trial, the location of the phreatic line is readjusted, and a new mesh is constructed. This method is tedious, and it is also based on the erroneous assumption that the phreatic line is the uppermost flow boundary.

A saturated-unsaturated model would appear to be superior to the saturated-only model. By considering water flow in both the saturated and unsaturated zones, the actual ground surface (rather than the phreatic line) can be used as the uppermost boundary. The phreatic line is obtained by joining points of zero water pressure in the flow region. The finite difference model proposed by Freeze (1971a) is an example of a saturated-unsaturated flow model. This model allows the calculation of flow and hydraulic heads in the unsaturated zone. It also allows the modeling of situations with a ground surface flux. As well, there is no need to adjust the mesh during the solution of the problem.

Much of the research concerning unsaturated flow has been undertaken by soil scientists. Geotechnical engineers have often accepted formulations from researchers with diverse backgrounds without evaluating the assumptions and objectives of their formulation. This paper presents the development of a transient finite element seepage

L. Lam. Graduate Student, Department of Civil Engineering, University of Saskatchewan, 57 Campus Drive, Saskatoon, SK, Canada S7N 5A9.

D.G. Fredlund, and S.L. Barbour. Professors, Department of Civil Engineering, University of Saskatchewan, 57 Campus Drive, Saskatoon, SK, Canada S7N 5A9.

Reproduced with permission from the *Canadian Geotechnical Journal*, 24: 565-580, 1987.

model using an approach consistent with that used by geotechnical engineers. The concepts pertinent to the understanding of unsaturated flow are reviewed. The general governing differential equation for transient seepage is derived and the finite element solution to the equation is presented.

Review of unsaturated flow concepts

Unsaturated flow is an example of multiphase flow through a porous media. Two phases, air and water, coexist in the pore channels. Two partial differential equations are required to rigorously describe the flow of air and water in unsaturated soil. Problems of this kind are referred to as two-phase flow problems (Fredlund 1981). However, for most seepage problems encountered in geotechnical engineering, only flow in the water phase of the unsaturated zone is of practical interest. This “single-phase” flow approach is used in this paper. The fundamental assumption is that the air phase is continuous and the pore-air pressure is equal to atmospheric pressure. This is generally the case when the degree of saturation is less than approximately 85%. In the case where the degree of saturation is larger than 85%, the air phase is occluded. However, the occluded air pressure will still be essentially atmospheric and will not introduce significant error into the “single-phase” flow approach. Freeze and Cherry (1979) stated that “the single-phase approach to unsaturated flow leads to techniques of analysis that are accurate enough for almost all practical purposes”.

Soils are porous materials, with water being free to flow through the interconnected pores between the solid particles. Regardless of the degree of saturation of the soil, water flows under the influence of a hydraulic gradient. The driving gradient can be identified by Bernoulli's theorem. Since seepage velocities in soils are normally small, the velocity head can be neglected, and the driving force is the sum of pore-water pressure head and elevation head.

$$[1] \quad h = \frac{u_w}{\rho_w g} + z$$

where:

- h = total head,
- u_w = pore-water pressure,
- z = elevation head above an arbitrary datum,
- ρ_w = density of water, and
- g = acceleration due to gravity.

The flow of water through a soil mass can be described using Darcy's law:

$$[2] \quad q = -ki$$

where:

- q = discharge per unit area,
- i = potential gradient, and
- k = coefficient of permeability (or hydraulic conductivity).

Darcy's law was originally derived for saturated soil, but can equally be applied to the flow of water through an unsaturated soil (Richards 1931; Childs and Collis-George 1950). The only difference is that for flow through an unsaturated soil, the coefficient of permeability is no longer a constant but is a function of the matric suction of the soil.

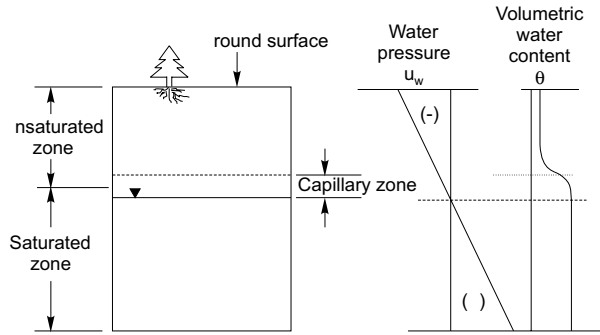
Figure 1 illustrates the pore-water pressure and moisture distribution within a soil profile under hydrostatic conditions. The water table (i.e., phreatic line) is an imaginary surface where the pore-water pressure is zero. Water may flow up and down across the water table if there is a hydraulic gradient between the saturated and unsaturated zones. Below the water table, the pore-water pressure is positive and increases linearly with depth. Above the water table, the pore-water pressure is negative and decreases with height. The amount of water retained in the unsaturated zone of a particular soil is a function of matric suction ($u_a - u_w$) of the soil (Fredlund and Morgenstern 1977). Since the pore-air pressure is atmospheric, the matric suction is also equal to the absolute value of the negative pore-water pressure.

Figure 2 shows the laboratory retention curve for fine sand, silt, and Regina clay obtained by Ho (1979). These retention curves were obtained using Tempe cells. The operating principles and the testing procedures can be found in the “Operating instructions for Tempe pressure cell” by Soil Moisture Equipment Corporation, Santa Barbara, California. In order to consider flow in both the saturated and unsaturated zones of a flow regime, the permeability of the soil at all points in both the saturated and unsaturated zones must be known. The saturated coefficient of permeability can be obtained using standard laboratory and field procedures. However, the direct measurement of the unsaturated permeability is often expensive and difficult to conduct. Considerable research has been done on evaluating the unsaturated permeability of a soil based upon its soil-water characteristic curve, which is relatively simple to obtain (Childs and Collis-George 1950; Marshall 1958; Green and Corey 1971; Elzefrawy and Cartwright 1981). It has been concluded that this method generally gives reliable predictions of experimentally measured permeability values.

The soil-water characteristic curve of a soil is of primary importance in understanding the transient flow of water in the unsaturated zone. The slope of the curve represents the storage characteristics of the soil (i.e., the m_2^w value in eq. [9]). The slope indicates the amount of water taken on or released by the soil as a result of a change in the pore-water pressure. The soil-water characteristic curve of a soil also provides a quantitative means of calculating the permeability function of the soil using procedures developed by Green and Corey (1971) and other researchers.

The soil-water characteristic curves and the calculated permeability functions as presented in Figs. 2 and 3 are typical for materials of different grain sizes. A coarser material (e.g., sand) will desaturate faster than a finer material (e.g., clay). Consequently, as anticipated, a sandy

Fig. 1. A saturated–unsaturated soil profile under hydrostatic conditions.



material will have a steeper permeability function than a clayey material.

General governing equation

Terzaghi’s (1943) one-dimensional consolidation theory for saturated soils introduced an approach to seepage problems that was particularly suitable to geotechnical engineering. The governing partial differential equation was derived by equating the net flow quantity from a soil element to the time derivative of the constitutive equation for the soil.

Fredlund and Morgenstern (1977) proposed the use of two independent stress state variables, $(\sigma - u_a)$ and $(u_a - u_w)$, to describe the state of stress for an unsaturated soil. Constitutive equations relating the volume change in the soil structure and fluid phases to stress state variable changes were also proposed (Fredlund and Morgenstern 1976).

The net flow through a two-dimensional element of unsaturated soil can be expressed as

$$[3] \quad \Delta q = \frac{\partial \theta_w}{\partial t} = -\frac{\partial}{\partial x} \left(k_x \frac{\partial h}{\partial x} \right) - \frac{\partial}{\partial y} \left(k_y \frac{\partial h}{\partial y} \right)$$

The constitutive equation for the water phase of an isotropic unsaturated soil is,

$$[4] \quad d\theta_w = m_1^w d(\sigma - u_a) + m_2^w d(u_a - u_w)$$

where:

- m_1^w = slope of the $(\sigma - u_a)$ versus θ_w plot when $d(u_a - u_w)$ is zero,
- m_2^w = slope of the $(u_a - u_w)$ versus θ_w plot when $d(\sigma - u_a)$ is zero,
- σ = total stress in the x - and (or) y -direction,
- u_a = pore-air pressure, and
- u_w = pore-water pressure.

Since m_1^w and m_2^w can be assumed to be constant for a particular time step during the transient process, the time derivative of the constitutive equation can be expressed as,

$$[5] \quad \frac{\partial \theta_w}{\partial t} = m_1^w \frac{\partial(\sigma - u_a)}{\partial t} + m_2^w \frac{\partial(u_a - u_w)}{\partial t}$$

Fig. 2. Soil-water characteristic curve for fine sand, silt and Regina clay.

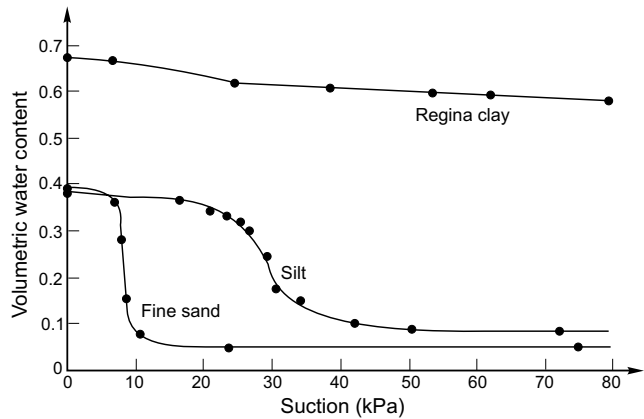
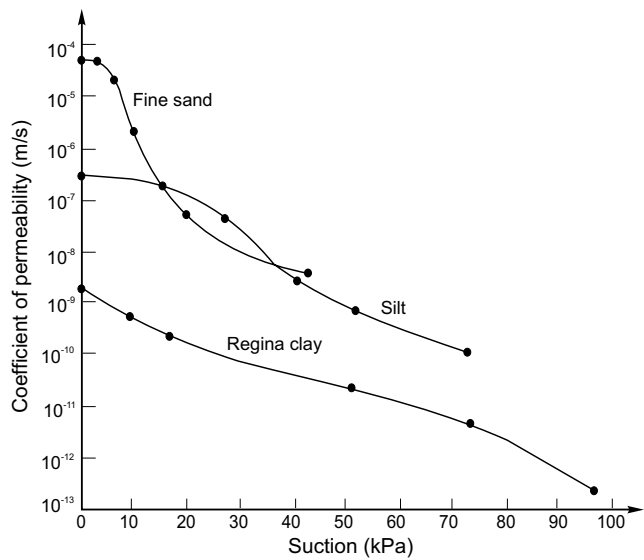


Fig. 3. Unsaturated permeability function of fine sand, silt and Regina clay.



Combining eqs. [3] and [5] gives,

$$[6] \quad -\frac{\partial}{\partial x} \left(k_x \frac{\partial h}{\partial x} \right) - \frac{\partial}{\partial y} \left(k_y \frac{\partial h}{\partial y} \right) = m_1^w \frac{\partial(\sigma - u_a)}{\partial t} + m_2^w \frac{\partial(u_a - u_w)}{\partial t}$$

If it is assumed that no external loads are added to the soil mass during the transient process, and that the air phase is continuous in the unsaturated zone (i.e., $\partial \sigma / \partial t = 0$ and $\partial u_a / \partial t = 0$), eq. [6] can be simplified as follows:

$$[7] \quad \frac{\partial}{\partial x} \left(k_x \frac{\partial h}{\partial x} \right) + \frac{\partial}{\partial y} \left(k_y \frac{\partial h}{\partial y} \right) = m_2^w \frac{\partial u_w}{\partial t}$$

Expressing the pore-water pressure term in eq. [7] in terms of total head, the governing differential equation for transient seepage can therefore be written as follows:

$$[8] \quad \frac{\partial}{\partial x} \left(k_x \frac{\partial h}{\partial x} \right) + \frac{\partial}{\partial y} \left(k_y \frac{\partial h}{\partial y} \right) = \rho_w g m_2^w \frac{\partial h}{\partial t}$$

After incorporating anisotropic soil conditions where the direction of the major coefficient of permeability is inclined at an arbitrary angle to the x -axis, eq. [8] becomes,

$$[9] \quad \frac{\partial}{\partial x} \left(k_{xx} \frac{\partial h}{\partial x} + k_{xy} \frac{\partial h}{\partial y} \right) + \frac{\partial}{\partial y} \left(k_{yx} \frac{\partial h}{\partial x} + k_{yy} \frac{\partial h}{\partial y} \right) = \rho_w g m_2^w \frac{\partial h}{\partial t}$$

where:

$$\begin{aligned} k_{xx} &= k_1 \cos^2 \alpha + k_2 \sin^2 \alpha, \\ k_{yy} &= k_1 \sin^2 \alpha + k_2 \cos^2 \alpha, \\ k_{xy} &= k_{yx} = (k_1 - k_2) \sin \alpha \cos \alpha, \\ k_1 &= \text{major coefficient of permeability,} \\ k_2 &= \text{minor coefficient of permeability, and} \\ \alpha &= \text{inclined angle between } k_1 \text{ and the } x\text{-axis.} \end{aligned}$$

The above governing partial differential flow equation (i.e., eq. [9]) has been developed in a manner most familiar to geotechnical engineers. The equation has been derived on the basis of unsaturated flow theory (Fredlund 1981) and can be used to describe continuous flow in saturated-unsaturated soil systems. The term m_2^w represents the rate at which a soil will absorb or release water when there is a change in matric suction. Figure 4 illustrates the variation in the value of the term m_2^w as the soil changes from saturated to unsaturated conditions. The value of m_2^w is equal to the slope of the soil-water characteristic curve. Under the assumptions of a constant total stress and a pore-air pressure equal to the pore-water pressure, m_2^w becomes equal to m_1^w in the saturated zone. The m_1^w value is equivalent to the coefficient of volume change, m_v , common to saturated soil mechanics.

Finite element formulation

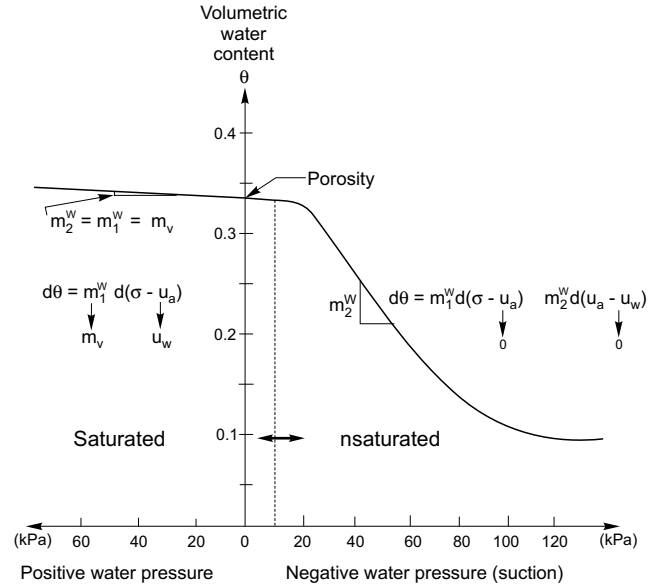
With the advance of high-speed digital computers, numerical methods provide practical solutions to complex seepage problems. The finite element method is the most powerful and widely used numerical method for two-dimensional problems. The following section presents the finite element formulation for the governing equation.

The Galerkin solution to eq. [9] is given by the following integrals over the area and boundary surface of a triangular element (Lam 1983):

$$[10] \quad \int_A [B]^T [K] [B] dA [h^n] + \int_A [L]^T \lambda [L] dA \frac{\partial [h^n]}{\partial t} - \int_S [L]^T q ds = 0$$

where:

Fig. 4. Soil-water characteristic curve and m_2^w for a saturated-unsaturated soil.



$$[B] = \frac{1}{2A} \begin{bmatrix} y_2 - y_3 & y_3 - y_1 & y_1 - y_2 \\ x_3 - x_2 & x_1 - x_3 & x_2 - x_1 \end{bmatrix}$$

with x_1, y_1 equal to the Cartesian coordinates of the nodes of the element;

$$[K] = \begin{bmatrix} k_{xx} & k_{xy} \\ k_{yx} & k_{yy} \end{bmatrix}$$

with $k_{xx}, k_{xy}, k_{yx}, k_{yy}$ equal to the components of the permeability tensor for the element;

$$[h^n] = \begin{bmatrix} h_1 \\ h_2 \\ h_3 \end{bmatrix}$$

with h_i equal to the total head at the element nodes;

$$[L]^T = [L_1, L_2, L_3]$$

with L_i equal to the area coordinates of the element;
 $\lambda = \rho_w g m_2^w$,
 q = flow across the perimeter of the element,
 A = area of the element,
 S = perimeter of the element, and
 t = time.

After numerical integration, eq. [10] can be simplified as follows:

$$[11] \quad [D][h^n] + [E][h^n] = [F]$$

where:

$$[D] = [B]^T [K] [B] A$$

is the stiffness matrix;

$$[E] = \frac{\lambda A}{12} \begin{bmatrix} 2 & 1 & 1 \\ 1 & 2 & 1 \\ 1 & 1 & 2 \end{bmatrix}$$

is the capacitance matrix;

$$[F] = \frac{ql}{2} \begin{bmatrix} 1 \\ 1 \\ 0 \end{bmatrix} \text{ or } \frac{ql}{2} \begin{bmatrix} 1 \\ 0 \\ 1 \end{bmatrix} \text{ or } \frac{ql}{2} \begin{bmatrix} 0 \\ 1 \\ 1 \end{bmatrix}$$

is the flux vector reflecting the boundary conditions;

$$[h^n]$$

is the time derivative of nodal total head.

For transient seepage, the time derivative of eq. [11] can be approximated by a finite difference procedure. Consequently, the relationship between the nodal heads of an element in two successive time steps can be expressed by the following equations:

$$[12] \quad \left([D] + \frac{2[E]}{\Delta t} \right) h^n_{t+\Delta t} = \left(\frac{2[E]}{\Delta t} - [D] \right) h^n_t - 2[F]$$

$$[13] \quad \left([D] + \frac{[E]}{\Delta t} \right) h^n_{t+\Delta t} = \frac{[E]}{\Delta t} h^n_t - [F]$$

Equation [12] is derived using the central difference approximation, and eq. [13] is derived using the backward difference approximation. Both of the above time approximations are considered to be unconditionally stable. Generally, solutions based on the central difference approximation are found to be more accurate than those of the backward difference approximation. However, the backward difference approximation is found to be more effective in dampening the numerical oscillations frequently encountered in highly non-linear flow systems, (Neuman and Witherspoon 1971; Neuman 1973).

After the matrices for each element are formed, the algebraic equations for the whole system can be constructed and solved for nodal total head. However, due to the non-linearity of the general seepage equation, an iterative procedure is required to obtain the correct nodal total heads. The iterative procedure involves a series of successive approximations. An initial estimate of the coefficient of permeability of an element is required in order to calculate a first approximation of the nodal total head. The computed nodal total head allows the calculation of the average pressure head of an element. Using the calculated average pressure heads and the input permeability function, an improved permeability value can be obtained for the element. The improved permeability value is used to compute a new set of nodal total heads. The procedure is repeated until both the total head and permeability differences for each element for two successive iterations are smaller than specified tolerances.

The convergency rate is highly dependent on the degree of non-linearity of the permeability function and the spatial discretization of the problem. A steep permeability

function requires more iterations and a larger convergency tolerance. A finer discretization in both element size and time step will assist in obtaining convergence faster with a smaller tolerance. Generally, the solution will converge to a tolerance of less than 1% in 10 iterations.

The seepage equation is considered solved for one time step once the converged nodal total heads of the system are obtained. Secondary quantities at a particular time step, such as pore-water pressure, gradients, velocities, and flux quantities, can then be calculated based on the nodal total heads. following equations apply:

The equation for nodal pore-water pressure,

$$[14] \quad [u_w]_t = ([h^n]_t - [z^n])\rho_w g$$

where :

$[z^n]$ = elevation at the nodes of the elements.

The equation for element gradient,

$$[15] \quad \begin{bmatrix} i_x \\ i_y \end{bmatrix}_t = [B][h^n]_t$$

The equation for element velocity,

$$[16] \quad \begin{bmatrix} v_x \\ v_y \end{bmatrix}_t = [K]_t [B][h^n]_t$$

The equation for flux,

$$[17] \quad [q_{ij}]_t = [D]_t (h_j^n - h_i^n)_t$$

where:

$[q_{ij}]_t$ = flux quantity to node i contributed from node j .

Implementation model, TRASEE

The finite element solution has been implemented into a computer program called TRASEE (Lam 1984). The computer facility used is a DIGITAL VAX 11/780 system in the College of Engineering, University of Saskatchewan, Saskatoon.

The implemented two-dimensional program can model both transient and steady state seepage through saturated-unsaturated soil systems. It can accommodate complex geometries with arbitrary degrees of heterogeneity and anisotropy for 20 different soils. A discretized soil system of up to 1500 elements and 1000 nodes can be modeled. Three iterative techniques, including the Secant method, have also been incorporated to ensure convergence for highly non-linear flow systems. Changing boundary conditions during a transient process can be accommodated by a prescribed step function. Special procedures are also included to automatically revise the boundary conditions along seepage faces and ponding surfaces. Flux quantities through any specified section of the flow system can be calculated. Furthermore, an auxiliary plotting and contouring program has also been developed for the presentation of computed results.

Table 1. Some transient seepage example problems modeled by TRASEE.

Problem	Remark [†]
Earth dam	With a horizontal drain With an impervious lower boundary* With a center core of lower permeability With anisotropic soil conditions With infiltration at dam surface Reservoir level increased at a constant rate Instantaneous reservoir drawdown
Lagoon	No anisotropy in the soil With anisotropy, $\alpha = -30^\circ$ *
Hill slope	Homogeneous, infiltration and evapotranspiration Heterogeneous, infiltration and evapotranspiration
Sandbox model, Rulon and Freeze (1985)	With a horizontal layer of lower permeability, transient seepage with infiltration*

*Example problem presented in this paper.

[†]Reference: Lam (1983).

Example problems

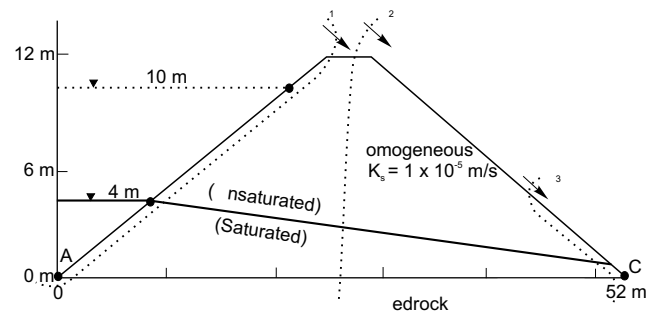
The developed program has been used to solve a wide variety of transient seepage problems (Table 1). In this paper, results of three example problems are presented.

The basic information required for a finite element seepage analysis are the definition of the flow regime, which includes the spatial dimensions of the material boundaries, the definition of the boundary conditions, and the definition of material parameters. Subsurface investigation will be required to delineate the different material strata and the lowest boundary of the flow regime. Piezometric records and hydrological data are used to define the boundary conditions. In most cases, *in situ* or laboratory permeability tests, laboratory evaluation of the soil-water characteristic curves of the unsaturated materials, and the calculations of unsaturated permeability functions are required. In some cases, a knowledge of the soil types, typical soil-water characteristic curves, and permeability functions can be used.

The first example, Example 1, illustrates transient seepage through a homogeneous earth dam with an impervious lower boundary (Fig. 5). An analytical solution to this problem has been attempted by Brahma and Harr (1962). Their solution was based on the assumption that the free surface is the uppermost flow line. Later studies (Freeze 1971b; Papagianakis and Fredlund 1984) have shown that the free surface is a specific isobar in the pressure head field, which is a component of the hydraulic head field that controls the flow of water in both the saturated and unsaturated zones. When solving this problem using the developed saturated–unsaturated model, no assumption is required regarding the free surface. Therefore, the actual external soil boundaries can be used in the analysis.

Figure 5 shows the geometry and boundary conditions for the problem. The material is assumed to be sandy soil with a saturated coefficient of permeability of 1×10^{-5} m/s, and a m_2^w value of 0.0001 m²/kN. To better illustrate the flow in the unsaturated zone, a moderately steep permeability function (i.e., a decrease of 1 order of

Fig. 5. Geometry and boundary conditions for Example 1, with seepage through an earth dam.



magnitude in permeability for every 5 m of negative pressure head) was assumed. Initially, the dam is at steady state conditions with the reservoir water level 4 m above datum. At time equal to zero, the water level is instantaneously raised to a level of 10 m. The water level remains constant at 10 m during the transient process.

Figure 6 illustrates the transient positions of the phreatic line as it advances from its initial steady state condition to a final steady state condition. Figures 7 and 8 present the computed results at times equal to 14, 107, 330, and 1007 min. Both the nodal total head plot and seepage velocity vector plot are presented for each time step.

The increase in reservoir level on the upstream face of the earth dam causes an increase in pore-water pressure with time. The change in pore-water pressure can be visualized by the changing position of the phreatic line and the equipotential lines at different times. The equipotential lines extend through the unsaturated zone as shown in Figs. 7 and 8, illustrating the presence of a hydraulic gradient and consequently water flow in the unsaturated zone. The fact that the phreatic line is not a flow line is confirmed by the seepage velocity vector plots. Figures 7 and 8 indicate that there is considerable flow across the phreatic line. These phenomena agree with the solution by Freeze (1971b).

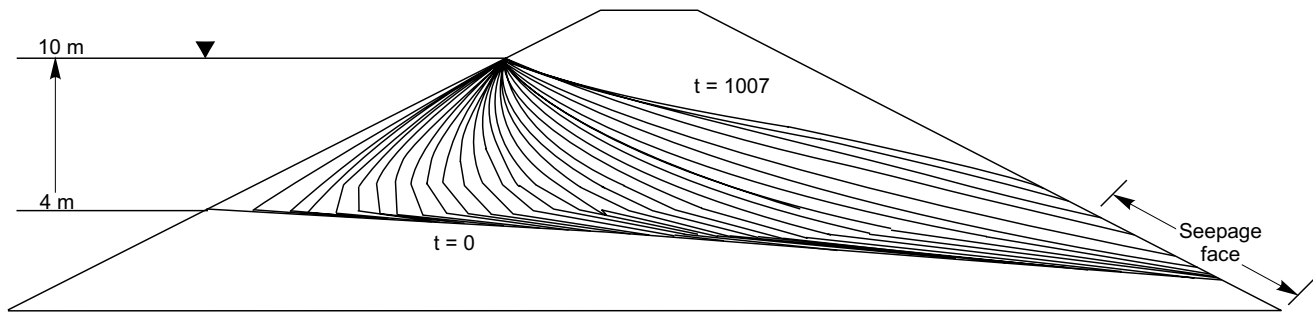
Fig. 6. Transient position of phreatic line from $t = 0$ to $t = 1007$ min.

Figure 9 shows the computed flux quantities Q_1 , Q_2 , and Q_3 through three sections (Fig. 6) of the earth dam during the transient process. Initially, the steady state flow quantity was equal to 3×10^{-6} ($\text{m}^3 \cdot \text{s}^{-1}$)/m as shown by Q_1 , Q_2 , and Q_3 . At times greater than zero, Q_1 increased rapidly to 3.5×10^{-4} ($\text{m}^3 \cdot \text{s}^{-1}$)/m due to the instantaneous increase in the reservoir level. The quantity Q_1 then decreased gradually with time to a final steady state flux; Q_2 increased gradually to 3×10^{-5} ($\text{m}^3 \cdot \text{s}^{-1}$)/m after 16 time steps and then decreased to a final steady state flux; Q_3 had no increase in flux during the early stages of the transient process, but after 10 time steps, began to increase gradually to the final steady state flux quantity.

In this example, final steady state conditions were achieved after 32 time steps or an elapsed time of 1007 min. The computed flux quantity at final steady state conditions was 1.7×10^{-5} ($\text{m}^3 \cdot \text{s}^{-1}$)/m. Using the flownet technique, a flux of approximately 1.3×10^{-5} ($\text{m}^3 \cdot \text{s}^{-1}$)/m was obtained. The difference in the two quantities is primarily due to the water flow through the unsaturated zone as computed by TRASEE. Unsaturated flow is not considered when using the flownet technique. The use of a steeper permeability function will allow less water flow in the unsaturated zone, and the computed result will be closer to the flownet solution (Lam 1983). The computed length of the seepage face above the downstream toe was 8.9 m. The flownet solution gave a length of 6.5 m. When a steep permeability function is used, the computed length of the seepage face is reduced to 6.7 m. Consequently, the flownet solution or the saturated-only model can be approximated as a special case of the saturated-unsaturated flow model.

The final steady state seepage condition achieved after 1007 min was also compared with the solution obtained from the steady state model called SEEP (Papagianakis and Fredlund 1984). The two models give almost identical solutions.

The second example, Example 2, illustrates transient groundwater seepage beneath a lagoon. Figure 10 illustrates the geometry and the boundary conditions of the problem. The material is to be anisotropic with the major coefficient of permeability 10 times larger than the minor coefficient of permeability. The direction of the major coefficient of permeability is at an angle of -30° with the horizontal. The major coefficient of permeability of the

soil at saturation was assumed to be 1×10^{-5} m/s. A 1 m thick liner was constructed on the bottom of the pond. The liner is assumed to be isotropic with a saturated coefficient of permeability equal to 1×10^{-6} m/s. The permeability function and m_2^w value used in example 1 are also used in this example.

An initial steady state condition with a water table located at 6.0 m below the ground surface was assumed. No flow conditions are assumed at the ground surface and the bottom boundary of the section. Furthermore, a hydrostatic condition was assumed to exist at both the left and right boundaries. At time equal to zero, the lagoon was filled with water. This provided a water head of 1.0 m.

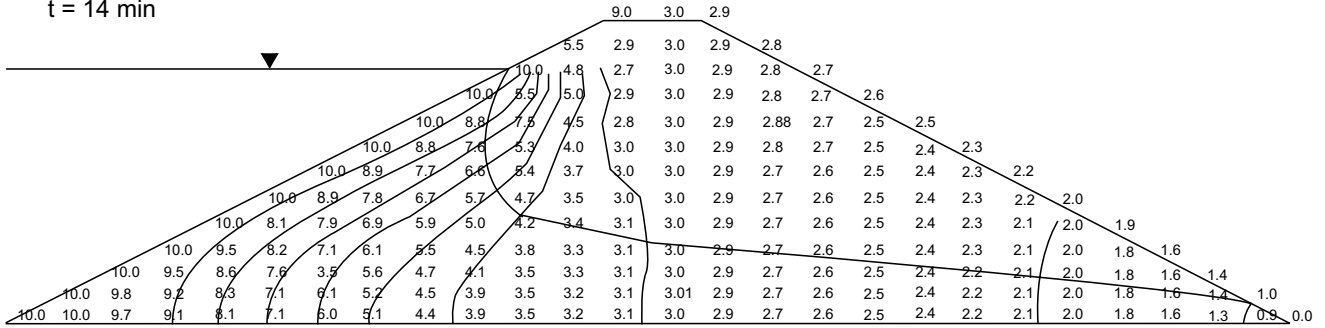
Figure 11 illustrates the transient position of the water table as seepage occurs from the lagoon. Figures 12 and 13 present solutions at different times. Both the pore-water pressure head and seepage velocity vector plots are presented. The contours show various pore-water pressure isobars.

It is difficult to visualize Example 2 as a conventional saturated-only analysis. In the early stages of the transient process (Fig. 12a), water flows in the unsaturated zone only and the water table is unaffected. After 66.5 min, water from the lagoon reaches the water table, which begins to mound towards the lagoon (Figs. 12b and 13a). The groundwater mound builds up to the point where the seepage from the lagoon is balanced by the seepage leaving the left and right boundaries. In this example, the new steady state condition was achieved after 1316 min (Fig. 13b). If more water would enter the flow system from the lagoon, the groundwater mound would build up higher and eventually come in contact with the lagoon (Lam 1983). The transient solution of Example 2 compares satisfactorily with the transient processes described by McWhorter and Nelson (1979).

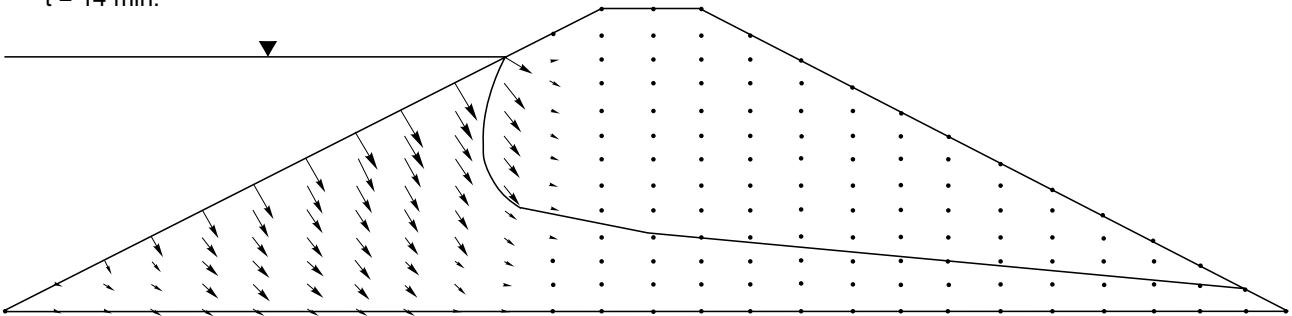
The effect of material anisotropy can be visualized from the seepage velocity vectors (Figs. 12 and 13). Under isotropic soil conditions, the flow system is symmetric with respect to the center line of the section. However, when the soil conditions are anisotropic, water flows along the axis of the major coefficient of permeability, causing an unsymmetric groundwater mound. Although the same boundary conditions are specified in both the left and right boundaries, water discharging from the right

Fig. 7. Nodal total head and velocity vector plots at $t = 14$ and 107 min.

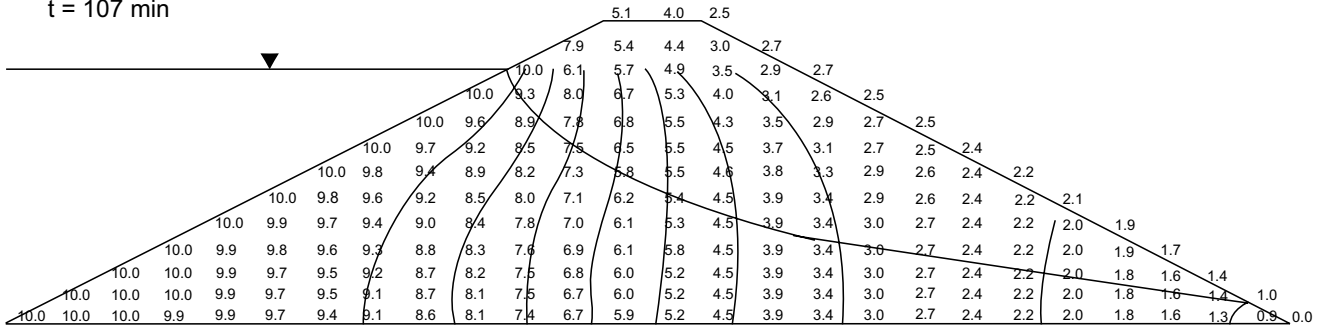
a) Nodal total head
 $t = 14$ min



b) Seepage velocity vector
 $t = 14$ min.



c) Nodal total head
 $t = 107$ min



d) Seepage velocity vector
 $t = 107$ min.

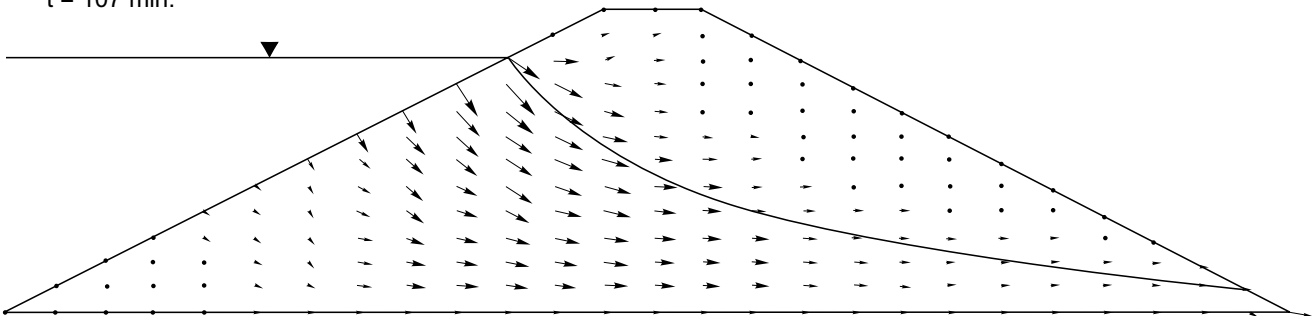
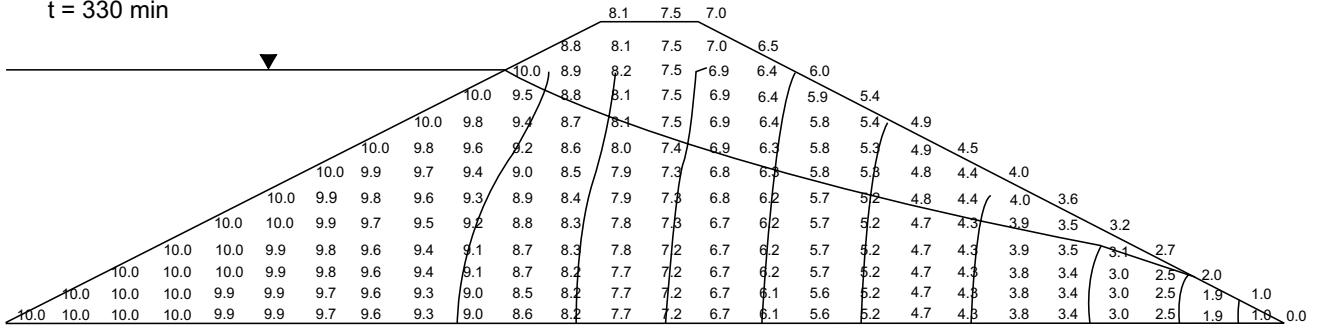
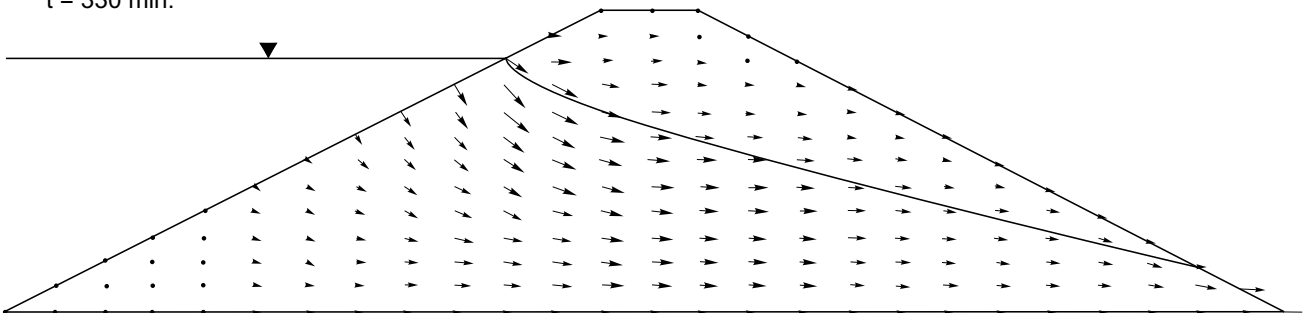


Fig. 8. Nodal total head and velocity vector plots at $t = 330$ and 1007 min.

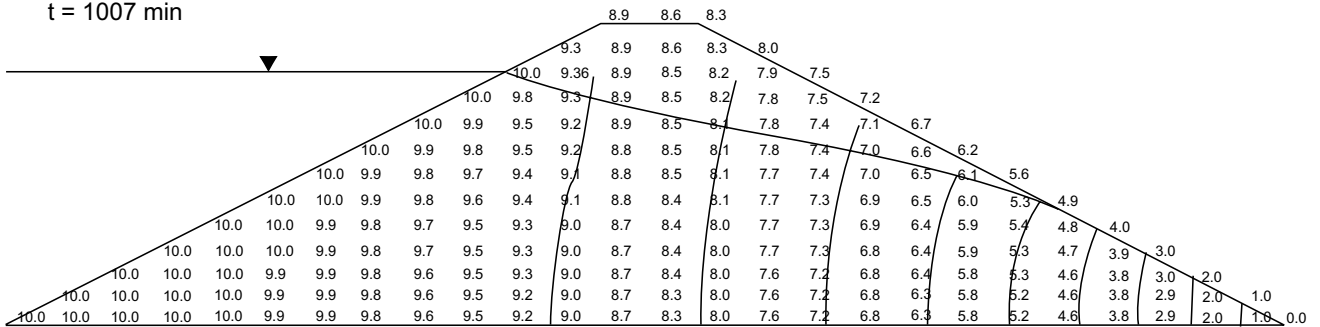
a) Nodal total head
 $t = 330$ min



b) Seepage velocity vector
 $t = 330$ min.



c) Nodal total head
 $t = 1007$ min



d) Seepage velocity vector
 $t = 1007$ min.

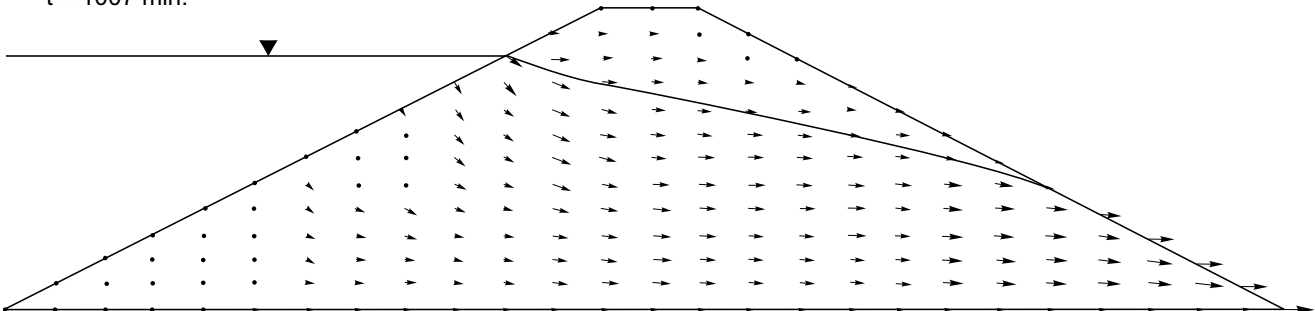


Fig. 9. Computed flux quantity at different time steps.

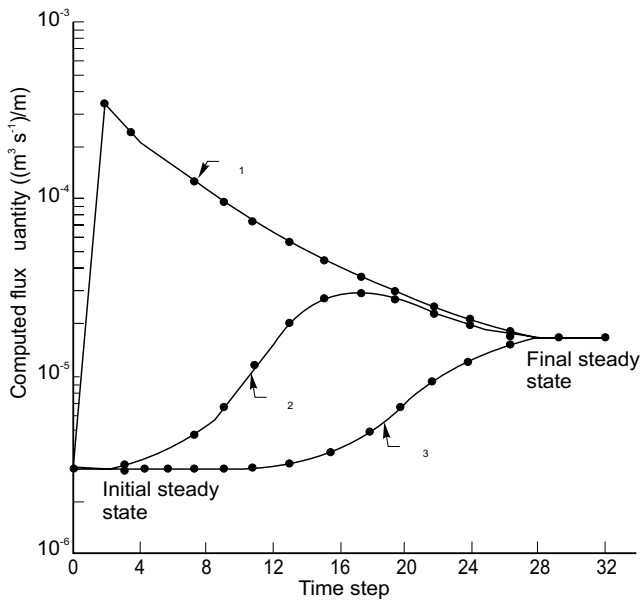
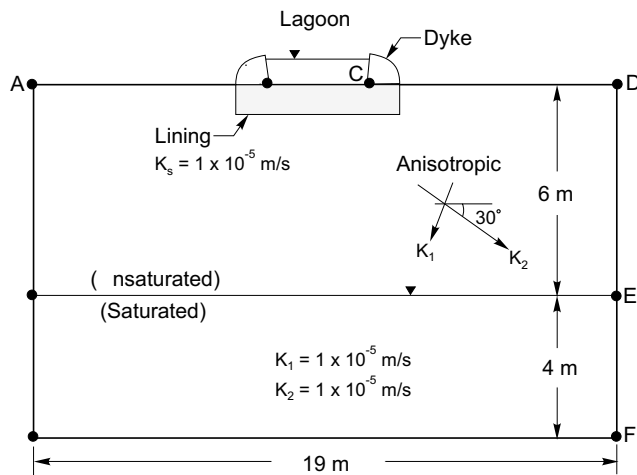


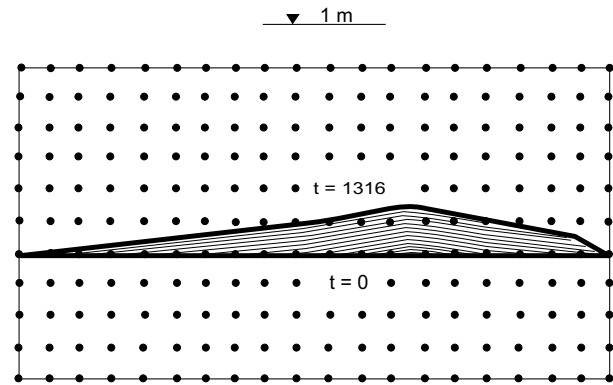
Fig. 10. Geometry and boundary conditions of Example 2, with seepage under a lagoon.



boundary is substantially higher than that from the left boundary because of anisotropy.

Rulon and Freeze (1985) studied the steady state seepage of a layered hill slope under constant infiltration conditions. A sandbox model of the layered hill slope was constructed and elaborately monitored. The sandbox model was composed of medium sand, within which there was a horizontal layer of fine sand. The fine sand was to impede flow and create a seepage face on the slope. A constant infiltration was imposed on the top portion of the hill slope. The observed results were then calibrated using Neuman's finite element model called UNSAT 1. The calibrated permeability values were 1.4×10^{-3} m/s for the medium sand and 5.5×10^{-5} m/s for the fine sand. The calibrated material permeabilities and an infiltration rate of 2.1×10^{-4} m/s produced a close com-

Fig. 11. Transient position of water table from $t = 0$ to $t = 1316$ min.



parison between the observed measurement and the results predicted by UNSAT 1 (Fig. 14).

The third example, Example 3, simulates the same layered hill slope problem using the developed model. Instead of solving only the steady state condition, the transient solution of the hill slope under infiltration was simulated. Figure 15 depicts the geometry and the boundary conditions of the sandbox model. The same permeability values and infiltration rate obtained by Rulon and Freeze (1985) were used in the transient simulation. An m_2^w value of $0.0005 \text{ m}^2/\text{kN}$ as estimated from the soil-water characteristic curve was used to represent the storage characteristic of the soils. An initial steady state condition was assumed with the water table located at 0.3 m. At time equal to zero, a constant infiltration rate was imposed on the top portion of the hill slope.

Figure 16 illustrates the development of the water table from its initial steady state condition to its final steady state condition. Figures 17 and 18 present the seepage velocity vector plots at various times after infiltration commenced.

The results indicate that the presence of the impeding layer creates a complex configuration to the position of the water table and the equipotential lines. At a time equal to 1 s, water infiltrates vertically toward the impeding layer, and the water table is essentially unaffected (Fig. 17a). The water table begins to rise at 2 s after infiltration commences (Fig. 17b). A perched water table on the impeding layer occurs at a time equal to 10 s (Fig 18a). At a time equal to 12 s, part of the impeding layer is saturated and a wedge-shaped unsaturated zone is formed (Fig. 18b). After 16 s, two seepage faces develop, one near the toe of the hill slope, the other just above the impeding layer (Fig. 18c). Finally, at 30 s, a steady state condition is achieved (Fig. 18d).

The computed final steady state results (Fig. 18d) are compared with the steady state results (Fig. 14) presented by Rulon and Freeze (1985). A close agreement between the two sets of results can be observed. The water table position and the developed seepage faces in both figures are almost identical. In other words, the numerical result computed using TRASEE compared closely with the nu-

Fig. 12. Nodal water pressure head and velocity vector plots at $t = 22.5$ and 66.5 min.

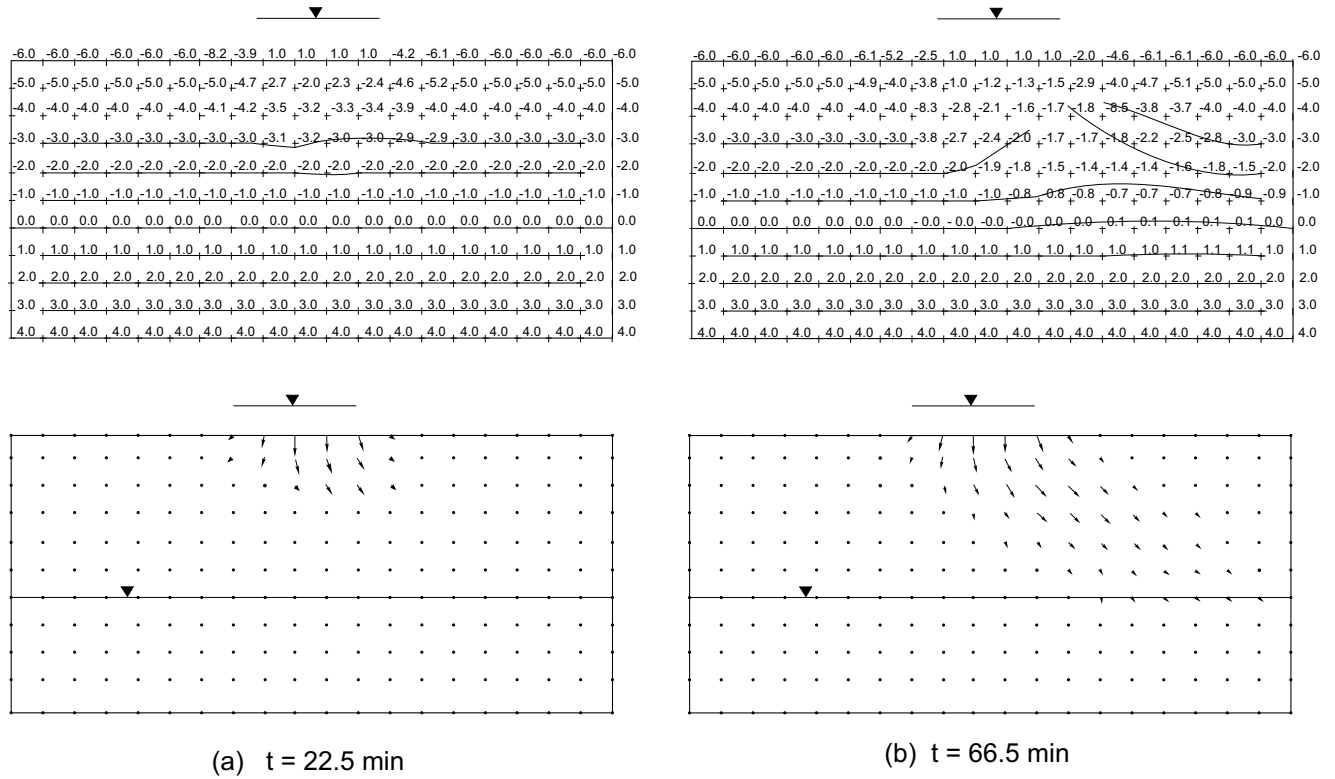


Fig. 13. Nodal water pressure head and velocity vector plots at $t = 174$ and 1316 min.

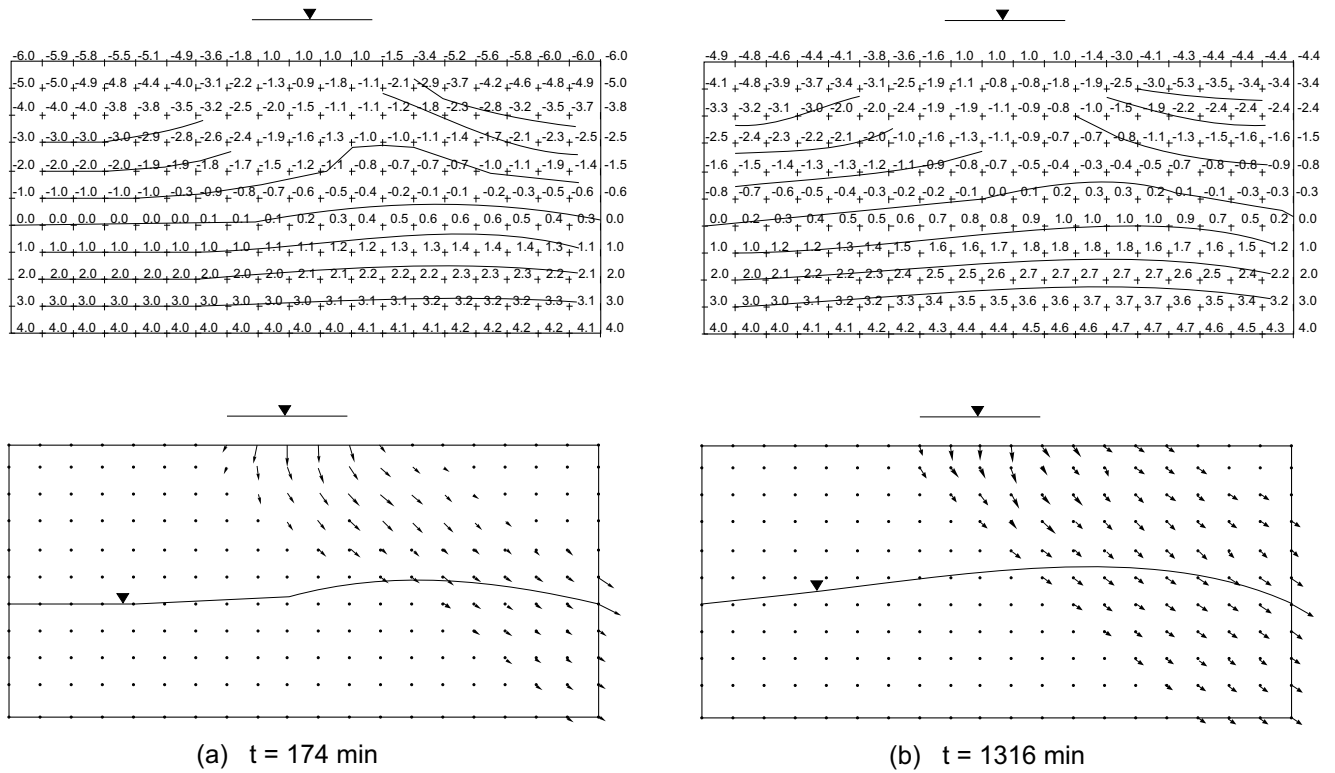
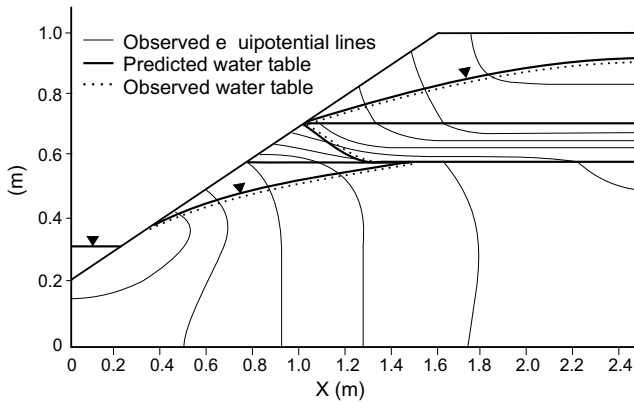


Fig. 14. Comparison of observed water table configuration in experimental sand tank with that predicted by Neuman's model, UNSAT 1 (after Rulon and Freeze 1985).



merical result computed using the UNSAT 1 model and the experimental result obtained by Rulon and Freeze (1985).

The developed model TRASEE is fundamentally different than the model UNSAT 1. UNSAT 1 seeks a solution in terms of pressure head. The governing partial differential equation is derived using a soil science approach. The storage characteristics of a material was expressed in terms of specific storage, S_s , and specific moisture capacity, C . TRASEE, however, seeks a solution in terms of total head, the governing partial differential equation is derived using a soil mechanics approach, and the storage characteristic of the material is expressed in terms of the water coefficient of volume change, m_2^w , as defined by Fredlund and Morgenstern (1976). Consequently, the transient solutions as predicted by the two models may be different; however, the steady state solutions should be the same.

Example 3 is also a class of seepage problem to which it is difficult to apply conventional saturated-only methods of analysis. The computed seepage velocity vectors indicate that water flows primarily in the unsaturated zone in the early stage of the infiltration process. Flow systems such as the above example can be complex depending on the position of the impeding layer and the permeability contrast between the soils. Features such as a perched water table, wedge-shaped unsaturated zones, and multiple seepage faces are difficult to handle without using a general saturated–unsaturated numerical model.

Conclusions and applications

The proposed finite element model offers a versatile tool for the analysis of a wide variety of seepage problems. Since water flow in both the saturated and unsaturated zones is considered there is no assumption required with respect to the phreatic line in unconfined seepage problems. Results from the examples indicate that the phreatic line is not a flow line since there can be considerable water flow across the phreatic line. Furthermore, the quantity of water flow in the unsaturated zone may be

Fig. 15. Geometry and boundary conditions of Example 3, with seepage in a layered hill slope.

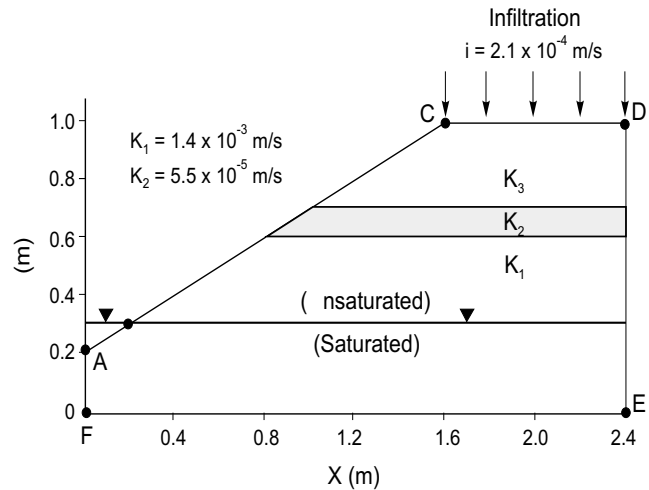
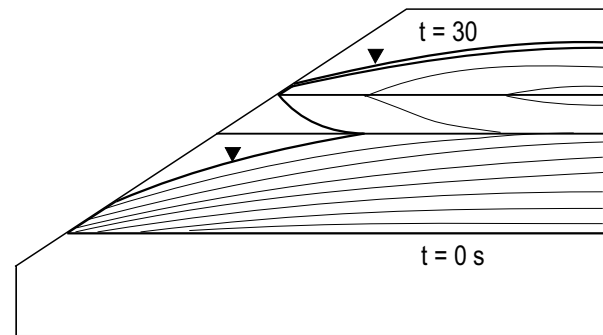


Fig. 16. Transient position of water table from $t = 0$ to $t = 30$ s.



substantial and failure to include the unsaturated zone may lead to unrealistic results.

Casagrande's flownet solution and the traditional saturated only flow models are shown to be a special case of the saturated–unsaturated flow model. The saturated–unsaturated model provides a more realistic and comprehensive representation of actual conditions. It can also be applied to a much wider range of engineering problems.

The computed results can be particularly valuable to practicing geotechnical engineers. The computed pore-water pressures throughout the flow region can be used to better understand the stress state in the soil. The stresses can then be applied in designs and analyses such as slope stability analyses. saturated–unsaturated flow models can also be of value in the design of dams and storage lagoons. The computed flow gradients in a region allow the calculation of critical points where gradients may be excessive. The computed seepage flux through a section is also of value in the designs of engineering structures such as drains, cut-offs, and liners. The defined seepage velocities throughout the region permit the determination of critical flow paths and serve as input to contaminant transport modelling (Lam and Barbour 1985).

Fig. 17. Velocity vector plots at $t = 1, 2, 5,$ and 8 s.

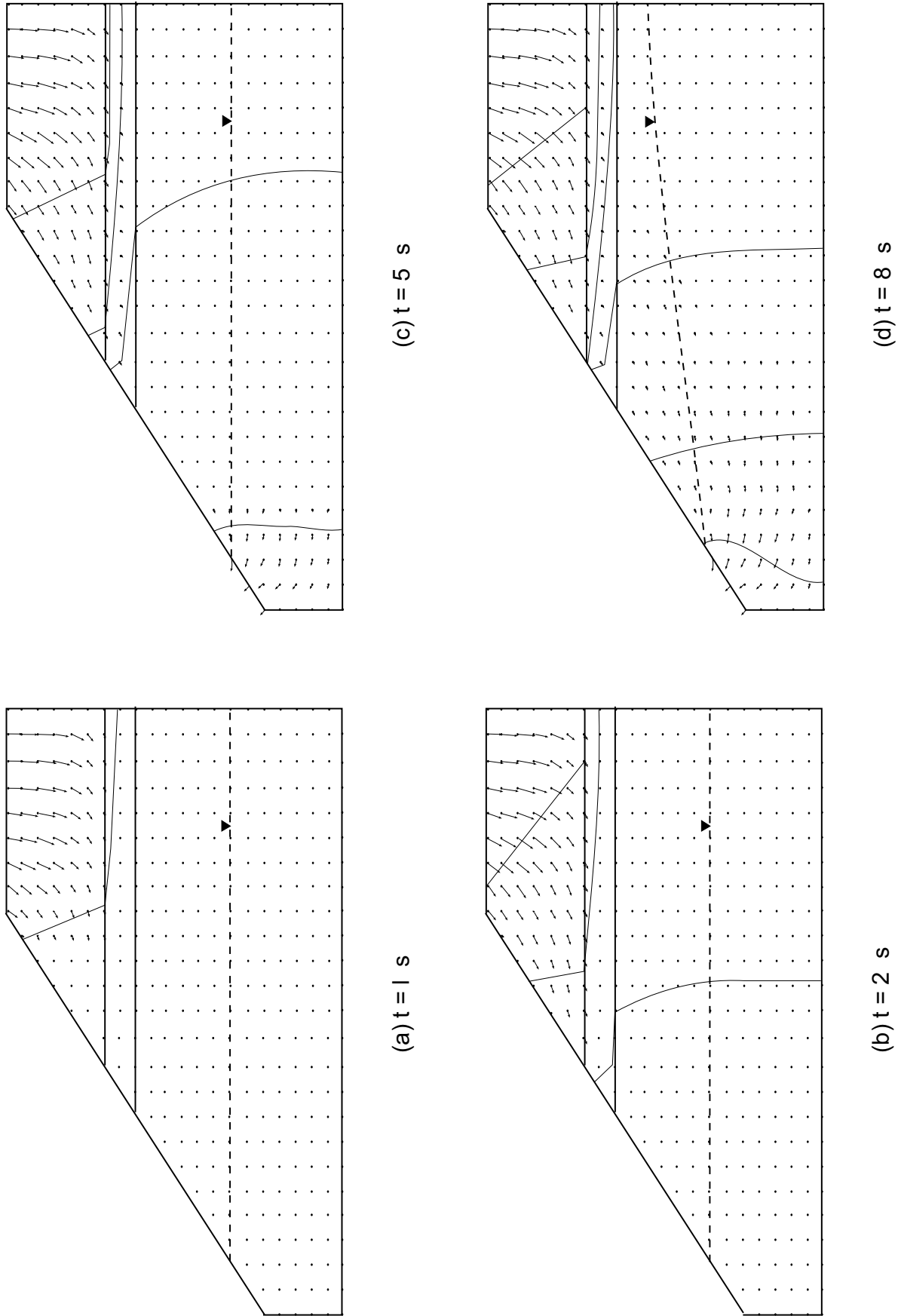
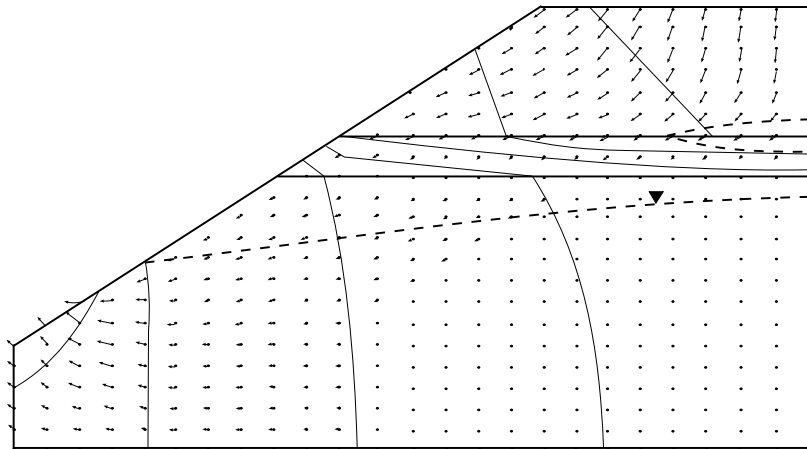
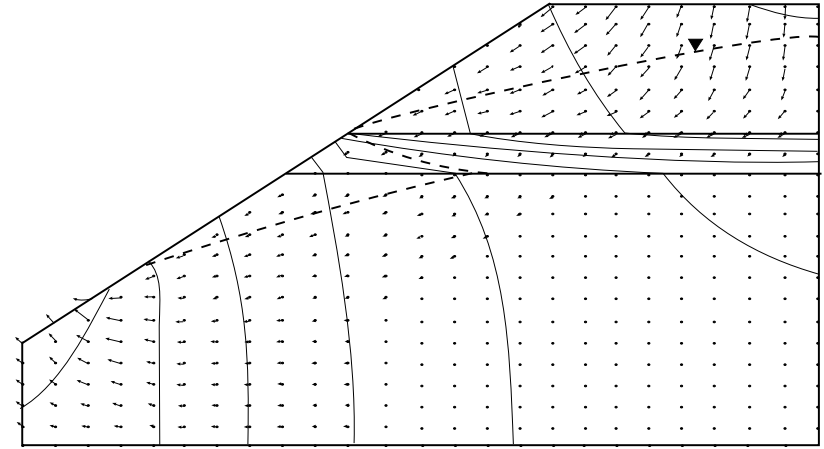


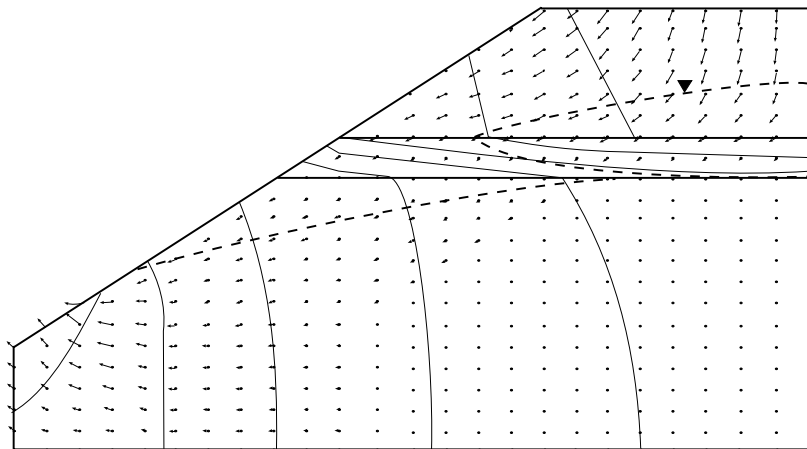
Fig. 18. Velocity vector plots at $t = 10, 12, 16,$ and 20 s.



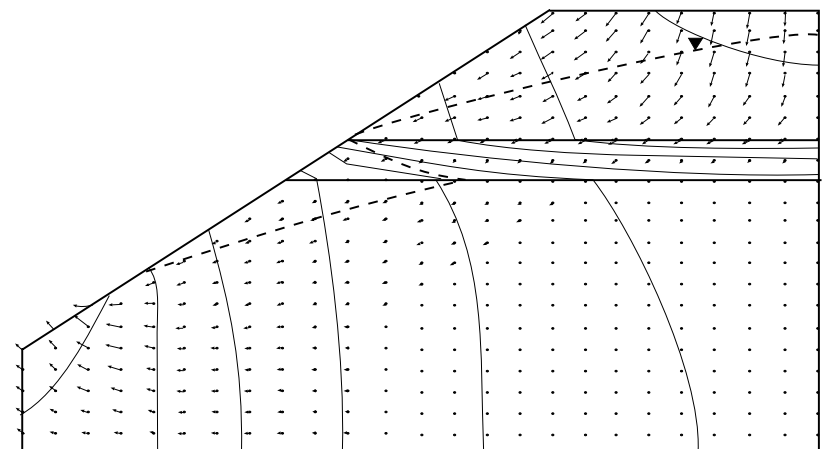
(a) $t = 10$ s



(c) $t = 16$ s



(b) $t = 12$ s



(d) $t = 30$ s

References

- Brahma, S.P., and Harr, M.E. 1962. Transient development of the free surface in a homogeneous earth dam. *Géotechnique*, **12**: 283–302.
- Casagrande, A. 1937. Seepage through dams. *New England Water Works*, **51**(2): 131–172.
- Childs, E.C., and Collis-George, N. 1950. The permeability of porous materials. *Proceedings of the Royal Society of London*, **201**: 392–405.
- Elzefrawy, A., and Cartwright, K. 1981. Evaluating the saturated and unsaturated hydraulic conductivity of soils. *In Permeability and groundwater contaminant transport. Edited by T.F. Zimmie, and C.D. Riggs. American Society for Testing and Materials, Special Technical Publication 146*, pp. 168–181.
- Fredlund, D.G. 1981. Seepage in saturated soils. Panel discussion: Groundwater and seepage problems. *Proceedings, 10th International Conference on Soil Mechanics and Foundation Engineering, Stockholm, Sweden, Vol. 4*, pp. 629–641.
- Fredlund, D.G., and Morgenstern, N.R. 1976. Constitutive relations for volume change in unsaturated soils. *Canadian Geotechnical Journal*, **13**: 261–276.
- Fredlund, D.G., and Morgenstern, N.R. 1977. Stress state variables for unsaturated soils. *ASCE Journal of the Geotechnical Engineering Division*, **103**(GT5): 447–466.
- Freeze, R.A. 1971*a*. Three dimensional transient saturated flow in a groundwater basin. *Water Resources Research*, **7**: 347–366.
- Freeze, R.A. 1971*b*. Influence of the unsaturated flow domain on seepage through earth dams. *Water Resources Research*, **7**(4): 929–940.
- Freeze, R.A., and Cherry, J.A. 1979. *Groundwater*. Prentice Hall, Englewood Cliffs, NJ.
- Green, R.E., and Corey, J.C. 1971. Calculation of hydraulic conductivity: A further evaluation of some predictive methods. *Soil Science Society of America Proceedings*, **35**: 3–8.
- Ho, P.G. 1979. The prediction of hydraulic conductivity from soil moisture suction relationship. B.Sc. thesis, University of Saskatchewan, Saskatoon, SK, Canada.
- Lam, L. 1983. Saturated–unsaturated transient finite element seepage model. M.Sc. thesis, University of Saskatchewan, Saskatoon, SK, Canada.
- Lam, L. 1984. Transient finite element seepage program, TRASEE, Users manual, CD-18, University of Saskatchewan, Saskatoon, SK, Canada.
- Lam, L., and Barbour, S.L. 1985. Saturated–unsaturated mass transport modelling by finite element method. *Proceedings, 7th Symposium on Management of Uranium Mill Tailings. Low-Level Waste and Hazardous Waste, Colorado State University, Fort Collins, CO*, pp. 431–440.
- Marshall, T.J. 1958. A relation between permeability and size distribution of pores. *Journal of Soil Science*, **9**: 1–8.
- McWhorter, D.B., and Nelson, J.O. 1979. Unsaturated flow beneath tailings impoundments, *ASCE Journal of the Geotechnical Engineering Division*, **105**(GT11): 1317–1334.
- Neuman, S.P. 1973. Saturated–unsaturated seepage by finite elements. *ASCE Journal of the Hydraulics Division*, **99**(HY12): 2233–2250.
- Neuman, S.P. and Witherspoon, P.A. 1971. Analysis of non-steady flow with a free surface using the finite element method. *Water Resources Research*, **7**: 611–623.
- Papagianakis, A.T. and Fredlund, D.G. 1984. A steady state model for flow in saturated–unsaturated soils. *Canadian Geotechnical Journal*, **21**: 419–430.
- Richards, L.A. 1931. Capillary conduction of liquids through porous mediums. *Physics (New York)*, **1**: 318–333.
- Rulon, J.J., and Freeze, R.A. 1985. Multiple seepage faces on layered slopes and their implications for slope-stability analysis. *Canadian Geotechnical Journal*, **22**: 347–356.
- Taylor, R.L., and Brown, C.B. 1967. Darcy flow with a free surface. *ASCE Journal of the Hydraulics Division*, **93**(HY2): 25–33.
- Terzaghi, K. 1943. *Theoretical soil mechanics*. John Wiley and Sons, New York, NY.

Effect of rainfall on matric suctions in a residual soil slope

T.T. Lim, H. Rahardjo, M.F. Chang, and D.G. Fredlund

Abstract: A slope stability study involving shallow slip surfaces should include the effect of negative pore-water pressures in a slope. A field instrumentation program was carried out to monitor negative pore-water pressure (i.e., *in situ* matric suction) in a residual soil slope in Singapore. Variations in matric suction and the matric suction profiles under: (1) a canvas-covered grassed surface, (2) a grassed surface, and (3) a bare ground surface, in response to rainfalls were investigated. Changes in matric suction due to changes in climatic conditions decrease rapidly with depth. The changes were found to be most significant in the bare slope and least significant under the canvas-covered slope. The amount of decrease in matric suction after a rainstorm was observed to be a function of the initial matric suction just prior to the rainstorm. Positive pore-water pressures were observed above the groundwater table, suggesting the development of a perched water table within the slope. These observations are also typical of other regions experiencing high seasonal rainfalls. The field monitoring program presented can be adopted for investigating rainfall-induced landslides in other parts of the world.

Key words: Matric suction, negative pore-water pressure, field instrumentation, rainfall, residual soil, slope stability.

Introduction

Slope stability problems in residual soils are receiving increasing attention. The occurrence of landslides in residual soil slopes is attributed to many factors. Rainfall has been considered to be the cause of the majority of landslides that occur in regions experiencing high seasonal rainfalls (Brand 1984). Most of the rainfall-induced landslides in residual soils consist of relatively shallow slips above the groundwater table.

The pore-water pressure in residual soil slopes is usually negative relative to atmospheric conditions during dry periods. The negative pore-water pressure, u_w , or matric suction when referenced to the pore-air pressure, u_a , (i.e., $(u_a - u_w)$), has been found to play a significant role in the stability of soil slopes.

Methods for computing the factor of safety of a slope with negative pore-water pressures have been illustrated by Fredlund and Rahardjo (1993). The application of these methods requires an understanding of the contribution of negative pore-water pressures to the shear strength of the soil and the variation of the *in situ* matric suction profiles with time in a soil slope.

Examples of simplified stability analyses for slopes involving negative pore-water pressures have illustrated the

effect of matric suction on the computed factor of safety (Rahardjo et al. 1995). It is important to study, through field measurements, the variation of *in situ* matric suction profiles with changes in the climatic condition.

This paper presents the results of matric suction monitoring in an instrumented slope in the residual soil of the sedimentary Jurong Formation in Singapore. The effect of rainfall on the matric suction in the slope is emphasized. Matric suction changes as observed under a canvas-over-grass surface, a grassed surface, and a bare ground surface provide useful information on maintaining the stability of slopes.

Literature review

Experimental results by Lumb (1962) have shown that changes in the *in situ* pore-water pressures as a result of infiltration are dependent on the duration and intensity of the rainfall, the soil properties, and the slope morphology. Equations presented by Lumb (1962) for the prediction of pore-water pressures are frequently used in slope designs in Hong Kong. The application of Lumb's equations requires the determination of the initial and final degrees of saturation; variables that are difficult to assess (Brand 1984). There is a need for a reliable and direct method for predicting and measuring *in situ* matric suctions. The method must be verified through field measurement techniques.

Field monitoring of *in situ* matric suction in slopes has been conducted by a number of researchers (Chipp et al. 1982; Sweeney 1982; Krahn et al. 1989; Macari et al. 1992; Affendi and Faisal 1994). Tensiometers are commonly used in the field instrumentation to measure matric suction in the soil, as long as the suctions are less than

T.T. Lim, H. Rahardjo, and M.F. Chang. School of Civil and Structural Engineering, Nanyang Technological University, Nanyang Ave., Singapore 2263.

D.G. Fredlund. Professor, Department of Civil Engineering, University of Saskatchewan, 57 Campus Drive, Saskatoon, SK, Canada S7N 5A9.

Reproduced with permission from the *Canadian Geotechnical Journal*, 33: 618–628, 1996.

100 kPa. In general, the fluctuation of matric suction in a slope in response to seasonal changes has been found to be less pronounced as the depth increases.

Small-scale hydrologic field studies have been initiated at the NASA Marshall Space Flight Center to study the spatial and temporal variability of surface and subsurface hydrologic processes (such as soil moisture distribution), particularly as influenced by vegetation (Macari et al. 1992). Examples showing the rate of flux exchange and the spatial variability of hydrologic parameters in the field have been presented. However, it appears that no attempt has yet been made to monitor and compare the variations of *in situ* matric suctions under different surface conditions for a particular slope morphology.

Engineering characteristics of the residual soil from the sedimentary Jurong Formation

The residual soil of the sedimentary Jurong Formation consists of materials ranging from silty clay and clayey silt to clayey sand. The liquid limits of the residual soil are between 30% and 60%, while the plastic limits are between 15% and 30%. The water content and the plasticity index generally decrease with depth. The fines content (i.e., percent finer than U.S. No. 200 sieve size) for the fine-grained residual soils ranges from 50% to 85%. The total density and dry density increase marginally with depth, with an average value of 2.05 Mg/m³ and 1.67 Mg/m³, respectively. The specific gravity of the soil averages 2.68 (Lim 1995).

Rahardjo et al. (1995) investigated the shear strength characteristics of the residual soil from the Jurong Formation using multistage, consolidated drained triaxial tests. Figure 1 shows that the fine-grained residual soils from the Jurong Formation have an average effective cohesion, c' , of 30 kPa. The effective angle of internal friction, ϕ' , has an average value of 26°. The angle associated with the matric suction, ϕ^b , also has an average value of 26° for matric suctions below 400 kPa. For matric suctions greater than 400 kPa, the ϕ^b angle appears to decrease slightly with an increase in matric suction.

The soil-water characteristic curves for the residual soils from the sedimentary Jurong Formation were investigated by Lim (1995). Results shown in Fig. 2 indicate that the fine-grained residual soil (i.e., silty clay) can maintain a high degree of saturation for matric suctions as high as 400 kPa. The predominantly silty sand residual soil begins to desaturate at a matric suction of between 150 kPa and 250 kPa. The sandy silt type residual soil begins to desaturate at a matric suction within the range of 200 kPa to 300 kPa.

Field instrumentation program

An instrumentation program was carried out to study the characteristics of *in situ* matric suction in a residual soil slope under three different surface conditions.

Fig. 1. Cohesion intercepts at τ versus $(u_a - u_w)$ plane (where $(\sigma - u_a) = 0$) for fine-grained residual soils of the Jurong Formation.

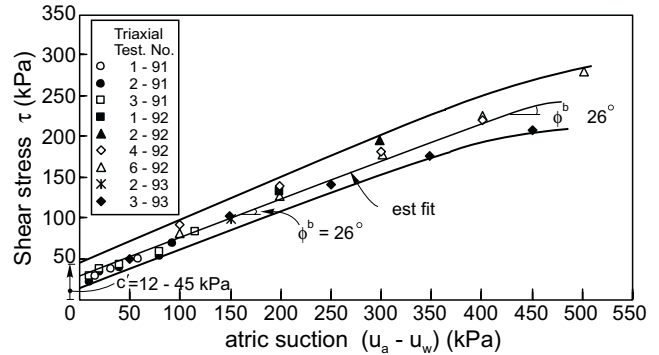
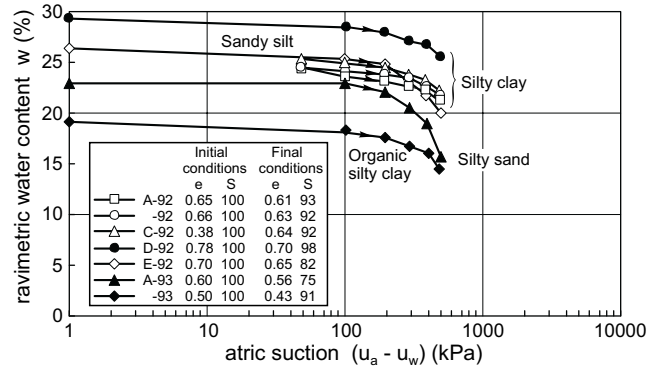


Fig. 2. Soil-water characteristic curves for residual soils from the sedimentary Jurong Formation; S , degree of saturation; e , void ratio.

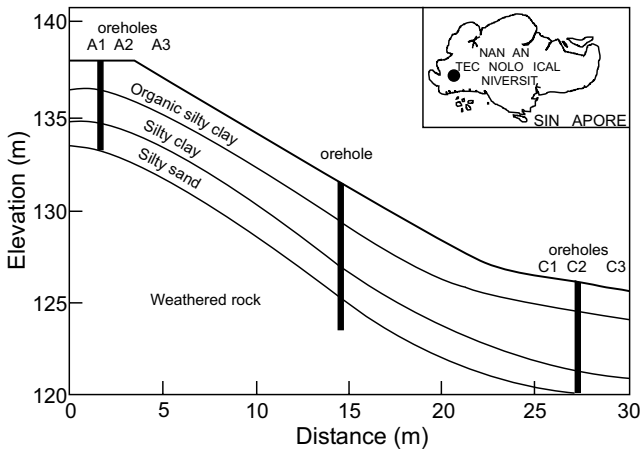


Site description

The instrumented site is located on a slope in an open grassed area on the campus of the Nanyang Technological University in the western part of Singapore. The site is underlain by the residual soil of the sedimentary Jurong Formation in Singapore. The geological formation of the residual soil has been described by Rahardjo et al. (1995). The typical engineering characteristics of the soil from this site have been discussed earlier. Figure 3 shows a generalized cross-section of the soil profile at the site. Field permeability measurements from the crest of the slope indicate that the saturated coefficient of permeability is 1.0×10^{-6} m/s. Laboratory tests on soil samples from depths of 1.7 m to 1.9 m indicate that the saturated coefficient of permeability is 1.0×10^{-9} m/s. The higher coefficient of permeability measured in the field can be attributed to the presence of cracks near to the ground surface.

An area of the slope, approximately 15 m wide (measured across the slope) and 25 m long (measured down the slope), was selected for the instrumentation. The selected area consisted of a horizontal crest, a uniform slope with an inclination of approximately 30°, and a toe

Fig. 3. Generalized soil profile through the instrumented slope.



with an inclination of 12° to 15° . The area was originally covered with grass.

The area was divided into three sections, each 5 m wide across the slope. The surface of each section of the slope was prepared to three different surface conditions. These surface conditions were (1) a canvas-over-grass surface (or simply referred to as canvas-covered surface); (2) a grassed surface, and (3) a bare ground surface. The canvas-covered surface was prepared merely by placing an impermeable canvas over the grassed surface. For the bare ground surface condition, 5 to 10 cm of top soil, containing the grass and most of the grass roots, was removed. Surface cracks and fissures on the slope were exposed after the removal of the covering grass. Trees and dense bushes were found near the toe of the slope adjacent to the canvas-covered area. Figure 4 is a photographic view of the three surface conditions.

Instrumentation layout

Figure 5 shows the locations and the layout of instruments installed in the area. Four standpipe piezometers (with Casagrande porous tips), A1, A3, C1, and C3, were installed on four corners of the instrumented area. Piezometers A1 and A3 were located at the crest of the slope, with their porous tips embedded at depths of 3.5 m and 3.7 m, respectively, below the ground surface. Piezometers C1 and C3 were located at the toe of the slope and embedded at depths of 5.3 m and 5.4 m, respectively. These piezometers were installed to monitor the fluctuation of the groundwater table below the instrumented slope. A tipping-bucket rain gauge¹ was installed at the crest of the slope to record the intensity and the duration of rainfall precipitation on the slope.

Jet-fill tensiometers² were used to monitor the matric suction changes in the slope. A typical jet-fill tensiometer is shown in Fig. 6. A total of 36 jet-fill tensiometers were installed, in 12 groups of 3 tensiometers per group. The

three tensiometers in each group were spaced at 0.5 m centers and were embedded vertically in the slope down to depths of 0.5, 1.0, and 1.5 m, respectively. Figure 6 shows one of the embedded jet-fill tensiometers equipped with a pressure transducer for automatic recording. The locations and spacing of the tensiometer groups are shown in Fig. 5. The cross-section of the instrumented slope is shown in Fig. 7. On each section of the slope there was a group of tensiometers at the crest as well as at the toe of the slope and two tensiometer groups at the mid-slope. All tensiometers were connected to an automatic recording system. An instrumentation hut was built on the crest of the slope to house the data acquisition systems for recording the matric suction and the rainfall precipitation measurements.

Jet-fill tensiometer

A jet-fill tensiometer consists of a high air entry ceramic cup, a plastic body tube with a port, a vacuum gauge, and a jet-fill reservoir cap (Fig. 6). When in use, the tensiometer is filled with deaired water. The vacuum gauge provides a measurement of the negative water pressure (i.e., suction) in the tensiometer. The reservoir cap is provided at the top of the tensiometer tube for air-bubble removal. A tensiometer is installed by inserting its ceramic cup into a precored hole.

At the tip of the tensiometer, capillary equilibrium is established between the water in the tensiometer and the soil pore-water via the high air entry ceramic cup. At equilibrium, the water in the tensiometer has the same negative pressure as the pore-water in the soil. This pressure is transmitted to the vacuum dial gauge connected to the port of the tensiometer through the water column in the tensiometer body.

The negative water pressure recorded by the vacuum gauge at the ground surface should be corrected for the elevation head difference corresponding to the height of the water column between the ceramic cup and the port (Stannard 1992). If water cavitates at approximately -90 kPa of pressure, the pressure limits that can be measured by tensiometers of 0.5, 1.0, and 1.5 m in length are approximately -85 , -80 , and -75 kPa, respectively. The measured negative pore-water pressure is numerically equal to the matric suction, since the pore-air pressure in the slope is atmospheric.

Data acquisition systems

A total of 36 pressure transducers³ were connected to the jet-fill tensiometers for recording the matric suction. The transducers were either connected directly to the port of each jet-fill tensiometer replacing the vacuum gauges or installed together with the vacuum gauges using a T-joint as shown in Fig. 6. The advantage of having both the current transducer and the vacuum gauge is that the negative water pressure in the tensiometer can be re-

¹Model 444A, manufactured by HANDAR, Sunnyvale, California.

²Model 2725, manufactured by Soilmoisture Equipment Corporation, Santa Barbara, California.

³Model 5301 Current Pressure Transducers, manufactured by Soilmoisture Equipment Corporation.

Fig. 4. Ground surface conditions on the instrumented slope.

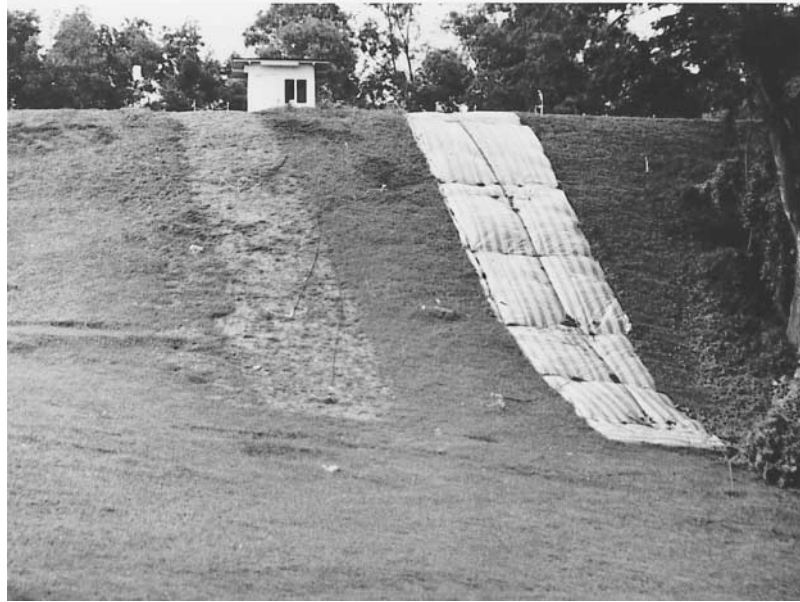
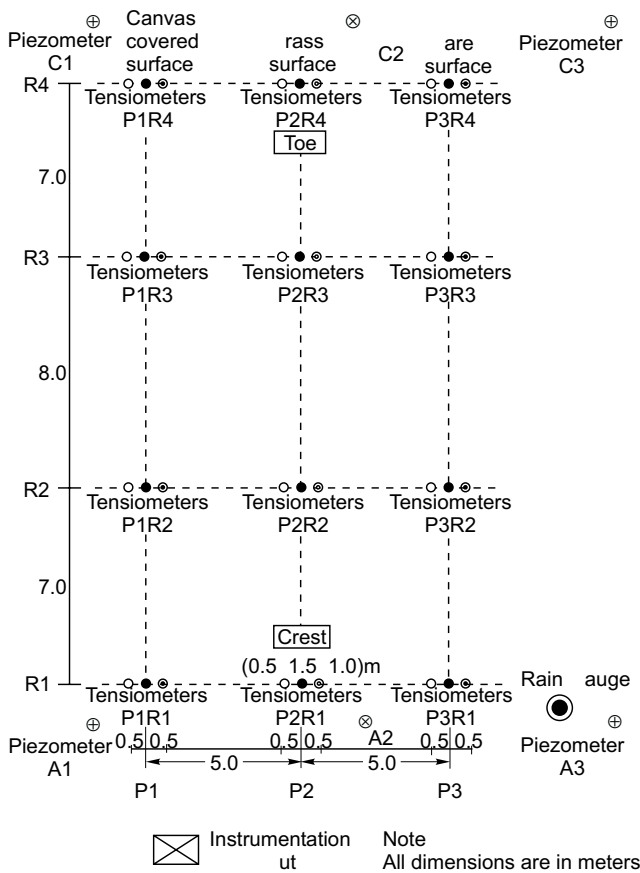


Fig. 5. Instrumentation layout. Measurements in meters.



corded automatically, remotely, and continuously using the current transducer as well as through direct manual readings using the vacuum gauge. Manual readings are useful for checking that the transducer is functional and reliable. Two data loggers⁴ were housed in the instrumentation hut to monitor the 36 tensiometers. The data were scanned and stored in the memory units of the data loggers at specified intervals (i.e., 10 or 15 min).

Rainfall data were monitored using a hydrologger,⁵ which was housed in the instrumentation hut. The hydrologger was connected by a cable to the tipping-bucket rain gauge located on the slope. The time intervals (i.e., 10 or 15 min) for logging rainfall data were programmed into the hydrologger. The total number of rain bucket tips occurring within each interval was counted and stored in the hydrologger.

Field monitoring results and discussion

Field measurement results are presented for the months of January and February, 1994. This period falls in the later part of the wet season when the Northeast Monsoon blows across the Straits of Malacca. Changes in matric suction, matric suction profiles, and total head profiles, in response to rainfall, are investigated.

In situ matric suction

Figures 8 to 10 show the typical daily variation of the *in situ* matric suction in the slope with respect to rainfall for the three different ground surface conditions. The P1R1, P2R1, and P3R1 locations were situated on the crest of the instrumented slope, while the P1R2, P2R2, and P3R2 locations were situated at the mid-slope, as shown in Figs. 5 and 7. Matric suction data were gener-

⁴Hydra Data Loggers, Model 2625A.

⁵HANDAR 550B Hydrologger manufactured by HANDAR, Sunnyvale, California.

Fig. 6. Jet-filled tensiometer equipped with a current pressure transducer.

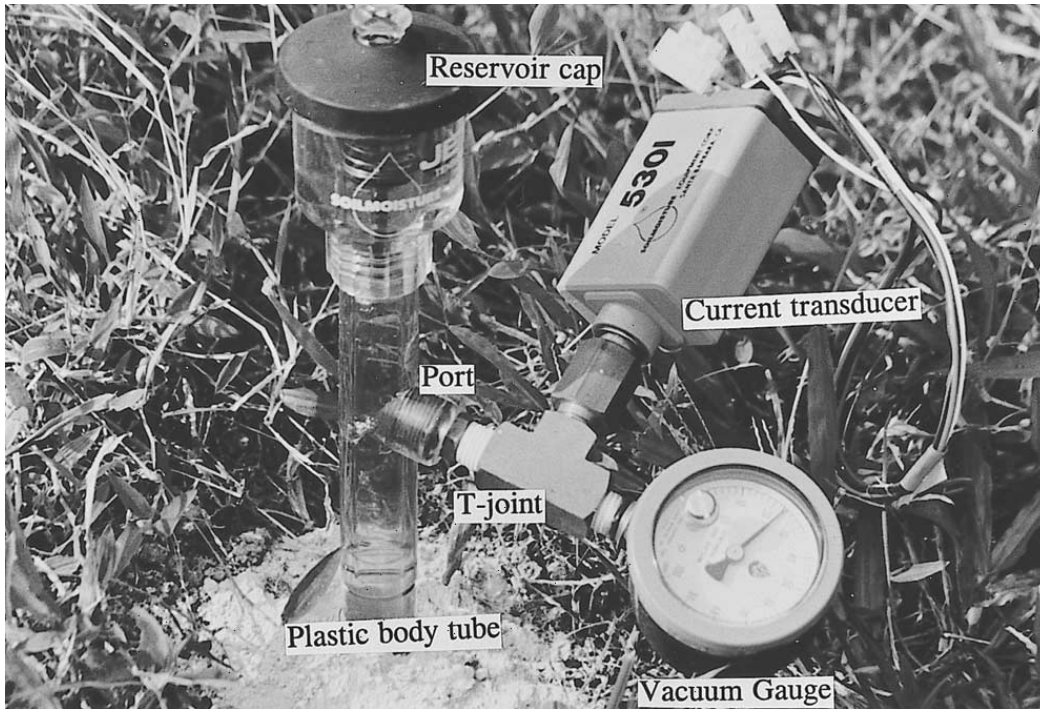
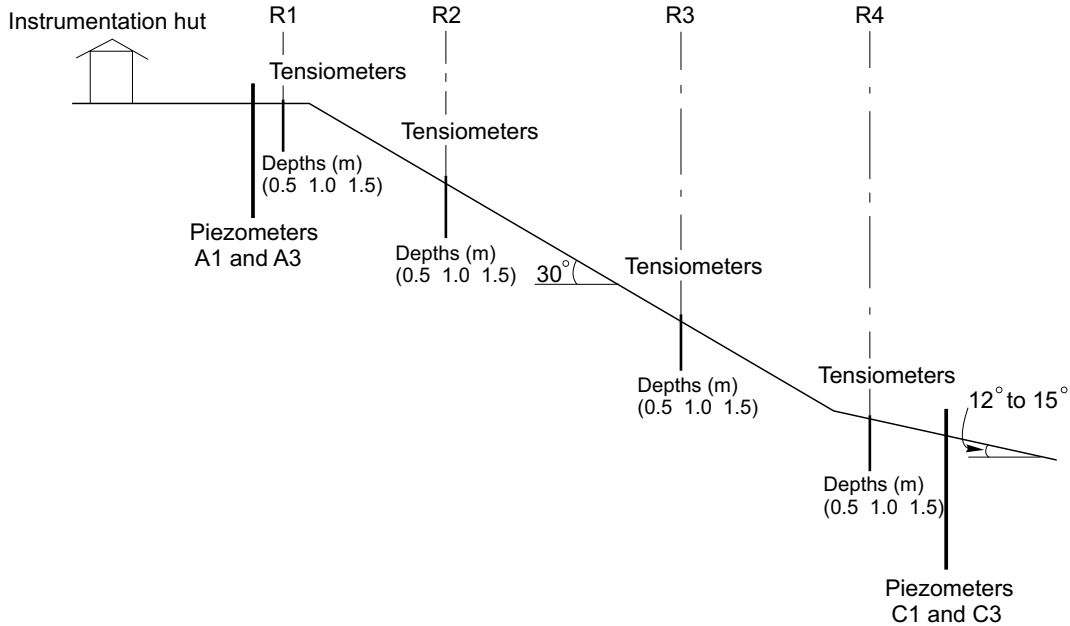


Fig. 7. Cross-section of the instrumented slope showing instrumentation details.



ally acquired at the end (i.e., 24:00) of each day, except for those acquired through manual readings.

The data (Figs. 8 to 10) indicated some similarities in the characteristics of *in situ* matric suction variations in the slope under the three different surface conditions. Maximum changes in matric suction often occurred near the ground surface (i.e., at a depth of 0.5 m), and the magnitude of the changes generally decreased with depth. The variation in matric suction due to periodic wetting

and drying was most significant in the bare slope section and least significant in the canvas-covered slope. Matric suctions near the ground surface were the first to be affected by changes in the climatic condition. Some delay in matric suction changes were exhibited at greater depths.

Matric suctions at some locations were found to have probably exceeded the limit of the tensiometers during the dry period. For example, the matric suction at P3R1

Fig. 8. *In situ* matric suction measurements in the slope with the canvas-covered surface: a) at P1R1; b) at P1R2.

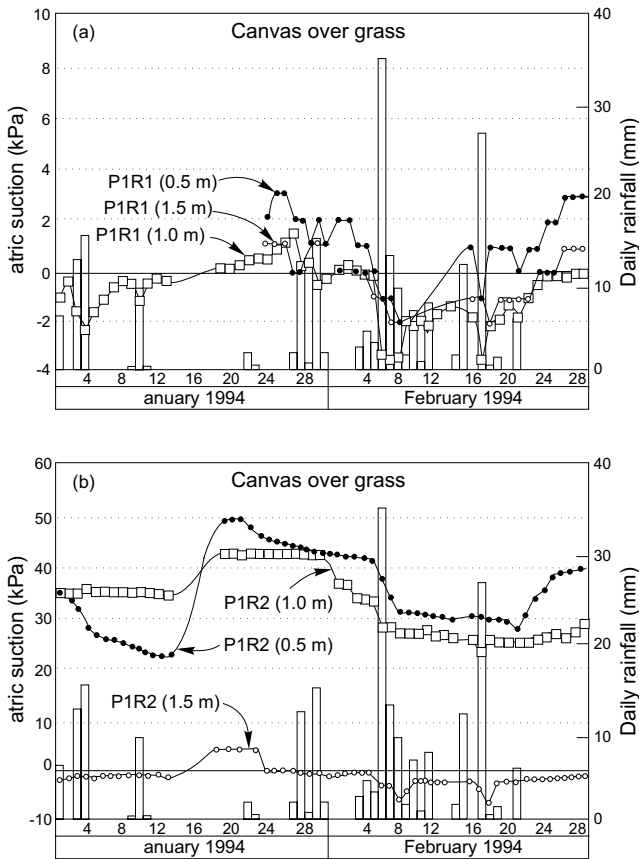
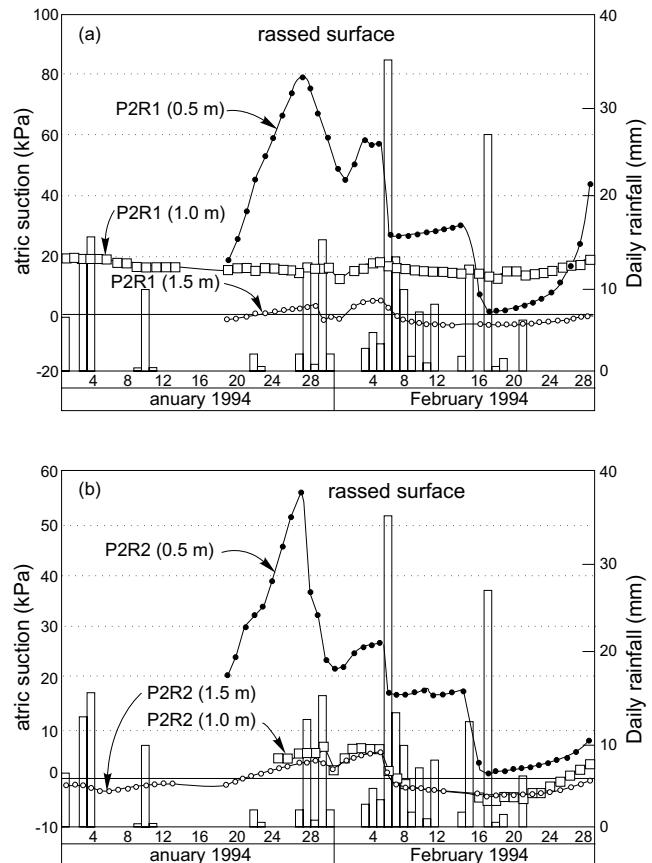


Fig. 9. *In situ* matric suction measurements in the slope with the grass-covered surface: a) at P2R1; b) at P2R2.



(i.e., at 0.5 m depth) would be higher than the matric suction readings indicated in Fig. 10, had cavitation not occurred.

For the canvas-covered slope, the vertical infiltration of water is prevented. However, the *in situ* matric suction was found to decrease during and after rainfalls (Fig. 8). The matric suction reduction was probably due to the lateral dispersion of percolating water from the infiltration beyond the edges of the canvas. Another factor that possibly affected the matric suction was the development of a perched water table in the slope. The matric suction increase observed under the canvas-covered section during the dry period could be attributed to the evapotranspiration process associated with the vegetation under the canvas.

The magnitude of decrease in matric suction during a particular rainstorm period appears to be a function of the matric suction profile just prior to the rainstorm. For example, the rainfall on January 28 led to a more significant decrease in matric suction than the rainfall on February 15 (Figs. 9 and 10), although the amount of precipitation of the two rainfall events were the same. This difference in response can be attributed to the different pressure gradients existing near the ground surface prior to each rainfall event. The higher pressure gradient on January 28 resulted in a higher infiltration rate into the soil.

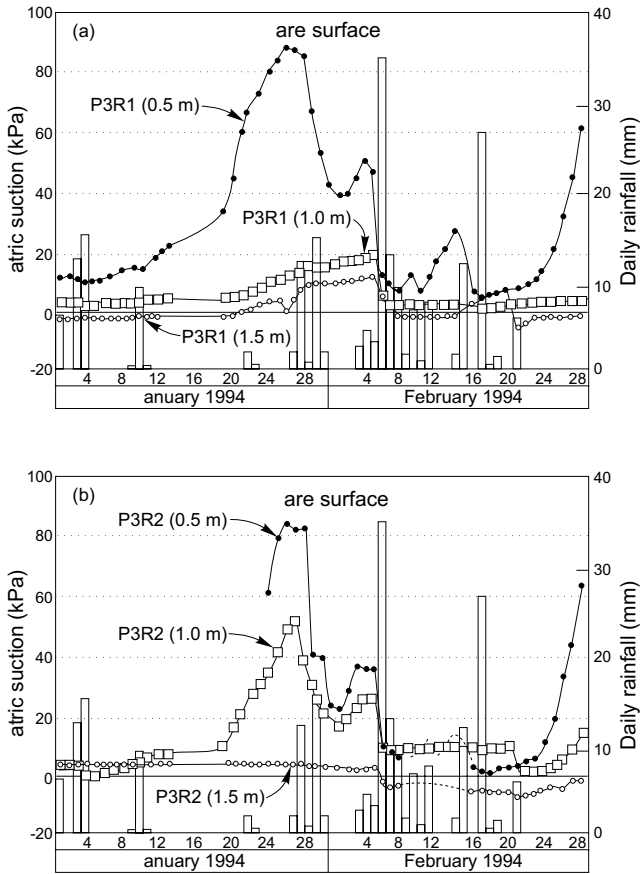
Rainstorms with large precipitation volumes (such as those on February 6) will affect the matric suction values at greater depths (i.e., 1.0 and 1.5 m). A small amount of precipitation (i.e., less than 3 mm) will not significantly affect the *in situ* matric suction at depth. This is shown in the observations made on the days of January 9, January 11, January 22, and January 23 (Figs. 9 and 10).

***In situ* matric suction profiles**

Variations in matric suction profiles and the associated total head profiles during a continuous wetting by rainwater infiltration were investigated. Observations made during the wet period from January 27 to February 18 were selected for discussion. Figure 11 shows typical results from the field measurements, which indicate the changes in matric suction profiles due to rainfalls under the canvas-covered area, the grass-covered area, and the bare surface area. The ranges of matric suction and their variations with depths at all 12 locations are presented in Fig. 12.

Prior to the commencement of the rainy period on January 27, the matric suction profiles generally showed a decrease in *in situ* matric suctions with depth. The *in situ* matric suctions near the ground surface under the grass-covered area and the bare surface area were much higher than those at greater depths. The matric suction profiles

Fig. 10. *In situ* matric suction measurements in the slope with the bare surface: a) at P3R1; b) at P3R2.

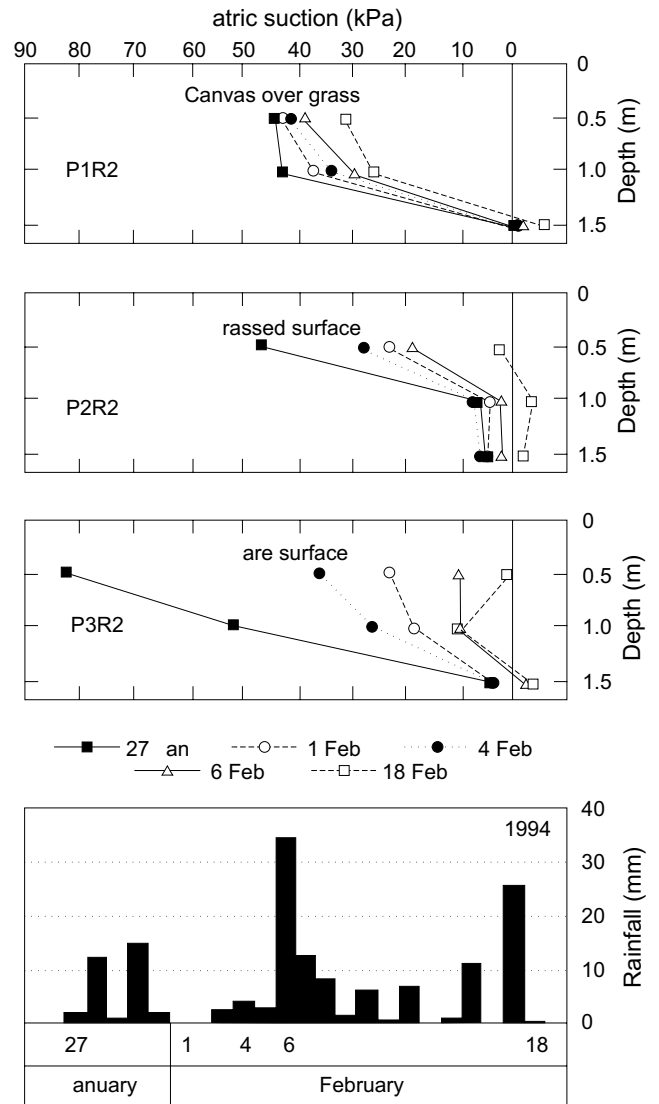


were found to deviate significantly from the theoretical hydrostatic line down to a depth of 1.5 m.

The progressive reductions in matric suction in the slope during the wet period are depicted in Fig. 11. A matric suction recovery, observed on February 4, was due to the drier period commencing on February 1. Changes in the matric suction profiles with time were more significant under the bare surface than they were under the grass-covered surface. The matric suction profile beneath the canvas-covered area showed little variation with respect to time. The fluctuation of matric suction in the canvas-covered area on the slope was generally more consistent with depth due to the negligible vertical infiltration from the ground surface.

For the grass-covered slope, the change in matric suction was significant near the ground surface (i.e., 0.5 m) but was insignificant at greater depths (i.e., 1.0 and 1.5 m). This may be attributed to the evaporation process caused by the thermal gradient across the ground surface and the evapotranspiration from the grass near the ground surface. The presence of vegetation accelerated the removal of the water from the soil and prevented the advancement of the wetting front from reaching greater depths. For the bare slope there is no evaporatranspiration and the removal of water from the soil was through surface evaporation alone. Surface evaporation does not ap-

Fig. 11. Changes of *in situ* matric suction profiles in response to rainfall at the mid-slope under three different ground surface conditions.



pear to be efficient in removing water at depth and the wetting front continued to greater depths after the end of each rainstorm. The reduction of matric suction in the bare slope due to the infiltration of rainwater propagated down to a depth of 1.5 m or deeper from the ground surface.

The ranges of matric suction changes at P1R4 and P2R4 and at 1.0 m depth at P1R3 (Fig. 12) were higher than those measured at other locations, probably due to the presence of roots from nearby trees.

Figures 8 to 12 indicate that most of the matric suctions measured at 1.5 m depth were relatively low. At times, positive pore-water pressures were observed to develop at this depth. Piezometric observations (Fig. 13) show that a perched water table had probably developed at about 1.5 m below the ground surface throughout the entire instrumented area during the wet period.

Fig. 12. Ranges of measured matric suction at instrumented site between January and February 1994.

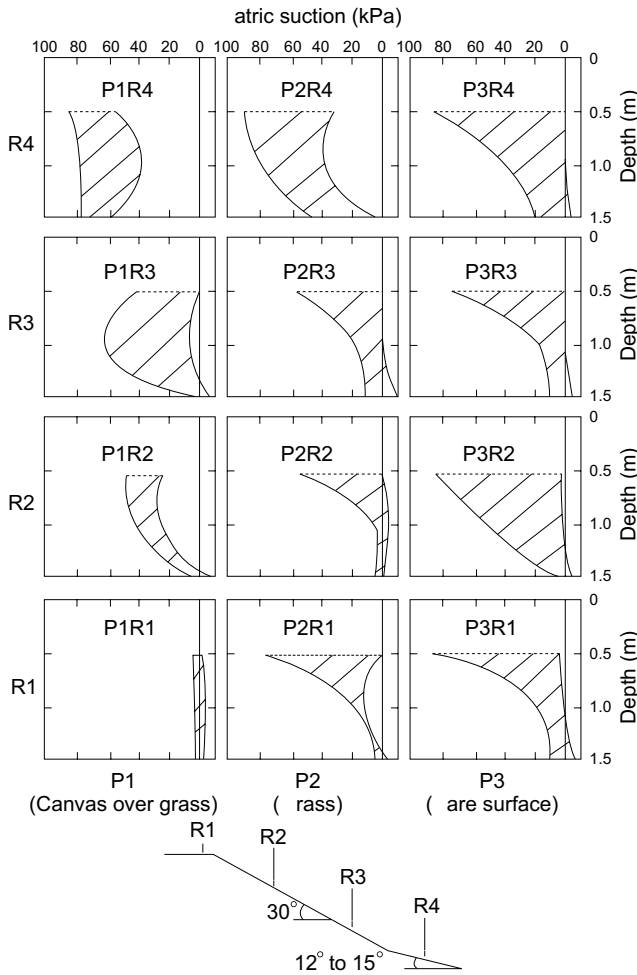
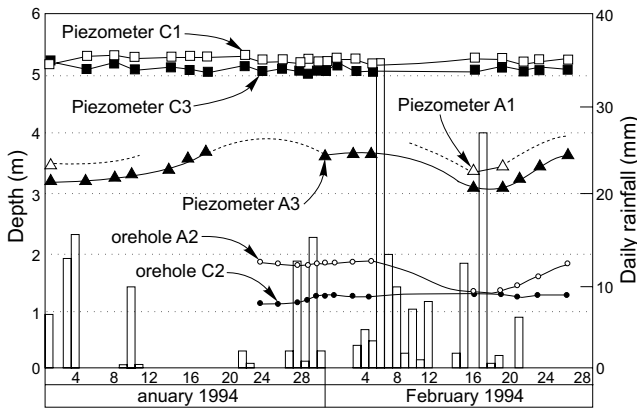


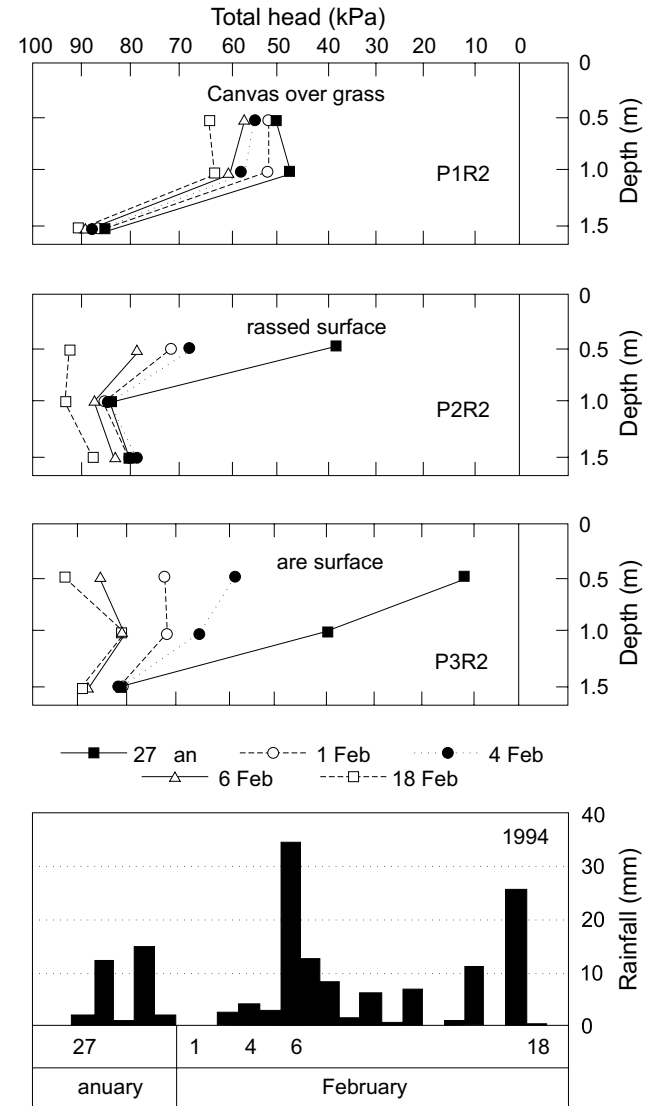
Fig. 13. Groundwater table measurements from piezometers and water levels encountered in boreholes in January and February 1994.



Total head profiles

Figure 14 shows the total head profiles associated with the matric suction profiles shown in Fig. 11. The total

Fig. 14. Changes of *in situ* total head profiles in response to rainfall at the mid-slope under three different ground surface conditions.



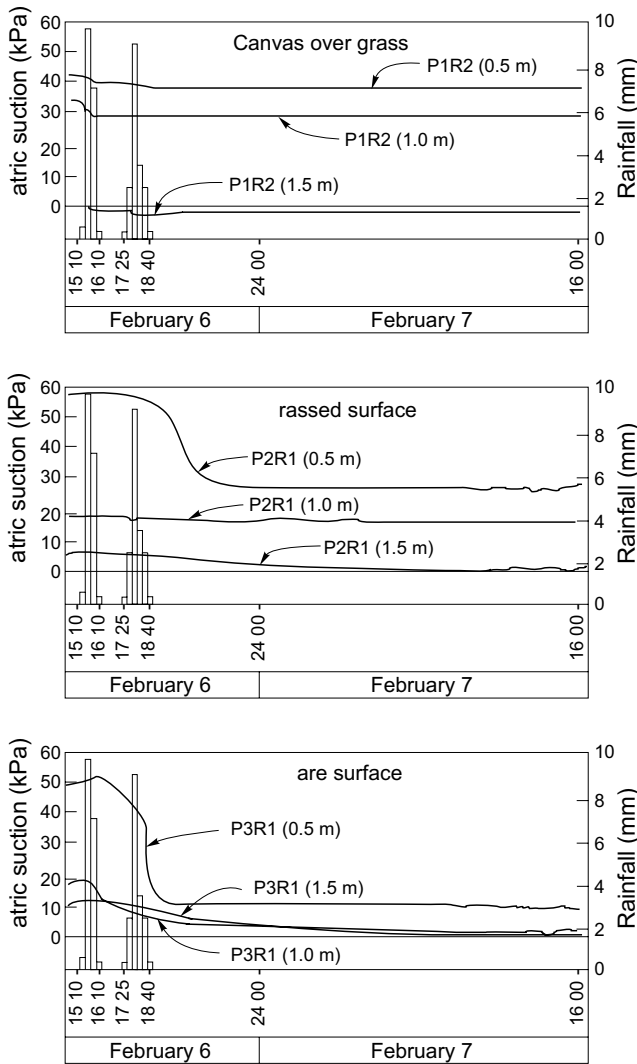
head profiles were constructed based on an assumed datum at 10 m depth below the ground surface.

A series of rainfall events from January 27 to February 18 resulted in a progressive change in the total head profiles shown in Fig. 14. There were gradual directional changes of moisture movement from the upward to the downward direction particularly under the bare ground surface. Rainfalls result in infiltration and reduce the soil matric suction near the ground surface. The total head at the ground surface will gradually increase until it becomes higher than the head at a greater depth.

Changes of matric suction due to heavy rainstorms

The variations in matric suction under the three different ground surface conditions in response to two consecutive rainstorms that commenced at 15:25 and ended at 18:40 on February 6 were investigated. The rainstorms

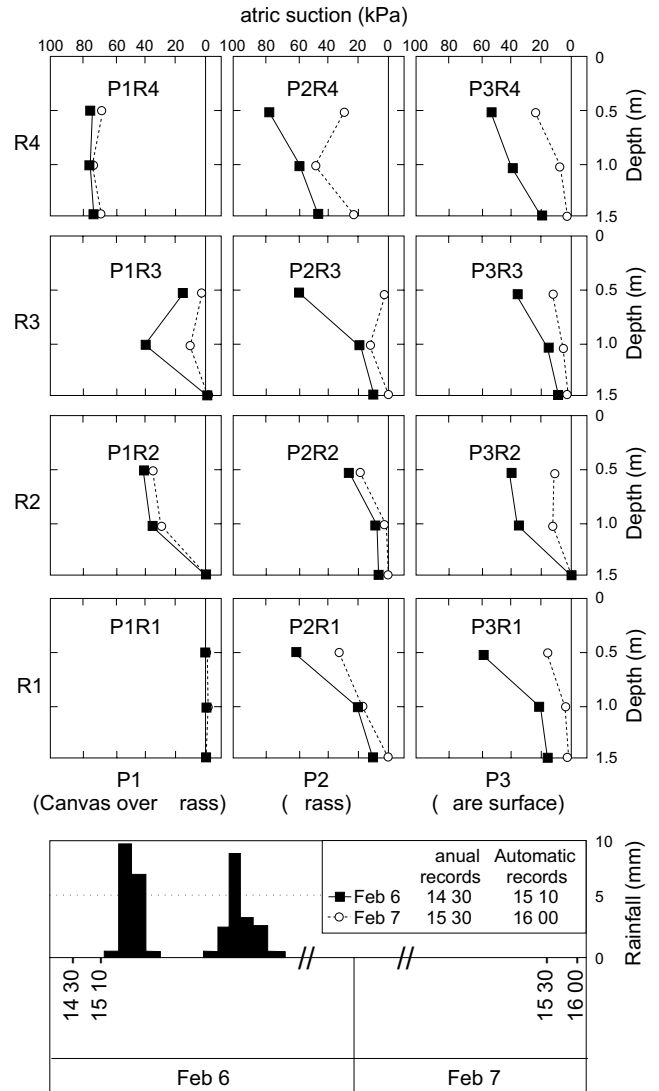
Fig. 15. Decrease in matric suction with the elapsed time at different depths during the rainstorms of February 6, 1994.



delivered a total of 35 mm of rainfall. Figure 15 shows the decrease in matric suction with time at P1R2, P2R1, and P3R1 during the rainstorms. The plots are extended to 16:00 h on February 7 to investigate the characteristics of water movement in the soil during and after the rainstorms. A comparison of the changes in matric suction profiles in the instrumented slope for all 12 locations are presented in Fig. 16. For each location, two matric suction profiles, one for the condition prior to the rainstorms (i.e., at 14:30 or 15:10 on February 6) and the other for the condition at approximately 1 day after the rainstorms (i.e., at 15:30 or 16:00 h on February 7) are shown.

In the canvas-covered section of the slope, there was an insignificant reduction in matric suction (Fig. 15). A significant decrease in matric suction occurred in the uncovered portion of the slope under the grassed and the bare surfaces. The magnitude of matric suction reduction decreased with depth. In the bare slope the matric suction reduced significantly soon after the storms. For the grassed portion, the decrease in matric suction generally

Fig. 16. Changes of *in situ* matric suction profiles under three different ground surface conditions due to the rainstorms of February 6, 1994.



occurred immediately after the rainstorms. Equalization in matric suction was generally achieved sooner at shallower depths. Equalization in matric suctions at greater depths (e.g., those observed at P2R1 and P3R1) were attained as late as 24 h after the rainstorms had stopped.

Figure 16 shows that matric suction generally decreased with depth (i.e., except that at P1R3) prior to the storms. The matric suction profiles shifted toward the direction of zero matric suction after being affected by the rainstorms. Except at P1R4 and P2R4, almost no matric suction was maintained at a depth of 1.5 m throughout the instrumented slope after the rainstorms. This was attributed to the possible existence of a perched water table at the 1.5 m elevation. At 0.5 m depth, a small magnitude of matric suction was maintained locally. It is expected that subsequent heavy rainstorms following the storm events as indicated in Fig. 16 will eliminate all the matric suctions in the slope. The matric suction profiles at P1R4,

P2R4, and at 1.0 m depth at P1R3 can be attributed to the roots from vegetation in the vicinity.

Conclusions

A field instrumentation program was carried out to continuously and simultaneously monitor the *in situ* matric suction and the rainfall on a residual soil slope. The slope was divided into three portions with different surface conditions. The measurements provided correlations between matric suction changes and climatic conditions.

Changes in the climatic conditions resulted in variations in the matric suction profile with time. The variation of the matric suction profile is less significant under the canvas-covered section than under the grass-covered and the bare sections of the slope. However, the presence of vegetation can significantly increase the *in situ* matric suction and alter the total head profile. A perched water table appears to have developed in the instrumented slope at a depth of about 1.5 m below the ground surface during the rainy period. The development of perched water tables results in shallow landslides, which occurred during the rainstorms. The field observations are useful in the study of the importance of flux boundary conditions on the changes of matric suction in a soil slope.

Acknowledgement

The authors acknowledged the assistance provided by Mr. Julian K-M. Gan, Research Engineer, University of Saskatchewan, in writing this paper.

References

Affendi, A.A., and Faisal, A. 1994. Field measurement of soil suction. Proceedings, 13th International Conference on Soil

- Mechanics and Foundation Engineering, New Delhi, India, January 5–10, pp. 1013–1016.
- Brand, E-W. 1984. Landslides in southeast Asia: A state-of-the-art report. Proceedings, 4th International Symposium on Landslides, Toronto, September, 16–21, Vol. 1, pp. 17–59.
- Chipp, P.N., Henkel, D.J., Clare, D.G., and Pope, R.G. 1982. Field measurement of suction in colluvium covered slopes in Hong Kong. Proceedings, 7th Southeast Asian Geotechnical Conference, Hong Kong, November 22–26, Vol. 1, pp. 49–61.
- Fredlund, D.G., and Rahardjo, H. 1993. Soil mechanics for unsaturated soils. John Wiley & Sons Inc., New York.
- Krahn, J., Fredlund, D.G., and Klassen, M.J. 1989. Effect of soil suction slope stability at Notch Hill. Canadian Geotechnical Journal, **26**: 269–278.
- Lim, T.T. 1995. Shear strength characteristics and rainfall-induced matric suction changes in a residual soil slope. M.Eng. thesis, Nanyang Technological University, Singapore.
- Lumb, P. 1962. Effects of rain storms on slope stability. Proceedings, Symposium Hong Kong Soils, Hong Kong, pp. 73–87.
- Macari, E.J., Laymon, C.A., and Costes, N.C. 1992. Hydrologic field instrumentation for a small-scale experiment with implications for rain-induced slope stability analyses. Proceedings, U.S.-Brazil Geotechnical Workshop: Application of Classical Soil Mechanics Principles to Structured Soils. Edited by A.S. Nieto, Belo Horizonte, Brazil, November 23–25., pp. 79–88.
- Rahardjo, H., Lim, T.T., Chang, M.F., and Fredlund, D.G. 1995. Shear strength characteristics of a residual soil. Canadian Geotechnical Journal, **32**: 60–77.
- Stannard, D.I. 1992. Tensiometer-theory, construction, and use. Geotechnical Testing Journal, **15**: 48–58.
- Sweeney, D.J. 1982. Some *in situ* soil suction measurements in Hong Kong's residual soil slopes. Proceedings, 7th Southeast Asian Geotechnical Conference, Hong Kong, November 22–26, Vol. 1, pp. 91–106.

One-dimensional consolidation theory: unsaturated soils

D.G. Fredlund and J.U. Hasan

Abstract: A one-dimensional consolidation theory is presented for unsaturated soils. The assumptions made are in keeping with those used in the conventional theory of consolidation for saturated soils, with the additional assumption that the air phase is continuous. Two partial differential equations are derived to describe the transient process taking place as a result of the application of a total load to an unsaturated soil.

After a load has been applied to the soil, air and water flow simultaneously from the soil until equilibrium conditions are achieved. The simultaneous solution of the two partial differential equations gives the pore-air and pore-water pressures at any time and any depth throughout the soil. Two families of dimensionless curves are generated to show the pore-air and pore-water dissipation curves for various soil properties.

For the case of an applied total load, two equations are also derived to predict the initial pore-air and pore-water pressure boundary conditions. An example problem demonstrates the nature of the results.

Key words: consolidation, pore-air pressures, pore-water pressures, unsaturated soils, finite difference, partial differential equations.

Introduction

Since the inception of modern soil mechanics, the theory derived by Terzaghi (1936) for the consolidation of saturated soils has formed an extremely useful conceptual framework in geotechnical engineering. Unfortunately, the study of the behavior of unsaturated soils has taken place in the absence of a similar theoretical framework. As a result, it has been difficult to envisage the transitions in theory when going from a saturated soil to an unsaturated soil.

Biot (1941) presented an analysis of the transient flow problem in unsaturated soils. He suggested two constitutive relations for the soil, and solved for changes in the pore-water pressure with time. Biot considered the air to be in an occluded state with no flow of air during the consolidation process.

Barden (1965) presented an analysis of the one-dimensional consolidation of compacted, unsaturated clay. The consolidation problem was subdivided into various categories depending upon the degree of saturation of the soil. The problem was stated as being indeterminate and, therefore, various assumptions were made in order to complete the analysis. The equation developed by Bishop (1959) is used to describe the stress conditions in the unsaturated soil.

Partial differential equations have been developed in the soil science discipline to describe unsteady moisture movement. More recently these equations have received increasing acceptance in the soil mechanics field (Aitchi-

son et al. 1965). These equations should be considered as a special case since the compressibility of the soil structure and the escape of air are not taken into consideration. These equations are generally not applied to transient processes associated with the application of an external load.

Fredlund and Morgenstern (1977) proposed stress state variables for unsaturated soils on the basis of the equilibrium equations for a multiphase system. These were also verified experimentally. An element of unsaturated soil was considered as a four phase system with two phases that come to equilibrium under applied stress gradients (i.e., soil particles and contractile skin or air-water interface) and two phases that flow under applied stress gradients (i.e., air and water). Fredlund and Morgenstern (1976) also proposed and experimentally tested constitutive relations for volume change in unsaturated soils. In addition, the continuity requirements for an element of unsaturated soil were outlined. The description of the stress, continuity, and constitutive relations, and suitable flow and compressibility laws for air and water, provide the necessary physical requirements for a more rigorous formulation of transient processes in unsaturated soils.

This paper presents a general one-dimensional consolidation (or swelling) theory for unsaturated soils within a theoretical framework similar to that for saturated soils. As well, equations are derived to predict the initial air and water boundary conditions associated with the application of an externally applied load. An example problem is included to demonstrate the solution of the above equations.

D.G. Fredlund. Professor, Department of Civil Engineering, University of Saskatchewan, 57 Campus Drive, Saskatoon, SK., Canada S7N 5A9.

J.U. Hasan. Graduate Student, Department of Civil Engineering, University of Saskatchewan, 57 Campus Drive, Saskatoon, SK., Canada S7N 5A9.

Reproduced with permission from the *Canadian Geotechnical Journal*, **16**: 521–531, 1979.

Physical requirements for the formulation

The state of stress in an unsaturated soil can be described by any two of a possible three stress state variables (Fredlund and Morgenstern 1977). Acceptable combinations are: (1) $(\sigma - u_a)$ and $(u_a - u_w)$; (2) $(\sigma - u_w)$ and $(u_a - u_w)$; and (3) $(\sigma - u_a)$ and $(\sigma - u_w)$. The stress variables selected to derive the consolidation equations in this paper are $(\sigma - u_a)$ and $(u_a - u_w)$, where σ = total stress; u_a = pore-air pressure; and u_w = pore-water pressure. Continuity of an unsaturated soil element requires that the overall volume change of the element must equal the sum of the volume changes associated with the component phases (Fredlund 1973). If the soil particles are considered incompressible and the volume change of the contractile skin (i.e., air-water interface) is considered as internal to the element, the continuity requirement can be written:

$$[1] \quad \Delta V / V = \Delta V_w / V + \Delta V_a / V$$

where:

- V = overall volume of the soil element,
- V_w = volume of water in the soil element, and
- V_a = volume of air in the soil element.

If any two of the volume changes are known, the third can be computed. In other words, it is necessary to have two constitutive equations to define volume change behavior in unsaturated soils.

Fredlund and Morgenstern (1976) proposed and tested constitutive relations to link the stress and deformation state variables. The proposed constitutive relationship for the soil structure is given by eq. [2] and the relationship for the water phase is given by eq. [3] (Fig. 1).

$$[2] \quad \Delta V / V = m_1^s d(\sigma - u_a) + m_2^s d(u_a - u_w)$$

$$[3] \quad \Delta V_w / V = m_1^w d(\sigma - u_a) + m_2^w d(u_a - u_w)$$

where:

- m_1^s = compressibility of the soil structure when $d(u_a - u_w)$ is zero,
- m_2^s = compressibility of the soil structure when $d(\sigma - u_a)$ is zero,
- m_1^w = slope of the $(\sigma - u_a)$ plot when $d(u_a - u_w)$ is zero, and
- m_2^w = slope of the $(u_a - u_w)$ plot when $d(\sigma - u_a)$ is zero.

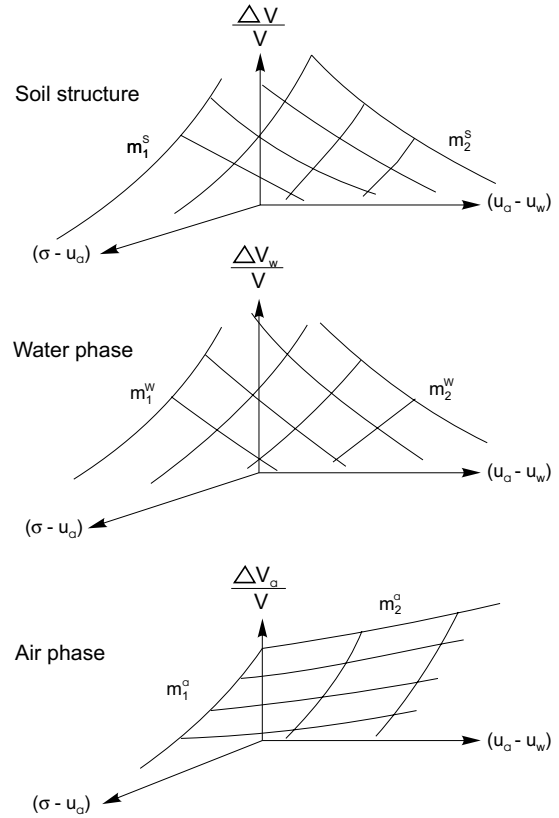
The constitutive relationship for the air phase is the difference between eqs. [2] and [3] because of the continuity requirement.

$$[4] \quad \Delta V_a / V = m_1^a d(\sigma - u_a) + m_2^a d(u_a - u_w)$$

where:

- m_1^a = slope of the $(\sigma - u_a)$ plot when $d(u_a - u_w)$ is zero, and
- m_2^a = slope of the $(u_a - u_w)$ plot when $d(\sigma - u_a)$ is zero.

Fig. 1. Constitutive surfaces for the various phases of an unsaturated soil.



Flow of the water phase is described by Darcy's law (Childs and Collis-George 1950).

$$[5] \quad v = (-k_w / \gamma_w)(\partial u_w / \partial y)$$

where:

- v = water velocity,
- k_w = coefficient of permeability with respect to the water phase,
- γ_w = unit weight of water, and
- y = depth in the y -direction.

Flow of the air phase is described by Fick's law (Blight 1971).

$$[6] \quad v_a = -D(\partial p / \partial y)$$

where:

- v_a = mass rate of air flow,
- D = a transmission constant having the same units as the coefficient of permeability,
- p = absolute air pressure (i.e., $u_a + u_{atm}$), and
- u_{atm} = atmospheric air pressure.

The isothermal compressibility equation for the air phase, β_a , is (Fredlund 1976):

$$[7] \quad \beta_a = 1 / (u_a + u_{atm})$$

and the isothermal compressibility equation of an air-water mixture (with no diffusion) in the presence of a particulate mass, β_m , is:

$$[8] \quad \beta_m = S\beta_w + B_{aw}(1 - S) / (u_a + u_{am})$$

where:

$$S = \text{initial degree of saturation, and}$$

$$B_{aw} = \text{pore-pressure coefficient equal to } \Delta u_a / \Delta u_w.$$

The above listed physical relationships are sufficient to derive the one-dimensional consolidation (or swelling) equations and the pressure boundary condition equations for an unsaturated soil.

Derivation of the Consolidation Equations

The one-dimensional consolidation equations for unsaturated soils are derived using the conventional assumptions for the consolidation theory by Terzaghi (1936) with the following additions:

- (1) The air phase is continuous.
- (2) The coefficients of permeability with respect to water and air, and the volume change moduli remain constant during the transient processes.
- (3) The effects of air diffusing through water and the movement of water vapor are ignored.

The above assumptions are not completely accurate for all cases; however, they are reasonable for a first attempt to derive a general consolidation theory for unsaturated soils (Hasan 1977).

After applying a load to an unsaturated soil, there will be a dissipation of the excess pore-air and pore-water pressures. In order to compute these values as a function of time, it is necessary to have two equations. This is accomplished by independently considering the continuity of the water and air phases. Then the derived equations are solved simultaneously to give the water and air pressures at any elapsed time.

Water phase partial differential equation

Let us consider a referential soil element as shown in Fig. 2. The water phase is assumed incompressible. For the consolidation process, water flows out of the element with time. The constitutive relationship for the water phase defines the volume of water in the element for any combination of total, air, and water pressures. The volume of water entering and leaving the element in the y -direction is described by Darcy's law as:

$$[9] \quad \text{Volume entering} = (-k_w / \gamma_w)(\partial u_w / \partial y) dx dz$$

The net flux of water in the element is:

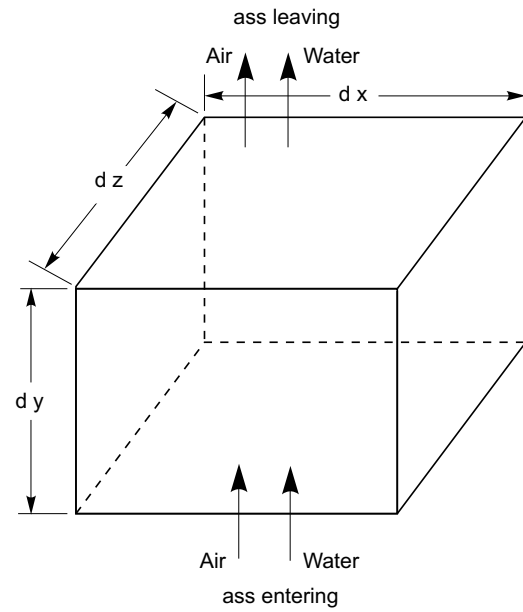
$$[10] \quad \partial(\Delta V_w / V) / \partial t = (-k_w / \gamma_w)(\partial^2 u_w / \partial y^2)$$

Equation [10] can be equated to the constitutive relationship for the water phase (eq. [3]) in accordance with the continuity requirement (eq. [1]).

$$[11] \quad m_1^w \frac{\partial(\sigma - u_a)}{\partial t} + m_2^w \frac{\partial(u_a - u_w)}{\partial t} = \frac{-k_w}{\gamma_w} \frac{\partial^2 u_w}{\partial y^2}$$

For the consolidation process the change in total stress with respect to time is set to zero. Simplifying and rear-

Fig. 2. A referential element in the soil mass.



ranging eq. [11], the water phase partial differential equation can be written:

$$[12] \quad \partial u_w / \partial t = -C_w(\partial u_a / \partial t) + c_v^w(\partial^2 u_w / \partial y^2)$$

where:

$$C_w = (1 - m_2^w / m_1^w) / (m_2^w / m_1^w); \text{ interactive constant associated with the water phase equation. This equation may be further simplified by defining } R_w \text{ as } m_2^w / m_1^w. \text{ When the soil is saturated, } R_w = 1, \text{ and}$$

$$c_v^w = (1 / R_w)(k_w / \gamma_w m_1^w); \text{ coefficient of consolidation with respect to the water phase.}$$

As a soil becomes saturated, the interactive constant approaches zero and eq. [12] reverts to the one-dimensional consolidation equation by Terzaghi (1936). The fact that the air phase cannot remain continuous as a soil goes towards saturation is a physical restriction; however, it does not pose a mathematical problem. Equation [12] also reverts to Terzaghi's equation whenever the air pressure induced is small.

Air phase partial differential equation

The air phase is compressible and flows independent of the water phase when subjected to an air pressure gradient. As well, the constitutive relationship for the air phase defines the volume of air in the element for any combination of the total, air, and water pressures. According to Fick's law the mass of air entering the element in the y -direction is:

$$[13] \quad \text{Mass entering} = -D(\partial p / \partial y) dx dz$$

The net mass flux of air in the element is:

$$[14] \quad \partial m / \partial t = -D(\partial^2 p / \partial y^2)$$

where:

m = mass of air in the element.

The mass rate of change is written in terms of a volume rate of change by differentiating the relationship between mass and volume.

$$[15] \quad \partial(V_a / V) / \partial t = \partial(m / \gamma_a) / \partial t$$

For isothermal conditions the density of air, γ_a , is:

$$[16] \quad \gamma_a = (w / R\theta)p$$

where:

w = molecular weight of the mass of air,
 R = universal gas constant, and
 θ = absolute temperature.

The mass of air is written in terms of the density of air, the degree of saturation, S , and the porosity of the soil, n .

$$[17] \quad m = (1 - S)n\gamma_a$$

Substituting eqs. [14], [16], and [17] into eq. [15] gives:

$$[18] \quad \frac{\partial(V_a / V)}{\partial t} = \frac{-DR\theta}{wp} \frac{\partial^2 u_a}{\partial y^2} + \frac{(1 - S)n}{p} \frac{\partial u_a}{\partial t}$$

Equating [18] to the constitutive relationship for the air phase (i.e., eq. [4]), gives:

$$[19] \quad m_1^a \frac{\partial(\sigma - u_a)}{\partial t} + m_2^a \frac{\partial(u_a - u_w)}{\partial t} \\ = \frac{-DR\theta}{wp} \frac{\partial^2 u_a}{\partial y^2} + \frac{(1 - S)n}{p} \frac{\partial u_a}{\partial t}$$

The change in total stress with respect to time can be set to zero for the consolidation process. Simplifying and rearranging eq. [19], the air phase partial differential equation can be written as follows.

$$[20] \quad \partial u_a / \partial t = -C_a (\partial u_w / \partial t) + c_v^a (\partial^2 u_a / \partial y^2)$$

where:

$$C_a = \frac{m_2^a / m_1^a}{(1 - m_2^a / m_1^a) + \frac{(1 - S)n}{(u_a + u_{am})m_1^a}}$$

and is called the interactive constant associated with the air phase equation. This equation may be further simplified by defining R_a as m_2^a / m_1^a .

$$c_v^a = \frac{DR\theta}{w} \frac{1}{(1 - R_a)(u_a + u_{am})m_1^a + (1 - S)n}$$

and is called the coefficient of consolidation with respect to the air phase.

As a soil becomes completely dry, the interactive constant approaches zero and eq. [20] reverts to the form presented by Blight (1971).

The dissipation of the excess pressure in the pore-air and pore-water phases is obtained by a simultaneous so-

lution of eqs. [12] and [20] using the finite difference technique described in the Appendix.

The results can be expressed in a dimensionless form by defining an average degree of consolidation and time factor for each of the fluid phases. The average degree of consolidation for the water phase is:

$$[21] \quad U_w = 1 - \frac{\int_0^{2H} u_w dy}{\int_0^{2H} u_{wi} dy}$$

where:

U_w = average degree of consolidation with respect to the water phase,
 u_{wi} = initial pore-water pressure,
 u_w = pore-water pressure at any time, and
 H = length of drainage path.

The time factor for the water phase is:

$$[22] \quad T_w = c_v^w t / H^2$$

where:

t = elapsed time.

Similarly, the average degree of consolidation and the dimensionless time factor with respect to the air phase are defined as:

$$[23] \quad U_a = 1 - \frac{\int_0^{2H} u_a dy}{\int_0^{2H} u_{ai} dy}$$

and

$$[24] \quad T_a = c_v^a t / H^2$$

where:

U_a = average degree of consolidation with respect to the air phase,
 T_a = time factor with respect to the air phase,
 u_{ai} = initial air pressure, and
 u_a = air pressure at any time.

Figure 3 shows the water phase degree of consolidation versus time factor curves for various air-water interaction constants. Similar curves for the air phase are shown in Fig. 4. The interactive constant in the air phase partial differential equation was assumed to be constant for the calculation of pore-air pressure dissipation. The curves cover anticipated reasonable ranges for the soil moduli. The consolidation curves also show a smooth transition towards the case of a completely saturated soil (Terzaghi 1936) and the case of a completely dry soil (Blight 1971).

Fig. 3. Dimensionless time factor versus degree of consolidation curves for the water phase.

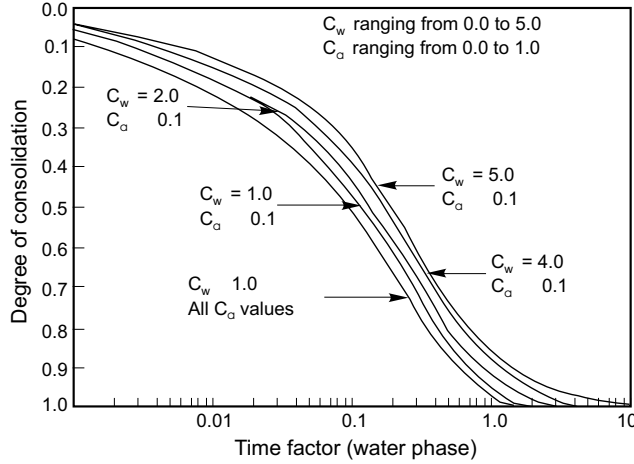
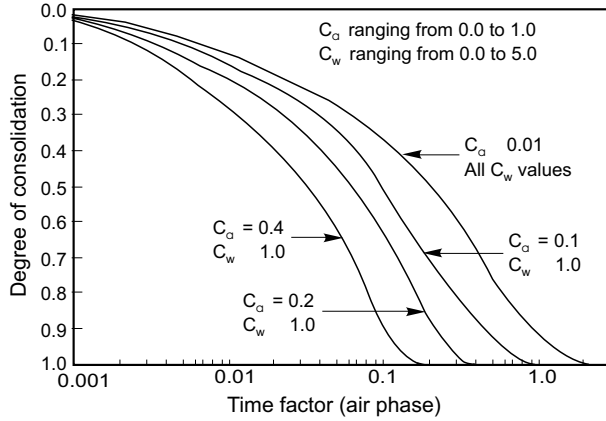


Fig. 4. Dimensionless time factor versus degree of consolidation curves for the air phase.



Varying permeabilities during consolidation

The partial differential equation for the pore-water and pore-air phases can also be derived for the case where the coefficients of permeability are variables during the process. The derivations follow a form similar to that presented above but the coefficients of permeability are treated as variables during differentiation. The pore-water partial differential equation now becomes:

$$[25] \quad \frac{\partial u_w}{\partial t} = -C_w \frac{\partial u_a}{\partial t} + c_{v1}^w \left[k_w \frac{\partial^2 u_w}{\partial y^2} + \frac{\partial u_w}{\partial y} \frac{\partial k_w}{\partial y} \right]$$

where:

$$c_{v1}^w = 1 / (R_w \gamma_w m_1^w)$$

The pore-air partial differential equation becomes:

$$[26] \quad \frac{\partial u_a}{\partial t} = -C_a \frac{\partial u_w}{\partial t} + c_{v1}^a \left[(u_a + u_{am}) \left(k_a \frac{\partial^2 u_a}{\partial y^2} + \frac{\partial u_a}{\partial y} \frac{\partial k_a}{\partial y} \right) + k_a \frac{\partial u_a}{\partial y^2} \right]$$

where:

$$c_{v1}^a = 1 / [(1 - R_a)(u_a + u_{am})m_1^a + (1 - S)n]$$

These equations can readily be solved using a finite difference technique; however, it is difficult to present the solutions in dimensionless form due to non-linearity.

Pore pressure boundary condition equations

When an external load is applied to an element of unsaturated soil, instantaneous compression occurs under undrained conditions and excess pressures are induced in the air and water phases. Two equations are necessary to predict the relative magnitudes of the excess pore-air and pore-water pressures. The pore pressures depend upon the compressibility of the soil structure, the air and water phases. In addition, the contractile skin has an effect on the relative changes in the pore-air and pore-water pressures. The induced pore pressures form the boundary conditions for the consolidation process.

The overall continuity requirement for the soil requires that the compression of the soil structure must equal the compression associated with the pore-fluid phases. This is satisfied by equating eqs. [2] and [8] and using the water phase as the reference phase for the pore-fluid pressure (Fredlund 1976).

$$[27] \quad m_1^s \Delta(\sigma - u_a) + m_2^s \Delta(u_a - u_w) =$$

$$\left[S\beta_w + \frac{\Delta u_a}{\Delta u_w} \frac{(1 - S)}{(u_a + u_{am})} \right] n \Delta u_w$$

Defining R_s as m_2^s / m_1^s , eq. [27] can be solved for the change in pore-water pressure.

$$[28] \quad \Delta u_w = \left[\frac{(R_s - 1) - \frac{(1 - S)n}{(u_a + u_{am})m_1^s}}{R_s + Sn\beta_w / m_1^s} \right] \Delta u_a + \left[\frac{1}{R_s + Sn\beta_w / m_1^s} \right] \Delta \sigma$$

Equation [28] involves two unknowns (i.e., Δu_w and Δu_a) and therefore another equation is required for its solution. A second equation is also logical since only one of two necessary constitutive relations has been used in formulating eq. [28]. The second constitutive relation can be incorporated by considering the continuity of the air phase. Volume change described by the compression of

the air phase must equal the volume change defined by the air phase constitutive relationship.

$$[29] \quad m_1^a \Delta(\sigma - u_a) + m_2^a \Delta(u_a - u_w) = (1 - S)n / (u_a + u_{atm}) \Delta u_a$$

Simplifying eq. [29] and solving for the change in pore-air pressure gives:

$$[30] \quad \Delta u_a = \left[\frac{R_a}{(R_a - 1) - \frac{(1 - S)n}{(u_a + u_{atm})m_1^a}} \right] \Delta u_w - \left[\frac{1}{(R_a - 1) - \frac{(1 - S)n}{(u_a + u_{atm})m_1^a}} \right] \Delta \sigma$$

Equations [28] and [30] can be solved for the changes in pore-air and pore-water pressures resulting from a change in the applied load. Let us simplify these equations by defining the following variables.

$$[31] \quad R_1 = \frac{(R_s - 1) - \frac{(1 - S)n}{(u_a + u_{atm})m_1^s}}{R_s + Sn\beta_w / m_1^s}$$

$$[32] \quad R_2 = 1 / (R_s + Sn\beta_w / m_1^s)$$

$$[33] \quad R_3 = \frac{R_a}{(R_a - 1) - \frac{(1 - S)n}{(u_a + u_{atm})m_1^a}}$$

$$[34] \quad R_4 = \frac{1}{(R_a - 1) - \frac{(1 - S)n}{(u_a + u_{atm})m_1^a}}$$

Therefore, eqs. [28] and [30] can be written:

$$[35] \quad \Delta u_w = R_1 \Delta u_a + R_2 \Delta \sigma$$

$$[36] \quad \Delta u_a = R_3 \Delta u_w + R_4 \Delta \sigma$$

Equations [35] and [36] are combined and solved to give two pore pressure coefficients that can be used to compute the boundary conditions.

$$[37] \quad B_w = \Delta u_w / \Delta \sigma = (R_2 - R_1 R_4) / (1 - R_1 R_3)$$

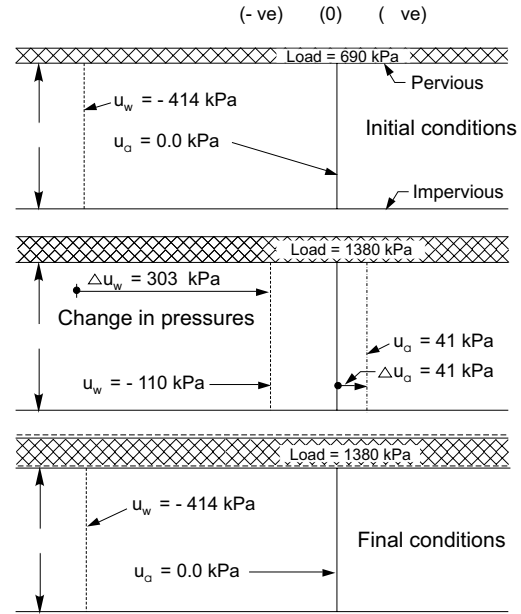
$$[38] \quad B_a = \Delta u_a / \Delta \sigma = (R_2 R_3 - R_4) / (1 - R_1 R_3)$$

Equations [37] and [38] require an iterative technique in their solution since R_1 , R_3 , and R_4 contain the absolute pore-air pressure value.

Example Problem

An example problem is solved to demonstrate the solution of boundary condition equations (i.e., eqs. [37] and [38]) and the partial differential equations for the pore-air and pore-water phases (i.e., eqs. [12] and [20]). Let us as-

Fig. 5. Initial and final boundary conditions for a consolidation process.



sume that a compacted soil layer overlying an impervious surface is initially in equilibrium with the stresses shown in Fig. 5. The initial equilibrium conditions are altered by changing the total stress applied to the top of the soil. The instantaneous change in total stress of 689 kPa (100 psi) produced a corresponding pore-air and pore-water pressure change of 41.4 kPa (6 psi) and 303 kPa (44 psi), respectively. The initial and final stresses (and stress state variables) with the assumed soil properties are shown in Table 1. The corresponding stress state variable changes on the constitutive surface are shown in Fig. 6. The dissipation of the excess pore-water and pore-air pressures is obtained by simultaneous solution of eqs. [12] and [20].

The average degree of consolidation with respect to the water phase (U_w) is plotted against the time factor for water phase (T_w) in Fig. 7. It shows that the U_w versus T_w plot is only slightly different than the conventional Terzaghi consolidation plot for saturated soils. This deviation of the U_w versus T_w plot from the conventional Terzaghi plot can be attributed to the interaction effect in the simultaneous solution of the two partial differential equations.

The average degree of consolidation with respect to the air phase (U_a) plotted against a time factor with respect to the air phase (T_a) is presented in Fig. 8. It also shows a slight deviation from the Terzaghi solution for saturated soils. It should be noted that the c_a^a term has been assumed constant during the consolidation process. To do this, the absolute air pressure has been set to a constant equal to the average air pressure during the consolidation process. The error involved for this example problem is negligible.

Figure 9 shows the percent mid-plane pore-water and pore-air pressures plotted against the dimensionless time

Table 1. Initial and final stress conditions in the soil.

Stresses	σ psi (kPa)	u_a psi* (kPa)	u_w psi (kPa)	$(\sigma - u_a)$ psi (kPa)	$(u_a - u_w)$ psi (kPa)
Initial condition	100.0 (690)	0.0 (0.0)	-60.0 (-414)	100.0 (690)	60.0 (414)
Instant after loading					
$\Delta u_a = +6$ psi (41 kPa);	200.0	6.0	-16.0	194.0	22.0
$\Delta u_w = +44$ psi (303 kPa)	(1380)	(41)	(-110)	(1338)	(152)
Final conditions	200.0 (1380)	0.0 (0.0)	-60.0 (-414)	200.0 (1380)	60.0 (414)

Notes: $S = 50\%$; $n = 50\%$; $m_1^a = 0.0008 \text{ in}^2/\text{lb}$ ($1.16 \times 10^{-4} \text{ m}^2/\text{kN}$); $m_1^s = 0.001 \text{ in}^2/\text{lb}$ ($1.45 \times 10^{-4} \text{ m}^2/\text{kN}$); $R_a = -0.01$; $R_w = 0.5$; and $R_s = 0.5$.
*Gauge.

Fig. 6. Initial and final stress points on a constitutive surface for the consolidation process.

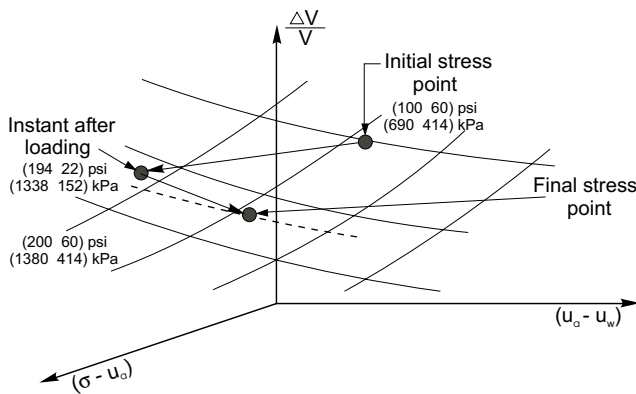
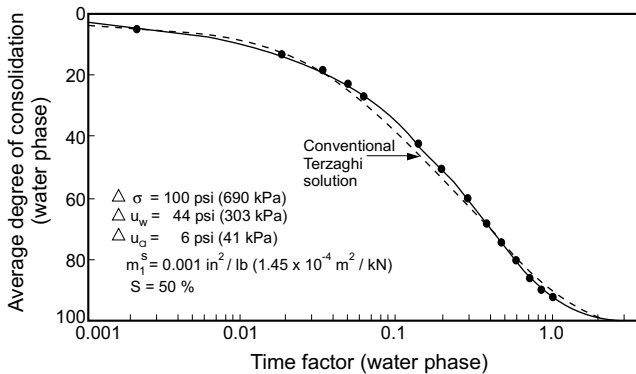


Fig. 7. Average degree of consolidation versus time factor for the water phase.



factors for both of the fluid phases. Dimensionless isochrones for both the water and the air phases are shown in Figs. 10 and 11, respectively. The plots show only slight deviations from the conventional Terzaghi plots. Other example problems have shown the interaction effects between the air and water phase partial differential equations to be more extreme.

Summary

All the necessary physical relationships are available for a complete formulation of the one-dimensional consolidation problem in unsaturated soils. The formulation

Fig. 8. Average degree of consolidation versus time factor for the air phase.

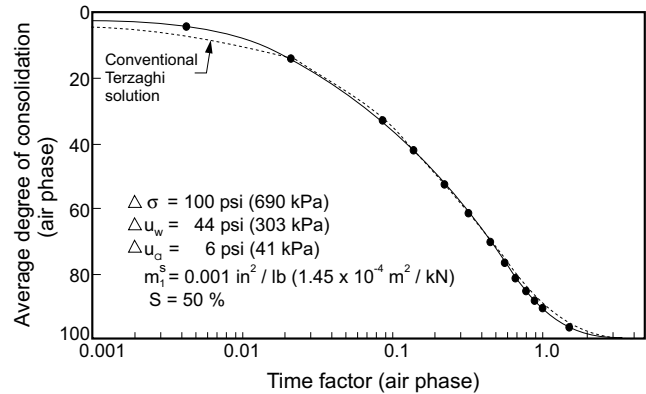
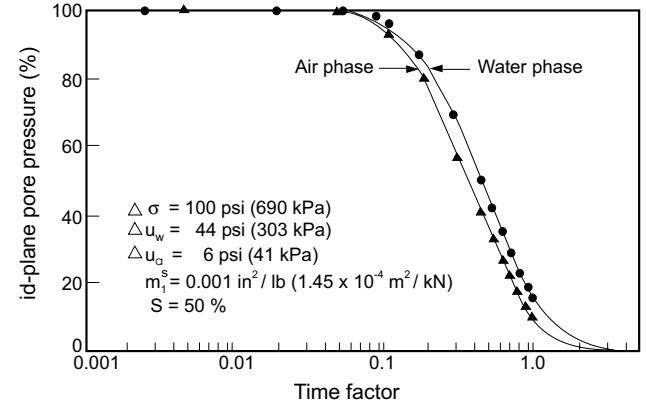
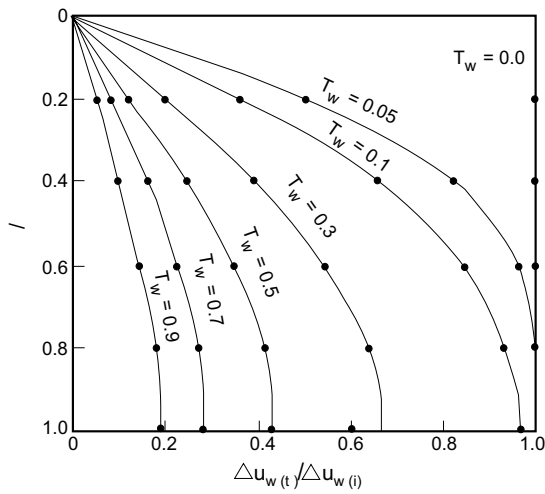


Fig. 9. Percent mid-plane pore-air and pore-water pressure versus time factor.



proceeds along lines similar to that of Terzaghi's conventional theory for saturated soils. However, it is necessary to have one partial differential equation for the air phase and another partial differential equation for the water phase (i.e., eqs. [12] and [20]). The two partial differential equations must be solved simultaneously.

For the completely dry and saturated cases, there is a smooth transition to the conventional solutions. At intermediate degrees of saturation there are varying amounts of interaction between the air and water phases during the dissipation process.

Fig. 10. Dimensionless isochrones for the water phase.

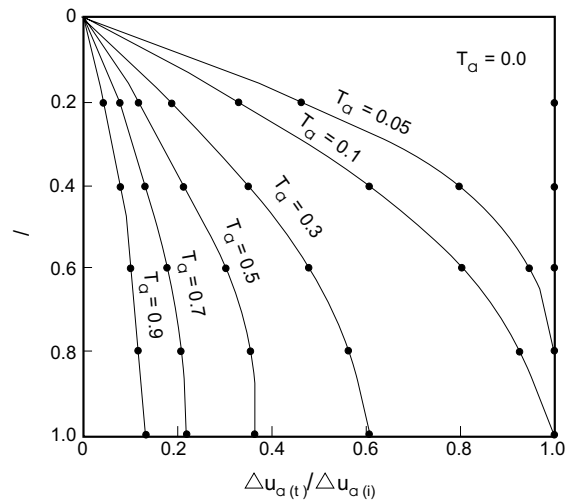
The necessary physical relationships are also available for a rigorous formulation of the pore-air and pore-water pressures generated during undrained loading. Once again two equations are formulated (i.e., eqs. [37] and [38]) that must be solved for the pore-air and pore-water boundary conditions to the consolidation problem.

Acknowledgements

The authors would like to acknowledge the Department of Highways and the Saskatchewan Research Council, Government of Saskatchewan, for their interest and financial support of research into transient processes in unsaturated soils.

References

- Aitchison, G.D., Russam, K., and Richards, B.G. 1965. Engineering concepts of moisture equilibria and moisture changes in soils. *In* Moisture equilibria and moisture changes in soils beneath covered areas. A Symposium in Print. Edited by G.D. Aitchison, Butterworth, Sydney, Australia, pp. 7–21.
- Barden, L. 1965. Consolidation of compacted and unsaturated clays. *Géotechnique*, **15**(3): 267–286.
- Biot, M.A. 1941. General theory of three-dimensional consolidation. *Journal of Applied Physics*, **12**(2): 155.
- Bishop, A.W. 1959. The principle of effective stress. Lecture delivered in Oslo, Norway, in 1955. *Teknisk Ukeblad*, **106**(39): 859–863.
- Blight, G.E. 1971. Flow of air through soils. *ASCE Journal of the Soil Mechanics and Foundations Division*, **97**(SM4): 607–624.
- Childs, E.C., and Collis-George, N. 1950. The permeability of porous material. *Proceedings of the Royal Society of London*, **201**: 392–405.
- Fredlund, D.G. 1973. Volume change behavior of unsaturated soils. Ph.D. thesis, University of Alberta, Edmonton, AB, Canada.
- Fredlund, D.G. 1976. Density and compressibility characteristics of air-water mixtures. *Canadian Geotechnical Journal*, **13**: 386–396.

Fig. 11. Dimensionless isochrones for the air phase.

Fredlund, D.G., and Morgenstern, N.R. 1976. Constitutive relations for volume change in unsaturated soils. *Canadian Geotechnical Journal*, **13**: 261–276.

Fredlund, D.G., and Morgenstern, N.R. 1977. Stress state variables for unsaturated soils. *ASCE Journal of the Geotechnical Engineering Division*, **103**(GT5), pp. 447–466.

Hasan, J.U. 1977. Transient flow processes in unsaturated soils. M.Sc. thesis, University of Saskatchewan, Saskatoon, SK, Canada.

Terzaghi, K. 1936. The shear resistance of saturated soils. *Proceedings, 1st International Conference on Soil Mechanics and Foundation Engineering*, Cambridge, MA, Vol. 1, pp. 54–56.

Appendix

An explicit finite difference technique is used to solve each of the partial differential equations. Since both equations must be solved simultaneously, the solution iterates between the two equations. In addition, one of the equations is non-linear.

Figure A1 shows the finite difference grids for the example problem and defines the related variables. Following are the finite difference forms for the partial differential equations.

Finite Difference Form of the Water Phase Partial Differential Equation

$$[A1] \quad u_w(i, j+1) = u_w(i, j) - C_w [u_a(i, j+1) - u_a(i, j)] + c_v^w \Delta t / (\Delta y)^2 [u_w(i+1, j) + u_w(i-1, j) - 2u_w(i, j)]$$

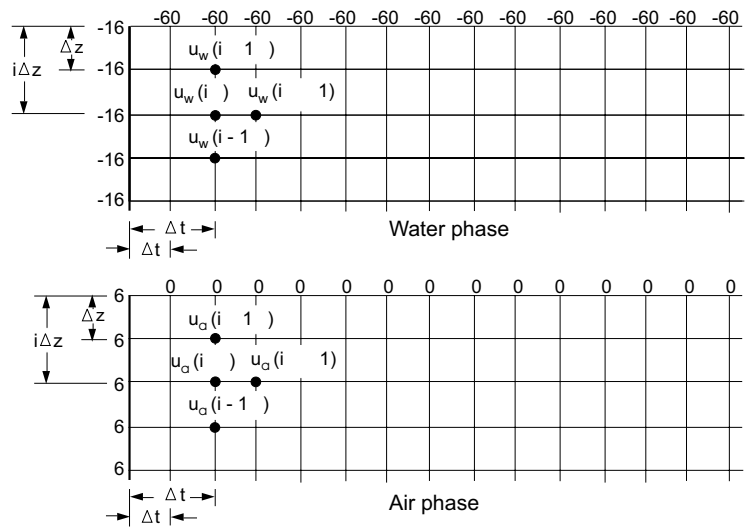
The $c_v^w \Delta t / (\Delta y)^2$ term has been set to 0.25 for the solution of the example problem.

Finite Difference Form of the Air Phase Partial Differential Equation

$$[A2] \quad u_a(i, j+1) = u_a(i, j) - C_a [u_w(i, j+1) - u_w(i, j)] + c_v^a \Delta t / (\Delta y)^2 [u_a(i+1, j) + u_a(i-1, j) - 2u_a(i, j)]$$

The $c_v^a \Delta t / (\Delta y)^2$ term has again been set to 0.25.

Fig. A1. Finite difference mesh for the consolidation equations.



The use of a rheological model for the visualization of unsaturated soil processes

D.G. Fredlund and A. Xing

Abstract: A rheological model is used to serve the role of aiding in visualizing the transient flow processes in an unsaturated soil subjected to various types of loading. The loadings may be due to an applied load or a change in the boundary flux or boundary pore pressure conditions. Two linear rheological elements connected in series were used to simulate each layer of an unsaturated soil in a strata with n layers. Two systems of n linear differential equations were required to characterize the flow processes in the unsaturated soil. Solutions to the two systems of linear differential equations are determined from the eigenvalues of the systems.

Key words: rheological model, unsaturated soil, flow processes, stress state variables, pore-water pressure, pore-air pressure, mathematical model.

Introduction

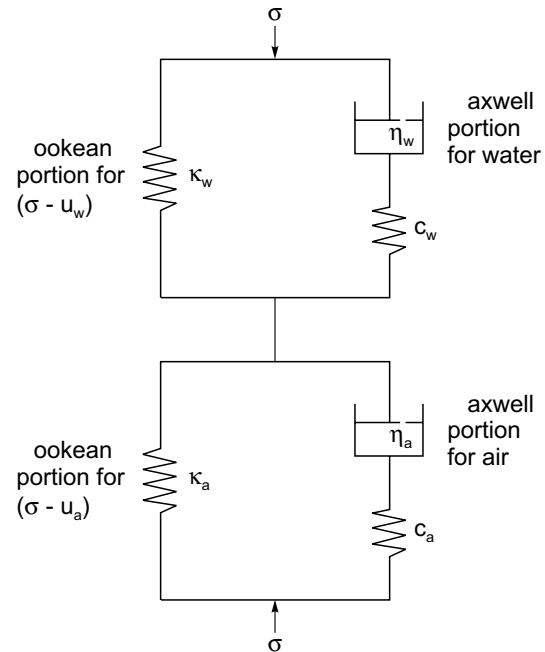
The primary value of rheological models lies in the role they serve as an aid in visualizing soil behavior. For example, a rheological model can illustrate how a load applied to a saturated soil is initially carried by the water phase and is slowly transferred to the soil structure as the pore-water pressure dissipates.

The proposed rheological model for unsaturated soils

Two linear rheological elements connected in series, one for the water phase and the other for the air phase were used to simulate the behavior of a layer of unsaturated soil (Fig. 1). The entire unsaturated soil strata can be simulated by interconnecting the rheological elements for both the air and water portions of the soil of subsequent layer, in series. In a non-homogeneous soil strata, the division of the strata into layers allows for the use of different soil parameters for each soil type.

Fredlund and Morgenstern (1977), showed on the basis of multiphase continuum mechanics principles that it was possible to use any two of the three possible stress state variables (i.e., $(\sigma - u_w)$, $(\sigma - u_a)$ and $(u_a - u_w)$) in order to describe soil behavior. When developing a rheological model to simulate unsaturated soil behavior, it appears that the $(\sigma - u_w)$ and $(\sigma - u_a)$ combination has advantages over other combinations.

Fig. 1. Two linear rheological elements in series representing the $(\sigma - u_w)$ and $(\sigma - u_a)$ stress state variables.



The Hookean constants, c_w and c_a , account for the compressibility of water and air, respectively. The fluids in the dashpots are assumed to be incompressible. The Hookean spring constants, κ_w and κ_a , account for the compressibility of the soil structure with respect to each of the stress state variables, $(\sigma - u_w)$ and $(\sigma - u_a)$, respectively, where σ is the total stress applied, u_w is the pore-water pressure and u_a is the pore-air pressure.

One linear rheological element is required to model the stress state variable which involves the solid and the water phase (i.e., $(\sigma - u_w)$) and another to model the stress state variable which involves the solid and the air phase (i.e., $(\sigma - u_a)$). The two linear elements are connected in series as the two stress state variables are independent.

D.G. Fredlund. Professor, Department of Civil Engineering, University of Saskatchewan, 57 Campus Drive, Saskatoon, SK, Canada S7N 5A9.

A. Xing. Research Associate, Department of Civil Engineering, University of Saskatchewan, 57 Campus Drive, Saskatoon, SK, Canada S7N 5A9.

Reproduced with permission from the *Proceedings, 6th National Congress on Mechanics*, Hanoi, Vietnam, December 3-5, 1997.

The hydraulic conductivity properties of the soil with respect to water and air are represented by the viscosity constants η_w and η_a , respectively. The total strain of a unit infinitesimal layer is denoted by ε . The strain of the linear rheological elements for the water phase and the air phase are denoted by ε_w and ε_a , respectively.

Boundary conditions

The total stress applied to a linear rheological model acts equally on both of the elements associated with each of the two stress state variables, $(\sigma - u_w)$ and $(\sigma - u_a)$, respectively.

The stress in the Maxwell and Hookean portions of each of the linear elements must always add up to the total stress applied to satisfies the conservation of energy requirement (i.e., $\sigma = \sigma_H + \sigma_M$ where σ_H = stress on the Maxwell portion of the linear element, σ_M = stress on the Hookean portion of the linear element which could represent either the pore-water pressure, u_w , or the pore-air pressure, u_a , σ = total stress applied to the linear element).

The total strain, ε , is always equal to the sum of the strain in the linear element associated with the $(\sigma - u_w)$ stress state variable, ε_w , and the strain in the linear element associated with the $(\sigma - u_a)$ stress state variable, ε_a (i.e., $\varepsilon = \varepsilon_w + \varepsilon_a$).

The Hookean portion and the Maxwell portion of each linear rheological element must always deform equal amounts.

Constitutive relations

First, consider only the linear rheological element associated with the stress state variable, $(\sigma - u_w)$. The total stress applied can be written in terms of the stress in the Hookean portion plus the stress in the Maxwell portion of the model:

$$[1] \quad \sigma = \sigma_H + \eta_w(\varepsilon_w - \varepsilon_c)$$

where:

ε_c = strain in the Hookean spring of the Maxwell portion of the model which is related to the compressibility of water,

ε_w = strain in the dashpot due to the flow of water,

$\dot{\varepsilon}_w, \dot{\varepsilon}_c$ = the derivatives of ε_w and ε_c , respectively, and

η_w = dashpot constant for the water phase.

Since

$$\sigma_H = \kappa_w \varepsilon_w$$

and

$$\sigma_M = c_w \varepsilon_c$$

where:

κ_w = Hookean spring constant related to the compressibility of the soil with respect to a change in $(\sigma - u_w)$, and

c_w = Hookean spring constant related to the bulk compressibility of water.

Equation [1] can be re-arranged to give a rate of strain condition for the linear rheological element associated with $(\sigma - u_w)$:

$$[2] \quad \varepsilon = \frac{\dot{\sigma}_M}{c_w} = \frac{\dot{\sigma} - \dot{\sigma}_H}{c_w} = \frac{0 - \dot{\sigma}_H}{c_w} = -\frac{\kappa_w}{c_w} \dot{\varepsilon}_w$$

A similar rate of strain condition can be written for the linear rheological element associated with $(\sigma - u_a)$.

Differential equations for the linear rheological elements of a single layer

The stress-strain equation for the linear rheological element associated with $(\sigma - u_w)$ can be written as:

$$[3] \quad \varepsilon_w = \frac{\sigma}{\kappa_w + c_w} \left\{ 1 + \frac{c_w}{\kappa_w} \left[1 - e^{-\frac{\kappa_w c_w}{\eta_w (\kappa_w + c_w)} t} \right] \right\}$$

The stress-strain equation for the linear rheological element associated with $(\sigma - u_a)$ can be written as:

$$[4] \quad \varepsilon_a = \frac{\sigma}{\kappa_a + c_a} \left\{ 1 + \frac{c_a}{\kappa_a} \left[1 - e^{-\frac{\kappa_a c_a}{\eta_a (\kappa_a + c_a)} t} \right] \right\}$$

Mathematical model for a multi-layer system

A transient flow process such as consolidation takes place as a result of the application of a total load to a soil. In an unsaturated soil with one way drainage through the top, both water and air would move upward from a lower layer to an upper layer. The water phase and the air phase are assumed to be continuous throughout the soil. For illustration, this process is simulated using the 3-layer system shown in Fig. 2.

The linear rheological elements associated with the stress state variables, $(\sigma - u_w)$ and $(\sigma - u_a)$, in the n -layer strata can be separated into two parts. An equivalency for the linear rheological elements is shown in Fig. 3. For simplicity, the compressibility of the air phase and the viscosity of the water phase are assumed linear in this paper.

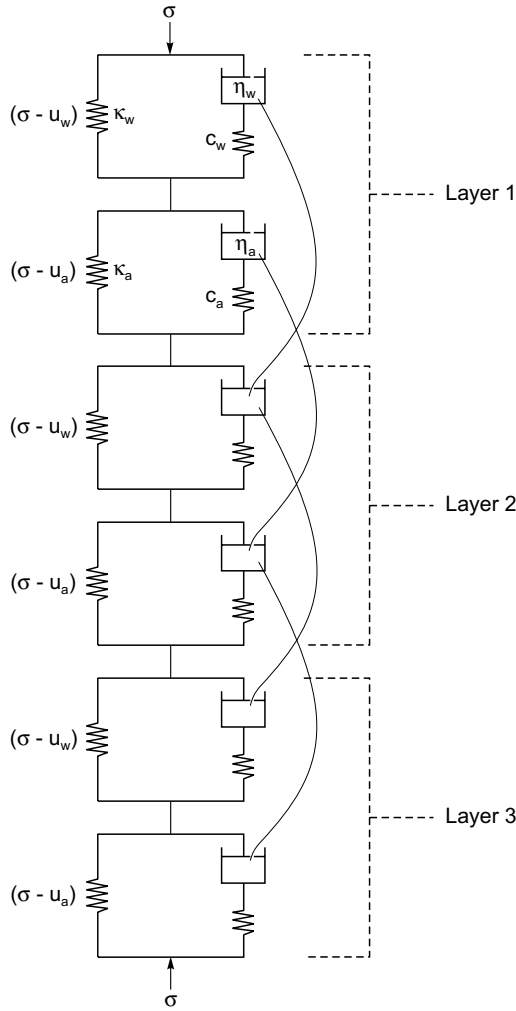
The compressibility of water and air is simulated using Hookean springs. In both the water and air phases, only the bottom layer is truly a linear rheological element. The other layers are a slight modification of the linear rheological element in that the pressure in one piston is fed into the adjacent piston in a series manner. Based on eq. [2], the water phase differential equations can be written as:

$$[5] \quad \dot{\varepsilon}_i = -\frac{\kappa_w}{c_w} (z_i - z_{i+1}), \quad i = 1, 2, \dots, n-1$$

$$[6] \quad \dot{\varepsilon}_n = -\frac{\kappa_w}{c_w} (z_n - 0)$$

where:

Fig. 2. A 3-layer system demonstrating 1-D consolidation process in an unsaturated soil.



$z_1(t), z_2(t), \dots, z_n(t)$ denote the positions of the n pistons, respectively (see Fig. 3), and $\epsilon_1(t), \epsilon_2(t), \dots, \epsilon_n(t)$ denote the strains of the n pistons, respectively.

In the first layer of the linear rheological element associated with the stress state variable, $(\sigma - u_w)$, the total stress, σ , is divided between the pore-water pressure and the stress acting in the spring representing the soil structure. That is,

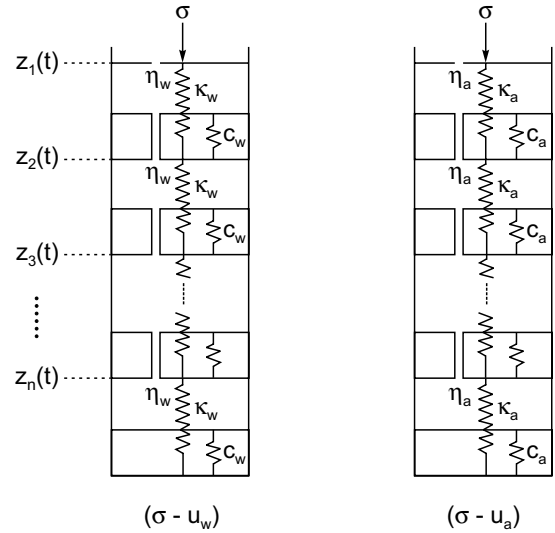
$$[7] \quad \sigma = \kappa_w(z_1 - z_2) + \eta_w(z_1 - \epsilon_1 - \epsilon_2 - \dots - \epsilon_n)$$

Substituting eqs. [5] and [6] into the conservation equation (i.e., eq. [7]) gives:

$$[8] \quad \sigma = \kappa_w(z_1 - z_2) + \eta_w \frac{c_w + \kappa_w}{c_w} z_1$$

The total stress, σ , also acts on the second piston associated with the linear rheological element for the stress state variable, $(\sigma - u_w)$, of the second layer. However, the Hookean stress, $\kappa_w(z_1 - z_2)$, developed in the first layer is the only stress which causes the piston in the element of

Fig. 3. Proposed rheological models for the $(\sigma - u_w)$ and $(\sigma - u_a)$ stress state variables.



the second layer to move downward. This stress is again divided between the spring stress and pore-water pressure increment in the second layer. The rates of strain for the second layer can be rewritten in terms of the water phase dashpot constant and the spring constants for the water and the soil structure as:

$$[9] \quad \kappa_w(z_1 - z_2) = \kappa_w(z_2 - z_3) + \eta_w \frac{c_w + \kappa_w}{c_w} z_2$$

Similar equations can be written for the third and subsequent layers. For the n -th layer:

$$[10] \quad \kappa_w(z_{n-1} - z_n) = \kappa_w z_n + \eta_w \frac{c_w + \kappa_w}{c_w} z_n$$

Equations [8] to [10] represent a system of linear differential equations for the linear rheological element associated with the stress state variable, $(\sigma - u_w)$, of the unsaturated soil. The system of linear differential equations for the response of the linear rheological element associated with the stress state variable, $(\sigma - u_w)$, can be written in matrix form as:

$$[11] \quad \dot{z} = \mathbf{A}z + b, z(0) = z^0$$

where:

$$\mathbf{A} = \frac{\kappa_w c_w}{\eta_w (\kappa_w + c_w)} \begin{bmatrix} -1 & 1 & 0 & 0 & \dots & 0 \\ 1 & -2 & 1 & 0 & \dots & 0 \\ \dots & \dots & \dots & \dots & \dots & \dots \\ 0 & \dots & \dots & 1 & -2 & 1 \\ 0 & \dots & \dots & 0 & 1 & -2 \end{bmatrix}$$

$$b = \frac{\sigma c_w}{\eta_w(\kappa_w + c_w)} \begin{bmatrix} 1 \\ 0 \\ \cdot \\ \cdot \\ \cdot \\ 0 \end{bmatrix}$$

$$z^0 = \frac{\sigma}{\kappa_w + c_w} \begin{bmatrix} n \\ n-1 \\ \cdot \\ \cdot \\ \cdot \\ 1 \end{bmatrix}$$

The non-zero initial condition (i.e., $z(0) = z^0$) is due to the compressibility of water. If water is assumed to be incompressible, the c_w term goes to infinity and z_0 becomes a zero vector and the system of linear differential equations (i.e., eq. [11]) reduces to the equation for the Kelvin model for saturated soils (Xing et al. 1995).

The system of linear differential equations for the linear rheological element associated with the stress state variable, $(\sigma - u_a)$, has the same form as eq. [11] for the stress state variable, $(\sigma - u_w)$, with all the subscripts w replaced by the subscripts a .

The total strain for the unsaturated soil is the summation of the solutions for the linear rheological elements associated with the stress state variables, $(\sigma - u_w)$, and $(\sigma - u_a)$. The total strain, $\varepsilon(t)$, is given by,

$$[12] \quad \varepsilon(t) = \frac{z_{w1}(t) + z_{a1}(t)}{z_{w1}(\infty) + z_{a1}(\infty)}$$

where:

$$z_w(t) = (z_{w1}(t), \dots, z_{wn}(t)), \text{ and}$$

$$z_a(t) = (z_{a1}(t), \dots, z_{an}(t)) \text{ denote the solutions for the } (\sigma - u_w) \text{ and } (\sigma - u_a) \text{ portions, respectively;}$$

$z_{w1}(\text{inf})$ and $z_{a1}(\text{inf})$ denote the limits of $z_{w1}(t)$ and $z_{a1}(t)$, respectively, as time goes to infinity.

The pore-water pressure, $u_{wi}(t)$, and the pore-air pressure, $u_{ai}(t)$, in the i -th layer are respectively given by the following eqs. [13] and [14].

$$[13] \quad u_{wi}(t) = \sigma - \kappa_w [z_{wi}(t) - z_{w(i+1)}(t)]$$

$$[14] \quad u_{ai}(t) = \sigma - \kappa_a [z_{ai}(t) - z_{a(i+1)}(t)]$$

Closed-form solution for the rheological model

The closed-form solution for eq. [11] can be expressed as,

$$[15] \quad z(t) = \begin{bmatrix} z_1(t) \\ z_2(t) \\ \cdot \\ \cdot \\ z_n(t) \end{bmatrix} = e^{At} z^0 + \int_0^t e^{A(t-s)} b \, ds$$

The coefficient matrix, A , of the initial value problem given by eq. [11] is tri-diagonal and satisfies the condition of a Jordan matrix. According to the Sturm theorem (Dickson 1939), A has n real distinct eigenvalues. The n corresponding eigenvectors form the fundamental matrix for the system of differential equations (i.e., eq. [11]). Using matrix theory, it can be further proved that all the eigenvalues are negative. The solution of eq. [11] has the following form:

$$[16] \quad z_1(t) = \alpha_0 + \sum_{i=1}^n \alpha_i e^{\lambda_i t}$$

where:

$$a_i = \text{constant } (i = 0, 1, \dots, n)$$

$$\lambda_i = \text{eigenvalue of } A (\lambda_i < 0; \quad i = 1, 2, \dots, n)$$

Equation [15] implies that the consolidation process is primarily governed by the eigenvalues of A . The n eigenvalues of A are uniquely determined by the soil parameters since only κ_w and η_w appear in the coefficient matrix, A . The external load or stress, σ , only affects the magnitude of the strain.

Numerical solution for the proposed rheological model

A numerical solution was formulated for solving the two systems of linear differential equations using the Runge-Kutta method. The unsaturated soil simulated using the rheological model does not have to be homogeneous. Each layer can have its own soil parameters. A numerical solution is preferred if the soil is divided into a large number of layers.

Comparison of the rheological model with experimental data

The rheological model was compared to experimental results for a compacted kaolin. The compacted kaolin has an initial dry unit weight of 13.19 kN/m³, an initial void ratio of 1.07, an initial water content of 34.3% and an initial degree of saturation of 78.9% (data from Fredlund and Rahardjo 1993). The soil specimen was simulated by a 10-layer rheological model using approximate soil parameters obtained from a consolidation test where the total stress was increased from 101.1 kPa to 202.2 kPa.

The water phase constitutive relation can be written as:

$$[17] \quad \frac{dV_w / V_0}{d(\sigma - u_a)} = m_1^w + m_3^w \frac{d(\sigma - u_w)}{d(\sigma - u_a)}$$

where:

Fig. 4. Percent consolidation versus logarithm of time plot for compacted kaolin (Fredlund and Rahardjo 1993).

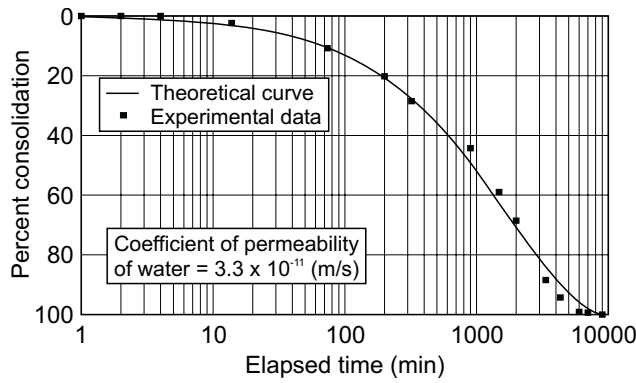
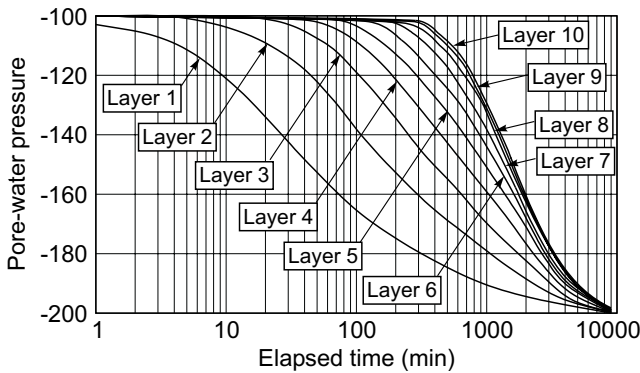


Fig. 5. Pore-water pressures in the compacted kaolin, from the linear rheological model.



dV_w / V_0 = change in the volume of water in the soil specimen with respect to the initial volume of the soil specimen,
 m_1^w = coefficient of water volume change with respect to a change in net normal stress,
 m_3^w = coefficient of water volume change with respect to a change in the stress state variable, $(\sigma - u_a)$.

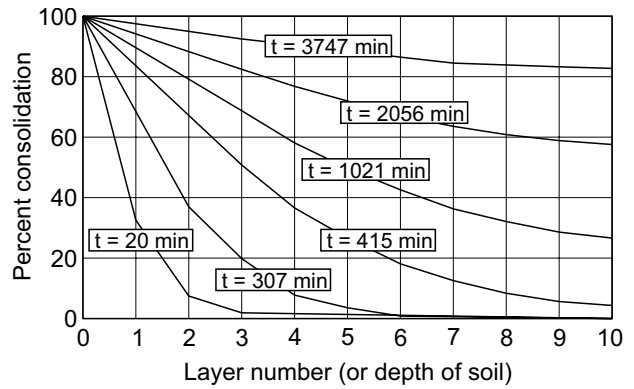
The following relationships for the water phase rheological model can be inferred:

$$[18] \quad \eta_w = \frac{\gamma_w}{k_w} \Delta z, \quad \kappa_w = \frac{1}{\Delta z} \left(\frac{1}{m_1^w + m_3^w} \right)$$

where:

k_w = coefficient of permeability with respect to water,
 γ_w = unit weight of water, and
 Δz = the thickness of each of the layers.

Fig. 6. Percent consolidation at different layers in the compacted kaolin, from the linear rheological model.



Similarly, for the air phase, the relationships are:

$$[19] \quad \eta_a = \frac{\gamma_a}{k_a} \Delta z, \quad \kappa_a = \frac{1}{\Delta z} \left(\frac{1}{m_1^a + m_3^a} \right)$$

where:

k_a = coefficient of permeability with respect to air,
 γ_a = unit weight of air,
 m_1^a = coefficient of air volume change with respect to a change in net normal stress,
 m_3^a = coefficient of air volume change with respect to a change in the stress state variable, $(\sigma - u_a)$.

The percent consolidation versus the logarithm of time plot is shown in Fig. 4. The pore-water pressures in each layer as a function of the logarithm of time are shown in Fig. 5. The percent consolidation versus the depth into the soil is shown in Fig. 6. It can be seen, from Fig. 4, that the theoretical curve computed using the rheological model (i.e., eq. [11]) is in good agreement with the experimental data.

References

Dickson, L. E. 1939. New first course in the theory of equations. John Wiley and Sons, Inc., New York, USA.
 Fredlund, D.G. and Rahardjo, H. 1993. Soil mechanics for unsaturated soils. John Wiley and Sons, New York.
 Fredlund, D.G. and Morgenstern, N.R. 1977. Stress state variables for unsaturated soils. ASCE Journal of Geotechnical Engineering, **103**(GT5): 447-466.
 Xing, A., Fredlund, D. G. and Gan, J. K-M. 1995. Use of a Kelvin rheological model to simulate the consolidation of a saturated soil strata. Proceedings, 15th Canadian Congress of Applied Mechanics, CANCAM 95, University of Victoria, May 28 to June 2. Edited by B. Jabbarok and S. Dost, Vol. 2, pp. 592-593.

Unsaturated soil consolidation theory and laboratory experimental data

D.G. Fredlund and H. Rahardjo

Abstract: The volume change process of an unsaturated soil was considered as a transient flow problem with water and air flowing simultaneously under an applied stress gradient. Laboratory experiments were performed to study the volume change behavior of unsaturated soils. Several compacted kaolin specimens were tested using modified Anteus oedometers and triaxial cells. Theoretical analyses were also made to best-fit the results from laboratory experiments. The fitting was accomplished by approximating the compressibility coefficients and adjusting the coefficients of permeability. The comparisons of the results obtained from the theory and the laboratory yield to a similar behavior of volume changes with respect to time.

Key words: unsaturated soil, volume change, consolidation, two-phase flow

Introduction

For saturated soils, a settlement analysis is usually performed using Terzaghi's theory of consolidation. In practice, many geotechnical problems involve unsaturated soils. The construction of earth-fill dams, highways, and airport runways always use unsaturated compacted soils. In addition, large portions of the earth's surface are covered with residual soils that are unsaturated. Heave and settlement problems are commonly encountered with these unsaturated soils.

The constitutive relations for volume change in an unsaturated soil were proposed by Fredlund and Morgenstern (1976). Laboratory experiments were also performed to study the volume change behavior of unsaturated soils (Fredlund 1973).

This paper presents theoretical analyses of the volume change process in unsaturated soils based on the proposed constitutive relations. Comparisons are made between the theoretical analyses and the laboratory time rate of deformation.

Theory

A stress gradient applied to an unsaturated soil will cause two phases (i.e., soil particle and contractile skin or air-water interface) to come to equilibrium, whereas the other two phases (i.e., air and water) will flow. The volume change process of an unsaturated soil can be treated

as a transient flow problem with water and air flowing simultaneously under an applied stress gradient.

The increase (swelling) or the decrease (consolidation) in the overall volume of an unsaturated soil can be predicted using the proposed constitutive relations (Fredlund and Morgenstern 1976). Assuming the soil particles are incompressible and the volume change of the contractile skin is internal to the element, the continuity requirement for a referential element can be written as

$$[1] \quad d\epsilon = d\theta_w + d\theta_a$$

where:

$d\epsilon$ = change in unit volumetric strain of the soil structure; that is, $d\epsilon = d\epsilon_x + d\epsilon_y + d\epsilon_z$ where ϵ_x , ϵ_y and ϵ_z , are the normal strains in the x -, y -, and z -directions, respectively,

$d\theta_w$ = net inflow or outflow of water from the unit element per unit volume, and

$d\theta_a$ = net inflow or outflow of air from the unit element per unit volume.

Equation [1] shows that only two of the three possible constitutive relations (i.e., the soil structure, water and air phases) are independent (Fredlund 1982). Therefore two constitutive relations are required to describe the volume change behavior in an unsaturated soil. The volume change constitutive relations for unsaturated soils were formulated using two independent stress-state variables, $(\sigma - u_a)$ and $(u_a - u_w)$ (Fredlund 1982), where, σ is the total normal stress, u_a represents the pore-air pressure, u_w the pore-water pressure, and $(u_a - u_w)$ the matric suction.

The constitutive equations for the soil structure, water and air phases are, respectively,

$$[2] \quad d\epsilon = m_1^s d(\sigma - u_a) + m_2^s d(u_a - u_w)$$

$$[3] \quad d\theta_w = m_1^w d(\sigma - u_a) + m_2^w d(u_a - u_w)$$

$$[4] \quad d\theta_a = m_1^a d(\sigma - u_a) + m_2^a d(u_a - u_w)$$

where:

D.G. Fredlund. Professor, Department of Civil Engineering, University of Saskatchewan, 57 Campus Drive, Saskatoon, SK, Canada S7N 5A9.

H. Rahardjo. Research Engineer, Department of Civil Engineering, University of Saskatchewan, 57 Campus Drive, Saskatoon, SK, Canada S7N 5A9.

Reproduced with permission from the American Society for Testing and Materials, Philadelphia, ASTM STP 892. *Consolidation of Soils: Testing and Evaluation.* Edited by R.N. Yong and E.C. Townsend, pp. 154-169, 1986.

- m_1^s = compressibility of soil structure with respect to a change in $(\sigma - u_a)$,
 m_2^s = compressibility of soil structure with respect to a change in $(u_a - u_w)$,
 m_1^w = slope of $(\sigma - u_a)$ versus θ_w ,
 m_2^w = slope of $(u_a - u_w)$ versus θ_w ,
 m_1^a = slope of $(\sigma - u_a)$ versus θ_a , and
 m_2^a = slope of $(u_a - u_w)$ versus θ_a .

Considering the volumetric continuity requirement shown in eq. [1], the following relationship for the compressibilities must be maintained:

$$[5] \quad m_1^s = m_1^w + m_1^a$$

$$[6] \quad m_2^s = m_2^w + m_2^a$$

The pore-water and pore-air pressures change with time and can be solved simultaneously using two independent partial differential equations. This method is called a two-phase flow approach and has been presented by Fredlund and Hasan (1979), Lloret and Alonso (1980) and Fredlund (1982).

In this paper, a one-dimensional transient flow process will be considered. The one-dimensional flow equations for the water and air phases can be derived by equating the time derivative of the relevant constitutive equation to the divergence of the velocity as described by the flow laws. Darcy's and Fick's laws are applied to the flow of water and air phases, respectively. The time derivative of the constitutive equation represents the amount of deformation that occurs under various stress conditions, while the divergence of velocity describes the rate of flow of the air and water.

Several assumptions are used in the derivations: (1) isotropic soil, (2) continuous air phase, (3) infinitesimal strains, (4) linear constitutive relations, (5) coefficients of permeability of water and air phases are functions of the volume-mass soil properties during the transient process, and (6) the effects of air diffusing through water, air dissolving in water, and the movement of water vapor are ignored.

The partial differential equation for the water phase in the y-direction can be written as (Fredlund 1982):

$$[7] \quad \frac{\partial u_w}{\partial t} = -C_w \frac{\partial u_a}{\partial t} + c_v^w \frac{\partial^2 u_w}{\partial y^2} + \frac{c_v^w}{k_w} \frac{\partial k_w}{\partial y} \frac{\partial u_w}{\partial y} + c_g \frac{\partial k_w}{\partial y}$$

where:

- t = time,
 $C_w = (1 - m_2^w / m_1^w) / (m_2^w / m_1^w)$ and is called the interaction constant associated with the water phase equation,
 $c_v^w = k_w / (\rho_w g m_2^w)$ and is called the coefficient of consolidation with respect to the water phase,
 k_w = coefficient of permeability with respect to the water phase,
 ρ_w = density of water,

- g = gravitational acceleration, and
 $c_g = 1 / m_2^w$ and is commonly referred to in the soil science literature as the gravity term constant.

The coefficient of permeability of water can vary significantly with space in the unsaturated soil. This variation is taken into account by the last two terms of eq. [7]. The volume-mass properties of the soil can be used to describe the variation in the coefficient of permeability (Corey 1957; Green and Corey 1971).

The air phase partial differential equation has the form (Fredlund 1982):

$$[8] \quad \frac{\partial u_a}{\partial t} = -C_a \frac{\partial u_w}{\partial t} + c_v^a \frac{\partial^2 u_a}{\partial y^2} + \frac{c_v^a}{D^*} \frac{\partial D^*}{\partial y} \frac{\partial u_a}{\partial y}$$

with:

$$C_a = \frac{m_2^a / m_1^a}{(1 - m_2^a / m_1^a) + \frac{(1 - S)n}{(u_a - u_{atm})m_1^a}}$$

and

$$c_v^a = \frac{D^* R \theta}{\omega} \frac{1}{(1 - m_2^a / m_1^a)(u_a + u_{atm})m_1^a + (1 - S)n}$$

where:

- C_a = interaction constant associated with the air phase equation,
 S = degree of saturation of the soil,
 n = porosity of the soil,
 u_{atm} = atmospheric pressure,
 c_v^a = coefficient of consolidation with respect to the air phase,
 $D^* = D / g$, the transmission constant of proportionality for the air phase,
 D = a transmission constant for the air phase having the same unit as coefficient of permeability,
 R = universal gas constant,
 θ = absolute temperature, and
 ω = molecular weight of the mass of air.

The last term in eq. [8] accounts for the variation of the transmission constant of proportionality for the air phase with respect to space. The constant of proportionality can be written as a function of the volume-mass properties of the soil.

The excess pore-air and pore-water pressures generated by a change in total stress can be computed using the pore pressure parameters associated with the air and water phases, respectively (Hasan and Fredlund 1980).

Laboratory tests

Laboratory experiments were performed on several compacted kaolin specimens using modified Anteus oedometers and triaxial cells (Fredlund 1973).

Equipment

The modified Anteus oedometers were used to perform one-dimensional consolidation tests. The modified Wykeham Farrance triaxial cells allowed isotropic volume change testing conditions.

A high air-entry ceramic disk was sealed to the lower pedestal. This disk allows the flow of water but prevents the flow of free air. Therefore the measurement of the pore-air and pore-water pressures can be made independently. A low air-entry disk was placed on the top of the specimen to facilitate the control of the pore-air pressure. This allowed the translation of the air and the water pressures to positive values in order to prevent cavitation of the water below the high air-entry disk (i.e., the axis-translation technique (Hilf 1948)). The total, pore-air, and pore-water pressure conditions can then be controlled to study the volume change behavior of unsaturated soils.

Two rubber membranes separated by a slotted tin foil were placed around the specimen. This composite membrane was found to be essentially impermeable for a long period of time.

Presentation of results

Five specimens of kaolin were compacted in accordance with the standard Proctor method. The initial volume-mass properties of each specimen are summarized in Table 1. Each experiment was performed by changing one of the stress state variable components: the total stress, σ , the pore-water pressure, u_w , or the pore-air pressure, u_a . The stress state component changes associated with each experiment are given in Table 2. In each case, the volume changes of soil structure and water phase were monitored.

Figure 1 shows a typical plot of volume changes due to an increment of total stress in Test 1. The plot exhibits a

decrease in volume of soil structure, air and water phases during the transient process. A large instantaneous volume decrease occurred at the time when the load was applied.

An increase in the pore-air pressure (Test 2) caused the soil structure to expand temporarily (Fig. 2). The increase in air pressure; however, resulted in an increase in matric suction ($u_a - u_w$), which in turn could cause a decrease in the soil structure at the end of the process.

A volume change process associated with a meta-stable structure is shown in Fig. 3. The decrease in air pressure (Test 3) reduced the matric suction ($u_a - u_w$) and allowed more water to flow into the specimen. The intake of water reduced the normal and shear stresses between the soil particles. As a result, the soil structure underwent a decrease in volume (i.e., collapse phenomenon).

An increase in water pressure could cause an increase in volume of the soil structure (Fig. 4 for Test 4) if the soil had a stable structure. On the other hand, when the soil structure was meta-stable, an increase in water pressures caused the soil structure to decrease in volume or collapse (Fig. 5).

Theoretical analyses

Attempts were made to best-fit the theoretical analyses of volume change with the results from laboratory experiments. This was accomplished by approximating the compressibilities of the soil structure, air, and water phases based on the laboratory results. Table 3 summarizes the approximate compressibilities for each of the five specimens.

The magnitudes of the compressibilities for each phase were obtained by dividing the amount of deformation at the end of each process by the change in the stress state variable. A sign (positive or negative) is attached to each

Table 1. Volume-mass relations for specimens tested.

Test No	Diameter cm	Height cm	Total volume cm ³	Water content %	Void ratio	Dry density kN/m ³	Degree of saturation %
1	10.006	11.815	929.09	34.32	1.0696	13.185	78.87
2	9.945	11.703	909.10	33.17	1.0251	13.298	80.61
3	10.543	5.867	503.53	29.62	1.2242	11.529	63.29
4	9.832	5.758	437.16	32.12	0.9310	13.281	90.25
5	6.350	2.283	72.29	31.18	1.1247	12.069	72.51

Table 2. Change in stress state variable components associated with each test.

Test No.	Total stress, σ kPa		Pore water pressure, u_w kPa		Pore-air pressure, u_a kPa		Pressure change kPa
	initial	final	initial	final	initial	final	
1	358.7	560.9	163.8	164.4	214.4	215.6	$\Delta\sigma = +202.2$
2	560.9	559.0	164.4	163.1	215.6	421.1	$\Delta u_a = +205.5$
3	475.1	476.8	42.9	42.2	397.8	206.5	$\Delta u_a = -191.3$
4	611.4	610.1	177.3	379.2	532.0	530.9	$\Delta u_w = +201.9$
5	606.7	605.2	216.5	323.6	413.8	413.8	$\Delta u_w = +107.1$

Fig. 1. Soil structure and water phase volume changes associated with Test 1.

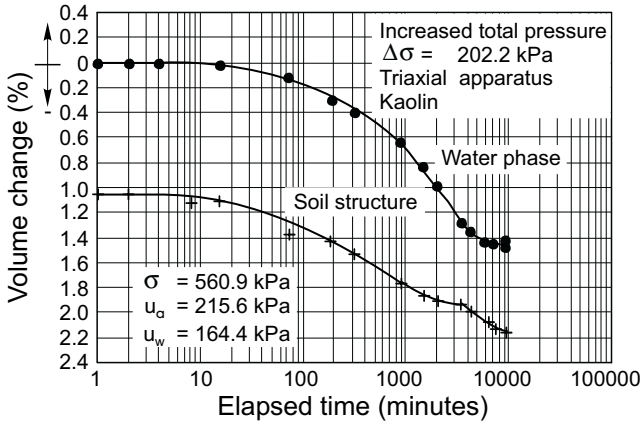


Fig. 2. Soil structure and water phase volume changes associated with Test 2.

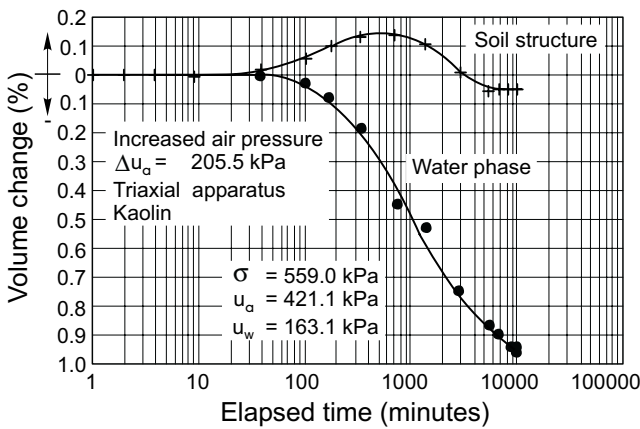
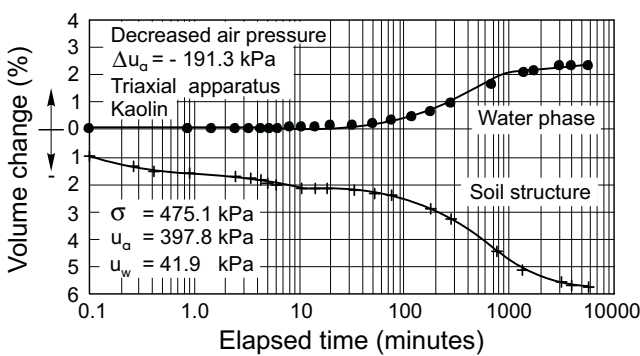


Fig. 3. Soil structure and water phase volume changes associated with Test 3.



of the compressibilities based on the direction (increase or decrease) of the volume change associated with each phase and the change of the stress state variables (Fredlund 1982). Table 3 indicates that the soil structure compressibilities have positive signs for a stable structured soil (Tests 1, 2, and 4) and negative signs for a meta-stable structured soil (Tests 3 and 5).

The theoretical analysis for each of the laboratory results was based upon the consideration of a one-

Fig. 4. Soil structure and water phase volume changes associated with Test 4.

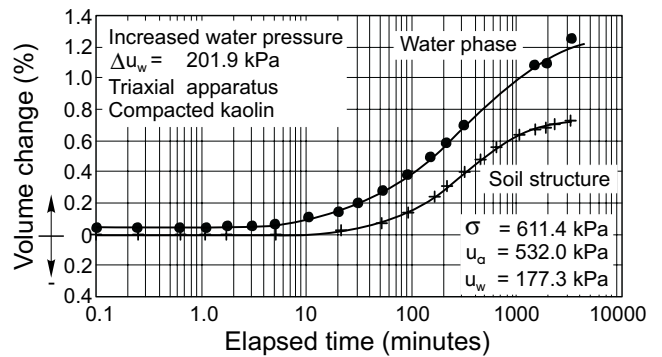
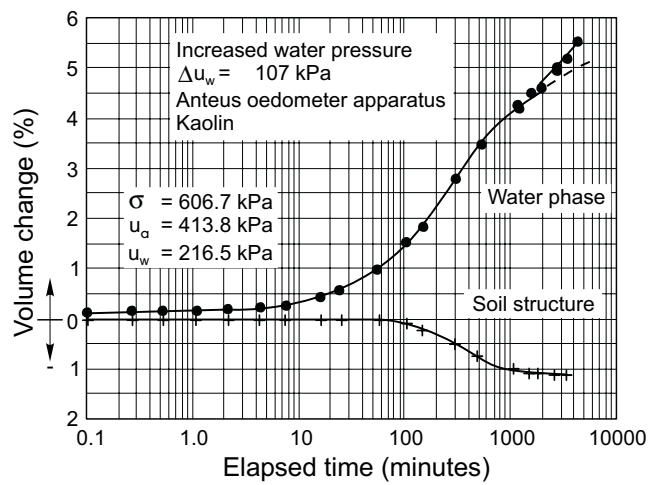


Fig. 5. Soil structure and water phase volume changes associated with Test 5.



dimensional transient flow process. The pore-water and pore-air pressures during the transient process were computed by solving simultaneously eqs. [7] and [8]. An explicit central difference technique was used for the calculations (Dakshanamurthy and Fredlund 1981). The coefficients of permeability of air and water were assumed to be constant during the transient process. Therefore the terms that account for the variation in coefficient of permeability in eqs. [7] and [8] were not used in the computations.

The volume changes associated with the water and the air phases during the transient process were computed according to eqs. [3] and [4]. The compressibilities used in the calculations were assumed to be constant throughout the process. The soil structure volume change was obtained by adding the volume changes associated with the water and air phases according to the continuity requirement in eq. [1].

Figures 6 to 10 show the theoretical analyses associated with Tests 1 to 5. The fitting was accomplished by using different combinations for the coefficients of permeability for the water and air phases. The combinations of the water and air coefficients of permeability that gave the best-fit results for each test are shown in each figure.

Table 3. Compressibilities for each specimen.

Test No.	Soil structure		Water phase		Air-phase	
	$m_1^s \times 10^{-4}$ kPa ⁻¹	$m_2^s \times 10^{-4}$ kPa ⁻¹	$m_1^w \times 10^{-4}$ kPa ⁻¹	$m_2^w \times 10^{-4}$ kPa ⁻¹	$m_1^a \times 10^{-4}$ kPa ⁻¹	$m_2^a \times 10^{-4}$ kPa ⁻¹
1	1.17	3.52	0.8	2.41	0.37	1.11
2	0.006	0.032	0.131	0.657	-0.125	-0.625
3	-0.76	-3.80	0.3	1.49	-0.106	-5.29
4	0.09	0.35	0.15	0.61	-0.06	-0.26
5	-0.26	-1.04	1.2	4.81	-1.46	-5.85

Fig. 6. Theoretical analysis associated with Test 1.

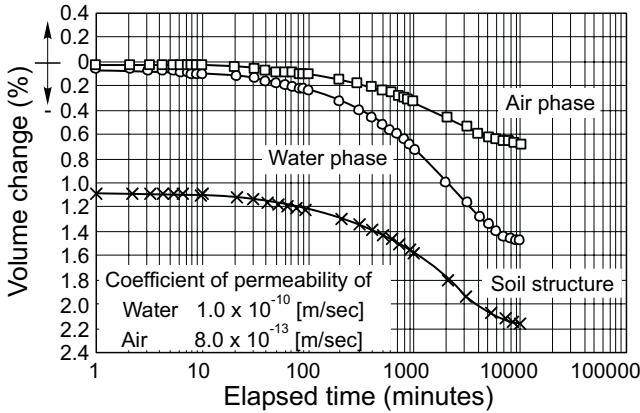
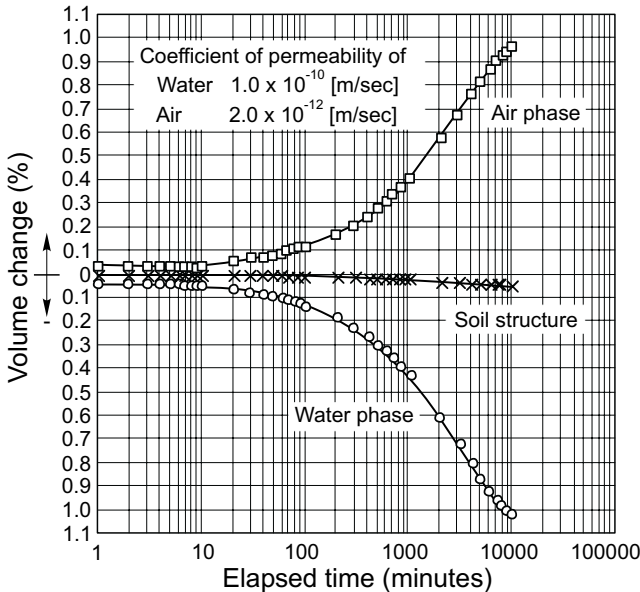


Fig. 7. Theoretical analysis associated with Test 2.



Comparisons between the theoretical analyses and laboratory results were made for Tests 4 and 3 (Figs. 11 and 12). The results indicate a close agreement between the theoretical analyses based on the constitutive equations and the results from the laboratory tests. Some discrepancies can be observed during the transient process. The disagreements may be due to one or more reasons. For example, the discrepancies may be due to the assumption of constant coefficients of permeability throughout the

Fig. 8. Theoretical analysis associated with Test 3.

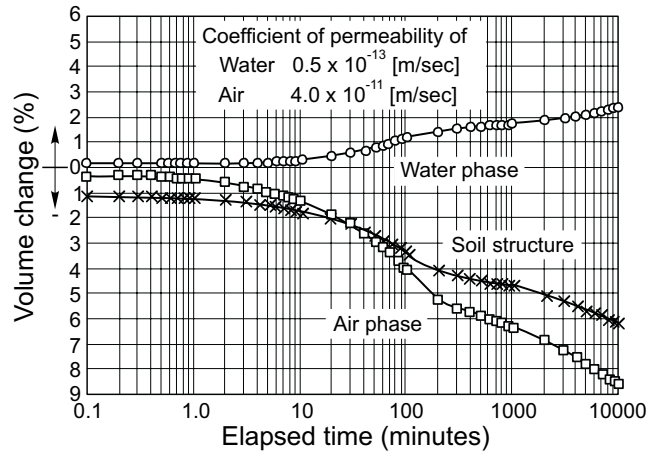
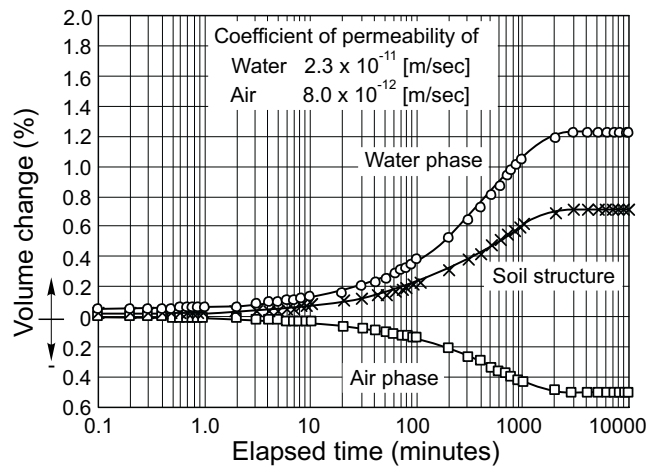


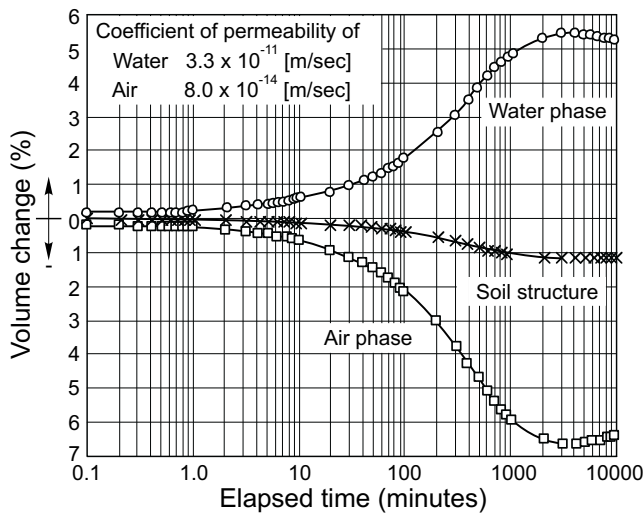
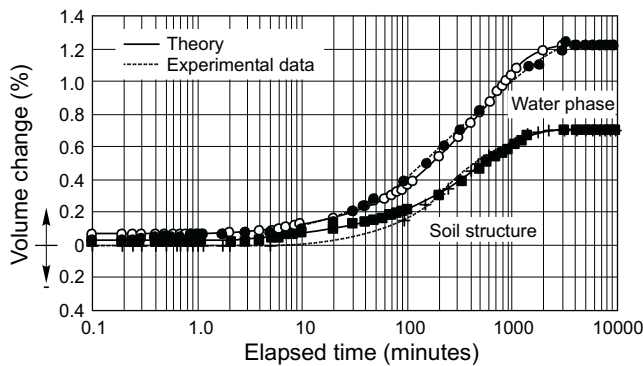
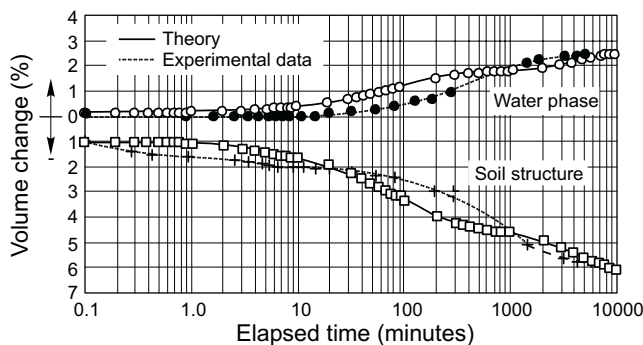
Fig. 9. Theoretical analysis associated with Test 4.



process. In spite of the difference during the process, the theoretical analyses and the laboratory results show similar trends.

Conclusions

The comparisons between the theoretical analyses of volume change in unsaturated soils with the experimental results are shown to yield similar behavior of volume changes with respect to time. The available theory for unsaturated soils can be used to describe the volume change behavior when appropriate coefficients are used. More re-

Fig. 10. Theoretical analysis associated with Test 5.**Fig. 11.** Comparison with theoretical analyses and laboratory results for Test 4 (Fig. 4).**Fig. 12.** Comparison with theoretical analyses and laboratory results for Test 3 (Fig. 3).

search should be conducted where each of the soil properties are independently measured and the time-dependent volume changes are predicted and independently monitored. The relationship between the coefficients of permeability and other soil properties also requires further study.

References

- Corey, A.T. 1957. Measurement of water and air permeability in unsaturated soil. *Proceedings of the Soil Science Society of America*, **21**(1): 7–10.
- Dakshnamurthy, V. and Fredlund, D.G. 1981. A mathematical model for predicting moisture flow in an unsaturated soil under hydraulic and temperature gradients. *Water Resources Research Journal*, **17**(3): 714–722.
- Fredlund, D.G. 1973. Volume change behavior of unsaturated soils. Ph.D. thesis, University of Alberta, Edmonton, AB, Canada.
- Fredlund, D.G. 1982. Consolidation of unsaturated porous media. *Proceedings, Symposium on the Mechanics of Fluid in Porous Media-New Approaches in Research*, NATO Advance Study Institute, Newark, DL.
- Fredlund, D.G. and Hasan, J.U. 1979. One-dimensional consolidation theory: Unsaturated soils. *Canadian Geotechnical Journal*, **16**(3): 521–531.
- Fredlund, D.G. and Morgenstern, N.R. 1976. Constitutive relations for volume change in unsaturated soils. *Canadian Geotechnical Journal*, **13**(3): 261–276.
- Green, R.E., and Corey, J.C. 1971. Calculation of hydraulic conductivity: A further evaluation of some predictive methods. *Soil Science Society of America Proceedings*, **35**: 3–8.
- Hasan, J.U. and Fredlund, D.G. 1980. Pore pressure parameters for unsaturated soils. *Canadian Geotechnical Journal*, **17**(3): 395–404.
- Hilf, J.W. 1956. An investigation of pore water pressures in compacted cohesive soils. Technical Memorandum 654, U.S. Department of the Interior, Bureau of Reclamation, Denver, CO.
- Lloret, A. and Alonso, E. E. 1980. Consolidation of unsaturated soils including swelling and collapse behavior. *Géotechnique*, **30**(4): 449–477.

Discussion

V. Drnevich, University of Kentucky, Lexington, KY (written discussion):

- (1) What is meant by the statement that permeability is a function of the volume-weight properties of the soil?
- (2) Why were the last two terms in eq. [7] omitted when trying to fit the theory and the laboratory results?

D.G. Fredlund and H. Rahardjo (authors' closure):

- (1) The coefficient of permeability with respect to the water phase can be written as a function of two of the commonly used volume-weight variables of the soil. It may take any one of the following forms: $k_w = f(S, e)$, $k_w = f(e, w)$, or $k_w = f(w, S)$, where e = void ratio, S = degree of saturation, and w = water content. For an unsaturated soil, the degree of saturation or the water content is taken as the predominant variable and void ratio is assumed to be of secondary importance. Also, permeability is often written as a function of the negative pore-water pressure or matric suction. Any of the above forms are satisfactory.
- (2) The laboratory tests were performed by placing specimens in contact with a high air-entry ceramic disk.

This disk has a low permeability and impedes the flow of water out of the specimen. In other words, the rate of volume change may be more an indication of the permeability of the high air-entry disks than the soil. The last two terms in eq. [7] refer to the spatial variation of permeability of the soil with time. These terms were not meaningful for the type of laboratory test performed.

Finally, we emphasize that the laboratory results presented do not provide a rigorous verification of the consolidation theory for an unsaturated soil. It is difficult to provide such a verification because of the low permeability of the high air-entry disk. A rigorous verification would require

an independent measurement of all soil properties involved in the formulation and a measurement of the pore-air and pore-water pressure with respect to time and space. Experimentally this is extremely demanding. A lower level of verification involves the independent measurement of total and water volume changes with respect to time rather than the measurement of the pore pressures. The verification provided in this paper simply demonstrates that two independent volume changes (e.g., total volume change and water flux) occur during consolidation and that these can be modeled using two partial differential equations. Certainly there is a challenge for further verification of the consolidation theory.

Consolidation apparatus for testing unsaturated soils

H. Rahardjo and D.G. Fredlund

Abstract: An apparatus for performing consolidation tests under K_0 conditions was designed and constructed for testing unsaturated soils. Three types of consolidation tests are of interest in unsaturated soils. These are: (1) constant water content loading tests, (2) consolidation under a net total stress, and (3) consolidation under a matric suction. The apparatus had been used for simultaneous and separate measurements of pore-air and pore-water pressures for all three types of consolidation tests. The experimental results demonstrate the pore pressure and volume change behavior of an unsaturated soil during these tests.

Key words: consolidation, K_0 loading, matric suction, unsaturated soils, pore-water pressure, pore-air pressure, volume change.

Introduction

Great strides have been made in the development of concepts, theories, and formulations for unsaturated soils during the last two decades. Much needed experimental verification; however, has not kept pace with theoretical development. Experimental work on unsaturated soils is demanding and time consuming. There are few pieces of equipment available for testing unsaturated soils because of the specialized nature of the tests.

The objective of this paper is to illustrate the development of a K_0 apparatus for conducting consolidation tests on unsaturated soils. The apparatus is capable of measuring pore-air pressure, pore-water pressure, and volume change during various loading stages. The experiments are limited to one-dimensional air and/or water flows under K_0 conditions. Detailed considerations on the design and construction of the K_0 apparatus for consolidation testing in unsaturated soils are outlined in the paper.

Theory

Theoretical formulations for the pore-pressure parameters and the consolidation equations for unsaturated soils are briefly summarized in this section. Detailed derivations are referenced to Rahardjo (1990) and Fredlund and Rahardjo (1993).

Pore-water pressure parameters for constant water content loading

The pore-air pressure parameter, \bar{B}_a , and pore-water pressure parameter, \bar{B}_w , under K_0 -loading are defined as follows:

$$[1] \quad \bar{B}_a = \frac{du_a}{d\sigma_y}$$

and

$$[2] \quad \bar{B}_w = \frac{du_w}{d\sigma_y}$$

where:

du_a = excess pore-air pressure,

du_w = excess pore-water pressure, and

$d\sigma_y$ = total stress increment in the vertical direction, which is the major principal stress direction in this case.

In the constant water content test, the water phase is undrained while the air phase is allowed to drain. In other words, no excess pore-air pressure is developed (i.e., $du_a = 0$). The \bar{B}_a pore-air pressure parameter is equal to zero.

Consolidation equations

The water volume change due to changes in net normal stress ($\sigma_y - u_a$) and matric suction ($u_a - u_w$) during a consolidation process can be formulated. During the consolidation process resulting from a change in net total stress (i.e., $\partial\sigma_y / \partial t = 0$). The excess pore-air pressure can be assumed to dissipate instantaneously (i.e., $\partial u_a / \partial t = 0$). The constitutive equation for the water phase for either of the above cases can be simplified as

$$[3] \quad \frac{dV_w}{V_0} = -m_2^w du_w$$

H. Rahardjo. Senior lecturer, School of Civil and Structural Engineering, Nanyang Technological University, Singapore 639798.

D.G. Fredlund. Professor, Department of Civil Engineering, University of Saskatchewan, 57 Campus Drive, Saskatoon, SK, Canada S7H 5A9.

Reproduced with permission from the *Geotechnical Testing Journal*, GTJODJ, 19(4): 341–353, 1996.

where:

- dV_w / V_0 = water volume change in the soil element with respect to the initial volume of the element,
 V_w = volume of water in the soil element,
 V_0 = initial volume of the soil element,
 m_2^w = coefficient of water volume change with respect to a change in matric suction, $d(u_a - u_w)$.

If the gravitational component of the hydraulic head is neglected, a simplified form of the governing differential equation for water flow in an unsaturated soil can be written as follows:

$$[4] \quad \frac{\partial u_w}{\partial t} = c_v^w \frac{\partial^2 u_w}{\partial y^2} + \frac{c_v^w}{k_w} \frac{\partial k_w}{\partial y} \frac{\partial u_w}{\partial y}$$

where:

- c_v^w = coefficient of consolidation with respect to the water phase (i.e., $k_w / (\rho_w g m_2^w)$); the c_v^w coefficient for an unsaturated soil varies with suction due to the dependence of k_w and m_2^w on suction,
 t = time, and
 y = distance in the vertical direction.

The pore-water pressure changes, du_w , computed from eq. [4] can be substituted into eq. [3] to calculate the water volume changes, dV_w , during the consolidation process under a net total stress or under a matric suction.

The equation for soil volume change, dV , during the consolidation process under a net total stress or under a matric suction is given as follows:

$$[5] \quad \frac{dV}{V_0} = -m_2^s du_w$$

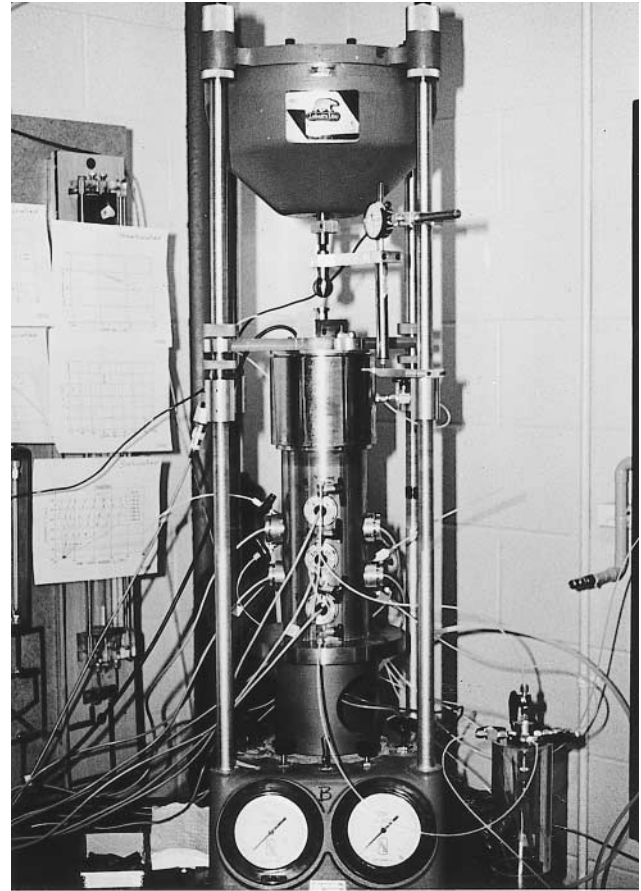
where:

- dV / V_0 = soil volume change referenced to the initial volume of the element,
 V = volume of the soil element,
 V_0 = initial volume of the soil element, and
 m_2^s = coefficient of the soil volume change with respect to a change in matric suction.

Equipment Design

An apparatus for conducting one-dimensional K_0 consolidation tests on an unsaturated soil was developed. The apparatus is capable of controlling, as well as independently measuring, pore-air and pore-water pressures in the soil specimen. The pore-air pressure, u_a , and the pore-water pressure, u_w , can be controlled to impose a matric suction, $(u_a - u_w)$, in the soil specimen using the axis-translation technique (Hilf 1956). During the consolidation process, the pore-air and pore-water pressures can be measured independently at various depths and time intervals to obtain the pore pressure isochrones.

Fig. 1. The K_0 cylinder set-up for consolidation testing of an unsaturated soil.

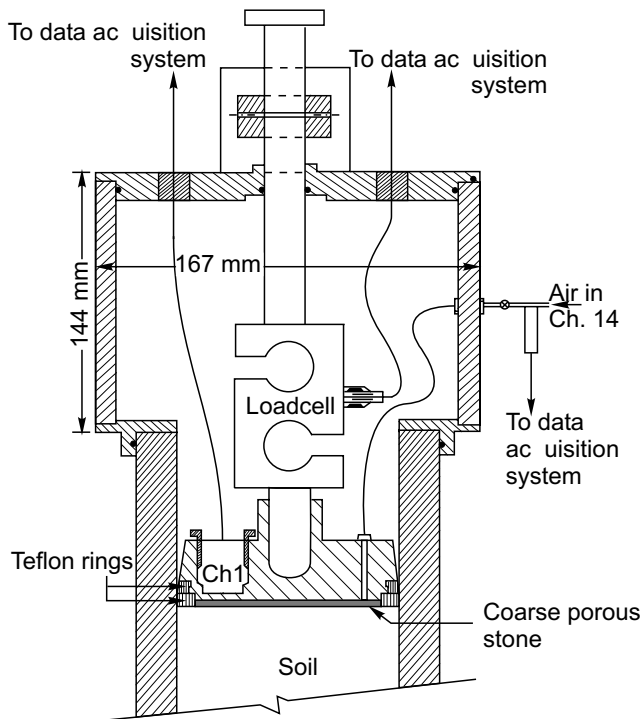


The apparatus consists of a bronze cylinder with a thick wall for maintaining a K_0 loading condition. The soil specimen has a diameter of 10.2 cm and a height of approximately 20 cm. The K_0 cylinder is placed in a Conbel loading frame¹ (Fig. 1). The maximum total stress applicable is about 3300 kPa. The Conbel loading frame provides a constant total stress, σ_y , using an air pressure applied through a rolling diaphragm and a piston below the diaphragm. The top of the cylinder is enclosed with an airtight chamber for pore-air pressure control. The loading piston goes through the pore-air pressure chamber and is seated on the loading cap (Fig. 2). A sealed super-mini load cell² is attached near the end of the piston for determining the net stress applied to the loading cap.

The loading cap has a smaller diameter at the top than at the base to minimize side friction (Fig. 2). Two Teflon[®] rings with sharp edges are attached around the base of the loading cap to prevent the entrapment of soil particles in between the cap and the wall (Fig. 3). These Teflon[®] rings have minimal contact with the wall and allow the passage of air during constant water content loading. The Teflon[®] rings can be replaced by rubber O-rings if

¹
²

Fig. 2. Piston-load cell-loading cap arrangements in an airtight chamber.

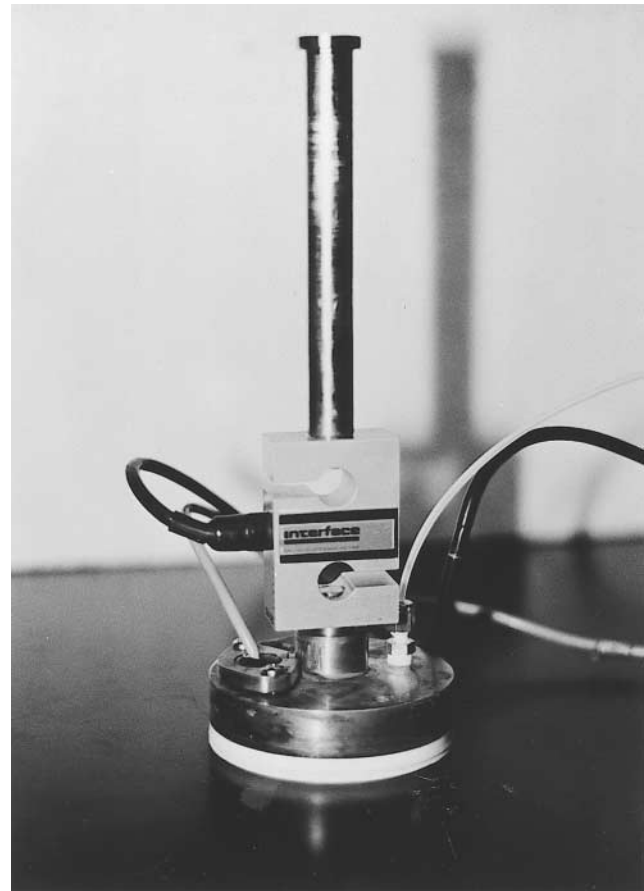


both the air and water phases are undrained during the test. A coarse porous disk with a low air entry value is placed at the base of the loading cap for controlling the pore-air pressure. This coarse porous disk is in contact with the top of the soil specimen. The disk is connected to the pore-air pressure control through a hole drilled in the loading cap. The controlled air pressure can be checked during tests using a pressure transducer mounted on the loading cap (i.e., Channel 1 in Fig. 2).

The pore-water pressure in the specimen is controlled through a high-air-entry ceramic disk located at the base of the specimen. The high-air-entry ceramic disk is placed on top of the spiral-grooved water compartment located in the pedestal. The water pressure in the compartment can be controlled. Saturation of the high-air-entry disk ensures continuity between the pore water in the soil specimen and the water in the compartment. The high-air-entry disk will remain saturated as long as the soil matric suction does not exceed the air entry value of the disk. The grooves in the compartment serve as water channels for flushing air bubbles that may diffuse through the disk. A pressure transducer is installed immediately below the compartment for checking the applied pressure.

Pore-air and pore-water pressure measuring ports are installed along the cylinder wall for pore pressure measurements during the consolidation process. Five holes are drilled through the cylinder wall for pore-air pressure measurements (Fig. 5). Another five holes at equal depths are drilled through the cylinder wall for pore-water pres-

Fig. 3. Loading cap with two Teflon® rings.



sure measurements. Pore-water pressures, u_w , are measured through the use of high-air-entry disks (i.e., Channels 3, 4, 5, 6, and 7 in Fig. 4), while the pore-air pressures, u_a , are measured using low-air-entry disks (i.e., Channels 8, 9, 10, 11, and 12 in Fig. 4).

Details of the pore-water pressure and pore-air pressure measuring ports are shown in Figs. 6 and 7, respectively. The pore pressure measuring ports are designed and constructed to conform to the curvature of the cylinder wall to minimize side friction between the soil specimen and the cylinder. High precision transducers³ with an accuracy of $\pm 0.25\%$ are installed in all pore pressure measuring ports. Each pore-water pressure port consists of a porous disk and a transducer that is connected through a water compartment (Fig. 6). The volume of the water compartment and the characteristics of the porous disk in each port are presented in Table 1. High-flow, high-air-entry ceramic disks⁴ with an air entry value of at least 100 kPa are used for the pore-water pressure measuring ports and for the water compartment at the base. Low-air-entry bronze disks are used for the pore-air pressure measuring ports.

A flushing system is provided for each of the pore-water pressure measuring ports to flush air bubbles that may be trapped or accumulated in the water compartment

Fig. 4. Locations of pore-air and pore-water pressure measuring ports along the cylinder wall.

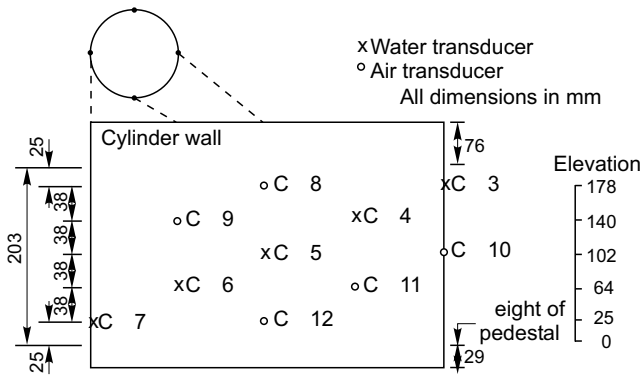
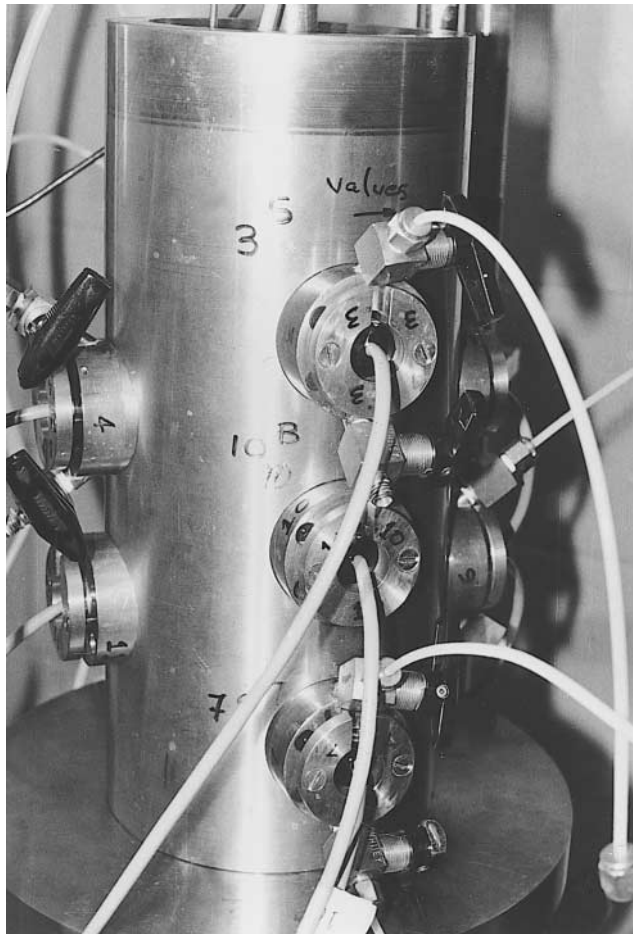
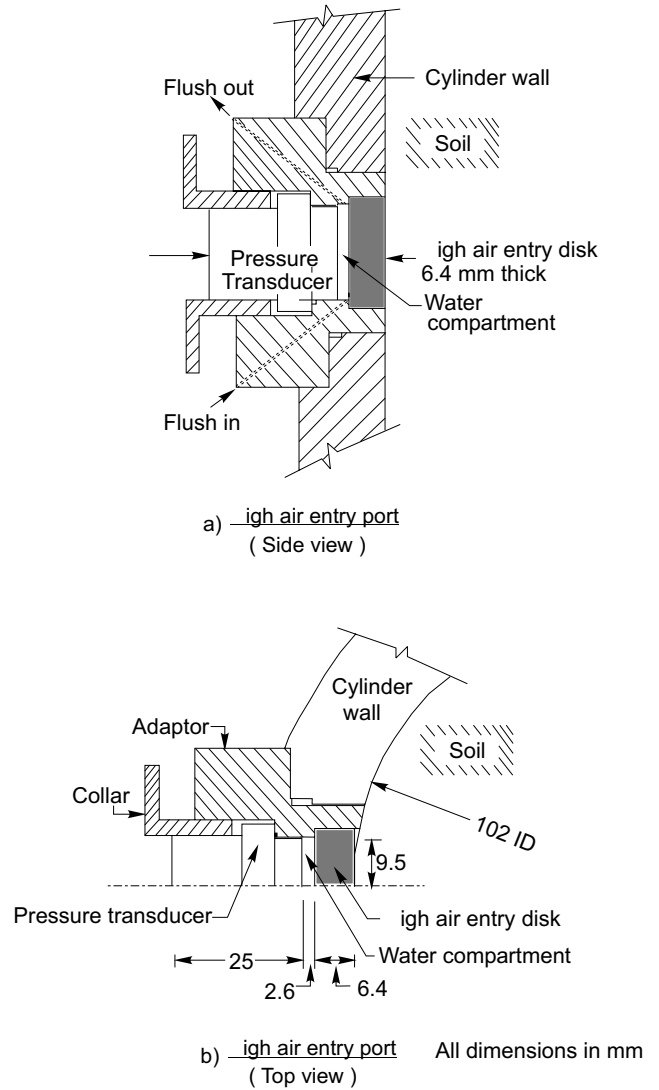


Fig. 5. Pore-air and pore-water pressure measuring ports along the cylinder wall.



as a result of air diffusion (Fig. 6). Two valves (i.e., the inlet and outlet valves) are provided for each pore-water pressure port to accommodate the flushing mechanism. The inlet valve is used to set the flushing pressure. The flushing pressure should be set approximately equal to the pressure being measured in order to minimize pressure disturbance. The entrapped air bubbles are flushed

Fig. 6. Pore-water pressure measuring system.



by momentarily opening the outlet valve several times to the atmospheric pressure.

The total volume change of the specimen is measured from the vertical deflection of the specimen using an LVDT (i.e., linear variable differential transformer) with a dial gauge as back up, the radial deformation being zero for a K_0 loading condition. The water volume change is measured using a twin-burette volume change indicator. A separate measurement of diffused air volume is performed at regular intervals using a diffused air volume indicator (DAVI) described by Fredlund and Rahardjo (1993). The measured volume of diffused air can be used to correct the water volume change measurement. In other words, the water volume changes during testing can be measured independently. The difference between the total volume change and the water volume change gives the air volume change. The layout of the plumbing associated with the control and the measuring systems for the consolidation equipment is illustrated in Fig. 8.

Table 1. Details on pore pressure ports.

Type of disk	Port No.	Compartment volume cm ³	Coefficient of permeability of disk, k_d m/s	Air entry value, $(u_a - u_w)_b$ kPa	Disk thickness, h_d mm
High air entry disks	2 (base plate)	4.95	4.20×10^{-8}	>200	10.0
	3	1.80	5.12×10^{-8}	115	6.4
	4	1.53	3.92×10^{-8}	130	6.4
	5	1.88	3.98×10^{-8}	110	6.4
	6	1.67	5.09×10^{-8}	130	6.4
	7	2.02	5.60×10^{-8}	150	6.4
Bronze	8	0.92	Decreases from 4.0×10^{-5} to 4.0×10^{-6}		6.4
	9	1.07		6.4	
	10	1.97		6.4	
	11	1.05		6.4	
	12	1.27		6.4	

Fig. 7. Pore-air pressure measuring system.

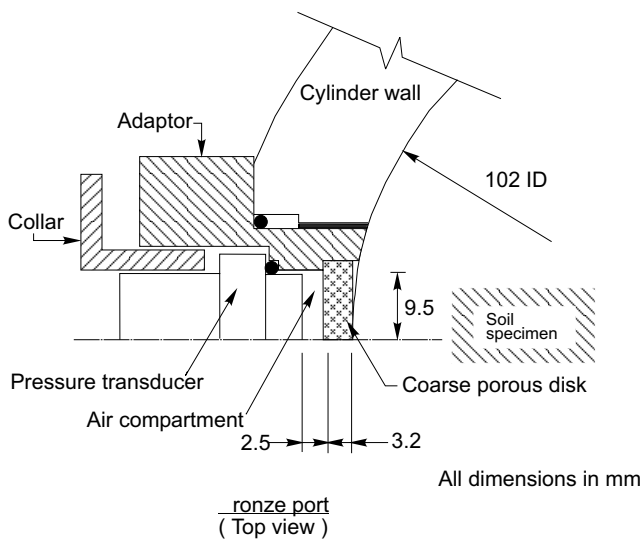


Table 2. Summary of index properties of the soil.

Grain size	
Sand =	52.5%
Silt =	37.5%
Clay =	10.0%
D_{10} =	0.002 mm
D_{30} =	0.02 mm
D_{60} =	0.09 mm
C_u =	$D_{60}/D_{10} = 45$
Atterberg limits	
w_L =	22.2
w_P =	16.6
I_P =	5.6
Specific gravity	
G_s =	2.68

Soil properties

A silty sand from Saskatchewan was used in the tests. Table 2 summarizes the properties of the soil. Pilot tests on initially slurried specimens indicate that the soil commences desaturation at a matric suction of approximately 10 kPa.

Testing program

A series of experiments (i.e., S_4 series) was conducted to study the pore pressure and volume change behavior during all three types of consolidation tests on unsaturated soil under the K_0 condition. The S_4 series consists of several “constant water content loadings”, “consolidation under net total stress”, and “consolidation under matric suction”. All three types of consolidation tests in the series were conducted alternately on a single specimen. The series was started using a slurried, saturated specimen (i.e., $(u_a - u_w)$ equal to 0). Figure 9 shows the

stress state, for the $(\sigma_y - u_a)$ and $(u_a - u_w)$ paths for the entire S_4 series. The points (e.g., M, N_1 , N_2 , etc.) indicate the stress states, while the lines (e.g., MN_1 , N_3O , OP) indicate the path for the type of tests (i.e., constant water content loading, consolidation under net total stress, and consolidation under matric suction, respectively).

Constant water content loading refers to the application of the total vertical stress, σ_y , under a condition where only the water phase is undrained while the air phase is drained. Excess pore-water pressure is developed during the loading while the pore-air pressure remains constant at the controlled pressure. In other words, the total stress increases and the matric suction decreases during loading. The loading is indicated by Paths MN_1 , N_1N_2 , and N_2N_3 in Fig. 9. The excess pore-water pressure dissipates with time and the matric suction returns to its initial value prior to loading (Path N_3O in Fig. 9). The soil will have a higher net normal stress at the end of consolidation as shown by comparison of Point O and Point M in Fig. 9.

On completion of the constant water content loading phase, the matric suction is increased by lowering the water pressure in the base plate compartment. The pore-air

Fig. 8. Schematic diagram of the control board and plumbing layout for the consolidation equipment.

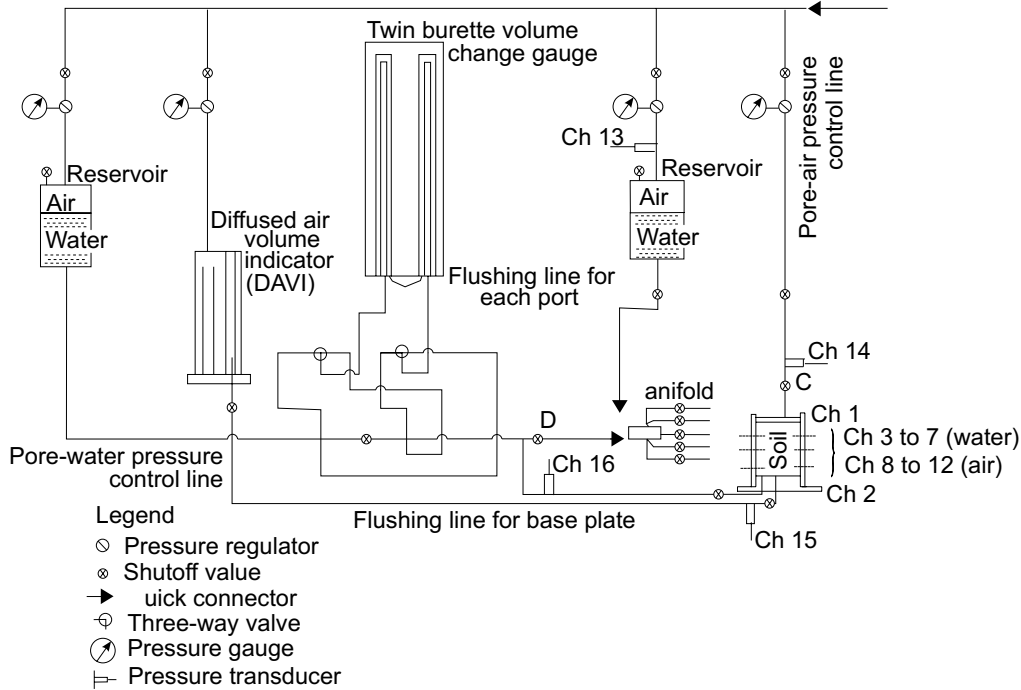
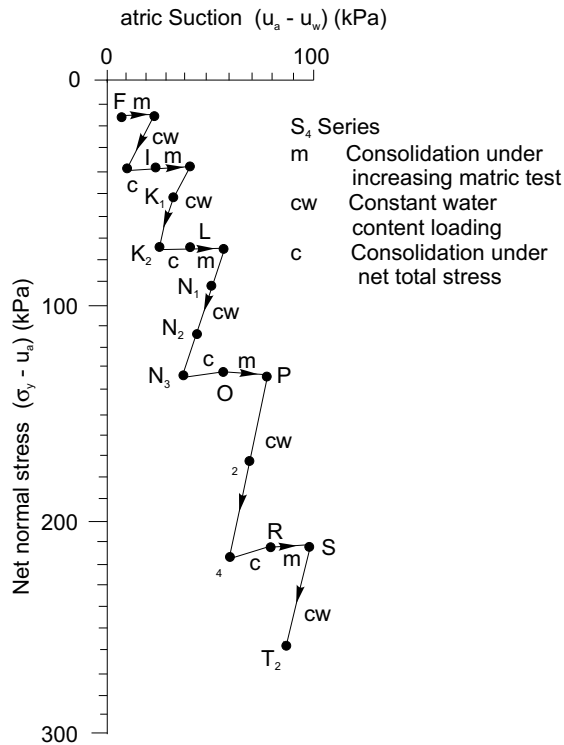


Fig. 9. Stress state path for S_4 series experiment.



pressure is maintained constant (i.e., the increasing matric suction process, for Path OP). The net normal stress ($\sigma_y - u_a$) is unchanged. The matric suction has increased to a new value (i.e., Point P). During the consolidation phase, the pore water will flow downward as a result of

the gradient between the water pressures in the specimen and in the base plate compartment. The above sequence of tests is repeated following the paths PQ_2 , Q_2Q_4 (constant water content loading), Q_4R (consolidation under net total stress), RS (consolidation under increasing matric suction), and so on (Fig. 9). Pore pressure changes and volume changes are measured continuously throughout the test.

Test results

Results from the S_4 series are presented. Figures 10 and 11 show the void ratio, e , and water content, w , of the specimen, respectively, at every point along the stress state path. The void ratio and water content values are plotted against the average net normal stress ($\sigma_y - u_a$) and matric suction ($u_a - u_w$) of the specimen at every equilibrium point along the proposed stress path. The void ratio appears to decrease little during constant water content loading (e.g., Path MN_3 in Fig. 10) as compared to the void ratio decrease during consolidation under net total stress (e.g. Path N_3O in Fig. 10), or consolidation under increasing matric suction (e.g., Path OP in Fig. 10). The decreases in void ratio during consolidation under net total stress and consolidation under matric suction are similar in magnitude.

The slope of the water content versus matric suction plot is much steeper during consolidation under increasing matric suction (e.g., slope of Path OP in Fig. 11) than the slope of the same plot for consolidation under net total stress (e.g., slope of Path N_3O in Fig. 11). A distinct change in the slope of the water content relationship occurs when the maximum past matric suction value of the soil (i.e., at the end of consolidation) is exceeded. This is

Fig. 10. Projection of the void ratio surface from the S_4 series onto the net normal stress and matric suction planes.

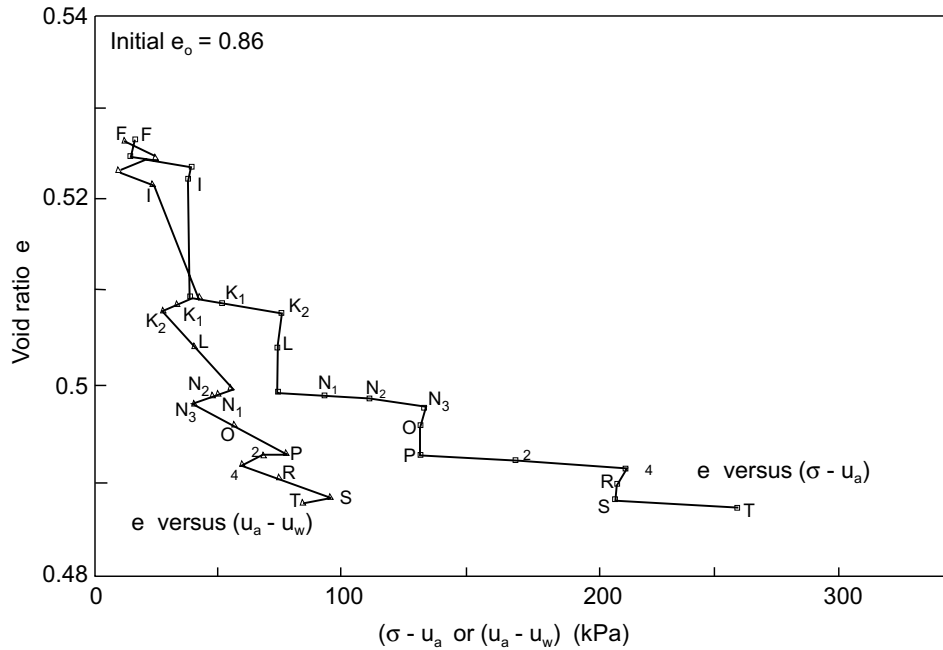
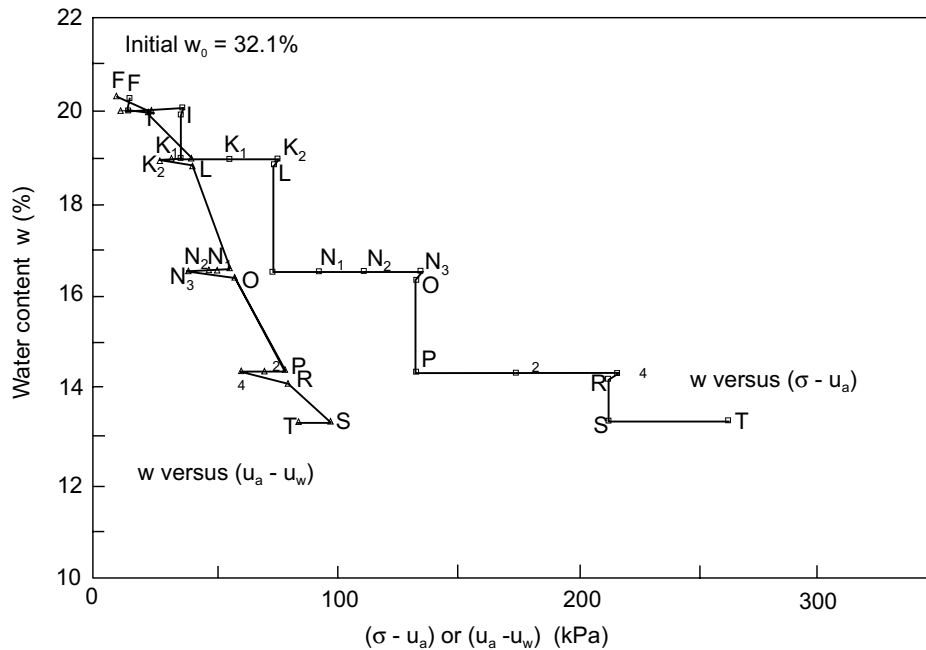


Fig. 11. Projection of the gravimetric water content surface from the S_4 series onto the net normal stress and matric suction planes.



similar to the preconsolidation concept in saturated soil mechanics. The consolidation under the net total stress test is similar to a reloading process, while the consolidation under the increasing matric suction test can be viewed as a loading process along the virgin curve of the water content versus matric suction relationship.

Test results from constant water content loading (i.e., Q_2Q_4 in Fig. 9), consolidation under net total stress (i.e.,

N_3O), and consolidation under increasing matric suction (i.e., OP) are summarized in Tables 3, 4, and 5, respectively. In the constant water content test (Q_2Q_4), an additional total stress of 43 kPa was applied to the soil specimen while the pore-air pressure remained essentially constant during loading. The average excess pore-water pressure developed during loading was about 8 kPa indicating a \bar{B}_w pore-water pressure parameter of 0.2 at a de-

Table 3. Soil properties and stress state variables corresponding to the constant water content test (Q_2Q_4).

Properties	Initial	Final
Soil properties		
S	78.0%	78.1%
e	0.493	0.492
w	14.3%	14.3%
n	0.330	0.330
Stress state variables, kPa		
σ_y	291.6	334.7
u_a (top)	118.7	117.7
u_w (bottom)	50.4	58.1
$\sigma_y - u_a$	172.9	217.0
$d(\sigma_y - u_a)$		44.1
$u_a - u_w$	68.3	59.6
$d(u_a - u_w)$		-8.7

Note: S = degree of saturation, e = void ratio, w = water content, and n = porosity.

Table 4. Soil properties and stress state variables corresponding to the consolidation under total stress test (N_3O).

Properties	Initial	Final
Soil properties		
S	88.8%	88.2%
e	0.498	0.496
w	16.5%	16.3%
n	0.332	0.331
Stress state variables, kPa		
σ_y	252.8	251.0
u_a (top)	117.5	118.2
u_w (bottom)	79.7	60.4
$\sigma_y - u_a$	135.3	132.8
$d(\sigma_y - u_a)$		-2.5
$u_a - u_w$	37.8	57.8
$d(u_a - u_w)$		20.0

gree of saturation of about 78% (Table 3). The result indicates low pore pressure parameter values for unsaturated soils (i.e., when the degree of saturation falls below 100%). The development of excess pore-water pressures throughout the specimen and the total volume changes during the constant water content loading (Q_2Q_4) are illustrated in Fig. 12. The plot indicates a uniform generation of excess pore-water pressures throughout the soil specimen. The pore-water pressure development in Fig. 12 was similar in behavior to the undrained pore-water pressure development reported by Barden and Sides (1970). Barden and Sides (1970) attributed the stepwise increase in the pore-water pressures during undrained loading to the structural viscosity or creep properties.

In the consolidation under total stress test (N_3O), an excess pore-water pressure of 20 kPa from the preceding

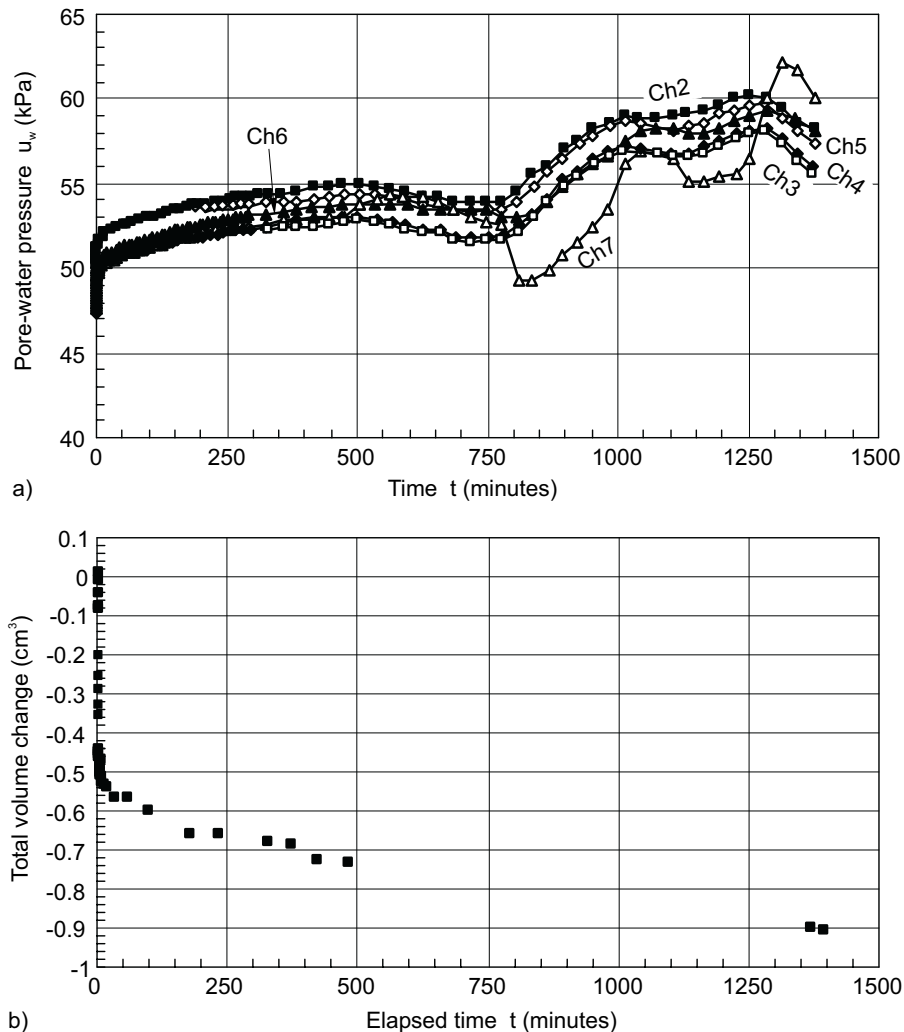
Table 5. Soil properties and stress state variables corresponding to the consolidation under increasing matric suction test (OP).

Properties	Initial	Final
Soil properties		
S	88.2%	77.9%
e	0.496	0.493
w	16.3%	14.3%
n	0.331	0.330
Stress state variables, kPa		
σ_y	251.0	251.0
u_a (top)	118.2	118.5
u_w (bottom)	60.4	40.8
$\sigma_y - u_a$	132.8	132.5
$d(\sigma_y - u_a)$		-0.3
$u_a - u_w$	57.8	77.7
$d(u_a - u_w)$		19.9

constant water content loading stage (i.e., MN_1 , N_1 , N_2 , and N_2N_3 in Fig. 9) was dissipated under constant total stress and constant pore-air pressure (Table 4). The pore-water pressure distributions and the volume changes during the consolidation process are depicted in Fig. 13 by individual data points. The measured pore-water pressures indicate some impedance to the flow at the bottom of the soil specimen (Fig. 13a). The pore-water pressures at the bottom of the specimen did not dissipate as fast as the theory would predict. The theoretical simulation of the consolidation under the total stress test (N_3O) using eqs. [2], [3], and [4] are also shown in Fig. 13. The simulation was conducted using an impeded flow boundary condition at the base by reducing the coefficient of permeability of the disk, k_d , one hundred times. Grain-size distribution analysis, after the completion of the test, indicated a higher percentage of fine particles at the bottom of the specimen. The higher fines content at the bottom of the specimen suggests that there was a downward migration of fine particles along with the downward flow of water during the consolidation test. As a result, the bottom soil layer would have a lower permeability than the soil layers at higher elevations (i.e., impeded boundary condition at the base). The simulation also required a varying water efflux at the top of the specimen to represent the evaporation across the top boundary.

In the consolidation under increasing matric suction test (OP), the matric suction was increased by 20 kPa by reducing the pore-water pressure under constant total stress and pore-air pressure (Table 5). The pore-water pressure decrease in the top, middle, and bottom sections of the specimen during the test (OP) is shown in Figs. 14a, 14b, and 14c, respectively. The pore-water pressures showed daily fluctuations, which were found to correlate closely with the daily temperature variations in the laboratory. Daily temperatures in the laboratory varied between 23 to 25°C (Rahardjo 1990). The temperature fluctuation caused volume changes in the measuring systems, which in turn resulted in changes in the measured

Fig. 12. Pore pressure build-up and volume changes during the constant water content loading test (Q_2Q_4): a) excess pore-water pressure build-up; b) total volume changes during loading.



pressures. The greatest fluctuation occurred in the bottom region (Fig. 14c), which was nearest to the base plate where the outside tubings were exposed to ambient temperature fluctuations. The upper regions of the soil specimen were buffered from the temperature effects as demonstrated by the smaller pressure variations in Figs. 14a and 14b. Regardless of these fluctuations, the mean pressures can be obtained from the plot of the measured pressures as indicated in Fig. 14c.

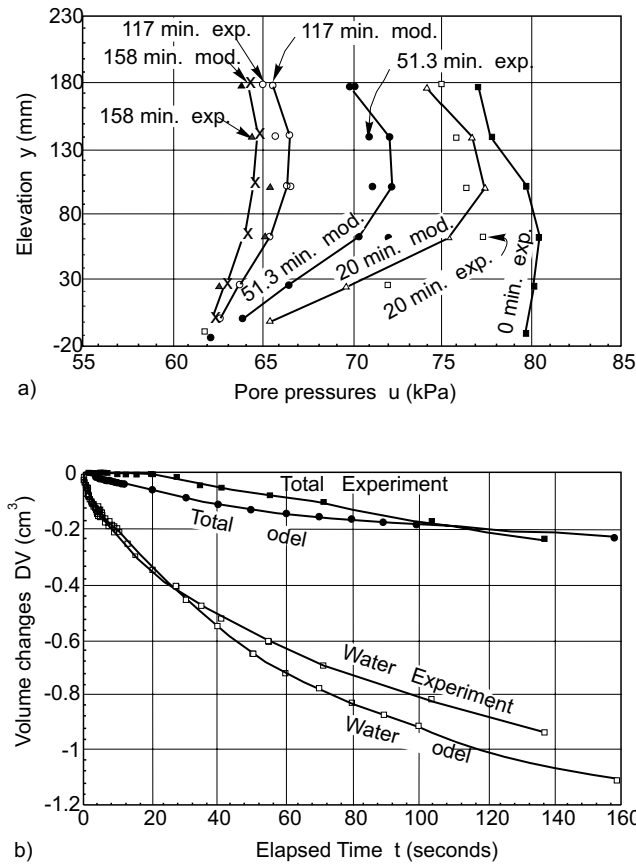
The total and water volume changes during the consolidation under increasing matric suction test (OP) are presented in Fig. 15. The ratio between the total volume change to the water volume change was typically small for the consolidation under increasing matric suction test as compared to the same ratio for the consolidation under total stress test (compare Figs. 15 and 13b). The water volume change during the consolidation under increasing matric suction test (Fig. 15) was significantly larger than the water volume change during the consolidation under total stress test (Fig. 13b). This was the reason for the

much steeper slope of the water content versus matric suction relationship during the consolidation under increasing matric suction test (Fig. 11). The equilibration time required for the consolidation under increasing matric suction test was typically much longer than the equilibration time for the consolidation under total stress test (compare Figs. 15 and 13). The consolidation under increasing matric suction test (OP) was conducted over approximately 19.5 days. Appreciable amounts of diffused air collected in the base plate were removed and measured daily. Details of the diffused air volume measurements are given in Fredlund and Rahardjo (1993). The diffused air volumes were used to correct the water volume changes as depicted in Fig. 15.

Conclusions

The following conclusions can be drawn from the results of the experimental program:

Fig. 13. Comparisons between theoretical analyses and experimental results for the consolidation under the net total stress test (N_3O): a) pore-water pressure profiles at different times; b) total and water volume changes during test.



- (1) The behavior of unsaturated soils during constant water content loading, consolidation under total stress, and consolidation under increasing matric suction can be studied using the K_0 cylinder described.
- (2) Separate measurements of pore-air and pore-water pressures along an unsaturated soil specimen can be carried out continuously during a consolidation test using the measuring systems and techniques described in this paper.
- (3) Temperature fluctuations in the laboratory affect the pore pressure measurements. It is important to maintain a constant ambient temperature in the laboratory throughout the testing period.
- (4) The B_w pore pressure parameter decreases significantly when the degree of saturation falls below 100%.
- (5) Significant water volume changes occur when a soil is subjected to a matric suction value greater than the maximum past matric suction that the soil has ever experienced (e.g., increasing matric suction test).
- (6) Unsaturated soil mechanics theory can be used to describe the pore pressure and volume changes of an unsaturated soil during undrained and drained processes.

Fig. 14. Decrease in pore-water pressures during the consolidation under the increasing matric suction test (OP): a) pressure decrease in the top region (arithmetic plot); b) pressure decrease in the middle region (arithmetic plot); c) pressure decrease in the bottom region (arithmetic plot).

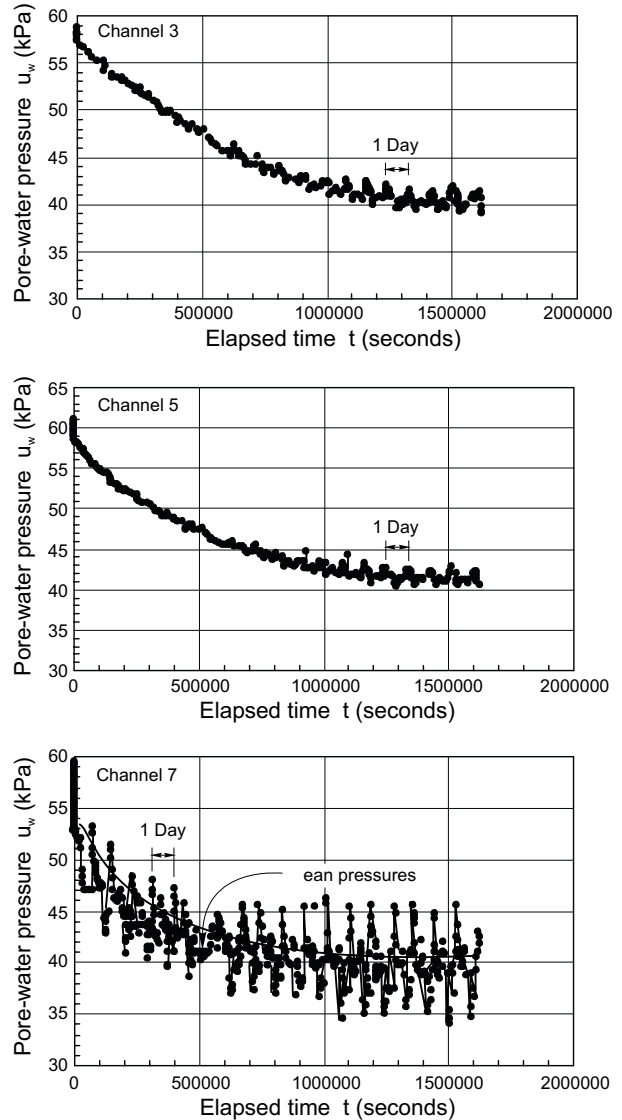
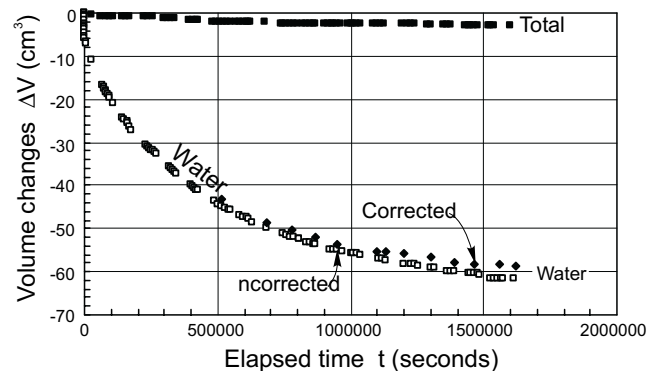


Fig. 15. Total and water volumes during the consolidation under increasing matric suction test (OP).



References

- Barden, L. and Sides, G.R. 1970. Engineering behavior and structure of compacted clay. *ASCE, Journal of Soil Mechanics and Foundation Engineering*, **96**: 1171–1200.
- Fredlund, D. G. and Rahardjo, H. 1993. *Soil mechanics for unsaturated soils*, John Wiley and Sons, New York.
- Hilf, J.W. 1956. An investigation of pore pressures in compacted cohesive soils. Technical Memo 654, U.S. Department of Interior, Bureau of Reclamation. Denver, CO.
- Rahardjo, H. 1990. The study of undrained and drained behaviour of unsaturated soils. Ph.D. thesis, University of Saskatchewan, Saskatoon, SK, Canada.

Experimental verification of the theory of consolidation for unsaturated soils

H. Rahardjo and D.G. Fredlund

Abstract: An experimental program was designed to study the behavior of unsaturated soils during undrained loading and consolidation. A K_0 cylinder was designed and built for the testing program. Simultaneous measurements of pore-air and pore-water pressures could be made throughout a soil specimen using this K_0 cylinder. Four types of tests were performed on a silty sand. These are (1) undrained loading tests where both the air and water are not allowed to drain, (2) constant water content tests where only the water phase is not allowed to drain, (3) consolidation tests where both the air and water phases are allowed to drain, and (4) increasing matric suction tests. Undrained loading tests or constant water content loading tests were conducted for measuring the pore pressure parameters for the unsaturated soil. Drained tests consisting of either consolidation tests or increasing matric suction tests were conducted to study the pore pressure distribution and volume change behavior throughout an unsaturated soil during a transient process. The experimental pore pressure parameters obtained from the undrained loadings and constant water content loadings agreed reasonably well with theory. The pore-air pressure was found to dissipate instantaneously when the air phase is continuous. The pore-water pressure dissipation during the consolidation test was found to be faster than the pore-water pressure decrease during the increasing matric suction test. The differing rates of dissipation were attributed to the different coefficients of water volume change for each of the tests. The water volume changes during the consolidation test were considerably smaller than the water volume changes during the increasing matric suction tests for the same increment of pressure change.

Key words: consolidation, K_0 loading, matric suction, pore-air pressures, pore-water pressures, unsaturated soils.

Introduction

Geotechnical engineers are increasingly challenged by problematic soils around the world. Some of the soils that have been identified as problematic are expansive soils, collapsible soils, and residual soils. These soils are generally unsaturated with pore-water pressures that are negative relative to atmospheric conditions. Another category of unsaturated soils is compacted soils used in the construction of roads, earth-filled dams, and other earth structures.

Many important issues in soil mechanics are related to an understanding of pore pressure and volume change behavior. The concept of pore pressure parameters for undrained loading and the consolidation theory for saturated soils have become classical theories in soil mechanics. There has been a significant increase in our understanding of the concepts, theories, and formulations of unsaturated soil mechanics during the past two decades. Laboratory tests on unsaturated soils have been found to be time-consuming and demanding. Consequently, experimental verifications have not kept pace with the theoretical developments. The application of the theories is also

limited by difficulties in measuring the required properties of the unsaturated soil. Difficulties associated with measuring the properties of unsaturated soils are primarily due to the fact that the pore-water pressures can be highly negative and the soil also contains an air phase. Conventional soil mechanics testing equipment is not built for testing unsaturated soils. There is a need to develop appropriate equipment and test procedures to experimentally study the behavior of unsaturated soils.

The primary objective of this research program is to study the pore pressure development and the consolidation behavior of an unsaturated soil caused by external loading of the soil. The study is limited to one-dimensional air and/or water flows under K_0 conditions and consists of both theoretical and experimental programs. In the theoretical study, the necessary formulations for describing the pore pressures and volume change behavior during undrained and drained loadings (e.g., consolidation) are presented. The experimental study involves the design and construction of appropriate equipment for undrained tests and consolidation tests on unsaturated soils. An extensive program of undrained tests and consolidation tests was conducted. The results

H. Rahardjo. Senior Lecturer, School of Civil and Structural Engineering, Nanyang Technological University, Nanyang Avenue, Singapore 2263.

D.G. Fredlund. Professor, Department of Civil Engineering, University of Saskatchewan, 57 Campus Drive, Saskatoon, SK, Canada S7N 5A9.

Reproduced with permission from the *Canadian Geotechnical Journal*, 32: 749–766.

are analyzed using the formulated theory. Typical pore pressure and volume change data (e.g., the rates and magnitudes of changes) during both processes constitute the primary data from the study.

Literature review

The total stress applied during the undrained loading of an unsaturated soil is carried by the soil structure, the pore-air, and the pore-water depending upon the relative compressibilities of the constituents involved. The excess pore pressures will dissipate with time as a function of the soil permeability with respect to air and water and the compressibility of the soil structure. This process is commonly referred to as consolidation. Several theories to describe the consolidation of an unsaturated soil have been proposed.

Pore pressure parameters

Skempton (1954) introduced the pore pressure parameter concept for describing pore-water pressure changes during undrained loading of a saturated soil. Bishop (1961) extended the pore pressure parameter concept to both the air and water phases of an unsaturated soil. The pore-air and pore-water pressures can be written with respect to a change in the major principal stress as follows:

$$[1] \quad du_a = \bar{B}_a d\sigma_1$$

$$[2] \quad du_w = \bar{B}_w d\sigma_1$$

where

du_a = pore-air pressure change,

du_w = pore-water pressure change,

\bar{B}_a = pore-air pressure parameter for an unsaturated soil,

\bar{B}_w = pore-water pressure parameter for an unsaturated soil, and

$d\sigma_1$ = change in the major principal stress.

The pore-air pressure change, du_a , during an undrained loading has been calculated using Boyle's law and Henry's law of solubility (Hamilton 1939; Brahtz et al. 1939; Hilf 1956; Bishop 1957). Hasan and Fredlund (1980) derived independent equations for the pore-air and pore-water pressure parameters. Laboratory experiments indicate that the development of excess pore-air and pore-water pressures during an undrained loading is a function of the soil structure compressibility and the pore fluid compressibility (Bishop and Henkel 1962; Barden and Sides 1970; Campbell 1973).

Consolidation

Terzaghi (1943) derived the classical theory for one-dimensional consolidation of saturated soils. The derivations incorporated a constitutive equation for saturated soils in terms of the effective stress and a flow law. The flow rate of water during consolidation was in accordance with Darcy's law.

Biot (1941) proposed a theory of consolidation for an unsaturated soil with occluded air bubbles. Two constitutive equations relating stress and strain were formulated in terms of the effective stress, $(\sigma - u_w)$, and the pore-water pressure, u_w , where σ is total stress. One equation relates the void ratio to the stress state and the other equation relates the water content to the stress state of the soil. For one-dimensional consolidation, Biot's theory resulted in an equation similar to Terzaghi's equation but the coefficient of consolidation, c_v , was modified to take into account the compressibility of the pore fluid. Larmour (1966), Hill (1967), Olson (1986), and Scott (1963) showed that Terzaghi's equation with a modified coefficient of consolidation can be used to describe the consolidation behavior of unsaturated soils with occluded air bubbles.

Blight (1961) derived transient flow equations for the air and water phases in a dry rigid-structured, unsaturated soil. Fick's law of diffusion was used to relate the mass transfer resulting from a pressure gradient. Barden (1965, 1974) presented an analysis of a one-dimensional consolidation of a compacted, unsaturated clay. Fredlund and Hasan (1979) presented two partial differential equations for solving the pore-air and pore-water pressures during the consolidation process of an unsaturated soil. The air phase was assumed to be continuous. Darcy's and Fick's laws were applied to the flow of water and air phases, respectively. The equations have been used to simulate the volume change behavior of compacted kaolin specimens during total stress change and matric suction change (Fredlund and Rahardjo 1986). Similar equations have also been proposed by Lloret and Alonso (1980).

Extensions of the consolidation theory for unsaturated soils to three-dimensional cases have been proposed by Richards (1974) and Dakshanamurthy et al. (1984). The continuity equations were coupled with the equilibrium equations by Dakshanamurthy et al. (1984), in deriving the three-dimensional formulation.

Theory

Theoretical formulations for the pore pressure parameters and the consolidation equations for an unsaturated soil are briefly summarized in this section.

Pore pressure parameters for K_0 loading

Consider the case of a vertical, total stress increment applied to a soil under K_0 conditions. The vertical, total stress increment is denoted as $d\sigma_y$. The pore-air and pore-water pressure parameters can be expressed in terms of the soil structure and pore-fluid compressibilities.

Analysis by Hilf (1948)

Hilf (1948) outlined a procedure based on the laws by Boyles and Henry to compute the change in pore pressure as a result of an applied total stress. The equation derived can be rearranged in the form of a pore pressure parameter equation. The derivation is based on the results of a one-dimensional oedometer test on a compacted soil. Hilf

(1948) assumed that the matric suction of the soil was negligible and that the change in the pore-air pressure was equal to the change in the pore-water pressure (i.e., $du_a = du_w$ or $\bar{B}_a = \bar{B}_w$). The constitutive relation for the soil structure was defined by saturating the soil in an oedometer test and measuring its volume change with increasing applied total stress (i.e., saturated consolidation).

The \bar{B} pore pressure parameter derived from the analysis by Hilf (1948) can be written as follows (Rahardjo 1990):

$$[3] \quad \bar{B}_a = \frac{1}{1 + \frac{(1 - S_0 + hS_0)n_0}{(u_{a0} + du_a)m_v}}$$

where

- \bar{B}_a = pore-air pressure parameter (i.e., $du_a / d\sigma_y$) for undrained K_0 loading,
- S_0 = initial degree of saturation,
- h = volumetric coefficient of solubility,
- n_0 = initial porosity,
- \bar{u}_{a0} = absolute initial pore-air pressure (i.e., $\bar{u}_{a0} = u_{a0} + \bar{u}_{atm}$),
- u_{a0} = gauge initial pore-air pressure,
- \bar{u}_{atm} = atmospheric pressure (i.e., 101 kPa), and
- m_v = coefficient of volume change measured on a saturated specimen in a one-dimensional oedometer test.

Pore-water pressure parameters for constant water content test

K_0 -loading can be applied to soils under constant water content conditions. Only the water phase remains undrained while the air phase is allowed to drain. No excess pore-air pressure will be developed (i.e., $du_a = 0$). In other words, the \bar{B}_a pore-air pressure is equal to zero. The \bar{B}_w pore-water pressure parameter has the following form (Bishop 1957):

$$[4] \quad \bar{B}_w = \frac{m_{1k}^s - C_{aw}n}{m_2^s}$$

where:

- \bar{B}_w = $du_w / d\sigma_y$ for K_0 loading under constant water content conditions,
- m_{1k}^s = coefficient of volume change with respect to a change in the net major principal stress under the K_0 loading conditions,
- C_{aw} = compressibility of air-water mixtures, which is a function of \bar{B}_a and \bar{B}_w parameters (Rahardjo 1990),
- n = porosity, and
- m_2^s = coefficient of volume change with respect to a change in matric suction.

Differential equation for water flow

Two partial differential equations for solving the pore-air and pore-water pressures during the consolidation process of an unsaturated soil have been presented by Fredlund and Hasan (1979). For the case of a continuous

air phase, the excess pore-air pressures commonly undergo an almost instantaneous dissipation during the consolidation process (Madedor 1967; Barden 1974). In other words, only the water phase undergoes a transient process during consolidation. This behavior can be attributed to the significantly greater coefficient of permeability for the air phase, k_a , over that of the water phase, k_w . Barden and Pavlakis (1971) reported that the coefficient of permeability with respect to the air phase, k_a , can be five to seven orders of magnitude higher than the coefficient of permeability with respect to the water phase, k_w .

The consolidation theory presented herein is based on the assumption of a continuous air phase and an instantaneous dissipation of the excess pore-air pressures. The differential equation for the water flow alone is required to describe the consolidation process. Several other assumptions used in the derivation are similar to those proposed by Terzaghi (1943) and Biot (1941). A summary of the assumptions are as follows: (1) isotropic soil; (2) infinitesimal strains; (3) linear constitutive relations for small strains; (4) the coefficient of permeability with respect to water is a function of matric suction during the transient process; (5) the effects of air diffusing through water, air dissolving in water, and the movement of water vapor are ignored.

The necessary physical relations required for deriving the differential flow equation are a flow law and a constitutive equation for the water phase. The flow law relates the flow rate to the driving potential that causes the water to flow. Darcy's law can be applied to the flow of water through an unsaturated soil (Buckingham 1907; Richards 1931; Childs and Collis-George 1950). However, the water coefficient of permeability, k_w , is not a constant but varies significantly with the pore-water pressure in the soil.

The constitutive equation for the water phase relates the water volume change to changes in net normal stress, $(\sigma - u_a)$, and matric suction, $(u_a - u_w)$. The total stress, σ , is assumed to remain constant during consolidation (i.e., $\partial\sigma / \partial t = 0$). The excess pore-air pressures are dissipated instantaneously (i.e., $\partial u_a / \partial t = 0$). As a result, the constitutive equation for the water phase can be simplified to

$$[5] \quad \frac{dV_w}{V_0} = -m_2^w du_w$$

where:

- dV_w / V_0 = water volume change in the soil element with respect to the initial volume of the element,
- V_w = volume of water in the soil element,
- V_0 = initial volume of the soil element, and
- m_2^w = coefficient of water volume change with respect to a change in matric suction, $d(u_a - u_w)$.

The differential equation for flow of water in an unsaturated soil can be formulated using a referential element. The net flux of water through the element can be computed from the volume rates of water entering and leaving the element within a given period of time. The net

flux of water per unit volume can be equated to the derivative of the water phase constitutive relation with respect to time, t , to give the differential equation for the water flow in an unsaturated soil. If the gravitational component of hydraulic head is neglected, a simplified form of the differential flow equation can be written as follows:

$$[6] \quad \frac{\partial u_w}{\partial t} = c_v^w \frac{\partial^2 u_w}{\partial y^2} + \frac{c_v^w}{k_w} \frac{\partial k_w}{\partial y} \frac{\partial u_w}{\partial y}$$

where:

- c_v^w = coefficient of consolidation with respect to the water phase (i.e., $k_w / (\rho_w g m_2^w)$), that varies with suction since k_w and m_2^w vary with matric suction,
- k_w = coefficient of permeability of the water phase,
- t = time,
- y = vertical coordinate, and
- g = gravitational acceleration.

The pore-water pressure changes, du_w , computed from eq. [6] can be substituted into eq. [5] to calculate the water volume changes, dV_w , during the transient process. Similarly, the soil volume changes, dV_v , during the transient process can be calculated as follows:

$$[7] \quad \frac{dV_v}{V_0} = -m_2^s du_w$$

where:

- dV_v / V_0 = soil volume change referenced to the initial total volume,
- V_v = volume of voids, and
- m_2^s = coefficient of soil volume change with respect to a change in matric suction.

The flow of water can also occur when the pore-water pressures are altered at the soil boundaries (i.e., top or bottom or both). For example, the lowering of the water table can cause the pore-water pressures in the unsaturated zone to become more negative (or the matric suction to increase). The changes in the pore-water pressure due to the increase in matric suction can also be described using the same differential flow equation derived for the consolidation process.

Finite difference form of the transient flow equation

Equation [6] can be written in a finite difference numerical form as follows:

$$[8] \quad u_w(i, j+1) = u_w(i, j) + \beta_w G_{1w} + \frac{\beta_w}{k_w} K_{1w} G_{2w}$$

where:

- i = the depth increment,
- j = the time step,
- $\beta_w = \Delta t c_v^w / \Delta y^2$,
- $G_{1w} = u_w(i+1, j) - 2u_w(i, j) + u_w(i-1, j)$,
- $K_{1w} = k_w(i, j) - k_w(i-1, j)$, and
- $G_{2w} = u_w(i, j) - u_w(i-1, j)$.

Equation [8] is an explicit finite difference scheme that can be solved using a marching forward technique from known initial and boundary conditions.

Finite difference solution

Consider one-dimensional water flow through a column of unsaturated soil as shown in Fig. 1. This case is typical of the tests performed in the experimental program. The initial pore-water pressures in the soil (i.e., $u_w(i, 0) = u_0$) constitute the initial conditions. The pore-water pressure in the soil can be changed by altering the water pressure in the compartment below the high air entry disk. As an example, the water pressure in the compartment is reduced from u_0 to u_1 causing the pore-water to flow downward in a one-dimensional manner. At the base of the column (i.e., at $i = 0$ in Fig. 1) the soil is in contact with the disk. The boundary condition at this node can be established by considering the continuity of water flow at this interface.

$$[9] \quad u_w(0, j+1) = \frac{(k_w / \Delta y) u_w(1, j) + (k_d / h_d) u_1}{(k_w / \Delta y + k_d / h_d)}$$

where:

- $u_w(0, j+1)$ = pore-water pressure at the base of the soil in contact with the high air entry disk,
- Δy = discretized layer thickness,
- k_d = coefficient of permeability of the disk with respect to water,
- h_d = thickness of the disk, and
- u_1 = controlled water pressures in the compartment below the disk.

The water vapor flux from the top of the soil column cannot be completely eliminated. This flux boundary condition at the top can be accommodated for in the analysis although the amount of water lost through vapor flux should likely be negligible.

$$[10] \quad u_w(n, j+1) = u_w(n-1, j+1) - \frac{\Delta y \rho_w g}{k_w} v_{w \text{ at top}}$$

where:

- $u_w(n, j+1)$ = pore-water pressure at the uppermost node,
- $u_w(n-1, j+1)$ = pore-water pressure at the node below the uppermost node, and
- $v_{w \text{ at top}}$ = water flow rate equivalent to water vapor flux at the top of the soil column; a function of the environments surrounding the soil column (i.e., temperature and relative humidity).

Equipment

A bronze cylinder for conducting various undrained and drained tests under K_0 loading conditions was designed and constructed as shown in Fig. 2. The soil specimens had a diameter of 10.2 cm and a height of approximately 20 cm. The soil specimen was placed into the cylinder between a high air entry ceramic disk at the

Fig. 1. One-dimensional water flow through an unsaturated soil.

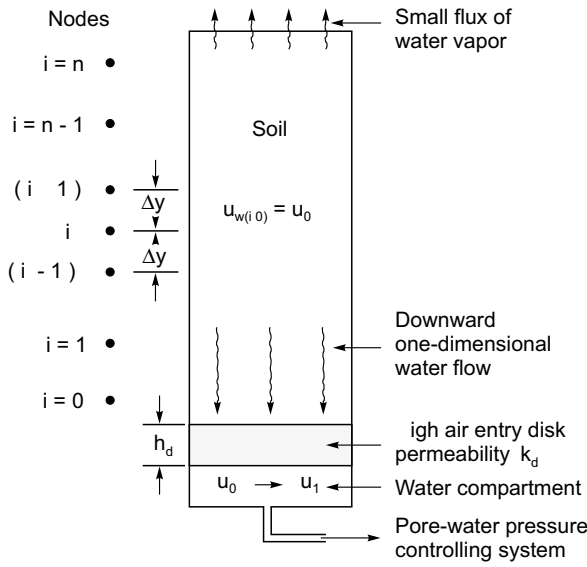
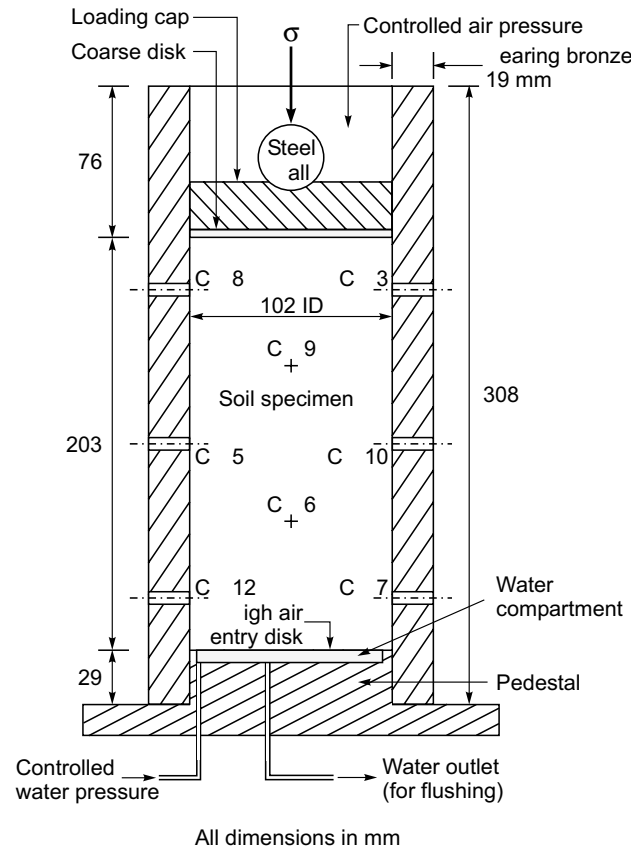
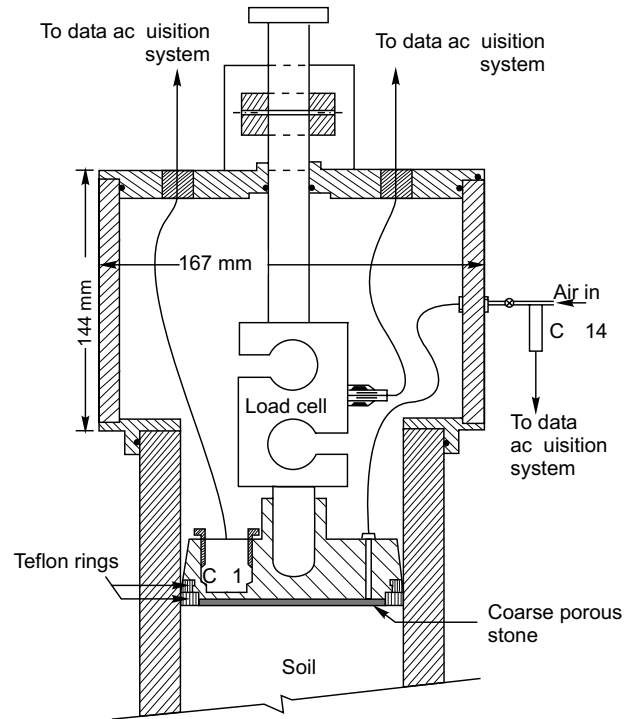


Fig. 2. K_0 cylinder for undrained loading and consolidation test.



bottom and a low air entry bronze disk at the top. The pore-air pressure, u_a , in the soil was controlled through the coarse bronze disk while the pore-water pressure, u_w , was controlled through the high air entry ceramic disk. All high air entry ceramic disks are of the high flow type

Fig. 3. Modified loading cap with load cell.

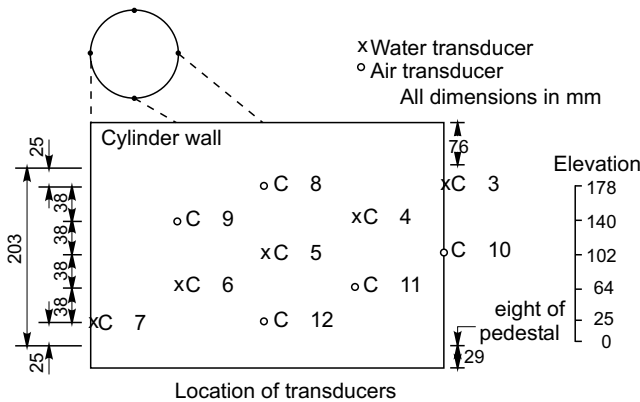


with a measured coefficient of permeability of 4×10^{-8} to 5×10^{-8} m/s. Simulated values for the coefficient of permeability during the laboratory tests were in the range of 1×10^{-10} to 1×10^{-11} m/s.

The total stress, σ , is applied to the specimen through a loading cap (Fig. 2) using a loading frame. The loading cap was originally built with two rubber O-rings to prevent leakage during undrained loadings (see Fig. 2). Side friction that developed around the loading cap, however, caused experimental problems during subsequent drained loadings. Therefore, the loading cap was later modified to minimize side friction during tests (Fig. 3). The diameter of the cap was made smaller at the top than at the base. The two rubber O-rings (Fig. 2) were replaced by two Teflon® rings with sharp edges (Fig. 3). The Teflon® rings were used to prevent the entrapment of soil particles in between the cap and the wall of the cylinder. The Teflon® rings have a minimal contact with the wall of the cylinder and yet are flexible enough to seal against air leakage at the top during undrained loading. It was later discovered that the Teflon® rings could not totally seal against air leakage. A sealed air chamber was eventually mounted on top of the cylinder (Fig. 3). The air chamber was pressurized to the same pressure as the controlled air pressure applied to the soil specimen. As a result, only the pore-water could be maintained undrained and subsequent tests were of the constant water content type. The pore-water could not leak around the loading cap because the pore-water was always less than the air pressure.

Pore-air and pore-water pressure measuring ports were installed along the cylinder as illustrated in Figs. 2 and 4. Five holes were drilled through the cylinder wall for the

Fig. 4. Pore-air and pore-water pressure measurement locations along the cylinder.



measurement of pore-air pressures. Another five holes at the same depths were drilled for the measurement of pore-water pressures. The pore-water pressures, u_w , were measured through the use of high air entry disks (i.e., channels 3, 4, 5, 6, and 7 in Figs. 2 and 4). The pore-air pressures, u_a , were measured through the use of coarse porous disks (i.e., channels 8, 9, 10, 11, and 12 in Figs. 2 and 4). A flushing system was provided in the pore-water pressure measuring system to flush air bubbles that may be trapped or accumulated in the water compartment as a result of air diffusion.

The total volume change and the water volume change were measured while the air volume change was computed as the difference between these two measured volumes. The total volume change of a specimen was obtained by measuring the vertical deflection of the specimen. The vertical deflection was measured using a conventional dial gauge and a LVDT (i.e., linear variable differential transformer) transducer. The water volume change was measured using a conventional twin-burette volume change indicator, which was connected to the water compartment in the pedestal.

Soil properties

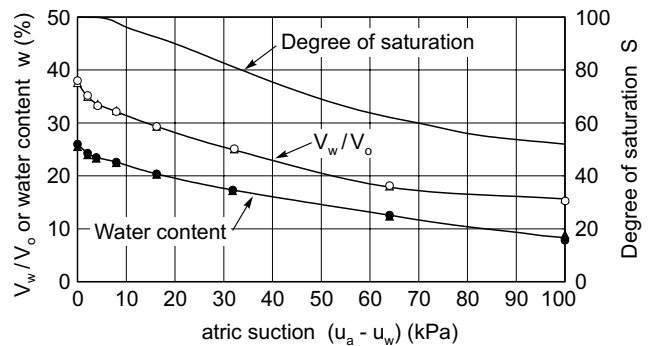
The soil used in the experimental program was a silty sand with properties as summarized in Table 1. Most tests were conducted on initially slurred specimens to ensure the homogeneity of the soil specimens tested. The soil-water characteristic curves for the Highway Pit soil are shown in Fig. 5 in terms of (V_w / V_0) and gravimetric water content, w . The slope of the (V_w / V_0) versus matric suction curve gives the coefficient of water volume change with respect to matric suction, m_2 . The degrees of saturation at various matric suctions are also illustrated in Fig. 5.

The coefficient of permeability with respect to water at saturation, k_s , was found to decrease from 10^{-8} to 10^{-9} m/s when the void ratio decreased from 0.55 to 0.40. The unsaturated permeability function was computed using the soil-water characteristic curve of the soil and the saturated coefficient of permeability. The theory and formulation associated with this method for obtaining the

Table 1. Index properties of the soil used in the experiment.

Saskatchewan Department of Highway Pit soil	
Grain size distribution	
Sand	52.5%
Silt	37.5%
Clay	10.0%
Atterberg limits	
Liquid limit, LL	22.2
Plastic limit, PL	16.6
Plasticity index, PI	5.6
Specific gravity, G_s	2.68

Fig. 5. Soil-water characteristic curves for the silty sand.



unsaturated permeability function are described in Fredlund and Rahardjo (1993).

Testing procedure

Direct measurements of pore-water pressures are limited to negative 101 kPa. The axis-translation technique (Hilf 1956) can be used to measure or to control pore-water pressures lower than negative 101 kPa. Using this method, both the pore-air and pore-water pressures are translated by an equal amount to positive pressures. The matric suction, $(u_a - u_w)$, is not affected by this translation process, which allows the pore-water pressures to be measured or controlled in the positive pressure range. The technique performs well as long as the matric suction does not exceed the air entry value of the air entry disks. The axis-translation technique was used in this program to prevent the possibility of cavitation as the matric suction approached negative 101 kPa.

Undrained loadings

Undrained tests were performed to observe pore pressure responses in an unsaturated soil as a result of a total stress increment. Consider the case of an unsaturated soil specimen that has been subjected to a specific stress state (i.e., $(\sigma_y - u_a)$ and $(u_a - u_w)$) under K_0 loading conditions. An additional total stress, $d\sigma_y$, is then applied to the specimen by maintaining undrained conditions for both the air and water phases. As a result, excess pore-air and pore-water pressures are generated, which can be written as pore-pressure parameters (i.e., $du_a = \bar{B}_a d\sigma_y$ and

$du_w = \bar{B}_w d\sigma_y$). At equilibrium, the net normal stress increases while the matric suction decreases. The excess pore pressures are measured (i.e., channels 3 to 12 in Fig. 4) and their values are compared with the additional total stress.

Constant water content tests

Constant water content tests refer to loading conditions where the air phase is allowed to drain while the water phase is maintained under undrained conditions. This loading condition was possible when using the modified loading cap (Fig. 3). The pore-air pressure in the soil specimen is maintained at equilibrium by the controlled pressure in the closed air chamber on top of the cylinder (Fig. 4). As a result, there was no excess pore-air pressure generated during the loadings. The excess pore-water pressure developed during the loading was used to calculate the \bar{B}_w parameter (i.e., $\bar{B}_w = du_w / d\sigma_y$).

Drained tests

The excess pore pressures generated during undrained or constant water content loading conditions were dissipated during the “consolidation” phase of the test. At the end of the consolidation process, the net normal stress, $(\sigma_y - u_a)$, was increased while the matric suction, $(u_a - u_w)$, returned to the initial value prior to undrained loading. The soil specimen was then subjected to an increase in matric suction while maintaining a constant net normal stress. This process is referred to as the “increasing matric suction” test. The matric suction is increased by reducing the pore-water pressure. The pore-air pressure remained constant during the process in order to maintain a constant net normal stress. In both tests, the air and water phases are free to flow in and out of the soil specimen.

Consolidation tests

During the consolidation test, the excess pore-air pressure was dissipated through the top of the specimen while the excess pore-water pressure was dissipated through the bottom of the specimen. In other words, single drainage conditions were established for both air and water phases during consolidation. The total stress, along with its additional stress, $(\sigma_y + d\sigma_y)$, remained constant during consolidation. Eventually, the pore-air and pore-water pressures returned to their initial values. The excess pore pressure dissipations are observed with respect to depth and time through pore pressure measurements along the cylinder (i.e., channels 3 to 12 in Fig. 4). At equilibrium, the net normal stress was increased by $d\sigma_y$ and the matric suction reverted back to its initial value.

Increasing matric suction tests

The increasing matric suction test was performed by reducing the pore-water pressure, u_w , while maintaining a constant pore-air pressure. The matric suction is increased while the net normal stress remains constant during the test. The pore-water pressure is decreased by lowering the water pressure in the base plate. The gradi-

ent between the water pressures in the soil and those in the base plate causes water to flow downward. The decreasing pore-water pressures are observed with respect to depth and time through pore-water pressure measuring ports along the cylinder walls (i.e., channels 3 to 7 in Fig. 4). At equilibrium, the net normal stress is unchanged and the matric suction increases to a new value.

Testing program

Five series of experiments were conducted to study the pore pressure and volume change behavior during undrained and drained loading under K_0 conditions. The series of experiments consisted of several undrained loadings, consolidation, and increasing matric suction tests. These tests were conducted alternately on a single specimen. Each series of tests was started using a slurried, saturated specimen. The specimen was brought to specific matric suctions and net normal stresses by applying various stresses. The stress path was followed by alternately performing the above mentioned three tests. Considerable test data were obtained from five series of experiments.

Test results

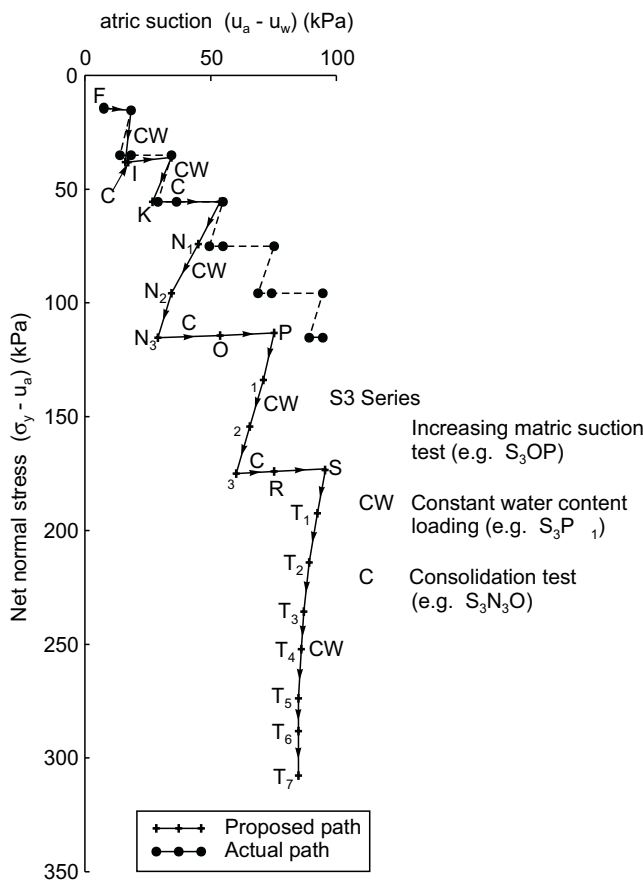
The first two series were part of a pilot study. The last three series were the actual experiments. The stress path followed during the third series of experiments (i.e., S_3 series) is shown in Fig. 6 for illustration purposes. The modified loading cap described earlier was used for the first time in this series. The problems associated with friction around the loading cap were essentially eliminated in the S_3 series. The modified loading cap; however, was not designed to seal against air. Therefore, loadings under constant water content conditions were conducted throughout the S_3 series.

Total stress applied was measured using a load cell. The equilibrium pore-air pressure at the top of the specimen, as measured on the loading cap, was used in calculating the boundary stress state variables. The equilibrium pore-water pressure at the base, as measured in the water compartment, was used in computing the boundary stress state variables. At equilibrium, the pore-air and pore-water pressure distributions were approximately uniform throughout the soil specimen. The vertical deflection measurements were obtained from dial gauge and LVDT readings while the water volume change measurements (i.e., dV_w) were taken from the twin-burette water volume change indicator.

Pore pressure parameters

Pore pressure parameters were calculated from the undrained and constant water content test results. The pore pressure measurements along the cylinder were averaged in accordance with the portion representative of each pressure measuring port. The difference between the average initial and final pore pressures was taken as being equal to the change in pore pressure due to the total stress

Fig. 6. Actual stress state path for the series 3 experiments.



increment. The ratio between the pore pressure change and the total stress increment was calculated as the pore pressure parameter. Calculations were performed for several multistage undrained or constant water content loadings to obtain an average pore pressure parameter.

The average \bar{B}_w parameters from the experimental results are plotted against matric suctions in Fig. 7. The \bar{B}_w parameters are shown to decrease with increasing matric suctions or decreasing degrees of saturation. In other words, most of the total stress increment is transferred directly to the soil structure at higher suctions. The stiffer soils at higher matric suctions will have lower pore pressure parameters, as suggested by eq. [4]. The \bar{B}_w parameters ranged from 0.2 to 0.5, which agreed closely with typical values suggested by Skempton (1954). The curve of \bar{B}_w parameters shown in Fig. 7 is similar to the results presented by Campbell (1973). In the case of the S_5 series, the \bar{B}_w parameters are close to unity, since the soil remained essentially saturated throughout the series (Rahardjo 1990).

The \bar{B}_w pore-water pressure parameters can also be computed based on the theory presented earlier. In all series (except the S_1 series), the loadings were conducted under constant water content conditions. The equation for the \bar{B}_w parameter under constant water content conditions was given in eq. [4]. Although excess pore-air pressures

do not develop during the constant water content test, the compressibility of the pore fluid is not zero. Therefore, eq. [4] can be used to estimate the \bar{B}_w parameter that is required to arrive at the experimental value for the \bar{B}_w parameter. The coefficients of volume change, m_{1k}^s and m_2^s in eq. [4] are calculated from the measured volume changes during the test. The estimated \bar{B}_a parameters corresponding to the experimental \bar{B}_w parameters are also plotted in Fig. 7.

The \bar{B}_a parameters are lower than the \bar{B}_w parameters, as shown in Fig. 7. The \bar{B}_a parameter also decreases with increasing matric suction (or decreasing degree of saturation). The decrease in the \bar{B}_a parameter does not appear to be as large as for the \bar{B}_w parameter.

Consolidation tests

The S_1 and S_2 series of consolidation tests were performed following the undrained loading tests. Both excess pore-air and pore-water pressures were developed during undrained loadings, which were then dissipated in the consolidation tests. In the S_3 , S_4 , and S_5 series, the consolidation tests were conducted following the constant water content loading tests. The excess pore-water pressures were developed during the constant water content tests. The excess pore-water pressures later dissipated during the consolidation tests. At the end of consolidation, the soil matric suction returned to the value established prior to the undrained or constant water content loadings.

The consolidation test results from the S_1 FG test (i.e., S_1 series) are presented in Fig. 8. The excess pore-air pressures were dissipated almost instantaneously while the excess pore-water pressures were dissipated with time (Fig. 8a). The instantaneous dissipation of the excess pore-air pressures occurred throughout the entire height of the soil specimen. The water volume changes were larger than the total volume changes during the test (Fig. 8b). As a result, the degree of saturation was decreasing during the consolidation process. Soil properties and stress state variables during the test are given in Table 2, together with those from other tests.

The S_3N_3O consolidation test results (i.e., S_3 series) are shown in Fig. 9. The pore-water pressures were dissipated from a pressure of approximately 96 to 71 kPa as shown in Fig. 9a. The most rapid dissipation occurred at the base of the soil specimen. The dissipation slowed towards the top of the specimen. The height of the specimen affected the equilibration rate of pore-water pressures at different depths, since the excess pressures were first dissipated at the base and then proceeded to the top of the specimen with time (i.e., one-dimensionally downward water flow). The ratio between the total and water volume changes (i.e., dV / dV_w) was approximately 0.3 (Fig. 9b) causing a further decrease in the degree of saturation at the end of the test (Table 3).

Increasing matric suction tests

The increasing matric suction tests were performed following the consolidation tests. The pore-water pressure in

Fig. 7. \bar{B}_a and \bar{B}_w pore pressure parameters versus matric suctions.

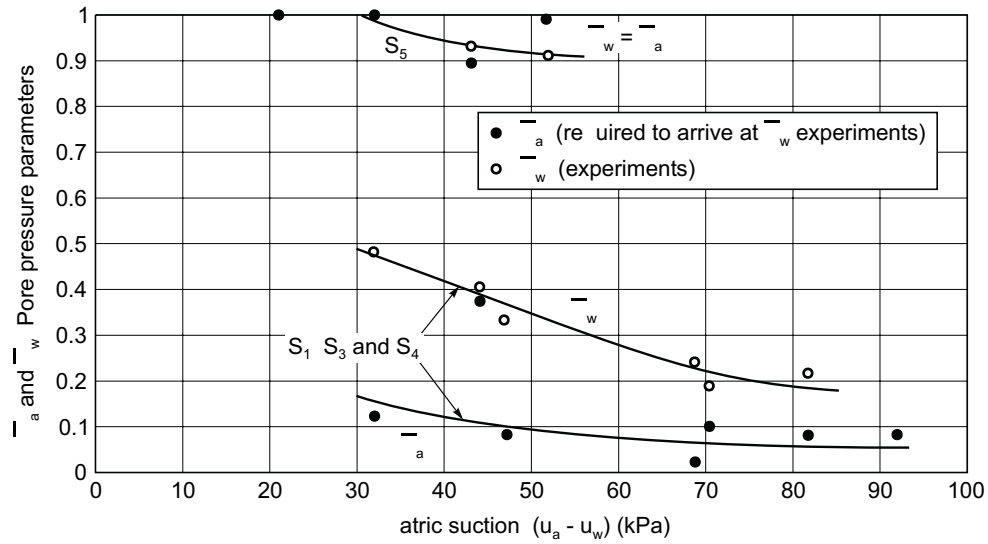


Fig. 8. Pore pressure dissipation and volume changes during the S_1 FG consolidation test: a) pore-air and pore-water pressure isochrones; b) total and water volume changes.

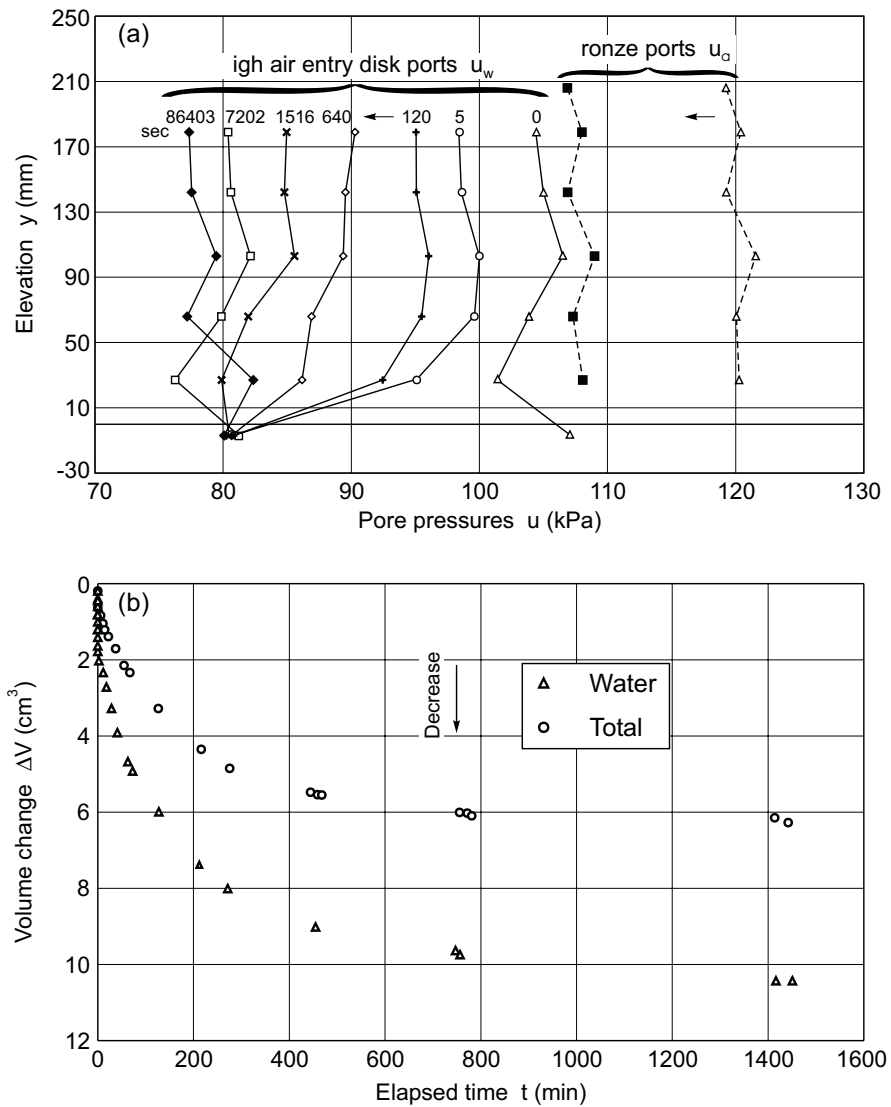


Table 2. Soil properties and stress state variables during the S₁FG test.

Test type: consolidation test		
	Initial	Final
Properties		
S	98.0%	97.2%
e	0.578	0.572
w	21.2%	20.7%
n	0.366	0.364
Stress state variables (kPa)		
σ	184.3	185.4
u_a (top)	119.5	107.5
u_w (bottom)	106.7	80.0
$\sigma - u_a$	64.8	77.9
$d(\sigma - u_a)$		13.1
$u_a - u_w$	12.8	27.5
$d(u_a - u_w)$		14.7

the soil specimen was reduced by decreasing the compartment pressure below the soil specimen. The total stress and the pore-air pressures were maintained constant. The soil matric suction increased to a new value under a constant net normal stress.

The pore-water pressure distributions at different times during the S₃OP increasing matric suction test (i.e., S₃ series) are shown in Fig. 10a. It should be noted that the pore-water pressures did not decrease as rapidly as the excess pore-water pressure dissipation during the consolidation test. The pore-water pressures decreased in a gradual manner. In addition, the pore-water pressure decrease near the bottom region of the specimen was faster than the pore-water pressure decrease near the top region.

The total and water volume changes during the S₃OP test are shown in Fig. 10b. The ratio between the total and water volume changes (i.e., dV / dV_w) was small (i.e., around 0.1) as compared with a similar ratio for the consolidation test. The small ratio indicated that the total volume changed little, while the water volume changed significantly when the matric suction is increased. In other words, the increase in matric suction was more effective in reducing the soil water content than in decreasing the soil void ratio. As a result, the degree of saturation decreased significantly during the increasing matric suction process (Table 4).

Observations from the test results

The following observations are made on the basis of the test results obtained from the five series of tests (Rahardjo 1990).

Pore pressure characteristics during drained tests

The excess pore-air pressures developed during undrained loadings in the S₁ and S₂ series have been shown to dissipate rapidly during the subsequent consolidation test. The essentially instantaneous dissipation of excess

pore-air pressure indicated that the air phase was continuous at matric suctions as low as 13 kPa (i.e., S₁FG test).

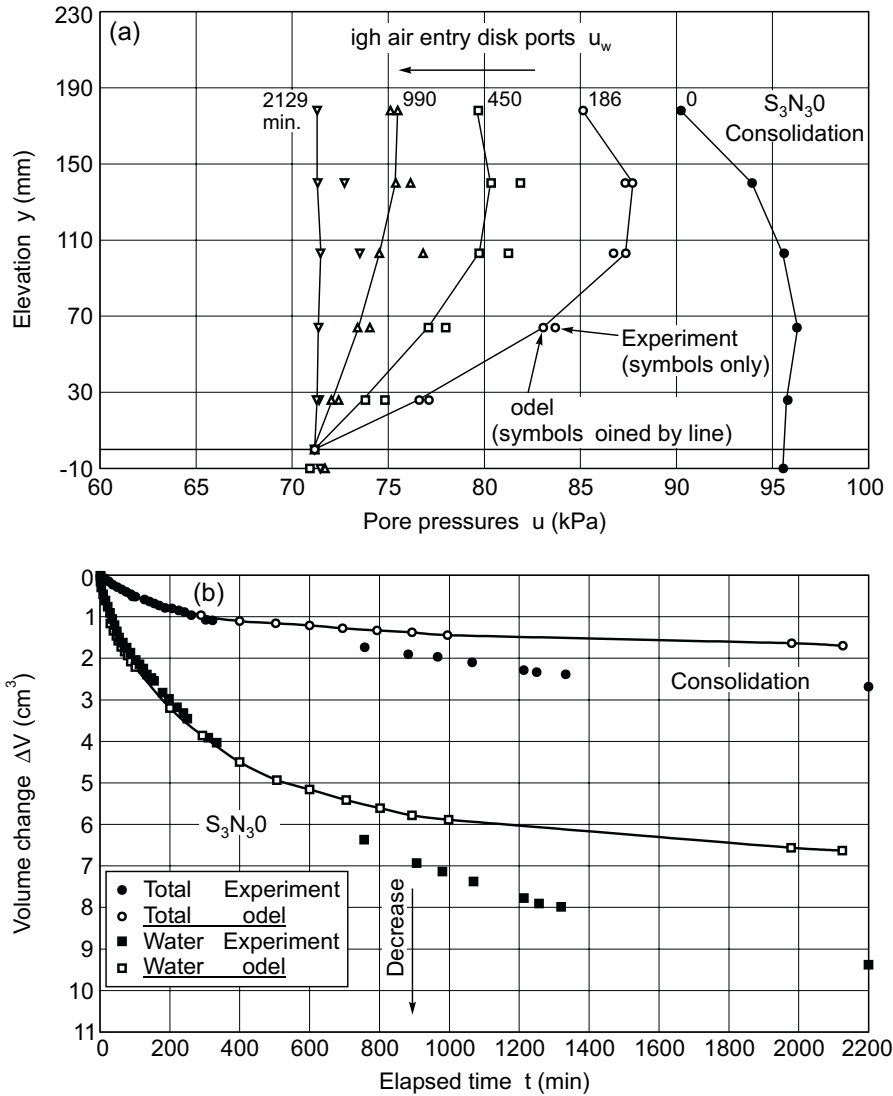
Comparisons between the consolidation and increasing matric suction test results revealed that the pore-water pressure dissipation in the consolidation test occurred at a faster rate than the pore-water pressure decrease in the increasing matric suction test. Figure 11a shows an idealized comparison between the differing pore-water pressure behavior during the consolidation and increasing matric suction tests for an equal reduction in the pore-water pressure. In the consolidation test, the pore-water pressures dissipated rapidly and equilibration was achieved within a short period of time. In the increasing matric suction test, the pore-water pressure dissipated gradually and equilibration required a long period of time.

The different rates of the pore-water pressure equalization between the consolidation and increasing matric suction tests are a reflection of the different coefficients of consolidation, c_v^w (i.e., $k_w / (\rho_w g m_2^w)$ in eq. [6]). The permeability, k_w , was essentially the same for both tests (Rahardjo 1990). Therefore, the differing coefficients of consolidation were primarily caused by the different m_2^w coefficients, for the consolidation and increasing matric suction tests. The m_2^w coefficient for the consolidation test was smaller than the m_2^w coefficient for the increasing matric test. As a result, the c_v^w value during the consolidation test was higher than the c_v^w value during the increasing matric suction test. In other words, the pore-water pressure dissipation during consolidation occurred at a faster rate than the pore-water pressure decrease during an increasing matric suction process.

Volume change characteristics during drained tests

Comparisons between volume change measurements during the consolidation and increasing matric suction tests are shown in an idealized manner in Fig. 11b. In both tests, the total volume changes were quite small. However, the water volume change during an increasing matric suction test was significantly larger than the water volume change during a consolidation test. In other words, the ratio of the total volume change to the water volume change during increasing matric suction tests is negligible. On the other hand, the total volume change during consolidation is significant when compared to its water volume change. Fig. 11b illustrates the effectiveness of an increasing matric suction in reducing the volume of water in the soil. The consolidation process caused by an increase in total stress is not as effective as the increasing matric suction process in expelling water from an unsaturated soil. An increase in total stress will not result in an equal change of pore-water pressure because of the low \bar{B}_w parameter for an unsaturated soil. As a result, for an equivalent change in total stress or matric suction, the pore-water pressure gradient during the consolidation process is much smaller than the pressure gradient during the increasing matric suction process. Consequently, the water volume change during the consolidation process is less significant than the water volume change during the increasing matric suction process.

Fig. 9. Comparison between theoretical analyses and experimental results from the S_3N_3O test: a) pore-water pressure profiles at different times; b) total and water volume changes during the test.



The time required for volume change equilibration during the consolidation process is smaller than the equilibration time required for the increasing matric suction process as illustrated in Fig. 11b. This difference is in agreement with the differing times required for pore-water pressure equalization shown in Fig. 11a.

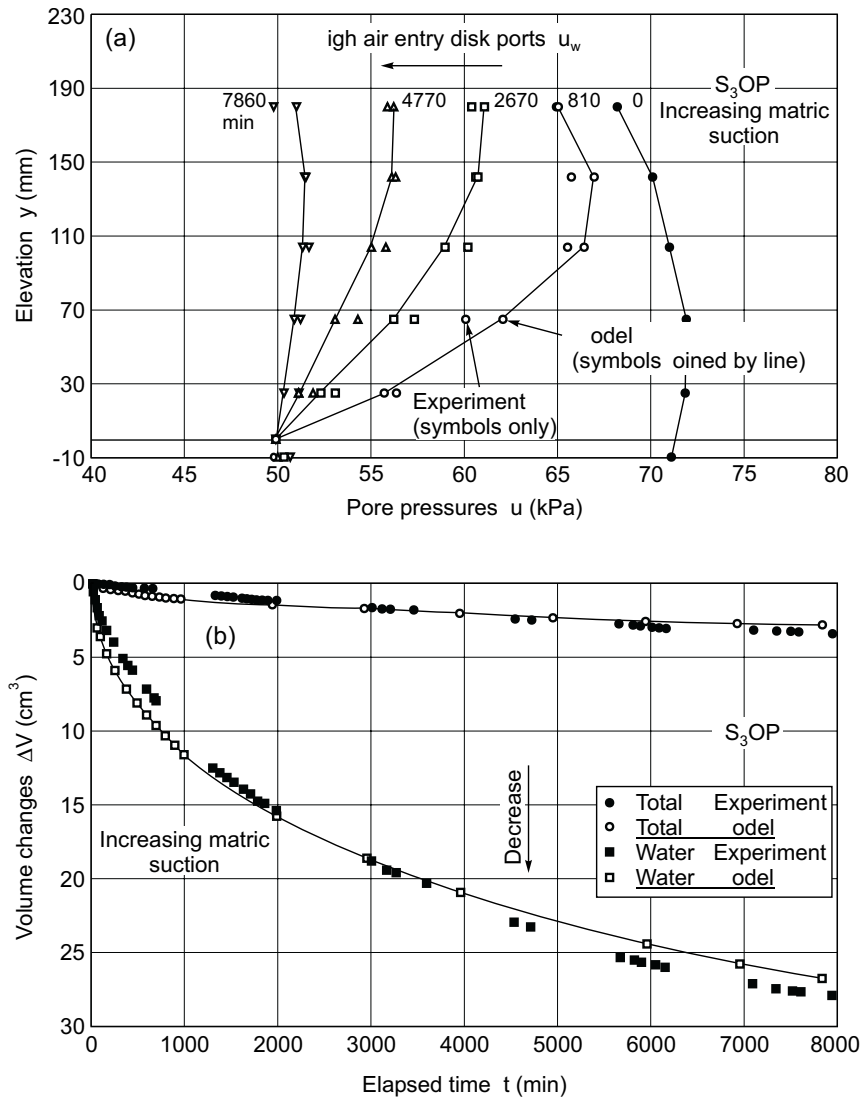
Theoretical analyses for drained tests

Two typical results of numerical simulations from the S_3 series are presented in this paper (i.e., S_3N_3O and S_3OP for consolidation and increasing matric suction tests, respectively). A constant coefficient of consolidation, c_v^w , was used during the simulation of each test (i.e., eq. [6] reduces to $\partial u_w / \partial t = c_v^w \partial^2 u_w / \partial y^2$). It was assumed that the soil properties (i.e., k_w , m_2^w and c_v^w) did not change significantly during each of the tests. The tests were performed over a relatively small change in matric suction (i.e., around 20 kPa). However, the c_v^w value was varied from one test to another since it involved a larger

Table 3. Soil properties and stress state variables during the S_3N_3O test.

Test type: consolidation test		
	Initial	Final
Properties		
S	76.2%	74.7%
e	0.510	0.507
w	14.5%	14.1%
n	0.338	0.336
Stress state variables (kPa)		
σ	240.3	239.4
u_a (top)	126.4	126.5
u_w (bottom)	95.8	71.4
$\sigma - u_a$	113.9	112.9
$d(\sigma - u_a)$		-1.0
$u_a - u_w$	30.6	55.1
$d(u_a - u_w)$		24.5

Fig. 10. Comparison between theoretical analyses and experimental results from the S_3OP test: a) pore-water pressure profiles at different times; b) total and water volume changes during the test.



change in matric suction. In other words, the soil properties were a function of matric suctions, but were considered to be constant within a single test.

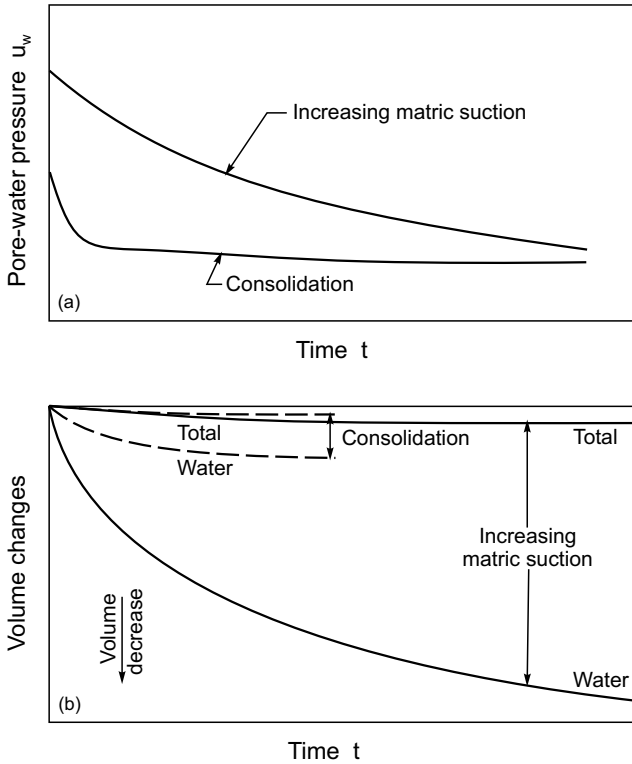
Figure 9 illustrates the comparisons between the theoretical and experimental results for the S_3N_3O consolidation test. The experimental pore-water pressures showed a lower pressure at the top than in the middle of the specimen. The results showed that a small water efflux appeared to be occurring at the top of the specimen. This water efflux could be attributed to the water vapor flow (i.e., evaporation) from the soil specimen to the air chamber on top of the cylinder. Therefore, a varying water efflux on the top of the specimen was used in order to more closely simulate the experimental profiles of pore-water pressures. The water efflux which produced the best simulation varied from 8×10^{-12} m/s down to 4×10^{-13} m/s as the elapsed time increased.

The theoretical simulations were commenced with a constant value of c_v^w that was estimated from the k_w and

Table 4. Soil properties and stress state variables during the S_3OP test.

Test type: increasing matric suction test		
	Initial	Final
Properties		
S	74.7%	70.0%
e	0.507	0.503
w	14.1%	13.1%
n	0.336	0.335
Stress state variables (kPa)		
σ	239.4	238.1
u_a (top)	126.5	126.4
u_w (bottom)	71.4	50.9
$\sigma - u_a$	112.9	111.7
$d(\sigma - u_a)$		-1.2
$u_a - u_w$	55.1	75.5
$d(u_a - u_w)$		20.4

Fig. 11. Comparison between consolidation and increasing matric suction tests: a) pore-water pressure behavior; b)



m_2^w values (i.e., $c_v^w = k_w / \rho_w g m_2^w$). The coefficient of permeability was first estimated from the unsaturated permeability function (Fig. 12). The coefficient of volume change, m_2^w , was first estimated from the soil-water characteristic curve (Fig. 5). The constant coefficients of consolidation were used to calculate the pore-water pressure profiles at different times during the test (i.e., $\partial u_w / \partial t = c_v^w \partial^2 u_w / \partial y^2$). The coefficients of volume change were used to compute the water volume changes in accordance with eq. [5] (i.e., $dV_w / V_0 = -m_2^s du_w$). The m_2^s values were estimated from the shrinkage curve. The m_2^s values were used to calculate the total volume change in accordance with eq. [7] (i.e., $dV_v / V_0 = -m_2^s du_w$).

The simulated pore-water pressure profiles and volume changes were compared with the experimental results. Attempts were made to closely match the earlier portion of the experimental results (i.e., pore-water pressure and volume changes). Deviations between the theoretical and experimental results during the later part of the test were anticipated as a result of temperature fluctuations. The effects of temperature fluctuations became more significant towards the end of the test when the rates of pressure change decreased. The experimental volume changes that were significantly affected by the cyclic temperature variations were larger in some cases than the simulated volume changes as illustrated in Fig. 9b. If the simulation results did not match the experimental results, the above simulation procedure was repeated using revised soil parameters for c_v^w , m_2^w and m_2^s . The above trial and error procedure was repeated until the best simulation of the

results was obtained as shown in Fig. 9. At this stage, the coefficient of permeability with respect to water, k_w , during the test was computed as $c_v^w(\rho_w g m_2^w)$.

The simulation results in Fig. 9 were obtained using a varying water efflux at the top of the specimen. It appeared that a varying water efflux was required to closely match the pore-water pressure profiles.

Similar simulations were applied on the increasing matric suction test results. Figure 10 shows good agreement between the theoretical and experimental results for the S₃OP test. A varying water efflux of 5×10^{-12} to 1×10^{-12} m/s at the top of the specimen, was used in the simulation.

The combined c_v^w values from the simulations of the S₃ and S₄ drained tests are plotted in Fig. 12 with respect to matric suctions. These values were obtained from simulations using a constant c_v^w value for each test. The curves in Fig. 12 clearly show the decreasing c_v^w values with increasing matric suctions and higher c_v^w values during the consolidation tests than during the increasing matric suction tests. The c_v^w values range from 8×10^{-6} m²/s to 3×10^{-7} m²/s for the consolidation tests. In the increasing matric suction tests, the c_v^w values ranged from 8×10^{-6} m²/s to as low as 3×10^{-8} m²/s (Fig. 12). The higher c_v^w values during the consolidation tests resulted in faster pore-water pressure dissipation during the consolidation process than during the increasing matric suction process.

The coefficients of permeability from the simulations of the S₃ and S₄ drained tests are plotted against matric suction in Fig. 13. The coefficients of permeability appear to decrease with increasing matric suctions at a slower rate than the rate suggested by the unsaturated permeability function obtained from the soil-water characteristic curve. This discrepancy could be attributed to the difference in void ratios during the experimental test series (i.e., S₃ and S₄ series) and the Tempe cell tests used to obtain the soil-water characteristic curves. The void ratios measured during the Tempe cell tests were higher than the void ratios during the experimental test series (i.e., S₃ and S₄ series). The difference in void ratio was due to the application of the net normal stress during the experimental series in the K_0 cylinder, while the Tempe cell tests were performed under a zero net normal stress. The Tempe cell specimens would be expected to have some large pores as well as the small pore sizes. On the other hand, the soil specimens of the S₃ and S₄ series probably contained mainly pores which were relatively small.

The large pores in the Tempe cell specimens would drain quickly with increasing matric suctions. This caused a more rapid reduction for the coefficients of permeability computed from the Tempe cell tests. The small pores in the S₃ and S₄ specimens would be expected to drain slowly with increasing matric suctions. As a result, the coefficient of permeability decreased gradually with increasing matric suctions during the S₃ and S₄ drained tests. It should also be noted that there was no significant difference between the permeabilities obtained from consolidation and increasing matric suction tests.

Fig. 12. Combined coefficients of permeability obtained from theoretical analyses of the S_3 and S_4 drained tests.

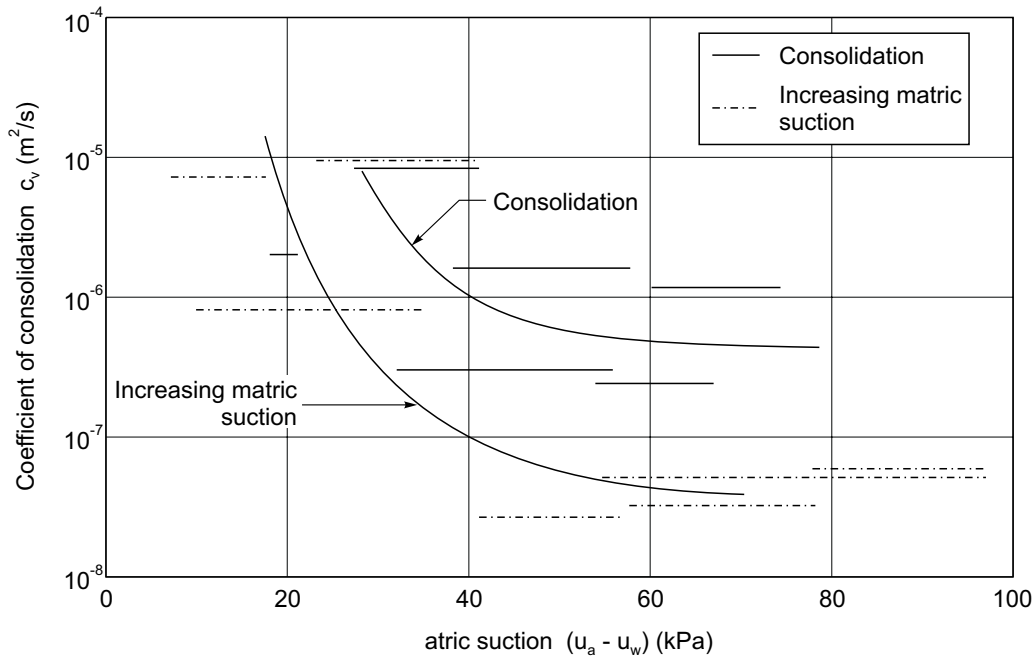
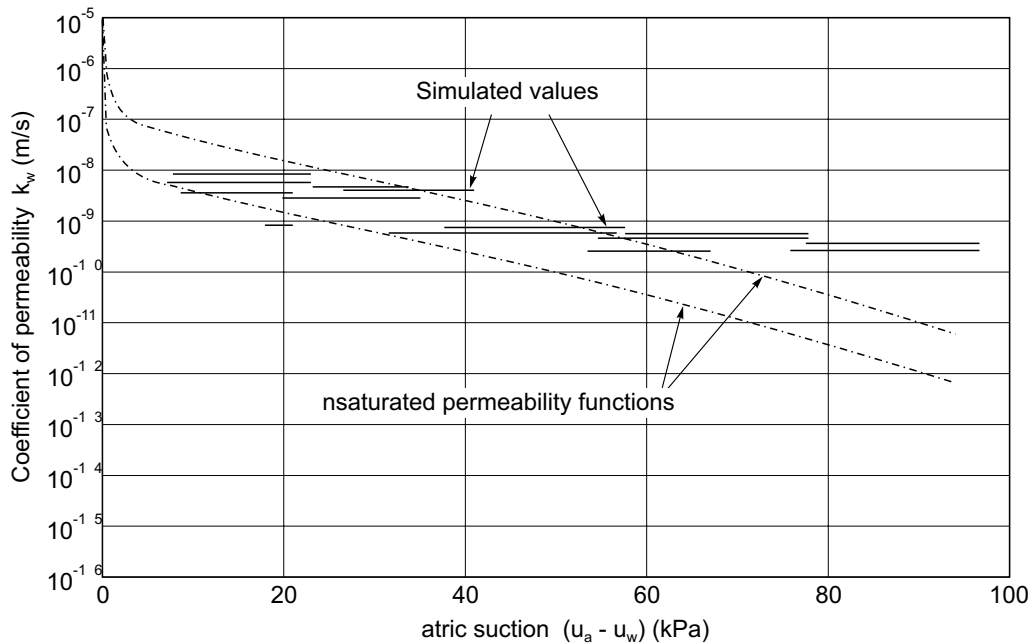


Fig. 13. Combined coefficients of consolidation obtained from theoretical analyses of the S_3 and S_4 drained tests.



The m_2^w and m_2^s coefficients of volume change used in the simulations of the S_3 and S_4 series are plotted in Figs. 14 and 15 for the consolidation and increasing matric suction tests, respectively. The m_2^w values are greater than the m_2^s values for both the consolidation and increasing matric suction tests, because the water volume change, dV_w , is always larger than the total volume change, dV_v , (Fig. 11b).

Comparisons between Figs. 14 and 15 reveal that the m_2^w coefficients from the increasing matric suction test are generally larger than the m_2^w coefficients from the

consolidation test. The differences in coefficients of volume change resulted in higher c_v^w values and faster dissipation rate during the consolidation test than during the increasing matric suction test.

The m_2^s and m_2^w coefficients from the consolidation and increasing matric suction tests appear to increase to a peak value and then decrease as the matric suction increases. This behavior can be illustrated by considering the constitutive surfaces on a constant net normal stress plane (Fig. 16). The m_2^s and m_2^w coefficients are the slopes of the soil structure and the water constitutive relations,

Fig. 14. Combined coefficients of volume change obtained from theoretical analyses of the S_3 and S_4 drained tests

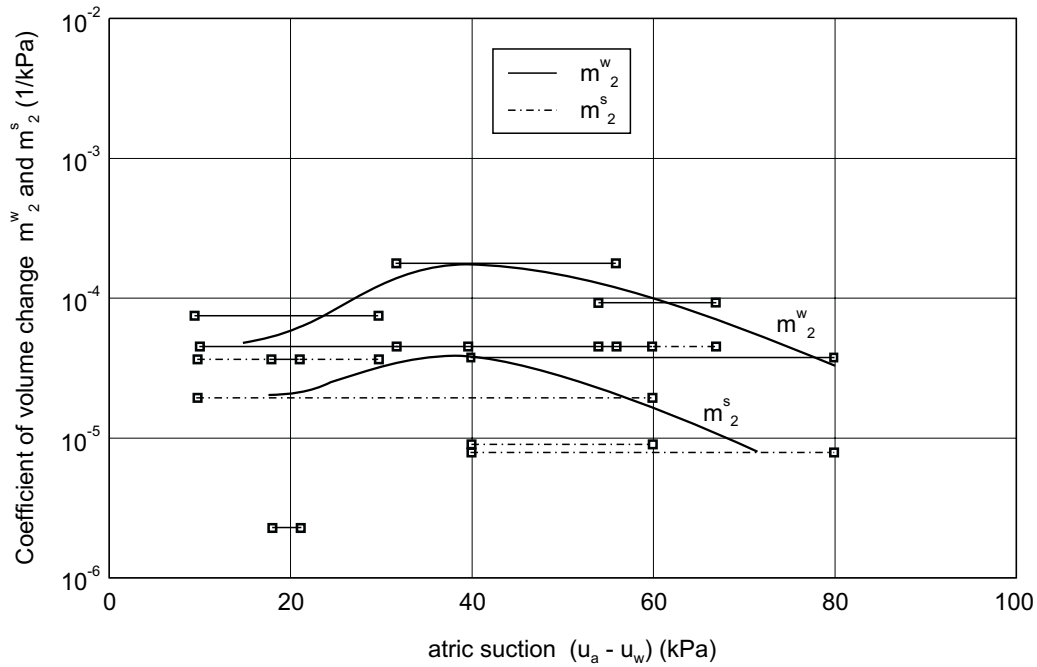
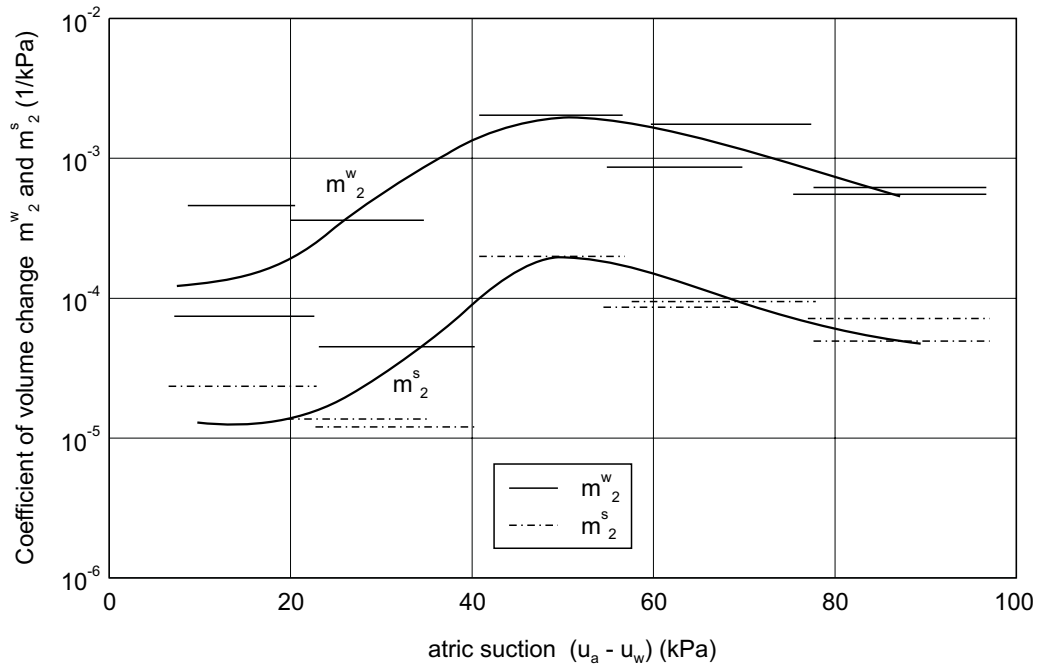


Fig. 15. Combined coefficients of permeability obtained from theoretical analyses of the S_3 and S_4 increasing matric suction tests.



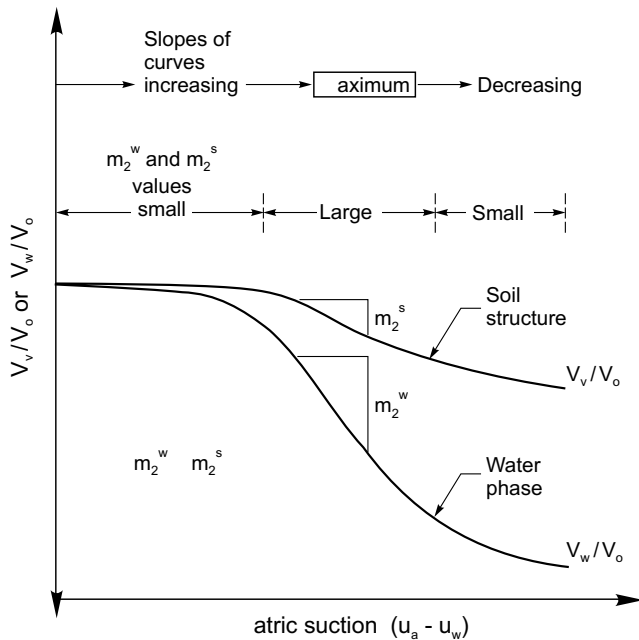
respectively. During initial stages of the tests, the soil structure and water volumes gradually decreased as the matric suction increased. Beyond a certain matric suction value, the total and water volumes decrease significantly and eventually slow down again at higher matric suctions. The changing rates of total and water volume changes at various matric suctions result in varying m_2^s and m_2^w coefficients with respect to matric suction as shown in Figs. 14 and 15.

Conclusions

Several conclusions can be made as a result of this study. These conclusions are related to the performance of the equipment and the behavior of the unsaturated soils during undrained and drained tests.

- (1) The designed and constructed K_0 apparatus can be used to observe the behavior of unsaturated soils during constant water content loading, consolidation, and increasing matric suction tests.

Fig. 16. Idealized constitutive surfaces at a constant net normal stress plane.



- (2) The pore-air and pore-water pressure measuring systems and techniques used in this experimental study performed satisfactorily. Independent measurements of pore-air and pore-water pressures throughout an unsaturated specimen, as well as at the surface of an unsaturated soil specimen can be achieved using the designed systems.
- (3) Pore pressure parameters for an unsaturated soil decrease rapidly as the degree of saturation decreases from 100 to 90%. These pore pressure parameters can be estimated from theory provided the soil structure and pore fluid compressibilities are known.
- (4) The change in matric suction as a result of a change in net normal stress under undrained or constant water content conditions becomes less significant as the soil becomes drier (i.e., at high matric suctions).
- (5) Pore-air pressure dissipation occurs essentially instantaneously when the air phase is continuous. When the air phase is occluded, the pore-air pressures could not be measured.
- (6) The pore-water pressure changes during the consolidation or the increasing matric suction process occurred in a time dependent manner (i.e., transient process) consistent with theory. The excess pore-water pressure dissipation during the consolidation process is faster than the pore-water pressure decrease in the increasing matric suction process. The differing rate is primarily due to the lower m_2^w coefficient for the consolidation process than for the increasing matric suction process. The coefficient of permeability, k_w , appears to be the same for both processes. As a result, the coefficient of consolidation, c_v^w is higher for the consolidation process (i.e., faster

pore-water pressure dissipation) than for the increasing matric suction process.

- (7) The water flow differential equation similar to Terzaghi's consolidation equation can be used to describe the transient flow of water in an unsaturated soil when the air phase is continuous (i.e., $S < 90\%$). In this case, the coefficient of permeability, k_w , and the coefficient of water volume change, m_2^w , used for computing the coefficient of consolidation, c_v^w , can be taken as a function of matric suction.
- (8) Water volume changes during an increasing matric suction process is considerably larger than the water volume changes during the consolidation process.

References

- Barden, L. 1965. Consolidation of compacted and unsaturated clays. *Géotechnique*, **15**(3): 267–286.
- Barden, L. 1974. Consolidation of clays compacted 'dry' and 'wet' of optimum water content. *Géotechnique*, **24**(4): 605–625.
- Barden, L., and Pavlakis, G. 1971. Air and water permeability of compacted unsaturated cohesive soil. *Journal of Soil Science*, **22**(3): 302–317.
- Barden, L., and Sides, G.R. 1970. Engineering behavior and structure of compacted clay. *ASCE, Journal of Soil Mechanics and Foundation Engineering*, **96**: 1171–1200.
- Biot, M.A. 1941. General theory of three dimensional consolidation. *Journal of Applied Physics*, **21**(2): 148–152.
- Bishop, A.W. 1957. Some factors controlling the pore pressures set up during the construction of earth dams. *Proceedings, 5th International Conference on Soil Mechanics and Foundation Engineering, Paris, France, Vol. 2, pp. 294–300.*
- Bishop, A.W. 1961. Discussion on general principles and laboratory measurements. *Proceedings, Conference on Pore Pressures and Suction in Soils, London. Butterworths, pp. 63–66.*
- Bishop, A.W., and Henkel, D.J. 1962. *The measurement of soil properties in the triaxial test. 2nd Edition, Edward Arnold (Publisher) Ltd., London, England, pp. 180–211.*
- Blight, G.E. 1961. *Strength and consolidation characteristics of compacted soils. Ph.D. thesis, University of London, London, England.*
- Brahtz, J.H.A., Zangar, C.N., and Bruggeman, J.R. 1939. *Notes on analytical soil mechanics. United States Bureau of Reclamation, Denver, Colorado. Technical Memorandum 592.*
- Buckingham, E. 1907. *Studies of the movement of soil moisture. USDA, Bureau of Soils, Bulletin No. 38.*
- Campbell, J.D. 1973. *Pore pressures and volume changes in unsaturated soils. Ph.D. thesis, University of Illinois at Urbana-Champaign, Urbana-Champaign, Ill.*
- Childs, E.C., and Collis-George, N. 1950. *The permeability of porous material. Proceedings of the Royal Society of London, Series A, 201: 392–405.*
- Dakshnamurthy, V., Fredlund, D.G., and Rahardjo, H. 1984. *Coupled three-dimensional consolidation theory of unsaturated porous media. Proceedings, 5th International Conference of Expansive Soils, Adelaide, Australia, 21–23 May.*
- Fredlund, D.G., and Hasan, J.U. 1979. *One-dimensional consolidation theory: Unsaturated soils. Canadian Geotechnical Journal, 16: 521–531.*
- Fredlund, D.G., and Rahardjo, H. 1986. *Unsaturated soil consolidation theory and-laboratory experimental data. In Con-*

- solidation of soil: testing and evaluation, ASTM STP 892. *Edited by* R.N. Yong and F.C. Townsend. ASTM, Philadelphia, pp. 154–169.
- Fredlund, D.G. and Rahardjo, H. 1993. Soil mechanics for unsaturated soils. John Wiley & Sons, New York.
- Hamilton, I.W. 1939. The effect of internal hydrostatic pressures on the shearing strength of soils. ASTM, Proceedings, Vol. 39.
- Hasan, J.U. and Fredlund, D.G. 1980. Pore pressure parameters for unsaturated soils. *Canadian Geotechnical Journal*, **17**: 395–404.
- Hilf, J.W. 1948. Estimating construction pore pressures in rolled earth dams. Proceedings, 2nd International Conference on Soil Mechanics and Foundation Engineering, Rotterdam, Vol. 3, pp. 234–240.
- Hilf, J.W. 1956. An investigation of pore-water pressure in compacted cohesive soils. Ph.D. thesis, Technical Memorandum No. 654, United States Department of the Interior Bureau of Reclamation, Design and Construction Division, Denver, Colorado, U.S.A.
- Hill, C.B. 1967. Consolidation of compacted clay. M.Sc. thesis, University of Manchester, Manchester, England.
- Larmour, Y. 1966. One dimensional consolidation of partially saturated clay. M.Sc. thesis, University of Manchester, Manchester, England.
- Lloret, A. and Alonso, E.E. 1980. Consolidation of unsaturated soils including swelling and collapse behavior. *Géotechnique*, **30**(4): 449–477.
- Madedor, A.O. 1967. Consolidation characteristics of compacted clay. M.Sc. thesis, University of Witwatersrand, South Africa.
- Olson, R.E. 1986. State-of-the-art: consolidation testing, consolidation of soils: testing and evaluation. ASTM STP 892. *Edited by* R.N. Yong and F.C. Townsend, ASTM, Philadelphia, pp. 7–70.
- Rahardjo, H. 1990. The study of undrained and drained behaviour of unsaturated soils. Ph.D, thesis, University of Saskatchewan, Saskatoon, SK, Canada.
- Richards, B.G. 1974. Behavior of unsaturated soils. *In* Soil mechanics-new horizons. *Edited by* I.K Lee. American Elsevier, New York, pp. 112–157.
- Richards, L.A. 1931. Capillary conduction of liquids through porous medium. *Physics*, **1**: 318–333.
- Scott, R.F. 1963. Principles of soil mechanics. Addison-Wesley Publishing Co. Inc., London, England.
- Skempton, A.W. 1954. The pore-pressure coefficient, A and B. *Géotechnique*, **4**(4): 143–147.
- Terzaghi, K. 1936. The shear resistance of saturated soils. Proceedings, 1st International Conference on Soil Mechanics and Foundation Engineering, Cambridge, Vol. 1.
- Terzaghi, K. 1943. Theoretical soil mechanics. John Wiley & Sons, New York.

Mechanisms of osmotic flow and volume change in clay soils

S.L. Barbour and D.G. Fredlund

Abstract: The mechanical behavior of compressible clay soils may be strongly influenced by physicochemical effects when concentrated pore fluids are introduced to the soil. Conceptual models have been used to explain the influence of pore fluid chemistry on the mechanical behavior of clays in a quantitative way. In this paper an alternative macroscopic description of the osmotic volume change behavior of a clay soil undergoing changes in a pore fluid chemistry is provided.

Theoretical descriptions of two potential mechanisms of osmotic volume changes (osmotic consolidation and osmotically induced consolidation) are presented. Osmotic consolidation occurs as a result of a change in the electrostatic repulsive-minus-attractive stress, $R - A$, between clay particles. Osmotically induced consolidation occurs because of fluid flow out of the clay in response to osmotic gradients.

A numerical simulation is used to demonstrate the characteristic behavior of a clay soil undergoing either of these volume change processes. The results of a laboratory testing program on two clay soils exposed to concentrated NaCl solutions are used to illustrate that the dominant mechanism of osmotic volume change in surficial clay soils is osmotic consolidation.

Key words: physicochemical, osmosis, volume change, NaCl salt, montmorillonite, clay, stress state variables, repulsive stress, active stress.

Introduction

The mechanical behavior of clay soils may be strongly influenced by physicochemical interactions between the clay particles and the pore fluid. Conceptual and analytical models have been proposed to explain the influence of pore fluid chemistry on the behavior of clays. These models have been developed at a microscopic scale and have provided a qualitative description of interactions.

A quantitative description of the behavior of clay soils in response to changes in pore fluid chemistry is required in current geotechnical practice. For example, in the design of containment facilities for concentrated electrolyte solutions (i.e., brine) or organic fluids, the impact that these fluids have on the hydraulic and mechanical properties of soil must be known. In this paper, the impact that strong NaCl solutions have on the volume change behavior of clay soils is used to illustrate the influence of inorganic salts on the mechanical behavior of clay soils.

The time-dependent volume change behavior of soil is controlled by two properties: first, the compressibility of the soil, that is, its change in volume related to changes in stress state; and second, the ability of the soil to conduct pore fluid. The ability of physicochemical (i.e., osmotic)

effects to influence both soil compressibility and fluid flow through soil has been demonstrated in the literature.

The presence of osmotic flow in clay aquitards has been studied by numerous researchers, including Hanshaw and Zen (1965), Marine and Fritz (1981), and Neuzil (1986). The influence of osmotic flow processes on the transport of salt has been studied by Kemper and van Schaik (1966), Kemper and Rollins (1966), Elrick et al. (1976), Greenberg et al. (1973), and others. Deviations from Darcy's law have also been attributed to osmotic flow by investigators such as Kemper (1961), Low (1955), Bolt and Groenevelt (1969), and Olsen (1985).

Extensive studies of the compressibility and swelling of clays in response to changing pore fluid concentrations have been conducted over the last 30 years, and include the work of Bolt and Miller (1955), Bolt (1956), Warkentin et al. (1957), Aylmore and Quirk (1962), Blackmore and Miller (1962), Warkentin and Schofield (1962), and Mesri and Olson (1971). Bailey (1965) and Mitchell (1973a) have provided reviews of this literature.

Up to the present, a comprehensive theoretical description of the combined influence of osmotic flow and volume change on the behavior of clay soils has been lacking. The objective of this paper is to provide a theoretical description of the two primary mechanisms for osmotic volume change, referred to in this paper as osmotically induced consolidation and osmotic consolidation.

When a clay is exposed to a concentrated salt solution the volume of the clay will change as a result of the combined influence of the processes of osmotic flow and osmotic compressibility. As salt is transported into the clay changes in the interparticle repulsive stresses will occur,

S.L. Barbour. Professor, Department of Civil Engineering, University of Saskatchewan, Saskatoon, SK, Canada S7N 5A9.

D.G. Fredlund. Professor, Department of Civil Engineering, University of Saskatchewan, Saskatoon, SK, Canada S7N 5A9.

Reproduced with permission from the *Canadian Geotechnical Journal*, **26**: 551–562, 1989.

which will in turn lead to suppression of the double layer and changes in void ratio. The time-dependent volume change associated with changes in the osmotic pressure of the pore fluid will be termed osmotic consolidation.

A second mechanism of volume change will occur; however, as a result of fluid flow that develops within the clay in response to osmotic gradients. As the clay is exposed to the electrolyte solution osmotic flow out of the sample will occur. These outward flows cause negative pore fluid pressures to develop within the specimen, which then lead to increases in effective stress, $\sigma - u_f$, and consequently volume change. The volume change that occurs is still in response to changes in effective stress. The changes in pore-water pressure; however, are induced as a result of osmotic pressures, this form of volume change is called osmotically induced consolidation.

Characteristic features of these two processes are demonstrated through the use of a numerical model, and the relative importance of these two independent processes is demonstrated from the results of a laboratory testing program. An analysis of these test results illustrates some practical applications of the proposed approach to geotechnical engineering design in situations in which changes in pore fluid chemistry are of concern.

Theoretical description of osmotic flow and compressibility

Consolidation is the result of the combined influence of fluid flow and soil compressibility. Changes in pore fluid chemistry may significantly influence both volume change and fluid flow through clay. Theoretical descriptions of these "osmotic" phenomena are presented in this section.

Osmotic flow

Osmosis is the term used to describe the phenomenon by which a solvent passes from a solution of lower solute concentration through a semipermeable membrane into a solution of higher solute concentration. A membrane is described as semipermeable if it allows the passage of solvent but not solute. If the flow of water is restricted, a pressure imbalance equal to the osmotic pressure difference between the two solutions would have to be present. The osmotic pressure can be calculated from thermodynamic principles (Robinson and Stokes 1968). The osmotic pressure can also be approximated by the van't Hoff equation (Metten 1966):

$$[1] \quad \Pi = RTC$$

where:

- Π = osmotic pressure (kPa),
- C = sum of the molar concentrations in solution (mol/L),
- R = universal gas constant = 8.32 (L kPa/K mol), and
- T = absolute temperature (K).

The osmotic flow of water in soil can be described using a flow law similar in form to Darcy's law:

$$[2] \quad q_\pi = k_\pi \frac{\Delta\pi}{\Delta x} = \sigma k_h \frac{\Delta\pi}{\Delta x}$$

where:

- q_π = water flux (m/s),
- k_π = coefficient of osmotic permeability (m/s),
- k_h = coefficient of (hydraulic) permeability (m/s),
- π = osmotic pressure head equal to $(\Pi / \rho_f g)$, (m),
- ρ_f = pore fluid density (kg/m³),
- g = gravitational acceleration (m/s²),
- σ = osmotic efficiency, and
- x = distance (m).

If the soil behaves as a perfect semipermeable membrane, the coefficient of osmotic permeability will be equal to the coefficient of hydraulic permeability. In this case only pure water will flow in response to osmotic gradients. However, if the membrane is "leaky", the osmotic permeability will be equal to the hydraulic permeability multiplied by an osmotic efficiency, and water, carrying with it some dissolved salts, will flow in response to osmotic gradients. The osmotic efficiency is a measure of the degree to which the clay behaves as a perfect semipermeable membrane.

The osmotic efficiency of clays has been studied by Kemper and Rollins (1966), Bresler (1973), Olsen (1972), and others. Results of these studies (Fig. 1) illustrate that osmotic efficiency is strongly dependent on pore fluid chemistry, pore fluid concentration, void ratio, and interparticle spacing. High osmotic efficiencies have been observed only at low pore fluid concentrations, or low void ratios.

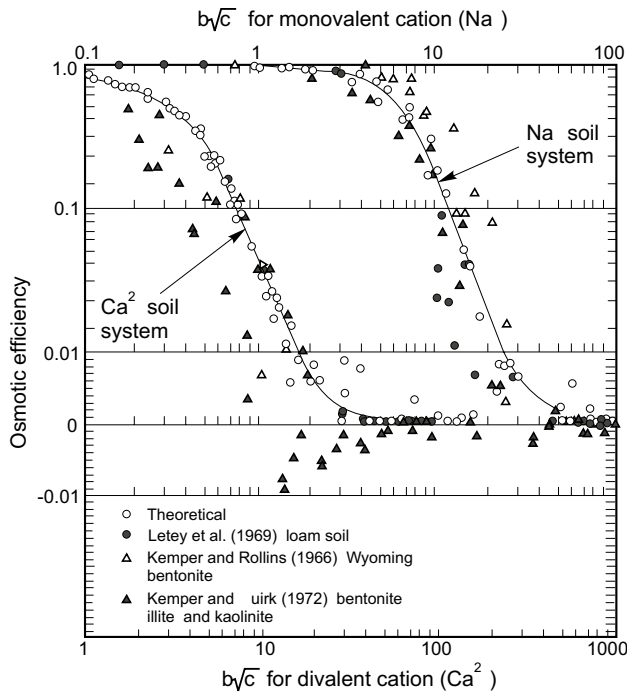
Figure 1 illustrates the dependence of osmotic efficiency of an unsaturated soil on pore fluid chemistry, pore fluid concentration, and fluid film thickness between soil particles. The film thickness is obtained by dividing the volumetric water content by half the soil surface area.

Osmotic compressibility

Volume changes in clays may occur as a result of changes in pore fluid chemistry due to the alteration of the electrostatic interactions between the clay particles. A conceptual model of the nature of the repulsive interparticle pressures is provided by the osmotic pressure concept and diffuse double layer theory.

Most clay minerals have a net negative surface charge. In the case of electroneutrality, a diffuse double layer of cations (and anions) develops around the clay particle. The negatively charged clay surface and the charge distribution adjacent to the clay particle are termed the diffuse double layer. Theoretical descriptions of the diffuse double layer were first proposed by Gouy (1910) and Chapman (1913) and later modified by Stern (1924). Detailed developments of diffuse double layer theory are provided by Mitchell (1976) and van Olphen (1977). The distribution of charge density and electric potential in the diffuse

Fig. 1. Osmotic efficiency for a monovalent anion, unsaturated soil system, as a function of $b\sqrt{C}$ (C is pore fluid concentration in normality, $2b$ is the film thickness in Ångstroms, Bresler 1973).



double layer are described by an equation known as the Poisson-Boltzman equation.

The charge density and electric potential vary as a function of distance from the clay surface, surface charge density, surface potential, electrolyte concentration and valence, dielectric constant of the fluid, and temperature. The influence of these factors can be seen in the equation for the distance to the center of gravity of charge density surrounding a semi-infinite negatively charged clay particle. This distance can be viewed as being representative of the “thickness” of the diffuse double layer (Mitchell 1976):

$$[3] \quad 1/K = (DkT / 8\pi n_0 \epsilon^2 v^2)^{1/2}$$

where:

- $1/K$ = “thickness” of the double layer (cm),
- D = dielectric constant,
- k = Boltzmann constant = 1.380662×10^{-23} (J/K),
- n_0 = bulk solution electrolyte concentration (ions/cm³),
- ϵ = unit electronic charge (esu),
- v = cation valence, and
- T = absolute temperature (K).

Equation [3] illustrates that the thickness of the diffuse double layer changes in response to changes in dielectric constant, concentration, and valence of the pore fluid. Changes in the behavior of clay soils due to changes in these pore fluid properties have been described by Mesri and Olson (1971).

In clay soils, long-range attractive and repulsive forces develop between particles. The long-range attractive force is primarily due to London van der Waals forces. The long-range repulsive force develops as a result of electrostatic repulsion between two adjacent clay particles. In many cases, the dominant long-range force between clay particles is electrostatic repulsion (Bailey 1965; Mitchell 1976).

The osmotic pressure concept can be used to calculate the repulsive stress between clay particles. The clay particle system is assumed to exist as a series of parallel clay particles. The Poisson-Boltzman equation for a single particle can be integrated to obtain the mid-plane electrolyte concentration and mid-plane potential between two clay particles. The half spacing between the clay particles can be estimated from the void ratio and the specific surface of the clay particles (Mitchell 1976).

In the osmotic pressure concept the overlapping diffuse double layers are considered as behaving as a semi-permeable membrane. The difference in osmotic pressure between the bulk pore fluid and the fluid between the clay particles is then taken to be equivalent to the electrostatic repulsive pressure between the particles. Detailed developments of the osmotic pressure concept are provided by Bolt (1956) and Mitchell (1976).

Researchers have attempted to use the osmotic pressure concept to predict the void ratio versus pressure relationship for clays containing low concentrations of homoionic pore fluid solutions. The osmotic pressure concept has been found; however, to provide a quantitative description of soil compressibility only for soils at high void ratios. The major limitation of this approach is the assumption of a perfectly dispersed parallel arrangement of individual clay particles, and the assumption that the dominant interparticle forces are the electrostatic repulsive force (Bailey 1965).

A second approach in dealing with osmotic compressibility considers the interparticle forces at a macroscopic scale. Barbour (1987a, b) and Barbour and Fredlund (1989) developed a set of stress state variables from a continuum mechanics approach for a saturated soil under physicochemical as well as mechanical stresses. A three-phase soil system consisting of the soil particles, the pore fluid, and the diffuse double hull surrounding each soil particle was considered. The three-dimensional stress state for this element was expressed as follows:

$$[4] \quad \begin{bmatrix} \sigma_x - u_f - (R - A) & \tau_{xy} & \tau_{xz} \\ \tau_{yx} & \sigma_y - u_f - (R - A) & \tau_{yz} \\ \tau_{zx} & \tau_{zy} & \sigma_z - u_f - (R - A) \end{bmatrix}$$

where:

- $\sigma_x, \sigma_y, \sigma_z$ = total normal stresses,
- τ_x, τ_y, τ_z = shearing stresses,
- u_f = pore fluid pressure, and
- $R - A$ = net interparticle repulsive-minus-attractive stress.

The stress state variable for the normal stress in eq. [4] can be subdivided into two components. The first component is the conventional effective stress for a saturated soil, $(\sigma - u_f)$. The second component is the net interparticle repulsive-minus-attractive stress, $(R - A)$. The two stress components can be visualized as a single stress state variable, $\sigma - u_f - (R - A)$. This is an expression similar to that for the "true" effective stress proposed by Balasubramonian (1972) and Chattopadhyay (1972):

$$[5] \quad \sigma^* = \sigma - u_f - (R - A)$$

where:

$$\sigma^* = \text{true effective stress.}$$

A similar expression based on static equilibrium along a wavy plane through a soil particle was also proposed by Lambe (1960), Bailey (1965), and Mitchell (1962).

Two requirements need to be met to accept a particular combination of stresses as a single stress state variable. The first requirement is that change in the value of one of the components of the stress state variable must be as effective in producing behavioral changes in the soil mass as the same magnitude of change in one of the other components of the stress state variable. Fredlund and Morgenstern (1977) demonstrated that a null type test could be used to confirm the correct components for the stress state variables for unsaturated soils using this technique. Testing by Balasubramonian (1972), Morgenstern and Balasubramonian (1980), and Chattopadhyay (1972) demonstrated that if $(R - A)$ could be calculated, changes in the effective stress were equal to changes in $(R - A)$ when the volume of the specimen was maintained constant.

The second requirement for the stress state variable; however, is that all components of the stress state variable be measurable. When using the true effective stress, σ^* , it is not possible to measure $(R - A)$ directly and the prediction of $(R - A)$ is possible only under ideal conditions. This is a severe restriction to the use of $(R - A)$ as a component of the stress state. Because of this, it may be necessary that a deduced quantity, which is more easily measured than $(R - A)$, be used.

The osmotic pressure concept relates the change in repulsive stress between clay particles to the change in the osmotic pressure difference between the interparticle fluid and the bulk pore fluid. Mitchell (1962) suggested that "double layer interactions and the consequent repulsion between opposing particles are reflected by the osmotic pressure". The osmotic pressure is described as having two components: one associated with the free salt in the bulk solution and the other caused by the additional ions required to satisfy double layer requirements. The osmotic pressure of the bulk solution can be readily eval-

uated using samples of the pore fluid; the osmotic pressure of the interparticle fluid; however, cannot be measured. Consequently, the difference between the osmotic pressure of the bulk fluid and that between the clay particles cannot be evaluated.

In most practical problems, the change of osmotic pressure is of more interest in regard to the process of osmotic compressibility than the absolute value of the components of osmotic pressure. In problems of osmotic compressibility, changes in the osmotic pressure of the bulk solution will be large relative to the initial osmotic pressure within the specimen. Consequently, it can be assumed that the change in the osmotic pressure of the bulk solution forms a satisfactory independent stress state variable. However, the osmotic pressure cannot be incorporated into the single stress state, $\sigma - u_f - (R - A)$, because osmotic pressure, Π , may not be as effective as $(\sigma - u_f)$ in producing behavioral changes in the soil.

The change in the osmotic pressure of the bulk pore fluid is the driving force for osmotic flow. Consequently, the use of osmotic pressure as a stress state variable provides for consistency in the stresses used for the description of volume change as well as for the flow of the pore fluid.

Constitutive relationship for volume change

A general form for the relationship linking the stress state variables and volumetric strain can be written as follows:

$$[6] \quad \epsilon = -\frac{dV}{V} = -\frac{1}{V} \left[\frac{\partial V}{\partial(\sigma - u_f)} d(\sigma - u_f) + \frac{\partial V}{\partial \Pi} d\Pi \right]$$

where:

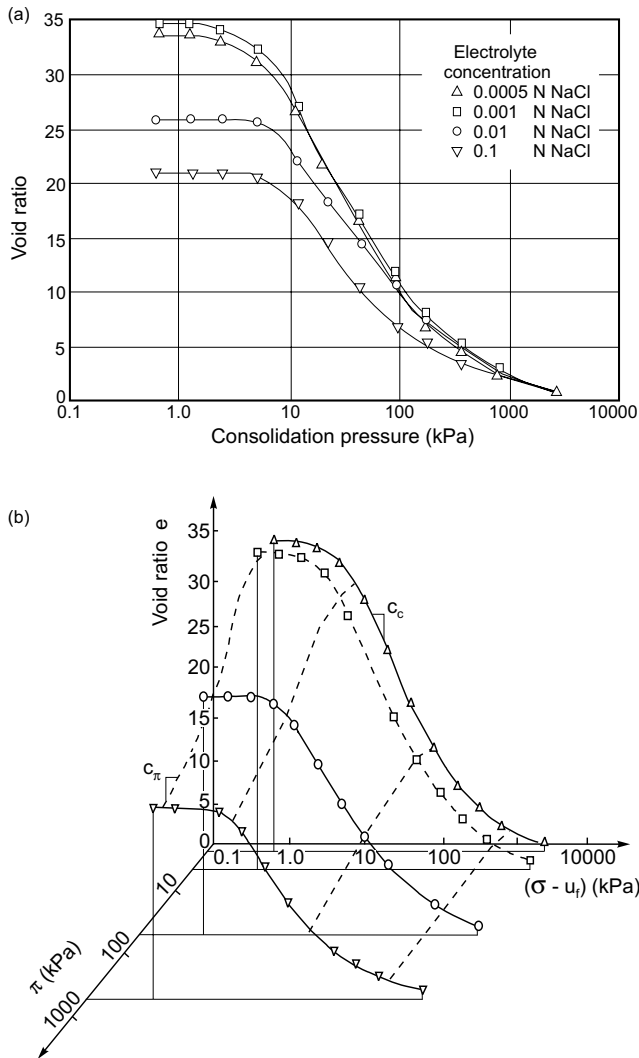
- ϵ = volumetric strain,
- V = initial soil volume and
- Π = osmotic pressure.

Equation [6] takes the form of a three-dimensional constitutive surface. The experimental data of Mesri and Olson (1971) illustrating the varying compressibility of a Na-montmorillonite clay with various concentrations of pore fluid are shown in Fig. 2a. Replotting this data using the osmotic pressure of the pore fluid as a stress state variable produces the three-dimensional constitutive surface shown in Fig. 2b. Along a plane in which Π is constant, the coefficient of volume change (compressibility), m_v , can be obtained. Along a plane in which $\sigma - u_f$ is constant, the slope can be used to define the osmotic coefficient of volume change (osmotic compressibility), m_π . The equation corresponding to a point on the constitutive surface can be written as:

$$[7] \quad d\epsilon = -m_v d(\sigma - u_f) - m_\pi d\Pi$$

It should be noted that m_v and m_π are not necessarily material constants. Just as m_v must be evaluated over an appropriate stress range, so must m_π be evaluated over an appropriate change in pore fluid chemistry.

Fig. 2. a) Consolidation curves for Na⁺-montmorillonite (after Mesri and Olson 1971); b) three-dimensional constitutive surface for Na⁺-montmorillonite.



Theoretical description of osmotic volume change-osmotic consolidation and osmotically induced consolidation

Osmotically induced consolidation occurs as a result of the flow of water out of a soil in response to chemical or osmotic gradients. This outward flow causes negative fluid pressure to develop within the clay, and consequently produces an increase in effective stress. The second osmotic volume change process is termed osmotic consolidation. In this process, volume change occurs because of a reduction in interparticle repulsive stresses as a result of changes in pore fluid chemistry.

Osmotically induced consolidation was addressed in a study by Greenberg (1971) and subsequently discussed by Greenberg et al. (1973) and Mitchell (1973*b*, 1976). The theoretical formulation of volume change due to osmotically induced consolidation was originally developed

Table 1. Summary of theoretical relationships for osmotic flow and volume change.

Flow laws

$$\text{For fluid: } q_h = -k_h (\partial h / \partial x)$$

$$q_\pi = -k_\pi (\partial \pi / \partial x)$$

$$q_f = q_h + q_\pi$$

$$\text{For salt: } q_s = q_f C - nD(\partial C / \partial x)$$

Constitutive relationships

$$\Delta e / (1 + e_0) = \Delta(\sigma - u_f) m_v$$

$$\Delta e / (1 + e_0) = \Delta \Pi m_\pi$$

Material properties

k_h = coefficient of permeability

k_π = coefficient of osmotic permeability

D = coefficient of diffusion

n = porosity

e = void ratio

m_v = coefficient of volume change

m_π = osmotic coefficient of volume change

m_{vs} = coefficient of volume change during swelling

C = concentration

by Greenberg (1971) using the theory of irreversible thermodynamics. Barbour (1987*a, b*) formulated the problem from a phenomenological basis more familiar to geotechnical engineers. This formulation described transient volume change due to both osmotic and osmotically induced consolidation.

Formulation for osmotic volume change-osmotic consolidation and osmotically induced consolidation

To predict transient volume change, changes in the stress state variables with time are related to volume change through the constitutive equation. Continuity is used to relate these volume changes to the divergence of the fluid flux from the element. These fluid fluxes are in turn defined by the flow laws for the fluid phase. It is assumed that only hydraulically and osmotically induced flows of the fluid occur. The potential of ion streaming to produce electrical gradients is not considered. The rate of movement of the dissolved salt is described by the advection-diffusion equation (Freeze and Cherry 1979). It is assumed that no geochemical interactions of individual ion species occur with the soil solids; however, retardation of dissolved salts due to adsorption onto the soil solids may be accommodated in this formulation.

Table 1 summarizes the flow laws and constitutive equations required to develop a description of transient volume change of clay soils due to osmotic or osmotically induced consolidation. The development and solution of the governing differential equations describing these phenomena were developed in detail by Barbour (1987*a*).

Numerical simulation

The equations given in Table 1 describing transient osmotic volume change were used to develop a one-dimensional numerical solution describing transient fluid

Table 2. Numerical simulation example cases.

General properties		Specific properties	
	$k_h = 1.0 \times 10^{-10}$ cm/s	Osmotically induced consolidation	
	$m_v = 5.0 \times 10^{-4}$ kPa ⁻¹	$k_\pi = 5.0 \times 10^{-13}$ m/s	
	$m_{vs} = 5.0 \times 10^{-5}$ kPa ⁻¹	$m_\pi = 0$	
	$c_v = 2.0 \times 10^{-4}$ cm ² /s	Osmotic consolidation	
	$D = 5.0 \times 10^{-10}$ m ² /s	$k_\pi = 0$	
	$n = 0.5$	$m_\pi = 2.5 \times 10^{-6}$ kPa	
Geometry and boundary conditions			
Sample thickness:	1 cm		
Initial conditions:	$u = 0, C = 0$ for all $y; t \leq 0$		
Boundary conditions:	Case 1	Case 2	
Top-flow boundary	1st type; $u = 0, t > 0$	1st type; $u = 0, t > 0$	
Bottom-flow boundary	2nd type; $q_f = 0; t > 0$	1st type; $u = 0, t > 0$	
Top-salt transport boundary	1st type; $C = 4$ M; $t > 0$	1st type; $C = 4$ M; $t > 0$	
Bottom-salt transport boundary	2nd type; $\partial C/\partial y = 0; t > 0$	3rd type; $qC = 0, t > 0$ $C = 0, t > 0$	

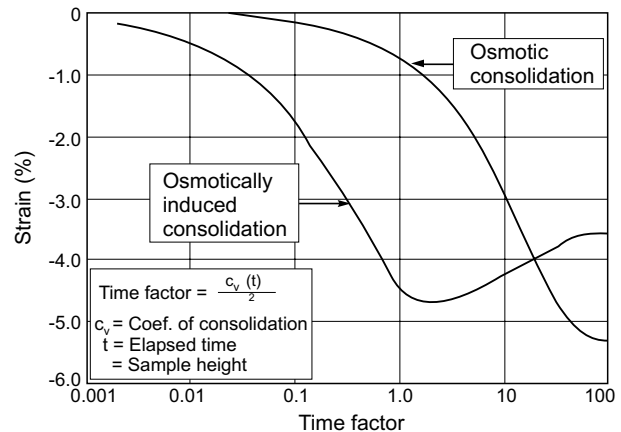
flow and salt migration during osmotic volume change (Barbour 1987a). The numerical model was verified by comparison of the results with the simulations of Greenberg (1971) and Mitchell (1973a, 1976) for osmotically induced consolidation, and with analytical solutions of one-dimensional conventional consolidation and contaminant transport. At present, no models of osmotic consolidation exist against which the present model can be verified. Rather, this model will be used to illustrate behavior that is typical of clay specimens undergoing either osmotic or osmotically induced consolidation.

The simulation was conducted for a 1 cm thick specimen of clay exposed to a 4.0 M NaCl brine along its upper surface. Two cases with different boundary conditions were analysed (Table 2). In case 1, the base of the specimen was considered to be sealed so that no fluid flow occurred across the base. In case 2, a zero pore pressure condition was maintained at the base. Salt flux across the base was not permitted in either case.

Two sets of material properties were used for the simulation cases to represent situations in which osmotically induced consolidation or osmotic consolidation was the dominant mechanism of volume change. In the first situation, osmotically induced consolidation will be the principal mechanism of volume change. The clay was assumed to behave as a semipermeable membrane with an osmotic efficiency of 0.005 (i.e., k_π is equal to $0.005k_h$). In the second situation, osmotic consolidation is the dominant mechanism of volume change. The clay was given an osmotic compressibility equal to 0.005 times the conventional compressibility of the specimen, but with an osmotic efficiency of zero. These values of osmotic compressibility and osmotic efficiency are typical of those obtained in laboratory tests described later in the paper.

The results of the simulations are illustrated in Figs. 3 and 4. For case 1 (Fig. 3) it is apparent that the time-

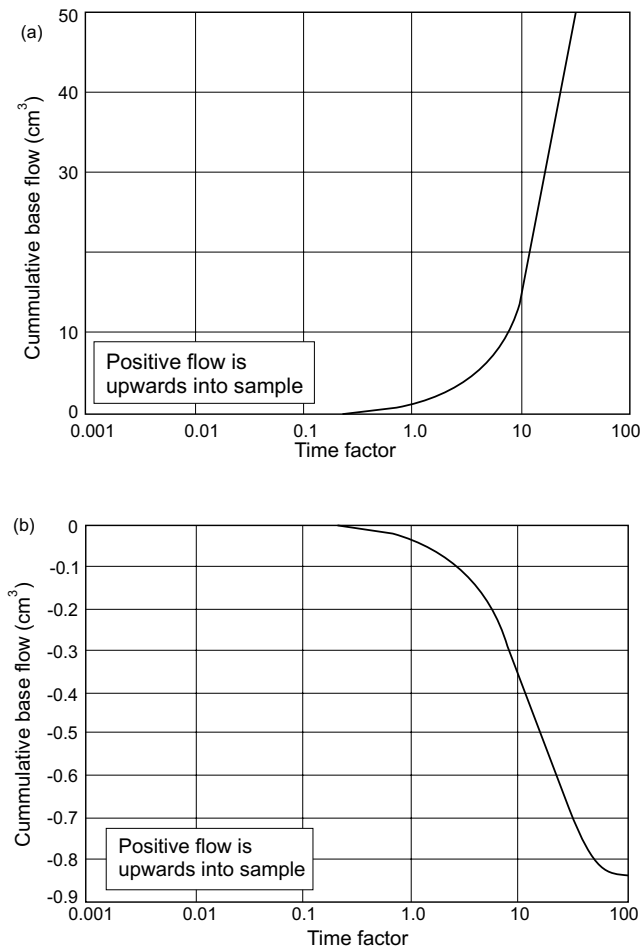
Fig. 3. Consolidation curves from numerical simulation of osmotic volume change for case 1, (no fluid from across the base).



deflection behavior is characteristically different in the two mechanisms. Osmotically induced consolidation occurs within the same time frame as conventional consolidation. The maximum deflection of the specimen occurs at a time factor of approximately 1. Rebound then occurs as the negative pore pressures induced by osmotic gradients dissipate as the salt diffuses into the soil specimen. Osmotic consolidation; however, develops slowly in response to the diffusion of salt into the clay.

In case 2 (Fig. 4), in which fluid flow across the base of the specimen was permitted, the results from the two simulations are quite different. For the case of osmotic consolidation (Fig. 4b), fluid is expelled from the base, as the advancing salt front causes a reduction in volume. However, in the case of osmotically induced consolidation (Fig. 4a), strong upward flows across the base begin at a time factor of approximately 1.0 in response to the

Fig. 4. Cumulative base flow curves from numerical simulation for case 2, (fluid flow across the base permitted): a) osmotically induced consolidation; b) osmotic consolidation.



strong osmotic gradients near the top of the specimen. The rate of flow through the base becomes nearly constant with time as the salt distribution reaches an equilibrium position. The final flow rate is approximately equal to the osmotic permeability times the osmotic pressure gradient across the soil specimen.

Laboratory testing

Laboratory testing was conducted to establish the dominant mechanism of osmotic volume change in two clay soils. A simple modified oedometer was used to consolidate a clay slurry to various confining stresses. The specimen was then exposed to concentrated NaCl solutions along either the upper soil surface only or the top and bottom of the specimen simultaneously. Measurements of specimen deflection were made for both cases. In the first case, the amount of osmotic flow across the base of the specimen or the pressure that developed along the base of

the sample when flow was prevented was also measured. The specimens tested were between 0.5 and 1.7 cm thick.

One natural soil and one artificial soil mixture were used in the tests. The natural soil was the minus No. 10 sieve fraction of air-dried samples of Regina Clay. The artificial soil was a mixture of 20% Na-montmorillonite and 80% Ottawa Sand. The slurries were prepared by mixing the air-dried soil to water contents 10 to 20% above the liquid limit. Tables 3 and 4 provide a summary of the physical and chemical characteristics of the two soil types. In contrast to the Na-montmorillonite – sand mixture, the Regina Clay is predominately a Ca-montmorillonitic soil.

Test results

Figure 5 illustrates a deflection curve for a specimen of Regina Clay undergoing normal effective stress consolidation from 100 to 200 kPa loading. At an elapsed time of 8000 min. the upper surface of the specimen is exposed to a 4.0 M NaCl solution, and further consolidation of the specimen takes place. Typical curves of specimen deflection versus time due to osmotic consolidation for the soils tested are illustrated in Figs. 6 and 7. These curves have been corrected for secondary consolidation as illustrated in Fig. 5. For the Regina Clay, the consolidation process is extremely slow and appears to be controlled by the rate of diffusion of salts into the specimen. The specimens of Na-montmorillonite – sand appear to undergo more rapid consolidation than the Regina Clay specimens. At first observation, this rapid consolidation would appear to be similar to that anticipated for osmotically induced consolidation (Fig. 3).

Figure 8 illustrates the effect of osmotic volume change as viewed on a conventional void ratio versus effective stress, $\sigma - u_f$ diagram. After osmotic volume change, the specimen appears to be overconsolidated to some higher stress level. Upon reloading, the specimen recompresses towards the original virgin branch.

For the cases where only the top of the specimen was exposed to brine, measurements were made of the flow across the base of the specimen. The reservoir for this flow was maintained at the same elevation as the brine level on the top of the specimen. Figure 9 illustrates typical patterns of cumulative flow with time for the Regina Clay and Na-montmorillonite – sand specimens. In the case of the Regina Clay, small flows into the specimen begin at time factors of approximately 1.0 and build to nearly constant flow rates. For the Na-montmorillonite – sand specimens, initial flow was out of the specimen. These flows reverse at a time factor of approximately 1.0 and begin to flow into the specimen, again increasing to essentially fairly constant flow rates.

Analyses of results

The test results may be interpreted in light of the theory presented previously, in order to evaluate the role played by osmotic flow (as represented by the osmotic ef-

Table 3. Summary of classification tests.

Test	Regina Clay	Na-montmorillonite	Ottawa Sand	Mixture of sand-montmorillonite
Specific gravity	2.83	2.56	2.65	2.63
Atterberg limits				
Liquid limit	75.5%	—	—	62.1%
Plastic limit	24.3%	—	—	Nonplastic
Plasticity index	51.2%	—	—	—
Grain-size distribution				
Sand sizes	0%	0%	100%	80%
Silt sizes	34%	0%	0%	0%
Clay sizes	66%	100%	0%	20%
Mineralogical composition – less than 2 μm ^a				
Montmorillonite	45.2%	80% ^b	—	—
Illite	27.7%	7%	—	—
Kaolinite	17.7%	7%	—	—
Trichlorite	9.4%	0%	—	—
Quartz	0%	8%	—	—
Gypsum	0%	3%	—	—
Carbonate	0%	2%	—	—
Specific surface (m ² /g)	53 ^c	700–840 ^d	—	140–168
Exchange capacity (meq/100 g) ^e	31.7	80–150 ^d	—	—
Total exchangeable base by NH ₄ Ac leaching (meq/100 g)				
Magnesium	15.3	—	—	—
Calcium	54.4	—	—	—
Potassium	0.59	—	—	—
Sodium	1.77	—	—	—

^a Test performed by Saskatchewan Research Council.

^b Quigley (1984).

^c Test performed by Department of Soil Science, University of Saskatchewan, by ethylene glycol sorption (Black 1965a).

^d Mitchell (1976).

^e Fredlund (1975).

Table 4. Chemical analysis of saturated extract.^a

Test result	Regina Clay	Na-montmorillonite
Water content of extract (%)	88	550
pH	7.4	8.8
Conductivity (mS/cm)	3.7	4.0
Ions in extract (μg/mL)		
Na ⁺	210	910
Ca ²⁺	546	23
Mg ²⁺	183	7
K ⁻	35	9
Cl ⁻	133	81
SO ₄ ²⁻	1700	1400
Sodium adsorption ratio	2.0	42.2

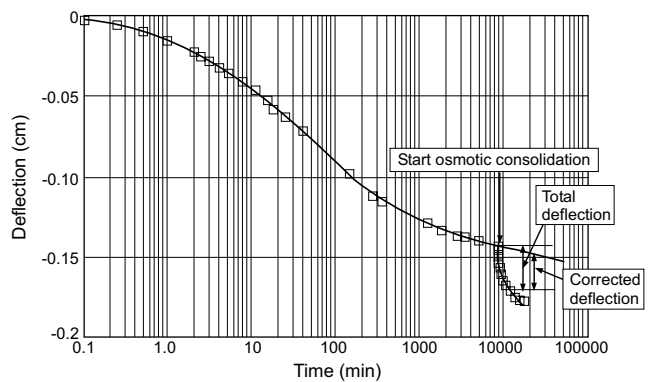
^a Tests performed by Saskatchewan Soil Testing laboratory (after Black 1965b).

iciency) and osmotic compressibility in producing volume change.

Osmotic efficiency

Nearly constant osmotic flow rates were developed in both soil types after the completion of volume change

Fig. 5. Effective stress consolidation and osmotic volume change of Regina Clay.



within the specimen. The osmotic flow rates were observed during exposure to different NaCl solution concentrations. Using eq. [2], the osmotic efficiency of the soils at different confining stresses and different solution concentrations was calculated. These efficiencies are shown in Figs. 10 and 11 along with osmotic efficiencies

Fig. 6. Time-dependent volume change of Regina Clay by 4.0 M NaCl solution (specimen preconsolidated to 200 kPa).

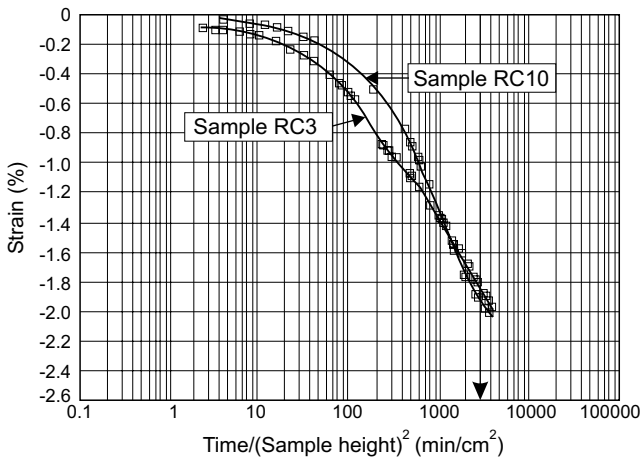
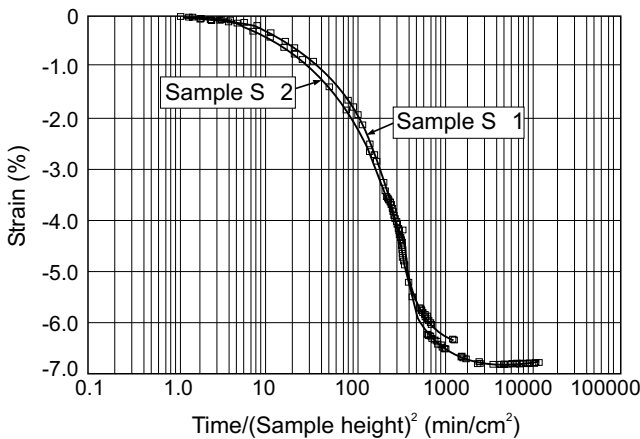


Fig. 7. Time-dependent volume change of sand-montmorillonite by 4.0 M NaCl solution (specimen preconsolidated to 200 kPa).



calculated from the work of Bresler (1973). The data of Bresler required an estimate of the film thickness of the solution between two charged soil particles. This value was obtained using estimates of specific surface, and the equation for interparticle spacing between packets of particles as given by Shainberg et al. (1971). With different values of specific surface the lines of efficiency shift to the right or left on the graph.

In spite of considerable scatter, a number of significant observations can be made. First, fairly high efficiencies are obtained at low solution concentrations and low efficiencies are obtained at high solution concentrations. This is consistent with the results described by Kemper and Rollins (1966). Second, the induced negative fluid pressures that would have occurred due to the observed flows are small. These pressures were calculated from eq. [2] using the osmotic pressure calculated using eq. [1], the full specimen thickness for ΔX , and the measured value of k_h . Efficiencies of 0.01 at 0.01 M and 0.001 at 1.0 M would only provide a negative pressure response in the

Fig. 8. Influence of osmotic consolidation on the virgin compression branch.

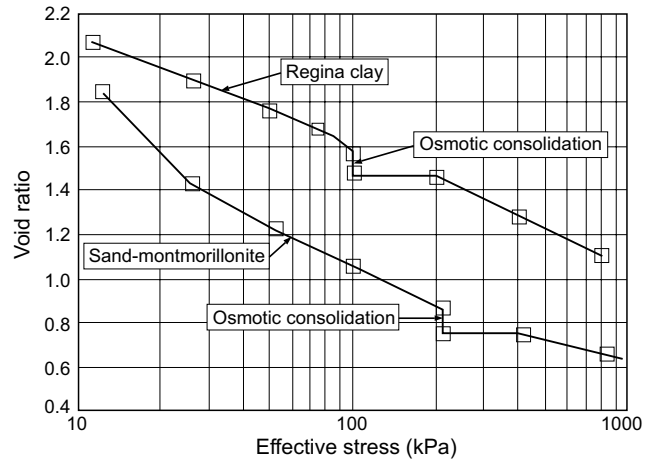
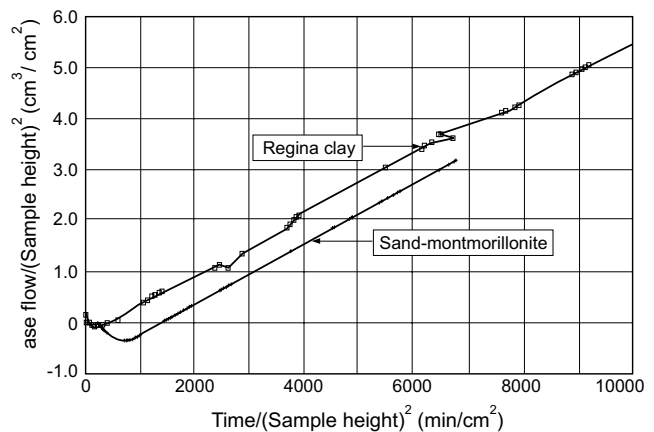


Fig. 9. Cumulative base flow for Regina Clay and sand-montmorillonite exposed to 4.0 M NaCl solution along upper surface (specimen preconsolidated to 200 kPa).

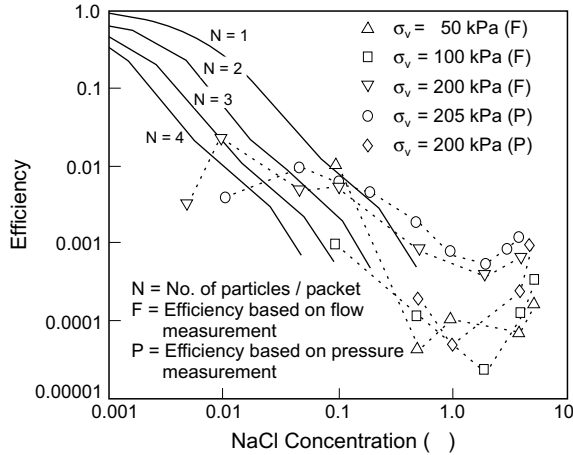


range 0.5 to 5 kPa. This would not be sufficient to account for the magnitude of volume change observed in Fig. 8. Finally, Fig. 10 indicates that for the Regina Clay, the number of particles bound into packets decreases as higher concentrations of NaCl are used. Although there are insufficient data, the pattern in the Na-montmorillonite – sand seems to indicate that the number of particles bound up in packets remains unchanged. Regina Clay is predominately a Ca-montmorillonite; consequently, the clay would be expected to form packets of clay particles bound together by adsorbed Ca^{2+} during sedimentation. However, as the pore fluid becomes concentrated these packets would begin to open up because of the dominance of Na^+ in the double layer, resulting in fewer particles per packet.

Osmotic compressibility

The analyses of the osmotic flow and pressure measurements indicate that the predominate mechanism of osmotic volume change for both types of soil cannot be

Fig. 10. Theoretical and experimental osmotic efficiencies for Regina Clay.



osmotically induced consolidation. However, if osmotic consolidation is the dominant mechanism, then the rate of consolidation will be controlled by the rate of salt transport into the specimen by diffusion.

Steady state diffusion tests were conducted on a single specimen of each material. The combined coefficient of diffusion for Na⁺ and Cl⁻ from tests on both materials was approximately 4×10^{-6} cm²/s. The coefficient of diffusion from steady state diffusion tests does not take into account the retardation of Na⁺ migration due to adsorption onto the soil solids. In that the Regina Clay is a Ca²⁺-dominated clay, it would be likely that the effective coefficient of diffusion during transient conditions would be lower than that measured in the steady state tests.

This lower rate of diffusion in the Regina Clay specimens may in part explain the more rapid changes in volume as a result of osmotic consolidation for the Na-montmorillonite – sand specimens (Fig. 7) over those for the Regina Clay specimens (Fig. 6). The difference in the time to 100% consolidation for the two soil types is large; however, and it is unlikely that this difference could be completely explained on the basis of the differences in the effective coefficients of diffusion.

A second explanation for the difference in the rates of osmotic volume change is that the magnitude of the osmotic compressibility of the two specimens is substantially different. The osmotic compressibility for each of these materials is illustrated in Fig. 12. Because of the high osmotic compressibility of the Na-montmorillonite – sand mixture at low salt concentrations, a majority of the osmotic volume change within the specimen would have occurred prior to full equalization of salt concentrations within the specimen.

In the case of Regina Clay, the constant value of osmotic compressibility would require nearly full equalization of salt concentrations within the specimen before osmotic consolidation is complete. Consequently, the time to the completion of osmotic consolidation of the Regina Clay was much longer than that for the sand-montmorillonite mixture.

Fig. 11. Theoretical and experimental osmotic efficiencies for sand-montmorillonite.

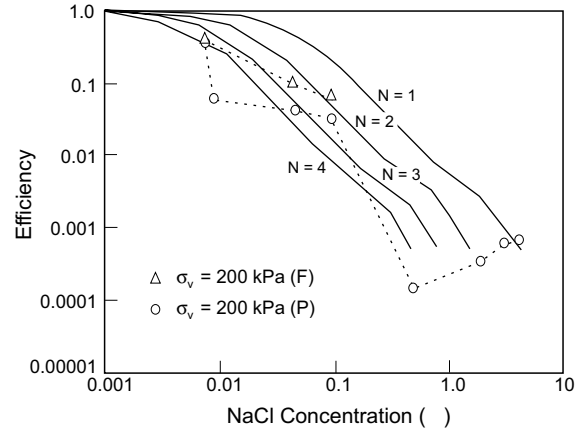
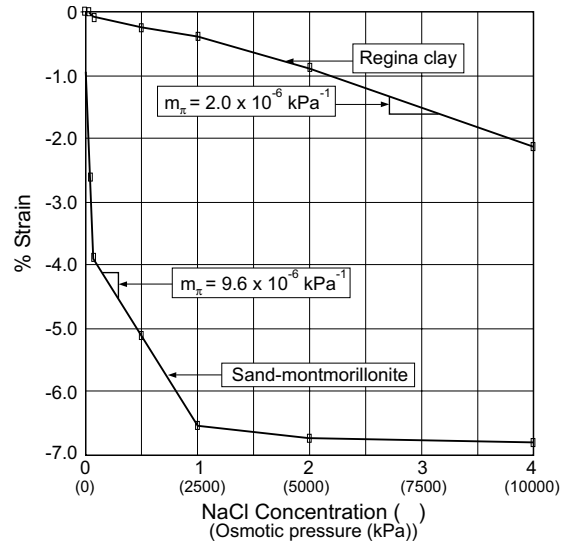


Fig. 12. Osmotic volumetric strain versus solution concentration.



The nearly linear relationship between strain and concentration for the Regina Clay does not appear to be consistent with the suppression of the double layer around individual clay particles. This linearity may be due to the dispersion of the clay packets within the Regina Clay as the concentration increases, as was also indicated by the osmotic efficiency data. The shapes of Na-montmorillonite – sand and Regina Clay curves (Fig. 12) are consistent with data described by Aylmore and Quirk (1962) for pure Na-montmorillonite and Ca-montmorillonite, respectively. These authors also attributed the anomalous behavior of the Ca-montmorillonite (similar to the Regina Clay) to the presence of clay packets.

Consolidation rates

When osmotic consolidation is the dominant mechanism, the time to 100% consolidation should coincide with the time for 100% equalization of salt concentrations within the specimen by diffusion. The osmotic deflection

versus time data for the Regina Clay was analyzed using this assumption, and the coefficient of diffusion for combined Na^+ and Cl^- was found to range from 1×10^{-6} to $9 \times 10^{-6} \text{ cm}^2/\text{s}$ with an average of approximately $5.0 \times 10^{-6} \text{ cm}^2/\text{s}$. Direct steady state diffusion testing was conducted by maintaining different salt concentrations within reservoirs above and below the specimen and measuring the salt flux through the specimen. The results of this testing indicated diffusion coefficients for combined Na^+ and Cl^- of between 3.6×10^{-6} and $4.2 \times 10^{-6} \text{ cm}^2/\text{s}$ with an average value of $3.9 \times 10^{-6} \text{ cm}^2/\text{s}$ for the Regina Clay specimens. These values of diffusion were not corrected for the small advective flux of salt due to osmotic flow, which would oppose the diffusive salt flux.

Apparent $R - A$ stress

The stress path followed during consolidation, osmotic consolidation, and then reloading, as viewed on the three-dimensional constitutive surface presented previously, is shown in Fig. 13a. When this pathway is viewed on the void ratio versus $(\sigma - u_f)$ plane (Fig. 13b), a path different from that presented in Fig. 8 develops. The actual observed behavior suggests that upon reloading, the osmotic pressure of the bulk pore fluid is not constant but is decreasing. In fact, the pore fluid concentration is unchanged during reloading. This behavior is consistent; however, with a view of using $(R - A)$ as the stress state variable representing physicochemical interactions. It would be reasonable that upon reloading, small decreases in void ratio would occur, which would produce an increase in the net repulsive stress between the particles as they are forced closer together.

An indirect estimate of the change in the net repulsive stress within the soil mass could be obtained from the void ratio versus stress plots. Figure 14 illustrates a typical virgin branch for the two soil types tested. A second line, below the virgin branch, was drawn by subtracting the volume changes due to osmotic consolidation under a 4.0 M NaCl solution (Fig. 12) from the virgin branch. The difference between these two virgin branches can be taken as a measure of the change in the $(R - A)$ stress present in the specimen at a particular void ratio when the soil is exposed to a 4.0 M NaCl solution.

Figure 15 illustrates how the change in the repulsive stress within the two soils varies with confining stress. Also shown is the predicted repulsive stress based on the osmotic pressure concept for the Na-montmorillonite - sand specimens. It is of interest that in the case of the Na-montmorillonite - sand specimens the theoretical values of $(R - A)$ agree reasonably well with the measured values when a value of specific surface equal to $580 \text{ m}^2/\text{g}$ is selected. Agreement between the theoretical and measured values for $(R - A)$ for Regina Clay was not obtained. Barbour (1987a) indicated that this may be due to the fact that the clay particles are bound up in packets and do not exist as individual parallel particles, as is assumed with the osmotic pressure concept method of calculating $(R - A)$.

Fig. 13. Stress paths during effective stress and osmotic consolidation: a) three-dimensional surface; b) projection onto effective stress axis.

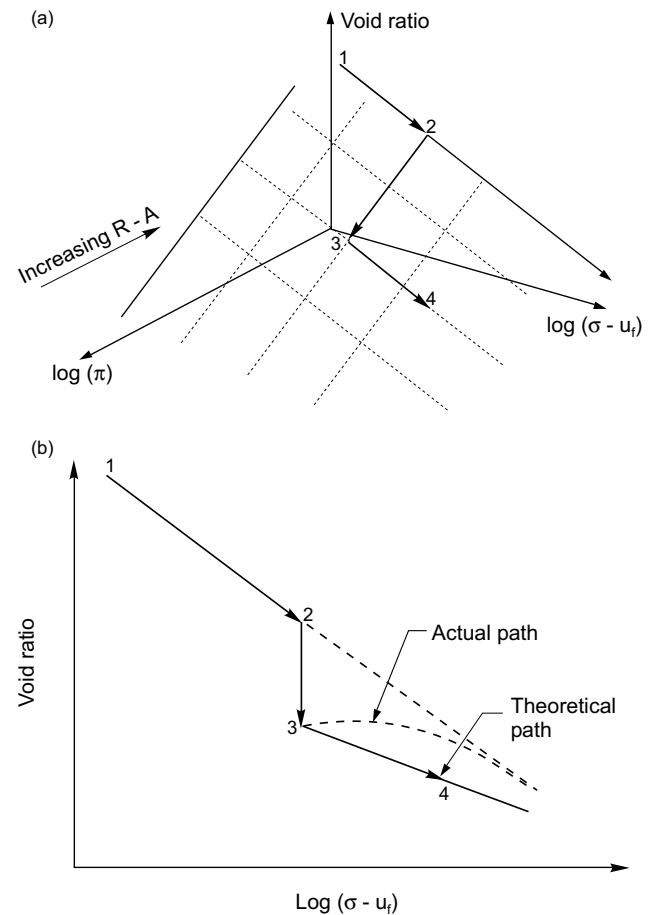
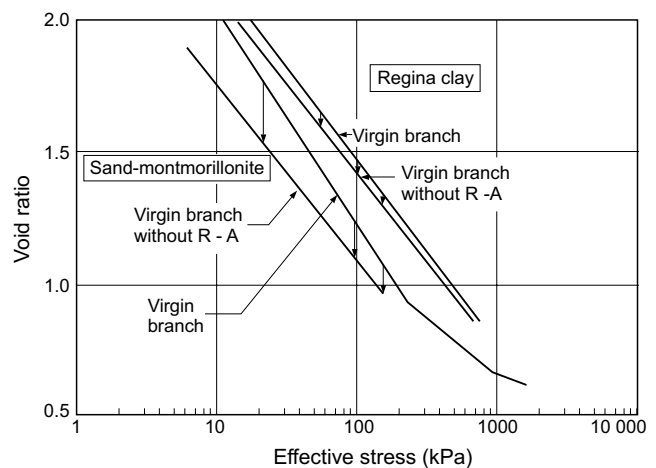


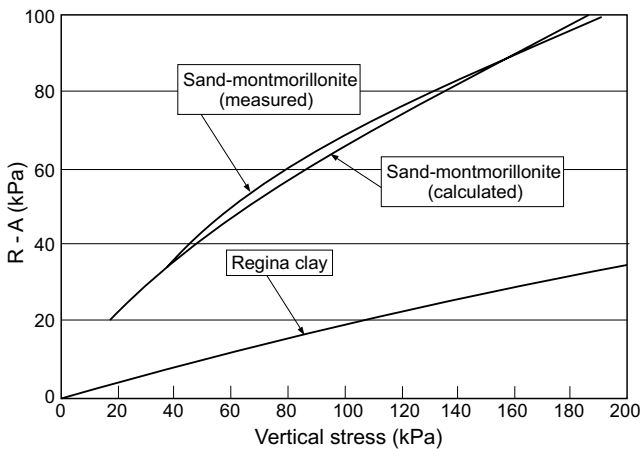
Fig. 14. Indirect evaluation of net $(R - A)$ stresses from the virgin curve.



Conclusions

The design of waste containment facilities requires that the mechanical and hydraulic properties of the barrier

Fig. 15. ($R - A$) versus vertical effective stress.



materials be defined. In many instances, alteration of these properties upon permeation with waste fluids will occur. Consequently, a methodology to incorporate these changes into the design is required.

The theoretical development highlighted in this paper provides for a generalized description of osmotic flow and volume change based on a continuum mechanics approach consistent with existing practice. The volume change behavior of a soil undergoing osmotically induced consolidation and osmotic consolidation can be described using the following properties: osmotic compressibility (m_π), compressibility (m_v), coefficient of permeability (k_h), coefficient of osmotic permeability (k_π), and coefficient of diffusion (D) for the dissolved salts. Laboratory tests on modified conventional oedometers can be used to establish the osmotic compressibility and permeability with techniques similar to those used to test for conventional compressibility and permeability.

In the soil specimens tested, the dominant mechanism of volume change associated with brine contamination was osmotic consolidation. This process is characterized by a slow rate of volume change controlled by the rate of transport of the dissolved salt into the specimen. Osmotically induced consolidation was shown to be of little significance with respect to volume change, although osmotic flow did occur.

The results of this study provide a comprehensive approach to dealing with the volume change processes that occur during permeation of clay soils with concentrated pore fluids. This understanding can be used to predict the magnitude and rate of associated volume changes. A second possible use of this approach is the incorporation of the effects of changing repulsive stresses within the soil mass into conventional geotechnical analyses through the use of true effective stress and an estimate of ($R - A$). Barbour (1987b) illustrated the potential use of this approach in analyses of the alteration of the permeability and shear strength of clays after permeation with brine.

The microscopic, mechanistic models such as diffuse double layer theory and the osmotic pressure concept have provided valuable insights into the role that pore

fluid chemistry has on soil behavior. Building on this understanding, a macroscopic, phenomenological model provides a way for this understanding to be quantified in design. Description of physicochemical interactions using the same phenomenological framework as conventional soil mechanics would allow existing analyses to include physicochemical interaction in design.

Further work is required to verify the use of "physicochemical" stress state variables and material properties. The present thrust of research into physicochemical interactions has to be expanded from "compatibility" testing of the permeability of clay barriers to a general characterization of hydraulic and mechanical behavior of clay soils within a verifiable, theoretical phenomenological framework.

References

- Aylmore, L.A.G., and Quirk, J.P. 1962. The structural status of clay systems. *Clays and Clay Minerals*, **9**: 104–130.
- Bailey, W.A. 1965. The effect of salt content on the consolidation behaviour of saturated remoulded clays. United States Army Engineer Waterways Experimental Station, Vicksburg, Contract Report 3-101.
- Balasubramonian, B.I. 1972. Swelling of compaction shale. Ph.D. thesis, Department of Civil Engineering, University of Alberta, Edmonton, AB, Canada.
- Barbour, S.L. 1987a. Osmotic flow and volume change in clay soils. Ph.D. thesis, Department of Civil Engineering, University of Saskatchewan, Saskatoon, SK, Canada.
- Barbour, S.L. 1987b. The role of physicochemical effects on the behavior of clay soils. Keynote address. Proceedings, 40th Canadian Geotechnical Conference, Regina, pp. 323–342.
- Barbour, S.L., and Fredlund, D.G. 1989. Physicochemical stress state variables to characterize the behavior of clay soils. Proceedings, 12th International Conference on Soil Mechanics and Foundation Engineering, Rio de Janeiro, Vol. 3, pp. 1839–1844.
- Black, C.A. (Editor). 1965a. Methods of soil analysis, Part 1. American Society of Agronomy, Inc., Madison, WI, Agronomy Series, No. 9.
- Black, C.A. (Editor). 1965b. Methods of soil analysis, Part 2. American Society of Agronomy, Inc., Madison, WI, Agronomy Series, No. 9.
- Blackmore, A.V., and Miller, R.D. 1962. Tactoid size and osmotic swelling in calcium montmorillonite. *Soil Science Society of America Proceedings*, **25**: 169–173.
- Bolt, G.H. 1956. Physico-chemical analyses of the compressibility of pure clay. *Géotechnique*, **6**: 86–93.
- Bolt, G.H., and Groenevelt, P.H. 1969. Coupling phenomena as a possible cause of "non-darcian" behavior of water in soil. *Bulletin of the International Association of Scientific Hydrology*, **14**(2): 17–28.
- Bolt, G.H., and Miller, R.D. 1955. Compression studies of illite suspensions. *Soil Science Society of America Proceedings*, **19**: 285–288.
- Bresler, E. 1973. Anion exclusion and coupling effects in nonsteady transport through unsaturated soils: I. Theory. *Soil Science Society of America Proceedings*, **37**: 663–669.
- Chapman, D.L. 1913. A contribution to the theory of electrocapillarity. *Philosophical Magazine*, **25**(6): 475–481.

- Chattopadhyay, P.K. 1972. Residual shear strength of some pure clay mineral. Ph.D. thesis, Department of Civil Engineering, University of Alberta, Edmonton, AB, Canada.
- Elrick, D.E., Smiles, D.E., Baumgartner, N., and Groenevelt, P.H. 1976. Coupling phenomena in saturated homo-ionic montmorillonite: I. Experimental. *Soil Science Society of America Journal*, **40**: 490–491.
- Fredlund, D.G. 1975. Engineering properties of expansive clays. Department of Civil Engineering, University of Saskatchewan, Saskatoon, SK, Transportation and Geotechnical Group Publication IR-7.
- Fredlund, D.G., and Morgenstern, N.R. 1977. Stress state variables for unsaturated soils. *ASCE Journal of the Geotechnical Engineering Division*, **103**: 447–466.
- Freeze, R.A., and Cherry, J.A. 1979. *Groundwater*, Prentice Hall, Englewood Cliffs, NJ.
- Gouy, G. 1910. Sur la constitution de la charge électrique à la surface d'un électrolyte. *Annales de Physique (Paris)*, Série 4, **9**: 457–468.
- Greenberg, J.A. 1971. Diffusional flow of salt and water in soils. Ph. D. thesis, Department of Civil Engineering, University of California, Berkeley, Berkeley, CA.
- Greenberg, J.A., Mitchell, J.K., and Witherspoon, P.A. 1973. Coupled salt and water flows in a groundwater basin. *Journal of Geophysical Research*, **78**: 6341–6353.
- Hanshaw, B.B., and Zen, E. 1965. Osmotic equilibrium and overthrust faulting. *Geological Society of America Bulletin*, **76**: 1379–1386.
- Kemper, W.D. 1961. Movement of water as affected by free energy and pressure gradients: I. Application of classic equations for viscous and diffusive movements to the liquid phase in finely porous media. *Soil Science Society of America Proceedings*, **24**: 244–260.
- Kemper, W.D., and Quirk, J.P. 1972. Ion mobilities and electric charges of external clay surfaces infrared from potential differences and osmotic flow. *Soil Science Society of America Proceedings*, **36**: 426–433.
- Kemper, W.D., and Rollins, J.B. 1966. Osmotic efficiency coefficients across compacted clays. *Soil Science Society of America Proceedings*, **30**: 529–534.
- Kemper, W.D., and van Schaik, J.C. 1966. Diffusion of salts in clay-water systems. *Soil Science Society of America Proceedings*, **30**: 534–540.
- Lambe, T.W. 1960. A mechanistic picture of shear strength in clay. *Proceedings, ASCE Research Conference on the Shear Strength of Cohesive Soil*, Boulder, CO, pp. 555–580.
- Letey, J., Kemper, W.D., and Noonan, L. 1969. The effect of osmotic pressure gradient on water movement in unsaturated soil. *Soil Science Society of America Proceedings*, **33**: 15–18.
- Low, P.F. 1955. The effect of osmotic pressure on diffusion rate of water. *Soil Science*, **80**: 95–100.
- Marine, I.W., and Fritz, S.J. 1981. Osmotic model to explain anomalous hydraulic heads. *Water Resources Research*, **17**: 73–82.
- Mesri, G., and Olson, R.E. 1971. Consolidation characteristics of montmorillonite. *Géotechnique*, **21**: 341–352.
- Metten, U. 1966. *Desalination by reverse osmosis*. M.I.T. Press, Cambridge, MA.
- Mitchell, J.K. 1962. Components of pore water pressure and their engineering significance. *Clays and Clay Minerals*, **10**: 162–184.
- Mitchell, J.K. 1973a. Recent advances in the understanding of the influence of mineralogy and pore solution chemistry on the swelling and stability of clays. *Proceedings, 3rd International Conference on Expansive Soil*. Vol. 2, pp. 11–25.
- Mitchell, J.K. 1973b. Chemico-osmotic effects in fine grained soils. *ASCE Journal of the Soil Mechanics and Foundations Division*, **99**: 307–322.
- Mitchell, J.K. 1976. *Fundamentals of soil behavior*. John Wiley and Sons, New York, NY.
- Morgenstern, N., and Balasubramanian, B.I. 1980. Effects of pore fluid on the swelling of clay-shale. *Proceedings, 4th International Conference on Expansive Soils*, Denver, pp. 190–205.
- Neuzil, C.E. 1986. Groundwater flow in low-permeability environments. *Water Resources Research*, **22**: 1163–1195.
- Olsen, H. 1972. Liquid movement through kaolinite under hydraulic, electric, and osmotic gradients. *American Association of Petroleum Geologists Bulletin*, **56**: 2022–2028.
- Olsen, H.W. 1985. Osmosis: a cause of apparent deviations from Darcy's law. *Canadian Geotechnical Journal*, **22**: 238–241.
- Quigley, R.M. 1984. Quantitative mineralogy and preliminary pore-water chemistry of candidate buffer and backfill materials for a nuclear fuel waste disposal vault. *Atomic Energy of Canada Ltd., Whiteshell Nuclear Research Establishment, Pinawa, MN*.
- Robinson, R.A., and Stokes, R.H. 1968. *Electrolyte solutions*. Second edition, Butterworths, London, United Kingdom.
- Shainberg, I., Bresler, E., and Klausner, Y. 1971. Studies on Na/Ca-montmorillonite systems. I. The swelling pressure. *Soil Science*, **3**(4): 214–219.
- Stern, O. 1924. Zur Theorie der elektrolytischen Doppelschicht. *Zeitschrift für Elektrochemie*; **30**: 508–516.
- van Olphen, H. 1977. *An introduction to clay colloid chemistry*. John Wiley and Sons, New York, NY.
- Warkentin, B.P., and Schofield, R.K. 1962. Swelling pressures of Na-montmorillonite in NaCl solution. *Journal of Soil Science*, **13**: 98.
- Warkentin, B.P., Bolt, G.H., and Miller, R.D. 1957. Swelling pressure of montmorillonite. *Soil Science Society of America Proceedings*, **21**: 495–497.

A new technique for diffusion testing of unsaturated soil

S.L. Barbour, P.C. Lim, and D.G. Fredlund

Abstract: A technique is proposed for determining the coefficients of diffusion and adsorption for ions in unsaturated soils. The method integrates the single reservoir diffusion testing of saturated soil with the axial-translation technique for the control of matric suction. The procedure allows for the application of a net total stress and matric suction to the soil during the diffusion test. The use of this technique to determine the coefficient of diffusion and adsorption from a single test is demonstrated. The effects of the degree of saturation on the coefficients of diffusion and adsorption were evaluated on a sandy soil with water contents ranging from saturation to near the residual degree of saturation. Potassium and chloride ions were used as the primary tracers.

The test results showed that both the coefficients of diffusion and adsorption can be determined from a single test. The results illustrate a decrease in both the effective diffusion and adsorption coefficients with a decrease in the degree of saturation. The extent of the decrease in the effective diffusion coefficient from saturation to near the residual degree of saturation was approximately 80%. The decrease in the adsorption coefficient was gradual and small from saturation to a degree of saturation of approximately 10%; however, it then decreased rapidly as the water content approached the residual degree of saturation.

Key words: unsaturated soil, diffusion test, inorganic chemicals, effective diffusion coefficient, adsorption coefficient.

Nomenclature

- J_d = diffusive mass flux, $ML^{-2} T^{-1}$,
 θ_w = volumetric water content, $L^3 L^{-3}$,
 D^* = effective diffusion coefficient of ion i in soil, $L^2 T^{-1}$,
 $\frac{dC_i}{dz}$ = concentration gradient, $ML^{-3} L^{-1}$,
 Q_i = mass of ion i adsorbed by the solids per unit mass of dry soil, MM^{-1} ,
 C_{e_i} = concentration of ion i at equilibrium, ML^{-3} ,
 K_f = Freundlich adsorption coefficient, $(L^3 M^{-1})^m$,
 m = Freundlich constant,
 σ = total stress, $ML^{-1} T^{-2}$,
 u_a = pore-air pressure, $ML^{-1} T^{-2}$, and
 u_w = pore-water pressure, $ML^{-1} T^{-2}$.

Introduction

Compacted, unsaturated soils are often present as one of the components in the design of barriers for the containment of waste. Zones of unsaturated soil can be found in covers or in the granular drainage layers in the leachate

collection system in landfills. Unsaturated layers of gravel are also being proposed as a backfill around subsurface nuclear and hazardous waste repositories (Conca and Wright 1990). Other geo-environmental problems such as remediation of hydrocarbon or chemical spills and prediction of the fate of agricultural-related contaminants in surficial soils and soil salinity also require an understanding of chemical transport in unsaturated soils.

The processes governing contaminant transport in saturated soils are also valid for unsaturated soils; however, the transport parameters may be quite different. Transport parameters such as hydraulic conductivity and the coefficients of diffusion and adsorption are generally assumed to be constant for saturated soils. In unsaturated soils; however, there needs to be functional relationships between these parameters and the water content.

This study focuses primarily on diffusion and adsorption as the dominant transport and attenuation processes governing the movement of contaminants in an unsaturated soil. A number of studies have emerged in the soil science literature which show that the effective diffusion coefficient varies with the water content of the soil. The

S.L. Barbour. Professor, Department of Civil Engineering, University of Saskatchewan, 57 Campus Drive, Saskatoon, SK, Canada, S7N 5A9.

P.C. Lim. Senior research fellow, Environmental Technology Research Institute, Innovation Centre #237, Nanyang Avenue, Singapore 639798.

D.G. Fredlund. Professor, Department of Civil Engineering, University of Saskatchewan, 57 Campus Drive, Saskatoon, SK, Canada, S7N 5A9.

Reproduced with permission from the American Society for Testing and Materials, *Geotechnical Testing Journal*, GTJODJ, 19(3): 247-258, 1996

shape of the functional relationships reported by different researchers vary for different textured soils; however, limitations in the test procedures used may have an effect on the measured diffusion coefficients. Existing data pertaining to the dependency of the adsorption coefficient on the degree of saturation are limited. Various hypotheses have been suggested by Bear and Verruijt (1987), but there has been no experimental verification to date.

The objective of this paper is to describe the principle and test procedure for a new technique for determining the coefficients of diffusion and desorption of ions for an unsaturated soil. The principle of the new test method is based on the integration of the single reservoir method for diffusion testing of saturated soil with the axis-translation technique (Hilf 1956) for the control of matric suction. With the axis-translation technique, the soil specimen can be brought to a specified degree of saturation by drainage of the soil-water. The new test method allows both the matric suction and the net total stress to be controlled independently before and during the diffusion test. For the purpose of evaluating the proposed test method, simple ions such as potassium and chloride were selected as the primary reactive and non-reactive tracers.

Background

The migration of contaminants in soil is governed by two key processes: transport and attenuation. In the absence of advection, movement by diffusion becomes the dominant transport process. Changes in concentration can also occur as a result of chemical or biological reactions within the liquid phase or by transfer of the contaminants to the solid phase of the soil matrix.

Diffusion in soils

Diffusion is a process whereby dissolved mass is transported from higher chemical potential toward lower by random molecular motion (Robinson and Stokes 1959). The equation describing a one-dimensional diffusive flux in soil given by Porter et al. (1960) is based on Fick's first law and is written as follows:

$$[1] \quad J_d = -\theta_w D_i^* \frac{dC_i}{dz}$$

where

J_d = diffusive mass flux,
 θ_w = volumetric water content,
 D_i^* = effective diffusion coefficient of ion i in soil,
 and

$\frac{dC_i}{dz}$ = concentration gradient.

The volumetric water content in eq. [1] represents the fraction of the total cross section of the soil that is occupied by water and through which diffusion takes place. The effective diffusion coefficient is a constant for a saturated soil. As the soil desaturates, numerous experimental data have shown that the effective diffusion coefficient decreases either linearly or non-linearly with a decrease

in the water content (Klute and Letey 1958; Porter et al. 1960; Graham-Bryce 1963; Romkens and Bruce 1964; Rowell et al. 1967; Warncke and Barber 1972; Barraclough and Tinker 1981).

The two methods used most widely by soil scientists in determining the effect of water content on the effective diffusion coefficient are the two half cell method (Klute and Letey 1958; Porter et al. 1960; Graham-Bryce 1963; Romkens and Bruce 1964; Rowell et al. 1967) and the one half cell method with ion-exchange resin paper (Warncke and Barber 1972) or ion-exchange membrane (Barraclough and Tinker 1981).

The two half cell method consists of two cells of soil. Soil specimens are either equilibrated with different salt solutions of the same molarity or the same salt solution, one of which is spiked with an isotope tracer. One face of each soil specimen is then exposed, and the two half cells are joined together to allow diffusion to proceed. At the end of the test, the water content and the quantity of the labelled ions in each half cell are measured. The effective diffusion coefficient is back-calculated based on the quantity of the labelled ions that had diffused into the other half cell (Barrer 1951; Carslaw and Jaeger 1959).

The one half cell method, which uses an ion-exchange resin paper or membrane, is essentially the same as the two half cell method, the difference being that one of the cells is replaced by an ion-exchange membrane or resin paper that acts as an ion sink. At the end of the test, the quantity of the cations or anions that has diffused into the resin paper or membrane is measured. The method for calculating the effective diffusion coefficient is described by Vaidyanathan and Nye (1966).

Various methods of soil specimen preparation have been used. In most procedures, the soil is first wetted to a predetermined water content (Porter et al. 1960; Rowell et al. 1967; Warncke and Barber 1972; Barraclough and Tinker 1981). The soil is then packed into the half cell, and, if necessary, additional water is added to the soil specimen. Although the soil specimen is compacted to a consistent dry density, soils with differing water contents have different soil structures and are therefore "different" soils (Fredlund 1989; Lambe 1958). Another approach that provides better control of the stress state of the soil is to drain the soil-water to the desired water content using a pressure plate apparatus, (Klute and Letey 1958; Romkens and Bruce 1964).

The coefficient of diffusion for unsaturated gravel has also been determined using electrical conductivity measurements (Conca and Wright 1990). The electrical conductance of the pore-water was measured under a steady-state-flow condition using a two-electrode method. The water content in the gravel was brought to the required degree of saturation by varying the speed of the centrifuge and the flow rate of a pump that feeds a 0.01 M potassium chloride solution continuously into the soil specimen. The diffusion coefficient is calculated based on the assumption that the electrical conductance is analogous to the diffusion coefficient using the Nerst-Einstein equation.

Adsorption

Adsorption is the phenomenon by which a portion of the mass of a disposed substance (e.g., contaminant) is held to the solid at a liquid-solid interface (Bear and Verruijt 1987). The partitioning characteristics of an ion between the liquid and the solid phases at constant temperature and pressure is described quantitatively by an adsorption function. The form of the adsorption function could be linear or non-linear depending upon the affinity of the solids for the adsorbate. Among the numerous empirical models for describing the adsorption characteristics of soil (Helfferich 1962), the Freundlich equation is quite widely used.

$$[2] \quad Q_i = K_f(C_{e_i})^m$$

where:

- Q_i = mass of ion i adsorbed by the solids per unit mass of dry soil,
- C_{e_i} = concentration of ion i at equilibrium,
- K_f = Freundlich adsorption coefficient, and
- m = Freundlich constant.

The coefficients K_f and m can be determined using a 24 hour batch type measurement or a short term batch method in accordance with ASTM Test Method for 24-hour Batch-Type Measurement of Contaminant Sorption by Soils and Sediments (D 4646–87) or ASTM Test Method for Distribution Ratios by the Short-Term Batch Method (D 4319–83), respectively. In both methods a high solution to solid ratio was specified. The affinity of the soil for the ion defined on the basis of D 4646–87 or D 4319–83, therefore, corresponds to the adsorption characteristics for a saturated soil.

Rowe et al. (1988) have also demonstrated that it is possible to back-calculate both the coefficients of diffusion and adsorption for a saturated soil using a single reservoir method. The test set-up consists of a soil column with a source reservoir at the top and a zero flux boundary at the base. The reservoir contains a mass source with some concentration, $C_{sub 0}$, at time equal to zero, and the decrease in concentration with time is monitored. The coefficients of diffusion and adsorption are determined by fitting a theoretical solution using POLLUTE/3.0 (Rowe and Booker 1983) to both the concentration versus time profile and the concentration versus depth profile in the soil specimen measured at the end of the test.

The effect of water content on the adsorption coefficient is not well defined for unsaturated soils. Brown (1953) tested the influence of water content on the adsorption characteristics of various geologic materials using a test set-up similar to the one half cell method with ion-exchange membrane. Synthetic Ca-exchange membranes are first washed with 4 N hydrochloric acid to displace Ca^{2+} with H^+ . Excess chlorides are removed by rinsing the membranes, with distilled water. The membranes are then placed into the bottom of a container, followed by 100 g of the moistened soil. The soil samples are pre-wetted to various water contents extending from

saturation to the wilting point. At the end of the test, the various major cations exchanged with H^+ were extracted from the membranes. An exchange period of 96 hours was established for each treatment. The results showed that the mass exchanged per unit mass of soil decreases with a decrease in the water content; however, the decrease in adsorption could also be related to a decrease in diffusive flux associated with a decrease in the effective diffusion coefficient.

Shortcomings of existing test methods

One of the key shortcomings for the two half cell method or the one half cell method with ion-exchange membrane is the lack of control of the stress state within the soil specimen. Soils with differing water contents and densities should be considered as “different” soils (Fredlund 1989) because of differences in the soil structures (Lambe 1958). Therefore, any measured changes in the effective diffusion coefficient could encompass both the effects of changing water content and soil structure. In addition, the soil suction was either not controlled during the test or there was no proper control of the water content of the resin paper or membrane. Consequently, mass flow of the contaminants due to a suction gradient could occur (Shackelford 1991; Barraclough and Tinker 1981). Hence, the movement of the contaminants is no longer driven by diffusion alone but rather by both advection and diffusion. Another limitation is related to the interconnectivity of the liquid phase along the soil-soil interface or the soil-membrane interface, particularly at low water contents.

In the case of reactive ions, the coefficient of diffusion determined from the two half cell method or the one half cell method with the ion-exchange paper method is not a fundamental parameter but is comprised of the effective diffusion and distribution coefficients. The need for an independent determination of the transport parameters was illustrated by Rowe et al. (1985). However, independent determination of the coefficients of diffusion and adsorption for a single test is not feasible because the effects of water content on these coefficients are both unknown.

A new method for diffusion testing of unsaturated soil

The design concept of the new test method evolves out of the need for a control of the stress state of the soil [i.e., net normal stress, $(\sigma - u_a)$ and matric suction $(u_a - u_w)$] and an independent measurement of the coefficients of diffusion and adsorption. One other problem encountered in the diffusion testing of unsaturated soil is related to the difficulty in determining the pore-water concentrations. Disturbances to the soil specimen in the course of extracting the pore-water will expose additional potential adsorption sites (i.e., sites associated with the soil particles that are isolated from the liquid phase under unsaturated

conditions). Consequently, the amount of adsorption would be overestimated.

Difficulties associated with the determination of the concentrations of the ions in the soil-water can be overcome by allowing the system to reach chemical equilibrium (i.e., when the rate of change in concentration, dC / dt , approached zero at large times). At equilibrium, the concentration of the ions would be uniform throughout the system. The amount of adsorption can then be computed using the principle of mass conservation if the equilibrium concentration is known. A procedure that allows the matric suction to be controlled throughout the test and the monitoring of the attainment of chemical equilibrium is therefore required for the diffusion testing of unsaturated soils. These requirements can be satisfied by integrating the principles of the single reservoir method with a flux-controlled boundary (Rowe et al. 1988) and the pressure plate apparatus [ASTM Test Method for Capillary-Moisture Relationships for Coarse- and Medium-Textured Soil by Porous Plate Apparatus (D 2325-68)].

The apparatus for diffusion testing of unsaturated soil

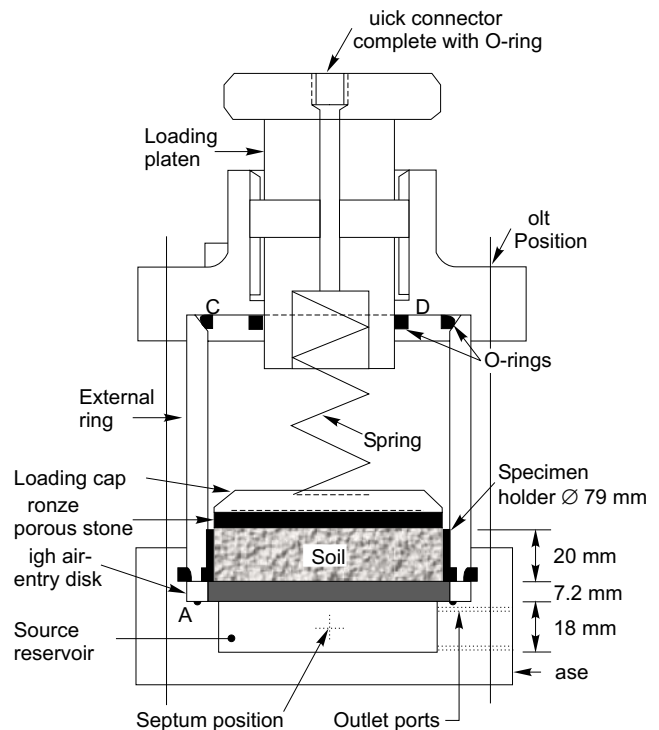
The apparatus for diffusion testing of unsaturated soils is shown in Fig. 1 (Lim 1995). The advantages of the apparatus include: (1) independent control of the stress state of the soil throughout the test duration; (2) no advection, and (3) independent determination of the coefficients of diffusion and adsorption from a single test.

The various components that make up the diffusion cell are a base, a high air-entry disk, a soil specimen holder, a bronze porous stone, a loading cap, a spring, an external ring, and a top with a loading platen and a quick connection to an air supply. The base houses a source reservoir of known volume, a septum for sampling purposes, two tapered plastic outlets, and O-rings at locations "A" and "B". The ends of each of the outlets are connected to another short piece of plastic tubing that can be opened or closed via a clamp. The outlet located just beneath the high air-entry disk functions both as a drainage outlet and an inlet during sampling. The lower outlet near the base of the reservoir is used for draining the source reservoir at the end of the test.

The external ring with an outside diameter of 9.525 cm and a wall thickness of 0.635 cm was made of acrylic. The external ring is pressure-sealed against the base and the top via the O-rings at locations "B" and "C". The top cover and the loading platen were fabricated from acetyl plastic. Potential air and moisture leakage between the top cover and the loading platen and at the quick connection were sealed with O-rings. The loading accessories, which include a porous stone, a plastic cap, and a spring, are placed over the soil specimen in the order shown in Fig. 1. Application of the preload is achieved by lowering the loading platen through a screw mechanism.

The high air-entry disks manufactured by Soilmoisture Equipment Corporation, Santa Barbara, CA 93105 were made from ceramic, formed from sintered kaolin. The

Fig. 1. A cross section of the apparatus for diffusion testing of unsaturated soil.



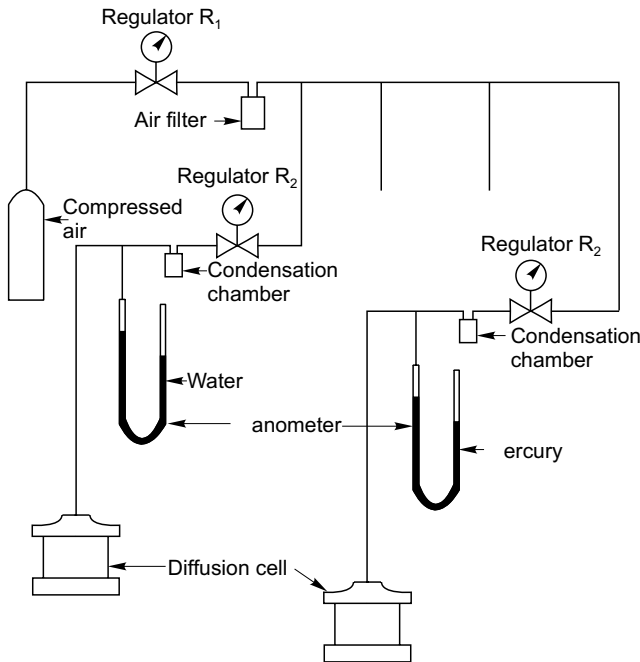
high air-entry disk is placed between the source reservoir and the soil specimen to facilitate the control of the matric suction through the use of the axis-translation technique. The high air-entry disk is encased in a stainless steel ring to provide a better sealing of the source reservoir. The soil specimen holder with an internal diameter of 7.9 cm and 2.0 cm high was made of stainless steel.

Test set-up

A schematic diagram of a typical set-up for diffusion testing of unsaturated soil is shown in Fig. 2. The incoming air was first regulated to a pressure of 80 kPa by Regulator R_1 . The air was then passed through an air filter that removes condensed water and dirt in the air pressure line. The air pressure was further regulated to the desired matric suction using Regulator R_2 . A condensation chamber was placed after Regulator R_2 for collecting the condensing water vapor. The magnitude of the air pressure was registered by either a water- or mercury-filled manometer for the low-pressure range or a pressure gauge for the high-pressure range.

Prior to the commencement of the test program, checks were undertaken to eliminate any leakage along the air pressure line and to ensure that the regulators and the pressure gauges were in good working condition. All the regulators and the gauges were calibrated against a standardized gauge and a manometer. The stability of the regulated air pressure was also checked prior to the diffusion tests by monitoring the fluctuation of the fluid levels in

Fig. 2. A schematic diagram of a typical set-up for diffusion testing of unsaturated soil.



the manometer or the needle position in the case of the pressure gauge. A small volume of distilled water was also placed in the condensation chamber to ensure that the air pressure line was saturated with water vapor.

Soil

The selection of the soil type for this study was based on two considerations. The two considerations are: (1) to evaluate the feasibility of the proposed apparatus in determining the coefficients of diffusion and adsorption; (2) to provide an understanding of the fundamental role of the liquid phase on the coefficients of diffusion and adsorption. A sand with low silt and clay content and with low water retention characteristics was therefore selected. The soil, called Beaver Creek Sand, is an olive brown, oxidized, uniform, fine-to-medium aeolian sand. The physical index characteristics, mineralogical composition, cation exchange capacity, and chemistry of this soil are summarized in Table 1.

The grain-size distribution of the soil was measured by mechanical sieving in accordance with ASTM Test Method for Particle Analysis of Soils (D 422–63). The fines content of the soil was determined by saturating the soil in a sodium hexametaphosphate solution in accordance to ASTM Test Method for Amount of Material in Soils Finer than the No. 200 (75 μ m) Sieve (D 1140–92). The fines in the soil were dispersed by shaking the soil solution mixture and then washing the mixture with distilled water through a U.S. No. 200 sieve. Tests for the mineralogy of the soil were performed by Saskatchewan Research Council, Saskatoon, Saskatchewan, Canada, using an X-ray diffraction method. The cation exchange ca-

Table 1. A summary of the physical index, mineralogical composition, cation exchange capacity and chemistry of the soil.

Grain size distribution	
Percentage of sand	98.9
% retained on 0.417 mm sieve	3.5
% retained on 0.297 mm sieve	30.0
% retained on 0.246 mm sieve	26.8
% retained on 0.149 mm sieve	37.3
% retained on 0.075 mm sieve	1.3
Percentage of silt and clay	1.1
Coefficient of uniformity	1.8
Specific gravity	2.67
Mineralogy, %	
Quartz	89.6
Plagioclase	8.71
Illite	1.24
Smectite	0.42
Fe-Mg chlorite	0.03
Cation exchange capacity, meq/100 g dry soil	1.30
Exchangeable cations, meq/100 g dry soil	
Ca ²⁺	0.86
Mg ²⁺	0.50
K ⁺	0.04
Na ⁺	0.06
Dissolved ionic species in the 5:1 solution extract, meq/100 g	
Ca ²⁺	0.45
Mg ²⁺	0.20
K ⁺	0.016
Na ⁺	0.014
Cl ⁻	0.003
SO ₄ ²⁻	0.009
HCO ₃ ⁻	0.19

capacity and the exchangeable cations provided by PLAINS-Innovative Laboratory Services, Saskatoon, SK, Canada, were determined based on the methods described by Page et al. (1982).

Chemical tracers

In order to illustrate the application of the diffusion cell in determining the coefficients of diffusion and adsorption, potassium and chloride ions prepared from potassium chloride salt were selected as the reactive and non-reactive tracers, respectively. Potassium is considered to be a relatively stable ion in that it does not complex with anions such as sulphates or carbonates. The diffusion coefficient of potassium and chloride in free water are also similar (Cussler 1984).

Test program and test procedure

Diffusion tests were conducted on the sand at six different values of suction (0, 2.75, 3.1, 3.6, 3.9 and 6.0 kPa). The procedure for soil specimen preparation, diffusion testing of the soil, and the high air-entry disk

are described in the following sections. Deaired, distilled, and de-ionized water was used throughout the test from preparation to sampling.

Soil specimen preparation

The soil specimen for the diffusion test was prepared from a slurry. This method of specimen preparation was adopted because it minimizes entrapped air bubbles and therefore ensures complete saturation of the soil specimen. After placing the saturated high air-entry disk into the base, the specimen holder was centered over the disk. A known weight of air-dried soil was then placed into the specimen holder in small increments, and water was added as the specimen height increased. The slurry was stirred intermittently to remove any entrapped air bubbles. To ensure consistency in the porosity and dry density, the mass of air-dried soil and the applied preload were approximately the same for each soil specimen.

Once the soil was in place, the bronze porous stone, loading cap, and spring were placed over the soil and the cell was assembled. A small preload was applied onto the soil specimen by lowering the loading platen, which in turn compressed the spring to give a required pressure of 10 kPa. Application of the preload was to ensure continuity between the liquid phase of the soil and the high air-entry disk. The soil specimen was left to equilibrate in a controlled environmental chamber for at least 24 hours. The relative humidity and temperature in the environmental chamber were maintained constant at $84 \pm 2\%$ and $19.6 \pm 0.2^\circ\text{C}$, respectively. Following the initial moisture equilibration, the upper outlet was opened to allow the soil to consolidate under the applied preload.

Procedure for the diffusion testing of soil

The preliminary preparation work involved the cleaning of the base, external ring, high air-entry disk, bronze porous stone, and loading cap to ensure chemical cleanliness. The base and external ring were washed with running water and then rinsed thoroughly with distilled de-ionized water. The high air-entry disk and the bronze porous stone were soaked in numerous pore volumes of distilled and de-ionized water. Chemical cleanliness of the high air-entry disk and the bronze porous stone was monitored by measuring the electrical conductance of the supernatant. Additional pore volumes of water were flushed through the high air-entry disk to ensure complete saturation and chemical cleanliness of the disk. Flushing was discontinued when the electrical conductance of the flushed-out water was less than $0.1 \mu\text{S}$.

After cleaning, the weight of the various components of the cell was measured and the source reservoir was filled with water. Upon filling the reservoir, a magnetic stir bar was placed into the reservoir, followed by the high air-entry disk and placement of the soil specimen. The cell was assembled, and, after consolidation, the upper outlet was left open and the cell was connected to a regulated air-pressure line via the quick connection to drain the soil-water to the required matric suction. At the end of drainage, the hydraulic head is a constant (i.e.,

zero hydraulic gradient), and since the pore-water pressure, u_w , is zero (i.e., the upper outlet is opened to atmosphere during drainage), the matric suction of the soil is therefore equal to the applied air pressure.

Once drainage was complete, the diffusion test was initiated by spiking the source reservoir with a stock solution containing potassium and chloride. The water in the source reservoir was spiked by injecting a known volume of the stock solution through the septum using a syringe. To accommodate the stock solution and without causing backflow of water from the source reservoir into the high air-entry disk and the soil specimen, the upper outlet was opened to allow drainage of the displaced water. In this manner, the volume of water in the source reservoir remained constant. To further ensure a uniform concentration at the start of the test, the solution was stirred gently for approximately 2 min. A 1 mL sample was then taken from the source reservoir to establish the initial concentrations of the various ions.

Changes in the concentrations of the various ions in the source reservoir were monitored continuously by sampling at various time intervals. The sample size was generally less than 1 mL. Prior to any sampling, a glass tube filled with de-aired, distilled and de-ionized water was first connected to the upper outlet port. Care was also taken to remove any air bubbles trapped between the outlet and the glass tube. During sampling, the upper outlet was opened and water in the source reservoir was withdrawn using a 1 mL gas-tight syringe. The sampled volume was replaced simultaneously with de-aired, distilled and de-ionized water. After each sampling, the upper outlet was closed immediately.

Various precautionary measures were undertaken to minimize moisture loss from the diffusion cell during the test: (1) stirring of the water in the source reservoir was carried out only during sampling; (2) the diffusion cell was housed in an insulated box to protect the cell from drafts; and (3) the complete test set-up was located in a controlled environmental chamber where it was maintained at a constant relative humidity of $84 \pm 2\%$ and room temperature of $19.6 \pm 0.2^\circ\text{C}$.

The test was terminated when the changes in the concentration of potassium in the source reservoir with time were insignificant. Upon completion of the test, the final weight of the diffusion cell was determined. To prevent possible flow of water from the source reservoir into the high air-entry disk and the soil specimen, the water in the source reservoir was first drained before dismantling the cell. After drainage, the cell was weighed again, and, as the cell was being dismantled, the weights of the various components were measured.

The soil specimen was extruded from the specimen holder with a specially designed extruder. The soil specimen was sectioned into three smaller slices approximately 4 to 5 mm thick for water content and chemical mass balance determinations. The rationale in sectioning the soil specimen was to check for possible variations of the water content and to verify the attainment of chemical equilibrium. For the case with a matric suction of 0 kPa.

the soil specimen was left whole since it was saturated and not stable during slicing.

Water contents of the sliced specimens were measured by air-drying the soil at a room temperature of $21 \pm 2^\circ\text{C}$. After drying, the total mass of chloride and also potassium in each sliced specimen were determined by saturating the soil in distilled de-ionized water. The supernatant was decanted after 48 hours. The remaining mass of potassium in each sliced specimen was extracted by saturating the soil in a barium chloride solution. The mixture was left to equilibrate for at least three days. At the end of each equilibration, the supernatant was decanted. The extraction process was repeated at least three times to ensure complete removal of the adsorbed potassium from the soil. During each saturation, the soil specimen was shaken periodically.

Procedure for the diffusion testing of the high air-entry disk

The high air-entry disk that was used for controlling the matric suction of the soil formed an integral part of the set-up for the diffusion testing of unsaturated soil. The effective diffusion and adsorption coefficients of the high air-entry disk are, therefore, pertinent to the determination of the coefficients of diffusion and adsorption for the soil. The general procedure for the diffusion testing of the high air-entry disk alone was done in a similar manner as the diffusion testing of the soil. In order to minimize the test duration, the water level over the high air-entry disk was kept to a minimum. The excess water above the high air-entry disk was flushed by applying a small air pressure to the cell. When the water level was drained to just above the high air-entry disk, the air-pressure line was disconnected, but the quick connector was left open to the atmosphere to allow continued drainage of the remaining water. Once drainage was complete, the quick connector was closed and the test was initiated by spiking the source reservoir.

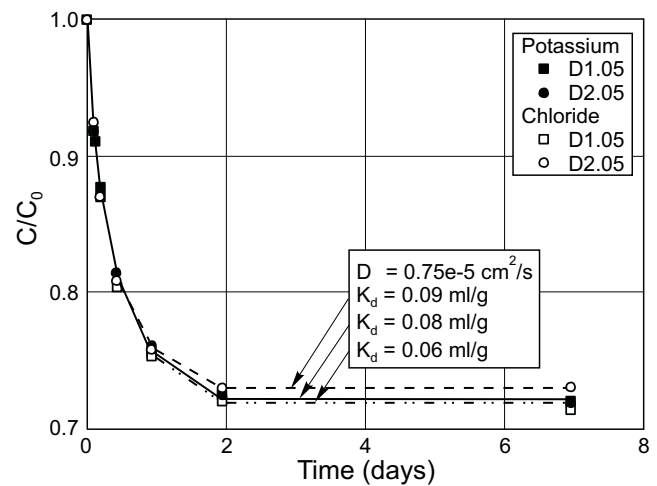
Analytical methods

The concentrations of the various tracers in the source reservoir were measured using various analytical methods. Concentrations of chloride and potassium in the samples and the distilled water extract were measured using ion chromatography and flame photometry, respectively. In the case of the barium chloride extract, the concentrations of potassium in the supernatant were measured using atomic adsorption spectrometry. Dilution of the samples was required to bring the concentration to within the measuring range of the equipment, and all samples were filtered through a $0.45 \mu\text{m}$ filter paper.

Test results

The test results for the high air-entry disk and the sand at different matric suctions, defined on the basis of a single reservoir diffusion test (Lim 1995), are presented in the following sections.

Fig. 3. Variations of the concentrations of potassium and chloride in the source reservoir normalized with respect to the initial concentration at time zero versus time for 0.5 bar high air-entry disks.



High air-entry disk

Diffusion tests were conducted on two 0.5 bar high air-entry disks designated as D1.05 and D2.05. The porosity and dry density of the high air-entry disks are 51.0% and 1550 kg/m^3 , respectively. The concentration versus time profiles for potassium and chloride in the source reservoir for D1.05 and D2.05 are given in Fig. 3. The concentrations were normalized with respect to the initial concentration at time equal to zero. The results showed that the variations in the concentrations of potassium and chloride in the source reservoir with time were characterized by a smooth decreasing trend, and the concentration profiles for potassium and chloride were almost identical.

A simple mass balance calculation at the end of the test showed that the final mass in the system was generally smaller than the initial mass after discounting the mass removed during sampling. The difference in mass, which ranged from 3.4 to 5.0% of the total mass, was relatively small and could be related to adsorption or small analytical errors. Regardless of the various possible causes, the difference in mass was represented mathematically as an adsorption reaction. The adsorption coefficient was calculated assuming a linear adsorption function and chemical equilibrium at the end of the test. The back calculated distribution coefficients of potassium and chloride for the 0.5 bar high air-entry disk were 0.1 and 0.07 mL/g, respectively.

The effective diffusion coefficients of potassium and chloride for the 0.5 bar high air-entry disk were determined by fitting a theoretical solution to the measured concentration versus time profile in the source reservoir. The diffusion coefficient corresponding to a profile that matched the measured concentration versus time profile would be the effective diffusion coefficient. The theoretical solution was obtained using CTRAN/W, a numerical solution based on a finite element formulation

(CTRAN/W 1991). CTRAN/W is a proprietary computer software developed and distributed by Geo-Slope International Ltd., Calgary, Alberta, Canada. The simulated concentration versus time profiles for potassium and chloride corresponding to an effective diffusion coefficient of $0.75 \times 10^{-5} \text{ cm}^2/\text{s}$, for both D1.05 and D2.05, are plotted on Fig. 3. The results showed that the match between the measured and the simulated profiles for the two disks were satisfactory.

Beaver Creek sand at various matric suctions

The soil-water retention characteristics and the variations of the degree of saturation across the soil specimen for cases at different matric suctions are shown in Figs. 4 and 5, respectively. The results showed that the variations in the degree of saturation, in general, were uniform except for the case with a matric suction of 3.9 kPa. The variations of the porosity and dry density among the various soil specimens and across the soil profile were also small. The average porosity and dry density of the soil specimen were 38.2% and 1650 kg/m^3 , respectively. The differences between the initial and final mass of water in the cell in general were less than 0.4 g (i.e., the moisture loss over the test duration was less than 0.4% of the total volume of water).

Plots of the concentration versus time profile for potassium and chloride in the source reservoir for the different cases are given in Figs. 6 and 7, respectively. The results showed that the concentration versus time profiles for potassium are characterized by a smooth decreasing trend. For chloride, the results also showed a smooth decreasing trend, but the concentration continued to decrease at a constant rate at larger times. In general, the results showed that the rate of change of the concentration in the source reservoir decreased with an increase in matric suction. For a non-reactive ion, the decreasing rate of change in concentration with increases in matric suction could be associated with a decrease in the effective diffusion coefficient. In the case of a reactive ion, the decreasing rate of change in concentration could also be related to a decrease in the adsorption coefficient.

Results of the total mass of potassium extracted from the soil specimen at the end of the test and the theoretical mass obtained from a simple mass calculation are plotted in Table 2. The theoretical total mass of potassium in the soil specimen was calculated based on the principle of mass conservation, assuming that chemical equilibrium was attained at the end of the test and assuming zero adsorption in the bronze porous stone. The mass removed during sampling was accounted for in the mass balance calculations. The results showed that except for the case with a matric suction of 0 kPa, the difference between the theoretical and the measured total mass ranged from 1 to 5%. The difference could be related to possible errors in the analytical method or the possible fixation of potassium by the smectite minerals. For the case with a matric suction of 0 kPa, the significant difference could be due to possible retention of a fraction of the soluble potassium on the tare during drying.

Fig. 4. The soil-water retention characteristics (characteristic curve) of the soil specimen at different matric suctions.

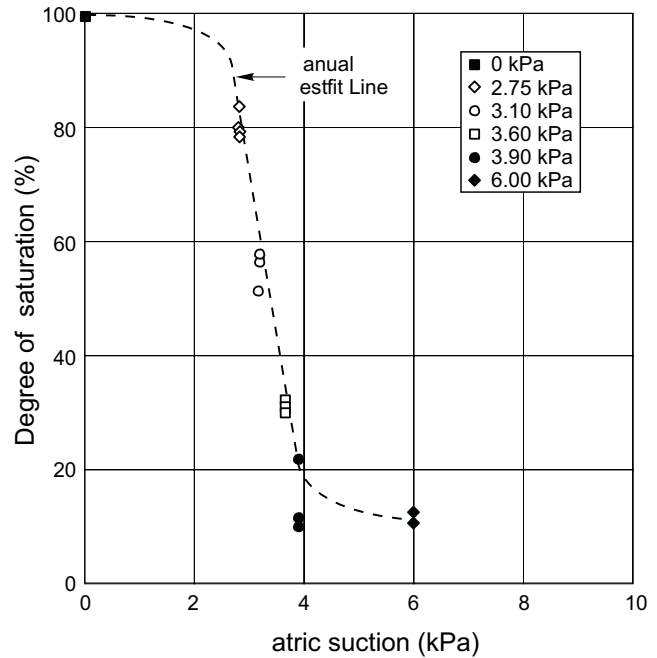
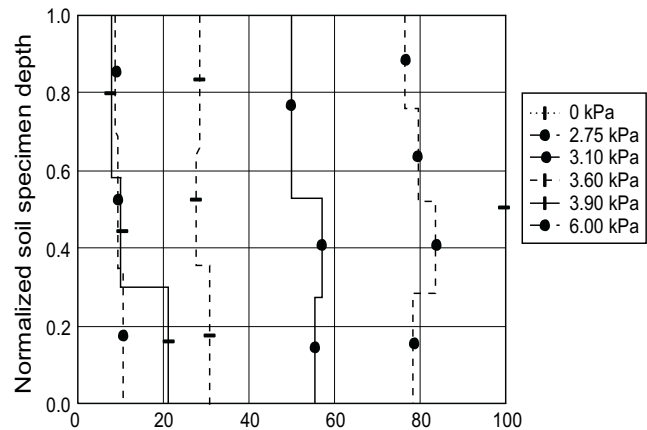


Fig. 5. Variations of the degree of saturation across the soil profile for cases at different matric suctions.



In the case of chloride, the final concentration in the source reservoir was also verified against a theoretical concentration calculated on the basis of mass balance at the end of the test. The results of the final and the theoretical concentrations for the different cases are given in Table 2. The results showed that the final concentrations were generally smaller than the theoretical concentrations except for cases with matric suctions of 0 and 6 kPa. The smaller measured concentrations would represent a loss of chloride.

The losses were quite significant and may be related to possible complexation-precipitation reactions between chloride and the upper bronze porous stone or the tin foil. For cases with matric suctions of 2.75, 3.1, and 3.9 kPa, additional tin foil was placed over the bronze porous

Fig. 6. Variations of the concentration of potassium in the source reservoir normalized with respect to the initial concentration at time zero versus time for cases at different matric suctions.

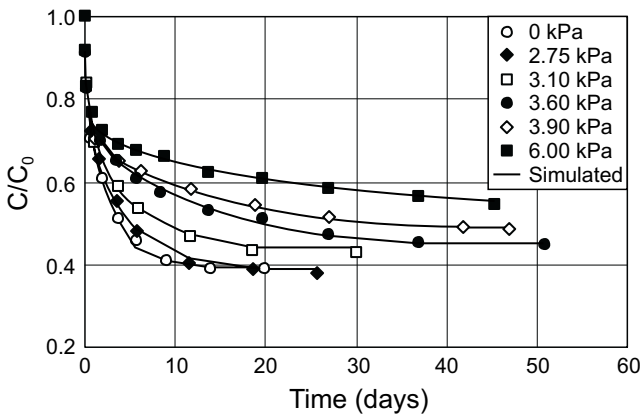


Fig. 7. Variations of the concentration of chloride in the source reservoir normalized with respect to the initial concentration at time zero versus time for cases at different matric suctions.

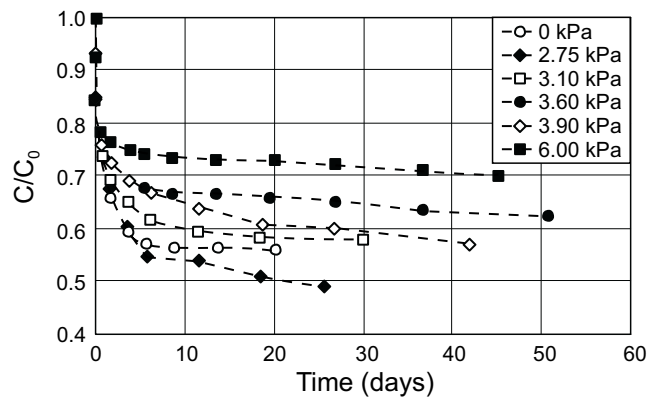


Table 2. A comparison of the measured and theoretical mass for potassium, and the final and theoretical concentration for chloride for cases at different matric suctions.

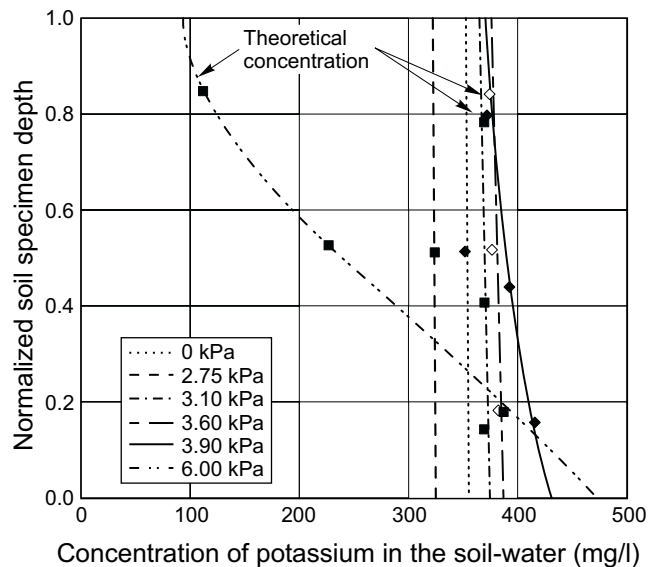
Case kPa	Total mass of K ⁺ in soil		Percent difference	Chloride concentration		
	extracted mg	theoretical mg		final mg/L	theoretical mg/L	Difference in Mass mg
0.00	29.3 ± 0.3	33.1	12 ± 1.0	426	448	-3 (-5%)
2.75	28.6 ± 0.1	29.8	4 ± 0.4	401	491	-11 (-18%)
3.10	25.0 ± 0.2	26.3	5 ± 0.7	476	533	-7 (-11%)
3.60	22.7 ± 0.1	24.0	5 ± 0.5	525	570	-5 (-8%)
3.90	19.1 ± 0.2	19.7	3 ± 0.8	480	584	-11 (-19%)
6.00	14.9 ± 0.1	15.1	1 ± 0.7	573	585	-1 (-2%)

stone to minimize the moisture loss from the soil specimen.

The effective diffusion coefficient was evaluated only for potassium. The method of the back-analysis for the coefficients of diffusion and adsorption differed somewhat depending on whether chemical equilibrium was reached at the end of the test. For cases in which chemical equilibrium was attained, the adsorption coefficient was calculated based on the principle of mass conservation. Once the adsorption coefficient was defined, the effective diffusion coefficient was obtained by fitting a theoretical solution to the measured concentration versus time profile using CTRAN/W. For cases in which chemical equilibrium was not attained, both the coefficients of diffusion and adsorption were unknown. The unknown coefficients were determined by fitting a theoretical solution to both the concentration versus time profile in the source and the concentration versus depth profile in the soil specimen simultaneously.

Plots of the simulated concentration versus time profiles for potassium for the various cases are given in Fig. 6. Plots of the simulated concentration versus depth profile and the average theoretical concentrations of potassium in the soil-water for the different cases are also shown in Fig. 8. The average theoretical concentration of potassium in the soil-water was calculated based on the

Fig. 8. Results of the simulated concentration versus depth profile and the theoretical concentration of potassium in the soil-water for cases at different matric suctions.



total mass of potassium in each sliced specimen and the adsorption coefficient assumed in the numerical simulation. The results showed that the match between the mea-

Fig. 9. Relationship between the effective diffusion coefficient normalized with respect to the effective diffusion coefficients at saturation and the degree of saturation.

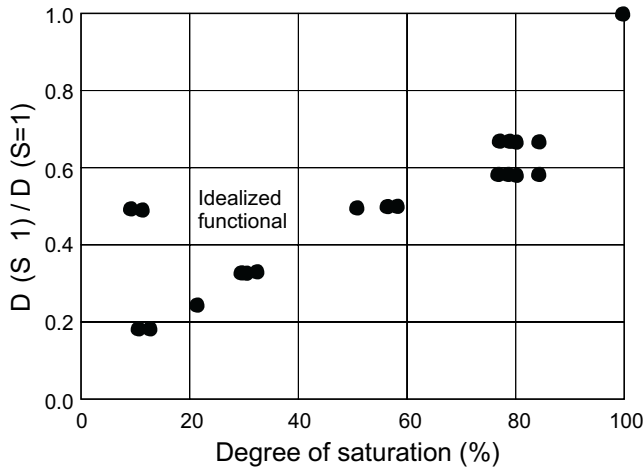
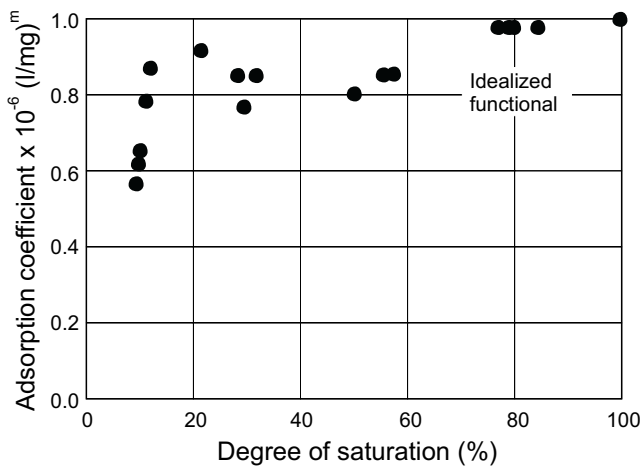


Fig. 10. Relationship between the adsorption coefficient and degree of saturation.



sured and the simulated profiles for the various cases was satisfactory.

The effects of matric suction on the coefficients of diffusion and adsorption plotted against the degree of saturation are given in Figs. 9 and 10, respectively. The effective diffusion coefficients were normalized with respect to the effective diffusion coefficient at saturation. The results in Fig. 9 showed that the normalized effective diffusion coefficient decreased with decreases in the degree of saturation. The decrease was quite rapid initially; however, beyond a degree of saturation of 60%, the normalized effective diffusion coefficient decreased almost linearly with a decrease in the degree of saturation. The extent of the decrease from saturation to near the residual degree of saturation was approximately 80%, less than one order of magnitude. The results showed an apparent anomaly in which the normalized effective diffusion coefficient increased and the water content approached the residual degree of saturation. A similar anomaly at low

water contents was also reported by Graham-Byce (1963) and Gillham et al. (1984). In general, the form of the functional relationship between the normalized effective diffusion coefficient and the degree of saturation was slightly non-linear.

The relationship between the adsorption coefficient and the degree of saturation given in Fig. 10 showed that the initial decrease was small as the soil desaturated from a degree of saturation of 100% to 60%. The adsorption coefficients; however, remained relatively constant from a degree of saturation of 60% to 20%. As the water content approached the residual degree of saturation, the adsorption coefficient decreased quite abruptly from 8×10^{-7} to $5.6 \times 10^{-7} \text{ (L/mg)}^m$ (i.e., a decrease of approximately 44%). In general, the form of the functional relationship between the adsorption coefficient and the degree of saturation was bi-linear.

Conclusions

A new technique for diffusion testing of unsaturated soil in which the stress state of the soil (i.e. the net total stress and the matric suction) can be controlled throughout the test duration is illustrated. The test results showed that a direct determination of the coefficients of diffusion and adsorption from a single test is feasible with the new technique.

The results determined from the single reservoir diffusion test for the sand showed that the concentration versus time profiles for potassium in the source reservoir were characterized by a well defined decreasing trend. At large times, the concentration versus time profiles began to level off, providing a clear indication of the attainment of chemical equilibrium. However, for cases with high matric suction, a long test duration would be required for complete attainment of chemical equilibrium.

In the case of chloride, the variations of the concentration in the source reservoir with time also showed a well defined decreasing trend. However, for most cases, the attainment of chemical equilibrium could not be established.

For cases with chemical equilibrium, the required adsorption coefficient could be calculated on the basis of mass balance at the end of the test, and the effective diffusion coefficient could be obtained by fitting a theoretical solution to the measured concentration versus time profile. For cases with incomplete chemical equilibrium, both the concentration versus time profile and the concentration versus depth profile in the soil specimen would be required to determine the unknown coefficients.

The results of this study showed that both the coefficients of diffusion and adsorption for potassium decreased with a decrease in the degree of saturation. For diffusion, the functional relationship between the normalized effective diffusion coefficient and the degree of saturation was slightly non-linear. In the case of adsorption, the effect of the degree of saturation on the adsorption coefficient was quite insignificant from saturation to a degree of saturation of 10%. A significant decrease in the

adsorption coefficient was evident only near the residual degree of saturation. The functional relationship between the adsorption coefficient and the degree of saturation was bi-linear.

References

- Barracough, P.B., and Tinker, P. B. 1981. The determination of ionic diffusion coefficients in field soils. I. Diffusion coefficients in sieved soils in relation to water content and bulk density. *Journal of Soil Science*, **32**: 225–236.
- Barrer, R.M. 1951. *Diffusion in and through solids*. University Press, Cambridge.
- Bear, J., and Verruijt, A. 1987. *Modeling groundwater flow and pollution*. Dordrecht D. Reide Publishing Company, Boston.
- Brown, D.A. 1953. Cation exchange in soils through the moisture range, saturation to the wilting percentage. *Proceedings of the Soil Science Society of America*, **17**: 92–96.
- Carslaw, H.S., and Jaeger, J.C. 1959. *Conduction of heat in solids*. Second edition, Oxford University Press, Oxford, England.
- Conca, J.L., and Wright, J. 1990. Diffusion coefficients in gravel under unsaturated conditions. *Water Resource Research*, **26**(5): 1055–1066.
- CTRAN/W, 1991. Version 2, Geo-Slope International Ltd., Calgary, AB, Canada.
- Cussler, E.L. 1984. *Diffusion-mass transfer in fluid systems*. University Press, Cambridge.
- Fredlund, D.G. 1989. The character of the shear strength envelope for unsaturated soils. The Victor de Mello Volume. *Proceedings, 12th International Conference on Soil Mechanics and Foundation Engineering, Rio de Janeiro, Brazil*. Editora Edgard Blucher, Ltda., Sao Paulo, Brazil, pp. 142–149.
- Gillham, R.W., Robin, M.J.L., and Dytynshyn, D.J. 1984. Diffusion of non-reactive and reactive solutes through fine-grained barrier materials. *Canadian Geotechnical Journal*, **21**: 541–550.
- Graham-Bryce, I.J. 1963. Effect of moisture content and soil type on self diffusion of ^{86}Rb in soils. *Journal of Agricultural Science*, **60**: 239–244.
- Helferich, F. 1962. *Ion exchange*. McGraw-Hill, New York.
- Hilf, J.W. 1956. An investigation of pore-water pressure in compacted cohesive soils. Ph.D. thesis. Technical Memorandum No. 654. U.S. Department of the Interior, Bureau of Reclamation. Design and Construction Division, Denver, CO.
- Klute, A. and Letey, J. 1958. The dependence of ionic diffusion on the moisture content of non-adsorbing porous media. *Proceedings of the Soil Science Society of America*, **22**: 213–215.
- Lambe, T.W. 1958. The engineering behavior of compacted clay. *ASCE, Journal Soil Mechanics and Foundations Division*, **84**(SM2, 1655): 1–35.
- Lim, P.C. 1995. Characterization and prediction of the functionals for the coefficients of diffusion and adsorption for inorganic chemicals. Ph.D thesis, University of Saskatchewan, Saskatoon, SK, Canada.
- Page, A.L., Miller, R.H., and Keeny, D.R. 1982. *Method of soil analysis. Part 2, Chemical and microbiological properties*. Monograph No. 9, 2nd edition., American Society of Agronomy, Madison, WI.
- Porter, L.K., Kemper, W.D., Jackson, R.D., and Stewart, B.A. 1960. Chloride diffusion in soils as influenced by moisture content. *Proceedings of the Soil Science Society of America*, **24**: 460–463.
- Robinson, R.A., and Stokes, R.H. 1959. *Electrolyte solutions*. Butterworths, London.
- Romkens, M.J.M., and Bruce, R.R. 1964. Nitrate diffusivity in relation to moisture content of non-adsorbing porous media. *Soil Science*, **98**: 332–337.
- Rowe, R.K., and Booker, J.R. 1983. Program POLLUTE-1D pollutant migration analysis program. ASCDA, Faculty of Engineering Science, The University of Western Ontario, London, ON, Canada.
- Rowe, R.K., Caers, C.J., and Barone, F. 1988. Laboratory determination of diffusion and adsorption coefficients of contaminants using undisturbed clayey soils. *Canadian Geotechnical Journal*, **25**: 108–118.
- Rowe, R.K., Caers, C.J., Booker, J.R., and Crooks, V.E. 1985. Pollutant migration through clayey soils. *Proceedings, 11th International Conference on Soil Mechanics and Foundation Engineering, San Francisco, A.A. Balkema, Boston*, pp. 1293–1298.
- Rowell, D.L., Martin, M.W., and Nye, P.H. 1967. The measurement and mechanism of ion diffusion in soils. III. The effect of moisture content and soil solution concentration on the self diffusion of ions in soils. *Journal of Soil Science*, **18**: 204–222.
- Shackelford, C.D. 1991. Laboratory diffusion testing for waste disposal-A review. *Journal of Contaminant Hydrology*, **7**: 177–217.
- Vaidyanathan, L.V., and Nye, P.H. 1966. An exchange resin paper method for measurement of the diffusive flux and diffusion coefficient of nutrient ions in soils. *Journal of Soil Science*, **17**: 175–183.
- Warncke, D.D., and Barber, S.A. 1972. Diffusion of zinc in soil: I. The influence of soil moisture. *Proceedings of the Soil Science Society of America*, **36**: 39–42.

Part VI
Volume Change Behaviour of
Unsaturated Soils



Dr. Robert L. Lytton
Department of Transportation Engineering
Texas A & M University
College Station, Texas

Introduction and Overview

Probably the most basic and at the same time complex theories for the understanding of unsaturated soil behaviour is that related to volume change. The study of volume change in unsaturated soils was the focus of D.G. Fredlund's Ph.D. thesis. Great strides have been made in our understanding of volume change in unsaturated soils; however, the subject still requires much more research.

The primary application for the volume change constitutive relations has been to the prediction of heave in expansive soils. This application has dominated the volume change scene because of the high cost associated with damages caused by swelling soils. There are also other soils, such as collapsing soils, that require volume change formulations. Numerous volume change prediction procedures have been proposed in the research literature. These procedures can be subdivided into procedures attempting to follow the actual suction change stress path in the field and procedures attempting to follow an equivalent total stress change during laboratory testing. Much of D.G. Fredlund's research focused on the use of the latter approach (i.e., the use of an equivalent total stress path for the prediction of heave). At the same time he supports suction measurements in the laboratory and the field and attempts to measure appropriate soil moduli to predict volume change in unsaturated soils.

The volume change constitutive behaviour of an unsaturated soil can be written in several possible forms; namely in terms of elastic parameters, compressibility parameters, and parameters historically adopted in classic soil mechanics. The classical soil mechanics form for the one-dimensional, K_0 , loading of a saturated soil involves the relationship between void ratio and effective stress.

$$[1] \quad de = a_v d(\sigma_y - u_w)$$

where:

- e = void ratio,
- a_v = coefficient of permeability,
- σ_y = total stress, and
- u_w = pore-water pressure.

Similar classical soil mechanics forms for the volume change constitutive relations for an unsaturated soil involve the use of void ratio, e , water content, w and/or degree of saturation, S . The need for two independent constitutive relations for an unsaturated soil can be demonstrated through the differentiation of the basic volume-mass relationship.

$$[2] \quad \int_{e_0}^{e_f} S de + \int_{S_0}^{S_f} e dS = G_s \int_{w_0}^{w_f} dw$$

where:

- G_s = specific gravity,
- S = degree of saturation, and
- w = water content.

The independent stress state variables can be used to formulate the constitutive relations for an unsaturated soil element. The volume change constitutive equation for isotropic loading, $(\sigma_c - u_a)$, written in terms of void ratio, e , is as follows:

$$[3] \quad de = a_t d(\sigma_c - u_a) + a_m d(u_a - u_w)$$

where

- $a_t = \frac{\partial e}{\partial(\sigma - u_a)}$; coefficient of compressibility with respect to a change in $(\sigma - u_a)$, and
- $a_m = \frac{\partial e}{\partial(u_a - u_w)}$; coefficient of compressibility with respect to a change in $(u_a - u_w)$.

The void ratio change can be independent of the water content change for an unsaturated soil element. For a complete volume-mass characterization, a second constitutive relationship is required. The water content constitutive relationship is generally used as the second constitutive relationship, and can be written as follows for the case of isotropic loading,

$$[4] \quad dw = b_t d(\sigma_c - u_a) = b_m d(u_a - u_w)$$

where

$$b_t = \frac{\partial w}{\partial(\sigma - u_a)}; \text{ coefficient of water content change with respect to a change in } (\sigma - u_a),$$

and

$$b_m = \frac{\partial w}{\partial(u_a - u_w)}; \text{ coefficient of water content change with respect to a change in } (u_a - u_w).$$

Similar sets of constitutive equations can also be written for non-isotropic loading conditions. When the net confining stress on the soil is equal to zero, the resulting equation is a relationship between water content and soil suction, commonly referred to as the soil-water characteristic curve.

$$[5] \quad dw = b_m d(u_a - u_w)$$

The equation is often written in terms of volumetric water content, θ_w , as follows:

$$[6] \quad d\theta_w = m_2^w (u_a - u_w)$$

The primary features of the soil–water characteristic curve are the air entry value and the residual water content. The soil exhibits hysteresis upon wetting and drying and the soil suction corresponding to zero water content is approximately 1 000 000 kPa.

A similar approach to the formulation of the constitutive relations can be applied within the critical state (or elasto-plastic) framework, which uses three parameters, p , q , r , along with two state parameters (i.e., water content, w , and specific volume, v). The specific volume, v , and void ratio, e , are related as follows:

$$[7] \quad v = 1 + e$$

The void ratio and water content constitutive surfaces corresponding to the above equations can be represented graphically as three-dimensional surfaces where the water content, w , and void ratio, e , are plotted as ordinates against the abscissas $(\sigma - u_a)$ and $(u_a - u_w)$. A study of the limiting conditions reveals the types of laboratory tests required to measure each of the limiting conditions on the two constitutive surfaces.

There are several stress paths along which an element of soil can be loaded. The most general loading stress path involves the independent control of stresses during three-dimensional loading. While this is the most general form, it is also the most difficult to perform and as a result it is desirable to revert to more specialized cases. The common stress paths for loading are: (1) isotropic loading, (2) uniaxial loading, (3) triaxial (actually biaxial) loading, and (4) K_0 loading. There are, however, benefits associated with using isotropic loading because changes in suction are always isotropic in nature, and isotropic loading has become the reference loading condition in critical state (or elasto-plastic) soil mechanics.

Three independent laboratory tests can be performed to define the extreme limits on the overall volume change and the water content constitutive relationships. The first laboratory test defines the basic relationship between void ratio and net total stress, $(\sigma - u_a)$. This relationship can be defined under zero suction conditions using a conventional saturated one-dimensional oedometer test or a triaxial test (isotropic test). The test results are referred to as the compression curve for the soil. This relationship is equivalent to the water content versus net total stress curve.

The second laboratory test involves the use of the pressure plate apparatus to define the relationship between gravimetric or volumetric water content and matric suction, $(\sigma - u_a)$. The test is most commonly performed with the net total stress equal to zero although testing can also be performed under various applied total stresses. The test results are referred to as the soil-water characteristic curve, SWCC, for the soil. At high suctions, (i.e., up to 1 000 000 kPa), vacuum desiccators can be used to complete the water content versus total suction relationship.

The third laboratory test is the shrinkage test for defining the ratio of the slope of the void ratio and the water content change of the soil in response to a change in soil suction. Data from

the above three tests can be used to define the extremes or limits on the void ratio and water content constitutive surfaces.

Little research has been done to define the shape of the constitutive surface between the extremes or limits, mentioned above. The remainder of the constitutive surfaces is generally assumed to have a particular character but this is a subject requiring further research. Research is required on soils with both a stable-structure and a meta-stable structure.

The relationship between soil suction and volume change of an unsaturated soil is referred to as the volume change function. To-date, little research has been done on an analytical prediction for the volume change function. However, it is anticipated that this relationship could also be predicted with sufficient accuracy for many engineering problems through use of the compression curve for the saturated soil and the soil-water characteristic curve.

While further research is still required in order to be able to estimate the relationship between the moduli along various stress paths, it has been possible to determine ways of relating the soil moduli on the void ratio constitutive surface. This relationship has been used to advantage for predicting heave in an expansive soils. As a result, an *in situ* stress state consisting of the overburden pressure and matric suction in the field, can be transferred onto the total stress plane to give the swelling pressure of the soil. The unloading moduli on the total stress plane can then be used in the prediction of heave upon wetting of an expansive soil.

Part VI

Volume Change Behaviour of Unsaturated Soils

- Fredlund, D.G., and Morgenstern, N.R. 1976. Constitutive relations for volume change in unsaturated soils. *Canadian Geotechnical Journal*, **13**(3): 261–276 515
- Ho, D.Y.F., Fredlund, D.G., and Rahardjo, H. 1992. Volume change indices during loading and unloading of an unsaturated soil. *Canadian Geotechnical Journal*, **29**(2): 195–207 . 528
- Pereira, J.H.F., and Fredlund, D.G. 1997. Constitutive modelling of a metastable-structured compacted soil. *Proceedings, International Symposium on Recent Developments in Soil and Pavement Mechanics, Rio de Janeiro, Brazil*, pp. 317–326 540
- Fredlund, D.G., Hasan, J.U., and Filson, H. 1980. The prediction of total heave. *Proceedings, Fourth International Conference on Expansive Soils, Denver, CO, June 16–18, Vol. 1*, pp. 1–17 550
- Fredlund, D.G. 1987. The prediction and performance of structures on expansive soils. *Proceedings, International Symposium on Prediction and Performance in Geotechnical Engineering, Calgary, Alberta*, pp. 51–60 559
- Fredlund, D.G. 1969. Consolidometer test procedural factors affecting swell properties. *Proceedings, International Conference on Expansive Soils, Texas A & M, College Station, Texas*, pp. 435–456 567
- Rao, R.R., Rahardjo, H., and Fredlund, D.G. 1988. Closed-form heave solutions for expansive soils. *Journal of Geotechnical Engineering*, **114**(5): 573–588 582
- Yoshida, R.T., Fredlund, D.G., and Hamilton, J.J. 1983. The prediction of total heave of a slab-on-grade floor on Regina clay. *Canadian Geotechnical Journal*, **20**(1): 69–81 . . . 590
- Ching, R.K.H., and Fredlund, D.G. 1984. A small Saskatchewan town copes with swelling clay problems. *Proceedings, 5th International Conference on Expansive Soils, Adelaide, Australia*, pp. 306–310 602
- Sattler, P.J., and Fredlund, D.G. 1990. Numerical modelling of vertical ground movements in expansive soils. *Canadian Geotechnical Journal*, **28**(2): 189–199 609
- Shuai, F., and Fredlund, D.G. 1997. Measured and simulated behavior of an expansive soil. *Proceedings, Third Brazilian Symposium on Unsaturated Soils, NSAT'97, Rio de Janeiro, Brazil, Vol. 1*, pp. 253–260 620
- Tadepalli, R., and Fredlund, D.G. 1991. The collapse behavior of a compacted soil during inundation. *Canadian Geotechnical Journal*, **28**: 477–488 626
- Fredlund, D.G., Bergan, A.T., and Wong, P.K. 1977. Resilient modulus constitutive relationships for cohesive soils. *Transportation Research Board, Transportation Research Record 642*, pp. 73–81 639

Constitutive relations for volume change in unsaturated soils

D.G. Fredlund and N.R. Morgenstern

Abstract: Volume change constitutive relations for unsaturated soils are proposed from a semi-empirical standpoint. One equation describes the deformation of the soil structure and a second equation defines the volume of water present in the element. Each equation can be viewed as a three-dimensional surface with two independent stress state variables forming the abscissas.

Uniqueness is tested by measuring volume changes resulting from stress changes in two orthogonal directions and comparing predicted and measured volume changes resulting from a stress change in a third direction. Specimens of undisturbed Regina Clay and compacted kaolin showed good agreement between the predicted and measured volume changes for monotonic deformation of the soil structure. The agreement was not as close for the water phase. The variation was attributed to difficulties in measuring water volume changes over a long period of time. The laboratory results indicate that the proposed constitutive equations are of the appropriate form for use in engineering practice.

Key words: volume change, constitutive relations, continuity, uniqueness, soil structure, water phase, air phase, unsaturated soil.

Introduction

Generally an unsaturated soil is considered to be a three-phase system. However, the independent properties and continuous bounding surfaces of the air-water boundary (i.e., contractile skin) require its consideration as a fourth phase (Davies and Rideal 1963). An element of unsaturated soil can therefore be considered as a mixture with two phases that come to equilibrium under applied stresses (i.e., soil particles and the contractile skin) and two phases that flow under applied pressures (i.e., the air and water). The air phase is assumed to be continuous.

Several effective stress equations have been proposed for unsaturated soils. However, these equations lack theoretical justification and have not proven satisfactory, as demonstrated by their limited application to engineering analyses. All equations have included a soil property in the description of the stress variable controlling soil behavior. Fredlund (1973*a, b*) used the principle of superimposition of coincident equilibrium stress fields to isolate the stress state variables associated with the soil particles and the contractile skin. The analysis indicated that any two of three possible normal stress variables can be used to define the stress state. Possible combinations are:

- (1) $(\sigma - u_a)$ and $(u_a - u_w)$
- (2) $(\sigma - u_w)$ and $(u_a - u_w)$
- (3) $(\sigma - u_w)$ and $(\sigma - u_a)$

where:

σ = total normal stress,
 u_a = air pressure, and
 u_w = water pressure.

Null experiments (i.e., $\Delta\sigma = \Delta u_a = \Delta u_w$) supported the theoretically proposed stress state variables (Fredlund 1973*a*).

The deformation variables required to describe the changes in each phase in an element can be derived from the continuity requirement for a multi-phase continuum (Fredlund 1973*a*, 1974). If the soil particles are assumed incompressible and the volume change of the contractile skin assumed internal to the element, the continuity requirement for an element reduces to,

$$[1] \quad \frac{\Delta V}{V} = \frac{\Delta V_w}{V} + \frac{\Delta V_a}{V}$$

where:

V = total volume,
 V_w = volume of water in the element, and
 V_a = volume of air in the element.

The measurement or prediction of any two of the above volume changes allows complete monitoring of the volume-weight change relationships. The amounts of air and water in the element can be represented respectively by one volumetric deformation state variable:

$$[2] \quad \theta_a = \frac{\Delta V_a}{V}$$

D.G. Fredlund. Professor, Department of Civil Engineering, University of Saskatchewan, 57 Campus Drive, Saskatoon, SK, Canada S7N 5A9.

N.R. Morgenstern. Professor, Department of Civil Engineering, University of Alberta, Edmonton, AB, Canada T6G 2G7.

Reproduced with permission from the *Canadian Geotechnical Journal*, **13**: 261–276.

$$[3] \quad \theta_w = \frac{\Delta V_w}{V}$$

The change in volume of the overall element (i.e., soil structure) can be written as the sum of the normal strain components.

$$[4] \quad \varepsilon = \frac{\Delta V}{V} = \varepsilon_x + \varepsilon_y + \varepsilon_z$$

where:

ε = volumetric strain,
 $\varepsilon_x, \varepsilon_y, \varepsilon_z$ = normal strain components in the x -, y -, and z - directions, respectively.

The independently derived stress and deformation state variables are linked by suitable constitutive relations. In the case of unsaturated soils, these are generally proposed from a semi-empirical standpoint and must be checked experimentally for uniqueness.

Literature review

In the considerations of three-dimensional consolidation by Biot (1941), the soil structure was assumed to behave as a linear, reversible, isotropic material. The soil was also assumed to be unsaturated in that the pore-water contained occluded air bubbles. The deformation was described in terms of the effective stress state variable ($\sigma - u_w$) and the pore fluid pressure, u_w . Biot (1941) also proposed a second constitutive relationship to describe the dependence of water content changes on the above stress variables. In total, four distinct physical soil properties were required to link the stress and deformation state variables.

Attempts to link the deformation of an unsaturated soil with the effective stress equation, proposed by Bishop (1959), have met with limited success (Jennings and Burland 1962). Bishop and Blight (1963) recognized these problems and concluded that the stress path of both components (i.e., $(\sigma - u_a)$ and $(u_a - u_w)$) must be considered. They suggested plotting volume change data versus both stress variables to form a three-dimensional plot. Burland (1965) reiterated his dissatisfaction with the effective stress equation by Bishop (1959) and proposed a set of constitutive relationships for the soil structure and the water phase.

Aitchison (1967) realized the importance of mapping volume changes with respect to the independent stress variables. Aitchison (1969) presented typical volume change curves obtained by following the $(\sigma - u_a)$ and $(u_a - u_w)$ stress paths, independently.

Matyas and Radhakrishna (1968) performed tests on identically prepared mixtures of 80% flint powder and 20% kaolin in which they controlled the total, air and water pressures in isotropic and K_0 compression tests. The constitutive surfaces of void ratio and degree of saturation versus the $(\sigma - u_a)$ and $(u_a - u_w)$ stresses were traced out using different stress paths to test their uniqueness. When the $(u_a - u_w)$ stress was decreased or the $(\sigma - u_a)$ stress was increased, the void ratio results traced out a

single warped surface with the soil structure always decreasing in volume. Normally, a reduction in suction ($u_a - u_w$), causes the soil to swell, but their results show overall volume decrease, indicating a metastable structured soil. Even though the soil structure indicates a collapse phenomenon, their results show a unique (i.e., soil structure) constitutive surface. The degree of saturation was always an increasing variable. When other stress paths were considered, the void ratio versus stress constitutive surface was not completely unique. Matyas and Radhakrishna (1968) state that the "restrictions on the paths arise from the fact that the hysteresis on the soil structure due to loading and unloading, wetting and drying, introduce certain non-unique characteristics". Their degree of saturation surfaces were not unique and the deviations were attributed to "incomplete saturation during the wetting process".

Barden et al. (1969) performed tests on low to highly plastic illite clay specimens. The total air and water pressures were controlled while investigating the effect of various stress paths during K_0 loading conditions. In all cases, the applied stress ($\sigma - u_a$) was increased subsequent to the initial conditions. In most cases the suction ($u_a - u_w$) was increased subsequent to the initial conditions; however, in a few cases it was decreased. Their results indicate that the soil structure volume change is dependent upon the direction of saturation. Barden et al. (1969) conclude "that hysteresis between saturation and desaturation processes is the major cause of stress path dependence". It was suggested that there is also a strong stress path dependence of the degree of saturation surface upon the reversal of the direction of saturation.

Brackley (1971) used two independent stress variables (i.e., $(\sigma - u_a)$ and $(u_a - u_w)$) in his study of partial collapse of unsaturated expansive clays. Difficulties were encountered in attempts to apply the effective stress equation presented by Bishop (1959). Subsequently, the description of volume change behavior was proposed as a function of the independent stress variables.

In this paper, the constitutive relations for an unsaturated soil are examined in the following manner:

- (1) the form and number of constitutive relationships for an unsaturated soil are proposed from a semi-empirical standpoint.
- (2) the constitutive surface is experimentally tested for uniqueness near a point. In other words, is the constitutive surface unique for small stress changes in various directions from a stress point? Limitations to uniqueness are established.

Proposed constitutive relations

(a) Soil structure

Insight to the constitutive relations for the soil structure may be obtained by inspecting incremental relations for a linear, elastic, isotropic material. Selecting $(\sigma - u_w)$ and $(u_a - u_w)$ as the stress state variables, the normal strain in the x -direction, ε_x , is,

$$[5] \quad \varepsilon_x = \frac{(\sigma_x - u_w)}{E_1} - \frac{\mu_1}{E_1} (\sigma_y + \sigma_z - 2\mu_w) + \frac{(u_a - u_w)}{H_1}$$

where:

E_1 = elastic modulus with respect to a change in $(\sigma - u_w)$,

μ_1 = Poisson's ratio with respect to relative strains in the x - and y - (or z -) directions, and

H_1 = elastic modulus with respect to a change in $(u_a - u_w)$.

Similar equations can be written for the y - and z - directions. The equations are essentially the same as those proposed by Biot (1941) and Coleman (1962). The volumetric strain of the soil structure, ε , is equal to the sum of the normal strain components (eq. [4]).

$$[6] \quad \varepsilon = C_t d(\sigma - u_w) + C_a d(u_a - u_w)$$

where:

C_t = compressibility of the soil structure with respect to a change in $(\sigma - u_w)$, and

C_a = compressibility of the soil structure with respect to a change in $(u_a - u_w)$.

For isotropic loading, σ is the all round stress.

$$C_t = 3 \left[\frac{1 - 2\mu_1}{E_1} \right]$$

For K_0 loading, σ is the major principal stress.

$$C_t = \frac{(1 + \mu_1)(1 - 2\mu_1)}{E_1(1 - \mu_1)}$$

For isotropic loading;

$$C_a = 3 / H_1$$

For K_0 loading;

$$C_a = \frac{(1 - \mu_1)}{H_1(1 + \mu_1)}$$

The above incremental equation (eq. [6]) can be written in a more general form to account for non-linear properties.

$$[7] \quad \varepsilon = \frac{1}{v} \frac{\partial v}{\partial(\sigma - u_w)} d(\sigma - u_w) + \frac{1}{v} \frac{\partial v}{\partial(u_a - u_w)} d(u_a - u_w)$$

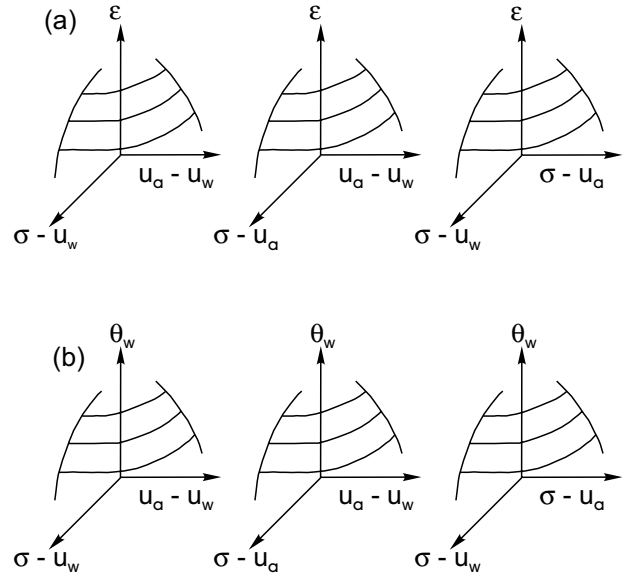
where:

v = unit volume

$\frac{1}{v} \frac{\partial v}{\partial(\sigma - u_w)}$ = compressibility of the soil structure when $d(u_a - u_w)$ is zero, and

$\frac{1}{v} \frac{\partial v}{\partial(u_a - u_w)}$ = compressibility of the soil structure when $d(\sigma - u_w)$ is zero.

All the above equations can be written using other combinations of stress state variables (Fig 1a). Using $(\sigma - u_a)$ and $(\sigma - u_w)$, the general equation for the soil structure takes the form,



$$[8] \quad \varepsilon = \frac{1}{v} \frac{\partial v}{\partial(\sigma - u_a)} d(\sigma - u_a) + \frac{1}{v} \frac{\partial v}{\partial(u_a - u_w)} d(u_a - u_w)$$

The stress state variables $(\sigma - u_a)$ and $(\sigma - u_w)$ can also be used to form similar equations. Any one of the above three forms can be used; however, only one of the equations is independent.

It must be emphasized that the soil structure (or void ratio) constitutive relationship is not sufficient to completely describe the change in state of an unsaturated soil. Either the air or water phase constitutive relations must also be formulated. Due to the compressible nature of the air phase, it is recommended that the water phase (or water content) constitutive relationship be formulated. The water content versus soil suction equation generally used in the soil physics area (Childs 1969) becomes a special case of the total description of state.

(b) Water phase

The water phase constitutive relation describes the volume of water present in the referential soil structure element. The water is assumed to be incompressible and the equation accounts for the net inflow or outflow of water from the element. The water phase constitutive relation can be formulated semi-empirically on the basis of a linear combination of the state variables.

$$[9] \quad \theta_w = \frac{(\sigma_x + \sigma_y + \sigma_z - 3u_w)}{3H_1} + \frac{(u_a - u_w)}{R_1}$$

where:

θ_w = net inflow or outflow of water,

R_1 = water volumetric modulus associated with a change in $(u_a - u_w)$, and

H_1 = water volumetric modulus associated with a change in $(\sigma - u_w)$.

Equation [9] can be written in a more general form to account for non-linear soil properties.

$$[10] \quad \theta_w = \frac{1}{v} \frac{\partial v_w}{\partial(\sigma - u_w)} d(\sigma - u_w) + \frac{1}{v} \frac{\partial v_w}{\partial(u_a - u_w)} d(u_a - u_w)$$

where:

v_w = volume of water in the element,

$\frac{1}{v} \frac{\partial v_w}{\partial(\sigma - u_w)}$ = slope of the water volume versus $(\sigma - u_w)$ plot when $d(u_a - u_w)$ is zero, and

$\frac{1}{v} \frac{\partial v_w}{\partial(u_a - u_w)}$ = slope of the water volume versus $(u_a - u_w)$ plot when $d(\sigma - u_w)$ is zero.

Equation [10] applies for isotropic and K_0 loading; however, the slopes contain different combinations of the water volumetric modulus. Other combinations of stress state variables can also be used to derive the volumetric representation of the change in the amount of water in the element (Fig. 1b). The specialization of eq. [10] used in soil physics relates water content to changes in matric suction $(u_a - u_w)$.

(c) Air phase

The change in volume of air present in an element can be written as the difference between the soil structure volume change and the change in the volume of water present in the element.

Sign convention for deformation soil properties

A positive or negative sign must be associated with each deformation (or compressibility) modulus since the direction of deformation is not necessarily known. That is, an increase in a stress state variable does not always produce a volume change in the same direction. For example, a decrease in suction $(u_a - u_w)$ in a stable-structured soil will result in swelling, whereas, it may cause a volume decrease in a meta-stable soil (Barden et al. 1969). Even for a particular soil, the direction of deformation is not fixed with respect to a single stress state variable. Rather, it can depend upon the component of the stress state variable that is changed. Consider, for example, the $(u_a - u_w)$ stress variable and the deformation of the soil structure. The suction can be increased by either increasing the air pressure or decreasing the water pressure. If the air pressure is increased in an unsaturated soil, the soil structure often expands. If the water pressure is decreased, the soil structure generally compresses. Therefore, when establishing the direction of deformation, it is necessary to either establish the stress component being changed (i.e., u_a or u_w) or else simultaneously consider

the stress state variables affected (e.g., $(\sigma - u_w)$ and $(u_a - u_w)$).

The suggested sign convention is as follows: if an increase in the stress state variable produces a phase volume decrease, the deformation modulus is POSITIVE. If the stress variable increase produces a volume increase, the compressibility modulus is NEGATIVE. The same sign convention is applicable to the soil structure, air and water phases.

Procedure to experimentally verify the uniqueness of the constitutive surface

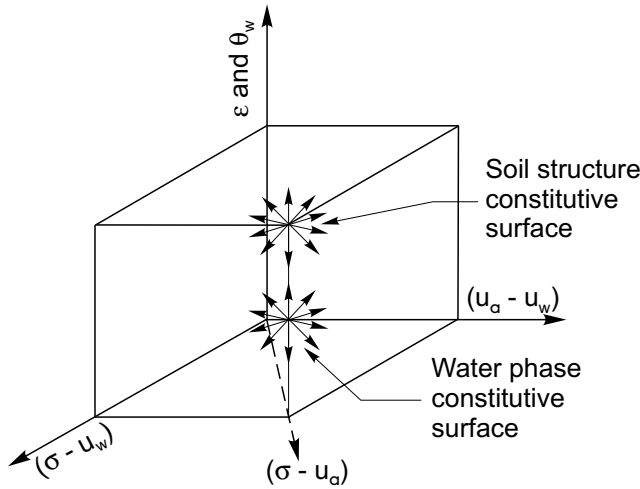
Two constitutive surfaces are required for the complete description of volume changes sustained by an unsaturated soil. Their uniqueness can be explored; first, in terms of small deviations from a stress point and second, in terms of larger stress state variable changes and reversals of stress. This paper examines only the uniqueness of the constitutive relations near a stress point. The term “uniqueness” is used to indicate that there is one and only one relationship between state variables. However, if complete “uniqueness” does not exist, the term “uniqueness” can be used in a more restrictive sense. For large stress changes, the drying and wetting of soils introduces hysteresis into the constitutive surfaces. In the restricted sense, the term “uniqueness” can be applied to either the drying surface or the wetting surface. The water phase constitutive surface can be tested for “uniqueness” in a similar manner.

Let us suppose that it is possible to prepare several “identical” unsaturated soil specimens that are subjected to the same total pressure and the same air and water pressures. Therefore, all specimens are at the same stress point in space and have the same initial volume-weight properties. Then let each specimen be subjected to varying stress changes, while monitoring the volume changes associated with each phase (Fig. 2). If the constitutive surface is essentially planar near a stress point, the deformation moduli associated with any orthogonal directions can be used to describe the deformations produced by other changes in the stress variables.

The above tests are somewhat fictitious since they would be difficult and extremely time consuming to conduct. Therefore, a simpler and more rapid procedure was adopted. One specimen was subjected to small stress increments along three stress paths. Using the deformations from any two of the increments, it is possible to compute two corresponding compressibility moduli. Now the deformation equation can be used to compute the anticipated deformation along any other stress path. The computed deformation is compared with the measured deformation. The constitutive surface at a point is unique if the measured and predicted deformations are essentially equal in all cases.

Three suitable stress paths are traced by changing the total, air and water pressures and allowing equalization after each pressure change (Fig. 3). The uniqueness tests can be applied to any of the proposed constitutive equa-

Fig. 2. Ideal tests to prove uniqueness of the soil structure and water phase constitutive surface at a point.



tions (i.e., soil structure, air and water phases). As an example, let us consider the soil structure deformations for the above case. One form of the constitutive equation for the soil structure is,

$$\frac{dv}{v} = C_t d(\sigma - u_w) + C_a d(u_a - u_w)$$

Suppose the first pressure increment is a decrease in the total stress. Therefore,

$$C_t = \frac{dv/v}{d(\sigma - u_w)}$$

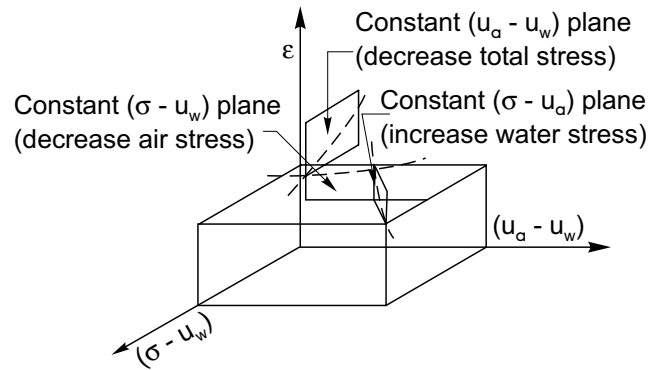
Let the second pressure change be an increase in the air pressure. Therefore,

$$C_a = \frac{dv/v}{d(u_a - u_w)}$$

Now that the two compressibility moduli are known (i.e., C_t and C_a), the volume change corresponding to a change in the pore-water pressure can be computed. This value can be compared with the measured volume change. Agreement indicates uniqueness of the constitutive surface at a point. Some discrepancy is anticipated since all stress changes do not initiate from the same stress point.

The procedure used in most of the tests was as follows. The specimen was allowed to come to equilibrium under an arbitrary set of stress conditions. An attempt was made to have a large initial suction. The water pressure was generally increased for the first pressure increment. After equalization, the air pressure was decreased. After equalization, the total pressure was decreased. The above procedure was repeated through several cycles as long as the suction remained positive. Throughout these steps, the water phase volume was continually increasing. The soil structure and air phase generally underwent a reversal in

Fig. 3. Stress path adhered to for the uniqueness test at a point.



their direction of volume change. The soil structure and water phase constitutive surfaces are analyzed in detail since they were measured independently in the laboratory.

Description of Equipment

Four pieces of equipment were used in the examination of volume change behavior of unsaturated soils (Fredlund 1973a). Two pieces of equipment consisted of modified Anteus oedometers¹ for one-dimensional strain conditions. The specimens were 2½ inch (6.4 cm) in diameter and approximately 1 inch (2.5 cm) in height. The other two pieces of equipment allowed isotropic volume change testing conditions in modified Wykeham Farrance triaxial cells. The specimens were 4 inch (10.2 cm) in diameter and approximately 2½ inch (6.4 cm) in height.

The air and water pressures were separated by means of a high air entry disk placed at the bottom of the specimen. Distilled, de-aired water was used below the high air entry disk. Although the high air entry disks do not leak air at pressures less than their air entry value, dissolved air diffuses through the water in the disk and collects below the base of the disk. For accurate water volume change measurements, it was necessary to measure the volume of diffused air and apply the appropriate correction. The diffused volume was measured by periodically flushing the base plate and measuring the volume of air displacing water in an inverted burette (Fredlund 1975).

The Anteus oedometer was selected for modification due to its versatile design. Figure 4 shows the layout of the modified Anteus oedometer and associated plumbing equipment. The chamber of the oedometer (normally filled with water for back pressuring the water phase of soils) was filled with air to regulate the air pressure in the soil specimen. All pressures were controlled using pressure regulators with an accuracy better than ±0.02 psi (0.14 kN/m²). The valves on Fig. 4 associated with the total air, water, and diffused air pressure control are labelled with a T, A, W, and D, respectively.

¹The Anteus oedometers are manufactured by Test-lab Corporation in the United States.

Fig. 4. Layout of modified Anteus oedometer.

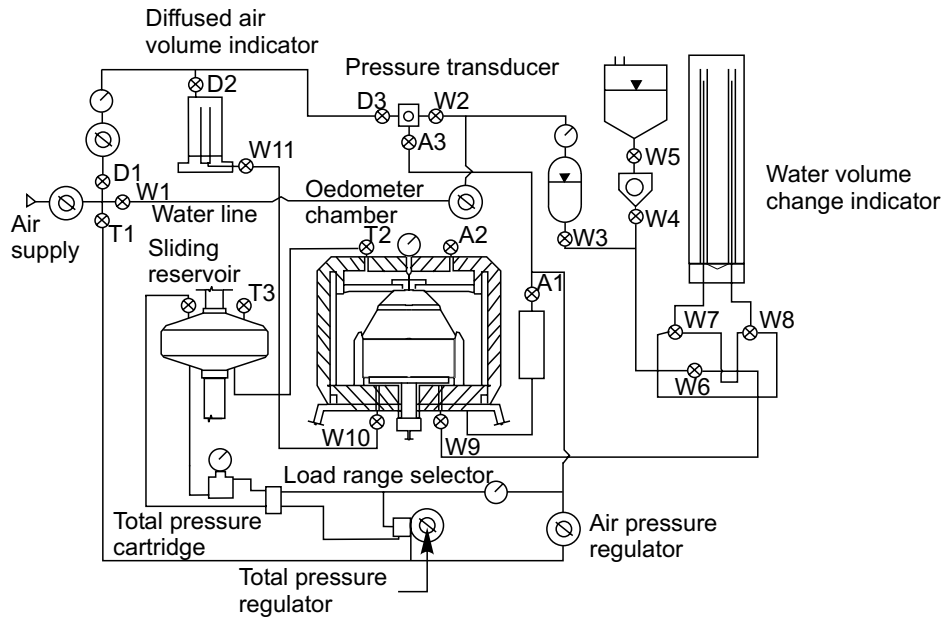
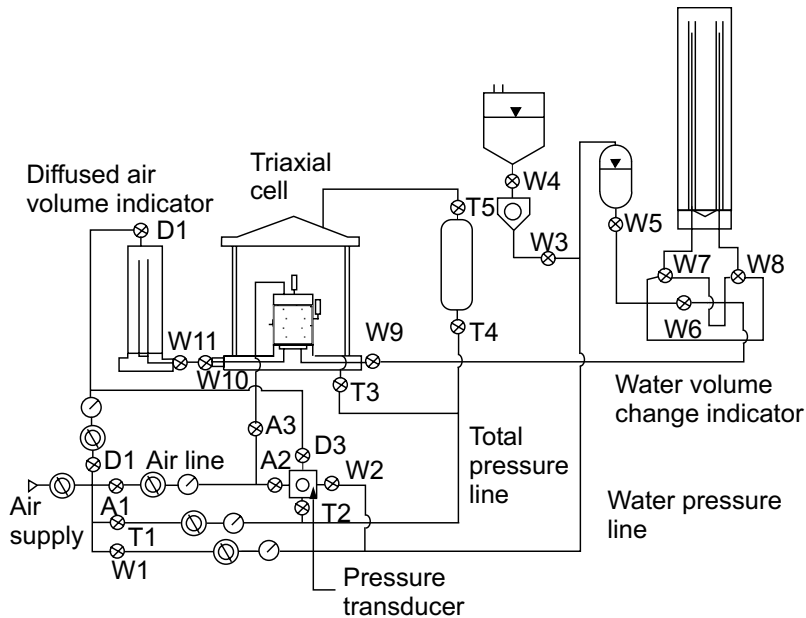


Fig. 5. Layout of modified triaxial tests.



The modified Wykeham Farrance triaxial cell is shown in Fig. 5. Linear voltage displacement transducers (LVDT's) were used to measure the vertical and lateral displacements. The cell was pressurized with air. A composite membrane consisting of slotted aluminum foil, vacuum grease, and two latex membranes was used to prevent the diffusion of air from the cell into the specimen.

Presentation of test data

Four series of experiments were run to test the constitutive surfaces for uniqueness. The first three specimens

(No. 15A, 16, and 17) were undisturbed Regina Clay, while specimen No. 21 was compacted kaolin. Specimens No. 15A and 17 were from a depth of 2 ft (0.6 m) and specimen No. 16 was from a depth of 15 ft (4.6 m) below a grassy area in north-west Regina, Saskatchewan. The shallow specimens exhibited a very nuggetty macro-fissured structure due to desiccation (Fredlund 1973a). The properties of the soils tested are shown in Table 1.

Table 2 summarizes the initial volume-weight properties and stress conditions at the start of each pressure change.

The volume changes observed as a result of the stress component changes are summarized in Table 3. The vol-

Table 1. Soil properties of specimens used for uniqueness tests.

Soil type	Sample numbers	Specific gravity	Liquid limit (%)	Plastic limit (%)	Sand sizes (%)	Silt sizes (%)	Clay sizes (%)
Regina clay	15A	2.78	75.0	26.0	5	30	65
	16	2.78	77.0	26.8	0	45	55
	17	2.78	76.3	25.4	—	—	—
Kaolin	21	2.62	64.2	34.7	2	35	63

Table 2. Initial volume-weight properties and initial stress conditions for uniqueness tests

Test No.	Initial pressures			Water content (%)	Void ratio (%)	Degree of saturation (%)
	σ (psi)	u_a (psi)	u_w (psi)			
Specimen No. 15A						
C-1	77.71	50.01	1.47	18.46	0.7990	64.21
C-2	77.91	50.14	12.19	21.56	0.8020	74.73
C-3	77.92	40.15	12.11	21.70	0.8014	75.28
C-4	67.63	40.16	12.11	22.09	0.8058	76.20
C-5	67.89	40.16	21.92	23.04	0.8106	79.02
C-6	67.92	30.19	22.21	23.54	0.8099	80.80
Specimen No. 16						
C-7	71.46	50.18	3.66	26.28	0.8354	87.44
C-8	71.39	50.16	13.57	26.51	0.8374	88.01
C-9	71.30	40.04	13.48	26.69	0.8321	89.18
C-10	61.11	39.72	13.18	26.92	0.8364	89.47
C-11	61.29	39.93	23.25	27.23	0.8404	90.08
C-12	61.44	30.11	23.39	27.68	0.8355	92.09
C-13	51.65	30.29	23.52	28.08	0.8435	92.53
Specimen No. 17						
C-14	77.72	50.01	1.50	22.51	0.7510	83.31
C-15	77.76	49.98	11.50	23.03	0.7577	84.48
C-16	77.84	39.99	11.45	23.20	0.7582	85.07
C-17	67.67	39.99	11.37	23.66	0.7646	86.04
Specimen No. 21						
C-18	82.04	61.20	4.36	31.60	1.0425	79.92
C-19	71.97	60.93	4.08	31.61	1.0441	79.86
C-20	72.06	51.09	4.22	31.56	1.0445	79.84
C-21	72.02	51.00	14.20	31.71	1.0453	79.81
C-22	62.41	51.23	14.24	31.83	1.0508	79.60
C-23	62.64	41.58	14.43	31.91	1.0510	79.59
C-24	62.46	41.34	24.13	32.29	1.0543	79.46
C-25	52.53	41.16	23.80	32.56	1.0717	78.79
C-26	52.53	31.13	23.80	33.26	1.0681	78.93
C-27	52.25	30.86	28.40	34.45	1.0682	78.94
C-28	43.06	31.46	28.91	35.10	1.0830	78.37
C-29	52.06	31.13	28.63	35.04	1.0749	78.67
C-30	52.02	31.09	23.76	34.32	1.0696	78.87
C-31	81.35	31.27	23.85	33.17	1.0251	80.61
C-32	81.07	61.07	23.66	32.44	1.0260	80.57

ume changes at two elapsed times are considered for each specimen since it is difficult to determine the point of complete equalization.

The object of the uniqueness analysis is to compute

two compressibility values and use these compressibilities to predict volume change in a third direction. The predicted volume change can be compared with a laboratory measured value.

Table 3. Volume-changes corresponding to stress component changes for uniqueness tests.

Test No.	Elapsed time (min)	Stress component changes			Percentage volume change		
		$\Delta\sigma$ (psi)	Δu_a (psi)	Δu_w (psi)	Soil structure	Air	Water
Specimen No. 15A							
C-1	1000	0	0	+10.54	-0.060	+0.080	-0.140
C-1	5000	0	0	+10.54	-0.188	+0.070	-0.258
C-2	1000	0	-9.96	0	+0.030	+0.190	-0.160
C-2	5000*	0	-9.96	—	+0.04	+0.44	-0.40
C-3	1000	-10.29	0	0	-0.110	-0.005	-0.105
C-3	5000	-10.29	0	0	-0.230	+0.280	-0.510
C-4	1000	0	0	+9.68	-0.050	+0.150	-0.200
C-4	5000	0	0	+9.68	-0.175	+0.565	-0.740
C-5	1000	0	-10.13	0	+0.045	+0.275	-0.230
C-5	5000	0	-10.13	0	+0.040	+0.860	-0.820
C-6	1000	-10.04	0	0	-0.110	+0.076	-0.185
C-6	5000	-10.04	0	0	-0.215	+0.385	-0.600
Specimen No. 16							
C-7	2000	0	0	+9.95	+0.035	+0.163	-0.128
C-7	15000	0	0	+9.95	-0.090	+0.202	-0.292
C-8	2000	0	-10.03	0	+0.315	+0.375	-0.060
C-8	15000	0	-10.03	0	+0.290	+0.570	-0.280
C-9	2000	-9.88	0	0	-0.160	-0.055	-0.105
C-9	15000	-9.88	0	0	-0.255	+0.060	-0.315
C-10	2000	0	0	+9.88	-0.075	+0.040	-0.115
C-10	15000	0	0	+9.88	-0.220	+0.235	-0.455
C-11	2000	0	-9.96	0	+0.225	+0.315	-0.090
C-11	15000	0	-9.96	0	+0.265	+0.790	-0.525
C-12	2000	-9.94	0	0	-0.210	-0.083	-0.127
C-12	15000	-9.94	0	0	-0.430	+0.150	-0.580
C-13	2000	-9.85	0	0	-0.335	-0.182	-0.153
C-13	15000	-9.85	0	0	-0.705	-0.058	-0.647
Specimen No. 17							
C-14	1000	0	0	0	-0.100	+0.090	-0.190
C-14	5000	0	0	0	-0.360	+0.230	-0.590
C-15	1000	0	-9.95	0	+0.018	+0.068	-0.050
C-15	5000	0	-9.95	0	-0.060	+0.230	-0.290
C-16	1000	-10.13	0	+10.04	-0.140	-0.050	-0.090
C-16	5000	-10.13	0	+10.04	-0.345	+0.135	-0.480
C-17	1000	0	0	0	-0.095	+0.105	-0.200
C-17	5000	0	0	0	-0.280	+0.320	-0.600
Specimen No. 21							
C-18	2000	-9.80	0	0	-0.110	-0.078	-0.032
C-18	10000†	-9.80	0	0	-0.070	-0.080	+0.010
C-19	2000	0	-9.95	0	-0.015	-0.015	0.000
C-19	10000†	0	-9.95	0	-0.015*	-0.015	0.000*
C-20	2000	0	0	+10.04	-0.033	+0.167	-0.200
C-20	10000†	0	0	+10.04	-0.020*	+0.350	-0.370*
C-21	2000	-9.75	0	0	-0.290	-0.120	-0.170
C-21	10000†	-9.75	0	0	-0.320	-0.170	-0.150
C-22	2000	0	-9.86	0	-0.037	+0.053	-0.090
C-22	10000†	0	-9.86	0	-0.010*	+0.090	-0.100*
C-23	2000	0	0	+9.91	-0.127	+0.258	-0.385
C-23	10000†	0	0	+9.91	-0.180*	+0.310	-0.490*
C-24	2000	-9.68	0	0	-0.700	-0.405	-0.295
C-24	10000	-9.68	0	0	-0.820	-0.494	-0.326
C-25	2000	0	-10.03	0	+0.235	+0.805	-0.570

Table 3. (Concluded).

Test No.	Elapsed time (min)	Stress component changes			Percentage volume change		
		$\Delta\sigma$ (psi)	Δu_a (psi)	Δu_w (psi)	Soil structure	Air	Water
Specimen No. 21							
C-25	10000	0	-10.03	0	+0.180	+1.067	-0.887
C-26	2000	0	0	+4.87	-0.005	+0.655	-0.660
C-26	15000	0	0	+4.87	-0.010	+1.510	-1.520
C-27	2000	-9.74	0	0	-0.595	-0.130	-0.465
C-27	15000	-9.74	0	0	-0.730*	+0.120	-0.850*
C-28	2000	+9.30	0	0	+0.315	+9.260	+0.055
C-28	10000†	+9.30	0	0	+0.360*	+0.280	+0.080*
C-29	2000	0	0	-4.83	+0.090	-0.390	+0.480
C-29	20000†	0	0	-4.83	+0.260*	-0.670	+0.930*
C-30	2000	+29.20	0	0	+1.890	+0.870	+1.020
C-30	10000	+29.20	0	0	+2.160	+0.710	+1.450
C-31	2000	0	+30.03	0	-0.080	-0.730	+0.650
C-31	15000	0	+30.03	0	+0.045	-0.910	+0.955
C-32	2000	0	0	+29.86	-0.526	+0.456	-0.982
C-32	12000	0	0	+29.86	-0.567	+0.663	-1.230*

*Deformations are very approximate.

† Estimated equilibrium conditions.

Comparison of predicted and measured volume changes

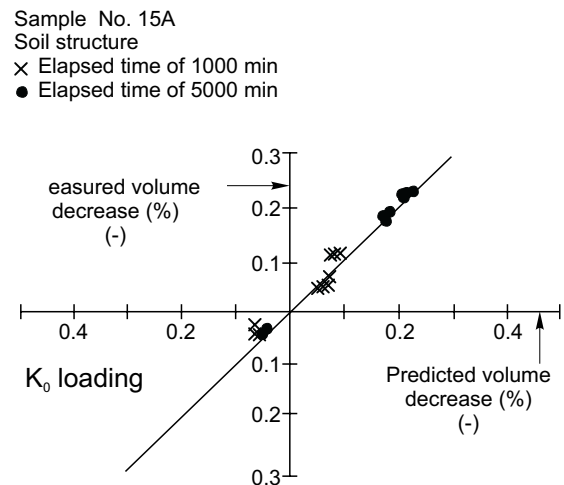
The predicted and measured volume changes can be visually assessed by plotting the predicted volume changes versus the measured volume changes. In addition, a statistical correlation between the predicted and measured volume changes helps quantify the agreement. The degree of correlation can be expressed in terms of the correlation coefficient, the slope, and intercept of the best-fit straight line (Neville and Kennedy 1966). Uniqueness would imply a slope of 1.0 and an intercept of 0. The correlation coefficient is a measure of the dispersion about the best-fit line. The significance of the correlation coefficient can be evaluated by comparing the computed value with the value that can be expected at a given level of significance. A high correlation coefficient implies causation and the existence of a reliable mathematical model for the constitutive surface.

Soil Structure

Figure 6 shows the agreement between the measured volume changes and the predicted volume changes for specimen No. 15A. Specimen No. 15A was tested under K_0 loading conditions. For elapsed times of 1000 and 5000 min, all points fall essentially along the 45° line, indicating virtually perfect correlation.

Specimen No. 16 (Fig. 7), tested under isotropic loading conditions, shows considerably more dispersion in the data. The correlation on the results at an elapsed time of 15000 min are superior to those at 2000 min. For some stress changes, it is possible to compare the predicted volume change with both a previous and subsequent measured volume change. In these cases, the graph shows a

Fig. 6. Comparison of predicted and measured soil structure volume changes for specimen No. 15A.



bar between the two comparisons. The accuracy of the volume measuring devices was such that it should not have caused discrepancies in the uniqueness analysis. The scatter in the results must be considered in terms of the demanding requirements of the test for uniqueness. For example, it would be anticipated that the effects of non-linearity of the constitutive surface and hysteresis are factors that could introduce significant scatter. These will be dealt with in more detail later.

Specimen No. 17 (Fig. 8) was tested under K_0 loading conditions. There is a good correlation between the predicted and measured soil structure volume changes. However, there are only a limited number of comparisons that can be made.

Fig. 7. Comparison of predicted and measured soil structure volume changes for specimen No. 16.

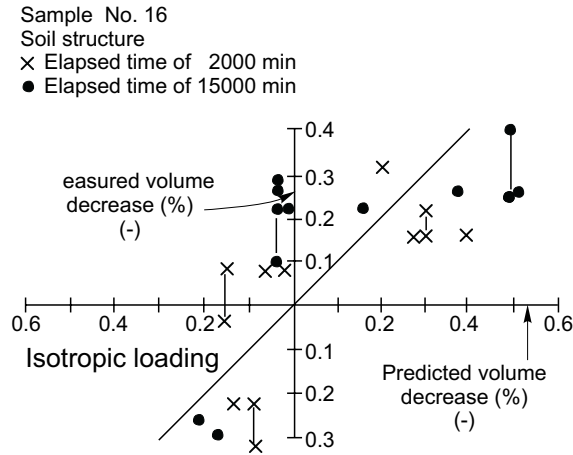


Fig. 8. Comparison of predicted and measured soil structure volume changes for specimen No. 17.

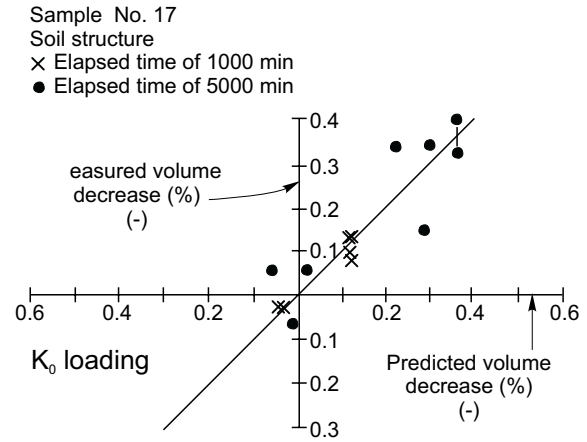


Table 4. Summary of regression analysis for soil structure assuming a linear constitutive surface.

Specimen No.	No. of comparisons	Critical coefficient of correlation 1% significance	Coefficient of correlation	Slope	Intercept
15A (1000 min)	12	0.68	0.961	0.901	-0.009
15A (5000 min)	12	0.68	0.999	0.993	-0.002
16 (2000 min)	12	0.68	0.750	0.678	+0.038
16 (15000 min)	12	0.68	0.779	0.763	+0.026
17 (1000 min)	6	0.91	0.961	0.850	-0.017
17 (5000 min)	6	0.91	0.904	0.650	-0.102
21 (2000 min)	30	0.46	0.293	0.230	-0.082
21 (Equilibrium conditions)	30	0.46	0.458	0.358	-0.090

Table 5. Summary of regression analysis using a logarithmic constitutive surface.

Specimen No.	No. of observations	Critical coefficient of correlation 1% significance	Correlation coefficient	Slope	Intercept
15A (5000 min)	12	0.68	0.983	1.049	+0.014
16 (15000 min)	12	0.68	0.820	0.928	+0.041
17 (5000 min)	6	0.91	0.858	0.609	-0.111
21 (Equilibrium conditions)	30	0.46	0.410	0.339	-0.095
	15*	0.62	0.390	0.293	-0.242

*Omission of first three and last four tests due to inconsistent order of changing stresses.

Specimen No. 21 was a compacted kaolin specimen tested under isotropic loading. The results indicated a low correlation. They are reviewed later in terms of the effect of non-linearity and hysteresis.

Table 4 shows a summary of the statistical properties for the soil structure, assuming a linear constitutive surface locally. Specimens No. 15A, 16, and 17 show correlation coefficients exceeding the critical correlation coefficient for a one percent level of significance. The weighted average intercept on the above specimens was -0.001 and the slope was 0.82. The average results show the intercept tending towards zero and the slope tending towards 1.0.

The correlation between the predicted and measured volume changes was also checked, assuming a non-linear constitutive surface (Table 5). The assumption made was that volume change varied as the logarithm of the stress state variables. The effect of a non-linear constitutive surface can be partly compensated for by correcting all slopes to the same stress point in space. Each compressibility is assumed to correspond to the mean of the initial and final stress points. All compressibilities are then corrected to the mean stress point.

Specimen No. 15A showed a virtually “perfect” correlation using the linear analysis and remains essentially the same for non-linear analysis. The non-linear analysis of

Table 6. Summary of regression analysis using a non-linear constitutive surface and applying a correction for hysteresis.

Specimen No.	No. of observations	Critical coefficient of correlation 1% significance	Correlation coefficient	Slope	Intercept
15A (5000 min)	12	0.68	0.969	0.971	-0.005
16 (15000 min)	13	0.66	0.868	1.145	-0.006
	12*	0.68	0.934	0.953	-0.006
17 (5000 min)	6	0.91	0.969	0.963	-0.008
21 (Equilibrium conditions)	30	0.46	0.831	0.829	+0.034
	15†	0.62	0.939	0.957	-0.056

*Omission of C-10 and C-11 due to inaccurate measurements.

†Omission of first three and last four tests since the order of changing stresses does not lend itself to a systematic comparison of measured and predicted deformations.

specimen No. 16 shows a marked improvement over the linear analysis. Specimen No. 17 showed a slight decrease in correlation coefficient when the compressibilities were corrected for non-linearity. Specimen No. 2 did not show any improvement in the statistical properties as a result of the correlations for non-linearity.

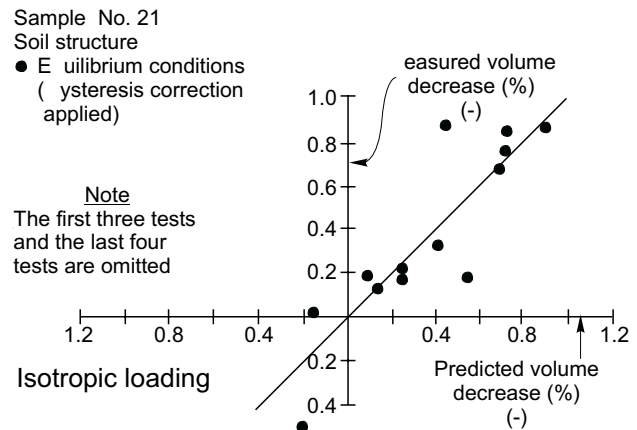
Tests No. 15A and 17 were performed on a heavily overconsolidated clay (i.e., Regina Clay). The effects of hysteresis should be small in the loading and unloading range considered. On the other hand, the kaolin specimen compacted to one-half standard compaction, should have pronounced hysteresis.

The change in air pressure generally resulted in a reversed direction of soil structure deformation. In the case of the compacted kaolin (specimen No. 21), there were considerably different amounts of volume change depending upon whether the volume was increasing or decreasing. It would appear that hysteresis associated with the change in the air pressure may be the key factor contributing to dispersion in the case of specimen No. 21. The effect of hysteresis due to an air pressure change was investigated by assuming that the predicted volume change due to an air pressure change was equal to the measured volume change. The deformation due to a change in total and water pressures remain the same. Obviously, this will produce an improvement in the correlation coefficient. However, conclusions must be based on the magnitude of the improvement of the correlation coefficient. Table 6 summarizes the statistical properties obtained when the above procedure is used to compensate for hysteresis.

The correlation coefficient for specimen No. 16 increased slightly to 0.87. By omitting the data from the check using tests C-10 and C-11, the correlation coefficient improved to 0.93. Although there is some improvement in the correlation coefficient, it is not dramatic and may indicate that the Regina Clay behavior approaches that of an elastic reversible material.

The statistical properties of specimen No. 21 show a dramatic improvement as a result of compensating for hysteresis. Considering all the data, the correlation coefficient improved from 0.41 to 0.83 (non-linear analysis). The slope of the best-fit line increased from 0.34 to 0.83 and the intercept changed from -0.09 to +0.03. Omitting

Fig. 9. Comparison of predicted and measured soil structure volume changes for specimen No. 21 (hysteresis correction applied).



the results from the first three and the last four pressure increments, the statistics are further improved (Fig. 9). The correlation coefficient rose to 0.94, the slope to 0.96, while the intercept went to -0.06. The analysis isolates soil structure hysteresis as the prime cause of dispersion between predicted and measured deformations.

Water Phase

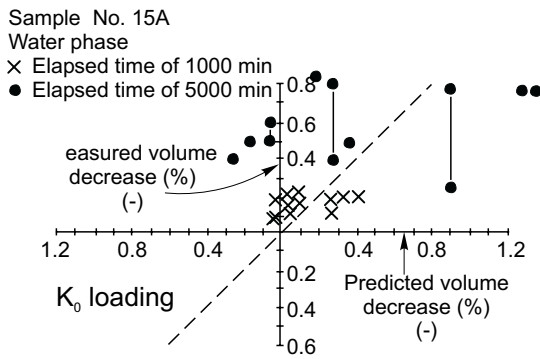
The laboratory testing technique associated with the water phase constitutive surface is considerably more difficult than for the soil structure constitutive surface. This factor influences the uniqueness analysis in addition to the effects of non-linearity and hysteresis.

The statistical properties on the water phase volume changes deviate more from those of "perfect" conditions than do the soil structure volume changes (Table 7). Figure 10 shows the comparison of predicted and measured water volume changes for specimen No. 15A. This test was performed in a one-dimensional oedometer and it was later discovered that some moisture was lost from the specimen by movement through the lucite walls of the chamber. The loss of even a small amount of moisture has a very pronounced affect on the uniqueness analysis. The excellent correlation from the uniqueness analysis on

Table 7. Summary of regression analysis for water phase assuming a linear constitutive surface.

Specimen No.	No. of comparisons	Critical coefficient of correlation of correlation 1% significance	Coefficient of correlation	Slope	Intercept
15A (1000 min)	12	0.68	0.484	0.124	-0.153
15A (5000 min)	12	0.68	0.514	0.116	-0.538
16 (2000 min)	12	0.68	0.645	0.168	-0.089
16 (15000 min)	12	0.68	0.153	0.027	-0.395
17 (1000 min)	6	0.91	0.583	2.028	+0.152
21 (2000 min)	30	0.46	0.582	0.606	-0.052
21 (Equilibrium conditions)	30	0.46	0.612	0.475	-0.227

Fig. 10. Comparison of predicted and measured water phase volume changes for specimen No. 15A.

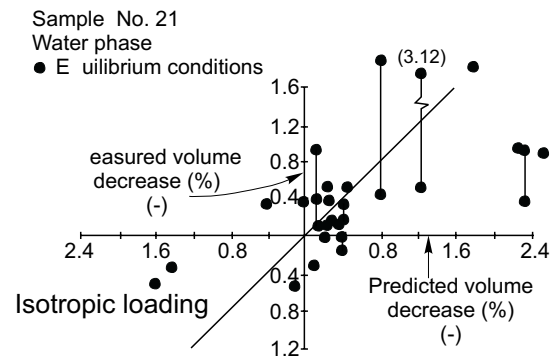


the soil structure (specimen No. 15A) showed that hysteresis cannot be considered as the factor causing the low correlation for the water phase. It is quite definite that specimen No. 15A experienced some loss of moisture during the test and this factor was investigated. An attempt was made to correct for the loss of moisture by observing the steady state rate of moisture loss at large elapsed times. When these corrections were applied, the correlation coefficient increased to 0.82 which is well above the critical correlation coefficient. However, the slope of the best-fit line is relatively low (0.55) and the intercept is quite far from zero (0.12).

Specimen No. 16 also showed relatively poor correlation between the predicted and measured water volume changes. When the results were corrected for the effects of soil structure hysteresis, the correlation coefficient increased from 0.15 to 0.89. This is well above the critical correlation coefficient of 0.71 for a 1% level of significance. The slope increased from 0.43 to 0.80. The marked improvement in statistical properties indicates that hysteresis in the soil structure produced dispersion in the water phase constitutive surface.

The results from specimen No. 17 showed a close agreement between the predicted and measured water volume changes. However, the total number of checks was only six. Specimen No. 21 (Fig. 11) showed relatively good agreement between the predicted and measured results. When the results are corrected for hysteresis (and the first three and the last four checks are omitted), the correlation coefficient increased to 0.82

Fig. 11. Comparison of predicted and measured water phase volume changes for specimen No. 21.



which is well above the critical correlation coefficient of 0.46 for a 1% level of significance. The slope of the best-fit line increased to 0.54. The intercept was -0.63 which is higher than desirable but appears related to two 'checks' showing a large discrepancy.

Conclusions

- (1) Two constitutive relations are required to describe the volume change behavior of an unsaturated soil. The first proposed equation is for the soil structure (eq. [8]).

$$\epsilon = \frac{1}{v} \frac{\partial v}{\partial(\sigma - u_a)} d(\sigma - u_a) + \frac{1}{v} \frac{\partial v}{\partial(u_a - u_w)} d(u_a - u_w)$$

The second proposed equation is for the change in volume of water in the element (eq. [10]).

$$\theta_w = \frac{1}{v} \frac{\partial v_w}{\partial(\sigma - u_a)} d(\sigma - u_a) + \frac{1}{v} \frac{\partial v_w}{\partial(u_a - u_w)} d(u_a - u_w)$$

The proposed constitutive equations were tested for uniqueness by determining the modulus of deformation in two directions and comparing the predicted and measured volume changes in a third direction.

- (2) Tests were performed on samples of over-consolidated, undisturbed Regina Clay and com-

pacted kaolin. These soils are typical of the range of properties commonly encountered.

(a) For the soil structure constitutive relationship, the volume changes predicted agreed well with the measured values for Regina Clay. Corrections for non-linearity of the constitutive surface and hysteresis upon loading and unloading showed further improvement in the correlation. The compacted kaolin showed relatively poor correlation between the predicted and measured volume changes. However, the correlation showed a dramatic improvement when corrections were applied for hysteresis.

Since hysteresis is a significant factor contributing to non-uniqueness, it is concluded that the proposed constitutive equation for the soil structure be used for monotonic deformations. Therefore, the compressibility moduli would be different for decreasing volume changes than for volume increases.

(b) The agreement between the predicted and measured water phase volume changes were not as close as those for the soil structure. The main cause of dispersion is associated with the difficulty in measuring minute water volume changes over long periods of time. This factor was in addition to the effects of non-linearity and hysteresis. Attempted corrections for the above factors showed a marked improvement in the correlation of predicted and measured water volume changes. It is concluded that the proposed water phase constitutive equation be used as well for monotonic water phase volume changes.

- (3) For complete monitoring of unsaturated soil behavior, laboratory testing should be done under conditions where the total, air and water pressures are controlled. The overall volume change should be measured.
- (4) The laboratory tests on unsaturated soils indicate that the proposed constitutive equations can be used for engineering practice.

References

- Aitchison, G.D. 1967. Separate roles of site investigation, quantification of soil properties, and selection of operational environment in the determination of foundation design on expansive soils. Proceedings, 3rd Asian Regional Conference on Soil Mechanics and Foundation Engineering, Haifa, Israel, Vol. 3, pp. 72–77.
- Aitchison, G.D. 1969. Soil suction in foundation design. Proceedings, 7th International Conference on Soil Mechanics and Foundation Engineering, Mexico, Vol. 2, pp. 1–8.
- Barden, L., Madedro, A.O., and Sides, G.R. 1969. Volume change characteristics of unsaturated clay. ASCE, Journal of Soil Mechanics and Foundation Division, **95**(SMI): 33–51.
- Biot, M.A. 1941. General theory of three dimensional consolidation. Journal of Applied Physics, **12**: 155–164.
- Bishop, A.W. 1959. The principle of effective stress. Lecture delivered in Oslo, Norway, in 1955. Teknisk Ukeblad, **106**(39): 859–863.
- Bishop, A.W. and Blight, G.E. 1963. Some aspects of effective stress in saturated and unsaturated soils. Géotechnique, **13**: 177–197.
- Brackley, I.J.A. 1971. Partial collapse in unsaturated expansive clay. Proceedings, 5th Regional Conference on Soil Mechanics and Foundation Engineering, South Africa, pp. 23–30.
- Burland, J.B. 1965. Some aspects of the mechanical behavior of partly saturated soils. In *Moisture equilibrium and moisture changes in soils beneath covered areas. A symposium in print. Edited by G.D. Aitchison, Butterworth and Company (Australia) Ltd., Sydney, Australia, pp. 270–278.*
- Childs, E.C. 1969. The physical basis of soil water phenomena. Wiley-Interscience, John Wiley and Sons Ltd., London, England.
- Coleman, J.D. 1962. Stress/strain relations for partly saturated soil. Correspondence, Géotechnique, **12**(4): 348–350.
- Davies, J.T., and Rideal, E.K. 1963. Interfacial phenomena. Second edition, Academic Press Inc., New York, N. Y.
- Fredlund, D.G. 1973a. Volume change behavior of unsaturated soils. Ph.D thesis, University of Alberta, Edmonton, AB, Canada.
- Fredlund, D.G. 1973b. Discussion at “The 2nd Technical Session Division Two (Flow shear Strength). Proceedings, 3rd International Conference on Expansive Soils, Vol. 2, Jerusalem Academic Press Ltd., Haifa, Israel, pp. 71–76.
- Fredlund, D.G. 1974. Engineering approach to soil continua. Proceedings, 2nd Symposium on the Applications of Solid Mechanics, Hamilton, ON, Vol. 1, pp. 46–59.
- Fredlund, D.G. 1975. A diffused air volume indicator for unsaturated soils. Canadian Geotechnical Journal, **12**(4): 533–539.
- Jennings, J.E., and Burland, J.B. 1962. Limitations to the use of effective stresses in partly saturated soils. Géotechnique, **12**(2): 125–144.
- Matyas, E.L., and Radhakrishna, H.S. 1968. Volume change characteristics of partially saturated soils. Géotechnique, **18**(4): 432–448.
- Neville, A.M., and Kennedy, J.B. 1966. Basic statistical methods for engineers and scientists. International Textbook Co., Scranton, PE.

Volume change indices during loading and unloading of an unsaturated soil

D.Y.F. Ho, D.G. Fredlund, and H. Rahardjo

Abstract: The paper presents the volume change theory and the designation of associated soil properties that must be measured for an unsaturated soil. The equipment required for the measurement of each of the relevant volume relationships is described. Several testing procedures for obtaining the volume change indices during loading and unloading of an unsaturated soil are presented. Typical results from loading and unloading tests on compacted silt and compacted glacial till specimens are presented and analyzed. The analysis is given in order to illustrate the application of the volume change theory to practical problems.

Key words: unsaturated soil, volume change indices, constitutive relations, coefficients of volume change, oedometer tests.

Introduction

Many geotechnical works involve soils with negative pore-water pressures, and often these soils are unsaturated. Natural soils above the groundwater table and compacted soils in roads and earth dams are typical examples of unsaturated soils. Volume changes in a soil due to applied loads or environmental changes (i.e., rainfall and evaporation) are of interest to practising engineers.

The volume change theory and testing procedures for saturated soils are well known to geotechnical engineers. Extensions to the theory and testing procedures are required for the prediction of volume changes in an unsaturated soil. These extensions are presented in the paper. Typical volume changes during loadings and unloadings of unsaturated, compacted silts and glacial tills are presented and analyzed to illustrate the application of the extended theory.

Constitutive relations for an unsaturated soil

In saturated soils, volume changes due to loading are usually presented as a relationship between void ratio, e , and effective stress, $(\sigma - u_w)$, where σ is the total normal stress and u_w is the pore-water pressure, expressed on a logarithmic scale¹ (Terzaghi 1943). The logarithmic slope of the loading curve is called the compression index, C_c , and the logarithmic slope of the unloading curve is called the swell index, C_s . The void ratio, e , versus $\log(\sigma - u_w)$ relationship is obtained from conventional consolidation

tests. The soil volume change associated with the soil structure of a saturated soil is always equal to the water volume change.

In an unsaturated soil, two stress state variables govern the volume change behavior; namely, net normal stress, $(\sigma - u_a)$, and matric suction, $(u_a - u_w)$, where u_a is pore-air pressure. Therefore, the void ratio, e , must now be related to the $(\sigma - u_a)$ and $(u_a - u_w)$ stress state variables (Fig. 1). In addition, an independent relationship for the water content, w , (Fig. 2) is required to obtain a complete description of the volume change in an unsaturated soil. These constitutive surfaces are the same as those proposed by Fredlund and Morgenstern (1976). The difference between the soil structure and water volume changes is equal to the air volume change.

Void ratio constitutive surface

The soil structure constitutive surface is a concave, warped surface when plotted on an arithmetic scale. The same surface resembles a quarter section of the convex surface of a vertical cone when plotted on a semi-logarithmic scale. A schematic diagram of the soil structure constitutive surfaces for monotonic volume changes is shown in Fig. 1. The intersection curves of the arithmetic surface of void ratio on the $(\sigma - u_a)$ and $(u_a - u_w)$ planes (Fig. 1a) result in the definition of four compressibility coefficients (i.e., a_t , a_{ts} , a_m , and a_{ms}) where a_t and a_{ts} are coefficients of compressibility and swelling with respect to the net normal stress for monotonic volume decrease and increase, and a_m and a_{ms} are coefficients of

D.Y.F. Ho. Geo-environmental Group, EBA Engineering Consultants Ltd., Civil, Geotechnical, and Materials Engineers, Edmonton, AB, Canada.

D.G. Fredlund. Department of Civil Engineering, University of Saskatchewan, 57 Campus Drive, Saskatoon, SK, Canada S7N 5A9.

H. Rahardjo. School of Civil and Structural Engineering, Nanyang Technological University, Singapore, Singapore.

Reproduced with permission from the *Canadian Geotechnical Journal*, **29**: 195–207, 1992.

¹Note that, for simplicity in this paper, variables expressed on a logarithmic scale are indicated as the log of the variables in question, e.g., the effective stress graphed on a logarithmic scale is indicated as $\log(\sigma - u_w)$.

Fig. 1. Proposed soil structure constitutive surfaces for an unsaturated soil. Schematic diagram of the void ratio constitutive surfaces for monotonic volume changes on *a*) an arithmetic scale and *b*) a semi-logarithmic scale; ---, swelling or rebound; —, compression.

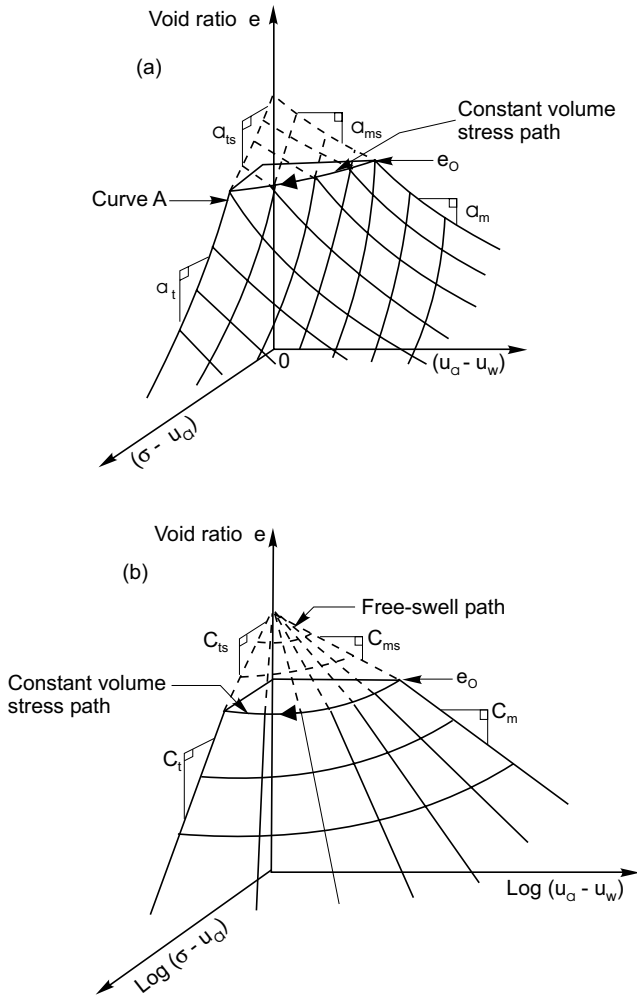
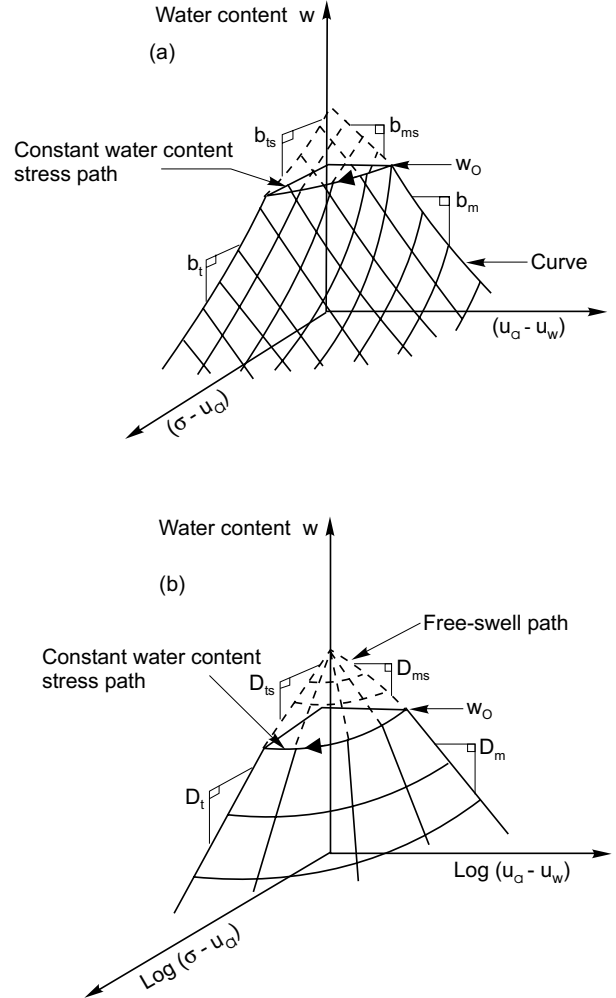


Fig. 2. Proposed water content constitutive surfaces for an unsaturated soil. Schematic diagram of the water content constitutive surfaces for monotonic volume changes on *a*) an arithmetic scale and *b*) a semi-logarithmic scale; ---, water content increase; —, water content decrease.



compressibility and swelling with respect to the matric suction for monotonic volume decrease and increase.

The shape of the intersection curve on the $(\sigma - u_a)$ plane is well established when matric suction is equal to zero (i.e., e versus $(\sigma - u_w)$ curve). This curve is the same as the conventional consolidation curve for a saturated soil. A typical compression of a natural, saturated soil consists of recompression and virgin compression branches (Terzaghi and Peck 1967). The virgin compression curve is exponential on an arithmetic scale and can be linearized on a semi-logarithmic plot. The rebound curves are approximately parallel to one another and can be linearized on a semi-logarithmic scale (Schmertmann 1955; Holtz and Gibbs 1956; Gilchrist 1963; Noble 1966; Lambe and Whitman 1979; Lidgren 1970; Chen 1975).

Soils can be overconsolidated by desiccation and rebounded due to a suction decrease. The virgin compression branch and rebound curves are essentially linear on a semi-logarithmic scale (Fredlund 1967; Aitchison and

Woodburn 1969; Escario 1969; Aitchison and Martin 1973; Richards et al. 1984). There are pressure range limits that must be kept to ensure linearity. A constant volume (i.e., constant void ratio) stress path, where an unsaturated soil is moving towards saturation, is essentially a straight line on an arithmetic plot of the stress state variables (Escario 1969). The same path becomes a convex asymptotic curve on a logarithmic scale.

Water phase constitutive surface

There is insufficient information in the literature to definitely define the form of the water phase constitutive surface. The water content and void ratio constitutive relations are interrelated by the specific gravity, G_s , when a soil is saturated (i.e., e is equal to wG_s , when S is equal to 100%). Conclusions arrived at for the void ratio constitutive relation are also assumed to apply to the water phase constitutive relation. There is evidence that the water content versus matric suction constitutive curves on a

semi-logarithmic scale are essentially linear when the net normal stress is equal to zero (Croney and Coleman 1954; Fredlund 1967; McWhorter and Nelson 1979; Mitchell and Avalle 1984). Once again, there are pressure limits within which there is linearity. The same curves are therefore approximately exponential on arithmetic plots.

There is no known experimental information available on the shape of a constant water content stress path on the constitutive surface. When a soil approaches saturation, a change in net normal stress becomes as effective as a change in matric suction in changing the water content. A constant water content stress path must therefore approach a 45° line when the matric suction tends to zero. This angle forms an upper limit. A constant water content stress path on the water phase constitutive surface will be assumed to be a straight line on an arithmetic plot of water content versus net normal stress and matric suction (Fig. 2a). The resulting constitutive surface is a concave surface when water content is increased or decreased. The same surface resembles a quarter section of the convex surface of a vertical cone on a water content versus the logarithm of net normal stress and matric suction.

A schematic diagram of the water phase constitutive surfaces for monotonic volume changes is presented in Fig. 2. The intersection curves of the arithmetic surface of water content on the $(\sigma - u_a)$ and $(u_a - u_w)$ planes (Fig. 2a) result in four coefficients of water change; namely, b_t , b_{ts} , b_m , and b_{ms} , where b_t and b_{ts} are the coefficient of water content change and rebound coefficient of water content change with respect to the net normal stress for monotonic water content decrease and increase, respectively; and b_m and b_{ms} are the coefficient of water content change and the rebound coefficient of water content change with respect to the matric suction for monotonic water content decrease and increase, respectively.

The above volumetric deformation coefficients vary from one state point to another along a non-linear constitutive surface. A direct method to determine these coefficients at a specific state point is to measure their magnitude at the stress point under consideration. The experimental measurements required are similar to those conducted for the verification of the constitutive surfaces. It may require numerous specimens and a long period of testing if the entire constitutive surface is to be defined.

A simpler procedure would be to assume that the constitutive surface is planar at a particular void ratio or water content. Therefore, every point on the surface corresponding to an equal void ratio or water content plane would have the same a_t and a_m coefficients or b_t and b_m coefficients, respectively. As a result, the a_t and b_t coefficients obtained from the saturation plane (i.e., $(u_a - u_w)$ equal to zero plane) can be used for other points on the surface as long as the void ratio (or water content) is constant. Similarly, the a_m and b_m coefficients obtained from the zero net normal stress plane (i.e., $(\sigma - u_a)$ equal to zero plane) can also be used for other points on the

surface along a constant void ratio or water content plane. In other words, the values of a_t , a_m , b_t , and b_m obtained on the saturation and zero net normal stress planes can be used for the entire constitutive surface.

The above method of determination of the volumetric coefficients is much simpler than defining the entire constitutive surface. However, it may be inferior to the use of the direct determination of volume change coefficients obtained at individual state points. The applicability of this approach will depend primarily on the character of the constitutive surfaces as established through laboratory experiments and on the reliability required in an analysis. The required level of accuracy in solving a problem must also be borne in mind when using the above assumption. In general, the suggested procedure may be sufficiently accurate for many geotechnical applications.

Semi-logarithmic forms of constitutive surfaces

The logarithmic plots of constitutive surfaces (Figs. 1b and 2b) exhibit linear curves on the extreme planes (i.e., the plane with $\log(u_a - u_w)$ approximately equal to zero and the plane with $\log(\sigma - u_a)$ approximately equal to zero). The slopes of the curves on these extreme planes are called indices. The volumetric deformation indices associated with the void ratio surface (Fig. 1b) are C_t , C_{ts} , C_m , and C_{ms} , where C_t and C_{ts} are the compressive and swelling indices with respect to the net normal stress for monotonic volume decrease and increase, respectively; and C_m and C_{ms} are the compressive and swelling indices with respect to the matric suction for monotonic volume decrease and increase, respectively.

The volumetric deformation indices associated with the water phase surface (Fig. 2b) are D_t , D_{ts} , D_m , and D_{ms} , where D_t and D_{ts} are the water content and the rebound water content indices with respect to the net normal stress for monotonic water content decrease and increase, respectively; and D_m and D_{ms} are the water content and the rebound water content indices with respect to the matric suction for monotonic water content decrease and increase, respectively.

The C_t , C_m , D_t , and D_m indices can be obtained from the same test data used to obtain the a_t , a_m , b_t , and b_m coefficients. The difference is in the manner in which the results are plotted. Using a conversion between a semi-logarithmic and an arithmetic scale (Lambe and Whitman 1979), the C_t , C_m , D_t , and D_m indices can be written in terms of the a_t , a_m , b_t , and b_m coefficients.

$$[1] \quad C_t = \frac{a_t(\sigma - u_a)_{ave}}{0.435}$$

$$[2] \quad C_m = \frac{a_m(u_a - u_w)_{ave}}{0.435}$$

$$[3] \quad D_t = \frac{b_t(\sigma - u_a)_{ave}}{0.435}$$

$$[4] \quad D_m = \frac{b_m(u_a - u_w)_{ave}}{0.435}$$

where:

$(\sigma - u_a)_{ave}$ = average of the initial and final net normal stresses for an increment, and

$(u_a - u_w)_{ave}$ = average of the initial and final matric suctions for an increment.

Despite the linear curves on the extreme planes, the cross-section of the constitutive surface on the $\log(\sigma - u_a)$ and $\log(u_a - u_w)$ planes is no longer a series of straight lines as are found on the $(\sigma - u_a)$ and $(u_a - u_w)$ planes. Figure 3 shows a comparison of the constitutive surface cross section at a constant void ratio when plotted using the arithmetic and logarithmic scales. An essentially linear cross section on the arithmetic plot becomes an asymptotic curve on the logarithmic plot.

The asymptotic cross-section curve suggests the logarithmic form of the void ratio constitutive surface as illustrated in Fig. 4a. An approximated form of the void ratio constitutive surface can be used in the analysis as shown in Fig. 4b. The approximated surface consists of three planes; namely, planes I, II, and III. The three planes converge at a void ratio ordinate corresponding to nominal values of the stress state variables (i.e., $\log(\sigma - u_a) \approx 0$ and $\log(u_a - u_w) \approx 0$). Planes I and III are referred to as the orthogonal planes. Plane I is perpendicular to the void ratio versus $\log(\sigma - u_a)$ plane, and the slope of plane I gives the C_t index. Plane III is perpendicular to the void ratio versus $\log(u_a - u_w)$ plane, and the slope of plane III gives the C_m index. In other words, only one index is required to describe the void ratio changes when the stress state variable changes occur within the regions defined by planes I and III. Therefore, the constitutive equation describing plane I can be written as:

$$[5] \quad de = C_t d[\log(\sigma - u_a)]$$

and the equation for plane III is as follows:

$$[6] \quad de = C_m d[\log(u_a - u_w)]$$

Plane II represents a transition zone between planes I and III. This plane intersects both the void ratio versus $\log(\sigma - u_a)$ plane and the void ratio versus $\log(u_a - u_w)$ plane. The slopes of the intersection lines define the slopes of plane II; namely, the C_t' , and C_m' , indices. In this case, two indices are required to describe void ratio changes when the stress state variable changes occur within the region of plane II. The constitutive equation describing plane II can be written as:

$$[7] \quad de = C_t' d[\log(\sigma - u_a)] + C_m' d[\log(u_a - u_w)]$$

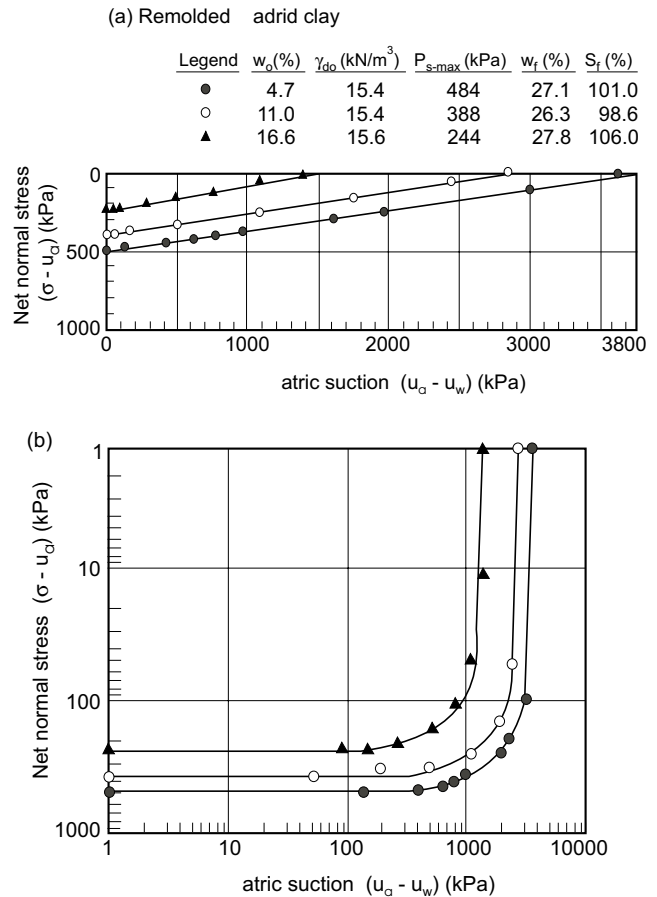
where:

C_t' = slope of the intersection line of plane II with the e versus $\log(\sigma - u_a)$ plane, and

C_m' = slope of the intersection line of plane II with the e versus $\log(u_a - u_w)$ plane.

It should also be noted that line B associated with plane II is assumed to be parallel to line A which joins planes I and III (Fig. 4b). This assumption is required in constructing the intersection lines of plane II on the ex-

Fig. 3. Cross sections of void ratio surfaces plotted on a) $(\sigma - u_a)$ and $(u_a - u_w)$ planes (arithmetic scale) and b) $\log(\sigma - u_a)$ and $\log(u_a - u_w)$ planes (logarithmic scale) (modified from Escario 1969).



treme planes as illustrated in Fig. 5. Line B intersects the extreme planes at points B_1 and B_2 . The lines joining the intersection points B_1 and B_2 to the convergence void ratio ordinate gives the C_t' and C_m' indices, respectively.

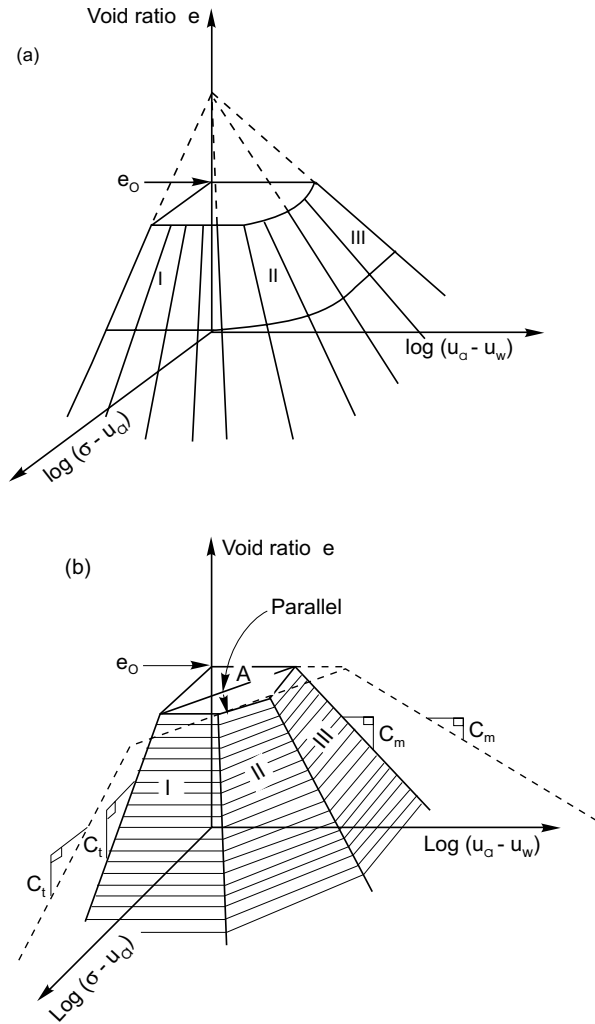
Unloading constitutive surfaces

The above approximation is also applicable to the unloading surface of void ratio (Ho 1988). The shape of the water content constitutive surface is not fully understood. It is a matter of speculation to assume that the water content constitutive surface is similar in shape to the void ratio constitutive surface. This assumption; however, is not substantiated by experimental data.

Relationships between volume change indices

The relationships between the volume change indices associated with the loading conditions can best be visualized by presenting the intersection curves on one plot (Ho and Fredlund 1989; Rahardjo et al. 1990). The intersection curves 1 and 2 from the void ratio surface (Fig. 6a) are combined in Fig. 6b. The slopes of curves 1 and 2 are called C_t and C_m volume change indices, respectively.

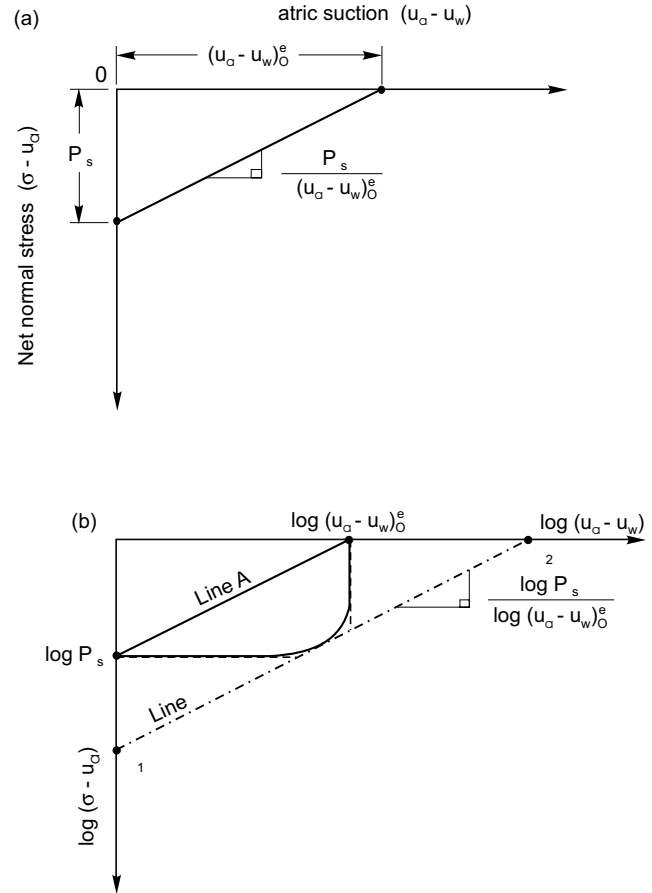
Fig. 4. Logarithmic forms of void ratio constitutive surface for loading conditions (from Ho 1088); *a*) void ratio constitutive surfaces for loading as plotted logarithmically; *b*) approximated form of the void ratio constitutive surface in the logarithmic plot.



The intersection curves 3 and 4 from the water content surface (Fig. 6c) are combined in Fig. 6d. The water content w can be multiplied by the specific gravity G_s (i.e., wG_s) to make use of the basic volume-mass relationship (i.e., $Se = wG_s$, where S is degree of saturation) in obtaining one of the index relationships. This means that curves 3 and 4 in Fig. 6c are translated vertically by a magnitude of G_s in Fig. 6d. As a result, the slopes of curves 3 and 4 in Fig. 6d are the products of G_s and the volume change indices (i.e., $D_t G_s$, and $D_m G_s$, respectively).

Curve 1 in Fig. 6 is essentially the consolidation curve for the soil in a saturated condition (i.e., $u_a - u_w = 0$, or $u_a = u_w$). The curve exhibits a linear relationship between void ratio and the logarithmic scale of net normal stress, over a wide loading range. The slope of curve 1, C_t , is equal to the compression index, C_c , of the saturated soil. Curve 3 in Fig. 6d coincides with curve 1 from Fig. 6b,

Fig. 5. Construction of lines A and B from constant-volume oedometer test results. Constant-volume path on *a*) an arithmetic scale and *b*) a logarithmic scale. P_s' , corrected swelling pressure; $(u_a - u_w)_0^e$, matric suction corresponding to zero net normal stress at a constant void ratio. —, actual stress path; - · - · -, approximate stress path.



since wG_s is equal to the void ratio when the soil is saturated (i.e., S is equal to 1). Therefore, the water content index, D_t , can be computed as C_t/G_s .

Curve 4 in Fig. 6 is called a soil-water characteristic curve that can be obtained from a pressure-plate test (see test procedures and equipment). A shrinkage test curve combined with the soil-water characteristic curve can be used to construct curve 2 in Fig. 6. In other words, the four volume change curves and their corresponding indices (i.e., C_t , D_t , D_m , and C_m) can be obtained from routine soil tests.

The combined plot of curves 1, 2, 3, and 4 is presented in Fig. 7, which is essentially a combination of Figs. 6b and 6d. The arrows in Fig. 7 indicate the direction of curves 2 and 4 approaching curve 1 as the initial degree of saturation of the soil increases. In this case, curve 1 is assumed to remain constant for various initial degrees of saturation. When the soil is saturated (i.e., $u_a - u_w = 0$, or $u_a = u_w$), the void ratio and wG_s vary only with respect to

Fig. 6. Void ratio and water content relationship for an unsaturated soil. *a)* void ratio relationship; *b)* intersection curves between void ratio surface and $\log(\sigma - u_a)$ or $\log(u_a - u_w)$ plane; *c)* water content relationship; *d)* intersection curves between water content surface and $\log(\sigma - u_a)$ and $\log(u_a - u_w)$ plane.

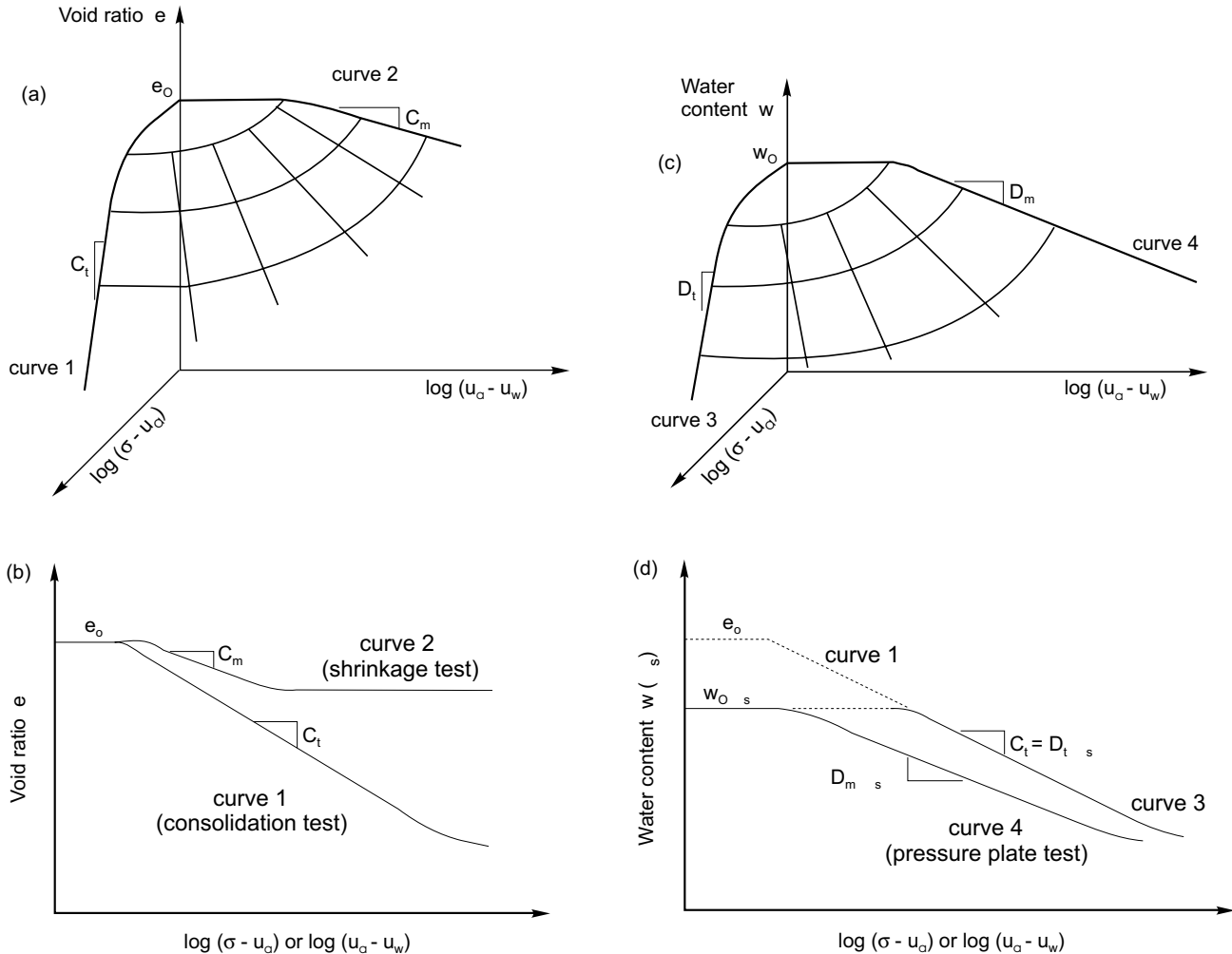
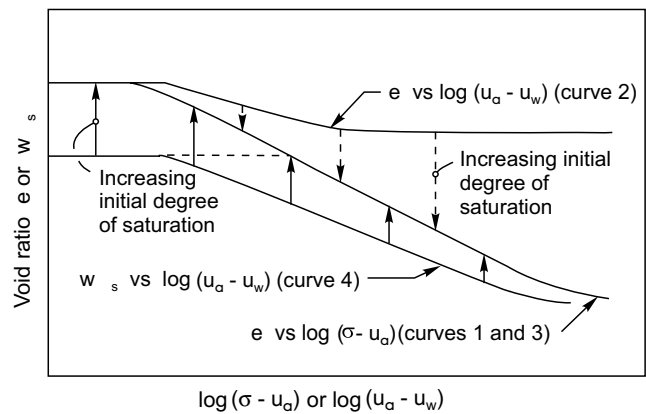


Fig. 7. Relationship between curves that define the volume change behavior of an unsaturated soil.

net normal stress or the effective stress $(\sigma - u_w)$ following the same curve (i.e., curve 1 in Fig. 7).

The volume change indices pertinent to the unloading conditions can be obtained from the unloading portion of the consolidation curve and the free-swell test. Unloading curves with respect to the net normal stress $(\sigma - u_a)$ are approximately parallel to one another (Lambe and Whitman 1979). Therefore, the unloading curve established at the end of the loading sequence can also be considered as the unloading curve of the specimen from its initial state. The slope of the unloading curve from the conventional consolidation test is commonly referred to as the swell index, C_s , which can be considered to be equal to the C_{ts} index. Similar to the loading conditions, the rebound water content index, D_{ts} , can be computed as C_{ts}/G_s .

The C_{ms} and D_{ms} indices are obtained from the free-swell test where the soil specimen undergoes a wetting process under a nominal applied load (i.e., $\sigma - u_a$). The soil matric suction $(u_a - u_w)$ is reduced to a nominal mag-



nitude at the end of the test. The state path followed during the free-swell test is indicated in Figs. 1 and 2. Measurements of void ratio and water content changes during

the free-swell test allow the determination of the C_{ms} and D_{ms} indices, respectively.

Test procedures and equipment

In addition to conventional oedometer tests, there are two other tests required for obtaining the volume change indices for an unsaturated soil. The other two tests are referred to as the pressure-plate test and the shrinkage test.

Oedometer tests

The procedures for performing oedometer tests on unsaturated soil specimens (e.g., compacted specimens) are outlined in ASTM D4546 (ASTM 1985a). This ASTM standard describes three methods for inundating the soil specimen prior to performing the compression test. During inundation, the soil matric suction is brought to zero, and the results can be used to calculate the swelling potential of the soil. The inundation can be conducted under either constant-volume or free-swell conditions. The test can be performed using regular consolidometers.

Curve 1 in Figs. 6 and 7 illustrates the oedometer test results with constant-volume inundation at the beginning of the test. Having inundated the soil specimen, the test can proceed using the conventional procedure used for saturated specimens (ASTM D2435, ASTM 1985b). The decreasing void ratios are plotted against the logarithmic scale of effective stress ($\sigma - u_w$) to yield curves 1 and 3 as shown in Figs. 6 and 7.

At the end of the loading process, the soil specimen can be unloaded with respect to the net normal stress. The increasing void ratios are plotted against the logarithmic scale of effective stress ($\sigma - u_w$) to yield the rebound curve with a slope equal to C_{ts} or $D_{ts}G_s$.

The void ratio versus $\log(u_a - u_w)$ curves at a nominal value of $\log(\sigma - u_a)$ are established by conducting the free-swell inundation with void ratio and water content measurements. In this case, more specialized equipment, such as a modified Anteus consolidometer for the K_σ loading condition, is required. The modified Anteus consolidometer allows the control of total, pore-air, and pore-water pressures and the measurements of total and water volume changes during the tests. The soil specimen can be wetted by injecting water through hypodermic needles installed in the loading cap. This procedure was found to be faster than introducing water to the specimen through the high air entry disk at the base of the specimen (Ho 1988).

Pressure-plate tests

The soil-water characteristic curve (i.e., curve 4 in Figs. 6 and 7) of a soil relates the water content to the applied matric suction in the soil. In an unsaturated soil, the pore-air pressure is usually atmospheric (i.e., u_a is equal to zero) and the pore-water pressure is negative. The difference in pressures is called the soil matric suction ($u_a - u_w$). In the laboratory, a matric suction is commonly applied to a soil specimen by maintaining a zero pore-water pressure (i.e., u_w is equal to zero) and applying a

positive pore-air pressure. Therefore, the matric suction in the soil specimen (i.e., $u_a - u_w$, where u_w is maintained at zero pressure in the compartment below a high air entry disk) can be varied by applying different air pressures to the specimen. This procedure is referred to as the axis-translation technique (Hilf 1956).

Pressure-plate extractors (Soilmoisture Equipment Corporation, Santa Barbara, CA) are used to establish the soil-water characteristic curve, and the equipment is shown in Figs. 8 and 9. The extractors are commonly used to apply the various matric suctions to the soil specimen, and the test is called a pressure-plate test (ASTM D2325-68, ASTM 1981). The pressure-plate extractor consists of a high air-entry ceramic disk contained in an air pressure chamber. The high air-entry disk is saturated and always in contact with water in a compartment below the disk which is maintained at zero water pressure.

A soil specimen is placed on top of the disk, and the airtight chamber is pressurized to a desired matric suction. The disk does not allow the passage of air as long as the applied matric suction does not exceed the air-entry value of the disk. This air-entry value is related to the diameter of the fine pores in the ceramic disk. Therefore, the air-entry value of the disk controls the maximum air pressure or matric suction that can be applied to the specimen.

The application of matric suction to the soil causes the pore water to drain to the water compartment through the disk. A burette can be connected to the compartment to measure the water volume changes. At equilibrium, the soil will have a reduced water content corresponding to the increased matric suction. The water content can also be computed at each equilibrium condition from the water volume change measurements if only one specimen is being tested. If more than one specimen is being tested, it is necessary to dismantle the chamber and measure the weight of the specimen at each applied pressure. This procedure is commonly used with 5 and 15 bar ceramic plate extractors, when several specimens are tested simultaneously. Plots of the equilibrium water contents versus the logarithms of the corresponding matric suctions give rise to curve 4 in Figs. 6 and 7.

Shrinkage tests

A shrinkage test gives the relationship between the void ratio and the water content for various matric suctions. A soil specimen can either be allowed to dry in the air or it can be subjected to various matric suctions using the pressure-plate extractors. In either case, the void ratio and water content of the specimen can be measured at various equilibrium states. When the specimen is allowed to dry in air, the process should be interrupted at various stages while the sample is covered and allowed to come to equilibrium.

Accurate measurements of void ratio can be performed following the techniques used in the shrinkage limit test (ASTM D427, ASTM 1985c). The shrinkage test involves the measurements of the total volume of the soil specimen using either direct measurements or the

Fig. 8. Volumetric pressure-plate extractor (i.e., maximum applied matric suction is 200 kPa) (photography courtesy of Soilmoisture Equipment Corporation, Santa Barbara, CA).

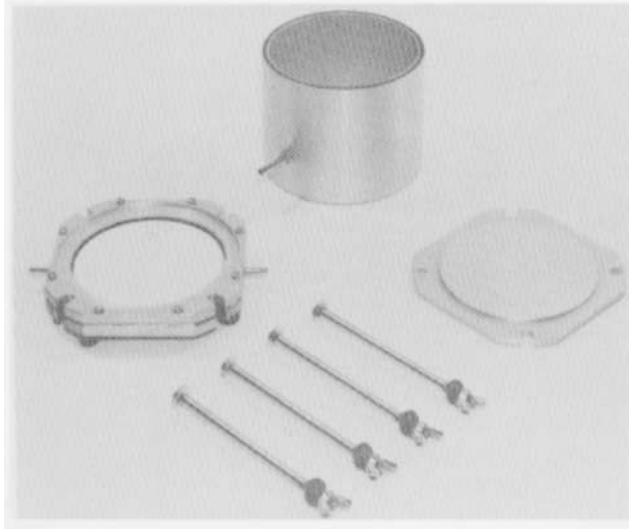
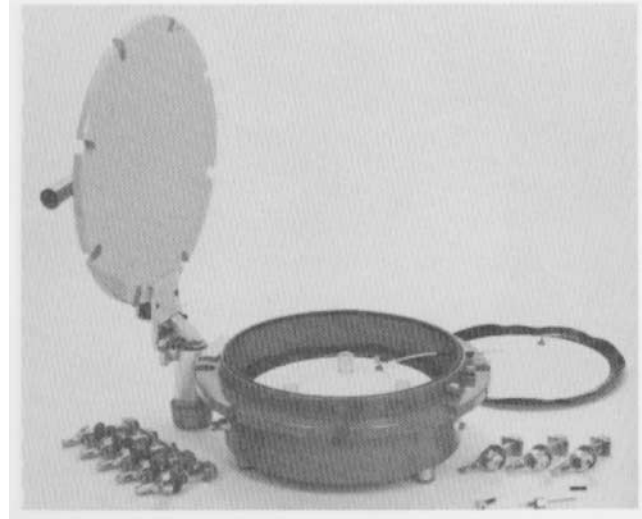


Fig. 9. Fifteen bar ceramic-plate extractor (i.e., maximum applied matric suction is 1500 kPa) (photography courtesy of Soilmoisture Equipment Corporation, Santa Barbara, CA).



mercury-displacement technique. Using the mercury-displacement technique, the volume of the displaced mercury during immersion is equal to the total volume of the specimen.

Direct measurements of total volume can be performed using callipers. The shrinkage curve can be constructed by plotting the void ratios against the water contents as the soil matric suction changes. The test is generally performed for the case of increasing matric suction.

A combination of the shrinkage test data and the water content versus matric suction test data can be used to compute the void ratio versus matric suction relationship for a soil.

Laboratory test program

Two soils, a uniform silt and a glacial till, were tested, and their index properties presented in Table 1. An attempt was made to prepare specimens with near identical initial conditions. Each soil was oven dried and hand mixed with a predetermined quantity of distilled water. The wet soil was placed in a sealed plastic bag and left to cure in a constant humidity and temperature room. The difference in water content between batches of the same soil was controlled to within 0.5%. Specimens were formed by static compaction at one-half standard Proctor compaction effort at either “dry of optimum” or “at optimum” initial water contents. The compaction characteristics of the silt and glacial till are given in Table 1.

Test results and discussion

The above tests were conducted on compacted silt and till specimens with initial properties corresponding to both the “dry of optimum” and “at optimum” conditions.

Table 1. Index properties of the silt and glacial till used in the test program.

	Silt	Glacial till
Liquid limit (%)	26.7	33.2
Plastic limit (%)	14.9	13.0
Plasticity index	11.8	20.2
Percent sand sizes	25.0	32.0
Percent silt sizes	52.0	39.0
Percent clay sizes	23.0	29.0
Specific gravity, G_s	2.72	2.76
Half-standard AASHTO compaction		
$w_{opt.}$ (%)	19.0	18.75
$\gamma_d \text{ max.}$ (kN/m ³)	16.65	17.12

The results are used to determine the volume change indices for the soils at both compaction conditions.

The set of results from compacted silt specimens at “dry of optimum” condition is used to illustrate the technique for obtaining the volume change indices. The consolidation test results for the silt specimens are shown in Fig. 10. The consolidation tests were performed in accordance with the constant volume test method. The loading curves are essentially curves 1 and 3 in Figs. 6 and 7, and their slopes are equal to C_t or $D_t G_s$. The soil-water characteristic curve of the silt (Fig. 11) was obtained from the pressure-plate tests. In this plot, the water content was multiplied by the specific gravity G_s for the purpose of plotting the void ratio and water content to the same scale as shown in Fig. 7 (i.e., curve 4). The slope of the curve is equal to $D_m G_s$.

The shrinkage curve for the compacted silt is shown in Fig. 12 where the water content is multiplied by the specific gravity G_s . The void ratios corresponding to the var-

Fig. 10. Results from one-dimensional constant volume tests on a compacted silt.

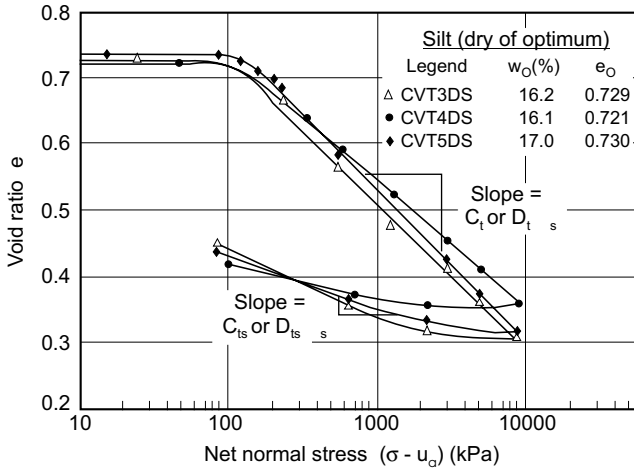
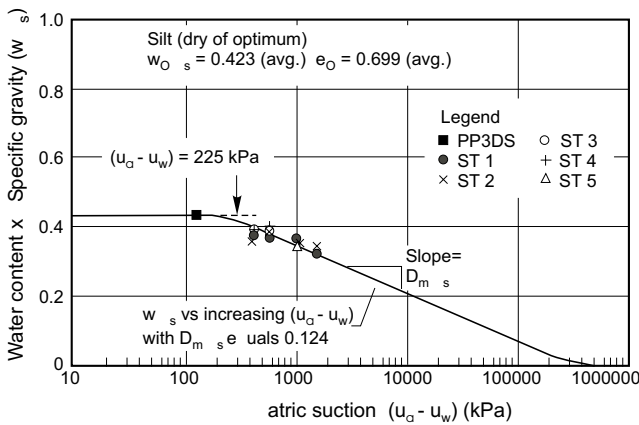


Fig. 11. Soil-water characteristic curve on a compacted silt.

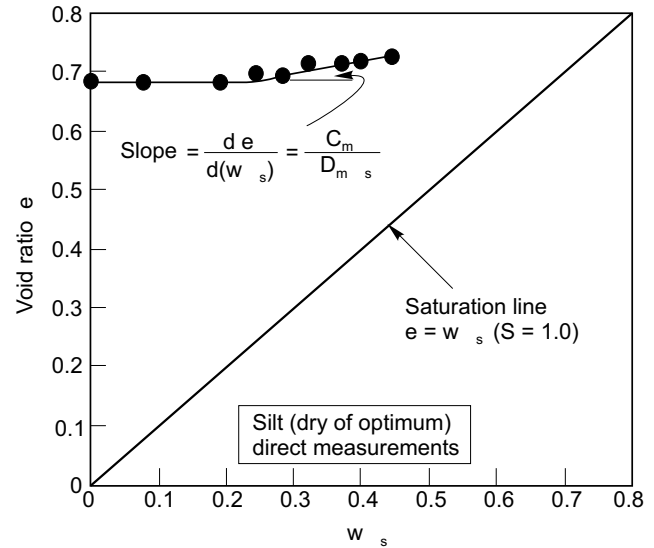


ious water contents in Fig. 11 can now be found using the shrinkage test relationship from Fig. 12. As a result, the void ratio versus matric suction relationship (i.e., curve 2 in Figs. 6 and 7) can be constructed using Figs. 11 and 12. The slope of the shrinkage curve (i.e., $de/d(wG_s)$ or $[\partial e / \partial(u_a - u_w)] / [\partial(wG_s) / \partial(u_a - u_w)]$) is equivalent to the ratio of volume change indices (i.e., C_m/D_mG_s).

The combined information from Figs. 10 to 12 is plotted in Fig. 13. Figure 13 illustrates the volume change characteristic of an unsaturated, compacted silt. The volume change indices (i.e., C_r , C_m , D_r , and D_m) can be computed from Fig. 13. Changes in void ratio and water content due to an increase in total stress or suction can now be predicted using the computed volume change indices.

The volume change indices for loading are shown in Table 2. Also shown in Table 2 are the volume change indices that are applicable to the limiting suction and net total stress planes (i.e., C'_t and C'_m). These indices are obtained using the graphical procedure illustrated in Figs. 4 and 5. In each case, these limiting condition indi-

Fig. 12. Shrinkage curve for the compacted silt. Initial conditions: $e_0 = 0.720$; $w_0 = 15.42\%$.



ces, C'_t and C'_m , are somewhat smaller in magnitude than the C_t and C_m indices.

The volume change indices associated with the unloading surface can be obtained from the rebound curve in Fig. 10 and from the free-swell test results in Fig. 14. As a result, the volume change indices associated with the loading and unloading surfaces for the silt specimen have been obtained from several basic soil tests.

The same test procedures were applied to other compacted silt and glacial till specimens. Figure 15 summarizes the results of shrinkage tests on the various compacted specimens. The lower the water content or the degree of saturation, the further away is the distance from the shrinkage test curve to the saturation line. Typical volume change relationships for the compacted silt and the glacial till are presented in Figs. 16 to 18. The relationships are similar to the one discussed in Fig. 13. The computed volume change indices for the compacted silt and glacial till are tabulated in Table 2.

Application of volume change coefficients and indices

The measured volume change coefficients and indices can be applied to the solution of geotechnical problems involving unsaturated soils. For example, the development of excess pore-air and pore-water pressures during undrained loading can be estimated using a knowledge of the volume change coefficients. Subsequently, the analysis of pore-pressure changes during a transient process (e.g., consolidation) also requires the use of volume change coefficients.

The amount of heave due to the unloading of a soil can be computed using the relevant volume change coefficients for the soil. The analysis for the prediction of heave is done differently for various geographic regions

Fig. 13. Volume change relationships for an unsaturated, compacted silt: $G_s = 2.72$, $e_0 = 0.720$; $w_0 = 15.5\%$, $w_0G_s = 0.420$.

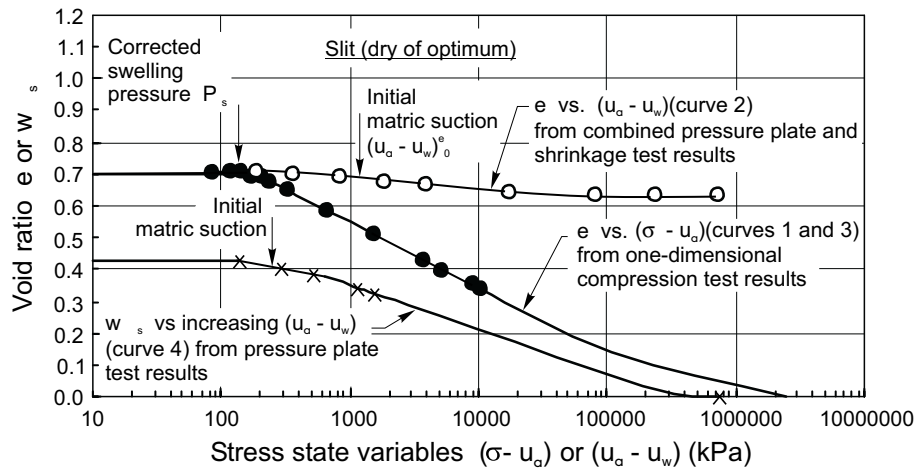


Table 2. A summary of the experimentally measured volumetric deformation indices.

Soil Type	One-dimensional loading							One-dimensional unloading					
	w_0G_s	e_0	C_i or D_iG_s	C'_i	C_m	C'_m	D_mG_s	w_0G_s	e_0	C_{ts}	$D_{ts}G_s$	C_{ms}	$D_{ms}G_s$
DS	0.420	0.699	0.196	0.155	0.030	0.023	0.124	0.419	0.702	0.040	0.126	0.033	0.263
DS	0.424	0.700						0.421	0.699				
OS	0.516	0.606	0.177	0.140	0.082	0.064	0.158	0.517	0.616	0.055	0.076	0.052	0.101
OS	0.511	0.609						0.514	0.609				
DT	0.427	0.642	0.206	0.162	0.089	0.066	0.159	0.436	0.693	0.066	0.084	0.056	0.122
OT	0.516	0.567	0.179	0.137	0.106	0.078	0.171	0.523	0.571	0.037	0.057	0.024	0.060

Note: All indices are negative, since an increase in stress state variable causes a decrease in volume. Soil types: DS, silt at dry of optimum initial water content; OS, silt at optimum initial water content; DT, till at dry of optimum initial water content; OT, till at optimum initial water content. C_a is the average slope of the unloading curve and D_a was calculated from the slope of the linear portion of the unloading curve.

Fig. 14. Results from one-dimensional free-swell test on a compacted silt.

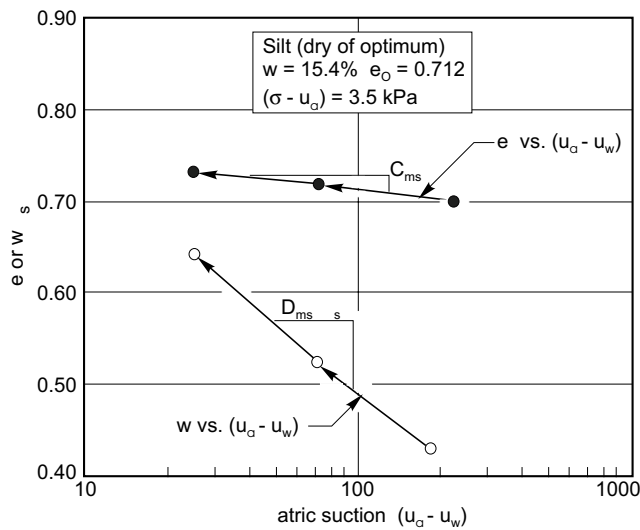
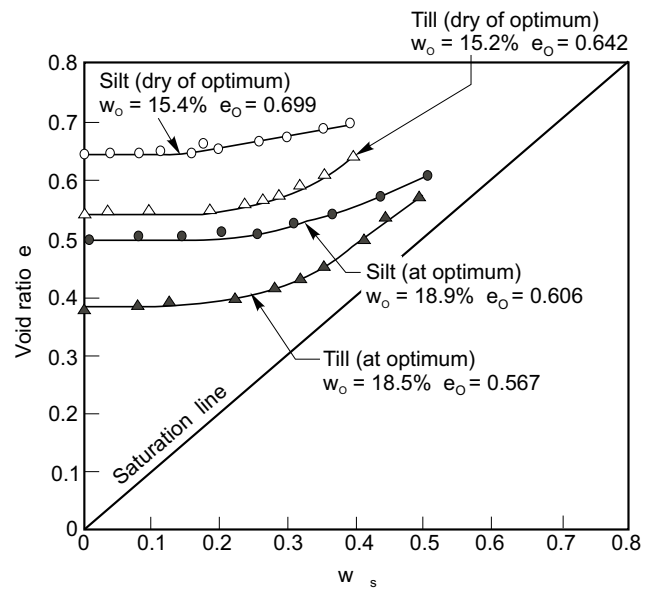


Fig. 15. Shrinkage curves for compacted silt and glacial tills.



of the world. Some analyses are performed in terms of void ratio change, whereas others are performed in terms of water content changes. Some analyses take the applica-

tion of total stress changes into account, whereas others only consider changes in matric suction. If any attempt is made to relate the various methods, it is necessary to

Fig. 16. Volume change relationships for silt at optimum water content under one-dimensional loading conditions. Average initial conditions: $G_s = 2.72$, $e_0 = 0.606$; $w_0 = 19.0\%$, $w_0G_s = 0.516$.

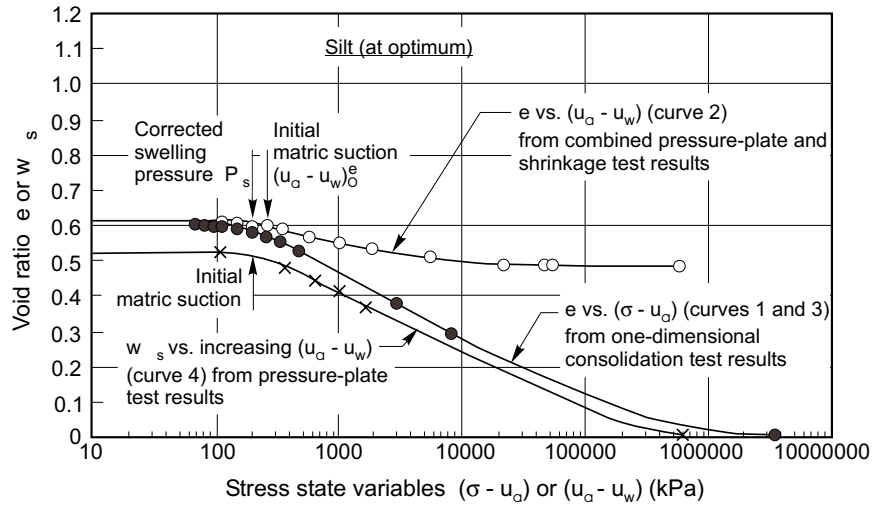


Fig. 17. Volume change relationships for glacial till with dry of optimum water content under one-dimensional loading conditions. Average initial conditions: $G_s = 2.76$, $e_0 = 0.642$; $w_0 = 15.4\%$, $w_0G_s = 0.427$.

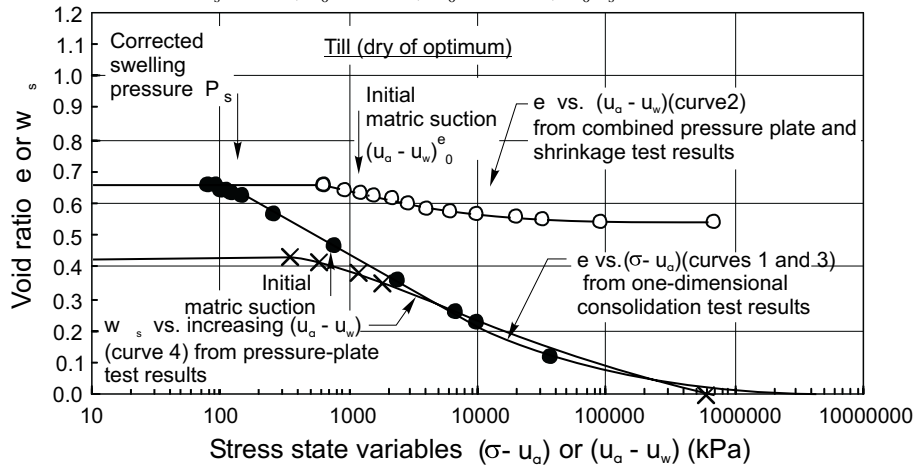
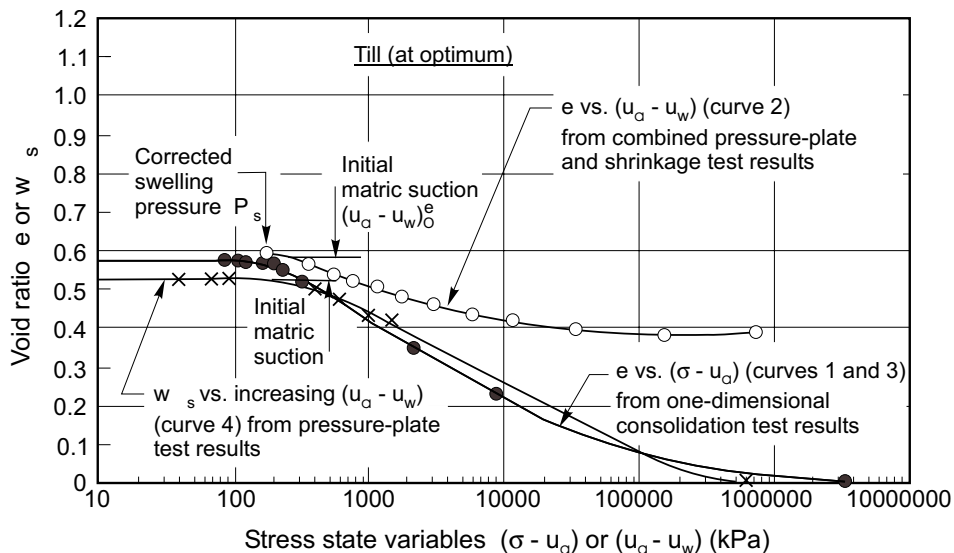


Fig. 18. Volume change relationships for glacial till with optimum water content under one-dimensional loading conditions. Average initial conditions: $G_s = 2.76$, $e_0 = 0.567$; $w_0 = 18.7\%$, $w_0G_s = 0.516$.



know the relationship between the various moduli on the constitutive surface for an unsaturated soil. The same reasoning can be applied to the case of settlement predictions for loading a soil.

In the study of the shear strength behavior of unsaturated soils, it is again of interest to know the relationship between changes in void ratio and water content for various applied loads and matric suction values.

Critical state soil mechanics is an area of considerable research in recent years. This area of study involves the presentation of a combination of the shear strength and volume change (and water content) properties of a soil. This means that a complete understanding of the volume change and water content versus stress state variables is an important part of a critical state model for unsaturated soils.

Summary

Oedometer, pressure-plate, and shrinkage tests are the experiments required for measuring the volume change indices corresponding to the loading of an unsaturated soil. These tests can be performed using conventional soil mechanics testing procedures. The test results provide an understanding of the volume change and water content relationships during the loading of an unsaturated soil.

The rebound portion of the oedometer test and the free-swell test are required for determining the volume change indices corresponding to the unloading portion of an unsaturated soil.

References

- Aitchison, G.D., and Martin, R. 1973. A membrane oedometer for complex stress-path studies in expansive clays. *Proceedings, 3rd International Conference on Expansive Soils, Haifa, Vol. 2*, pp. 83–88.
- Aitchison, G. D., and Woodburn, J.A. 1969. Soil suction in foundation design. *Proceedings, 7th International Conference on Soil Mechanics and Foundation Engineering, Mexico City, Vol. 2*, pp. 1–8.
- ASTM. 1981. Standard test method for capillary-moisture relationships for coarse and medium textured soils by porous plate apparatus. ASTM D2325–68. American Society for Testing and Materials, Philadelphia.
- ASTM. 1985a. Standard test method for one-dimensional swell or settlement potential of cohesive soils. ASTM D4546. American Society for Testing and Materials, Philadelphia.
- ASTM. 1985b. Standard test method for one-dimensional consolidation properties of soils. ASTM D2435. American Society for Testing and Materials, Philadelphia.
- ASTM. 1985c. Standard test method for shrinkage factors of soils. ASTM D427. American Society for Testing and Materials, Philadelphia.
- Chen, F.H. 1975. *Foundation on expansive soils*. 1st edition. Elsevier Science Publishing Co. Inc., New York.
- Crone, D., and Coleman, J.D. 1954. Soil structure in relation to soil suction. *Journal of Soil Science*, 5: 75–84.
- Escario, V. 1969. Swelling of soils in contact with water at a negative pressure. *Proceedings, 2nd International Research and Engineering Conference on Expansive Soils*. Texas A & M University, College Station, pp. 207–218.
- Fredlund, D.G. 1967. Comparison of soil suction and one-dimensional consolidation characteristics of a highly plastic clay. National Research Council of Canada, Division of Building Research, Technical Report 245.
- Fredlund, D.G., and Morgenstern, N.R. 1976. Constitutive relations for volume change in unsaturated soils. *Canadian Geotechnical Journal*, 13: 261–276.
- Gilchrist, H.G. 1963. A study of volume change of a highly plastic clay. M. Sc. thesis, University of Saskatchewan, Saskatoon, SK, Canada.
- Hilf, J.W. 1956. An investigation of pore-water pressure in compacted cohesive soils. Ph.D. thesis. Technical Memorandum No. 654. U.S. Department of the Interior, Bureau of Reclamation. Design and Construction Division, Denver, CO.
- Ho, D.Y.F. 1988. The relationship between the volumetric deformation moduli of unsaturated soils. Ph.D. thesis, University of Saskatchewan, Saskatoon, SK, Canada.
- Ho, D.Y.F., and Fredlund, D.G. 1989. Laboratory measurement of the volumetric deformation moduli for two unsaturated soils. *Proceedings, 42nd Canadian Geotechnical Conference, Oct. 23–25, Winnipeg, MB.*, pp. 50–60.
- Holtz, H.G., and Gibbs, H.J. 1956. Engineering properties of expansive clays. *Transactions of the American Society of Civil Engineers*, 121: 641–663.
- Lambe, T.H., and Whitman, R.V. 1979. *Soil mechanics*. John Wiley & Sons Inc., New York.
- Lidgren, R.A. 1970. Volume change characteristics of compacted till. M.Sc. thesis, University of Saskatchewan, Saskatoon, SK, Canada.
- McWhorter, D.B., and Nelson, J.D. 1979. Unsaturated flow beneath tailings impoundments. *ASCE Journal of the Geotechnical Engineering Division*, 105: 1317–1334.
- Mitchell, P.H., and Avalle, D.L. 1984. A technique to predict expansive soil movements. *Proceedings, 5th International Conference on Expansive Soils, Adelaide, Australia*, pp. 124–130.
- Noble, C.A. 1966. Swelling measurements and prediction of heave for a lacustrine clay. *Canadian Geotechnical Journal*, 3: 32–41.
- Rahardjo, H., Ho, D.Y.F., and Fredlund, D.G. 1990. Testing procedures for obtaining volume change indices during loading of an unsaturated soil. *Proceedings, 1990 Canadian Society of Civil Engineers Annual Conference, Hamilton, ON, Vol. II-2, May 15–18*, pp. 558–573.
- Richards, B.G., Peter, P., and Martin, R. 1984. The determination of volume change properties in expansive soils. *Proceedings, 5th International Conference on Expansive Soils, Adelaide, Australia*, pp. 179–186.
- Schmertmann, J.M. 1955. The undisturbed consolidation of clay. *Transactions of the American Society of Civil Engineers*, 120: 1201.
- Terzaghi, K. 1943. *Theoretical soil mechanics*. John Wiley & Sons Inc., New York.
- Terzaghi, K., and Peck, R.B. 1967. *Soil mechanics in engineering practice*. John Wiley & Sons Inc., New York.

Constitutive modeling of a metastable-structured compacted soil

J.H.F. Pereira and D.G. Fredlund

Abstract: The influence of wetting-induced collapse on the mechanical and hydraulic properties of a residual gneiss soil compacted as a metastable-structured material was experimentally investigated. Volume changes and coefficient of permeability were investigated using a triaxial permeameter system where the stress state variables were independently controlled. The compacted specimens were consolidated isotropically. Measurements of total volume change, water content change, and coefficient of permeability were made at specified matric suction values following a wetting stress path. The experimental data were analyzed to define volume change and water permeability constitutive relationships for the metastable-structured soil. A constitutive model is proposed for predicting the volume change behavior of the compacted metastable-structured residual soil during wetting-induced collapse. The proposed constitutive model is applied to the prediction of the volume change behavior of a compacted metastable-structured soil under different external loading conditions. Prediction is compared to experimental results.

Key words: collapsible soil, metastable-structured soil, unsaturated soil, numerical modeling, mechanical properties, hydraulic properties.

Introduction

A collapsible soil is commonly referred to as a metastable-structured soil. An increase in pore-water pressure results in swelling for an unsaturated stable-structured soil, whereas an increase in pore-water pressure may cause a volume decrease for an unsaturated metastable-structured soil (Barden et al. 1969). The research literature is in agreement that collapse is a behavior that any unsaturated soil may undergo under particular conditions of stress and saturation (Barden et al. 1973; Lawton et al. 1991).

The collapse behavior of compacted and cohesive soils depends on several factors; namely, the percentage of fines (especially clay fraction), the initial water content, the initial dry density, and the energy and process used in compaction (Jennings and Burland 1962; Barden et al. 1973).

In Terzaghi's theory, the mechanical behavior of a saturated soil is governed by the principle of effective stress. Initial attempts to extend such a theory to unsaturated soils had limited success (Bishop and Blight 1963). In recent years, a more sound theory has been established by Fredlund and Morgenstern (1976). Such a theory is con-

sistent with a multiphase, continuum mechanics approach and describe the mechanical behavior of an unsaturated soil as a function of two independent sets of stress variables; namely, the net normal stress ($\sigma - u_a$) and the matric suction ($u_a - u_w$) wherein u_a and u_w are the pore-air and the pore-water pressures in the soil voids. In this theory, the saturated condition is a special case where the "effective stress" (i.e., $(\sigma - u_w)$) becomes the governing stress state variable. The collapsing behavior of soils during saturation is one of the complex aspects to be developed through application of the unsaturated soil theory. The prediction of the performance of collapsing earth structures during saturation is one of the engineering problems depending upon these developments.

Current practice in geotechnique recognizes an unsaturated soil as a four-phase material composed of air, water, soil skeleton and contractile skin (Fredlund and Morgenstern 1976). Under this idealization and from a mechanical viewpoint, two phases can flow (i.e., air and water), and two phases come to equilibrium under imposed loads (i.e., soil skeleton and contractile skin).

Darcy's law has been used to describe the water flow through soils in both the saturated and unsaturated conditions (Freeze and Cherry 1979). The variation of the soil permeability with void ratio for saturated conditions is well established. For unsaturated soils, water flows through the pore spaces filled with water. Therefore, there is a rapid decrease of the soil permeability to water as the degree of saturation decreases (Gardner 1961).

Studies have been attempted to explain the collapse of soils during saturation as a result of changes in the effective stress and in the stress-strain relationships of the material (Lourens and Czaplá 1987). Recently, studies have attempted to explain these phenomena by using the two independent stress state variables for an unsaturated soil

J.H.F. Pereira. Department of Civil Engineering, University of Brasilia, Brasilia, Brazil.

D.G. Fredlund. Professor, Department of Civil Engineering, University of Saskatchewan, 57 Campus Drive, Saskatoon, SK, Canada S7N 5A9.

Reproduced with permission from the *Proceedings, International Symposium on Recent Developments in Soil and Pavement Mechanics*. 1997. Edited by Márcio Almeida, Balkema, Rotterdam, ISBN90 5410 885 1, pp. 317-326.

(Miranda 1988; Lloret and Ledesna 1993). However, these studies have experienced difficulties in reproducing available experimental results in terms of the stress-strain behavior of collapsing soils during saturation. This is particularly true for the condition of collapse of the soil structure under a constant vertical load and K_0 -conditions. Under these conditions a collapsing soil undergoes an increase in mean net confining stress (Maswoswe 1985; Lawton et al. 1991). However, those studies have encountered difficulties to reproduce the increase in horizontal stress during saturation of a collapsing soil. Hence, there exists a need for a better understanding of the mechanical behavior of collapsing soils in view of current theories for unsaturated soils. The primary objective of this paper is to develop a theoretical understanding of the mechanical behavior of a collapsing soil during saturation by using the theory of consolidation for unsaturated soils as presented by Fredlund and Rahardjo (1993).

Mechanical behavior of collapsing soils

Matyas and Radhakrishna (1968) showed that the state of a soil element could be graphically represented as a point in a system of coordinate axis representing the state parameters. This point is called a state point and its displacement, when the element state changes, is called the state path. All the possible state paths would form the state surface of the soil. It was proposed that changes in the void ratio and degree of saturation of an unsaturated soil must be expressed as functions of the stress variables, $(\sigma - u_a)$ and $(u_a - u_w)$, forming three-dimensional constitutive surfaces.

Continuity requirements for an unsaturated soil

The continuity requirement for an unsaturated soil, deforming under an applied stress gradient, can be expressed (Fredlund and Rahardjo 1993) as follows,

$$[1] \quad \frac{\Delta V_v}{V_0} = \frac{\Delta V_w}{V_0} + \frac{\Delta V_a}{V_0} + \frac{\Delta V_c}{V_0}$$

where:

- V_0 = initial overall volume of the soil element,
- V_v = volume of soil skeleton voids,
- V_w = volume of water phase,
- V_a = volume of air phase, and
- V_c = volume of the contractile skin (i.e., air-water interface).

By neglecting the volume changes in the contractile skin, the above relationship shows that only the volume changes associated with two phases must be measured, while the third can be computed. In practice, changes in void volume and water phase volume are usually measured. By using a rectangular Cartesian coordinate system and referencing deformation to an elemental volume, the total volumetric deformation, $d\varepsilon_v$, of an unsaturated soil element can be expressed as,

$$[2] \quad d\varepsilon_v = d\varepsilon_x + d\varepsilon_y + d\varepsilon_z = dV_v / V_0$$

where:

$\varepsilon_x, \varepsilon_y, \varepsilon_z$ = deformations on the x -, y -, z - directions.

Assuming infinitesimal deformations on the soil element, the deformation variable associated with the water phase can be defined as dV_w / V_0 .

Volume change behavior of unsaturated soils

Moduli and compressibility forms of the constitutive relationships have been used by researchers to illustrate discrete or incremental constitutive models. In these relationships, the deformation variables for total volume change and water volume change of the soil element are associated to changes in the stress state variables by means of elasticity modulus.

Assuming the soil as an incrementally isotropic, linear and elastic material, the moduli constitutive relationships have been presented (Fredlund and Morgenstern 1976), in accordance with the generalized Hooke's law, as follows (Fung 1965):

$$[3] \quad d\varepsilon_{ij} = \frac{1}{E} [(1 + \mu) d\sigma_{ij} - \mu d\sigma_{\alpha\alpha} \delta_{ij}] + \frac{1}{H} d(u_a - u_w) \delta_{ij}$$

where:

- σ_{ij} = total stress tensor,
- $\sigma_{\alpha\alpha} = \sigma_{ii} + \sigma_{jj} + \sigma_{kk}$,
- ε_{ij} = total deformation tensor,
- H = elasticity modulus for the soil structure relative to a change in $(u_a - u_w)$,
- E = elasticity modulus for the soil structure associated to a change in $(\sigma - u_a)$,
- μ = Poisson ratio for the soil, and
- δ_{ij} = Kronecker delta.

A similar semi-empirical approach has been used to the water phase constitutive relationship:

$$[4] \quad \frac{dV_w}{V_0} = \frac{1}{E_w} d(\sigma_{ii} - 3u_a) + \frac{1}{H_w} d(u_a - u_w)$$

where:

- E_w = water volumetric change modulus associated with a change in $(\sigma - u_a)$, and
- H_w = water volumetric change modulus associated with a change in $(u_a - u_w)$.

The above forms of the constitutive equations can be applied to general cases where non-linear stress versus strain relationships occur by means of incremental procedures.

In an alternative way to the moduli form, Fredlund and Rahardjo (1993) presented the compressibility equations, for soil structure and water phase for a triaxial stress state, as follows:

$$[5] \quad dV_v / V_0 = m_1^s d(\sigma_m - u_a) + m_2^s d(u_a - u_w)$$

$$[6] \quad dV_w / V_0 = m_1^w d(\sigma_m - u_a) + m_2^w d(u_a - u_w)$$

where:

- $m_1^2 = 3(1 - 2\mu) / E$, is the coefficient of total volume change with respect to mean net normal stress,
- $m_2^s = 3 / H$, is the coefficient of total volume change with respect to matric suction,
- $m_1^w = 3 / E_w$, is the coefficient of water volume change with respect to mean net normal stress,
- $m_2^w = 1 / H_w$, is the coefficient of water volume change with respect to matric suction, and
- σ_m = mean net normal stress.

In the state surfaces defined by Fredlund and Rahardjo (1993), both compressive net normal stresses and matric suction were assumed as positive. Therefore, this implied negative signs for the four parameters m_1^s , m_2^s , m_1^w and m_2^w for a soil which undergoes volume decrease due to increases in any stress variable. It was stated that the four negative parameters characterize a stable soil. In turn, the stable soil swelled upon decrease in any stress variables. These sign conventions are also valid for the corresponding elasticity parameters.

Collapsing soils

Nowadays, geotechnique recognizes the following facts regarding the mechanical behavior of compacted collapsing soils:

- Any type of soil compacted at dry of optimum conditions and at a low dry density may develop a collapsible fabric or metastable structure (Barden et al. 1973).
- A compacted and metastable soil structure is supported by microforces of shear strength (i.e., bonds) which are highly dependent upon capillary action. With the increase of the water content the bonds start losing strength and at a critical water content the soil structure collapses (Jennings and Knight 1957; Barden et al. 1973).
- There is a gradual increase in compressibility as well as a gradual decrease in shear strength of a collapsible soil during the saturation process (Jennings and Burland 1962; Barden et al. 1973),
- The soil collapse progresses as the degree of saturation increases. There is; however, a critical degree of saturation for a given soil above which negligible collapse will occur regardless of the magnitude of the pre-wetting overburden pressure (Booth 1977).
- The collapse is associated with localized shear failures rather than an overall shear failure of the soil mass (Maswoswe 1985).
- During wetting-induced collapse, under a constant vertical load and under K_0 -oedometer conditions, a soil specimen undergoes an increase in horizontal stresses (Maswoswe 1985).
- From a phenomenological point of view, there is an increase in the Poisson ratio of the collapsing soil during saturation (Pereira 1996).
- Under a triaxial stress state, the magnitude of volumetric strain, resulting from a change in stress state or from wetting, depends on the mean normal total

stress and is independent of the principal stress ratio (σ_a / σ_r). However, the individual components of volumetric strain (i.e., axial and radial strain) depend on the principal stress ratio. For a given mean normal total stress, the magnitude of axial collapse increases and the magnitude of radial collapse decreases with an increasing stress ratio (Lawton et al. 1991).

A soil collapse model must be able to properly reproduce the progress and magnitude of the soil collapse as a function of the two independent stress variables governing the mechanical behavior of unsaturated soils. It is worth emphasizing that Lawton et al. (1991) observations provide valuable information for the modeling of the collapsing soil behavior since it relates the total volumetric wetting-induced collapse to the mean net normal total stress. In addition, it illustrates that depending on the applied stress ratio a collapsing soil can even undergo expansion to the direction of the minor total stress during saturation.

According to eq. [5], if the mean net normal stress is kept constant, the collapsible soil structure must undergo a volume decrease due to a decrease in its matric suction. Therefore, a collapsible soil has a positive compressibility modulus (i.e., m_2^s) associated with a change in matric suction (Fredlund and Rahardjo 1993). Depending on the initial degree of saturation and the reduction in porosity during the soil collapse, it is possible that the volumetric water content may decrease as the matric suction decreases. In this case, the water phase compressibility modulus associated with a change in matric suction is also positive (i.e., m_2^w).

Equation 3 assumes isotropic mechanical properties for an unsaturated soil. This implies a positive value for the isotropic elasticity modulus for the soil structure relative to a change in matric suction (i.e., H) for a collapsible soil, since m_2^s is positive. An isotropic modulus, H , results in isotropic wetting-induced collapse of a soil element in response to a decrease in matric suction, independent on the total stress state applied on the soil element. Such a prediction contradicts the previously presented available experimental data reported by Maswoswe (1985).

Isotropic wetting-induced soil collapse can occur on a soil specimen under an isotropic total stress state (Lawton et al. 1991). In addition, Lawton et al. (1991) findings predict that during triaxial wetting-induced collapse a soil specimen undergoes anisotropic deformations which are functions of the applied anisotropic stress state. Therefore, a stress induced anisotropic modulus, H , appears to be a reasonable alternative to the theory of unsaturated soils to properly model the collapsing behavior of a soil during saturation. By using a rectangular Cartesian system, the proposed stress induced anisotropic constitutive equations for the normal deformations are as follows:

$$[7] \quad \varepsilon_x = \frac{(\sigma_x - u_a)}{E} - \frac{\mu}{E} (\sigma_y + \sigma_z - 2u_a) + \frac{(u_a - u_w)}{H_x}$$

$$[8] \quad \varepsilon_y = \frac{(\sigma_y - u_a)}{E} - \frac{\mu}{E} (\sigma_x + \sigma_z - 2u_a) + \frac{(u_a - u_w)}{H_y}$$

$$[9] \quad \varepsilon_x = \frac{(\sigma_z - u_a)}{E} - \frac{\mu}{E}(\sigma_x + \sigma_y - 2u_a) + \frac{(u_a - u_w)}{H_z}$$

where:

$H_i = H / (1 + H\xi_i)$, is the elasticity modulus for the soil structure in the i -direction relative to a change in matric suction (i.e., $u_a - u_w$),

H = isotropic elasticity modulus (function of the mean net total stress) for the soil structure relative to a change in $(u_a - u_w)$,

ξ_i = stress induced anisotropic collapse factor in the i -direction (function of the stress ratios σ_i / σ_j and σ_i / σ_k) for the soil structure relative to a change in $(u_a - u_w)$, and

i, j, k = directions of a three-orthogonal coordinate system (e.g., x, y, z).

In addition, and a consequence of the assumption that the volumetric wetting-induced collapse is a unique function of the applied mean net stress, comparison between eq. [5] and eqs. [7] to [9] allows a definition of the following relationships for the soil parameters, m_2^s , H_i , ξ_i .

$$[10] \quad m_2^s = \frac{1}{H_x} + \frac{1}{H_y} + \frac{1}{H_z}$$

$$[11] \quad x_z + x_y + x_x = 0$$

Besides, it can also be concluded that ξ_i are non-linear soil parameters with values equal to zero for an isotropic stress state.

Flow law and hydraulic properties for unsaturated soils

The soil permeability to air remain significantly greater than the soil permeability to water for all water contents in a compacted soil (Barden and Pavlakis 1971). This study is related to the practical cases wherein the pore-air phase can be considered at constant atmospheric pressure.

Some unsaturated soils do not undergo significant changes in void ratio in response to changes in the stress state variables. For these soils, the water coefficient of permeability can be expressed as a sole function of their degree of saturation. Therefore, the soil-water characteristic curve has been used to derive semi-empirical relationships for the permeability to water, as a function of the soil matric suction, for such soils (Brooks and Corey 1964). Relationships between the soil permeability to the water and matric suction are strongly dependent on the stress path. However, hysteresis has relatively little influence on the relationships between the water coefficient of permeability and the degree of saturation for soils with a non-deforming soil structure.

A metastable soil may undergo a considerable rearrangement of its structure due to wetting-induced collapse. Therefore, the water coefficient of permeability for a collapsible soils must be investigated as a function of its volume mass properties (i.e., void ratio and degree of saturation). In engineering practice, a collapsible soil maintains a relatively open structure even for relatively

low matric suctions. This means that the soil possesses a low degree of saturation and, consequently, a low permeability with respect to the water phase and a high permeability with respect to the air phase even at low levels of matric suction.

Physics involved in the problem of wetting of collapsing soils

Dakshanamurthy et al. (1984) extended the theory by Biot for consolidation of saturated soils to unsaturated soils. In their work, the air continuity equation was explicitly included as a continuous and compressible phase. Their basic physics equations were as follows.

(a) Equilibrium equations:

$$[12] \quad \sigma_{ij,j} + b_i = 0$$

where:

b_i = body forces.

(b) Air continuity equation:

$$[13] \quad \frac{\partial}{\partial t} [\rho_a n(1 - S + H_c S)] + \nabla[\mathbf{J}_a] = 0$$

where:

\mathbf{J}_a = mass rate of air flowing across a unit area of the soil,

ρ_a = mass density of air,

n = porosity,

S = degree of saturation,

H_c = Henry's constant ($nH_c S$ = air volume dissolved in the pore-water phase), and

$\nabla = \frac{\partial}{\partial x} \mathbf{i} + \frac{\partial}{\partial y} \mathbf{j} + \frac{\partial}{\partial z} \mathbf{k}$, the divergence operator.

(c) Water continuity equation.

$$[14] \quad \frac{\partial(\rho_w \theta_w)}{\partial t} + \nabla(\rho_w \mathbf{v}_w) = 0$$

where:

ρ_w = mass density of water,

$\theta_w = nS$, the volumetric water content, and

$\mathbf{v}_w = v_w^x \mathbf{i} + v_w^y \mathbf{j} + v_w^z \mathbf{k}$, macroscopic velocity vector of water.

The coupled flow and stress equations involved in the behavior of a collapsing soil mass requires a numerical solution. In the present paper, the finite element method was used in the development of a numerical model dealing with a coupled solution. Comparison between experimental and numerical results are later illustrated. Details of the coupled solution involving water flow-mechanical equilibrium in soils are presented in Pereira (1996).

Laboratory testing results and soil modeling

The soil utilized in this research study is a residual silty sand derived from a granitic gneiss of the Ceara

group in Northeast Brazil. Table 1 illustrates the index properties of the soil tested.

Laboratory tests were performed to define the constitutive relationships for the collapsing soil. Soil specimens were statically compacted at dry of optimum and low dry density conditions as compared to the AASHTO compaction energy. The collapsing soil specimens were compacted at a gravimetric water content of 10.5% (i.e., minus 4% dry of optimum conditions) and at a dry density of 14.75 kN/m³ (i.e., compacted at 90% of the AASHTO compaction energy).

Double-oedometer tests in the range of vertical stresses from 0 to 800 kPa were performed on the compacted soil specimens. The soil showed low compressibility when loaded under unsaturated conditions. The soil specimens did not present any collapsing behavior when saturated under vertical stresses lower than 50 kPa. A vertical stress of 100 kPa produced soil collapse amounting to 3.0%. The volumetric collapse reached about 7.2% and 11% when loaded under vertical stresses of 200 kPa and 400 kPa, respectively.

A drying soil-water characteristic curve showed that the soil specimen started desaturating at a matric suction of about 3.0 kPa. The degree of saturation of the specimens dropped to values of less than 50% for suction values of about 60 kPa. The coefficient of permeability of compacted soil specimens at saturated conditions varied from $k_w = 1.5 \times 10^{-6}$ to $k_w = 4.0 \times 10^{-9}$ m/s, for applied vertical stresses from 25 kPa to 800 kPa. A relationship between the logarithm of the water coefficient of permeability versus the void ratio was non-linear. Low values for the permeability with respect to water would be expected for unsaturated soil specimens under suction values higher than 80 kPa. The method of Brooks and Corey (1964) was used to estimate the soil permeability of the unsaturated soil. A coefficient of permeability equal to 10^{-11} m/s was predicted at a matric suction of 80 kPa. At the as-compacted initial matric suction of about 370 kPa, the coefficient of permeability was predicted to be of about 10^{-13} m/s.

A triaxial permeameter system was utilized in the definition of the volume change constitutive relationships for the compacted collapsing soil. This equipment allowed for the performance of isotropic consolidation tests on unsaturated soils. The testings followed stress paths wherein the as-compacted soil specimen was firstly loaded and then gradually wetted (i.e., by reducing the applied matric suction). The coefficient of permeability could be measured using the triaxial permeameter using the constant head, steady-state, controlled head method (Pereira 1996).

Laboratory test results

To establish the constitutive relationships required, four triaxial permeability tests were conducted on four statically compacted collapsing soil specimens. Each soil specimen, at its as-compacted initial condition, was isotropically loaded under a given net normal confining pressure. The pore-air pressure was controlled in a

Table 1. Index properties of the soil.

Soil	Residual silty sand
Grain size distribution	Sand = 52% Silt = 35% Clay = 13%
Atterberg limits	Liquid limit, $w_l = 29$ Plastic limit, $w_p = 17$ Plasticity index, $PI = 12$
Specific gravity USCS	$G_s = 2.64$ SW-SM; well-graded sand with silt

drained mode. The specimens were allowed to consolidate at various steps of decreasing matric suction (i.e., following a wetting stress path under a constant net confining pressure) until saturation was reached. Applied net confining pressures of about 20 kPa, 50 kPa, 100 kPa and 200 kPa were utilized, respectively, for the four specimens tested. The changes in the total volume of the specimens were monitored during each step of the tests. The outflow and inflow of water to the specimen was also monitored in order to determine the changes in its water content. This allowed the computation of the soil coefficient of permeability at each applied matric suction. The specimen for the tests had a height of 44.8 mm and a diameter of 101.1 mm. The as-compacted soil specimens showed a void ratio of about 0.754 and a degree of saturation of about 36.7%.

A typical collapse behavior illustrated that a stress path, which follows decreasing matric suction at a given net confining pressure, shows that there are three distinct phases in the collapse mechanism. In the first phase (pre-collapse phase), at relatively high matric suctions, the soil does not collapse and only small deformations occur in response to a decrease in matric suction. In the second phase (collapse phase), at intermediate matric suctions, large deformations are observed in response to a decrease in matric suction. In the third phase (post-collapse phase), at low matric suctions, there is an absence of deformations as the matric suction is reduced to zero.

In terms of water volume changes, it was observed that, for the range of confining stresses used, the wetting curve is practically independent of the soil collapse. The influence of the soil collapse was only noticed as the soil approached complete saturation. It was observed that, the lower the porosity of the collapsed soil, the less is the increase in water content in response to further decreases in matric suction.

The small amounts of water flow involved made it difficult to determine the influence of the gradual soil collapse on the water coefficient of permeability of the unsaturated soil specimens.

Soil modeling

The soil models were defined by using best-fit analyses in the search for continuous functional relationships that could capture the essential characteristics of the behavior

of the soil as observed from the available data. A superior curve-fitting was obtained by using a five parameter logistic function. Equation [15] shows this function in terms of void ratio as a function of matric suction at a given net confining stress.

$$[15] \quad e = e_u + (e_s - e_u) / \left[1 + \left(\frac{(u_a - u_w)}{c} \right)^b \right]^a$$

where:

- e_u = initial void ratio of a soil specimen under a given net confining stress,
- e_s = void ratio at saturated conditions of a soil specimen under a given net confining stress,
- c = matric suction value at the inflection point (i.e., middle point of the “collapse” phase),
- b = slope parameter (i.e., slope of the “collapse” phase), and
- a = the symmetry parameter which makes the logistic function asymmetric.

Equation [16] is the mathematical model, for net confining stresses higher than 45 kPa, for the void ratio state surface of the collapsing soil resulting from the best-fit analysis of the available data.

$$[16] \quad e = e_u + (e_s - e_u) / \left[1 + \left(\frac{(u_a - u_w)}{c} \right)^b \right]$$

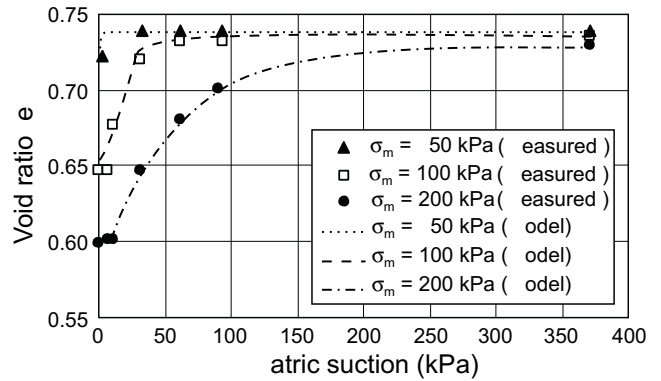
where:

- $e_u = 0.76 - 0.0073 \ln(\sigma^*)$,
- $e_s = 1.226 (\sigma^*)^{-0.1359}$
- $c = c_1 (\sigma^*)^2 + c_2 (\sigma^*) + c_3$,
- $b = b_1 (\sigma^*)^{b_2}$,
- $c_1 = 9.4 \times 10^{-4}$,
- $c_2 = 7.46 \times 10^{-2}$,
- $c_3 = -4.07$,
- $b_1 = 49.01$,
- $b_2 = -6.1 \times 10^{-1}$, and
- σ^* = net confining stress.

Figure 1 illustrates the best-fit model in terms of void ratio versus matric suction relationships under different net confining stresses. The available experimental data are also illustrated in this figure and show a comparison of the best-fit surface provided by eq. [16]. The void ratio state surface allows for the evaluation of the compressibility parameter, m_v^s , which expresses (see eq. [5]) a relationship between the soil elasticity modulus (i.e., E) and the Poisson ratio (i.e., μ). Therefore, a Poisson ratio relationship is required in order to completely define the mechanical behavior of the soil structure.

A Poisson ratio equal to 0.3 may reflect the as-compacted conditions of a loosely compacted soil (Miranda 1988). However, changes in the structure of a metastable-structured soil upon saturation, results in corresponding changes in the Poisson ratio (Maswoswe 1985).

Fig. 1. Void ratio best fit modeling.



In this research study, the first step involved the establishment of a relationship between the Poisson ratio and the mean normal stress of the collapsing soil at saturated conditions. Such a relationship was defined by combining the available triaxial and double-oedometer test results with the experimental observation that: “the volumetric collapse of a soil mass is truly a function of the acting mean total stress” (Lawton et al. 1991). Approximate values for mean total stress (i.e., σ_m) in the oedometer test at various values of vertical stresses (i.e., σ_v), were determined by selecting values of vertical stress for various void ratios on the oedometer curve. Then, the corresponding value of mean net stress on the saturated curve of the isotropic triaxial test was determined for the corresponding void ratio. A given combination of mean total stress and vertical stress allowed an evaluation of the horizontal stress (i.e., σ_h) in the oedometer test. Then, for a given mean confining stress, the Poisson ratio for the saturated collapsing soil (i.e., μ_s), was evaluated as follows:

$$[17] \quad \mu_s = (3\sigma_m - \sigma_v) / (\sigma_v + 3\sigma_m)$$

where

$$\sigma_m = (\sigma_v + 2\sigma_h) / 3, \text{ and}$$

$$\sigma_h = [\mu / (1 - \mu)] \sigma_v.$$

The Poisson ratio for the collapsing soil at unsaturated conditions was determined as follows: *a*) at a given mean net stress (i.e., net confining stress) a constant Poisson ratio equal to 0.3 is assumed for the as-compacted soil condition; *b*) at a given mean total stress, it is assumed that the Poisson ratio increases with soil collapse.

This implies an increase of the Poisson ratio when the matric suction decreases, which reflects experimental evidence (Maswoswe 1985).

In this research study, the same relationship used to simulate the soil collapse versus matric suction (i.e., eq. [16]) is used to simulate the change in Poisson ratio in response to a change in matric suction. This assumption implies a variation in the Poisson ratio of the collapsing soil from an initial value of about 0.3 (i.e., at the as-compacted conditions) to a value calculated, by using eq. [17], when the soil reaches saturated conditions. Therefore, the Poisson ratio for the collapsing soil under unsaturated conditions is calculated as:

$$[18] \quad \mu = 0.3 + (\mu_s - 0.3) / \left[1 + \left(\frac{(u_a - u_w)}{c} \right)^b \right]$$

where:

$$\mu_s = 0.092 \ln(\sigma_m) - 0.021; \text{ the Poisson ratio equation for the saturated soil obtained by using eq. [17].}$$

The degree of saturation state surface was also defined using a best-fit analysis. The logistic function provided the best-fit results of the available data. The mathematical model obtained is expressed as follows:

$$[19] \quad S = S_0 + (1 - S_0) / \left[1 + \left(\frac{(u_a - u_w)}{c} \right)^d \right]$$

where:

$$\begin{aligned} S_0 &= a + b \ln(\sigma^*), \\ a &= 0.354, \\ b &= 3.65 \times 10^{-3}, \\ c &= 7.91, \text{ and} \\ d &= 0.977. \end{aligned}$$

A phenomenological model for the degree of saturation already includes both the effect of changes in the soil structure (i.e., pore size changes) and the water inflow when the collapsible soil is saturating. Figure 2 shows the resulting best-fit model in terms of the degree of saturation versus matric suction relationship under different net confining stresses.

In terms of soil permeability to water versus stress state variables, the Brooks and Corey (1964) equation provided a satisfactory best-fitting relationship for the collapsing soil. A relationship between the coefficient of permeability at saturated conditions, k_s , and the net confining stress was previously defined and used as a constraint in the best-fit analysis. Equation [20] expresses the best-fit mathematical equation for the water coefficient of permeability.

$$[20] \quad k_w = k_p \left(\frac{\Psi_{cr}}{(u_a - u_w)} \right)^\lambda$$

where:

$$\begin{aligned} k_w &\leq k_s, \\ k_p &= -1.39 \times 10^{-7} + 6.259 \times 10^{-8} \ln(\sigma^*), \\ k_s &= 1.17 \times 10^{-6} - 1.8 \times 10^{-7} \ln(\sigma^*), \text{ is the coefficient of permeability for the soil at saturated conditions,} \\ \Psi_{cr} &= 3.0, \text{ and} \\ \lambda &= 2.90. \end{aligned}$$

Figure 3 shows the best-fit results for the collapsing soil in terms of the water coefficient of permeability versus matric suction relationship for different net confining stresses. The figure also shows the available data for the net confining stress of 200 kPa, in order to show the accuracy of the predicting model.

Fig. 2. Degree of saturation best-fit modeling.

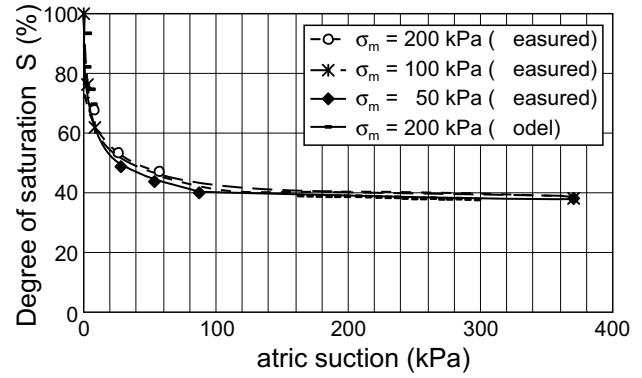
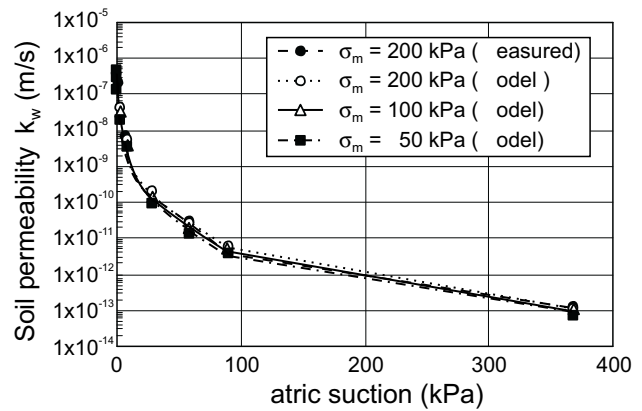


Fig. 3. Soil permeability best-fit modeling.



Numerical modeling of a metastable-structured soil

A finite element model, developed in a computer program hereafter called COUPSO (Pereira 1996), was utilized to solve the coupled equations for the consolidation of unsaturated soils (i.e., eqs. [12] and [14]). The numerical solution takes into account the stress induced anisotropic constitutive relationships for a collapsing soil (i.e., eqs. [7] to [9]). In this paper, the ability of the model to handle soils that undergo collapsing behavior is firstly demonstrated by using results of laboratory tests presented by Maswoswe (1985). Then, the numerical model is applied to the analysis of the mechanical behavior of the residual silty soil compacted at metastable-structured conditions.

Maswoswe (1985) conducted tests on soil specimens compacted at metastable-structured conditions. Test SK2 is one of the tests that corresponded to a soil compacted to an initial void ratio of about 0.66. In this test, the soil specimen was loaded to a vertical stress of 190.4 kPa and then wetted under K_0 conditions. Table 2 shows the measured data from Maswoswe (1985).

The soil parameters required for the COUPSO computer program were defined by using the following procedures:

a) State surfaces for void ratio, e , and degree of saturation, S .

Table 2. SK2 test results from Maswoswe (1985).

Point	$(\sigma_v - u_a)$ (kPa)	$(u_a - u_w)$ (kPa)	$(\sigma_h - u_a)$ (kPa)	Void ratio, e	$(\sigma_m - u_a)^*$ (kPa)
A	0.1			0.66	
B	190.4	250	50.9	0.65	97.4
C	190.4	220	80.4	0.61	117.0
D	190.4	150	89.6	0.56	123.2
E	190.4	0	110	0.45	136.8
F	220.4	0	120.9	0.45	154.0

$$*(\sigma_m - u_a) = [(\sigma_v - u_a) + 2(\sigma_h - u_a)] / 3$$

The available data in Table 2 were used to define a plane for the void ratio state surface of the collapsing soil. This plane was adjusted for the stress states corresponding to the initial point (i.e., B) and the final point (i.e., E) of the wetting-induced collapse. The void ratio state surface was established as follows:

$$[21] \quad e = a_0 + a_1(\sigma_m - u_a) + a_2(\sigma_m - u_a)(u_a - u_w)$$

where:

$$\begin{aligned} a_0 &= 0.66, \\ a_1 &= -1.53 \times 10^{-3}, \text{ and} \\ a_2 &= 5.70 \times 10^{-6}. \end{aligned}$$

For the degree of saturation state surface a relationship from Alonso (1993), based on the data by Maswoswe (1985), was used. The state surface for the degree of saturation was expressed as:

$$[22] \quad S = 1 - m \tan h[n(u_a - u_w)]$$

where:

$$\begin{aligned} m &= 0.64 \\ n &= 5.38 \times 10^{-3} \text{ kPa}^{-1}. \end{aligned}$$

b) Poisson ratio, μ , coefficient of permeability, k_w , and factors ξ_i .

Since the horizontal stress increases when the soil collapses under K_0 -conditions and at a constant vertical stress, the following linear relationship between the Poisson ratio, μ , and the matric suction was established based on the initial and final stress states (i.e., points B and E) of the wetting-induced collapse:

$$[23] \quad \mu = \mu_s + d_0(u_a - u_w)$$

where:

$$\begin{aligned} \mu_s &= 0.37, \\ d_0 &= (u_0 - u_{fs}) / (u_a - u_w)_{max}, \\ \mu_0 &= 0.21, \text{ and} \\ (u_a - u_w)_{max} &= 250 \text{ kPa}. \end{aligned}$$

The coefficient of permeability (i.e., k_w) was considered constant and equal to 1.36×10^{-8} m/s. The stress-induced anisotropic factors, ξ_i , were defined in a trial and error process, using the computer program COUPSO, in such a way that the wetting-induced collapse (i.e., from point B to point E) was exactly reproduced. In this process, equal values were used for the horizontal-direction anisotropic factors (i.e., ξ_x and ξ_z), simulating the confining

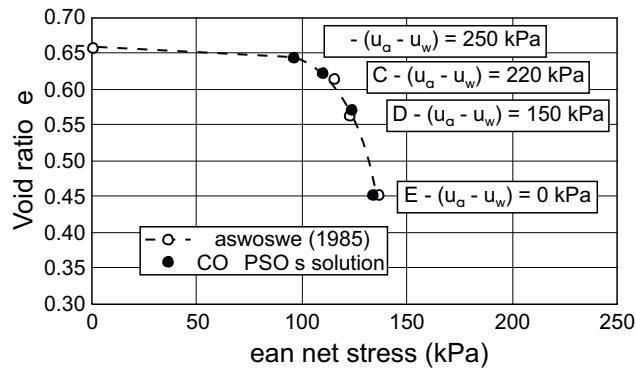
oedometric conditions. The closed-form relationship ξ_y equal to minus $(\xi_x + \xi_z)$ (i.e., eq. [11]) defined the anisotropic factor in the vertical direction. The trial and error process defined horizontal-direction anisotropic factors ξ_x and ξ_z equal to minus 1.28.

Figure 4 presents a comparison between the results obtained using COUPSO and the measured values obtained by Maswoswe (1985). Figure 4 shows the capability of COUPSO to reproduce a wetting induced soil collapse where the vertical stress is kept constant. The intermediate values (i.e., points C and D) were calculated by keeping the previously defined soil parameters and changing the boundary conditions to reproduce the partial wetting collapse. Figure 4 shows that despite the assumptions involved, especially a constant value for the factors ξ_i , the numerical and experimental results are in good agreement. It is also illustrated that there is an increase in the mean net stress, as a result of an increase in the net horizontal stress during soil collapse as measured by Maswoswe (1985). These results show the importance of the stress induced anisotropic factors ξ_i , to the constitutive relationships for a collapsing soil.

A second application of COUPSO is related to the behavior of the metastable-structured compacted residual silty soil during saturation. The soil properties are based on the laboratory results previously discussed. The constitutive relationships for void ratio, e , Poisson ratio, μ , degree of saturation, S , and permeability to water for the collapsing soil are the previously presented equations [16], [18], [19] and [20], respectively.

The stress induced anisotropic factors ξ_i , (i.e., ξ_x , ξ_y and ξ_z) were defined in a trial and error process using the computer program COUPSO and the available double-oedometer tests. This trial and error procedure consisted of the reproduction of the wetting-induced (i.e., matric suction from 360 to 0 kPa) collapse of the soil specimen under K_0 -conditions and under an applied vertical stress of 200 kPa. A value of about minus 2.60 was calculated for the anisotropic factors ξ_x and ξ_z from the above trial and error procedure.

The numerical analyses were performed by discretizing the soil specimen, which had a height equal to 0.02 meters, using a mesh of 5 equal axis-symmetric finite elements (Pereira 1996). The analysis was transient and required time steps varying from 5 to 0.5 seconds. Figure 5 illustrates the simulation of the wetting-induced soil collapse by using the above defined anisotropic factors. It

Fig. 4. Soil collapse during saturation.

shows the wetting induced soil collapse of residual silty soil specimens under K_0 -loading conditions and under vertical loads of 100 and 200 kPa. Both the unsaturated and saturated loading paths were obtained from the triaxial permeameter tests.

The intermediate values (i.e., points B, C, D and E) correspond to values of matric suction of 200, 100, 50 and 10 kPa, respectively. These points were calculated by changing the boundary conditions to reproduce the partial wetting collapse. The results demonstrate the generality of the stress induced anisotropic collapse factors in simulating the collapsing soil behavior under different vertical loads.

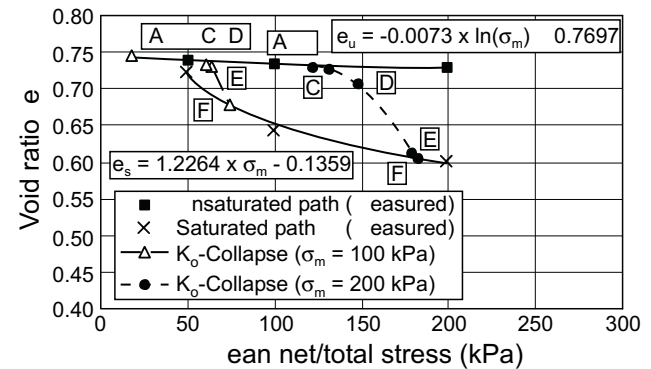
In this wetting-induced collapse test, it is worth noting the monotonic stress path followed by the collapsing soil specimen. For this loading condition, the concept of stress state surfaces is fulfilled and reasonable predictions of changes in void ratio and degree of saturation of an unsaturated soil can be expected.

Conclusions

- (1) The theory by Fredlund and Rahardjo (1993) for the consolidation of an unsaturated soil in its more generalized form (i.e., introducing a stress-induced anisotropic behavior of an unsaturated soil element in response to a change in matric suction), can be used to simulate the stress-strain behavior of a collapsing soil during saturation. The mechanical behavior of a stable soil is a special case of this more generalized theory.
- (2) Additional studies on the anisotropic collapsing factors (i.e., ξ_i factors) are required. More research is needed to completely understand these factors and their influence on the stress-strain behavior of a metastable-structured soil.
- (3) The numerical model COUPSO is able to simulate K_0 -condition triaxial tests on metastable soils. The predicted results show reasonable accuracy to the measured data.

References

Alonso, E. 1993. Constitutive modeling of unsaturated soils. Civil Engineering European Courses, Barcelona, Spain, June.

Fig. 5. Residual soil collapse during saturation.

Barden, L., and Pavlakis G. 1971. Air and water permeability of compacted unsaturated cohesive soil. *Journal of Soil Science*, **22**(3): 302–317.

Barden, L., Madedor A.O., and Sides, G.R. 1969. Volume change calculations of unsaturated clay. *ASCE, Journal of Soil Mechanics and Foundations Engineering Division*, **95**: 33–51.

Barden, L., McGown, A., and Collins, K. 1973. The collapse mechanism in partially saturated soil. *Engineering Geology*, **7**(1): 49–60.

Bishop, A.W., and Blight, G.E. 1963. Some aspects of effective stress in saturated and partly saturated soil. *Géotechnique*, **13**(13): 177–197.

Booth, A.R. 1977. Collapse settlement in compacted soils. CSIR Research Report 324, Council for Scientific and Industrial Research, Pretoria, South Africa.

Brooks, R.H., and Corey, A.T. 1964. Hydraulic properties of porous media. Colorado State University Hydrology Paper, Fort Collins, Nr. 3, Vol. 27, March.

Dakshnamurthy, V., Fredlund, D.G., and Rahardjo, H. 1984. Coupled three-dimensional consolidation theory of unsaturated porous media. *Proceedings, 5th International Conference on Expansive Soils, Adelaide, Australia, May*, pp. 99–104.

Fredlund, D.G., and Rahardjo, H. 1993. *Soil mechanics for unsaturated soils*. John-Wiley and Sons, New York.

Fredlund, D.G., and Morgenstern, N.R. 1976. Constitutive relations for volume change in unsaturated soils. *Canadian Geotechnical Journal*, **13**(3): 261–276.

Freeze, R.A., and Cherry, J.A. 1979. *Groundwater*. Englewood Cliffs, Prentice-Hall, NJ.

Fung, Y.C. 1965. *Foundations of solid mechanics*. Prentice-Hall, Incorporated, Englewood Cliffs, NJ.

Gardner, W.R. 1961. Soil suction and water movement. *In Pore Pressure and Suction in Soils*. London, Butterworths, pp. 137–140.

Jennings, J.E.B., and Burland, J.B. 1962. Limitations to the use of effective stresses in partly saturated soils. *Géotechnique*, **12**(2): 125–144.

Jennings, J.E.B., and Knight, K. 1957. The additional settlement of foundations due to collapse of structure of sandy subsoil on wetting. *Proceedings, 4th International Conference on Soil Mechanics and Foundation Engineering, Vol. 1*, pp. 316–319.

Lawton, E.C., Fragaszy, R.J., and Hardeastle, J.H. 1991. Stress ratio effects on collapse of compacted clayey sand. *Journal of Geotechnical Engineering*, **117**(5): 714–730.

- Lloret, A., and Ledesna, A. 1993. Unsaturated soils: recent developments and applications. Civil Engineering European Courses, Barcelona, June.
- Lourens, J.P., and Czapla, H. 1987. Prediction of collapse settlement of a high embankment. *Civil Engineer in South Africa*, **29**(2): 49–57.
- Maswoswe, J. 1985. Stress paths for a compacted soil during collapse due to wetting. Ph.D. thesis, Imperial College of Science and Technology, London, England.
- Matyas, E.L., and Radhakrishna, H.S. 1968. Volume change characteristics of partially saturated soils. *Géotechnique*, **18**(4): 432–448.
- Miranda, A.N. 1988. Behavior of small earth dams during initial filling. Ph.D. thesis, Colorado State University, Fort Collins, USA.
- Pereira, J.H. 1996. Numerical analysis of the mechanical behavior of small collapsing earth dams during first reservoir filling. Ph.D. thesis, University of Saskatchewan, Saskatoon, SK, Canada.

The prediction of total heave

D.G. Fredlund, J.U. Hasan, and H.L. Filson

Abstract: Numerous methods have been proposed in various geographic regions for the prediction of total heave. This paper provides a theoretical context within which the various methods can be visualized with respect to the stress path followed.

The effect of sampling disturbance is isolated as a significant factor affecting the prediction of heave. An empirical procedure is proposed to compensate for the effect of sampling disturbance. The determination of the *in situ* state of stress from the constant volume oedometer test is also described. This information is used in a method proposed in this paper for the prediction of total heave.

Key words: total heave, stress path, one-dimensional heave analysis, boundary stress conditions, sampling disturbance, swelling soils.

Introduction

Engineers are well aware of the severe distress that lightly loaded structures can suffer when placed on a swelling soil that is subjected to environmental changes. The prediction of heave of such structures has probably received more attention than any other analysis associated with swelling soils. As a result, numerous methods have been proposed and utilized for the prediction of total heave. Table 1 lists most of the proposed analytical procedures for predicting heave (McKeen 1976) along with their country of origin. Each method for predicting heave has been used in a restricted geographical region and little attempt has been made to embrace the various procedures within one consistent theoretical context.

The objectives of this paper are as follows:

- (1) to formulate a general one-dimensional, theoretical framework that will embrace all methods of heave analysis and thereby allow their comparison.
- (2) to review some of the methods of heave analysis within the proposed theoretical context and demonstrate the stress paths followed.
- (3) to propose another method for the prediction of heave. The method is based on one-dimensional oedometer tests and differs from previous procedures primarily in the manner of interpretation of the data.

Theoretical considerations

Two independent stress variables are required to describe the state of stress in an unsaturated soil (Fredlund and Morgenstern 1977). The preferable stress state variables are $(\sigma - u_a)$ and $(u_a - u_w)$ where σ is the total stress, u_a is the pore-air pressure and u_w is the pore-water pressure. $(\sigma - u_a)$ is herein called the total stress term and

$(u_a - u_w)$ is called the matric suction term. Although other combinations are feasible for the stress state variables, this combination is most satisfactory since the effects of externally applied loads and the effects of environmental changes can readily be separated in terms of stress changes. The pore-air pressure in the prediction of heave analysis will be approximately atmospheric. The assumption is made that the osmotic suction of the soil remains constant or else is simulated between the laboratory and the *in situ* conditions. In either case it will not appear in the analysis.

The continuity requirement that must be satisfied for an unsaturated soil is as follows:

$$[1] \quad \frac{\Delta V}{V} = \theta_w + \theta_a$$

where:

V = volume of a referential element,

θ_w = change in the amount of water (by volume) in the referential element, and

θ_a = change in the amount of air (by volume) in the referential element.

The continuity requirement demonstrates that constitutive relations are required for at least two of the volume change variables. The change in the volume of the referential element (i.e., strain of the soil structure) can be written as the sum of the orthogonal linear strains (Fredlund 1973).

$$[2] \quad \frac{\Delta V}{V} = \epsilon_x + \epsilon_y + \epsilon_z$$

where:

$\epsilon_x, \epsilon_y, \epsilon_z$ = strain in the x-, y-, and z-directions.

D.G. Fredlund. Professor, University of Saskatchewan, 57 Campus Drive, Saskatoon, SK, Canada, S7N 5A9.

J.U. Hasan. Graduate Student, University of Saskatchewan, 57 Campus Drive, Saskatoon, SK, Canada, S7N 5A9.

H.L. Filson. Yellowhead Consulting Engineers Ltd., Saskatoon, SK, Canada.

Reproduced with permission from the *Proceedings, 4th International Conference on Expansive soils*, Denver, CO, USA, June 16–18, Vol. 1, pp. 1–17, 1980.

Table 1. Proposed methods of predicting heave.

Name of Method	Reference		
	Year	Author	Country
Methods utilizing the Oedometer			
1. Double Oedometer Method	1957	Jennings and Knight	South Africa
	1969	Jennings	
2. Salas and Serratosa Method	1957	Salas and Serratosa	Spain
3. Volumeter Method	1961	DeBruijn	South Africa
4. Mississippi Method	1962	Clisby	USA
	1972	Teng et al.	
	1973	Teng et al.	
	1975	Teng and Clisby	
5. Sampson, Schuster and Budge's Method	1965	Sampson et al.	USA
6. Noble Method	1966	Noble	Canada
7. Sullivan and McClelland Method	1969	Sullivan and McClelland	USA
8. Holtz Method	1970	Holtz	USA
9. Navy Method	1971	NAVFAC	USA
10. Direct Model Method (Texas Highway Department)	1973	Smith	USA
11. Simple Oedometer Method	1973	Jennings et al.	South Africa
12. USBR Method	1973	Gibbs	USA
Other Methods			
1. McDowell Method	1956	McDowell	USA
2. Van der Merwe Method	1964	Van der Merwe	South Africa
3. Richards Method	1967	Richards	Australia
4. Australian Method	1969	Atchison and Woodburn	Australia
5. Corps of Engineers Method	1974	Johnson	USA
	1977	Snethen et al.	
	1977	Johnson	
	1978	Johnson	
	1978	Johnson and Snethen	

The linear strains can be linked to the stress state variables in a semi-empirical manner to give suitable constitutive equations. The equations are an extension of the elasticity formulation used for saturated soils (Fredlund and Morgenstern 1976).

$$[3a] \quad \varepsilon_x = \frac{(\sigma_x - u_a)}{E_1} - \frac{\mu_1}{E_1}(\sigma_y + \sigma_z - 2u_a) + \frac{(u_a - u_w)}{H_1}$$

$$[3b] \quad \varepsilon_y = \frac{(\sigma_y - u_a)}{E_1} - \frac{\mu_1}{E_1}(\sigma_x + \sigma_z - 2u_a) + \frac{(u_a - u_w)}{H_1}$$

$$[3c] \quad \varepsilon_z = \frac{(\sigma_z - u_a)}{E_1} - \frac{\mu_1}{E_1}(\sigma_x + \sigma_y - 2u_a) + \frac{(u_a - u_w)}{H_1}$$

where:

E_1 = Young's modulus with respect to $(\sigma - u_a)$,

μ_1 = Poisson's ratio, and

H_1 = elastic modulus with respect to $(u_a - u_w)$.

The constitutive equation for the water phase can be written:

$$[4] \quad \theta_w = \frac{(\sigma_x + \sigma_y + \sigma_z - 3u_a)}{3H_1'} + \frac{(u_a - u_w)}{R_1}$$

where:

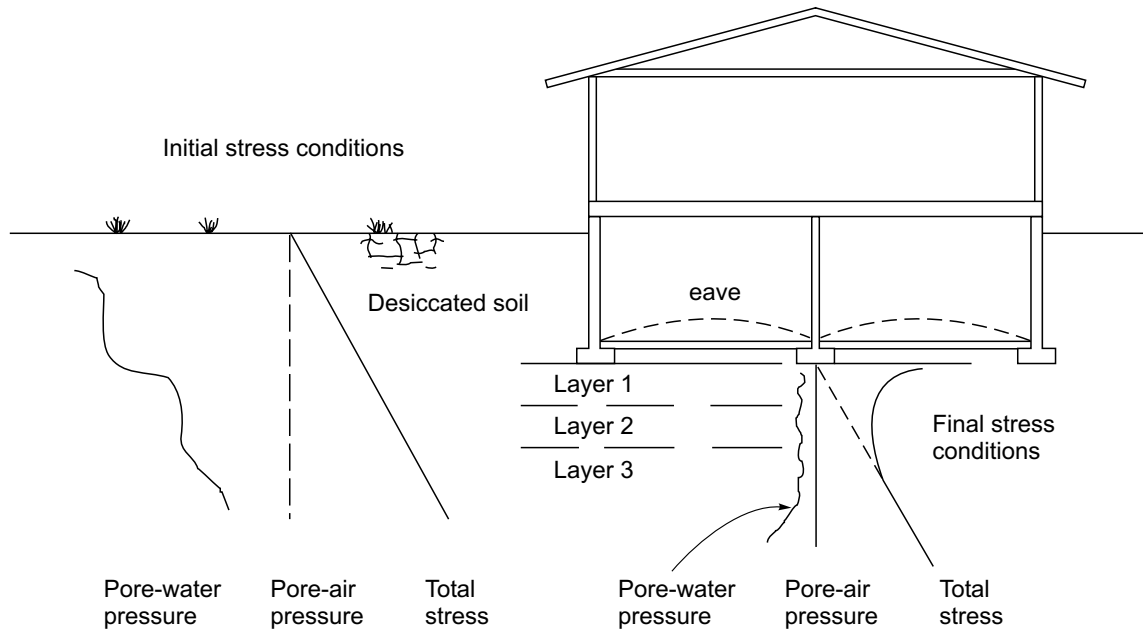
H_1 = water phase modulus with respect to $(\sigma - u_a)$, and

R_1 = water phase modulus with respect to $(u_a - u_w)$.

The proposed constitutive equations have been experimentally tested for uniqueness near a point (Fredlund and Morgenstern 1976) and for uniqueness when larger stress increments are used (Matyas and Radhakrishna 1968; Barden et al. 1969). The results indicate uniqueness as long as the deformation conditions are monotonic. This means that the soil parameters must change for increases and decreases in their respective volumes.

Example problem

Let us consider the construction of a light residential building on desiccated, unsaturated soil (Fig. 1). Prior to construction the pore-water will be in a state of tension due to evaporation and evapotranspiration at the ground surface. The unloading due to excavation will further induce tension in the water phase. The pore-air pressure will be approximately equal to atmospheric conditions. The construction of the house essentially curtails moisture movement away from the region below the basement

Fig. 1. Initial and final stresses below a light residential building.

floor slab. With time, water accumulates below the house resulting in a decrease in the pore-water tension and subsequent heaving of the house.

An analysis for the prediction of heave must utilize the constitutive equations to relate the initial and final stress states. In fact, all methods for the prediction of heave can be viewed in terms of (1) the procedure used to evaluate the initial state of stress, (2) the manner in which the final state of stress is estimated and (3) the constitutive model used to relate the initial and final stress states.

Derivation of the one-dimensional heave analysis

Let us consider an element of an unsaturated soil from below the house basement. The strain in the y -direction (i.e., vertical direction) is given by eq. [3b]. For the one-dimensional case, the strains in the x - and y - directions are zero while their changes in total stress are equal. The $(\sigma_x - u_a)$ and $(\sigma_z - u_a)$ terms can be computed by equating eqs. [3a] and [3c].

$$[5] \quad (\sigma_x - u_a) = (\sigma_z - u_a) \\ = \frac{\mu_1}{(1 - \mu_1)} (\sigma_y - u_a) - \frac{E_1}{(1 - \mu_1)} (u_a - u_w)$$

Substituting eq. [5] into eq. [3b] gives,

$$[6] \quad \varepsilon_y = m_1^s d(\sigma_y - u_a) + m_2^s d(u_a - u_w)$$

where:

$$m_1^s = \frac{1}{E_1} - \frac{(1 + \mu_1)(1 - 2\mu_1)}{E_1(1 - \mu_1)}$$

soil structure compressibility modulus associated with a change in $(\sigma_y - u_a)$, and

$$m_2^s = \frac{1 + \mu_1}{H_1(1 - \mu_1)} ;$$

soil structure compressibility associated with a change in $(u_a - u_w)$.

It is often more convenient to use the change in void ratio, Δe , rather than strain. In this case,

$$[7] \quad \Delta e = \varepsilon_y(1 + e_0)$$

where:

$$e_0 = \text{initial void ratio.}$$

The amount of heave associated with each arbitrary layer (i.e., the i -th layer; Fig. 1) is computed as the vertical strain, ε_y , multiplied by the thickness of the layer, h_i . The total heave for each layer, Δh_i is,

$$[8] \quad \Delta h_i = h_i [m_1^s d(\sigma_y - u_a) + m_2^s d(u_a - u_w)]$$

The stress state variable changes must be computed for each layer from measured, assumed or computed initial and final stress boundary conditions. Appropriate moduli must be assigned for each layer. The total heave is equal to the sum of the heaves computed for each layer.

$$[9] \quad \Delta h = \sum_{i=j}^{i=1} \Delta h_i$$

A change in the volume of water in the referential element can be computed on the basis of the assumptions associated with one-dimensional strain.

$$[10] \quad \theta_w = m_1^w d(\sigma_y - u_a) + m_2^w d(u_a - u_w)$$

where:

$$m_1^w = \frac{1 + \mu_1}{3H_1'(1 - \mu_1)} ;$$

slope of the $(\sigma_y - u_a)$ versus water volume plot when $d(u_a - u_w)$ is zero, and

$$m_2^w = \frac{3(1 - \mu_1)H_1' H_1 - 2E_1 R_1}{3(H_1' H_1 R_1(1 - \mu))} ;$$

slope of the $(u_a - u_w)$ versus water volume plot when $d(\sigma_y - u_a)$ is zero.

The change in volume of water in the soil can be written as a change in water content as follows:

$$[11] \quad w = \frac{\theta_w(1 + e_0)}{G_s}$$

where:

w = water content, and
 G_s = specific gravity.

The degree of saturation, as well as all other volume-weight relations can now be computed.

A total of four compressibility moduli have been defined to completely describe the volume-weight soil properties under any set of stress conditions. However, in general this can be reduced. When predicting total heave, it is not necessary to compute change in water content. Therefore, only the m_1^s and m_2^s moduli are required. In addition, if changes in total stress are negligible, only the m_2^s modulus is required. It should also be noted that the final water contents can be estimated since the final degree of saturation will approach 100 percent (Fredlund 1979).

$$[12] \quad \Delta w = S_f \Delta e / G_s - e_0 \Delta S / G_s$$

where:

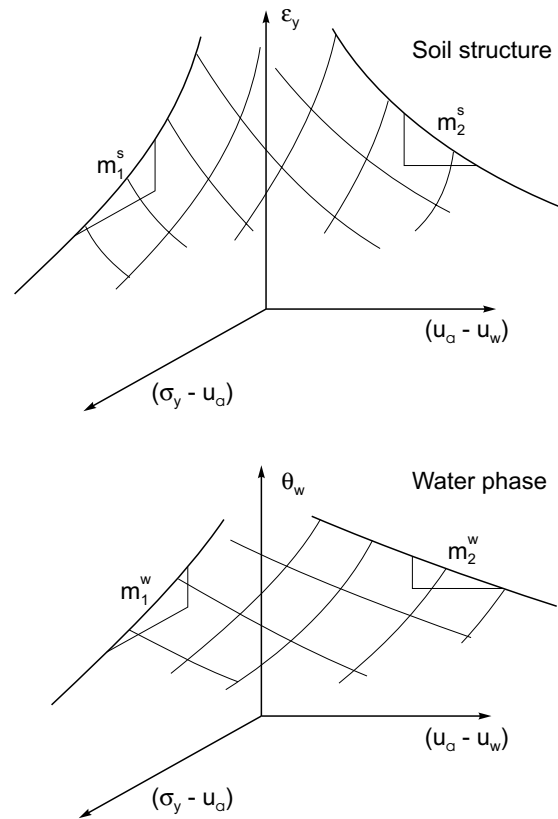
S_f = final degree of saturation, and
 ΔS = change in degree of saturation.

Equations [6] and [10] can be visualized as two three-dimensional surfaces (Fig. 2). The surfaces differ for loading and unloading conditions, and for increasing and decreasing matric suction.

Initial and final boundary stress conditions

In order to perform a heave analysis, the initial and final stress conditions must be known. The initial total stress, σ_y , can be computed using conventional total stress theory. The initial pore-air pressure can be estimated as equal to atmospheric pressure. The initial pore-water pressure is highly negative and difficult to evaluate. Attempts have been made to measure the pore-water pressure *in situ* using devices such as tensiometers and psychrometers. Tensiometers have the disadvantage that their range is limited to one atmosphere negative. Psychrometers have the limitation that the soil must have a relatively high pore-water tension and be in an equilibrium temperature condition (Krahn 1970). As well, the

Fig. 2. Constitutive surfaces for an unsaturated soil.



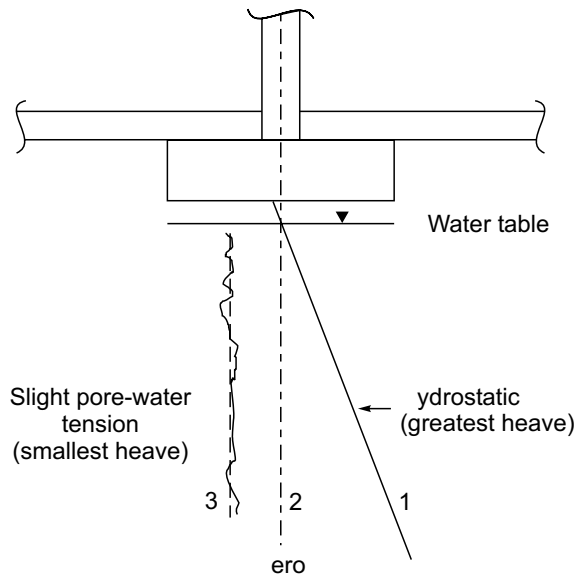
measured value is total suction and must be corrected for osmotic suction unless the soil moduli are measured in terms of total suction.

Axis-translation, null type tests can be performed in the laboratory on undisturbed samples. However, if these results are used to estimate the *in situ* pore-water pressure it is necessary to correct the measured value for changes in pore-water pressure due to unloading and sample disturbance.

One-dimensional oedometer tests can be performed on undisturbed samples to estimate the pore-water pressure. The test procedures used are variable and subjected to diverse interpretations. In particular, the effects of sample disturbance must be taken into consideration and it must be realized that measurements are being performed on the total stress plane.

The final total stress can be computed using the elastic stress theory. The final pore-air pressure is atmospheric. The final pore-water pressure conditions must be estimated. One of three possibilities provide the most logical assumption for the final pore-water pressure (Fig. 3). First, it can be assumed that the water table will rise to the surface, creating a hydrostatic condition. This assumption produces the greatest heave prediction. Second, it can be assumed that the pore-water pressure approaches zero throughout its depth. This may be a realistic assumption; however, it is not an equilibrium condition. Third, it can be assumed that under long-term equilibrium conditions the pore-water pressure will remain slightly nega-

Fig. 3. Final pore-water pressure boundary conditions.



tive. This assumption produces the smallest prediction of heave. Any one of the above three assumptions produce relatively similar predictions of heave in most cases. This is due to the fact that most of the heave occurs in the uppermost soil layers where the change in matric suction is largest and the soil modulus is largest. The choice of a final pore-water pressure boundary condition could vary from one geographic location to another depending upon the climate conditions.

Visualization of procedures for heave analysis

Each of the procedures for predicting heave mentioned in Table 1 can be visualized in terms of the stress paths followed on the constitutive surfaces. Only a few of the methods will be used to demonstrate the stress path followed.

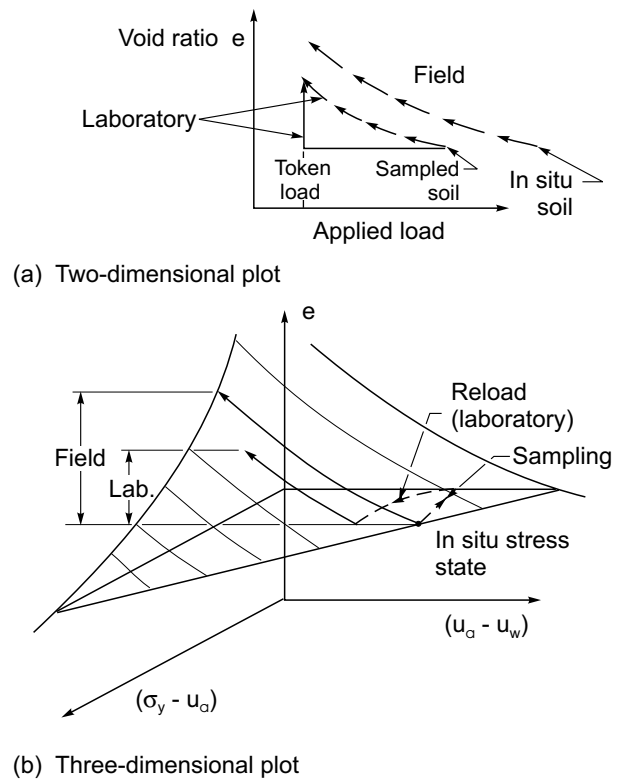
Direct model method

The direct model method is based on free-swell consolidation tests on undisturbed samples placed in an oedometer (Fig. 4). Specimens are subjected to the overburden pressure (or the load that will exist at the end of construction) and allowed free access to water. The predicted heaves are generally significantly below actual field heaves. The stress path followed by the test procedure is shown in Fig. 4b. The conventional two-dimensional manner for plotting the test data is shown in Fig. 4a. The under-estimation of heave appears to be primarily due to sampling disturbance.

Sullivan and McClelland consolidometer method

The prediction of heave is based on a constant volume oedometer test on an undisturbed sample initially subjected to the overburden pressure. Once the swelling pressure has been reached, the specimen is rebound. The

Fig. 4. Stress path for the direct model method.



stress path followed is shown in Fig. 5. There are limited case histories published but in general the authors would expect this method to under-estimate heave since sample disturbance has not been taken into account.

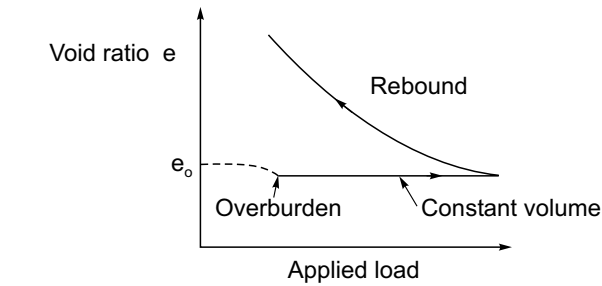
Richards method

Richards method is based on a laboratory suction test which yields a water content versus matric suction curve. The suction measured at the 10 foot depth is used as the final equilibrium suction. A change in water content is computed which is empirically converted to a change in volume (Fig. 6). The authors are not aware of substantiating case histories.

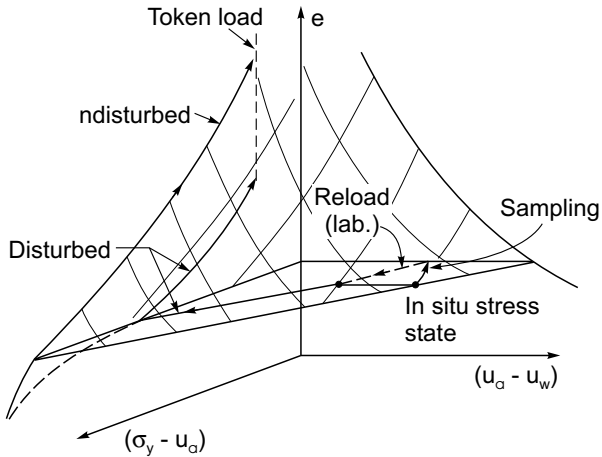
Jennings and Knight double oedometer method

This method is based on the two oedometer tests; namely, a free-swell oedometer test that is initially under a token load of 0.01 t/ft² (1 kPa) and a natural water content oedometer test. The natural water content oedometer test data are adjusted vertically to match the free-swell test results at high applied loads. Various loading conditions and final pore-water pressures can be simulated in the analysis. In general, the analysis shows over-prediction of the actual heave (Jennings and Knight 1957). The stress paths followed by the two tests are shown in Fig. 7. The authors suggest that the predicted heave is generally satisfactory since the method of analysing the data compensates for the effects of sample disturbance. In other words, the natural water content curve reflects the effect of sampling disturbance. The stress

Fig. 5. Stress path for the Sullivan and McClelland method.



(a) Two-dimensional plot



(b) Three-dimensional plot

paths of more recent, up-to-date versions of the double oedometer method can be visualized on similar three-dimensional plots.

Proposed method on heave analysis

The procedure proposed for the prediction of heave is based on constant volume oedometer tests performed on undisturbed samples. The data required from the laboratory test are the rebound modulus (and sometimes the loading modulus) and an estimate of the *in situ* pore-water pressure. The rebound modulus is relatively insensitive to sample disturbance (Schmertmann 1955). The main problem is to estimate the *in situ* pore-water pressure from the deformation characteristics measured in the laboratory. Prior to the interpretation of the laboratory results, the data should be corrected for the effects of compressibility of the apparatus (Fredlund 1969).

The constant volume oedometer tests are performed on specimens that are at least 2½ inch diameter, taken from the upper portion of the soil profile. The specimens are placed in an oedometer with an initial load approximately equal to the existing overburden load. After initial dial readings are taken, the specimen is immersed in water. As the specimen attempts to swell, increased load is applied to the soil in order to maintain its initial volume. At some point the specimen has no further tendency to swell under the applied load. This applied load is called the swelling

Fig. 6. Stress path for Richards method.

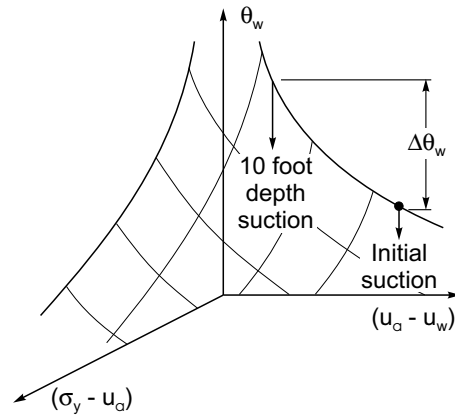
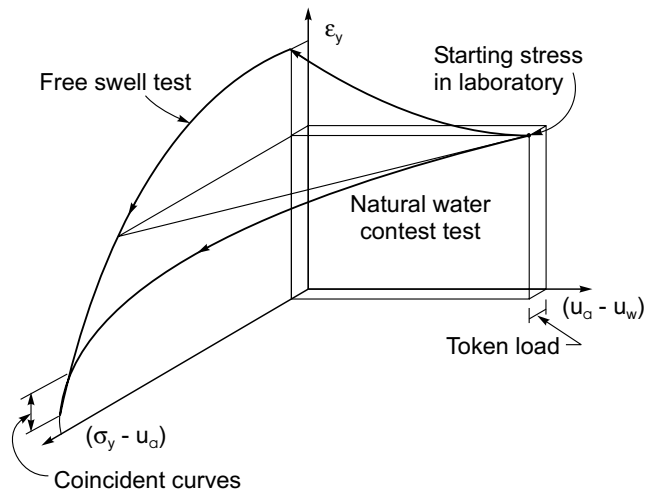


Fig. 7. Stress paths for double oedometer test (Jennings and Knight 1957).



pressure of the soil, P_s . The specimen is then loaded logarithmically up to approximately 16 t/ft² (1700 kPa). The specimen is subsequently rebound in double increments, to a token load.

The data is commonly plotted as a total pressure versus void ratio curve but the actual stress path can be more easily visualized on a three-dimensional plot using the stress state variables as abscissas. Figure 8 shows an idealized interpretation of the constant volume oedometer results where sampling is assumed to not produce disturbance to the soil. Sampling; however, does cause disturbance and the actual stress path is shown in Fig. 9. The net result of sample disturbance is a reduction in the swelling pressure, P_s . Therefore, the laboratory swelling pressure cannot be directly related to the *in situ* stress state.

No procedure has previously been proposed to correct the swelling pressure for the effect of sampling disturbance. However, the procedures commonly used to estimate the pre-consolidation pressure of a saturated soil are actually procedures which account for the effects of sample disturbance (Leonards 1962). Figure 10 shows a modified form of the Casagrande construction that is

Fig. 8. Ideal interpretation of the constant volume oedometer test.

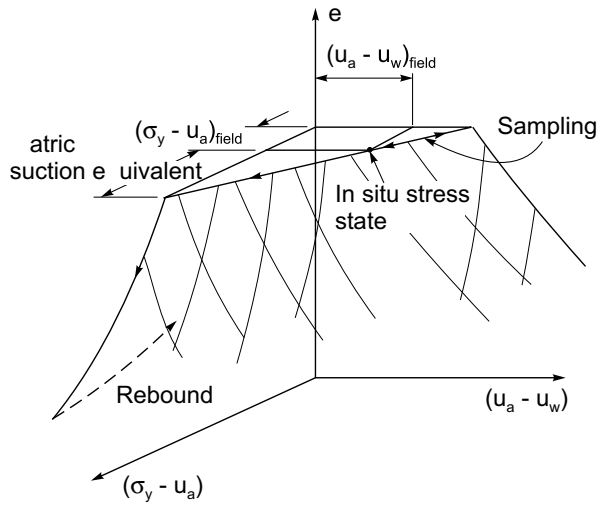
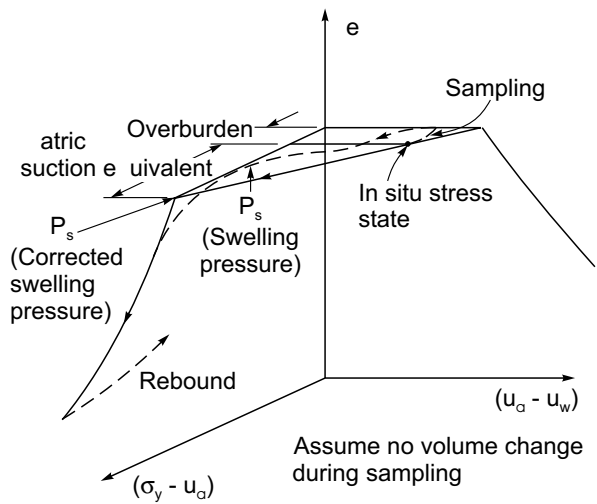


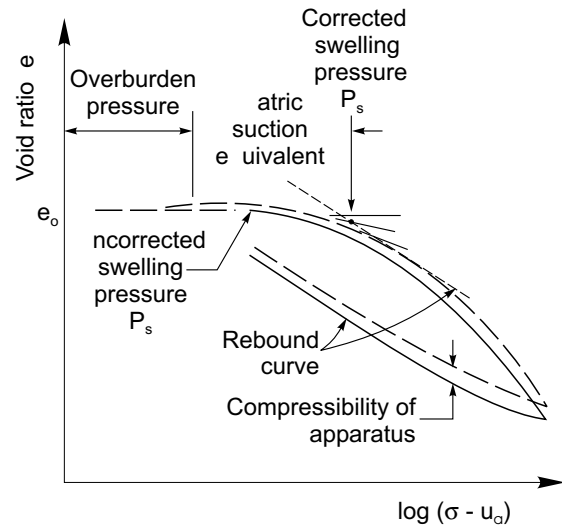
Fig. 9. Actual stress path during sampling and constant volume test.



proposed to compensate for the effect of sample disturbance in desiccated soils.

The construction procedure involves first locating the point of maximum curvature on the void ratio versus total pressure curve. The point of concern is the maximum curvature immediately past the swelling pressure. On some laboratory test results it is difficult to determine this point but in general it is readily discernible. Horizontal, tangential and bisector lines are drawn from this point. A line parallel to the rebound curve is then drawn tangent to the recompression curve. The intersection of this line with the bisector gives an abscissa that approximates the undisturbed state of stress. This point is designated as the corrected swelling pressure, P_s' . Figure 11 shows uncorrected and corrected swelling pressure results obtained on samples of compacted Regina clay. Also shown are the results of a series of free-swell oedometer tests performed

Fig. 10. Construction to compensate for sample disturbance.

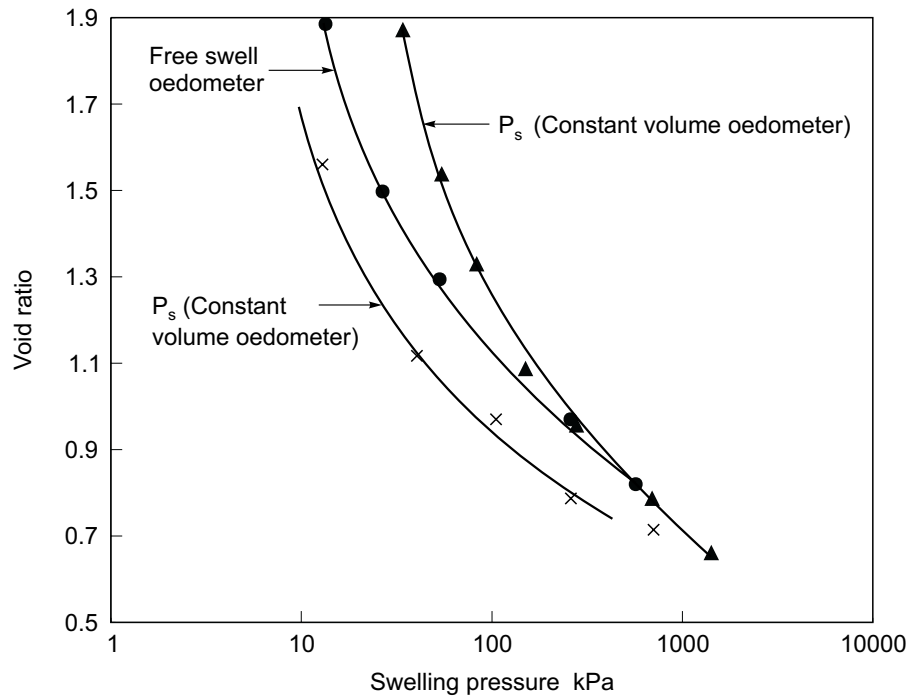
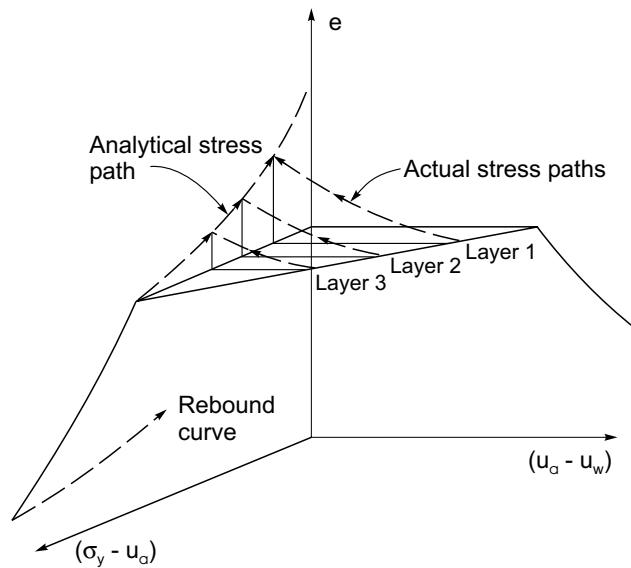


on the same soil (Fredlund 1975). The swelling pressure from the corrected constant volume oedometer tests are slightly greater than those from the free-swell oedometer tests.

The magnitude of the corrected swelling pressure, P_s' , can be subdivided into two parts. These are the overburden pressure and the matric suction equivalent, $(u_a - u_w)_L$, on the total stress plane. The matric suction equivalent is not equal in magnitude to the *in situ* matric suction. However, since the soil modulus is measured on the total stress plane, (i.e., $(\sigma - u_a)$ plane), the matric suction equivalent can be used in an analysis to predict heave (Fig. 12).

The corrections for sampling disturbance significantly effect the prediction of heave (Fredlund 1975). The predicted heave using corrected swelling pressure values may be twice the predicted heaves when the correction is not applied. It is noteworthy that attempts to use constant volume oedometer tests without accounting for the effect of sampling disturbance corrections, result in heave predictions that are generally low. The use of free-swell oedometer tests has produced greater predicted heave values which appear to be more consistent with observed heave measurements. The reason being that the free-swell swelling pressure value incorporates hysteresis which gives the effect of overcoming sample disturbance. The authors; however, do not advocate the use of the free-swell oedometer test due to the hysteresis effects incorporated in the measurement of swelling pressure.

The presentation of detailed case histories to support the above procedure are beyond the scope of this paper. Numerous case histories have been analyzed and in general the predicted heaves slightly exceed the measured heaves. The interpretation of the stress conditions statistically analyzed for undisturbed Regina clay (Fredlund et al. 1980) also support the proposed procedure for predicting heave.

Fig. 11. Void ratio versus swelling pressure for compacted Regina clay.**Fig. 12.** Comparison of the actual stress path and the stress path used in the analysis.

References

- Aitchison, G.D., and Woodburn, J.A. 1969. Soil suction in foundation design. Proceedings, 7th International Conference on Soil Mechanics and Foundation Engineering, Vol. 2, pp. 1–8.
- Barden, L., Madedor, A.D, and Sides, G.R. 1969. Volume change characteristics of unsaturated clay. ASCE, Journal of Soil Mechanics and Foundation Engineering Division, **95**(SM1): 33–51.

- Clisby, M.B. 1962. An investigation of the volumetric fluctuations of active clay soils. Ph.D. thesis, University of Texas, Austin, TX.
- DeBruijn, D.M.A. 1961. Swelling characteristics of a transported soil profile in Leeveh of Vereeniging (Transvaal), Proceedings, 5th International Conference on Soil Mechanics and Foundation Engineering, Vol. 1, pp. 43–49.
- NAVFAC 1971. Soil mechanics foundation and earth structures. Design Manual. NAVFAX DM-7, Naval Facilities Engineering Command. Department of the Navy, Bureau of Yards and Docks, Washington, D.C.
- Fredlund, D.G. 1969. Consolidometer test procedural factors affecting swell properties. Proceedings, 2nd. International Conference on Expansive Clay Soils, Texas A & M Press, College Station, TX, pp. 435–456.
- Fredlund, D.G. 1973. Volume change behavior of unsaturated soils. Ph.D. thesis, University of Alberta, Edmonton, AB, Canada.
- Fredlund, D.G. 1975. Engineering properties of expansive clays. Seminar on Shallow Foundations on Expansive Clays, Regina, SK, Canada.
- Fredlund, D.G. 1979. Second Canadian geotechnical colloquium: Appropriate concepts and technology for unsaturated soils. Canadian Geotechnical Journal, **16**(1): 121–139.
- Fredlund, D.G., and Morgenstern, N.R. 1976. Constitutive relations for volume change in unsaturated soils. Canadian Geotechnical Journal, **13**(3): 261–276.
- Fredlund, D.G., and Morgenstern, N.R. 1977. Stress state variables for unsaturated soils. ASCE, Journal of the Geotechnical Engineering Division, **103**(G75): 447–466.
- Fredlund, D.G., Krahn, J., and Hasan, J.V. 1980. Variability of an expansive clay deposit. Proceedings, 4th International Conference on Expansive Soils, Denver, CO, USA, Vol. 1, pp. 322–338.

- Gibbs, H.J. 1973. Use of consolidometer for measuring expansion potential of soils. Proceedings, Workshop on Expansive Clays and Shales in Highway Design and Construction, Vol. 1, pp. 206–213.
- Holtz, W.G. 1970. Suggested method of test for one-dimensional expansion and uplift pressure of clay soils. *In* Special Procedures for Testing Soil and Rock for Engineering Purposes. 5th Edition, ASTM Special Technical Publication 479.
- Jennings, J.E. 1969. The prediction of amount and rate of heave likely to be experienced in engineering construction on expansive soils. Proceedings, 2nd International Conference on Expansive Clay Soils, Texas A & M Press, College Station, TX, pp. 99–109.
- Jennings, J.E., and Knight, K. 1957. The prediction of total heave from the double oedometer test. Transactions of the South African Institution of Civil Engineers, 7(9): 13–19.
- Jennings, J.E., Firth, R.A., Ralph, T.K., and Nager, N. 1973. An improved method for predicting heave using the oedometer test. Proceedings, 3rd International Conferences on Expansive Clay Soils, Vol. 2, Haifa, Israel, pp. 149–156.
- Johnson, L.D. 1974. An evaluation of the thermocouple psychrometric technique for the measurement of suction in clay soils. Technical Report S-74-1, U.S. Army Corps of Engineers Waterways Experiment Station, Vicksburg, MS.
- Johnson, L.D. 1977. Evaluation of laboratory suction tests for prediction of heave in foundation soils. Technical Report S-77-7, U.S. Army Corps of Engineers Waterways Experiment Station, Vicksburg, MS.
- Johnson, L.D. 1978. Predicting potential heave and heave with time in swelling foundation soils. Technical Report S-78-7, U.S. Army Corps of Engineers Waterways Experiment Station, Vicksburg, MS.
- Johnson, L.D., and Sneten, D.R. 1978. Prediction of potential heave of swelling soil. ASTM, Geotechnical Testing Journal, 1(3): 117–124.
- Krahn, J. 1970. Comparison of soil pore water potential components. M.Sc. thesis, University of Saskatchewan, Saskatoon, SK, Canada.
- Leonards, G.A. 1962. Foundation engineering. McGraw-Hill Book Co. Inc. New York.
- Matyas, E.L., and Radhakrishna, H.S. 1968. Volume change characteristics of partially saturated soils. Géotechnique, 18(4): 432–448.
- McDowell, C. 1956. Interrelationship of load, volume, change and layer thickness of soils to the behavior of engineering structures. Proceedings of the Highway Research Board, Washington, DC, 35: 754–772.
- McKeen, R.G. 1976. Design and construction of airport pavements on expansive soils. Report No. FAA-RD-76-66 U.S. Department of Transportation, Washington, USA.
- Noble, C.A. 1966. Swelling measurements and prediction of heave for lacustrine clays. Canadian Geotechnical Journal, 3(1): 32–41.
- Richards, B.G. 1967. Moisture flow and equilibria in unsaturated soils for shallow foundations. ASTM, Special Technical Publication No. 417, Philadelphia, USA.
- Salas, J.A.J., and Serratos, J.M. 1957. Foundations on swelling clays. Proceedings, 4th International Conference on Soil Mechanics and Foundation Engineering, London, Vol. 1, pp. 424–428.
- Sampson, E., Schuster, B.L., and Budge, W.D. 1965. A method of determining swell potential of an expansive clay. Proceedings, International Conference on Expansive Clays, College Station, TX, pp. 225–275.
- Schmertmann, J.H. 1955. The undisturbed consolidation behavior of clay. ASCE Transactions, 120: 1201–1227.
- Smith, A.W. 1973. Method for determining the potential vertical rise, PVR. (Texas Test Method Tex-126-E). Proceedings, Workshop on Expansive Clays and Shales in Highway Design and Construction. Edited by Lamb, D.R. and Hanna, S.J., Vol. 1, pp. 189–205.
- Sneten, D.R., Johnson, L.D., and Patrick, D.M. 1977. An investigation of the natural microscale mechanisms that cause volume change in expansive clays. Federal Highway Administration Report FHWA-RD-77-75, available from National Technical Information Service, Springfield, VA.
- Sullivan, R.A., and McClelland, B. 1969. Predicting heave of buildings on unsaturated clay. Proceedings, 2nd International Conference on Expansive Clay Soils, Texas A & M Press, College Station, TX, pp. 404–420.
- Teng, T.C.P., Mattox, R.M., and Clisby, M.B. 1972. A study of active clays as related to highway design. Final Report MSHD-RD-72-045, Vol. 1 and 2, Mississippi State Highway Department.
- Teng, T.C.P., Mattox, R.M., and Clisby, M.B. 1973. Mississippi experimental work on active clays. Proceedings, Workshop on Expansive Clays and Shales in Highway Design and Construction. Edited by Lamb, D.R. and Hanna, S.J., Vol. 2, pp. 1–27.
- Teng, T.C.P., and Clisby, M.B. 1975. Experimental work for active clays in Mississippi. ASCE, Transportation Engineering Journal, 101(TE1, Proc. Paper No. 11105(6798)): 77–95.
- Van der Merwe, D.H. 1964. Prediction of heave from the plasticity index and percentage clay fraction of soils. Civil Engineer in South Africa, 6(6): 103–107.

The prediction and performance of structures on expansive soils

D.G. Fredlund

Abstract: Numerous analytical procedures have been proposed for the prediction of heave in swelling soils. These procedures have recently been examined within the context of unsaturated soil theory. This paper describes the theory related to the swelling of soils, outlines the procedure for testing these soils in a one-dimensional oedometer, and also explains how the data should be interpreted. Two case histories are presented.

Key words: expansive soils, heave prediction, analytical procedure, unsaturated soil, one-dimensional oedometer, case history.

Introduction

Lightly loaded structures commonly suffer severe distress subsequent to their construction. Changes in the environment around the structure result in changes in the (negative) pore-water pressure, thereby producing volume changes in the soil. Soils with a high swelling index, C_s , in a changing environment are commonly found to be highly swelling soils.

Krohn and Slosson (1980) estimated that 7 billion dollars are spent each year in the United States as a result of damage to all types of structures built on swelling soils. Jones and Holtz (1973) pointed out that more than twice as much is spent on damage due to swelling soils as is spent on damage from floods, hurricanes, tornadoes and earthquakes. Certainly the problem is of enormous financial proportions.

The prediction of heave of light structures has probably received more attention than any other analysis associated with swelling soils. Numerous analytical procedures have been proposed in various countries. Most methods have been used to a limited extent within a restricted geographical region. Only recently has there been an attempt to embrace the different methods for predicting heave within one consistent theoretical context.

It is necessary to relate soil behavior to the stress state in the soil, in order to develop a transferable science for swelling soils. The engineer must be able to visualize volume changes in terms of appropriate stress state variable changes. The success of the practice of saturated soil mechanics can be attributed largely to the ability of engineers to relate soil behavior to changes in the effective stress state variables. Swelling soils are generally unsaturated and engineers have found it much more difficult to relate soil behavior to stress state variable changes.

The primary objective of this paper is to assist engineers in relating the volume change behavior of unsaturated, swelling soils to changes in the stress state. Specifically, the objectives can be summarized as follows:

- (1) To explain how past, present and future behavior of a swelling soil can be explained in terms of stress state variables. An attempt will be made to maintain a similar philosophical framework to that used in saturated soil mechanics.
- (2) To describe a method that can be used to predict heave. The method involves the use of one-dimensional oedometer tests. Emphasis will be placed on the interpretation of the laboratory results.
- (3) To briefly present two case histories involving swelling soils. The results of these studies are used to confirm the reasonableness of the proposed method.

Stress state variables controlling behavior

Three stresses must be measured, estimated or predicted in order to describe the behavior of an unsaturated soil. These are the total stress, σ , the pore-water pressure, u_w , and the pore-air pressure, u_a . These variables can be combined into two independent stress state variables for unsaturated soils (Fredlund and Morgenstern 1977). Although various combinations of independent stress variables are possible, the $(\sigma - u_a)$ and $(u_a - u_w)$ combination has proven to be most advantageous since the effects of total stress changes and pore-water pressure changes can be separated. This is beneficial both from a conceptual and analytical standpoint since pore-air pressure can generally be assumed to be atmospheric. The $(\sigma - u_a)$ term is referred to as the net total stress and the $(u_a - u_w)$ term is referred to as the matric suction. These stress state variables provide a smooth transition when going from the unsaturated to the saturated soil case. As the degree of saturation approaches 100 percent, the pore-air pressure and the pore-water pressure become approximately equal in magnitude. When the matric suction term goes to zero,

D.G. Fredlund. Professor, University of Saskatchewan, 57 Campus Drive, Saskatoon, SK, Canada S7N 5A9.

Reproduced with permission from the *Proceedings, International Symposium on Prediction and Performance in Geotechnical Engineering*, Calgary, AB, June 17–19, 1987. pp. 51–60.

the pore-air pressure, u_a , in the $(\sigma - u_a)$ term equals the pore-water pressure, u_w .

The independent stress state variables can be used to assist in understanding the behavior of a swelling clay deposit. Let us consider a deposit of proglacial, lacustrine origin. The present physical properties and state of stress of the clay are dependent upon stress influences subsequent to deposition. When studying a potential heaving problem, the engineer must evaluate the present state of stress in the soil and determine suitable physical properties to predict future behavior.

Stress history

Deposits in a proglacial lake are initially consolidated by the buoyant weight of the overlying sediments. The drainage of the lake and the subsequent evaporation of water over the lake sediments commences a desiccation of the underlying sediments. The term "desiccation" is used to mean the drying of the soil by evaporation and evapotranspiration. The water table is simultaneously drawn below the ground surface. The total stress on the sediments remains essentially constant, while the stress in the water phase is reduced (i.e., it becomes negative above the water table). This gives rise to an increase in effective stress and the soil consolidates. The tension in the water phase acts in all directions and as a result, there is a tendency for cracking and overall desaturation of the upper portion of the profile (Fig. 1).

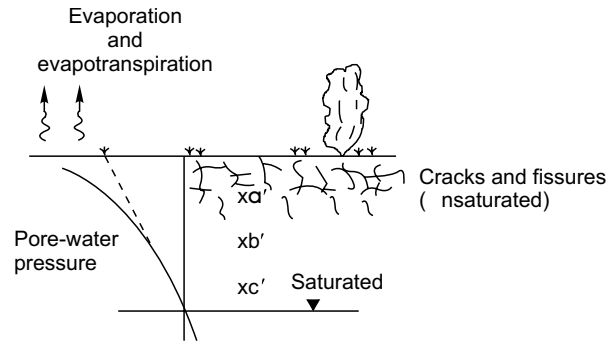
Grass, trees, and other plants also start to grow on the surface with the net effect of further drying the soil by applying a tension to the water phase. Most plants are capable of applying 10 to 20 atmospheres of tension to the water phase prior to reaching their wilting point. A high tension in the water phase (i.e., high matric suction) means that the soil is highly desiccated. The drying results in an affinity of the soil for water (Fig. 1a).

Year after year, the surface deposit is subjected to varying and changing environmental conditions. In response to these changes, the upper portion of the deposit swells and shrinks. Volume changes may extend to depths in excess of 10 feet (3 m). Environmental changes transmit a change in stress to the pore-water. The stress changes are isotropic. On the other hand, changes in total stress imposed by man are generally anisotropic. It is advantageous to separate the effects of total and pore-water pressure changes in accordance with the stress state variables involved.

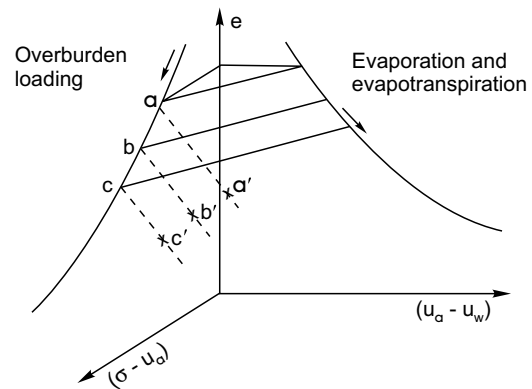
Evaporation and evapotranspiration are depicted as movements in the matric suction plane, whereas loads applied to the soil structure are shown in the net total stress plane (Fig. 1b). Wetting and drying due to environmental effects are visualized as changes along hysteresis loops in the matric suction plane. In arid and semi-arid regions, the natural water content gradually decreases.

Low water contents in clay deposits indicate that the soil has the potential to swell if evaporation and evapotranspiration from the ground surface are not permitted as a result of covering the area with a building, asphalt, etc.

Fig. 1. Stress representation after the lake sediments are subjected to evaporation and evapotranspiration.



a) Pore-water pressure during drying



b) Stress path during drying

Present state of stress

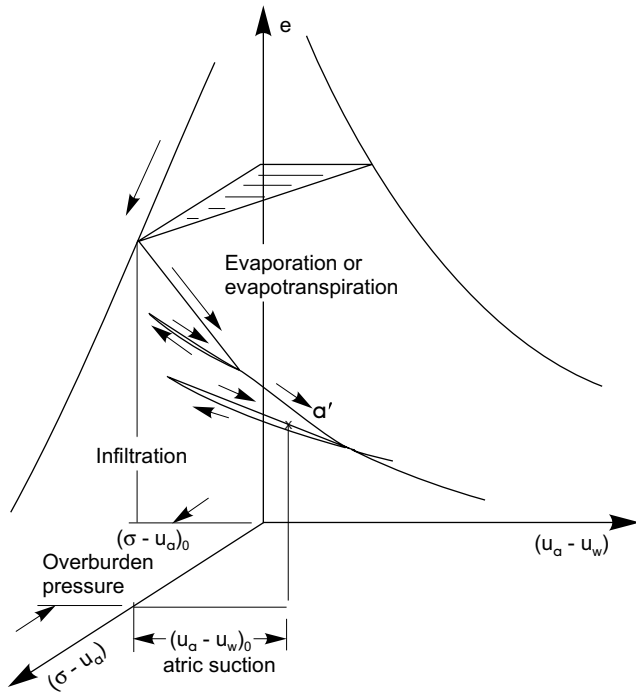
When the soil is sampled for laboratory testing purposes, the *in situ* state of stress may be anywhere along either a drying or wetting portion of the void ratio versus stress relationship. Figure 2 illustrates a typical, complex stress history. In reality, the soil has undergone thousands of cycles of drying and wetting. At the point of sampling, the soil is subjected to a specific net total stress and a specific *in situ* matric suction.

The primary laboratory information desired by the engineer for analysing a swelling problem is an assessment of: (1) the *in situ* state of stress, and (2) the swelling properties with respect to changes in matric suction. It is necessary to develop a simple, rapid, and economical procedure to obtain the information required for solving practical swelling clay problems.

Several laboratory testing procedures are used in practice to obtain the required soils information. These generally involve the use of the one-dimensional consolidation apparatus (i.e., oedometer) and are classified as the constant volume and free swell testing procedures (Noble 1966).

The oedometer can test the soil on the total stress plane. The assumption is made that it is possible to eliminate the matric suction in the soil by immersing of the specimen in water and obtaining the necessary soil properties and stress values from the total stress plane.

Fig. 2. Stress representation after soil has undergone a complex stress history caused by drying and wetting.



Let us first consider the constant volume oedometer test procedure. The specimen is subjected to a token load and submerged in water. As the specimen attempts to swell, the applied load is increased to maintain the specimen at a constant volume. This procedure is continued until there is no further tendency for swelling. The applied load at this point is referred to as the uncorrected swelling pressure, P_s . The specimen is further loaded and unloaded in the conventional manner.

The test results are commonly plotted as shown in Fig. 3a. The actual stress paths followed during the test can be more clearly understood by use of a three-dimensional plot with the stress state variables forming abscissas (Fig. 3b). An understanding of the stress paths followed during the test assist in the interpretation of the data. The void ratio and water content stress paths are shown for the situation where there is a minimum of disturbance due to sampling. Even so, the loading path displays some curvature as the total stress plane is approached. In actuality, the stress path may show even more influence from sampling (Fig. 4). Engineers have long recognized the significance of sampling disturbance when determining the preconsolidation pressure for a saturated clay. Only recently; however, has the significance of sampling disturbance been recognized in evaluating the swelling pressure of a soil (Fredlund et al. 1980a).

Sampling disturbance causes the conventional swelling pressure, P_s , to fall well below the ideal or corrected swelling pressure, P'_s . The corrected swelling pressure represents the *in situ* stress state translated to the total stress plane. It is equal to the overburden pressure plus the *in situ* matric suction translated onto the total stress

Fig. 3. Interpretation of data from a constant volume oedometer test; a) Conventional procedure for plotting constant volume oedometer data; b) ideal stress path representation of constant volume oedometer data.

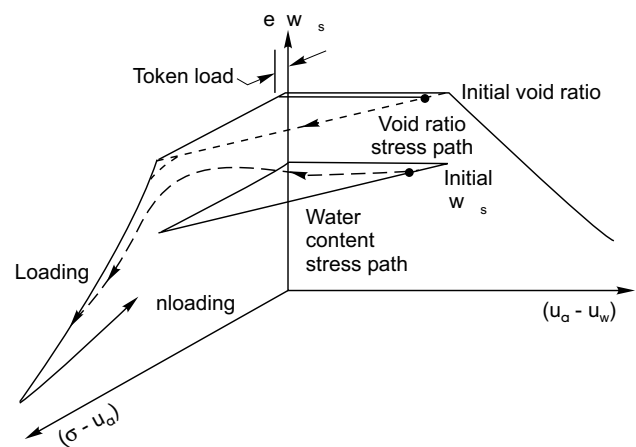
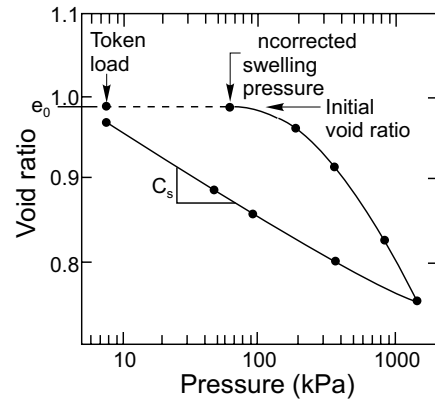
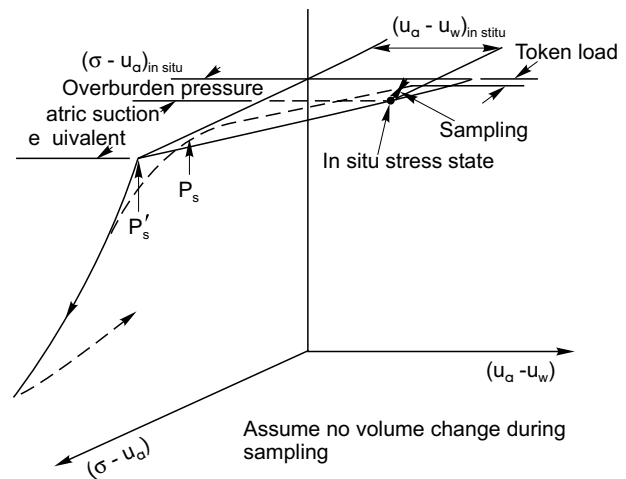


Fig. 4. Actual stress path showing the effect of sampling disturbance.



plane. The translated suction is called the matric suction equivalent (Yoshida et al. 1982). The magnitude of the matric suction equivalent will be lower than the *in situ*

matric suction; the difference being primarily a function of the *in situ* degree of saturation. The engineer needs to obtain the corrected swelling pressure from the oedometer test in order to reconstruct the *in situ* stress conditions. The procedure for accounting for sampling disturbance is discussed later in this paper.

The free swell oedometer test can also be used to measure the swelling pressure and swelling properties of a soil. The specimen is initially allowed to swell freely with a token load applied (Fig. 5). The load required to bring the specimen back to its original void ratio is termed the swelling pressure. The stress paths adhered to can be understood from a three-dimensional plot of stress state variables versus void ratio and water content. This test has the limitation that it allows volume change and incorporates hysteresis into the estimation of the *in situ* stress state (i.e., swelling pressure). On the other hand, this procedure somewhat compensates for the effect of sampling disturbance.

Future ground movements

The prediction of future ground movements requires a knowledge of (1) the initial *in situ* state of stress, (2) the swelling moduli and (3) the final state of stress. The initial state of stress can be quantified from the corrected swelling pressure. The swelling moduli can be obtained from the rebound data. The final state of stress corresponding to several years after construction must be estimated on the basis of local experience. Possible final pore-water pressure profile are discussed under final boundary conditions.

For discussion purposes, let us assume that the final pore-water pressures go to zero. Figure 6 shows the stress path that would be followed by a soil element at a specific depth. Swelling would follow a path from the initial void ratio, e_0 , to the final void ratio, e_f , along the rebound surface of the matric suction plane. The rebound surface can be assumed to be unique (Matyas and Radhakrishna 1968; Fredlund and Morgenstern 1976). Therefore, it is also possible to follow a stress path from the *in situ* stress state to the corrected swelling pressure and then proceed along the rebound curve in the total stress plane to the final stress condition. The advantage of the latter stress path is that the soil properties determined in the total stress plane can be used to predict total heave.

The effects of excavation, replacement of soil with a relatively inert material (e.g., gravel) and loadings can also be taken into account by using appropriate moduli for loading and unloading. However, it is preferable to assume that there is insufficient time for the soil to respond to each loading and unloading, and that long term heave is in response to the net loading or unloading.

Determination of *in situ* consolidation/swelling curve

When testing saturated clays, the laboratory oedometer test is used to reconstruct the *in situ* void ratio versus effective stress plot. Likewise, the laboratory oedometer test on desiccated soils can be used to construct a void ratio versus pressure plot for analysis purposes. Often the

Fig. 5. Stress path representation for the free swell oedometer test; a) conventional free swell data plot; b) three-dimensional stress path plot.

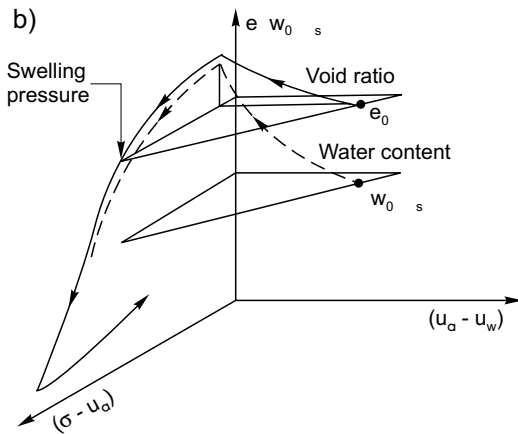
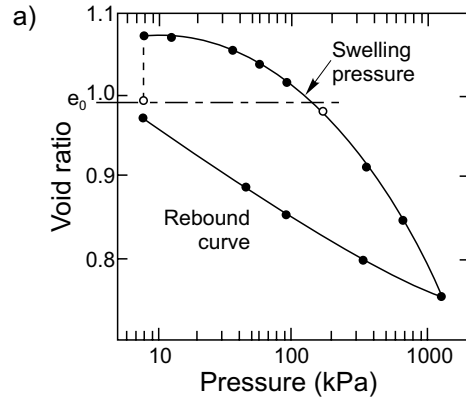
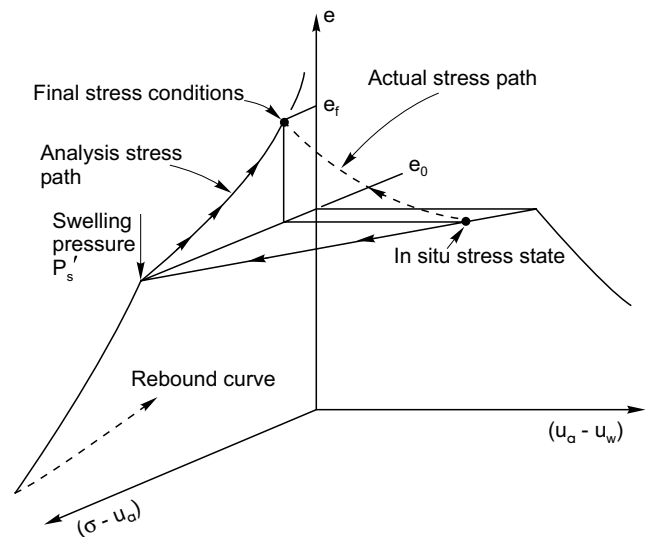


Fig. 6. Actual and analysis stress paths representing swelling of the soil.



entire laboratory loading curve is on the recompression portion; not even reaching the virgin compression branch. The preconsolidation pressure of the clay may exceed the

highest load applied in the laboratory. The corrected swelling pressure indicates the present *in situ* state of stress on the total stress plane. The lower, uncorrected swelling pressure shows the effect of sampling disturbance. Upon access to water in the field, the soil swells along the rebound curve. The laboratory rebound curve in the vicinity of the initial void ratio, e_0 , must be translated upward to pass through the corrected swelling pressure in order to show the stress path that would be followed.

The following procedure is suggested for obtaining the corrected swelling pressure. First, an adjustment should be made to the laboratory data in order to account for the compressibility of the oedometer apparatus. Desiccated, swelling soils have a low compressibility and the compressibility of the apparatus can significantly affect the evaluation of *in situ* stresses and the slope of the rebound curve (Fredlund 1969). Second, a correction must be applied for sampling disturbance. Sampling always increases the compressibility of a soil and does not permit the laboratory specimen to return to its *in situ* state of stress at its *in situ* void ratio. Casagrande (1936) proposed an empirical construction on the laboratory curve to account for the effect of sampling disturbance when assessing the preconsolidation pressure of a soil. Other construction procedures have also been proposed (Schmertmann 1955). A modification of the Casagrande (1936) construction is suggested for finding the corrected swelling pressure (Fig. 7).

The need for applying a correction to the laboratory measured swelling pressure is revealed in numerous ways. First, it would be anticipated that such a correction is necessary as a result of experience in determining preconsolidation pressure. Second, attempts to use the uncorrected swelling pressure in the prediction of total heave results in predictions which are too low. Predictions using corrected swelling pressure may often be twice the magnitude of those predicted when no correction is applied. Third, the analysis of oedometer results from desiccated deposits often produce results which are difficult to interpret if no correction is applied for sampling disturbance (Fredlund et al. 1980b).

Figure 8 shows a comparison of corrected and uncorrected swelling pressure data from two soil deposits. The results indicate that it is possible for the corrected swelling pressures to be more than 300 percent of the uncorrected swelling pressures.

Theoretical derivation for prediction of heave

An equation for the prediction of heave has been previously derived using the unsaturated soil theory (Fredlund et al. 1980a). In this paper, reference is made only to the theory necessary to use the results of an oedometer test to predict total heave. All stress paths considered are transferred to the total stress plane.

The rebound portion of the oedometer test data, plotted in a semi-logarithmic form, is essentially a straight line.

$$[1] \quad e_f = e_0 - C_s \log P_f / P_0$$

Fig. 7. Construction procedure to correct for the effect of sampling disturbance.

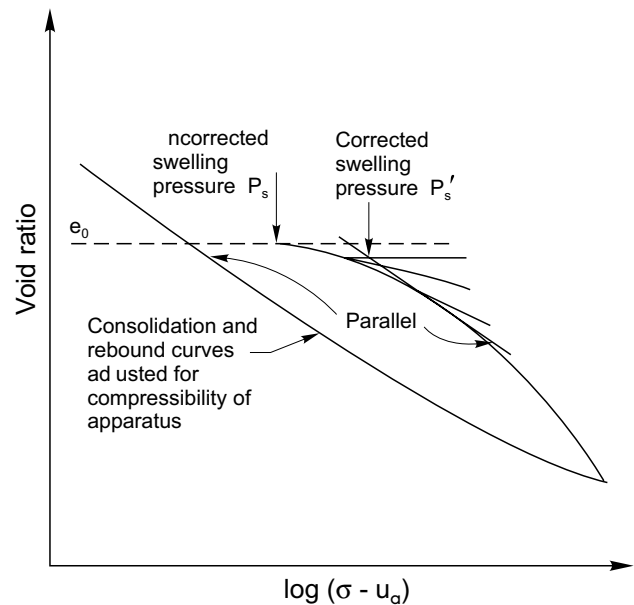
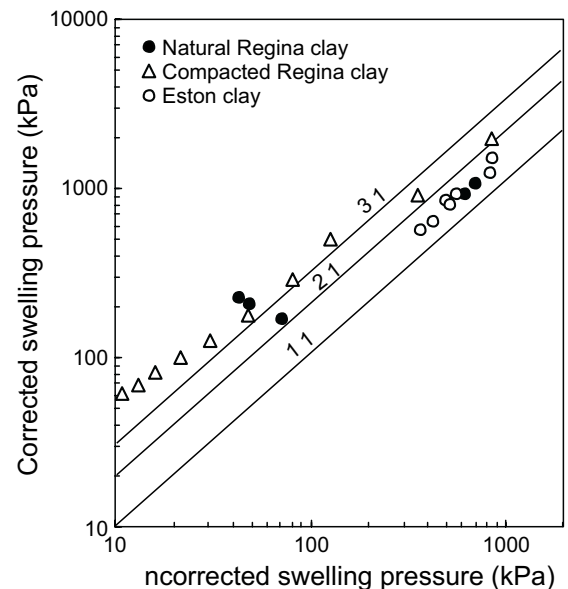


Fig. 8. Change in swelling pressure due to correction for sampling disturbance.



where:

- e_f = final void ratio,
- e_0 = initial void ratio,
- C_s = swelling index,
- P_f = final stress state, and
- P_0 = initial stress state.

The initial stress state, P_0 , is the sum of the overburden pressure and the matric suction transferred to the total stress plane (i.e., matric suction equivalent). The initial stress state is always equal to the corrected swelling pressure.

$$[2] \quad P_0 = \sigma_v + (u_a - u_w)_e$$

where:

σ_v = original overburden pressure, and
 $(u_a - u_w)_e$ = matric suction equivalent.

It is necessary to have some understanding of the corrected swelling pressure versus depth relationship for the deposit under consideration. The final stress state, P_f , must account for total stress changes and the final pore-water pressure conditions.

$$[3] \quad P_f = \sigma_v \pm \Delta\sigma - u_{wf}$$

where:

$\Delta\sigma$ = change in total stress due to excavation or placement of fill, and
 u_{wf} = estimated final pore-water pressure.

The heave in an individual soil layer can be written in terms of changes in void ratio.

$$[4] \quad \Delta h_i = h_i \Delta e / (1 + e_0)$$

where:

Δh_i = heave in a layer,
 h_i = thickness of the layer under consideration,
 and
 Δe = change in void ratio (i.e., $e_f - e_0$)

The heave in a layer in a strata can be written as:

$$[5] \quad \Delta h_i = h_i \frac{C_s}{1 + e_0} \log P_f / P_0$$

$$[6] \quad \Delta h_i = h_i \frac{C_s}{1 + e_0} \log \frac{(\sigma_v \pm \Delta\sigma - u_{wf})}{(\sigma_v + (u_a - u_w)_e)}$$

The total heave, Δh , is the sum of the heaves computed for each layer.

$$[7] \quad \Delta h = \sum \Delta h_i$$

The matric suction is often a maximum near the ground surface of a deposit. This is also the zone of lowest overburden pressure. Therefore, the ratio of P_f and P_0 is most negative in this region, resulting in the largest amount of heave.

Initial and final pore-water pressure boundary condition

The initial and final stress states must be known in order to perform a heave analysis. The initial and final total stresses can be computed using conventional total stress theory. The initial and final pore-air pressure is equal to atmospheric pressure. The need to know the initial *in situ* pore-water pressures is circumvented through the manner in which the laboratory oedometer test data is interpreted.

One of three possibilities provides the most logical estimation of the final pore-water pressure conditions. First, it can be assumed that the water table will rise to ground surface, creating a hydrostatic condition. This assumption produces the greatest heave prediction. Second, it can be

assumed that the pore-water pressure approaches zero throughout its depth. This may be a realistic assumption; however, it should be noted that it is not an equilibrium condition. Third, it can be assumed that under long-term equilibrium conditions the pore-water pressure will remain slightly negative. This assumption produces the smallest prediction of heave. It is also possible to have variations of the above assumptions with depth. As well, there may be a limit placed on the depth to which wetting will occur. Any of the above assumptions produce similar predictions of heave in most cases. This is due to the fact that most of the heave occurs in the uppermost soil layer where the matric suction change is largest.

The choice of a final pore-water pressure boundary condition can vary from one geographic location to another depending upon the climatic conditions. Russam and Coleman (1961) related the equilibrium suction below asphalt pavements to the Thornthwaite Moisture Index. On many smaller structures; however, it is often man-made causes such as leaky water lines and poor drainage that control the final pore-water pressure in the soil.

Example calculations

An example problem is presented to illustrate the calculations required to predict heave (Fig. 9, Table 1). Let us consider a 2-metre layer of swelling soil with an initial void ratio of 0.8, a total unit weight of 18.0 kN/m³ and a swelling index of 0.21.

Three oedometer tests were performed which show a decrease in the corrected swelling pressure with depth (Fig. 9).

Suppose the engineering design suggests the removal of 1/3 metre of swelling clay from the surface, prior to the placement of 2/3 metre of gravel. The unit weight of the gravel is assumed as being equal to that of the clay. The 1-2/3 metres of swelling clay is subdivided into 3 strata as shown in Fig. 9.

The initial stress state, P_0 , can be obtained by interpolation of the laboratory data to the midpoint of each layer. The final stress state, P_f , must take into account changes in the total stress and the final pore-water pressure. The final pore-water pressure is assumed to be -7.0 kPa. Equations [5] or [6] can be used to calculate the heave in each layer. The total amount of heave is computed to be 22.1 cm.

Two assumptions are made concerning the heave analysis in the example. First, it is assumed that the independent processes of excavation and placement of the gravel fill do not allow sufficient time for equilibrium to be established. Therefore, the soil responds only to the net changes in stress. Second, the designation of a final negative pore-water pressure assumes that near saturation, the slopes of the rebound curves on the matric suction plane and the total stress plane approach the same value. This assumption is reasonable provided the final pore-water pressures are relatively small.

Fig. 9. Calculations for example.

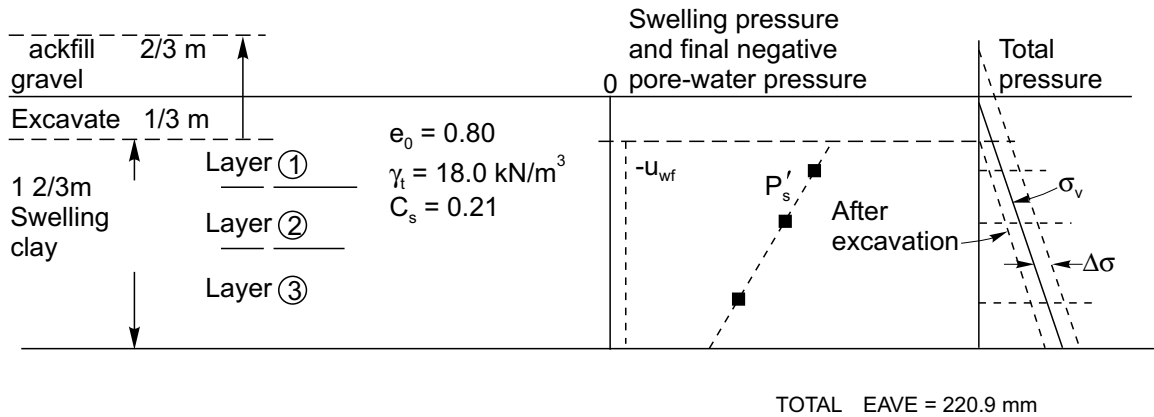


Table 1. Data for example calculation.

Layer No.	Initial stress state			Change in total stress $\Delta\sigma$ (kPa)	Final stress state		
	Thickness (mm)	$P_0 = P'_s$ (kPa)	Initial overburden stress σ (kPa)		Final pore-water pressure u_{wf} (kPa)	$P_f = \sigma_v \pm \Delta\sigma - u_{wf}$ (kPa)	Δh_i (kPa)
1	333	800	9.0	+6.0	-7.0	22.0	60.6
2	500	608	16.4	+6.0	-7.0	29.4	76.7
3	833	300	28.4	+6.0	-7.0	41.4	83.6

Case histories

Two case histories are briefly presented to demonstrate that the proposed method for predicting total heave can be used with a reasonably high degree of confidence.

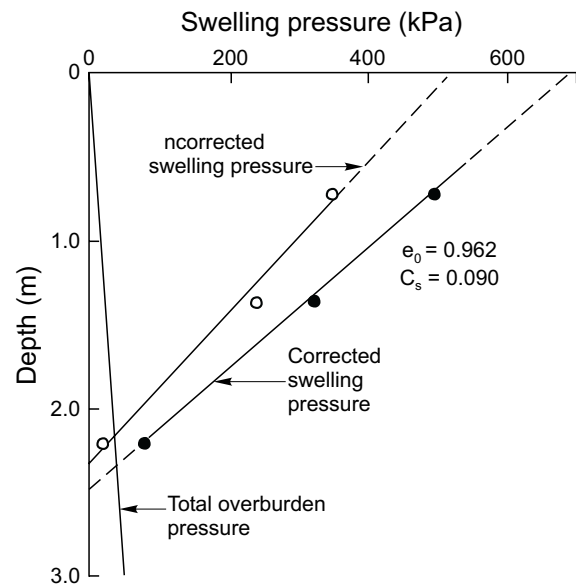
Slab-on-grade floor, Regina, Saskatchewan

In 1961, the Division of Building Research, National Research Council, undertook to monitor the performance of a light industrial building which was being constructed in north-central Regina. Details of the study have been presented by Yoshida et al. (1983). Instrumentation was installed to monitor ground movements at various depths below the slab. Water content changes were monitored using a neutron moisture meter probe. Undisturbed samples were taken as part of the subsurface exploration prior to the construction of the building. Constant volume oedometer tests were performed on three specimen and the swelling pressures are shown in Fig. 10. The average swelling index was 0.09.

Approximately one year after construction, the owner noticed considerable cracking of the floor slab. Precise level surveys showed the maximum total heave to be 106 mm. The owner had also noticed a significant increase in water consumption (i.e., 35 000 litres). It was discovered that a leak had occurred in the hot water line beneath the floor slab, at the location of maximum heave. The leak was immediately repaired.

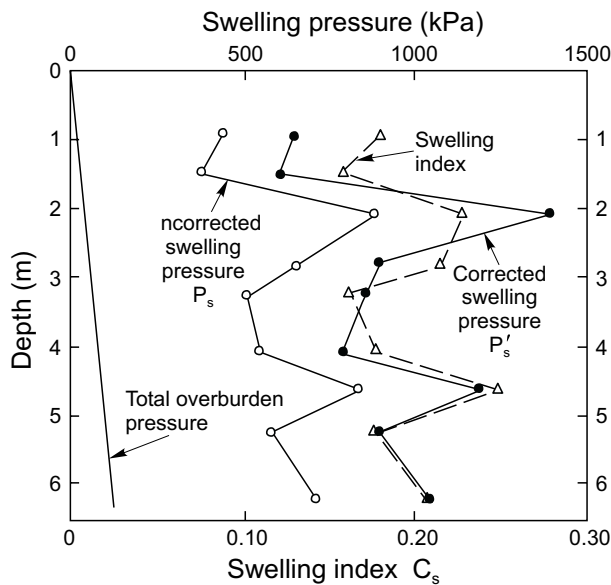
Heave analyses were performed using the laboratory oedometer data. Various assumptions were made concerning the final pore-water pressures. When it was assumed that the soil had become saturated and the water table had

Fig. 10. Swelling pressure versus depth for Regina clay (from Yoshida et al. 1983).



risen to the base of the floor slab, the predicted heave was 141 mm. Assuming that the negative pore-water pressures were reduced to zero gave a total heave prediction of 118 mm. Assuming a final pore-water pressure of -50 kPa, gave a total heave prediction of 66 mm. On the basis of the heave analysis, it appeared that the assumption of zero pore-water pressure was probably the most realistic for this case history. It appeared that further heave would likely have taken place had the leak not

Fig. 11. Swelling index and swelling pressure versus depth for Eston clay.



been repaired. The prediction of heave at various depths also showed close agreement with the actual measurements.

Eston School, Eston, Saskatchewan

Soils in the Eston area of Saskatchewan have long been known as extremely high swelling. The stratigraphy consists of approximately 7-1/2 metres of highly plastic, brown clay overlying the glacial till. Many light structures in the area have undergone serious distress. The building of particular interest was the Old Eston School constructed in the late 1920's.

The school building was constructed on concrete strip footings and a wooden basement floor was supported by interior surface concrete footings. The school was a two-storey structure with classrooms in both, the lower and upper levels. The lower floor was approximately 1.2 m (4 feet) below grade. The exterior concrete walls were founded approximately 1.8 m (6 feet) below grade.

A substantial amount of heave had taken place below the interior footings. Although the performance had not been precisely recorded, the heave in one portion of the basement area had been severe. On two occasions during the history of the school, 15 cm to 30 cm (6 to 12 inches) of soil had been removed from below the interior footings. As much as 45 cm to 90 cm (1-1/2 to 3 feet) of total heave had occurred during the life of the school, according to maintenance records. Large amounts of differential heaving of the floor (i.e., 15 cm or 6 inches) were measured in 1960. The school was demolished in 1967.

In 1981, a subsurface investigation was conducted adjacent to the location of the old school. Undisturbed soil samples were taken and constant volume oedometer tests

were performed. The results are presented in Fig. 11. The average natural water content throughout the profile was 25 percent. The average plastic limit was 27 percent and the average liquid limit was 100 percent. The average swelling index was 0.21. Due to a lack of detailed information on the soil and performance conditions of the school, it was not possible to do a precise total heave analysis. It was of interest; however, to perform an approximate analysis. Using the corrected swelling pressure from Fig. 11 and assuming the negative pore-water pressures went to zero, the predicted heave would be in excess of 90 cm (3 feet).

Further case history studies would be useful in confirming the proposed procedure for predicting total heave.

References

- Casagrande, A. 1936. The determination of the pre-consolidation load and its practical significance. Discussion D-34. Proceedings, 1st International Conference on Soil Mechanics and Foundation Engineering, Cambridge, Vol. 3, pp. 60-64.
- Fredlund, D.G. 1969. Consolidometer test procedural factors affecting swell properties. Proceedings, 2nd Conference on Expansive Clay Soils, Texas A & M Press, College Station, TX, pp. 435-456.
- Fredlund, D.G., and Morgenstern, N.R. 1976. Constitutive relations for volume change in unsaturated soils. Canadian Geotechnical Journal, **13**(3): 261-276.
- Fredlund, D.G., and Morgenstern, N.R. 1977. Stress state variables for unsaturated soils. ASCE, Journal of the Geotechnical Engineering Division, **103**(G75): 441-466.
- Fredlund, D.G., Hasan, J.U., and Filson, H. 1980a. The prediction of total heave. Proceedings, 4th International Conference on Expansive Soils, Denver, CO, Vol. 1, pp. 1-17.
- Fredlund, D.G., Krahn, J., and Hasan, J.V. 1980b. Variability of an expansive clay deposit. Proceedings, 4th International Conference on Expansive Soils, Denver, CO, Vol. 1, pp. 322-338.
- Jones, D.E., and Holtz, W.G. 1973. Expansive soils - the hidden disaster. ASCE, Civil Engineering, **43**: 87-89.
- Krohn, J.P., and Slosson, J.E. 1980. Assessment of expansive soils in the United States. Proceedings, 4th International Conference on Expansive Soils, Denver, CO, pp. 596-608.
- Matyas, E.L., and Radhakrishna, H.S. 1968. Volume change characteristics of partially saturated soils. Géotechnique, **18**(4): 432-448.
- Noble, C.A. 1966. Swelling measurements and prediction of heave for a lacustrine clay. Canadian Geotechnical Journal, **3**: 32-41.
- Russam, K., and Coleman, J.D. 1961. The effect of climatic factors on subgrade moisture condition. Géotechnique, **11**(1): 22-28.
- Schmertmann, J.H. 1955. The undisturbed consolidation behavior of clay. Transactions, ASCE, **120**: 1201-1227.
- Yoshida, R.T., Fredlund, D.G., and Hamilton, J.J. 1983. The prediction of total heave of a slab-on-grade floor on Regina clay. Canadian Geotechnical Journal, **20**: 69-81.

Consolidometer test procedural factors affecting swell properties

D.G. Fredlund

Abstract: The one-dimensional oedometer was originally designed to test soft, compressible soils. The use of the oedometer for testing expansive soils has meant that a number of procedural factors must be taken into account. For example, the compressibility of the apparatus has a significant effect upon the measured swelling properties of a soil.

The apparatus compressibility characteristics of a number of oedometer were measured and the data were statistically analyzed. The compressibility characteristics of the filter paper placed above and below a specimen are also presented. Recommendations are presented regarding the corrections that should be applied to oedometer test data from expansive soils.

Key words: one-dimensional oedometer, compressibility characteristics, expansive soils, filter paper, porous stone, swelling pressure.

Test procedures for evaluating swelling properties

The one-dimensional consolidometer has become widely accepted for testing swelling soils. Holtz and Gibbs (1956), Jennings and Knight (1957–58) and Lambe and Whitman (1959) were among the first to report the use of consolidometer tests for predicting heave in swelling soils. Sampson et al. (1965) reported the use of the consolidometer to predict heave in heavily over-consolidated shales. The PVR (potential vertical rise) meter as mentioned by McDowell (1965) is a special type of consolidometer used primarily to measure swelling pressure, which in turn is correlated with the potential amount of volume change. The test, performed on remolded soil, has been used extensively by the Federal Housing Administration in the United States (Henry 1965). The swelling properties of compacted, unsaturated soils have also been investigated by use of the consolidometer (Seed et al. 1961; Gizienski and Lee 1965; Noble 1966). It appeared that the consolidometer had become widely accepted for evaluating swelling soils and predicting the problems that may be encountered during and after construction (Kassiff et al. 1965).

Although the consolidometer test is used extensively for evaluating swelling clays, it should be noted that the procedures used are quite varied. In Western Canada two types of swelling tests have been used extensively (Dyregrov and Hardy 1962; Gilchrist 1963). These are the free swell (FS) and the constant volume (CV) tests. In either test, the specimen is placed in the consolidometer

and subjected to a token pressure of approximately 0.08 kg/cm^2 (7.84 kPa). The specimens are then submerged in water.

In the free swell test the specimen was allowed to change volume until equilibrium was reached. The specimen was then loaded and unloaded in the conventional manner. The pressure required to reduce the volume of the specimen to its original volume was termed the swelling pressure of the soil. In the constant volume test, the total stress on the specimen was increased after submersion in order to keep it at a constant volume. In this case, the pressure at which there was neither a tendency for volume increase or decrease was termed the swelling pressure of the soil.

The typical results shown in Fig. 1 are plotted using dashed and solid lines to show those portions of the curve which are only total stresses and those portions which are effective stresses. Additional construction lines are shown to demonstrate the interpretation of the results. The construction is based primarily on the assumption that the rebound curves remain parallel when shifted vertically on the void ratio versus pressure plot (Schmertmann 1953; Rutledge 1944; Sampson et al. 1965).

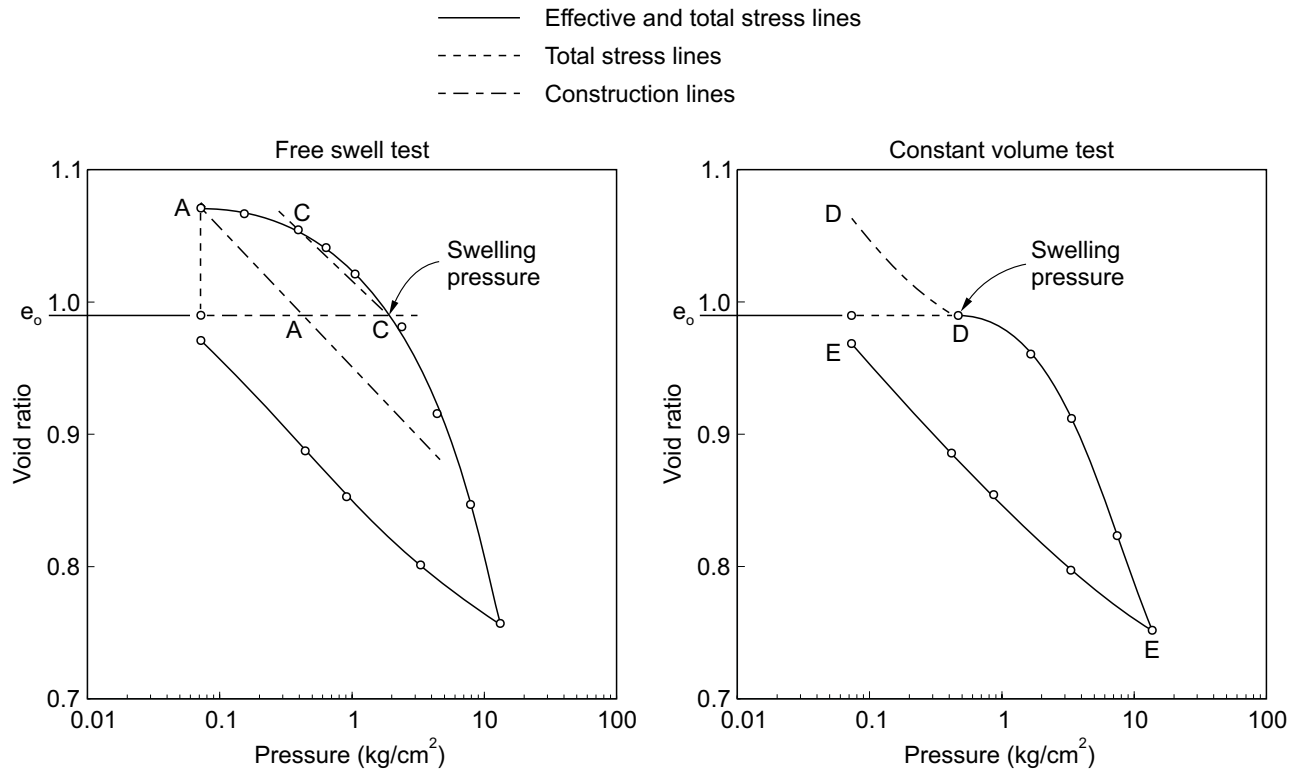
In the constant volume test, the initial effective stress in the soil was assumed equal to the value at point *D*. During submersion with water, the negative stresses in the pore water were released until atmospheric pressure was attained. Release of the total stress on the specimen allowed rebound along line *D–D'*. Using the same line of reasoning for the free swell test lead us to assume that point *A* should be of similar magnitude to point *D* from the CV test. However, a prediction of heave analysis, based upon the FS test, generally assumed the initial field effective stress equal to point *C*.

The two procedures outlined produced swelling pressure values which were considerably different in magnitude (Noble 1966). The swelling pressure obtained from the FS test (Point *C*) appeared to be incorrectly inter-

D.G. Fredlund. Professor, Department of Civil Engineering, University of Saskatchewan, 57 Campus Drive, Saskatoon, SK, Canada S7N 5A9.

Reproduced with permission from the *Proceedings, 2nd International Conference on Expansive Clay soils*. College Station, TX, Texas A&M Press, pp. 435–456, 1969.

Fig. 1. Typical consolidation test results; a) Free swell, b) constant volume.



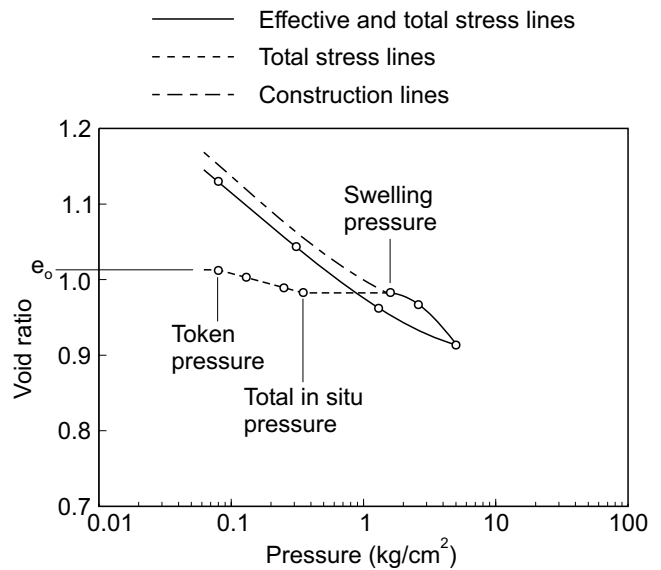
preted. In practice; however, the results are continued to be used, since they produce a more conservative design, and also appear more realistic when compared to the total pressure *in situ*.

Skempton (1961) stated that the value obtained for swelling pressure from a constant volume consolidation test gave an indication of the negative pore pressures *in situ*, if the sample had not been disturbed or allowed to dry after sampling. Applying this reasoning to the interpretation of the CV tests performed on desiccated lacustrine clays in Western Canada would indicate that in many cases the *in situ* pore pressure was actually positive. Since the water table was well below the depth under consideration, the most logical error appeared to be in the measurement of swelling pressure. In other words, the measured swelling pressure was too low. This; however, did not mean that the FS test was a more accurate simulation of field conditions but, rather, that procedural factors produced an under-estimation of the swelling pressure measured in the CV test.

Seed et al. (1961) showed that small changes in volume during testing produce a pronounced decrease in the measured swelling pressure. Even while keeping the dial gauge on a consolidometer at a constant value immediately after submersion (CV test), the meniscii are released by the water and volume change is actually occurring in the specimen as it seats against the porous disks and compresses the components of the consolidation pot.

It should also be noted that the soil specimen has actually undergone some rebound between the time of sampling and testing. This rebound also decreases the

Fig. 2. Modified constant volume consolidation test.



measured swelling pressure below that of the *in situ* value. Figure 2 shows typical results using a modified constant volume test procedure which is superior. In this procedure, the sample is trimmed, placed in the consolidation pot and a token pressure applied for initial dial reading. The specimen is covered to prevent evaporation and the load on the specimen is doubled in increments (allowing each to come to equilibrium) until the load on the sample is equal to the total vertical pressure existing

in the field (Hvorslev 1949). The specimen is then submerged with water and the test continued according to the constant volume test procedure. However, there is generally no need to load the specimen any greater than a pressure approximately twice the swelling pressure since the desired information has been obtained and the testing time can be kept to a minimum.

Test procedures used by other authors will not be dealt with here since they are felt to be outside the scope of this paper. It should be noted; however, that most of the procedural factors discussed in this paper apply to other procedures since, in all cases, an attempt is being made to reproduce *in situ* stress-strain conditions that will occur due to changes produced by construction or environmental changes. Using the above analysis, it is necessary to establish the initial stress conditions, estimate the final stress conditions and produce the proper stress-strain relationship for the problem.

Procedural factors

The procedural factors of importance when testing soft, sensitive clays are not necessarily of prime concern when testing swelling clays. Factors such as side friction, sample disturbance, sample size and temperature, are dealt with in the literature (Taylor 1942; Matlock and Dawson 1951; Finn 1951; Leonards and Girault 1961) mainly in connection with testing soft, sensitive soils. Procedural factors of concern when testing swelling clays include loading procedure (load-increment ratio and duration of load), apparatus friction, compressibility of consolidometer and the “seating” of soil and porous disks.

Loading procedure

The effects of the loading procedure are presently under investigation and the results are still incomplete. However, the results have shown that a considerable length of time is required to reach equilibrium at the swelling pressure of a soil. Specimens have been run with varying amounts of back pressure and the measurement of pore pressure at the base of the specimen. For specimen approximately 3/4 inch in thickness several days are required for equilibrium rather than the one day normally used.

Apparatus friction

Friction in the mechanical components of the apparatus is of interest since it affects the shape of the lower pressure end of the recompression and rebound curves. Figure 3 shows average results for the relationship between load applied to the hanger and load transmitted to the specimen for four light frame consolidometers. (Each of the consolidometers gave almost identical results.) A small, highly sensitive proving ring with strain gauges was substituted for the soil specimen and used to measure the load reaching the specimen. The theoretical mechanical advantage is obtained by precise measurement of lengths of the lever arms.

Fig. 3. Portion of the load transmitted to soil specimen.

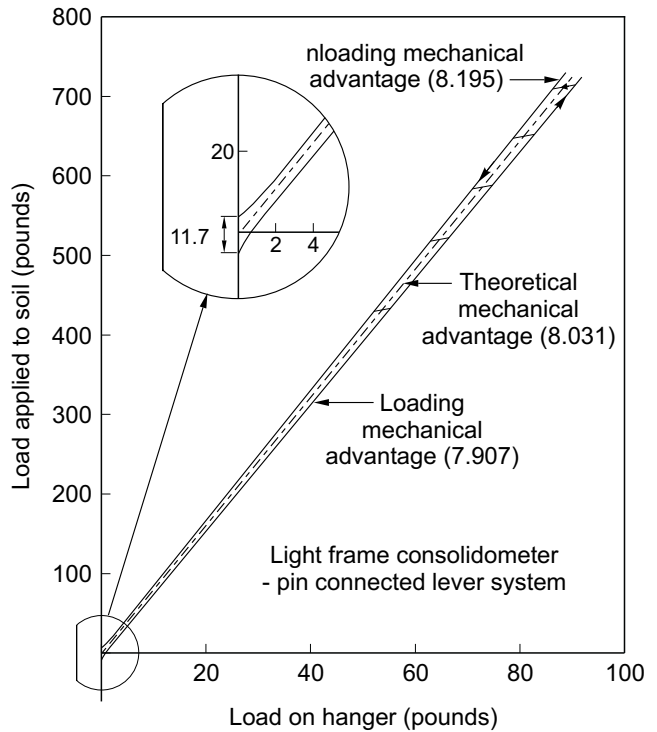
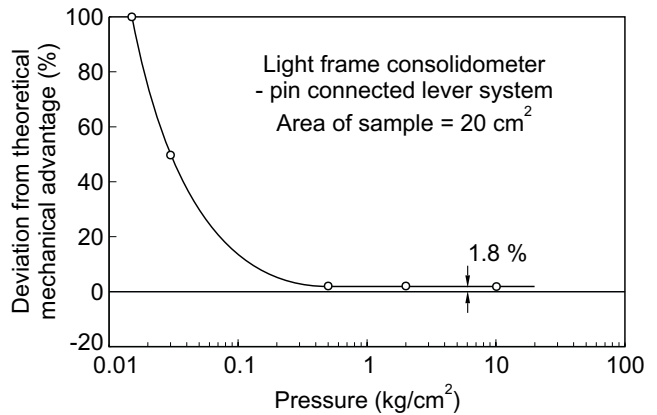


Fig. 4. Error in pressure measuring system due to friction.

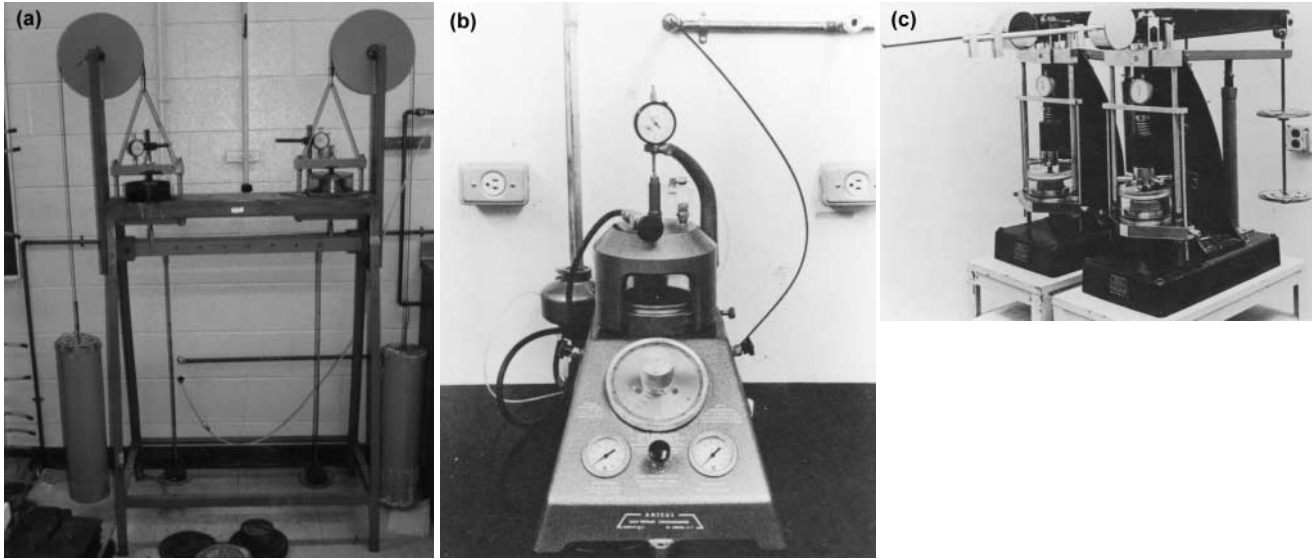


Throughout the loading and unloading range greater than 0.5 kg/cm² (49 kPa), the load applied to the specimen is within 1.8% of the theoretical value. However, at lower pressures the percent error increases rapidly (Fig. 4). At a pressure of 0.01 kg/cm² (0.98 kPa) the load applied to the sample may be in error by 100%.

Similar results on the Wykeham-Farrance bench model consolidometers showed an error of approximately 1.2% for pressure above 0.2 kg/cm² (19.6 kPa). There was a slight decrease in the frictional component due to the use of knife edges rather than pin-connectors on the loading mechanism.

The accuracy of the applied load using consolidometers with air pressure regulators depends on the accuracy of the pressure regulator. One regulator generally does

Plate 1. Low load capacity consolidometers: *a)* Light frame consolidometers, *b)* Anteus Testlab consolidometer, *c)* bench model consolidometer.



not provide accurate pressures for the entire range of loading. Two, and preferably three, pressure regulators are more satisfactory. The Anteus Testlab consolidometer uses a constant pressure head of water at low pressures which allows precise pressure measurements.

Irregular behavior often noticeable in the low range of loading may be largely attributable to inaccuracies in the load transmitted to the specimen. This problem is further discussed in connection with the seating of the soil specimen and the porous disks. Also, in the free swell test the interpretation of the results depends upon an accurate determination of the token pressure. Friction in the loading mechanism may be a primary factor in the flattening of the rebound curve often noticeable at low pressures. However, the above problems should not only be viewed from the standpoint of apparatus friction since factors such as friction between the consolidation ring and the soil are also of importance. The testing procedure for swelling clays should be one that tends to suppress inaccuracies in pressure measurements, if possible.

Compressibility of apparatus

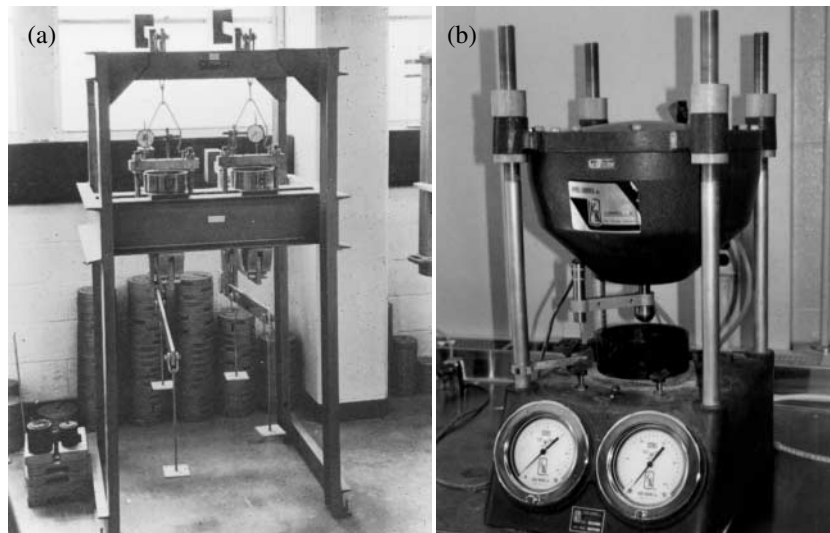
If a portion of the deflections measured during a consolidation test are due to volume changes in the apparatus rather than the soil specimen, the test results will be in error unless corrections are made. Compressibility of apparatus affects the measurement of swelling pressure and the slope of the compression and rebound curve. Attempts have been made to increase the stiffness of the measuring device (Seed et al. 1961; Kassiff et al. 1965) in order to more accurately measure swelling pressure by the constant volume procedure. Hveem (1958) in his suggested method for determining the expansive pressures of remolded soils states that a pressure measuring system with a stiffness of 0.04% per 0.5 psi (3.45 kPa) is satisfactory. However, at 30 psi (207 kPa) this would mean

2.4% volume change. This can cause serious errors in the measurement of swelling pressure. Increasing stiffness increases the swelling pressure; however, the problem of seating and compressibility of the various components of the apparatus between the points of measurement have still not been accounted for. The compression of the apparatus can be measured by substituting a steel plug for the soil specimen and performing the loading and unloading cycle. The effects of filter paper and seating of the soil and porous disks are discussed later.

Although the reliability of the above procedure has been questioned, it appears to be the best method available. Matlock and Dawson (1951) concluded that the evaluation of compressibility of apparatus is seldom justified, "first because there are no results except to alter the shape of the void ratio-pressure curves slightly; and second, because the deformations measured during such calibrations are usually only partially elastic and cannot be depended upon to repeat themselves during the actual consolidation test". Others (Means and Parcher 1963; Hamilton and Crawford 1960) have suggested that the compressibility of apparatus be determined prior to running the consolidation test and that corrections be applied to the results obtained. It is the author's opinion that the effects of compressibility should be taken into consideration when testing swelling soils.

The compressibility characteristics of the consolidometers tested are presented in terms of statistical properties. Deformations occurring for each logarithmic cycle of pressure were tabulated for five types of equipment. They are:

- (1) Light Frame Consolidometer — Lever arm loading system with pin-connectors; with a mechanical advantage of 8 (Plate 1*a*).
- (2) Anteus Testlab Consolidometer — Compressed air loading with one regulator; constant head water pot at low pressures (Plate 1*b*).

Plate 2. High load capacity consolidometers; a) Large frame consolidometers, b) Conbel consolidometer.

- (3) Bench Model Consolidometer — Manufactured by Wykeham-Farrance; lever arm loading system with knife edges; mechanical advantage of 11:1 (Plate 1c).
- (4) Large Frame Consolidometer — Lever arm loading system with knife edges; mechanical advantages of 40:1 and 50:1 (Plate 2a).
- (5) Conbel Consolidometer — Manufactured by Karol Warner; compressed air loading with two regulators; capacity of 120 kg/cm² (11.76 MPa) on a 2-½ inch (63.5 mm) diameter sample (Plate 2b).

First cycle of loading and unloading

Generally only one cycle of loading and unloading is run in a consolidation test. To simulate this it would appear that only the first cycle in the compressibility tests should be considered. Several pieces of apparatus for each type of equipment mentioned were tested (Table 1).

The consolidometers do not compress in an elastic manner since too much deflection occurs at low pressures (Fig. 5). However, their shapes on a semi-logarithmic plot are similar to those expected from testing soil specimen. The light frame and bench model consolidometers show similar compressibility curves with approximately 0.0045 inches (0.114 mm) occurring at 10 kg/cm² (980 kPa). The large frame and Conbel consolidometers show considerably more compression. The Anteus Testlab consolidometer shows only 0.0016 inches (0.06 mm) at 10 kg/cm² (980 kPa).

The standard deviation of the compressibility for each log cycle of pressure increases as the pressure increases. However, when expressed as a percentage of the mean (i.e., coefficient of variation) it decreases.

All apparatuses, except the Anteus Consolidometer, show considerable hysteresis between loading and unloading. The larger the hysteresis, the more residual deflection there is remaining when the pressure is 0.01 kg/cm² (0.98 kPa). Although there is a wide variation in residual deflection, it should be noted that this value is dependent upon the maximum pressure applied.

Since this varied from one apparatus to another, the residual deflections can also be expected to vary. Due to hysteresis and residual effects, there should be one compressibility correction curve for loading and another for the unloading of the specimen.

Comparison of first and second cycle of loading

Table 2 shows the change in compressibility that occurs upon the second cycle of loading. It is noteworthy that there is an insignificant difference in compressibility up to 1.0 kg/cm² (98 kPa) upon loading the second time and that only a slight decrease occurs with pressures up to 10 kg/cm² (980 kPa). The results on the unloading portion are not significantly different; however, the residual deformation is greater on the first cycle. Also, the standard deviations are not significantly different between the two cycles of loading. It appears that several cycles of loading and unloading could be performed on one apparatus and the average results used for the compressibility correction.

Cycling load on one apparatus

Since there appears to be only a small amount of difference in the deflection from the first and second cycle of loading, several runs were made on a single apparatus to check the reproducibility of the results (Table 3).

A high degree of reproducibility is shown by the low coefficients of variation and standard deviations. The highest variation occurs in the value for residual deformation. It would appear most satisfactory to apply the compressibility corrections from the loading end of the consolidation curve.

Components of compressibility

Calculations of deflection based on the elastic moduli of the materials involved shows that many times as much deflection occurs when loading as would theoretically be expected. For example, at 10 kg/cm² (980 kPa) on the light frame consolidometers, the average ratio of the actual deflection to the theoretical deflection was 4.0. It is

Table 1. Compressibility of consolidometers. First cycle of loading and unloading.

Type of equipment	No. of observations	Pressure range ² (kg/cm ²)	Deflection ³ (inches)				Coeff. of variation (%)
			Mean	Median	Standard deviation	95% Confid. limits	
Light frame consolidometer	25	0.0 to 0.1	0.0002	0.0002	0.0001	0.0002	39.9
		0.1 to 1.0	0.0010	0.0010	0.0003	0.0006	30.3
		1.0 to 10.	0.0033	0.0033	0.0010	0.0019	28.7
		10. to 1.	0.0029	0.0030	0.0010	0.0020	34.7
		1.0 to 0.1	0.0010	0.0011	0.0004	0.0007	32.0
		0.1 to 0.01	0.0004	0.0004	0.0002	0.0004	44.5
		Residual ¹	0.0007	0.0006	0.0005	0.0010	65.9
Bench model consolidometer	6	0.0 to 0.1	0.0005	0.0004	0.0004	0.0009	88.5
		0.1 to 1.0	0.0009	0.0009	0.0003	0.0006	34.0
		1.0 to 10.	0.0030	0.0035	0.0010	0.0019	32.5
		10. to 1.	0.0024	0.0025	0.0005	0.0009	20.1
		1.0 to 0.1	0.0010	0.0010	0.0004	0.0007	34.6
		0.1 to 0.01	0.0007	0.0005	0.0006	0.0012	87.0
		Residual ¹	0.0007	0.0002	0.0012	0.0023	159.0
Anteus Test Lab consolidometer	3	0.0 to 0.1	0.0003				
		0.1 to 1.0	0.0005				
		1.0 to 10.	0.0008				
		10. to 1.	0.0008				
		1.0 to 0.1	0.0004				
		0.1 to 0.01	0.0001				
		Residual ¹	0.0004				
Large frame consolidometer	10	0.0 to 0.1	0.0015	0.0017	0.0009	0.0018	61.4
		0.1 to 1.0	0.0023	0.0026	0.0012	0.0024	53.8
		1.0 to 10.	0.0048	0.0052	0.0021	0.0041	43.2
		10. to 1.	0.0022	0.0021	0.0012	0.0023	51.8
		1.0 to 0.1	0.0029	0.0032	0.0014	0.0028	49.4
		0.1 to 0.01	0.0017	0.0019	0.0010	0.0020	57.4
		Residual ¹	0.0021	0.0012	0.0019	0.0037	87.1
Conbel consolidometer	2	0.0 to 0.1	0.0008				
		0.1 to 1.0	0.0023				
		1.0 to 10.	0.0028				
		10. to 100.	0.0065				
		100. to 10.	0.0050				
		10. to 1.	0.0021				
		1.0 to 0.1	0.0009				
Residual ¹	0.0041						

¹Residual is the term used for the difference between starting and finishing dial readings.

²1 kg/cm² is equal to 98 kPa.

³1 inch is equal to 25.4 mm.

therefore, of interest to observe the basis of the deflections measured.

Figure 6 shows the components giving rise to the deflections occurring during the loading and unloading of the Conbel consolidometer. At 30 kg/cm² (2941 kPa) approximately 13% of the deflection occurred in the loading ram and the base of the loading frame of the consolidation apparatus. Forty-eight percent occurred in the porous disks which also are the main contributors to the hysteresis effect and residual deformation. The remaining 39% of deformation occurred in the consolidation pot, loading cap and the seating of the ball on the loading cap. Due to

the large deformation in the porous disks, their properties were further investigated.

Commercial manufacturers list the elastic modulus of corundum porous disks at approximately 10×10^6 psi. Measured values in the laboratory are shown in Fig. 7 and the computed moduli summarized in Table 4. Only the thick porous disks show a deformation modulus approaching the theoretical value. Factors such as roughness and warp in the disks appear to introduce high deflections and hysteresis.

Another factor producing a variation in results is the size and smoothness of the consolidation pot. All contact

Fig. 5. Compressibility of consolidometers.

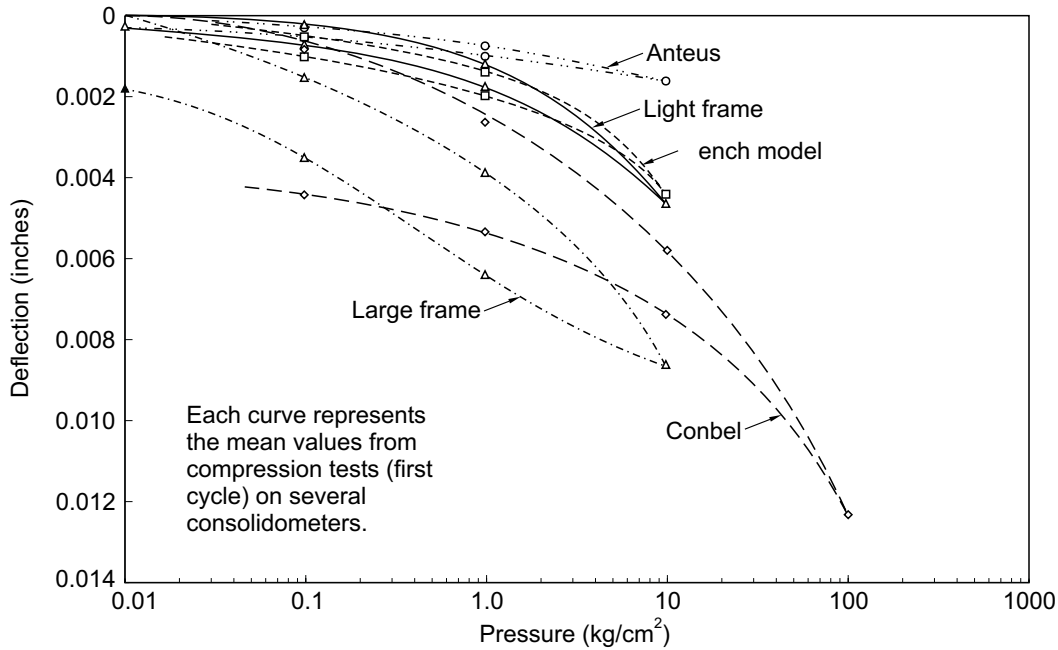


Table 2. Compressibility of consolidometers. Comparison of the first and second cycle of loading (Light frame consolidometer).

No. of observations	Pressure range ² (kg/cm ²)	Cycle #1		Cycle #2	
		Deflection ³ (inches)			
		Mean	Standard deviation	Mean	Standard deviation
6	0.0 to 0.1	0.0002	0.0001	0.0002	0.0001
	0.1 to 1.0	0.0008	0.0002	0.0008	0.0003
	1.0 to 10.0	0.0030	0.0011	0.0026	0.0012
	10.0 to 1.0	0.0021	0.0009	0.0023	0.0011
	1.0 to 0.1	0.0009	0.0003	0.0008	0.0003
	0.1 to 0.01	0.0003	0.0001	0.0003	0.0001
	Residual ¹	0.0010	0.0003	0.0003	0.0001

¹Residual is the term used for the difference between starting and finishing dial readings.

²1 kg/cm² is equal to 98 kPa.

³1 inch is equal to 25.4 mm.

areas should be machined smooth; however this is difficult to do on large size consolidation pot.

Even after machining the bases of several consolidation pots smooth, three times as much deformation occurred for a consolidation pot with a contact area of 150 cm² as one with a contact area of 30 cm², when loaded to 10 kg/cm² (980 kPa). The interchanging of any parts of the consolidometer pots between loading frames is poor practice since it changes the compressibility.

Prediction of compressibility of apparatus

By using the *t*-distribution for small samples it is possible to predict the number of compressibility tests necessary to statistically predict deformations within a certain limit of accuracy (Neville and Kennedy 1966).

$$Limit\ of\ Accuracy = \frac{t \cdot Standard\ Deviation}{\sqrt{Number\ of\ tests}}$$

where “*t*” is taken from tables in accordance with the number of observations used to define standard deviations. (A 95% level of significance is used in this paper).

Limit of accuracy curves could be drawn for each pressure range; however, it is better to have only one curve for each consolidometer or each type of consolidometer. For this reason, the standard deviation associated with the total deflection for the 0 to 10 kg/cm² (0 to 980 kPa) loading and 10 to 0.01 kg/cm² (980 to 0.98 kPa) unloading have been used. Table 5 shows a summary of the standard deviations for the various apparatus tested. The limit of accuracy curves for the first cycle of loading on various types of apparatus are shown in Fig. 8 and similar curves for individual consolidometers are shown in Fig. 9.

Depending upon the criteria set up, the number of compressibility tests necessary for a certain limit of accuracy can be established. For example, the curves show that for

Table 3. Compressibility of consolidometers. Repeated load cycling of a consolidometer.

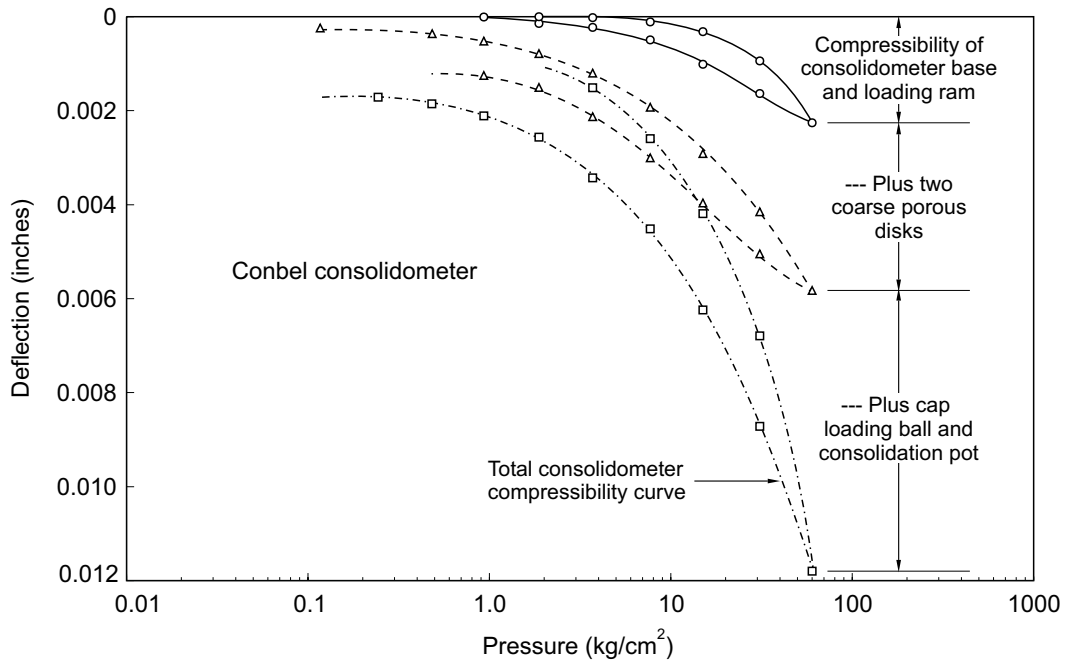
Type of equipment	No. of observations	Pressure range ² (kg/cm ²)	Deflection ³ (inches)				
			Mean	Median	Standard deviation	95% Confid. limits	Coeff. of variation (%)
Light frame consolidometer #1	12	0.1 to 1.0	0.0012	0.0012	0.0002	0.0004	15.8
		1.0 to 10.0	0.0047	0.0047	0.0004	0.0008	8.3
		10.0 to 1.0	0.0040	0.0041	0.0002	0.0004	5.5
		1.0 to 0.1	0.0012	0.0012	0.0001	0.0002	9.0
		0.1 to 0.01	0.0003	0.0002	0.0001	0.0002	43.5
Light frame consolidometer #2	6	Residual ¹	0.0007	0.0006	0.0005	0.0010	73.4
		0.0 to 0.1	0.0001	0.0001			
		0.1 to 1.0	0.0007	0.0007	0.0002	0.0005	32.3
		1.0 to 10.0	0.0034	0.0035	0.0004	0.0008	12.3
		10.0 to 1.0	0.0029	0.0032	0.0005	0.0009	15.9
Large frame consolidometer #1	5	1.0 to 0.1	0.0010	0.0010	0.0003	0.0005	25.3
		0.1 to 0.01	0.0023	0.0021	0.0008	0.0016	35.0
		Residual ¹	0.0010	0.0007	0.0009	0.0017	86.9
		0.0 to 0.1	0.0026	0.0026	0.0002	0.0003	6.3
		0.1 to 1.0	0.0049	0.0046	0.0005	0.0009	9.5
		1.0 to 10.0	0.0059	0.0054	0.0013	0.0025	21.5
		10.0 to 1.0	0.0046	0.0047	0.0002	0.0004	4.2
		1.0 to 0.1	0.0049	0.0049	0.0002	0.0004	3.7
		0.1 to 0.01	0.0034	0.0035	0.0004	0.0008	11.6
		Residual ¹	0.0006	0.0003			

¹Residual is the term used for the difference between starting and finishing dial readings.

²1 kg/cm² is equal to 98 kPa.

³1 inch is equal to 25.4 mm.

Fig. 6. Factors contributing to compressibility of consolidometer.



six compressibility tests on the light frame consolidometers, the total compressibility can be predicted within approximately 0.0012 inches (0.03 mm) using the first cycles of loading from several apparatus or within approximately 0.0005 inches (0.013 mm) using the results

of six cycles on an individual consolidometer. The standard deviations for the loading and unloading portion of the compressibility curves are somewhat different but the highest standard deviation should be used to establish the number of tests necessary for a certain limit of accuracy.

Table 4. Elastic moduli of porous disks.

Type of porous disk	Pressure range ¹		
	0 to 0.1 kg/cm ²	0.1 to 1.0 kg/cm ²	1.0 to 10.0 kg/cm ²
	Modulus of Elasticity in psi ²		
Coarse corundum porous disks			8.28 × 10 ⁴
2 — Fine, Norton porous disks	0.397 × 10 ⁴	0.926 × 10 ⁴	6.65 × 10 ⁴
8 — Fine, Norton porous disks	0.339 × 10 ⁴	0.802 × 10 ⁴	3.85 × 10 ⁴
Fine, thick Norton porous disks (Anteus)	9.26 × 10 ⁴	46.3 × 10 ⁴	160 × 10 ⁴

¹1 kg/cm² is equal to 98 kPa.

²1 psi is equal to 6.895 kPa.

Table 5. Compressibility of consolidometers. Data for limit of accuracy curves.

Type of consolidometer and procedure	No. of observations	Pressure range ¹ (kg/cm ²)	Deflection ² (inches)	
			Mean	Standard Deviation
First cycle of loading	25	0.0 to 10.0	0.0046	0.00113
Light frames		10.0 to 0.01	0.0044	0.00130
Bench models	6	0.0 to 10.0	0.0046	0.00298
		10.0 to 0.01	0.0044	0.00211
Large frames	10	0.0 to 10.0	0.0097	0.00384
		10.0 to 0.01	0.0074	0.00309
Cycling on one consolidometer				
Light frame #1	12	0.0 to 10.0	0.0062	0.00052
		10.0 to 0.01	0.0056	0.00060
Large frame #1	5	0.0 to 10.0	0.0135	0.00107
		10.0 to 0.01	0.0137	0.00205

¹1 kg/cm² is equal to 98 kPa.

²1 inch is equal to 25.4 mm.

The lower load capacity consolidometers tested have lower standard deviations and, therefore the compressibilities can be predicted more accurately than for the higher load capacity consolidometers.

Compressibility of filter paper

Filter paper is often placed above and below the soil specimen during a consolidation test (Goris 1963; Fredlund 1962). However, its compressibility is of significant proportion. It not only has an instantaneous compression when the load is applied but also compresses with time (Fig. 10). The effects of varying the pressure and the load increment ratio on the slope of the log time deflection curves are shown in Fig. 11.

Figure 12 shows a plot of total compression after one day of loading versus applied load for a load increment ratio of one. At a pressure of 1 kg/cm² (98 kPa) the compression in the filter paper is approximately five times that of the apparatus and approximately 2½ times at a pressure of 10 kg/cm² (980 kPa).

The relatively large amount of compression and hysteresis effects make it advisable not to use filter paper when testing swelling soils. Various types of filter paper have been tested and each gives different results, although the general behavior is the same.

Seating of the porous stones and the soil specimen

Even after the compressibility of the apparatus is accounted for, there is still the problem of seating between the porous disks and the soil specimen (Seed et al. 1961). This is a volume change measured on the dial gauge but one which does not occur in the sample.

Commercial porous disks of coarse texture have a roughness (difference between the peaks and depressions) in the order of 0.05 inches (1.27 kPa) and the finer textured disks with smooth surfaces have a roughness in the order of 0.02 inches (0.5 mm). Measurements on trimmed soil samples showed roughness values varying from 0.001 to 0.02 inches (0.025 to 0.5 mm). Placing the two rough surfaces together and applying pressure permits seating. Seating occurs as the peaks from the soil surface fail and fit into the porous disk. In addition to sample roughness on a local scale there is the unevenness of the specimen surface on a larger scale.

To more accurately understand the seating of the specimen, the time-deflection curves of a number of consolidation tests were analyzed. After subtracting the compressibility of apparatus and the theoretical correction to zero reading from the instantaneous deflection, the remaining compression was assumed to be due to compressibility of air in the specimen and seating of the porous disks and the soil. If no seating is occurring, a plot

of accumulated deflection versus pressure should approximate a straight line in accordance with Boyle's Law (Hilf 1948; Hamilton and Crawford 1959).

Fig. 7. Stress-strain properties of porous disks.

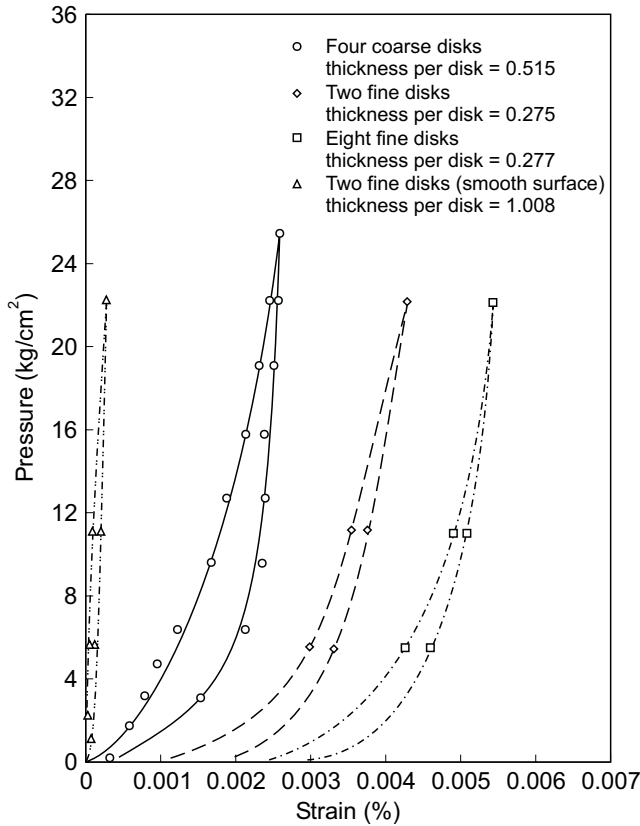


Fig. 8. Limit of accuracy curves for first cycle of loading of consolidometers.

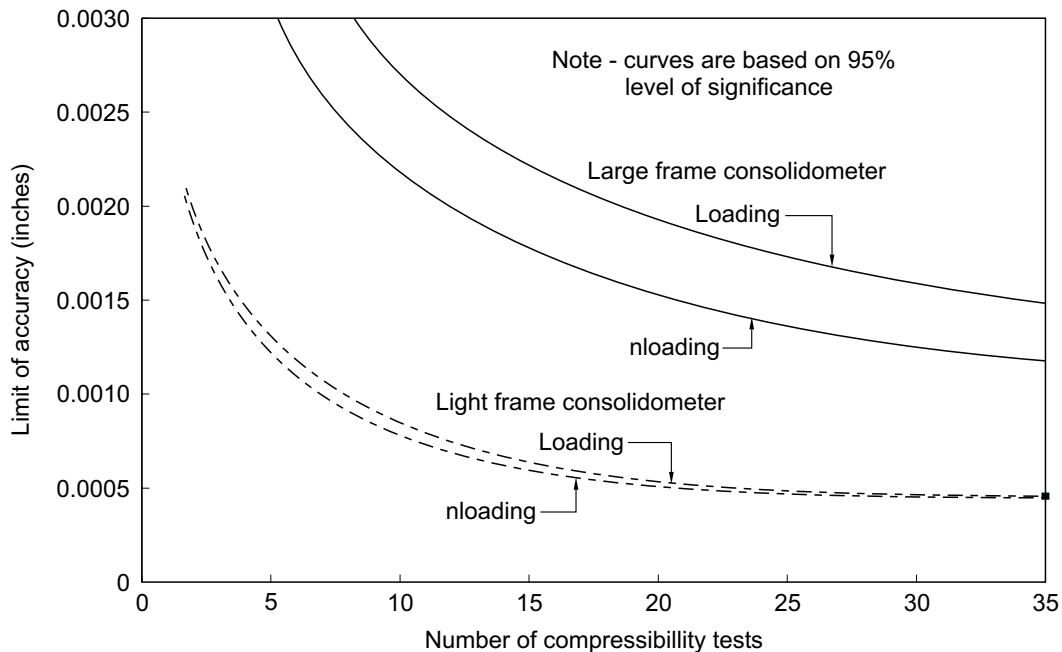


Figure 13 shows typical plots of accumulated deflection versus pressure for a constant volume and a free swell test. It should be noted that in the constant volume test, seating during the application of load up to the swelling pressure cannot be determined by this method. The free swell test shows the effects of seating during the lower loads. However, seating can also occur at higher pressures as shown by the example. Part of the deflection noticed at lower loads may be attributed to compression of air voids produced by cavitation as a result of sampling,

If no seating has occurred, the accumulated deflection versus pressure plot shows a straight line or a slightly concave shape. However, when seating is superimposed at various pressures, the plot shows distinct increases in accumulated deflection.

Since most seating occurs under low pressures, the modified procedure for the CV test gives a more accurate value for swelling pressure. Also, the seating correction does not appear to affect the rebound curve and therefore no correction for seating is necessary.

Discussion and applications

Compressibility of the consolidometer and accessories has a significant effect upon the interpretation of swell tests data. Two main properties are affected: first, the measurement of swelling pressure and second, the slope of the rebound curve.

Corrections for both properties can be made by subtracting deflections due to compressibility from the deflections measured during the test. In the FS test, deflections due to seating can also be evaluated and subtracted. In the conventional CV test the seating correction cannot be applied below the swelling pressure whereas in

Fig. 9. Limit of accuracy curves for several cycles on one apparatus.

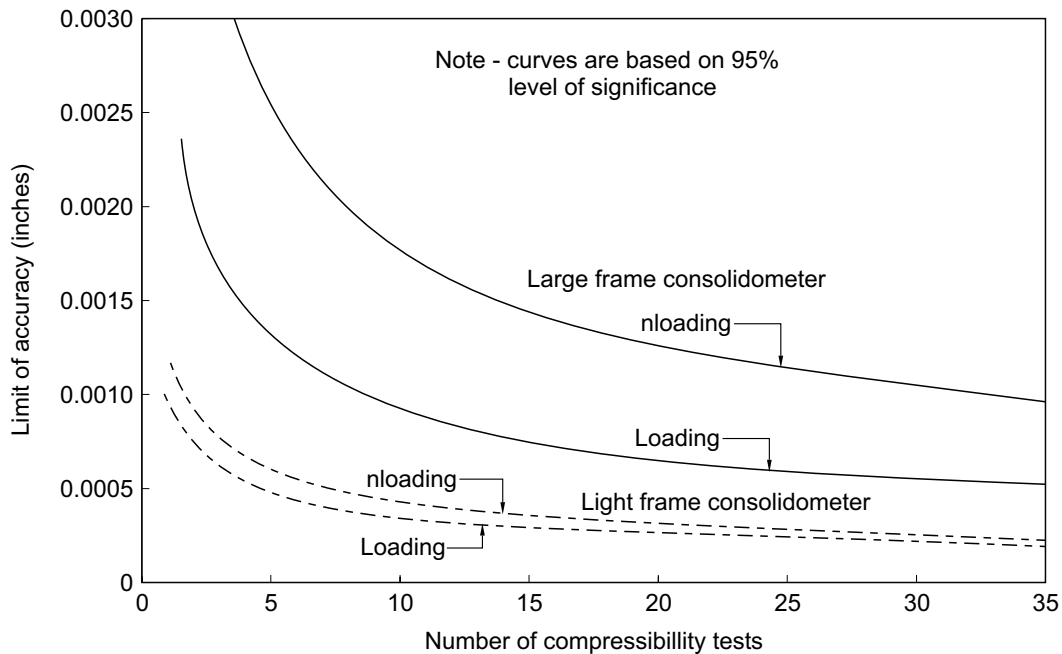
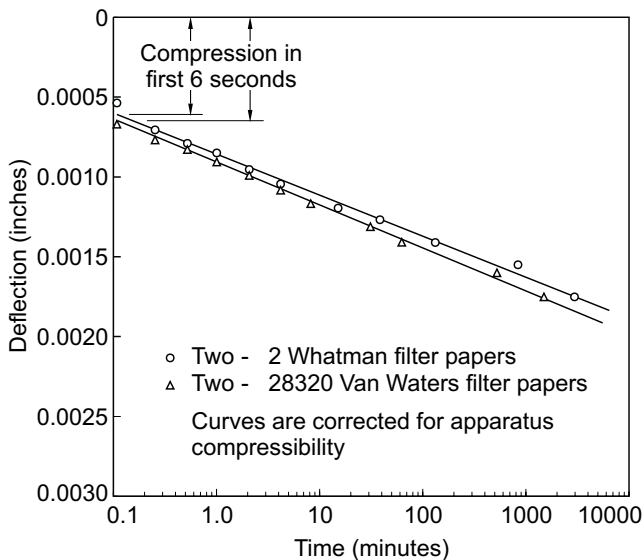


Fig. 10. Typical time-deflection curves for filter paper.



the modified CV test most of the seating has occurred while applying pressures up to the *in situ* total pressure.

Seed et al. (1961) showed that volume changes even in the order of a fraction of one percent cause significant changes in swelling pressure. Goris (1965) performed swell tests on Bearpaw shale and found compressibility of apparatus and filter paper to have a very pronounced effect on the swelling pressure measured (Fig. 14). Due to the low compressibility of the shale, the swelling changed from an uncorrected value of 2.05 kg/cm² to 11.7 kg/cm² (200 to 1147 kPa) when corrected. This figure also demonstrates the manner in which the swelling

pressure can be evaluated when taking into account compressibility.

Taking into account compressibility always increases the swelling pressure. An analysis of 244 free swell consolidation tests performed in a commercial laboratory shows that more realistic values of swelling pressure are obtained after compressibility corrections are applied (Figure 15). The results at the 15 foot depth are low even after the corrections for compressibility are applied. This is believed mainly due to the more silty nature of the soil and the possibility of cavitation during sampling. In this case, seating and recompression of the soil when loaded to its *in situ* total stress are probably significant factors which have not been taken into consideration.

Hamilton (1965, 1968) reported the rapid swelling beneath an industrial building in Regina, Saskatchewan. Consolidation tests were performed from three depths below the concrete slab (Fig. 16). Ground movement gauges were also installed at three depths and precise elevation readings taken with time. Flooding due to a break in the water line occurred during the summer of 1962 and the floor heaved in excess of three inches in approximately one week. The results of the classification tests and consolidation test data are summarized in Table 6.

Table 7 compares the predicted heave and actual heaves measured. The swelling pressure was assumed to be the initial effective stress in the field while the final effective stress was assumed equal to the total stress. In other words, the final pore-water pressure is assumed equal to zero.

The results show relatively good agreement between the actual and the predicted movement. It appears from this case that underestimating the swelling pressure results in too low a prediction of heave.

Fig. 11. Slope of the time-deflection curves for filter paper.

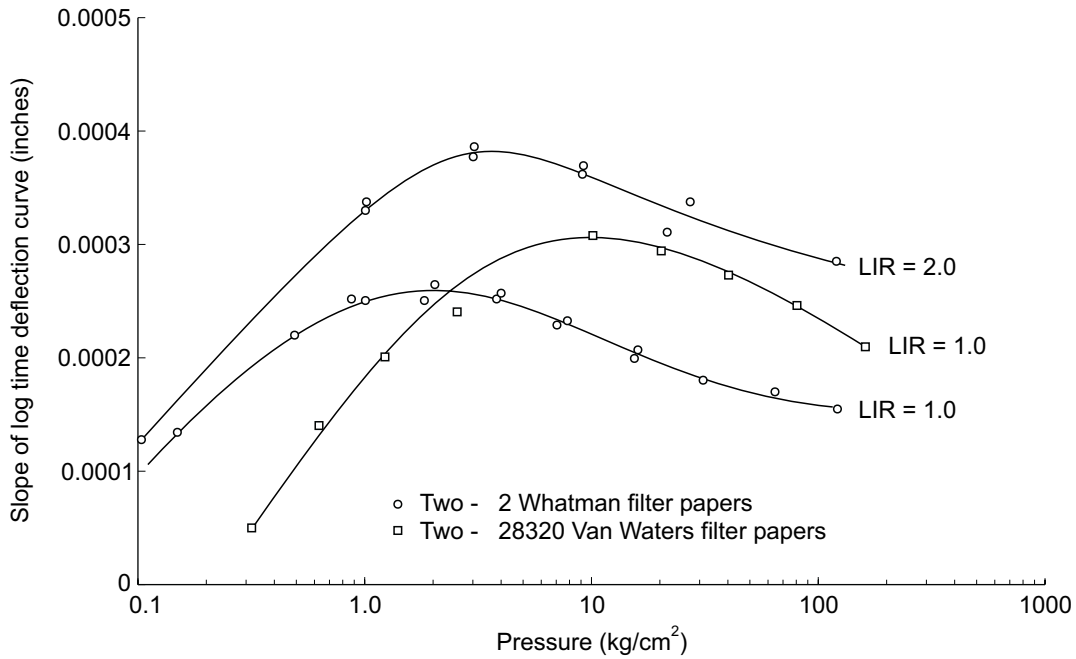
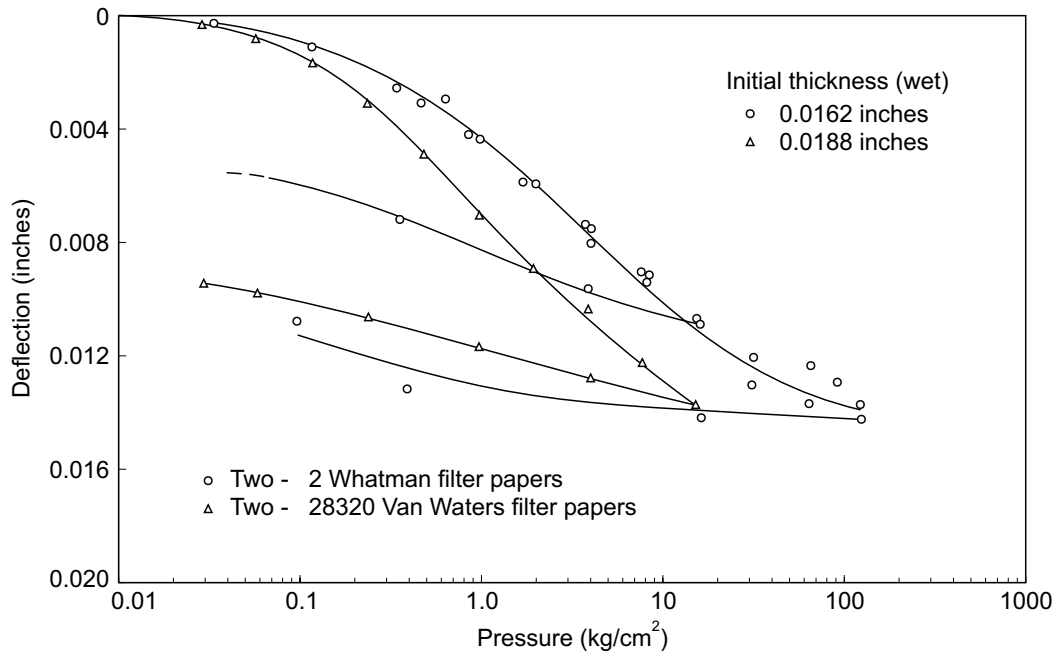


Fig. 12. Compressibility of filter paper.



Conclusions

The test procedure and apparatus used when testing for the properties of swelling clays have a significant effect upon the results obtained. The proposed modified CV swell test procedure overcomes many of the adverse procedural problems. The compressibility correction for the consolidometer should be applied to the results.

The characteristics of the consolidometer being used should be established prior to performing swell tests:

- (1) Friction in the pressure measuring device appears to be of significance only under small pressures. Special significance should not be placed on the shape of the rebound curve at low pressures unless the applied pressures can be precisely determined.
- (2) Consolidometer compression for both loading and unloading is of the same order of magnitude for apparatus produced by a specific manufacturer. However, the compressibility can be determined approximately twice as accurately by performing

Fig. 13. Typical plots of accumulated seating of porous disks and soil, and compression of the air in the soil.

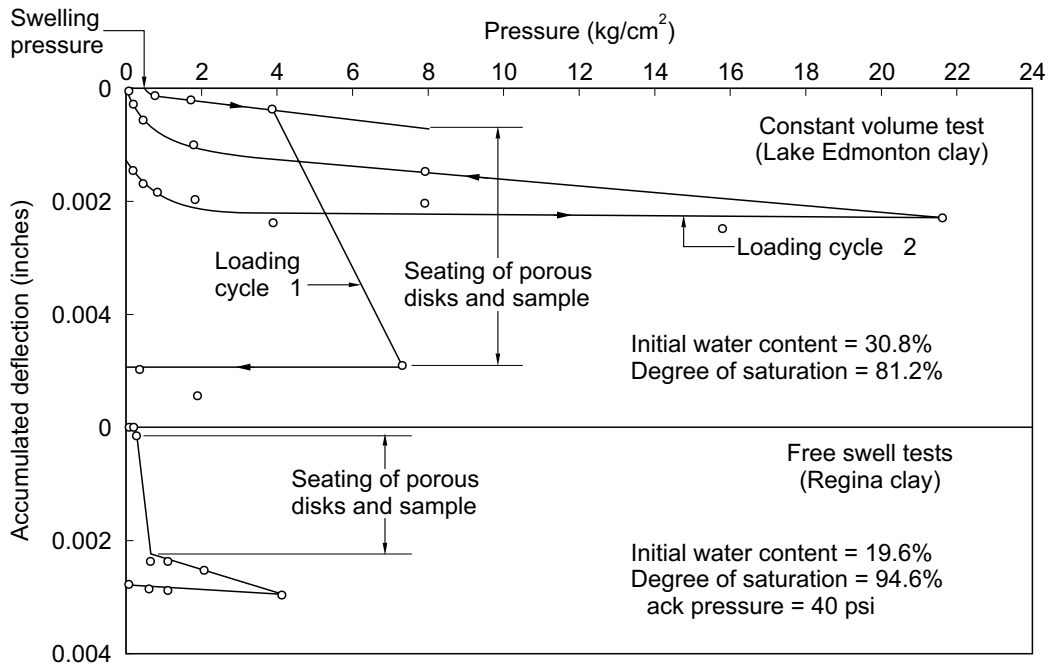
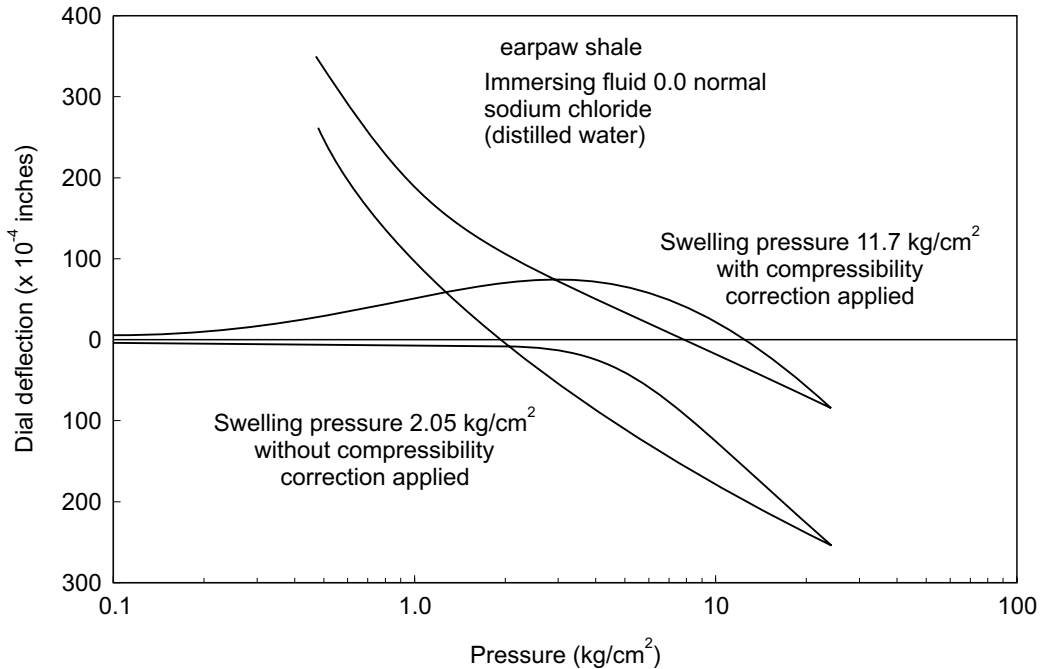


Fig. 14. Comparison of constant volume consolidation curves with and without compressibility correction applied (after Goris 1965).



- (3) A high percentage of the compressibility is produced by the porous disks. Smoothly ground, thick stones appear to be the most satisfactory.
- (4) Filter paper undergoes several times as much compression as the consolidometer upon loading and should not be used when testing for the swelling properties of soils.
- (5) The seating of the porous disks and the soil specimen is difficult to evaluate and is of significance primarily under low pressures. Attempts should always be made to evaluate the compressibility characteristics of the consolidometer when

Table 6. Summary of classification and constant volume consolidation test data.

Test No.	Depth ¹ (feet)	Atterberg limits			Initial water content	Initial void ratio	Corrected slope of rebound curve C_s	Swelling pressure	
		Liquid limit	Plastic limit	% clay				Uncorrected ² (psf)	Corrected (psf)
1	2.4	82	34	49	27.4	0.859	0.0940	6400	9240
2	4.6	74	32	46	27.9	0.983	0.0848	5200	7000
3	7.4	73	32	52	30.0	0.975	0.0962	1400	1700

¹1 foot equals 0.3048 m.

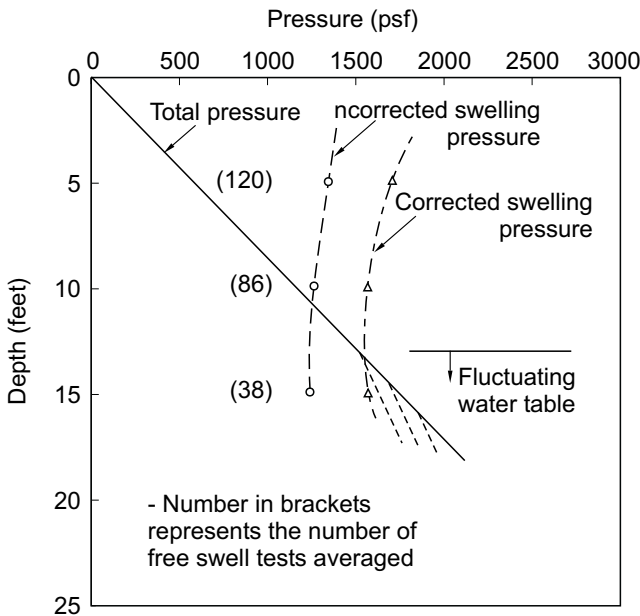
²1 psf equals 48 Pa.

Table 7. Summary of predicted and actual heave (industrial building in Regina, SK, Canada).

Layer No.	Actual heave ¹ (feet)	Predicted heave ¹ (no corrections)(feet)	Predicted heave (%)	Corrected swelling pressure and rebound curve	
				Predicted heave ¹ (feet)	Predicted heave ¹ (%)
1	0.175	0.0778	106	0.096	84
2	0.0333	0.0481		0.061	55
3	0.0667	0.1630	69	0.227	29
4	0.2750	0.3767	41	0.497	

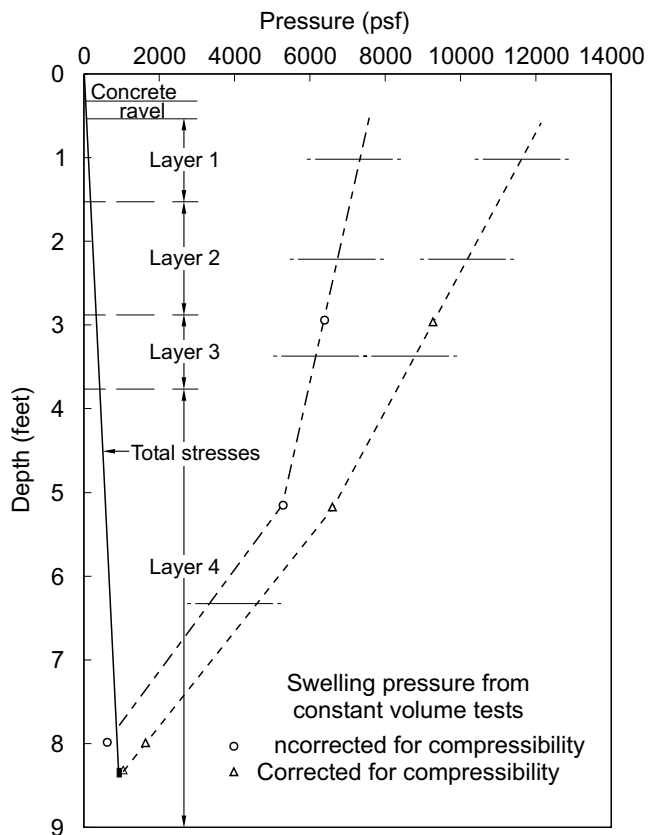
¹1 foot equals 0.3048 m.

Fig. 15. Uncorrected and corrected mean swelling pressured for Lake Edmonton clay.



testing swelling soils. Compressibility corrections should then be applied to the test data to determine a corrected swelling pressure and corrected swelling index, C_s . Percentage errors without the corrections can be in excess of 100% for the swelling pressure and generally 10 to 50% for the swelling index.

Fig. 16. Stresses below industrial building floor slab.



Acknowledgements

The author is indebted to the Prairie Regional Station, Division of Building Research, National Research Council for their technical assistance; to the Associate Committee on Geotechnical Research for their financial assistance (Grant No. A4218); to R.M. Hardy & Associates for test data and the various laboratories who allowed compressibility tests to be performed on their equipment; to the undergraduate students S. Williams, D. Allenback and G. Hodges who undertook portions of this study as their research topic.

References

- Carothers., H.P. 1965. Engineered foundations in expansive clays. Proceedings, International Research and Engineering Conference on Expansive Clay Soils, College Station, TX.
- Dyregrov, A.O., and Hardy, R.M. 1962. Practical experience with highly swelling soil types. Paper presented to Prairie Regional Soils Conference, September 1962, unpublished.
- Finn, F.N. 1951. The effect of temperature on the consolidation characteristics of remolded clay. Symposium on Consolidation Testing of Soils, American Society for Testing Materials, Special Technical Publication No. 126, pp. 65–71.
- Fredlund, D.G. 1964. Comparison of soil suction and one-dimensional consolidation characteristics of a highly plastic clay. National Research Council Technical Report No. 245.v, Division of Building Research, Ottawa, ON, Canada.
- Gilchrist, H.G. 1963. A study of volume change of a highly plastic clay. M.Sc. thesis, University of Saskatchewan, Saskatoon, SK, Canada.
- Gizinski, S.F., and Lee, L.J. 1965. Comparison of laboratory swell tests to small scale field tests. Proceedings, International Research and Engineering Conference on Expansive Clays, College Station, TX.
- Goris, J. 1965. Pressures associated with swelling in soils. M.Sc. thesis, University of Alberta, Edmonton, AB, Canada.
- Hamilton, J.J. 1965. Shallow foundations on swelling clays in Western Canada. Proceedings, International Research and Engineering Conference on Expansive Clay Soils. College Station, TX.
- Hamilton, J.J. 1968. Effects of natural and man-made environments on the performance of shallow foundations. Proceedings, 21st Annual Canadian Soil Mechanics Conference, Winnipeg, MB.
- Hamilton, J.J., and Crawford, C.B. 1959. Improved determination of preconsolidation pressure of a sensitive clay. American Society For Testing Materials, Special Technical Publication No. 254, pp. 254–271.
- Henry, E.F. 1965. The federal housing administration's program for handling the problem of expansive clays. Proceedings, International Research and Engineering Conference on Expansive Clays, College Station, TX.
- Hilf, J.W. 1948. Estimating construction pore pressures in rolled earth dams. Proceedings, 2nd International Conference on Soil Mechanics and Foundation Engineering, Rotterdam, Vol. 3, pp. 234–240.
- Holtz, W.G., and Gibbs, H.J. 1956. Engineering properties of expansive clays. Transactions, American Society of Civil Engineers, **121**: 641–663.
- Hveem, F.N. 1958. Suggested method of test for expansion pressures of remolded soils. *In* Procedures for Testing Soils, American Society For Testing Materials, pp. 285–286.
- Hvorslev, M.J. 1949. Sub-surface exploration and sampling of soils for civil engineering purposes. Waterways Experimental Station, Vicksburg, MS.
- Jennings, J.E., and Knight, K. 1957–58. The prediction of total heave from the double oedometer test. Symposium on Expansive Clays, South African Institution of Civil Engineers, Johannesburg, pp. 13–19.
- Kassiff, G., Komornik, A., Wiseman, G., and Zeitlen, J.G. 1965. Studies and design criteria for structures on expansive clays. Proceedings, International Research and Engineering Conference on Expansive Clays, College Station, TX.
- Lambe, T.W., and R.V. Whitman, 1959. The role of effective stress in the behavior of Expansive soils. Quarterly, Colorado School of Mines, **54**(4): 33–60.
- Leonards, G.A., and Girault, P. 1961. A study of the one-dimensional consolidation test. Proceedings, 5th International Conference on Soil Mechanics and Foundation Engineering. Vol. 1, pp. 213–218.
- Matlock, H., and Dawson, R.F. 1951. Aids in the interpretation of the consolidation test. Symposium on Consolidation Testing of Soils, American Society for Testing Materials, Special Technical Publication No. 126, pp. 43–52.
- McDowell, C. 1965. Remedial procedures used in the reduction of detrimental effects of swelling soils. Proceedings, International Research and Engineering Conference on Expansive Clay Soils, Texas A&M Press, pp.239–254.
- Means, R.E., and Parcher, J.V. 1963. Physical properties of soils. Charles E. Merrill Books, Inc., Columbus, OH.
- Neville, A.M., and Kennedy, J.B. 1964. Basic statistical methods for engineers and scientists. International Textbook Co., Scranton, PN.
- Noble, C.A. 1966. Swelling measurements and prediction of heave for a lacustrine clay. Canadian Geotechnical Journal, **3**(1): 32–41.
- Rutledge, P.C. 1944. Relation of undisturbed sampling to laboratory testing. Transactions, American Society of Civil Engineers, **109**: 1155–1183.
- Sampson, E., Schuster, R.L., and Budge, W.D. 1965. A method of determining swell potential of an expansive clay. Proceedings, International Research and Engineering Conference on Expansive Clays, College Station, TX.
- Schmertmann, J.M. 1953. Estimating the true consolidation behavior of clay from laboratory test results. American Society of Civil Engineers, Proceedings, **79**: 311.
- Seed, H.B., Mitchell, J.K., and Chan, C.K. 1961. Studies of swell and well pressure characteristics of compacted clays. Proceedings, 40th Annual Meeting. Highway Research Board Bulletin, **313**: 12–39.
- Skempton, A.W. 1961. Horizontal stresses in an over-consolidated eocene clay. Proceedings, 5th International Conference on Soil Mechanics and Foundation Engineering, **1**: 351–357.
- Taylor, D.W. 1942. Research on consolidation of clays. Massachusetts Institute of Technology, Serial 82, Boston, MA.

Closed-form heave solutions for expansive soils

R.R. Rao, H. Rahardjo, and D.G. Fredlund

Abstract: During the past decade, the theory for heave prediction has developed within the context of unsaturated soil behavior and has become a valuable tool for geotechnical practice. The laboratory procedures for testing expansive soils have also been essentially standardized. The heave prediction theory is briefly reviewed in this paper, and the importance of sampling disturbance is emphasized. Closed-form solutions are presented for several possible situations that can be applied to engineering practice. In all cases, the soil deposit is assumed to be homogeneous, and the swelling pressure is assumed to be constant with depth. The closed-form solutions are presented for the calculation of total heave when: (1) a portion or the entire active depth is wetted; (2) a portion of the expansive soil is excavated, and (3) the excavated portion is backfilled with a nonexpansive soil.

Key words: expansive soils, heave prediction, unsaturated soil, sampling disturbance, swelling pressure.

Introduction

Lightly loaded structures founded on desiccated, unsaturated soils commonly suffer severe distress subsequent to their construction. Changes in the environment around the structure result in changes in the (negative) pore-water pressure, thereby producing volume changes in the soil. Unsaturated soils with a high swelling index, C_s , in a changing environment are referred to as highly swelling soils (i.e., expansive soils).

It was estimated that seven billion dollars were spent each year in the United States as a result of damage to all types of structures built on swelling soils (Krohn and Slosson 1980). The cost associated with damage due to swelling soils was more than twice as much as the cost associated with damage from floods, hurricanes, tornadoes, and earthquakes (Jones and Holtz 1973). It is obvious that the problems associated with swelling soils are of enormous financial proportions.

The prediction of heave of light structures has received more attention than any other analysis associated with swelling soils. The heave prediction requires a knowledge of (1) the initial *in situ* state of stress; (2) the swelling index; and (3) the final state of stress (Fredlund 1983). The initial stress state and the swelling index are commonly obtained from one-dimensional oedometer tests. The final stress state may be strongly influenced by local experience (Fredlund 1983). The stress state variable change

between the initial and the final conditions together with the swelling index are used to predict the amount of heave.

An important variable required in the prediction of heave in swelling soils is the swelling pressure. The swelling pressure represents the initial stress state of the soil *in situ*. The swelling pressure is generally measured in a one-dimensional oedometer test using either the constant volume or the free swell procedures (Fredlund 1969). Geotechnical engineers have only recently recognized the importance of accounting for sampling disturbance when measuring the swelling pressure of expansive soils (Fredlund et al. 1980; ASTM 1986). Sampling disturbance is of particular importance when using the constant volume testing procedure, since it results in a significant reduction in the measured swelling pressure (Fredlund 1983).

One of the objectives of this paper is to emphasize the need to apply a correction for sampling disturbance when interpreting oedometer test data. The second and main objective is to present a closed-form solution to the equation for the prediction of total heave. This solution is then applied to several typical, practical examples. These solutions can be used to compare the effectiveness of various remedial measures on heave reduction.

Sampling disturbance and use of corrected swelling pressure

The free swell oedometer test has a limitation in that it allows volume change and incorporates hysteresis into the estimation of the *in situ* stress state. The constant volume oedometer test has an advantage in this respect. It suffers; however, a substantial reduction in the measured swelling pressure due to sampling disturbance. The effect of sampling disturbance on the measured swelling pressure is similar to the effect of sampling disturbance on the measurement of preconsolidation pressure. In the oedometer test, it is impossible for the soil specimen to

R.R. Rao. Reader, Department of Civil Engineering, Andhra University, Waltair, India, 530 003.

H. Rahardjo. Research Engineer, Department of Civil Engineering, University of Saskatchewan, Saskatoon, 57 Campus Drive, Canada, S7N 5A9.

D.G. Fredlund. Professor, Department of Civil Engineering, University of Saskatchewan, Saskatoon, 57 Campus Drive, Canada, S7N 5A9.

Reproduced with permission from the *Journal of Geotechnical Engineering*, 114(5): 573-588, 1988.

return to an *in situ* stress state after sampling without displaying some curvature in the void ratio versus effective stress plot (i.e., compression curve). A construction has been proposed on the data that provides a correction to account for the effect of sampling disturbance on the measured swelling pressure (Fredlund 1983).

The ideal and actual stress-deformation paths followed during the constant volume test can be more readily understood by use of a three-dimensional plot with the net normal stress and matric suction forming independent axes (Fig. 1). The ideal stress-deformation path is shown for the situation in which there is a minimum of disturbance due to sampling. Even so, the loading path will display some curvature as the net normal stress plane is approached. In reality, the actual stress-deformation path will be even more significantly affected by sampling.

Sampling disturbance causes the conventionally measured swelling pressure, P_s , to fall well below the ideal or corrected swelling pressure, P'_s . The corrected swelling pressure represents the *in situ* state translated to the net normal stress plane. It is equal to the overburden pressure plus the matric suction equivalent (Yoshida et al. 1983). The engineer only needs to know the corrected swelling pressures versus depth in order to predict total heave. The corrected swelling pressure is obtained by applying a correction to the measured swelling pressure (ASTM 1986).

The constant volume test results are generally plotted two-dimensionally as shown in Fig. 2. The slope of the rebound curve is referred to as the swelling index, C_s . The procedure suggested for determining the corrected swelling pressure can be summarized (Fredlund 1983). An adjustment is first applied to the laboratory data to account for the compressibility of the apparatus (Fredlund 1969). Then the correction for sampling disturbance can be applied. Sampling always increases the compressibility of a soil and does not permit the laboratory-tested specimen to return to its *in situ* state of stress at its measured void ratio. Casagrande (1936) proposed an empirical construction that should be applied to saturated soils to compensate for the effect of sampling disturbance. The construction was for the determination of the correct preconsolidation pressure. The suggested procedure for finding the corrected swelling pressure has only a slight deviation from Casagrande's procedure as shown in Fig. 2. The deviation lies in the use of the slope of the rebound curve (rather than the slope of the virgin compression curve) in the construction.

The evidence supporting the need for correcting for sampling disturbance has been previously explained by Fredlund (1983). For example, two case histories involving Regina and Eston clays in Saskatchewan, Canada, were analyzed using the corrected swelling pressure. A slab-on-grade floor on Regina clay experienced a maximum total heave of 106 mm. The analysis resulted in a total heave prediction of 118 mm based on the assumption that the final negative pore-water pressures increased to zero (Yoshida et al. 1983). Without the correction for sampling disturbance, the predicted heave was significantly less than the measured total heave. A school build-

Fig. 1. Ideal and actual stress-deformation paths showing effect of sampling disturbance.

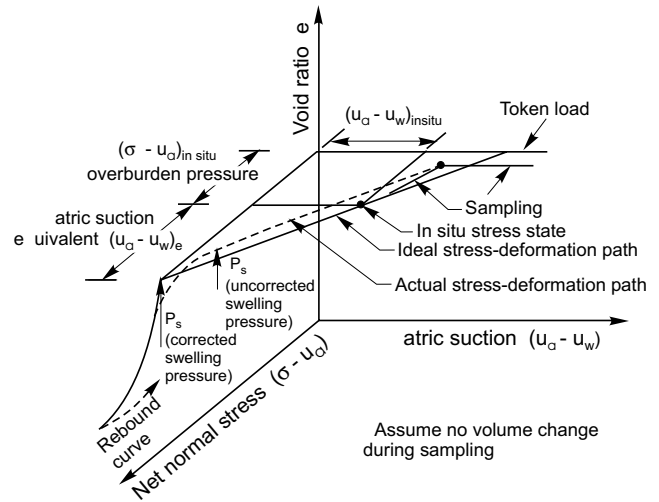
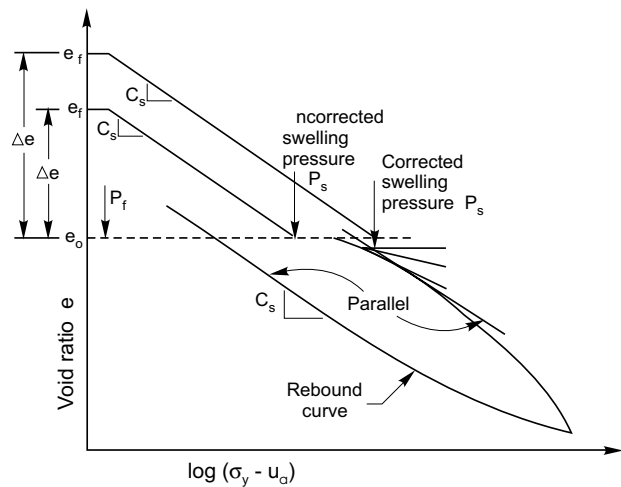


Fig. 2. One-dimensional oedometer test showing effect of sampling disturbance.



ing founded in Eston clay had undergone as much as 90 cm of heave. The total heave was predicted to be approximately 90 cm when the final negative pore-water pressures was assumed to increase to zero. Heave analyses using the uncorrected swelling pressure were too low.

Theory of heave predictions

A general equation for the prediction of heave was published by Fredlund et al. (1980). In this paper, reference will only be made to the theory necessary to predict total heave from one-dimensional oedometer test results. The equations presented correspond to all stress paths being projected to the net normal stress plane (Fig. 2). The heave stress path follows the rebound curve (i.e., C_s) from the initial stress state to the final stress state. The equation for the rebound portion of the oedometer test data can be written, as:

$$[1] \quad \Delta e' = C_s \log \left(\frac{P_f}{P_0} \right)$$

where:

- $\Delta e'$ = change in void ratio (i.e., $e_f' - e_0$) corresponding to the corrected swelling pressure, P_s' ,
 e_0 = initial void ratio,
 e_f' = final void ratio corresponding to the corrected swelling pressure, P_s' ,
 C_s = swelling index,
 P_f = final stress state, and
 P_0 = initial stress state or the corrected swelling pressure, P_s' .

The initial stress state, P_0 , can be formulated as the sum of the overburden pressure and the matric suction equivalent (see Fig. 1) as follows:

$$[2] \quad P_0 = (\sigma_y - u_a) + (u_a - u_w)_e$$

where:

- σ_y = total overburden pressure,
 $(\sigma_y - u_a)$ = net overburden pressure,
 u_a = pore-air pressure,
 $(u_a - u_w)_e$ = matric suction equivalent, and
 u_w = pore-water pressure.

The pore-air pressure in the field is commonly atmospheric. Therefore, eq. [2] can be simplified as

$$[3] \quad P_0 = \sigma_y - u_{we}$$

In practice, the initial stress state, P_0 , is measured as the corrected swelling pressure, P_s' , in the oedometer test. The final stress state, P_f , must account for total stress changes and the final pore-water pressure conditions.

$$[4] \quad P_f = \sigma_y \pm \Delta \sigma_y - u_{wf}$$

where:

- $\Delta \sigma_y$ = change in total stress due to the excavation or placement of fill, and
 u_{wf} = estimated final pore-water pressure.

One of the three possibilities provide the most logical estimation of the final pore-water pressure conditions. First, it can be assumed that the water table will rise to ground surface, creating a hydrostatic condition. This assumption produces the greatest heave prediction. Second, it can be assumed that the pore-water pressure approaches zero throughout its depth. This may be a realistic assumption; however, it should be noted that it is not an equilibrium condition. Both case histories mentioned previously show a good agreement between heave analyses and field data when zero final pore-water pressures were assumed. Third, it can be assumed that under long-term equilibrium conditions the pore-water pressure will remain slightly negative. This assumption produces the smallest prediction of heave. It is also possible to have variations of these given assumptions with depth. There may be a limit placed on the depth to which wetting will occur as well. Any of these assumptions produces relatively similar pre-

dictions of heave in most cases. This is due to the fact that most of the heave occurs in the uppermost soil layer where the matric suction change is largest.

The choice of a final pore-water pressure boundary condition can vary from one geographic location to another depending upon the climatic conditions. Russam and Coleman (1961) related the equilibrium suction below asphaltic pavements to the Thornthwaite Moisture Index. On many smaller structures; however, it is often man-made causes such as leaky water lines and poor drainage that control the final pore-water pressure in the soil.

The heave of an individual soil layer can be written in terms of a change in void ratio as follows:

$$[5] \quad \Delta h_i = \frac{\Delta e_i'}{1 + e_{0i}} h_i$$

where:

- Δh_i = heave of an individual layer,
 h_i = thickness of the layer under consideration,
 $\Delta e_i'$ = change in void ratio of the layer under consideration (i.e., $e_{fi}' - e_{0i}$),
 e_{0i} = initial void ratio of the soil layer, and
 e_{fi}' = final void ratio of the soil layer.

The change in void ratio, $\Delta e_i'$, in eq. [5] can be substituted by eq. [1] to give the following form:

$$[6] \quad \Delta h_i = \frac{C_s}{1 + e_{0i}} h_i \log \frac{P_{fi}}{P_{0i}}$$

where:

- P_{fi} = final stress state in the soil layer, and
 P_{0i} = initial stress state in the soil layer.

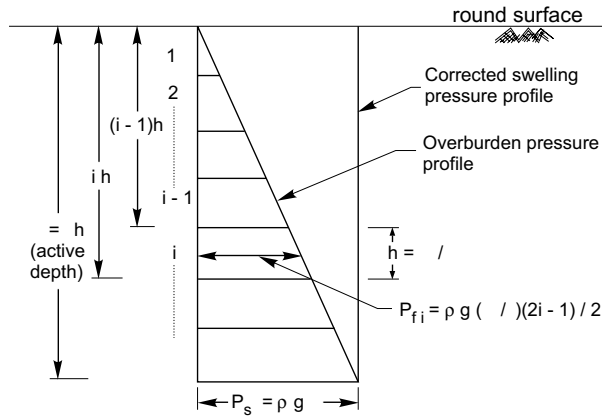
The total heave from several layers, ΔH , is equal to the sum of the heave for each layer.

$$[7] \quad \Delta H = \sum \Delta h_i$$

Closed-form heave equation when swelling pressure is constant

A case where the corrected swelling pressure, P_s' , is constant with depth is shown in Fig. 3. The soil is assumed to be homogeneous (i.e., e_0 , ρ and C_s are constant with depth). These assumptions apply to all cases presented in this paper. Sufficient water is supplied to the soil such that the pore-water pressure is assumed to go to zero for the entire soil profile. The final stress state, P_f , is assumed to be equal to the total overburden pressure. The unsaturated, expansive soil swells upon wetting. Most of the heave will occur near ground surface where there is the largest difference between the corrected swelling pressure and the total overburden pressure. The heave continues to occur until a depth where there is no difference between the corrected swelling pressure and the total overburden pressure. In this paper, the depth at which the corrected swelling pressure equals the total overburden pressure will be defined as the active depth H .

Fig. 3. Overburden and swelling pressure distributions versus depth for case of constant swelling pressure.



$$[8] \quad H = \frac{P_s'}{\rho g}$$

where:

- H = active depth,
- ρ = total density of the soil which is assumed to remain constant (e.g., kg/m³, lb/ft³), and
- g = gravitational acceleration (e.g., 9.8 m/s², 32 ft/s²).

The heave analysis can be performed by first subdividing the computed active depth into j number of layers of equal thickness (i.e., $h_i = h$).

$$[9] \quad h = \frac{H}{j}$$

where:

h = thickness of a soil layer.

An attempt is first made to determine the number of layers required to accurately predict total heave. The initial stress state, P_{0i} , is equal to the corrected swelling pressure, P_s' , defined in terms of the active depth in eq. [8].

$$[10] \quad P_{0i} = \rho g H$$

The final stress state, P_{fi} , in the i -th layer from ground surface is computed as the average overburden pressure of the layer.

$$[11] \quad P_{fi} = \rho g \frac{(i-1)h + ih}{2}$$

where:

i = soil layer number (i.e., 1, 2, ..., j).

The thickness of soil layer, h , in eq. [11] can be substituted by eq. [9].

$$[12] \quad P_{fi} = \frac{\rho g H (2i-1)}{2j}$$

The heave equation is written for each soil layer and then summed to give the total heave. The amount of heave in each layer can be computed by substituting eqs. [9], [10], and [12] for h_i , P_{0i} , and P_{fi} respectively, into eq. [6].

The total heave for the entirely wetted active depth is the summation of the individual heave in each layer.

$$[13] \quad \Delta H = \frac{C_s H}{1 + e_0} \frac{1}{j} \sum_{i=1}^j \log \left(\frac{2i-1}{2j} \right)$$

The computed total heave changes very little when using more than 35 layers (i.e., $j = 35$). Figure 4 shows the percentage of total heave, referenced to the case of 35 layers, versus the number of layers used in the analysis. If we assume the number of layers in the analysis to be 35, eq. [13] can be simplified as follows:

$$[14] \quad \Delta H = (-0.430) \frac{C_s H}{1 + e_0}$$

with (-0.430) being the computed value for the second term in eq. [13];

$$[15] \quad \left[\frac{1}{35} \sum_{i=1}^{35} \log \left(\frac{2i-1}{70} \right) \right]$$

The total heave expressed in eq. [14] will later be used as the reference when comparing the amount of heave computed for different field conditions (i.e., partly wetted active depth, excavation and backfill). In practice, heave analysis can be performed using ten layers with an accuracy within practical limits.

Substituting eq. [8] into eq. [14] and assuming a unit weight (i.e., ρg) of 20 kN/m³ and an initial void ratio e_0 of 1.0 yields;

$$[16] \quad \Delta H = -10.75 \times 10^{-3} C_s P_s'$$

P_s' and ΔH have a unit of kPa and m, respectively.

Figures 5 and 6 show the types of plots that can be drawn from eq. [16] to illustrate approximate amounts of heave for various swelling indices and swelling pressures. The total heave varies linearly with both of the above variables, or viewed in another way, it is equally important to accurately assess both the swelling pressure and the swelling index of an expansive soil.

Effect of correcting swelling pressure on prediction of heave

Correcting the swelling pressure for the effect of sampling disturbance increases the change in void ratio as shown in Fig. 2. As a result, the calculation of heave also increases (see eq. [5]). The change in void ratio corresponding to the corrected swelling pressure can be computed from eq. [1] by substituting P_s' for P_0 (see also Fig. 2).

Fig. 4. Percentage of total heave with respect to number of layers.

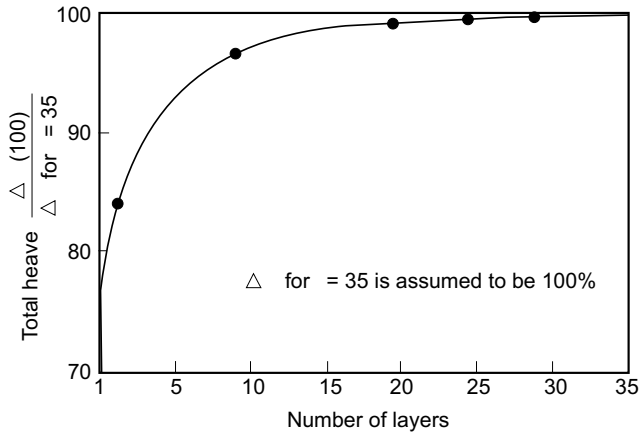
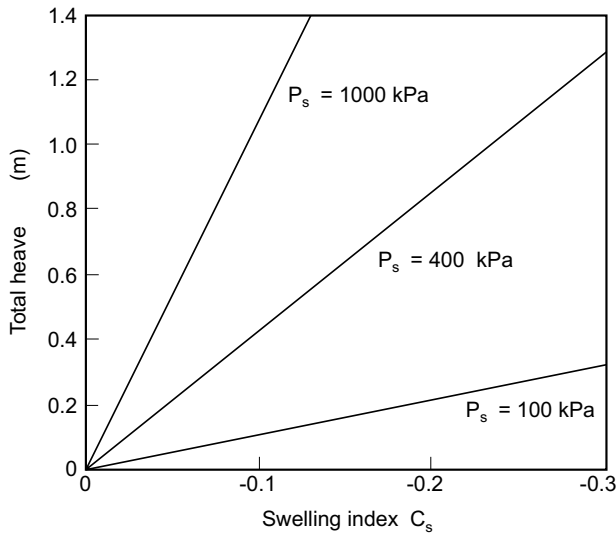


Fig. 5. Total heave versus swelling index for various corrected swelling pressures.



$$[17] \quad \Delta e' = C_s \log \left(\frac{P_f}{P_s'} \right)$$

The change in void ratio corresponding to the uncorrected swelling pressure, P_s , is written as (see Fig. 2);

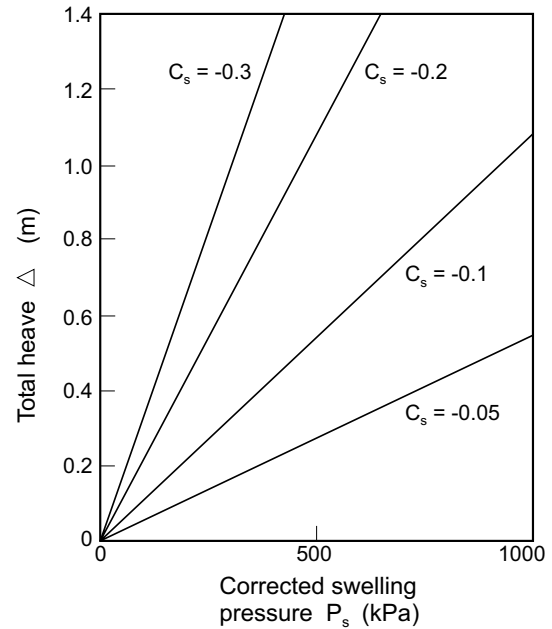
$$[18] \quad \Delta e = C_s \log \left(\frac{P_f}{P_s} \right)$$

The difference in heave or in void ratio change can be obtained by subtracting eq. [18] from eq. [17].

$$[19] \quad \Delta e' - \Delta e = C_s \log \left(\frac{P_s}{P_s'} \right)$$

Expressing the difference with respect to Δe gives;

Fig. 6. Total heave versus corrected swelling pressure for various swelling indices.



$$[20] \quad \frac{\Delta e' - \Delta e}{\Delta e} = \frac{\log \left(\frac{P_s}{P_s'} \right)}{\log \left(\frac{P_f}{P_s} \right)}$$

Equation [20] is shown graphically in Fig. 7 for various ratios of (P_s'/P_s) and (P_f/P_s) . The plot shows that the relative difference between heave predictions increases as the difference between the corrected and uncorrected swelling pressures increases (i.e., P_s'/P_s increases). It is common for the corrected swelling pressure to be two to three times greater than the uncorrected swelling pressure [i.e., P_s'/P_s can be 2–3 (Fredlund 1983)]. The relative difference in heave also increases as the overburden pressure increases (i.e., P_f/P_s increases). Note that the difference between the two heave computations can be substantial.

Example with wetting from top to specified depth

Figure 8 shows the variables involved in studying the effect of wetting of the soil from the ground surface to some specified depth (e.g., by flooding the surface). For example, an insufficient amount of water infiltration into the ground may result in only a portion of the active depth being wetted. H_r is the portion of the active depth that has been wetted (i.e., rH). The wetted zone is also subdivided into j number of layers in computing the heave. The heave for any layer in the wetted zone can be calculated by substituting the variables in Fig. 8 into eq. [6].

Fig. 7. Effect of correction for swelling pressure on change in void ratio for various overburden pressures.

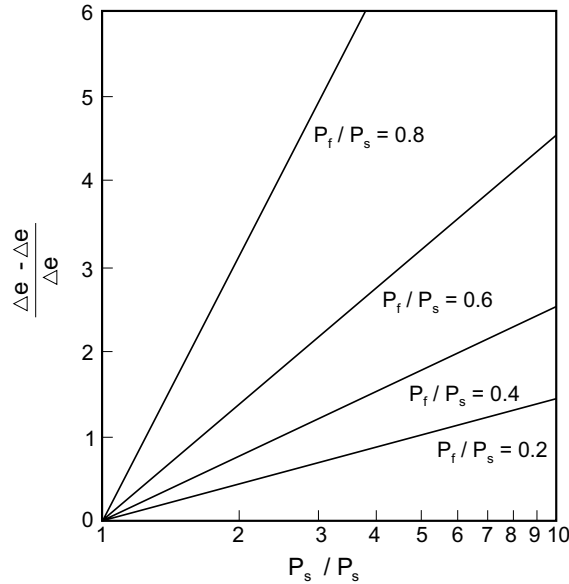
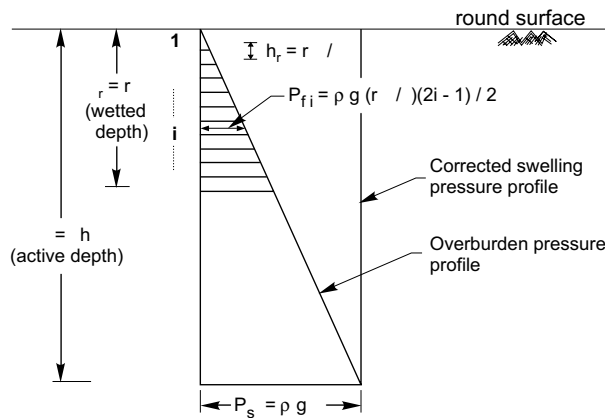


Fig. 8. Pressure distributions and definition of variables for case of wetting a portion of active depth.



$$[21] \quad \Delta h_{ri} = \frac{C_s}{1 + e_0} \frac{rH}{j} \log \left[\frac{\rho g r H (2i - 1)}{2j \rho g h} \right]$$

where:

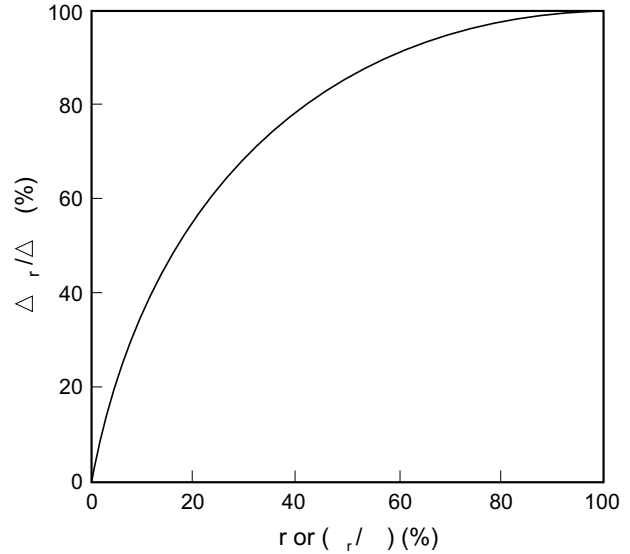
Δh_{ri} = heave of an individual layer when a portion of the active depth is wetted; and
 r = the portion of the profile wetted (i.e., H_r / H).

Equation [21] reduces to the following form;

$$[22] \quad \Delta h_{ri} = \frac{C_s}{1 + e_0} \frac{rH}{j} \left[\log \left(\frac{(2i - 1)}{2j} \right) + \log r \right]$$

Equation [22] can be applied to all layers in the wetted zone to give the total heave.

Fig. 9. Ratio of total heave predicted for wetting over partial depth to total heave for wetting to full depth.



$$[23] \quad \Delta H_r = \frac{C_s H}{1 + e_0} r \left[\frac{1}{j} \sum_{i=1}^j \log \left(\frac{2i - 1}{2j} \right) + \log r \right]$$

Substituting eq. [14] into eq. [23] for j equal to 35, gives;

$$[24] \quad \Delta H_r = \frac{C_s H}{1 + e_0} r (-0.430 + \log r)$$

When r is equal to one, the entire active depth is wetted and eq. [24] reverts to eq. [14]. A comparison between eq. [24] and eq. [14] is as follows:

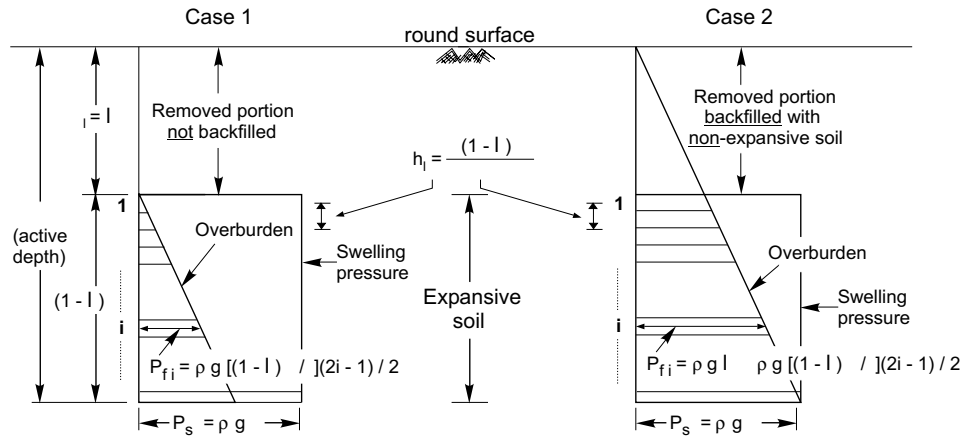
$$[25] \quad \frac{\Delta H_r}{\Delta H} = r (1 - 2.326 \log r)$$

Figure 9 shows a plot of eq. [25] where various percentages of the profile are wetted. The relationship is unique for all values of swelling pressure and swelling index. As an example, it can be seen that 80% of the total heave occurs if the depth of wetting is 40–50% of the active depth. Therefore, it may be possible to flood an area prior to construction until a significant percentage of total heave has occurred. Whether this is a practical engineering solution may depend on other factors associated with the soil properties and the design of the structure.

Example with portion of profile removed by excavation and backfilled with nonexpansive soil

This section considers the possibility of excavating the upper portion of the profile. This is considered under the title of case 1. If the excavated portion is backfilled with nonexpansive soil, the heave calculations are considered as case 2. These two cases are shown in Fig. 10. In case 1, it is assumed that the active depth is unaffected by the

Fig. 10. Pressure distributions and definition of variables for case of partial excavation and backfilling of active depth.



removal of the soil. In both cases, the heave calculations are made for the condition where the entire active depth is wetted.

Case 1 will be considered first. The heave for any layer in the expansive soil can be computed by substituting the variables for case 1 in Fig. 10 into eq. [6].

$$[26] \quad \Delta h_{li} = \frac{C_s}{1 + e_0} \frac{(1+l)H}{j} \log \left[\frac{\rho g(1-l)H(2i-1)}{2j \rho g H} \right]$$

where:

Δh_{li} = heave in an expansive soil layer when the active depth is partially excavated, and
 l = the portion of the profile excavated (i.e., H_l / H).

Equation [26] can be rearranged to the following form:

$$[27] \quad \Delta h_{li} = \frac{C_s}{1 + e_0} \frac{(1-l)H}{j} \left[\log \left(\frac{2i-1}{2j} \right) + \log(1-l) \right]$$

The total heave for case 1 is computed by summing the individual heave in each soil layer.

$$[28] \quad \Delta H_l = \frac{C_s H}{1 + e_0} (1-l) \left[\frac{1}{j} \sum_{i=1}^j \log \left(\frac{2i-1}{2j} \right) + \log(1-l) \right]$$

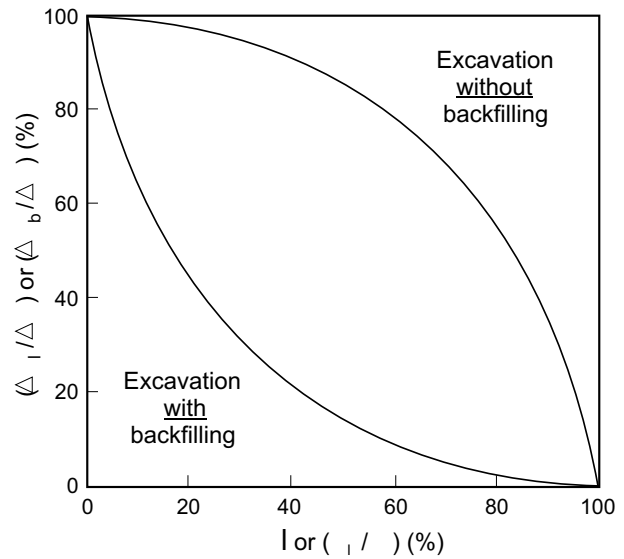
Substituting eq. [14] into eq. [28] for j equal to 35, gives;

$$[29] \quad \Delta H_l = \frac{C_s H}{1 + e_0} (1-l) [-0.430 + \log(1-l)]$$

If l is equal to zero, there is no removal, and eq. [29] reverts to eq. [14]. If l is equal to one, the entire active depth has been excavated, and there is no more tendency for heaving. A comparison between eq. [29] and eq. [14] can be written as:

$$[30] \quad \frac{\Delta H_l}{\Delta H} = (1-l) [1 - 2.326 \log(1-l)]$$

Fig. 11. Ratio of total heave for partial excavations and backfilling to total heave for wetting of entire active depth.



Equation [30] is graphically shown in Fig. 11 for various percentages of removal.

Let us now consider case 2 in which the excavated portion of the profile is backfilled with an inert or non-expansive soil. The total density of the backfill is assumed to be equal to the expansive soil density. Similarly, the total heave, ΔH_b , for case 2 can be calculated using the variables given in Fig. 10.

$$[31] \quad \Delta H_b = \frac{C_s H}{1 + e_0} (1-l) \left\{ \frac{1}{j} \sum_{i=1}^j \log \left[l + \frac{2i-1}{2j} (1-l) \right] \right\}$$

If l is equal to zero, the maximum heave is computed, and if l is equal to one, the heave is zero. A comparison between eq. [31] and eq. [14] can be written as:

$$[32] \quad \frac{\Delta H_b}{\Delta H} = -2.326(1-l) \left\{ \frac{1}{j} \sum_{i=1}^j \log \left[l + \frac{2i-1}{2j} (1-l) \right] \right\}$$

Dimensionless plots illustrating cases 1 and 2 are shown in Fig. 11. These plots apply for all swelling indices and swelling pressures and show the relative influence of excavation and backfill on the computed heave.

Figure 11 shows, for example, that if 50% of the active depth were removed, the total heave would still be 86% of that anticipated for no excavation. However, if the excavated portion is backfilled with a nonexpansive soil, the total heave would be only 15% of that anticipated if no material were excavated. In other words, partial excavation of the expansive soil depth does not significantly reduce the total heave unless there is backfilling with an inert soil.

Other possible boundary conditions could be assumed, but these examples illustrate the type of plots that can readily be generated using the heave prediction equation. The plots are of assistance in making engineering decisions when placing structures on expansive soils. Possible remedial measures for heave reduction by flooding, excavation, and backfilling can be readily compared using these types of plots.

Conclusions

A brief review of the heave prediction theory has been presented. A closed-form equation for computing heave in an expansive soil was derived for the condition with a constant swelling pressure. The variation in the computed total heave is small if a sufficient number of layers is used in the analysis. The effect of sampling disturbance on the measurement of swelling pressure was illustrated graphically.

Several other closed-form solutions were presented for cases of wetting a portion of the active depth, partial excavation, and partial excavation with backfilling of the active depth. The study indicated that 80% of the total heave occurred within 50% of the active depth. Therefore, the replacement of the top portion of the expansive soil depth can significantly reduce the potential heave that could occur during the lifetime of the structure. The results also indicated that partial excavation of the expan-

sive soil depth alone did not help in reducing the total heave. The excavation must be accompanied by backfilling with a nonexpansive soil in order to significantly reduce the total heave.

Similar closed-form solutions can also be generated for other typical swelling pressure distributions encountered in the field. Various factors affecting the total heave prediction can also be studied from the generated plots before making an engineering decision.

References

- Casagrande, A. 1936. The determination of the preconsolidation load and its practical significance. Proceedings, 1st International Conference on Soil Mechanics and Foundation Engineering, Cambridge, MS, Vol. 3, pp. 60–64.
- Fredlund, D.G. 1969. Consolidometer test procedural factors affecting swell properties. Proceedings, 2nd International Conference on Expansive Clay Soils, Texas A & M University, College Station, TX, pp. 435–456.
- Fredlund, D.G. 1983. Prediction of ground movements in swelling clays. Proceedings, 31st Annual Soil Mechanics and Foundation Engineering Conference, Minneapolis, MN.
- Fredlund, D.G., Hasan, J.U., and Filson, H.L. 1980. The prediction of total heave. Proceedings, 4th International Conference on Expansive Soils, Denver, CO, pp. 322–338.
- Jones, D.E., and Holtz, W.G. 1973. Expansive soils - the hidden disaster. ASCE, Civil Engineering, **43**(8): 49–51.
- Krohn, J.P., and Slosson, J.E. 1980. Assessment of expansive soils in the United States. Proceedings, 4th International Conference on Expansive Soils, Denver, CO, pp. 596–608.
- Russam, K., and Coleman, J.D. 1961. The effect of climatic factors on subgrade moisture conditions. Géotechnique, **11**: 22–28.
- ASTM 1986. Standard test methods for one-dimensional swell or settlement potential of cohesive soils. Annual book of ASTM standards, Vol. 04.08, ASTM Committee D-18 on Soil and Rock, Subcommittee D18.05 on Structural Properties of Soils, Philadelphia, PA.
- Yoshida, R.T., Fredlund, D.G., and Hamilton, J.J. 1983. The prediction of total heave of a slab-on-grade floor on Regina clay. Canadian Geotechnical Journal, **20**(1), 69–81.

The prediction of total heave of a slab-on-grade floor on Regina clay

R.T. Yoshida, D.G. Fredlund, and J.J. Hamilton

Abstract: Several analytical methods for the prediction of total heave of desiccated, expansive soils have been proposed for various geographic regions. The proposed method herein is based on a general theory for unsaturated soil. The *in situ* stress conditions as assessed from the corrected swelling pressure and the required soil moduli, are deduced from the constant volume oedometer test.

Verification of the proposed method was accomplished using data accumulated from the monitoring of movements of a door slab in a light industrial building in north-central Regina, Saskatchewan. A leak in a water line buried under the floor slab resulted in a maximum heave of about 106 mm. Of the three final pore-water pressure distributions assumed, the one where pressure is constant with depth and equal to atmospheric pressure appears to be representative of the field conditions corresponding to the maximum measured heave. The measured heave represents 89% of the predicted heave for the zero pore-water pressure distribution. It is concluded that the proposed method of analysis, based upon a general theory for unsaturated soils, provides a practical method to accurately assess total heave.

Key words: heave analysis, swelling pressure, swelling index, matric suction, slab-on-grade, oedometer test.

Introduction

The construction of buildings on unsaturated soils can result in damage from excessive volume changes in the soil. Costs associated with damage to all types of structures built on expansive soils in the United States have been estimated at \$7 billion per year (Krohn and Slosson 1980). The magnitude of this problem has necessitated the development of practical engineering solutions. Thus, much research has been undertaken regarding expansive soils throughout the world. The area of research most often addressed has been the prediction of total heave.

Methods for the prediction of total heave have been proposed in many parts of the world, but the empiricism upon which they have been based limits their use to specific geographic regions. Fredlund et al. (1980a) attempted to provide a general theoretical basis that would allow comparison of the various methods proposed. A predictive method developed on a more theoretical basis provides a more favourable analytical procedure.

In Western Canada, as in other parts of the world, predictive methods have generally utilized the oedometer (i.e., the consolidation apparatus) for the identification of

swelling soils (Hardy 1965; Noble 1966). The tests most commonly performed are referred to as constant volume and free swell oedometer tests. For the prediction of total heave, these methods have been considered to be more qualitative than quantitative.

This paper describes an analytical procedure for the prediction of total heave. The procedure is based on a general theory for unsaturated soils and utilizes the results of the constant volume oedometer test to represent the *in situ* state of stress and the relevant soil parameters for analysis. The predictive method is verified by using data collected by the Prairie Regional Station of the Division of Building Research (DBR), National Research Council of Canada, located in Saskatoon, Saskatchewan. In a program to investigate volume change problems associated with expansive soils in western Canada, the performance of the floor slab of a light industrial building in north-central Regina, Saskatchewan, was monitored. A leak in a water line buried under the floor slab resulted in a maximum heave of about 106 mm. Laboratory tests on samples taken from beneath the floor slab provided data for the calculation of heave using the proposed method for the prediction of total heave.

R.T. Yoshida. Graduate Student, Department of Civil Engineering, University of Saskatchewan, Saskatoon, SK, Canada S7N 5A9.

D.G. Fredlund. Professor, Department of Civil Engineering, University of Saskatchewan, Saskatoon, SK, Canada S7N 5A9.

J.J. Hamilton. Division of Building Research, National Research Council of Canada, Saskatoon, SK, Canada S7N 0W9.

Reproduced with permission from the *Canadian Geotechnical Journal*, 20: 69–81, 1983.

History of the study site

As part of a larger study of shallow foundation performance in expansive soils in the Prairies, the DBR initiated measurements of vertical slab and subsoil movements at a typical single-storey commercial building in north-central Regina, Saskatchewan. The building superstructure was placed on a perimeter grade beam supported by cast-in-place concrete piers. About 180 mm of gravel fill was placed to raise the grade to a suitable elevation for the floor slab and a concrete slab with a thick-

ness of 100 mm was then placed. Construction of the building and instrumentation took place during the month of August, 1961. Instrumentation installed at the site included a deep bench-mark (DBM), vertical movement gauges, and a neutron moisture meter (NMM) access tube (Fig. 1). For the installation of the deep bench-mark, a 100-mm diameter auger boring was made which was logged visually, with four 75-mm Shelby tube samples taken at depths of 0.5, 1.2, 2.4, and 4.3 m from the original ground surface. At a depth of 14.6 m, the boring was halted and a deep bench-mark was lowered into the boring and pushed into the soil to refusal at a depth of 16.8 m (Bozozuk et al. 1962).

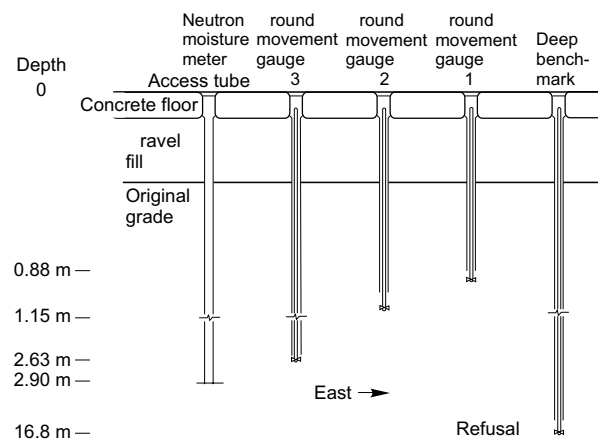
Three spiral-foot ground movement gauges (GMG) (Bozozuk 1968) were installed near the benchmark (Fig. 1) at depths of 0.88 m, 1.15 m, and 2.69 m below the design elevation of the floor slab. The ground movement gauges and bench-mark were accessed through floor clean-outs cast in the floor. A neutron moisture meter access tube was installed next to the ground movement gauges to a depth of 2.90 m; this tube allowed the use of the meter to monitor soil moisture contents adjacent to the tube without removing soil samples.

Whereas the ground movement gauges were used to measure vertical movements at specific depths, vertical movement of the floor slab surface was measured by taking level shots at a number of predetermined positions on the slab. Initial level readings were made on the ground movement gauges on August 23, 1961, with initial readings on the surface of the floor slab being made on September 22, 1961. Between these two dates, the shallow ground movement gauge indicated a heave of 6.4 mm. Thus, it is assumed that the floor slab was heaved by an equal amount, and a correction has been applied to the initial floor surface level readings. Later measurements of ground movement and water content of the soil using the gauges and neutron moisture meter were made about twice a year up to 1968, with additional measurements using the vertical ground movement gauges up to 1972. Level surveys of the floor slab were made in August of 1962.

Heaving and cracking of the floor slab was first noticed by the building owner in early August, 1962. The owner also noticed an unexpected increase in water consumption of approximately 35 000 L. The loss of water was traced to a leak, in a hot-water line beneath the floor slab, which was subsequently repaired. The location of the cracking and contours of heave for the floor slab are shown in Fig. 2, with vertical ground movements indicated in Fig. 3. Changes in the water content are shown in Fig. 4 and correspond to changes measured at the location of the neutron moisture meter access tube.

The maximum amount of heave for the floor slab, as shown in Fig. 3, has been approximated because elevation readings made by others between August 22, 1961 and August 15, 1962 were found to be unreliable. The shape of the curve has been made similar to that of a plot of heave over time for another test area in Regina (Hamilton 1969). This latter test area was flooded intentionally

Fig. 1. Instrumentation at the site.



and showed that heaving took place almost immediately. Thus, it has been assumed that the break in the hot-water line took place in late July or early August, 1962, and that no heave other than the initial 6.4 mm had occurred until that time. It has been assumed that after August, 1962 an additional 9 mm of heave took place, an amount corresponding to vertical movement measured by the shallow vertical movement gauge. Thus, it has been estimated that the maximum heave of the floor slab was at least 106 mm. It appears that unmeasured quantities of products stored around the perimeter of the floor slab, as well as the loads applied by the perimeter wall, restricted the amount of heave in such a way that most of the vertical movement occurred in the lightly loaded central portion of the floor slab.

It is likely that the gravel fill under the slab facilitated the movement of water from the plumbing trench to a larger area. A loss of 35 000 L of water can be equated to 100 mm of water over the entire 355 m² of floor area. However, most of the vertical movement took place near the centreline of the floor in the vicinity of the water line, with the greatest distress to the floor slab indicated by cracking directly over the subfloor plumbing trench. It does not appear that complete saturation had occurred over the entire area of the door, rather that only the area surrounding the water leak was immediately affected. Water content profiles as indicated in Fig. 4, measured using the neutron moisture meter, show a more gradual increase over a 7-year period at a point a short distance from the plumbing trench.

From these observed changes in volume and water content, sufficient information is available to evaluate a method for the prediction of total heave. As is the practice in soil mechanics for saturated soils, the proposed method relates changes in the stress state of the soil to its volume change. In order to accomplish this, the variable describing the state of stress at a point in an unsaturated soil must be known, as must the constitutive relations necessary to relate stress to deformation.

Fig. 2. Floor plan of study site (NMM = neutron moisture meter; GMG = ground movement gauge; DBM = deep benchmark).

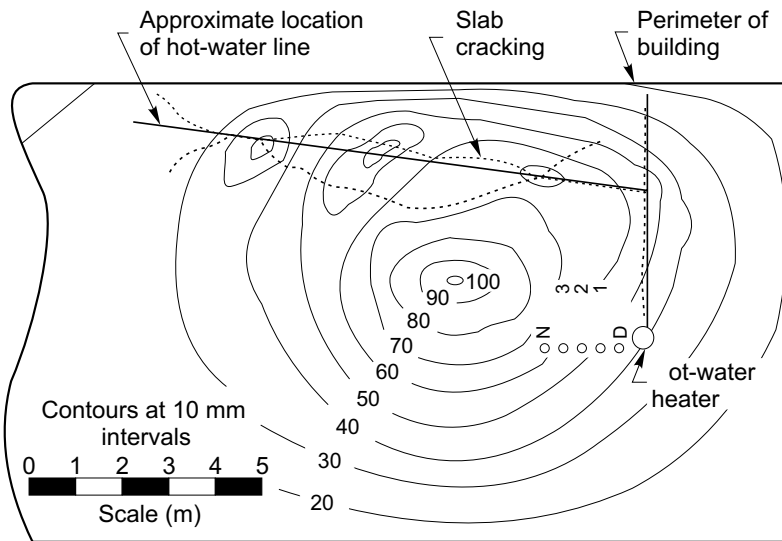


Fig. 3. Measured ground movement (GMG = ground movement gauge).

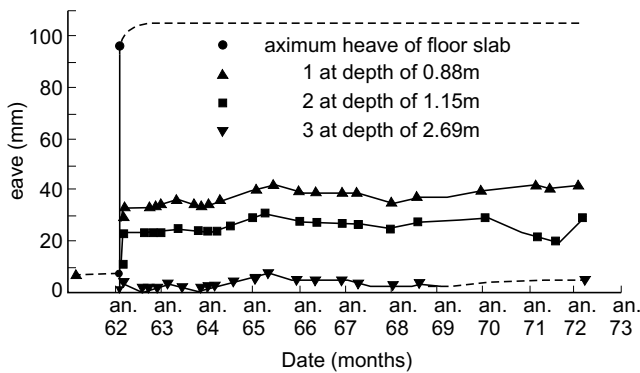
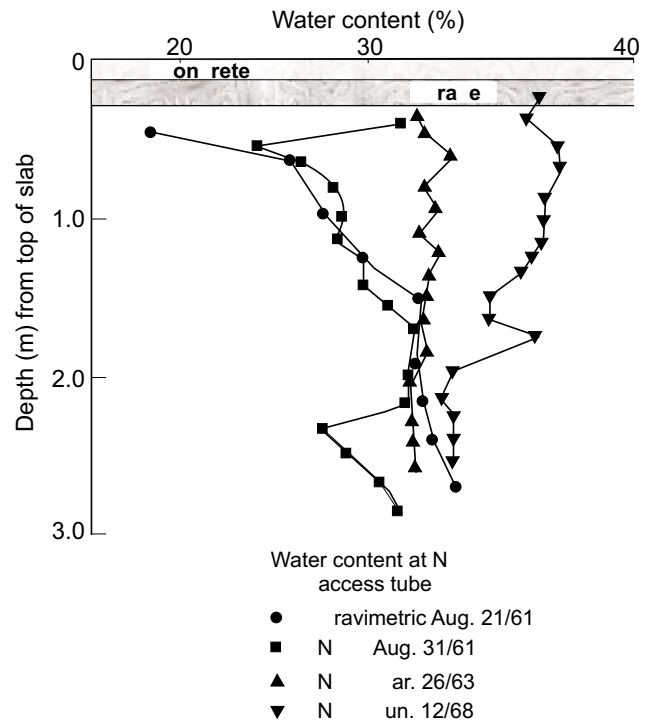


Fig. 4. Measured water content (NMM = neutron moisture meter).



Theoretical aspects

The unsaturated and highly expansive soils of the Regina area are typical of lacustrine deposits. The climate is cool and semiarid. Although these soils were deposited in a saturated state, subsequent evaporation and evapotranspiration has left the water table well below the surface. Although the total stress conditions have not changed, pore-water pressures above the water table are generally less than atmospheric (or negative), resulting in desaturation, fissuring, and shrinkage of the deposit to a considerable depth. Influences such as precipitation, evapotranspiration, or freezing alter the pore-water pressure distribution with time.

The analysis of the behavior of unsaturated soils is best visualized by separately considering changes in stress due to mechanical processes and those due to variations in the water content. Although the volume change of unsaturated soils has been described in terms of effective stress, degree of saturation, or water content, these empirical relationships have been found to be difficult to utilize in a general sense. Other investigators (Aitchison 1969;

Fredlund 1973; Fredlund and Morgenstern 1976, 1977) have indicated the importance of relating volume change to independent stress variables.

Although various combinations of stress state variables can be used to define the stress state in an unsaturated soil, the most satisfactory ones are $(\sigma - u_a)$ and $(u_a - u_w)$ where σ is the total stress, u_a is the pore-air pressure, and u_w is the pore-water pressure (Fredlund 1973, 1979; Fredlund and Morgenstern 1976, 1977). The use of these two stress state variables allows the separation of changes in total stress from those in pore-water pressure. The

$(\sigma - u_a)$ term is referred to as the net total stress and the $(u_a - u_w)$ term is called the matric suction. The usefulness of these stress state variables has been experimentally verified (Fredlund 1973). Although two constitutive surfaces are necessary to fully describe the volumetric changes in an unsaturated soil, one constitutive surface relating the stress state variables to the void ratio, e , is sufficient to describe the method for the prediction of total heave. A more detailed description of the theoretical concepts of unsaturated soil mechanics and of the prediction of total heave can be found elsewhere (Fredlund and Morgenstern 1976; Fredlund et al. 1980a).

The void ratio constitutive surface (Fig. 5) can be linearized over a relatively wide range of stress if the logarithm of the stress state variables is used. The change in void ratio, Δe , is then expressed:

$$[1] \quad \Delta e = C_t \log \frac{(\sigma - u_a)_f}{(\sigma - u_a)_0} + C_m \log \frac{(u_a - u_w)_f}{(u_a - u_w)_0}$$

where:

C_t = compressive index with respect to net total stress,

C_m = compressive index with respect to matric suction,

f = subscript indicating final conditions, and

0 = subscript indicating initial conditions.

If the soil profile is divided into n layers of finite thickness, h_i , then for the i -th layer the heave, Δh_i , is:

$$[2] \quad \Delta h_i = h_i \frac{\Delta e}{(1 + e_0)}$$

where:

e_0 = initial void ratio.

The total heave, Δh , is then expressed as:

$$[3] \quad \Delta h = \sum_{i=1}^n \Delta h_i$$

Since the final degree of saturation will approach 100% (Fredlund 1979), the change in water content, Δw , and therefore the final water content can be calculated, where:

$$[4] \quad \Delta w = S_f \Delta e / G_s + e_0 \Delta S / G_s$$

and:

S_f = final degree of saturation,

ΔS = change in degree of saturation, and

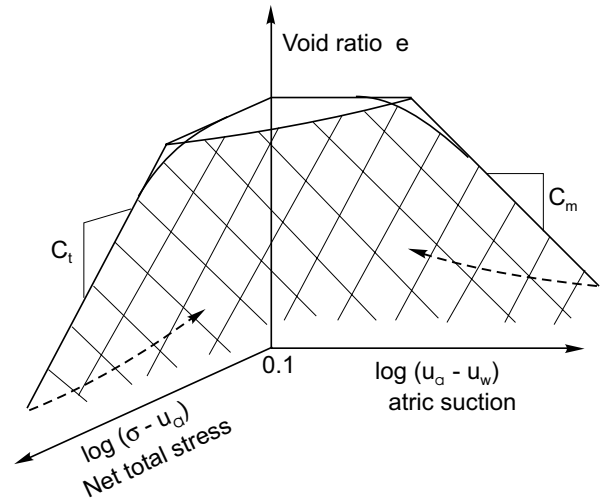
G_s = specific gravity of the soil.

For each layer considered in the analysis, the appropriate moduli must be known, as must the initial and final net total stress and matric suction.

Initial stress boundary conditions

Of particular interest and concern in establishing the initial stress boundary conditions for an unsaturated soil is the matric suction profile. If the pore-air pressure is as-

Fig. 5. Logarithm of stress variables versus void ratio.



sumed initially to be in equilibrium and equal to atmospheric pressure, then the distribution of pore-water pressure is equivalent to the matric suction distribution. The initial stress boundary conditions will vary, depending upon the changes in the environment that have taken place over several decades or centuries. For a cumulative moisture depletion, pore-water pressures will be negative relative to atmospheric pressure. Therefore, the matric suction will be high and the propensity for swelling accompanying an influx of moisture will be large.

The distribution of matric suction can be established in a number of ways, including the use of psychrometers, axis-translation matric suction methods, and oedometer tests on undisturbed soil samples. The method of analysis proposed herein makes use of a constant volume oedometer test on undisturbed samples. Although this method does not directly evaluate the *in situ* matric suction, an equivalent matric suction is measured. This is done on the net total stress plane, but can be used for the calculation of total heave since the measured modulus is on the net total stress plane as well. The details of the constant volume oedometer test are discussed further in a later section.

Final stress boundary conditions

The final stress boundary conditions, like the initial stress boundary conditions, are generally controlled by environmental factors such as geography, climate, and land use. As is the case for the initial stress boundary conditions, air pressure is assumed to be atmospheric or zero gauge and the net total stress can be determined by considering the depth of overburden, the soil density, and the applied loads.

In general, one of the three following assumptions is used regarding the final pore-water pressures (Fredlund 1979).

- (1) The water table will rise to some elevation near or at the soil surface. Thus, a hydrostatic pore-water pres-

sure distribution will result. This assumption will give the highest prediction of heave.

- (2) Pore-water pressure is constant and atmospheric or zero gauge with depth. Although this profile is an unsteady state boundary condition, it could occur if water has been made available from the soil surface.
- (3) The pore-water pressure profile is slightly negative. Such a distribution would be related to the soil type and climatic conditions imposed by the building placed on the ground surface.

Predictions of heave using any one of these three assumptions generally do not differ appreciably from predictions using any other of the assumptions (Fredlund et al. 1980a) because most of the heave occurs in the uppermost layers of the soil where the soil modulus is highest and the change in the matric suction is the largest. Figure 6 illustrates both the initial and final boundary conditions.

Proposed method of analysis

The proposed method of analysis utilizes the constant volume oedometer test to evaluate the rebound modulus and to infer the *in situ* stress state. By making use of the oedometer test data, the proposed method of analysis utilizes equipment and techniques readily available in soil mechanics laboratories.

Heaving of an expansive unsaturated soil is equivalent to the rebound that is experienced due to the unloading of a saturated soil. On the three-dimensional void ratio constitutive surface, the rebound surface is unique (Fig. 7). Thus, starting at the initial void ratio, e_0 , at the *in situ* stress state defined by the net total stress, $(\sigma - u_a)_0$, and the matric suction, $(u_a - u_w)_0$, the field swelling follows the stress path to e_f , the final void ratio corresponding to the stress state represented by the net total stress, $(\sigma - u_a)_f$, which equals the initial net total stress, $(\sigma - u_a)_0$, and the matric suction, $(u_a - u_w)_f$, which is equal to zero.

Knowledge of the rebound modulus with respect to a change in the matric suction, $(u_a - u_w)$, in conjunction with the initial *in situ* stress state allows the calculation of total heave. However, the evaluation of these quantities is not easy. In order to simplify the analysis, the proposed method uses an alternative stress path.

Because the constitutive surface is unique for monotonic stress changes, between the initial and the final stress states there is an infinite number of possible stress paths. The path followed in the proposed method of analysis (Fig. 7) first proceeds along the constitutive surface at a constant volume as the matric suction decreases and the net total stress increases. When the matric suction becomes zero the net total stress plane is reached and there can be no further increase in the net total stress without a decrease in volume. The net total stress at this point is commonly referred to as the swelling pressure.

The swelling pressure is not actually a characteristic or a property of the unsaturated soil, but is an indicator of the *in situ* stress state. The components of the swelling

Fig. 6. Initial and final boundary stress conditions.

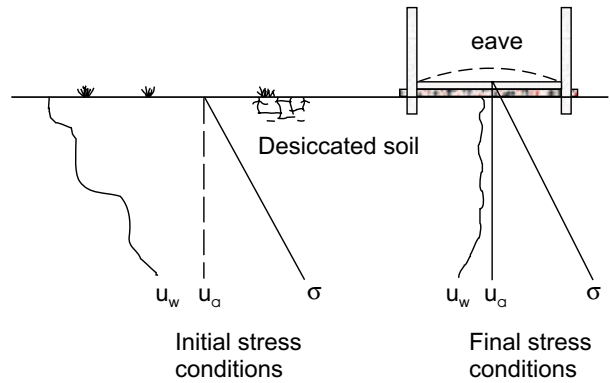


Fig. 7. Comparison of the actual stress path and the stress path used in the analysis.

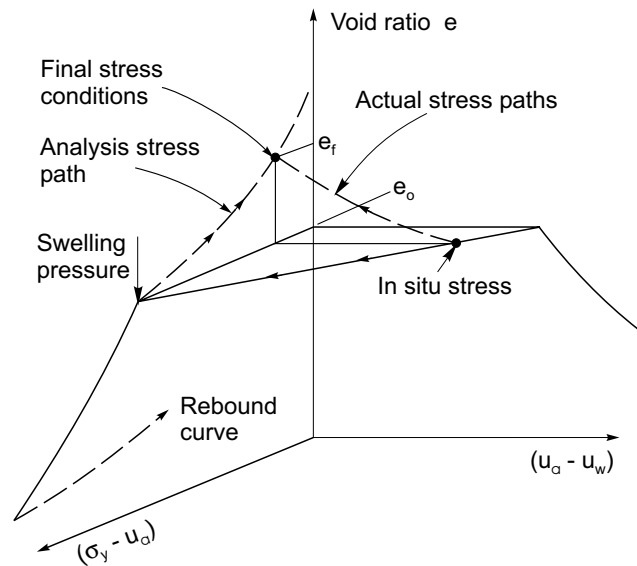
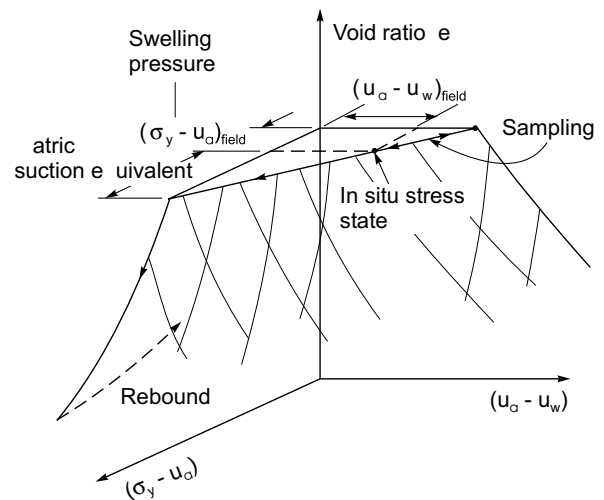


Fig. 8. Ideal interpretation of sampling and constant volume.



pressure are the overburden pressure and the matric suction equivalent (Fig. 8). The matric suction equivalent is not equal to the *in situ* matric suction but, as the equiva-

lent matric suction is reduced to zero and the soil is allowed to swell, the subsequent rebound to the overburden pressure corresponds to the rebound due to the reduction in the matric suction. Thus, the stress path for the analysis is complete (Fig. 7).

Invariably, there is some disturbance of the soil as a result of sampling (Fig. 9). If no volume change due to sampling is assumed with the overburden pressure removed, the state of stress in the sample is largely unknown. If a specimen is loaded to the overburden pressure in the oedometer, flooded with water, and allowed to swell freely as in the free-swell oedometer test, the resulting heave would be less than the actual field swelling, due to sample disturbance (Fredlund et al. 1980a). A suitable correction to the matric suction to compensate for sampling disturbance was proposed by Fredlund et al. (1980a).

In the constant volume oedometer test, the point at which no further swelling takes place may be much less than the actual swelling pressure (Fig. 10). A procedure that is a correction for sample disturbance is used to evaluate the actual or corrected swelling pressure. The procedure is similar to that used to evaluate the preconsolidation pressure of a saturated soil. The correction, shown in Fig. 10, is a modified form of the Casagrande construction (Leonards 1962).

To evaluate the corrected swelling pressure, the point of maximum curvature of the curve of void ratio versus logarithm of total pressure is located. The point can readily be found immediately past the uncorrected swelling pressure. From this point, horizontal and tangential lines are drawn and the angle formed is bisected. The intersection of a line parallel to the rebound portion of the curve and the bisector indicates the corrected swelling pressure. It is noted that no correction is required for the rebound modulus because it is not altered significantly by the stress level or sample disturbance (Schmertmann 1955).

For the soil profile being analyzed, several samples from varying depths are required to properly define the initial void ratio, the initial state of stress represented by the corrected swelling pressure, and the rebound modulus. Next, the final stress conditions must be determined.

The final stress state is determined by calculating the overburden pressure, any surcharges that may be applied, and the final pore-water pressure distribution. In order to simplify the analysis, it is assumed that a surcharge causes a constant increase in total stress with an increase in depth. Also, any hysteretic effects due to unloading from the removal of overburden and due to loading from a surcharge are neglected. However, these hysteretic effects could be taken into account by using appropriate compressive indices. Final pore-water pressures assumed for the analysis are subtracted from the total stress.

Analysis

The engineering properties of the highly plastic, expansive proglacial lake sediments upon which the city of Re-

Fig. 9. Actual stress path during sampling and constant volume oedometer test (assuming no volume change during sampling).

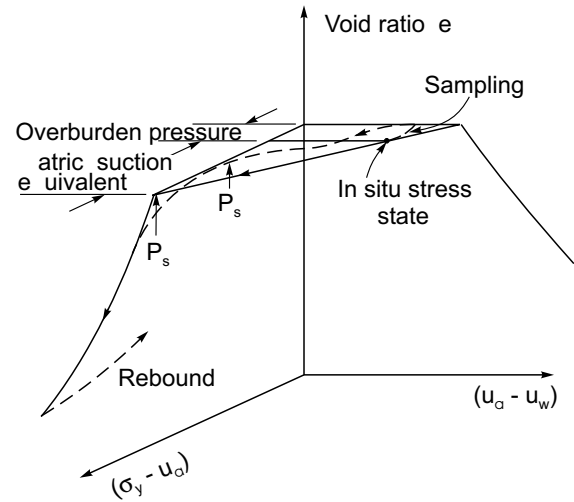
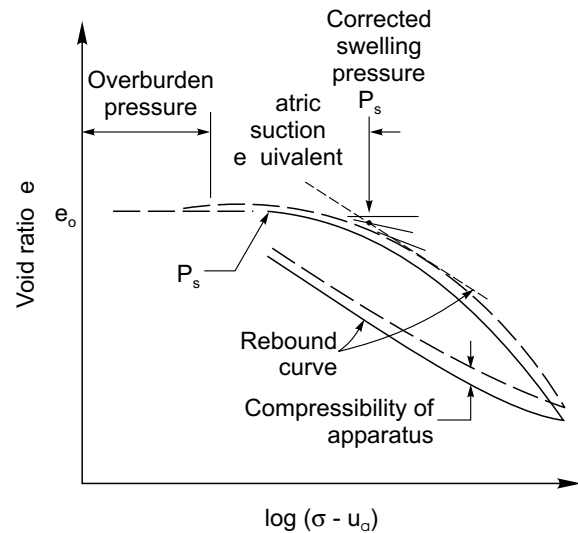


Fig. 10. Construction to compensate for sample disturbance.



gina, Saskatchewan is built have been well documented (Fredlund and Hasan 1979; Fredlund et al. 1980b). The statistical analysis of data accumulated from numerous boreholes advanced in the Regina area indicates that the sediments are relatively uniform. For the study site being considered, laboratory analyses were performed on samples from the borehole made in August, 1961 for the installation of the deep benchmark. The tests evaluated the Atterberg limits, water contents *in situ*, grain-size distribution, swelling indices, and *in situ* stress state as represented by the corrected swelling pressure. Figure 11 indicates the results of index tests on the samples taken. On the average, the liquid limit was found to be 77%, with a plastic limit of 33% and a water content of 29%.

Constant volume oedometer tests on three samples were used to evaluate the initial void ratios, the swelling indices, and the corrected swelling pressures. Although there was some variation in the initial void ratio and the

Fig. 11. Soil profile at the study site.

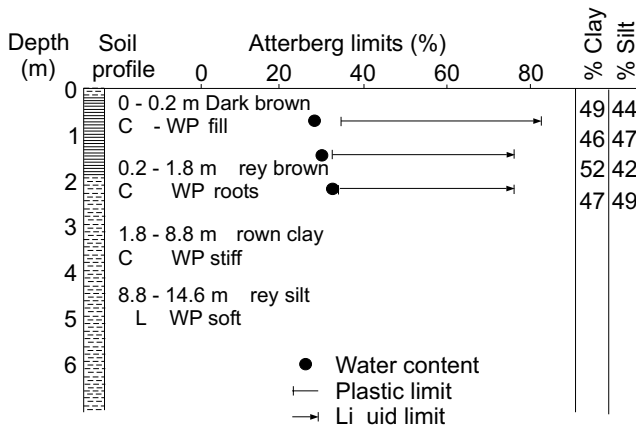


Table 1. Constant volume oedometer data.

Depth (m)	Initial void ratio	Swelling index	Uncorrected swelling pressure (kPa)	Corrected swelling pressure (kPa)
0.69	0.927	0.095	350	490
1.34	0.985	0.081	240	325
2.20	0.974	0.094	22	81

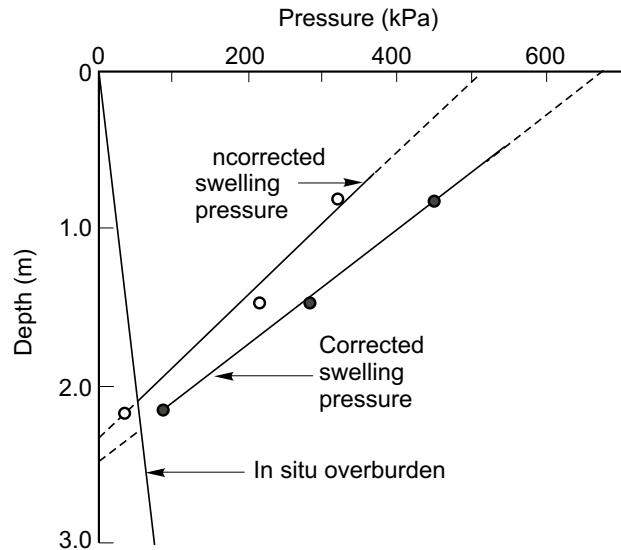
swelling index (Table 1), average values of 0.962 for the initial void ratio and 0.090 for the swelling index will be used in the analyses. The distribution of the corrected swelling pressure with depth is shown in Fig. 12. A straight line can be used to represent the apparent distribution of the corrected swelling pressure with depth for purposes of analysis.

Other considerations for the analyses are as follows:

- (1) The thickness of the layers used is 0.3 m; eight layers are considered. The lower boundary is the point where the initial stress state is equal to the final stress state, a point at which there is no apparent tendency for swelling. This lower boundary may also be selected on the basis of the lowest depth to which changes in matric suction may be expected to take place.
- (2) A change in total stress equal to 5.76 kPa is applied. This surcharge is made up of 180 mm of fill with a unit weight of 18.88 kN/m³ and 100 mm of concrete with a unit weight of 23.60 kN/m³. The analyses will examine a central portion of the slab known to be essentially unloaded. Although loads were placed at the perimeter of the floor slab, their magnitudes are not accurately known.
- (3) The specific gravity for the soil profile is 2.82.
- (4) The unit weight for the soil profile is 18.88 kN /m³.
- (5) The final degree of saturation is 100%.
- (6) The initial and final air pressure is assumed to be 0 kPa gauge.

In general, the final stress state, FST, can be expressed as:

Fig. 12. Distribution of swelling pressure with depth.



$$FST = OB + \Delta\sigma - u_w$$

where:

OB = overburden pressure,

$\Delta\sigma$ = change in total stress, and

u_w = final pore-water pressure, all expressed in kPa.

The change in void ratio, Δe , for the i -th layer is found using a reformulation of eq. [1] that is consistent with the stress path used for the analysis. Since this stress path is in the net total stress plane, the change in void ratio can be written as follows.

$$[5] \quad \Delta e = -C_s \log \frac{FST}{IST}$$

where:

C_s = swelling index, and

IST = initial stress state represented by the corrected swelling pressure.

The swelling index, C_s , is the slope of the rebound curve when the constant volume oedometer test results are plotted on semilogarithmic paper. The change in thickness, Δh_i , for the i -th layer is computed using eq. [2] and the appropriate initial void ratio, e_0 . Equation [3] is used to calculate the total heave.

Since the initial water content profile has been established (see Fig. 4), the initial degree of saturation can also be calculated. Assuming a final degree of saturation, the change in water content for each layer and hence the final water content can be calculated by using the change in void ratio, Δe , the initial void ratio e_0 , and eq. [4]. The final water contents can then be compared with those measured using the neutron moisture meter.

Case 1: Final pore-water pressure equal to zero

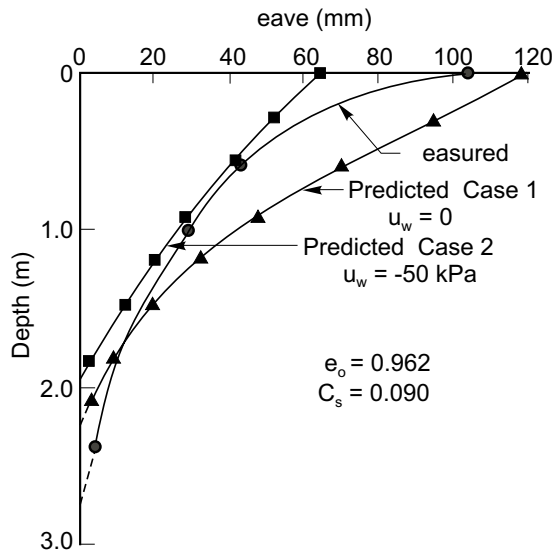
Assuming that the final pore-water pressure increases from a negative value to zero results in a calculated heave

Table 2. Prediction of heave assuming final pore-water pressure is zero.

Depth (m)	Δe	e_f	S_o (%)	w_f (%)	Δh_i (mm)	$\sum \Delta h$ (mm)
0.15	0.169	1.131	55.1	40.1	26	118
0.45	0.143	1.105	78.1	39.2	22	92
0.75	0.124	1.086	81.1	38.5	19	70
1.05	0.107	1.069	85.0	37.9	16	51
1.35	0.090	1.052	92.4	37.3	14	35
1.65	0.072	1.035	91.6	36.7	11	21
1.95	0.050	1.012	92.3	35.9	8	10
2.25	0.015	0.977	92.9	34.6	2	2

Note: $e_o = 0.962$; $C_s = 0.090$; $S_f = 100\%$.

Fig. 13. Measured and predicted ground movements.

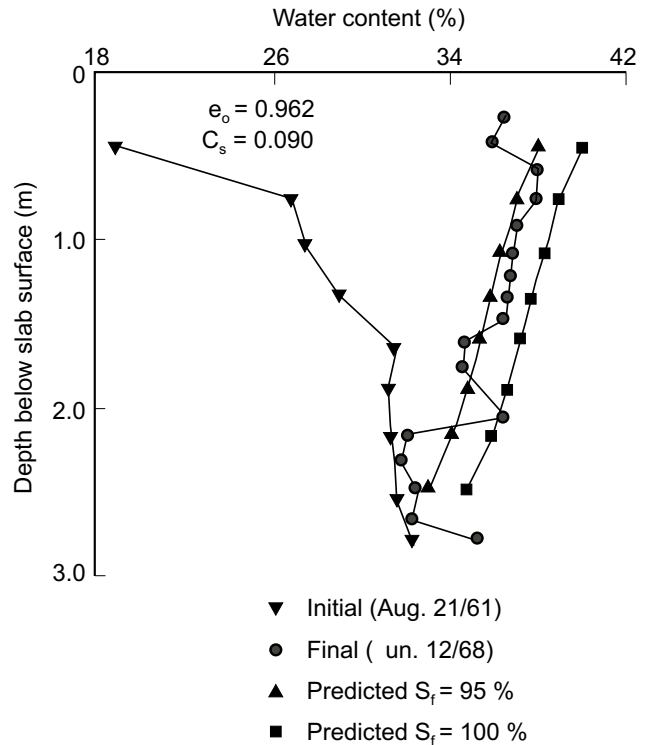


of 118 mm (Table 2). Figure 13 indicates the measured and predicted heave. However, the agreement between the predicted and measured heave at different depths is not completely satisfactory. A variation in the initial void ratio from 0.920 to 1.000 results in a change of less than $\pm 2\%$ in the calculated total heave. Thus it appears that, within the range of initial void ratios measured in the laboratory, relatively insignificant error results. For further analyses, an initial void ratio of 0.962 will be used.

Values of the swelling index for Regina clay based on a statistical study of the entire lake basin (Fredlund et al. 1980b) are somewhat lower than those found at this study site. The statistical study showed a mean value of 0.062 and the 95% significance limits were about 0.024 – 0.097 at an average depth of 3.3 m in Regina clay. The standard deviation reported is ± 0.015 . The relative consistency of the values for the swelling index evaluated for this paper are deemed sufficient to place confidence in their use in the analyses. At the site under consideration, the mean value is 0.090, with a standard deviation of ± 0.006 .

A variation in the swelling index affects the calculated heave in direct proportion to the magnitude of the variation. Therefore, for one standard deviation change from

Fig. 14. Measured and predicted water contents.



C_s , equal to 0.090, there will be a change in the predicted heave equal to $\pm 7\%$. This results in a range of total heave from 110 to 125 mm. The predicted heave using the uncorrected swelling pressure to represent the *in situ* stress state as shown in Fig. 13 and Table 1 is 100 mm. This prediction is about 15% lower than that using the corrected swelling pressure.

A comparison between the calculated final water content and the measured values shows good agreement for an assumed 100% saturation. For an assumption of 95% for the final saturation, Fig. 14 shows that the calculated final water content decreases by 2%. The change in the calculated final water content for the variation in the initial void ratio assumed is less than $\pm 1.5\%$. For a change in the swelling index of $\pm 7\%$, the resulting variation in the water content is less than $\pm 1\%$.

Table 3. Prediction of heave assuming final pore-water pressure is -100 kPa.

Depth (m)	Δe	e_f	S_0 (%)	w_f (%)	Δh_i (mm)	$\sum \Delta h$ (mm)
0.15	0.069	1.031	55.1	36.6	11	44
0.45	0.062	1.024	78.1	36.3	9	33
0.75	0.054	1.016	81.1	36.0	8	24
1.05	0.045	1.007	85.0	35.7	7	16
1.35	0.034	0.996	92.4	35.3	5	9
1.65	0.021	0.983	34.9	34.9	3	4
1.95	0.003	0.965	92.3	34.2	1	1

Note: $e_0 = 0.962$; $C_s = 0.090$; $S_f = 100\%$.

Table 4. Prediction of heave assuming final pore-water pressure is hydrostatic.

Depth (m)	Δe	e_f	S_0 (%)	w_f (%)	Δh_i (mm)	$\sum \Delta h$ (mm)
0.15	0.176	1.138	55.1	40.4	27	141
0.45	0.158	1.120	78.1	39.7	24	114
0.75	0.142	1.104	81.1	39.2	22	90
1.05	0.127	1.089	85.0	38.6	19	68
1.35	0.112	1.074	92.4	38.1	17	49
1.65	0.095	1.057	91.6	37.5	14	32
1.95	0.073	1.035	92.3	36.7	11	17
2.25	0.039	1.001	92.9	35.5	6	6

Note: $e_0 = 0.962$; $C_s = 0.090$; $S_f = 100\%$.

Case 2: Final pore-water pressure is negative

A negative final pore-water pressure represents a possible long-term net loss of moisture from the site. For a final pore-water pressure of -100 kPa the predicted total heave is 44 mm. When the final pore-water pressure is increased to -50 kPa the predicted heave increases to 66 mm. Results of the calculations for a final pore-water pressure of -100 kPa are shown in Table 3.

Case 3: Final pore-water pressure is hydrostatic

The upper limit for a prediction of total heave is represented by the case in which the water table rises to the surface resulting in a hydrostatic pore-water pressure distribution. In such a case, the heave that takes place can be considered to be composed of a portion where the pore-water pressure increases from a negative value to zero, and a portion that results from a rebound on the net total stress plane due to a decrease in the effective stress. In the analysis, the modulus used to calculate the latter portion is equal to the swelling index, which has been measured on the net total stress plane. For this case the predicted heave amounts to 141 mm. The results of the calculations are shown in Table 4.

Discussion

It appears from the analyses that, of the several components required for calculations, the evaluation of the swelling index and the *in situ* stress state, as represented by the corrected swelling pressure, are the most important for accurate predictions. Reasonable errors could be tolerated in the initial void ratio without affecting the predic-

Table 5. Summary of the prediction of heave.

Final pore-water pressure	Predicted total heave (mm)
-100 kPa	44
-50 kPa	66
0 kPa	118
Hydrostatic	141

Note: $e_0 = 0.962$; $C_s = 0.090$.

tion of total heave substantially. However, errors in the evaluation of the swelling index will affect the prediction of total heave in direct proportion to the error. Errors in the evaluation of the corrected swelling pressure can also affect the analysis substantially. Without corrections for the disturbance of the sample and compression of the equipment, predicted quantities of heave will be low.

It is obvious that the assumption used to define the final pore-water pressure conditions will affect the prediction of total heave (Table 5). When dealing with volume changes in an unsaturated, expansive soil, it is apparent that the physical environment is a major factor. The definition of the equilibrium state must reflect the temperature, relative humidity, and wind and precipitation conditions in the area. The natural environment of the upper soil profile is dynamic with changes in the thermal and moisture conditions occurring diurnally, seasonally, and over several years. Furthermore, this dynamic environment is usually significantly altered by the activities of man. Therefore, an equilibrium pore-water pressure distribution must at best be considered as a range of the

expected environmental conditions determined for each individual site.

For the case study presented here, it is concluded that the maximum heave that took place near the centreline of the floor slab (Fig. 2) corresponds to a final pore-water pressure distribution that is constant with depth and approaching zero (Fig. 13). However, Fig. 13 seems to indicate that in the vicinity of the ground movement gauges the final pore-water pressure was slightly negative and approximately equal to -50 kPa. From Fig. 2, the estimated heave in the vicinity of the ground movement gauges is approximately 50–60 mm, agreeing reasonably well with the calculated heave. However, for a final pore-water pressure distribution that is constant with depth and approaching zero, and an assumed increase in total stress equal to approximately 75 kPa, a heave of 60 mm is calculated. Thus, a reduced quantity of heave away from the central area of the floor slab may be due to the effect of perimeter loads on the floor slab.

Conclusions

- (1) The proposed method of analysis based upon a general theory for unsaturated soils provides a practical method to accurately assess total heave. The maximum measured heave (i.e., 106 mm) represents 89% of the 118 mm of heave predicted for an assumed final pore-water pressure that is constant with depth and equal to zero.
- (2) It is important, in the evaluation of the *in situ* stress state represented by the corrected swelling pressure and the swelling indices, that corrections be made to account for sample disturbance and the compressibility of the apparatus. The empirical procedure proposed appears to compensate for this disturbance to give a reliable indication of the initial *in situ* stress state.
- (3) Assumptions regarding the final pore-water pressure distribution will depend upon the environmental conditions encountered at the site. For the limited flooding situation encountered, an assumed final pore-water pressure that is constant with depth and equal to zero seems adequate for a prediction of the maximum heave.
- (4) The general theory for unsaturated soil behavior provides a good framework for the prediction of total heave in expansive soils. This behavior can be related to independent changes due to mechanical processes and changes in matric suction. Further case history studies would be beneficial.

Acknowledgements

Funding for this paper was made available through a Technology Transfer Contract No. 080-018/0-0612. This was an agreement between the Program for Industry/Laboratory Projects (PILP) of the National Research Council of Canada, the Canadian Geotechnical Society, and the University of Saskatchewan.

Laboratory testing and field data collection was performed by the staff and summer assistants of the Prairie Regional Station of the Division of Building Research, National Research Council of Canada, Saskatoon.

References

- Aitchison, G.D. 1969. A statement of the problems the engineer faces with expansive soils. Proceedings, 2nd International Research and Engineering Conference on Expansive Clay Soils. Texas A & M University, College Station, pp. 33–51.
- Bozozuk, M. 1968. The spiral foot settlement gauge. Canadian Geotechnical Journal, **5**: 123–125.
- Bozozuk, M., Johnston, G.H., and Hamilton, J.J. 1962. Deep bench marks in clay and permafrost areas. *In* Field testing of soils. ASTM Special Technical Publication No. 322, pp. 265–279.
- Fredlund, D.G. 1969. Consolidometer test procedural factors affecting swell properties. Proceedings, 2nd International Conference on Expansive Clay Soils, Texas A & M University, College Station, pp. 435–456.
- Fredlund, D.G. 1973. Volume change behavior of unsaturated soils. Ph.D. thesis, University of Alberta, Edmonton, AB, Canada.
- Fredlund, D.G. 1979. Second Canadian Geotechnical Colloquium: Appropriate concepts and technology for unsaturated soils. Canadian Geotechnical Journal, **16**: 121–139.
- Fredlund, D.G., and Hasan, J.U. 1979. One-dimensional consolidation theory: Unsaturated soils. Canadian Geotechnical Journal, **16**: 521–531.
- Fredlund, D.G., and Morgenstern, N.R. 1976. Constitutive relations for volume change in unsaturated soils. Canadian Geotechnical Journal, **13**: 261–276.
- Fredlund, D.G., and Morgenstern, N.R. 1977. Stress state variables for unsaturated soils. ASCE, Journal of the Geotechnical Engineering Division, **103**(GT75): 447–466.
- Fredlund, D.G., Hasan, J.U. and Filson, H. 1980a. The prediction of total heave. Proceedings, 4th International Conference on Expansive Soils, Denver, CO, Vol. 1, pp. 1–17.
- Fredlund, D.G., Krahn, J., and Hasan, J.V. 1980b. Variability of an expansive clay deposit. Proceedings, 4th International Conference on Expansive Soils, Denver, CO, Vol. 1, pp. 322–338.,
- Hamilton, J.J. 1969. Effects of environment on the performance of shallow foundations. Canadian Geotechnical Journal, **6**: 65–80.
- Hardy, R.M. 1965. Identification and performance of swelling soil types. Canadian Geotechnical Journal, **11**: 141–153.
- Krohn, J.P., and Slosson, J.E. 1980. Assessment of expansive soils in the United States. Proceedings, 4th International Conference on Expansive Soils, Denver, CO, pp. 596–608.
- Leonards, G.A. 1962. Foundation engineering. McGraw-Hill Book Co. Inc., New York, NY, pp. 148–155.
- Noble, C.A. 1966. Swelling measurements and prediction of heave for a lacustrine clay. Canadian Geotechnical Journal, **3**: 32–41.
- Schmertmann, J.H. 1955. The undisturbed consolidation behavior of clay. Transactions of the American Society of Civil Engineers, **120**: 1201–1227.

Appendix

This appendix describes in detail the procedure for computing total heave.

Field sampling

Field sampling consists of taking suitable undisturbed samples from the upper 4 m or more of the site. The sampling depth will depend upon several factors. These include the depth at which the soil has been desiccated as well as the depth to which moisture flow can be expected.

The depth to which there has been desiccation will determine the depth to which volume change can be a problem. However, if within reasonable environmental conditions moisture flow is not expected to penetrate past an assumed depth, the determination of the *in situ* stresses below this depth is not critical. The final boundary conditions are up to the discretion of the engineer.

Sufficient samples should be obtained to properly characterize the distribution of the swelling index and the *in situ* stress state within the expansive clay portion of a profile.

Evaluation of *in situ* parameters

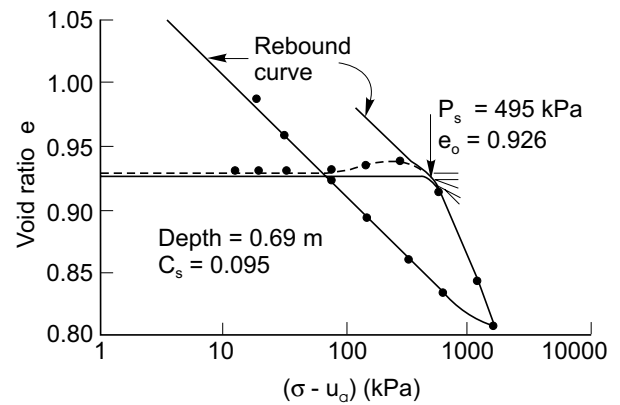
Suitable specimens are trimmed and placed in the oedometer apparatus. A load equivalent to the *in situ* overburden pressure is placed on the specimen and an initial dial gauge reading is taken. The sample is then immersed in distilled water. Additional loads are added to counteract the tendency for the sample to swell. When this tendency ceases, loads are applied using conventional increments to properly define the swelling pressure. The maximum load should be at least two load increments (logarithmic scale) beyond the swelling pressure. The specimen is then unloaded in suitable increments to the token load.

Interpretation of the oedometer data

The data accumulated from the oedometer tests are plotted as void ratio versus logarithm of pressure. It is important to apply corrections for the compressibility of the apparatus (Fredlund 1969). By examining the plot of void ratio versus logarithm of pressure shown in Fig. A1, the corrected swelling pressure can be determined as follows:

- (1) The curve of void ratio versus logarithm of pressure is first corrected for the compressibility of the apparatus. The corrected curve will show a slight upward bulge in the vicinity of the swelling pressure. A corrected void ratio versus pressure curve should be sketched by drawing a line, from the initial void ratio, that is horizontal at first and then curves downward and joins the recompression curve which has been corrected for apparatus compressibility.
- (2) The point of maximum curvature is located at the point where the void ratio versus pressure curve bends downward onto the recompression curve.
- (3) At the point of maximum curvature, a horizontal line and a tangent are drawn. The corrected swelling pres-

Fig. A1. Example problem to illustrate the determination of the corrected swelling pressure.



sure is then found at the intersection of the bisector of the angle formed by these lines and a line tangent to the curve and parallel to the rebound portion of the curve.

Calculation of total heave

For the calculation of total heave, the following equations are used:

$$[A1] \quad \Delta e = -C_s \log \frac{FST}{IST}$$

where:

Δe = change in void ratio,

C_s = swelling index,

FST = final stress state accounting for overburden pressure, surcharge, and final pore-water pressure (kPa), and

IST = initial stress state represented by the corrected swelling pressure (kPa).

$$[A2] \quad \Delta h_i = h_i \frac{\Delta e}{1 + e_0}$$

where:

Δh_i = change in thickness of the i -th layer,

h_i = thickness of the i -th layer, and

e_0 = initial void ratio.

$$[A3] \quad \Delta h = \sum_{i=1}^n \Delta h_i$$

where:

n = number of layers.

To calculate the final water contents, the change in water content, Δw , is computed as:

$$[A4] \quad \Delta w = S_f \Delta e / G_s + e_0 \Delta S / G_s$$

where:

S_f = final assumed degree of saturation,

G_s = specific gravity, and

ΔS = change in degree of saturation.

Example problem

The predicted total heave is calculated in detail using data from the study site presented in this paper.

- (1) The initial void ratio $e_0 = 0.962$.
- (2) The initial water content distribution is shown in Fig. 4.
- (3) The corrected swelling pressure can be represented by a best-fit line (Fig. 13).
- (4) The swelling index used is $C_s = 0.090$.
- (5) The surcharge is 5.76 kPa.
- (6) The analysis will consider eight layers, each 0.3 m thick.
- (7) The specific gravity $G_s = 2.82$.
- (8) The assumed final degree of saturation $S_f = 1.0$.
- (9) The final pore-water pressure distribution assumed is equal to zero.
- (10) The overburden is assumed to have a density of 1.92 kg/m^3 .
- (11) The pore-air pressure $u_a = 0.0 \text{ kPa}$ (i.e., atmospheric).

The results of the calculations are shown in Table 2. For the first layer, the depth to the centre of the layer from the original ground surface is 0.15 m. Therefore,

$$\begin{aligned} \text{FST} &= \text{OB} + \Delta\sigma - u_w \\ &= (0.15)(1.92)(9.81) + 5.76 - 0.0 \\ &= 8.59 \text{ kPa} \end{aligned}$$

From Fig. 12, at a depth of 0.15 m the initial stress state represented by the corrected swelling pressure is 640.8 kPa. Therefore, using [A1],

$$\Delta e = -0.090 \log \frac{8.59}{640.8} = 0.1685$$

and using [A2],

$$\Delta h_i = 0.3 \frac{0.1685}{(1 + 0.962)} 1000 = 26 \text{ mm}$$

To calculate the final water content, the initial water content must be known. In Fig. 4, a depth of 0.15 m below the original ground surface corresponds to a depth of 0.43 m, which accounts for the thickness of slab and fill. The initial water content, w_0 , is 18.8%. The initial degree of saturation, S_0 , is:

$$S_0 = \frac{(0.188)(2.82)}{0.962} 100 = 55.1\%$$

Using [A4],

$$\begin{aligned} \Delta w &= (1.0)(0.1685)/2.82 \\ &\quad + (0.962)(1.0 - 0.551)(2.82)(100) \end{aligned}$$

$$\Delta w = 21.3\%$$

Therefore, the final water content, w_f , is 40.1%.

A small Saskatchewan town copes with swelling clay problems

R.K.H. Ching and D.G. Fredlund

Abstract: This paper presents the problems and solutions associated with construction on an expansive soil deposit in the Eston area of Saskatchewan, Canada. The results of laboratory testing and records of field investigations are presented. The investigation showed the soil to be extremely expansive in nature and that a school building had undergone approximately one meter of heave during its history. This magnitude of heave is reasonable only if the measured swelling pressures are corrected for sampling disturbance.

Key words: expansive soils, swelling, foundation, soil suction, heave design.

Introduction

A large portion of the area in Western Canada is covered by expansive soil deposits. Foundation problems are often encountered as a result of swelling of these soils (Hamilton 1966; Fredlund 1975). The soils are unsaturated due to desiccation and the environment is changed when a structure is constructed on the soil. With time, moisture accumulates in the soil as it tends to approach saturation. As a result, the soil undergoes volume change which causes damage to the structure.

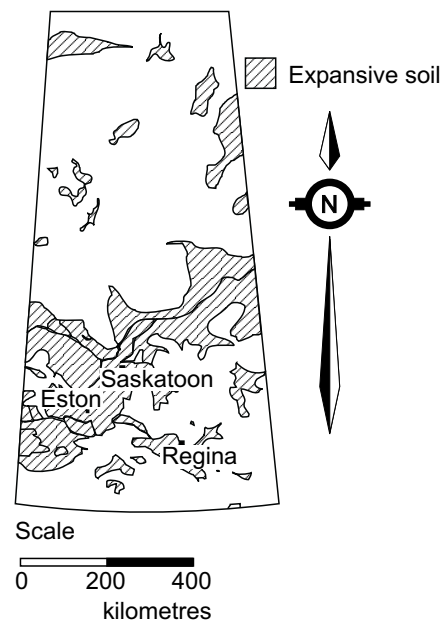
A study was initiated in the 1950's to investigate the problems of the swelling soil in the Eston area of Saskatchewan, Canada. This study also included the monitoring of ground movements in the field and the performance of structural foundations. This paper presents the results of laboratory tests and field measurements at several sites. Special construction techniques have been developed for small structures to accommodate the ground movements. These techniques are described in this paper.

Description of study area and soil material

Eston is situated within the Snipe Lake Plain physiographic region which was a proglacial lake basin (Christiansen 1965) in the south-western part of Saskatchewan. Figure 1 shows the location of Eston and the distribution of expansive soils in Saskatchewan.

The climate in Eston is classified as sub-arid. The monthly precipitation varies widely. The highest precipitation occurs in June and July with an average rainfall of 55 mm. The monthly evapotranspiration over the summer months ranges from 70 mm to 130 mm and usually ex-

Fig. 1. Location of the town of Eston and distribution of expansive soils in Saskatchewan, Canada.



ceeds the monthly precipitation. As a result, a net moisture deficit occurs. The monthly average temperature ranges from -18°C in January to $+18^{\circ}\text{C}$ in July.

The surficial material is a uniform and highly plastic clay known as the Eston clay. The clay is highly overconsolidated due to desiccation. Large shrinkage cracks are present to well below the ground surface. Underlying the lacustrine clay is a layer of calcareous till. A groundwater table is usually not observed during a

R.K.H. Ching. Research Engineer, Department of Civil Engineering, University of Saskatchewan, 57 Campus Drive, Saskatoon, SK, Canada S7N 5A9.

D.G. Fredlund. Professor, Department of Civil Engineering, University of Saskatchewan, 57 Campus Drive, Saskatoon, SK, Canada S7N 5A9.

Reproduced with permission from the *Proceedings, 5th International Conference on Expansive Soils*, Adelaide, South Australia, May 21–23, 1984. pp. 306–310.

subsurface investigation in the general area of Eston. Figure 2 shows a typical soil profile in Eston.

Soil properties and soil suction measurement

Atterberg limits tests, grain size distributions and constant volume oedometer tests were performed to obtain the physical properties of the Eston clay. Filter paper tests were also conducted to give an estimation of the total suction of the soil (McQueen and Miller 1968).

Classification tests

The average liquid limit of the Eston clay is about 94 percent and its average plasticity index is 63 percent. The Eston clay is classified as a highly plastic clay. The natural water content of the soil ranges from 20 to 35 percent, slightly below the plastic limit of the soil. The void ratio of the soil remains consistent at approximately 1.0 throughout the clay soil profile as shown in Fig. 2.

The Eston clay consists of approximately 90 percent clay sizes, 8 percent silt sizes and 2 percent sand sizes. The clay has an activity index of 0.7 which indicates a high swelling potential.

Constant volume oedometer test

One-dimensional oedometer tests were performed to establish the volume change properties of the Eston clay. The swelling index and the swelling pressures were obtained for predicting volume change. Two swelling pressures are defined; the corrected swelling pressure, P_s' , and the uncorrected swelling pressure, P_s (Fredlund et al. 1980). Figure 3 shows the typical results of a constant volume oedometer test performed on an undisturbed sample. Both the corrected and the uncorrected swelling pressures greatly exceed the overburden pressure. The large swelling pressures indicate the highly expansive nature of the soil.

Figure 4 presents a typical swelling index and swelling pressure profile for the Eston clay. Both profiles exhibit a similar pattern of variations. The corrected swelling pressure varies from 500 and 1400 kPa with an average of approximately 950 kPa. The larger variation in the swelling pressures in the upper strata is possible due to surface effects of infiltration, desiccation and cracking.

Soil suction measurements

The soil suction can be used to indicate the swelling potential of a soil because the volume change associated with a soil is related to the change in the soil suction. Numerous techniques have been devised for measuring soil suction. The filter paper technique seems to be a simple means for estimating the suction (McQueen and Miller 1968). Although further refinement is required for this method, the results can be used as an indication of the negative pore-water pressures in the soil. Figure 5 shows the soil suction profiles performed on the Eston clay samples, using the filter paper technique. Soil suction values generally range from 2000 to 6000 kPa. A comparison

Fig. 2. Soil properties of Eston clay.

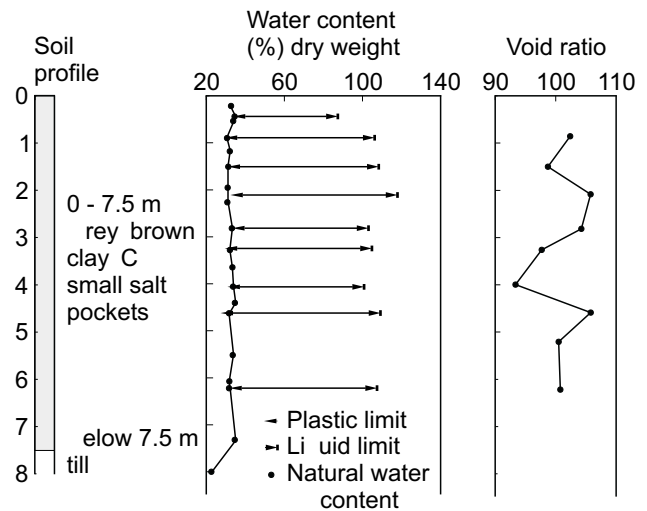


Fig. 3. Typical consolidation results for Eston clay.

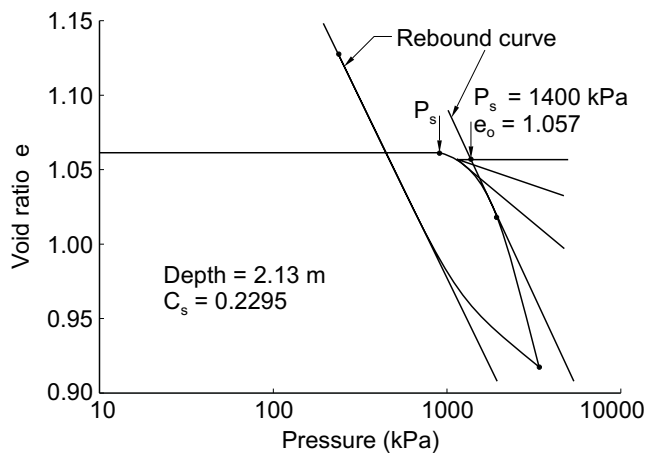


Fig. 4. Profile and swelling properties for Eston clay.

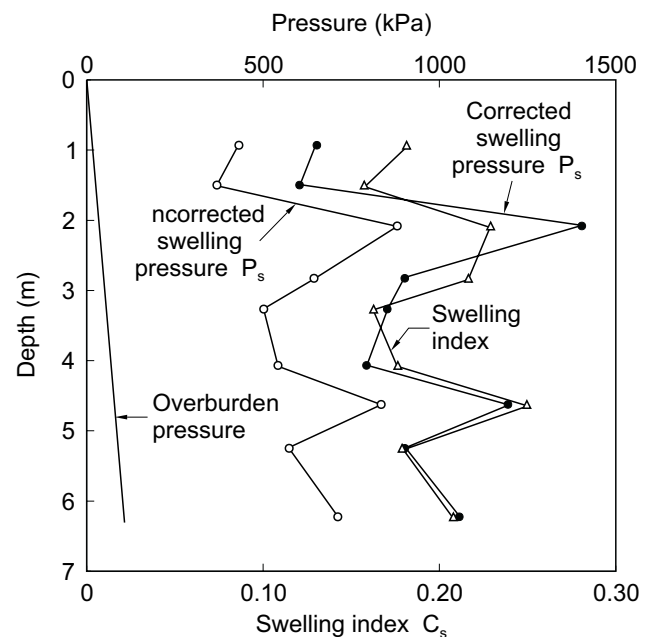
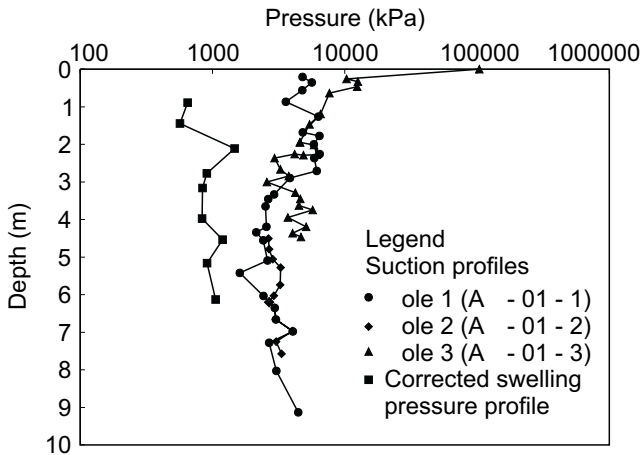


Fig. 5. Soil suction profile for Eston clay.



given in Fig. 5 shows that there is a correlation between the corrected swelling pressures and the soil suctions. The soil suctions are higher than the swelling pressures as would be expected. However, the accuracy of the measured suctions is not known.

Results of the laboratory tests for the Eston clay are summarized in Table 1.

Record of swelling soil problems at Eston

A study program was initiated in the 1950's to investigate the problems associated with the swelling soil in the Eston area. Studies included the monitoring of ground movements in an undisturbed field plot and the performance of foundations on the expansive Eston clay. The results of these studies are presented to provide some quantitative measures for the swelling soil problems that have been encountered in this region.

The open field test plot was used to collect field data relating ground movements to climatic factors (Hamilton 1963). Instrumentation consisted of a deep bench mark, a neutron moisture meter access tube, a rain gauge and vertical ground movement gauges. These were installed as illustrated in Fig. 6. Six movement gauges were embedded at different depths below the ground surface. Ground movements were obtained from levelling surveys on the movement gauges with reference to the deep bench mark. The neutron moisture meter did not perform satisfactorily. Instead, the soil-moisture conditions were obtained by gravimetric determination of soil samples. Precipitation was recorded by the storage rain gauge.

Ground movements obtained from three of the movement gauges as well as the rainfall records during the period of June, 1961 to April, 1970 are given in Fig. 7. Maximum ground movements were found to occur during the wet season from March to September. Settlements usually occurred following a long dry period. This pattern of ground movements agreed closely with the precipitation record obtained from the storage rain gauge. The maximum movement recorded is approximately 80 mm.

Table 1. Summary of test results for Eston clay.

Test	Results
Atterberg limits	
Liquid limit	94%
Plastic limit	31%
Plasticity index	63%
Grain size distribution	
Sand sizes	2%
Silt sizes	8%
Clay sizes	90%
Constant volume oedometer test	
Swelling index	0.19
Corrected swelling pressures	500 – 1400 kPa
Matric suction measurement using filter paper	2000 – 6000 kPa

Fig. 6. Instrumentation in Eston test plot.

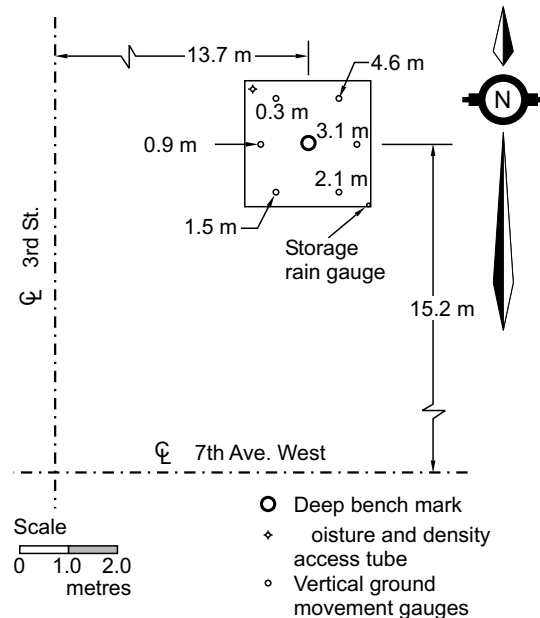
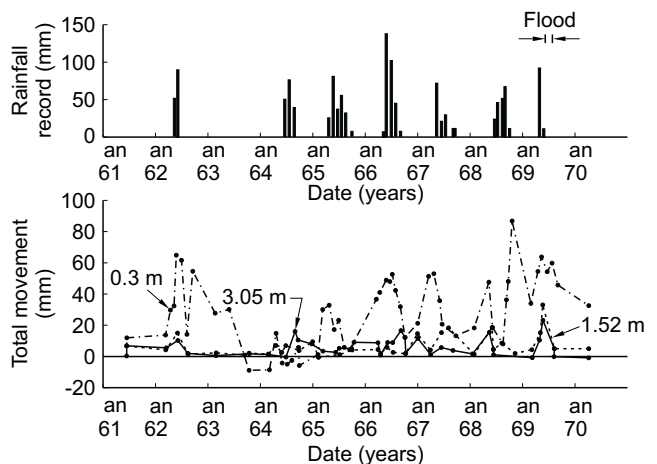


Fig. 7. Ground movements in Eston test plot.



Comparatively large movements varying from 10 to 30 mm were found to take place at a depth of 3 metres. This signifies that the available moisture is effective in penetrating down to a considerable depth. The records of soil moisture contents agreed well with this observation. After a rainfall, the soil moisture contents in the upper 3 metres were usually increased by 5 to 25 percent. This finding is of particular interest because the zone of influence exceeds the common depth used for shallow foundations. Any foundation located within this depth is vulnerable to the effect of soil movements.

The results from the test plot indicate that ground movement problems can occur even under undisturbed conditions. The problem is expected to be greatly aggravated if a change in the soil environment is introduced by the construction of a structure. As a result, moisture will gradually accumulate in the subsoil and cause a reduction in the soil suction and an increase in the soil volume.

The excessive ground displacements associated with a change in the soil environment can be illustrated by the record of the foundation performance of the old Eston school building. This structure was monitored as part of the study program. The basement floor of this building continued to heave since the completion of construction. Figure 8 shows the basement floor heave when the initial measurements were made in August, 1960. Although the maximum differential movement was only about 150 mm, a much larger total heave of approximately 600 to 800 mm had already taken place before the commencement of the monitoring program (Hamilton 1966). The maintenance records indicate that the deformation was severe. As a result, the concrete floor slab had to be removed and approximately 300 mm of the subsoil had to be excavated. The soil was then levelled to allow the reconstruction of the floor slab. This upgrading operation was executed twice before the building was finally demolished in 1969.

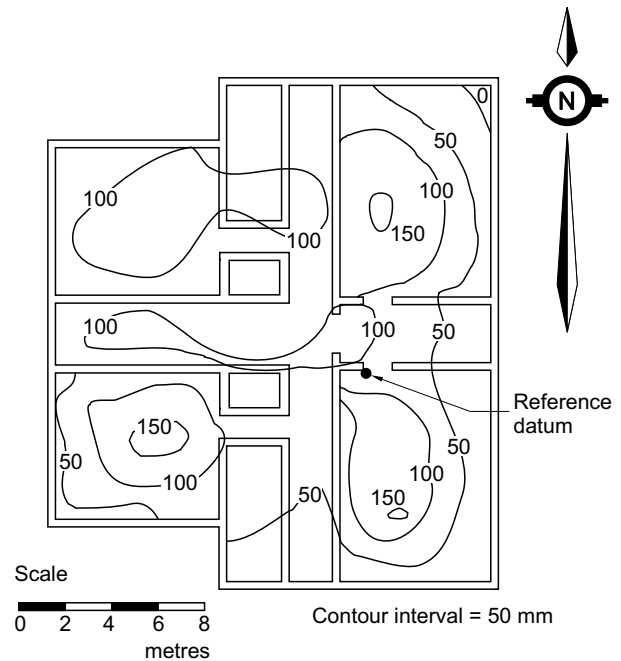
Using the prediction method for heave proposed by Fredlund et al. (1980) and the results from the constant volume oedometer tests, a total heave of 780 mm can be computed. Detailed calculation procedures are outlined by Yoshida et al. (1983). The computed total heave agrees well with the actual heave that had taken place at the structure.

The data collected from the monitoring of this structure indicated the severe ground movements that can be caused by environmental changes. Ground movements of such large magnitude can inflict serious damages to structures and are difficult to take into account in the design.

Special construction techniques used in Eston

Special construction techniques for small structures have been developed by residents of the area to accommodate the problem of swelling soils. These methods have been derived largely on the basis of experience. Both deep foundation and shallow foundation are used. The type of foundation selected is usually based on the

Fig. 8. Floor heave in the old Eston school building.



loading requirements and the importance of the structure. The unit costs of the two foundation types are approximately the same.

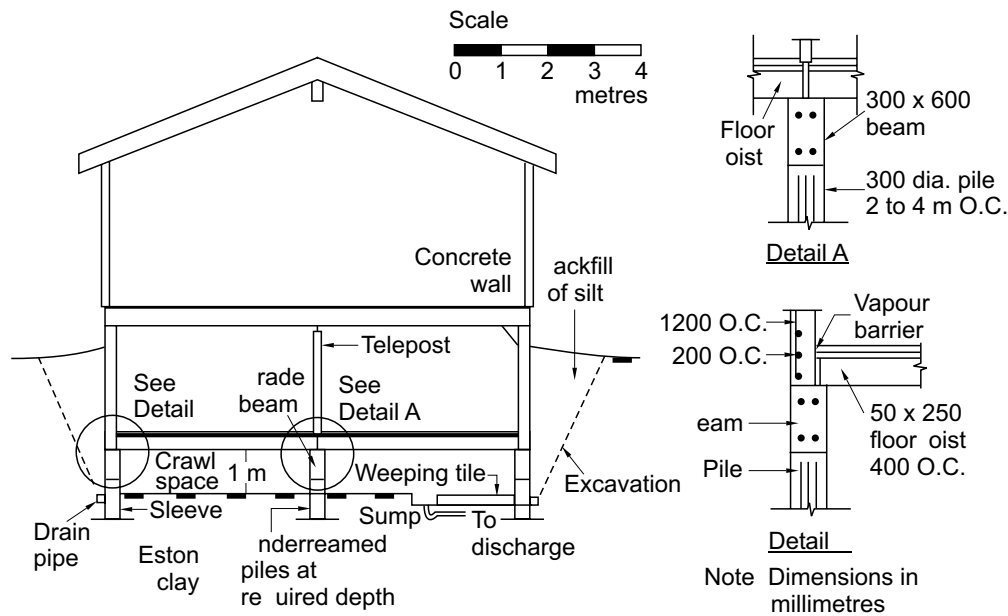
Numerous other foundation treatments have been tried with poor success. For example, tin cans, tires and straw bales placed beneath the concrete slabs have not proven effective in eliminating the heave problem.

Deep foundation

Deep foundations are generally used for more heavily loaded structures where unsightly structural damages are of major concern to the public. Cast-in-place augered piles with diameters of 250 mm or larger are commonly founded on the underlying till layer. The upper portion of the pile is encased with a sleeve to avoid the development of skin friction which may be reversed due to soil expansion. Piles are reinforced with several vertical bars of 12 to 25 mm diameter to resist the tensile forces produced in an uplift action. The lower portion of the pile is generally bell-shaped. Structural concrete beams are constructed spanning across adjacent piles. Styrofoam boards are utilized to fill the gap beneath the perimeter structural beams. These boards may be crushed as the swelling pressure of the soil develops.

Structural walls are built with concrete heavily reinforced in both horizontal and vertical directions to resist the tensile forces caused by differential movements. Wooden floor joists are simply supported on structural beams and a wooden floor is laid on these floor joists. Typically, the floor unit is not rigidly affixed to the load carrying members. In this manner, the entire structure is flexible and can tolerate large distortions without detrimental results.

Fig. 9. Structure with a deep foundation.



A building can be constructed with or without a basement. In the latter case, an unusually large crawl space of approximately 1 metre is provided beneath the lower floor to allow room for the anticipated soil expansion. If a basement is needed, the basement walls must be reinforced to provide resistance against the lateral swelling pressures. Typical horizontal and vertical reinforcement spacings are 200 mm and 1200 mm, respectively. Heated air outlets have been sometimes installed in the crawl space. Hot dry air can be periodically circulated in order to maintain a consistent environment for the foundation soil. A weeping tile system is constructed around the building at the lower floor level for collecting large volumes of water that may infiltrate through the soil. The water is drained into a sump in the crawl space where it is discharged into the public storm sewers. The excavation is backfilled with a non-swelling silt, which is locally referred to as "river clay," borrowed from the nearby region. The compacted backfill is less permeable compared to the fissured clay and is more effective in reducing the infiltration of water. Figure 9 illustrates a typical structure supported on piles.

Shallow foundation

For lightly loaded structures, a shallow foundation is preferred. The basic foundation unit is a continuous strip footing of approximately 0.5 metres wide by 0.2 metres high. The footing is heavily reinforced to increase its flexural strength in resisting the detrimental effect of differential movements. A wooden form is then constructed on the spread footing for the perimeter structural wall. Slots are cut into the wooden form approximately 1 metre above the footing level. Joists are inserted into these slots. Concrete is cast *in situ* to form the structural walls. A wood floor is placed on top of the structural floor joists. Using this procedure, the floor and walls form a

single, integral unit. The wall unit is locally called a "stub wall." The stub wall may require two form works and concrete pours to attain the desired height for the foundation wall. Figure 10 shows a typical structure using this construction technique.

A variation in the shallow foundation construction technique shown in Fig. 11 has also been used. The basic foundation unit is also a continuous strip footing of 0.5 metres wide by 0.2 metres high. In addition, another strip footing of smaller dimensions (i.e., 0.4 metres wide by 0.2 metres high) is constructed on top of the larger strip footing. The wood floor unit used in this construction is laid on the bottom spread footing instead of bonding it to the structural walls.

In both shallow foundation types, a crawl space of 1 metre is provided beneath the lower floor to allow room for possible soil heave. The underground drainage system and backfilling operation are essentially the same as those for the deep foundation described previously.

Observations of performance of different types of foundations

Performance records for the Eston school building are cited to show the effectiveness of deep foundations to overcome the swelling clay problem. The Eston school was erected in 1954-55. Its construction made use of deep foundations along with a crawl space, as described in the previous sections. Attention was given to the design and construction of this building in an attempt to reduce the detrimental effect resulting from the anticipated soil movements. The boiler room was built on a mat foundation to support heavy boiler machinery and vibrations induced by the boiler operation.

The deep foundations with the one-metre crawl space performed satisfactorily and no structural movement oc-

Fig. 10. Structure with stub wall construction.

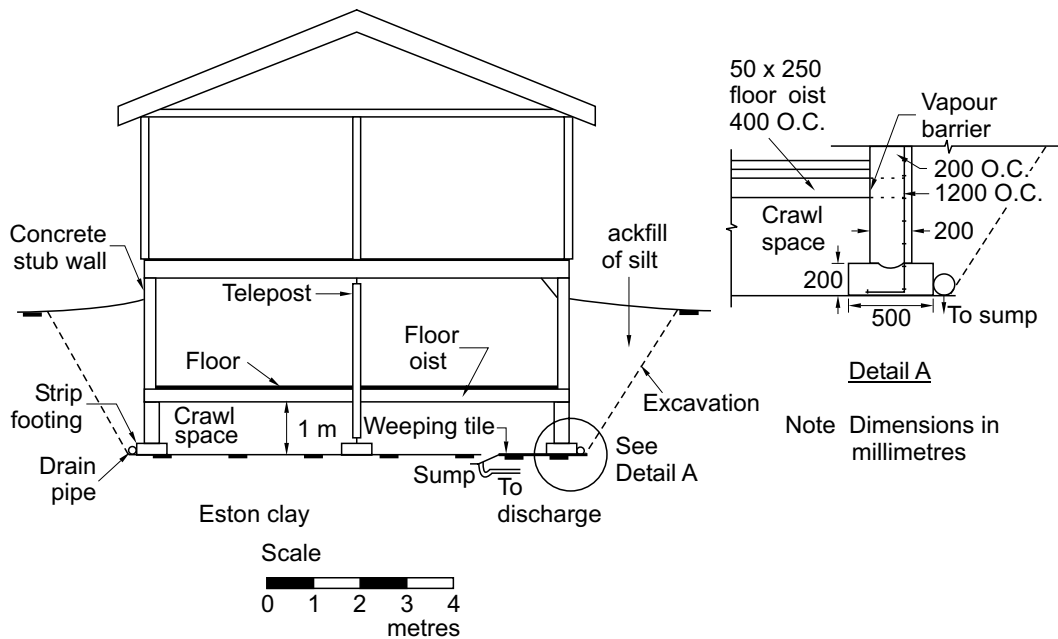
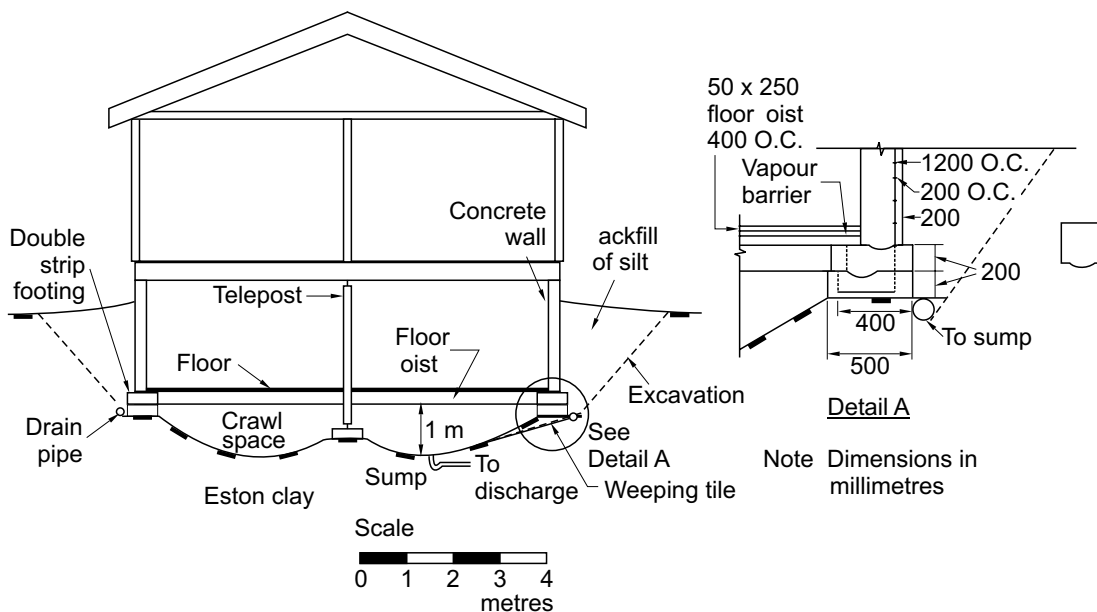


Fig. 11. Structure with double strip footings.

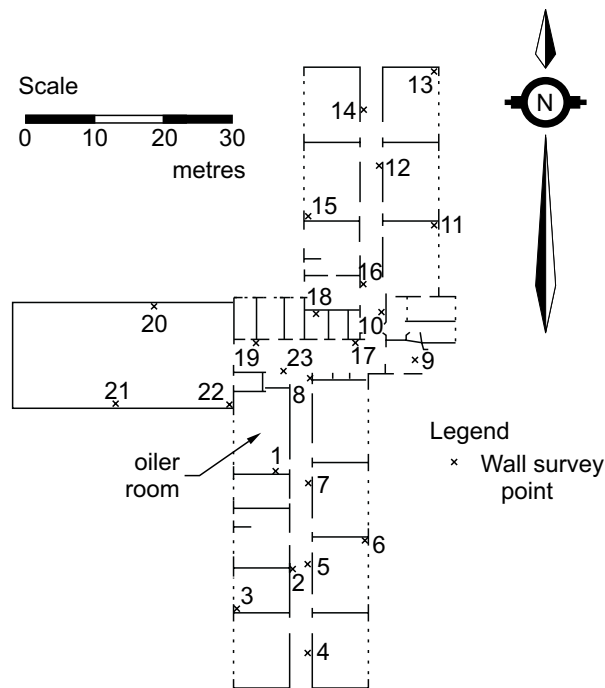


curred on the main floor. However, the structural floor slab in the boiler room was observed to heave continuously after construction. The movements were monitored by means of levelling surveys. Survey points were installed on the walls in the main building and on the floor in the boiler room. Figure 12 shows the locations of the wall survey points. Large differential movements took place in the floor slab of the boiler room. Slab movements amounting to 75 mm were measured in the middle of the floor. The structural grade beams around the perimeter of the boiler room restrained the floor movements

along the edges of the room. As a result, the floor slab bulged upward toward the middle of the room.

As a result of the heaving of the boiler room floor the structures neighbouring the boiler room tilted. Some structural members were badly damaged and continuous repairs were required. Figure 13 illustrates the movements observed from several of the survey points. Structural movements in excess of 50 mm occurred in the main floor area adjacent to the boiler room. Only slight movement was observed in the main floor area which was further away from the boiler room.

Fig. 12. Survey points in Eston public school.



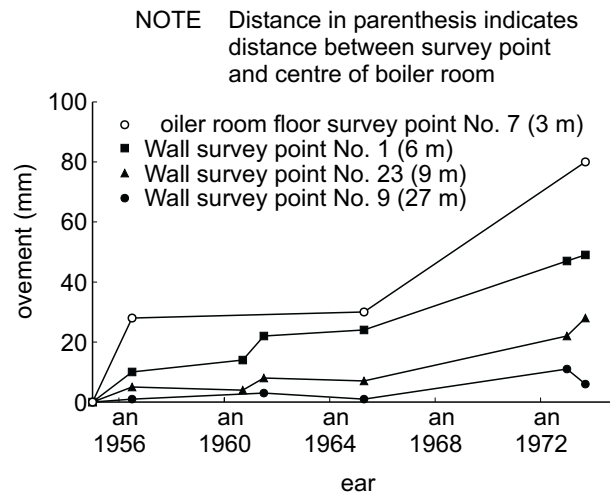
The record for the Eston school building provides a history typical of the performance of the deep foundations in the Eston area. The deep foundations minimize the effect of environmental changes in the swelling subsoil since the structural loads are transferred down to the underlying till layer. The provision of the crawl space appears to be effective in reducing the amount of soil movement.

Discussion

The expansive Eston clay is highly desiccated. A change in the soil moisture conditions can cause substantial volume change to occur. From the investigations in the open field test plot, it is evident that substantial ground movements can occur even under the natural cycles of drying and wetting. The ground movement problem is greatly magnified due to the construction of a structure. This is verified by monitoring of floor movements in the old school building in Eston. In this case, an estimated heave in the range of 600 to 800 mm had occurred during its service life.

Foundations in direct contact with the swelling soil generally suffer excessive structural damages due to soil movements. When designing structures in the Eston area, the potential of large volume change of the clay must be taken into consideration. Special construction techniques have been developed for small structures. Both deep and shallow foundations are used in these designs. The key elements involve a large crawl space beneath the floor and flexible connections between structural members. The crawl space is used to isolate the superstructure from the expansive soil. The building can tolerate some differential movements to occur without harmful conse-

Fig. 13. Wall movements due to boiler room floor heave.



quences. A relatively less permeable silt backfill has been used to reduce excessive seepage into the cracked subsoil. Adequate subsurface drainage around the outside perimeter of the foundation is provided to divert seepage water from the subsoils. These measures are essential in minimizing the magnitude of the soil movements.

Acknowledgements

The financial support for the research works provided by the Supply and Services, Government of Canada, is gratefully acknowledged. The authors would like to acknowledge the staff members of the Division of Building Research, National Research Council, Saskatoon, for their involvement in the collection of field data. Special thanks are extended to R.T. Yoshida for his involvement in the field investigation.

References

- Christiansen, E.A. 1965. Geology and groundwater resources at the Kindersley area (72-N) Saskatchewan. Report No. 7, Geology Division, Saskatchewan Research Council, Saskatoon.
- Fredlund, D.G. 1975. Engineering properties of expansive clay. Proceedings, Seminar on Shallow Foundations on Expansive Soils: Design, Construction and Performance. Regina, SK, Oct. 27-28, pp. 3-64.
- Fredlund, D.G., Hasan, J.U., and Filson, H.L. 1980. The prediction of total heave. Proceedings, 4th International Conference on Expansive Soils, Denver, CO, Vol. 1, pp. 1-17.
- Hamilton, J.J. 1963. Volume change in undisturbed clay profiles in Western Canada. Canadian Geotechnical Journal, 1: 27-42.
- Hamilton, J.J. 1966. Swelling and shrinking subsoils. Canadian Building Digest, Ottawa. Report No. 84.
- McQueen, I.S., and Miller, R.F. 1968. Calibration and evaluation of a wide range method for measuring moisture stress in field soil samples. Soil Science, 106(3): 225-231.
- Yoshida, R.T., Fredlund, D.G., and Hamilton, J.J. 1983. The prediction of total heave on a slab-on-grade floor on Regina clay. Canadian Geotechnical Journal, 20(1): 69-81.

Numerical modelling of vertical ground movements in expansive soils

P.J. Sattler and D.G. Fredlund

Abstract: A numerical model was developed to relate matric suction changes and vertical ground movements. The research considers one-dimensional vertical ground movements under open-vegetated fields subject to changing climatic conditions. A percentage of the Thornthwaite potential evapotranspiration model proved to be adequate to characterize the surface flux boundary condition. The infiltration and exfiltration processes were modelled separately for the field conditions. During infiltration, shrinkage cracks and the macrostructure of the soils dominate behavior. During this process, bulk permeabilities in the order of 10^{-6} – 10^{-8} m/s were required to simulate measured ground movements. Exfiltration processes are dominated by flow in the vapour phase as drying occurs in the soil. Bulk permeabilities in the order of 10^{-9} – 10^{-11} m/s were required to simulate the measured ground movement. The simulations of ground movements would also indicate that thermally induced suctions (i.e., winter freezing conditions) could account for a significant portion of the seasonal vertical ground movements. The numerical model can also be used to predict seasonal ground movements beneath light engineered structures. Further research; however, is required to better understand how to establish the surface flux boundary condition. As well, there is need for more case histories to enlarge the database of unsaturated soil parameters.

Key words: vertical ground movement, matric suction, modelling, evapotranspiration, field permeabilities.

Introduction

The development of a numerical model to quantify the relationship between meteorological information and vertical ground movements (i.e., heave and shrinkage) has only recently become possible as a result of advances in our understanding of unsaturated soil behavior. A simple numerical model has been developed to illustrate how increases in matric suction result in shrinkage and decreases in matric suction result in swelling. The present research focuses on the one-dimensional simulation of vertical ground movements under open-vegetated fields subject to changing climatic conditions. The long-term objective of the study is to be able to predict the vertical movement of light engineered structures such as building foundations and highway pavements (Fig. 1).

Background

Geotechnical engineers throughout the world are familiar with the challenges posed by expansive soils. Vertical ground movements associated with expansive soil deposits cause more damage to light engineered structures than

all other natural disasters combined (Jones and Holtz 1973). Documented case histories and a better comprehension of unsaturated soils behavior have contributed significantly to our understanding of expansive soils.

During the late 1950's and 1960's, the Division of Building Research of the National Research Council of Canada in Saskatoon, Saskatchewan, conducted a long-term study involving vertical ground movements in open fields and the performance of building foundations on expansive soils. Vertical ground movement gauges were installed at four open-field locations in Manitoba and Saskatchewan; namely, the Elmwood district of Winnipeg, Manitoba; and Regina, Tisdale, and Eston, Saskatchewan (Hamilton 1963) (Fig. 2). The ground movements were measured using precise survey equipment and deep benchmarks. Measurements of vertical ground movement were taken on approximately a monthly basis for a period of several years at each location. Water content changes were also measured periodically over the span of several years (Hamilton 1963).¹

The recorded measurements for each location are presented in Figs. 3 to 6. Figure 3 illustrates that between 1960 and 1968, the maximum change in ground elevation

P.J. Sattler. Graduate Student, Department of Civil Engineering, University of Saskatchewan, 57 Campus Drive, Saskatoon, SK, Canada S7N 5A9.

D.G. Fredlund. Professor, Department of Civil Engineering, University of Saskatchewan, 57 Campus Drive, Saskatoon, SK, Canada S7N 5A9.

Reproduced with permission from the *Canadian Geotechnical Journal*, **28**: 189–199, 1991.

Fig. 1. Objective of the research: to predict vertical ground movements with time.

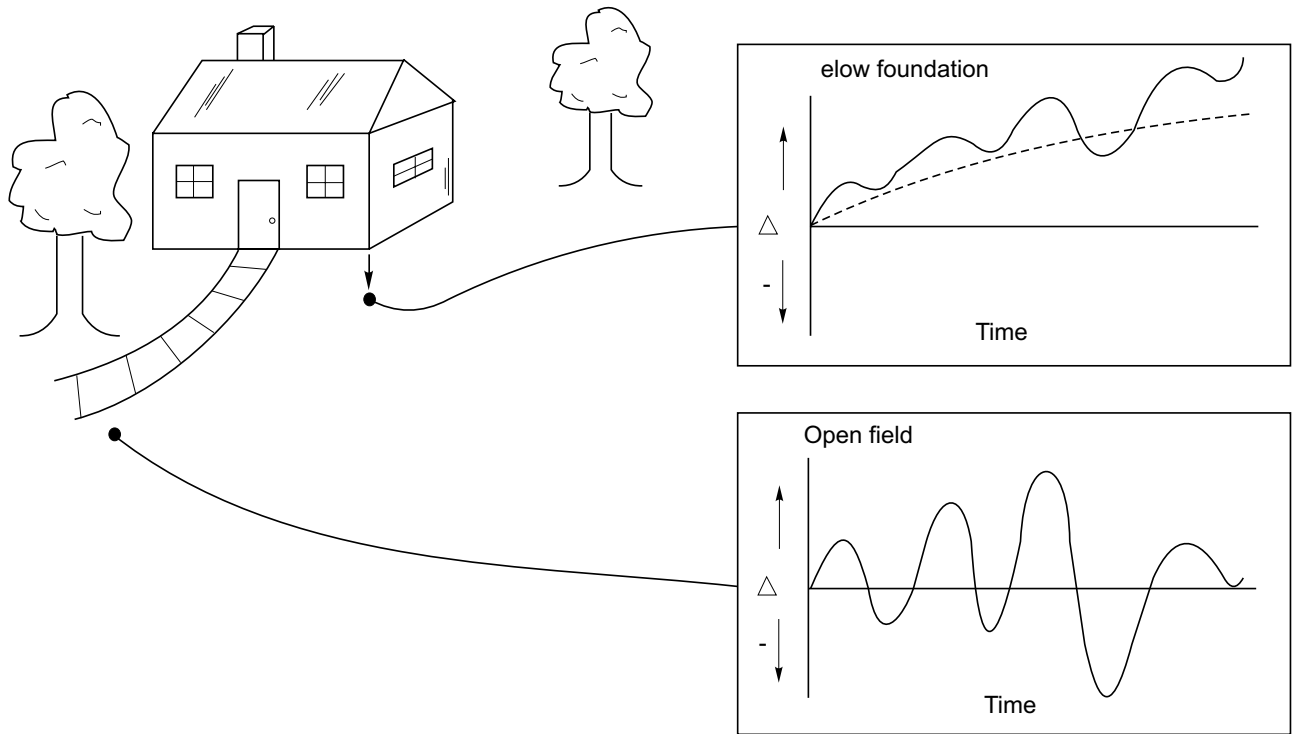
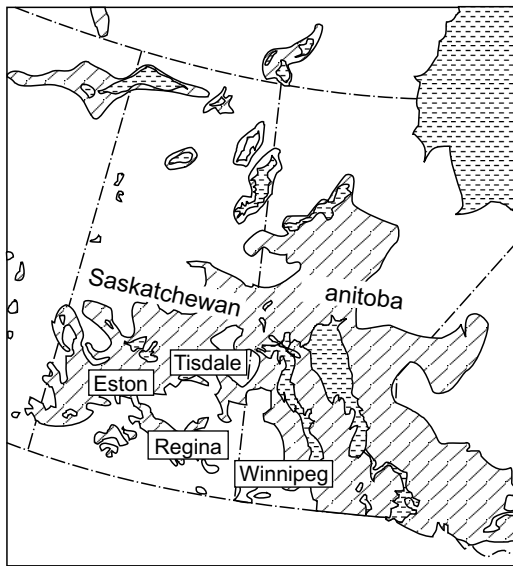


Fig. 2. Glacial lake deposits and associated expansive soil deposits (Hamilton 1965).



for the open-field test plot at Regina, Saskatchewan, was in the order of 50 mm at a depth of 0.3 m. Measured vertical ground movements for the open-field test plot at Tisdale, Saskatchewan, were characteristically less severe than at Regina (Fig. 4), whereas measured vertical ground movements for Eston, Saskatchewan, were more severe than at Regina (Fig. 5). The maximum vertical rise in ground elevation for Eston was recorded as 63 mm at a depth of 0.3 m in 1962. Measurements recorded for Win-

nipeg, Manitoba, include 3 years of surface measurements. The maximum recorded vertical ground movement for Winnipeg was about 75 mm at the ground surface in 1963 (Fig. 6).

Hamilton (1965) summarized the results of the research and illustrated a relationship between meteorological observations and vertical ground movements. Data records indicated that building slabs showed a gradual heave over long periods of time, whereas open-field test plots exhibited more of an upward and downward movement (Hamilton 1968).

It was observed that increases in the water content of the soil were associated with upward ground movements. During wet periods, both the open field and the building slab exhibited upward movement. During dry periods in which the demands of the vegetation become predominant, concrete-slab elevations remained essentially constant, whereas the open-field gauges indicated a downward movement.

The amplitudes of measured vertical ground movements were in the order of 75 mm near the ground surface. Under severe drought, movements were recorded to depths exceeding 2.5 m. Both vertical and horizontal shrinkage were observed in winter. Hamilton (1963) concluded that the magnitude of vertical movement “increases during periods of extremes in weather conditions and wanes during periods of more or less average weather conditions.”

The ground-movement measurements have proven to be a valuable record of the magnitude of shrinking and swelling which can be anticipated on the prairies. Some of the data has been used to illustrate correlations with

Fig. 3. Measured vertical ground movements for an open-field test plot at Regina, Saskatchewan (Hamilton 1968).

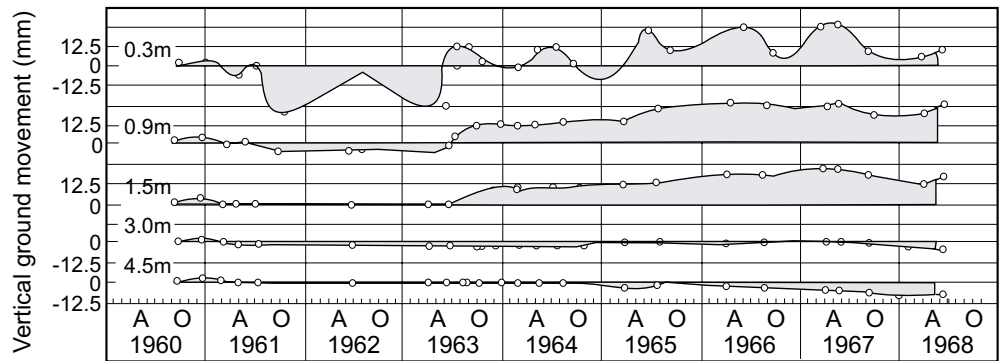


Fig. 4. Measured vertical ground movements for an open-field test plot at Tisdale, Saskatchewan (Hamilton 1968).

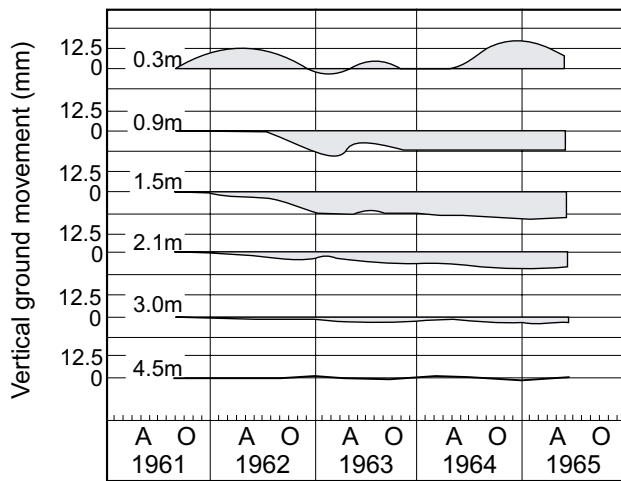
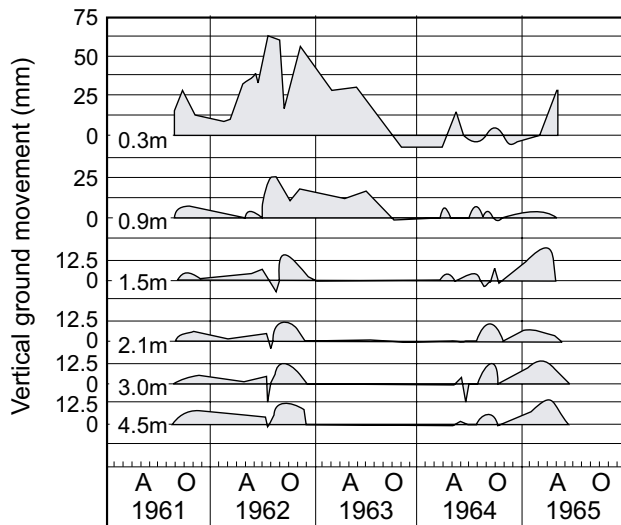
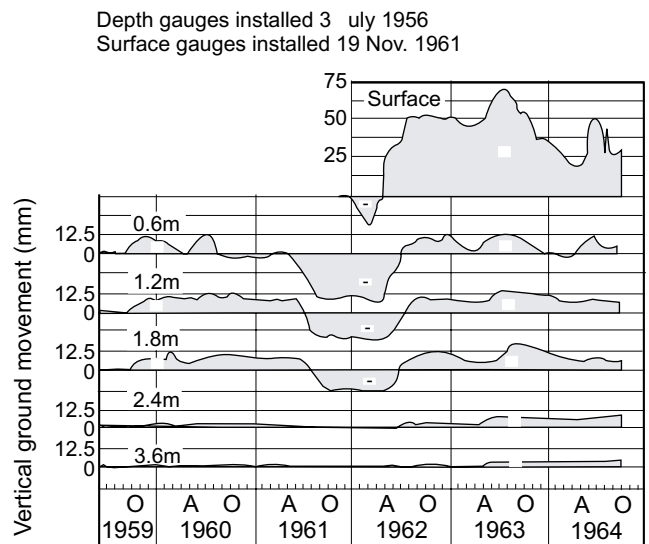


Fig. 5. Measured vertical ground movements for an open-field test plot at Eston, Saskatchewan (Hamilton 1968).



climatic conditions. Hamilton (1966) performed soil moisture depletion calculations for the Winnipeg study site based on Thornthwaite's evapotranspiration model (1948) and precipitation data for Winnipeg. A definite

Fig. 6. Measured vertical ground movements for an open-field test plot at Winnipeg, Manitoba (Hamilton 1968).



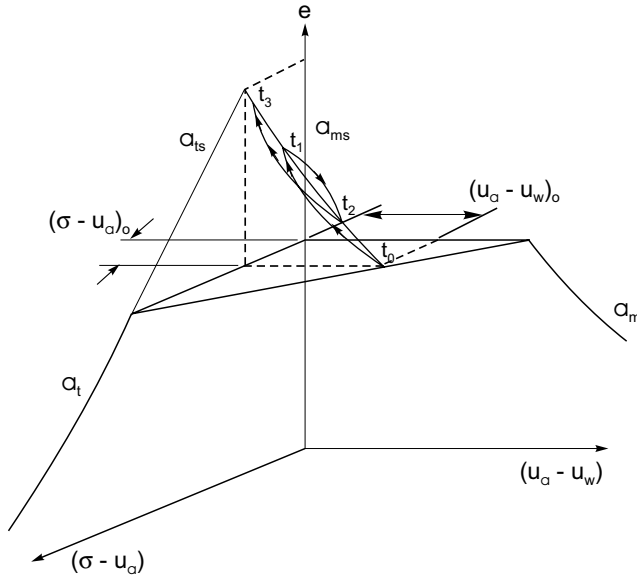
correlation was shown between climatic conditions and vertical ground movements.

Physical relationships required for a ground-movement model

The derivation of an equation to describe vertical ground movements in expansive soils is based on unsaturated soil mechanics theories (Fredlund 1979). Two independent stress state variables are used to describe the engineering behavior of the soil mass; namely, (1) net normal stress ($\sigma - u_a$) and (2) matric suction ($u_a - u_w$) (Fredlund and Morgenstern 1977). Matric suction is the negative pore-water pressure referenced to the air pressure. Changes in the negative pore-water pressure occur as a result of changes in the climate and can be related to changes in soil volume through the use of constitutive relations.

The form of the constitutive equation linking the stress state variables to soil volume change is illustrated in Fig. 7. Swelling in the field occurs along the rebound curve (i.e., with slope a_{ms}), at an overburden pressure

Fig. 7. Schematic diagram of the constitutive relationship for void ratio in terms of matric suction and net normal stress.



(i.e., $(\sigma - u_a)_0$) and an *in situ* matric suction (i.e., $(u_a - u_w)_0$). Shrinkage occurs along either a recompression branch or the virgin compression branch. The arithmetic form of the constitutive equation for the virgin branch can be written as follows:

$$[1] \quad de = a_t d(\sigma - u_a) + a_m d(u_a - u_w)$$

where:

- de = change in void ratio,
- a_t = coefficient of compressibility with respect to a change in $(\sigma - u_a)$, and
- a_m = coefficient of compressibility with respect to a change in $(u_a - u_w)$.

The form of the constitutive equation for the rebound curve is similar to eq. [1] except that the moduli are from the rebound branch (i.e., a_{ms} and a_{ts}). One-dimensional volume change (i.e., vertical ground movement) for a soil mass of n layers is equal to the sum of the volume changes in individual layers of thickness, H_{i0} , for each of the n layers. The change in layer thickness for each layer is computed from the following expression:

$$[2] \quad \Delta H_i = H_{i0} \frac{\Delta e_i}{1 + e_{i0}}$$

where:

- i = number of the soil layer, with soil layers ranging from 1 to n , the total number of layers,
- ΔH_i = change in thickness of an individual layer,
- H_{i0} = initial layer thickness,
- Δe_i = change in void ratio for the layer, and
- e_{i0} = initial void ratio for the layer.

The change in void ratio for each layer is computed from eq. [1].

The sum of the changes in layer thickness (i.e., vertical ground movement) is written as:

$$[3] \quad \Delta H = \sum \Delta H_i$$

Changes in matric suction occur throughout the soil mass as water flows from a greater to a lower hydraulic head. The classic seepage equation for a saturated soil can be extended to describe the flow of water in an unsaturated soil. As a first approximation, the transient flow equation can be written as:

$$[4] \quad \frac{\partial h}{\partial t} = \frac{k_y}{\rho_w g m_2^w} \frac{\partial^2 h}{\partial y^2}$$

where:

- h = total hydraulic head,
- $\frac{\partial h}{\partial t}$ = derivative of total hydraulic head with respect to time,
- k_y = coefficient of permeability of the soil in the vertical direction,
- ρ_w = density of water,
- g = acceleration due to gravity,
- m_2^w = coefficient of water volume change, which is equal to $a_{ms} / (1 + e_{i0})$ on the rebound branch, and
- $\frac{\partial^2 h}{\partial y^2}$ = second derivative of total hydraulic head with respect to depth above the datum.

The coefficient of permeability, k_y , for an unsaturated soil is a function of matric suction, which in turn is a function of hydraulic head. A more rigorous formulation of the unsaturated-seepage equation was presented by Lam and Fredlund (1984). However, for the purposes of developing a first-approximation model, the linear form of the seepage equation (i.e., eq. [4] above) is proposed.

The total hydraulic head in an unsaturated soil is written the same as for a saturated soil:

$$[5] \quad h = \frac{u_w}{\rho_w g} + y$$

where:

- y = elevation head above the chosen datum.

Conventionally, the air pressure, u_a , is assumed to be equal to zero. Therefore, the matric suction stress state variable (i.e., $u_a - u_w$) is equal in magnitude and opposite in sign to the pore-water pressure (i.e., u_w).

The volume-change moduli, a_{ms} and m_2^w can be estimated from experimental data. To a large extent, estimates of the volume-change moduli were used for the four field-site locations. The volume-change modulus, a_{ms} , was estimated from a knowledge of the swelling index data (i.e., C_s) and the shrinkage limit of the soil. Modulus values were in the order of 1×10^{-2} to 1×10^{-5} per kPa. Further details regarding the estimation of the soil parameters and initial conditions are described in Sattler (1989).

Initial boundary conditions

Initial conditions required for the model include the negative pore-water pressure, the void ratio, the water content, and the degree of saturation. Profiles of initial negative pore-water pressure were estimated from typical swelling pressure profiles (Yoshida et al. 1983) and field soil suction data for prairie locations (van der Raadt 1988). Profiles of the initial void ratio, water content, and degree of saturation with depth were established from summaries of statistical properties (Fredlund and Hasan 1979) and measured water contents for the study locations (Hamilton 1968).

For the numerical modelling, the lower boundary below which volume changes are negligible was set at 7.5 m, in accordance with observations by Hamilton (1965). The surface boundary was subjected to a transient flux computed from precipitation and evapotranspiration data.

Surface flux boundary condition

The flow of water across the surface boundary was assumed to conform to Darcy's law:

$$[6] \quad q = k_y \frac{\Delta h}{\Delta y}$$

where:

- q = rate of water flow or surface boundary flux in units of distance per time,
- k_y = coefficient of permeability in the vertical direction at ground surface,
- Δh = change in total hydraulic gradient across the surface layer, and
- Δy = distance across the surface layer.

The surface boundary flux is computed from the difference between the infiltration and exfiltration processes at the surface. For the flat prairie locations under study, runoff was assumed to be negligible. Therefore, infiltration was equal to precipitation. Exfiltration was computed from estimates for actual evapotranspiration (i.e., the sum of evaporation from the soil and transpiration by plants).

The Thornthwaite model was used to estimate the potential evapotranspiration based upon simple calculations using temperature and day length (Thornthwaite 1948):

$$[7] \quad \text{PET} = 1.6F \left[\frac{10t}{I} \right]^a$$

where:

- PET = monthly potential evapotranspiration (cm),
- F = sunlight duration correction factor based upon Thornthwaite and Mather (1957),
- t = mean monthly temperature ($^{\circ}\text{C}$), and
- I = sum of the 12 monthly heat indices, j , with $j = (t/5)^{1.515}$ and
- a = constant dependent on the heat indices, which varies from 0 to 4.25; with

$$a = 6.75\text{E-}07 I^3 - 7.71\text{E-}05 I^2 + 1.792\text{E-}02 I + 0.49239.$$

Potential evapotranspiration is defined as the moisture loss from a surface completely covered with vegetation when there is an unlimited supply of water available for plant use (Thornthwaite and Mather 1955). Potential evapotranspiration can be considered as an upper limit on actual evapotranspiration, since actual evapotranspiration is dependent upon the available soil moisture. Actual evapotranspiration can be estimated from computations of potential evapotranspiration and empirical correlations between actual and potential values for evapotranspiration (Granger and Gray 1989).

The actual evapotranspiration was estimated as a percentage of potential evapotranspiration based upon concurring results from several analyses, including (1) the use of net groundwater recharge observations for Saskatchewan, (2) the use of historic temperature and precipitation data, and (3) the use of long-term mean values for precipitation and temperature (Sattler 1989). Results of the analyses indicated that a ratio of 0.70 between actual and potential evapotranspiration was reasonable for the four prairie locations that were studied. In hydrology, a value of 0.70 is also used to represent the ratio of the classic pan evaporation as a percentage of actual lake evaporation (Gray and Male 1980). Just as actual evapotranspiration is less than potential evapotranspiration because of limited available water in the soil, likewise, pan evaporation is less than lake evaporation because of natural limitations on the pan measuring ability.

Numerical solution

The marching forward finite-difference numerical technique was used to solve the transient flow equation (i.e., [4]) in terms of hydraulic head, subject to the boundary conditions:

$$[8] \quad \frac{h_1 - h_0}{\Delta t} = \frac{k_y}{\rho_w g m_2^w} \frac{h_2 - 2h_0 + h_3}{(\Delta y)^2}$$

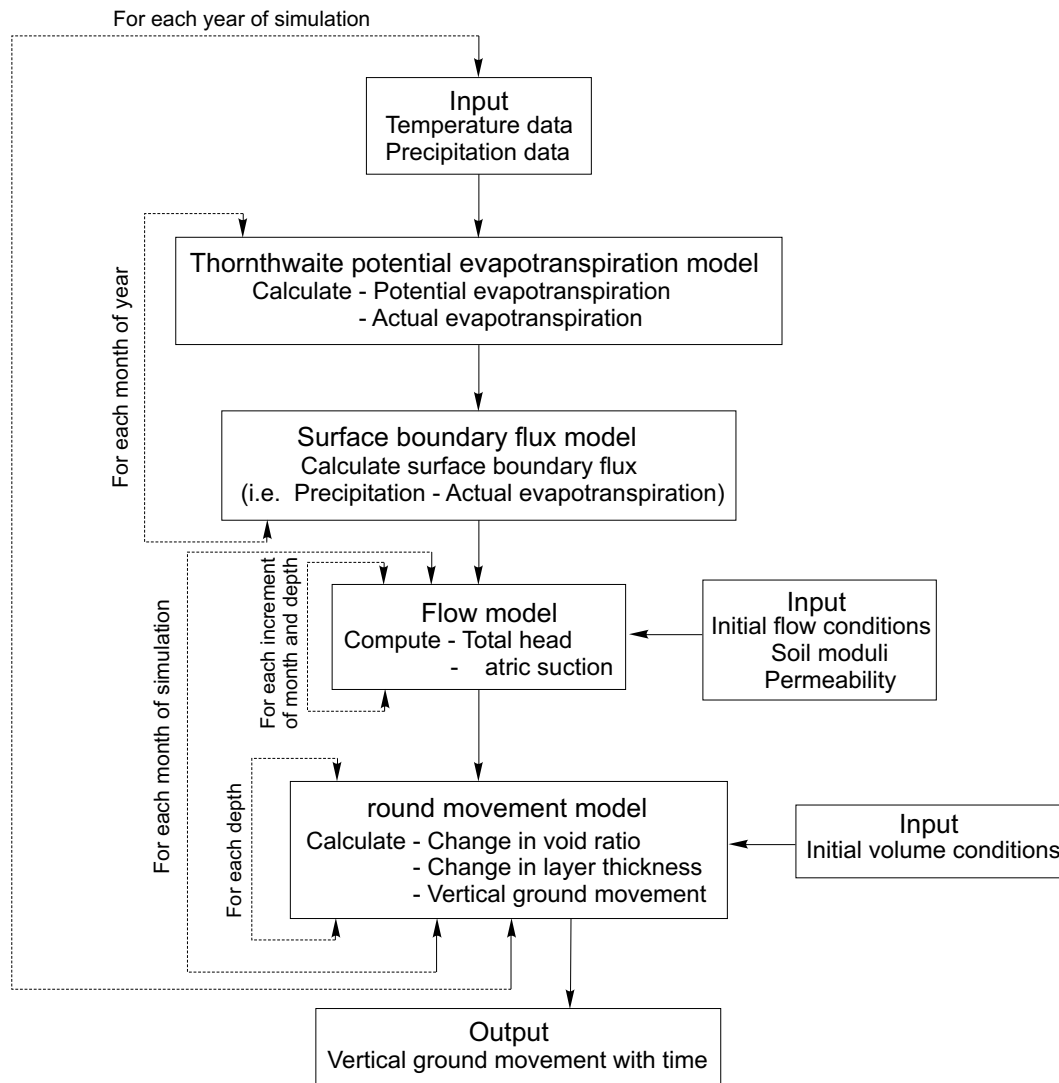
where:

- h_0 = total hydraulic head at time j and depth k ,
- h_1 = total hydraulic head at time $j + 1$ and depth k ,
- h_2 = total hydraulic head at time j at depth $k - 1$,
- h_3 = hydraulic head at time j and depth $k + 1$,
- Δy = increment of vertical depth, and
- Δt = increment of time.

Equation [6] was rewritten to solve for the hydraulic head at ground surface corresponding to the computed surface boundary flux. The corresponding pore-water pressure profiles were computed using eq. [5].

Figure 8 shows a flow chart of the steps undertaken by the computer model. The surface boundary flux is computed on a monthly basis and applied proportionally to each time increment within a month. The marching forward procedure is used for each time increment within a month to compute the next set of values for hydraulic head. At the end of the month, values are computed for

Fig. 8. Flow chart for the computer model used to predict vertical ground movements with depth and time.



pore-water pressure, degree of saturation, water content, void ratio, and vertical ground movement. The ground movements are accumulated for the duration of months simulated.

The accuracy of the solution is dependent upon the value of the β parameter, which is defined as follows:

$$[9] \quad \beta = \frac{k_y \Delta t}{\rho_w g m_2^w (\Delta y)^2}$$

Von Neumann (Smith 1975) concluded that the value of β must be less than one-third to one-half to avoid computational instability. Twenty-six nodes were considered the optimal discretization in the vertical direction. The time discretization was changed during the solution to ensure that the value of β would fall within the limits imposed by the surface boundary flux.

To accommodate a layered soil profile in which the permeability and modulus varied with depth, the geometric mean was used to average the values of the param-

eters (Haverkamp and Vauclin 1981). The geometric mean for the coefficient of permeability was defined as:

$$[10] \quad k^* = (k_1 \times k_2)^{1/2}$$

where:

k^* = geometric mean of the coefficient of permeability between the layers,

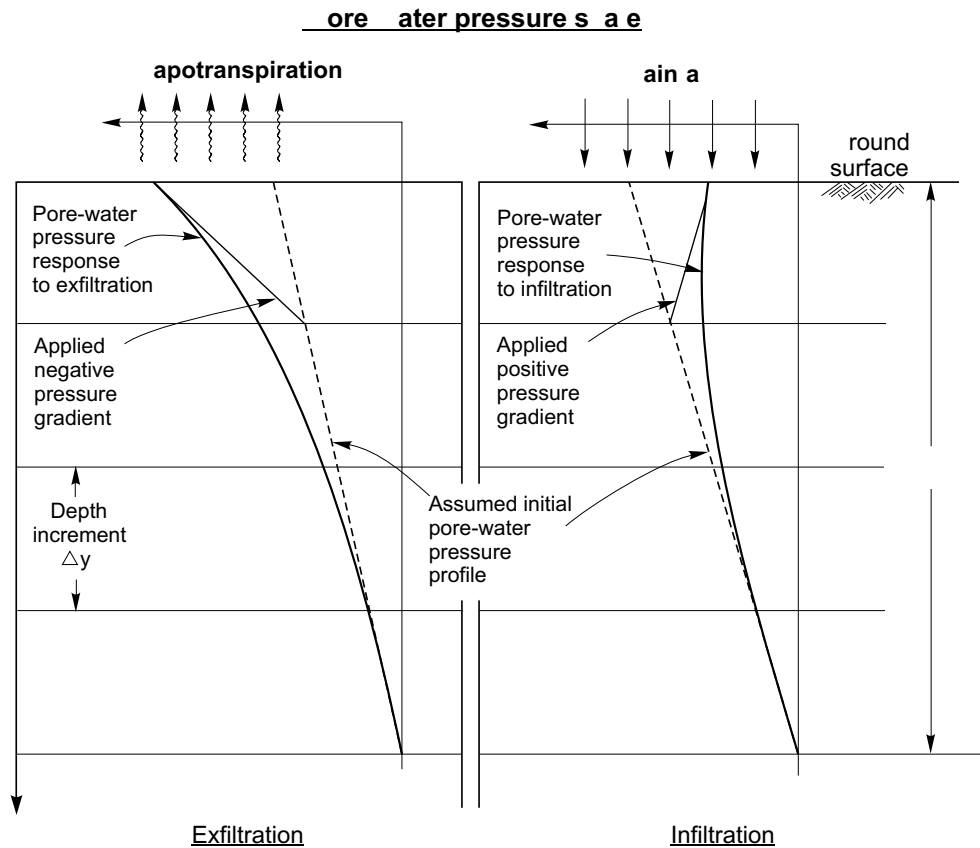
k_1 = coefficient of permeability of layer 1, and

k_2 = coefficient of permeability of layer 2.

The geometric mean for the water volume change modulus was defined similarly. The use of the geometric mean compensates for sharp changes in permeability or modulus between nodes in the finite-difference grid.

Figure 9 shows a schematic representation of the pore-water pressure response to a changing surface boundary flux, assuming that the initial conditions do not establish a gradient that controls the response. During exfiltration, the matric suction or negative pore-water pressure becomes greater at the surface, and the remainder of the

Fig. 9. Schematic representation of pore-water response to a changing surface boundary flux (after Fredlund and Dakshanamurthy 1982).



profile adjusts accordingly. During infiltration, the matric suction decreases at the surface (i.e., the pore-water pressure increases), and the negative pore-water pressures continue to decrease as water infiltrates to greater depths.

Presentation and discussion of results

The numerical model can be used to illustrate the relationship between matric suction and vertical ground movements. The model shows how increases in matric suction result in shrinkage and decreases in matric suction result in swelling. Simulated vertical ground movements can be fit to measured vertical ground movements using estimated soil properties and reasonable initial boundary conditions.

A preliminary investigation was conducted to determine the range of reasonable matric suction values at the surface for reasonable permeabilities and surface boundary fluxes. The preliminary results suggested that two independent ranges for the coefficient of permeability were required: one permeability for infiltration and one permeability for exfiltration. Permeability values in the order of 10^{-6} – 10^{-8} m/s were required for modelling infiltration events for the four prairie locations. These permeability values suggest that the soil profile behaves as though it were sand during the infiltration process. This can be attributed to the presence of shrinkage cracks as evident in

the field into which the water can readily flow (Fig. 10). The associated volume-change behavior is mostly related to the macrostructure of the soil mass during the infiltration event.

For the exfiltration process, considerably smaller coefficients of permeability (i.e., in the order of 10^{-9} – 10^{-11} m/s) were required during the simulation. This low coefficient of permeability can be attributed to the form of water flow that occurs during exfiltration. Exfiltration occurs primarily as a vapor transport process from the intact clay clods into the fractures in the soil (Fig. 11). The volume change behavior during exfiltration is more closely linked to the microstructure of the soil.

To model an infiltration event, the permeability was chosen to equal the infiltration rate. In other words, the permeability of the cracked soil profile was assumed to be large enough to accommodate all water flow into the cracks during the infiltration process. The initial matric suction profile was assumed to remain constant with depth, corresponding to a hydraulic head gradient of 1.0.

Exfiltration occurs as a result of evaporation from the ground surface and transpiration through plants drawing water out of the soil. To match vertical ground movements with measured ground movements, large matric suction values were generated at the surface during the exfiltration process, corresponding to the low coefficients of permeability.

Fig. 10. Example of fissured Regina clay.

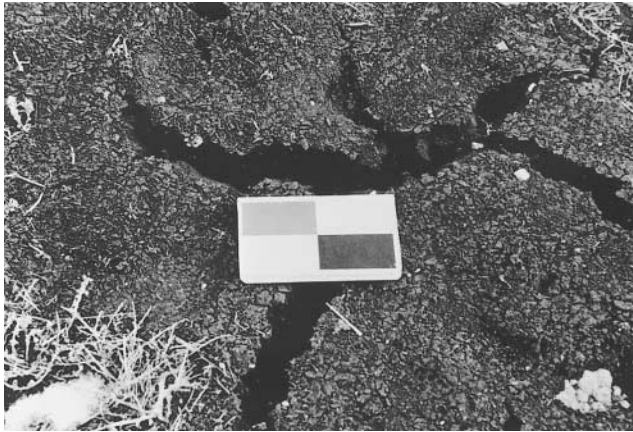
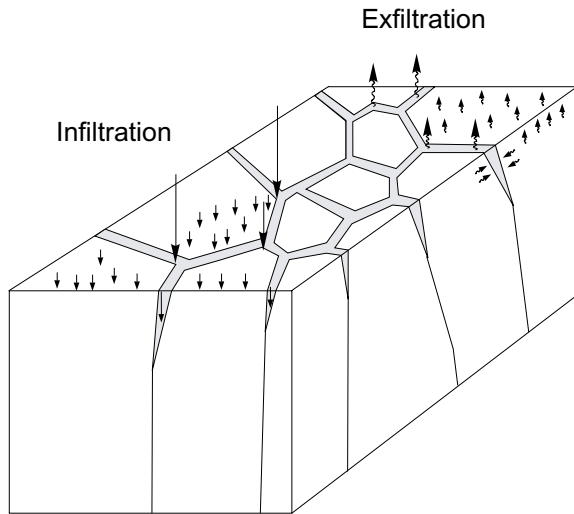


Fig. 11. Schematic diagram illustrating infiltration and exfiltration in a cracked clay soil.



The coefficient of permeability is usually expressed as a function of the matric suction, which in turn is a function of the hydraulic head. However, the characterization of the coefficient of permeability solely in terms of matric suction is not sufficient for the cracked nature of the soil and the difference between the infiltration and the exfiltration processes. The extreme ranges in simulated permeability values suggest the inadequacy of expressing the coefficient of permeability in terms of matric suction for simulation of field conditions. The use of a constant permeability value in eq. [4] and two modelling processes is therefore felt to be justified, particularly for first-order approximation in highly fissured and fractured clays.

Figure 12 shows the simulated vertical ground movement for the Regina site for a simple infiltration event (i.e., one in which the surface boundary flux is positive for each of the 3 months of simulation). Figure 13 presents the corresponding matric suction values required to model the infiltration event. The majority of movement occurs during April as the accumulated winter snowfall melts and penetrates the soil profile. The simulated vertical ground movement is in the order of 50 mm at surface.

Fig. 12. Predicted vertical ground movements for an infiltration event.

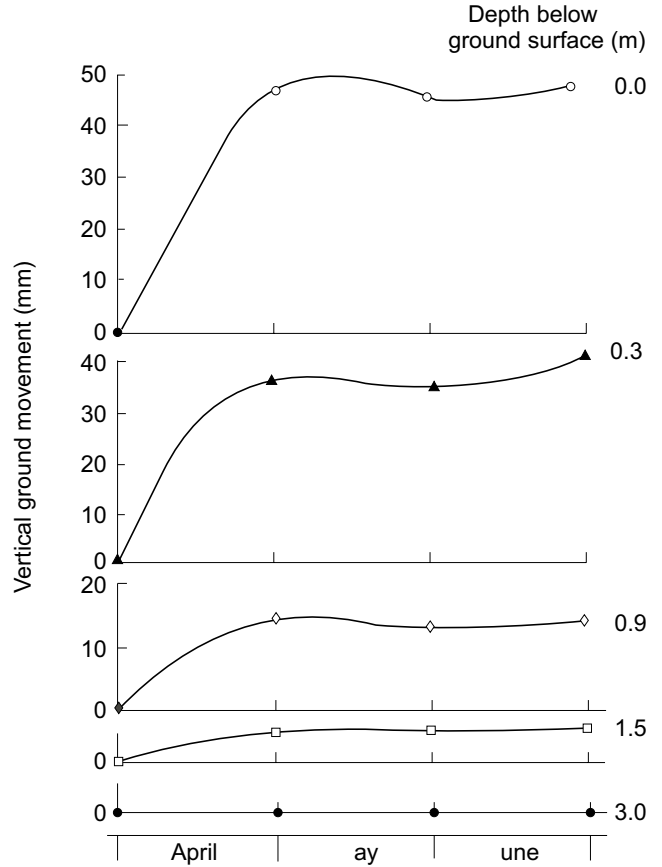
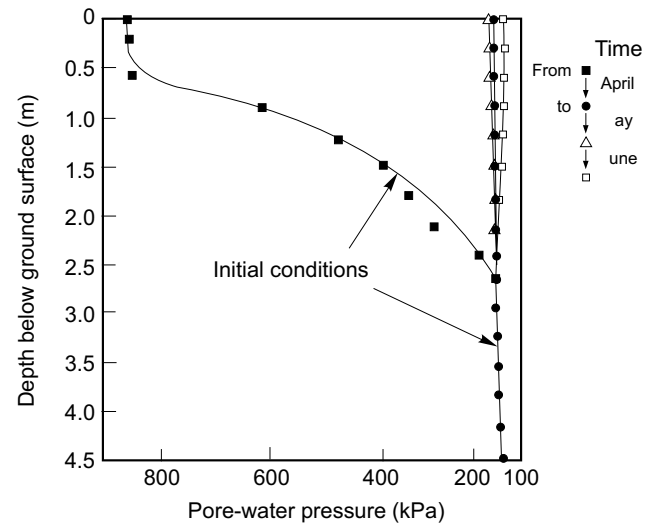


Fig. 13. Corresponding negative pore-water pressures for an infiltration event.



At depths of 0.3, 0.9, and 1.5 m, respectively, the predicted vertical ground movement is in the order of 40, 18, and 7 mm. The measured movements for these depths over the same period were in the order of 41, 18, and 7 mm, respectively.

Figure 14 illustrates the predicted vertical ground movement for a simple exfiltration event for the Regina site. The corresponding matric suction profiles are presented in Fig. 15. Extreme changes in matric suction occur at the surface as the soil profile dries. In reality, there is significant lateral volume change (i.e., cracking) in addition to vertical volume change. However, simulation of the ground movements still appears to be possible.

Figure 16 shows the predicted and measured vertical ground movements for each of the 10 events modelled for the Regina site. In general, the correspondence between measured and predicted vertical ground movements was readily accomplished using reasonable soils parameters and initial boundary conditions. However, the matching of volume-change behavior becomes more difficult for winter conditions and for complex events (i.e., events in which the surface boundary flux fluctuated from positive to negative during the simulation period). This suggests that the winter temperature phenomenon is significant to the estimation of seasonal vertical ground movements. The difficulty in matching complex events is most likely the result of over-simplifications and accumulated errors related to the event being modelled.

There was insufficient meteorological data for the 1960's for the sites located at Tisdale and Eston. An attempt was made to use meteorological data from nearby sites, but the results showed that it was important to have a meteorological station located reasonably close to the site for which vertical ground movement estimates were required.

The results for the Winnipeg site were satisfactory but have been excluded from the discussion because of their similarity to those at Regina.

Average seasonal ground movements were postulated for the Regina site based upon the information gathered during the simulation of the individual events. The average seasonal vertical ground movements for Regina are presented in Fig. 17. The assumption was made that there should be neither a net positive nor a net negative shrinkage during an average year. To satisfy this assumption, approximately 40 mm of temperature shrinkage was required during the winter months.

The corresponding suction profiles are presented in Fig. 18. Typical seasonal matric suction values are suggested to vary between 50 and 1400 kPa at the soil surface. During the summer months, the negative pore-water pressure at the surface becomes large, resulting in the formation of shrinkage cracks. During the winter months, the matric suction also becomes large because of temperature gradients induced during freezing. In the spring, the accumulated snowmelt penetrates the dry soil, resulting in large positive vertical ground movements.

Conclusions and recommendations

The numerical model illustrates the relationship between vertical ground movement and matric suction changes. The model shows how increases in matric suc-

Fig. 14. Predicted vertical ground movement for an exfiltration event.

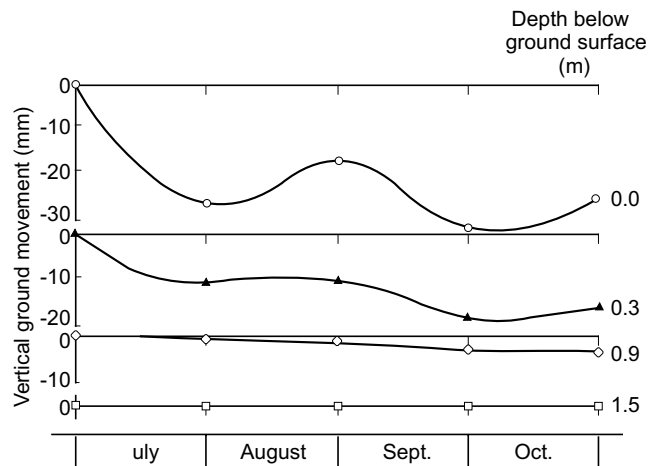
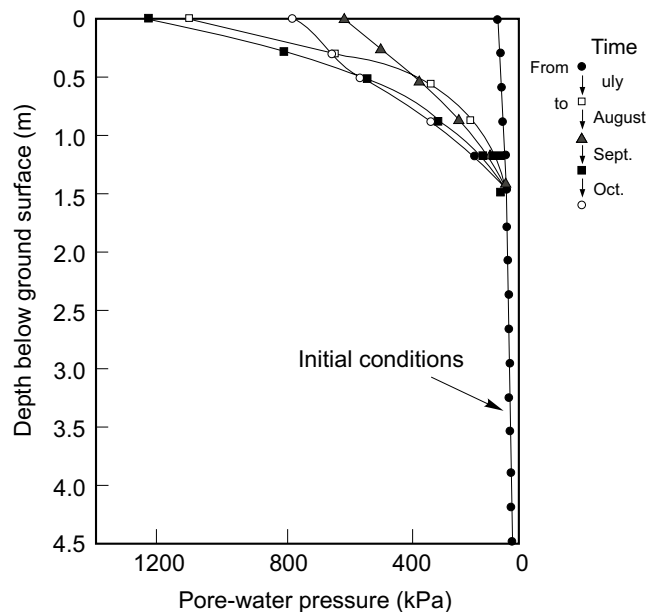


Fig. 15. Corresponding negative pore-water pressures for an exfiltration event.



tion result in shrinkage and decreases in matric suction result in swelling.

Reasonable agreement between measured and predicted vertical ground movements was achieved using soil parameters that vary with depth. The modelling studies indicated that the infiltration and exfiltration processes were characteristically different. Bulk coefficients of permeability were required to simulate measured ground movements during infiltration. These were relatively high, in the order of 10^{-8} – 10^{-9} m/s. The high values are probably due to the formation of shrinkage cracks and the associated macrostructure of the soil.

Bulk coefficients of permeabilities required for the exfiltration processes were in the order of 10^{-9} to 10^{-11} m/s. These lower values possibly reflect the change

Fig. 16. Comparison of predicted and measured vertical ground movements for each of the 10 events modelled for Regina, Saskatchewan.

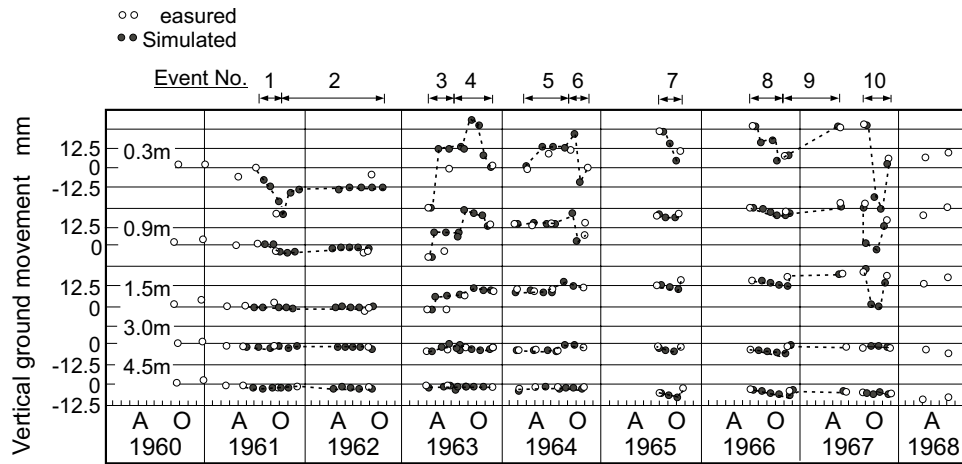


Fig. 17. Simulated average vertical ground movements for Regina, Saskatchewan.

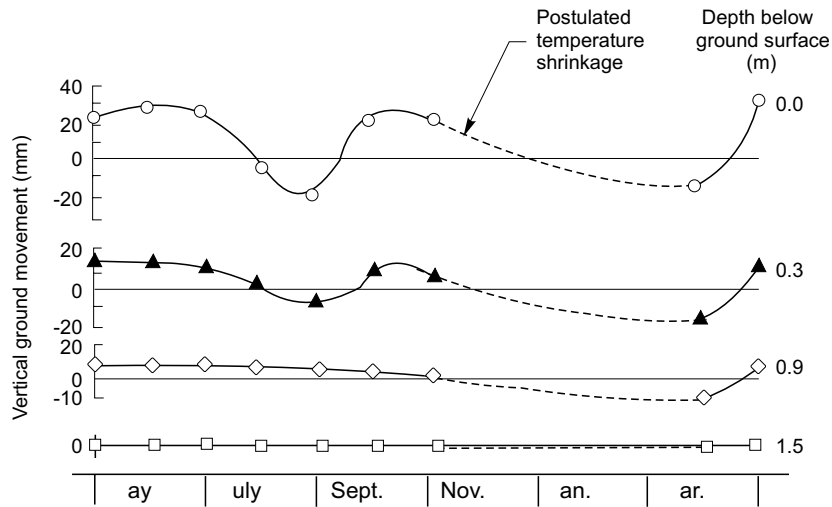
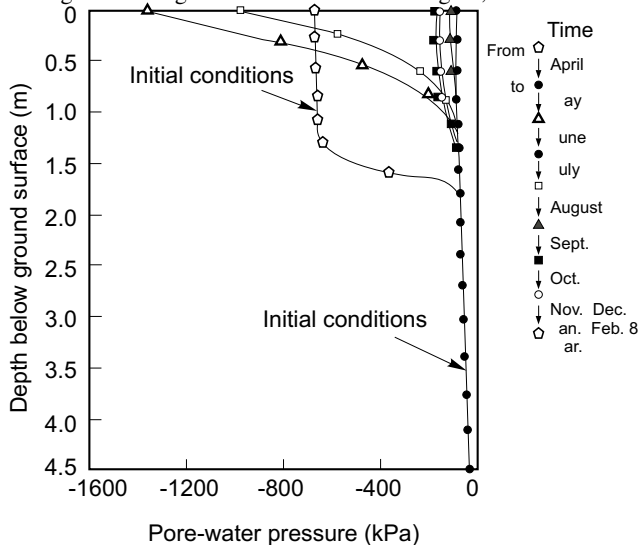


Fig. 18. Corresponding negative pore-water pressures for average vertical ground movements for Regina,



from water flow in the liquid phase during infiltration to water flow primarily in the vapour phase during exfiltration.

The Thornthwaite potential evapotranspiration model provided a reasonable characterization of the surface boundary flux, with the actual evapotranspiration estimated to be 70% of potential evapotranspiration based upon several methods.

The model could be extended to predict seasonal ground movements beneath light-engineered structures using available meteorological data (e.g., precipitation and temperature) and appropriate boundary conditions.

Further research is required to better establish the surface boundary conditions and to enlarge on the database of typical soil properties.

Thermally induced matric suctions should be studied and included in the modelling of vertical ground movements. The cracking phenomena exhibited in the field and the associated flow processes for the cracked profile should be examined in further detail.

References

- Fredlund, D.G. 1979. Appropriate concepts and technology for unsaturated soils. Proceedings, 2nd Canadian Geotechnical Colloquium. *Canadian Geotechnical Journal*, **16**: 121–139.
- Fredlund, D.G., and Dakshanamurthy, V. 1982. Transient flow processes in unsaturated soils under flux boundary conditions. Proceedings, 4th International Conference on Numerical Methods in Geomechanics, Edmonton, AB, pp. 307–317.
- Fredlund, D.G., and Hasan, J.U. 1979. Statistical geotechnical properties of Lake Regina sediments. Transportation and Geotechnical Group, Internal Report, Department of Civil Engineering, University of Saskatchewan, Saskatoon, SK.
- Fredlund, D.G., and Morgenstern, N.R. 1977. Stress state variables for unsaturated soils. *ASCE Journal of the Geotechnical Division*, **103**(GT5): 447–466.
- Granger, R.J., and Gray, D.M. 1989. Evaporation from natural nonsaturated surfaces. *Journal of Hydrology*, **111**: 21–29.
- Gray, D.M., and Male, D.H. 1981. *Handbook of snow. Principles, processes, management and use.* Pergamon Press Canada, Willowdale, ON.
- Hamilton, J.J. 1963. Volume changes in undisturbed clay profiles in Western Canada. *Canadian Geotechnical Journal*, **1**: 27–41.
- Hamilton, J.J. 1965. Shallow foundations on swelling clays in Western Canada. Proceedings, The International Research and Engineering Conference on Expansive Clay Soils, Texas A&M University, College Station, TX, pp. 183–207.
- Hamilton, J.J. 1966. Soil moisture depletion calculations for Winnipeg, 1950–1963. National Research Council of Canada, Division of Building Research, Technical Paper 229.
- Hamilton, J.J. 1968. Effects of natural and man-made environments on the performance of shallow foundations. Proceedings, 21st Annual Canadian Soil Mechanics Conference, Winnipeg, MB.
- Haverkamp, R., and Vauclin, M. 1981. A comparative study of three forms of the Richard equation used for predicting one-dimensional infiltration in unsaturated soil. *Soil Science Society of America Journal*, **45**: 13–20.
- Jones, D.E., and Holtz, W.G. 1973. Expansive soils - the hidden disaster. ASCE, Civil Engineering, New York, **43**: 87–89.
- Lam, L., and Fredlund, D.G. 1984. Saturated-unsaturated transient finite element seepage model for geotechnical engineering. *Advances in Water Resources*, **7**: 132–136.
- Sattler, P.J. 1989. Numerical modelling of vertical ground movements. M.Sc. thesis, Department of Civil Engineering, University of Saskatchewan, Saskatoon, SK, Canada.
- Smith, G.D. 1975. *Numerical solution of partial differential equations.* Oxford University Press, Ely House, London, England.
- Thornthwaite, C.W. 1948. An approach toward a rational classification of climate. *Geographical Review*, **38**: 55–94.
- Thornthwaite, C.W., and Mather, J.R. 1955. *The water balance.* Second edition, Publications in Climatology, Vol. 8, No. 1. Drexel Institute of Technology, Centerton, NJ.
- Thornthwaite, C.W., and Mather, J.R. 1957. Instructions and tables for computing potential evapotranspiration and the water balance. Publications in Climatology, vol. 10, No. 3. Drexel Institute of Technology, Centerton, NJ.
- van der Raadt, P.W. 1988. Field measurement of soil suction using thermal conductivity matric potential sensors. M.Sc. thesis, University of Saskatchewan, Saskatoon, SK, Canada.
- Yoshida, R.T., Fredlund, D.G., and Hamilton, J.J. 1983. The prediction of total heave of a slab-on-grade floor on Regina clay. *Canadian Geotechnical Journal*, **20**: 69–81.

Measured and simulated behavior of an expansive soil

F. Shuai and D.G. Fredlund

Abstract: In this paper, a theoretical model for describing the changes of soil volume, vertical total stress, and matric suction with time during various swelling oedometer tests is formulated. The model is based on the equilibrium equation, the constitutive equations for unsaturated soils and the continuity equation for the pore fluids. The transient water flow process is coupled with the load-deformation process. The proposed model has been used to simulate the results from Free Swell oedometer tests, Constant Volume oedometer tests, and Loaded Swell oedometer tests. The computed values of volume change, vertical total stress and pore-water pressure are in good agreement with measured values.

Key words: swelling pressure, free swell oedometer tests, constant volume oedometer tests, transient flow, matric suction.

Introduction

Expansive soils exhibit significant volumetric expansion upon wetting due to a decrease in the matric suction. A pressure will develop if an attempt is made to stop the swelling. Such pressures are sometimes sufficiently large to cause serious damage to structures. In order to predict the pressure or amount of heave, numerous laboratory testing procedures have been proposed. These procedures generally involve the use of a one-dimensional consolidation apparatus (i.e., oedometer). The most commonly used testing procedures are: (1) Free Swell oedometer test, (2) Loaded Swell oedometer test and (3) Constant Volume oedometer test.

Free Swell oedometer test method

In the Free Swell oedometer test, the soil specimen is brought in contact with water and allowed to swell freely under an applied token load. The soil is then gradually consolidated back to its original volume in the conventional manner used for consolidation test (Fig. 1a). The swelling pressure is defined as the stress required to consolidate the specimen back to its original volume (Hardy 1965; Sridharan et al. 1986). The stress paths in the swelling and subsequent consolidation process can be more clearly understood using a three-dimensional plot with the stress state variable forming the abscissas (Fig. 1b).

Loaded Swell oedometer test method

In the Loaded Swell oedometer test, a series of identical specimens are subjected to different initial applied loads and allowed to swell freely. The resulting final volume changes are then plotted against the corresponding applied load or stresses. The stress corresponding to zero volume change is termed the swelling pressure (Skempton 1961; Gizienski and Lee 1965; Noble 1966; Matyas 1969). The stress path followed is shown in Fig. 2.

Constant Volume oedometer test method

In the Constant Volume test, a specimen is subjected to a token load and immersed in water. The specimen volume is maintained constant throughout the first part of the test by varying the load applied to the specimen, as required. This procedure is continued until there is no further tendency for swelling. The applied load at this point is referred to as the uncorrected swelling pressure, P_s . The soil specimen is then further loaded and unloaded following the conventional oedometer test procedure. The test results are commonly plotted as shown in Fig. 3a. The stress paths followed during the test can be visualized using a three-dimensional plot of the stress state variables versus void ratio and water content (Fig. 3b).

In order to account for the effect of sampling disturbance, Fredlund et al. (1980) defined a correction to the data to give a corrected swelling pressure.

A large amount of test results and experience involving these three methods have been reported. In contrast, little attempt has been made to theoretically and analytically simulate the testing procedures.

Theoretical model

Processes involved in swelling tests

Swelling oedometer tests primarily involve two processes; namely, the transient water flow process and the load-deformation process. The load-deformation process

F. Shuai. Research Engineer, Department of Civil Engineering, University of Saskatchewan, 57 Campus Drive, Saskatoon, SK, Canada S7N 5A9.

D.G. Fredlund. Professor, Department of Civil Engineering, University of Saskatchewan, 57 Campus Drive, Saskatoon, SK, Canada S7N 5A9.

Reproduced with permission from the *Proceedings, Third Brazilian Symposium on Unsaturated Soils, NSAT'97*, Rio de Janeiro, Brazil, April 22–25, Vol. 1, pp. 253–260.

Fig. 1. Stress path representation for the Free Swell oedometer test; a) conventional free swell data plot, b) three-dimensional stress path plot (after Fredlund 1995).

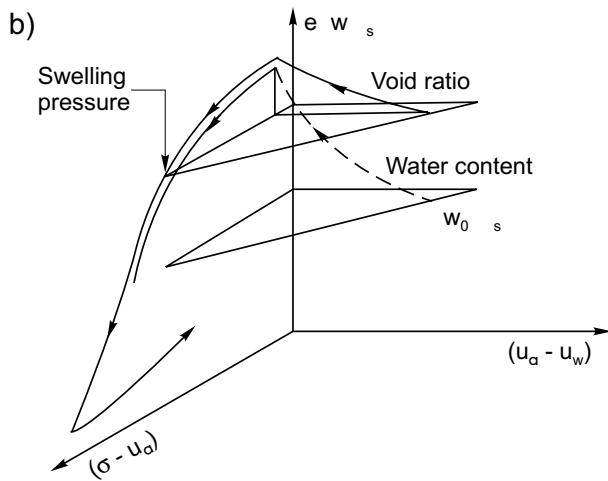
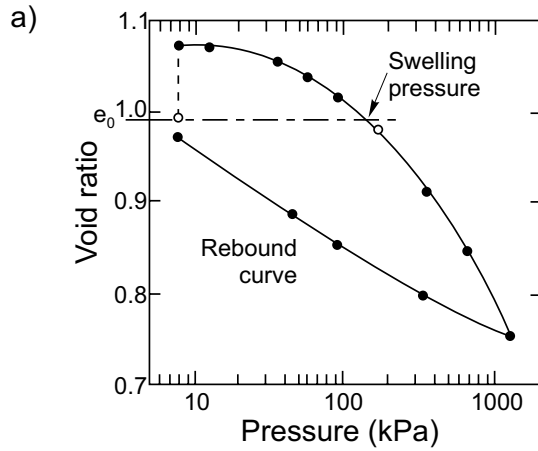
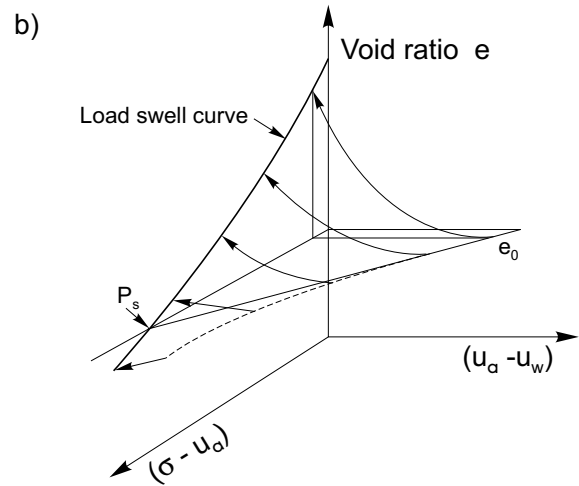
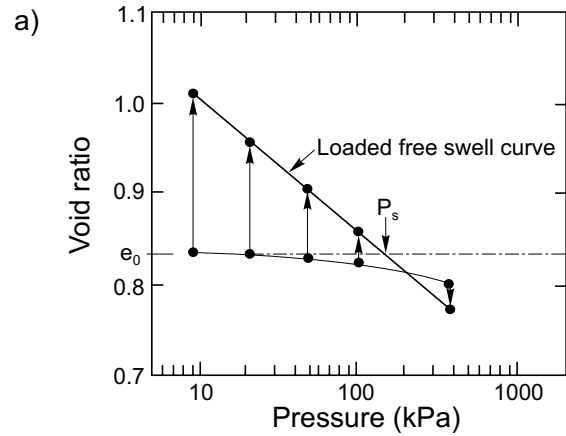


Fig. 2. Stress path followed in the Loaded Swell oedometer test; a) two-dimensional plot, b) three-dimensional plot.



describes the deformation response of the soil as a result of a change of load or matric suction and is governed by the equilibrium equations and the constitutive equations for unsaturated soils. For one-dimensional case, the equilibrium equations can be written in incremental form as follows:

$$[1] \quad \frac{\partial \Delta \sigma_z}{\partial z} = 0$$

where:

$\Delta \sigma_z$ = increment of total normal stress in the z-direction (i.e., vertical direction).

The constitutive equations for an unsaturated soil were proposed by Fredlund (1979) and are written as: for the soil structure:

$$[2] \quad \epsilon_z = \frac{\Delta V_v}{V_0} = m_1^s \Delta(\sigma_z - u_a) + m_2^s \Delta(u_a - u_w)$$

for the water phase:

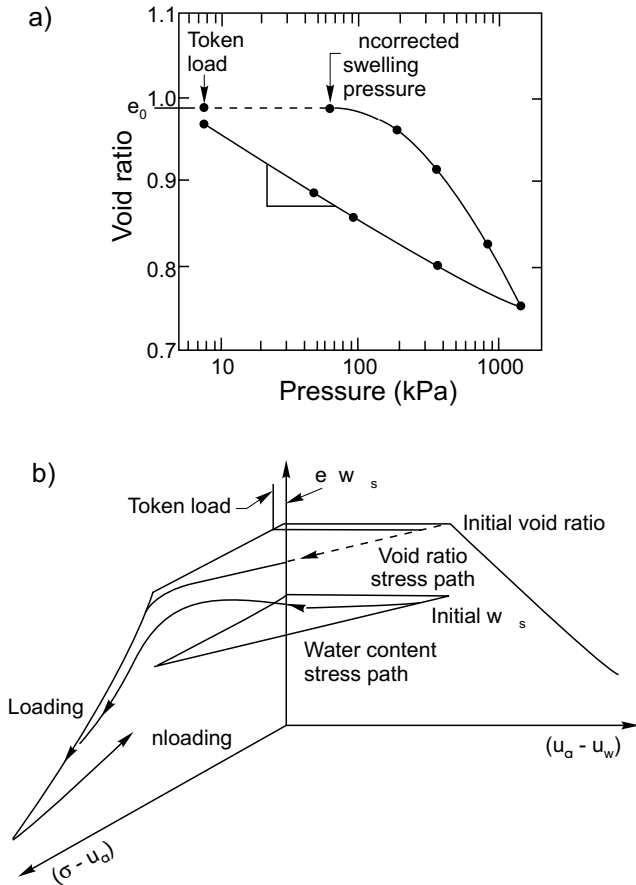
$$[3] \quad \frac{\Delta V_w}{V_0} = m_1^w \Delta(\sigma_z - u_a) + m_2^w \Delta(u_a - u_w)$$

where:

- ϵ_z = strain in the z-direction,
- σ_z = total normal stress in the z-direction,
- V_0 = initial overall volume of the soil element,
- ΔV_v = change in the volume of voids in the soil element,
- m_1^s = coefficient of volume change with respect to a change in net normal stress,
- m_2^s = coefficient of volume change with respect to a change in matric suction,
- ΔV_w = change in the volume of water in the soil element,
- m_1^w = coefficient of water volume change with respect to a change in the net normal stress,
- m_2^w = coefficient of water volume change with respect to a change in matric suction.

The transient water flow process is governed by the continuity equation which can be written as:

Fig. 3. Stress path followed in the Constant Volume oedometer test; a) conventional constant volume data plot, b) three-dimensional stress path plot (after Fredlund 1995).



$$[4] \quad \frac{\partial}{\partial t} \left(\frac{V_w}{V_0} \right) = \frac{1}{\rho_w g} \frac{\partial}{\partial z} \left(k_w \frac{\partial u_w}{\partial z} \right)$$

where:

k_w = coefficient of permeability with respect to the water phase in the z -direction (which is a function of the negative pore-water pressure),

z = elevation,

u_w = pore-water pressure,

ρ_w = density of water,

g = gravitational acceleration.

For some swelling tests (i.e., Constant Volume oedometer test) the water flow process and load-deformation process are not independent. During the constant volume test, the total stress increases with respect to time. The increase in the total stress results in a tendency for the soil to decrease its volume and hence results in a decrease in the negative pore-water pressure. Alternatively, the water content increase due to transient water flow causes the negative pore-water pressure to decrease. The decrease in the negative pore-water pressure results

in a tendency for the soil to increase in volume and consequently results in a further increase in the total stress because of the requirement to maintain a constant volume. Therefore, it is difficult to separate the two processes (i.e., the transient water flow process and the soil load-deformation process) during the constant volume test. In order to simulate various swell testing procedures, the simultaneous equations coupling the transient water flow process with the load-deformation process must be formulated.

Governing differential equation for swelling test

In order to simplify the derivation, the following assumptions are made: (1) isotropic soil, (2) infinitesimal strain, (3) linear constitutive relations for a small change in net normal stress or matric suction, (4) the permeability with respect to the air phase, k_a , is significantly greater than the permeability with respect to the water phase, k_w , which means that the pore-air pressure is always equal to the surrounding air pressure (i.e., $u_a = 0$). According to assumption (4) the net normal stress, $(\sigma_z - u_a)$, becomes equal to the total vertical stress, σ_z , and matric suction, $(u_a - u_w)$, becomes equal to the negative pore-water pressure, $-u_w$. The constitutive eqs. [2] and [3] for an unsaturated soil become:

$$[5] \quad \epsilon_z = \frac{\partial V_v}{V_0} = m_1^s \Delta \sigma_z - m_2^s \Delta u_w$$

$$[6] \quad \frac{\partial V_w}{V_0} = m_1^w \Delta \sigma_z - m_2^w \Delta u_w$$

Differential equation for water flow

The continuity requirement for the water phase is given by eq. [4] and the constitutive relation for the water phase of an unsaturated soil is given by eq. [6].

Substituting eq. [6] into Eq.[4] gives:

$$[7] \quad m_1^w \frac{\partial \sigma_z}{\partial t} - m_2^w \frac{\partial u_w}{\partial t} = \frac{1}{\rho_w g} \frac{\partial}{\partial z} \left(k_w \frac{\partial u_w}{\partial z} \right)$$

Differentiating eq. [5] with respect to time yields,

$$[8] \quad \frac{\partial \epsilon_z}{\partial t} = m_1^s \frac{\partial \sigma_z}{\partial t} - m_2^s \frac{\partial u_w}{\partial t}$$

Equation [8] can be rewritten as:

$$[9] \quad \frac{\partial \sigma_z}{\partial t} = \frac{1}{m_1^s} \left(\frac{\partial \epsilon_z}{\partial t} + m_2^s \frac{\partial u_w}{\partial t} \right)$$

Substituting eq. [9] into eq. [7] gives:

$$[10] \quad \frac{m_1^w}{m_1^s} \frac{\partial \epsilon_z}{\partial t} - \left(m_2^w - \frac{m_2^s m_1^w}{m_1^s} \right) \frac{\partial u_w}{\partial t} = \frac{1}{\rho_w g} \frac{\partial}{\partial z} \left(k_w \frac{\partial u_w}{\partial z} \right)$$

Written in terms of displacement, the strain in the z -direction can be expressed as:

$$[11] \quad \varepsilon_z = \frac{\partial \delta_z}{\partial z}$$

where:

δ_z = displacement in the z -direction.

Substituting the strain in eq. [11] into eq. [10] gives:

$$[12] \quad \frac{m_1^w}{m_1^s} \frac{\partial}{\partial t} \left(\frac{\partial \delta_z}{\partial z} \right) - \left(m_2^w - \frac{m_2^s m_1^w}{m_1^s} \right) \frac{\partial u_w}{\partial t} = \frac{1}{\rho_w g} \frac{\partial}{\partial z} \left(k_w \frac{\partial u_w}{\partial z} \right)$$

Equation [12] can be rewritten as:

$$[13] \quad \alpha \frac{\partial}{\partial t} \left(\frac{\partial \delta_z}{\partial z} \right) - \beta \frac{\partial u_w}{\partial t} = \frac{1}{\rho_w g} \frac{\partial}{\partial z} \left(k_w \frac{\partial u_w}{\partial z} \right)$$

where:

$$\alpha = \frac{m_1^w}{m_1^s}$$

$$\beta = m_2^w - \frac{m_2^s m_1^w}{m_1^s}$$

Equation [13] is the transient flow equation for the water phase in terms of displacement and negative pore-water pressure.

Differential equation for soil volume change

The constitutive relation for the volumetric strain of an unsaturated soil under one-dimensional case is given by eq. [5] and the deformation equation for the one-dimensional case is given by eq. [11]. Substituting the strain in eq. [11] into eq. [5] allows the displacement to be written as:

$$[14] \quad \frac{\partial \delta_z}{\partial z} = m_1^s \Delta \sigma_z - m_2^s \Delta u_w$$

Rearranging eq. [14] results in,

$$[15] \quad \Delta \sigma_z = \frac{1}{m_1^s} \frac{\partial \delta_z}{\partial z} + \frac{m_2^s}{m_1^s} \Delta u_w$$

Substituting eq. [15] into the equilibrium equation (i.e., eq. [1]) and differentiating it with respect to z gives:

$$[16] \quad \frac{\partial^2 \delta_z}{\partial z^2} = -m_2^s \frac{\partial u_w}{\partial z}$$

Equation [16] is the load-deformation equation for the swelling oedometer test.

Simultaneous equations for Constant Volume oedometer test

The load-deformation equation and the transient water flow equation for the swelling tests are given by eq. [16] and eq. [13], respectively. Equation [13] is used to define the negative pore-water pressure, $-u_w$, when solving for

soil volume change in eq. [16]. The displacement, δ_z , required in eq. [13] depends on the deformation given by eq. [16]. Equations [16] and [13] must be solved simultaneously.

The governing equations for swelling tests, eq. [16] and eq. [13], can be written in the form of simultaneous equations as follows:

$$[17] \quad \begin{cases} \frac{\partial^2 \delta_z}{\partial z^2} = -m_2^s \frac{\partial u_w}{\partial z} \\ \alpha \frac{\partial}{\partial t} \left(\frac{\partial \delta_z}{\partial z} \right) = \frac{1}{\rho_w g} \frac{\partial}{\partial z} \left(k_w \frac{\partial u_w}{\partial z} \right) + \beta \frac{\partial u_w}{\partial t} \end{cases}$$

There are two equations in eq. [17] with two unknowns (i.e., δ_z and u_w). These equations can be used to compute the negative pore-water pressure and displacement at various depths and times during the swelling process. The negative pore-water pressure change, Δu_w , and the displacement, δ_z , computed from eq. [17] can be substituted into eq. [15] to compute the change in vertical stress, $\Delta \sigma_z$, required to maintain constant volume condition during the constant volume test.

The relationships required to solve eq. [17] are the compression or rebound curve (i.e., V_w / V_0 versus $(\sigma_z - u_w)$), the soil-water characteristic curve, shrinkage or swelling curve and the permeability function (i.e., $k_w(u_w)$).

Experimental results and numerical simulations

The governing differential equation describing the pore pressure and volume change behavior during various swelling tests (i.e., eqs. [16] and [13]) are non-linear. The coefficients of permeability, k_w , the coefficients of soil volume change, m_1^s and m_2^s , and the coefficients of water volume change, m_1^w and m_2^w , vary with vertical position and time due to changes in total stress, and negative pore-water pressure. A closed-form solution is not available; a computer program called SWELL was developed using the finite element method for predicting the pore-water pressure and volume change behavior during a swell test (Shuai 1996).

The proposed theoretical model was used to simulate the results from several oedometer swelling tests (i.e., Free Swell oedometer test, Constant Volume oedometer test, and Loaded Swell oedometer test) on compacted Regina Clay. The specimens used in the tests have a moulding water content of 26% and an initial void ratio of 0.96. Comparisons are given in this section of the paper between measured and predicted matric suction, vertical total stress and volume change values for the swelling oedometer tests.

Figure 4 shows the measured and computed deflection versus time curves for Free Swell oedometer tests on two 100 mm high specimens and two 20 mm height specimens. A comparison between the computed and measured curves shows reasonably good agreement for the full du-

Fig. 4. Computed and measured deflection versus time curves for Free Swell oedometer tests.

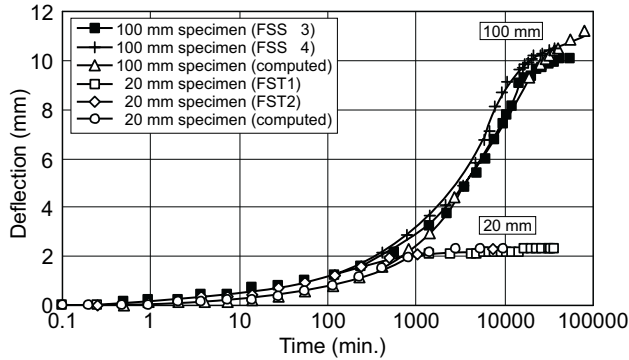
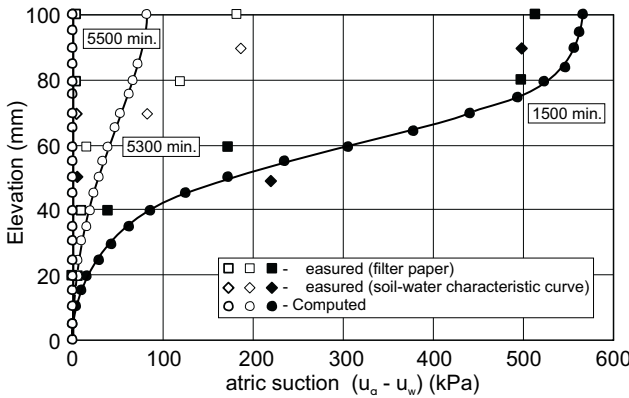


Fig. 5. Computed and measured matric suction profiles for Free Swell oedometer tests.



ration of the test for these specimens. The predicted total heaves are almost the same as those measured.

A comparison between the computed and measured matric suction profiles for Free Swell oedometer test on the 100 mm high specimen is presented in Fig. 5. The matric suction was measured by placing Whatman No. 42 filter papers between each layers of specimen and measuring the water content of the filter papers after each test. Good agreement was found between the measured and computed matric suctions for the early (i.e., $t = 1500$ min.) and latter stages (i.e., $t = 54\,700$ min.) of the test. Some differences were noted during the intermediate stage (i.e., $t = 5300$ min.) of the test. The matric suctions predicted at the upper part of the specimen are somewhat lower than the measured suctions. The poor prediction could be attributed to the filter paper which were placed in the specimen. Since the water retention of the filter paper is much higher than that of the soil, the filter paper may absorb more water than the soil for a given decrease in matric suction. As a result, the filter papers in the soil retard the advance of the saturated zone resulting in a slower decrease of matric suction.

The measured and computed vertical total stress versus time curves for Constant Volume oedometer tests on two 100 mm high specimen and two 20 mm height specimen are shown in Fig. 6. Good agreement was found between

Fig. 6. Computed and measured vertical normal stress versus time curves for Constant Volume oedometer tests.

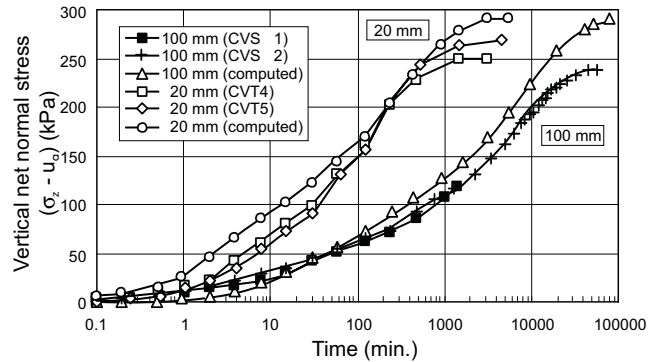


Fig. 7. Computed and measured matric suction profiles for Constant Volume oedometer tests.

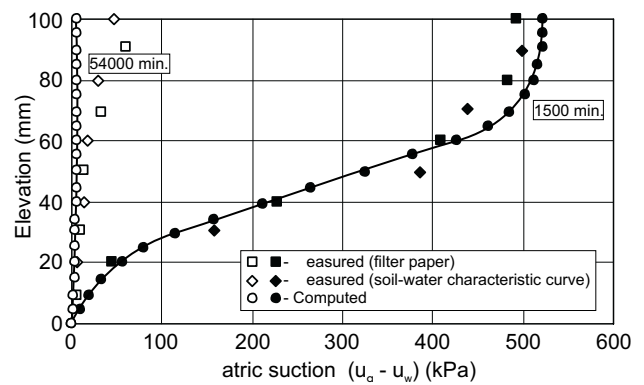
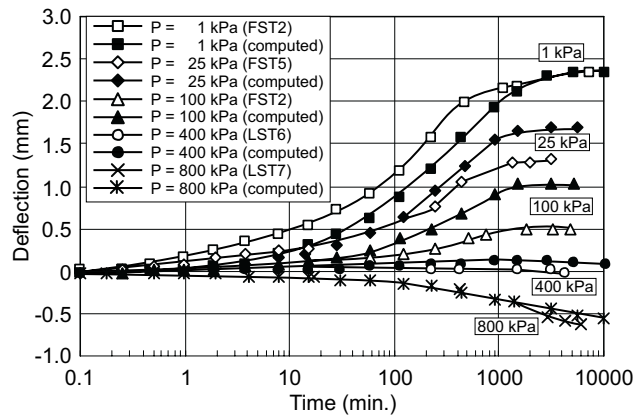


Fig. 8. Computed and measured time-heave relationship for Loaded Swell oedometer tests.



the computed and measured curves for the full duration of the test for all specimens.

The measured and computed profiles of matric suction are presented in Fig. 7. The correlation between the measured and computed matric suctions are good.

The measured and computed deflection versus time curves for the Loaded Swell oedometer tests are shown in Fig. 8. The computed and measured deflection-time curves show good agreement when the applied load is higher than 300 kPa and lower than 20 kPa. The correla-

tion between the measured and computed deflection-time curves is not as good during the latter stages of the test when the applied load is lower than 300 kPa and higher than 20 kPa. The discrepancy could be contributed to the high ratio of horizontal to vertical stress (i.e., σ_h / σ_v) at the end of the test.

Komornik and Zeitlen (1965) used a special oedometer to measure the lateral swelling pressure under different vertical loads. The results obtained indicated that the ratio of horizontal to vertical stress at the end of the test increased as the amount of swell increased. In other words, under a constant vertical stress, the mean normal stress applied to the soil increases at the end of the test. The test results obtained by Dakshanamurthy (1979) showed that total heave decreased with increasing mean normal stress. Therefore, the increase in the mean normal stress due to the increasing stress ratio (i.e., σ_h / σ_v) will decrease the total heave at the end of the loaded swell test. Since the increase in the ratio of horizontal to vertical stress has not been taken into account in this theoretical simulation, it should be expected that the calculation results will overestimate the total heave. The amount of the overestimation will decrease as the applied load increase since the ratio of horizontal to vertical stress decrease with the increasing vertical applied load and decreasing amount of swell.

Conclusions

The swelling oedometer tests primarily involve two processes; namely, the transient water flow process and the load-deformation process. These processes are governed by following basic equations:

- (1) The equilibrium equations for an element of soil;
- (2) The constitutive equations for unsaturated soils; and
- (3) The continuity equations for the pore fluids.

The transient water flow process and the load-deformation process are not independent for the Constant Volume oedometer test. The simultaneous equations coupling the transient water flow process with the load-deformation process are required for simulation of swell testing procedures.

The simultaneous equations for describing the processes which occur during a swelling oedometer test are formulated. These equations are non-linear with respect to position and time and should be solved using a numerical method. The soil properties required in the theoretical model are the coefficient of permeability function (i.e., k_w); the coefficients of volume change (i.e., m_1^s and m_2^s) and the coefficients of water volume (i.e., m_1^w and m_2^w). These soil properties can be obtained using ordinary laboratory methods.

The proposed theoretical model was used to simulate the results from Free Swell oedometer test, Constant Volume oedometer test, and Loaded Swell oedometer test. In

general, good agreement was found between the computed and measured values of volume change, vertical total stress and pore-water pressure. Some over-estimation of total heave was noted for Loaded Swell oedometer tests when the surcharge loads were significantly lower than the swelling pressure. This poor prediction is attributed to the increasing ratio of horizontal to vertical stress at the end of the test which is not possible to simulate using a one-dimensional model.

The work presented in this paper concentrated on the simulation of swell testing processes performed in the laboratory. However, the proposed theoretical model is also of value in prediction of *in situ* total heave or collapse, the swelling pressure and the rate of swell or collapse.

References

- Dakshanamurthy, V. 1979. A stress-controlled study of swelling characteristics of compacted expansive clays. *Geotechnical Testing Journal*, 2(1): 57–60.
- Fredlund, D.G. 1979. Second Canadian geotechnical colloquium: Appropriate concepts and technology for unsaturated soils. *Canadian Geotechnical Journal*, 16(1): 121–139.
- Fredlund, D.G. 1995. The prediction of heave in expansive soils. Proceedings, Canada-Kenya Symposium on Unsaturated Soil Behaviour and Applications, August 22–23, University of Nairobi, Kenya, pp. 105–119.
- Fredlund, D.G., Hasan, J.U. and Filson, H. 1980. The prediction of total heave. Proceedings, 4th International Conference on Expansive Soils, Denver, CO, Vol. 1, pp. 1–17.
- Gizienski, S.F. and Lee, L.J. 1965. Comparison of laboratory swell tests to small scale field tests. Proceedings, 1st International Conference on Expansive Soils, Texas A&M University Press, College Station, pp. 108–119.
- Hardy, R.M. 1965. Identification and performance of swelling soil types. *Canadian Geotechnical Journal*, 2(2): 141–153.
- Komornik, A. and Zeitlen, J.G. 1965. An apparatus for measuring lateral soil swelling pressure in the laboratory. Proceedings, 6th International Conference on Soil Mechanics and Foundation Engineering, Montreal, Vol. 1, pp. 278–281.
- Matyas, E. L. 1969. Some properties of two expansive clays from Western Canada. Proceedings, 2nd International Conference on Expansive Clay Soils, Texas A&M University Press, College Station, pp. 263–278.
- Noble, C. A. 1966. Swelling measurements and prediction of heave for lacustrine clay. *Canadian Geotechnical Journal*, 3(1): 32–41.
- Shuai, F. 1996. Simulation of swelling pressure measurements on expansive soils. Ph.D. thesis, University of Saskatchewan, Saskatoon, SK, Canada.
- Skempton, A.W. 1961. Horizontal stresses in an over-consolidated Eocene clay. Proceedings, 5th International Conference Soil Mechanics and Foundation Engineering, Vol. 1, pp. 351–357.
- Sridharan, A., Rao, A.S. and Sivapullaiah, P.V. 1986. Swelling pressure of clays. *Geotechnical Testing Journal*, 9(1): 24–33.

The collapse behavior of a compacted soil during inundation

R. Tadepalli and D.G. Fredlund

Abstract: The collapse behavior of a compacted, uncemented soil is studied within a theoretical context consistent with the concepts of unsaturated soil mechanics. Experimental data are presented relating the initial matric suction of a compacted soil to its volume decrease during inundation. The laboratory results indicate a unique relationship between the changes in matric suction (i.e., $\Delta(u_a - u_w)$, where u_a is the pore-air pressure and u_w is the pore-water pressure) of the compacted soil and the resulting volume reduction during inundation. Changes in the matric suction and total volume with respect to time were modeled using the theory of transient flow through an unsaturated soil. The predicted results show reasonable agreement with the experimental observations. The comparisons between the simulated results and the experimental data indicate that the coefficient of consolidation of the soil varies linearly with matric suction during the inundation process.

Key words: unsaturated soil, matric suction, collapsible soils, negative pore-water pressures.

Introduction

The concept of effective stress, useful in predicting the behavior of saturated soils, fails to explain the collapse behavior of unsaturated soils during inundation. The principle of effective stress would indicate that the overall volume of the soil should increase during inundation, as a result of a decrease in the effective stress. However, the overall volume decreases, producing what is termed as collapse, during the inundation process. Soils that exhibit collapse during inundation are initially unsaturated and subsequently become saturated after inundation for a period of time.

It would appear to be appropriate to use the concepts of unsaturated soil mechanics in an attempt to explain the collapse behavior. Two independent stress state variables; namely, net normal stress ($\sigma - u_a$) and matric suction ($u_a - u_w$) (where σ is the total normal stress, u_a is the pore-air pressure, and u_w is the pore-water pressure), have been found to be suitable for predicting the mechanical behavior of unsaturated soils (Matyas and Radhakrishna 1968; Fredlund and Morgenstern 1976). The stress state variable that changes during inundation is matric suction ($u_a - u_w$). The total stress does not change during inundation, and the pore-air pressure is commonly assumed to remain at atmospheric conditions (Rahardjo 1990). A typical compression curve for a soil specimen exhibiting collapse subsequent to inundation is shown in Fig. 1. The idealized compression curve is plotted with respect to net normal stress and matric suction. The stress path before

inundation is shown by the line AB, during inundation by the line BC, and after inundation by the lines CD and DE.

A research program was established with the intention of verifying whether or not the stress state variables for an unsaturated soil could be used to describe the collapse mechanism in an unsaturated soil. In other words, is there a relationship between matric suction change and the total volume change during inundation, as shown on the idealized plot (Fig. 1). The uniqueness of such a relationship between matric suction and collapse was studied by means of the laboratory program.

Literature review

Man-made earth structures such as embankments, road fills, and earth dams often exhibit collapse when compacted dry of optimum (Holtz 1948). It is commonly assumed that only sandy or silty soils exhibit collapse; however, in recent years it has been reported that compacted soils in general can exhibit collapse (Barden et al. 1973; Cox 1978). Clayton (1980) reported the occurrence of collapse in a compacted chalk-fill. It is now generally accepted that any type of soil compacted dry of optimum may develop a collapsible fabric or metastable structure at low densities.

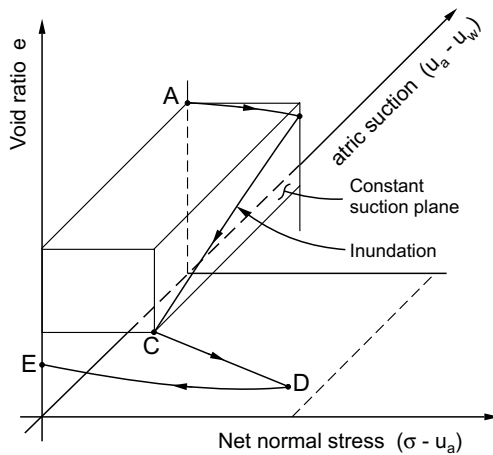
Qian and Lin (1988) reported that naturally occurring collapsing soils can be divided into two categories. There are those that collapse upon inundation under a total pressure equal to their overburden, and there are those which require a total pressure greater than their overburden to exhibit the collapse phenomenon. The later category involves soils that have significant cementation or bonding at the particle contacts. This paper deals only with collapsing soils with insignificant cementation at the particle contacts.

Compacted soils that exhibit collapse typically have an open type of structure with many void spaces, which give rise to a metastable structure. Many researchers have hy-

R. Tadepalli. Engineer, Clifton Associates Ltd., 101-108 Research Drive, Saskatoon, SK., Canada S7N 3R3
D.G. Fredlund. Professor, Department of Civil Engineering, University of Saskatchewan, 57 Campus Drive, Saskatoon, SK, Canada S7N 5A9

Reproduced with permission from the *Canadian Geotechnical Journal* 28: 477-488, 1991.

Fig. 1. Compression curve for a soil exhibiting collapse behavior with respect to net normal stress and matric suction.



pothesized regarding the structural arrangement of the particles for these soils. Common to these postulations is the description of the soil structure which states that the bulky grains are held together in a honeycomb type of fabric by some type of bonding material or force at the points of contact. The various postulated structural arrangements generally differ with respect to the size and orientation of the bonding material.

The dry density and water content of soil specimens at the time of compaction are generally considered as the primary soil properties that control the amount of collapse. Several researchers have reported that soils exhibit collapse if the dry density of the soil specimen is less than 1.6 Mg/m^3 . Jennings and Knight (1975) reported that the above conclusion is a misconception and should be dispelled. It was also suggested that the collapse behavior is also dependent on other variables such as clay content and clay type. An extensive laboratory testing program has been carried out on residual clays from Kenya by Foss (1973). Popescu (1986) conducted similar test on a loess soil from Romania. Lefebvre and Benbelfadhel (1989) also conducted studies on glacial till to investigate the effect of a wide range of placement conditions on the collapse of a soil.

The soils tested by Foss (1973) were compacted at a constant water content with varying densities. The soils indicated a linear inverse relationship between the dry density and the percentage of collapse (i.e., dH/H_0 , where dH = decrease in height of the specimen subsequent to inundation, and H_0 = initial height of the specimen). Popescu (1986) compacted the loess specimens at a constant density and varying water contents to study the effect of water content on the amount of collapse. The relationship observed between the water content and the percentage of collapse was essentially linear. However, the results presented by Lefebvre and Benbelfadhel (1989) show a more parabolic relationship, particularly at low water contents. Obviously, the form of the relationship may vary from one soil to another.

Meckechnie (1989) stated that unsaturated soils having a dry density lower than 1.6 Mg/m^3 are liable to collapse. However, he also noted that not all the soils with low densities are necessarily collapsible in nature. At the same time, he stated that an initially unsaturated condition is a prerequisite for collapse.

Most research has concentrated on the development of laboratory testing methods for identifying soils that exhibit collapse.

The tests are also used to estimate the probable amount of collapse. The probable mechanisms involved in the collapse phenomena have been suggested by several researchers (Holtz and Hilf 1961; Burland 1965; Larinov 1965; Dudley 1970; Barden et al. 1973). Collapse mechanisms differ considerably from the classical consolidation process. In the consolidation process, the total volume change of the saturated soils occurs as a transient process. Collapse, on the other hand, appears to occur in a relatively short period of time in response to the infiltration of water at a constant vertical stress. Collapse can result in a radical rearrangement of the soil particles, resulting in a significant reduction in total volume of the soil mass.

Holtz and Hilf (1961) described the mechanism of collapse accompanying wetting as the result of capillary pressures approaching zero and the degree of saturation increasing to 100%. The mechanism for cohesionless soils was explained on the basis of the reduction of shear factor (i.e., shear strength - shear stress) against collapse. It was postulated that during inundation, the Mohr circle translates horizontally by an amount equal to the negative pore-water pressure existing in the soil before inundation. Due to this transition, the effective stress path intersects the Mohr-Coulomb failure envelope, resulting in a general shear failure and associated settlement.

Burland (1965) explained the collapse mechanism in terms of the stability at the interparticle contact points. Due to inundation, the negative pore-water pressure at the contact points decreases, giving rise to grain slippage and distortion. This results in an irrecoverable decrease in total volume.

Larinov (1965), Dudley (1970), and Barden et al. (1973) described the collapse phenomena in terms of the bonding materials present at the contact points. It was suggested that in the case of silt bonds (i.e., bonding material is of silt-sized particles) the temporary strength was mainly due to capillary tension. In this case, the temporary strength would be lost during inundation, resulting in a decrease in volume. However, it was suggested that, in general, the bonding material for collapsible soils was clay. Dudley (1970) postulated that the capillary forces provided temporary strength to the clay bonds when in a dry state.

The underlying principles associated with all postulated mechanisms are: (1) the soil must be unsaturated and (2) the pore-water pressures must be negative. The fact that soils must be unsaturated to exhibit collapse encourages the consideration of the unsaturated soil mechanics principles. However, few researchers have attempted to describe collapse behavior in this manner.

Matyas and Radhakrishna (1968) and Escario and Saez (1973) provided experimental data that relates the volume change of a collapsible soil to changes in matric suction while controlling the pore-air and pore-water pressures. Matyas and Radhakrishna (1968) proposed using the concept of state surfaces relating void ratio and degree of saturation of the stress state variables of the soil.

Fredlund and Morgenstern (1977) provided further theoretical and experimental justification for the use of two independent stress state variables (i.e., $(\sigma - u_a)$ and $(u_a - u_w)$) for unsaturated soils, in general. Fredlund and Morgenstern (1977) proposed constitutive relationships for volume changes of an unsaturated soil using the two stress state variables. The equations were equally applicable for either volume increases or decreases in response to a change in the stress state variables. Fredlund and Hasan (1978) proposed a one-dimensional consolidation theory for unsaturated soils. Independent partial differential equations were derived for the water phase and the air phase. Both equations were to be solved simultaneously when a significant excess pore-air pressure was generated. Miranda (1988) simulated the collapse behavior of small earth dams during their first filling, using the concepts of unsaturated soil mechanics.

Theory

The volume change constitutive relationships for an unsaturated soil proposed by Fredlund and Morgenstern (1978) can be written as follows:

$$[1] \quad \frac{dV_v}{V_0} = m_1^s d(\sigma - u_a) + m_2^s d(u_a - u_w)$$

$$[2] \quad \frac{dV_w}{V_0} = m_1^w d(\sigma - u_a) + m_2^w d(u_a - u_w)$$

where:

- dV_v = change in total volume,
- V_0 = initial volume of soil,
- dV_w = change in volume of water,
- $d(\sigma - u_a)$ = change in net normal stress,
- $d(u_a - u_w)$ = change in matric suction,
- m_1^s = coefficient of total volume change with respect to a change in net normal stress at a constant matric suction,
- m_1^w = coefficient of water volume change with respect to a change in net normal stress at a constant matric suction,
- m_2^s = coefficient of total volume change with respect to a change in matric suction at a constant net normal stress, and
- m_2^w = coefficient of water volume change with respect to a change in matric suction at a constant net normal stress.

During inundation, volume change occurs under a constant vertical stress. The pore-air pressures in the soil will be assumed to remain unchanged during collapse. It has been shown experimentally that the pore-air pressure in

the soil may build up by a slight amount but will then quickly dissipate (Rahardjo 1990). For practical purposes, it can then be considered that the variable which changes during inundation is the negative pore-water pressure. Therefore, the constitutive equations applying to inundation can be written as:

$$[3] \quad \frac{dV_v}{V_0} = m_2^s d(-u_w)$$

$$[4] \quad \frac{dV_w}{V_0} = m_2^w d(-u_w)$$

The sign convention for the coefficients in the above equations are in accordance with the suggestions made by Fredlund and Morgenstern (1976). That is, if the change in the stress state variable is in the same direction as the volume change for a particular phase, the sign of the corresponding coefficient is negative. Therefore, the signs for the coefficients m_2^s and m_2^w are negative and positive, respectively, during the collapse mechanism.

The one-dimensional water flow equation during inundation can be derived by equating the divergence of the hydraulic head (as described by the flow law) to the time derivative of the water phase constitutive equation. Darcy's law can be used to describe the flow of water in an unsaturated soil (Childs and Collis-George 1950) and will be assumed to be applicable during the collapse process. The divergence of the hydraulic head describes the rate of water flow, and the time derivative of the water phase constitutive equation represents the water volume changes during inundation.

For the derivation, the soil is assumed to (1) be isotropic, (2) have a continuous air phase with free flow to the boundaries, (3) have a linear constitutive relationship, (4) undergo infinitesimal strains, (5) have coefficients of volume change and permeability that are the functions of matric suction during inundation, and (6) have no effects of air diffusing through water, air dissolving in water, and water vapor movements. The partial differential equation for the water phase in the y -direction can be written as follows:

$$[5] \quad \frac{\partial u_w}{\partial t} = \frac{1}{c_v^w} \frac{\partial^2 u_w}{\partial^2 y} + \frac{\partial c_v^w}{\partial y} \frac{\partial u_w}{\partial y} + \rho_w g \frac{\partial c_v^w}{\partial y}$$

where:

- u_w = pore-water pressure,
- c_v^w = coefficient of consolidation,
- ρ_w = density of water, and
- g = acceleration due to gravity.

Ignoring the effect of the elevation heads, eq. [5] can be rewritten as follows:

$$[6] \quad \frac{\partial u_w}{\partial t} = \frac{1}{c_v^w} \frac{\partial^2 u_w}{\partial^2 y} + \frac{\partial c_v^w}{\partial y} \frac{\partial u_w}{\partial y}$$

Equation [6] can be written in an explicit, finite-difference form as follows:

$$[7] \quad u_w(i, j+1) = u_w(i, j) + \frac{\Delta t}{2\Delta y} [(c_v^w(i+1, j)u_w(i+1, j)) + (c_v^w(i, j)u_w(i-1, j)) - (c_v^w(i, j)u_w(i, j)) - (c_v^w(i+1, j)u_w(i, j))]$$

A computer program can be written for eq. [7] which can be used to predict changes in negative pore-water pressure with respect to time and depth, subsequent to inundation. The variables used in eq. [7] are shown in Fig. 2. The changes in the total volume and water volumes during inundation are computed using eq. [3] and eq. [4].

Experimental program

Laboratory tests on compacted specimens were conducted in two phases (i.e., phase 1 and phase 2). Tests in phase 1 were performed to relate the amount of collapse to the soil properties (i.e., dry density and water content). Tests in phase 2 were conducted to study the effect of initial matric suction on collapse behavior. Six tests were performed to study the effect of initial water content on the amount of collapse at an initial dry density of around 1.6 Mg/m³. Eight tests were conducted to study the effect of initial dry density on the amount of collapse at initial water contents of 12.8 and 7.3% (i.e., four tests on each initial water content).

The soil properties for the phase 2 series of tests were selected to have initial matric suctions within a range that could be measured using tensiometers.¹ At the same time, it was desirable to have a soil that would exhibit a reasonable amount of collapse. Seven tests were performed to study the transient processes of matric suction and volume changes during inundation.

Properties of the soil tested

Indian Head silt, procured from the Saskatchewan Department of Highways, was used for the laboratory testing program. The index properties of the Indian Head silt are shown in Table 1.

The optimum water content for the soil was 13.4% for full standard compaction (AASHTO) and 14.4% for half standard compaction. The maximum dry density for full standard compaction was 1.87 and 1.29 Mg/m³ for half standard compaction.

Equipment

Specimens were statically compacted into an oedometer ring using the compaction mold shown in Fig. 3. The mold is similar to that used by Booth (1977) and Maswoswe (1985). Tensiometers were used to measure the initial matric suction. AGWA-II² thermal conductivity sensors were used to check the measurements of initial matric suction.

Fig. 2. Variables used in the finite-difference method.

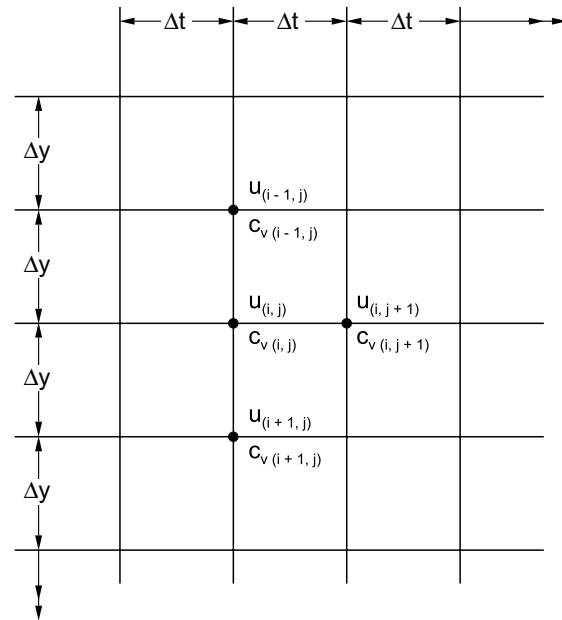


Table 1. Summary of index properties for Indian Head silt.

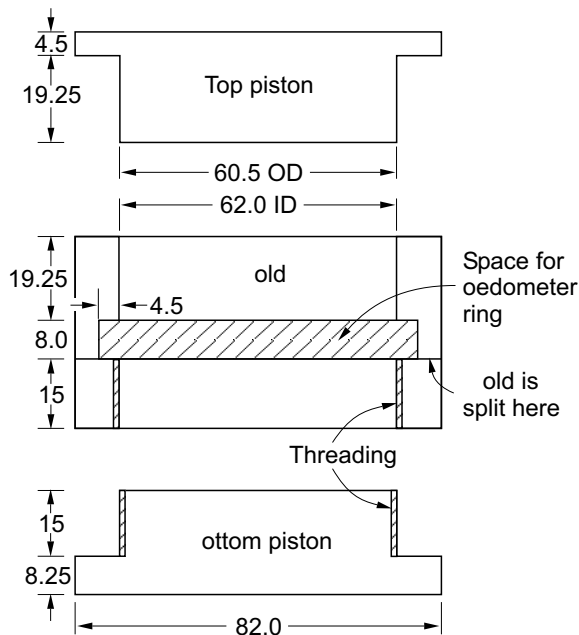
Grain-size distribution	
Sand	62%
Silt	32%
Clay	6%
D_{10}	0.0034 mm
D_{30}	0.025 mm
D_{60}	0.090 mm
Coefficient of uniformity, $C_u = D_{60}/D_{10}$	26.4
Atterberg limits	
Liquid limit, w_L	22.2%
Plastic limit, w_P	16.6%
Plasticity index, PI	5.6
Relative density, G_s	2.68

Three sizes of oedometer rings (types 1, 2, and 3) were used in the laboratory testing program. Oedometer ring type 1 was used in the study of the effect of the soil properties on the amount of collapse. The dimensions of the ring were 19.0 mm in height and 63.0 mm in diameter.

Oedometer ring types 2 and 3 were used in the study of the transient processes involving a change in matric suction and volume change during inundation. The height of oedometer ring type 2 was 25.4 mm and the diameter was 63.0 mm. A hole with a diameter of 7.5 mm was drilled through the side of the oedometer ring. This hole was used to insert the tensiometer tip into the compacted specimen.

Oedometer ring type 3 was used to perform tests, with matric suction measurements (i.e., using tensiometers) taken at different heights along the compacted specimen.

Fig. 3. Compaction mold with oedometer ring inside; dimensions in mm.



The height and diameter of the oedometer ring were 60.0 and 84.9 mm, respectively. Two holes were drilled at a distance of 12.5 mm from the top and bottom of the ring. The third hole was drilled diametrically opposite at the mid-height of the ring.

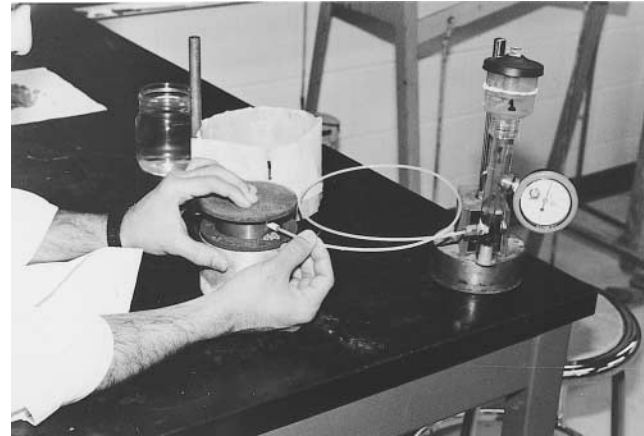
The oedometer pot was adapted with a flexible extension to accommodate the flexible tubing associated with the tensiometers.

Specimen preparation

A soil mass of a known water content was compacted statically into the oedometer ring. The mold shown in Fig. 3 was used to compact the specimens into ring types 1 and 2. After compaction, the soil specimen and the ring were weighed to obtain the initial density of the specimen.

The oedometer ring containing the soil specimen was then firmly held between two porous stones. The specimen was held in this configuration to avoid disturbance when drilling the hole(s) for the tensiometer(s). A hole was drilled horizontally into the compacted specimen through the hole provided in the ring. The drill bit was slightly smaller than the diameter of the tensiometer tip to ensure a good contact between the tensiometer tip and the soil. The depth of the hole was slightly more than the length of the ceramic tip. The ceramic tip of the flexible tube type tensiometer³ was carefully inserted into the compacted specimen as shown in Fig. 4. The slight gap between the end of the ceramic tip and the outer edge of the oedometer ring was filled with representative soil.

Fig. 4. Installation of the tensiometer tip into oedometer ring type 2.



The outer edge of the hole was sealed with silicone gel to prevent water from coming in contact with the tensiometer tip through the hole in the ring. Porous stones were then placed on the top and bottom of the soil specimen. The slight gap between the outer edge of the porous stones and the edge of the ring was sealed with silicone gel to avoid the entry of water into the specimen through this gap. This procedure was used in an attempt to provide uniform wetting of the specimen.

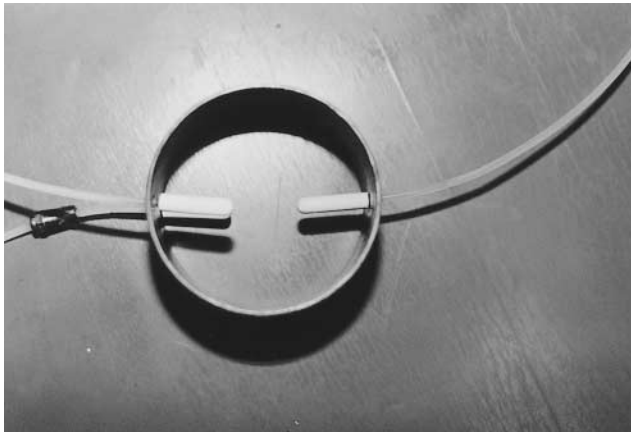
Similar procedures were adopted for the preparation of the specimens for ring type 3. However, the soil was compacted directly into the ring instead of being compacted into the compaction mold. The installation of the tensiometers and the sealing procedures were similar to those used in the preparation of ring type 2 specimens. The arrangement of the three tensiometers along with the cylinder is shown in Fig. 5.

Testing methods

The collapse tests for phase 1 were conducted in a conventional oedometer. The specimen was placed between two air-dried porous stones. The top of the oedometer pot was covered with Saran wrap to minimize moisture loss. The assembly was left for 24 h. The specimen was then loaded every 2 h by doubling the previous load. When the settlement under the applied load was complete, the specimen was inundated with distilled water. Subsequent to saturation of the specimen for 24 h, further loads were applied to the specimen under the saturated condition after the end of 24 h of inundation.

The collapse tests with matric suction measurements were conducted in the modified oedometer with the flexible oedometer pot extension. The entire oedometer pot was covered with Saran wrap. The specimen was left in the above condition until the tensiometer readings came to equilibrium. After reaching the equilibrium condition, a total load was applied to the specimen. The load was in-

Fig. 5. Details of the three tensiometers at different heights in the oedometer ring type 3.



creased every 2 h with a load-increment ratio of approximately 1.0.

The specimen was inundated either from both the top and bottom or from the bottom only. During inundation the matric suction and the dial gauge readings were recorded simultaneously with times, until the matric suction dropped to zero. The final settlement at the end of 24 h of inundation was then recorded and the specimen was unloaded. The ceramic tip was carefully removed from the specimen after unloading and serviced properly for the next test.

Three collapse tests (S1M, S2M, and S3M) were conducted using one tensiometer measurements (i.e., oedometer ring type 2), and one test (S4M) was performed using three tensiometers (i.e., oedometer ring type 3). Initial soil properties (i.e., dry density, ρ_d , water content, w) used for all the four collapse tests are shown in Table 2.

Test results

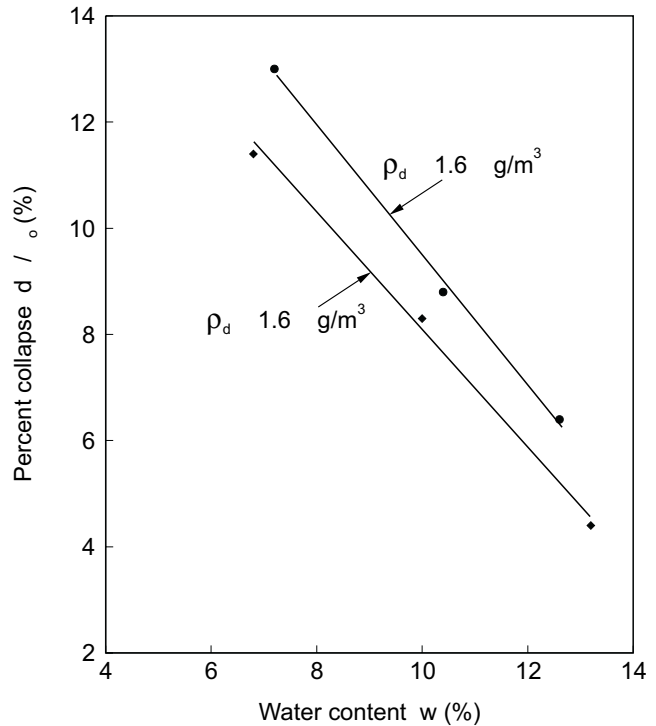
The effect of the initial water content on the amount of collapse of a soil with an initial dry density around 1.6 Mg/m^3 is shown in Fig. 6. The results indicate that the amount of collapse for compacted specimens varies inversely, in a linear fashion, with initial water content for a particular initial dry density. Similarly, the relationship between the initial dry density and the amount of collapse at a constant initial water content also indicates an inverse and linear relationship (Fig. 7). The linear relationships between the amount of collapse and the initial soil properties are in agreement with the observations made by Popescu (1986) and Foss (1973).

The initial matric suction measurements indicated that an initial water content of approximately 12.0% would correspond to a matric suction of approximately 60 kPa, irrespective of the initial dry density. Changes in the matric suction and the total volume during inundation for tests S1M, S2M, and S3M are presented in Figs. 8, 9, and

Table 2. Summary of index properties, inundation pressure, and percent collapse for collapse tests.

Test identification	Description			
	S1M	S2M	S3M	S4M
Dry density, ρ_d (t/m^3)	1.598	1.506	1.405	1.394
Water content, w (%)	11.8	11.79	11.8	12.75
Inundation pressure (kPa)	97	96	99	55
Collapse, dH/H_0 (%)	5.84	11.62	15.26	18.62

Fig. 6. Effect of the initial water content on the amount of collapse.



10, respectively. The inundation pressure and the percent collapse for all the collapse tests are shown in Table 2.

The results obtained from the S1M test indicate that the initial matric suction at the centre of the specimen during inundation was 58 kPa. The results show that there was a significant change of the matric suction during the first minute after inundation. The matric suction continued to drop at a significant rate in the next 6 min and came close to zero in the following 3 min. This implies that the matric suction of the entire specimen dropped to zero in approximately 12 min.

The total volume of the specimen decreased slightly within 6 s after inundation. The volume decreased significantly from 6 s to 5.5 min after inundation. The volume decreased at a slower rate in the next 6–7 min and remained almost constant, 12 min after inundation. The results indicate that the decrease in total volume ceased as the matric suction at the centre of the specimen approached zero. Similar observations can be made from

Fig. 7. Effect of the initial dry density on the amount of collapse.

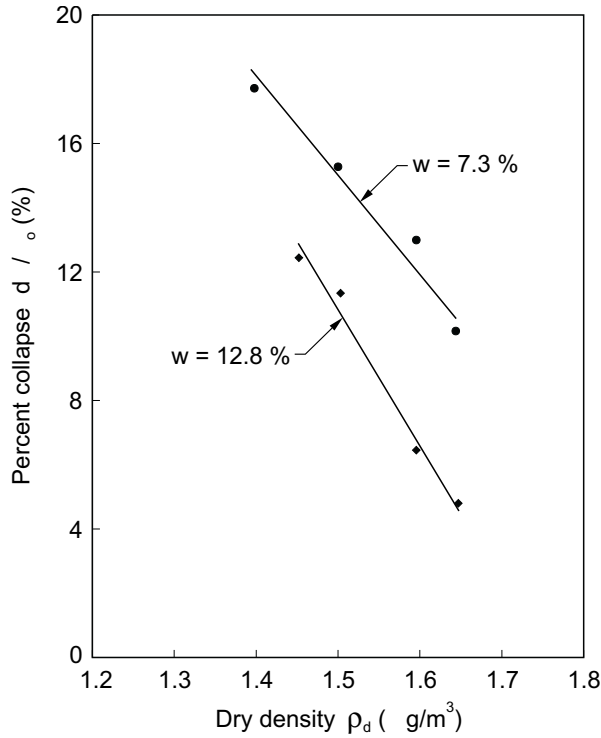


Fig. 8. Matric suction and total volume changes versus time during inundation of test S1M.

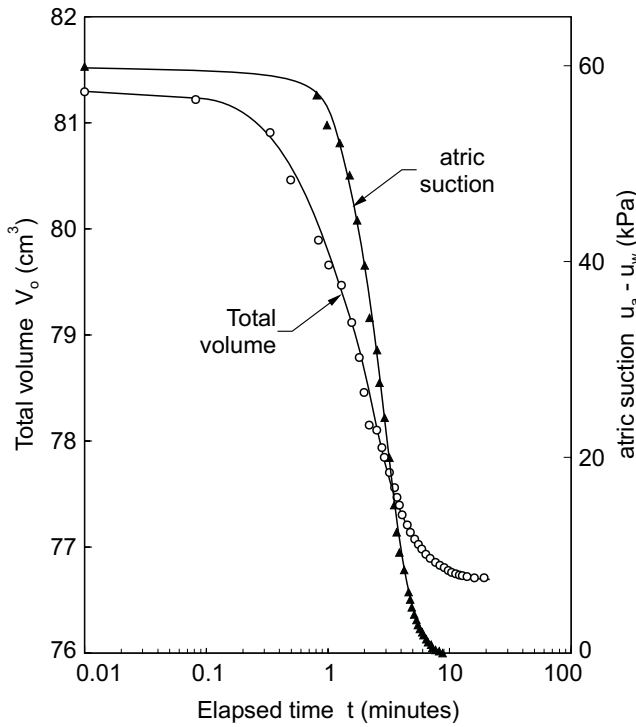


Fig. 9. Matric suction and total volume changes versus time during inundation of test S2M.

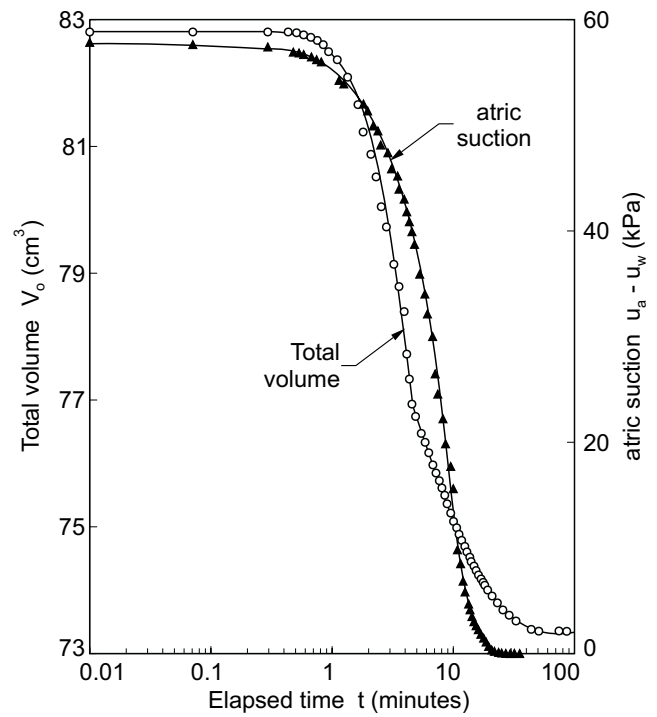
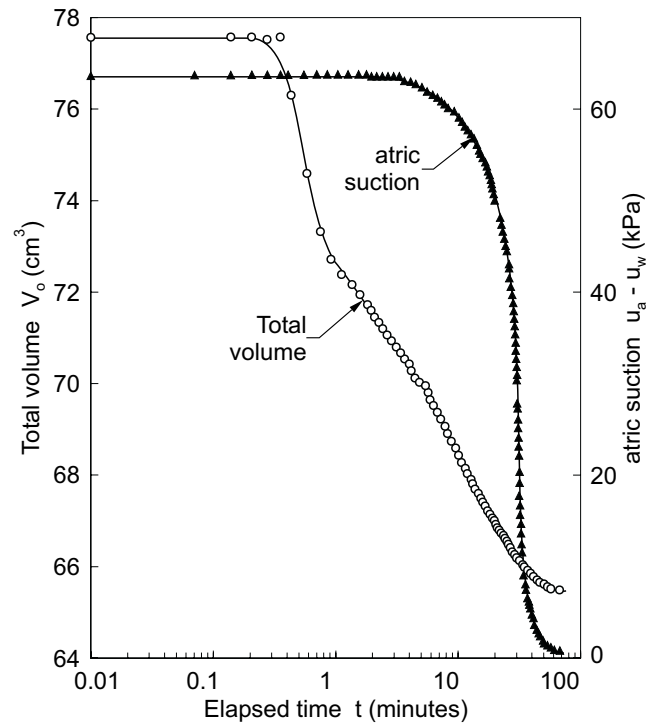
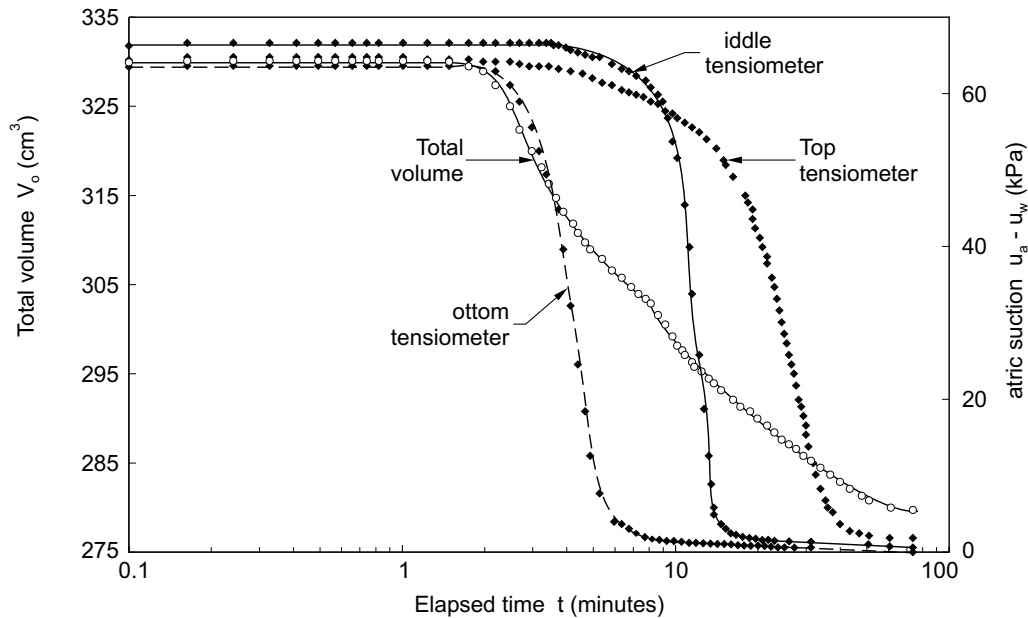


Fig. 10. Matric suction and total volume changes versus time during inundation of test S3M.



the S2M and S3M test results. This observation would appear to indicate that there exists a one-to-one relationship between matric suction changes and total volume changes for collapsible soils during inundation.

Test S4M was conducted using larger specimens in which the changes in the matric suction were measured at three different heights. This test was performed to further verify the one-to-one correspondence of the relationship

Fig. 11. Matric suction and total volume changes versus time during inundation of test S4M.

between matric suction changes and the total volume change during collapse upon inundation. The soil specimen was inundated from the bottom, unlike the previous tests (i.e., S1M to S3M) that were inundated from top and bottom. The changing matric suction at the top, middle, and bottom of the specimen along with the total volume changes are shown in Fig. 11.

The results indicate that the initial matric suction of 64 kPa prior to inundation has dropped to zero around bottom tensiometer in about 9.5 min after inundation. The matric suction at the middle of the specimen did not change significantly during the first 5.5 min after inundation. It then dropped to zero at a significant rate in the following 12 min. The matric suction around the top tensiometer dropped by 7 kPa in the first 10 min after inundation. This was due to the accidental application of a small amount of water to the top of the specimen at the beginning of the test. The wetting of the specimen can be considered as being predominantly from the bottom of the specimen. The matric suction around the top tensiometer dropped to zero by 1 h after inundation. The matric suction in the portion of the specimen above the top tensiometer would have dropped to zero in a couple of minutes after the matric suction around the top tensiometer dropped to zero as the wetting front moved upwards.

The total volume of the specimen remained unchanged during the first 2 min after inundation and then decreased significantly between 2 and 60 min after inundation. The volume of the specimen decreased at a slow rate in the next 20 min, and no further volume change was noticed 80 min after inundation.

The experimental results indicate that there is a one-to-one correspondence relationship between the matric suction and the total volume changes during collapse due to inundation. The volume of the specimen decreased signif-

icantly within 2 min after inundation, and the matric suction around the bottom tensiometer began to drop at about 2.5 min after inundation. The centre of the bottom tensiometer was located at 12.5 mm from the base of the specimen. A decrease in the total volume occurred prior to a decrease being registered on the bottom tensiometer. This decrease in volume was due to the decrease in matric suction in the region below the bottom tensiometer.

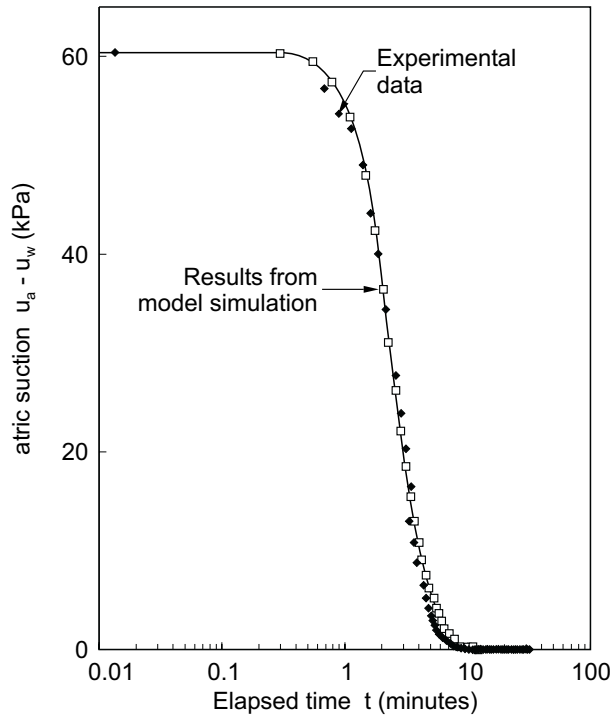
The soil volume decreased at a continuous rate during the next several minutes as the wetting front moved from the bottom to the top of the specimen. The matric suction around the top tensiometer dropped initially because of the accidental leakage of water onto the top of the specimen.

The matric suction around the top tensiometer dropped to zero slightly earlier than the time when no further change in total volume was noticed. This indicates that the volume changes during the last few minutes were due to the decreasing matric suctions in the region above the top tensiometer. The top tensiometer was located at 12.5 mm from the top surface of the specimen. The experimental results clearly indicate that the total volume of the specimen started and continued to decrease until the matric suction in the entire specimen decreased to zero.

Theoretical simulations

Theoretical simulations between the matric suction and the total volume changes during collapse were carried out in accordance with the theory suggested earlier in the paper. A computer program was written to solve the water flow, partial differential equation that was written in a finite-difference form in eq. [7]. The theoretical simulations of all test results indicated that the coefficient of consolidation, c_v^w , varied during inundation. It was higher

Fig. 12. Comparison between the theoretical simulations and experimental results for matric suction changes for test S1M.



than the value deduced from the experimental data using the semilog-plot method suggested by Casagrande (1938) for saturated soils. Best-fit theoretical simulations using a linear variation of the coefficient of consolidation value with respect to matric suction are compared with the experimental results for the S1M test (Fig. 12). The coefficient of consolidation values required to obtain a best-fit are shown in Table 3 against matric suction.

The varying matric suctions at the bottom, middle, and top of the specimen during the S4M test, obtained from the theoretical simulations, are compared with the experimental results in Figs. 13 to 15. The coefficient of consolidation was assumed to vary linearly with matric suction, and the values used to obtain the best-fit are shown in Table 4. Large variations in the coefficient of consolidation and the technique used in programming are the main reasons for numerical instability and scatter in the simulated results shown in Figs. 14 and 15. The accidental application of a small amount of water to the top of the specimen at the beginning of the test is also partly responsible for the scatter in the simulated results, particularly around the top tensiometer.

Matric suction isochrones obtained for the theoretical simulations of test S1M, by using the best fit values of c_v , are shown in Fig. 16. It can be observed from the isochrones that suction is dropping at the top and bottom of the specimen as the specimen was inundated from both ends. These results are in good agreement with the observations from numerical modelling studies by Lloret and Alonso (1980).

Table 3. Summary of coefficients used in S1M test simulation.

Matric suction, $u_a - u_w$ (kPa)	Coefficient of consolidation, c_v^w (cm ² /s)	Coefficient of volume change, m_s^s (L/kPa)
0	6.87E-3	4.7E-4
60.2	1.77E-3	4.7E-4

Theoretical simulations for the total volume changes were computed once the changes in the matric suction in the specimen had been predicted. Best-fit results of the total volume changes for test S1M were obtained using a constant value of m_s^s throughout the process. The measured total volume changes are compared with the “best-fit” simulations in Fig. 17, for test S1M.

The best-fit simulation values obtained for the S4M test are compared with the experimental results in Fig. 18. The simulations were obtained using a linearly varying value of m_s^s with respect to matric suction. The m_s^s values are shown against the respective matric suction values in Table 4.

The comparison between the simulated and the experimental results for changes in the matric suction with respect to time indicate that the theory of the consolidation equation for unsaturated soils can be used to simulate changes in matric suction for soils exhibiting collapse behavior. The values for the coefficient of consolidation were found to vary (usually within about one order of magnitude) during the collapse process. The values of the coefficient of consolidation appear to vary by two orders of magnitude for specimen S4M. This was the thicker soil specimen. The coefficient of consolidation values were found to increase as the degree of saturation of the specimen increased during inundation.

Volume change comparisons between the theoretical simulations and the experimental results also support the use of unsaturated soil theories to predict collapse behavior. Constant values of m_s^s could be used in simulations for higher density soil specimens (i.e., specimens having a dry density equal to or higher than 1.5 t/m³). The m_s^s values were found to be varying linearly with respect to matric suction for the lower density specimens. There was good agreement of the total volume decreases due to inundation for all the tests irrespective of their initial dry density or water content. The m_s^s values were found to decrease with decreasing matric suctions during inundation of the lower density specimens.

The experimental results and the theoretical analyses provide evidence that a reduction in matric suction is the primary cause of a reduction in overall volume when a soil collapses upon inundation. The collapse phenomenon is a gradual process with respect to time, although it does occur over a relatively short period of time. The decrease in volume and changes in matric suction during inundation can be satisfactorily simulated using the concepts and formulations associated with unsaturated soil behavior.

Fig. 13. Comparison between the theoretical analysis and experimental results for matric suction changes at the bottom tensiometer of large specimen from test S4M.

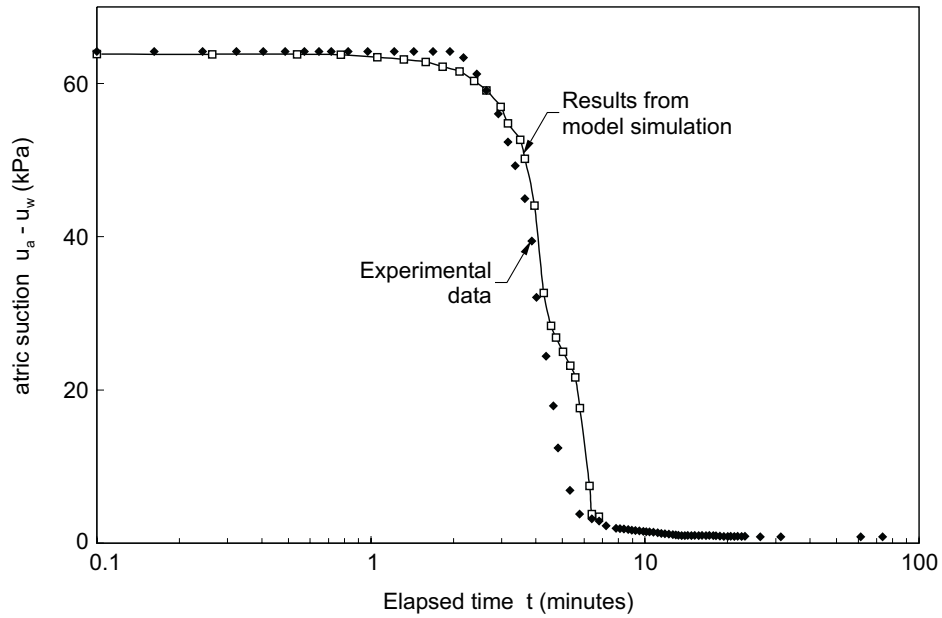
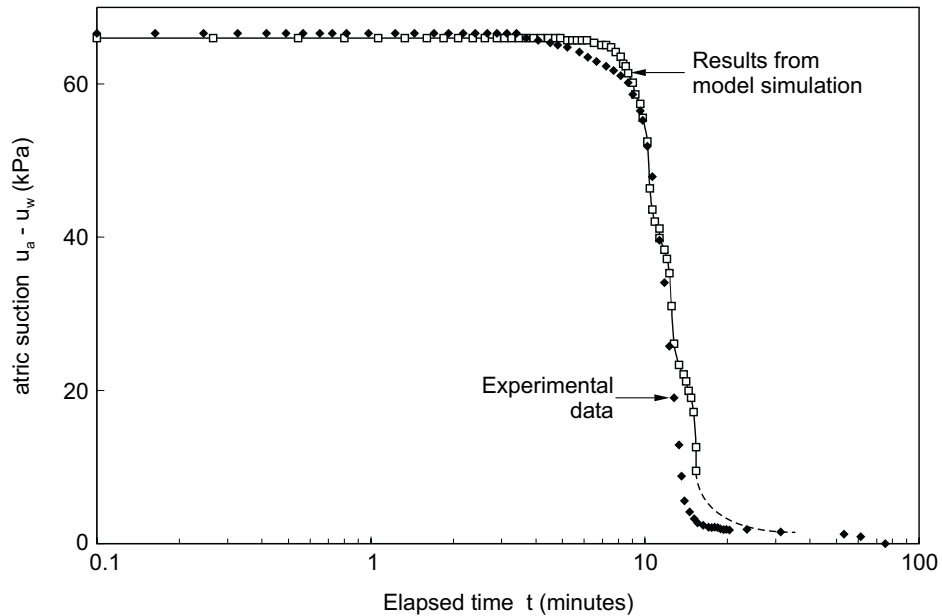


Fig. 14. Comparison between the theoretical analysis and experimental results for matric suction changes at the middle tensiometer of large specimen from test S4M.



Conclusions

The following conclusions can be drawn from the results presented in this paper.

- (1) The collapse phenomenon is primarily related to the reduction of the matric suction during inundation. Matric suction is one of the two stress state variables that control the behavior of an unsaturated soil.
- (2) There is a one-to-one relationship between matric suction and total volume change for a soil exhibiting collapse behavior during inundation.

Table 4. Summary of coefficients used in S4M test simulation

Matric suction, $u_a - u_w$ (kPa)	Coefficient of consolidation, c_v^w (cm ² /s)	Coefficient of volume change, m_2^s (L/kPa)
0	1.0E-2	3.0E-5
20	5.0E-3	8.0E-4
40	4.6E-4	1.6E-3
66.8	1.0E-4	2.6E-3

Fig. 15. Comparison between the theoretical analysis and experimental results for matric suction changes at the top tensiometer of large specimen from test S4M.

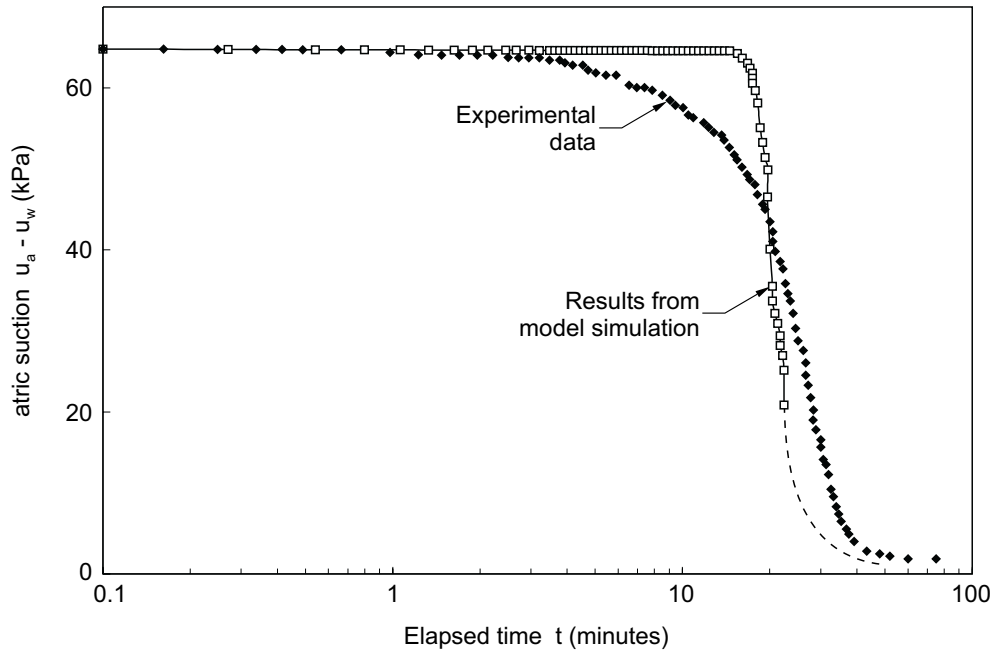


Fig. 16. Matric suction isochrones from S1M test.

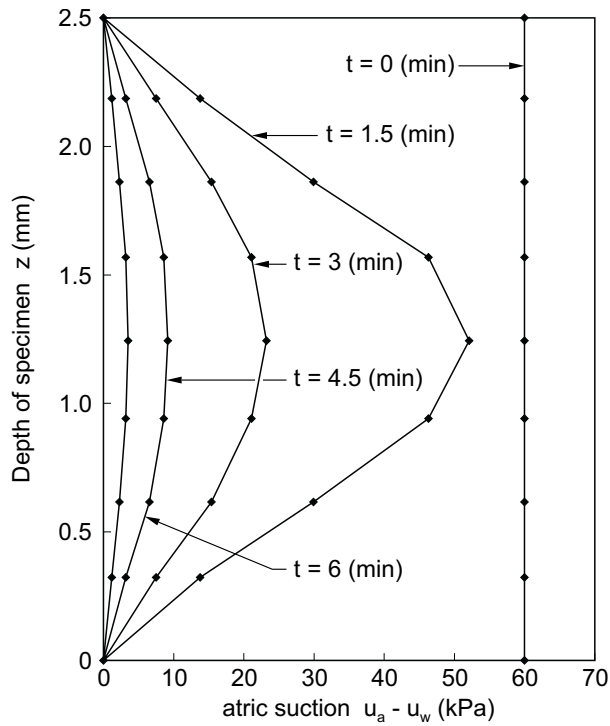
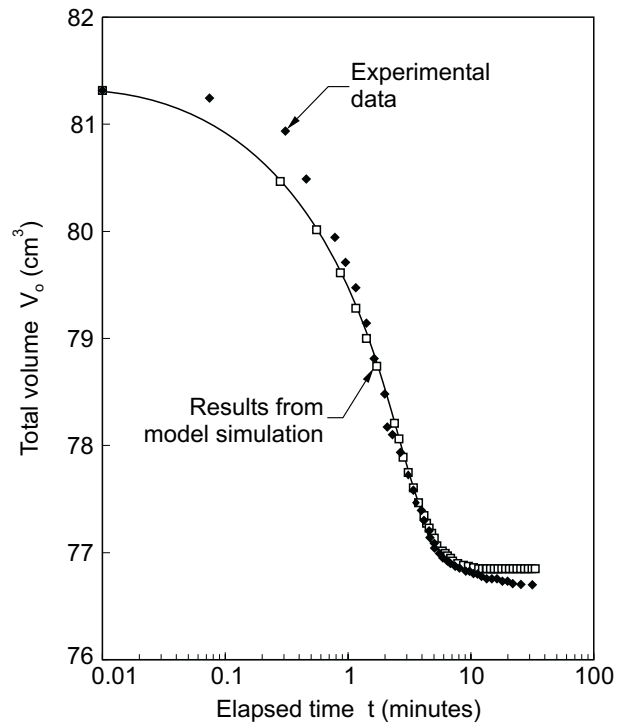


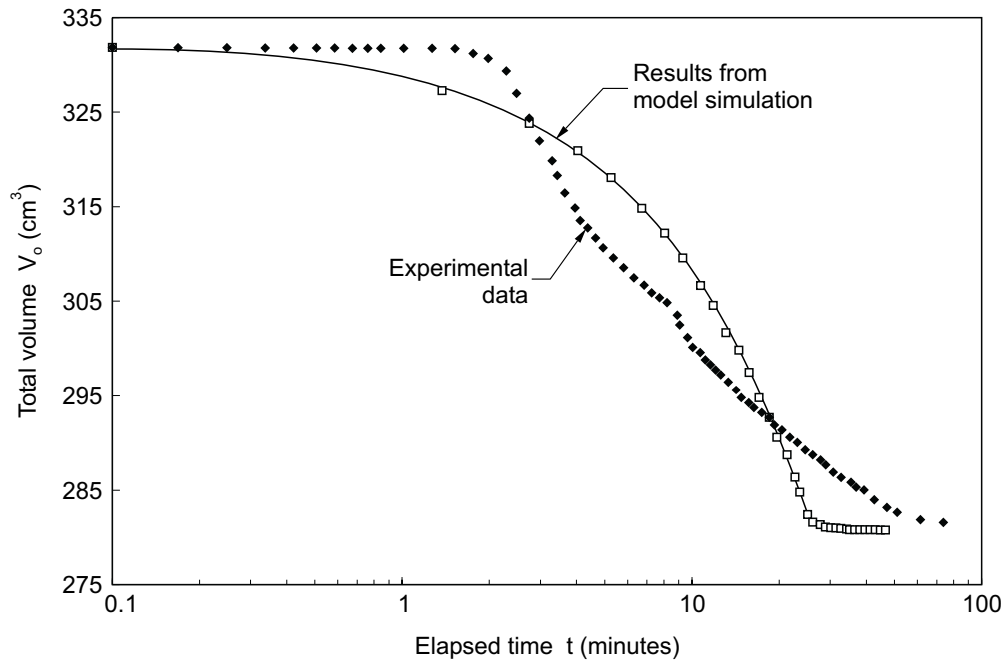
Fig. 17. Comparison between the theoretical analysis and experimental results for total volume changes from test S1M.



- (3) The theory of consolidation for an unsaturated soil can be used to predict the matric suction and total volume changes with respect to time during inundation, for a collapsing soil.
- (4) The experimental data relating matric suction and total volume change during collapse can be obtained

using slight modifications of a conventional oedometer.

- (5) Theoretical situations of matric suction changes indicate that the coefficient of consolidation, c_v^w , of the collapsing soil increases during inundation.

Fig. 18. Comparison between the theoretical analysis and experimental results for total volume changes from test S4M.

- (6) The theoretical simulations of total volume change during collapse indicate that the coefficient of volume change with respect to matric suction, m_v^s , is either constant or decreases (in an absolute sense) with the reduction in matric suction during collapse.

References

- Barden, L., McGown, A., and Collins, K. 1973. The collapse mechanism in partly saturated soil. *Engineering Geology* (Amsterdam), **7**: 49–60.
- Booth, A.R. 1977. Collapse settlement in compacted soils. Council for Scientific and Industrial Research, Research Report 324, National Institute for Transport and Road Research Bulletin **13**: 1–34.
- Burland, J.B. 1965. Some aspects of the mechanical behavior of partly saturated soils. In *Moisture equilibria and moisture changes in soils beneath covered areas*. Butterworths, Sydney, Australia, pp. 270–278.
- Casagrande, A. 1938. Notes on soil mechanics - first semester. Harvard University, Cambridge, MA.
- Childs, E.C., and Collis-George, N. 1950. Permeability of porous materials. *Proceedings of the Royal Society London*, **201**(A): 392–405.
- Clayton, C.R.I. 1980. The collapse of compacted chalk fill. *Proceedings, International Conference on Compaction, Paris, Session 2*.
- Cox, D.W. 1978. Volume change of compacted clay fill. *Proceedings, Institution of Civil Engineers Conference on Clay Fills, London*, pp. 79–86.
- Dudley, J.H. 1970. Review of collapsing soils. *ASCE Journal of the Soil Mechanics and Foundations Division*, **96**(SM3): 925–947.
- Escario, V., and Saez, J. 1973. Measurement of the properties of swelling and collapsing soils under controlled suction. *Proceedings, 3rd International Conference on Expansive Soils, Haifa, Israel, Vol. 1*, pp. 195–200.
- Foss, I. 1973. Red soil from Kenya as a foundation material. *Proceedings, 8th International Conference on Soil Mechanics and Foundation Engineering, Moscow, USSR, Vol. 2.3*, pp. 73–80.
- Fredlund, D.G., and Hasan, J.U. 1978. One-dimensional consolidation theory: unsaturated soils. *Canadian Geotechnical Journal*, **16**: 521–531.
- Fredlund, D.G., and Morgenstern, N.R. 1976. Constitutive relations for volume change in unsaturated soils. *Canadian Geotechnical Journal*, **13**: 261–276.
- Fredlund, D.G., and Morgenstern, N.R. 1977. Stress state variables for unsaturated soils. *ASCE Journal of the Geotechnical Engineering Division*, **103**(GT5): 447–466.
- Holtz, W.G. 1948. The determination of limits for the control of placement moisture in high rolled earth dams. *Proceedings American Society for Testing and Materials*, **48**: 1240–1248.
- Holtz, W.G., and Hilf, J.W. 1961. Settlement of soil foundations due to saturation. *Proceedings, 5th International Conference on Soil Mechanics and Foundation Engineering, Paris, Vol. 1*, pp. 673–679.
- Jennings, J.E., and Knight, K. 1975. A guide to construction on or with materials exhibiting additional settlement due to “collapse” of grain structure. *Proceedings, 6th Regional Conference for Africa on Soil Mechanics and Foundation Engineering, Durban, South Africa, Vol. 1*, pp. 99–105.
- Larionov, A.K. 1965. Structural characteristics of loess soils for evaluating their structural properties. *Proceedings, 6th International Conference on Soil Mechanics and Foundation Engineering, Montréal*, pp. 64–68.
- Lefebvre, G., and Benbelfadhel, M. 1989. Collapse at permeation for a compacted non plastic till. *Proceedings, 12th International Conference on Soil Mechanics and Foundation Engineering, Rio de Janeiro*, pp. 619–622.

- Lloret, A., and Alonso, E.E. 1980. Consolidation of unsaturated soils including swelling and collapse behavior. *Géotechnique*, **30**: 449–477.
- Maswoswe, J. 1985. Stress paths for a compacted soil during collapse due to wetting. Ph.D. thesis, Imperial College, London.
- Matyas, E.L., and Radhakrishna, H.S. 1968. Volume change characteristics of partially saturated soils. *Géotechnique*, **18**: 432–448.
- Meckechnie, W.R. 1989. General report of discussion on collapsible soils. Session 7. Proceedings, 12th International Conference on Soil Mechanics and Foundation Engineering, Rio de Janeiro, Balkema.
- Miranda, A.N. 1988. Behavior of small earth dams during initial filling. Ph.D. thesis, Colorado State University, Fort Collins, CO.
- Popescu, M.E. 1986. A comparison between the behavior of swelling and of collapsing soils. *Engineering Geology (Amsterdam)*, **23**: 145–163.
- Qian, H.J., and Lin, Z.G. 1988. Loess and its engineering problems in China. *In* Engineering Problems of Regional Soils. Proceedings, International Conference on Engineering Problems of Regional Soils, Beijing, China, pp. 136–153.
- Rahardjo, H. 1990. The study of pore-pressure parameters and consolidation behavior of unsaturated soils. Ph.D. thesis, University of Saskatchewan, Saskatoon, SK, Canada.

Resilient modulus constitutive relationships for cohesive soils

D.G. Fredlund, A.T. Bergan, and P.K. Wong

Abstract: The relationships between stress conditions and resilient modulus, which is a necessary input parameter in fatigue design of asphalt concrete pavements, is established. For a cohesive subgrade soil there are relationships between resilient modulus and deviator stress, confining pressure, and matric suction. Proposed constitutive relationships were experimentally checked by using specimens of compacted glacial till from the Qu'Appelle Moraine in Saskatchewan, Canada. Four series of repeated triaxial tests were performed on a repeated-load triaxial system developed at the University of Saskatchewan, Saskatoon. Matric suctions were measured on a pressure plate device immediately after each repeated-load test. Experimental data indicate a good correlation between the resilient modulus and the stress variables. The stress variables of most significance with respect to changes in resilient modulus are deviator stress and matric suction. An equation is proposed by which the resilient modulus of a compacted subgrade soil can be linked to the stress variables.

Key words: cohesive soil, constitutive relationships, resilient modulus, deviator stress, confining pressure, matric suction, triaxial test.

Introduction

The necessity of developing a complete fatigue design program for asphaltic concrete pavements has become increasingly evident in recent years. One of the important input parameters to such a design program is the resilient modulus of the subgrade. Because fatigue prediction is highly sensitive to changes in subgrade resilient modulus, it is not enough to assume one resilient-modulus value for the year; rather a relationship must be established between stress conditions and resilient modulus (Bergan 1972). Previous attempts to develop realistic fatigue simulation may have failed because of inadequate characterization of the subgrade soils.

The research presented here includes a theory that establishes the relationship between stress conditions and resilient modulus. Results of laboratory tests on a subgrade soil are also presented to compliment the developed theory.

Theory

Previous research has shown relations between the volume and weight, the method of sample preparation, the deviator stress, and the resilient modulus of compacted soils (Monismith et al. 1967). However, the authors are not aware of any unique relationships having been estab-

lished among these variables. Establishing a relationship between the resilient modulus and the stress conditions in a soil is imperative in the fatigue design of asphalt concrete pavements.

Fredlund et al. (1975) showed from a stress analysis standpoint that the resilient modulus is a function of three stress variables.

$$[1] \quad M_R = f[(\sigma_3 - u_a), (\sigma_1 - \sigma_3), (u_a - u_w)]$$

where:

M_R = resilient modulus,

σ_3 = confining pressure,

σ_1 = major (vertical) principal stress during the application of the repeated load,

u_a = pore-air pressure (approximately atmospheric),

u_w = pore-water pressure,

$(\sigma_3 - u_a)$ = net confining pressure,

$(\sigma_1 - \sigma_3)$ = deviator stress, and

$(u_a - u_w)$ = matric suction.

In other words, if the above three stress variables were known during a repeated-load test, it would be reasonable to attempt to relate resilient modulus to these variables. Unfortunately, there are serious technical problems associated with measuring air and water pressure under dynamic loading conditions. Relating the resilient modulus to the stresses before or after the repeated-load test may be sufficient.

Under repeated-load conditions, the first 100 repetitions of load have been found to be sufficient to ensure proper seating of the specimen in the testing apparatus (Culley 1971; Dehlen 1969; MacLeod 1971). Continuing to load the specimen up to 100 000 repetitions produces a further change in resilient modulus, and this change is probably related to changes in the stress variables. How-

D.G. Fredlund and A.T. Bergan, Department of Civil Engineering, University of Saskatchewan, 57 Campus Drive, Saskatoon, SK, Canada S7N 5A9.

P.K. Wong, Mitchell McFarlane Brentnall and Partners, Hong Kong.

Reproduced with permission from the Transportation Research Board, *Transportation Research record* 642, 77.73-81, 1977.

ever, because the stresses cannot readily be monitored, it is proposed that the number of repetitions (N) be designated as a further state variable. This paper considers only the effect of the first 100 repetitions.

Figure 1 shows the anticipated linear relationship between resilient modulus and confining pressure for specimens compacted at various water contents. The normal range of confining pressure of interest in the field is approximately 20.7 to 41.4 kPa (3 to 6 psi) and linearity is anticipated in this range (Weimer 1972). At water contents above optimum (i.e., low matric suction), the voids are largely filled with water and an increase in confining pressure produces little change in the resilient modulus. At low water contents (i.e., high matric suction), confining pressure increases produce more substantial increases in resilient modulus.

Figure 2 shows typical variations in resilient modulus for various deviator stresses. The resilient modulus does not vary as much with deviator stress for conditions dry of optimum water content, as it does for conditions wet of optimum water content. The results from previous investigations show relationships that are curved. At high deviator stresses an increase in resilient modulus has sometimes been observed. The practical range of deviator stress is 0 to 83 kPa (0 to 12 psi). In Fig. 3 the relationship between resilient modulus and deviator stress is linearized over the above stress range by plotting resilient modulus on a logarithm scale.

In extending the logarithmic resilient modulus versus deviator stress back to a deviator stress equal to zero, two variables can be used to define each line: namely, the slope of the line on the semilogarithmic plot (m_{1d}) and the intercept on the ordinate (c_{1d}). Each line is therefore described by the equation,

$$[2] \quad \log M_R = c_{1d} - m_{1d}(\sigma_1 - \sigma_3)$$

where:

c_{1d}, m_{1d} = functions of matric suction.

In this way, the resilient modulus is also related to the third stress variable, ($u_a - u_w$).

Since the resilient modulus is expected to be more highly affected by deviator stress and matric suction than by net confining pressure, the effect of confining pressure could either be ignored or a correction could be applied for confinement. The correction equation would take the following form (Fig. 1):

$$[3] \quad \Delta M_R = m_c \Delta(\sigma_3 - u_a)$$

where:

ΔM_R = change in resilient modulus,

m_c = slope of the plot for confining pressure versus resilient modulus, and

$\Delta(\sigma_3 - u_a)$ = change in confining pressure from that used to define the plot for resilient modulus versus deviator stress.

The relationships between c_{1d}, m_{1d} and matric suction must be experimentally determined. The form is not yet definite but should become better established with further

Fig. 1. Anticipated relation between resilient modulus and confining pressure.

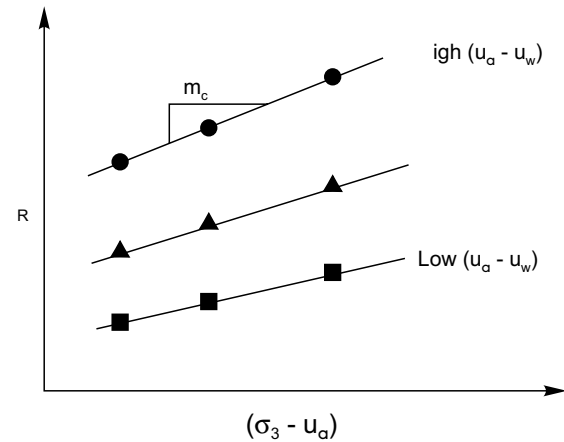


Fig. 2. Anticipated relation between resilient modulus and deviator stress.

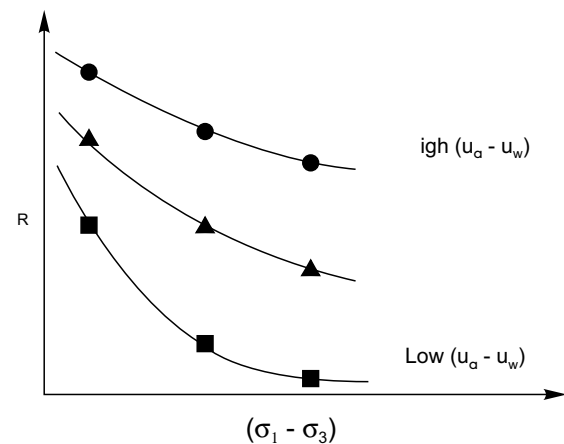
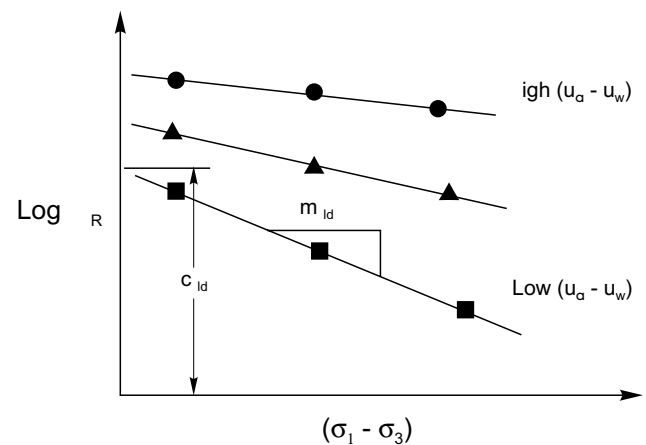


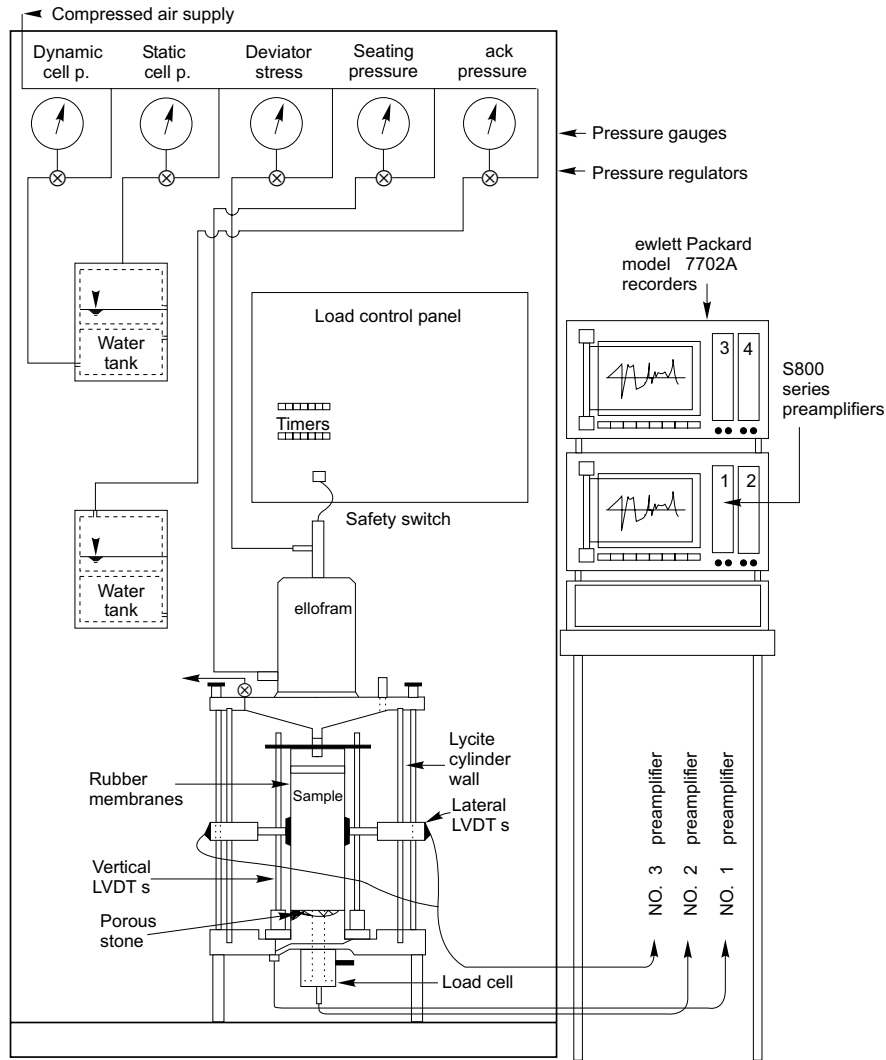
Fig. 3. Linearization of relation between resilient modulus and deviator stress.



testing. The degree of uniqueness of the proposed equations must be established experimentally by subjecting specimens to varying stress paths or methods of sample preparation and comparing the results by using the proposed equation. The relationship between resilient modu-

lus and matric suction (for a particular deviator stress)

Fig. 4. Repeated-load triaxial system.



can also be obtained by cross-plotting for resilient modulus versus water content and matric suction versus water content (Fredlund et al. 1975).

Laboratory equipment

The repeated-load apparatus (Fig. 4) consists of a reinforced triaxial cell with a bellofram operated on compressed air to apply the deviator load. The cell was filled with air. The loading frequency was 20 repetitions/min with a load duration of 0.1 s. The load applied to the specimen was measured by a load cell in the base plate of the triaxial cell. The vertical and lateral displacements of the specimen were measured using linear variable differential transducers. The matric suctions were measured by placing the specimen on a high-air-entry disk [i.e., either 0.5 or 1.5 MPa (5 or 15 bars)] and using the axis-translation procedure to nullify the negative water pressures.

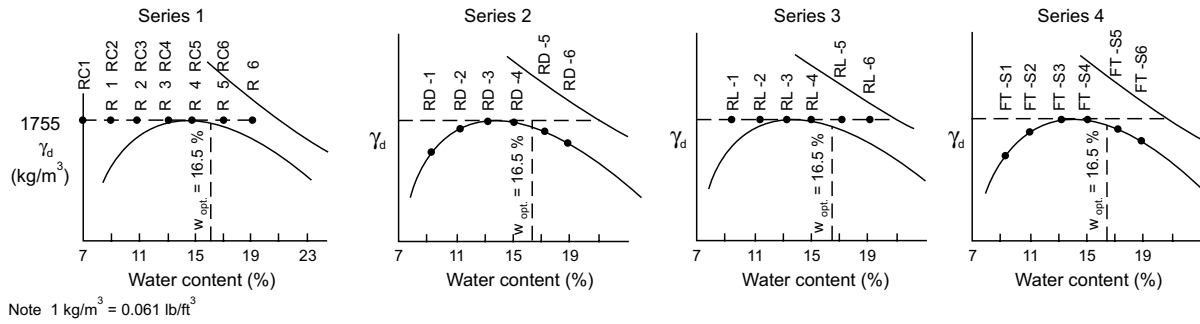
Soil samples

The soil used in the study was a glacial till obtained from the Qu'Appelle Moraine in Saskatchewan. Its properties are summarized in Table 1.

The soil specimens were prepared by air drying, pulverizing, sorting on a 2-mm (No. 10) sieve, and then mixing with the appropriate amount of distilled water. The wet soil was placed in a plastic bag and stored in a high humidity room for 24 h. The specimens were 15.2 cm (6 in) in length and 7.1 cm (2.8 in) in diameter and were formed by static compaction in three lifts. The specimens were wrapped in plastic, waxed, and stored for at least 7 days before testing.

Test program

The test program was designed to evaluate the relationships between resilient modulus, M_R , deviator stress, $(\sigma_1 - \sigma_3)$, confining pressure, $(\sigma_3 - u_a)$, and matric suc-

Fig. 5. Dry density and water contents for four test series.**Table 1.** Soil properties of Qu'Appelle Moraine, Saskatchewan.

Property	Measurement
Liquid limit, %	33.9
Plastic limit, %	17.0
Sand, %	31.8
Silt, %	38.5
Clay, %	29.7
Specific gravity	2.77
Maximum standard density, kg/m ³	1767
Optimum water content, %	16.5
Modified AASHO density, kg/m ³	1967
Optimum AASHO water content, %	11.9

Note: 1 kg/m³ = 0.06 lb/ft³

tion, ($u_a - u_w$). The resilient modulus was calculated after 100 load repetitions; the effect of larger numbers of repetitions was not evaluated.

The test program consisted of four test series; data for dry density, γ_d , and water content are given in Table 2 and shown in Fig. 5 (Wong 1975). For all specimens, an attempt was made to measure the matric suction at the top, middle, and bottom of the specimen (in some cases only two measurements were possible).

Series 1 specimens were prepared at maximum standard density and water contents ranging from 7 to 19 percent. Each specimen was tested for deviator stresses, σ_d , of 20.6, 48.2, 82.7, and 103.4 kPa (3, 7, 12, and 15 psi). The confining pressure, ($\sigma_3 - u_a$), was kept at 20.7 kPa (3 psi) in all cases. The results from Series 1 allowed a study of the resilient modulus versus deviator stress and matric suction relationships when the dry density is kept constant.

Series 2 was the same as the first series except that the dry density varied with water content in accordance with the standard compaction curve. The results allowed a study of the resilient modulus, M_R , versus deviator stress and matric suction relationships when the dry density varied.

Series 3 specimens were prepared at maximum standard density. Tests were run at deviator stresses of 48 and 69 kPa (7 and 10 psi). The confining pressures on each specimen were 20.7, 68.9, 137.9, and 275.8 kPa (3, 10, 20, and 40 psi). Each confining pressure was allowed 8 h for equalization. The results allowed a study of the resilient

Table 2. Dry densities and water contents for four test series.

Specimen	Water content (%)	γ_d (kg/m ³)
Series 1		
RC-1	7	109.6
RB-1 and RC-2	9	109.6
RB-2 and RC-3	11	109.6
RB-3 and RC-4	13	109.6
RB-4 and RC-5	15	109.6
RB-5 and RC-6	17	109.6
RB-6	19	109.6
Series 2		
RD-1	9	90.0
RD-2	11	97.2
RD-3	13	102.8
RD-4	15	108.0
RD-5	17	109.4
RD-6	19	104.4
Series 3		
RL-1	9	109.6
RL-2	11	109.6
RL-3	13	109.6
RL-4	15	109.6
RL-5	17	109.6
RL-6	19	109.6
Series 4		
FT-S1	9	90.0
FT-S2	11	97.2
FT-S3	13	102.8
FT-S4	15	108.0
FT-S5	17	109.4
FT-S6	19	104.4

Note: 1 kg/m³ = 0.06 lb/ft³.

modulus versus confining pressure and matric suction relationships.

Series 4 specimens were prepared at a constant dry density and varying water contents and then subjected to three freeze-thaw cycles. The purpose of freeze-thaw cycles was to check the consistency of the resilient modulus versus stress-variable relationships when the soil structure was modified or disturbed. The confining pressure was 21 kPa (3 psi) and the deviator stresses were 20.7, 34.5, 48.3, and 82.7 kPa (3, 5, 7, and 12 psi).

Table 3. Results of test Series 1.

Specimen	Water content (%)	γ_d (kg/m ³)	S^1 (%)	$(\sigma_3 - u_a)$ (kPa)	$(u_a - u_w)^2$ (kPa)	M_R (kPa)			
						$\sigma_d = 20.6$ kPa	$\sigma_d = 48.2$ kPa	$\sigma_d = 82.7$ kPa	$\sigma_d = 103.4$ kPa
RB-1	11.4	1751	55.4	20.7	469	32 476	28 476	25 443	23 443
RB-2	13.5	1752	65.5	20.7	345	61 021	43 301	22 616	28 270
RB-3	15.2	1772	76	20.7	269	52 057	47 713	33 027	28 339
RB-4	17.7	1749	85.6	20.7	207	61 917	39 991	15 376	6 619
RB-5	20.8	1703	93.2	20.7	186	41 715	12 066	10 687	5 902
RB-6	21.9	1740	104.5	20.7	172	3 068	3 254	3 652	—
RC-1	9	1693	40	20.7	896	124 041	109 424	100 391	89 635
RC-2	11	1664	46.6	20.7	558	99 564	129 626	90 531	93 358
RC-3	13.1	1732	61.6	20.7	355	54 677	39 026	34 958	32 131
RC-4	15.3	1700	68.5	20.7	293	80 465	46 472	28 683	19 720
RC-5	17	1728	79.4	20.7	217	32 613	18 134	7 495	6 268
RC-6	19.4	1703	87.1	20.7	205	31 579	8 481	6 019	6 392

Note: 1 kg/m³ = 0.06 lb/ft³; 1 kPa = 0.145 psi.

¹ Degree of saturation.

² Values estimated from matric suction versus water content plot.

Table 4. Results of test Series 2.

Specimen	Water content (%)	γ_d (kg/m ³)	S^1 (%)	$(\sigma_3 - u_a)$ (kPa)	$(u_a - u_w)$ (kPa)	M_R (kPa)			
						$\sigma_d = 20.7$ kPa	$\sigma_d = 48.3$ kPa	$\sigma_d = 82.7$ kPa	$\sigma_d = 103.4$ kPa
RD-1	11.3	1414	33.1	20.7	751	37 785	—	—	—
RD-2	13.1	1530	45.7	20.7	530	46 334	36 337	23 167	—
RD-3	15	1586	56.5	20.7	262	34 475	31 441	21 099	17 375
RD-4	17.3	1727	80.6	20.7	188	70 329	38 129	15 790	12 273
RD-5	19	1735	90	20.7	131	24 408	13 170	7 240	—
RD-6	21.2	1653	88.1	20.7	93	—	—	—	—

Note: 1 kg/m³ = 0.06 lb/ft³; 1 kPa = 0.145 psi.

¹ Degree of saturation.

Table 5. Results of test Series 3.

Specimen	Water content (%)	γ_d (kg/m ³)	S^1 (%)	$(u_a - u_w)$ (kPa)	$(\sigma_1 - \sigma_3)$ (kPa)	M_R (kPa)			
						$(\sigma_3 - u_a) = 20.7$ kPa	$(\sigma_3 - u_a) = 68.9$ kPa	$(\sigma_3 - u_a) = 137.9$ kPa	$(\sigma_3 - u_a) = 275.8$ kPa
RL-1	11.7	1711	51.2	792	48	97 564	112 871	115 078	143 899
RL-2	12.1	1749	58.3	800	48	65 916	106 666	117 284	156 448
RL-3	14.3	1725	66.5	778	69	116 457	116 526	95 978	162 998
RL-4	15.1	1767	74.9	734	69	53 092	66 744	72 811	88 049
RL-5	17.4	1764	86.2	469	69	26 684	29 580	28 270	32 544
RL-6	19.4	1759	95.2	262	69	14 273	20 340	22 823	27 097

Note: 1 kg/m³ = 0.06 lb/ft³; 1kPa = 0.145 psi.

¹ Degree of saturation.

Presentation and discussion of data

The resilient modulus values for Series 1, 2, 3, and 4 are summarized in Tables 3, 4, 5, and 6, respectively.

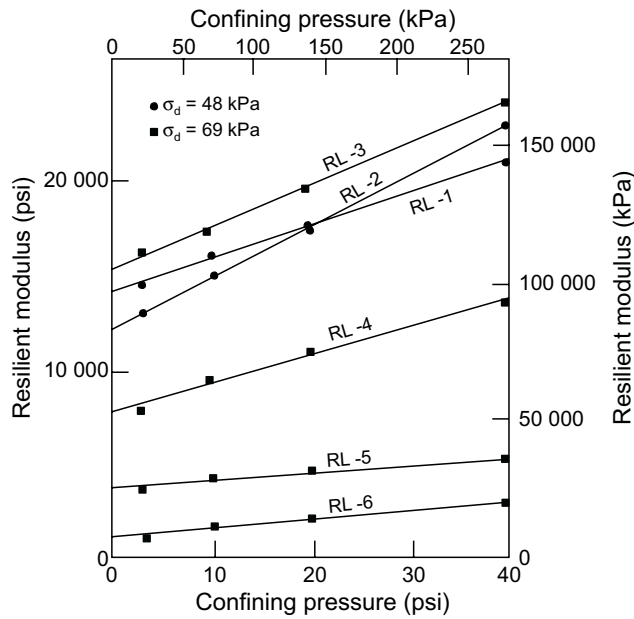
Figure 6 shows the changes in resilient modulus versus confining pressure ($\sigma_3 - u_a$) for a wide range of water contents (Series 3). The changes in resilient modulus with confining pressure are linear and more pronounced for water contents below optimum. The slopes of the resilient

Table 6. Results of test Series 4.

Specimen	Water content (%)	γ_d (kg/m ³)	S^1 (%)	$(\sigma_3 - u_a)$ (kPa)	$(u_a - u_w)$ (kPa)	M_R (kPa)			
						$\sigma_d = 20.7$ kPa	$\sigma_d = 34.5$ kPa	$\sigma_d = 48.3$ kPa	$\sigma_d = 82.7$ kPa
FT-S1	11.4	1296	33.9	21	731	14 342	—	—	—
FT-S2	13.2	1506	44	21	483	42 473	—	21 237	11 101
FT-S3	15.2	1624	57.8	21	272	29 511	—	10 412	—
FT-S4	17.5	1724	81.4	21	169	9 239	4 013	5 364	9 998
FT-S5	19.5	1719	89.9	21	97	3 186	—	3 944	—
FT-S6	19.9	1680	86.4	21	66	8 412	15 721	11 101	—

Note: 1 kg/m³ = 0.06 lb/ft³; 1kPa = 0.145 psi.
¹Degree of saturation.

Fig. 6. Resilient modulus versus confining pressure for specimens of test series 3, labelled RL-1 to RL-6.

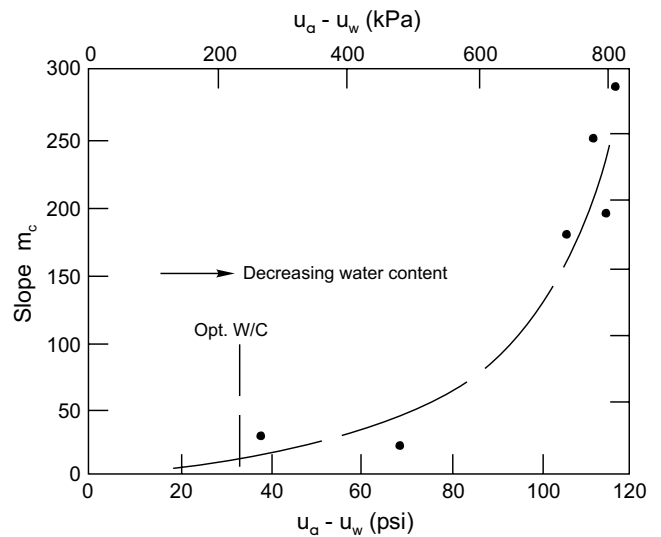


modulus versus confining pressure relation are plotted versus matric suction in Fig. 7. The slopes decrease to a relatively low value as the water content is increased. It should be noted that the confining pressure has been varied over a wide range and that field water contents will generally be in the vicinity of (or above) optimum conditions.

The results confirm that the confining pressure is relatively insignificant. Therefore, the proposed procedure of applying a correction for the confining pressure appears justifiable. The authors recommend that a constant slope, m_c , corresponding to the optimum water content conditions be used in the correction equation.

The resilient modulus versus deviator stress, $(\sigma_1 - \sigma_3)$, can be plotted from Series 1, 2, and 4. Figure 8 shows an arithmetic plot of the tests on the specimens of test series 1, labelled RC-1 to RC-6. The plots exhibit a charac-

Fig. 7. Slope of confining pressure versus resilient modulus for various matric suctions.



teristic decrease in resilient modulus with increasing deviator stress. At water contents above optimum there is some strain-hardening effect at deviator stresses greater than 83 kPa (12 psi). The curves for resilient modulus versus deviator stress can be linearized on a semi-logarithmic plot. Figures 9, 10, and 11 show the semi-logarithmic plots of test series 1 (RB and RC specimens) and test Series 2. Test series 4 was not plotted because of the erratic results following freeze-thaw cycles.

The slopes and intercepts of the semi-logarithmic plots of resilient modulus versus deviator stress are given in Table 7 and are shown plotted versus matric suction in Figures 12 and 13, respectively. The slope, m_{1d} , is shown to increase as matric suction decreases. The scatter within an individual series shows that it is not possible to differentiate between the specimens prepared at constant dry densities and those with dry densities that vary according to the standard compaction curve. One result from the freeze-thaw specimens indicates an increase in slope, m_{1d} .

Fig. 8. Arithmetic plot of resilient modulus versus deviator stress for specimens of test Series 1, labelled RC-1 to RC-6.

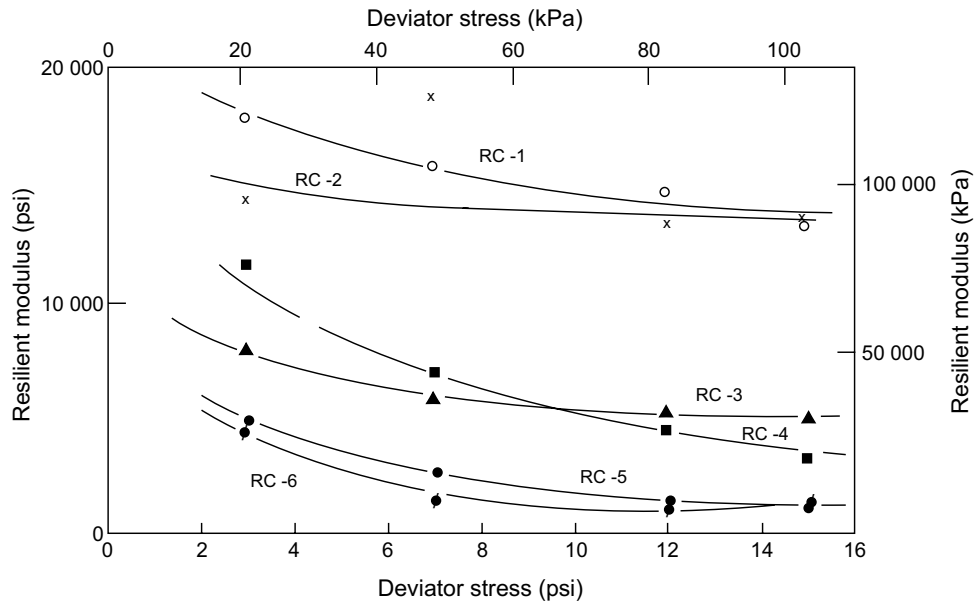
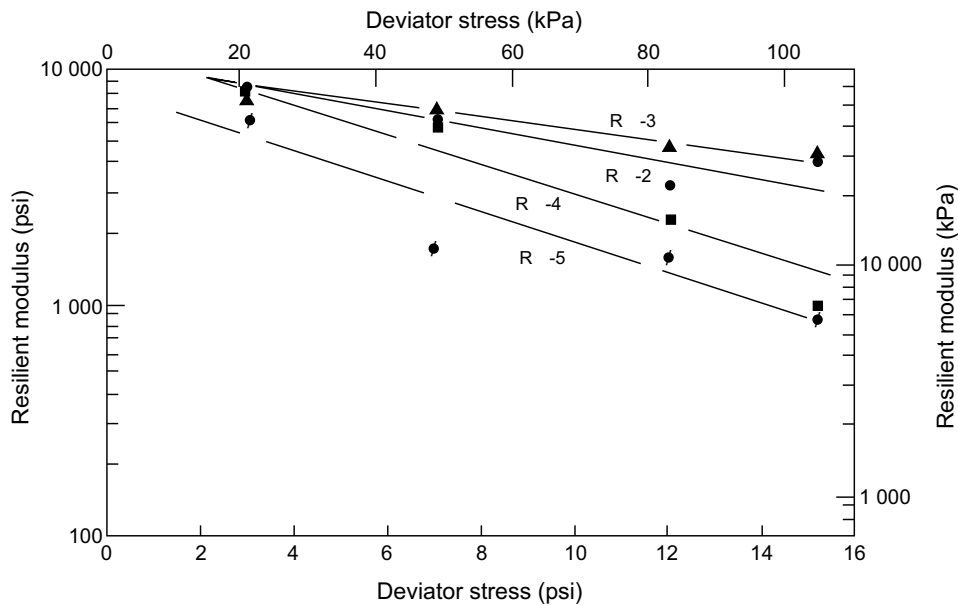


Fig. 9. Resilient modulus versus deviator stress for specimens of test Series 1, labelled RB-2 to RB-5.



The logarithm of the intercept corresponding to zero deviator stress, c_{1d} , shows a decrease as matric suction decreases (Fig. 13). Again, the scatter within a test series is greater than the variations produced by varying the dry density.

The best-fit lines (dashed portion) from Figs. 12 and 13 were used to obtain the intercept, c_{1d} , and slope, m_{1d} , values to be substituted into eq. [2]. By assuming various deviator stresses, a family of curves of resilient modulus versus matric suction was derived (Fig. 14). The trend of the plots is similar to that presented in the cross-plotting technique of Fredlund et al. (1975).

Figure 15 shows the relationships between matric suction and water content, and Fig. 16 shows the relationship between resilient modulus and water content for the specimens tested. The best-fit lines through each set of data were cross-plotted, and the results are superimposed in Fig. 13. The resilient-modulus values used in cross-plotting correspond to a deviator stress of 48 kPa (7 psi). The results from eq. [2] show good agreement with the results obtained by the cross-plotting technique.

The results from the proposed eq. [2] show that the plot of resilient modulus versus matric suction can be highly non-linear in the region of low matric suction. That non-linearity grows more pronounced as the deviator

Fig. 10. Resilient modulus versus deviator stress for specimens of test Series 1, labelled RC-1 to RC-6.

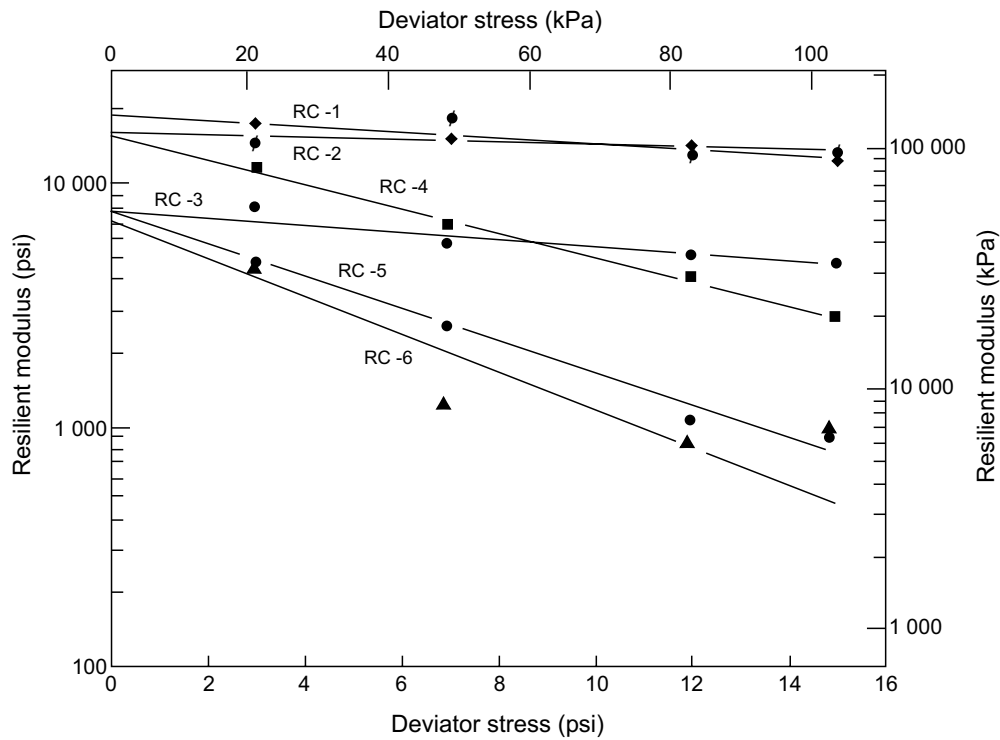
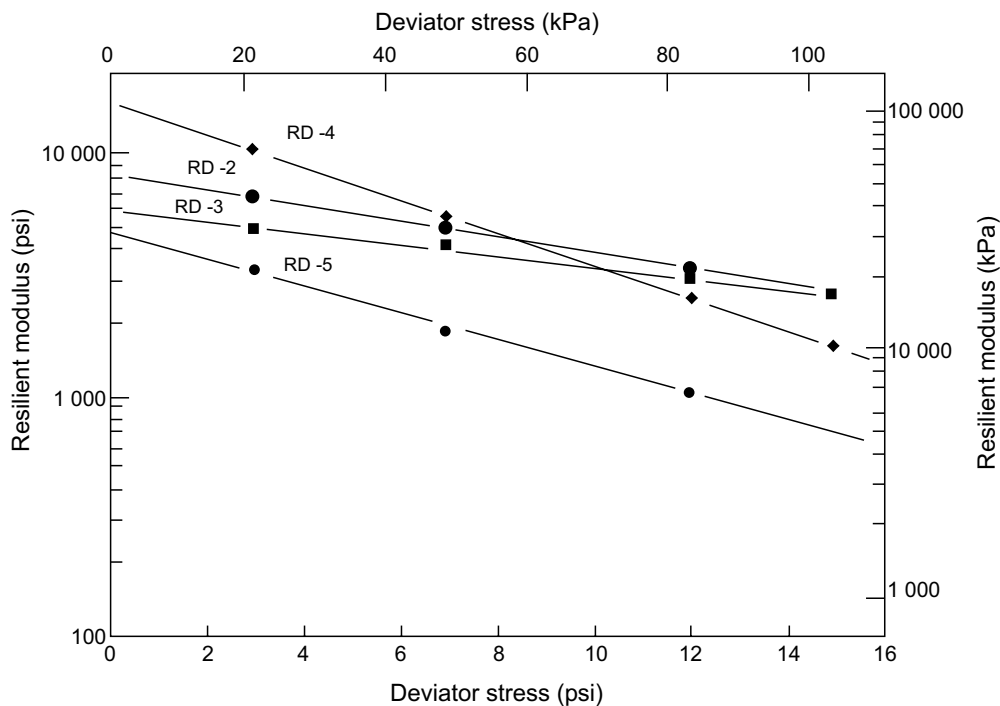


Fig. 11. Resilient modulus versus deviator stress for specimens of test Series 2, labelled RD-2 to RD-5.



tor stress is increased. There is also a reversed non-linearity in the high matric suction range.

The slopes, m_{1d} , (Fig. 12) and intercepts, c_{1d} , (Fig. 13) showed that the scatter within one series of tests was similar to that experienced between the different series.

Therefore, eq. [2] appeared to be unique in its accuracy in representing resilient modulus.

Considering the typical ranges for the stress variables, it is possible to assess the significance of each stress in terms of corresponding changes in resilient modulus. As

Fig. 12. Slopes versus matric suction.

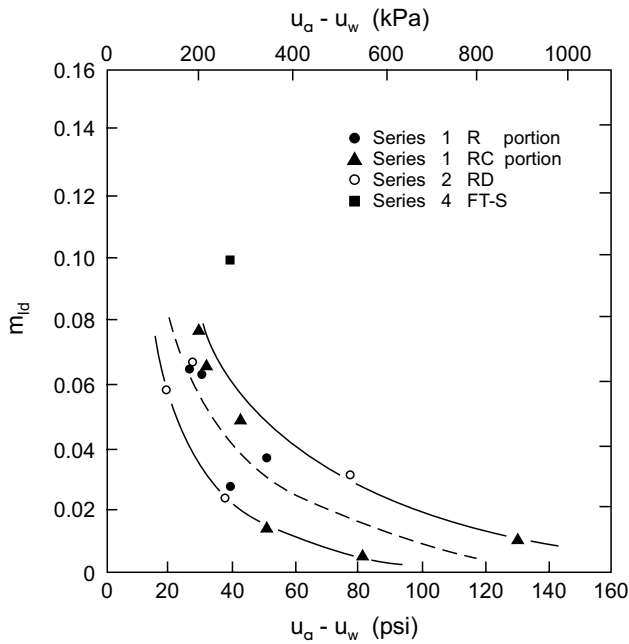
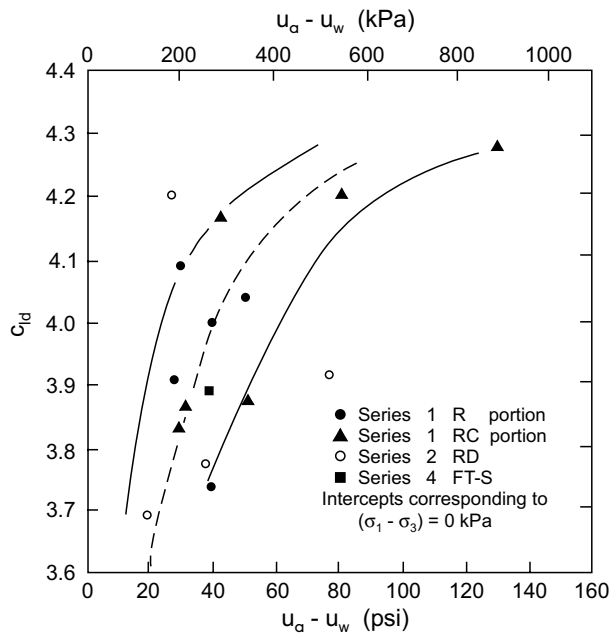


Fig. 13. Logarithm of resilient modulus for zero deviator stress versus matric suction.



given in Table 8, at a water content near optimum, the deviator stress is the most significant stress variable, the matric suction is also significant, but the confining pressure has little significance (1 kPa = 0.145 psi)

Summary

The resilient modulus of a compacted subgrade soil can be linked to the stress variables by eq. [2], which ap-

Table 7. Slopes and intercepts of resilient modulus versus log of deviator stress plots.

Specimen	$(u_a - u_w)^1$ (kPa)	m_{1d}	M_r intercept (kPa)	c_{1d}
RB-2	345	0.0360	75 845	4.041
RB-3	269	0.0272	71 019	4.013
RB-4	207	0.0624	84 119	4.086
RB-5	186	0.0641	55 850	3.908
RC-1	896	0.0108	131 005	4.279
RC-2	559	0.0052	110 320	4.204
RC-3	355	0.0140	52 402	3.881
RC-4	293	0.0477	103 425	4.176
RC-5	217	0.0649	51 023	3.869
RC-6	205	0.0764	46 886	3.832
RD-2	530	0.0312	56 539	3.914
RD-3	262	0.0234	41 370	3.778
RD-4	188	0.0668	112 389	4.212
RD-5	131	0.0578	34 475	3.699
FT-S2	483	0.0854	77 914	4.053
FT-S3	272	0.0989	53 781	3.892

Note: 1 kPa = 0.145 psi.
¹ Matric suction value is in doubt.

Table 8. Significance of stress variables.

Stress variable	Approximate change in field (kPa)	Change in resilient modulus (kPa)
$(\sigma_1 - \sigma_3)$	0 to 83	43 439
$(u_a - u_w)$	227 to 0	24 132
$(\sigma_3 - u_a)$	21 to 41	69

pears to be unique within the limits of accuracy of the resilient modulus measurements. The effect of confining pressure appears to be negligible for the soil tested.

The recommended testing program to evaluate c_{1d} and m_{1d} for eq. [2] is as follows:

- (1) Specimens should be compacted at various water contents and densities and a compactive-energy input comparable to field placement conditions should be used.
- (2) Each specimen should be subjected to at least 100 repetitions of deviator stresses ranging from 21 to 83 kPa (3 to 12 psi).
- (3) After the completion of the repeated-load test, two or three matric-suction tests should be performed on smaller specimens cut from the tested specimens.

Because of the difficulty of obtaining reproducibility in the measurements of resilient modulus, the procedure should be repeated on three carefully prepared specimens at each chosen water content and density. The testing program showed that it was extremely difficult to get reproducibility of resilient modulus on specimens in cases in which the structure had been modified by freeze-thaw cycles.

Fig. 14. Cross-plotted relationships for resilient modulus versus matric suction.

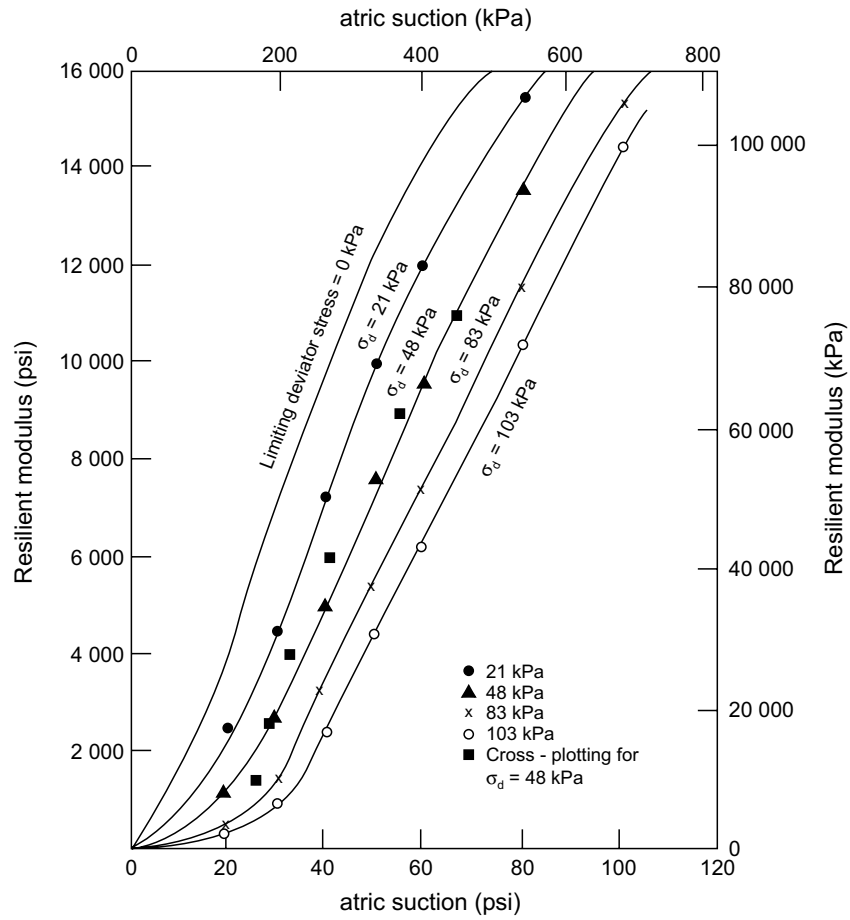


Fig. 15. Matric suction versus water content.

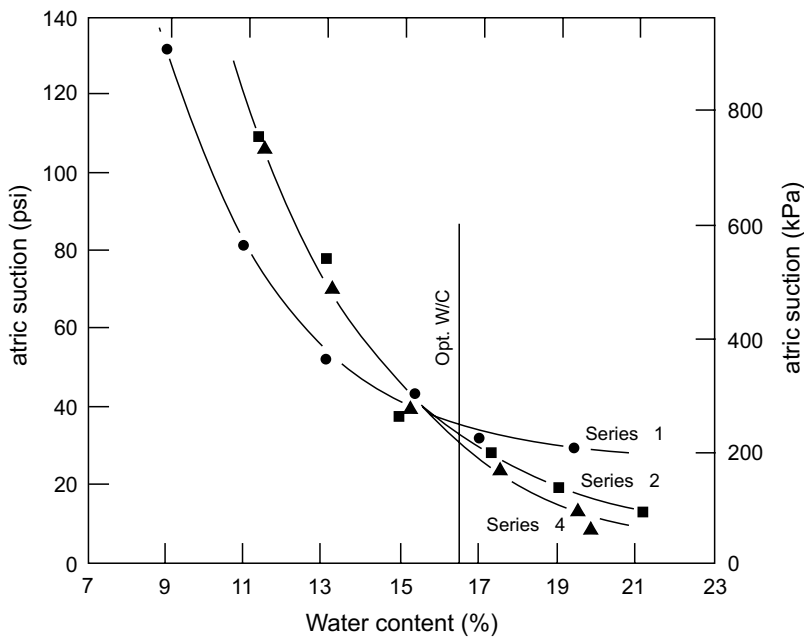
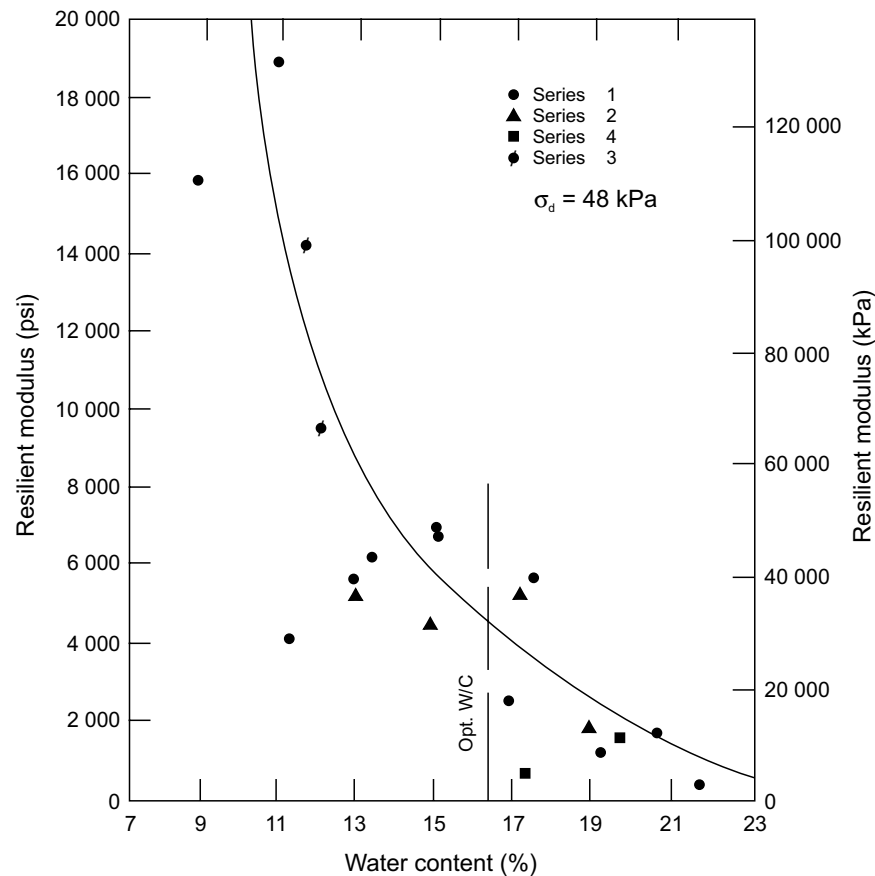


Fig. 16. Resilient modulus versus water content.

Acknowledgements

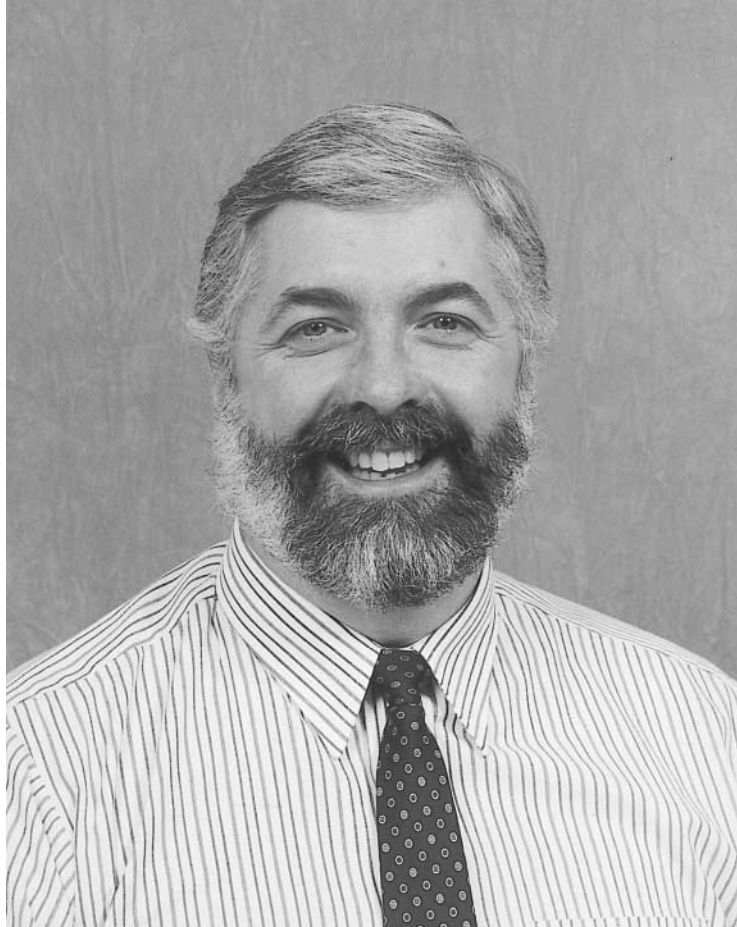
The authors wish to thank the Saskatchewan Department of Highways for their financial support of the resilient modulus research studies at the University of Saskatchewan, Saskatoon. The data used in this paper are taken from a thesis written by P.K. Wong at the University of Saskatchewan, Saskatoon, Canada.

References

- Bergan, A.T. 1972. Some considerations in the design of asphalt concrete pavements in cold regions. Ph.D. thesis, University of California, Berkeley, CA.
- Culley, R.W. 1971. Effect of freeze-thaw cycling on stress-strain characteristics and volume change of a till subjected to repetitive loading. *Canadian Geotechnical Journal*, **8**(3): 359–371.
- Dehlen, G.L. 1969. The effect of non-linear material response on behavior of pavements subjected to traffic loads. Ph.D. thesis, University of California, Berkeley, CA.
- Fredlund, D.G., Bergan, A.T., and Sauer, E.K. 1975. Deformation characteristics of subgrade soils for highways and runways in northern environments. *Canadian Geotechnical Journal*, **12**(2): 213–223.
- MacLeod, D.R. 1971. Some fatigue considerations in the design of thin pavements. M.Sc. thesis, University of Saskatchewan, Saskatoon, SK, Canada.
- Monismith, C.L., Seed, H.B., Mity, F.G., and Chan, C.K. 1967. Prediction of pavement deflections from laboratory tests. Proceedings, 2nd International Conference on Structural Design of Asphalt Pavements, University of Michigan, Department of Civil Engineering, College of Engineering, Ann Arbor, MI, August 7 - 11, pp. 109–140.
- Weimer, H.F. 1972. The strength, resilience and frost durability characteristics of a lime-stabilized till. M.Sc. thesis, University of Saskatchewan, Saskatoon, SK, Canada.
- Wong, P.K. 1975. Resilient modulus constitutive relationships for cohesive subgrade soils. M.Sc. thesis, University of Saskatchewan, Saskatoon, SK, Canada.

Part VII

Moisture Flux Boundary Conditions at Ground Surface



Dr. G. Ward Wilson
Department of Civil Engineering
University of Saskatchewan
Saskatoon, Saskatchewan, Canada

Introduction and Overview

The behaviour of unsaturated soils is described using constitutive relationships and stress state variables. Soil properties such as the coefficient of permeability and the coefficients of volume change, for example, are used together with the change in stress state to determine the amount of heave and associated rate of volume change. It can generally be said that soil properties remain relatively constant for the design life of most engineered structures. If this is true, it can also be said that changes in soil behaviour can be attributed to changes in the stress state variables (i.e., total stress ($\sigma - u_a$) and matric suction ($u_w - u_a$)). This would be the case for problems such as heave under a floor slab or the loss of shear strength in an earth embankment.

The ability to predict the behaviour of unsaturated soils requires the ability to predict changes in the stress state variables, particularly those changes related to matric suction. Changes in total stress are easily calculated. Changes in pore-water pressure and pore-air pressure are more difficult to determine as they respond to flow in the water and air phases. These flows are controlled by both the short-term and long-term stress state boundary conditions at the ground surface.

The ground surface is a dynamic boundary which is driven by short-term atmospheric forcing conditions. While the ground surface is truly a moisture flux boundary condition, it is also useful to understand the meaning of long-term equilibrium conditions. The location of the groundwater table is a measure of this condition; while at the same time noting that the suction conditions near to the surface are related to climatic conditions.

The saturated soil, unsaturated soil, and atmosphere profile is a continuous system with respect to the flow of energy and mass. Thermal dynamic equilibrium exists at most time scales between the liquid pore-water and water vapour in the matrix of an unsaturated soil profile. Water flow is the dominant mass flux between the water table and the atmosphere. Conductive heat flow and latent heat transfer due to water changing phase between liquid water and water vapour are the primary heat fluxes. Heat and mass transfer in unsaturated soil is coupled through the latent heat term associated with flow in the vapour phase.

Water is delivered to the ground surface through rainfall and snow melt as liquid but can only be removed as vapour through the processes of evaporation and evapotranspiration. Thermal dynamic continuity between soil and atmospheric waters at the soil/atmosphere boundary is provided by the vapour phase.

The well known Lord Kelvin relationship can be used to relate negative pore-water pressure to relative humidity for water vapour in air. For example, a value of matric suction of 1500 kPa at 20°C in the soil at the ground surface corresponds to a vapour pressure of 2.3 kPa and a relative humidity of 98.9% in the air phase of the soil. Given an air temperature of 20°C with a relative humidity of 50% in the atmosphere above the soil surface, an equivalent value of suction of approximately 100 000 kPa is computed for the water vapour in the atmosphere. A gradient exists for the stress state of the water in the soil and the overlying air. Whether it is expressed as water vapour pressure, relative humidity, or suction, the flow of water to the atmosphere from the soil will occur through the vapour phase. Evaporation of liquid pore-water in the soil occurs in response to this vapour flux.

The key to solving heat and mass transfer problems in the unsaturated soil profile between the water table and the ground surface is the definition of the flux boundary condition at the soil-atmosphere boundary. The infiltration of liquid water can be readily calculated on the basis of precipitation events. Precipitation events, while responsible for all water delivered to the ground surface, are usually a short-term flux boundary condition. The flux boundary condition at the soil surface is an evaporative flux boundary condition most of the time, particularly in arid and semi-arid regions of the world.

The primary hindrance to the evaluation of ground surface moisture fluxes is related to the prediction of the “actual” evaporation and evapotranspiration from the ground surface. Recent studies using a couple heat and mass transport theory for the soil-atmosphere zone have shown that it is possible to estimate the actual evapotranspiration from the ground surface.

Four papers that provide a rational basis for the evaluation of the moisture flux boundary condition at the ground surface and the associated heat and mass transfer in the unsaturated soil profile below the ground surface are presented in this section. The first paper by Dakshanamurty

and Fredlund provides a comprehensive flow model for air, water, water vapour, and heat in unsaturated swelling soils. Three partial differential equations describing the flow of water, air, and heat are presented. The equations for moisture flow and air flow are coupled and solved simultaneously.

The other papers present a coupled soil-atmosphere model for soil evaporation. A method of analysis for predicting the actual rate of evaporation from unsaturated non-vegetated soil surfaces is given. The model uses a system of equations for coupled heat and mass transfer in soil. The study shows that Dalton's Law and a modified form of the Penman Equation can be used to compute the actual rate of evaporation based on suction at the soil surface.

The relationship between soil suction and the ratio of the actual evaporation to the potential evaporation from a soil surface is a function of the total suction (i.e., matric suction plus osmotic suction) at the soil surface. This is shown to be true for all soil types including clay, sand, and silt with experimental results presented in the third paper for the effect of soil suction on evaporative fluxes from soil surfaces. This finding is of great significance for the analysis of ground surface moisture flux boundary conditions and has been successfully applied in engineering design.

A method of analysis to predict plant transpiration for problems in geotechnical engineering is also presented. A vegetative canopy is normally found at the surface of the soil. Plants extract liquid water in the soil through their roots and transpire the water as vapour to the atmosphere through their leaves. The value of total suction in the root zone is usually between 0 and 1500 kPa (i.e., 1500 kPa is the permanent wilting point for most plants). In contrast, the value of total suction at the surface of the leaves is typically in the range of 100 000 kPa (i.e., RH of 50% at 20°C), thus a gradient for moisture movement and transpiration is created. A model is presented for computing the actual rate of transpiration on the basis of the potential rate of evaporation established by climatic conditions and the suction values in the root zone. The validity of the method is demonstrated with experimental results.

In summary, the studies presented in this section provide a rational basis for the analysis of moisture flux boundary conditions at the ground surfaces. The ability to evaluate flux boundary conditions is paramount for problems in unsaturated soils where transient conditions with respect to matric suction prevail. These problems included the analysis of heave in expansive soils, the stability of unsaturated-saturated soil slopes, the bearing capacity of pavement structures, and the analysis of seepage through various soil structures.

Part VII
Moisture Flux Boundary Conditions at Ground Surface

- Wilson, G.W., Fredlund, D.G., and Barbour, S.L. 1994. Coupled soil-atmosphere modeling for soil evaporation. *Canadian Geotechnical Journal*, **31**(2): 151–161 657
- Wilson, G.W., Barbour, S.L., and Fredlund, D.G. 1997. The effect of soil suction on evaporative fluxes from soil surfaces. *Canadian Geotechnical Journal*, **34**(1): 145–155 . . . 670
- Tratch, D.J., Fredlund, D.G., and Wilson, G.W. 1995. An introduction to analytical modeling of plant transpiration for geotechnical engineers. *Proceedings, 48th Canadian Geotechnical Conference, Vancouver, B.C., Vol. 2*, pp. 771–780 681
- Dakshanamurthy, V., and Fredlund, D.G. 1981. A mathematical model for predicting moisture flow in an unsaturated soil under hydraulic and temperature gradients. *Water Resources Journal*, **17**(3): 714–722 687

Coupled soil-atmosphere modeling for soil evaporation

G.W. Wilson, D.G. Fredlund, and S.L. Barbour

Abstract: Traditional methods of evaluating evaporation provide an estimate of the maximum or potential rate of evaporation determined on the basis of climatic conditions. Methods such as these are appropriate for open water or fully saturated soil surfaces. Actual rates of evaporation from unsaturated soil surfaces are generally greatly reduced relative to the potential rate of evaporation. A theoretical model for predicting the rate of evaporation from soil surfaces is presented in this paper. The model is based on a system of equations for coupled heat and mass transfer in soil. Darcy's Law and Fick's Law are used to describe the flow of liquid water and water vapour, respectively. Heat flow is evaluated on the basis of conductive and latent heat fluxes. Dalton's Law is used to calculate the rate of soil water evaporation to the atmosphere based on the suction at the soil surface. The soil-atmosphere model was used to predict evaporation rates, water content profiles, and temperature profiles for a controlled column evaporation test over a 42 day period. The values computed by the soil-atmosphere model agreed well with the values measured for two columns of Beaver Creek sand in the evaporation test.

Key words: modeling, evaporation, unsaturated soil, soil surfaces, moisture flux.

Introduction

Prediction of the moisture flux boundary condition with respect to water flow across the soil-atmosphere boundary is essential for many problems in geotechnical engineering. Examples include the design of soil cover systems for the long-term closure of hazardous-waste sites, saturated-unsaturated groundwater flow modeling, and the prediction of heave for shallow foundations on expansive soils.

Two principal processes govern the exchange of water between the soil surface and the atmosphere. Water enters the soil surface as liquid through the process of infiltration. Alternately, water exfiltrates from the soil surface as vapour through the process of evaporation. The process of infiltration depends primarily on soil properties such as hydraulic conductivity and is reasonably well understood. The evaluation of the evaporative fluxes from a soil surface is more difficult, since the rate of evaporation depends on both soil properties and climatic conditions. Accurate prediction of evaporative fluxes is critical, for example, in the design of soil cover systems which are to function as oxygen barriers for mine tailings that produce acid drainage.

This paper presents a theoretical approach for the evaluation of evaporative fluxes based on measured soil properties and climatic conditions. The theoretical model is

used to simulate evaporative fluxes for comparison with the measured results from a sand column evaporation test conducted under controlled climatic conditions. The theoretical approach presented considers nonvegetated or bare soil surfaces. This work forms the basis of a more general formulation that could incorporate the effects of a vegetative cover on evaporation rates from soil surfaces.

Background

Engineers have traditionally used a term defined as potential evaporation, PE, to estimate evaporation or evapotranspiration rates. The term, which has been in use for at least 40 years, was first introduced by Thornthwaite (1948). Potential evaporation may be defined as the upper limit or maximum rate of evaporation from a pure water surface under given climatic conditions. The potential rate of evaporation may be computed using the Dalton-type equation (Gray 1970);

$$[1] \quad E = f(u)(e_s - e_a)$$

where:

E = rate of evaporation (mm/day),

e_s = saturation vapour pressure of water at the temperature of the surface (mm Hg or kPa),

e_a = vapour pressure of the air in the atmosphere above the water surface (mm Hg or kPa), and

$f(u)$ = turbulent exchange function that depends on the mixing characteristics of the air above the evaporating surface.

The use of the apparently simple expression given in eq. [1] is considered a direct approach (van Bavel 1967; Granger 1989). However, the application of eq. [1] to field problems can be difficult. Accurate evaluation of the turbulent exchange function requires either an empirical

G.W. Wilson. Assistant Professor, Department of Civil Engineering, University of Saskatchewan, Saskatoon, SK, Canada, S7N 5A9.

D.G. Fredlund, and S.L. Barbour. Professors, Department of Civil Engineering, University of Saskatchewan, Saskatoon, SK, Canada S7N 5A9.

Reproduced with permission from the *Canadian Geotechnical Journal*, 31: 151-161, 1994.

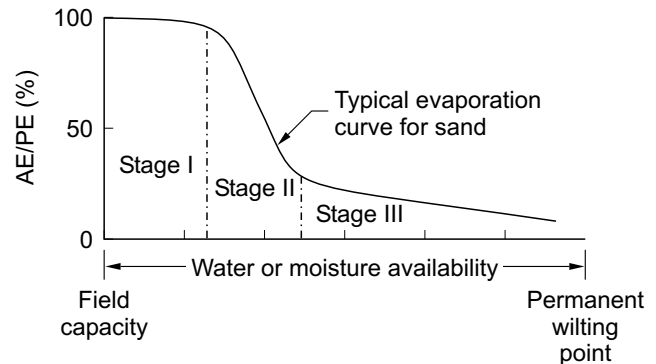
approach or the application of rigorous aerodynamic profile methods. Furthermore, eq. [1] is often indeterminate when applied to field studies because of difficulties associated with the evaluation of surface temperatures and vapour pressure (Granger 1989). The Dalton equation is generally not applied in the elementary form stated in eq. [1]. However, eq. [1] forms the basis for the widely used Penman method. Penman (1948) resolved the difficulty associated with surface temperature in eq. [1] by combining it with a second simultaneous equation for the sensible heat flux at the surface. Penman (1948) also provides a relatively simple method for determining the turbulent exchange function on the basis of mean wind speed. The Penman method assumes the surface to be saturated at all times and therefore provides an estimate of the potential rate of evaporation.

Numerous other methods are available for calculating the rate of potential evaporation. These include the temperature-based method proposed by Thornthwaite (1948) and the energy-based method developed by Priestley and Taylor (1972). Although all of the various methods for potential evaporation may predict different rates of evaporation when applied to a specific site (Granger 1989), all methods attempt to predict a maximum or potential rate of evaporation. The fundamental assumption used by the methods outlined above is that water is freely available at the surface for evaporation. In other words, the surface is an open water surface or a saturated soil surface.

The actual rate of evaporation, AE, begins to decline as the surface becomes unsaturated and the supply of water to the surface becomes limited (Gray 1970; Morton 1975; Brutsaert 1982). Figure 1 shows a typical relationship for the ratio of actual evaporation and potential evaporation, AE/PE, versus water availability for a sand surface. Gray (1970) presents similar curves for sand and clay surfaces. The rate of actual evaporation is approximately equal to the potential rate (i.e., AE/PE equal to 100%) when the sand is saturated or nearly saturated (i.e., water content at or above the field capacity). The rate of AE/PE decreases as the sand surface becomes drier and eventually falls to a low, relatively constant residual value as the sand surface desiccates to the permanent wilting point for plants.

The shape of the drying curve shown in Fig. 1 is well known and has been described by others including Hillel (1980). In general, the curve is described as having three stages of drying. Stage I drying is the maximum or potential rate of drying that occurs when the soil surface is at or near saturation and is determined by climatic conditions. Stage II drying begins when the conductive properties of the soil no longer permit a sufficient flow of water to the surface to maintain the maximum potential rate of evaporation. The rate of evaporation continues to decline during Stage II drying as the surface continues to desiccate and reaches a slow residual value defined as Stage III drying. Hillel (1980) states that the slow rate of evaporation during Stage III drying occurs after the soil surface becomes sufficiently desiccated to cause the liquid-water phase to become discontinuous. The flow of liquid water to the surface ceases and water molecules may only migrate to the surface through the process of

Fig. 1. The relationship between the rate of actual evaporation and potential evaporation (i.e., AE/PE) and water availability.



vapour diffusion. In summary, it can be seen that the rate of actual evaporation from a soil surface is controlled by both climatic conditions, which define the potential rate of evaporation, and soil properties such as hydraulic conductivity and vapour diffusivity.

Since the actual rate of evaporation is controlled by both climatic conditions and soil properties, accurate prediction of the actual rate of evaporation from soil surfaces requires a method of analysis that includes both factors. The methods previously outlined (i.e., the use of eq. [1] or the Penman method) are based on climatic conditions such as temperature, relative humidity, wind speed, and net radiation. These methods are reliable only for special conditions where the rate of evaporation is controlled solely by climatic conditions (i.e., Stage I drying). The climate-based methods of analysis for potential evaporation often over-estimate actual evaporation rates, since the actual rate of evaporation is soil limited. This is frequently the case for unsaturated soil surfaces in arid and semi-arid environments (Wilson 1990). Geotechnical engineers are often required to predict evaporative fluxes under these conditions. A method that includes both atmospheric conditions and soil properties is required.

The method given by Penman (1948) for predicting the potential rate of evaporation has been modified a number of times for application to nonpotential conditions (Monteith 1965; Shuttleworth and Wallace 1985; Choudhury and Monteith 1988). These extended forms of the Penman equation incorporate a number of soil and canopy resistance terms to reduce the computed rate of evaporation and evapotranspiration (Stannard 1993). In general, the resistance terms for the soil surface are determined using either empirical methods or simplified assumptions for vapour diffusion in the drying soil at the surface. Properties of the soil profile below the surface such as hydraulic conductivity are not considered. Geotechnical engineers are interested in predicting the movement of groundwater in the soil below the surface, and require a soil-atmosphere model based on the explicit hydraulic properties of the soil.

A variety of soil-atmosphere-based models for the evaluation of soil evaporative fluxes have been proposed (Passerat De Silans et al. 1989). Most of the methods pro-

posed calculate actual evaporative fluxes from bare soil surfaces using a system of coupled heat and water transport equations. The actual rates of evaporation are predicted using equations similar to eq. [1]. The actual vapour pressure of the soil surface replaces the saturated vapour pressure. In most cases the vapour pressure at the soil surface is calculated using the well-known Philip and de Vries (1957) formulation for the transport of heat and moisture in soil.

The soil-atmosphere models proposed by Schieldge et al. (1982), Camillo et al. (1983), Witono and Bruckler (1989), and Passerat De Silans et al. (1989) use the Philip and de Vries (1957) formulation. In general, the models appear to provide good estimates of evaporative fluxes, water content profiles, and temperature profiles for drying events ranging between 2 and 7 days. Few difficulties have been reported when the models are applied to relatively short periods of evaporation. However, the accuracy of the models with respect to extended periods of evaporation has not been demonstrated. The results of field tests and model simulations do not show the development of Stage III drying previously described. Periods of continuous evaporation in arid and semi-arid regions of the world commonly extend over several weeks. The application of these soil-atmosphere models to the prolonged evaporative events can be questioned.

In addition to the lack of experimental verification, the soil-atmosphere models based on the Philip and de Vries (1957) formulation have other shortcomings with respect to application to geotechnical problems. The most important difficulty relates to the Philip and de Vries (1957) formulation that assumes flow in response to a volumetric water content gradient. This is fundamentally incorrect, since the flow of liquid water occurs in response to a hydraulic-head gradient. Because of this limitation, the formulation is applicable only to the analysis of homogeneous and isotropic systems. Geotechnical engineers are commonly required to analyze multilayered, anisotropic systems. In fact, the design of covers is by definition a multilayer system. For these reasons the Philip and de Vries (1957) formulation is not acceptable for application to problems in geotechnical engineering.

Attempts have been made to modify the volumetric water content based Philip and de Vries (1957) formulation. Sophocleous (1979) and Milly (1982, 1984a, 1984b) use a matric head based formulation. Sophocleous (1979) conducted model simulations to study the effects of coupled and uncoupled heat and moisture flow on evaporative fluxes. Milly (1984a, 1984b) provided model simulations of evaporative fluxes under atmospheric forcing. Sophocleous (1979) and Milly (1984a, 1984b) did not compare field and/or laboratory observations with the theory and as such it is difficult to determine the accuracy of these models.

The objective of this paper is to provide a basis for the development of a soil-atmosphere model to predict evaporative fluxes from soil surfaces. The model should be formulated in a manner suitable for application in geotechnical engineering. In this paper, a model is formulated using stress state variables and conventions suitable

for application to problems in geotechnical engineering. The accuracy of the assumptions used in the proposed model are tested using a controlled column drying test. The surfaces of two identical columns of fine uniform sand are allowed to desiccate in an arid laboratory chamber. The rates of actual evaporation from the sand surfaces are measured directly along with water content changes in the soil profile of the columns. The drying test was conducted over a prolonged time such that the third stage of drying was fully developed. The measured results from the column drying tests are compared with theoretical simulations obtained from the proposed soil-atmosphere model.

Soil-atmosphere model formulation

The development of a soil-atmosphere model for the evaluation of evaporative fluxes requires a system of equations which describe the flux of water vapour into the atmosphere and the flow of liquid water and water vapour below the soil surface.

Wilson (1990) provides a modification to the Penman method for the calculation of nonpotential evaporation from unsaturated soil surfaces;

$$[2] \quad E = \frac{\Gamma Q_n + \eta E_a}{\Gamma + \eta A}$$

where:

E = evaporative flux (mm/day),

Γ = slope of the saturation vapour pressure versus temperature curve at the mean temperature of the air (mm Hg/°C),

Q_n = all net radiation at the soil surface (mm/day of water),

η = psychrometric constant, and

$E_a = f(u)e_a (B - A)$, with

$f(u) = 0.35 (1 + 0.146 Wa)$,

Wa = wind speed (km/h),

e_a = water vapour pressure of the air above the soil surface (mm Hg),

B = inverse of the relative humidity in the air, and

A = inverse of the relative humidity at the soil surface.

The fundamental assumption made in the formulation of eq. [2] is that the term e_s for the saturated vapour pressure of water at the soil surface in eq. [1] can be replaced using the actual vapour pressure at the soil surface. It may be noted that eq. [2] transforms to the original Penman equation if the soil surface is saturated (i.e., A is equal to unity for a relative humidity of 100%). The actual vapour pressure at the soil surface is in turn calculated on the basis of the flow of liquid water and water vapour below the soil surface.

Application of the extended form of the Penman equation given in eq. [2] is not suited to the laboratory column drying test described in this paper. However, the Dalton-type equation shown in eq. [1] can readily be applied to the column drying test. In general, eq. [1] is the most fun-

damental expression which describes soil evaporation. Since eq. [1] provides the basis for the modified form of the Penman equation in eq. [2], it will be used for the formulation of the soil-atmosphere model presented in this paper.

Examination of eq. [1] which is used to calculate the rate of evaporation, shows evaporation to be a function of the vapour-pressure gradient between the soil surface and the overlying air. The vapour pressure in the air is computed as the product of the saturation vapour pressure of water at the measured air temperature and the measured relative humidity of the air. The vapour pressure at the soil surface, which may be saturated or unsaturated, is calculated as the product of the saturation vapour pressure of water at the temperature of the soil and the relative humidity of the pore air. The relative humidity of the soil surface is evaluated on the basis of the total suction of the soil (Wilson 1990). The turbulent exchange function, $f(u)$, may be evaluated either empirically or through the use of aerodynamic profile methods (Gray 1970). An empirical method was adopted for the present work since it is the most direct.

The total suction at the soil surface depends on the evaporative flux to the atmosphere (i.e., as specified by eq. [1]) and the flow of groundwater to the soil surface. In most cases, the process is transient. Water may flow to the ground surface as liquid water or water vapour. The vapour pressure in the soil is a function of both the soil temperature and soil suction. In general, a system of equations is required to describe the coupled flow of liquid water, water vapour, and heat in the soil under transient conditions.

The flow of liquid water in saturated or unsaturated soils occurs in response to a hydraulic gradient and can be described using Darcy's Law (Childs and Collis-George 1950);

$$[3] \quad q_1 = -k_w \frac{\partial h_w}{\partial y}$$

where;

q_1 = volumetric liquid water flux (m/s),
 k_w = coefficient of hydraulic conductivity (m/s),
 h_w = hydraulic head in the water phase (m), i.e.,

$$\left(\frac{u_w}{\rho_w g} + y \right),$$

u_w = pore-water pressure (kPa),
 y = position (m),
 g = acceleration due to gravity (m/s²), and
 ρ_w = density of liquid water (kg/m³).

The flow of water vapour in an unsaturated soil can be described using Fick's law (Philip and de Vries 1957; de Vries 1975; Fredlund and Dakshanamurthy 1982);

$$[4] \quad q_v = -D_v \frac{\partial P_v}{\partial y}$$

where:

q_v = water vapour flux (kg/(m²·s)),
 P_v = partial pressure due to water vapour (kPa),
 and

$D_v = (\alpha)(\beta) \left(D_{vap} \frac{W_v}{RT} \right)$ the diffusion coefficient of the water vapour through soil (kg · m/(kN · s)) (Wilson 1990),
 $\alpha = \beta^{2/3}$, tortuosity factor of soil (Lai et al. 1976),
 β = cross-sectional area of soil available for vapour flow (i.e., $(1 - S)n$),

$$D_{vap} = 0.229 \times 10^{-4} \left(1 + \frac{T}{273} \right)^{1.75}, \text{ molecular}$$

diffusivity of water vapour in air (m²/s) (Kimball et al. 1976),

W_v = molecular weight of water (0.018 kg/mol),
 R = universal gas constant (8.314 J/(mol · K)),
 T = temperature (K),
 n = porosity, and
 S = degree of saturation.

The combined transient flow of liquid water and water vapour in unsaturated soil results in a change in the volume of the soil structure, the water phase, and/or the air phase. In the case of a uniform sand, volume change in the soil structure is small and a decrease in the volume of the water phase is approximately equal to the increase in volume of the air phase and vice versa. Fredlund and Morgenstern (1976) provide a constitutive relationship for the change in volume of water in an element;

$$[5] \quad \frac{\Delta V_w}{V} = [m_1^w d(\sigma_y - u_a) + m_2^w d(u_a - u_w)]$$

where:

$\frac{\Delta V_w}{V}$ = change in volumetric water content,

σ_y = vertical stress (kPa),

u_a = pressure in the air phase (kPa),

u_w = pressure in the water phase (kPa),

m_1^w = slope of the $d(\sigma_y - u_a)$ versus volumetric water content plot for $d(u_a - u_w)$ equal to zero (m²/kN), and

m_2^w = slope of the $d(u_a - u_w)$ versus volumetric water content plot for $d(\sigma_y - u_a)$ equal to zero (m²/kN).

Combining eqs. [3] and [4] and differentiating with respect to vertical position y , describes the divergence of flux (i.e., change in volumetric water content with respect to time) in one-dimensional space due to imposed hydraulic and vapour pressure gradients in the soil. This relationship may be equated to the time differential of the constitutive relationship given in eq. [5]. Assuming the change in vertical stress σ_y and air pressure u_a equal to

zero and setting pore-water pressure u_w equal to $\rho_w g(h - y)$, rearranging and simplifying, leads to a transient equation for the one-dimensional flow of liquid water and water vapour as follows;

$$[6] \quad \frac{\partial h}{\partial t} = C_w \frac{\partial}{\partial y} \left(k_w \frac{\partial h_w}{\partial y} \right) + C_v \frac{\partial}{\partial y} \left(D_v \frac{\partial P_v}{\partial y} \right)$$

where the modulus of volume change with respect to the liquid phase, C_w , is defined as:

$$C_w = \frac{1}{\rho_w g m_2^w}$$

and the modulus of volume change with respect to the vapour phase, C_v , is defined as:

$$C_v = \frac{1}{(\rho_w)^2 g m_2^w} \left(\frac{P + P_v}{P} \right)$$

where:

- $(P + P_v)P$ = a correction factor for vapour diffusion,
- P = the total atmospheric pressure (kPa), and
- P_v = partial pressure in the soil due to water vapour (kPa).

Equation [6] has two variables (i.e., hydraulic head and vapour pressure). These variables are not independent. The vapour pressure P_v may be related to the pressure head in the water phase (i.e., $u_w = \rho_w g(h - y)$) by using the widely accepted thermodynamic relationship given by Edlefsen and Anderson (1943);

$$[7] \quad P_v = P_{vs} h_r$$

where:

- P_v = partial pressure due to water vapour within the voids of the unsaturated soil (kPa),
- P_{vs} = saturation vapour pressure (kPa) of the soil water at the soil temperature T ,
- $h_r = e^{\psi g_s W_s / RT}$, relative humidity, and
- ψ = total potential in the liquid water phase expressed as on equivalent matric potential (m).

The calculation of the vapour pressure in eq. [7] depends on the saturation vapour pressure and the temperature of the soil. Hence the temperature profile of the soil must be evaluated simultaneously with eqs. [6] and [7]. Wilson (1990) used the following equation for heat flow:

$$[8] \quad C_h \frac{\partial T}{\partial t} = \frac{\partial}{\partial y} \left(\lambda \frac{\partial T}{\partial t} \right) - L_v \left(\frac{P + P_v}{P} \right) \frac{\partial}{\partial y} \left(D_v \frac{\partial P_v}{\partial y} \right)$$

where:

- C_h = volumetric specific heat ($J/(m^3 \cdot ^\circ C)$),
- λ = thermal conductivity ($W/(m \cdot ^\circ C)$), and
- L_v = latent heat of vaporization for water (J/kg).

Equation [8] describes heat flow due to conductive and latent heat transfer. Convective heat flow is not included. Andersland and Anderson (1978), Jame and Norum (1980), Milly (1984a), and others point out that this term

is negligible for most applications. Philip and de Vries (1957) and de Vries (1987) used an equation for heat flow similar to eq. [8].

Equations [6], [7], and [8] describe the transfer of liquid water, water vapour, and heat, respectively, in a porous medium. These equations assume the soil structure to be rigid and neglect secondary effects due to flow in the air phase and storage changes in the air and liquid phases. These assumptions are reasonable for the application in this paper as the theory is used to simulate heat and mass transfer processes in a fine to medium, uniform sand that shows little volume change during the evaporation process. Wilson (1990) provides a more rigorous system of equations to account for the effects of volume change in the soil structure and secondary fluxes.

The term $(P + P_v)/P$ used in eqs. [6] and [8] is a correction factor used by Wilson (1990) to account for combined flow due to vapour diffusion and bulk air advection. Philip and de Vries (1957) used a similar mass-flow factor equal to $P / (P - P_v)$. In most applications, the correction factor is approximately equal to unity and has little effect on the solution.

The soil-atmosphere model computes the evaporation rate from soil by solving eqs. [1], [6], [7] and [8], simultaneously. The vapour pressure at the soil surface in eq. [1] (i.e., e_s) is set equal to the vapour pressure at the soil surface (i.e., P_v) computed by solving eqs. [6], [7], and [8]. The numerical results subsequently presented were obtained using an explicit finite difference technique.

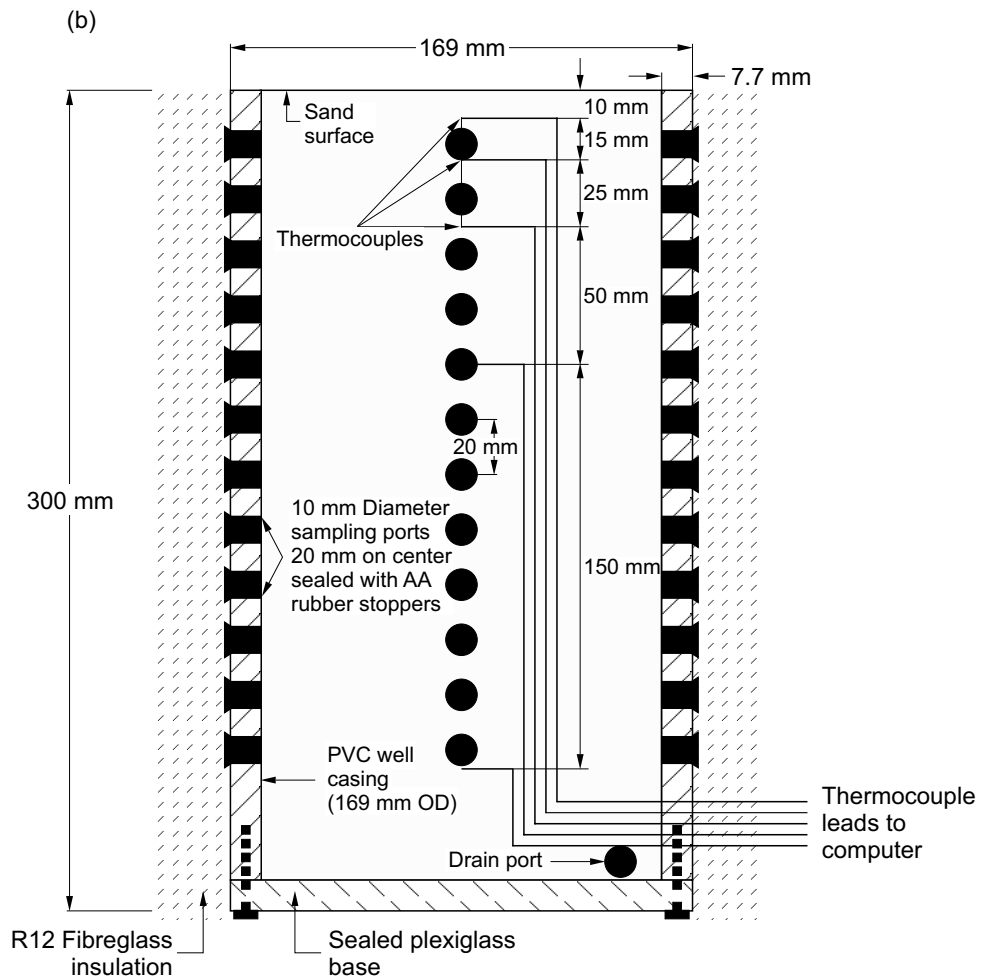
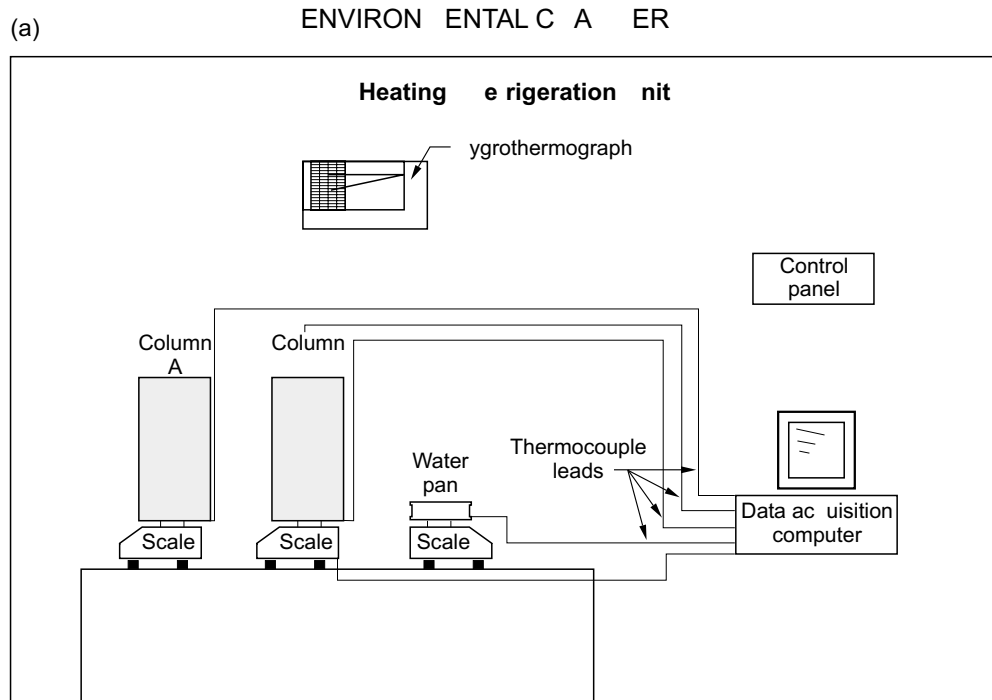
Column drying test

The objective of the column drying test was to measure the actual rates of evaporation from a soil profile and to compare these with the predicted values of evaporation obtained from the proposed soil-atmosphere model. The exposed surfaces of two identical columns of a fine to medium aeoline sand (Beaver Creek sand) were allowed to evaporate under controlled laboratory conditions. The columns were filled with saturated sand and were allowed to drain to a hydrostatic condition. The columns were then sealed at the base and the upper surfaces were allowed to desiccate for a period of 42 days.

Figure 2 illustrates the apparatus used to conduct the column drying test. Two columns were constructed using 169 mm outside diameter PVC casing. The columns were 300 mm in height and sealed at the base. Sampling ports in the sidewall of the PVC casing were installed vertically down the columns to allow for sample extraction and the measurement of water content. Conventional thermo-couples were also installed along a vertical profile in the centre of the columns as shown in Fig. 2b. A modified PC computer with a data-acquisition board was used to automatically record the temperatures at 15 min intervals. The sand columns were wrapped with insulation to minimize the effects of lateral heat flow.

The sand columns were supported on scales to give a continuous measurement of their mass and, therefore, their change in mass. The actual rate of soil evaporation

Fig. 2. a) Apparatus used for the column drying test; b) details of the sand-filled column A and associated instrumentation.



was determined on the basis of change in mass for each column which was automatically recorded at 15 min intervals. An evaporation pan filled with water and having an identical surface area and geometry to that of the columns was installed adjacent to the columns to determine the potential rate of evaporation. The entire test apparatus was installed within a climatically controlled environmental chamber with a constant temperature of 38°C and a relative humidity of approximately 10%. The resulting potential rate of evaporation in the environmental chamber was approximately 8 mm/day. The temperatures of the water surface and chamber air were monitored continuously along with the relative humidity of the ambient air. Soil samples were taken through the sampling ports at various times to obtain a direct measurement of water content along the column profiles.

Figure 3 shows the measured rates of evaporation from the evaporation pan, column A, and column B with respect to time. The measured rate of evaporation from the water pan is shown as the potential rate of evaporation. Figure 4 shows the measured water contents in columns A and B at the start of the tests and at various times throughout the duration of the test.

The actual rate of evaporation from both sand columns was approximately equal to the potential rate of evaporation for the first 3 or 4 days. This corresponds to the Stage I drying phase as previously defined. During this period, the water contents of the sand surfaces were observed to decline continuously from the initial values of 13–14% but remained wet in visual appearance. It can be seen that the initial high rate of actual soil evaporation was slightly below the potential rate defined by the water-filled evaporation pan. In general, saturated soils evaporate at the potential rate (Wilson 1990). However, both sand surfaces were observed to be approximately 1°C cooler than the surface of the water-filled evaporation pan. This resulted in a slightly lower saturation vapour pressure at the surfaces of the sand columns compared with the water and hence a slightly lower rate of evaporation (i.e., as defined by eq. [1]).

The actual rate of evaporation for columns A and B declined rapidly after the initial high rate Stage I phase. The rapid decline in the rate of evaporation continued for approximately 11 days. The drying period between 3 and 11 days corresponds to Stage II drying as previously discussed. The onset of Stage II drying was observed to begin at the same time that the surface of the sand became visually dry. This corresponded to a water content at the sand surface slightly less than 2%. The drying surface was initially very thin. The water content of the sand immediately below the dry surface remained relatively high, as can be seen in Fig. 4 (i.e., after 5 and 9 days). The dry surface layer was observed to gradually increase in thickness as the rate of evaporation continued to decline.

The decline in the actual rates of evaporation slowed after approximately 11 days for columns A and B. This may be defined as the onset of Stage III drying, which is defined as the slow residual rate of evaporation. The water content of the sand at both surfaces was measured to

Fig. 3. Measured rates of evaporation from the evaporation pan and columns A and B versus time.

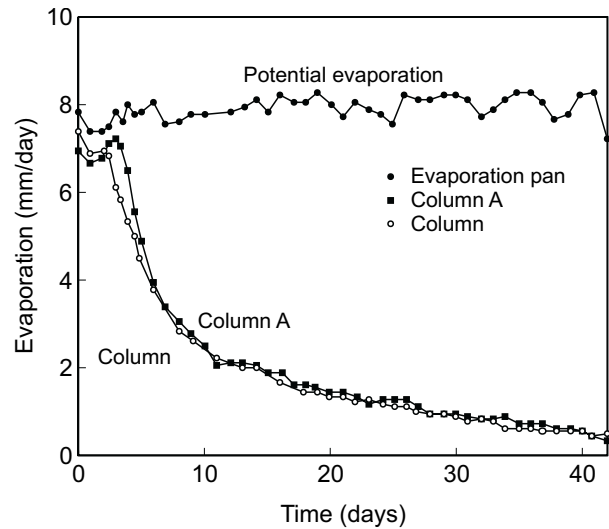
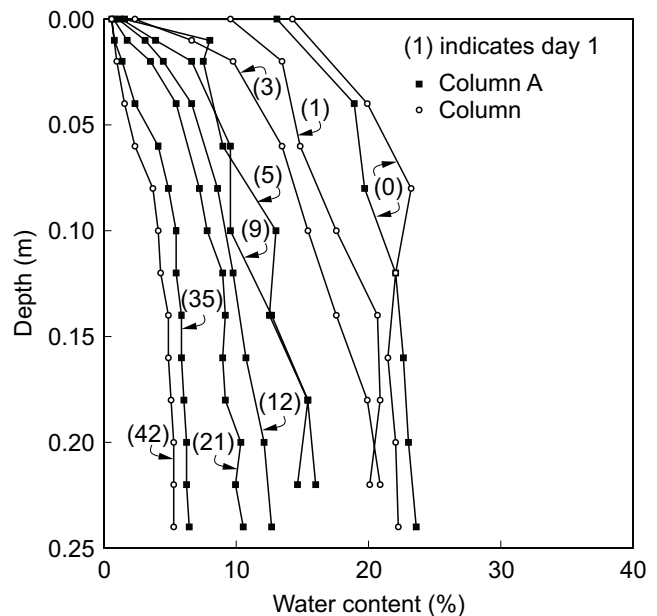


Fig. 4. Measured water content profiles in columns A and B at various times during the column drying test.



be approximately 1% after 12 days of drying. Distinct drying fronts developed which extended to a depth of approximately 1 cm after 21 days and advanced to a depth of approximately 8 cm after 42 days of continuous evaporation. The sand within the drying fronts was extremely dry, and the liquid phase appeared to be absent. The final rate of actual evaporation was approximately 0.4 mm/day compared with the potential evaporation rate equal to approximately 8 mm/day.

Analysis and discussion

The proposed soil-atmosphere model was used to calculate the evaporative fluxes measured in the column dry-

ing test. The coefficients for the solution of eqs. [1], [6], and [8] include the turbulent exchange function, $f(u)$, hydraulic conductivity, k_w , the modulus of volume change with respect to the liquid and vapour phases, C_w and C_v , specific heat capacity, C_h , and thermal conductivity, λ . The turbulent exchange function was calculated directly on the basis of the measured evaporative flux from the water-filled evaporation pan (i.e., $f(u) = E / (e_s - e_a)$), given that the vapour pressures at the water surface and in the air were known. The remaining coefficients were calculated on the basis of measured soil properties.

The moduli of volume change with respect to the liquid and vapour phases were calculated on the basis of the slope m_2^w of the water content characteristic curve. Figure 5 shows the soil-water characteristic curve for the Beaver Creek sand determined in the laboratory. The Tempe cell method was used to establish the soil-water characteristic curve between 0 and 100 kPa suction. Vapour-equilibrium desiccators were used for the higher values of suction to a maximum of approximately 300 000 kPa. It should be noted that the soil-water characteristic curve shown in Fig. 5 corresponds to drying or drainage of the sand. In addition to calculating the coefficient of consolidation, the soil-water characteristic curve was also used to determine the values of suction based on water contents measured in the profile of the sand columns.

The hydraulic conductivity, k_w , for the Beaver Creek sand depends on the water content and therefore, in turn, on matric suction. The relationship between the coefficient of hydraulic conductivity and matric suction was evaluated using the method described by Laliberte et al. (1968) and is shown in Fig. 6. The functional relationship shown in Fig. 6 is determined on the basis of the measured saturated hydraulic conductivity and the soil-water characteristic curve shown in Fig. 5. The effect of hysteresis associated with wetting and drying of the sand was not evaluated, since the sand columns were subjected only to continuous drying due to evaporation. The diffusion coefficient, D_v , for water vapour in the soil was calculated directly as shown in eq. [4] on the basis of porosity and degree of saturation.

The thermal conductivity, λ , and the volumetric specific heat of the Beaver Creek sand were determined using the method described by de Vries (1963), who provides the following equation for the calculation of the specific heat capacity of a soil;

$$[9] \quad C_h = C_s \theta_s + C_w \theta_w + C_a \theta_a$$

where:

C_s = volumetric specific heat capacity of the soil solids ($2.24 \times 10^6 \text{ J}/(\text{m}^3 \cdot ^\circ\text{C})$);

C_w = volumetric specific heat capacity of the liquid water phase ($4.15 \times 10^6 \text{ J}/(\text{m}^3 \cdot ^\circ\text{C})$);

C_a = volumetric specific heat capacity of the air phase, which can be assumed to be negligible (de Vries 1963); and

$\theta_s, \theta_w, \theta_a$ = volumetric fractions of the soil solids, water, and air, respectively.

Fig. 5. Water content characteristic curve for Beaver Creek sand.

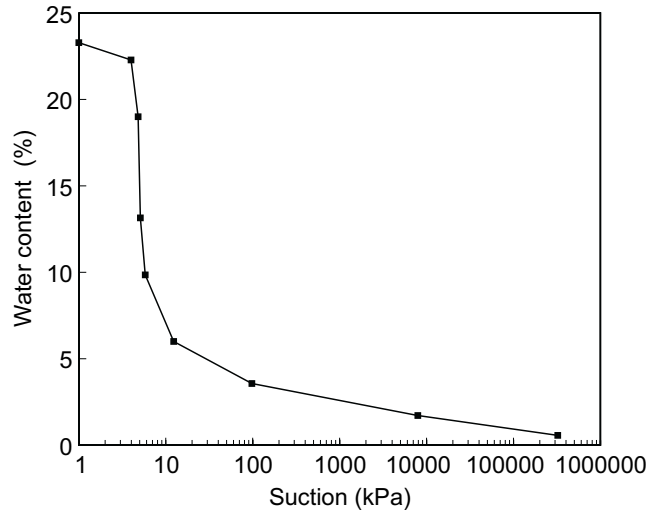
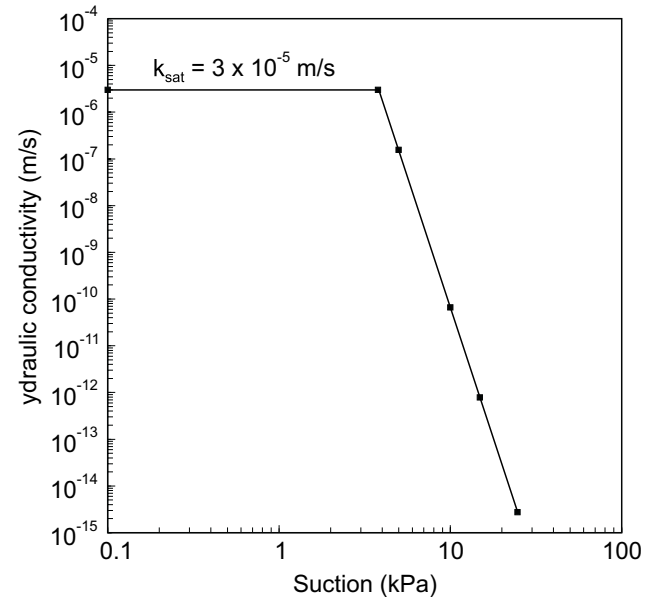


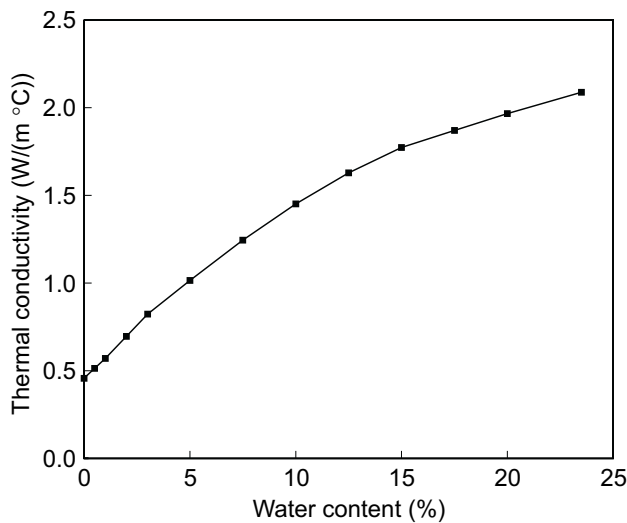
Fig. 6. Hydraulic conductivity versus matric suction for Beaver Creek sand; k_{sat} is the hydraulic conductivity of saturated soil.



The thermal conductivity, λ , of the Beaver Creek sand is also a function of the water content of the soil. The method used for calculating thermal conductivity was more rigorous than that given in eq. [9] and the reader is referred to de Vries (1963). Figure 7 shows the computed relationship between thermal conductivity and water content on the basis of de Vries (1963). The methods for calculating volumetric specific heat capacity and thermal conductivity provided by de Vries (1963) are theoretical. Jame (1977); however, found that the theoretical model given by de Vries (1963) provided good agreement with measured values.

The soil-atmosphere model was applied using the coefficients evaluated as described above. Equations [6] and

Fig. 7. Thermal conductivity versus water content for Beaver Creek sand.

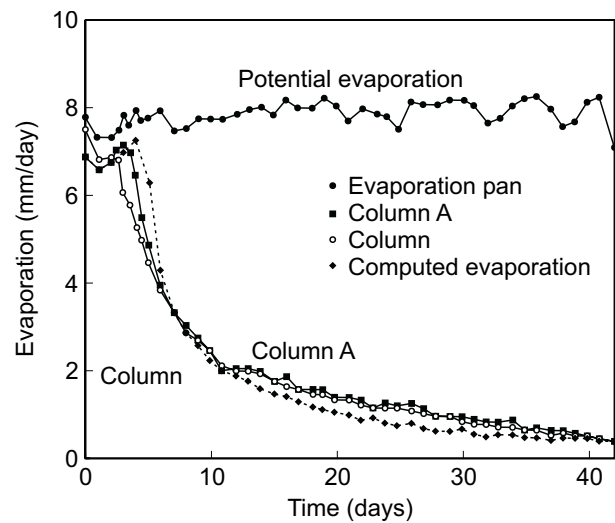


[8] are nonlinear. All of the functional relationships for the soil coefficients depend on either matric suction or water content. Furthermore, the analysis of the column drying test was for transient conditions. Soil evaporative fluxes, water content, soil suction, and soil temperature are all nonsteady. Extremely small time steps of approximately 0.1 s were selected for the explicit finite difference solutions, and soil coefficients were evaluated at each time step.

Figure 8 shows the computed rate of soil evaporation and the measured rates of soil evaporation for the 42 day column drying test. A good correlation between the computed rate of evaporation and the measured rate of evaporation was observed when using the measured soil properties. Figures 9a and 9b show the computed and measured water content and temperature profiles, respectively, at various times during the test. Again, the correlation between the values computed by the soil-atmosphere model appears to be good. The proposed soil-atmosphere model appears capable of predicting soil evaporation rates, water content profiles, and temperature profiles on the basis of measured atmospheric conditions and soil properties with reasonable accuracy. This indicates that the theoretical model based on the Dalton-type equation for evaporation, Darcy's Law for liquid transfer in soil, and Fick's Law for vapour diffusion in soil was appropriate.

The mechanisms for water transport to the soil surface should be considered because water may flow upward to the soil surface as liquid water and/or water vapour. During Stage I evaporation over the first 3–4 days, the surface of the sand and underlying soil were very moist or nearly saturated. Suctions were relatively low and the corresponding hydraulic conductivity was at or near the saturated hydraulic conductivity. As can be seen in Fig. 6, the hydraulic conductivity of the Beaver Creek sand remains equal to the saturated value until matric suction exceeds the air entry value, AEV, of 3.8 kPa. In other

Fig. 8. Measured and computed rates of evaporation versus time for the column drying test.



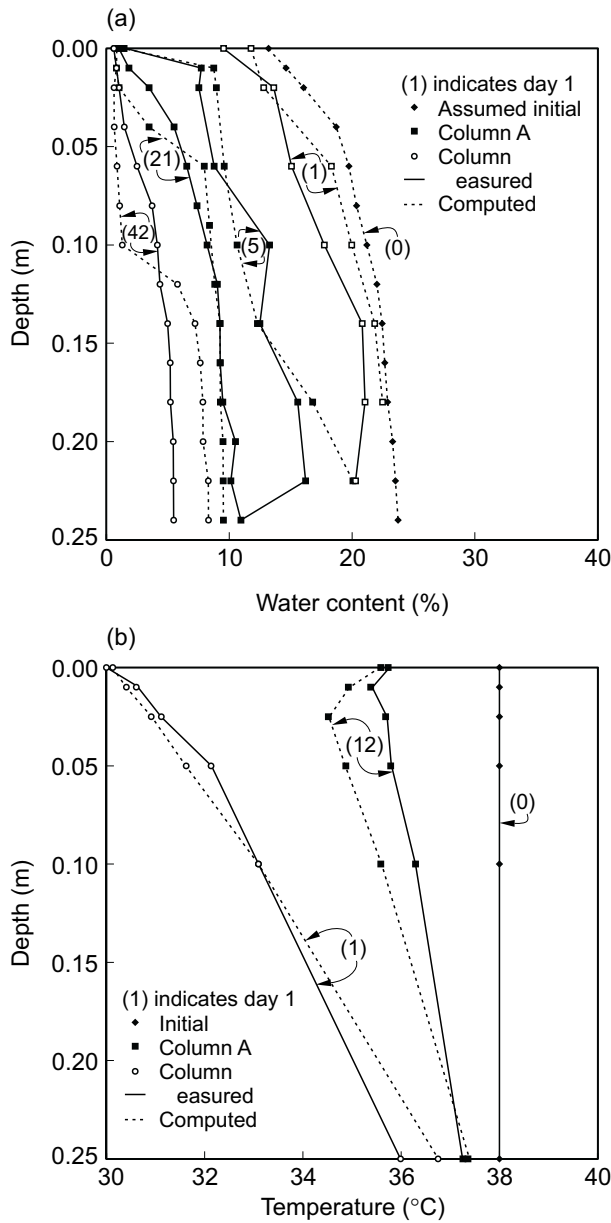
words, the flow of water in the liquid phase was not restricted. The values of suction increased as Stage I evaporation continued, and the hydraulic conductivity decreased rapidly once the value of matric suction exceeded the air entry value. This caused the flow of liquid water to become increasingly restricted as evaporation continued. The development of this restriction in the flow of liquid water to the soil surfaces most likely corresponds to the transition from the high rate Stage I drying to the falling rate Stage II drying.

Stage II drying or the falling rate stage was observed to begin once a dry zone of sand appeared on the surface of the columns after approximately 4 days of drying. The soil surfaces were sufficiently dry such that the liquid water phase was absent. The continuation of the evaporation can be explained by the process of water molecules diffusing to the surface of the sand through the vapour phase in the dry sand. The actual rate of evaporation declined rapidly after 5 days as the thickness of the dry zone increased. The formation of a dry soil surface was important, as it signalled the rapid decline in evaporative flux and the transition to vapour diffusion.

The transition from Stage II drying to Stage III is somewhat arbitrary. However, Hillel (1980) describes Stage III as a vapour-diffusion process. The thickness of the dry surface zone increased to form a distinct drying front approximately 0.5 cm thick after 11 or 12 days of drying. The rate of decline in the evaporation rate appears to decrease after this point in time and can be defined as the onset of Stage III drying. The drying front or zone of vapour diffusion slowly increased in thickness with time to approximately 1 cm after 21 days and 6–8 cm after 42 days. The evaporative flux decreased from approximately 2 mm/day to 0.4 mm per/day during the same period of time.

Figure 10 helps illustrate the transition from liquid flow to vapour flow across the drying front after 29 days of evaporation. Figure 10a shows the suctions based on

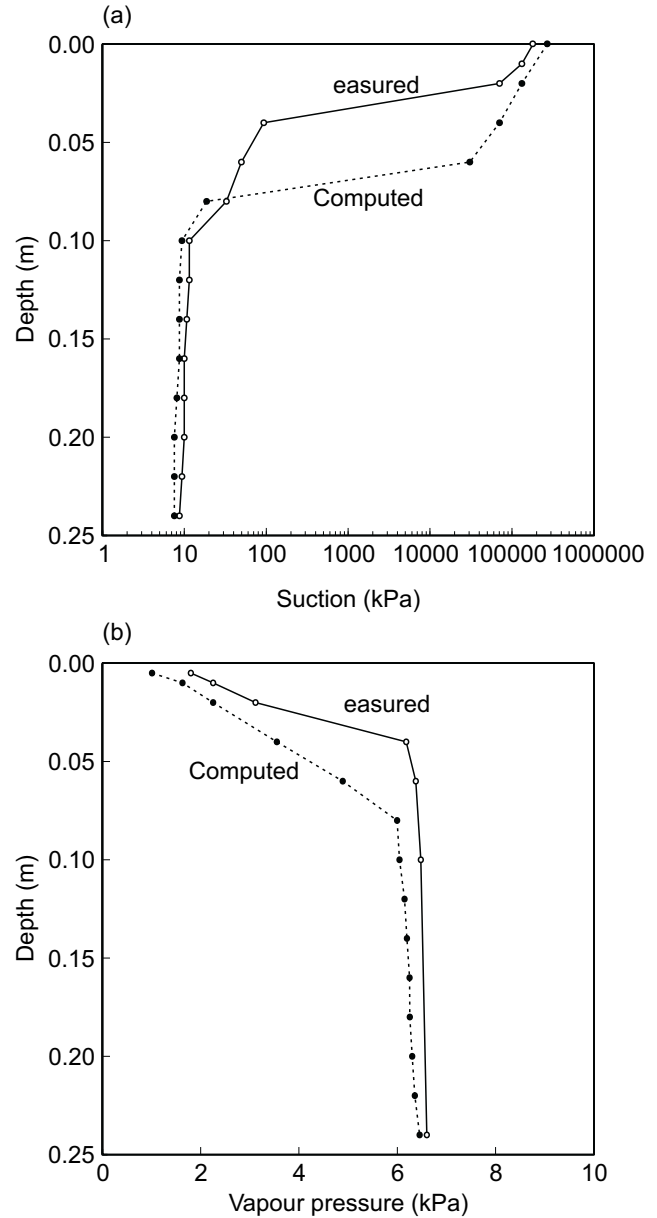
Fig. 9. *a)* Measured and computed water content profiles after 1, 5, 21, and 42 days of evaporation; *b)* measured and computed temperature profiles after 1 day and 12 days of evaporation.



measured water contents (i.e., using Fig. 5) and the suctions computed by the soil-atmosphere model. Both computed and measured suctions within the top 2 cm compare well. Suctions in the drying front exceed 100 000 kPa. The corresponding hydraulic conductivity (i.e., Fig. 7) and liquid flow at these values of suction are virtually zero. The flow of water to the surface must be predominantly by vapour diffusion.

Both computed and measured suctions in Fig. 10a decreased from approximately 100 000 to 20 kPa between 2 and 8 cm in depth. This zone may be noted as the transition zone from predominant vapour flow to predominant

Fig. 10. *a)* Measured and computed suctions in the sand after 29 days of evaporation; *b)* measured and computed vapor pressures in the sand after 29 days of evaporation.



liquid flow. The correlation between the measured and computed suctions is not as good within this zone. This may be attributed to the limitation of the function used to define the relationship between hydraulic conductivity and matric suction.

Laliberte et al. (1968) stated that the proposed function for hydraulic conductivity is accurate only for water contents above the residual water content. The residual water content for the Beaver Creek sand based on the method described by Laliberte et al. (1968) is approximately 5.7% at 20 kPa suction. This corresponds approximately to the suctions where the inaccuracy becomes apparent in Fig. 10a. The correlations between the measured and the

computed suctions are good below the transition zone when the values of suction are less than 20–30 kPa. A similar inaccuracy may be noted in Fig. 9a for the measured and predicted water contents for the sand profile after 42 days of drying as the entire sand profile approaches the residual water content.

Figure 10b shows the mechanism that drives vapour flow across the transition and vapour flow zones (i.e., drying front). The measured vapour pressures shown in Fig. 10b were determined on the basis of the measured suction shown in Fig. 10a (i.e., which gives relative humidity using eq. [7]) and the measured soil temperature. The curve showing computed vapour pressure was computed by the soil-atmosphere model. A distinct pressure difference of approximately 4 kPa may be noted for both curves between the surface of the sand and the top 4 to 8 cm. This pressure gradient is the mechanism that drives vapour diffusion as described by Fick's law in eq. [4]. The gradient decreases to a small value below approximately 8 cm and hence vapour diffusion decreases to a small value in the zone where liquid flow predominates.

The transition zone at the drying front is the location where evaporation occurs and water molecules move from the liquid water phase to the vapour phase. At the start of the test, evaporation initially occurs at the surface of the sand. It may be noted in Fig. 9b that this is the coldest point in the sand column profile after 1 day of evaporation. Evaporation provides a heat sink where energy is required for latent heat of vaporization. The location of the evaporation surface advanced into the column with the drying front. It can be seen in Fig. 9b, for example, that the coldest points in the temperature profile after 12 days of evaporation for the measured and computed temperatures occurred at approximately 1.0 and 2.5 cm, respectively, below the sand surface. The temperatures were coldest at these points because of the latent heat required to transfer water from the liquid phase to the vapour phase. The location of the measured and computed cold front varies somewhat. This may be attributed to the difficulty previously described with respect to the accuracy of determining hydraulic conductivity in the transition zone.

The soil-atmosphere model appears to predict the actual evaporative fluxes with accuracy when compared with the measured values. All simulations were conducted using the measured soil properties for the Beaver Creek sand. Questions may be asked regarding the importance or significance of the various material properties. Laboratory tests were not conducted with other soil types; however, model simulations were conducted with different soil properties. The coefficient of hydraulic conductivity is one of the most important soil properties, as it controls the flow of liquid water. The value of the saturated hydraulic conductivity for determining the functional relationship between hydraulic conductivity and matric suction for the Beaver Creek sand (i.e., Fig. 6) was set equal to a low value of 4×10^{-6} m/s and a high value of 8×10^{-5} m/s. All other soil properties were set equal to values previously used.

Figure 11 shows the rate of soil evaporation versus time computed for the different values of saturated hydraulic conductivity. It can be seen that varying the saturated hydraulic conductivity has a significant impact on the computed rates of soil evaporation. Decreasing the saturated hydraulic conductivity to 4×10^{-6} m/s reduces the time for high-rate Stage I drying previously established for the column drying test from approximately 4 days to 1 day. Alternately, increasing the saturated hydraulic conductivity to 8×10^{-5} m/s extends Stage I drying to approximately 6 days. It may be noted that in all cases the magnitude of the slow residual rate of evaporation in Stage III drying is not significantly effected. This is considered reasonable, as this stage of drying is controlled by vapour diffusion through the drying front.

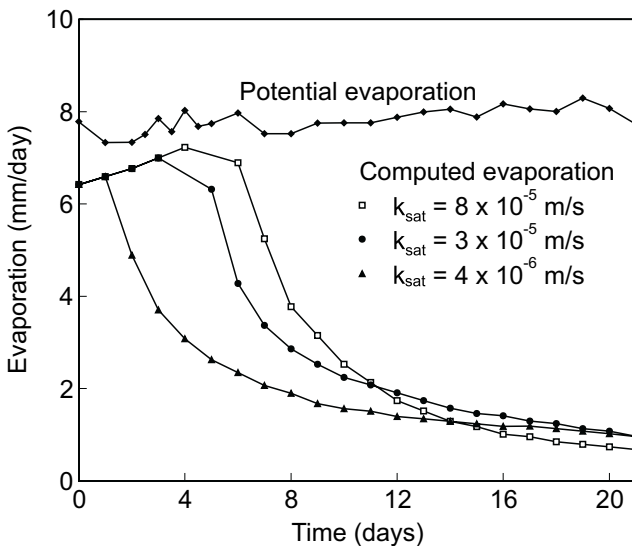
Summary and conclusions

A soil-atmosphere model for the evaluation of soil evaporative flux has been developed. The theoretical formulation of the model is based on the Dalton-type equation for evaporation from a surface into the atmosphere. Darcy's Law for the flow of liquid water and Fick's Law for the flow of water vapour in the soil below the surface were also used. The values for actual evaporation rates, water content profiles, and temperature profiles predicted by the soil-atmosphere model were compared with the values measured in a controlled column evaporation test over a 42-day period. The results of the model simulations agree well with the measured values of the column drying test for the Beaver Creek sand.

Both the soil-atmosphere model and the laboratory test showed the development of the three stages of drying described by Hillel (1980). The high rate of evaporation for saturated or nearly saturated soil during Stage I is approximately equal to the potential rate of evaporation for a free water surface. This high rate of evaporation is controlled primarily by atmospheric conditions. Stage I drying was found to continue until a dry surface zone developed. The development of the dry surface zone greatly reduced the rate of evaporation during the falling-rate phase of Stage II drying. Simulations conducted with the soil-atmosphere model showed the length of time for Stage I drying is strongly controlled by the hydraulic conductivity of the soil. The column drying test and the soil-atmosphere model also showed the long term development of Stage III drying. The rate of evaporation from the sand surface during Stage III drying was reduced by a factor of approximately 20 when compared with the initial high rate of evaporation (i.e., 8 mm/day versus 0.4 mm/day after 42 days).

The ability to predict evaporative fluxes is useful to geotechnical engineers, for example, in the design of soil covers for mine tailings. Conventional methods of evaluating evaporation such as the Penman method (1948) provide only estimates of the potential rate of evaporation (i.e., Stage I). This could result in considerable error if applied to a soil surface over extended periods of drying between rainfall events. However, comparison of the

Fig. 11. Computed rates of soil evaporation versus time for various values of saturated hydraulic conductivity.



evaporative fluxes computed using the Dalton-based soil-atmosphere model with the results measured in the column drying test indicates using the actual vapour pressure corrects the difficulties associated with predicting evaporation from unsaturated soil surface. Furthermore, it suggests the Penman equation may be extended as shown in eq. [2] for field problems where the rate of evaporation is less than the potential rate of evaporation. This could be achieved by computing the actual vapour pressure at the soil surface using eqs. [6] to [8]. Field tests; however, will be required to demonstrate this application.

References

- Andersland, O.B., and Anderson, D.M. 1978. *Geotechnical engineering for cold regions*. McGraw-Hill Inc., New York.
- Brutsaert, W.H. 1982. *Evaporation into the atmosphere: theory, history and applications*. P. Reidel Publishing Company, Dordrecht, The Netherlands.
- Camillo, P.J., Gurney, R.J., and Schmutge, T.J. 1983. A soil and atmospheric boundary layer model for evapotranspiration and soil moisture studies. *Water Resources Research*, **19**(2): 371–380.
- Childs, E.C., and Collis-George, N. 1950. The permeability of porous materials. *Proceedings of the Royal Society of London*, **201**: 392–405.
- Choudhury, B.J., and Monteith, J.L. 1988. A four-layer model for the heat budget of homogeneous land surfaces. *Quarterly Journal of the Royal Meteorology Society*, **114**: 373–398.
- de Vries, D.A. 1963. Thermal properties of soils. *In Physics of plant environment*. Edited by W.R. Van Wijk, North Holland Publishing Company, Amsterdam, The Netherlands, pp. 210–235.
- de Vries, D.A. 1975. Heat transfer in soil. *In Heat and mass transfer in the biosphere*. 1. Transfer processes in plant environment. Edited by D.A. de Vries and N.H. Afgan. Scripta Book Company, Washington, D.C., pp. 5–28.
- de Vries, D.A. 1987. The theory of heat and moisture transfer in porous media revisited. *International Journal of Heat and Mass Transfer*, **30**(7): 1343–1350.
- Edlefsen, N.E., and Anderson, A.B.C. 1943. Thermodynamics of soil moisture. *Hilgardia*, **15**(2): 31–298.
- Fredlund, D.G., and Dakshanamurthy, V. 1982. Prediction of moisture flow and related swelling or shrinking in unsaturated soils. *Geotechnical Engineering*, **13**: 15–49.
- Fredlund, D.G., and Morgenstern, N.R. 1976. Constitutive relations for volume change in unsaturated soils. *Canadian Geotechnical Journal*, **13**: 261–276.
- Granger, R.J. 1989. An examination of the concept of potential evaporation. *Journal of Hydrology*, **111**: 9–19.
- Gray, D.M. 1970. *Handbook on the principals of hydrology*. Canadian National Committee for the International Hydrological Decade, National Research Council of Canada, Ottawa.
- Hillel, D. 1980. *Applications to soil physics*. Academic Press, New York.
- Jame, Y.W. 1977. *Heat and mass transfer in freezing unsaturated soil*. Ph.D. thesis, University of Saskatchewan, Saskatoon, SK, Canada.
- Jame, Y.W., and Norum, D.I. 1980. Heat and mass transfer in a freezing unsaturated porous medium. *Water Resources Research*, **16**(4): 811–819.
- Kimball, B.A., Jackson, R.D., Reginato, R.J., Nakayama, F.S., and Idso, S.B. 1976. Comparison of field-measured and calculated soil-heat fluxes. *Soil Science Society of America Proceedings*, **40**(1): 18–25.
- Lai, S., Tiedje, J.M., and Erickson, A.E. 1976. In situ measurement of gas diffusion coefficient in soils. *Soil Science Society of America Proceedings*, **40**(1): 3–6.
- Laliberte, A.M., Brooks, R.H., and Corey, A.T. 1968. Permeability calculated from desaturation data. *ASCE Journal of the Irrigation and Drainage Division*, **94**: 57–71.
- Milly, P.C.D. 1982. Moisture and heat transport in hysteretic, inhomogeneous porous media: A matric head-based formulation and a numerical model. *Water Resources Research*, **18**(3): 489–498.
- Milly, P.C.D. 1984a. A linear analysis of thermal effects on evaporation from soil. *Water Resources Research*, **20**(8): 1075–1085.
- Milly, P.C.D. 1984b. A simulation analysis of thermal effects on evaporation from soil. *Water Resources Research*, **20**(8): 1087–1098.
- Monteith, J.L. 1965. Evaporation and environment. *In The State and Movement of Water in Living Organisms, Symposium: Society of Experimental Biology*. Vol. 19. Edited by G.E. Fogg. Academic Press, San Diego, CA, pp. 205–234.
- Morton, F.I. 1975. Estimating evaporation and transpiration from climatological observations. *Journal of Applied Meteorology*, **14**(4): 488–497.
- Passerat De Silans, A., Bruckler, L., Thory, J.L., and Vaublin, M. 1989. Numerical modelling of coupled heat and water flows during drying in a stratified bare soil-comparison with field observations. *Journal of Hydrology*, **105**: 109–138.
- Penman, H.L. 1948. Natural evapotranspiration from open water, bare soil and grass. *Proceedings of the Royal Society of London, Series A*, **193**: 120–146.
- Philip, J.R., and de Vries, D.A. 1957. Moisture movement in porous materials under temperature gradients. *Transactions, American Geophysical Union*, **38**(2): 222–232.

- Priestley, C.H.B., and Taylor, R.J. 1972. On the assessment of surface heat flux and evaporation using large-scale parameters. *Monthly Weather Review*, **100**: 81–92.
- Schildge, J.P., Kahle, A.B., and Alley, R.E. 1982. A numerical simulation of soil temperature and moisture variations for a bare field. *Soil Science*, **133**: 197–207.
- Shuttleworth, W.J., and Wallace, J. S. 1985. Evaporation from sparse crops - an energy combination theory. *Quarterly Journal of the Royal Meteorology Society*, **111**: 839–855.
- Sophocleous, M.A. 1979. Analysis of water and heat flow in unsaturated-saturated porous media. *Water Resources Research*, **15**(5): 1195–1206.
- Stannard, D.I. 1993. Comparison of Penman-Monteith, Shuttleworth-Wallace, and modified Priestley-Taylor evapotranspiration models for wildland vegetation in semi-arid rangeland. *Water Resources Research*, **29**(5): 1379–1392.
- Thornthwaite, C.W. 1948. An approach toward a rational classification of climate. *Geographical Review*, **38**: 55–94.
- van Bavel, C. H. M. 1967. Changes in canopy resistance to water loss from alfalfa induced by soil water depletion. *Agricultural Meteorology*, **4**: 165–176.
- Wilson, G. W. 1990. Soil evaporative fluxes for geotechnical engineering problems. Ph.D. thesis, University of Saskatchewan, Saskatoon, SK, Canada.
- Witono, H., and Bruckler, L. 1989. Use of remotely sensed soil moisture content as boundary conditions in soil-atmosphere water transport modelling 1. Field validation of a water flow model. *Water Resources Research*, **25**(12): 2423–2435.

The effect of soil suction on evaporative fluxes from soil surfaces

G.W. Wilson, D.G. Fredlund, and S.L. Barbour

Abstract: This paper presents a theoretical approach in which a Dalton type mass transfer equation was used to predict the evaporative fluxes from non-vegetated soil surfaces. Soil evaporation tests were conducted in the laboratory on three different soil samples of Beaver Creek sand, Custom silt and Regina clay. The soil surfaces were saturated and allowed to evaporate to a completely air-dried state. The actual evaporation rate, AE, for each soil surface was measured along with the potential evaporation rate, PE, for an adjacent water surface. The ratio of actual evaporation to potential evaporation or the normalized soil evaporation, AE/PE, was then evaluated with respect to drying time, soil water content and soil suction.

The value of AE/PE was found to be approximately equal to unity for all soils until the total suction in the soil surfaces reached approximately 3000 kPa. The rate of actual soil evaporation was observed to decline when the total suction exceeded 3000 kPa. A relationship between the actual evaporation rate and total suction was found to exist for all three soil types which appears to be unique and independent of soil texture, drying time, and water content.

Key words: actual evaporation, potential evaporation, soil suction, evaporative flux.

Introduction

Engineered soil covers cannot be designed without evaluating the evaporative fluxes at the soil surface. The purpose of any soil cover system is to control the mass flux of water entering the underlying waste materials. Net water fluxes are a function of the infiltration entering the soil cover due to precipitation and exfiltration leaving the soil cover due to atmospheric evaporation. A clear rationale for predicting infiltration is available. However, a suitable methodology for evaluating soil evaporation has yet to be demonstrated. The need for the development of an appropriate geotechnique is strong since geotechnical engineers in many regions of the world find that the frequency and duration of evaporative events greatly exceed that of infiltration events.

Recent studies have illustrated the need for predictive techniques to evaluate evaporation rates from soil surfaces. Yanful et al. (1993) provides design criteria and performance modeling for a composite soil cover system constructed on an acid generating waste rock dump in New Brunswick. The cover was designed to minimize water and oxygen fluxes to the underlying waste rock. Cover efficiency with respect to oxygen fluxes depended on maintaining high saturation since moisture losses due to evaporation may have led to failure. Empirical labora-

tory tests were required in order to achieve an estimate for the appropriate evaporation function for the cover.

Barbour et al. (1993) evaluated the saturated-unsaturated groundwater conditions of a sulphide-rich, thickened tailings deposit in Ontario. Oxidation of the tailings at the surface is known to increase as the degree of saturation decreases. The analysis showed that increased evaporative fluxes during the summer months decreased the thickness of the tension-saturated zone above the water table resulting in the increased potential for desaturation of the tailings surface. The evaporative fluxes used for the analysis were assumed on the basis of empirical pan evaporation rates. Since actual evaporative fluxes were not evaluated, the accuracy of the analysis can be questioned.

Other applications exist in geotechnique where evaporative fluxes at the soil surface must be evaluated. Silvestri et al. (1990) showed settlement problems in lightweight structures founded on Champlain clays in Montreal to be strongly controlled by potential evapotranspiration and associated rainfall deficits. Sattler and Fredlund (1989) demonstrated how heave and settlement for expansive clay soils are affected by evaporation.

Most of the previous work for describing evaporation is found outside the traditional area of geotechnical engineering in disciplines such as hydrology and soil science. In response to the need to develop a clear rationale for geotechnical applications, this paper reviews the necessary background for evaluating evaporation found in these other disciplines. Laboratory data are presented where actual evaporation rates from initially saturated soil surfaces of sand, silt and clay were measured. A simple theoretical approach for the prediction of evaporation from soils is presented and comparisons are made with measured values.

G.W. Wilson. Assistant Professor, Department of Civil Engineering, Unsaturated Soils Group, University of Saskatchewan, Saskatoon, SK, Canada, S7N 5A9.

D.G. Fredlund, S.L. Barbour. Professors, Department of Civil Engineering, Unsaturated Soils Group, University of Saskatchewan, Saskatoon, SK, Canada, S7N 5A9.

Reproduced with permission from the *The Canadian Geotechnical Journal*, 34(4): 145-155, 1997.

Definitions

The concept of potential evaporation, PE, has been used in engineering practice for nearly 50 years (Thornthwaite 1948). In the most simple terms, PE is considered to be an upper limit or maximum rate of evaporation. The International Glossary of Hydrology (World Meteorological Organization 1974) defines potential evaporation as:

“The quantity of water vapor which could be emitted by a surface of pure water per unit surface area and unit time under the existing atmospheric conditions.”

Evaporation from a water surface can be computed by the simple and well known equation for mass transfer, first given by Dalton in 1802 (Gray 1970):

$$[1] \quad E = f(u)(e_s - e_a)$$

where:

E = rate of evaporation (mm/day),

e_s = saturation vapor pressure at the temperature of the water surface (kPa),

e_a = vapor pressure of the air in the atmosphere above the water surface (kPa), and

$f(u)$ = transmission function which depends on the mixing characteristics of the air above the evaporating surface.

The transmission function $f(u)$ can be established empirically (Gray 1970).

Many contemporary mass transfer equations in use take the same basic form as Dalton's equation with the function $f(u)$ evaluated on the basis of aerodynamic profile and eddy diffusion similarity theory.

In simple terms, the mass transfer given in eq. [1] describes evaporation as a function of the difference in vapor pressure between the water surface and overlying air. The vapor pressure of the evaporating water surface, e_s , is the saturation vapor pressure of the water given by the Clausius-Clapeyron equation (Brutsaert 1982) which is a function of temperature. The vapor pressure in the air above the water, e_a , is determined on the basis of the saturated vapor pressure at the measured air temperature and relative humidity. Determining the surface temperature of the water can be extremely difficult (Gray 1970) and as a result, eq. [1] often becomes indeterminate. Penman (1948) rendered the problem determinant by incorporating the energy budget and net radiation available to the evaporating water surface.

The actual rate of evaporation from vegetated and bare soil surfaces is stated to be approximately equal to the rate of evaporation from an open or free water surface (i.e., PE) provided the supply or availability of water to the surface is unlimited (Penman 1948). This suggests that the rate of evaporation from a wet soil surface can be evaluated using the same techniques as used for free water surfaces. However, the approach becomes inaccurate once the soil surface begins to dry and becomes unsaturated. As a result, traditional methods for predicting potential evaporation from saturated surfaces such as the

Penman method provide over-estimates of evaporation for unsaturated soil surfaces (Morton 1985; Granger 1989a).

Literature review

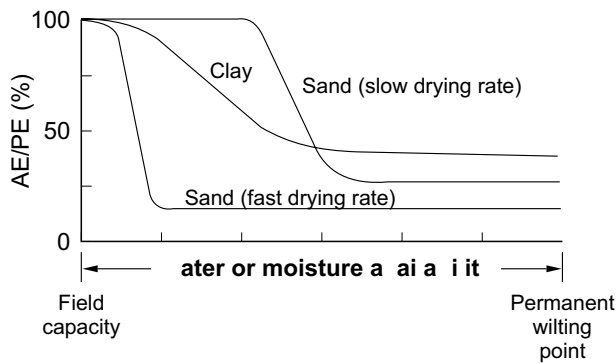
Hydrologists, soil scientists and engineers have been attempting to evaluate evaporation from unsaturated soils for a number of decades. Figure 1, after Holmes (1961) and Gray (1970), shows the relationship between potential evaporation, PE, from a free water surface and actual evaporation, AE, for typical sand and clay soil surfaces which are allowed to evaporate from initially wet or nearly saturated states. Holmes (1961) showed that the AE is equal to the PE (i.e., AE/PE equals unity) for both the sand and clay soils when the water content is high or near the field capacity. The ratio of AE/PE for each soil type begins to decline as the availability of water decreases to the permanent wilting point for plants. Holmes (1961) and Gray (1970) do not explicitly state the units of water or moisture availability, but the limit of the permanent wilting point (i.e., approximately equal to 15 atmospheres of suction) implies that the soil has negative pore-water pressures or suction.

Figure 1 shows that as water becomes less available, the decline in the ratio AE/PE varies significantly depending on the soil texture and drying rate. For example, the ratio AE/PE for the sand undergoing rapid drying is significantly less than that for the slow drying sand when the water availability is at the midpoint between the field capacity and the permanent wilt point. The curve for the clay indicates a higher rate of actual evaporation than either the fast or slow drying sand as the water availability approaches the permanent wilt point. In summary, Fig. 1 indicates that the actual evaporation rate from soil surfaces relative to the potential evaporation rate is a function of water availability, soil texture and drying rate. No single variable or soil property appears to control the evaporation rate from the soils.

The difficulty with respect to defining the soil properties that control evaporation from unsaturated soil surfaces has resulted in the development of empirical methods. For example, Hillel (1980) suggests the drying of a soil surface may be simulated using square root time relations. The function is purely empirical and the actual mechanisms that control soil evaporation are not identified. Yanful et al. (1993) essentially adopted an empirical approach for evaluating the performance of a soil cover system for acid generating waste rock.

A few attempts have been made to define the dependent variables which control evaporation from unsaturated soil. Barton (1979) suggested soil evaporation can be estimated on the basis of the humidity and water content of the near surface soil. Hammel et al. (1981) also described actual evaporation from soil as a function of soil water content and included water flow processes in the soil with combined moisture and temperature gradients. Granger (1989b) stated that evaporation from unsaturated soil surfaces is a function of the actual vapor pressure at the soil

Fig. 1. Typical drying curves for sand and clay showing actual evaporation, AE, as a percentage of potential evaporation, PE, versus water availability (after Holmes 1961).



surface. This behavior is in agreement with eq. [1]. The actual vapor pressure for unsaturated soil surfaces is less than the vapor pressure that would occur at full saturation of the soil, hence, evaporation is suppressed. However, Granger (1989b) did not provide a means for evaluating the actual vapor pressure at the unsaturated soil surface.

Wilson et al. (1994) developed a coupled soil-atmosphere model for soil evaporation. The model solved for evaporation using eq. [1] with the vapor pressure at the soil surface determined on the basis of solving coupled heat and mass transfer equations for the soil profile below the surface. Model predictions for a sand profile were compared to laboratory measurements with good correlations. However, the laboratory tests were conducted using a column of ideal cohesionless uniform sand. The suitability of the theoretical model for other soils such as a fine grained silt or cohesive clay was not demonstrated.

In general, the work described above shows that for given climatic conditions, the evaporation rate from unsaturated soils is less than the evaporation rate from saturated soils or water. The mass transfer (i.e., eq. [1]), that defines evaporation, indicates that a reduction in the evaporation rate from a soil surface that is drying from an initial state of saturation under constant climate conditions will occur only if the vapor pressure at the soil surface, e_s , decreases during drying. However, this basic principle has not been clearly demonstrated. Instead, the decline in evaporation rates for unsaturated soil surfaces has been explained on the basis of a variety of other factors such as soil water availability or water content, soil texture, drying rate and drying time.

The present work evaluates the process of evaporation from soil surfaces composed of various soil types that were allowed to evaporate under controlled laboratory conditions. The laboratory testing program carried out used two identical evaporation pans. One pan contained water to measure the potential evaporation rate and the second pan contained soil to measure the actual soil evaporation rate. The simultaneously measured actual and potential evaporation rates were compared as the soil surfaces desiccated from wet to dry. The influence of soil

parameters such as texture, drying time, water content and soil suction were also evaluated.

Laboratory test program

Evaporation tests were carried out using three texturally distinct soil types selected to represent the clay, silt and sand soil groups. The soils were as follows:

- (1) Beaver Creek sand
- (2) Custom silt
- (3) Regina clay

The Beaver Creek sand was a fine, uniform, natural aeolian soil consisting of 98 percent sand and 2 percent silt and clay. This material was selected to represent granular, cohesionless soils. Regina clay which is a highly plastic lacustrine deposit was the natural soil selected to represent fine-grained, cohesive soils. A silt material was also included to represent a fine-grained cohesionless soil intermediate to the extremes of a clean sand and a highly plastic clay. The silt was a custom material containing 84 percent silt produced in the laboratory. A summary of the soil properties for each soil type are presented in Table 1.

Water retention characteristics

The soil-water characteristic curves were determined for each of the selected soil types. The soil-water characteristic curve of a soil is a measure of the availability of water since it provides a relationship between water content and soil suction. The soil-water characteristic curves for the Beaver Creek sand, Custom silt and Regina clay were evaluated using pressure plates and glass desiccators containing electrolyte solutions.

Pressure plates were used to determine water contents at various values of matric suction between 0 and 100 kPa. Soil water contents for high values of suction were determined using osmotic pressures induced by electrolyte solutions. The osmotic pressure of the electrolyte solutions in the glass desiccators was calculated using the well known expression for thermodynamic equilibria of solvents given by Robinson and Stokes (1955) as follows:

$$[2] \quad \pi = \frac{RT}{V_A} \ln a_w$$

where:

π = osmotic pressure or suction (kPa),

R = universal gas constant (8.314 J/mol·K),

T = absolute temperature (K),

V_A = molar volume, and

a_w = activity of water for the aqueous solution.

Five aqueous solutions were selected to give a suitable range of osmotic suction. Table 2 provides a summary of the salt solutions used and the corresponding values of osmotic suction.

Each soil type was slurried with distilled water and placed into the pressure plate in a saturated state. The air pressure in the pressure plate was increased by increments of 25 kPa allowing the samples to reach an equilib-

Table 1. Summary of material properties used for each soil type in the evaporation tests.

Item	Beaver Creek sand	Custom silt	Regina clay
Description	fine, uniform clean sand; aeolian	coarse to medium clean silt; laboratory produced	highly plastic clay; lacustrine
Texture	98.0% sand 2.0% silt and clay	7.0% sand 84.0% silt 9.0% clay	8.0% sand 41.0% silt 51.0% clay
Atterberg limits	non-plastic	plastic	plastic
Liquid limit	—	26.8%	75.5%
Plastic limit	—	25.4%	24.9%
Plasticity index	—	1.4	50.6
USCS	SP	ML	CH
Specific gravity	2.67	2.72 (estimated)	2.83
Void ratio at 100 kPa suction	0.63	0.85	1.34

Table 2. Summary of saturated salt solutions, activity coefficients and osmotic suctions used for the vacuum desiccators at 20°C.

Salt solution	Activity coefficient	Osmotic suction (10 ⁻³ kPa)
Lithium chloride [LiCl H ₂ O] and [LiCl 2H ₂ O]	0.115	292.4
Magnesium chloride [MgCl ₂ 6H ₂ O]	0.330	152.4
Magnesium nitrate [Mg(NO ₃) ₂ 6H ₂ O]	0.543	84.0
Sodium chloride [NaCl]	0.755	38.6
Potassium sulphate [K ₂ SO ₄]	0.970	4.19

rium water content for each increment of matric suction to a maximum of 100 kPa. Small specimens of soil weighing approximately 1 gram each were then removed from the pressure plate at the end of the procedure. These specimens were placed directly into each of the five glass desiccators and the soil water contents allowed to come to equilibrium with the osmotic suction established in the desiccators. The specimens were separated from the electrolyte solutions in the reservoirs of the glass desiccators by an air space which functioned as a semi-permeable membrane. The temperature was maintained at 20°C for the samples in the pressure plate and glass desiccators. Figures 2, 3 and 4 show the measured soil-water characteristic curves for the Beaver Creek sand, Custom silt and Regina clay, respectively, for suctions ranging from 25 kPa to approximately 300 000 kPa.

The soil-water characteristic curve for the Regina clay at 20°C (Fig. 4) was established using several additional values of water content and corresponding values of suction obtained from Fredlund (1964). Fredlund (1964) determined these points by the pressure plate glass desiccator method as described above.

Evaporation tests

The second stage of the testing program was to conduct evaporation tests using sections of each soil type.

Thin soil sections were selected in order to minimize the influence of soil water below the evaporating soil surface. Hillel (1980) states:

“the actual evaporation rate is determined either by external evaporativity or by the soil’s own ability to deliver water, whichever is the lesser (and hence the limiting factor).”

The objective of the test procedure described herein was to determine the soil properties at the soil surface or the soil boundary layer that control evaporation. The soil sections were therefore made as thin as possible to minimize potential flow processes in the soil below the surface from influencing the rate of evaporation from the surface of the soil.

The thin soil section evaporation tests were conducted such that the actual evaporation rate from the soil surfaces was continually measured as drying took place from an initially saturated state to a completely air-dried state. The thin soil sections were artificially formed on a circular, 258 mm diameter, evaporation pan as shown in Fig. 5. Each evaporation test was carried out using two identical evaporation pans. One pan contained the thin section of soil surface to determine the actual evaporation rate, while the second identical pan contained distilled water that provided the reference for the potential evaporation rate. The mass and change in mass of each pan was continually monitored to determine the rate of evaporation from the pans. The water contents of the soil specimens at various times during each test were determined using the final mass of dry soil and water at the end of the test plus the instantaneous masses measured during the test. The temperature of the soil surfaces, the water surface and the air was also monitored continuously along with the relative humidity of the air above the evaporating surfaces. All tests were conducted at room temperature in the geotechnical laboratory at the University of Saskatchewan, Saskatoon.

Two thin section drying tests were completed for each soil type, (i.e., sand, silt and clay). Numerous attempts were required in order to develop a procedure that provided a thin layer of soil with a uniform thickness and initial water content. The thin soil sections were prepared by gently dusting a layer of soil on to the pan using a

Fig. 2. Soil-water characteristic curves for Beaver Creek sand at 20°C.

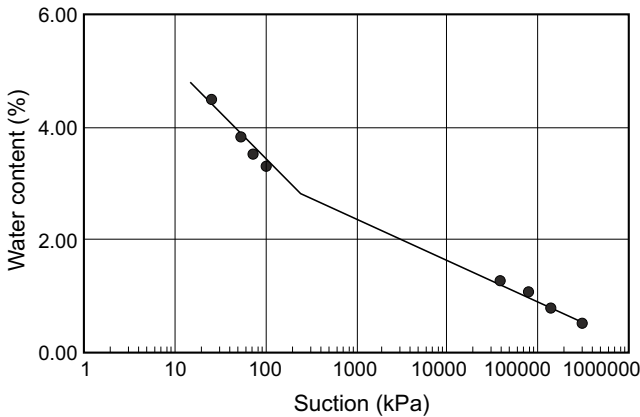


Fig. 3. Soil-water characteristic curves for Custom silt at 20°C.

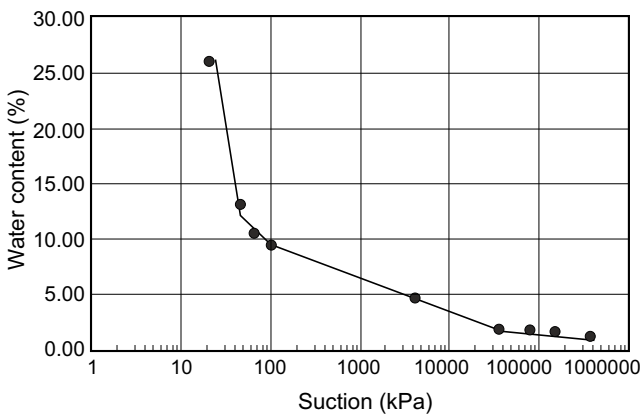
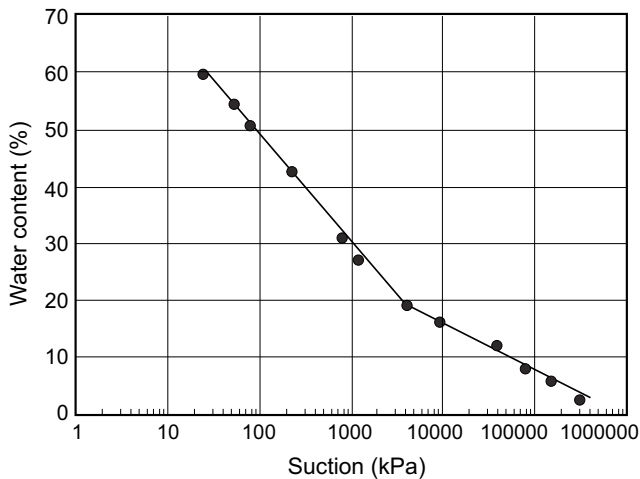


Fig. 4. Soil-water characteristic curves for Regina clay at 20°C.



hand-held sieve filled with powdered dry soil. An 850 μm sieve was used to apply the Beaver Creek sand, while a 425 μm sieve was used to apply the Custom silt and Regina clay. The dusted soil layers were applied uniformly

until a thickness just adequate to visually cover the aluminum surface of the pan was achieved. The final layer thickness for the two Beaver Creek sand specimens were 0.5 mm and 0.7 mm, while the final layer thicknesses for the two Custom silt and one of the Regina clay surfaces was 0.3 mm. A layer thickness of 0.2 mm was used for the second Regina clay specimen.

The dry soil layers were wet to saturation with a fine uniform mist of distilled water. The mass of the soil specimens were then monitored while evaporating to an air dry state. Table 3 provides a summary of the six thin soil section drying tests. Figure 6 shows the normalized evaporation, AE/PE, obtained for the soil and water surfaces measured with respect to time for the Beaver Creek sand, Custom silt and Regina clay. The normalized evaporation parameter is selected for convenience since the potential evaporation is controlled primarily by atmospheric conditions and surface temperature that are the same for both the water and soil surfaces during each evaporation test.

Discussion and analysis

The soil-water characteristic curves for each soil are shown in Figs. 2, 3 and 4. These drying curves are important because the graphs show the amount of water retained in the soil over the total range of soil suction. Wetting the soils from a dry state to a wet state (i.e., high suction to low suction) would result in slightly different curves due to the effects of hysteresis. The drying curves shown are most applicable to the thin soil section evaporation test.

Geotechnical engineers are most familiar with soil suctions that are relatively low when compared with those shown in Figs. 2, 3 and 4. The unsaturated soils dealt with usually have values of matric suction not exceeding 500 kPa. In nature; however, soils at the ground surface commonly have extremely high values of suction. The permanent wilting point of plants found in semi-arid climates is approximately 1500 kPa. Even at large values of suction, considerable water may still be present in the soil. For example, in Fig. 4, Regina clay has a water content of approximately 25 percent at 1500 kPa of suction. This corresponds approximately to the water content at the plastic limit. Natural soils commonly reach a completely air dried state at the ground surface. This would be the case for the exposed soil surface of a cover for a municipal landfill after several days of continuous drying without precipitation. The water content for Regina clay, for example, may be as low as 6 per cent at the ground surface. Figure 4 shows that this water content would correspond to a value of total suction of approximately 200 000 kPa. Oven drying at a temperature of 105°C results in a suction approaching 1 000 000 kPa. Although the physical properties of soil water at extremely high values of suction are not yet fully explained (Fredlund 1991), it can be argued that understanding the behavior of natural soils at and near the ground surface requires the acceptance of soil suctions far in excess of 500 kPa.

Fig. 5. a) Thin soil section drying test apparatus. b) Detailed section of the evaporation pan used for the thin soil section evaporation test.

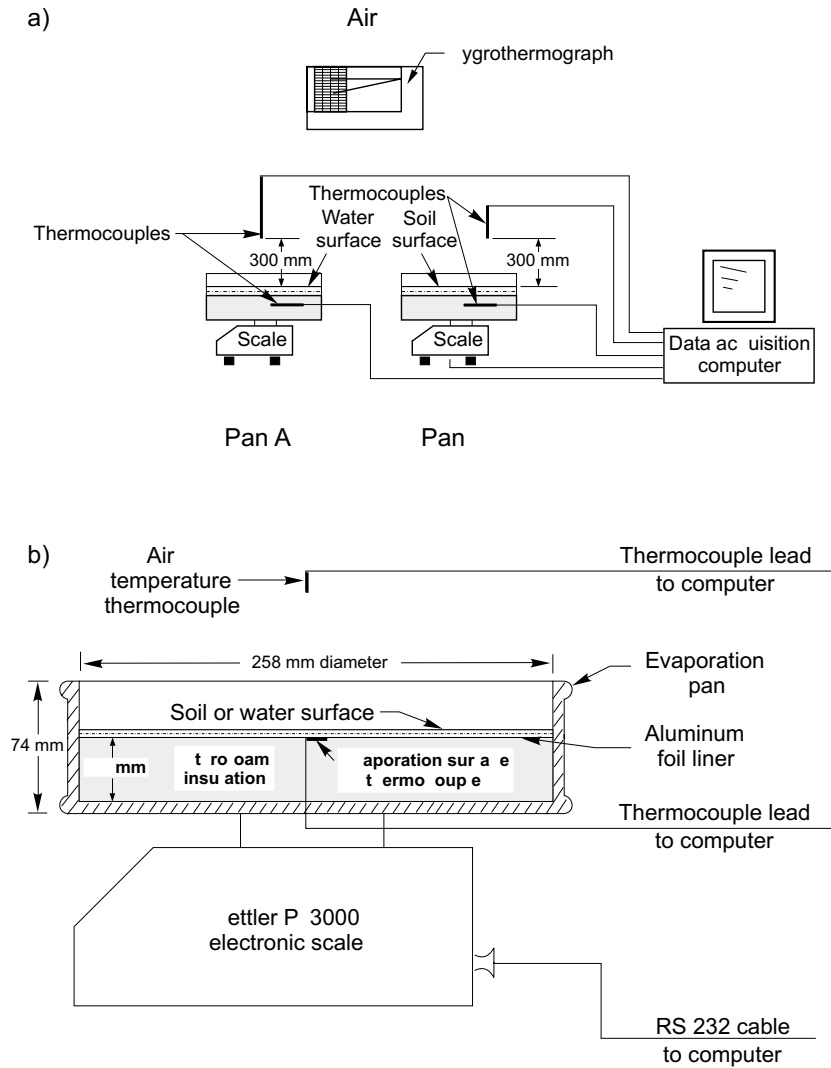


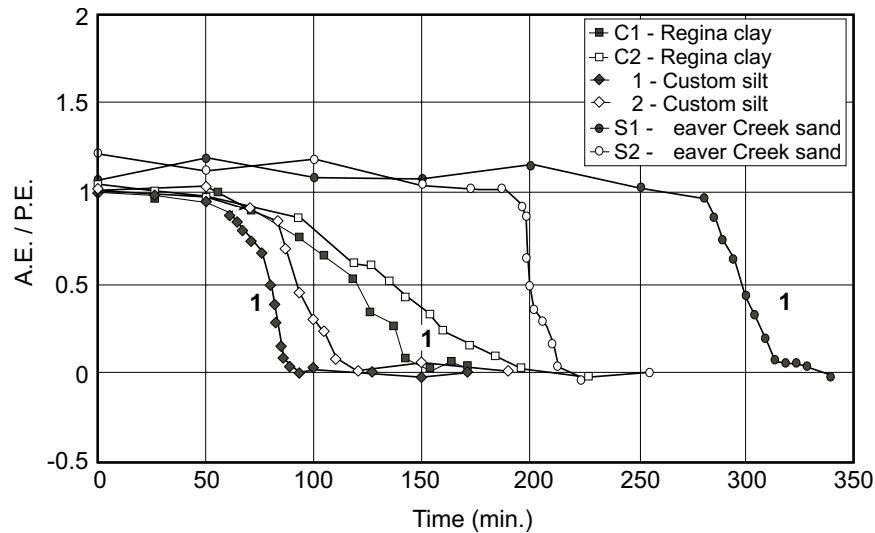
Table 3. Summary of thin soil section evaporation tests.

Specimen No.	Soil type	Sample thickness (mm)	Initial water content (%)	Test duration (min.)	Mean room air temp. (°C)	Mean relative humidity of air (%)	Mean water pan evaporation (mm/day)
S1	Beaver Creek sand	0.7	25.0	330	23.1	53	1.31
S2	Beaver Creek sand	0.5	25.5	250	22.7	44	1.40
M1	Custom silt	0.3	30.0	125	22.5	39	1.71
M2	Custom silt	0.3	28.8	190	23.0	62	1.16
C1	Regina clay	0.3	63.5	195	22.8	35	1.54
C2	Regina clay	0.2	61.2	225	25.5	50	1.29

It should be noted that a distinction has been made between matric suction and total suction in Figs. 2, 3 and 4. The suctions established using the pressure plate method correspond to values of matric suctions (i.e., $u_a - u_w$). Osmotic suction due to the presence of dissolved solids is not included. Distilled water was used for all test proce-

dures, therefore, the value of osmotic suction for the Beaver Creek sand and Custom silt may be assumed to be relatively small. This assumption may not, however, be true for the Regina clay due to its geochemical nature. Krahn (1970) showed osmotic suction to be approximately 200 kPa for Regina clay having a water content of

Fig. 6. The ratio of actual evaporation and potential evaporation, AE/PE, versus drying time for the Beaver Creek sand, Custom silt and Regina clay.



30 percent. This indicated that a high level of dissolved solids was present in the clay. The use of distilled water during sample preparation diluted but did not remove the salts. In summary, the values of matric suction established by the pressure plate method for the Regina clay may under-estimate total suction.

The soil water contents shown in Figs. 2, 3 and 4 that correspond to high values of suction (i.e., greater than 1500 kPa) were established in the desiccators through vapor equilibrium with the osmotic suction of the electrolyte solutions. The soil water contents actually correspond to total suction which includes both matric and osmotic suction. It is difficult to establish the relative components of matric and osmotic suction at such high values of total suction, but it is reasonable to assume that the magnitude of osmotic suction will increase at lower water contents since the mass of dissolved solids remains constant.

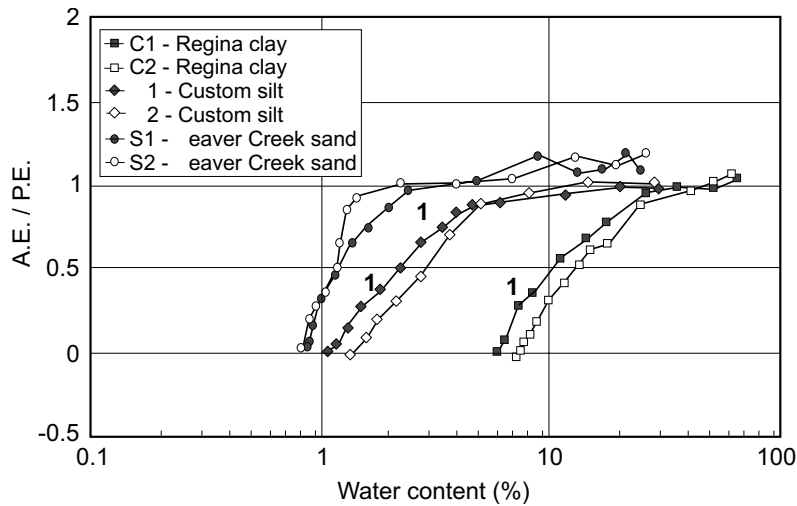
Figure 6 shows the ratio of AE/PE, versus time for each sample of Beaver Creek sand, Custom silt and Regina clay. The curves are similar to those given by Holmes (1961) in Fig. 1 except that the AE/PE ratio is plotted as a function of time rather than water availability. Time zero in Fig. 6 corresponds to a nearly saturated state (or a high water availability) which is similar to the field capacity in Fig. 1. The normalized evaporation, AE/PE, is approximately unity for all specimens at the start of the evaporation test. It can be seen that the ratio is slightly greater than 1.0 for the Beaver Creek sand specimens S1 and S2. This deviation can be attributed to slight variations in the aerodynamic resistance in the air spaces above the water and soil evaporation pans as well as the surface temperatures at the time of the tests. All specimens continue to evaporate at a near potential rate and then begin to decline after a period of time. The rate of evaporation decreases first for the silt, followed by the clay and finally the sand. The evaporation rate for all soils fall to zero after each soil specimen reaches an air

dry state. It is difficult to understand and compare all of the controlling variables for Fig. 6 since each soil type has a different initial water content, sample thickness and volume of water available for evaporation.

Figure 7 shows a plot of the AE/PE ratio versus water content for each specimen. The break or decline in evaporation rate occurs at a specific water content for each soil type. For example, the decline in evaporation for Regina clay specimens C1 and C2 occurs at a water content of approximately 20 percent. The Custom silt and Beaver Creek sand have a break in the evaporation rate at water contents of 5 and 2 percent, respectively. When the plots for the clay specimens C1 and C2, and for the silt specimens M1 and M2, are compared, they show slight variations. Specimens C1 and M1 reach zero evaporation at slightly lower water contents than specimens C2 and M2. This slight variation can be attributed to a difference in the relative humidity of the air at the time of each test since relative humidity control in the test area was not available. Table 3 shows the relative humidity in the air at the time of each test and it can be seen that tests C1 and M1 were performed at significantly lower relative humidities than tests C2 and M2. Hence, the air-dried soils for tests C1 and M1 have less hygroscopic moisture. Tests S1 and S2 were performed with similar humidities and therefore show closer agreement for the final water content corresponding to zero evaporation (or an AE/PE ratio equal to zero).

The data shown in Fig. 7 suggests that the water content of the soil influences the rate of evaporation for each soil type. However, water content alone cannot be identified as the unique independent variable controlling the actual rate of evaporation for all soil types. Soil texture must also be taken into consideration. Water content may, however, be used to determine the value of total suction in the soil. The soil-water characteristic curves shown in Figs. 2, 3 and 4 were used to determine corresponding values of total suction at each measured water content

Fig. 7. The ratio of actual evaporation and potential evaporation, AE/PE, versus water content for Beaver Creek sand, Custom silt and Regina clay.



during the evaporation tests. Figure 8 shows a plot of the AE/PE ratio versus total suction for the Beaver Creek sand specimen S1, Custom silt specimen M1, and Regina clay specimen C2. The tests for specimen S1 and C2 were conducted at a relative air humidity of approximately 50 percent. The tests for specimen M1 were performed at a lower relative air humidity of approximately 40 percent.

Figure 8 shows a reasonably good correlation between the ratio of AE/PE and total suction. This correlation is independent of time, water content and soil texture. The ratio of AE/PE is approximately constant and equal to unity for values of total suction less than approximately 3000 kPa. The actual rate of evaporation begins to decline once the value of the total suction exceeds approximately 3000 kPa. The rate of actual evaporation continues to decrease as the value of total suction increases. The AE/PE ratio then falls to zero for the three soil types at values of total suctions slightly larger than 100 000 kPa.

The relationship between total suction and AE/PE can be explained by considering the relationship between relative humidity and total suction given by Edlefsen and Anderson (1943):

$$[3] \quad h_r = e^{\left(\frac{\psi g W_v}{RT}\right)}$$

where:

h_r = relative humidity in the unsaturated soil voids (i.e., actual vapor pressure divided by saturation vapor pressure),

ψ = total suction in the liquid water phase expressed as equivalent matric suction and as a negative value (m),

W_v = molecular weight of water (0.018 kg/mol), and

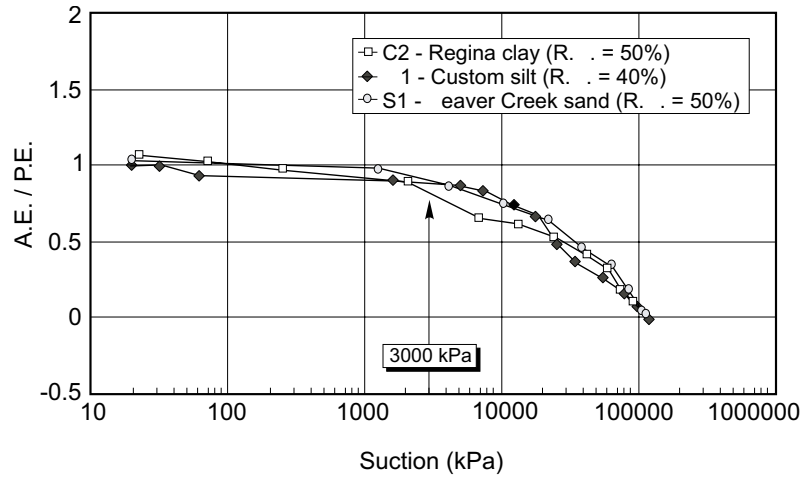
g = acceleration (m/sec²).

Figure 9 shows this relationship graphically on a semi-logarithmic plot. Relative humidity is an exponential function of total suction and the decline in relative humidity with increasing suction is initially small. A substantial decrease in the relative humidity occurs only after the value of total suction exceeds 2000 to 3000 kPa (i.e., 3000 kPa of total suction corresponds to a relative humidity of approximately 98 percent). The suppression of relative humidity results in an equivalent decline in the absolute vapor pressure at the soil surface. Since eq. [1] shows the rate of evaporation to be a function of the vapor pressure at the evaporation surface, the rationale that suggests that the actual rate of evaporation depends on the total suction at the soil surface appears valid.

Figure 8 has illustrated that the AE/PE ratio is equal to zero for a value of total suction slightly greater than 100 000 kPa. This point of zero evaporation is controlled by the relative humidity in the air. The evaporating soil surface dries to a point which is in equilibrium with the air. For example, test C2 was performed with a room air relative humidity of 50 percent. As shown in Fig. 9, this corresponds to a total suction of approximately 100 000 kPa. Soil evaporation should cease when the relative humidity in the soil reaches equilibrium with the relative humidity of the air above the soil. Hence, zero evaporation should correspond to a suction of 100 000 kPa as shown in Fig. 8. Alternately, evaporation would have continued to a higher value of total suction if the humidity in the air were less. A room air relative humidity of 20 percent would have resulted in a total suction of approximately 200 000 kPa for the soil surface to reach air dry equilibrium.

The relationship between actual soil evaporative fluxes and total suction in the soil is important to geotechnical engineers since it forms the basis for the prediction of actual evaporative fluxes. Predicting the values of AE/PE as a function of total suction shown in Fig. 8 can be achieved by combining eqs. [1] and [3]. Using eq. [1] and

Fig. 8. The ratio of actual evaporation and potential evaporation, AE/PE, versus total suction for the Beaver Creek sand, Custom silt and Regina clay.



assuming $f(u)$ is the same for both the soil surface and the water surface gives:

$$[4] \quad \frac{AE}{PE} = \frac{(e_o - e_a)}{(e_s - e_a)}$$

where:

- e_o = actual vapor pressure of the soil surface, equal to the product of h_r and e_s (kPa),
- e_s = saturation vapor pressure, defined by the temperature of the soil, water and air; and
- e_a = vapor pressure of the air, equal to the product of the relative humidity measured in the air (i.e., Table 3) and e_s .

Assuming the air, water and soil are at approximately the same temperature so that e_s cancels out and substituting eq. [3] into eq. [4] gives:

$$[5] \quad \frac{AE}{PE} = \left(\frac{\frac{\psi_g W_c}{e^{RT}} - h_a}{1 - h_a} \right)$$

where:

- h_a = relative humidity of the air above the evaporating soil and water surfaces.

It is important to note that should the soil, water and air temperatures not be equal, eqs. [3] and [4] must be solved using the saturated vapor pressure corresponding to each temperature.

Equation [5] provides the value of AE/PE as a function of total suction at the soil surface. The accuracy of the functional relationship can be tested through comparison with the experimental data. Figure 10 shows the curve for AE/PE as a function of total suction computed using [5], along with the values measured for the sand, silt and clay surface. It can be seen that the predicted curve compares reasonably well to the measured values. The principle that soil suction controls the normalized evaporation for a soil surface appears valid. Furthermore, this principle is

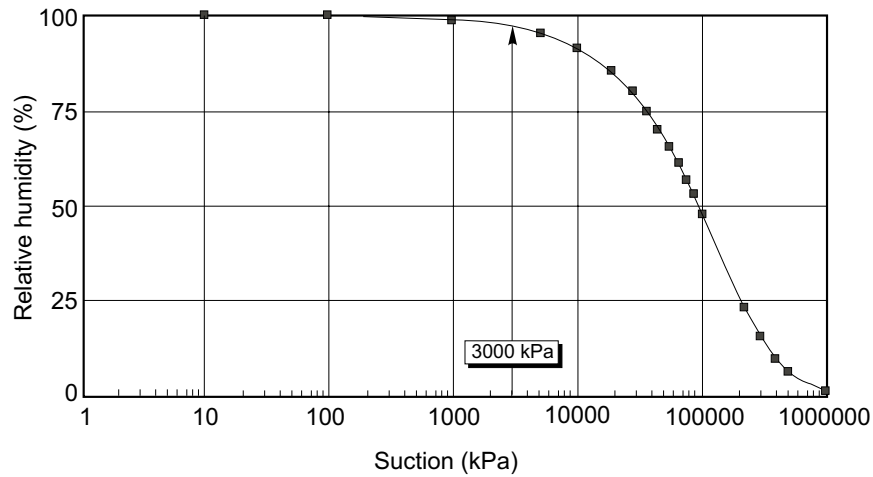
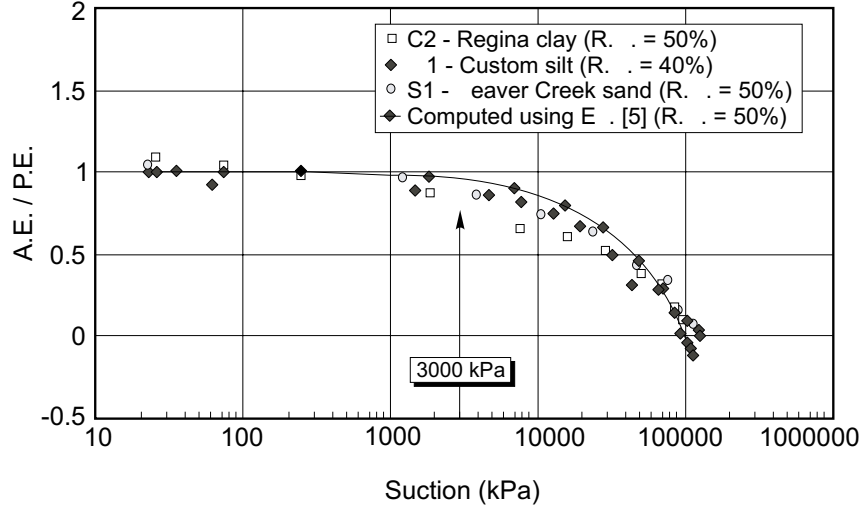
independent of other soil properties such as moisture content, texture and mineralogy.

It should be noted that this discussion has addressed only the properties of soil surfaces which control evaporative fluxes into the atmosphere. The soil evaporation tests considered only thin soil sections in the absence of the influence due to soil water below the surface. Increasing the thickness of the soil layers would greatly influence evaporative fluxes as deeper soil water would be available as recharge to the desiccating soil surfaces. The analysis of this more complex problem would require a theoretical approach which includes the influence of flow processes below the soil surface.

Summary and conclusions

Many problems in geotechnical engineering require that the exchange of water between the atmosphere and ground surface be known. The process of evaporation from soil surfaces in particular has not been clearly defined in the past. This study has found that a relationship between the actual or normalized evaporation rate and total suction does exist for three different soil types.

Evaporation from a soil surface is a function of the vapor pressure gradient between the soil surface and the ambient atmosphere. The mass transfer equation, eq. [1], initially proposed by Dalton for evaluating evaporation from water surfaces, can be modified and applied to soil surfaces. Saturated and nearly saturated soil surfaces evaporate at a potential rate approximately equal to the evaporation rate from free water surfaces. It has been found that the actual rate of evaporation from a soil surface falls below this potential rate of evaporation once the soil becomes unsaturated and the value of total suction exceeds a value of approximately 3000 kPa. This relationship occurs independently of water content. The rate of evaporation continues to decline as the total suction increases. In general, total suction (i.e., matric suction plus osmotic suction) appears to be a suitable state variable for describing soil atmosphere evaporative fluxes. This is

Fig. 9. Relative humidity versus total suction calculated on the basis of eq. [3] (20°C).**Fig. 10.** Comparison of the measured AE/PE versus total suction for the Beaver Creek sand, Custom silt and Regina clay to the curve computed using eq. [5].

consistent with the stress state variables generally used in unsaturated soil mechanics.

In summary, evaporative fluxes from soil surfaces can be evaluated on the basis of easily measured soil properties. The measured water content can be used in conjunction with the soil-water characteristic curve for total suction to calculate the vapor pressure at the soil surface. Evaporative fluxes from unsaturated soil surfaces at high values of suction are less than those from saturated surfaces under identical climatic conditions. This is an important consideration with respect to the design, for example, of soil cover systems for the control of water fluxes into underlying waste materials. In such an application, the geotechnical engineer could use a conventional method for evaluating the potential rate of evaporation (i.e., the Penman method) and modify it to obtain the actual evaporation for unsaturated conditions using eq. [5].

References

- Barbour, S.L., Wilson, G.W., and St-Arnaud, L.C. 1993. Evaluation of the saturated-unsaturated groundwater conditions of a thickened tailings deposit. *Canadian Geotechnical Journal*, **30**: 935–946.
- Barton, I.J. 1979. A parameterization of the evaporation from nonsaturated surfaces. *Journal of Applied Meteorology*, **18**: 43–47.
- Brutsaert, W.H. 1982. *Evaporation into the atmosphere*. P. Reidel Publishing Company, Dordrecht, Holland.
- Edlefsen, N.E., and Anderson, A.B.C. 1943. Thermodynamics of soil moisture. *Hilgardia*, **15**(2): 31–298.
- Fredlund, D.G. 1964. Comparison of soil suction and one-dimensional consolidation characteristics of a highly plastic clay. M.Sc. thesis, University of Alberta, Edmonton, AB, Canada.
- Fredlund, D.G. 1991. How negative can pore-water pressures get? *Geotechnical News*, Canadian Geotechnical Society, **9**(3): 44–46.

- Granger, R.J. 1989a. An examination of the concept of potential evaporation. *Journal of Hydrology*, **111**: 9–19.
- Granger, R.J. 1989b. Evaporation from natural non-saturated surfaces. *Journal of Hydrology*, **111**: 21–29.
- Gray, D.M. 1970. Handbook on the principals of hydrology. Canadian National Committee for the International Hydrological Decade. National Research Council of Canada.
- Hammel, J.E., Papendick, R.I., and Campbell G.S. 1981. Fallow tillage effects on evaporation and seedzone water content in a dry summer climate. *Soil Science of America Journal*, **45**: 1016–1022.
- Hillel, D. 1980. Applications to soil physics. Academic Press, New York.
- Holmes, R.M. 1961. Estimation of soil moisture content using evaporation data. Proceedings, Hydrology Symposium, No. 2 Evaporation. Queen's Printer, Ottawa, pp. 184–196.
- Krahn, J. 1970. Comparison of soil Pore water potential components. M.Sc. thesis, University of Saskatchewan, Saskatoon, SK, Canada.
- Morton, F. I. 1985. The complementary relationship areal evapotranspiration model: How it works. Proceedings, National Conference on Advances in Evapotranspiration, American Society of Agricultural Engineers, Chicago, IL, pp. 377–384.
- Penman, H.L. 1948. Natural evapotranspiration from open water, bare soil and grass. Proceedings Royal Society of London, Series A. **193**: 120–145.
- Robinson, R.A., and Stokes, R.H. 1955. Electrolyte solutions: The measurement and interpretation of conductance, chemical potential and diffusion in solutions of simple electrolytes. Academic Press, New York.
- Sattler, P., and Fredlund, D.G. 1989. Use of thermal conductivity sensors to measure matric suction in the laboratory. *Canadian Geotechnical Journal*, **26**: 491–498
- Silvestri, V., Soulie, M., Lafleur, J., Sarkis, G., and Bekkouche, N. 1990. Foundation problems in Champlain clays during droughts. 1: Rainfall Deficits in Montreal (1930–1988). *Canadian Geotechnical Journal*, **27**: 285–293.
- Thorntwaite, C.W. 1948. An approach toward a rational classification of climate. *Geographical Review*, **38**: 55–94.
- Wilson, G.W., Fredlund, D.G., and Barbour, S.L. 1994. Coupled soil-atmosphere modeling for soil evaporation. *Canadian Geotechnical Journal*, **31**: 151–161.
- World Meteorological Organization. 1974. International glossary of hydrology. World Meteorological Organization Report No. 385.
- Yanful, E.K., Bell, A.V., and Woysner M.R. 1993. Design of a composite soil cover for an experimental waste rock pile near Newcastle, New Brunswick, Canada. *Canadian Geotechnical Journal*, **30**: 578–587

An introduction to analytical modeling of plant transpiration for geotechnical engineers

D.J. Tratch, G.W. Wilson, and D.G. Fredlund

Abstract: Geotechnical engineers have been historically concerned with groundwater flow, particularly within the saturated zone. More recently, geotechnical engineers have identified the importance of unsaturated flow and the flux boundary condition with respect to water flow across the soil-atmosphere interface. Plant transpiration is an important component of the surface flux rate.

This paper outlines a theoretical approach for the prediction of transpiration rates. A laboratory experiment was conducted to measure evapotranspiration rates and analytical modeling was performed to simulate laboratory data. The experimental results identify the significance of including the transpiration flux in the surface flux boundary condition. The analytical modeling results show the proposed methodology for the prediction of transpiration to be reasonably accurate.

Key words: unsaturated flow, soil-atmosphere interphase, modeling, plant transpiration, evapotranspiration

Introduction

The science of geotechnical engineering must, with an ever expanding knowledge base, continually apply theory developed by other disciplines. The evaluation of plant transpiration is one such area where the research has been conducted primarily by Soil Scientists. Geotechnical engineers often overlook the surface flux component related to the vegetative cover. The flux boundary condition at the soil surface is a critical factor for problems in geotechnical engineering related to soil cover system design, saturated/unsaturated groundwater flow, slope stability and volume change in expansive soils. In such engineered systems, the transpiration component may be critical in the success of the design.

The design of soil covers involves the placement of multiple soil layers over hazardous wastes. The arrangement allows for the control of oxygen diffusion and moisture percolation into the underlying waste to reduce leachate production. Vegetation is placed on the soil cover for aesthetic as well as design purposes. Vegetation promotes the integrity of the soil against erosion due to surficial runoff waters. The resulting influence of the vegetative cover on the performance of the cover system with respect to moisture flow must be evaluated. A re-

view of literature on existing transpiration prediction methodologies identifies a science that although has had immense research conducted does not have consensus on an acceptable method to predict transpiration. Methods to predict transpiration vary between highly empirical (de Jong 1974) to physically based models that are highly theoretical (Federer 1979). Marker and Mein (1985) state that empirical based models lack accuracy whereas theoretical methods are too complicated for routine use.

Methodology to predict transpiration

The computer program SoilCover (MEND 1993) was developed by researchers of the Unsaturated Soils Group at the University of Saskatchewan, Saskatoon. SoilCover is a one-dimensional, transient, heat and mass transfer finite element model. One of the special features of SoilCover is the ability to evaluate bare soil evaporation from unsaturated soil surfaces as given in eq. [1] by Wilson et al. (1994).

$$[1] \quad E = f(u)(e_s - e_a)$$

where:

E = actual evaporation from the saturated/unsaturated soil surface (mm/s),

$f(u)$ = turbulent mixing parameter (units),

e_s = vapour pressure at the soil surface (units), and

e_a = vapour pressure in the overlying atmosphere (units).

The partial differential equation describing mass movement through porous media, including its modification to include the transpiratory root uptake flux is presented in eq. [2] (Wilson 1990). Wilson (1990) also provides a heat transfer equation which is solved simultaneously with eq. [2].

D.J. Tratch. Geotechnical Engineer, Clifton Associates Ltd., 340 Maxwell Crescent, Regina, SK, Canada, S4N 5Y5.

G.W. Wilson. Assistant Professor, Department of Civil Engineering, University of Saskatchewan, 57 Campus Drive, Saskatoon, SK, Canada S7N 5A9.

D.G. Fredlund. Professor, Department of Civil Engineering, University of Saskatchewan, 57 Campus Drive, Saskatoon, SK, Canada S7N 5A9.

Reproduced with permission from the *Proceedings, 48th Canadian Geotechnical Conference*, Vancouver, BC, September 25–27, 1995, Vol. 2, pp. 771–780.

$$[2] \quad \frac{\partial h_w}{\partial t} = C_w^1 \frac{\partial}{\partial y} \left(k_w \frac{\partial h_w}{\partial y} \right) + C_w^2 \frac{\partial}{\partial y} \left(D_v \frac{\partial P_v}{\partial y} \right) + S$$

where:

h_w = total hydraulic head (m),

k_w = coefficient of permeability as a function of matric suction (m/s),

D_v = coefficient of water vapour diffusion through the soil (kg·m/kN·s),

$C_w^1 = \left(\frac{1}{\rho_w g m_w^2} \right)$ modulus of volume change of water with respect to the liquid phase,

$C_w^2 = \left(\frac{1}{(\rho_w)^2 g m_w^2} \right)$ modulus of volume change of water with respect to the vapour phase,

m_w^2 = slope to soil-water characteristic curve (1/kPa),

ρ_w = mass density of water (kg/m³),

P = total pressure in the bulk air phase (kPa),

P_v = actual vapour pressure in the bulk air phase (kPa),

t = time (s),

y = vertical position (m), and

S = root uptake sink term (m/s).

The first term on the right hand side of eq. [2] describes the flow of liquid phase water according to Darcy's law. The second term describes the flow of vapour phase water according to Fick's law. The third term describes the root uptake sink term which occurs as a flux from each influenced node. The methodology to evaluate the sink term will be briefly discussed in the following paragraphs.

The methodology to predict transpiration has been based upon the method proposed by Feddes et al. (1978). The semi-empirical method to evaluate the transpiration flux was selected due to its ability to be adapted to bare soil and partitioned cover evaporation and evapotranspiration.

The first step in evaluating the transpiration flux involves determination of the potential evaporation rate. The term potential evaporation has been well defined in the past, hence only a brief discussion will be presented herein. The exact definition of potential evaporation differs between disciplines and various authors. However, it is generally agreed to be the maximum potential cumulative sum of bare soil evaporation and plant transpiration (Granger 1989).

The second step in evaluating the transpiration flux involves the determination of potential transpiration flux. Because the evaporation and transpiration components must be evaluated individually, the potential evaporation flux must be distributed into its evaporation and transpiration components. Ritchie (1972) observed that the transpiration component was dependent upon the leaf area

index values of the plant canopy. From his research, three degrees of vegetative cover were identified with the resulting influence upon the potential transpiration flux presented in eqs. [3], [4] and [5].

$$[3] \quad E_p = 0.0, \quad \text{LAI} < 0.1$$

$$[4] \quad E_p = E_0 (-0.21 + 0.70 \text{ LAI}^{1/2}), \quad 0.1 < \text{LAI} < 2.7$$

$$[5] \quad E_p = E_0, \quad 2.7 < \text{LAI}$$

where:

E_p = potential transpiration rate per unit time (mm/day),

$\text{LAI} = \left(\frac{\text{surface area}_{\text{leaf}}}{\text{surface area}_{\text{soil}}} \right)$ leaf area index of the vegetative cover, and

E_0 = the potential evaporation rate per unit time (mm/day).

Depending on the ratio of the surface area of the leaves to the soil surface area covered, the surface flux condition described by either eqs. [3], [4] and [5] assumes either; evaporation only, a combined evaporation and transpiration flux or solely transpiration flux conditions. The three phases of vegetative cover are identified as bare soil, partial cover and full cover conditions, respectively. Ritchie (1972) describes the leaf area index values which define lower and upper limits of the partial cover condition as 0.1 and 2.7 respectively.

The mass flux due to transpiration, being a surface potential flux, must be distributed through the soil profile which is occupied by the vegetative root structure. The proposed method of distributing the potential transpiration is presented in Fig. 1 as a decreasing uptake rate with depth (Prasad 1988).

The potential transpiration flux, defined in Fig. 1, is distributed into nodal fluxes. The potential nodal flux rates are then dependent upon the potential transpiration flux, the location of the node with respect to the top and bottom of the active root zone and the node spacing. The potential nodal fluxes are then modified to determine the actual nodal root uptake flux as required in eq. [2]. The potential root uptake flux is modified by a reducing term given in eq. [6], which is in turn based upon the matric suction at that nodal locations by the relationship presented in Fig. 2.

$$[6] \quad S = \text{PRU} \cdot \text{PLF}$$

where:

S = actual nodal root uptake sink term, required in eq. [1] (m/s),

PRU = potential root uptake flux (m/s), and

PLF = plant limiting factor, dependent upon the nodal matric suction as defined in Fig. 2.

Fig. 1. The shape function used to calculate the potential root uptake distribution through the above root zone (after Prasad 1988).

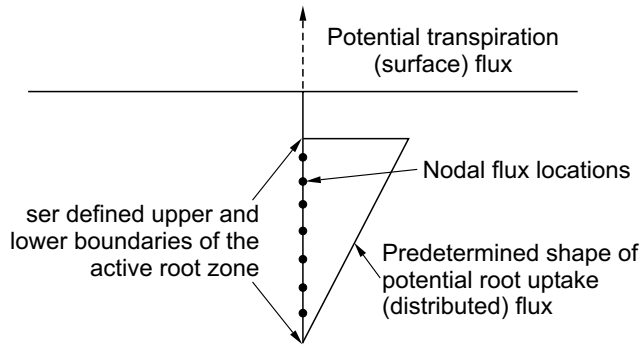


Fig. 2. Definition of plant limiting factor from the nodal matric suction. Generally accepted values for the limiting and wilting points range from 50 to 100 kPa and 1500 to 2000 kPa, respectively (Feddes et al. 1978).

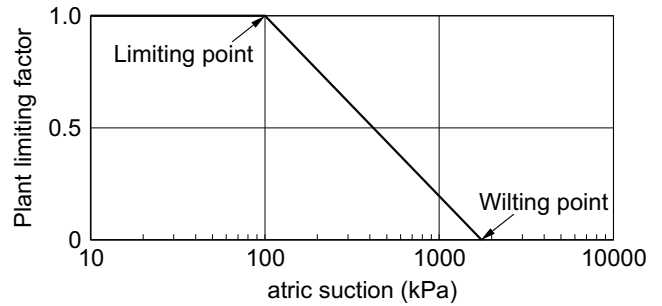
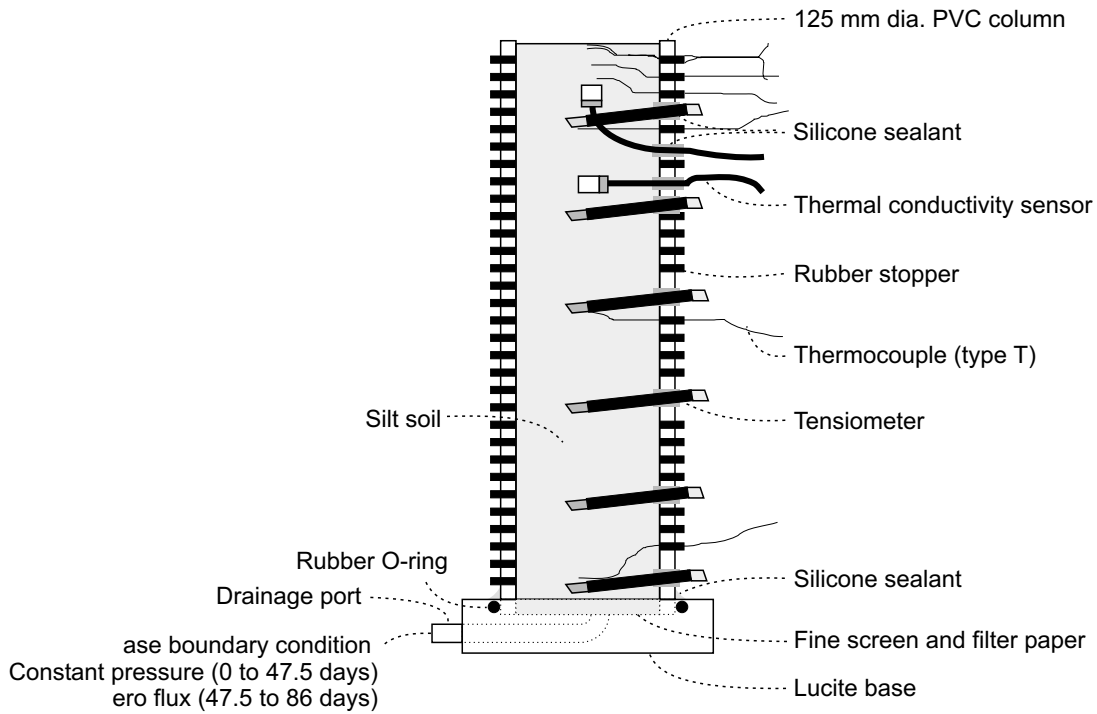


Fig. 3. Diagram of the PVC column used in the evapotranspiration study, displaying the general construction and instrumentation details.

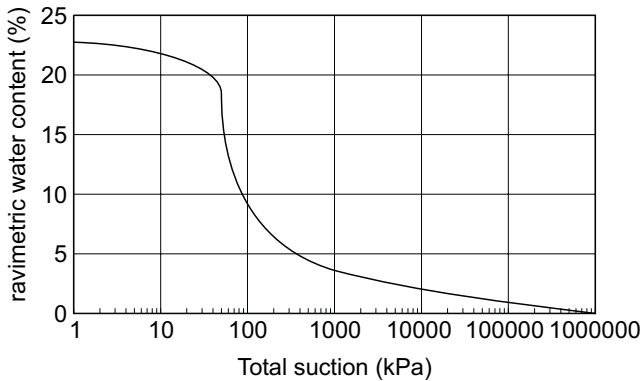


Laboratory program

A laboratory program was conducted to evaluate the physical responses of a soil profile to plant vegetation as well as to provide a data set for the verification of the transpiration equations presented in eqs. [2] through [6]. The experiment consisted of one-dimensional evapotranspiration from a soil column system placed within an environmental chamber. The soil column surface was vegetated and allowed to evapotranspire in the prevailing controlled atmospheric conditions. The surface flux as well as the subsurface moisture conditions were monitored to evaluate the influence of the vegetative cover. The soil column system, including some of the construction and instrumentation details, is presented in Fig. 3.

The surface evapotranspiration flux condition was evaluated directly by measuring the flow of moisture into the soil column and the change in mass of the entire soil column system. The soil profile was instrumented for the measurement of matric suction using thermal conductivity sensors and tensiometers. The soil column was also instrumented for temperature using type T thermocouples. Manual water content profiles were evaluated using the PVC column port holes sealed with rubber stoppers. Climatic characterization included pan (potential) evaporation rates as well as ambient relative humidity and temperature. The vegetative canopy leaf area index was measured directly and the subsurface rooting characteristics were determined on the basis of water content profiles.

Fig. 4. Soil-water characteristic curve for the silt material used in the soil column evapotranspiration study.



The soil used in the experiment was characterized as a low plasticity silt material. The soil-water characteristic curve for the silt material is presented in Fig. 4. The soil was observed to consolidate slightly under desiccation conditions, however, the soil was otherwise found to perform well throughout the experiment.

Analytical modeling results

The measured surface flux results obtained through the experimental program are presented in Fig. 5. Figure 5 also shows the computed rate of evaporation, transpiration and evapotranspiration on the basis of eqs. [1] through [6]. Good agreement is apparent between the measured and computed rates of evapotranspiration. The individual components of evaporation and transpiration were not measured, however, the computed trends may be discussed in general terms.

Six surface flux stages were observed to occur through the experimental period, three involving evaporation only and three involving both evaporation and transpiration fluxes. During the first two days from initiation of the experiment, the soil surface was saturated and the flux continued at potential evaporation rates. Between days 3 and 10, the soil surface was desaturating and the evaporative flux continually decreased. Between days 10 and 17 the soil column system appeared to be near equilibrium for evaporative conditions. After day 17, the vegetative leaf area index exceeded 0.1, causing the transpiration flux to increase. On day 40, the vegetative canopy reached a leaf area index value of 2.7 and the potential transpiration flux was found to equal the potential evaporation flux. Between day 40 and day 47, the total evapotranspiration continued at potential evaporation rates. The flux supplying the column base was discontinued on day 47 which induced moisture limiting conditions. Almost immediately, the surface flux condition responded to the increased matric suctions caused by continuous drying conditions. The limiting conditions for evapotranspiration continued to the conclusion of the experiment on day 86. The increase in evapotranspiration after day 70 coincides with an increase in potential evaporation.

The simulated evaporation component in Fig. 5 was found to continuously decrease with increasing transpiration fluxes. The decreasing evaporation flux was directly related to the desaturating surface due to the interception of moisture by the root system before it could reach the soil surface.

The measured and simulated water content profiles on select days are presented in Fig. 6. The four days shown represent evaporation flux conditions only (day 16), non-limiting transpiration with full vegetative cover conditions (day 47), and evapotranspiration in moisture limiting conditions (days 72 and 86). The water content profile trends indicate the influence of transpiration and root water uptake. The water content profile on day 16 represents steady state conditions with an evaporative flux. Changes in the water content profiles after day 16 are related to the transpiration flux and the resulting root water uptake patterns.

Comparisons of the simulated and measured water content results indicate the computed water uptake patterns were representative of the actual root uptake conditions. The computed root uptake trends on 10 day intervals are presented in Fig. 7. The y-axis of Fig. 7 is in units of mm/day/mm, hence the uptake distribution must be integrated over the entire depth to determine the surface flux in units of mm/day.

The various phases of the surface flux conditions are identified in Fig. 7. Between initiation and day 17, the surface flux consisted totally of evaporation, hence root uptake was zero. Between days 20 and 40, the root uptake pattern is shown to increase substantially with increasing vegetative cover. After day 50, the matric suctions through the root system increase to moisture limiting conditions, hence the fluxes near the surface progressively decrease to the conclusion of the experiment. Also of interest is the increase in depth of the root system indicating the progressive growth of the root system.

Conclusions

An experiment was conducted to evaluate the influence of transpiration on the surface flux and subsurface moisture conditions. The experiment was successful in evaluating the surface flux through six surface flux stages including bare soil evaporation and cumulative evaporation and transpiration fluxes. A good correlation was found between measured and computed evapotranspiration. Unfortunately, the evaporation and transpiration components of the surface flux could not be identified except by theoretical means. Moisture redistribution patterns under the influence of transpiration withdrawal of moisture were also successfully documented.

The proposed methodology to predict the transpiratory flux and root uptake rates appears to properly evaluate the measured data trends observed in the soil column experiment. The methodology follows a simple solution which conforms to geotechnical engineering nomenclature. The terms required for the transpiration flux solution

Fig. 5. Comparison of the measured and perspired evapotranspiration fluxes. Also presented are the simulated evaporation and transpiration flux partitions.

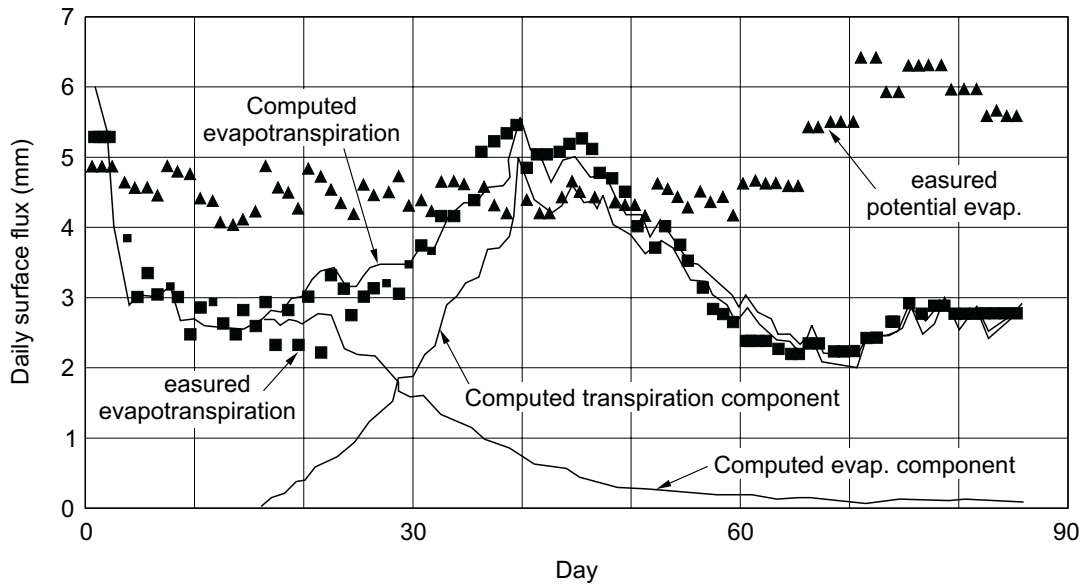


Fig. 6. Simulated and measured water content profiles on days 16, 47, 72 and 86.

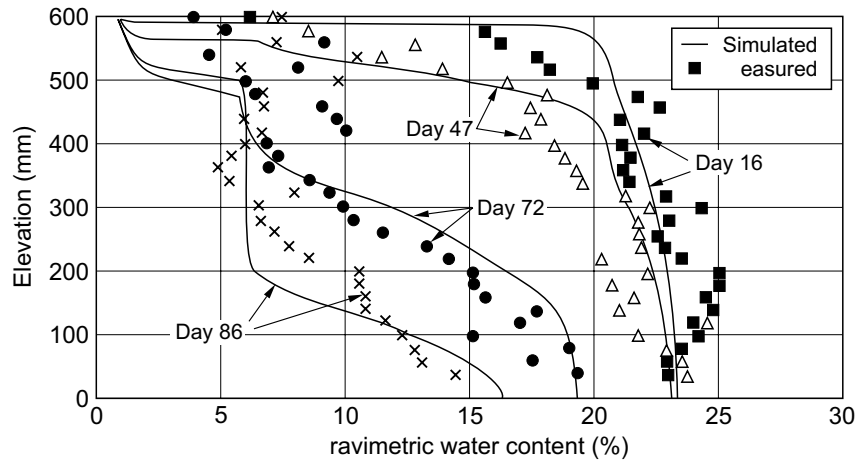
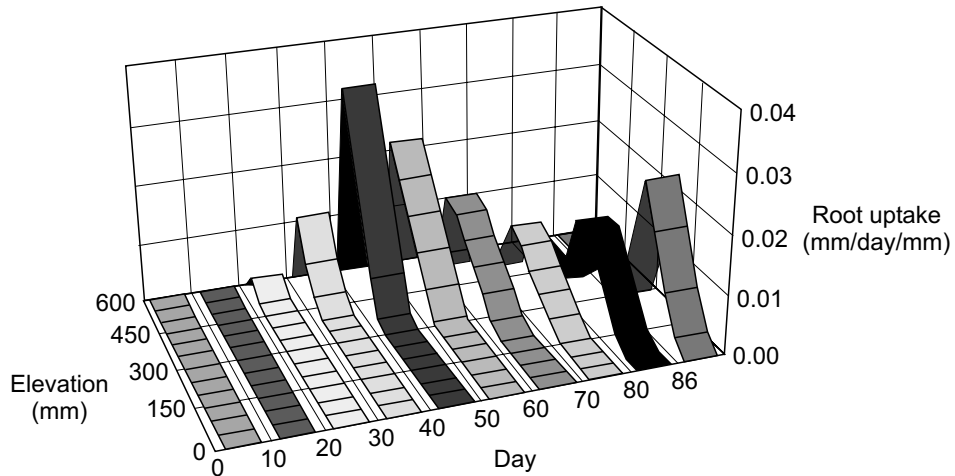


Fig. 7. Presentation of simulated root extraction patterns through the soil depth, displaying trends on 10 day intervals.



are easy to define and measure and the results do not require a sophisticated biological interpretation.

References

- de Jong, E. 1974. Technical Report No. 61. Modeling: VII. Soil water simulation models. Matador Project, University of Saskatchewan, Saskatoon, SK, Canada.
- Feddes, R.A., Kowalik, P.J., and Zaradny, H. 1978. Simulation of field water use and crop yield. John Wiley and Sons, Toronto.
- Federer, C.A. 1979. A soil-plant atmosphere model for transpiration and availability of soil water. *Water Resources Research*, **15**(3): 555–562.
- Granger, R.J. 1989. An examination of the concept of potential evaporation. *Journal of Hydrology*, **111**: 9–19.
- Marker, M.S., and Mein, R.G. 1985. A practical model for evaporation, transpiration and redistribution. *Proceedings, Hydrology and Water Resources Symposium*, Sidney, Australia, May 14–16, pp. 182–186.
- MEND 1993. SoilCover user's manual for evaporative flux model. University of Saskatchewan, Saskatoon, SK, Canada.
- Prasad, R. 1988. A linear root uptake model. *Journal of Hydrology*, **99**: 297–306.
- Ritchie, J.T. 1972. Model for predicting evaporation from a row crop with incomplete cover. *Water Resources Research*, **8**(5): 1204–1213.
- Wilson, G.W. 1990. Soil evaporative fluxes for geotechnical engineering problems. Ph.D. thesis, University of Saskatchewan, Saskatoon, SK, Canada.
- Wilson, G.W., Fredlund, D.G. and Barbour, S.L. 1994. Coupled soil-atmosphere modeling for soil evaporation. *Canadian Geotechnical Journal*, **31**: 151–161.

A mathematical model for predicting moisture flow in an unsaturated soil under hydraulic and temperature gradients

V. Dakshanamurthy and D.G. Fredlund

Abstract: A theoretical model is presented to predict the moisture flow in an unsaturated soil as the result of hydraulic and temperature gradients. A partial differential heat flow equation (for above-freezing conditions) and the two partial differential transient flow equations (one for the water phase and the other for the air phase), are derived in this paper and solved using a finite difference technique. Darcy's law is used to describe the flow in the water phase, while Fick's law is used for the air phase. The constitutive equations proposed by Fredlund and Morgenstern are used to define the volume change of an unsaturated soil. The simultaneous solution of the partial differential equations gives the temperature, the pore-water pressure, and the pore-air pressure distribution with space and time in an unsaturated soil. The pressure changes can, in turn, be used to compute the quantity of moisture flow.

Key words: moisture flow, thermal gradients, hydraulic gradients, vapor flow, matric suction, unsaturated soil.

Introduction

Increasing interest has been shown in recent years in understanding the behavior of unsaturated soils, especially those exhibiting high swelling or shrinking characteristics. The prediction of moisture flow under transient conditions is important in both soil science and civil engineering. Geotechnical engineers are interested in moisture flow when considering such practical problems as the design of shallow foundations, highway and airfield pavements, and the stability of unsaturated soil slopes. The prediction of changes in moisture content for any given climate and topographic location involves many complex variables such as varying soil properties, the type of ground cover and surrounding vegetation, groundwater table depth, wind velocity, solar radiation, and atmospheric conditions. Because of the complex nature of the problem, research work in this area has largely remained semi-empirical with serious approximations.

The theory by Terzaghi (1943) of one-dimensional consolidation for saturated soils has formed an extremely useful transient flow formulation for geotechnical engineering. However, there has been difficulty in extending the transient flow solutions to embrace unsaturated soils. In general, proposed analyses for transient flow have assumed that the volume change of the soil is inconsequential. Most transient flow analyses presently used in

geotechnical engineering have been borrowed from the soil science literature without careful consideration of the differences associated with the geotechnical engineering problems.

By the early 1950's there was a considerable interest in the physics of moisture movement in porous media, under both isothermal and non-isothermal conditions. The complex nature of the pore space in soil and the water held therein made it difficult to understand the force fields acting on the water. Philip and de Vries (1957) presented the following equation, which describes moisture and heat transfer under combined moisture content and temperature gradients.

$$[1] \quad Q = D_{\theta} \nabla \theta + D_T \nabla T + K_{\theta}$$

where:

Q = net water flux,
 D_{θ} = isothermal moisture diffusivity,
 $\nabla \theta$ = moisture content gradient,
 D_T = thermal diffusivity,
 ∇T = temperature gradient, and
 K_{θ} = gravity term.

The terms D_{θ} and D_T are each made up of two components: one for vapor flow and the other for liquid flow.

Taylor and Cary (1964) proposed linear flow equations based on the law of irreversible thermodynamics. The formulation considers the flux of one component of a system to influence the flux of other components of the system. For example, the calculation of the heat flux is affected by the calculation of the water flux.

Cassel et al. (1969) reviewed the theoretical models proposed for predicting the movement of water in soils in response to an imposed temperature gradient and concluded that the work by Philip and de Vries (1957) showed acceptable agreement of the predicted and ob-

V. Dakshanamurthy, Graduate Student, Department of Civil Engineering, University of Saskatchewan, 57 Campus Drive, Saskatoon, SK, Canada S7N 5A9.

D.G. Fredlund, Professor, Department of Civil Engineering, University of Saskatchewan, 57 Campus Drive, Saskatoon, SK, Canada S7N 5A9.

Reproduced with permission from the *Water Resources Research*, 17(3): 714-722, 1981.

served water movement. It was concluded that the Taylor-Cary equation (Taylor and Cary 1964) under-predicted the observed water movement.

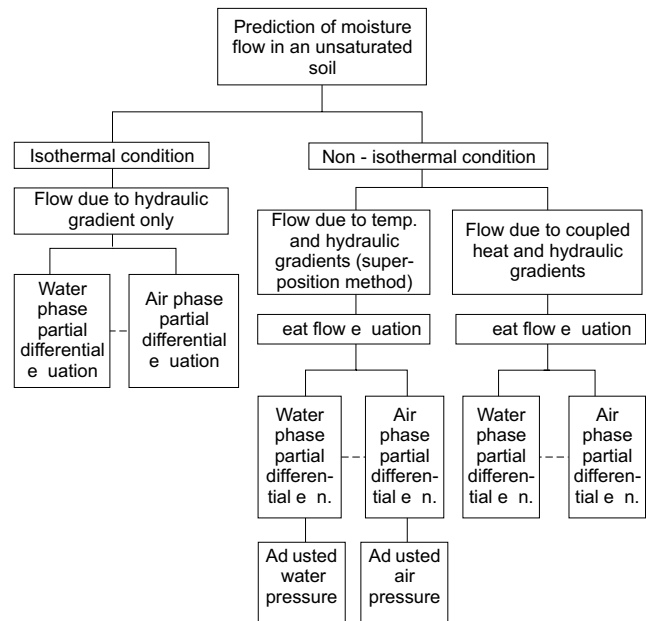
Nachlinger and Lytton (1969) proposed two coupled differential equations representing an isothermal case and three coupled differential equations representing the non-isothermal case for flow through a porous medium. The formulation was based on the principle of superimposed continuum mechanics. The driving forces associated with the liquid and gas phases were the hydraulic and thermal gradients.

Researchers in soil sciences (Cassel et al. 1969) and geotechnical engineering (Aitchison et al. 1965; Dempsey and Elzeftawy 1976; Dempsey 1978; Sophocleous 1978) have appeared to generally accept the theory of Philip and de Vries (1957). However, the adoption of the Philip-de Vries model in geotechnical engineering practice has some limitations. For example, the assumption that the soil is incompressible is not realistic. This creates difficulty in analysing geotechnical problems such as the dissipation of pore pressures in the compacted core material of an earthfill dam. Here the total stress is increasing with time (during placement of fill) and the pore-water and pore-air pressures induced are a function of the applied load and the compressibility of the soil. In order to solve this problem, the soil must be assumed to be compressible and the constitutive relations for the soil must be known in terms of total stress and pore-water and pore-air pressure. Generally, the flow of the air phase is ignored. However, fundamentally the air and water phases flow independently under total hydraulic heads. Consequently, it is not matric suction that produces flow in the water phase. In fact, it is possible to have the flow of water in one direction while the flow of air is in another direction.

Fredlund and Hasan (1979) presented a one-dimensional consolidation theory for unsaturated soils. Two partial differential equations were derived, one for the water phase and the other for the air phase. These were shown to describe the transient flow processes taking place as a result of the application of an external load to an unsaturated soil. Dakshanamurthy and Fredlund (1980a) further developed the model to predict the moisture flow in an unsaturated soil under isothermal and non-isothermal conditions. The model proposed was also extended to two-dimensional geometrical conditions. Two partial differential equations, one for the water phase and the other for the air phase, were again used to describe the moisture flow under transient conditions. In addition, a partial differential heat flow equation was solved and the corresponding pore-water and pore-air pressures were adjusted by the method of superposition, in order to account for the imposed temperature gradient. The flow chart shown in Fig. 1 illustrates the various stages in the formulation of the moisture flow model.

This paper combines the effect of the thermal gradient and the hydraulic gradient to obtain a modified form of the pore-air and pore-water partial differential equations. In total, three partial differential equations, namely, (1) heat flow, (2) water phase, and (3) air phase equa-

Fig. 1. Flow chart for prediction of moisture flow.



--- Signifies simultaneous solution
 Fredlund and Hasan (1979)
 Dakshanamurthy and Fredlund (1980a)
 Adjusted using pore pressure parameters
 Adjusted for temperature using gas law

tions, are solved simultaneously for changes in the combined thermal and hydraulic boundary conditions. Temperature changes in the soil are converted to a change in pore-air pressure. The changes in pore-air pressure produce changes in the pore-water pressure in accordance with the B_{aw} pore pressure parameter defined in geotechnical engineering (Fredlund 1976; Hasan and Fredlund 1980).

$$[2] \quad B_{aw} = \frac{\nabla u_a}{\nabla u_w}$$

where:

Δu_a = change in pore-air pressure, and
 Δu_w = change in pore-water pressure.

The B_{aw} pore pressure parameter is a function of the compressibility of the air-water mixture and the compressibility of the soil structure. B_{aw} is less than 1 for an unsaturated soil and approaches a value of 1 as saturation is approached.

In this study, attention is given to solving example problems typical of the conditions which would exist in an unsaturated soil layer below ground surface. The examples reflect changes that would occur in a subgrade either due to continuous evaporation or infiltration, coupled with increases or decreases in temperatures. It is assumed that the boundary conditions are known at all times and, in fact, remain constant during the process under consideration. Only one-dimensional heat and moisture flow is presently considered. The distribution of moisture flow

enables the prediction of the overall volume change, the degree of saturation, and the void ratio with time.

The proposed model

All the necessary physical equations required for the formulation of a moisture flow model have been previously proposed and experimentally verified (Fredlund 1973; Fredlund and Morgenstern 1976, 1977). These are the continuity equation and the constitutive relations for the soil structure, the water phase, and the air phase. $(\sigma_y - u_a)$ and $(u_a - u_w)$ are used as the stress state variables for an unsaturated soil where σ_y is the total stress in the y -direction, u_a is the pore-air pressure, and u_w is the pore-water pressure. The flow equation for the water phase is described by Darcy's law (Childs and Collis-George 1950), and Fick's law is used to describe flow in the air phase (Blight 1971).

The one-dimensional transient flow equations for an unsaturated soil are derived in a manner so as to reflect the form of derivation used in geotechnical engineering for saturated soils. The conventional assumptions for the consolidation theory developed by Terzaghi (1943) are adhered to along with the following additions:

- (1) The air phase is continuous. This is generally the case when the degree of saturation is less than approximately 85%. At higher degrees of saturation the air phase generally becomes occluded and the formulation would need to treat the soil as having one compressible fluid phase.
- (2) The coefficients of permeability with respect to the water and air phases are functions of the volume-weight properties of the soil (Corey 1957). The coefficients are assumed to be constant in the derivation of the partial differential equations; however, they can be revised in accordance with any proposed function throughout the transient process.
- (3) The volume change moduli remain constant during the transient process.
- (4) Vapor pressure gradients and the dissolving of air in the water are not considered in the analysis.

The above assumptions are not completely accurate throughout the processes being considered. For example, the coefficient of permeability with respect to the water phase is a function of both water content and degree of saturation. However, the coefficient of permeability is assumed to be constant in the derivation of the transient flow equation. The derived equations are later solved using a finite difference technique. During the solution of the equations it is possible to update the coefficient of permeability in accordance with any desired functional relationship. For example, the coefficient of permeability could be written as a function of the degree of saturation (Corey 1957). The degree of saturation (as well as water content and void ratio) are known at all times since the constitutive relations for the unsaturated soil are known in terms of the stress state variables. The coefficient of permeability with respect to the air phase is also a function of water content and degree of saturation, but it is

likewise assumed to be constant. The above approach can again be justified since the partial differential equations are being solved using a finite difference technique which allows for the adjustment of the coefficients of permeabilities with time. The constitutive relations for the unsaturated soil have non-linear soil moduli; however, they are assumed linear for the example problems presented. These values could also be adjusted during the finite difference solution, if desired.

The proposed model does not include the effect of vapor moisture movement as a result of a vapor pressure gradient. In other words, it is assumed that the vapor pressure above the boundary of the layer under consideration is the same as the vapor pressure within the soil. However, moisture vapor can be assumed to be carried in or out of the soil as a result of air movement. Further research presently underway at the University of Saskatchewan in Saskatoon considers a more rigorous analysis of vapor pressure gradients.

Water phase partial differential equation

Let us consider a differential soil element as shown in Fig. 2. In the transient flow process, water flows out of the element with time. The constitutive relationship for the water phase defines the volume of water in the element for any combination of total, water, and air pressures (Fredlund and Morgenstern 1976).

The volume of water entering and leaving the element can be described by Darcy's law as follows:

$$[3] \quad V_{WE} = - \left[k \frac{\partial h_w}{\partial y} \right] dx dz$$

$$[4] \quad V_{WL} = - \left[k \frac{\partial h_w}{\partial y} + \frac{\partial}{\partial y} \left(k \frac{\partial h_w}{\partial y} \right) dy \right] dx dz$$

where:

V_{WE} = volume of water entering the element,

V_{WL} = volume of water leaving the element,

k = coefficient of permeability with respect to the water phase,

h_w = hydraulic head in the water phase, and

y = direction of flow.

The net flux of water per unit volume of the element is

$$\frac{\partial(V_w / V)}{\partial t} = - \left[\frac{k}{\gamma_w} \frac{\partial^2 u_w}{\partial y^2} \right]$$

where:

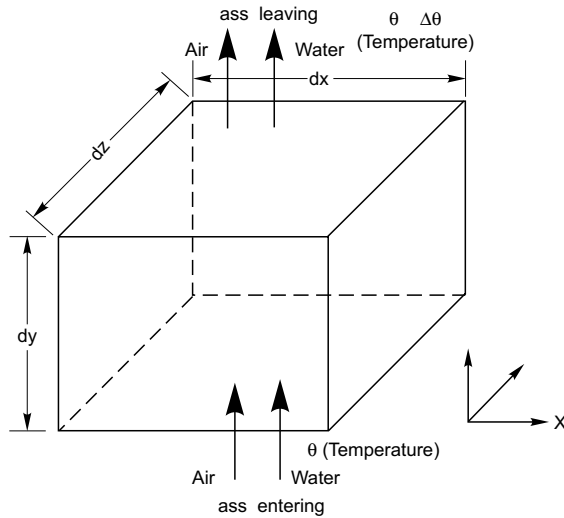
γ_w = unit weight of water,

V = total volume of a referential element of the soil mass, and

t = time.

Equation [5] is equated to the time differential of the constitutive relationship for the water phase:

Fig. 2. A differential element in the soil mass, showing coupled heat, air, and water flow.



$$[6] \quad m_1^w \frac{\partial(\sigma_y - u_a)}{\partial t} + m_2^w \frac{\partial(u_a - u_w)}{\partial t} = - \left[\frac{k}{\gamma_w} \frac{\partial^2 u_w}{\partial y^2} \right]$$

where:

m_1^w = slope of $(\sigma_y - u_a)$ versus volume of water plot when $d(u_a - u_w)$ is zero, and

m_2^w = slope of $(u_a - u_w)$ versus volume of water plot when $d(\sigma_y - u_a)$ is zero.

The change in total stress with respect to time is set to zero for the type of example problems being considered. By simplifying and rearranging eq. [6], the water phase partial differential equation can be written:

$$[7] \quad \frac{\partial u_w}{\partial t} = C_w \frac{\partial u_a}{\partial t} + c_v^w \frac{\partial^2 u_w}{\partial y^2}$$

where:

$C_w = -(1 - m_2^w / m_1^w) / (m_2^w / m_1^w)$, interactive constant associated with the water phase equation.

This equation is further simplified by letting $R_w = m_2^w / m_1^w$. As the soil approaches saturation, R_w approaches unity.

$$[8] \quad c_v^w = \frac{1}{R_w} \frac{k}{\gamma_w} \frac{1}{m_1^w}$$

where:

c_v^w = coefficient of consolidation for the water phase.

Air phase partial differential equation

The air phase is compressible and flow occurs in response to a pressure gradient. The constitutive relationship for the air phase defines the volume of air in the element for any combination of the total water, and air

pressures. Quantitatively, the air phase constitutive relationship is equal to the difference between the soil structure constitutive relationship and the water phase constitutive relationship.

According to Fick's law, the masses of air entering and leaving the element are:

$$[9] \quad M_{AE} = -D \frac{\partial p}{\partial y} dx dz$$

$$[10] \quad M_{AL} = - \left[D \frac{\partial p}{\partial y} + \frac{\partial}{\partial y} \left(D \frac{\partial p}{\partial y} \right) dy \right] dx dz$$

where:

M_{AE} = mass of air entering the element,

M_{AL} = mass of air leaving the element,

D = transmission constant, equal to $D^* (\omega / R\theta)$, having the same units as coefficient of permeability,

D^* = mass diffusivity of gases in air,

p = absolute air pressure (i.e., $u_a + u_{atm}$), and

u_{atm} = atmospheric air pressure.

The net flux of air through the element is,

$$[11] \quad \frac{\partial m}{\partial t} = - \left(D \frac{\partial^2 p}{\partial y^2} \right)$$

where:

m = the mass of air in the element.

The mass rate of change is written in terms of a volume rate of change by differentiating the relationship between the mass and volume of air.

$$[12] \quad \frac{\partial(V_a / V)}{\partial t} = \frac{\partial(m / \gamma_a)}{\partial t} = \frac{1}{\gamma_a} \frac{\partial m}{\partial t} - \frac{1}{\gamma_a^2} \frac{\partial \gamma_a}{\partial t} m$$

The density of air can be written in terms of pressure and temperature using the gas law.

$$[13] \quad \gamma_a = \frac{\omega}{R\theta} p$$

where:

ω = molecular weight of air,

R = universal gas constant, and

θ = absolute temperature.

The mass of air is written in terms of the density of air, γ_a , the degree of saturation, S , and the porosity of the soil, n .

$$[14] \quad m = (1 - S)n\gamma_a$$

By differentiating eq. [13] and substituting eqs. [11] and [14] and by simplifying and rearranging, eq. [12] can be written as:

$$[15] \quad \frac{\partial(V_a / V)}{\partial t} = - \frac{D}{\gamma_a} \frac{\partial^2 p}{\partial y^2} - \frac{(1 - S)n}{p} \frac{\partial p}{\partial t} + \frac{(1 - S)n}{\theta} \frac{\partial \theta}{\partial t}$$

Equation (15) can be equated to the time differential of the air phase constitutive relationship:

$$[16] \quad m_1^a \frac{\partial(\sigma_y - u_a)}{\partial t} + m_2^a \frac{\partial(u_a - u_w)}{\partial t} = - \left[\frac{DR\theta}{\omega p} \frac{\partial^2 u_a}{\partial y^2} + \frac{(1-S)n}{p} \frac{\partial p}{\partial t} - \frac{(1-S)n}{\theta} \frac{\partial \theta}{\partial t} \right]$$

where:

m_1^a = compressibility moduli of the air phase associated with the $(\sigma_y - u_a)$ stress state variable, and

m_2^a = compressibility moduli of the air phase associated with the $(u_a - u_w)$ stress state variable.

As in the water phase equation the change in total stress with respect to time is set to zero. By simplifying and rearranging eq. [16] the air phase partial differential equation can be written as:

$$[17] \quad \frac{\partial u_a}{\partial t} = C_a \frac{\partial u_w}{\partial t} + C_\theta \frac{\partial \theta}{\partial t} + c_v^a \frac{\partial^2 u_a}{\partial y^2}$$

where:

$$[18] \quad C_a = \frac{-m_2^a / m_1^a}{(1 - m_2^a / m_1^a) + \{[(1-S)n] / [m_1^a(u_a + u_{am})]\}}$$

(which is the interactive pressure constant associated with the air phase equation). This equation is further simplified by letting $R_a = m_2^a / m_1^a$. When the soil is saturated, R_a is equal to unity.

$$[19] \quad C_\theta = \frac{1}{\theta} \left[\frac{(1-S)n(u_a + u_{am})}{(1-R_a)(u_a + u_{am})m_1^a + (1-S)n} \right]$$

(which is the interactive thermal constant associated with the air phase equation).

$$[20] \quad c_v^a = \frac{DR\theta}{\omega} \left[\frac{1}{(1-R_a)(u_a + u_{am})m_1^a + (1-S)n} \right]$$

(which is the coefficient of consolidation for the air phase).

The dissipation of the excess pressure of the pore-air and pore-water phases are obtained by solving eqs. [7] and [17] simultaneously, using the explicit finite difference method described in the Appendix. However, prior to solving eqs. [7] and [17] it is necessary to obtain the thermal gradient within the soil.

Heat flow equation

The heat flow equation for one-dimensional conditions is as follows (Aldrich 1956):

$$[21] \quad \frac{\partial \theta}{\partial t} = \alpha \frac{\partial^2 \theta}{\partial y^2}$$

where:

θ = temperature,

λ = thermal conductivity,

c = heat capacity,

α = thermal diffusivity factor, equal to $(\lambda / c\gamma)$, and

γ = soil density.

The heat flow equation is solved using an explicit finite difference method (see Appendix). The solution gives the change in temperature with one-dimensional space and time (Fig. 3).

Example problems

Particular emphasis is given to solve four example problems involving the prediction of moisture flow in an unsaturated subgrade soil such as that below a highway or airfield pavement. The model simulates the effect of environmental change on a layer of soil within the subgrade. It is assumed that the subgrade system is initially in a state of equilibrium. Then a sudden environmental change is imposed at the boundary. Changes considered are: evaporation, infiltration, and temperature changes. The environmental changes either due to evaporation or infiltration builds up an excess (either positive or negative with respect to the equilibrium state) pore-water pressure at the boundary. Similarly, the maximum or minimum temperature change also results in an excess pore-air pressure. It is assumed, under non-isothermal conditions, that the change in excess pore-water pressure consequent to the change in excess pore-air pressure is zero. In other words, the pore pressure parameter, B_{aw} , relating pore-air pressure and pore-water pressure, is assumed to be large. Other, more realistic, lower B_{aw} values could also have been assumed. These excess pore-water and pore-air pressures build up at the surface and cause simultaneous flow in the water and the air phases independently. An unsaturated soil mass will equilibrate to a new set of pore pressure conditions dependent on the assumed final boundary conditions. The boundary conditions used in the four example problems discussed below are presented in Table 1. The solution to the transient flow conditions is obtained by solving simultaneously the three partial differential equations, namely, eqs. [7], [17], and [21]. The details of the simultaneous solutions of these equations are given in the Appendix.

A computer program has been developed to solve these partial differential equations (Dakshanamurthy and Fredlund 1980b). Solutions are presented for various initial and final pore-water and pore-air pressures boundary conditions and various initial and final surface temperatures. The effect of various compressibility moduli for the water and air phase constitutive relations is also investigated along with the effect of degree of saturation, porosity, and thermal conductivity and heat capacity.

In the example problems solved, the soil properties used are typical of Regina clay found near Regina, SK, Canada (Fredlund 1964) (Table 2). For this study a 10 cm

Table 1. Boundary conditions for example problems.

Example number	Corresponding figure number	Pore-water pressure, kPa		Pore-air pressure, kPa		Temperature, °C		Remarks
		Initial	Final	Initial	Final	Initial	Final	
1	4, 6	-280	-420	102	102	20	20	isothermal, consolidation
2	3, 4, 6	-280	-420	102	102	10	25	non-isothermal, consolidation
3	5, 7	-420	-280	102	102	20	20	isothermal, swelling
4	3, 5, 7	-420	-280	102	102	10	25	non-isothermal, swelling

Table 2. Summary of classification tests, compressibility, and permeability properties of Regina clay.

	Value
Specific Gravity	2.83
Atterberg limits	
Liquid limit	75.5%
Plastic limit	24.9%
Shrinkage limit	13.1%
Plasticity index	50.6
Grain size distribution	
Sand sizes	8%
Silt sizes	41%
Clay sizes	51%
Compressibility*	
m_v^w	0.0007614/kPa
m_v^a	0.0003263/kPa
$R_w = R_a$	0.7
Permeability*	
k	0.6×10^{-10} m/s
D^*	1.0×10^{-9} m ² /s
Volume-weight properties	
Soil density (γ)	1.8g/cm ³
Porosity (n)	50%
Degree of saturation (S)	70%
Thermal properties	
λ = thermal conductivity	0.4574 cal/m s °C
c = heat capacity	30 cal/g K
Physico-chemical properties	
ω = molecular weight of air	18.015 g/mol
R = universal gas constant	847.825 J/mol K

*Estimated values.

thick layer of compacted Regina clay is used in the example problems.

Results and discussions

The distribution of temperature, pore-water pressure, and pore-air pressure are obtained by solving eqs. [21], [7], and [17], respectively. The water content (volumetric) is obtained by back substitution into the water phase constitutive relationship. Because of the assumption that the change in excess pore-water pressure is zero under non-isothermal conditions, the water content (volumetric) distribution with space and time is essentially the same for isothermal and non-isothermal conditions. The results

are presented by the family of curves shown in Figs. 3 to 8.

Figure 3 shows the temperature isotherms within the clay layer as a result of an increase in the temperature from 10°C (283.2 K) to 25°C (298.2 K). The figure illustrates how the imposed thermal gradient at the surface slowly dissipates to the bottom of soil and eventually equilibrates to the new boundary condition.

Figure 4 shows the pore-water pressure distribution throughout the clay layer due to a change in the pore-water pressure at the boundary. The initial (i.e., equilibrium) pore-water pressure was -280 kPa, and the boundary pore-water pressure was changed to a value of -420 kPa at the surface instantaneously. The change in pore-water pressure is assumed to be due to evaporation. However, this is a special case of evaporation where the boundary pore-water pressure is kept constant. Figure 5 shows the numerically identical but reverse process to that presented in Figure 4. In other words, the surface of the soil is kept moistened to maintain the pore-water pressure at -280 kPa.

Figures 6 and 7 show the pore-air pressure distributions throughout the clay layer due to changes in the pore-water pressure under isothermal and non-isothermal conditions. Figure 6 shows the distribution under the volume decrease or consolidation process, and Fig. 7 shows the distribution under the volume increase or swelling process.

Figures 4 to 6 show that it takes considerable time (i.e., 854 hours) to dissipate the excess pore-water and pore-air pressure to the bottom of 10 cm thick clay layer. This is understandable, since the permeability and compressibility moduli are low for the soil considered. However, the system reaches a new equilibrium condition, and the example demonstrates the interaction between the effects of a thermal and hydraulic gradient.

Figure 8 shows the distribution of water content (volumetric) throughout the clay layer considered, under both the consolidation and the swelling process. The magnitude of the changes in water content are equal for the swelling and consolidation process because the compressibility moduli have been chosen as equal. In other words, hysteretic effects are not considered for this example problem. The final water content throughout the clay layer equilibrates to a value consistent with the change in pore-water pressure at the surface. It is also possible to predict changes in overall volume of the soil or heave of the soil surface. The distribution of moisture

Fig. 3. Temperature isotherms for an example problem.

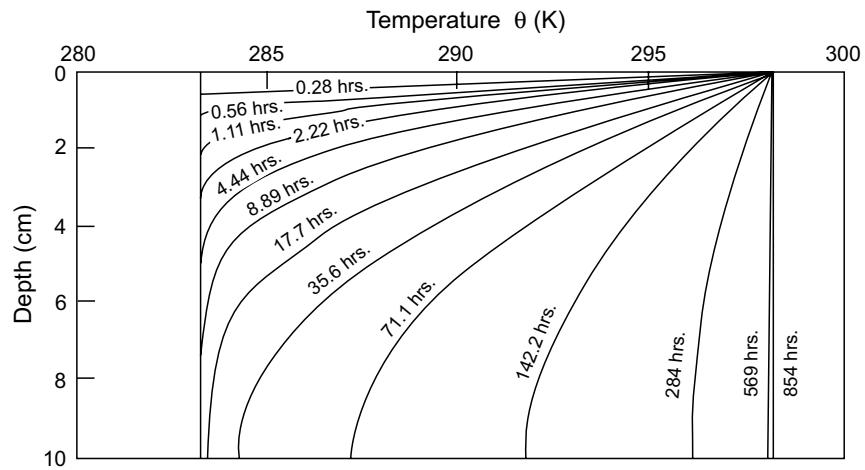


Fig. 4. Pore-water pressure distribution under consolidation.

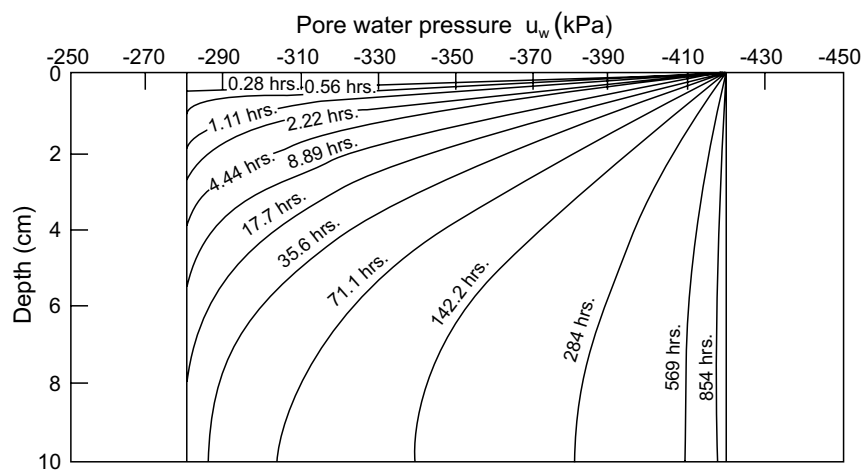
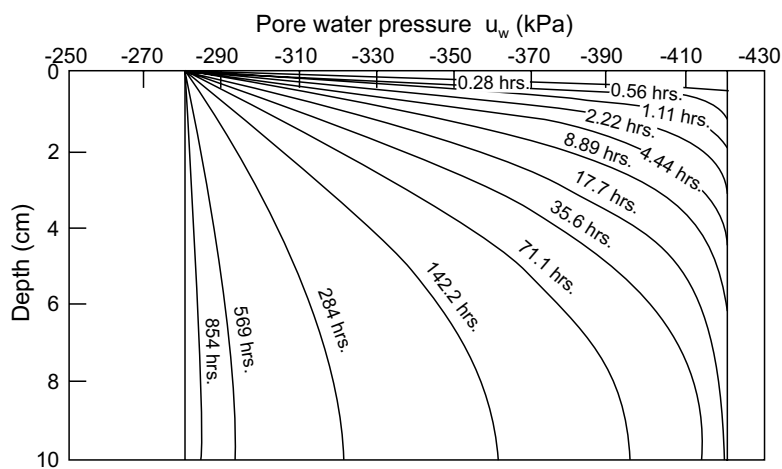


Fig. 5. Pore-water pressure distribution under swelling.



content with space and time and the changes in overall volume of the saturated soil system under varying boundary conditions enables the prediction of the degree of saturation, S , and the void ratio, e , during the transient processes.

The boundary conditions can be changed at any time during one process and the effects will be superimposed on one another. This results in highly complex thermal and pore pressure distributions throughout the soil layer.

Fig. 6. Pore-air pressure distribution under consolidation.

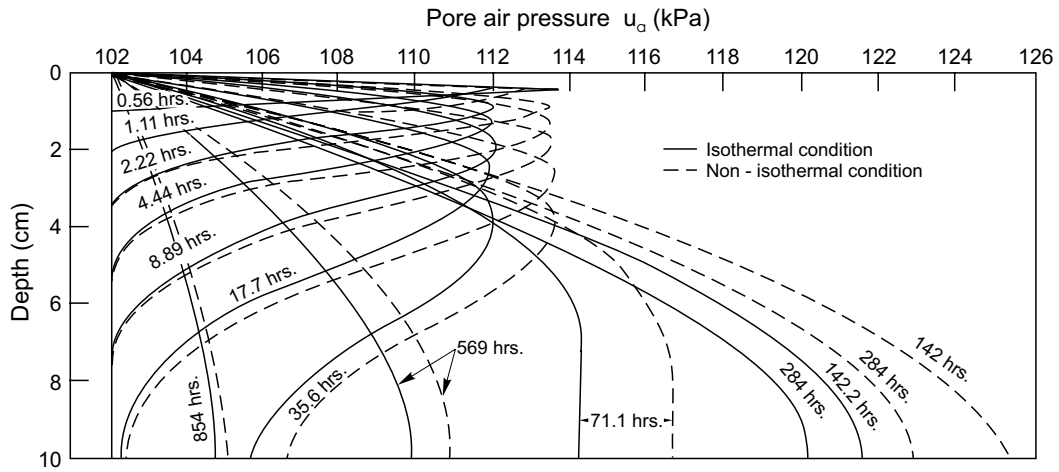


Fig. 7. Pore-air pressure distribution under swelling.

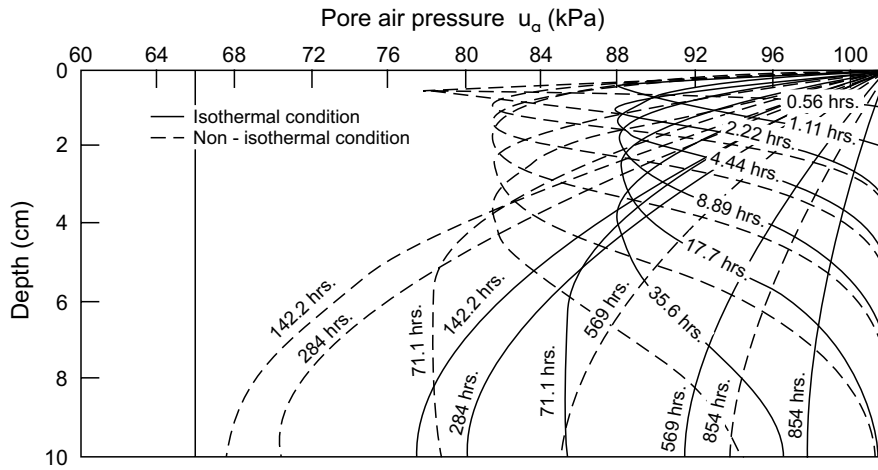
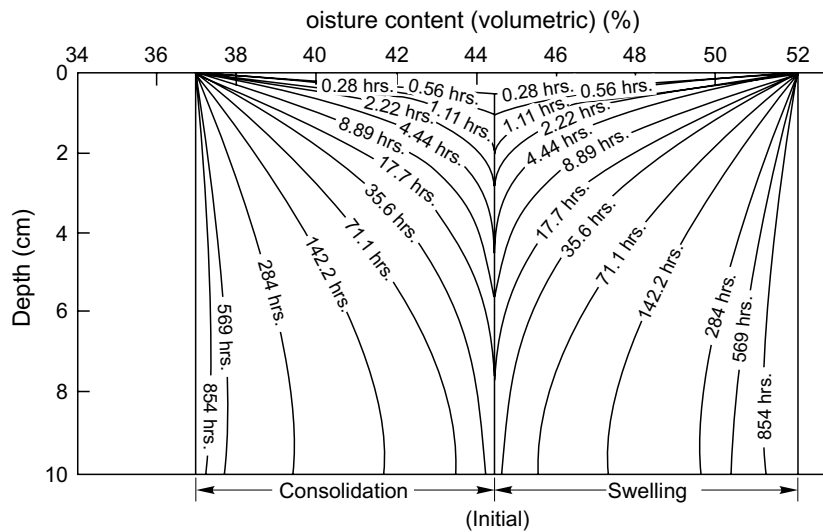


Fig. 8. Water content (volumetric) distribution.



Summary

All the necessary physical relations are available to formulate a rigorous theoretical model to describe the transient flow process under coupled hydraulic and thermal gradients in an unsaturated soil. The heat flow equation is first solved by a forward finite difference technique. Then two partial differential equations (i.e., one for the water phase and the other for the air phase) are solved simultaneously using a special finite difference procedure. Families of curves show temperature, pore-water pressure, pore-air pressure, and water content (volumetric) distribution throughout the clay layer considered, as a result of coupled hydraulic and temperature gradients in an unsaturated soil. The purpose of the example problems is to demonstrate the form of the resulting processes under various changes in the boundary conditions. Present analyses being performed at the University of Saskatchewan, Saskatoon, involve the refining of the coefficients of permeability during the transient processes.

The distribution of water content and overall volume change enables the prediction of overall volume-weight properties of the soil throughout the transient process. The model shows good promise for describing the behavior of unsaturated soil systems under highly complex environmental changes.

Appendix

Figure A1 shows the finite difference designations for the example problems. Prior to solving the water phase and air phase equations the heat flow eq. [21] is solved. The finite difference form of the heat flow equation is as follows:

$$[A1] \quad \frac{(\theta_{i,j+1} - \theta_{i,j})}{\Delta t} = \alpha \frac{(\theta_{(i+1,j)} - 2\theta_{(i,j)} + \theta_{(i-1,j)})}{\Delta y^2}$$

where:

i = array used for depth increments, and
 j = array used for time increments.

$$[A2] \quad \theta_{(i,j+1)} = \theta_{(i,j)} + \beta_t (\theta_{(i+1,j)} - 2\theta_{(i,j)} + \theta_{(i-1,j)})$$

where:

$$\beta_t = \alpha \frac{\Delta t}{\Delta y^2}$$

A special numerical procedure is adapted to obtain the simultaneous solution of the water phase and air phase partial differential equations (i.e., eqs. [7] and [17]). These two equations are solved using an explicit forward difference technique. Since the air phase and water phase equations formulated in this paper are non-linear, this procedure is advantageous because this procedure transforms the non-linear partial differential equation into a linear partial differential equation. The following steps are used to solve the water phase and air phase transient flow equations.

Write the transient flow equation for the water phase in a finite difference form:

$$[A3] \quad \frac{u_{w(i,j+1)} - u_{w(i,j)}}{\Delta t} = C_w \left[\frac{u_{a(i,j+1)} - u_{a(i,j)}}{\Delta t} \right] + c_v^w \left[\frac{u_{w(i+1,j)} - 2u_{w(i,j)} + u_{w(i-1,j)}}{\Delta y^2} \right]$$

Write the transient flow equation for the air phase in a finite difference form:

$$[A4] \quad \frac{u_{a(i,j+1)} - u_{a(i,j)}}{\Delta t} = C_a \left[\frac{u_{w(i,j+1)} - u_{w(i,j)}}{\Delta t} \right] + C_\theta \frac{(\theta_{(i,j+1)} - \theta_{(i,j)})}{\Delta t} + c_v^a \left[\frac{u_{a(i+1,j)} - 2u_{a(i,j)} + u_{a(i-1,j)}}{\Delta y^2} \right]$$

Equation [A4] is multiplied by C_w and eqs. [A3] and [A4] are solved simultaneously for pore-water pressure (u_w). The resulting eq. [A5] is simplified and rearranged such, that the unknown pore-water pressure at the given time step (i.e., $j + 1$ -th) is on the left-hand side and all known variables at the previous time step (i.e., j -th) are on the right-hand side of the equation:

$$[A5] \quad u_{w(i,j+1)} = u_{w(i,j)} + \frac{\beta_w g_1^w}{(1 - C_a C_w)} + \left(\frac{C_w}{1 - C_a C_w} \right) \beta_a f_1^a + \frac{C_w C_\theta}{(1 - C_a C_w)} \theta_1$$

where:

$$\beta_w = c_v^w \left(\frac{\Delta t}{\Delta y^2} \right) \quad \beta_a = c_v^a \left(\frac{\Delta t}{\Delta y^2} \right)$$

$$g_1^w = u_{w(i+1,j)} - 2u_{w(i,j)} + u_{w(i-1,j)}$$

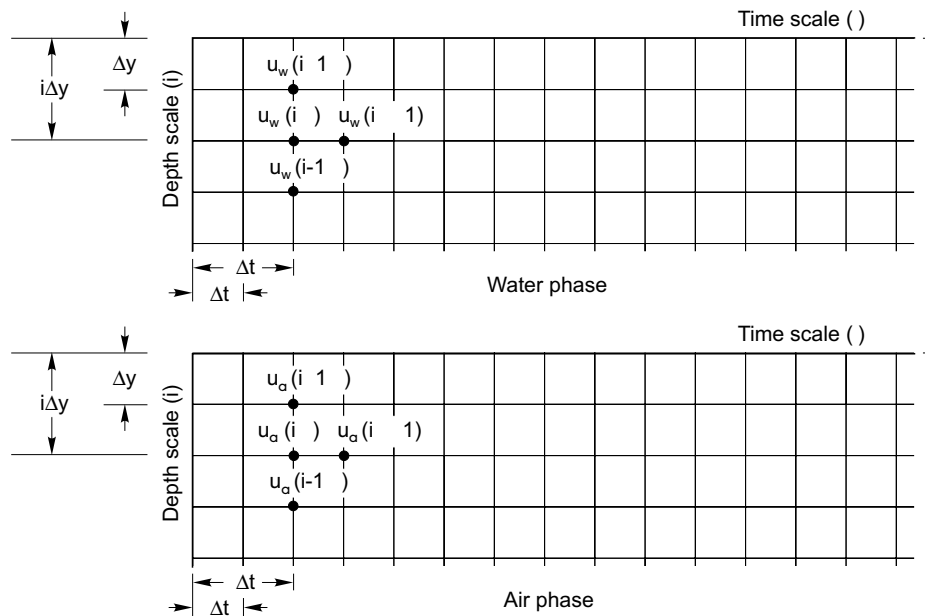
$$f_1^a = u_{a(i+1,j)} - 2u_{a(i,j)} + u_{a(i-1,j)}$$

$$\theta_1 = [\theta_{(i,j+1)} / \theta_{i,j} - 1]$$

Equation [A3] is multiplied by C_a and eqs. [A3] and [A4] are solved simultaneously for pore-water pressure (u_w). The resulting eq. [A6] is simplified and rearranged such, that unknown pore-air pressure at the given time step (i.e., $j + 1$ -th) is on the left-hand side and all known variables at the previous time step (i.e., j -th) are in the right hand side of the equation:

$$[A6] \quad u_{a(i,j+1)} = u_{a(i,j)} + \left(\frac{C_a}{1 - C_a C_w} \right) \beta_w g_1^w + \frac{\beta_a f_1^a}{(1 - C_a C_w)} + \frac{C_\theta}{(1 - C_a C_w)} \theta_1$$

Fig. A.1. Finite difference mesh for the transient flow equations.



Compute the pore-water and the pore-air pressures at the given time step from the known values at the previous time step. When computations for both pore-water and pore-air pressures for all depth steps are completed, then march forward to the next time step. Repeat the above procedure up to the desired time interval. The solution of all the above example problems are obtained by setting the values of β_r , β_w and β_a , terms ≤ 0.5 in order to satisfy the stability conditions of the partial differential equations.

Acknowledgements

This study was supported under a research grant from the Saskatchewan Highways and Transportation Department, Government of Saskatchewan, Regina, SK. Acknowledgement is made to Dr. R. Manohar, Professor of Mathematics, University of Saskatchewan, for his assistance during this study.

References

- Aitchison, G.D., Russam, K., and Richards, B.G. 1965. Engineering concepts of moisture equilibria and moisture changes in soils. *In* Moisture equilibria and moisture changes in soils beneath covered areas. A Symposium in Print. Edited by G.D. Aitchison, Butterworth, Sydney, Australia, pp. 7–21.
- Aldrich, H.P., Jr. 1956. Frost penetration below highway and airfield pavements. Highway Research Board Bulletin, National Research Council, Washington, DC, **135**: pp. 124–149.
- Blight, G.E. 1971. Flow of air through soils. ASCE, Journal of Soil Mechanics and Foundation Division, **97**(SM4): 607–624.
- Cary, J.W. 1966. Soil moisture transport due to thermal gradients: Practical aspects. Soil Science Society of America Journal, **30**: 428–433.
- Cassel, D.K., Nielsen, D.R., and Biggar, J.W. 1969. Soil-water movement in response to imposed temperature gradients. Soil Science Society of America Journal, **33**: 493–500.
- Childs, E.C., and Collis-George, N. 1950. The permeability of porous material. Proceedings Royal Society of London, Series A, **201**: 392–405.
- Corey, A.T. 1957. Measurement of water and air permeability in unsaturated soil. Soil Science Society of America Journal, **21**: 7–10.
- Dakshnamurthy, V., and Fredlund D.G. 1980a. Moisture and air flow in an unsaturated soil. Proceedings, 4th International Conference on Expansive Soils, American Society of Civil Engineering, Denver, CO, Vol. 1, pp. 514–532.
- Dakshnamurthy, V., and Fredlund, D.G. 1980b. Transient flow processes in unsaturated soils (temperature, relative humidity, evaporation and infiltration). CD-16.4, Transportation and Geotechnical Group, Department of Civil Engineering, University of Saskatchewan, Saskatoon, SK, Canada.
- Dempsey, B.J. 1978. A mathematical model for predicting coupled heat and water movement in unsaturated soil. International Journal of Numerical Analytical Methods in Geomechanics, **2**: 19–36.
- Dempsey, B.J., and Elzeftawy, A. 1976. Mathematical model for predicting moisture movement in pavement systems. Transportation Research Records, National Academy of Sciences, Washington, DC, **612**, pp. 48–55.
- Fredlund, D.G. 1964. Comparison of soil suction and one-dimensional consolidation characteristics of a highly plastic clay. M.Sc. thesis, University of Alberta, Edmonton, AB, Canada.
- Fredlund, D.G. 1973. Volume change behavior of unsaturated soils. Ph.D. thesis, University of Alberta, Edmonton, AB, Canada.
- Fredlund, D.G. 1976. Density and compressibility characteristics of air-water mixtures. Canadian Geotechnical Journal, **13**(4), 386–396.
- Fredlund, D.G., and Hasan, J.U. 1979. One-dimensional consolidation theory: Unsaturated soils. Canadian Geotechnical Journal, **16**(3), 521–531.

- Fredlund, D.G., and Morgenstern, N.R. 1976. Constitutive relations for volume change in unsaturated soils. *Canadian Geotechnical Journal*, **13**(3), 261–276.
- Fredlund, D.G., and Morgenstern, N.R. 1977. Stress state variables for unsaturated soils. *ASCE, Journal Geotechnical Engineering Division*, **103**(GT5): 447–466.
- Hasan, J.U., and Fredlund, D.G. 1980. Pore pressure parameters for unsaturated soils. *Canadian Geotechnical Journal*, **17**(3), 395–404.
- Nachlinger, R., and Lytton, R.L. 1969. Continuum theory of moisture movement and swell in expansive clays. Centre for Highways Research, University of Texas, Austin, TX, Research Report 118.2.
- Philip, J.R., and de Vries, D.A. 1957. Moisture movement in porous materials under temperature gradients. *Transactions American Geophysical Union*, **38**(2):222–232.
- Taylor, S.A., and Cary J.W. 1964. Linear equation for the simultaneous flow of matter and energy in a continuous soil system. *Soil Science Society of America Journal*, **28**, 167–172.
- Terzaghi, K. 1943. *Theoretical Soil Mechanics*. John Wiley, New York.
- Sophocleous, M.A. 1978. Analysis of heat and water transport in unsaturated-saturated porous media. Ph.D. thesis, University of Alberta, Edmonton, AB, Canada.

Part VIII

Epilogue

Dr. A.W. Clifton
Dr. D.G. Fredlund

After the presentation of the R.F. Leggett Award, October 1998. From left to right: Del Fredlund, JoAnne Fredlund, Anita Clifton, and Wayne Clifton.



Introduction by Dr. A.W. Clifton

As this monograph was nearing completion, Dr. Fredlund received the most senior and prestigious award of the Canadian Geotechnical Society, the R.F. Leggett Award, at the 51st Annual Conference of the Society in Edmonton, Canada, in October 1998. This award is presented only to those who have made outstanding contributions to the field of geotechnical engineering in Canada. In his acceptance remarks, which follow below, Dr. Fredlund laid out briefly, but with great clarity, the significance of his work to date and his vision for the future. For many present, it underlined both the accomplishments of this lifetime of achievement and the potential for his work to substantially change the way geotechnical engineering is practiced, both in Canada and internationally. His acceptance remarks provide further insights into both his personal values and his comprehensive understanding of the unsaturated soils area. They are a fitting epilogue to this book, summarizing progress in unsaturated soil mechanics to date, while outlining the vision of even greater achievements in this field in the future.

Remarks of Dr D.G. Fredlund upon accepting the R.F. Leggett Award, October 1998:

When I received the notice by e-mail that I was the recipient of the Leggett Award, my first response was to write back to the sender and ask if he had possibly, accidentally sent the notice to the wrong person. It is truly a great honor for me to receive this award and I do so with deep and sincere humility.

I am sure that as I received the notice of the award, my mind went through the same thought processes that recipients have gone through in previous years. I began to think of all the people who have helped me in so many ways, along the way. There are many graduate students, research engineers, practicing engineers, and colleagues who have been an integral part of my professional development. There are colleagues such as Lee Barbour, Moir Haug, Dennis Pufahl, Karl Sauer, and Ward Wilson.

When I graduated from the University of Saskatchewan in 1962, I recall receiving two job offers. The lower paying job was with the National Research Council of Canada in Saskatoon, and

the pay was \$425 per month. I worked for Jim Hamilton and we instrumented buildings to measure the heave associated with expansive soils. One day Jim announced that a very important person would be coming to visit from Ottawa and he briefed us on how to behave. That person was none other than Robert F. Legget. His visit was by no means stressful and I can still remember the interest he took in my measurements of water content versus soil suction on Regina Clay. In fact, he suggested that I put the information together in the form of a research paper to be published by the National Research Council. And so, that became my first research paper, back in 1963. To me, the best part was the Preface to the paper that was personally written by Robert Legget. And as I read the Preface, I can remember thinking, "How does he know so much about expansive soils?". Well, such was the man, Robert F. Legget.

My career started with the measurement of the relationship between water content and soil suction, a relationship now commonly referred to as the soil-water characteristic curve. One month ago, I was asked to give the opening keynote address in Beijing, China, at the Second International Conference on Unsaturated Soils, and my topic was the "Importance of the Soil-Water Characteristic Curve in Bringing Unsaturated Soil Mechanics into Geotechnical Engineering". And so, it would appear that I have spent my entire career studying the same topic. Wayne Clifton, in one of his complimentary moments referred to me as a very focused person, others may have thought that I was simply a very persistent person, but my wife might say that I must be a slow learner.

And speaking about my wife, I want to publicly say thank you to JoAnne for her endurance and patience over the past 34 years. Patience when my airplanes never came in and when I missed birthdays and anniversaries. And I also want to say thanks to my three sons and one daughter. Three boys who provided me with hundreds upon hundreds of hockey games and baseball games to watch and a daughter who provided dressage horseback competitions to watch. It is rewarding to have my daughter Jocelyn here today. And it is also personally rewarding to also have one son who felt that geotechnical engineering would be interesting and it is a delight to have him here today. I once teasingly commented to my wife that Murray must have gotten my brains because his marks were quite high. My wife replied, "I agree because I still have mine!".

I have immensely enjoyed research work and teaching at university. I was fortunate to have excellent supervisors on my M.Sc. and Ph.D. programs. Dr. Stan Thomson supervised me on my Masters program and Dr. Morgenstern supervised me on my Ph.D. program. When I decided to go back for my Ph.D. degree, I applied to two universities; the University of Alberta and a university in the United States.

I was having some difficulty deciding which university I should go to. However, one day I received a letter from the American university informing me that I would have to write the dreaded TOEFL English exam. I think that it was the fear of failing the TOEFL exam that made me select the University of Alberta. That is not really what happened. I spent some time discussing the area of research that was of interest to me with Dr. Morgenstern, and from the start I admired his perception and insight into the subject of unsaturated soils. It was a subject that I had been studying for some time but a subject about which he seemed to know exactly the direction the research needed to go. And so I embarked on my research program and one day I explained to him that I had some insights on the use of independent stress state variables. He listened and, at the end, he made a remark that has remained with me throughout my career. He may not even remember the remark but I remember it clearly. He said that he felt that the concept of independent stress state variables was so powerful and so important that I could spend my entire career convincing the world that this was the approach to use in understanding unsaturated soil mechanics. And so, I guess I would say that he was right (he was a Prophet), and that is what I have done and that is basically the story of my life.

I have had the good fortune of seeing unsaturated soil mechanics emerge from a few theoretical concepts to the point where it now plays an important role in numerous geotechnical engineering design procedures. One example involves the design of covers for waste disposal where the cover design involves obtaining the right unsaturated soil properties for the local climate. So much of our infrastructure design and environmental control measures involve near ground surface soils that are unsaturated, and as a result, unsaturated soil mechanics provides a door of opportunity for geotechnical engineering.

My goal during the 1970s was to establish the fundamental physical relationships for seepage, shear strength, and volume change behaviour of unsaturated soils. My goal in the 1980s was to develop the necessary computational tools for unsaturated seepage modelling, slope stability analyses, and the prediction of heave and collapse. My goal for the 1990s has been to work towards the implementation of unsaturated soil mechanics into conventional geotechnical engineering practice. I have had a vision for a long time, that unsaturated soil mechanics could be understood and practiced as a relatively simple extension of saturated soil mechanics. It was a vision that was quite dim in the 1970s, became feasible in the 1980s, and is emerging as a reality in the 1990s. I believe that we now have a window of opportunity to show internationally what can be done through the application of unsaturated soil mechanics.

During the ISSMFE presidency of Dr. Morgenstern, there was a reorganization of some of the technical committees. There was a combination of the expansive soils committee, the collapsible soils committee, and the committee on arid soils. These committees were reorganized into a new committee called the unsaturated soils committee. I have had the good fortune to chair this committee for three terms. Only one month ago, this committee sponsored the Second International Conference on Unsaturated Soils in Beijing, China. The conference was personally rewarding to me for two reasons. First, it was rewarding to see the rapid rate at which the unsaturated soils theories are finding their way into routine geotechnical engineering applications. Second, it was personally rewarding to have the conference held in a developing country. Many of the more severe unsaturated soils problems are found in arid and semi-arid regions, and these regions are often in developing countries with few financial resources to send engineers to conferences.

I would like to bring my comments to a close by saying a few words about my involvement in programs of collaboration with developing countries. As personally rewarding as my theoretical studies on unsaturated soils have been, they have not meant as much to me as the programs of collaboration with needy, developing countries. Many of you will recall the collection of civil and geotechnical engineering books that filled almost two 20-foot containers that were sent to Hanoi, Vietnam.

When the first container was being unloaded in Hanoi, the Vietnamese customs officer said to one of the Vietnamese engineers, "Where did you find a friend who would do this for you?" I wanted to mention this today because you are the people who donated the books for Vietnam; you are their friends, and I thank you. In addition, it is rewarding to have two graduate students and one visiting scholar from Vietnam here today.

Almost a year after the books arrived in Vietnam, government officials provided a banquet to express their thanks. At the end of the evening they asked me to speak on "Why did I come to Vietnam and why did I do what I had done for the Vietnamese people?" They gave me 45 minutes to speak but today I want to conclude with the tribute that I paid to my mother and father when I spoke that day. I said that it was my mom and dad who taught me that,

"If I live for myself, I will feed my ego, and when life is over I will have nothing,
If I live for others, I will feed the soul, and life will have meaning."
And this, I still believe more strongly than ever.

And finally, I want to say "thank you" to God, for being my personal God, for making life exciting and meaningful. And "thank you" to the Canadian Geotechnical Society for bestowing this treasured award on me.

Part IX

Bibliography of Publications

1969

Fredlund, D.G. 1969. Consolidometer test procedural factors affecting swell properties. Proceedings, Second International Conference on Expansive Soils, College Station, Texas, Texas A&M Press, pp. 435–456.

1971

Fredlund, D.G., and Dahlman, A.E. 1971. Statistical geotechnical properties of glacial Lake Edmonton sediments. Proceedings, First International Conference on Application of Statistics and Probability to Soil and Structural Engineering, September, Hong Kong. pp. 212–228.

1972

Krahn, J., and Fredlund, D.G. 1972. On total, matric and osmotic suction. *Soil Science*, **114**(5): 339–348.

1973

Bergan, A.T., and Fredlund, D.G. 1973. Characterization of freeze-thaw effects on subgrade soils. Symposium on Frost Action on Roads, Organization for Economic Cooperation and Development, Oslo, Norway.

Fredlund, D.G. 1973. Discussion on The Second Technical Session, Division Two (Flow and Shear Strength), Proceedings, Third International Conference on Expansive Soils, II, Jerusalem Academic Press, Israel Institute of Technology, Technion City, Haifa, Israel, pp. 71–76.

Fredlund, D.G., and Morgenstern, N.R. 1973. Pressure response below high air entry disks. Proceedings, Third International Conference on Expansive Soils, I, Jerusalem Academic Press, Israel Institute of Technology, Technion City, Haifa, Israel, pp. 97–108.

1974

Fredlund, D.G. 1974. Engineering approach to soil continua. Second Symposium, Application of Solid Mechanics, McMaster University, Hamilton, Ontario, pp. 46–59.

1975

Fredlund, D.G. 1975. A diffused air volume indicator for unsaturated soils. *Canadian Geotechnical Journal*, **12**(4): 533–539.

Fredlund, D.G. 1975. Prediction of heave in unsaturated soils. Proceedings, Fifth Asian Regional Conference, Bangalore, India, December 19–22, pp. 19–22.

Fredlund, D.G., Bergan, A.T., and Sauer, E.K. 1975. Deformation characterization of subgrade soils for highways and runways in northern environments. *Canadian Geotechnical Journal*, **12**(2): 213–223.

Kent, D.D., Fredlund, D.G., and Watt, W.G. 1975. Variables controlling behavior of a partly frozen soil. Proceedings, Conference on Soil Water Problems in Cold Regions, May, Calgary, Alberta, pp. 70–88.

1976

Fredlund, D.G. 1976. Computer software for slope stability analysis. Proceedings, 90th Annual EIC Congress, Halifax, Nova Scotia, October 4–8.

Fredlund, D.G. 1976. Density and compressibility characteristics of air-water mixtures. *Canadian Geotechnical Journal*, **13**(4): 386–396.

Fredlund, D.G., and Morgenstern, N.R. 1976. Constitutive relations for volume change in unsaturated soils. *Canadian Geotechnical Journal*, **13**(3): 261–276.

Hasan, J., and Fredlund, D.G. 1976. Discussion on J. Uzan: Analysis of swelling-soil column infiltration test. *Journal of the Geotechnical Engineering Division, American Society of Civil Engineers*, **103**(GT7): 829–831.

1977

- Fredlund, D.G. 1977. Slope stability software usage in Canada. Proceedings, Specialty Session on Computing in Soil Mechanics: Present and Future, Specialty Session No. 12, Ninth International Conference on Soil Mechanics and Foundation Engineering, Tokyo, Japan, July, pp. 289–302.
- Fredlund, D.G., and Krahn, J. 1977. Comparison of slope stability methods of analysis. Canadian Geotechnical Journal, **14**(3): 429–439.
- Fredlund, D.G., and Morgenstern N.R. 1977. Stress state variables for unsaturated soils. Journal of the Geotechnical Engineering Division, American Society of Civil Engineers, **103**(GT5): 447–466.
- Fredlund, D.G., Bergan, A.T., and Wong, P.K. 1977. Resilient modulus constitutive relationship for cohesive soils. Annual Meeting of the Transportation Research Board, Washington, D.C., Transportation Research Record **642**: 73–81.
- Hasan, J., and Fredlund, D.G. 1977. Consolidation theory for unsaturated soils. Symposium on Water Movement and Equilibrium in Swelling Soils, Committee on Water in the Unsaturated Zone, Section of Hydrology of the American Geophysical Union, San Francisco, California.
- Haug, M.D., Sauer, E.K., and Fredlund, D.G. 1977. Retrogressive slope failures at Beaver Creek, south of Saskatoon, Saskatchewan, Canada. Canadian Geotechnical Journal, **14**(3): 288–301.

1978

- Fredlund, D.G. 1978. Book review: *Foundation on Expansive Soils*, by Fu Hua Chen. Canadian Geotechnical Journal, **15**(1): 135–136.
- Fredlund, D.G. 1978. Usage, requirements and features of slope stability computer software (Canada, 1977). Canadian Geotechnical Journal, **15**(1): 83–95.
- Fredlund, D.G., and Morgenstern, N.R. 1978. Closure to paper entitled stress state variables for unsaturated soils. American Society of Civil Engineering, Geotechnical Division (GT11), pp. 1415–1416.
- Fredlund, D.G., Morgenstern, N.R., and Widger, R.A. 1978. Shear strength of unsaturated soils. Canadian Geotechnical Journal, **15**(3): 313–321.

1979

- Bocking, K.A., and Fredlund, D.G. 1979. Use of the osmotic tensiometer to measure negative pore-water pressure. Geotechnical Testing Journal, GTJODJ, **2**(1): 3–10.
- Fredlund, D.G. 1979. Appropriate concepts and technology for unsaturated soils. Canadian Geotechnical Journal, **16**(1): 121–139.
- Fredlund, D.G., and Hasan, J. 1979. One-dimensional consolidation theory: Unsaturated soils. Canadian Geotechnical Journal, **16**(2): 521–531.
- Krahn, J., Johnson, R.F., Fredlund, D.G., and Clifton, A.W. 1979. A highway cut in cretaceous sediments at Maymont, Saskatchewan. Canadian Geotechnical Journal, **16**(4): 703–715.
- Morrison, J., and Fredlund, D.G. 1979. Discussion: Emploi d'une methode psychrométrique dans des essais triaxiaux sur un limon remanié non saturé. Canadian Geotechnical Journal, **16**(3): 614–615.
- Widger, R.A., and Fredlund, D.G. 1979. Stability of swelling clay embankments. Canadian Geotechnical Journal, **16**(1): 140–151.

1980

- Bocking, K.A., and Fredlund, D.G. 1980. Limitation of the axis-translation technique. Proceedings, Fourth International Conference on Expansive Soils, Denver, Colorado, Vol. 1, pp. 117–135.

- Dakshanamurthy, V., and Fredlund, D.G. 1980. Moisture and air flow in an unsaturated soil. Proceedings, Fourth International Conference on Expansive Soils, Denver, Colorado, Vol. 1, pp. 514–532.
- Fredlund, D.G. 1980. Use of computers for slope stability analysis. Proceedings, International Symposium on Landslides, April 7–11, New Delhi, India, Vol. 2, pp. 129–138.
- Fredlund, D.G. 1980. Discussion: Consolidation of unsaturated soils including swelling and collapse behavior, by Lloret A. and Alonso, *Géotechnique* **30**(4): 449–477.
- Fredlund, D.G., Hasan, J.U., and Filson, H. 1980. The prediction of total heave. Proceedings, Fourth International Conference on Expansive Soils, Denver, Colorado, Vol. 1, pp. 1–17.
- Fredlund, D.G., Krahn, J., and Hasan, J.U. 1980. Variability of an expansive clay deposit. Proceedings, Fourth International Conference on Expansive Soils, Denver, Colorado, Vol. 1, pp. 332–338.
- Hasan, J.U., and Fredlund, D.G. 1980. Pore-pressure parameters for unsaturated soils. *Canadian Geotechnical Journal*, **17**(3): 395–404.

1981

- Clifton, A.W., Krahn, J., and Fredlund, D.G. 1981. Riverbank instability and development control in Saskatoon. *Canadian Geotechnical Journal*, **18**(1): 95–105.
- Dakshanamurthy, V., and Fredlund, D.G. 1981. A mathematical model for predicting moisture flow in an unsaturated soil under hydraulic and temperature gradients. *Water Resources Journal*, **17**(3): 714–722.
- Fredlund, D.G. 1981. Seepage in saturated soils. Panel discussion: Groundwater and seepage problems. Proceedings, Tenth International Conference on Soil Mechanics and Foundation Engineering, Stockholm, Sweden, Vol. 4, pp. 629–641.
- Fredlund, D.G. 1981. The shear strength of unsaturated soils and its relationship to slope stability problems in Hong Kong. *The Hong Kong Engineer*, **9**(4): 37–45.
- Fredlund, D.G., and Dakshanamurthy, V. 1981. Transient flow theory for geotechnical engineering. Presented at a Special Session entitled Impact of Richards' Equation. A semi-centennial session organized by the Hydrology Section, American Geophysical Union, San Francisco, California, December.
- Fredlund, D.G., Krahn, J., and Pufahl, D.E. 1981. The relationship between limit equilibrium slope stability methods. Proceedings, International Conference on Soil Mechanics and Foundation Engineering, Stockholm, Sweden, Vol. 3, pp. 409–416.
- Yoshida, R., Fredlund, D.G., and Hamilton, J.J. 1981. The prediction of heave of a slab-on-grade floor on Regina Clay. *Canadian Geotechnical Journal*, **20**(1): 69–81.

1982

- Fredlund, D.G. 1982. Closure: The shear strength of unsaturated soils and its relationship to slope stability problems in Hong Kong. *The Hong Kong Engineer*, June, pp. 57–59.
- Fredlund, D.G., and Dakshanamurthy, V. 1982. Prediction of moisture flow and related swelling or shrinking in unsaturated soils. *Geotechnical Engineering*, **13**: 15–49.
- Fredlund, D.G., and Dakshanamurthy, V. 1982. Transient flow process in unsaturated soils under flux boundary conditions. Proceedings, Fourth International Conference on Numerical Methods in Geomechanics, Edmonton, Alberta, Vol. 1, pp. 307–318.
- Ho, D.Y.F., and Fredlund, D.G. 1982. Multi-stage triaxial tests for unsaturated soils. *ASTM, Geotechnical Testing Journal*, **5**(1/2): 18–25.
- Ho, D.Y.F., and Fredlund, D.G. 1982. Strain rates for unsaturated soils shear strength testing. Proceedings, Seventh Southeast Asian Geotechnical Conference, Hong Kong, November 22–26, Vol. 1, pp. 787–803.
- Ho, D.Y.F., and Fredlund, D.G. 1982. The increase in shear strength due to soil suction for two Hong Kong soils. Proceedings, American Society of Civil Engineers, Geotechnical Conference on Engineering and Construction in Tropical and Residual Soils, Honolulu, Hawaii, January, pp. 263–295.

1983

- Ching, R., and Fredlund, D.G. 1983. Some difficulties associated with the limit equilibrium method of slices. *Canadian Geotechnical Journal*, **20**(4): 661–672.
- Fredlund, D.G. 1983. Prediction of ground movements in swelling clays. Proceedings, Thirty-first Annual Soil Mechanics and Foundation Engineering Conference, American Society of Civil Engineers, Minneapolis, Minnesota.
- Fredlund, D.G., and Rahardjo, H. 1983. A comprehensive limit equilibrium software package for geotechnical engineering. Presented at the Computer Applications Technical Session of the Canadian Society of Civil Engineers Annual Meeting, Computer Systems in Civil Engineering, Ottawa, Canada.
- Goodall, D.C., Fredlund, D.G., and Lamb, K. 1983. Methods and implications of a state-of-the-art geotechnical field investigation of potash tailings near Lanigan, Saskatchewan. Proceedings, First International Potash Technology Conference, Saskatoon, Saskatchewan, October 3–5. *Edited by R.M. McKercher*, pp. 781–786.
- Krahn, J., and Fredlund, D.G. 1983. Variability of the engineering properties of natural soil deposits. Proceedings, Fourth International Conference on Applications of Statistics and Probability in Soil and Structural Engineering, Florence, Italy, June 13–17, Vol. 2, pp. 1017–1029.
- Papagianakis, A.T., and Fredlund, D.G. 1983. A steady state model for flow in saturated-unsaturated soils. Proceedings, Ninth Canadian Congress of Applied Mechanics, Saskatoon, Saskatchewan, May 30 – June 3.
- Papagianakis, A.T., Lam, L., and Fredlund, D.G. 1983. Steady state and transient mass transport models for saturated-unsaturated soil. Proceedings, First International Potash Technology Conference, Saskatoon, Saskatchewan, October 3–5. *Edited by R.M. McKercher*, pp. 741–747.
- Pufahl, D.E., Fredlund, D.G., and Rahardjo, H. 1983. Lateral earth pressures in expansive unsaturated clay soils. *Canadian Geotechnical Journal*, **20**(2): 228–241.
- Rahardjo, H., and Fredlund, D.G. 1983. Lateral earth force theory using limit equilibrium. Proceedings, Ninth Canadian Congress of Applied Mechanics, Saskatoon, Saskatchewan, May 30 – June 3.
- Wilson, G.W., and Fredlund, D.G. 1983. The evaluation of the interslice side forces for slope stability analysis by the finite element method. Proceedings, Ninth Canadian Congress of Applied Mechanics, Saskatoon, Saskatchewan, May 30 – June 3.
- Yoshida, R., Fredlund, D.G., and Hamilton, J.J. 1983. The prediction of heave of a slab-on-grade floor on Regina Clay. *Canadian Geotechnical Journal*, **20**(1): 69–81.

1984

- Ching, R., and Fredlund, D.G. 1984. A small Saskatchewan town copes with swelling clay problems. Proceedings, Fifth International Conference on Expansive Soils, Adelaide, Australia, May 21–23, pp. 306–310.
- Ching, R.K.H., and Fredlund, D.G. 1984. Quantitative comparisons of limit equilibrium methods of slices. Proceedings, Fourth International Symposium on Landslides, Toronto, Ontario, September 16–21, 1984, pp. 373–379.
- Ching, R., Sweeney, D.J., and Fredlund, D.G. 1984. Increase in factor of safety due to soil suction for two Hong Kong slopes. Proceedings, Fourth International Symposium on Landslides, Toronto, Ontario, September 16–21, pp. 617–623.
- Clifton, A.W., Yoshida, R., Fredlund, D.G., and Chursinoff, R.W. 1984. Performance of Darke Hall, Regina, Canada, constructed on a highly swelling clay. Proceedings, Fifth International Conference on Expansive Soils, Adelaide, Australia, May 21–23, pp. 197–201.
- Dakshnamurthy, V., Fredlund, D.G., and Rahardjo, H. 1984. Coupled three-dimensional consolidation theory of unsaturated porous media. Proceedings, Fifth International Conference on Expansive Soils, Adelaide, South Australia, May 21–23, pp. 99–104.

- Fredlund, D.G.. Analytical methods for slope stability analysis. State-of-the-art address to the Fourth International Symposium on Landslides, Toronto, Ontario, September 16–21, 1984, pp. 229–250.
- Lam, L., and Fredlund, D.G. 1984. Saturated–unsaturated transient finite element seepage model for geotechnical engineering. Proceedings, Fifth International Conference on Finite Elements in Water Resources, University of Vermont, Burlington, Vermont, pp. 113–122.
- Lee, R.K., and Fredlund, D.G. 1984. Measurement of soil suction using the MCS 6000 gauge. Proceedings, Fifth International Conference on Expansive Soils, Adelaide, Australia, May 21–23, pp. 50–54.
- Papagianakis, A.T., and Fredlund, D.G. 1984. A steady state model for flow in saturated–unsaturated soils. *Canadian Geotechnical Journal*, **21**(3): 419–430.
- Rahardjo, H., and Fredlund, D.G. 1984. General limit equilibrium theory for lateral earth force. *Canadian Geotechnical Journal*, **21**(1): 166–175.

1985

- Fredlund, D.G. 1985. Soil mechanics principles that embrace unsaturated soils. Proceedings, Eleventh International Society for Soil Mechanics and Foundation Engineering, San Francisco, California, August 11–15, Vol. 2, pp. 465–473.
- Fredlund, D.G. 1985. Theory formulation and application for volume change and shear strength problems in unsaturated soils. Session 9C, Problems in Areas with Special Geological Conditions, Foundation Problems in Arid Areas, Eleventh International Conference on Soil Mechanics and Foundation Engineering, San Francisco, California, August 11–16, Vol. 6, pp. 2835–2838.
- Fredlund, D.G., and Rahardjo, H. 1985. Theoretical context for understanding unsaturated residual soil behavior. Proceedings, First International Conference on Geomechanics in Tropical Lateritic and Saprolitic Soils, Brasilia, Brazil, February 11–14, pp. 295–306.
- Fredlund, D.G., and Rahardjo, H. 1985. Unsaturated soil consolidation theory and laboratory experimental data, consolidation of soils: Testing and evaluation. ASTM STP 892. *Edited by* R. Yong and F.C. Townsend, Fort Lauderdale, Florida, January, pp. 154–169.

1986

- Clifton, A.W., Mickleborough, O., and Fredlund, D.G. 1986. Highwall stability analysis under dragline loadings at a Saskatchewan coal mine. International Symposium on Geotechnical Stability in Surface Mining, Calgary, Alberta, Nov. 6–7, pp. 341–353.
- Fan, K., Fredlund, D.G., and Wilson, G.W. 1986. An interslice force function for limit equilibrium slope stability analysis. *Canadian Geotechnical Journal*, **23**(3): 287–296.
- Fredlund, D.G. 1986. Slope stability analysis incorporating the effect of soil suction. *In Slope Stability. Edited by* M.G. Anderson and K.S. Richards, John Wiley and Sons Ltd., pp. 105–136.

1987

- Arenicz, R.M., and Fredlund, D.G. 1987. A note on reinforced earth design. Engineering Conference on Developing Remote Areas. The Institution of Engineers (Australia) Canberra, Darwin, May 11–15, pp. 199–203.
- Fredlund, D.G. 1987. Book review: *The Stability of Slopes* by E.N. Bromhead. Surrey University Press (1986), *Canadian Geotechnical Journal*, **24**(2): 323–324.
- Fredlund, D.G. 1987. The prediction and performance of structures on expansive soils. Keynote Address, International Symposium on Prediction and Performance in Geotechnical Engineering, Calgary, Alberta, June 17–19. *Edited by* R.C. Joshi and F.J. Griffiths, pp. 51–60.
- Fredlund, D.G. 1987. The stress state for expansive soils. Keynote Address, Sixth International Conference on Expansive Soils, New Delhi, India, December 1–4, pp. 1–9.

- Fredlund, D.G., and Fredlund, L.D. 1987. The PC-SLOPE family of software for slope stability analysis. Proceedings, First Canadian Symposium on Micro-Computer Applications to Geotechnique, Regina, Saskatchewan, October 22–23, pp. 173–181.
- Fredlund, D.G., and Fredlund, M.D. 1987. The PC-SLIN family of software for slope inclinometer data reduction. Proceedings, First Canadian Symposium on Micro-Computer Applications to Geotechnique, Regina, Saskatchewan, October 22–23, pp. 163–171.
- Fredlund, D.G. and Rahardjo, H., 1987. Soil mechanics principles for highway engineering in arid regions. Session on Geotechnical Problems in Arid Region, Transportation Research Board, Committee A2L06TRB, Washington, D.C., January, Transportation Research Record **1137**: 1–11.
- Fredlund, D.G., Rahardjo, H., and Gan, J.K-M. 1987. Non-linearity of strength envelope for unsaturated soils. Proceedings, Sixth International Conference on Expansive Soils, New Delhi, India, December 1–4, Vol. 1, pp. 49–56.
- Gan, J.K-M., and Fredlund, D.G. 1987. Multistage direct shear testing of unsaturated soils. ASTM Geotechnical Testing Journal, **11**(2): 132–138.
- Krahn, J., Fredlund, D.G., Lam, L., and Barbour, S.L. 1987. PC-SEEP: A finite element program for modelling seepage. Proceedings, First Canadian Symposium on Micro-Computer Applications to Geotechnique, Regina, Saskatchewan, October 22–23, pp. 243–251.
- Lam, L., Fredlund, D.G., and Barbour, S.L. 1987. Transient seepage model for saturated-unsaturated soils systems: A geotechnical engineering approach. Canadian Geotechnical Journal, **24**(4): 565–580.
- Rao, R.R., and Fredlund, D.G. 1987. Interpretation of expansive soils data and its application to the prediction of heave. Proceedings, Sixth International Conference on Expansive Soils, New Delhi, India, December 1–3, pp. 207–210.
- Rao, R.R., Rahardjo, H., and Fredlund, D.G. 1987. Closed form heave solutions for expansive soils. American Society of Civil Engineers, Geotechnical Journal, **114**(5): 573–588.
- van der Raadt, P., Fredlund, D.G., Clifton, A.W., Klassen, M.H., and Jubien, W.E. 1987. Soil suction measurements at several sites in Western Canada. Session on Geotechnical Problems in Arid Regions, Transportation Research Board, Committee A2L06TRB, Washington, D.C., January, Transportation Research Record **1137**: 24–35.

1988

- Fredlund, D.G., and Barbour, S.L. 1988. The role of kriging in slope stability analysis. Annual Conference on Canadian Society of Civil Engineers, Computer Applications in Civil Engineering, Calgary, Alberta, May 25–27, pp. 41–57.
- Fredlund, D.G., and Rahardjo, H. 1988. State-of-development in the measurement of soil suction. Proceedings, First International Conference on Engineering Problems of Regional Soils, August 11–15, Beijing, China, pp. 582–588.
- Gan, J.K-M., Fredlund, D.G., and Rahardjo, H. 1988. Determination of the shear strength parameters of an unsaturated soil using the direct shear test. Canadian Geotechnical Journal, **25**(3): 500–510.
- Pufahl, D.E., and Fredlund, D.G. 1988. Lateral movements and deformation properties of a potash tailings pile in Saskatchewan, Canada. Hydraulic Fill Structures '88, American Society of Civil Engineers, Geotechnical Specialty Conference, CSU, Fort Collins, CO, August 14–17, pp. 956–970.
- Sauer, E.K., and Fredlund, D.G. 1988. Effective stress, limit equilibrium, back-analysis of failed slopes: An evaluation. Proceedings, Fourth International Symposium on Landslides, Lausanne, Switzerland, July 10–15, pp. 763–770.
- Sweeney, D.A., Wong, D.K.H., and Fredlund, D.G. 1988. The effect of lime on a highly plastic clay with special emphasis on aging. Transportation Research Board, Washington, D.C., January, Transportation Research Record **1190**: 13–23.
- Wong, D.K.H., Barbour, S.L., and Fredlund, D.G. 1988. Modelling of flow through potash tailings piles. Canadian Geotechnical Journal, **25**(2): 292–306.

1989

- Barbour, S.L., and Fredlund, D.G. 1989. Mechanics of osmotic flow and volume change in clay soils. *Canadian Geotechnical Journal*, **26**: 551–562.
- Barbour, S.L., and Fredlund, D.G. 1989. Physico-chemical state variables for clay soils. Proceedings, Twelfth International Conference on Soil Mechanics and Foundation Engineering (ICSMFE), Rio de Janeiro, Brazil, August, pp. 1839–1843.
- Fredlund, D.G. 1989. Soil suction monitoring for roads and airfields. Symposium on the State-of-the-Art of Pavement Response Monitoring Systems for Roads and Airfields, sponsored by the U.S. Army Corps. of Engineers, Hanover, New Hampshire, March 6–9, pp. 24–39.
- Fredlund, D.G. 1989. The character of the shear strength envelope for unsaturated soils. The Victor de Mello Volume, Proceedings, Twelfth International Conference on Soil Mechanics and Foundation Engineering (ICSMFE), Rio de Janeiro, Brazil, August, pp. 142–149.
- Fredlund, D.G. 1989. The role of negative pore-water pressures in slope stability analyses. Proceedings, First South American Symposium on Landslides, Bogota, Columbia, August 8–10, pp. 226–256.
- Fredlund, D.G., and Wong, D.K.H. 1989. Calibration of AGWA-II thermal conductivity sensors for measuring soil suction. *ASTM Geotechnical Testing Journal*, **12**(3): 188–194.
- Fredlund, D.G., Rahardjo, H., and Loi, J. 1989. Typical matric suction measurements in the laboratory and the field using thermal conductivity sensors. Proceedings, Indian Geotechnical Conference, Visakhapatnam, India, December 14–16, pp. 127–131.
- Ho, D.Y.F., and Fredlund, D.G. 1989. Laboratory measurement of the volumetric deformation moduli for two unsaturated soils. Proceedings, Forty-second Canadian Geotechnical Conference, Winnipeg, Manitoba, October 23–25.
- Krahn, J., Fredlund, D.G., and Klassen, M.J. 1989. Effect of soil suction on slope stability at Notch Hill. *Canadian Geotechnical Journal*, **26**(2): 269–278.
- Rao Rama, R., Rahardjo, H., and Fredlund, D.G. 1989. Closure on: Closed-form heave solutions for expansive soils. Discussion by K.S. Li, Binnie and Partners, Hong Kong, American Society of Civil Engineers, *Geotechnical Journal*, **115**(12): 1822–1833.
- Sattler, P.J., and Fredlund, D.G. 1989. Use of thermal conductivity sensors to measure matric suction in the laboratory. *Canadian Geotechnical Journal*, **26**: 491–498.
- Sweeney, D.A., Fredlund, D.G., Gan, J.K.-M., and Widger, R.A. 1989. Evaluation of environmental influences on a lime-modified highly plastic clay. Presented to the RTAC meeting, Calgary, Alberta, September 17–21.
- Wong, D.K.H., Fredlund, D.G., Imre, E., and Putz, G. 1989. Difficulties associated with the use of AGWA-II thermal conductivity sensors to measure suction. Transportation Research Board, Washington, D.C., January, *Transportation Research Record* **1219**: 131–143.

1990

- Fredlund, D.G. 1990. Theory and research related to the use of thermal conductivity sensors. Soil Physics Symposium on the Measurement of Soil Physical Properties, San Antonio, Texas, October 21–26.
- Fredlund, D.G., Rahardjo, H., and Gan, J.K.-M. 1990. Discussion on the paper entitled, “A framework for unsaturated soils behavior” by D.G. Toll (1990). *Géotechnique*, **40**(1): 31–44.
- McClarty, D.V.B., and Fredlund, D.G. 1990. Spline interpolation: A means of interfacing finite element analysis and limit equilibrium analysis. Proceedings, Annual Conference of the Canadian Society of Civil Engineering, Hamilton, Ontario, May 15–18, Vol. II-2, pp. 779–798.
- Rahardjo, H., Ho, D.Y.F., and Fredlund, D.G. 1990. Testing procedures for obtaining volume change indices during loading of an unsaturated soil. Proceedings, Annual Conference of the Canadian Society of Civil Engineering, Hamilton, Ontario, May 15–18, Vol. II-2, pp. 558–573.
- Sattler, P., and Fredlund, D.G. 1990. Numerical modelling of vertical ground movements in expansive soils. *Canadian Geotechnical Journal*, **28**(2): 189–199.

- Sattler, P., Fredlund, D.G., Klassen, M.J., and Rowan, W.G. 1990. Bearing capacity approach to railway design using subgrade matric suction. Transportation Research Board, Washington, D.C. Transportation Research Record **1241**: 27–33.
- Sattler, P., Fredlund, D.G., Lam, L.W., Clifton, A.W., and Klassen, M.J. 1990. Implementation of a bearing capacity design procedure for railway subgrades: A case study. Transportation Research Board, Committee on Railroad Track Structure System Design. Presented to Transportation Research Board 69th Annual Meeting, Washington, D.C., January 7–11, Transportation Research Record **1288**: 191–197.

1991

- Barbour, S.L., and Fredlund, D.G. 1991. Integrated seepage and limit equilibrium analyses to assess the possibility of slope instability. *In Geomechanics and Water Engineering in Environmental Management*. The University of Wollongong, Australia, pp. 3–36.
- Barbour, S.L., Fredlund, D.G., and Pufahl, D.E. 1991. The osmotic role in the behavior of swelling clay soils. NATO Advanced Research Workshop, Korfu, Greece, July 1–6, pp. 97–139.
- Fredlund, D.G. 1991. How negative can pore-water pressure get? Canadian Geotechnical Society, Geotechnical News, September, **9**(3), pp. 44–46.
- Fredlund, D.G. 1991. Long term stability of potash tailings piles on soft foundations. Presentation, Second International Potash Technology Conference, KALI '91, Hamburg, Germany, May 26–29.
- Fredlund, D.G., and Ning Yang. 1991. The mechanical properties of unsaturated soil and their engineering application. Journal of China Academy of Building Research. Chinese Journal of Geotechnical Engineering, Beijing, China, **13**(5): 24–35.
- Fredlund, D.G., Gan, J.K.-M., and Rahardjo, H. 1991. Measuring negative pore-water pressures in a freezing environment. Presented to the Transportation Research Board (TRB) meeting in January; Session on Moisture Migration in Freezing and Thawing Soils, sponsored by the Committee on Frost Action, Transportation Research Record **1307**, pp. 291–299.
- Khogali, W.E.I., Anderson, K.O., Gan, J.K.-M., and Fredlund, D.G. 1991. Installation and monitoring of moisture suction sensors in a fine-grained subgrade soil subjected to seasonal frost. Second International Symposium, “State-of-the-Art” of Pavement Response-Monitoring Systems for Roads and Airfields, Sponsored by U.S. Army Cold Regions, Research and Engineering Laboratory, Hanover, New Hampshire and Federal Aviation Administration, Washington, D.C., West Lebanon, New Hampshire, September 10–13.
- Lau, J.T.K., Fredlund, D.G., and Rahardjo, H. 1991. Comparison of elastic and plastic approaches to the prediction of depth of cracking. Abstract, Proceedings, CANCAM '91, Thirteenth Canadian Congress of Applied Mechanics, University of Manitoba, Winnipeg, Manitoba, June 2–6, Vol. 1, p. 388.
- McClarty, D.V.B., Fredlund, D.G., and Barbour, S.L. 1991. The use of spline interpolation in slope stability analysis. Proceedings, Forty-fourth Canadian Geotechnical Conference, Calgary, Alberta, September 29 – October 2, pp. 20-1 to 20-10.
- Rahardjo, H., and Fredlund, D.G. 1991. Calculation procedures for slope stability analyses involving negative pore-water pressures. Slope Stability Engineering: Development and Applications. Proceedings, International Conference on Slope Stability Engineering. Edited by R. Chandler, organized by the Institution of Civil Engineers, Shanklin, Isle of Wight, England, April 15–19, pp. 43–49.
- Robinsky, E., Barbour, S.L., Wilson, G.W., Bordin, D., and Fredlund, D.G. 1991. Thickened sloped tailings disposal — an evaluation of seepage and abatement of acid drainage. Proceedings, Second International Conference on the Abatement of Acidic Drainage, Montreal, Quebec, September 16–18, Vol. 1, pp. 529–549.
- Sattler, P.J., and Fredlund, D.G. 1991. Modelling vertical ground movements using surface climatic flux. Proceedings, ASCE, Geotechnical Engineering Congress, Boulder, Colorado, June 9–12, pp. 1292–1306.
- Tadepalli, R., and Fredlund D.G. 1991. The collapse behavior of a compacted soil during inundation. Canadian Geotechnical Journal, **28**: 477–488.

Wilson, G.W., Fredlund, D.G., and Barbour, S.L. 1991. The evaluation of evaporative fluxes from soil surfaces for problems in geotechnical engineering. Proceedings, Forty-fourth Canadian Geotechnical Conference, Calgary, Alberta, September 29 – October 2, pp. 68.1–68.9.

1992

Barbour, S.L., Fredlund, D.G., Gan, J.K-M., and Wilson, G.W. 1992. Prediction of moisture movement in highway subgrade soils. Proceedings, Forty-fifth Annual Canadian Geotechnical Conference, Keynote address, Toronto, Ontario, October 26–28, pp. 41A.1 – 41A.13.

Fan, K.K., Fredlund, D.G., and Wilson, G.W. 1992. Finite element analysis of interslice force functions for lateral earth force problems. Presented to the seventeenth South West Geotechnical Workshop, sponsored by American Society of Civil Engineers, Honolulu, Hawaii, April 22–24.

Fredlund, D.G. 1992. Background theory and research related to the use of thermal conductivity sensors for matric suction measurements. *In* Advances in Measurement of Soil Physical Properties; Bringing Theory into Practice, SSSA Special Publication No. 30, Soil Science of America, 677 S. Segoe Road, Madison, Wisconsin. pp. 249–262.

Fredlund, D.G., Sattler, P.J., and Gan, J.K-M. 1992. *In situ* suction measurements using thermal sensors. Proceedings, Seventh International Conference on Expansive Soils, Dallas, Texas, August 3–5, pp. 325–330.

Fredlund, D.G., Zhang, Z.M., and Lam, L. 1992. Effect of the axis of moment equilibrium in slope stability analysis. Canadian Geotechnical Journal, **29**: 456–465.

Ho, D.Y.F., Fredlund, D.G., and Rahardjo, H. 1992. Volume change indices during loading and unloading of an unsaturated soil. Canadian Geotechnical Journal, November, **29**(2): 195–207.

Loi, J., Fredlund, D.G., Gan, J.K-M., and Widger, R.A. 1992. Monitoring soil suction in an indoor test track facility. Transportation Research Record, **1362**: 101–110.

Rahardjo, H., and Fredlund, D.G. 1992. Slope stability and lateral earth force interslice functions based on finite element analysis. Proceedings, ASCE Speciality conference on Stability and Performance of Slopes and Embankments-II, University of California at Berkeley, California, USA, June 29 – July 1, Vol. 1, pp. 325–341.

Rahardjo, H., and Fredlund, D.G. 1992. Mechanics of soils with matric suction. Proceedings, International Conference on Geotechnical Engineering. GEOTROPIKA '92, Universite Teknologi, Johor Bahru, Malaysia, April 21–25, pp. 593–605.

Rahardjo, H., Fredlund, D.G., and Vanapalli, S.K. 1992. Use of linear and non-linear shear strength versus matric suction relations in slope stability analysis. Proceedings, Sixth International Symposium on Landslides, Christ Church, New Zealand, February 10–14, pp. 531–537.

Szafron, B.J., and Fredlund, D.G. 1992. Monitoring matric suctions in the subgrade of gravel roads. Proceedings, Forty-fifth Canadian Geotechnical Conference, Toronto, Ontario, October 26–28, pp. 52.1–52.10.

Tadepalli, R., Fredlund, D.G., and Rahardjo, H. 1992. Soil collapse and matric suction change. Proceedings, Seventh International Conference on Expansive Soils, Dallas, Texas, August 3–5, pp. 286–191.

Tadepalli, R., Rahardjo, H., and Fredlund, D.G. 1992. Measurements of matric suction and volume changes during inundation of collapsible soil. Journal of American Standards for Testing Materials, ASTM, **15**(2): 115–122.

1993

Fredlund, D.G., and Fredlund, L.D. 1993. Computing and geotechnical engineering; the 1990's and beyond. Geotechnical News, Bi-Tech Publishers, Canadian Geotechnical Society, April.

Fredlund, D.G., and Rahardjo, H. 1993. An overview of unsaturated soil behavior. Keynote Address. Proceedings, American Society of Civil Engineers Specialty Session on Unsaturated Soil Properties, Dallas, Texas, October 24–28, pp. 1–31.

Fredlund, D.G., and Rahardjo, H. 1993. Soil mechanics for unsaturated soils. John Wiley & Sons, New York.

- Fredlund, D.G., and Rahardjo, H. 1993. The role of unsaturated soil behavior in geotechnical practice. Keynote Address. Proceedings, Eleventh Southeast Asian Geotechnical Conference, Singapore, May 4–8, pp. 37–49.
- Fredlund, D.G., Rahardjo, H., and Ng, T. 1993. Effect of pore-air and negative pore-water pressures on stability at the end-of-construction. Proceedings, International Conference on Dam Engineering, Johor Bahru, Malaysia, January 12–13, pp. 43–51.
- Fredlund, D.G., Zhang, Z.M., and MacDonald, K. 1993. Analysis for the stability of potash tails piles. *Canadian Geotechnical Journal*, **30**(3):491–505.
- Kasap, S.O., Lakhanpal, D., Patzer, C., Mandziak, T., and Fredlund, D.G. 1993. Ultrasonic measurements on a porous ceramic to determine soil suction. *Ultrasonics*, Butterworth-Heinemann Ltd., Oxford, UK, **32**(5): 379–383.
- Lam, L., and Fredlund, D.G. 1993. A general limit equilibrium model for three-dimensional slope stability analysis. *Canadian Geotechnical Journal*, **30**(6): 905–919.
- McClarty, D.V.B., Fredlund, D.G., and Barbour, S.L. 1993. Use of spline interpolation in slope stability analysis. *Journal of Microcomputers in Civil Engineering*, Elsevier Science Publishers Ltd., Essex, England, No. 8, pp. 439–452
- Rahardjo, H., and Fredlund, D.G. 1993. Stress paths for shear strength testing of unsaturated soils. Proceedings, Eleventh Southeast Asian Geotechnical Conference, Singapore, May 4–8, pp. 187–192.
- Yang, Dai, Fredlund, D.G., and Stolte, W.J. 1993. A probabilistic slope stability analysis using deterministic computer software. Proceedings, Conference on Probabilistic Methods in Geotechnical Engineering, Canberra, Australia, February 10–12, pp. 267–274.

1994

- Adams, B.A., Wulfsohn, D., and Fredlund, D.G. 1994. Unsaturated soil mechanics for agricultural conditions. Paper No. 94-1037. American Society of Agricultural Engineers, International Summer Meeting, Kansas City, Missouri, June 19–22.
- Fredlund, D.G. 1994. Visualization of the world of soil mechanics. Proceedings, Sino-Canadian Symposium on Unsaturated/Expansive Soils, Wuhan, China, June 7–8, pp. 1–21.
- Fredlund, D.G., and Gan, J.K.-M. 1994. The collapse mechanism of a soil subjected to one-dimensional loading and wetting. *Genesis and Properties of Collapsible Soils*, NATO Advanced Research Workshop, Loughborough University of Technology, United Kingdom, April 11–16, pp. 173–205.
- Fredlund, D.G., and Xing, A. 1994. Equations for the soil-water characteristic curve. *Canadian Geotechnical Journal*, **31**(3): 521–532.
- Fredlund, D.G., Gan, J.K.-M., and Li, W-X. 1994. Thermal conductivity suction sensors — design considerations. Proceedings, Thirteenth International Conference on Soil Mechanics and Foundation Engineering, New Delhi, India, pp. 291–296.
- Fredlund, D.G., Xing, A., and Huang, S.Y. 1994. Predicting the permeability function for unsaturated soils using the soil-water characteristic curve. *Canadian Geotechnical Journal*, **31**(4): 533–546.
- Gan, J.K.-M., and Fredlund, D.G. 1994. The shear strength characteristics of two saprolitic soils from Hong Kong. Proceedings, Sino-Canadian Symposium on Unsaturated/Expansive Soil, Chinese Institution for Soil Mechanics and Foundation Engineering, CEES, Wuhan, China, June 7–8, pp. 81–107.
- Gan, J.K.-M., Fredlund, D.G., Xing, A., and Li, W-X. 1994. Design and data acquisition for thermal conductivity matric suction sensors. *Transportation Research Records* **1432**: 68–75.
- Huang, S., Barbour, S.L., and Fredlund, D.G. 1994. A history of the coefficient of permeability function. Proceedings, Sino-Canadian Symposium on Unsaturated/Expansive Soil, Chinese Institution for Soil Mechanics and Foundation Engineering, CEES, Wuhan, China, June 7–8, pp. 57–80.
- Jichun, Sun, Rahardjo, H., and Fredlund, D.G. 1994. A technique to perform coupled consolidation analysis using two independent softwares. *Computing in Civil Engineering*. Proceedings,

- First Congress on Computing in Civil Engineering, American Society of Civil Engineers, Washington, D.C., June 20–22, Vol. 1, pp. 849–856.
- Lam, L., and Fredlund, D.G. 1994. Reply: A general limit equilibrium model for three-dimensional slope stability analysis. *Canadian Geotechnical Journal*, **31**(4): 795–796.
- Lim, P.C., Barbour, S.L., and Fredlund, D.G. 1994. Laboratory determination of diffusion and adsorption coefficients of inorganic chemicals for unsaturated soil. Proceedings, First International Congress on Environmental Geotechnics, Edmonton, Alberta, July 10–15, pp. 319–324.
- Wilson, G.W., Fredlund, D.G., and Barbour, S.L. 1994. Coupled soil-atmosphere modelling for soil evaporation. *Canadian Geotechnical Journal*, **31**(2): 151–161.
- Wulfsohn, D., Adams, B.A., and Fredlund, D.G. 1994. Triaxial testing of unsaturated agricultural soils. American Society of Agricultural Engineers, International Summer Meeting, Kansas City, Missouri, June 19–22, Paper No. 94-1036.
- Xing, A., and Fredlund, D.G. 1994. Numerical modelling of a thermal conductivity matric suction sensor. *ASTM Geotechnical Testing Journal*, **17**(4): 415–424.

1995

- Barbour, S.L., Fredlund, D.G., Gan, J.K-M., and Wilson, G.W. 1995. Moisture movement in highway subgrade soils, prediction and measurement. Proceedings, Symposium on Unsaturated Soil Behavior and Applications, Nairobi, Kenya, August 22–23, pp. 21–40.
- Clifton, A.W., Misfeldt, G.A., and Fredlund, D.G. 1995. Experiences with two tills on clay shale. Proceedings, Tenth Panamerican Conference on Soil Mechanics and Foundation Engineering, Mexico, October 29 – November 3.
- Fredlund, D.G. 1995. Engineering Mission to Vietnam. *Geotechnical News*, Vancouver, **13**(2): 39–40.
- Fredlund, D.G. 1995. Unsaturated soil behaviour within generalized soil mechanics context. Proceedings, Symposium on Unsaturated Soil Behaviour and Applications, Nairobi, Kenya, August 22–23, pp. 1–20.
- Fredlund, D.G. 1995. The prediction of heave in expansive soils. Proceedings, Symposium on Unsaturated Soil Behaviour and Applications, Nairobi, Kenya, August 22–23, pp. 105–119.
- Fredlund, D.G. 1995. The prediction of unsaturated soil functions using the soil-water characteristic curve. Proceedings, Bengt Broms Symposium in Geotechnical Engineering, Singapore, December 13–16, pp. 113–133.
- Fredlund, D.G. 1995. The scope of unsaturated soils problems. Proceedings, Keynote Address, 1st International Conference on Unsaturated Soils, Paris, France, September 6–8, A.A. Balkema. *Edited by* E.E. Alonso and P. Delage, Vol. 3, pp. 1155–1177.
- Fredlund, D.G. 1995. The stability of slopes with negative pore-water pressures. The Ian Boyd Donald Symposium on Modern Developments in Geomechanics. *Edited by* C.M. Haberfield, Monash University, Department of Civil Engineering, Clayton, Victoria, Australia, pp. 99–116.
- Fredlund, D.G. 1995. Unsaturated soils behaviour within a generalized soil mechanics context. Proceedings, Canada–Kenya Symposium on Unsaturated Soil Behaviour and Applications, University of Nairobi, Nairobi, Kenya, August 22–23, pp. 1–20.
- Fredlund, D.G., and Lim, P.C. 1995. Discussions: Matrix suction and diffusive transport in centrifuge models, by R.J. Mitchell. *Canadian Geotechnical Journal*, **32**(1): 178–180.
- Fredlund, D.G., Gan, J.K-M., and Gallen, P. 1995. Suction measurements on compacted till specimens and an indirect filter paper calibration technique. *Transportation Research Record* **1481**: 3–9.
- Fredlund, D.G., Huang, S.K., Clifton, A.W., Wang, Q., Barbour, S.L., Ke, Z.J., and Fan, Q.Y. 1995. Matric suction and deformation monitoring at an expansive soil site in southern China. Proceedings, First International Conference on Unsaturated Soils, Paris, France, September 6–8, A.A. Balkema. *Edited by* E.E. Alonso and P. Delage, Vol. 2, pp. 855–862.
- Fredlund, D.G., Vanapalli, S.K., Xing, A., and Pufahl, D.E. 1995. Predicting the shear strength function for unsaturated soils using the soil-water characteristic curve. Proceedings, First In-

- ternational Conference on Unsaturated Soil, Paris, France, September 6–8, A.A. Balkema. *Edited by* E.E. Alonso and P. Delage, Vol. 1, pp. 63–70.
- Fredlund, D.G., Xing, A., and Gan, J.K.-M. 1995. Use of a Kelvin rheological model to simulate the consolidation of a saturated soil strata. Proceedings, Fifteenth Canadian Congress of Applied Mechanics CANCAM '95. May 28 – June 1. *Edited by* B. Jabarrok and S. Dost, University of Victoria, British Columbia, Canada, Vol. 2, pp. 592–593.
- Gan, J.K.-M., and Fredlund, D.G. 1995. Shear strength behavior of two saprolitic soils. proceedings, First International Conference on Unsaturated Soils, Paris, France, September 6–8, A.A. Balkema. *Edited by* E.E. Alonso and P. Delage, Vol. 1, pp. 71–76.
- Ho, D.Y.F., and Fredlund, D.G. 1995. Determination of the volume change moduli and respective inter-relationships for two unsaturated soils. Proceedings, First International Conference on Unsaturated Soils, Paris, France, September 6–8, A.A. Balkema. *Edited by* E.E. Alonso and P. Delage, Vol. 1, pp. 117–122.
- Huang, S.Y., Fredlund, D.G., and Barbour, S.L. 1995. Measurements of the coefficient of permeability of an unsaturated soil. Proceedings, First International Conference on Unsaturated Soils, Paris, France, September 6–8. A.A. Balkema. *Edited by* E.E. Alonso and P. Delage, Vol. 2, pp. 505–512.
- Lim, P.C., Barbour, S.L., and Fredlund, D.G. 1995. Effect of degree of saturation on the adsorption characteristics of inorganic chemical in unsaturated soils. Geoenvironment 2000, Specialty Conference sponsored by the Geotechnical and Environmental Divisions of American Society of Civil Engineers, New Orleans, Louisiana, February 24–26, pp. 815–828.
- Rahardjo H., and Fredlund, D.G. 1995. Procedures for slope stability analyses involving unsaturated soils. Proceedings, Developments in Deep Foundations and Ground Improvement Schemes. *Edited by* Balasubramaniam et al. Balkema, Rotterdam, pp. 33–56.
- Rahardjo, H., and Fredlund, D.G. 1995. Experimental verification of the theory of consolidation for unsaturated soils. *Canadian Geotechnical Journal*, **32**(5): 749–766.
- Rahardjo, H., and Fredlund, D.G. 1995. Pore pressure and volume change behavior during drained and undrained loadings of unsaturated soils. Proceedings, First International Conference on Unsaturated Soils, Paris, France, September 6–8, A.A. Balkema. *Edited by* E.E. Alonso and P. Delage, Vol. 1 pp. 177–182.
- Rahardjo, H., and Fredlund, D.G. 1995. Procedures for slope stability analyses involving unsaturated soils. Lecture Series on Slope Failures and Remedial Measures, Asian Institute of Technology, Bangkok, Thailand, June.
- Rahardjo, H., Lim, T.T., Chang, M.F., and Fredlund, D.G. 1995. Shear strength characteristics of a residual soil with suction. *Canadian Geotechnical Journal*, **32**: 60–77.
- Tratch, D.J., Wilson, G.W., and Fredlund, D.G. 1995. The prediction of moisture uptake in the root zone due to transpiration for problems in geotechnical engineering. Proceedings, Forty-eighth Canadian Geotechnical Conference, Vancouver, British Columbia, September 25–27, Vol. 2, pp. 771–780.
- Vanapalli, S.K., Pufahl, D.E., and Fredlund, D.G. 1995. A rational approach for the design of forest slopes. Proceedings, Forty-eighth Canadian Geotechnical Conference, Vancouver, British Columbia, September 25–27, Vol. 2, pp. 781–788.
- Wilson, G.W., Barbour, S.L., and Fredlund, D.G. 1995. The prediction of evaporative fluxes from unsaturated soil surfaces. Proceedings, First International Conference on Unsaturated Soils, Paris, France, September 6–8, A.A. Balkema. *Edited by* E.E. Alonso and P. Delage, Vol. 1, pp. 423–429.
- Wilson, G.W., Fredlund, D.G., and Barbour, S.L. 1995. A theoretical approach for evaluating evaporative fluxes from unsaturated soil behavior and applications. Proceedings, Symposium on Unsaturated Soil Behavior and Applications, Nairobi, Kenya, August 21–40, pp. 88–104.

1996

- Adams, B.A., Wulfsohn, D., and Fredlund, D.G. 1996. Air volume change measurement in unsaturated soil testing using a digital pressure-volume-controller. *ASTM Geotechnical Testing Journal*, **19**(1): 12–21.

- Barbour, S.L., Lim, P.C., and Fredlund, D.G. 1996. A new technique for diffusion testing of unsaturated soil. American Society for Testing and Materials, Geotechnical Testing Journal, **19**(3): 247–258.
- Fredlund, D.G. 1996. Geotechnical problems associated with swelling clays. In *Vertisol and Technologies for their Management, Developments in Soil Science 24*, Chapter 14, pp. 501–526. Edited by N. Ahmad and A.R. Mermut, Elsevier Science.
- Fredlund, D.G. 1996. Microcomputers and saturated/unsaturated continuum modelling in geotechnical engineering. Keynote Address, Proceedings, Symposium on Computers in Geotechnical Engineering, INFOGEO'96, Sao Paulo, Brazil, August 28–30. pp. 29–50.
- Fredlund, D.G. 1996. The emergence of unsaturated soil mechanics. Fourth Spencer J. Buchanan Lecture, College Station, Texas, November 8, Texas A&M Press. 39 p.
- Fredlund, D.G., Xing, A., Fredlund, M.D., and Barbour, S.L. 1996. The relationship of the unsaturated shear strength to the soil-water characteristic curve. Canadian Geotechnical Journal, **33**(3): 440–448.
- Fredlund, M.D., Sillers, W.S., Fredlund, D.G., and Wilson, G.W. 1996. Design of a knowledge-based system for unsaturated soil properties. Proceedings, Third Canadian Conference on Computing in Civil and Building Engineering, Montreal, Quebec, August 26–28, pp. 659–677.
- Gan, J.K-M., and Fredlund, D.G. 1996. Shear strength characteristics of two saprolitic soils. Canadian Geotechnical Journal, **33**(4): 595–609.
- Krahn, J., Fredlund, D.G., and Lam, L. 1996. The use of finite element computed pore-water pressure in a slope stability analysis. Proceedings, Seventh International Symposium on Landslides, Trondheim, Norway, June 17–21, Vol. 2, pp. 1277–1282.
- Lam, L., and Fredlund, D.G. 1996. Appropriate intercolumn force functions and lambda values for three-dimensional slope stability analyses. Proceedings, Seventh International Symposium on Landslides, Trondheim, Norway, June 17–21, Vol. 2, pp. 1283–1288.
- Lim, T.T., Rahardjo, H., Chang, M.F., and Fredlund, D.G. 1996. Effect of rainfall on matric suctions in a residual soil slope. Canadian Geotechnical Journal, **33**(4): 618–628.
- Oloo, S.Y., and Fredlund, D.G. 1996. A method for the determination of ϕ^b for statically compacted soils. Canadian Geotechnical Journal, **33**(2): 272–280.
- Rahardjo, H., and Fredlund, D.G. 1996. Consolidation apparatus for testing unsaturated soils. American Society for Testing and Materials, Geotechnical Testing Journal, **19**(4): 341–353.
- Skibinsky, D., and Fredlund, D.G. 1996. A centrifuge method to obtain the soil-water characteristic curve. Proceedings, Forty-ninth Canadian Geotechnical Conference, St. John's, Newfoundland, September 23–25, Vol. 2, pp. 753–760.
- Stoicescu, J.T., Haug, M.D., and Fredlund, D.G. 1996. The soil-water characteristics and unsaturated hydraulic conductivity of various sand-bentonite mixtures. Proceedings, Forty-ninth Canadian Geotechnical Conference, St. John's, Newfoundland, September 23–25, Vol. 2, pp. 721–728.
- Vanapalli, S., Fredlund, D.G., and Barbour, S.L. 1996. A rationale for an extended soil-water characteristic curve. Proceedings, Forty-ninth Canadian Geotechnical Conference, St. John's, Newfoundland, September 23–25, Vol. 1, pp. 457–464.
- Vanapalli, S.K., Fredlund, D.G., and Pufahl, D.E. 1996. The relationship between the soil-water characteristic curve and the unsaturated shear strength of a compacted glacial till. American Society for Testing and Materials, Geotechnical Testing Journal, **19**(2): 259–268.
- Vanapalli, S.K., Fredlund, D.G., Pufahl, D.E., and Clifton, A.W. 1996. Model for the prediction of shear strength with respect to soil suction. Canadian Geotechnical Journal, **33**(3): 379–392.
- Wulfsohn, D., Adams, B.A., and Fredlund, D.G. 1996. Application of unsaturated soil mechanics for agricultural conditions. Canadian Agricultural Engineering, **38**(3): 173–181.

1997

- Fredlund, D. G. 1997. An introduction to unsaturated soil mechanics. American Society of Civil Engineers, Geotechnical Engineering Division, GeoLogan Conference, Special Geotechnical

- Publication No. 86 entitled *Unsaturated Soils Engineering Practice*, Logan, Utah, July 16–19, pp. 1–37.
- Fredlund, D.G. 1997. Inauguration of the Vietnamese Geotechnical Journal. Letter to the Editor, First Issue of the Vietnamese Geotechnical Journal, April, pp. 11–12.
- Fredlund, D.G. 1997. From theory to the practice of unsaturated soil mechanics. Invited Lecture, Proceedings, Third Brazilian Symposium on Unsaturated Soils, NSAT'97, Rio de Janeiro, Brazil, April 21–25, Vol. 2.
- Fredlund, D.G., and Xing, A. 1997. The use of a rheological model for the visualization of processes in unsaturated soils. Proceedings, Sixth National Congress on Mechanics, Hanoi, Vietnam, December 3–5. pp. 221–227.
- Fredlund, D.G., Gan, J.K-M., Guan, Y., and Richardson, N. 1997. Suction measurement on a Saskatchewan soil using a direct measurement, high suction sensor. *Transportation Research Record* **1596**: 84–92.
- Fredlund, M.D., Fredlund, D.G., and Wilson, G.W. 1997. Estimation of unsaturated soil properties using a knowledge-based system. Proceedings, Fourth Congress on Computing in Civil Engineering, ASCE, Philadelphia, Pennsylvania., June 16–18. pp. 501–510.
- Fredlund, M.D., Wilson, G.W., and Fredlund, D.G. 1997. Prediction of soil-water characteristic curve from grain-size distribution. Proceedings, Third Brazilian Symposium on Unsaturated Soils, NSAT'97, Rio de Janeiro, Brazil, April 21–25, Vol. 1, pp. 13–24.
- Fredlund, M.D., Wilson, G.W., and Fredlund, D.G. 1997. Indirect procedures to determine unsaturated soil property functions. Proceedings, Fiftieth Canadian Geotechnical Conference, Golden Jubilee, Ottawa, Canada, October 20–22, pp. 407–414.
- Guan, Y., and Fredlund, D.G. 1997. Direct measurement of high soil suction. Proceedings, Third Brazilian Symposium on Unsaturated Soils, NSAT'97, Rio de Janeiro, Brazil, April 21–25, Vol. 2.
- Guan, Y., and Fredlund, D.G. 1997. Use of the tensile strength of water for the direct measurement of high soil suction. *Canadian Geotechnical Journal*, **34**(4): 604–614.
- Huang, S., Fredlund, D.G., and Barbour, S.L. 1997. Measurement of the coefficient of permeability for a deformable unsaturated soil using a triaxial permeameter. *Canadian Geotechnical Journal*, **35**(3): 426–432.
- Huang, S., Barbour, S.L., and Fredlund, D.G. 1997. Development and verification of a coefficient of permeability function for a deformable unsaturated soil. *Canadian Geotechnical Journal*, **35**(3): 411–425.
- Newman, L.L., Barbour, S.L., and Fredlund, D.G., 1997. Mechanisms for preferential flow in vertically layered, unsaturated waste rock. Proceedings, Fiftieth Canadian Geotechnical Conference, Golden Jubilee, Ottawa, Canada, October 20–22, Vol. 1, pp. 201–208.
- Newman, L.L., Herasymuk, G.M., Wilson, G.W., Fredlund, D.G., and Smith, T. 1997. Hydrogeologic characterization and the mechanisms for preferential flow in waste rock dumps. Proceedings, International Conference on Acid Rock Drainage, Vancouver, British Columbia, May 31 – June 6, Vol. 2, pp. 551–565.
- Oloo, S.Y., Fredlund, D.G., and Gan, J.K-M. 1997. Bearing capacity of unpaved roads. *Canadian Geotechnical Journal*, **34**(3): 398–407.
- Oloo, S.Y., Fredlund, D.G., and Gan, J.K-M. 1997. Shear strength design of thin pavements and unbound roads. Proceedings, International Symposium on Thin Pavements, Surface Treatments, Unbound Roads, University of New Brunswick, Fredericton, New Brunswick, June 24–25, pp. 135–142.
- Pereira, J.H.F., and Fredlund, D.G. 1997. Constitutive modeling of a metastable-structured compacted soil. Proceedings, Conference on Recent Developments in Soil Mechanics, Rio de Janeiro, Brazil, June 25–27, pp. 317–326.
- Pereira, J.H.F., and Fredlund, D.G. 1997. Numerical analyses of the post-filling performance of small collapsing dams. Proceedings, Third Brazilian Symposium on Unsaturated Soils, Rio de Janeiro, Brazil, April 21–25.

- Shuai, F., and Fredlund, D.G. 1997. Measured and simulated behavior of an expansive soil. Proceedings, 3rd Brazilian Symposium on Unsaturated Soils, NSAT'97, Rio de Janeiro, Brazil, April 21–25, Vol. 1, pp. 253–260.
- Tang, X.G., Graham, J., and Fredlund, D.G. 1997. Effect of osmotic suction on strength of unsaturated highly plastic clays. Proceedings, Fiftieth Canadian Geotechnical Conference, Golden Jubilee, Ottawa, Canada, October 20–22, pp. 641–648.
- Vanapalli, S.K., and Fredlund, D.G. 1997. Interpretation of undrained shear strength of unsaturated soils in terms of stress state variables. Proceedings, Third Brazilian Symposium on Unsaturated Soils, NSAT'97, Rio de Janeiro, Brazil, April 21–25, Vol. 1, pp. 35–46.
- Vanapalli, S.K., Fredlund, D.G., and Pufahl, D.E. 1997. Comparison of saturated-unsaturated shear strength and hydraulic conductivity behavior of a compacted sandy clay till. Proceedings, Fiftieth Canadian Geotechnical Conference, Golden Jubilee, Ottawa, Canada, October 20–22, 1997, pp. 625–632.
- Wilson, G.W., Fredlund, D.G. and Barbour, S.L., 1997. The effect of soil suction on evaporative fluxes from soil surfaces. *Canadian Geotechnical Journal*, **34**(4): 145–155.
- Wilson, G.W., Fredlund, D.G., Barbour, S.L. and Pufahl, D.E. 1997. The use of ground surface moisture flux boundary conditions in geotechnical engineering, Proceedings, Fourteenth International Conference on Soil Mechanics and Foundation Engineering, ISSMFE, Hamburg, Germany, September 6–12, Vol. 3, pp. 1861–1864.

1998

- Chen, T.H., Fredlund, D.G., Gan, J.K-M, and Zhou, H.Q. 1998. Non-linear model for unsaturated soils. Proceedings, Second International Conference on Unsaturated Soils, UNSAT2, Beijing, China, August 27–30, Vol. 1, pp. 461–466.
- Cook, D., and Fredlund, D.G. 1998. TDR matric suction measurements. Proceedings, Second International Conference on Unsaturated Soils, UNSAT2, Beijing, China, August 27–30, Vol. 1, pp. 338–343.
- Feng, M., Gan, J.K-M., and Fredlund, D.G. 1998. A study of swelling pressure from consolidometer tests using various loading paths. Proceedings, Second International Conference on Unsaturated Soils, UNSAT2, Beijing, China, August 27–30, Vol. 1, pp. 350–355.
- Fredlund, D.G. 1998. Bringing unsaturated soil mechanics into engineering practice. Invited Keynote lecture. Proceedings, Second International Conference on Unsaturated Soils, UNSAT2, Beijing, China, August 27–30, Vol. 2.
- Fredlund, D.G. 1998. Computer modelling for unsaturated soil mechanics problems. Invited Lecture to the Eleventh Danube-European Conference on Soil Mechanics and Foundation Engineering, Porec, Croatia, May 25–29.
- Fredlund, M.D., Fredlund, D.G., and Wilson, G.W. 1998. Application of knowledge-based systems in estimating unsaturated soil property functions for numerical modelling. Proceedings, Second International Conference on Unsaturated Soils, UNSAT2, Beijing, China, August 27–30, Vol. 1, pp. 479–484.
- Guan, Y., Fredlund, D.G., and Gan J.K-M. 1998. Behavior of water subjected to high tensile stress. Proceedings, Second International Conference on Unsaturated Soils, UNSAT2, Beijing, China, August 27–30, Vol. 1, pp. 356–361.
- Ho, D.Y.F., and Fredlund, D.G. 1998. Shrinkage measurements for two unsaturated soils. Proceedings, Second International Conference on Unsaturated Soils, UNSAT2, Beijing, China, August 27–30, Vol. 2.
- Kasim, F., Fredlund, D.G., and Gan, J.K-M. 1998. The effect of steady state rainfall on the matric suction conditions in a slope. Proceedings, Second International Conference on Unsaturated Soils, UNSAT2, Beijing, China, August 27–30, Vol. 1, pp. 78–83.
- Kasim, F., Fredlund, D.G., and Gan, J.K-M. 1998. The effect of steady state rainfall on the matric suction conditions in soil. *In Slope engineering in Hong-Kong. Edited by K.S. Li, J.N. Kay and K.K.S. Ho, Balkema, Rotterdam, pp. 75–85.*
- Lim, P.C., Barbour, S.L., and Fredlund, D.G. 1998. The influence of the degree of saturation on the coefficient of aqueous diffusion. *Canadian Geotechnical Journal*, **35**(5): 811–827.

- Newman, L.L., Barbour, S.L., and Fredlund, D.G. 1998. Preferential flow in vertically layered, unsaturated systems. Proceedings, Second International Conference on Unsaturated Soils, UNSAT2, Beijing, China, August 27–30, Vol. 1, pp. 586–589.
- Shuai, F., and Fredlund, D.G. 1998. A model for the simulation of swelling pressure measurements in expansive soils. *Canadian Geotechnical Journal*, **35**(1): 96–114.
- Shuai, F., and Fredlund, D.G. 1998. Theoretical model for the simulation of the swelling process. Proceedings, Second International Conference on Unsaturated Soils, UNSAT2, Beijing, China, August 27–30, Vol. 1, pp. 509–514.
- Stoicescu, J.T., Haug, M.D., and Fredlund, D.G. 1998. The soil-water characteristic curves of sand-bentonite mixtures used for liners and covers. Proceedings, Second International Conference on Unsaturated Soils, UNSAT2, Beijing, China, August 27–30, Vol. 1, pp. 143–148.
- Stoicescu, J.T., Haug, M.D., and Fredlund, D.G. 1998. Laboratory techniques used to measure the soil-water characteristic curves for soil liners and covers. Proceedings, Fifty-first Canadian Geotechnical Conference, Edmonton, Alberta, October 4–7.
- Vanapalli, S.K., and Fredlund, D.G. 1998. Influence of compaction conditions on the unsaturated shear strength behavior of a sandy clay till. Proceedings, Second International Conference on Unsaturated Soils, UNSAT2, Beijing, China, August 27–30, Vol. 1, pp. 161–166.
- Vanapalli, S.K., Pufahl, D.E. and Fredlund, D.G. 1998. The effect of stress state on the soil-water characteristic behavior of a compacted sandy clay till. Proceedings, Fifty-first Canadian Geotechnical Conference, Edmonton, Alberta, October 4–7. pp. 87–94.
- Wang, Q., Huang, S., Ke, Z., Fan, Q., Chen, Z., and Fredlund, D.G. 1998. Long term field monitoring of climatic impact on matric suction and ground movement in Nanning, China. Proceedings, Second International Conference on Unsaturated Soils, UNSAT2, Beijing, China, August 27–30, Vol. 1, pp. 444–449.
- Wulfsohn, D., Adams, B.A., and Fredlund, D.G. 1998. Triaxial testing of unsaturated agriculture soils. *Journal of Agriculture Engineering Research*, **69**: 317–330.

1999

- Lim, P.C., Barbour, S.L., and Fredlund, D.G. 1999. Characterization and prediction of the coefficient of diffusion for unsaturated soils. *Canadian Geotechnical Journal*.
- Zakerzadeh, N., Pufahl, D.E., and Fredlund, D.G. 1999. Lateral earth force calculations using general limit equilibrium. Proceedings, Eleventh Pan American Conference on Soil Mechanics and Geotechnical Engineering, Iguazu Falls, Brazil, August 8–12.

In progress (April 1999)

- Feng, M., and Fredlund D.G. 1999. The effects of capillary hysteresis on the suction measurement using thermal conductivity sensors. Proceedings, 52th Canadian Geotechnical Conference, Regina, Saskatchewan, October 24–27.
- Fredlund, D.G., 1999. The implementation of unsaturated soil mechanics into geotechnical engineering. R.M. Hardy Address, 52th Canadian Geotechnical Conference, Regina, Saskatchewan, October 24–27.
- Fredlund, D.G., Scoular, R.E.G., and Zakerzadeh, N. 1999. Using a finite element stress analysis to compute the factor of safety. Proceedings, 52th Canadian Geotechnical Conference, Regina, Saskatchewan, October 24–27.
- Fredlund, D.G. Pentland, J., and Fredlund, M.D. 1999. Use of a knowledge-based system in the design, construction and management of pipelines. Proceedings, 18th International Offshore Mechanics & Arctic Engineering Conference (OMAE 99), St. John's, Newfoundland, Canada, July 11–16.
- Fredlund, D.G, and Scoulr, R.E.G. 1999. Using limit equilibrium concepts in finite element slope stability analysis. Invited Keynote paper, Proceedings, International Symposium on Slope Stability Engineering- IS- Shikoku'99, Matsuyama, Shikoku, Japan, November 8–11.
- Kodikara, J., Barbour, S.L., and Fredlund, D.G. 1999. Changes in clay structure and behaviour due to wetting and drying. Proceedings, 8th Australian-New Zealand Conference in Geomechanics, Hobart, February 15–17.

- Khanzode, R.M., Fredlund, D.G., and Vanapalli, S.K. 1999. An alternative method for the measurement of soil-water characteristic curves for fine-grained soils. Proceedings, 52th Canadian Geotechnical Conference, Regina, Saskatchewan, October 24–27.
- Nishimura, T., and Fredlund, D.G. 1999. Unconfined shear strength of a compacted unsaturated silty soil applied high total suctions. Proceedings, International Symposium on Slope Stability Engineering- IS- Shikoku'99, Matsuyama, Shikoku, Japan, November 8–11.
- Nishimura, T., Fredlund, D.G., Gan, J.K-M., and Hirabayashi, Y. 1999. Total stress ratio and shear strength parameters for an unsaturated compacted soil. Proceedings, 11th Asian Regional Conference, Seoul, Korea, August 16–20.
- Pereira, J.H.F., and Fredlund, D.G. 1999. Numerical analysis of the post-filling performance of small collapsing dams. Proceedings, Eleventh Pan American Conference on Soil Mechanics and Geotechnical Engineering, Iguazu Falls, Brazil, August 8–12.
- Pereira, J.H.F., and Fredlund, D.G. 1999. Shear strength behavior of a residual soil of Gneiss compacted at metastable-structured conditions. Proceedings, Eleventh Pan American Conference on Soil Mechanics and Geotechnical Engineering, Iguazu Falls, Brazil, August 8–12.
- Thu, T.M., and Fredlund, D.G. 1999. Modelling subsidence in the Hanoi city area, Vietnam. Canadian Geotechnical Journal, **36** (In press).
- Thu, T.M., and Fredlund, D.G. 1999. Subsidence in the city of Hanoi, Vietnam. Proceedings, Canadian Society of Civil Engineers Annual Conference, Regina, Saskatchewan, Canada, June 2 01505.
- Vanapalli, S.K., and Fredlund D.G., 1999. Empirical procedures to predict the shear strength of unsaturated soils. Proceedings, 11th Asian Regional Conference, Seoul, Korea, August 16–20.
- Vanapalli, S.K., Fredlund, D.G., and Pufahl, D.E 1999. Relationship between soil water characteristic curves and the as compacted water content versus soil suction for a glacial till. Proceedings, Eleventh Pan American Conference on Soil Mechanics and Geotechnical Engineering, Iguazu Falls, Brazil, August 8–12.
- Vanapalli, S.K., Fredlund, D.G., and Pufahl, D.E 1999. The influence of soil structure and stress state on the soil-water characteristic curve behavior of a statically compacted glacial till. Geotechnique, (In press).
- Vanapalli, S.K., Pufahl, D.E., and Fredlund, D.G. 1999. Interpretation of the shear strength of unsaturated soils in undrained loading conditions. Proceedings, 52th Canadian Geotechnical Conference, Regina, Saskatchewan, October 24–27.
- Zakerzadeh, N., Fredlund, D.G., and Pufahl, D.E. 1999. Interslice force functions for computing active and passive earth force. Canadian Geotechnical Journal, **36** (In press).

Part X

Theses Supervised

In progress

- Khanzode, Ravindra. "An Alternative Centrifuge Method to obtain the Soil-Water Characteristic Curve," M.Sc. (in progress).
- Nguyen, Thieu Thi Minh. "Use of Unsaturated Soil Property Functions in Seepage Modelling," M.Sc. (in progress).
- Pessarar, A. "Effects of Wet-Dry Cycles on the Soil-Water Characteristic Curve of Clay Soils," Ph.D. (in progress).
- Reinson, Jeff. "The Permeability Function for Coars-grained Soils," M.Sc. (in progress).
- Vu Quang Hung. "A Numerical Model for Two-Dimensional Heave Analysis," M.Sc. (in progress).
- Wang, Qing. "A Laboratory Study of Elasto-plastic Models for Unsaturated Soils," M.Sc. (in progress).
- Wog, Karyn, M. "Numerical Simulation of *In Situ* Unsaturated Permeability Tests," M.Sc. (in progress).

1999

- Feng, Man. "Study of Hysteresis Associated with Thermal Conductivity Matric Suction Sensor," M.Sc., 1999.
- Newman, Lori. "Preferential Flow in Unsaturated Vertical Layered Systems," M.Sc., 1999.

1998

- Thu, Trinh Minh. "Subsidence Due to Pumping Groundwater in the City of Hanoi, Vietnam," M.Sc., 1998.
- Scoular, Edward. "Limit equilibrium Slope Stability Analysis Using a Stress Analysis," M.Sc., 1998.
- Zakerzadeh, Noshin. "Combining Stress Analysis and Limit Equilibrium for Lateral Earth Pressure Problems," M.Sc., 1998.

1997

- Sillers, Warren Scott. "The Mathematical Representation of the Soil-Water Characteristic Curve," M.Sc., 1997.
- Deutscher, Michael Stanley. "The Development of a New Air Permeability Testing Apparatus," M.Sc., 1997.
- Stoicescu, Jeffrey Todd. "Properties of Unsaturated Soil-Bentonite Mixtures Used for Liners and Covers," M.Sc., 1997.

1996

- Cook, David Lyle. "Development of a TDR Matric Suction Sensor," M.Sc., 1996.
- Guan, Yun. "The Measurement of Soil Suction," Ph.D., 1996.
- Pereira, Jose Henrique Feitosa. "Numerical Analysis of the Mechanical Behavior of Collapsing Earth Dams During First Reservoir Filling," Ph.D., 1996.
- Shuai, Fangsheng. "Simulation of Swelling Pressure Measurements on Expansive Soils," Ph.D., 1996.
- Skibinsky, Darren Nicholas. "A Centrifuge Method to Obtain the Soil-Water Characteristic Curve," M.Sc., 1996.

1995

- Tratch, David Jonathan. "A Geotechnical Engineering Approach to Plant Transpiration and Root Water Uptake," M.Sc., 1995.
- Lim, Puai Choo. "Characterization and Prediction of the Functional for the Coefficients of Diffusion and Adsorption for Inorganic Chemicals in Unsaturated Soils," Ph.D., 1995.

1994

- Vanapalli, Sai Krishna. "Simple Test Procedures and their Interpretation in Evaluating the Shear Strength of an Unsaturated Soil," Ph.D., 1994.
- Oloo, Simon Youno. "A Bearing Capacity Approach to the Design of Low-Volume Traffic Roads," Ph.D., 1994.
- Huang, Shangyan. "Evaluation and Laboratory Measurement of the Coefficient of Permeability in Deformable, Unsaturated Soils," Ph.D., 1994.

1993

Meidl, Dan. "Hydraulic Conductivity of Railway Ballast," M.Eng., 1993

1992

Dai, Yang. "Applying Probabilistic Theory to a Deterministic Solution in Slope Stability Analysis," 1992.

1991

Lam, Leonard Wai-Leung. "Generalized Three-dimensional Slope Stability Analysis Using Method of Columns," Ph.D., 1991.

Szafron, Brent Joseph. "The Measurement of Soil Suctions and its Influence on the Bearing Capacity of Subgrades," M.Sc., 1991.

McClarty, Darrell Vaughan Basil. "A Comparison of Estimation Methods for Predicting Quantity and Quality of Aggregate Reserves," M.Sc., 1991.

Mandziak, Terry. "Development of a Matric Suction Sensor," M.Sc., 1991.

1990

Tadepalli, Rambabu. "The Study of Collapse Behavior of Soils during Inundation," M.Sc., 1990.

Wilson, G. Ward. "Soil Evaporative Fluxes for Geotechnical Engineering Problems," Ph.D., 1990.

Rahardjo, Harianto. "The Study of Undrained and Drained Behavior of Unsaturated Soils," Ph.D., 1990.

1989

Sattler, Pamela J. "Numerical Modelling of Vertical Ground Movements," M.Sc., 1989.

1988

Ho, David Yip-Fei. "The Relationship Between the Volumetric Deformation Moduli of Unsaturated Soils," Ph.D. 1988.

Ng, Tony Nam-Sang. "The Effect of Negative Pore-Water Pressures on Slope Stability Analysis," M.Sc., 1988.

Sweeney, Douglas Alan. "The Effect of Lime on the Properties of Regina Clay," M.Sc., 1988.

van der Raadt, Paul. "Field Measurement Soil Suction using Thermal Conductivity Matric Potential Sensors," M.Sc., 1988.

1987

Lau, Jacky Tak Kwai. "Desiccation Cracking of Soils," M.Sc., 1987.

1986

Gan, Julian Koo-Ming. "Direct Shear Strength Testing of Unsaturated Soils," M.Sc., 1986.

Barbour, Sidney Lee. "Osmotic Flow and Volume Change in Clay Soils," Ph.D., 1986.

1985

Wong, Daniel Kam Hong. "A Study of Brine Flow Through Saturated/Unsaturated Potash Tailings," M.Sc., 1985.

Poon, Andy W.K. "Design of Anchor Systems Using Limit Equilibrium Methods," M.Sc., 1985.

Gallén, Peter M. "The Measurement of Soil Suction Using the Filter Paper Method," M.Sc., 1985.

1983

Lam, Leonard Wai-Leung. "Saturated-Unsaturated Transient Finite Element Seepage Model," M.Sc., 1983.

Fan, Kenneth K. "Evaluation of the Interslice Side Forces for Lateral Earth Force and Slope Stability Problems," M.Sc., 1983.

Lee, Rudy, K.C. "Measurement of Soil Suction Using the MCS 6000 Sensor," M.Sc., 1983.

1982

- Rahardjo, Harianto. "Lateral Earth Force Calculations Using Limit Equilibrium," M.Sc., 1982.
Papagiannakis, A. Thomas. "A Steady State Model for Flow in Saturated-Unsaturated Soils," M.Sc., 1982.
Wilson, G. Ward. "The Evaluation of the Interslice Side Forces for Slope Stability Analysis by the Finite Element Method," M.Sc., 1982.

1981

- Ching, Raymond. "A Theoretical Examination and Practical Applications of the Limit Equilibrium Methods to Slope Stability Problems," M.Sc., 1981.
Ho, David Yip-Fei. "The Shear Strength of Unsaturated Hong Kong Soils," M.Sc., 1981.

1980

- Filson, Harvey Leroy. "A Study of Heave Analysis Using the Oedometer Test," M.Sc., 1980.
Morrison, John Alan. "Psychrometric Measurements on Unsaturated Soils during Repetitive Loading," M.Sc., 1980.

1977

- Naderi, Farhad. "Examination of the "SLOPE" Computer Program", M.Sc., 1977.
Hasan, Jamshed. "Transient Flow Processes in Unsaturated Soils," M.Sc., 1977.
Bocking, Kenneth Arthur. "Methods of Measurement of Negative Pore-Water Pressures," M.Sc., 1977.

1976

- Widger, Robert Allan. "Slope Stability in Unsaturated Soils," M.Sc., 1976.

1975

- Wong, Peter K. "Resilient Modulus Constitutive Relationships for Cohesive Subgrade Soils," M.Sc., 1975.

1974

- Kent, David Douglas. "State Variables for a Partly Frozen Soil," M.Sc., 1974.

1970

- Pufahl, Dennis Edward. "Evaluation of Effective Stress Components in Non-Saturated Soils," M.Sc., 1970.
Krahn, Johny. "Comparison of Soil Pore Water Potential Components," M.Sc., 1970.
Tao, Shannon Sai-Ling. "Soil Testing Data Reduction," M.Sc., 1970.
Lidgren, Ray Alan. "Volume Change Characteristics of Compacted Till," M.Sc., 1970.

1969

- Lu, Yi-Ming. "Swell Properties of Desiccated Regina Clay," M.Sc., 1969.
Wiesner, William Raymond. "Residual Shear Strength of Over-Consolidated Clay Shales," M.Sc., 1969.

Index

air

diffused, 16, 237–238, 246–247, 460, 465, 519
 free, 237–238, 347–348, 353, 355, 452
 air volume change, 449, 460, 473, 528
 coefficient of, 449
 air-water interphase, 33
 analysis
 stability, 122, 129–130, 133, 135, 168–169, 175, 300, 313, 316, 318–322, 324–326, 329, 331, 333, 335–336, 340, 352–353, 358, 411
 transient, 169
 apparatus
 modified direct shear, 219, 247, 269–270, 286, 293–294, 322–323
 modified triaxial, 17, 219
 axis-translation, 15, 31, 36, 79–83, 115, 123, 130, 139, 231, 238, 244–245, 273, 300, 304, 314, 323, 385, 452, 458, 473, 499, 501, 534, 593, 641
 boundary, flux, 141, 145, 154, 175, 209, 289, 321, 326, 334, 375, 435, 471, 500, 609, 613, 653–654, 657, 681
 capacity, bearing, 108, 122–123, 155, 286, 333–334, 373–382, 654
 capillary, 32, 47–48, 73, 92, 121, 142, 145, 181–182, 184, 208, 237, 334, 385, 399–400, 428, 542, 627
 cavitation, 48, 53, 74, 79, 85–86, 96, 115, 244, 431, 452, 473, 576–577
 centrifuge, 499
 change
 air volume, 449, 460, 473, 528
 overall volume, 16, 22, 32, 108, 287, 345, 437, 512, 527, 689, 695
 soil structure volume, 453, 516, 518, 523–525
 volume, 9, 14–22, 30, 32–33, 35, 42, 45, 49, 60, 70, 78, 96, 107–108, 111, 113–114, 121, 123, 125, 127, 129, 133, 135–136, 140–143, 148, 152, 154–155, 157, 164, 166, 169–170, 174, 181, 193–195, 207–209, 223, 238–239, 246–247, 250, 273, 277, 279, 287, 344–346, 348, 353–356, 371, 385, 389, 392–393, 413–414, 422, 436–438, 441, 449–450, 452–454, 456–458, 460–462, 464–466, 468–471, 473–483, 485–497, 511–513, 515–521, 523–536, 539–542, 544, 550, 559, 562, 567–568, 570, 575, 577, 582, 590–592, 595, 598, 600, 602–603, 608, 611–615, 617, 620–621, 623, 625–629, 632–637, 653, 660–661, 664, 681–682, 687, 689, 695
 characteristic curve, soil-water, 10, 99, 108, 140, 149–153, 156, 158, 160–164, 166–167, 169–174, 177–178, 181–191, 202–204, 206–209, 211–214, 219–220, 255–257, 263, 265–266, 269, 277–298, 333, 338–340, 342, 385, 389–395, 397, 412, 414, 416, 420, 427, 473, 480, 512–513, 532, 534–535, 543–544, 623, 664, 672–674, 676, 679, 682, 684
 climate, 27, 145, 175, 193–194, 321, 326, 375, 386, 592–593, 602, 611, 658, 672, 674, 687
 coefficient, adsorption, 498–500, 504–508
 coefficient of air volume change, 449
 coefficient of compressibility, 107, 117, 119, 129, 136–137, 348, 511, 612
 coefficient of consolidation, 137, 197–198, 239, 438–439, 451, 458, 469, 471, 478, 483, 626, 628, 633–634, 636, 664, 690–691
 coefficient of diffusion, 209, 489, 494–496, 498–500

coefficient of earth pressure at rest, 121
 coefficient of permeability, 107–108, 127–128, 133–134, 137, 141, 144–146, 149, 151, 166–170, 181, 244, 269, 277, 291, 294, 321, 323, 326–327, 333–335, 339, 349, 385–386, 389–402, 406, 409, 411–412, 414–417, 427, 437, 449, 451, 453, 455, 464, 470–473, 480, 483, 489, 496, 511, 540, 543–544, 546–547, 612–616, 622, 625, 653, 682, 689–690
 coefficient of solubility, volumetric, 273, 470
 coefficient of volume change, 107, 355–356, 385, 414, 422, 470, 480, 488–489, 621, 637
 coefficient of water content change, 129, 137, 512, 530
 coefficient
 pore pressure, 344, 441
 water content, 119
 compressibility, 29, 43, 45, 107, 117, 119, 123, 129, 135–138, 142, 144, 197, 344–345, 347–351, 436–437, 440, 445–446, 448, 450–451, 469–470, 475, 485–488, 490, 493–494, 496, 511, 517–519, 521, 524, 527–529, 541–542, 544–545, 552–553, 555, 563, 567, 569–571, 573–579, 581, 583, 599–600, 612, 688, 691–692
 coefficient of, 107, 117, 119, 129, 136–137, 348, 511, 612
 isothermal, 437
 compression
 confined, 333
 unconfined, 333
 compression index, 294, 528, 532
 computer, 5, 141, 166, 168, 174–176, 178, 181, 202, 208–209, 211, 215, 324–327, 334, 348, 352, 369, 396, 399, 401, 409, 411, 414–415, 505, 546–547, 613–614, 623, 629, 633, 661, 681, 691
 condition, surface boundary, 618
 conductivity, thermal, 10, 48–50, 53–62, 65–66, 68, 70, 72–73, 75–83, 85–86, 96–97, 102, 139, 207, 209–210, 326, 629, 661, 664, 683, 691–692
 consolidation, 3, 16, 108, 113, 118–119, 123, 127, 129, 133, 137, 193–201, 213, 239, 247, 250, 259, 261–262, 265, 270, 272–274, 294, 305, 344, 352, 368, 413, 436–444, 446–453, 455–466, 468–483, 485–486, 489–496, 503, 516, 528–529, 532–533, 535–536, 541, 543–544, 546, 548, 554–555, 560–563, 568, 570–573, 575, 577, 579–580, 582–583, 590, 595, 603, 620, 626–628, 633–636, 664, 687–694
 coefficient of, 137, 197–198, 239, 438–439, 451, 458, 469, 471, 478, 483, 626, 628, 633–634, 636, 664, 690–691
 one-dimensional 3, 108, 118, 193–201, 294, 352, 413, 436, 438, 442, 452, 469, 560, 620, 628, 687–688
 constitutive surface
 void ratio, 149, 513, 529, 531–532, 593–594
 water content, 119, 138, 149, 512–513, 529, 531
 continuity requirement, 114, 136, 345, 436–438, 440, 450–451, 453, 515, 541, 550, 622
 continuum mechanics, 9, 13–14, 22, 27–32, 42–43, 112, 114, 127, 286, 445, 487, 496, 540, 688
 multiphase, 32, 42, 112, 127, 445
 crack, tension, 81, 360–361, 365–366, 369–372
 cracking, depth of, 155
 curve fitting, 181, 187, 202, 214, 394
 curve, soil-water characteristic, 10, 99, 108, 140, 149–153, 156, 158, 160–164, 166–167, 169–174, 177–178, 181–191, 202–204, 206–209, 211–214, 219–220, 255–257, 263, 265–266, 269, 277–298, 333, 338–340, 342, 385,

- 389–395, 397, 412, 414, 416, 420, 427, 473, 480, 512–513, 532, 534–535, 543–544, 623, 664, 672–674, 676, 679, 682, 684
- dam, earthfill, 13, 154, 169–170, 352, 356, 396, 416–417, 528, 626, 628, 688
- database, 108, 173–175, 178, 202–203, 206–209, 211, 213, 215, 220, 609, 618
- deformation, volumetric, 111, 346, 515, 530, 541
- degree of saturation, residual, 291–292, 338–340, 498, 507–508
- depth, active, 582, 584–589
- desaturation, 113, 150, 157, 170, 181, 183, 207–208, 234–235, 256–257, 287–288, 290, 294, 296, 339–340, 461, 516, 560, 592, 670
- desiccation, 68
- difference, finite, 375–376, 400, 411, 415, 436, 439–440, 443, 471, 661, 665, 687, 689, 691, 695
- diffusion, 16–17, 48, 141–142, 207, 209, 215, 437, 460, 469, 473, 489–491, 494–496, 498–507, 520, 658, 660–661, 664–667, 671, 681–682
- coefficient of, 209, 489, 494–496, 498–500
- diffusivity, 54, 72–74, 77, 207, 658, 660, 687, 690–691
- direct shear, 160, 170, 219, 231–232, 244–251, 253, 255–256, 258–263, 265, 267, 269–275, 280, 286, 293–295, 302, 322–325, 337–338, 340, 375
- disk, high air entry, 16, 219, 231, 237, 244–247, 270, 300, 302, 323, 471, 473, 519, 534
- distribution
- grain size, 71, 97, 108, 166, 170–171, 173–174, 176–179, 220, 234, 265, 302, 603
 - particle size, 176, 178, 202
 - pore size, 55, 170, 176, 178, 181–186, 189, 203–204, 208, 289, 389–390
- disturbance, 123, 164, 194, 242, 258, 263–264, 268, 309, 460, 550, 553–556, 561–563, 569, 582–583, 585, 589, 595, 598–599, 602, 620, 630
- sampling, 550, 554–556, 561–563, 582–583, 585, 589, 595, 602, 620
- earth pressure, 79, 111, 113–114, 121–123, 125, 155, 237, 360–361, 365–368, 370, 376
- active, 121, 365
 - lateral, 79, 361, 365, 370, 376
 - passive, 121, 123, 363, 368, 370
- elasticity form, 116, 121, 135–136, 551
- element, finite 168, 209, 213, 215, 326–327, 336, 376, 380, 386, 399–401, 409, 411–412, 414–416, 420, 422, 504, 543, 546–547, 623, 681
- equation
- continuity, 469, 543, 620–621, 625, 689
 - equilibrium, 13–14, 22–25, 29, 32–33, 43–44, 313, 436, 469, 620–621, 623, 625
 - partial differential, 135, 137, 175, 385, 412–413, 422, 436, 438–443, 451, 456, 469–470, 628, 633, 681, 687–691, 695–696
- equations, coupled 546
- equilibrium
- limit, 121–122, 125, 168, 313, 320, 324, 326–327, 331, 335, 353, 376, 378, 381
 - plastic, 121, 361, 370
- evaporation, 27, 63, 66, 80–81, 83, 86, 113, 145–146, 193–197, 270, 273, 326, 432, 464, 479, 528, 551, 560, 568, 592, 613, 615, 653–654, 657–661, 663–665, 667–679, 681–685, 688, 691–692
- evapotranspiration, 113, 145, 326, 416, 431–432, 551, 560, 592, 602, 609, 611, 613, 618, 653, 657–658, 670, 681–685
- excavation, unsupported, 360
- failure plane, 120, 148–149, 158, 219, 230, 232, 240, 245, 255–256, 269, 307, 321, 361, 368
- failure, time to, 244
- field, stress, 9, 13–14, 24, 28–29, 32, 43, 223, 515
- filter paper, 10, 50–51, 73–74, 79–83, 85–86, 96–102, 123, 197, 504, 567, 570, 575, 577–578, 603–604, 624
- flow, moisture, 51, 70, 600, 659, 681, 687–689, 691
- flow
- saturated-unsaturated, 325–326, 331, 397
 - transient, 137, 326, 344, 385, 400, 412, 436, 445–446, 450–451, 453, 469, 471, 483, 612–613, 620, 623, 626, 660, 687–689, 691, 695–696
 - two-phase, 412, 450–451
 - unsaturated 325–326, 331, 375, 385–386, 390, 397, 400, 411–412, 414, 417, 422, 681
 - vapour, 51, 96, 100, 102, 479, 660, 665–667, 687
- flownet, 411, 417, 422
- flux boundary, 141, 145, 154, 175, 209, 289, 321, 326, 334, 375, 435, 471, 500, 609, 613, 653–654, 657, 681
- flux
- evaporative, 145, 175, 653–654, 657–660, 663, 665, 667, 670–671, 673, 675, 677–679, 684
 - moisture, 146, 155, 167, 175, 653–654, 657
- force function, interslice, 336–337
- force, shear, 323–324, 335–336
- foundation, 3, 6, 61, 97, 107, 141, 146, 155, 193, 209, 277, 286, 333, 376, 590, 602, 604–606, 608–609, 657, 687
- shallow, 6, 141, 590, 605–606, 608, 657, 687
- freezing, 3, 70–78, 209, 592, 609, 617, 687
- function
- interslice force, 336–337
 - permeability, 108, 144–145, 149, 151, 153–154, 166–170, 181, 183, 277, 291, 321, 327, 331, 334, 385, 389–395, 397–398, 402, 411–413, 415–417, 473, 480, 623, 625
 - shear strength, 150–151, 170, 172, 219–220, 277, 279, 281–283, 291–292
 - unsaturated soil property, 108, 149, 166–171, 173–175, 178, 207–208
- gradient
- hydraulic, 154, 385, 412, 416, 503, 613, 660, 687–688, 692
 - thermal, 70, 432, 687–688, 691–692, 695
- ground movement, vertical, 591, 604, 609–619
- groundwater table, 27, 107, 140–142, 145–146, 154–155, 175, 255, 320–321, 328–330, 333–334, 426, 428, 528, 602, 653, 687
- head, 31, 127–128, 133–134, 145, 149, 166, 169, 204, 244, 321, 326–330, 334, 385, 389, 391, 397, 399–402, 409, 411–419, 422, 428–429, 431, 433, 435, 458, 471, 486, 503, 544, 550, 570, 612–613, 615–616, 628, 659–661, 682, 688–689
- heave, 27, 107, 119, 123–125, 127, 129, 133, 193–194, 197, 511, 513, 536, 550–557, 559, 562–567, 577, 580, 582–591, 593–602, 605–606, 608–610, 620, 625, 653–654, 657, 670, 692
- prediction of, 119, 129, 193–194, 197, 511, 513, 536, 550, 552, 554–556, 559, 563–567, 577, 582–586, 589, 593, 598, 657

- total, 123–124, 194, 550–553, 555, 557, 562–566, 582–591, 593–594, 596–601, 605, 625
- heave analysis, one-dimensional, 550, 552
- humidity, relative, 36, 47, 50, 57, 74, 182, 278, 294, 471, 503, 598, 653, 658–661, 663, 667, 671, 673, 676–678, 683
- hysteresis, 55, 96, 102, 149, 158, 182, 394, 512, 516, 518, 523–527, 543, 556, 560, 562, 571–572, 575, 582, 664, 674
- index
 - compression, 294, 528, 532
 - swelling, 27, 528, 294, 533, 559, 563–566, 580, 582–587, 590, 595–598, 600–601, 603, 612
- indices, volume change, 528, 531–536, 539
- infiltration, 62, 65–66, 129, 145, 154–155, 176, 194, 313–314, 318–319, 326, 333, 416, 420, 422, 426, 431–433, 586, 603, 606, 609, 613, 615–618, 627, 653, 657, 670, 688, 691
- instrumentation, 3, 61, 320, 426–430, 435, 662, 683
 - field, 426, 435
- interphase
 - air-water, 33
 - soil-atmosphere, 681
- knowledge-based system, 108, 167, 173–174, 203, 207–211, 213, 215
- laws, flow 129, 137, 166, 451, 489
- limit equilibrium, 121–122, 125, 168, 313, 320, 324, 326–327, 331, 335, 353, 376, 378, 381
- line, phreatic, 154, 169, 399, 401–402, 409, 411–412, 416–417, 422
- loading
 - drained 117, 138, 219, 344, 351–353, 355, 361, 443, 468–469, 472–475, 477, 536
 - isotropic, 117, 148–149, 344, 346–347, 351, 511–512, 517, 523–524
 - K₀, 468–471, 473
 - three-dimensional, 346, 512
 - undrained, 117, 138, 344, 351–353, 355, 443, 468–469, 472, 474–475, 477, 536
 - uniaxial, 512
 - wheel, 60, 62, 67
- measurement
 - matric suction, 38–39, 53–56, 58, 66, 83, 85, 87–88, 92, 123, 129, 431–432, 630–631
 - suction, 35–36, 38–40, 49–51, 53–56, 58, 66, 70, 73, 75–76, 80–83, 85, 87–88, 92, 97, 99, 102, 123, 129–130, 314, 318, 334, 432, 511, 603–604, 630–631
- mechanics
 - continuum, 9, 13–14, 22, 27–32, 42–43, 112, 114, 127, 286, 445, 487, 496, 540, 688
 - multiphase continuum, 32, 42, 112, 127, 445
- membrane, pressure, 35, 193, 195–197
- method
 - double oedometer 554–555
 - General Limit Equilibrium, 313, 335
- model
 - finite element, 213, 215, 400, 411, 420, 422, 546, 681
 - mathematical 445, 523, 545–546, 687
 - rheological, 108, 445–449
- modeling, numerical, 5, 166, 168, 178, 540, 613, 634
- modulus
 - elastic, 28, 116, 136, 373, 517, 551, 572
 - resilient, 639–649
- shear, 162
- Mohr-Coulomb, 111, 120–122, 128, 135, 152, 158–159, 219, 223, 232, 235, 237, 245, 247, 249, 249, 255, 277, 286, 301, 321, 337–340, 360–361, 370, 627
 - extended, 120, 135, 232, 235, 245, 321, 361
- moisture flow, 51, 70, 600, 659, 681, 687–689, 691
- moisture flux, 146, 155, 167, 175, 653–654, 657
- movement, vertical ground, 591, 604, 609–619
- non-linearity, 96, 231–235, 244–245, 250–253, 256, 263, 275, 322, 337–338, 411, 415, 440, 523–525, 527, 645–646
- non-uniqueness, 233, 527
- null test, 13, 15–17, 22, 43
- numerical modeling, 5, 166, 168, 178, 540, 613, 634
- oedometer, one-dimensional, 16, 348, 353–354, 512, 525, 550, 559, 567, 582–583, 469–470
- osmosis, 485
- parameter
 - pore pressure, 28, 123, 138, 344–351, 353, 355, 451, 466, 468–470, 475–476, 483, 688, 691
 - shear strength, 92, 120–121, 130, 159–161, 219, 223–224, 229, 231, 233, 241, 244–247, 249–251, 253, 269–270, 273, 275, 277, 279, 286–287, 290–291, 294–296, 298, 300–301, 309, 314, 318, 320–321, 329, 338, 340, 342, 373, 375–376, 379
- path, stress, 133–134, 233, 272, 367, 371, 462, 474, 495, 511–512, 516, 518, 529–530, 532, 540, 543–544, 548, 550, 554–557, 561–563, 583, 594–596, 620–622, 626–627, 640
- pavement, 60–63, 65–66, 97, 269, 286, 373–376, 379–382, 564, 584, 609, 639, 654, 687, 691
- permeabilities, field, 609
- permeability, coefficient of, 107–108, 127–128, 133–134, 137, 141, 144–146, 149, 151, 166–170, 181, 244, 269, 277, 291, 294, 321, 323, 326–327, 333–335, 339, 349, 385–386, 389–402, 406, 409, 411–412, 414–417, 427, 437, 449, 451, 453, 455, 464, 470–473, 480, 483, 489, 496, 511, 540, 543–544, 546–547, 612–616, 622, 625, 653, 682, 689–690
- permeameter, 540, 544, 548
- phreatic line, 154, 169, 399, 401–402, 409, 411–412, 416–417, 422
- physicochemical, 42–43, 45, 485, 487, 495–496
- plane, failure, 120, 148–149, 158, 219, 230, 232, 240, 245, 255–256, 269, 307, 321, 361, 368
- plate, pressure 35–36, 48–49, 55, 75, 79–83, 86, 97, 158, 161, 193, 195–197, 239, 245, 269, 273, 293–297, 340, 499, 501, 512, 639, 672–673, 675–676
- point, stress, 14, 32, 120, 147–148, 224, 229–230, 442, 516, 518–519, 524, 530
- porosity, 14, 23, 149, 151, 202–204, 206, 210, 273, 287, 339, 344–345, 348, 351, 353, 439, 451, 464, 470, 489, 503–505, 542–544, 660, 664, 690–691
- potential evaporation, 27, 146, 654, 657–659, 663, 670–674, 676–678, 682, 684
- precipitation, 27, 145, 154, 300, 326, 333–334, 428, 431, 505, 592, 598, 602, 604, 611, 613, 618, 653, 670, 674
- prediction, heave 129, 553, 556, 559, 564–565, 582–584, 586, 589
- pressure
 - active earth, 121, 365
 - confining, 113, 120–121, 228, 234–235, 228, 234–235, 261–262, 281, 297, 323, 349, 544, 639–644, 647

- earth, 79, 111, 113–114, 121–123, 125, 155, 237, 360–361, 365–368, 370, 376
- lateral earth, 79, 361, 365, 370, 376
- osmotic, 43–45, 52, 486–488, 491, 493, 495–496, 672
- passive, 122, 360, 362, 364, 376–377, 379
- passive earth, 121, 123, 363, 368, 370
- preconsolidation, 197–198, 561–563, 582–583, 595
- swelling, 139, 513, 532, 554–557, 561–570, 576–577, 580, 582–587, 589–590, 594–606, 613, 620, 625
- properties, classification, 174, 207, 212
- property function, unsaturated soil, 108, 149, 166–171, 173–175, 178, 207–208
- psychrometer, 10, 35–36, 38–39, 50–51, 73–74, 96–97, 99, 102, 115, 117, 123, 553, 593
- rainfall, 3, 129, 155, 168, 255, 313, 320, 327–329, 331, 333–334, 407, 426–429, 431–435, 528, 602, 604–605, 653, 667, 670
- ratio, principal stress 542
- relation, phase, 108
- relationship
- stress-strain, 540, 569
 - volume-mass, 163, 209, 294, 511, 532
- relative humidity, 36, 47, 50, 57, 74, 182, 278, 294, 471, 503, 598, 653, 658–661, 663, 667, 671, 673, 676–678, 683
- requirement, continuity 114, 136, 345, 436–438, 440, 450–451, 453, 515, 541, 550, 622
- response, pore pressure, 344, 348, 351, 473
- road, unpaved, 373–375, 377, 379–381
- safety, factor of, 107, 122–123, 129–130, 135, 300, 313–320, 324–329, 331, 333, 335–336, 340–342, 352, 357–358, 369, 371, 373, 379, 426
- sampling disturbance, 550, 554–556, 561–563, 582–583, 585, 589, 595, 602, 620
- seepage, 33, 65, 79, 107–108, 127–128, 133–134, 141–142, 144–145, 154, 166–170, 174, 209, 327–329, 331, 361, 385–386, 389, 396–397, 399–402, 411–417, 419–422, 425, 608, 612, 654
- transient, 174, 328, 385, 411–413, 415–416
- sensor, 10, 48–50, 53–63, 65–70, 73, 75–83, 85–89, 91–92, 96–102, 326, 629, 683
- shear, direct 160, 170, 219, 231–232, 244–251, 253, 255–256, 258–263, 265, 267, 269–275, 280, 286, 293–295, 302, 322–325, 337–338, 340, 375
- shear force, 323–324, 335–336
- shear modulus, 162
- shear strength
- undrained, 269
 - unsaturated, 158, 160, 172, 219–220, 255, 260, 265, 269, 275, 278, 286–287, 293–296, 309, 314, 321, 333, 337–339
- shear strength versus matric suction, 151, 160–161, 255–258, 260, 263–266, 274–275, 302, 321–323, 325, 337–338
- site, investigation of, 86, 96, 240, 320
- skin, contractile, 13–14, 18, 22–25, 33, 107–108, 111, 113, 125, 127, 157, 161, 345, 436–437, 440, 450, 515, 540–541
- slip surface, 313, 316, 318, 320, 325, 333, 335–337, 341–343, 426
- critical, 313, 316, 333, 341–343
- slope, stability of, 5, 31, 79, 111, 122–123, 127, 129–131, 133, 135, 155, 168–169, 175, 237, 286, 300–301, 309, 312, 313, 320–321, 323–329, 331, 333–335, 337, 340, 353, 356, 376, 411, 422, 426, 681
- soil
- collapsible, 468, 540, 542–543, 546, 626–628, 632
 - compacted, 13, 39, 41–42, 55, 96–97, 102, 111–112, 123, 133, 142, 232, 244, 269, 271, 273, 275, 352–353, 356, 358, 441, 450, 468–469, 528, 540–541, 543–545, 547, 549, 626, 639
 - dry 39, 82, 142, 439, 498, 500, 502, 617, 665, 673–674
 - expansive, 3, 5–6, 27, 33, 111–112, 121, 123, 133, 141, 231, 360, 468, 511, 513, 559, 561, 563, 565, 567, 582–585, 587–590, 592, 598–599, 602, 608–611, 613, 615, 617, 619–621, 623, 625, 654, 657, 681
 - metastable structured, 453, 516
 - residual, 5, 47, 53, 79, 127, 129–131, 133, 144, 237, 240, 245, 300–302, 304, 309, 314, 319, 327–328, 391, 426–427, 429, 431, 433, 435, 450, 468, 540
 - saprolitic, 255, 257, 259–261, 263, 265–268
 - stable-structured, 149, 155, 453, 516, 518, 540, 545–546, 548
 - structure of, 13–14, 16, 22, 29, 44, 113, 115–116, 122, 129, 133, 135–137, 154, 158, 161–163, 194, 197, 241, 275, 293, 309, 345, 347, 360–361, 370, 378, 385, 389, 392–393, 413, 436–437, 440, 445, 447, 450–453, 469–470, 475, 481–483, 499–500, 515–519, 523–529, 541–543, 545–546, 550, 552, 560, 621, 642, 654, 660–661, 688–690
 - swelling, 53, 79, 107, 111, 129, 193, 511, 550, 559, 563–564, 567, 570, 575, 580, 582, 590, 602, 604–605, 608
- soil structure volume change, 453, 516, 518, 523–525
- solubility, 273, 345, 353, 469–470
- specific volume, 47, 71, 149, 392, 512
- squeezer, pore fluid, 51
- state, steady, 124, 133–134, 154, 169, 174, 328–329, 385, 399–401, 403, 405, 407, 409, 411, 415–417, 420, 422, 494–495, 594, 684
- statically compacted, 81, 160, 258, 269–271, 273, 275, 286, 293–294, 301, 340, 544, 629
- steady state, 124, 133–134, 154, 169, 174, 328–329, 385, 399–401, 403, 405, 407, 409, 411, 415–417, 420, 422, 494–495, 594, 684
- stone, porous 196, 501, 503, 505–506, 567, 575, 630
- strain
- normal, 450, 516–517
 - volumetric 31, 136, 160, 450, 488, 494, 516–517, 542, 623
- strain rate, 239, 295, 305
- strength
- unsaturated shear, 158, 160, 172, 219–220, 255, 260, 265, 269, 275, 278, 286–287, 293–296, 309, 314, 321, 333, 337–339
 - undrained shear , 269
- stress
- deviator, 238–241, 262, 264–265, 302, 305, 308, 323, 344, 351, 639–642, 644–647
 - net horizontal, 547
 - net normal, 9, 149, 159–160, 209, 215, 231–235, 245–247, 250–252, 255–256, 258–261, 263–265, 267, 269–271, 273–274, 278, 286, 290–291, 293–294, 296–298, 321, 338, 340, 378, 449, 457, 461–462, 470, 474, 477, 480–481, 483, 500, 528, 530–534, 540, 542, 583, 611–612, 621–622, 626–628
- stress field, 9, 13–14, 24, 28–29, 32, 43, 223, 515
- stress history, 118, 158, 182, 293, 560–561
- stress path, 133–134, 233, 272, 367, 371, 462, 474, 495, 511–512, 516, 518, 529–530, 532, 540, 543–544, 548, 550, 554–557, 561–563, 583, 594–596, 620–622, 626–627, 640

- stress point, 14, 32, 120, 147–148, 224, 229–230, 442, 516, 518–519, 524, 530
- stress ratio, principal, 542
- suction
- measurement of, 52
 - osmotic 10, 35–36, 38, 40, 47, 51–52, 102, 115–116, 123, 142, 182, 278, 287, 289, 326, 338, 390, 550, 553, 654, 672–673, 675–676, 678
 - total, 10, 35–36, 38, 40–41, 47, 50–51, 96–97, 99, 102, 115, 123, 142, 149, 182, 278, 287, 289, 326, 338, 390, 392, 512, 553, 603, 654, 660, 670, 674–679
- surface
- constitutive, 9, 42, 45, 111, 117–119, 138, 149, 151, 441–442, 481, 483, 488–489, 495, 512–513, 516–520, 523–532, 537, 541, 554, 593–594
 - slip, 313, 316, 318, 320, 325, 333, 335–337, 341–343, 426
 - void ratio constitutive, 149, 513, 529, 531–532, 593–594
- surface tension, 157, 184, 344, 391
- swelling index, 27, 528, 294, 533, 559, 563–566, 580, 582–587, 590, 595–598, 600–601, 603, 612
- system
- knowledge-based, 108, 167, 173–174, 203, 207–211, 213, 215
 - multiphase 9, 13, 22, 28, 32–33, 43, 436
- technique, squeezing, 10, 38–39
- Tempe cell, 158, 412, 480, 664
- tensile strength of water, 79, 85
- tension, surface, 157, 184, 344, 391
- test
- CD 303
 - consolidated drained, 231, 244–245, 302
 - consolidation, 108, 119, 123, 193–194, 196–199, 294, 352, 448, 452, 457–458, 461, 464, 466, 468, 472, 474–481, 528, 533, 535, 544, 554, 568, 570–571, 575, 577, 580, 620
 - constant volume, 535–536, 556, 567–569, 576, 582–583, 622–623
 - constant volume oedometer, 125, 550, 554–556, 561, 566, 582, 590, 593–596, 603, 605, 620
 - constant water content 231, 233, 245, 251, 274, 301–302, 457, 463–464, 468, 470, 474–475
 - free swell, 123, 197, 560, 567, 570, 576
 - free swell oedometer, 562, 582, 590, 620
 - multistage, 219, 231, 239, 241, 244, 246–247, 250, 294–295, 305, 308–309, 314
 - multistage triaxial, 237, 300, 302, 305–307, 309, 314
 - null, 13, 15–17, 22, 43
 - oedometer, 123–125, 348, 353–354, 356, 469–470, 512, 528, 534, 539, 544–545, 547, 550, 553–556, 559, 561–567, 582–584, 590, 593–596, 600, 603–605, 620–625
 - permeability, 134, 416, 544
 - shrinkage, 193–194, 512, 532, 534–536, 539
 - triaxial, 30, 130, 160–161, 223–225, 231–233, 237, 239–245, 253, 255, 258–259, 261, 264–265, 300–302, 305–307, 309, 314, 427, 512, 545, 548, 639
- theory
- consolidation 133, 413, 436–439, 441, 443, 450–451, 453, 455–456, 468–470, 628, 688–689
 - non-linear, 373
 - time to failure, 244
 - transpiration, plant, 193, 654, 681–683, 685
 - triaxial test, multi-stage, 237, 300, 302, 305–307, 309, 314
- uniqueness, 117, 129, 137, 140, 203, 231, 233, 251, 515–516, 518–523, 525–527, 551, 626, 640
- value, air entry, 16, 53, 144, 149–151, 159, 195, 197, 208, 219, 231, 234–235, 237, 244, 252, 257, 263, 265, 278–279, 281, 291–292, 323, 338–339, 377–379, 459, 473, 512, 519, 665
- variable
- deformation state, 13, 28, 31, 158, 437, 515–516
 - stress state, 6, 9–10, 13–14, 16, 18, 22, 25, 27–33, 42–45, 53, 108, 111, 114–115, 117–119, 127–129, 140–142, 146–149, 157–159, 166, 174, 219, 223–224, 231–232, 234, 237, 239, 245, 255–256, 269, 272, 277, 286, 301, 305, 313, 321–322, 337, 344, 360–361, 378, 390, 411, 413, 436–437, 441, 445–449, 452–453, 464, 474–475, 477–479, 485, 487–489, 495–496, 511, 515–518, 524, 528–529, 531, 537, 539–541, 543, 546, 550–552, 555, 559–562, 582, 592–593, 611–612, 620, 626, 628, 635, 653, 659, 689, 691
 - volume change, 9, 14–22, 30, 32–33, 35, 42, 45, 49, 60, 70, 78, 96, 107–108, 111, 113–114, 121, 123, 125, 127, 129, 133, 135–136, 140–143, 148, 152, 154–155, 157, 164, 166, 169–170, 174, 181, 193–195, 207–209, 223, 238–239, 246–247, 250, 273, 277, 279, 287, 344–346, 348, 353–356, 371, 385, 389, 392–393, 413–414, 422, 436–438, 441, 449–450, 452–454, 456–458, 460–462, 464–466, 468–471, 473–483, 485–497, 511–513, 515–521, 523–536, 539–542, 544, 550, 559, 562, 567–568, 570, 575, 577, 582, 590–592, 595, 598, 600, 602–603, 608, 611–615, 617, 620–621, 623, 625–629, 632–637, 653, 660–661, 664, 681–682, 687, 689, 695
 - coefficient of, 107, 355–356, 385, 414, 422, 470, 480, 488–489, 621, 637
 - overall, 16, 22, 32, 108, 287, 345, 437, 512, 527, 689, 695
 - soil structure, 453, 516, 518, 523–525
 - volume, specific, 47, 71, 149, 392, 512
- walls, retaining, 121, 141, 360, 371
- water content change, coefficient of, 129, 137, 512, 530
- water content test, constant, 231, 233, 245, 251, 274, 301–302, 457, 463–464, 468, 470, 474–475
- water content, volumetric, 150–153, 170, 181–184, 186–188, 203, 207–210, 212, 219–220, 278–279, 281, 287, 289–291, 296, 328, 338–340, 390–393, 395, 397, 486, 498–499, 512, 542–543, 659–660
- water, tensile strength of, 79, 85